1959 PERIODICAL
1959
LIBRARY
22 1959
FISH & WILDLIFE

WOODS HOLE OCEANOGRAPHIC INSTITUTION

COLLECTED REPRINTS

1958

JULY, 1959

LIBRARY
BUREAU OF COMMERCIAL FISHERIES
U. S. FISH AND WILDLIFE SERVICE
P. O. BOX 3830
HONOLULU 12, HAWAII

Digitized by the Internet Archive
in 2025

https://archive.org/details/collected-reprints-woods-hole-oceanographic-institution_1958

WOODS HOLE OCEANOGRAPHIC INSTITUTION

COLLECTED REPRINTS

1958

JULY, 1959

LIBRARY
BUR. OF COMM. FISH.
HON. BIOL. LAB.

Periodical
Woods Hole Oceanog. Instit.
Collected Reprints,
1958
2311

This volume contains contributions from the Woods Hole Oceanographic Institution which were published in 1958; also the Annual Report of the Director for the year 1958.

TABLE OF CONTENTS

Contribution No.

BARNES, H.
Regarding the Southern Limits of *Balanus balanoides* (L) 998

BARNES, H. and MARGARET BARNES
The Rate of Development of *Balanus balanoides* (L) Larvae 928

BARNES, H. and MARGARET BARNES
Further Observations on Self-Fertilization in *Chthamalus* sp. 949

BIGELOW, HENRY B. and WILLIAM C. SCHROEDER
Four New Rajids from the Gulf of Mexico 932

BLANCHARD, DUNCAN C.
Electrically Charged Drops from Bubbles in Sea Water and their Meteorological Significance 849

BOWEN, VAUGHAN T. and T. T. SUGIHARA
Marine Geochemical Studies with Fallout Radioisotopes 970

BRESLAU, L. R. and H. E. EDGERTON
The Luminescence Camera 1001

DAY, C. GODFREY
Surface Circulation in the Gulf of Maine Deduced from Drift Bottles 977

FALLER, ALAN J.
An Optical Method for the Measurement of Surface Waves in the Laboratory 945

HERSEY, J. B. and M. S. RUSTEIN
Reconnaissance Survey of Oriente Deep (Caribbean Sea) with a Precision Echo Sounder 944

ICHIYE, TAKASHI
A Theory of Vertical Structure of Density in the Ocean 951

ICHIYE, TAKASHI
Tsunami Waves — What are known about them — How we have studied them 952

ICHIYE, TAKASHI
The Response of a Stratified, Bounded Ocean to Variable Wind Stresses 963

ICHIYE, TAKASHI
On Convective Circulation and Density Distribution in a Zonally Uniform Ocean 981

KETCHUM, BOSTWICK H. and VAUGHAN T. BOWEN
Biological factors determining the distribution of radio-isotopes in the sea 968

KETCHUM, BOSTWICK H., JOHN H. RYTHER, CHARLES S. YENTSCH and NATHANIEL CORWIN
Productivity in Relation to Nutrients 946

LEWIN, JOYCE C.
The Taxonomic Position of *Phaeodactylum tricornutum* 936

Contribution No.

LEWIN, JOYCE C., R. A. LEWIN and D. E. PHILPOTT
Observations on *Phaeodactylum tricornutum* 935

MALKUS, JOANNE STARR
On the Structure and Maintenance of the Mature Hurricane Eye 915

MALKUS, W. V. R. and G. VERONIS
Finite Amplitude Cellular Convection 943

MATHER, FRANK J., III, and ROBERT H. GIBBS, JR.
Distribution of the Atlantic Bigeye Tuna, *Thunnus obesus*, in the western North Atlantic and the Caribbean Sea 942

McLEOD, G. C.
Delayed Light Action Spectra of several Algae in Visible and Ultraviolet Light 955

MILLER, ARTHUR R.
The Effects of Winds on Water Levels on the New England Coast 900

MILLER, ROBERT L. and JOHN M. ZEIGLER
A Model Relating Dynamics and Sediment Pattern in Equilibrium in the Region of Shoaling Waves, Breaker Zone, and Foreshore 958

MOULTON, JAMES M.
The Acoustical Behavior of some Fishes in the Bimini Area 957

MOULTON, JAMES M.
A Summer Silence of Sea Robins, *Prionotus* spp 960

REDFIELD, ALFRED C.
Preludes to the entrapment of organic matter in the sediments of Lake Maracaibo 784

REDFIELD, ALFRED C.
The Inadequacy of Experiment in Marine Biology 923

REDFIELD, ALFRED C.
The Biological Control of Chemical Factors in the Environment 976

RICHARDSON, WILLIAM S. and CHARLES H. WILKINS
An Airborne Radiation Thermometer 934

RYTHER, JOHN H. and CHARLES S. YENTSCH
Primary Production of Continental Shelf Waters off New York 906

RYTHER, JOHN H., CHARLES S. YENTSCH, E. M. HULBURT and RALPH F. VACCARO
The Dynamics of a Diatom Bloom 978

SANDERS, HOWARD L.
Benthic Studies in Buzzards Bay. I. Animal-Sediment Relationships 940

SCHOLANDER, P. F.
Counter Current Exchange: A Principle in Biology 983

SMAYDA, THEODORE J.
Biogeographical Studies of Marine Phytoplankton 965

Contribution No.

SOULE, FLOYD M. and R. M. MORSE
Physical Oceanography of the Grand Banks Region and the Labrador Sea in 1957 959

SOULE, FLOYD M. and J. E. MURRAY
Physical Oceanography of the Grand Banks Region and the Labrador Sea in 1956. (Dated 1957) 877

SPENCER, A. T. and D. C. BLANCHARD
A Portable Raindrop Recorder for Semi-Continuous Determination of Size Distributions 979

STOMMEL, HENRY
Letter to the Editors: The Abyssal Circulation 953

STOMMEL, HENRY, A. B. ARONS and A. J. FALLER
Some Examples of Stationary Planetary Flow Patterns in Bounded Basins 939

TURNER, HARRY J., JR.
The Effect of Nutrition on the Color of the Callus of *Polinices duplicatus* 938

VERONIS, G.
On the Transient Response of a β-plane Ocean 933

von ARX, WILLIAM S.
"Dister": A Displacement Sequence Stereoscope 930

von ARX, WILLIAM S.
Synoptic Photography 931

VOSS, GILBERT L.
The Cephalopods Collected by the R/V Atlantis during the West Indian Cruise of 1954 994

WOODCOCK, A. H.
The Release of Latent Heat in Tropical Storms Due to the Fall-Out of Sea-Salt Particles 920

YENTSCH, CHARLES S. and RALPH F. VACCARO
Phytoplankton Nitrogen in the Oceans 972

THE WOODS HOLE OCEANOGRAPHIC INSTITUTION
Report for the Year 1958

LIST OF CONTRIBUTIONS

The following contributions are not included in this volume:

HERSEY, J. B.
Electronics in Oceanography (Dated 1957) 874

MALKUS, JOANNE STARR
On the Structure of the Trade Wind Moist Layer 969

Contribution No. 784

PRELUDES TO THE ENTRAPMENT OF ORGANIC MATTER IN THE SEDIMENTS OF LAKE MARACAIBO

BY

ALFRED C. REDFIELD

Reprinted for private circulation from
HABITAT OF OIL
The American Association of Petroleum Geologists
June 1958

PRELUDES TO THE ENTRAPMENT OF ORGANIC MATTER IN THE SEDIMENTS OF LAKE MARACAIBO[1]

ALFRED C. REDFIELD[2]
Woods Hole, Massachusetts

ABSTRACT

Sedimentation has continued in the Maracaibo Basin since the formation of its earliest oil-bearing strata. The present lake is reputed to be one of the most productive waters in the world. Perhaps no more favorable place can be found for examining the conditions presumed to precede the accumulation of organic matter in sedimentary deposits.

The lake appears to have been fresh in the recent past. Sea water gained access to the basin when the rising sea level drowned its approaches to a present depth of 60 feet. Since then marine sediments have greatly reduced the sill depth. Escaping fresh water limits the entrance of sea water, which occurs only during three months of the dry season.

The lake water contains about one part in thirty of sea water, uniformly distributed by an active wind-driven circulation. In the deeper basin, with depths of 100 feet, the salt content is substantially higher. The oxygen content of this "deep water" is reduced and over a large area of bottom is anaerobic.

The fauna of the lake on superficial observation is limited in variety and numbers. Marine forms are restricted to species adapted to life at very low salinities. The significant bulk of organic matter is produced by fresh-water species of planktonic algae. These at times produce prominent surface blooms.

The potential fertility of the lake water is revealed by its phosphorous content. The total phosphorous is about 1.4 microgram atoms per liter in the mixed layers above the "deep water." This is more than commonly found in surface waters of the sea, but is less than that of the deep water of the Pacific and Indian Oceans. The phosphorus, and presumably other nutrients, are derived from land drainage and are accumulated in the lake by evaporation and by the sinking of organisms into the deep water.

One third of the phosphorus is present in inorganic form available for plant nutrition. Consequently, growth is not limited by its availability in the photic zone. In the "deep water" the phosphorus content is manifoldly increased by the sinking of organisms. The oxygen available is insufficient to oxidize this accumulation, and conditions unusually favorable for the entrapment of organic matter in sediments result.

Sedimentation is active in the lake, particularly in the southwest quarter, where the Catatumbo River is building an extensive delta. Its water discolors the lake for a great distance along the shore. The lake bottom consists of soft blue mud which, in the anaerobic region, is black for several inches below the surface and smells strongly of H_2S. The mud is sufficiently unconsolidated to permit a test pile to sink 30 feet under its own weight.

It is concluded that Lake Maracaibo is an unusually favorable place to study the processes which lead to the entrapment and the subsequent transformation of organic matter in sediments.

> "Petroleum in its natural occurrence is closely associated with marine or semi-marine near-shore sediments. The relation is practically universal and has persisted since Cambrian time, very probably without material alteration. The study of the depositional zones of present-day seas and oceans therefore appears essential to an understanding of oil occurrence, particularly in its initial stages." Eugene Stebinger (1950).

The Maracaibo Basin in Venezuela is the site of one of the world's most productive oil fields. The greater part of the production is drawn from under the water of the present lake. Lake Maracaibo itself is noted for its exceptional plant productivity. An experienced limnologist, Dr. Fritz Gessner, has stated that this lake may well be the richest in plankton of all the waters of the earth (1953a). The possibility that these two aspects of Lake Maracaibo may be related is strengthened by its geological history.

Lake Maracaibo lies in a geosynclinal basin of sedimentation which is almost completely surrounded by mountains. The basin has been slowly sinking and

---

[1] Read before the Association at New York, March 30, 1955. Manuscript received, May 2, 1956. Contribution No. 784 from the Woods Hole Oceanographic Institution.

[2] Woods Hole Oceanographic Institution.

simultaneously accumulating a tremendous volume of sediments while the bordering mountains have been rising at the same rate. The lake is underlain by a total thickness of some 16,000 feet of post-Eocene sediments (Zuloaga, 1950). The topographic depression in which the present lake lies has had nearly the same size and shape since some time in the Oligocene, but the actual area covered by water has varied in position. The connection with the sea has been variable also and the sediments show a continual alternation between marine, brackish, fresh water, and terrestrial deposits (Sutton, 1946).

The present lake thus appears to represent one of a series of alternating conditions which have recurred in the past. Let us examine what the present condition is and whether it is one favorable to the initial process on which the formation of petroleum is assumed to depend; namely, the entrapment of organic matter in the sediments.

The topography of the outlet suggests that in comparatively recent times Lake Maracaibo stood above sea level, and that its water was fresh. The form of the Strait of Maracaibo resembles a river valley eroded under arid conditions. A deeper trough along its western side represents the actual course of the river which once drained the lake. A rise of sea level of at last 60 feet would be required to drown this valley to the present lake level, and would have given access of salt water to the lake. Such a rise is well within the limits thought to have occurred with the decline of glaciation (Kuenen, 1950). Subsequently, marine deposits filled the bight in which Tablazo Bay lies and built the barrier islands and bars which separate it from the outer sea (U. S. A. Corps of Engineers, 1938). The marine deposits at the entrance to the lake restrict the inlet to such an extent that it is only during the dry season, when the outflow of lake water slackens, that appreciable quantities of sea water enter the lake. This salt water is mixed with lake water by the tides as it enters. The resulting mixture, however, is denser than the lake water and flows down along the bottom to form a pool of saline water in the deeper basin.

Although the restricted entrance to the lake reduces the tide to insignificance, the lake water is in active circulation. A current with an average speed of half a knot flows around the lake in an anticlockwise direction (Fig. 1). It is driven presumably by the distribution of the prevailing winds and supported by the distribution of density in the lake water and the influence of the Corioli force. Its result is to mix the water thoroughly down to the upper limit of the pool of saline water over the bottom, and to produce almost uniform conditions from one end of the lake to the other. Its further effect is to spin the pool of saline water up into a cone which rises to within 50 feet of the surface at the center of the lake, and to withdraw it from around the margins, where the mixed water extends to the bottom, even in places where the depth is as great as anywhere—that is, about 100 feet (Fig. 2).

The chloride content of the mixed water of the lake, which accounts for more than nine tenths of its volume, is between 700 and 800 ppm. This corresponds to a salinity a little greater than one part per thousand or to about one part of sea

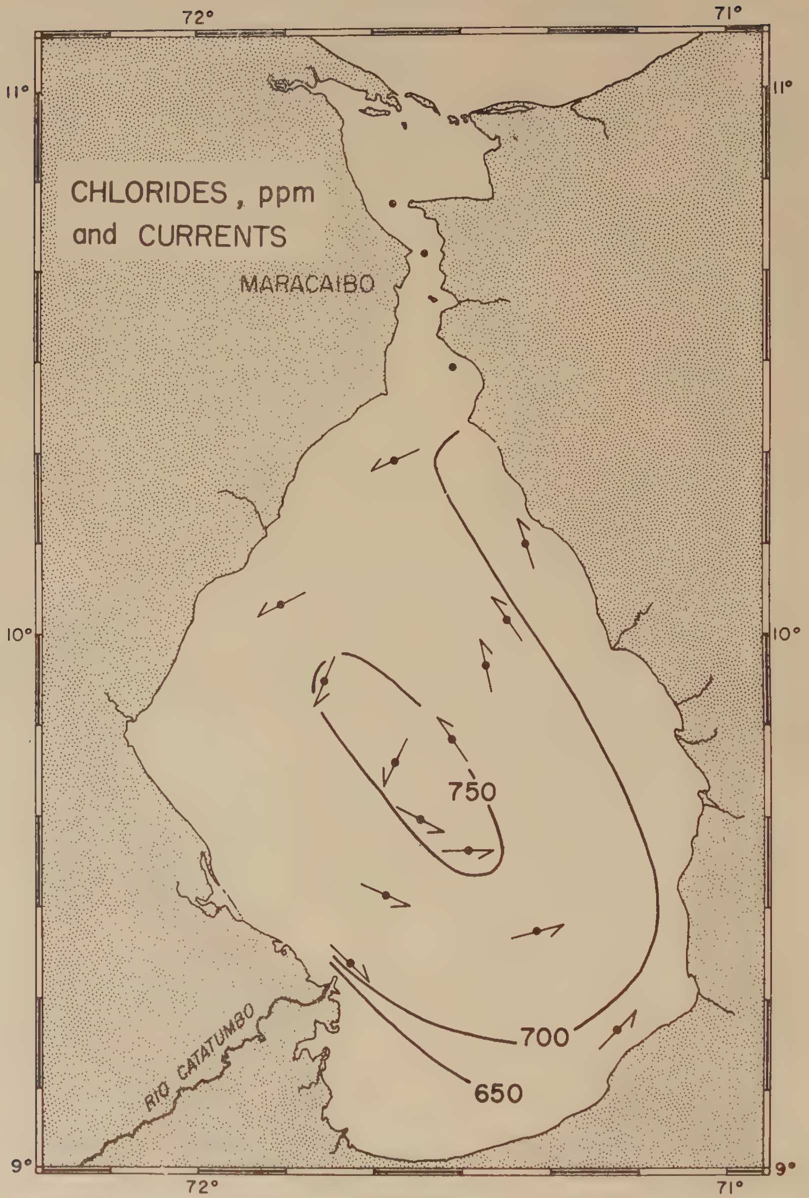
72°
71°
11°
10°
9°
CHLORIDES, ppm
and CURRENTS
MARACAIBO
750
700
650
RIO CATATUMBO

FIG. 1.—Direction of current and concentration of chloride in the surface of Lake Maracaibo. March 1954.

water in thirty. A few years ago, presumably because of deficient rainfall, the chlorides of the mixed water rose to about 1,200 ppm, but this condition did not persist. In the pool of salt water over the bottom, the chloride concentration is greater than 2,000 ppm at the center. This relatively high salt content gives this mass of water stability which leads to a depletion of its oxygen content and favors the accumulation of organic matter at the bottom.

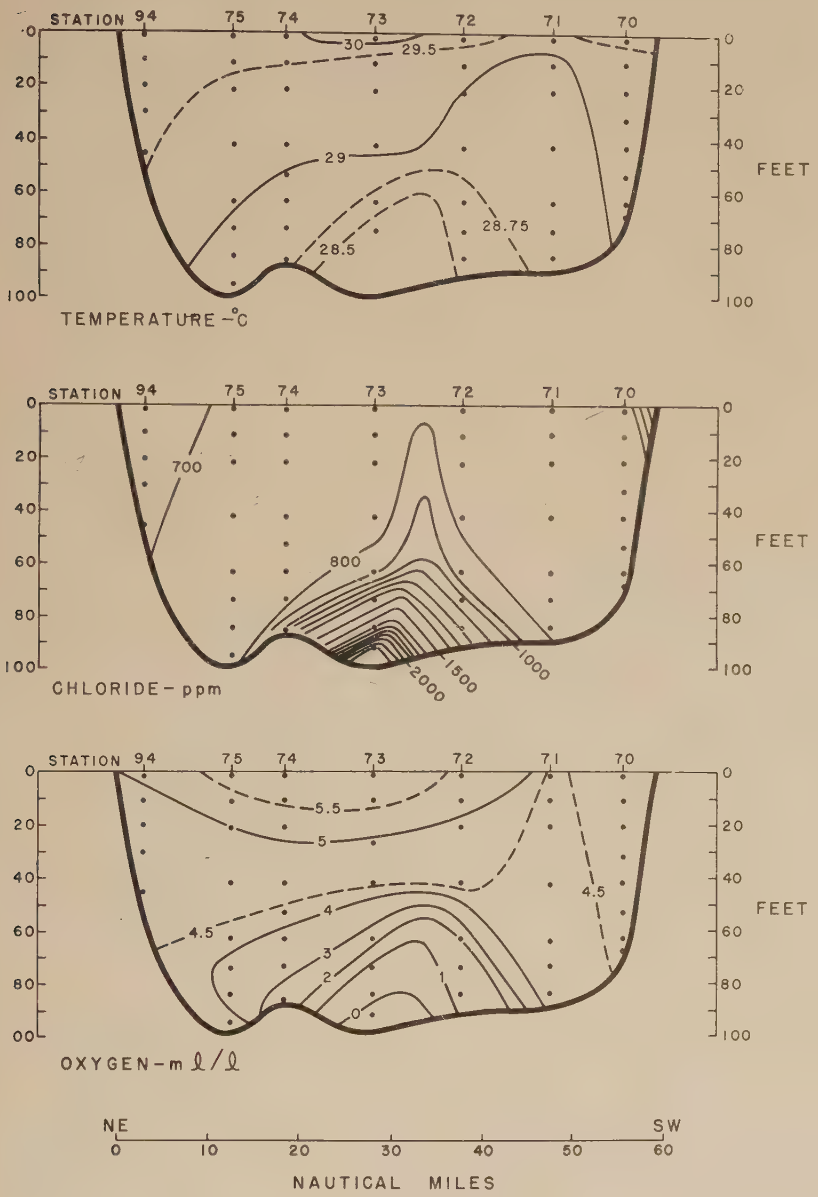

FIG. 2.—Distribution of temperature, chloride, and oxygen in a vertical section running NE to SW across Lake Maracaibo. March 1954.

On superficial observation the lake does not appear to support a particularly rich fauna. Marine invertebrates are excluded except for a few forms, such as blue crabs and teredos which are adapted to live at very low salinities. Doubtless the reciprocal relation excludes many fresh-water species which cannot tolerate the existing salinity. Fish are present in variety and numbers sufficient to provide good angling, and supply a food source for the lakeside villages (Schultz, 1949).

The only extensive fishery in evidence, however, is conducted in the more saline water of Tablazo Bay. In the same way, sea birds which obtain their food from pelagic sources are scarce on the lake in contrast to the waters of its approaches.

The bulk of organic matter present in the lake is unquestionably in the form of planktonic algae and their decomposition products. Many observers, like Gessner, have been impressed by the conspicuous blooms, or even scums, of algae which appear on the lake at times. Such blooms as we have observed, in May and June, were limited to a very thin layer at the surface. No blooms were noted in March. To the eye the lake water was clearly more turbid than is usual in open coastal waters or lakes of comparable size. In the open lake a white disk cannot be seen below depths of 8–10 feet. The turbidity was not greater, however, than we have observed among the San Juan Islands (at Friday Harbor, Washington) and was less than we have seen in the polluted water of Great South Bay, Long Island.

The phytoplankton of the lake are characteristic fresh-water species, but include a few known to occur in brackish environments. The dominant forms are a species of *Macrocystitis,* a colonial blue-green, *Aulacoidiscus,* a diatom, and *Lyngbia,* a filamentous blue-green. The surface blooms observed were due to *Anabaena circinolis,* which was the only species recorded which is commonly associated with such blooms. The counts of the dominant forms ranged from 40 to 110 billion per cubic meter in the mixed water and were as high as 22 billion in a sample from a depth of 98 feet. These are exceptionally high counts. It is noteworthy that the numbers are large even over the bottom in the deep part of the lake.[3]

The only precise means of estimating the organic production of a body of water are biochemical. For the purpose one would like to know the quantities and the rates of transformation of the principal elements which enter into the synthesis and decomposition of organic matter; that is, of carbon, oxygen, nitrogen, and phosphorus. One needs to know also the rates of movement of dissolved substances and of organisms between the illuminated layers near the surface, where photosynthesis takes place, and the deeper layers where processes of decomposition occur.

Lacking full information, as we do, useful knowledge can be obtained from measurement of the phosphorus fractions in the water and a comparison of their values with the oxygen content of the water. The potential fertility, that is, the quantity of organic matter which could be formed in the water assuming no other element became limiting, is indicated by the total phosphorus content (Harvey, 1946). The fraction of the potential fertility which is realized is given by the difference between the total phosphorus and the inorganic phosphorus of the water, and represents phosphorus in organic combination, either as living organisms or products of their decomposition.

The phosphorus of the lake water is derived almost exclusively from land drainage, as shown by the proportions of fresh and salt water in the lake and the relatively small amounts of phosphorus in the off-lying sea. The total phosphorus content of the Caribbean, off the Gulf of Venezuela, is about 0.3 microgram atoms per liter, whereas in the lake it is four or five times as great. Water remains in the lake basin for some five years and nonvolatile solutes for ten years on the average, so that the nutrients which produce organic matter in the lake remain there and may be recycled many times in the course of its production and decomposition. Photosynthesis exceeds respiration in only the upper 10–20 feet of water, as shown by the depth to which the water is completely saturated with oxygen. Below these depths decomposition exceeds synthesis, as shown by the decreasing oxygen content of the water.

---

[3] I am indebted to Mr. John T. Conover for examining the phytoplankton in water samples collected by Nansen bottle in May-June 1953, and providing the information given in this paragraph. See also Gessner (1953b, 1955) for information on the flora and fauna of Lake Maracaibo.

The total phosphorus content of the mixed water, which lies above the pool of saline water near the bottom, is about 1.4 microgram atoms per liter. Of this about three quarters is in organic combination. The remaining 0.3 or 0.4 microgram atoms is present as inorganic phosphate, which has not been assimilated in the production of organic matter. Gessner (1953b, 1955) suggests that this residue may be due to the deficiency of some other nutrient, such as nitrogen. We believe, however, that it is more likely the result of the relatively rapid mixing of the water in the upper layers of the lake, so that no parcel of water remains long enough in the illuminated region to have its phosphates completely absorbed by the plant cells.

This view is consistent with the distribution of temperature and density with depth and explains why the surface waters do not become substantially oversaturated with oxygen. If it is correct, it indicates that nutrients are not the limiting factor in organic production, and that its rate is limited primarily by the rate of insolation of the lake's surface. Considering the tropical location of Lake Maracaibo, which provides high and uniform temperatures throughout the year and high annual illumination, it seems probable that conditions in the surface waters are nearly optimal for realizing the highest rates of production which its potential fertility will permit.

In the deeper parts of the lake the total phosphorous content increases—to maximal values of more than 6 microgram atoms per liter, or four times the quantity in the mixed water near the surface (Fig. 3). This fact can be explained by the sinking of organisms or their partially decomposed fragments, from the site of synthesis near the surface. From this accumulation of organic matter only about one half of the combined phosphorus has been liberated in the form of inorganic phosphate ions. It is evident that accumulation is taking place faster than oxidation of the organic matter can liberate the combined phosphorus of the material. A consideration of the dissolved oxygen in lake water shows that this must be so.

The statistical composition of plankton shows that 1 milliliter of oxygen is required to oxidize the organic matter containing 0.42 microgram atoms of phosphorus (Fleming, 1941). The surface water of Lake Maracaibo contains about 5 milliliters per liter of oxygen. If this water leaves the surface its contained oxygen can oxidize organic matter containing not more than about 2.1 microgram atoms of phosphorus per liter. This is sufficient to oxidize all the organic matter which can be formed in a liter of surface water. It is, however, entirely inadequate to oxidize the quantities of organic matter which accumulate near the bottom. As a result, the oxygen is entirely depleted in these layers and a substantial residue of unoxidized organic matter remains.

The depletion of oxygen and the accumulation of organic phosphorus in the deep water are closely correlated with the concentration of chlorides in these layers of water. (Fig. 3). There can be little doubt that the greater density, and consequent stability, of the pool of more saline water near the bottom is a critical factor in reducing vertical mixing and thus allowing organic matter to accumulate there.

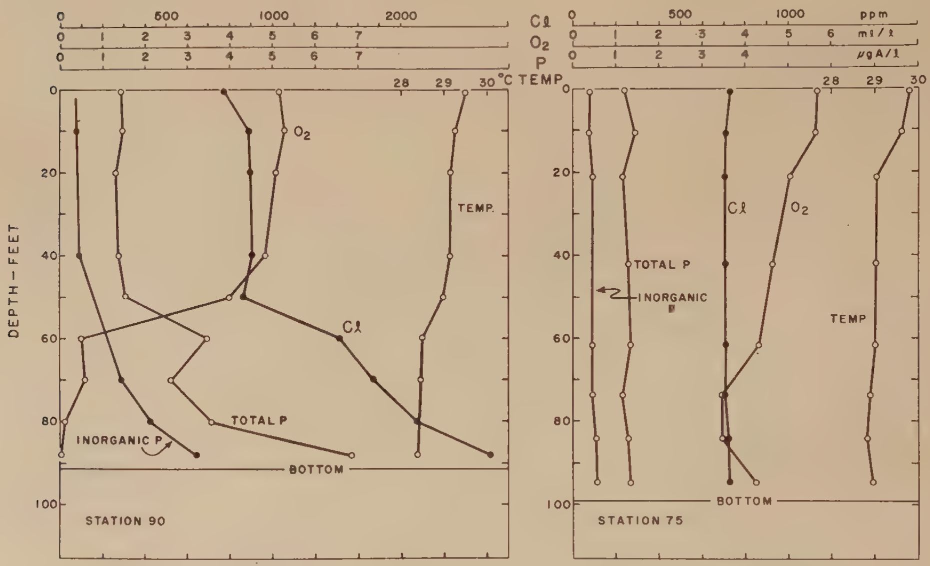

Fig. 3.—Distribution of temperature, chloride, oxygen, and phosphorus with depth at Station 90 near the center of Lake Maracaibo, and at Station 75 ten miles from the NE shore. March 1954.

Two conclusions emerge from these considerations which bear on our problem—1. The conditions for the synthesis of organic matter in the surface waters of Lake Maracaibo are nearly optimal, given the quantities of nutrients available in the water; and 2. the quantitative relations of oxygen solubility and nutrient concentration are such that very substantial quantities of unoxidized organic matter exist over the bottom.

Because of current concern with sedimentary processes on the continental shelves in relation to the sources of petroleum, it is of interest to compare the hydrobiological conditions observed in the ocean with those described for Lake Maracaibo. Figure 4 shows the distribution with depth of oxygen content, total phosphorus, inorganic phosphorus, and, by difference in the latter two, the organic phosphorus at a number of coastal positions. In general it may be said that—

1. In the surface waters the potential fertility as shown by the total phosphorus

content is not superior in the lake to the coastal situations. It is inferior to the Strait of Juan de Fuca where somewhat exceptional conditions obtain, and is superior to the Gulf of Maine where the surface phosphates have been depleted

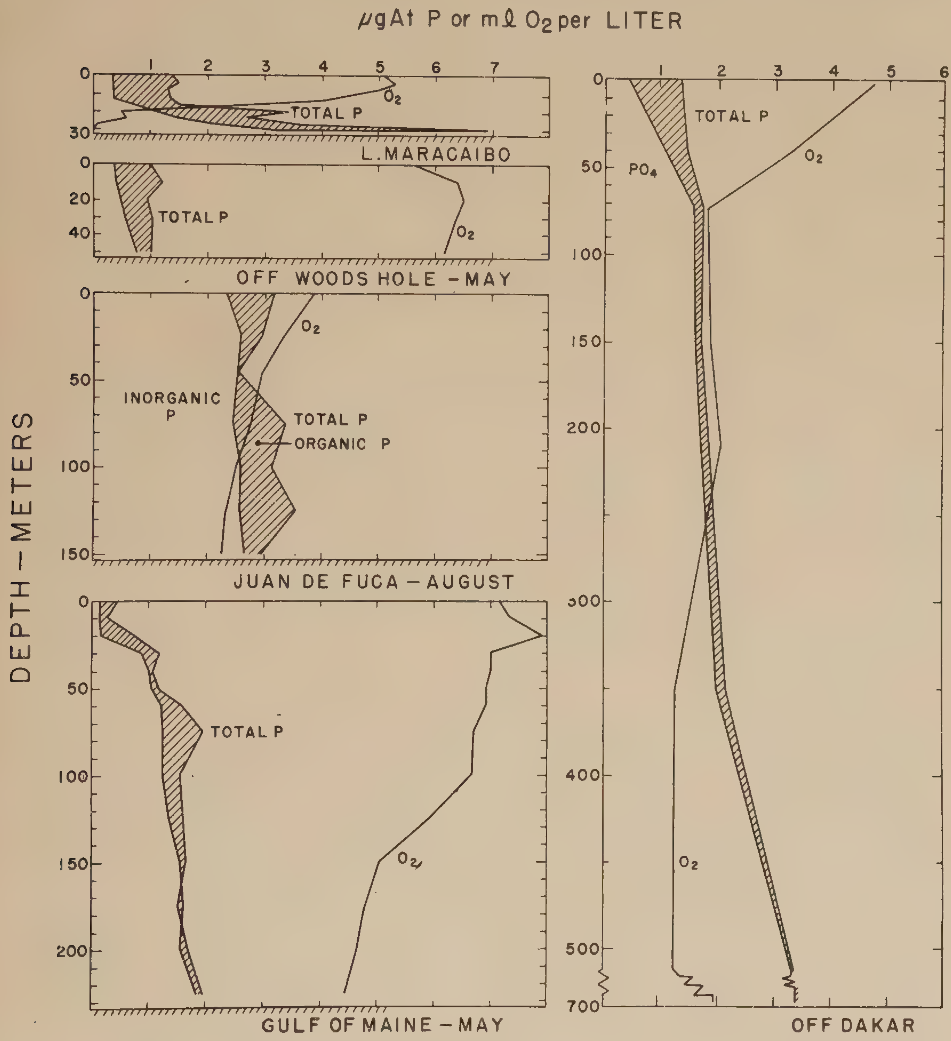

FIG. 4.—Distribution of phosphorus fractions and oxygen with depth in Lake Maracaibo, in coastal and in oceanic water. The crosshatched area represents the organic phosphorus content.

by a seasonal bloom which has sunk carrying phosphate out of the surface (Redfield, *et al.*, 1937).

2. In the surface waters the concentration of organic phosphate is very much the same in the lake as in the coastal situations.

3. The consistent difference is in the deeper water where in the ocean no substantial accumulation of organic phosphate occurs at depth.

4. Correlated with this is the fact that in all cases the oceanic water contains substantial quantities of dissolved oxygen even down to the bottom.

Accumulating evidence indicates that in the sea most of the organic matter produced at the surface is decomposed before sinking more than a few hundred meters. At such depths mixing processes keep the water well oxygenated and retard the accumulation of organic matter on the bottom. It appears that only in basins separated from the ocean by shallow sills and devoid of strong tidal action, such as the Scandinavian fjords and the Black Sea, are conditions encountered along the ocean coast which approach those in Lake Maracaibo in favoring the accumulation of unoxidized organic matter at the bottom. The importance of the oxygen content of the overlying water to the organic content of sediments is suggested by recent findings in the Gulf of Mexico where it has been shown that the depths at which the organic content is highest correspond closely to those where the oxygen content of the water is minimal (Richards and Redfield, 1954).

The concentrations at which organic matter is entrapped in sediments naturally depend upon the relative rates of sedimentation and of the accumulation of organic matter at the bottom. In Lake Maracaibo the principal source of sediment is undoubtedly the Catatumbo River, which drains the greater part of the watershed lying in the region of heavy rainfall to the south and west of the lake. This river has built a delta which extends prominently into the lake, and from which the depths drop sharply to the level of the lake bottom at more than 80 feet. The sediment load of the river water is so great that a white disk cannot be seen 6 inches below the surface. On emerging into the lake, the river water is carried southward and eastward along the lake shore by the circulation of the lake, forming a wide band of muddy water sharply delineated by its color from the clear green water of the lake.

Short cores of the bottom sediments show that the bottom consists of soft blue mud. A sample taken under the muddy outflow off the mouth of the Catatumbo River had the yellow color of well-oxidized silt for a depth of 2 inches below the surface. In the central area of the lake, where anaerobic conditions were found in the deep water, the sediment was black to a depth of several inches, and smelled strongly of hydrogen sulfide. Test piles driven at water depths of 100 feet in the northeastern quarter of the lake sink into the lake bottom under their own weight to a depth of some 30 feet and may be driven easily for another 20 feet. In shallower water, where the circulation is more active, the unconsolidated sediment is thinner.

These observations suggest that sedimentation is occurring at quite different rates in different parts of the lake basin. It must be most rapid in the southern area, beneath the outflow of the rivers draining the region of high rainfall. It must be least rapid in the shallower areas along the northern margins of the lake, where the circulation tends to keep the sediment in suspension and where the cores were sandier than elsewhere. The tendency of unoxidized organic matter to accumulate in the sediment as it is deposited must also vary regionally. The oxygen content of the water over the bottom decreases in general with depth. However, it is only in the central portion of the lake, where the pool of saline water is concentrated by the rotatory circulation of the water, that truly anaerobic conditions exist (Fig. 5[4]).

An account of the sediments of Lake Maracaibo and the Gulf of Venezuela which deals primarily with the mechanical properties and nitrogen content of the deposits is given by Trask (1933). In order to examine the relation between the oxygen concentration above the bottom of the lake, the source of the sediment and its composition, cores have been collected along two traverses of the lake and at several positions along the outlet. The analyses of some of the constituents of these cores are given in Table I and their distribution is shown in Figure 6.[5]

TABLE I. ANALYSES OF SEDIMENTS FROM LAKE MARACAIBO

	Southwest—Northeast Section						
Station No.	69	70	71	73	74	75	94
Latitude, N	9–20.4	9–23.8	9–31.2	9–48.2	9–56.4	10–01.4	10–10
Longitude, W	71–44.5	71–42.6	71–38.4	71–30.9	71–27.2	71–24.7	71–22.5
Depth, feet	6	71	90	98	92	99	50
Carbonate Carbon, %	<0.01	0.03	<0.01	0.06	<0.01	0.02	<0.01
Organic Carbon, %	1.33	2.04	3.82	4.37	4.59	3.56	1.50
Nitrogen, %	0.15	0.22	0.39	0.37	0.47	0.39	0.15
Phosphorus as P_2O_5, %	0.115	0.129	0.196	0.060	0.077	0.060	0.097
Sulfur, %	0.02	0.21	0.51	1.80	1.03	2.22	1.60
Organic Extract, ppm	606	1902	4000	5907	4703	6224	1538
	Northwest—Southeast Section						
Station No.	92	91	90	72	89	88	87
Latitude, N	10–03.3	9–54.7	9–45.7	9–39.6	9–36	9–27.2	9–16.7
Longitude, W	71–50.4	71–45.5	71–37.5	71–34.6	71–29.1	71–21.4	71–12.4
Depth, feet	45	87	93	87	86	90	61
Carbonate Carbon, %	<0.01	0.09	<0.01	0.05	0.01	0.01	0.01
Organic Carbon, %	1.16	0.68	3.60	4.27	4.68	5.20	3.50
Nitrogen, %	0.035	0.025	0.33	0.41	0.43	0.51	0.30
Phosphorus as P_2O_5, %	0.773	0.102	0.057	0.074	0.104	0.108	0.253
Sulfur, %	0.12	0.08	1.96	1.75	0.99	0.79	0.68
Organic Extract, ppm	568	86	4834	4816	8963	5002	2105
	Strait of Maracaibo—North-South Section						
Station No.	31	76	25				
Latitude, N	10–47.5	10–42	10–29.5				
Longitude, W	71–37.6	71–34	71–30.8				
Depth, feet	41	44	27				
Carbonate Carbon, %	0.13	0.03	0.05				
Organic Carbon, %	0.50	1.07	3.05				
Nitrogen, %	0.07	0.10	0.32				
Phosphorus as P_2O_5, %	0.036	0.088	0.054				
Sulfur, %	0.25	1.05	1.28				
Organic Extract, ppm	903	1205	4799				

The organic carbon increases toward the center of the lake, where maximal values of more than 5 per cent occurred (Fig. 6-*A*). This corresponds to about 10 per cent of organic matter in the dry sediment and is an unusually high value. Around the margins the organic carbon is about one fifth as plentiful and corresponds to the values commonly found in marine sediments. This pattern follows the distribution of the oxygen deficiency in the water over the bottom, but the pattern is skewed toward the eastern side of the lake in a way which suggests that the greater rate of sedimentation, which probably occurs on that side, is influencing the entrapment of organic matter.

[4] Fig. 5 is based on data obtained in May 1953. In March 1954, when the bottom cores described in Fig. 6 were collected, the oxygen concentrations near the bottom in the southeastern quarter of the lake were higher than are shown in Fig. 5. It is believed that the May data are more representative of the year-round condition.

[5] The chemical analyses of the sediments were made by Mrs. Maxine Brenneman of the Esso Research and Engineering Company, with the exception of the phosphate determinations which were made by Mr. Nathaniel Corwin of the Woods Hole Oceanographic Institution.

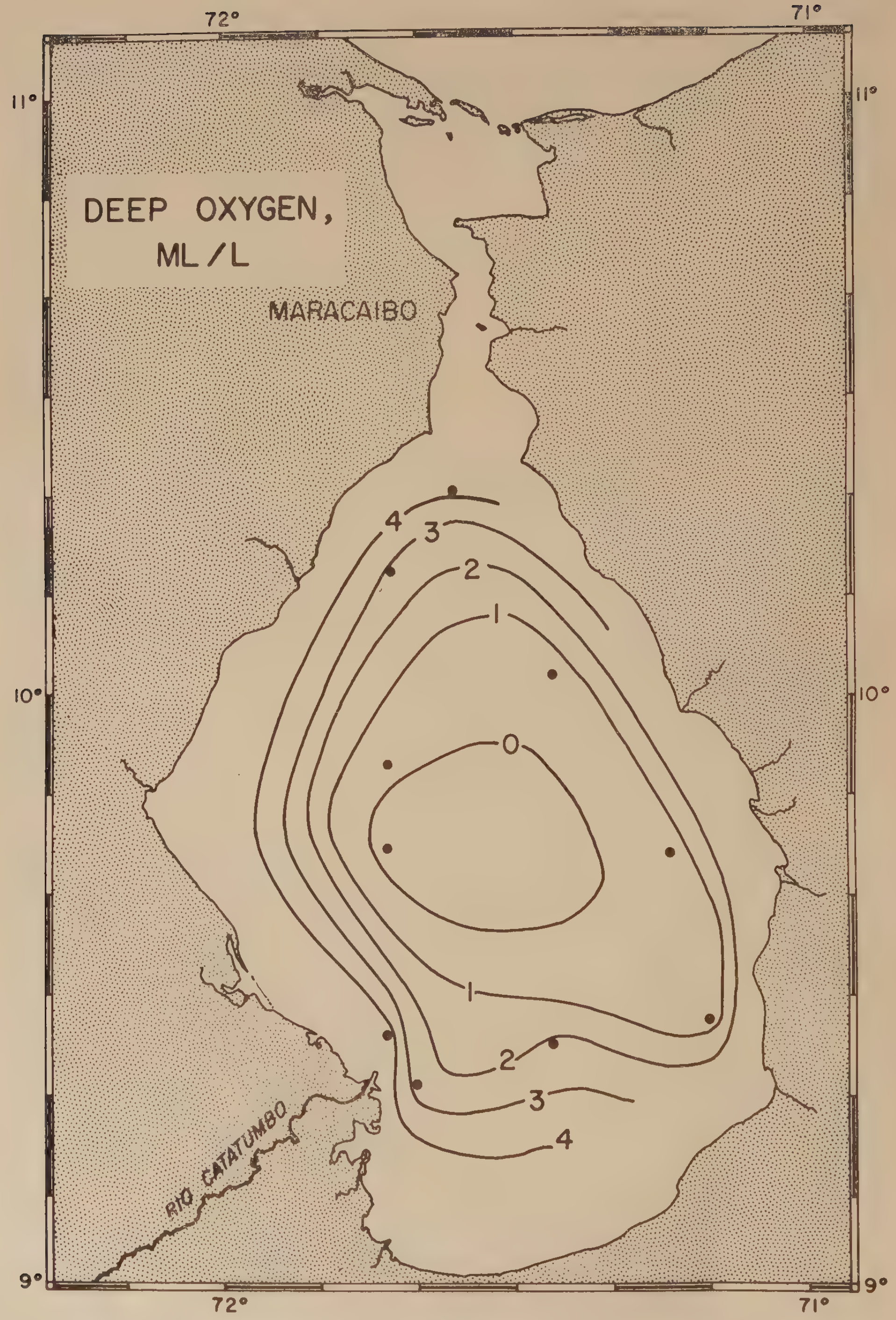
72°
71°
11°
10°
9°
DEEP OXYGEN, ML/L
MARACAIBO
RIO CATATUMBO
4
3
2
1
0
1
2
3
4

FIG. 5.—Concentration of oxygen, as milliliters per liter, in water a few feet from the bottom of Lake Maracaibo. May 1953.

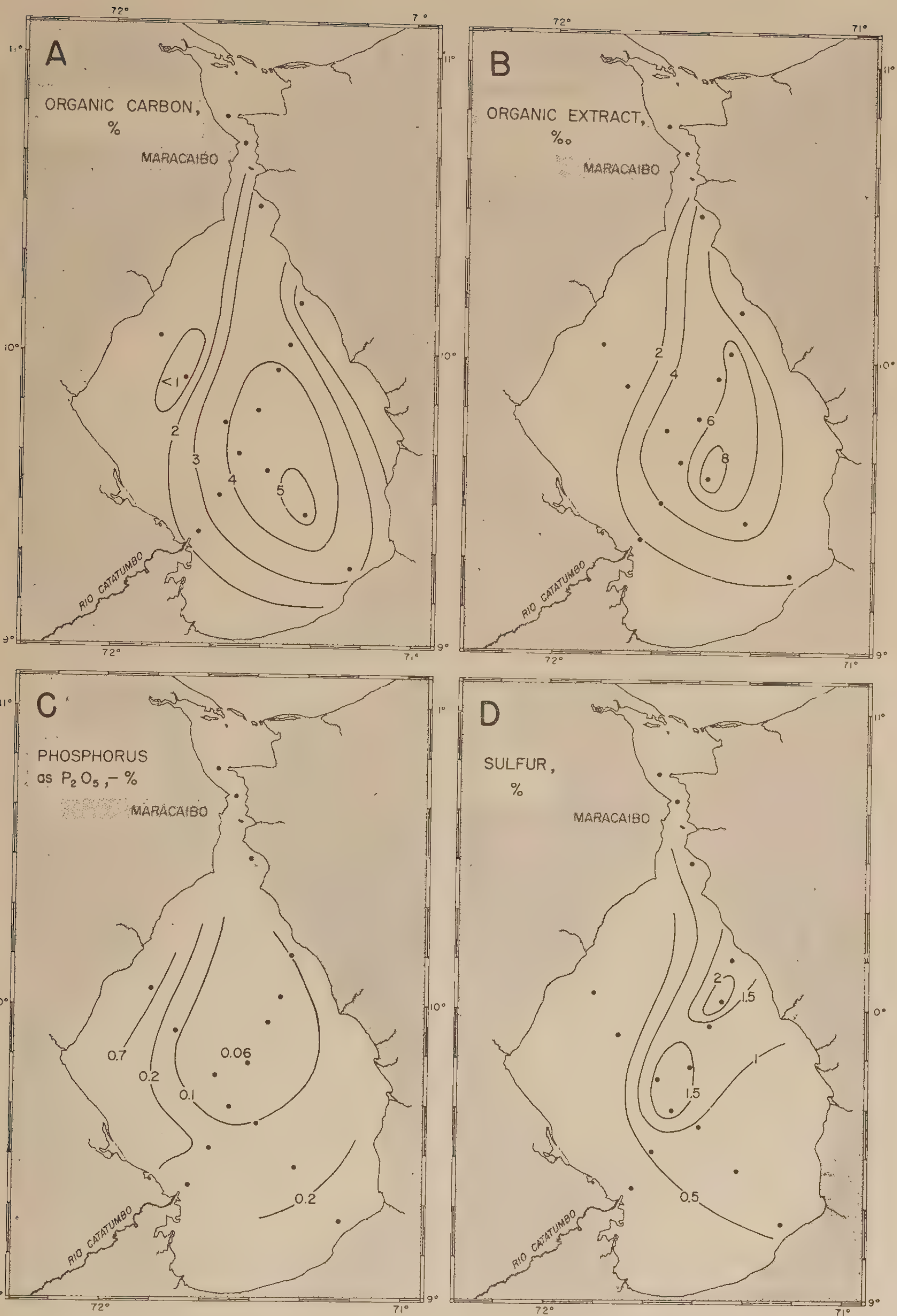
A
ORGANIC CARBON, %
MARACAIBO
<1
2
3
4
5
RIO CATATUMBO
B
ORGANIC EXTRACT, ‰
MARACAIBO
2
4
6
8
RIO CATATUMBO
C
PHOSPHORUS as P_2O_5, – %
MARACAIBO
0.7
0.2
0.1
0.06
0.2
RIO CATATUMBO
D
SULFUR, %
MARACAIBO
2
1.5
1
1.5
0.5
RIO CATATUMBO
72°
71°
11°
10°
9°

FIG. 6.—*A*—Distribution of organic carbon, as per cent dry weight, in bottom sediments of Lake Maracaibo; *B*—Distribution of material extracted with an organic solvent, as parts per thousand dry weight, from bottom sediments in Lake Maracaibo; *C*—Distribution of phosphorus, as P_2O_5 in per cent dry weight, in bottom sediments of Lake Maracaibo; *D*—Distribution of sulfur, as per cent dry weight, in bottom sediments of Lake Maracaibo.

The material extracted by an organic solvent follows a similar pattern (Fig. 6-*B*). The distribution of nitrogen in the sediment is also like that of organic carbon, there being about one part of nitrogen to ten parts of carbon.

The quantity of phosphorus in the sediment varies symmetrically with distance from the center of the lake, but unlike the other constituents the phosphorus content is lowest in the center and increases toward shore (Fig. 6-*C*).

This distribution appears to be related to the phenomena described by Einsele (1936, 1938; and Vetter, 1938) and Mortimer (1941–1942) for lakes in which the oxygen of the deep water becomes depleted during a period of stagnation in summer. At that time phosphorus is freed from the sediments and goes into solution in the water over the bottom. In autumn, when the deep water becomes oxygenated, phosphorus is redeposited in the sediment. Iron follows a similar cycle. It is consequently believed that the phenomenon depends on the oxidation and reduction of iron phosphates and the resulting change in solubilities. In Lake Maracaibo the permanent depletion of oxygen in the center of the lake appears to favor the solution of phosphorus from the sediment, whereas its presence around the margin causes its retention in the deposits.[6]

The distribution of sulfur in the sediment is peculiar also. Although high sulfur contents occurred in the center of the lake, where hydrogen sulfide was present in the water, the highest values were found toward the northeastern side of the lake (Fig. 6-*D*). The sulfur probably has its origin from sulfates, derived from sea water, which are reduced by anaerobic bacteria. Consequently it is deposited in the sediment, not as a part of the organic matter, but as a precipitate resulting from reactions of hydrogen sulfide with metallic elements in the sediment either before or after its deposition. It would be premature to speculate further on the cause of the peculiar distribution of sulfur without more information.

The hydrography and chemistry of Lake Maracaibo indicate that conditions are not only favorable for a high rate of production of organic matter, but also that they are equally favorable in all parts of the basin. The entrapment of organic matter in the sediments, in contrast, is much greater in the center of the lake than along its margin. This condition appears to arise from those peculiarities of the circulation which cause organic derivatives to accumulate there over the bottom, and to the attendant reduction in oxygen content of the water. There is indication also that the varied rate of sedimentation, which is presumed to decrease as the water moves around the basin from its source in the Catatumbo River, influences the organic content of the bottom deposits. Finally, reactions taking place in the water itself, involving phosphates and hydrogen sulfide, further modify the composition of the sediment.

At the present time conditions in Lake Maracaibo, at least locally, are highly favorable for the processes which are assumed to initiate the accumulation of the source materials of petroleum. Within the basin the richness of the sediments varies fivefold in a simple pattern apparently controlled by oxygen concentration and rate of sedimentation. The processes leading to organic deposition are active. The sediments are being laid down under a variety of hydrobiological influences. The record between present processes and the reserves of petroleum laid down in former times is almost unbroken. The writer believes the chief contribution which he may have made to the discussion on modern sedimentary basins is to call attention to the opportunity which exists in the Maracaibo Basin for advancing knowledge of these processes.

---

[6] The present analyses indicate that the carbon-phosphorus ratio may be a very sensitive indicator of the presence or absence of oxygen in the water from which sediment is deposited. The C/P_2O_5 ratio varies from more than 60 in the anaerobic area in the center of the lake, to 10 or less around the margin. The value of this ratio as an indicator of the conditions under which sediments were deposited deserves further study.

REFERENCES

Einsele, W. (1936), "Ueber die Beziehungen des Eisen Kreislaufes zum Phosphor Kreislauf im Eutrophen See.," *Arch. Hydrobiol.*, Bd. 29, 664–86.

——— (1938), "Über Chemische und Kolloidchemische Vorgänge in Eisen-Phosphat-Systemen unter Limnochemischen und Limnogeologischen Gesichtpunkten." *ibid.*, Bd. 33, H. 3, 361–87.

———, and Vetter, H. (1938), "Untersuchungen Über die Entwichlung der Physikalischen und Chemischen Verhaltnisse im Jahreszyklus in Einen Massig Eutrophen See. (Schleinsee bei Laugenargen)." *Internat. Rev. Hydrobiol.*, Vol. 36, 285–324.

Fleming, R. H. (1941), "Composition of Plankton and Units for Reporting Populations and Production," *Proc. Sixth Pacific Sci. Congress*, 535–40.

Gessner, Fritz (1953a), "Auf den Spuren Alexander von Humboldts in Venezuela," *Natur und Wissenschaft*, No. 138, 20.

——— (1953b), "Investigaciones Hydrograficas en el Lago de Maracaibo," *Acta Cientifica Venezolana*, Vol. 4, 173–77.

——— (1955), "Die Limnologischen Verhaltnisse in den Seen und Flüssen von Venezuela," *Verhandlung der Internat. Vereininigung für Theoretische und Augewandte Limnologie*, Vol. 12, 284–95.

Harvey, H. W. (1946), "Fertility of the Ocean," *Discussion on Oceanography*, The Linnean Society of London, 5–8.

Kuenen, P. H. (1950), *Marine Geology*, John Wiley & Sons, Inc., New York.

Mortimer, C. H. (1941–42), "The Exchange of Dissolved Substances Between Mud and Water in Lakes," *Jour. Ecol.*, Vol. 29, 280–328, 1941; and Vol. 30, 147–201, 1942.

Redfield, A. C., Smith, H., and Ketchum, B. H. (1937), "The Cycle of Organic Phosphorus in the Gulf of Maine," *Biol. Bull.*, Vol. 72, 421–43.

Richards, F. A., and Redfield, A. C. (1954), "Correlation Between Oxygen Content of Sea Water and the Organic Content of Marine Sediments," *Deep-Sea Research*, Vol. 1, 279–81.

Schultz, L. P. (1949), "A Further Contribution to the Ichthyology of Venezuela," *Proc. U. S. Nat. Mus.*, Vol. 99, pp. 1–211.

Stebinger, Eugene (1950), "Petroleum in the Ground," *World Geography of Petroleum*, edited by Wallace E. Pratt and Dorothy Good, Amer. Geogr. Soc., Spec. Publ. No. 31.

Sutton, F. A. (1946), "Geology of Maracaibo Basin, Venezuela," *Bull. Amer. Assoc. Petrol. Geol.*, Vol. 30, No. 10, 1621–1741.

Trask, P. D., assisted by Hammer, H. E., and Wu, C. C. (1932), *Origin and Environment of Source Sediments of Petroleum*, Amer. Petrol. Inst. (printed by Gulf Publ. Co., Houston).

U. S. Army Corps of Engineers (1938), "Model Study of Channel Improvements at Outer Bar, Lake Maracaibo, Venezuela," *Tech. Memo. No. 106–1, U. S. Waterways Experiment Station*, Vicksburg, Miss.

Zuloaga, Guillermo (1950), "Venezuela," *World Geography of Petroleum*, edited by Wallace E. Pratt and Dorothy Good, Amer. Geogr. Soc., Spec. Pub. No. 31.

Contribution No. 849

ELECTRICALLY CHARGED DROPS FROM BUBBLES IN SEA WATER AND THEIR METEOROLOGICAL SIGNIFICANCE

By Duncan C. Blanchard

Woods Hole Oceanographic Institution[1]

(Original manuscript received 13 September 1957; revised manuscript received 3 April 1958)

ABSTRACT

A modification of Millikan's classic oil-drop experiment was used to determine the electric charge and radius of drops that were ejected from a bursting bubble at an air-sea water interface. Charge measurements were made of both the natural and the induced charge. Drops of 2 to 20 microns in radius carry natural charges of at least 2×10^2 to 5×10^3 elementary units, respectively. The induced charges are considerably higher, reaching 10^6 elementary units on drops of 50 microns radius. The sign of the natural charge is positive on drops < about 4 microns. For larger drops both the sign and magnitude of the charge appear to be a function of the depth of water through which the bubble rises.

The meteorological significance stems from the fact that rain and snow, as well as whitecaps, can produce great numbers of small bubbles in the surface waters of the oceans. Both laboratory and field work suggest that the majority of these bubbles produce positively charged drops that contribute to the atmospheric space-charge. Of special significance is the fact that, for positive induction fields less than about 25 v cm^{-1}, a positive charge is found on the small drops. For fields greater than 25 v cm^{-1} the induced negative-charge exceeds the natural positive-charge and so the drops carry a net negative-charge. Consequently, small bubbles breaking at the surface of the sea in the presence of the earth's fair-weather positive field of about 1 v cm^{-1} will produce drops that carry a positive charge. Calculations based on measurements of the bubble spectrum produced by whitecaps indicate that the charge on the drops may, under some conditions, provide a counter-current of the same order of magnitude as the fair-weather conduction current. Thus the sea may be a source as well as a sink for the charge that maintains the earth's positive electric-field.

1. Introduction

The origin of the sea-salt particles that are so numerous in marine atmospheres [1, 2, 3] is most likely to be found in the bubbles that are produced in the water near the sea surface. The production of these bubbles can be modified by many factors including precipitation, wind force, and supersaturation of the surface waters [4]. If the evolution of rain in marine clouds is intimately connected to the salt-particle distribution in the free air [5], then the physical and chemical properties of these bubbles and their disintegration products should be of the utmost concern to the cloud physicist. This paper will be concerned with the electric charge that is carried from the water surface by the drops that are ejected from the bubble as it bursts at the air-water interface [6].

A number of papers have dealt with the charging of the aerosols that are produced by bubbling air through various liquids, but none of these investigations was aimed at a determination or understanding of the charge production from a single bubble. Chapman [7, 8, 9, 10], in a series of careful researches, determined the carrier mobility spectra of liquids electrified by bubbling and spraying. Köhler [11] obtained the charge on individual drops that were created by directing an air blast tangentially at a sea water surface. These drops apparently were formed by mechanical disruption of the water surface. Dinger and Gunn [12], who were interested in the electrical effects associated with the freezing and melting of water, measured the charge given off to the air by bubbles that were released from a melting block of ice. Aliverti and Lovera [13] carried out a laboratory study of the charge given off to the air by a disintegrating foam patch on a sea-water surface. Only the latter investigation appeared to be concerned mainly with the production of charged particles by the ocean surface and the resultant modification of the earth's electric field.

2. Experimental technique

Before attempting to discuss the methods used for charge determination, it might be well to describe just how the charged drops that we will be concerned with are ejected from the sea-water surface. Stuhlman [14], in a study of effervescence, had observed the breaking of bubbles at the surface of fresh water and the subsequent ejection of several small drops. He postulated that the drops came from the breakup of a vertical jet of water that rose from the bottom of a

---

[1] Contribution Number 849 from the Woods Hole Oceanographic Institution. This paper represents the results of research carried out by the Woods Hole Oceanographic Institution under contract with the Office of Naval Research. Reproduction in whole or in part is permitted for any purpose of the United States Government.

collapsing bubble. This hypothesis was verified in this laboratory by taking high-speed motion pictures of the collapse of bubbles [15]. Fig. 1a shows a side view of the collapse of a 1.7-mm-diameter bubble and the formation of the jet. The bottom photo of the sequence shows a drop just at the point of separating itself from the jet. Fig. 1b shows the final stages of collapse of a 1-mm-diameter bubble with three drops detached from the jet. The time interval from the initiation of the collapse of the bubble to the separation of the five or six drops from the jet is of the order of 10^{-3} sec. The drops from bubbles <100-μ diameter are ejected with computed speeds that exceed 30 m $\sec^{-1}$. This high ejection speed precludes visual observation of the upward flight of the drops and they only become visible when frictional retarding forces stop the upward motion and allow them to fall at a speed defined by Stokes' law.

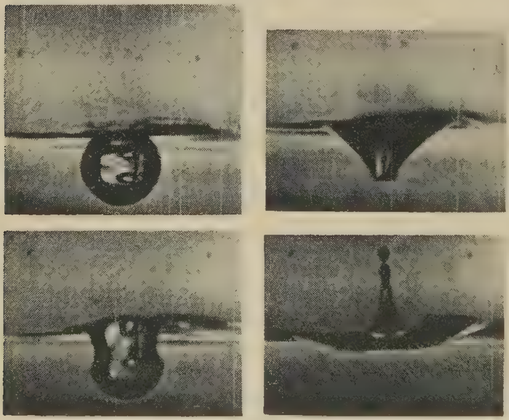

FIG. 1a. Composite photograph of high-speed motion pictures illustrating some of the stages in the collapse of a 1.7-mm diameter bubble and the formation of the jet. The time interval between top and bottom frames is about 2.3 milliseconds. The angle of view is horizontal through a glass wall. The surface irregularities are due to meniscus.

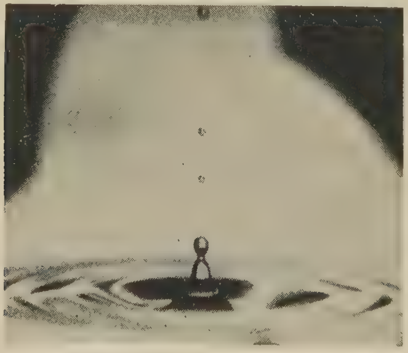

FIG. 1b. Oblique view of the jet from a 1-mm-diameter bubble. The diameter of the smallest drop shown is 0.09 mm. The exposure time was 30 μsec.

Each of the several drops is ejected to a characteristic height which is a function of bubble size. The experimental study illustrated in fig. 2 shows how the ejected height of the top drop is roughly 100 times the bubble diameter up to the maximum of about 18.5 cm at a bubble diameter of 1.9 mm. The diameters of the top two drops coming off the jet are approximately 0.1 the bubble diameter while the lower drops are somewhat larger. For a given bubble size, the drop diameters and the heights to which they are ejected are amazingly reproducible. In fact, this reproducibility provides a very simple method for the production of homogeneous water drops down to one-micron radius [16]. More important, perhaps, it implies identical chemical and electrical properties of drops from similar positions on the jets from bubbles of similar size.

The first observations of a charge on the drops were made by simply holding a charged comb a few cm above an area where bubbles were breaking. All of the ejected drops were attracted to the comb regardless of the sign of the charge on the comb. This, of course, indicated that charging by induction was taking place. Electrostatic induction occurred

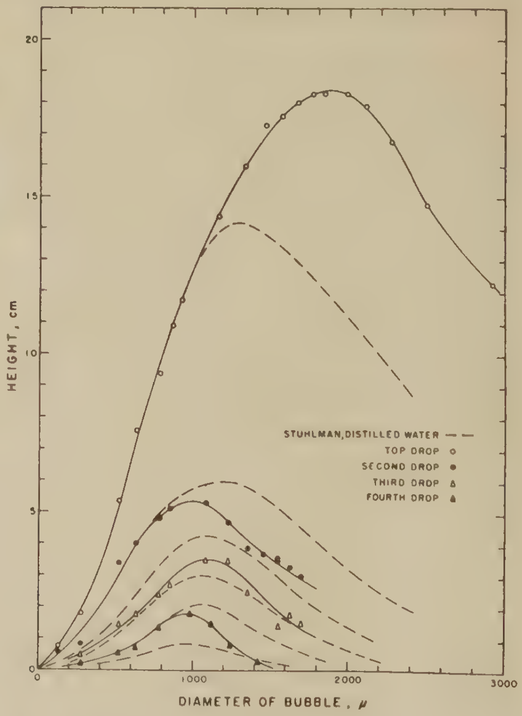

FIG. 2. Illustration of the heights of ejection of the several drops from the jet of a bubble bursting in sea water. Stuhlman's (14) findings are shown by dotted lines for drops from bubbles bursting in distilled water, while the solid lines represent the data obtained by Dr. C. Keith from bubbles bursting in sea water.

when the jet (bottom photo, fig. 1a) rose in the electric field of the charged comb, and induction charging took place as the drops were separated from the jet. It was desired to determine the magnitude of not only the induction charging but of any natural charging that might occur as the drops separated from the jet in a field-free region.

A. *The Millikan-type chamber.*—A device embodying the principle of Millikan's classic experiment on the charge of the electron was constructed and used to obtain both the charge and radius of an individual drop. A schematic sketch of the apparatus is shown in fig. 3. The bubbles were created by forcing air under 10- to 30-psi pressure through a finely drawn-out section of glass capillary tubing. The bubbles rose through the sea water in the inner container A, broke at the water surface, and ejected electrically charged drops into the observation region between A and the horizontally mounted, rectangular (5.7×8 cm) brass plate B. Plate B was rigidly attached to, but electrically insulated from, a rectangular open-bottomed plexiglas housing C. This housing sealed the observation region off from room air by making contact with the sea water in the cylindrical (12-cm diameter) outer container D. The electric field E could be controlled by varying the voltage on the plate or by changing the plate-water distance. A simple switching circuit, not shown in fig. 3, allowed the plate to be at any desired ±DC voltage up to 12 kv with respect to the grounded sea water in A. The plate-water distance could be varied from 0 to 2.5 cm by raising or lowering C.

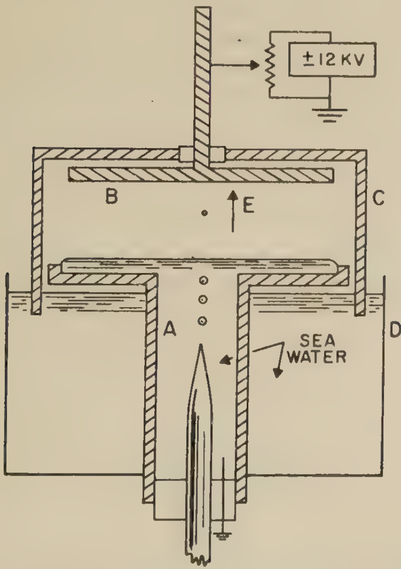

FIG. 3. A schematic sketch of the apparatus that was used to determine the charge and radius of small drops from bursting bubbles. The charged drops were suspended, as shown, in the electric field *E*. See text for details.

The observations leading to the charge and radius of an ejected drop were made in the following way. The air-supply value (not shown in fig. 3) was turned on and bubbles began to issue from the glass tip. With clean, filtered sea water and a bubble production rate of 3 to 10 sec^{-1} most of the bubbles would break as they reached the surface and eject charged drops into the air. If a voltage of the proper sign is now applied to the plate while one is observing a particular drop as it falls toward the water surface, the resulting vertically-oriented electric field will exert an upward-directed force on the charged drop. The air supply is turned off and the plate voltage adjusted until the upward-directed electric force just balances the gravitational force and the drop remains stationary in the electric field. At this point we can write

$$\tfrac{4}{3}\pi R^3 p g = E_s Q, \qquad (1)$$

where R is the drop radius in cm; $p = 1.025$, the density of sea water; $g = 980$ cm sec^{-2}, the acceleration of gravity; E_s, the electric field in esu cm^{-1}; Q, the drop charge in esu. As both R and Q are unknown in (1), more information is required. This may be obtained by turning off the plate voltage and, with a stopwatch and a cathetometer, determining the fall speed V of the drop from the time it takes to fall a known distance to the water surface. With the cathetometer telescope, the drop is easily followed and its entry into the water can be anticipated by watching the drop approach its reflection from the water surface. While the drop is falling, the gravitational attraction must be balanced by the frictional force as given by Stokes' Law and so we obtain

$$\tfrac{4}{3}\pi R^3 p g = 6\pi\eta R V \qquad (2)$$

where $\eta = 1.83 \times 10^{-4}$ g sec^{-1} cm^{-1}, the viscosity of the air; V, the fall velocity of the drop in cm sec^{-1}. With the observed value of V, equation (2) can be solved for R and, with this value, (1) may be solved for Q. The validity of this method depends upon using sufficiently small drops such that Stokes' Law will apply and that the time required for the drop to attain terminal velocity is negligible compared to the total time of fall to the water surface. In regards to the latter requirement, calculation indicated that drops as large as 10 microns radius essentially attain terminal velocity within about 0.2 sec after starting from rest. As this time is sufficiently small compared to the total fall-time of several seconds, the drop may be assumed to be at terminal velocity during the entire fall. Drops of this size are well within the range where Stokes' Law applies.

Drops > about 10 microns radius fall much too rapidly to enable one to obtain an accurate value of the terminal velocity over the short fall path that is available. Thus after the drop has been suspended in the electric field E_s, and (1) applies, the voltage on the plate is not turned off but only decreased a slight amount. The electric field is now E_m where $E_m < E_s$ and the drop will move slowly downward. The gravitational force is balanced by the frictional force plus the upward-directed force due to the field E_m and we can write

$$\tfrac{4}{3}\pi R^3 \rho g = 6\pi\eta R V + E_m Q. \qquad (3)$$

This equation can be solved simultaneously with (1) to obtain an expression for R

$$R^2 = \frac{9\eta V}{2\rho g}\left(\frac{E_s}{E_s - E_m}\right). \qquad (4)$$

Note that the $9\eta V/2\rho g$ term follows directly from Stokes' Law when (2) is solved for R^2. As E_m approaches zero, (4) approaches Stokes' Law.

The production of bubbles by a glass tip provides a simple way to produce any desired bubble size, but it obviously is not the manner in which bubbles are produced on the open sea. In an attempt to approach this natural method of bubble production, the glass capillary tip was removed and the inner container A of fig. 3 was extended downward about 35 cm and closed off at the bottom. Housing C was removed and sea water was allowed to fall down the extension tube in such a way as to produce as much splashing as possible. By the time A was full of water, many hundreds of minute bubbles were distributed through the entire water column. Housing C was replaced immediately with a minimum of plate-water separation (<1 cm) to insure rapid saturation of the chamber. The saturation process is undoubtedly hastened by the partial evaporation of the hundreds of drops that are ejected into the chamber during the first few minutes after the chamber is sealed. At the end of about four minutes, only a relatively small number of minute bubbles remain and these, upon bursting, produce drops that rise a maximum of about 0.3 cm. With the techniques already outlined, the charge and radius of the drop are easily determined.

B. *Qualitative charge measurements.*—The Millikan-type chamber that was just described was used to obtain the charge and radius of drops that were

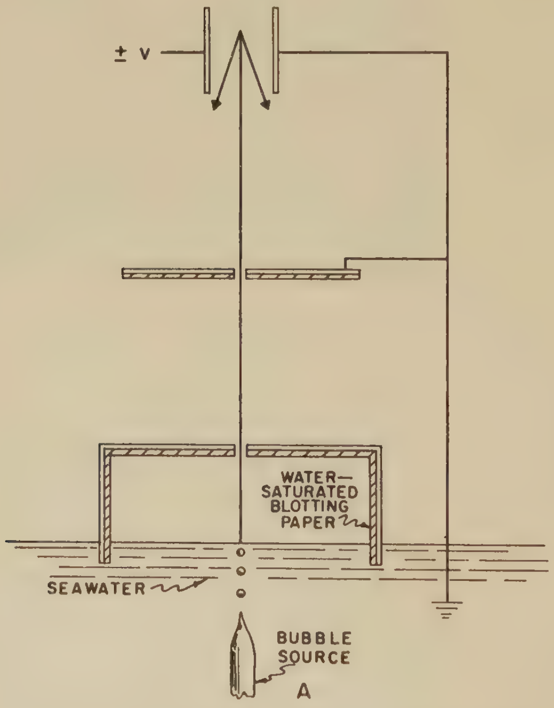

FIG. 4a. A schematic sketch of the apparatus used to determine the sign of the charge on the drops from large bubbles. The vertical line rising up through the pillbox represents the upward motion of the drop, and the arrows at the top indicate its direction of fall in the horizontal electric field that exists between the vertical plates. The charged drop is deflected to one side or the other depending on the sign of the voltage V.

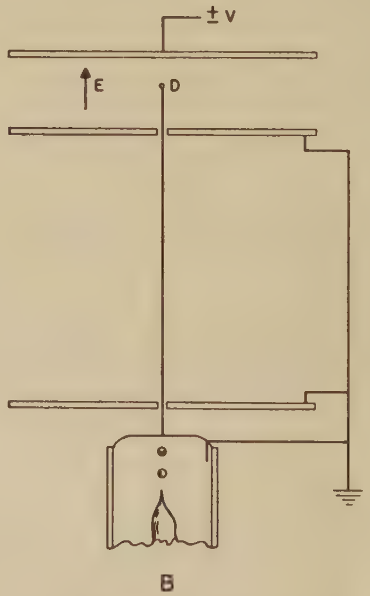

FIG. 4b. Similar to 4a with the exception that here the drop is suspended between the upper two plates by the electric field E and the pillbox has been replaced by a flat metal plate.

ejected from small bursting bubbles to heights of about 2 cm or less. It was not feasible to use this apparatus for the larger drops that were ejected to heights >2 cm as the plate-water distance became too great. This, plus the increased drop mass, required prohibitive plate voltages far in excess of the available 12 kv to produce the necessary electric fields for drop suspension. In addition, such high plate voltages produce corona and sparking at the regions of sharp curvature on the plate. It is thus perhaps fortunate that these large drops have such a high settling rate that they have little probability of remaining air-borne over the oceans and, therefore, will contribute little to the net separation of charge at the air-water interface. More details of this will come later. At any rate, a knowledge of the qualitative and semi-quantitative nature of the charge of the large drops would certainly be of interest in attempting to understand the fundamentals of the charging process.

It was pointed out earlier that the detection of any natural charge on the drops by their attraction or repulsion for a charged probe is overshadowed by an induced charge that is obtained during the jet to drop evolution. It is evident that the jet from the bursting bubble must be shielded from the electric field of the "test" charge. Two very effective yet simple experimental setups for this purpose are shown schematically in fig. 4. In fig. 4a, the region in which the bubbles burst is covered by an open-bottom, 9-cm diameter, 3-cm deep, brass cylinder. Any electric fields within the cylinder due to potentials at the brass-water interface are eliminated by lining it with blotting paper which is then saturated with sea-water [17]. To minimize the penetration of lines of force through the 3-mm hole at the top of the cylinder a 6-cm square, blotting-paper-lined brass plate was placed horizontally above the cylinder. The drops from the bursting bubbles passed up through the hole in the cylinder and a similar hole in the brass plate and entered the horizontal electric field between two vertical plates. If no field was present the drops would fall vertically down between the plates, but in the presence of a field they experienced a deflection to the left or right depending on the sign of their charge.

The apparatus shown in fig. 4b is similar in principle to that of fig. 3 except that here a grounded plate takes the place of the water surface. By moving the upper plates close together, a relatively low voltage V can produce a sufficiently high electric field to suspend the charged drop. The two grounded lower plates prevent induction charging of the drop. It is apparent that the rapid evaporation of the drops will allow only a crude estimate of the magnitude of the charge.

As some of the experiments with the drops from the smallest bubbles were aimed at obtaining only the sign of the charge, a far simpler device than those discussed so far was used. This consisted of nothing more than a large (11×21 cm) insulated copper plate that was lined on the bottom side with sea-water-saturated blotting paper and placed horizontally about 1 cm above the area where small bubbles were breaking. During the instant a bubble broke and drops were being ejected into the air, a copper wire was used to short-out the plate and the water surface. Thus, no electric fields could be formed due to sea water-copper potentials. While the drop was still in the air, the wire was removed and a voltage applied to the plate. The motion of the drop in the resultant electric field indicated the sign of the charge.

C. *Space charge measurements.*—If bursting bubbles at the sea surface are ejecting charged drops into the overlying air, then any net charge should be amenable to measurement by some type of space-charge measuring device. Although a number of methods are available for measuring space charge [18], the method used here, first suggested by Kelvin [18], consists of measuring a potential due to the space charge. The air containing the space charge is allowed to flow through a cylindrical cage made of 14-mesh copper window screening, on the axis of which a small amount of radioactive material is attached to a conducting rod. The space charge will create a potential difference between the cage and the radioactive point. The function of the radioactivity is rapidly to bring the rod to which it is attached to the potential of the center of the cage with respect to the periphery. Assuming a uniform distribution of space charge it can be shown that

$$V=\pi R^2\rho. \tag{5}$$

With (5), the space charge ρ can be determined from the radius of the cage R and the voltage V.

3. Results

A. *Natural charge from artificially created bubbles.*—By artifically created bubbles we mean bubbles that are produced by forcing air through fine glass tips as contrasted to bubble production on the open sea by the entraining of air by breaking waves. The apparatus shown in fig. 3 was used for the measurements discussed here, and some results are shown in fig. 5 in the curves marked B, C, and D.

Most of these data were obtained with bubbles that were ejecting drops to heights of 5 to 15 mm although the drops used were not necessarily the ones that rose to these heights. It was usually the case that several drops were in the air when the electric field was applied, and the drop that was most nearly balanced was the one selected for the test. Consequently, nothing can be said of the initial position of the drop in respect to the others rising from the same bubble.

Curve B is for the charge found on small drops that appeared to be ejected only a few mm above the water surface. Other larger drops that were created at the same time rose much higher. Curves C and D show the charge from experiments with larger drops. Note that curve B indicates higher charges for drops of 3 to 4μ than does curve C and that the data of curve D suggest a different grouping from that of curve C. The most probable explanation of this is based on the fact that the charge on the several drops from a bursting bubble is a function of the depth of water through which the bubble has risen (see section C). This fact was not discovered until after most of the work described in this paper had been done and therefore no record was made of the length of time that the bubbles existed before they arrived at the surface and broke. It is possible that the bubbles used to obtain the data of curves B, C, and D were released at different depths and thus the charge on a drop size common to two of the curves might be expected to be different. It will be shown in the next two sections that the data for the small drops (curve A) probably represent the maximum charge on drops from small bubbles and that curves C and D most likely represent charges that are less than the maximum charge that could be obtained on drops from large bubbles.

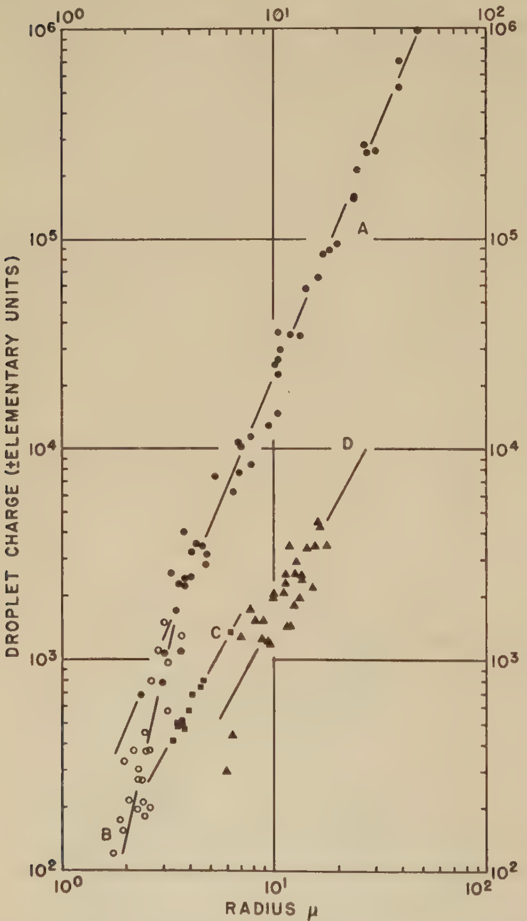

Fig. 5. Natural and induced charge on drops from bursting bubbles. Curve A is for induced charge while the others represent the natural charge. See text for further discussion.

The charge for the drops of curves B and C is mostly positive and reaches about 10^3 fundamental units while that for curve D is negative and attains a value of several thousand fundamental units. It will be shown presently that the charge is positive on drops from small bubbles and either positive or negative on drops from large bubbles. In the case of the large bubbles, the sign of the charge is a function of bubble age and the position of the drop in the bubble jet.

B. *Natural charge produced by bubbles created by splashing.*—One might argue that the charge of the drops of fig. 5 is a direct result of a charge-separation process that occurs as the bubble is formed and detached from the capillary tip. To investigate this effect, bubbles were created, as described earlier, by the splashing of water to simulate bubble formation at sea. As the drops from these bubbles were all <5-μ radius, the bubbles from which they originated were probably <50-μ. The charge-radius correlation that was found was not significantly different from that obtained with drops of similar size from bubbles from capillary tips (see curve B, fig. 5). The sign of the charge for all of the drops investigated here was positive, and it appeared that most, if not all, of the drops from bubbles of this size carried a positive charge.

It was conceivable that the existence of surface films and the concomitant lowering of surface tension might play a major part in the drop-charging process. To check this, data were obtained from sea water with surface tensions varying from 40 to 74 dynes cm^{-1}. The surface films were produced by oleic acid, unknown contamination on the water container, Aerosol OT, and by simply touching the water surface with one's finger. Several surface-tension values were made at the end of each run with a standard du Nouy tensiometer but, as errors of an uncertain magnitude were associated with this method [19], these values can only be considered approximate ones. Although in general it was found that the nature of the surface film has little effect on the magnitude of the charging and no effect on the sign of the charge, at least one experiment showed a reversal of charge which appeared to be a result of surface film effects.

It can be simply and convincingly demonstrated that the positive charge is most likely characteristic of a majority of the drops from small bubbles created by splashing sea water. When many tens of bubbles are breaking sec^{-1}, the stratum of air in the first millimeter or two above the water becomes filled with a "haze" of drops. If a strong field is applied, the drops move up or down depending on the direction of the field and the sign of the charge on the drop. It appears that all of the drops that are ejected from these small bubbles are positively charged. Consecutive observations on twenty breaking bubbles showed no exception to this. These observations have been repeated on many occasions with the same results.

C. *Natural charge on drops from large bubbles.*—It was pointed out earlier that the apparatus shown in fig. 3 could not be adapted easily for the large drops that were ejected more than about 2 cm from the water surface. As only a semi-quantitative knowledge of the charge was desired, the experimental setups of fig. 4 were used. All bubbles were produced by a capillary tip as it was not feasible to produce large bubbles by splashing and expect them to break directly beneath the holes in the cylinder and horizontal plates of fig. 4.

The drops from various-sized bubbles were ejected from 0.4 to 8 cm. Fig. 2 shows that the drops ejected to the maximum height, 8 cm, came from bubbles of about 700-μ diameter. In using the apparatus shown in fig. 4a, the drop that rose the maximum height from each bubble indicated a negative charge. To eliminate the possibility that this negative charge was being caused by surface films or by some other action of the cylinder-blotter-water contact, the apparatus of fig. 4b was used. After the 5-cm plastic cylinder was full, the sea water was allowed to drain over the paraffined edges to remove surface films. A clean platinum wire was used to ground the water.

Observations were made of the electric field that was required to suspend the top drop as a function of the depth of water through which the bubble rose. As the field required to suspend a given drop is inversely proportional to the charge, it is a simple matter to obtain the relative charge of the drop as a function of bubble depth. It was found that the charge on the top drop of a jet was positive if the bubble rose from a depth of at least a centimeter and increased with the bubble-release depth. Some preliminary experiments indicate that, with bubbles that produced jets of 30 to 40 mm, the top drop from a bubble released at a depth of 100 cm carried a positive charge at least ten times as great as the same drop from a bubble released at a depth of only 1 cm. In most of the experiments where the bubble release depth was <0.2 to 1 cm, the top drop was weakly charged either positive or negative. This appeared to be true for the top drop from jets not only in the 30- to 40-mm range but in the entire range studied to date; *i.e.*, 6 to 50 mm.

The second drop in the jet in the 30- to 40-mm range is strongly negative if it comes from bubbles that are released near the surface but becomes increasingly less negative and finally positive as the depth of bubble release is increased. The point at which the charge on the second drop goes positive is not well known but it appears to be for bubble-release depths in excess of 5 cm. At the present time nothing can be said of the variations of charge on the lower drops of the jet as a function of the bubble-release depth.

With these findings in mind, it is unlikely that the positively charged drops of curve C or the negatively charged drops of curve D, fig. 5, represent the maximum possible charge for drops of this size that originate from bubbles in sea water. If we carry this reasoning to the small bubbles, it is puzzling to find that the charge on drops from bubbles released near the surface (curve B, fig. 5) is similar to that from bubbles that rose from much greater depths (section B). No explanation can be given at the present time, but this point will be considered in future work.

D. *Induced charge.*—The technique of the measurement of an induced charge involves the use of the apparatus of fig. 3 to measure the charge and radius of drops that originated from bubbles that burst at an air-water interface above which existed a known electric field. Electric fields from about 100 to nearly 300 volts cm^{-1} were used, and the major results are shown on curve A of fig. 5. The data fall on essentially a straight line and indicate that charges reaching 10^6 elementary units can be obtained on drops of 50-μ radius. With the exception of one point, all of the data for drops $>20\mu$ were obtained with fields of 225 to 280 volts cm^{-1} while the data for drops $<20\mu$, plus the above exception, were obtained in fields of 110 to 135 volts cm^{-1}. The linearity of the graph and the merging of one set of data into another suggests that the induction charging is fairly independent of field strength within the above-mentioned values. The drops $>20\mu$ probably are amongst the last of the several to arise from a breaking bubble. These are known to be the largest and are observed to rise only a small fraction of the distance attained by the other drops. When the electric field is high enough to induce charges sufficient to suspend these large drops, the smaller drops are carried rapidly to the upper plate. Using the data of curve A, one can calculate that a field of 200 to 300 volts cm^{-1} will suspend the largest drops while only about 50 volts cm^{-1} are necessary for the drops of about 3μ.

E. *Induced charges and "bucking" fields at low field strengths.*—The results of part B of this section showed that the small bubbles produced by the splashing of water will burst at the water surface and eject positively charged drops into the air. As this process occurs in the absence of an electric field, induction charging cannot be the cause and, therefore, we must assume that some type of charge separation process is occurring at the air-water interface. Inasmuch as part D shows that induction charging can be appreciable, it is reasonable to suspect that a field strength of the proper value could be found such that an induced negative charge would be equal to the naturally occurring positive charge. Thus the drop will have a net-zero charge. In other words, there should exist a positive electric field such that, for fields smaller or larger, small bubbles will eject positively or negatively charged drops, respectively. By a positive field we mean one in which the potential increases with distance from the water surface.

This hypothesis was tested in the following way. Bubbles were produced by splashing water in a manner already described. An electric field, either positive or negative, was produced in the region above the breaking bubbles so as to insure an induced charge on the drops. While the drops were still in the air, a much larger electric field, of the order of several thousand volts cm^{-1}, was applied. The observed motion of the drops in this test field was used to indicate the sign of the charge. Now the bubble spectrum created by splashing water is such that only a relatively few bubbles eject drops as high as a centimeter while the great majority eject drops <2 mm. These later drops are <5-μ radius and are the ones that we shall discuss below.

Let us consider the charging effects of these small drops. For all negative induction fields, the induced charge plus the natural positive charge gives, as must be the case, a net positive charge. This was shown by a pronounced up-and-down motion in a negative and positive test field, respectively. This same behavior was indicated for positive induction fields less than about 15 volts cm^{-1}, thus indicating that the induced negative charge is not sufficiently great to exceed the natural positive charge. As the induction field went from negative to positive, the upward motion of the drops in a negative test field became progressively less pronounced until, at about $+15$ volts cm^{-1}, the cloud of drops was observed to rise very slowly, if at all. At an induction field of >30 volts cm^{-1}, the induced negative charge exceeds the natural charge and a net negative charging occurs. A reversal of the motion of the drops in the test field is observed, and they are now accelerated up or down in a positive or negative test field, respectively. Consequently, it is to be expected that the critical field necessary to produce a net-zero charge will vary, depending on drop sizes and charge, from about 15 to 30 volts cm^{-1}.

These findings do indeed show that drops can leave the water surface with a net positive charge in spite of the existence of a positive bucking electric field. It would seem that the induced charge is a function of only the induction field and is independent of the natural charge. With this assumption, one can build up a simple qualitative model of the charge variation with induction field. This is shown in fig. 6 where the net drop charge is represented by the ordinate and the induction field by the abscissa. The graph of fig. 6 can be considered to represent the relative contributions of the natural and induced charge for a given small drop. The origin of the natural positive charge is not known but as it is most likely a manifestation of the chemistry of the bubble-water interface plus the manner in which the drops are formed, it can be represented by the arbitrarily placed horizontal line showing it to be independent of induction fields. The induced charge, shown as a dashed line through the origin, is here assumed, at least for positive or negative fields whose absolute value does not exceed 50 volts cm^{-1}, to be a linear function of the field. This is in accord with the usual classroom experiments to demonstrate the existence of an induced charge. By algebraically adding the two charges, the net charge may be obtained and is shown as the solid line. This model is in agreement with the basic findings discussed above in that the net charge is increasingly positive as the electric field algebraically decreases from a certain positive value but is increasingly negative for larger positive fields. It should be noted that the field for which the net charge is zero was selected to be in agreement with the observational data.

F. *Space charge above the surf.*—If, as the present work indicates, positively charged drops are ejected from the small bursting bubbles and if the bubbles

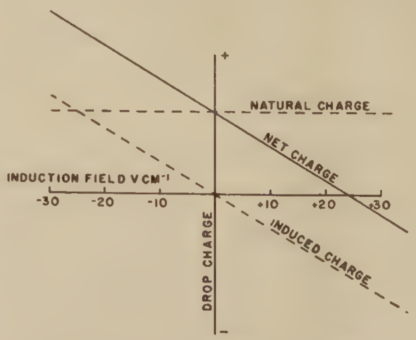

FIG. 6. Illustration of an hypothesis of the charging of a drop from a bursting bubble. It assumes that the natural charge is independent of the induction charge. The net charge is simply the algebraic sum of these two processes.

formed at sea by natural processes are predominantly of this size, then it is reasonable to suspect that one should be able to find a positive space charge in the atmosphere over the sea. This should be especially true over regions of intense bubbling. Using the space charge apparatus described earlier, the writer, in connection with the field studies of Project Shower [20], carried out several experiments over large surf-producing regions on the east coast of the island of Hawaii. The results of one such experiment, shown in fig. 7, indicate that a large positive space charge was found downwind from regions where breaking waves had produced such great numbers of bubbles that the water appeared a milky white. In this case, the wind was blowing nearly parallel to the surf line and across a shallow inlet about 100 m in width. Large waves were breaking about 50 m offshore and produced foam and bubble-filled water that were carried nearly into the beach. The space-charge measurements were made on the downwind side of the inlet and curve A of fig. 7 shows the time variation of space charge near the beach where little bubbling had occurred. This is somewhat higher than the readings that were found inland away from the surf. Curve B shows how the positive space charge rises to average values of nearly 2000 fundamental units cc^{-3} as one approaches the area just downwind from the region of pronounced bubbling produced by the breaking waves. Curve C, obtained directly downwind, indicates even higher values and rapid fluctuations reaching peak space charges of about +5000 units cc^{-3}. Here the high concentration of drops from bursting bubbles produced a marked salt haze that was easily visible against the dark vegetation near the shore.

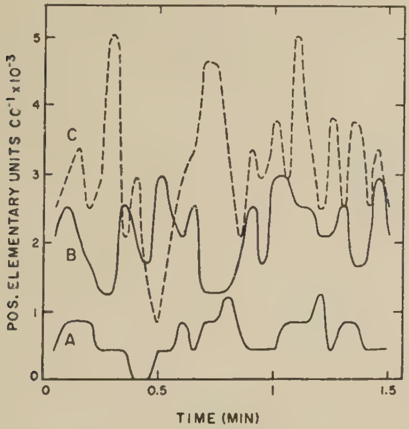

Fig. 7. Space charge downwind from whitecaps and bubble producing areas in an inlet on the island of Hawaii on 26 November 1954. See text for explanation of curves A, B, and C.

Additional evidence for the production of a positive space charge from the bursting of bubbles was obtained in the same area by Schaefer [21] who made observations of the current flow into a grounded radioactive point. He found that the positive current increased when the point was held near the breaking surf and observed the current "to have a definite relationship to the mass breaking of bubbles following the shoreward rush of foam from a breaking wave." This increase of positive current with bubble breakage seems certain to be the result of an increase in positive space charge.

4. Discussion

A. *Origin of the drop charge.*—At this point it will be well to review some of the literature to show that the charging described in this paper cannot be explained by existing hypotheses. The charging of drops created by spraying or other disintegration methods has usually been explained by the Lenard [22] spray-electrification mechanism in which it is postulated that the charge arises from a rupture of the double layer [19] that is believed to exist at the surface of most liquids. This double layer, in the case of pure water, consists of a negatively charged surface layer of a depth of about 20 molecules with an underlying positive layer of similar depth [23]. During a spray-disintegration process the smallest drops, considered to originate from the outer negative layer, should be charged negative. Other drops, although relatively few, are positive and originate from the deeper positive layer. According to this mechanism, the charging of drops >0.1-micron diameter should not occur for then the drop should be composed of water from both layers. This hypothesis failed when Chapman [7, 10], using the Millikan oil-drop method and an Erikson mobility tube, found relatively high charges of both signs on drops up to 5 microns radius.

In 1953, Dodd [23] found analogous results when he showed that charged drops that were created by spraying various nonconducting liquids had a net neutral Gaussian distribution. Dodd carried out an investigation to find out if this symmetrical charging might be expected to result "from statistical fluctuations of the electrolytic ion concentrations of both signs present in relatively low concentrations compared to those in aqueous solutions." The results indicated that this hypothesis could indeed be used to explain the charging that was not predicted on the basis of the Lenard theory but it appears that it cannot account for the large charges that were found by Chapman [7].

The present findings of charge on micron-sized drops cannot be explained by the Lenard mechanism and as the charge on a collection of drops is, for the most part, either positive or negative but not both, we cannot appeal to statistical fluctuations of charge within the bulk water. The writer will attempt to show that the charge originates from some action at the bubble-water interface and is apparently independent of the inductive charging process that occurs when the bubble breaks in a region containing an electric field.

After the preliminary findings [6] were published, Prof. L. B. Loeb, aware that they could not be explained on the basis of existing theories, suggested[2] that stray fields or voltages caused by electrode potentials might possibly account for the charging. The writer devised the type of experiment as illustrated in fig. 4a to eliminate any such effects. The continued occurrence of charged drops with this setup plus the production of positively charged drops in a bucking electric field removed any doubt that the drops could become charged by processes other than by induction.

Experiments with bubbles produced in a more natural manner by splashing were carried out to determine if any bubble charging was occurring at the capillary tip. As reported earlier in the paper, no significant difference in drop charge was found. The charge mechanism either was controlled by some double-layer phenomena at the bubble surface or else at the surface of the bulk water in the immediate vicinity of the bubble. These latter effects, although present, do not appear to be the main charging mechanism. The finding of a large increase of drop charge as a function of bubble-release depth definitely precludes bulk water surface effects as a major charge-producing mechanism and strongly suggests that the charge arises from phenomena at the bubble-water interface.

The charging of a gas bubble in water and its relative motion or cataphoresis during the application of an electric field is well known [24]. In this and later work, McTaggart [25] showed that a bubble in distilled water behaved as if it carried a net negative charge but, with concentrations as low as 8×10^{-6} N thorium nitrate, the charge appeared to be positive, and in the region of 6×10^{-6} N a bubble initially negative became positive as the bubble decreased in size. After experimenting with various gases, Alty [26] concluded that the composition of the gas plays very little part in surface electrification. In attempting to explain the charging, he presented a model that postulated the existence of a double layer that formed as a result of selective absorption of ions of one sign on the bubble. Polar water molecules were considered to be partly or completely orientated at the bubble surface and to attract negative ions from the water. These ions gave the bubble its negative charge. A partial "covering up" of the negative ions by a diffuse cloud of positive ions was considered to extend some distance from the bubble surface.

During an investigation of the electrification accompanying the melting of ice, Dinger and Gunn [12] observed that ice made from distilled water showed electrification upon melting only if bubbles were present within the ice. They concluded that the bubbles on being released from the ice would carry a negative charge to the surface of the water and, upon bursting, somehow transfer this charge to the air and leave the water with a positive charge. The observed charge transfer was in the right direction to lend support to Alty's hypothesis. In general, they found that only bubbles coming from melting ice made from distilled water indicated a negative cataphoresis charge. If the same experiment was performed with ice made from tap water or aqueous solutions of HCL or NaOH such that the pH was <2.5 or >10, no electrification was noted. These significant observations are analogous, in some respects, to the findings of workers in spray electrification [8, 27, 28] who, in general, found that the addition of various contaminants to distilled water greatly reduced the net spray electrification. Chapman [8] stated "the fact that the amount of electrification from salt solutions decreased with increasing concentration (above 10^{-4} N) makes it impossible to account for much of the ionization observed over the oceans by a spray electrification process, since sea water is about 0.7 normal and even with 0.2 normal KCL the electrification is very slight."

To return now to the cataphoresis of bubbles, it would be well to consider the increase of charge of the drops (part 3, section C) as a function of bubble-release depth in the light of the findings of an appreciable bubble-charging time [26, 29, 30, 31]. Now inasmuch as the present work indicated that an increase in bubble-release depth showed no significant changes in bubble size, as evidenced by no change in the ejection heights of the drops, it seems reasonable to suppose that the effects of bubble-release depth are actually effects of the age of the bubble. Thus if the charge of the drops is a result of the charge of the bubble, then the present findings would indicate that a bubble-charging time is to be expected. Although the writer is unaware of any similar experiments with bubbles in sea water, other investigators have observed bubble charging in relatively pure water. Currie and Alty [30] found that bubbles of the order of 2-mm diameter required about 2000 seconds before an equilibrium charge had been obtained. Whybrew, Kinzer, and Gunn [31] observed that bubbles of about 300-microns diameter in water of a resistivity of from 0.8 to 5×10^6 ohm cm carried about four times the surface charge after 15 min of existence as compared to less than 20 sec.

---

[2] Personal communication.

The statement made earlier to the effect that the net charge on a drop ejected from a bubble can be attributed to two independent charging mechanisms, that of induction charging and that of the natural charge, is based on two considerations. First, the findings of a positive charge in the face of a bucking electric field, as illustrated in fig. 6 make the idea appear qualitatively reasonable and, secondly, a similar phenomenon has been found by other investigators [27, 32]. For example, Banerji [27], in studying spray electrification, applied ± voltages to his atomizer (and hence to the water) and observed the net charge on drops that were sprayed from a given quantity of water. He obtained a net charge that varied linearly with the applied voltage in the same manner as shown on fig. 6.

It now seems quite evident that the electrification observed in the present study can be considered as arising from two independent processes with the most important being the charge separation as a result of double layer or other effects at the bubble surface. Any future work would do well to proceed along two separate lines. First, one should pay close attention to the work of Alty [29] but with considerations of the high conductivity of sea water. Secondly, it appears to be most important that we have a much better understanding of the details of the formation of the drops from the bubble jet. The high-speed camera studies [15] were quite inadequate to give any detail of the drop formation from bubbles of the order of 100-microns diam. A camera taking pictures at a rate of 10,000 sec^{-1} or more would be necessary to give information on the manner in which the bubble jets are formed.

B. *Possible atmospheric electrical effects.*—If one is to make an attempt to evaluate the atmospheric electrical effects that might result from a collection of charged drops from bursting bubbles, it is apparent that in addition to a knowledge of the magnitude and sign of the charge on a given-sized drop one would have to have an idea of the size distribution and rate of production of the drops. This, in turn, implies an understanding of their source, the spectrum of bubbles in the sea. Recent experimental studies [4] have shown that whitecaps are a most potent mechanism for the production of a bubble spectrum in which, in the size range of about 70- to 500-microns diameter, the number of bubbles m^{-3} is inversely proportional to the fifth power of the bubble diameter. From these experimentally determined values it was computed, assuming that 10 per cent of the sea surface was producing bubbles, that over a given area the average production rate for bubbles <100-microns diameter was 3 $\mathrm{cm}^{-2}\,\mathrm{sec}^{-1}$ while the production rate for bubbles from 100–200 microns was only about 0.3 $\mathrm{cm}^{-2}\,\mathrm{sec}^{-1}$, or 10 times less. The production rate for bubbles >200 microns was negligibly small, being about 0.06 $\mathrm{cm}^{-2}\,\mathrm{sec}^{-1}$. It is evident, assuming that bubbles are the source, that the great majority of the airborne drops that are observed over the open sea should be <20 microns diameter. (This is determined from the rule of thumb, mentioned earlier, of 10 as the ratio of bubble- to ejected-drop diameter.) This agrees with the experimental work of Woodcock [1].

We can now make a rough but conservative estimate, based on the above and present studies, of the charge transfer that might be expected to take place at the sea surface. Let us assume that only one drop from each bubble remains airborne. If each of the drops from the 3 bubbles $\mathrm{cm}^{-2}\,\mathrm{sec}^{-1}$ that are <100 microns carries a positive charge of 10^3 fundamental units while each of the drops from the bubbles >100 microns transports an average negative charge of 3×10^3 units (see fig. 5), then a net positive charge of about 2×10^3 fundamental units will be transferred from the sea to the air $\mathrm{cm}^{-2}\,\mathrm{sec}^{-1}$. This would appear to be a minimum value as the above assumptions of all drops from bubbles >100 microns remaining airborne and carrying a negative charge is most unlikely.

The production of a net positive space charge should not be confined to the breaking of bubbles that are produced solely by wave action. In addition to the obvious whitecaps, Blanchard and Woodcock [4] have found that snow, hail, and raindrops are capable of producing great quantities of bubbles, predominantly <100 microns, whose ejected drops should carry a positive charge. As all of these natural methods for the production of bubbles in the sea, and especially those involving precipitation, produce a spectrum of bubbles the majority of which are <100-microns diameter, it follows that most of the ejected drops, according to the present study, will be positive in charge and <10-microns diameter. The significance of the net positive charge of 2×10^3 fundamental units $\mathrm{cm}^{-2}\,\mathrm{sec}^{-1}$ that has been estimated to be leaving the sea as a result of breaking bubbles from wave action can be seen when we compare it to the average air-earth conduction current that prevails in areas of fair weather. The upward flow of a positive charge of 2×10^3 fundamental units $\mathrm{cm}^{-2}\,\mathrm{sec}^{-1}$ is equivalent to about 10^{-6} statamperes cm^{-2} which is the same value that has been calculated to be flowing into the oceans wherever fair weather prevails [33]. Now it is generally assumed that the mechanism by which the atmosphere regains the positive charge that is lost as a fair weather conduction current has its origin only in thunderstorms while the sea has been considered only as a sink for the positive charge. In view of the above calculation, it appears that the sea, which comprises about 70 per cent of the earth's surface, may be far from being a complete charge sink and might, during intense wave action or snow showers, contribute an appreciable net positive charge to the atmosphere. The positive space charge (fig. 7) found over the surf in Hawaii suggests that this is true for intense wave action. The calculated contribution of 10^{-6} statampere cm^{-2} of positive current from sea to atmosphere certainly cannot be considered as an average for the ocean as a whole but only for those regions where the above effects would cause moderate bubble formation. The transfer of charge from sea to atmosphere was discussed by Aliverti and Lovera [13] who bubbled air through sea water and found a net positive charge transferred to the air. They did not get their data from individual bubbles but from an artifically created foam patch that, in the opinion of the writer, is not representative of bubble phenomena on the open sea. Thus it is hard to interpret their results in a quantitative manner.

The postulated net positive charge transfer from sea to atmosphere by breaking bubbles becomes especially significant in view of the fact expressed earlier in the paper that it can occur in the presence of bucking electric fields up to about 25 volts cm^{-1}. Inasmuch as the average fair-weather field over the oceans is about 1 volt cm^{-1} [34], it is plain that the transfer of positive charge will be relatively unaffected by such small fields. Once airborne, the motion of the charged drops due to the electric field will be equally insignificant with respect to the motion due to gravity and turbulent processes. For example, a 3-micron-radius drop carrying a charge of 10^3 fundamental units will have a mobility of only 1.6×10^{-3} cm sec^{-1}, some three orders of magnitude less than that of the small ions in the atmosphere and 70 times less than the fall velocity due to gravity. Thus, in opposition to the force due to the earth's electric field, turbulent mixing and convective updrafts could carry the positive charge into clouds. Here the process envisaged by Vonnegut [35] may reverse the electric field at the top of the cloud and effectively cause a transfer of positive charge to the higher regions of the atmosphere where it spreads out and returns to the earth as a part of the fair-weather conduction current.

Let us consider the electric fields at the surface of these charged drops with the view that under some conditions they may be high enough to cause corona discharge and neutralization of the drop charge. Consider the case of a 3-micron-radius drop carrying 1000 fundamental units of charge (see fig. 5) when it leaves the sea and again when it is subjected to humidities <75 per cent. Using Gauss' Law we find that the electric field E at the surface of a drop of radius R carrying a charge Q is $E = Q/R^2$ which, in the above case of the drop as it leaves the sea, gives a field of 1600 volts cm^{-1}. As the humidity of the air is decreased, the drops will become smaller and more saline. For humidities >75 per cent, an equilibrium drop size will exist where the vapor pressure of the saline drop is identical with that of the air. At about 75 per cent relative humidity the drop becomes a saturated salt solution and further reduction of the vapor pressure of the air will cause the NaCl to crystallize [36]. A spherical crystalline sea-salt nucleus has a radius about 25 per cent of the initial radius [37]. Gauss' Law shows that a 16-fold increase of the electric field will occur and, consequently, the above-mentioned field of 1600 volts cm^{-1} will rise to 25,600 volts cm^{-1}. It might be well to note that the charge of a drop will diminish the tendency of the drop to evaporate [38]. It can be shown, however, that the effect is negligible when we consider magnitudes of charge and radius as given above.

If an electrical storm occurs that produces fields of 100 volts cm^{-1} at the sea surface, it can be shown from the data of fig. 5 that all drops <10-microns radius will have a sufficiently high induced charge to enable them to be carried upward in the electric field. The field at the surface of these 10-micron drops, assuming a charge of 2.2×10^4 fundamental units, would be 3200 volts cm^{-1}, becoming about 51,000 volts cm^{-1} on the crystalline nucleus at a humidity <75 per cent.

It has been assumed that the crystalline nucleus (not entirely crystalline as magnesium and calcium salts are still in solution long after the major salt NaCl precipitates out) is spherical, but this is not the case as examination under the microscope reveals many sharp edges and protuberances [39]. As the surface charge density will vary in direct proportion to the reciprocal of the radius of curvature [40], the edges and points will attain a proportionately higher surface charge σ. Consequently, the field strength $E = 4\pi\sigma$ may well attain values far in excess of those computed on the basis of a spherical drop.

Although in the case of phase change and at points of high curvature the surface electric field may well exceed 30,000 volts cm^{-1} (the critical value for spark discharge in air at atmospheric pressure), it will not necessarily break down. The breakdown of an electric field results from ionization produced by the collision of ions with the molecules of the gas. In the case of spherical drops, the electric field falls off inversely with the square of the distance from the drop center. Thus, the smaller the drop the faster will the field decrease over a given distance from the drop surface. The probability of ionization by collision will, therefore, decrease, and the electric field required for corona will increase. This was shown by the investigation of Zeleny [41] and more recently by the work of English [42]. It appears then that the charge on these drops will not experience a neutralization by electric-field breakdown. The only method by which charge can be lost is by the diffusion onto the drops of the small ions that exist in the atmosphere over the oceans [43]. The relaxation time for the charge on drops in the lower atmosphere will vary, depending upon the conductivity, from 5 to 40 min [44]. Thus, under some conditions it is to be expected that drops could be carried by air current into clouds and still retain much of their original charge. In any event, any decrease with time of the charge of the drops does not change the net charge per unit volume of space but merely transfers the charge to smaller carriers.

5. Conclusion

Probably the most significant aspect of the present findings is the charge-separation process that appears to be occurring at the bubble-water interface of a small bursting bubble which results in a positive charge on the ejected drops. The observations cannot be explained on the basis of known phenomena and make further work imperative.

The suggestion that the sea need not be considered as a complete sink for the atmospheric space charge, but also as a source, leads to consideration of the sea as a source of the supply current to maintain the earth's electric field. This should be followed up with more laboratory and field studies of the net charge transfer under various simulated and natural bubbling conditions. It would be well to investigate the charge transfer by the small drops that are created by the bursting of the films of the relatively few large bubbles that are produced by wave action [45].

Finally, it is well to keep in mind that the large electric fields, associated with thunderstorms and perhaps snow showers at sea, would induce high charges on the ejected drops from bursting bubbles. Due to an increase of local winds and precipitation in these storm areas, the bubble formation would be increased and a high local concentration of space charge should occur. It may be that such pronounced local effects will be of more importance in the atmosphere electrical balance than the charge transfer from a relatively quiet sea in areas of low surface winds and fair weather.

Acknowledgments.—The writer is indebted to his colleague, Mr. A. H. Woodcock, for the many helpful discussions on the problem and for help in obtaining some of the data. His former colleague, Dr. C. H. Keith, is responsible for the work relating bubble diameter to the mass and height of the ejected drops. To Prof. Leonard B. Loeb of the University of California, the writer would like to express his thanks for the many helpful ideas that evolved from an extended correspondence. Finally, he would like to thank Dr. Bernard Vonnegut who, on several occasions, loaned his apparatus for the determination of space charge.

REFERENCES

1. Woodcock, A. H., 1953: Salt nuclei in marine air as a function of altitude and wind force. *J. Meteor.*, **10**, 362–371.
2. Twomey, S., 1955: The distribution of sea-salt nuclei in air over land. *J. Meteor.*, **12**, 81–86.
3. Lodge, J. P., 1955: A study of sea-salt particles over Puerto Rico. *J. Meteor.*, **12**, 493–499.
4. Blanchard, D. C., and A. H. Woodcock, 1957: Bubble formation and modification in the sea and its meteorological significance. *Tellus*, **9**, 145–158.
5. Woodcock, A H , and D. C. Blanchard, 1955: Tests of the salt-nuclei hypothesis of rain formation. *Tellus*, **4**, 437–448.
6. Blanchard, D. C., 1955: Electrified droplets from the bursting of bubbles at an air-sea water interface. *Nature*, **175**, 334–336.
7. Chapman, S., 1934: The charges on droplets produced by the spraying of liquids as revealed by the Millikan oil drop method. *Physics*, **5**, 150–152.
8. Chapman, S., 1937: Carrier mobility spectra of spray electrified liquids. *Phys. Rev.*, **52**, 184–190.
9. Chapman, S., 1938: Carrier mobility spectra of liquids electrified by bubbling. *Phys. Rev.*, **54**, 520–527.
10. Chapman, S., 1938: Interpretation of carrier mobility spectra of liquids electrified by bubbling and spraying. *Phys. Rev.*, **54**, 528–533.
11. Köhler, H., 1941: An experimental investigation on sea water nuclei. *Nova Acta Regiae Soc. Sci. Upsaliensis*. Ser. 4, **12**, 55 pp.
12. Dinger, J. E., and R. Gunn, 1946: Electrical effects associated with a change of state of water. *Terr. Mag. and atmos. Elec.*, **51**, 477–494.
13. Aliverti, G., and G. Lovera, 1939: I fenomeni meteorologica sull Oceano e il campo elettrico terrestre. *Atti della Reale Accademia delle Sci. di Torino*, **74**, 573–590.
14. Stuhlman, O., 1932: The mechanics of effervescence. *Physics*, **2**, 457–466.
15. Kientzler, C. F., A. B. Arons, D. C. Blanchard, and A. H. Woodcock, 1954: Photographic investigation of the projection of droplets by bubbles bursting at a water surface. *Tellus*, **6**, 1–7.
16. Blanchard, D. C., 1954: A simple method for the production of homogeneous water drops down to 1 micron radius. *J. Colloid Sci.*, **9**, 321–328.
17. Chalmers, J. A., and F. Pasquili, 1937: The potential difference at an air-water interface. *Philosophical Mag.*, **23**, 88–96.
18. Chalmers, J. A., 1950: *Atmospheric electricity*. London, Oxford Univ. Press, 175 pp.
19. Adam, N. K., 1941: *The physics and chemistry of surfaces*. London, Oxford Univ. Press, 436 pp.
20. Squires, P., 1955: Project "Shower": an investigation on warm rain in the Hawaiian Islands. *Nature*, **175**, 748–750.
21. Schaefer, V. J., 1956: Atmospheric electrical measurements in the Hawaiian Islands. *Geofis. pura e Applicata*, **34**, 209–220.
22. Lenard, P., 1915: Über Wasserfall-elektrizität und über die Oberflächenbeschaffenheit der Flüssigeiten. *Annalen der Phys.*, **47**, 463–524.
23. Dodd, E. E., 1953: The statistics of liquid spray and dust electrification by the Hopper and Laby method. *J. appl. Phys.*, **24**, 73–80.

24. McTaggart, H. A., 1914: The electrification at liquid-gas surfaces. *Philosophical Mag.*, **27**, 297–314.
25. McTaggart, H. A., 1922: On the electrification at the boundary between a liquid and a gas. *Philosophical Mag.*, **44**, 386–395.
26. Alty, T., 1924: The cataphoresis of gas bubbles in water. *Proc. r. Soc.* (A), **106**, 315–340.
27. Banerji, S. K., 1938: On the interchange of electricity between solids, liquids and gases in mechanical action. *Indian J. Phys.*, **12**, 409–436.
28. Nolan, J. J., and J. Enright, 1922: Experiments on the electrification produced by breaking up water, with special application to Simpson's theory on the electricity of thunderstorms. *Sci. proc. r. Dublin Soc.*, **17**, 1–11.
29. Alty, T., 1926: The origin of the electrical charge on small particles in water. *Proc. r. Soc.* (A), **112**, 235–251.
30. Currie, B. W., and T. Alty, 1929: Absorption at a water surface. *Proc. r. Soc.*, **122**, 622–633.
31. Whybrew, W. E., G. D. Kinzer, and R. Gunn, 1952: The electrification of small air bubbles in water. *J. geophys. Res.*, **57**, 459–471.
32. Peterson, J. W., 1954: Contact charging between borosilicate glass and nickel. *J. appl. Phys.*, **25**, 501–504.
33 Gish, O. H., 1951: *Compendium meteor.* Boston, Amer. meteor. Soc., pp. 101–119.
34. Bauer, L. A., and W. F. G. Swann, 1917: *Results of atmosphericel-ectric observations made aboard the Galilee (1907–1908) and the Carnegie (1909–1916). Carnegie Inst. of Washington Publ. No. 175*, **3**, 361–422.
35. Vonnegut, B., 1955: *Possible mechanism for the formation of thunderstorm electricity.* Geophys. Res. Pap. No. *42*, Geophys. Res. Dir., AFCRC, 169–181.
36. Twomey, S., 1954: The composition of hygroscopic particles in the atmosphere. *J. Meteor.*, **11**, 334–338.
37. Woodcock, A. H., 1952: Atmospheric salt particles and raindrops. *J. Meteor.*, **9**, 200–212.
38. Thomson, J. J., and G. P. Thomson, 1928: *Conduction of electricity through gases.* London, Cambridge Univ. Press, Vol. I.
39. Woodcock, A. H., and M. M. Gifford, 1949: Sampling atmospheric sea–salt nuclei over the ocean. *J. marine Res.*, **8**, 177–197.
40. Loeb, L. B., 1938: *Fundamentals of electricity and magnetism.* New York, John Wiley and Sons, Inc., 544 pp.
41. Zeleny, J., 1920: Electrical discharges from pointed conductors. *Phys. Rev.*, **16**, 102–125.
42. English, W. N., 1948: Corona from a water drop. *Phys. Rev.*, **74**, 179–189.
43. Gish, O. H., 1939: *Terrestial magnetism and electricity.* New York, McGraw-Hill Book Co., Inc.
44. Chalmers, J. A., 1957: *Atmospheric electricity.* London, Pergamon Press, 327 pp.
45. Knelman, F., N. Dombrowski, and D. M. Newitt, 1954: Mechanism of the bursting of bubbles. *Nature*, **173**, 261.

Contribution No. 877

PHYSICAL OCEANOGRAPHY OF THE GRAND BANKS REGION AND THE LABRADOR SEA IN 1956[1]

By Floyd M. Soule and J. E. Murray
(U. S. Coast Guard)

The *USCGC Evergreen* served as oceanographic vessel of the International Ice Patrol again in 1956. Descriptions of instruments, and deck and laboratory arrangements have been published in earlier bulletins of this series. No new gear was used nor were any major changes in arrangement made in 1956.

Temperature and salinity data were collected during three surveys made during the season and on a postseason cruise. The first survey, intended to develop the dynamic topography of the waters over and immediately seaward of the eastern and southern slopes of the Grand Banks from the latitude of Flemish Cap to the Tail of the Grand Banks and westward of the Tail to about 52°W., took place between 31 March and 14 April (Argentia to Argentia) with the work of collection of data confined to the period from 1 April to 13 April. The weather did not require the suspension of oceanographic work at any time during the survey. The only delay was a six-hour period on 12 April during which a fathometer fault was located and repaired. During the first survey 86 stations (6037 to 6122) were occupied.

Because of necessary engine repairs, departure for the second survey was from Boston on 15 May instead of from Argentia on 25 April as had been planned. On completion of the survey the *Evergreen* returned to Argentia on 2 June. The actual work of collection of data took place between 19 May and 1 June. The area covered by the 95 stations of the survey was the same as that of the first survey plus a westward extension westward of the Tail of the Banks to about longitude 53° W. A delay of about 3 hours was caused by gales on 27 May and another 1 hour delay on 31 May was occasioned by the replacement of a GEK electrode cable which had been cut by the screw.

The third survey, from 11 to 21 June (Argentia to Argentia) developed the dynamic topography of the waters over and immediately seaward of the northeastern slope of the Grand Banks

---

[1] To be reprinted as Contribution No. 877 in the Collected Reprints of the Woods Hole Oceanographic Institution.

Extract from U. S. Coast Guard Bulletin No. 42, pages 35-100. Reprinted as Contribution No. 877 in the Collected Reprints of the Woods Hole Oceanographic Institution.

from Flemish Cap to and including the Bonavista triangle. No delays were encountered from weather or other causes and the 67 stations were occupied between 12 and 19 June.

The postseason cruise, 6 to 23 July (Boston to Argentia) comprising 29 stations in the occupation of the Bonavista triangle, 10 to 13 July, and 22 stations in the occupation of the section from South Wolf Island, Labrador to Cape Farewell, Greenland, 15 to 20 July, was delayed 2 hours on 15 July for fathometer repairs, 2½ hours on 17–18 July for radar repairs and 19 hours on 18–19 July by weather.

The oceanographic work was under the supervision of Oceanographer Floyd M. Soule who was assisted by LT John E. Murray. Other assistants in the observational work were Francis N. Brown, yeoman first class; Elwood C. Gray, aerographer's mate first class; Lewis M. Lawday, aerographer's mate second class; Hugh R. McCartney Jr., aerographer's mate second class; and Bruce M. McCluskey, boatswain mate second class.

Of the 299 stations occupied during the season and postseason surveys, the 22 stations forming the section across the Labrador Sea were occupied from the surface to as near bottom as was practicable, and at the other 277 stations the observations extended to about 1,500 meters where the depth of water permitted. As in previous years, the intended depths of observation in meters, were 0, 25, 50, 75, 100, 150, 200, 300, 400, 600, 800, 1,000 and thence by 500-meter intervals. The dynamic heights have been referred to the 1,000-decibar surface, except for the section across the Labrador Sea where the 1,500-decibar surface has been used for reference. Temperature and salinity were measured at each observation level.

Deep sea reversing thermometers were used to measure temperatures and determine depths of observation. The protected thermometers used were, for the most part, of Richter and Wiese manufacture but a small percentage were made by Negretti and Zambra, G.M. Manufacturing Co., and the Kahl Scientific Instrument Corp. The unprotected thermometers used were made by Richter and Wiese and by Kahl. The thermometers were used in pairs and the individual instruments making up the pairs were shifted periodically to permit intercomparison of the protected thermometers. From a total of 1,993 comparisons, the probable difference between the corrected readings of a pair of protected thermometers was ±0.010°C. Many of the thermometers had recently been compared in the laboratory with thermometers tested by the National Bureau of Standards. As in most cases the temperatures are the means of the corrected readings of a pair of thermometers it is considered that the observed temperatures listed in the table of oceanographic data have a probable error of ±0.01°C.

Routine measurements of salinity were made, as in previous years, with a Wenner salinity bridge using a substitution method. From measurements and tests of the instrument prior to the beginning of the 1956 field work it was concluded that there was no need for a redetermination of its calibration curve. Water from an oil-sealed carboy of sea water was used as a working standard of salinity for the routine measurements. At least twice during each run samples of Copenhagen normal sea water were measured as unknowns. At the end of each survey these measurements of Copenhagen water were used to compute any necessary corrections to the salinities of the samples measured during the survey. At the beginning of the season Copenhagen water of the batch P_{17} was used. Samples of Copenhagen water of the batch P_{22} were also measured as unknowns to get the conductivity-salinity relationship of this batch in terms of the batch P_{17}, thus enabling a shift to batch P_{22} as the reference standard at the beginning of the 3rd survey. For the three surveys made during the season the corrections did not exceed 0.005°/oo and no corrections have been applied. The correction for the post season cruise was +0.006°/oo and corrections have been applied in the table of oceanographic data. The dynamic topography of the Bonovista triangle shown in figure 15 however, has not been corrected and the dynamic heights shown in this figure are consequently 4 mm too high. The calibration curve of the salinity bridge is determined by the measurement of samples of sea water whose salinities are known from silver nitrate titration. The accuracy of the salinities determined by the bridge is therefore no better than the accuracy of the silver nitrate titration method used in determining the calibration curve. The precision of the bridge measurements, however, is much better and is about ±0.005°/oo in salinity.

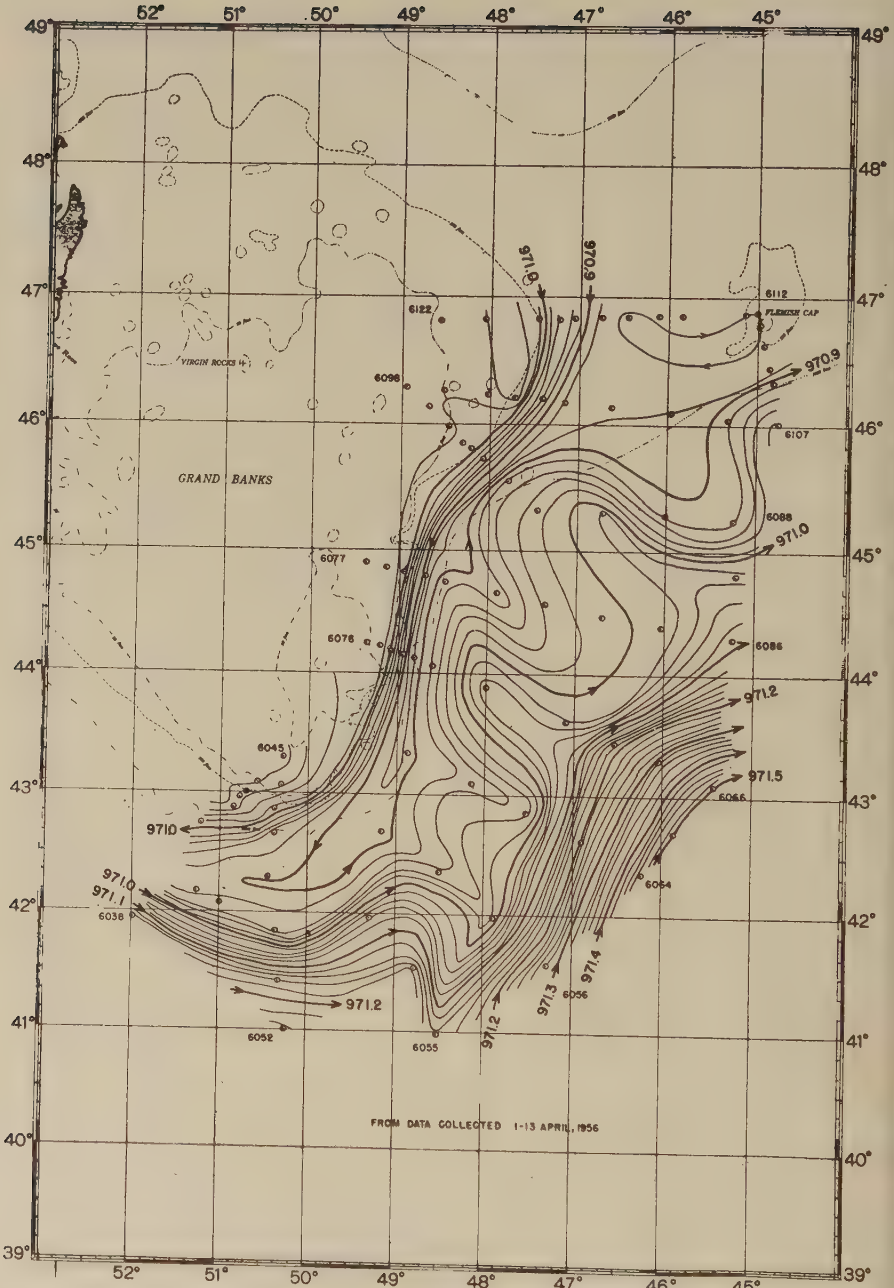
52°
51°
50°
49°
48°
47°
46°
45°
49°
48°
47°
46°
45°
44°
43°
42°
41°
40°
39°
VIRGIN ROCKS
GRAND BANKS
FLEMISH CAP
6122
6112
6098
6107
6088
6077
6076
6086
6045
6066
6064
6038
6056
6052
6055
971.0
970.9
970.9
971.0
971.2
971.5
9710
971.0
971.1
971.2
971.2
971.3
971.4
FROM DATA COLLECTED 1-13 APRIL, 1956

FIGURE 12.—Dynamic topography of the sea surface relative to the 1000-decibar surface from data collected 1–13 April 1956. Oceanographic station positions are indicated and the station numbers given at turning points.

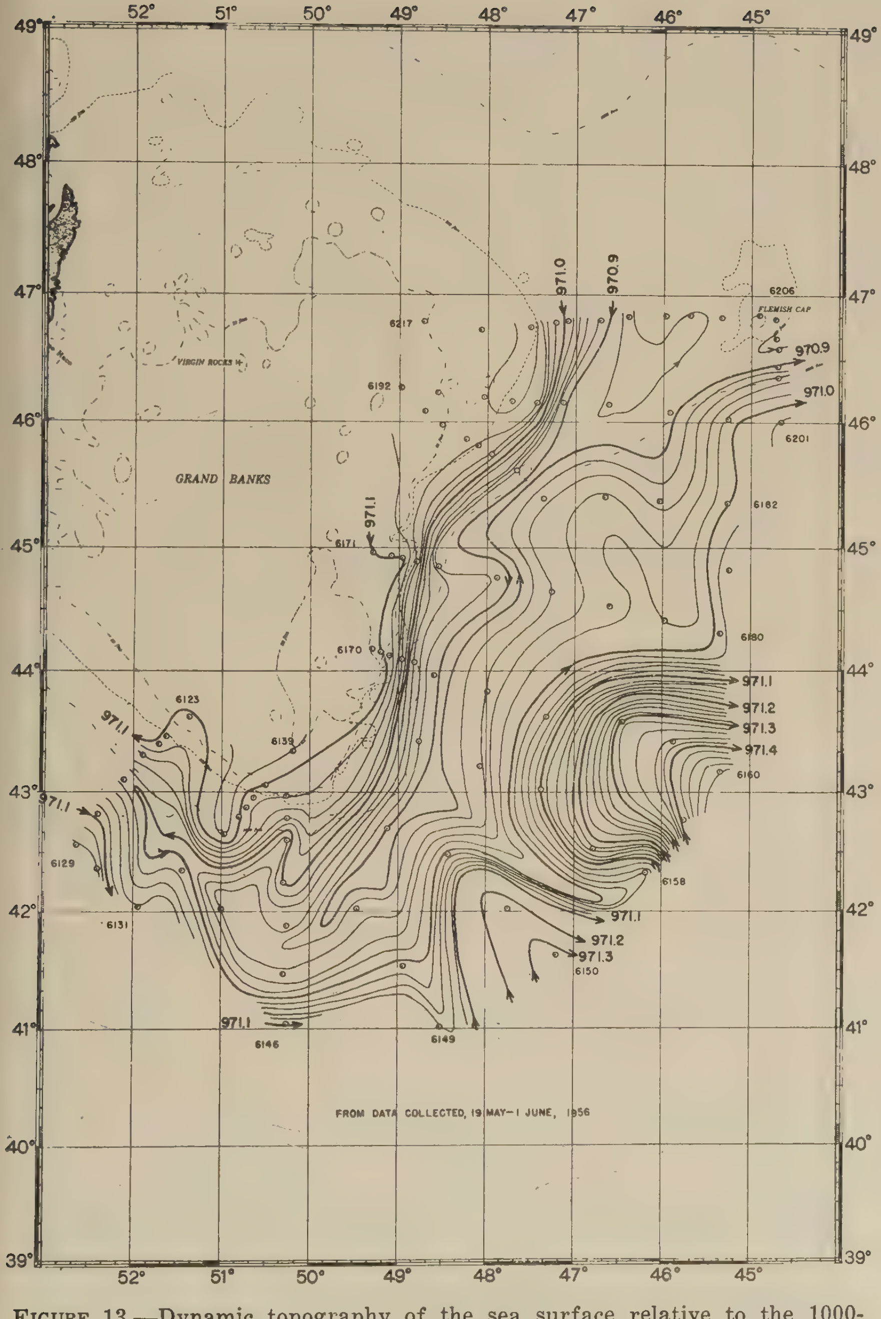
49°
48°
47°
46°
45°
44°
43°
42°
41°
40°
39°
52°
51°
50°
49°
48°
47°
46°
45°
GRAND BANKS
VIRGIN ROCKS
FLEMISH CAP
971.0
970.9
971.1
971.2
971.3
971.4
6206
6217
6192
6201
6182
6171
6170
6180
6123
6139
6160
6129
6131
6158
6150
6146
6149
FROM DATA COLLECTED, 19 MAY–1 JUNE, 1956

FIGURE 13.—Dynamic topography of the sea surface relative to the 1000-decibar surface from data collected 19 May–1 June 1956. Oceanographic station positions are indicated and the station numbers given at turning points.

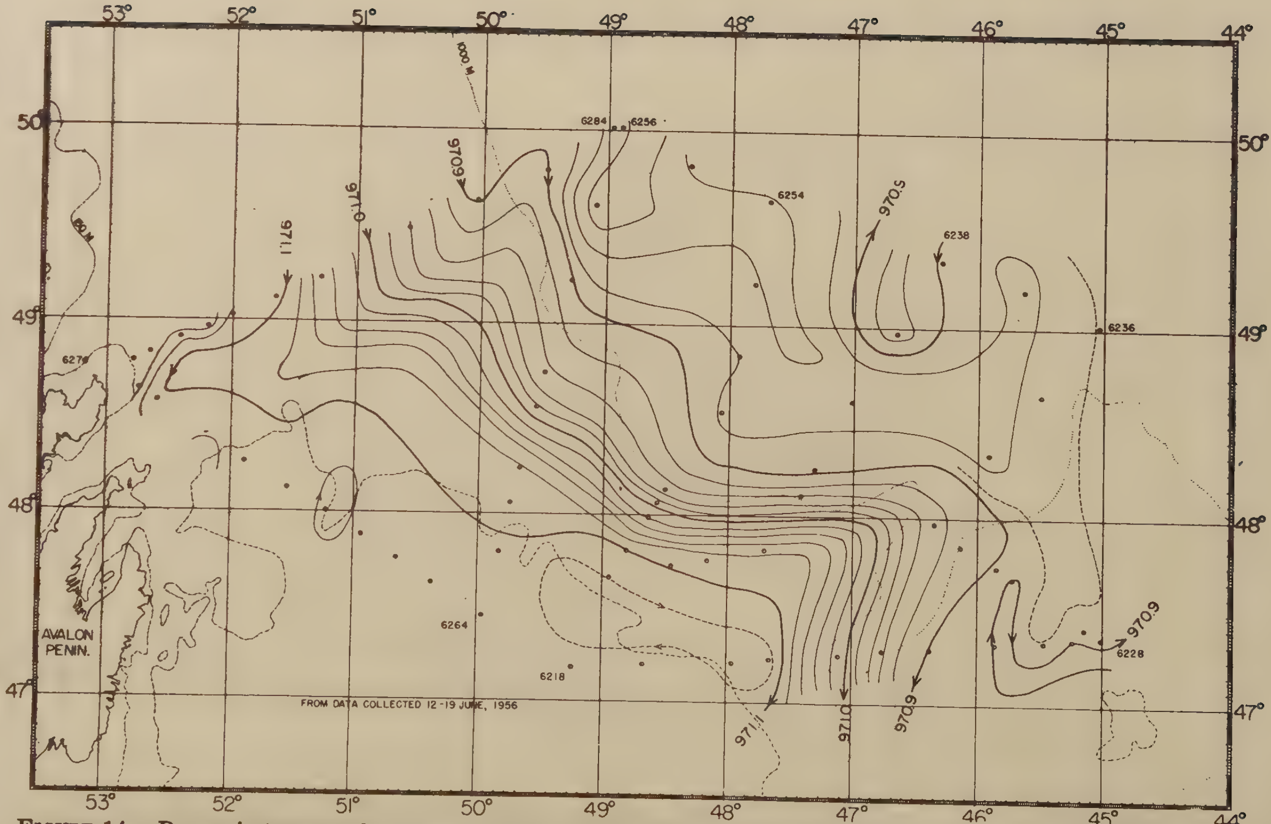
53°
52°
51°
50°
49°
48°
47°
46°
45°
44°
50°
49°
48°
47°
1000 M
60 M
6284
6256
6254
6238
6236
6228
6218
6264
6278
970.5
970.9
971.0
971.1
AVALON PENIN.
FROM DATA COLLECTED 12-19 JUNE, 1956

FIGURE 14.—Dynamic topography of sea surface relative to the 1000-decibar surface from data collected 12–19 June 1956. Oceanographic station positions are indicated and station numbers given at turning points.

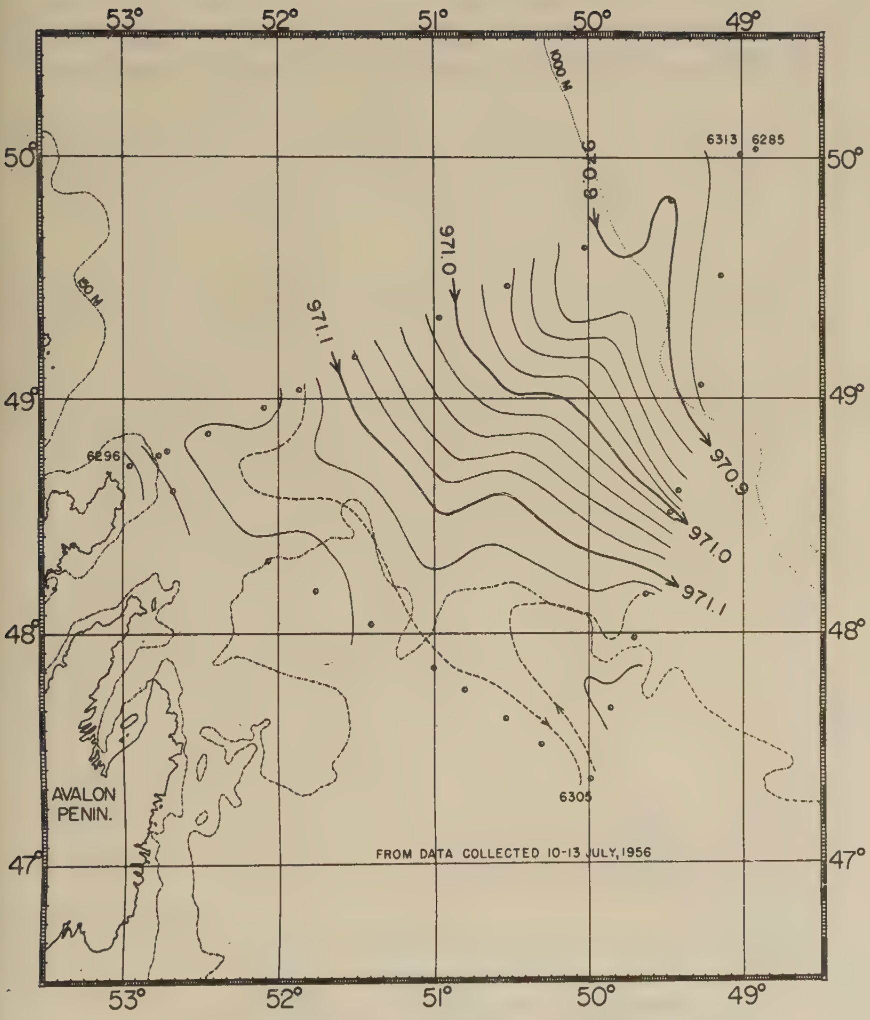
53°
52°
51°
50°
49°
1000 M
6313
6285
50°
970.9
971.0
971.1
150 M
49°
6296
970.9
971.0
971.1
48°
AVALON PENIN.
6305
FROM DATA COLLECTED 10-13 JULY, 1956
47°

FIGURE 15.—Dynamic topography of the sea surface relative to the 1000-decibar surface from data collected 10–13 July 1956. Oceanographic station positions are indicated and the station numbers given at turning points.

The dynamic topography found during the three surveys made during the season and during the postseason occupation of the Bonavista triangle is shown in figures 12, 13, 14 and 15 presented in chronological order. It will be seen from figure 12 that during the first survey except at the two northernmost sections the Labrador Current was flowing with about normal surface speeds all the way to and westward of the Tail of the Banks. This water continued westward of the Tail beyond the limits of the surveyed area before recurving to the south and east. The temperature structure of the Labrador Current was not normal and the temperature minimum was atypically warm and poorly defined except at the northern sections. Here the abnormality seemed to be confined to that part of the current which was eastward of the 100-fathom curve.

Figure 13 shows the considerable northwestward extension of the Labrador Current beyond the Tail of the Banks. The surface speed of the Labrador Current remained strong along the eastern edge of the Banks and in the northwestern part of the surveyed area the pattern of set onto the Banks inside the 100-fathom curve shown in figure 12 was repeated. The temperature minimum of the Labrador Current was about 0.6°C colder than the abnormally warm temperatures found during the first survey. While these colder minimum values showed a recovery to about normal, this recovery was limited to the inshore half of the current.

During the third survey (figure 14) the abnormally warm minimum temperatures in the offshore half of the Labrador Current continued. The only station where negative temperatures were found seaward of the 971.0 dynamic meter contour was station 6260 on the southeastern side of the Bonavista triangle and the lowest dynamic height at which a temperature minimum as cold as —1.0°C was found was 971.05 dynamic meters on the northern side of the triangle. Along the southernmost section of the survey the dynamic topography indicated little change from that found in the northern part of the second survey.

The current pattern in the Bonavista triangle found during the post-season cruise (figure 15) was much the same as that found during the third survey, the principle change being a seaward shift of the current pattern. From the topography shown in figure 15 any bergs crossing the 49th parallel eastward of about longitude 51–45° W. Would have followed the eastern branch of the Labrador Current and those crossing westward of that longitude would have followed the western branch.

Labrador Current water and Atlantic Current water found in the Grand Banks region have temperature-salinity characteristics which identify them as water masses. Here also these parent water masses mix in a sufficiently constant proportion so that the mixed water can be regarded as a virtual water mass. Mean T–S curves for these three water masses have been derived from observations made during the 8-year period 1934–41. Conditions found during the recent postwar years were compared with these prewar means for want of any better normals. We now have a postwar series of observations of comparable length made during the 9-year period 1948–56. The mean T-S relationships for each of the three water masses is shown for each of the two periods in figure 16.

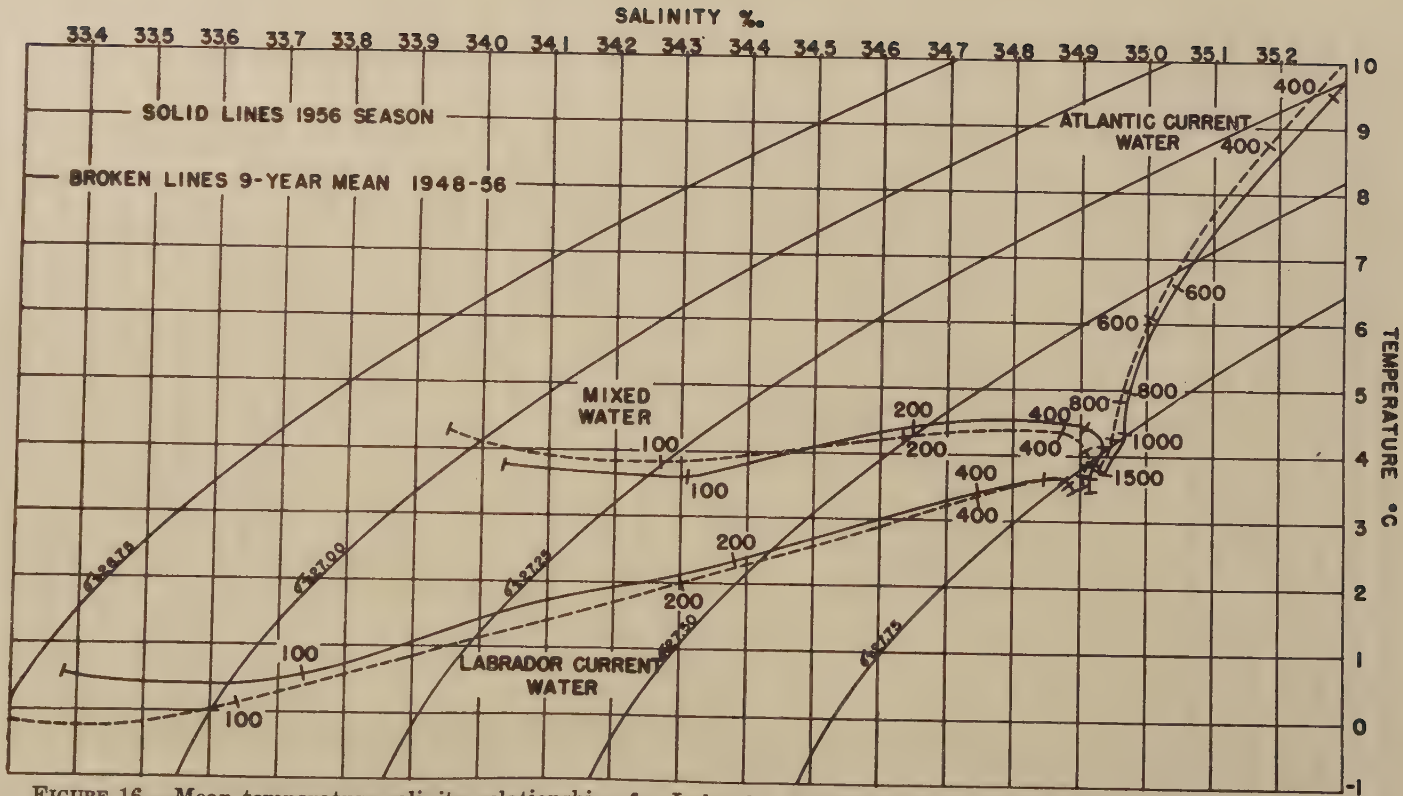

FIGURE 16.—Mean temperature-salinity relationships for Labrador Current water, Atlantic Current water, and mixed water found in the Grand Banks region during the period 1948–56 (shown as solid lines) compared with means for the period 1934–41 (shown as broken lines).

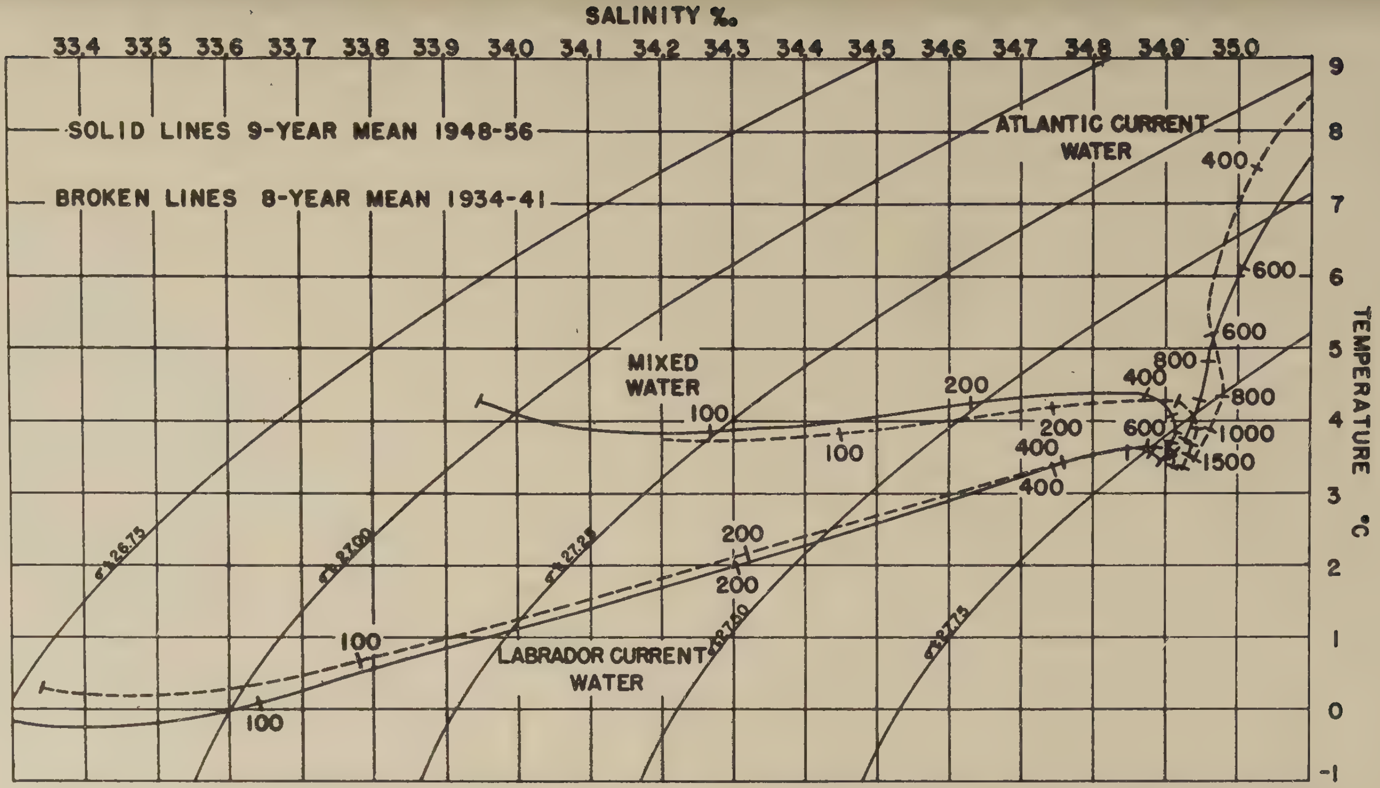

FIGURE 17.—Temperature-salinity relationships for Labrador Current water, Atlantic Current water, and mixed water found in the Grand Banks region. Solid lines show conditions found during the first and second surveys in 1956 and broken lines represent the 9-year means for the period 1948–56. An approximate depth scale in meters is given.

The density is less in each water mass level for level in the recent period than in the earlier period. In Labrador Current water the postwar observations show fresher and colder water at the levels above 600 meters and fresher water of about the same temperatures at the levels below 600 meters. The postwar mixed water is fresher and warmer at all levels. In Atlantic Current water the postwar observations show saltier and warmer water at levels above 600 meters and fresher and warmer water at 800 meters and below. The prewar salinity inversion with a minimum at about 5.5° is not present in the postwar curve. The salinity difference between the prewar and postwar curves at 1,000 meters is about 0.02°/oo, being somewhat less in Atlantic Current water and somewhat more in Labrador Current water and mixed water. While it is possible that this may represent a shift in instrument standardization it is considered to be at least partly a real change in salinity of the water. The temperature changes are considered to be real. The differences in the curves for Atlantic Current water are not as significant as those in the curves for the other two water masses since most of the surveys do not get far enough into the Atlantic Current to get a representative sampling of the entire current.

In figure 17 the T-S relationships found in 1956 are compared with the means for the period 1948–56. It will be seen that in 1956 the Labrador Current water was denser, warmer and saltier than the mean at levels above 600 meters and was the same as the mean at levels below 600 meters. The mixed water was denser and saltier than the mean at all levels and colder above about 150 meters, warmer from 150 to 800 meters and about the same below 800 meters. The Atlantic Current water was denser, saltier and warmer than the mean at all levels.

The position of the cold wall was estimated for each of the first two surveys, using as a criterion the horizontal projection of the line along which a temperature of 6°C corresponds to a salinity of 34.95°/oo. To permit a simple numerical expression of the position of this cold wall with respect to its advance toward or retreat from the Grand Banks we have used the area between it and the fixed rhumb lines of the 45th parallel, the 49th meridian from 45° N., to 43° W., and a line from 43° N., 49° W., through 42° N., 47° W., extended. This area was 7.7 and 7.5 (x 10^4 square kilometers) for the first and second surveys respectively. Reasoning that the position of the cold wall is determined by the relative strengths of the Labrador Current and the Atlantic Current the effect of the latter is approximated by adjusting the area by 10^4 square kilometers for each 10^6 cubic meters per second of Labrador Current entering the area past the 45th parallel. The resulting adjusted area, A, was 4.10 and 2.63 for the first and second surveys respectively. These figures are to be compared with 3.62 and 1.60 respectively, computed from the 1952 prediction formula $A=6.97(H-5.07)-1.67$ where H, expressed in feet, is the sea level at Charleston minus the departure from average sea level at Bermuda 11½ months earlier.

The Labrador Current has been studied in some detail for a number of years through the examination of the velocity and temperature distribution in vertical sections which have been repeatedly occupied. The section across the West Greenland Current off Cape Farewell also has been studied in the same manner although the dates of the various occupations and those of the section across the Labrador Current are not as widely distributed over the spring and summer months as are those for the sections in the Grand Banks region. The various sections have been designated as follows. Sections NW, SW and SE are the northwestern, southwestern and southeastern sides of the Bonavista triangle which is defined by its corners located just off Cape Bonavista, Newfoundland, 50° N., 49° W., and about 47°20′ N., 50°00′ W. Section H is roughly parallel to the southeastern side of the Bonavista triangle and extends north-northeasterly from about 47°10′ N., 49°15′ W. Section G extends northeasterly from about 47°10′ N., 48°40′ W. Section F_2 is an east-west section between the Grand Banks and Flemish Cap along the parallel of 47°15′ N. Section F is similar to F_2 but about 30 miles farther south. Section T extends southeasterly from about 46°20′ N., 49°00′ W. Section U extends easterly from the Grand Banks at about 45°00′N. Section W extends southerly from the Grand Banks along the meridian of 50°15′ W.

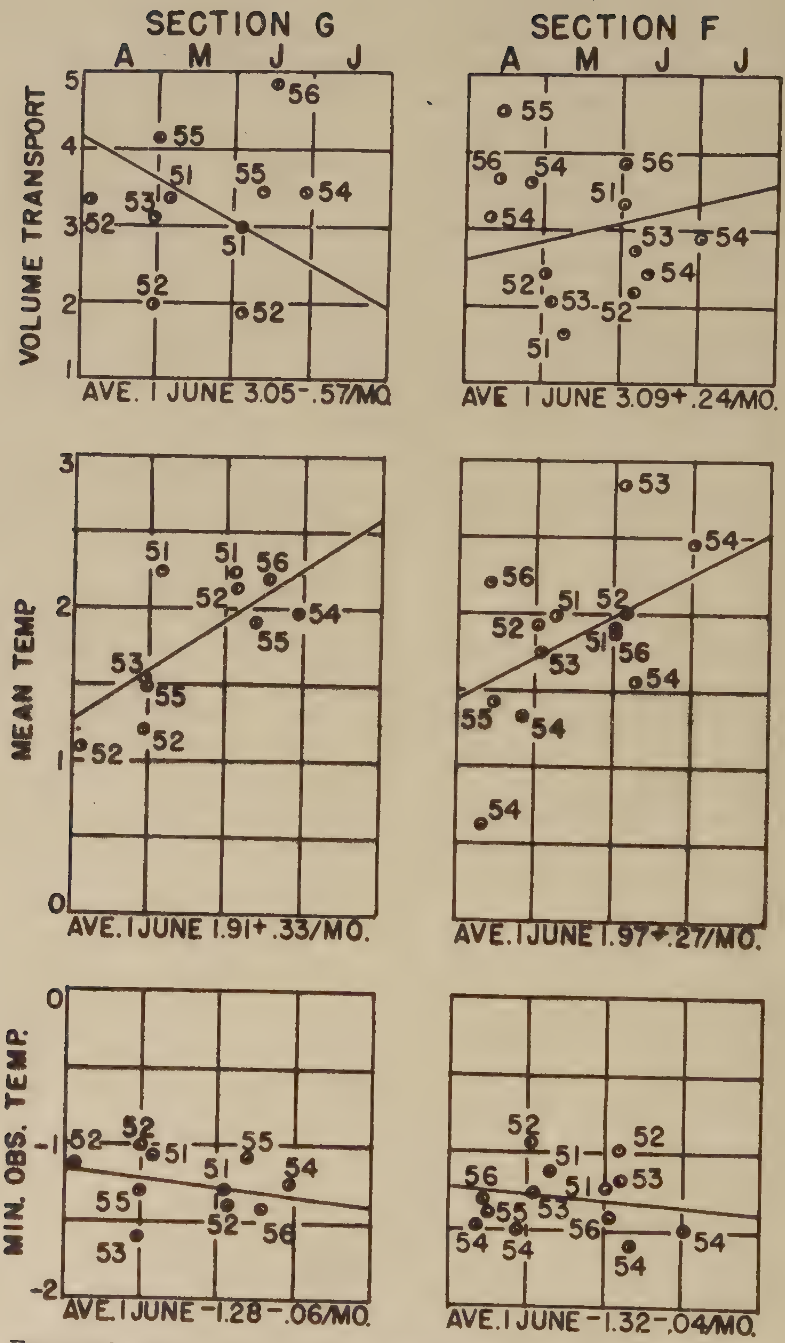

FIGURE 18.—Tentative normal seasonal change in volume transport, mean temperature, and minimum observed temperature of the Labrador Current at sections G and F.

The data from these sections, while not numerous, have permitted the development of some tentative normal seasonal variation relationships for a part of the year. Those for the West Greenland Current off Cape Farewell were published in bulletin 35 of this series. These data for the section across the Labrador Current off South Wolf Island, Labrador, have so far been treated as of a common date and average values are used for comparison with those for an individual occupation. Tentative normal seasonal variation curves for sections T, U and W have been published in bulletin 36 and those for the Bonavista triangle appear in bulletin 39. Data from sections H and F_2 are still insufficient for the development of even tentative normals. Figure 18 gives the approximate normal seasonal variation relationships at sections F and G. The seasonal increase in volume transport for section F does not agree with the seasonal decrease found for section G. All three sections of the Bonavista triangle show a seasonal increase in volume transport. It is to be expected that section F would show either a seasonal decrease or a smaller seasonal increase than that at the Bonavista triangle. These curves are therefore looked upon with suspicion and additional data may show that the seasonal decrease at section G is less than shown in figure 18 and that the volume transport at section F normally has a seasonal decrease.

Table 1.—Summary of velocity sections across Labrador Current occupied in 1956

Section	Volume transport			Mean temperature			Minimum observed temperature			Heat transport		
	1956	Normal	Anomaly	1956	Normal	Anomaly	1956	Normal	Anomaly	1956	Normal	Anomaly
1st Survey:												
F	3.65	2.71	+0.94	2.21	1.55	+0.66	−1.30	−1.26	−0.04	8.07	4.19	+3.88
T	2.59	3.31	−0.72	2.01	1.95	+0.06	−0.73	−1.40	+0.67	5.20	6.45	−1.25
U	3.58	5.34	−1.76	2.72	1.47	+1.25	−0.46	−1.22	+0.76	9.77	7.85	+1.92
W	5.53	4.24	+1.29	2.37	2.02	+0.35	+0.14	−0.51	+0.65	13.10	8.56	+4.54
2d Survey:												
F	3.86	3.10	+0.76	1.87	1.98	−0.11	−1.43	−1.32	−0.11	7.22	6.14	+1.08
T	3.76	2.67	+1.09	2.10	1.73	+0.37	−1.38	−1.55	+0.17	7.90	4.62	+3.28
U	4.87	3.84	+1.03	1.75	2.31	−0.56	−1.04	−1.22	+0.18	8.49	8.87	−0.38
W	5.20	4.13	+1.07	2.93	3.10	−0.17	−0.54	−0.41	−0.13	15.25	12.80	+2.45
3d Survey:												
NW	4.11	3.76	+0.35	1.40	1.23	+0.17	−1.60	−1.67	+0.07	5.76	4.62	+1.14
SW	0.68	0.52	+0.16	−0.82	−0.27	−0.55	−1.61	−1.64	+0.03	−0.56	−0.14	−0.42
SE	3.78	3.15	+0.63	2.02	1.74	+0.28	−1.38	−1.54	+0.16	7.63	5.48	+2.15
H	4.44	-------	-------	2.18	-------	-------	−1.45	-------	-------	9.67	-------	-------
G	4.87	2.74	+1.93	2.19	2.09	+0.10	−1.42	−1.31	−0.11	10.69	5.73	+4.96
F2	4.54	-------	-------	1.77	-------	-------	−1.52	-------	-------	8.05	-------	-------
Postseason:												
NW	4.71	4.04	+0.67	1.88	1.41	+0.47	−1.62	−1.61	−0.01	8.86	5.70	+3.16
SW	0.42	0.62	−0.20	0.15	0.06	+0.09	−1.57	−1.64	+0.07	0.06	0.04	+0.02
SE	4.82	3.32	+1.50	2.35	1.98	+0.37	−1.47	−1.58	+0.11	11.34	6.57	+4.77
South Wolf Island	4.18	4.72	−0.54	1.75	2.46	−0.71	−1.50	−1.49	+0.01	7.33	11.61	−4.28

There were 18 occupations of various of these sections across the Labrador Current in 1956. Table 1 gives the volume transport, mean temperature, minimum observed temperature and heat transport found during these occupations in comparison with the seasonal normal values where they are available. In the table, as well as in the text, the volume transport is given in millions of cubic meters per second, mean temperature and minimum observed temperature are in degrees Centigrade, and heat transport is given in millions of cubic meter degrees Centigrade per second.

In volume transport, table 1 shows a preponderance of positive anomalies, the exceptions being sections T and U during the first survey and the South Wolf Island section occupied during the post season cruise. The mean temperatures were all higher than normal during the first survey and except for section T were below normal during the second survey. The Labrador Current at the Bonavista triangle was warmer than normal during both occupations and at South Wolf Island it was colder than average. The percentage of the volume transport following the eastern branch of the Labrador Current at the Bonavista triangle during the 3d survey was 84.7 which was close to the seasonal normal of 85.1 percent. At the time of the post season cruise, however, this had increased to 92.0 percent whereas the normal seasonal change is a reduction to 83.6 percent. As the volume transport at the triangle increased from 4.28 to 4.98 between the two occupations, whereas the normal seasonal increase is from 3.72 to 4.00 during this period, the positive anomaly increased from 0.56 to 0.98. This, together with the increase in the positive anomaly in mean temperature shown in table 1, indicates that the anamalous increase in the percentage following the eastern branch was caused by an increase in the warmer offshore part of the Labrador Current, from which an increased activity in the circulation of the Labrador Sea is inferred.

In bulletin 39 of this series it was noted that the minimum observed temperature at the South Wolf Island section was slightly warmer and its corresponding salinity somewhat fresher than these values at the Bonavista triangle. Following is a tabulation of the minimum observed temperatures and their corresponding salinities at the South Wolf Island section and at the Bonavista triangle for each of the 9 years from which nearly synoptic observations are available.

	South Wolf Island			Bonavista triangle		
Year	Depth	Temperature	Salinity	Depth	Temperature	Salinity
1948	81	−1.55	32.72	189	−1.61	33.17
1949	73	−1.70	32.98	99	−1.62	33.29
1950	50	−1.68	32.82	64	−1.76	33.17
1951	69	−1.34	32.66	96	−1.58	33.00
1952	74	−1.68	32.78	95	−1.63	33.13
1953	51	−1.21	32.88	92	−1.67	33.06
1954	102	−1.58	32.85	98	−1.67	33.15
1955	103	−1.66	32.95	100	−1.66	33.08
1956	75	−1.50	33.01	75	−1.62	32.96
Average	75	−1.54	32.85	101	−1.65	33.11

Only in 1949 and 1952 was the minimum observed temperature at the South Wolf Island section colder than that at the Bonavista triangle. Except for 1956 the corresponding salinities at the South Wolf Island section were fresher than at the Bonavista triangle. The direction of the salinity difference is not surprising since the average depth of the minimum temperature was about 26 meters greater at the Bonavista triangle than at the South Wolf Island section. The previously offered explanation of colder water at the Bonavista triangle being brought about by winter time concentration through the removal of water by freezing is not completely satisfactory and while it no doubt plays an important part in producing the temperatures and salinities found at the Bonavista triangle in the summertime, it seems probable that the T-S characteristics of the water found off South Wolf Island in summer are decidedly affected by the discharge of fresh water from Hamilton Inlet. Nutt and Coachman[2] have estimated that the winter's precipitation at Hebron Fjord, Labrador is released into the Fjord between May 15 and July 15.

These same authors found a trend toward lower salinity and a slight warming from measurements made in late July and early August in 1949, 1952, and 1954 over which span the total freshening amounted to 0.34$°/_{oo}$. While the foregoing table shows salinity fluctuations of about the same range a T–S plot of the nine annual points in chronological sequence does not show any such pronounced trend either at South Wolf Island or at the Bonavista triangle. Remembering that these are points of minimum observed temperature and that the temperature minimum over the continental shelf is probably the least disturbed of any part of the Labrador Current during the warmer part of the year by onshore or offshore winds, they may reasonably be taken as representative of the inshore frigid component of the Labrador Current. Because of the various depths of the different observations, however, scaled values from the same stations at constant level were plotted (at 75 meters off South Wolf Island and at 100 meters for the Bonavista triangle) this plot showed similarly negative results as to any consistent trend.

---

[2] The Oceanography of Hebron Fjord, Labrador—Nutt, David C. and Lawrence K. Coachman. J. Fish. Res. Bd. Canada. vol. 13 no. 5; 1956.

Referring again to table 1 it will be noted that the volume transport of the Labrador Current at the South Wolf Island section was 4.18 whereas that at the Bonavista triangle a few days earlier was 4.98. Usually there is some loss of volume transport to the eastward between the South Wolf Island section and the Bonavista triangle. With the volume transport some 0.8 higher at the Bonavista triangle than at South Wolf Island the explanation would seem to be that at least 0.8 were involved in a cyclonic closed eddy northeastward of the Bonavista triangle. This has been indicated in figure 19 which schematically presents the volume transports listed in table 1.

Table 2

Ship	Year	Occupations of sections across—									
		Labrador Current off South Wolf Island					West Greenland Current off Cape Farewell			
		Date	Vol. Trans.	Mean Temp.	Min. Obs. temp.	Heat Trans.	Date	Vol. Trans.	Mean Temp.	Heat Trans.
Godthaab	1928	--------	--------	--------	--------	--------	.92 May	4.0	4.1	16.4
Marion	1928	.73 July	5.1	3.3	−1.45	16.5	.05 Sept.	4.4	5.5	24.1
General Greene	1931	.34 July	1.3	1.7	−1.41	2.2	.05 Aug.	3.7	5.3	19.5
Do	1933	.73 July	7.60	3.41	−1.06	25.90	.27 July	5.76	4.19	24.13
Do	1934	.31 July	5.03	2.68	−1.60	13.50	.40 July	2.91	5.1	14.86
Meteor	1935	--------	--------	--------	--------	--------	.24 March	7.5	4.0	30.0
General Greene	1935	.73 Aug.	4.22	2.76	(−1.50)	11.65	.60 Aug.	8.50	4.99	42.44
Do	1936	.65 June	3.32	1.27	−1.61	4.22	.75 June	6.37	4.05	25.83
Do	1938	.79 July	4.20	2.92	−1.56	12.25	.89 July	5.43	4.69	25.04
Do	1939	.34 July	4.56	2.69	−1.51	12.27	.45 July	6.31	4.19	26.46
Do	1940	.82 June	2.75	1.52	−1.72	4.17	--------	--------	--------	--------
Do	1941	.79 July	2.32	2.60	−1.08	6.03	.89 July	6.46	4.87	31.46
Evergreen	1948	.37 July	3.01	2.21	−1.55	6.65	.50 July	1.52	3.93	5.97
Do	1949	.18 July	5.16	2.3	−1.70	11.87	.27 July	2.52	3.62	9.12
Do	1950	.02 Aug.	5.92	2.63	−1.68	15.57	.11 Aug.	7.76	4.26	33.06
Do	1951	.60 July	5.30	2.63	−1.34	13.93	.69 July	5.28	3.68	19.41
Do	1952	.53 July	6.37	2.63	−1.68	16.76	.63 July	5.93	3.79	22.50
Do	1953	.50 July	6.41	2.64	−1.21	16.94	.63 July	7.35	3.84	28.22
Do	1954	.82 Aug.	7.84	2.39	−1.58	18.72	.92 Aug.	8.95	4.95	44.33
Do	1955	.51 July	5.02	2.62	−1.66	13.15	.60 July	5.66	4.74	26.85
Do	1956	.50 July	4.18	1.75	−1.50	7.33	.62 July	7.32	4.10	30.01
Average	------	.59 July	4.72	2.46	−1.49	11.61				

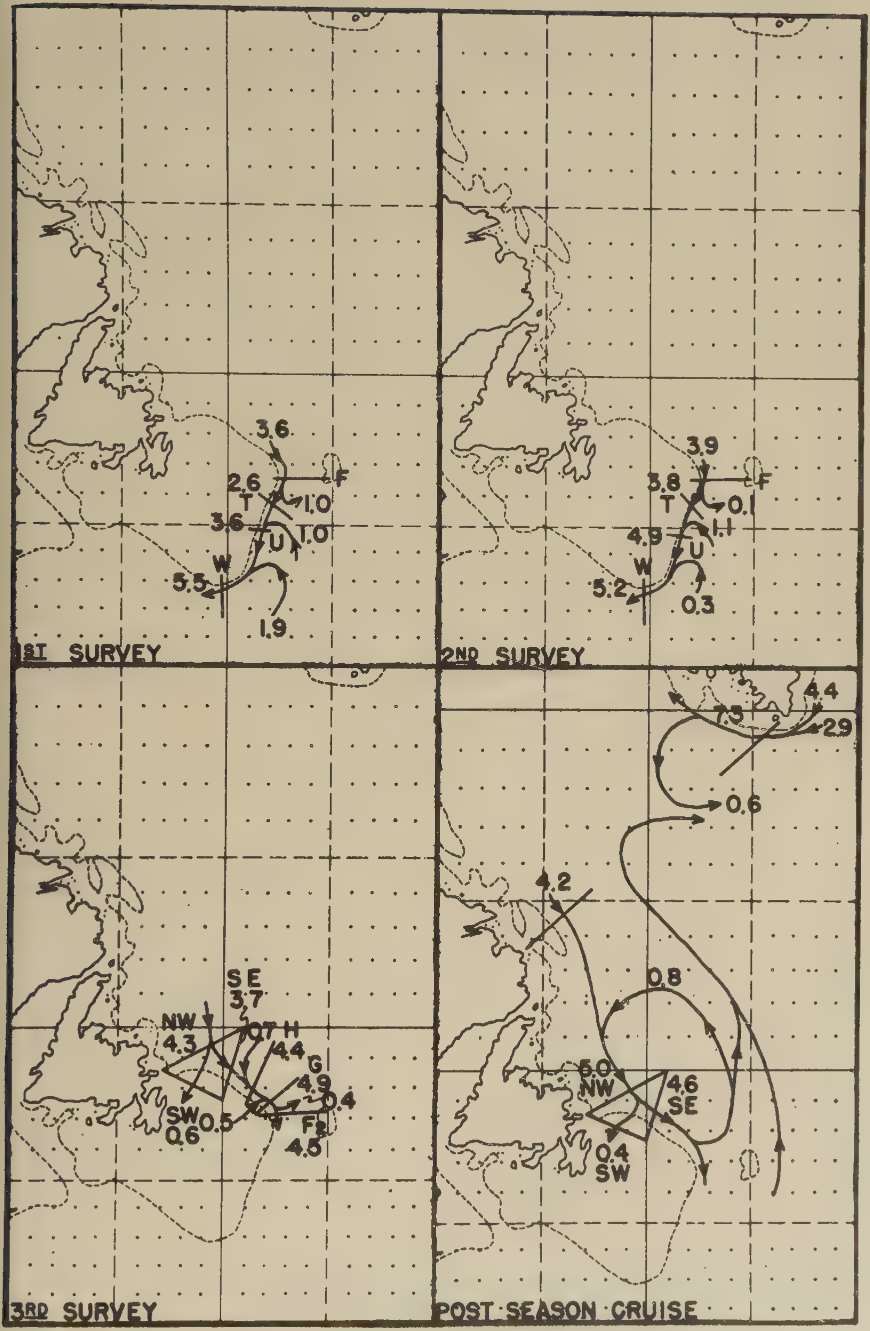
3.6
2.6
T
F
1.0
3.6
U
1.0
W
5.5
1.9
1ST SURVEY
3.9
3.8
T
F
0.1
4.9
H
U
W
5.2
0.3
2ND SURVEY
SE
3.7
NW
4.3
0.7 H
4.4
G
4.9
0.4
SW
0.6
0.5
W
F
4.5
3RD SURVEY
4.4
7.5
29
0.6
4.2
0.8
5.0
NW
4.6
SE
0.4
SW
POST SEASON CRUISE

FIGURE 19.—Schematic representation of circulation deducted from sections occupied during 1956. Numerals indicate volume transport in units of cu.m/sec X 10^{-6}.

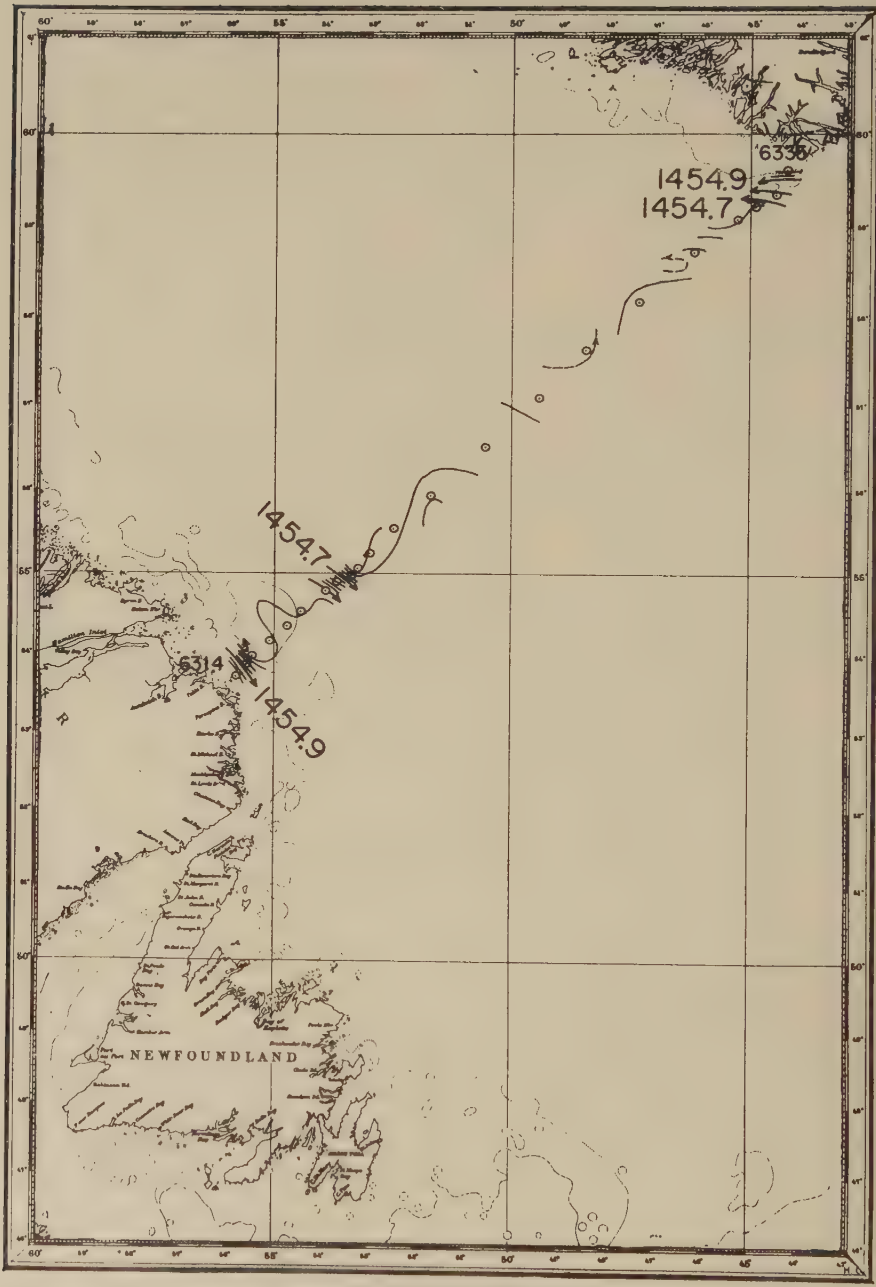
60°
55°
50°
45°
60°
55°
50°
6335
1454.9
1454.7
1454.7
6314
1454.9
NEWFOUNDLAND
Hamilton Inlet

Figure 20.—Dynamic topography of the sea surface relative to the 1500-decibar surface from data collected 15–20 July 1956. Oceanographic station positions are indicated and the station numbers given at turning points.

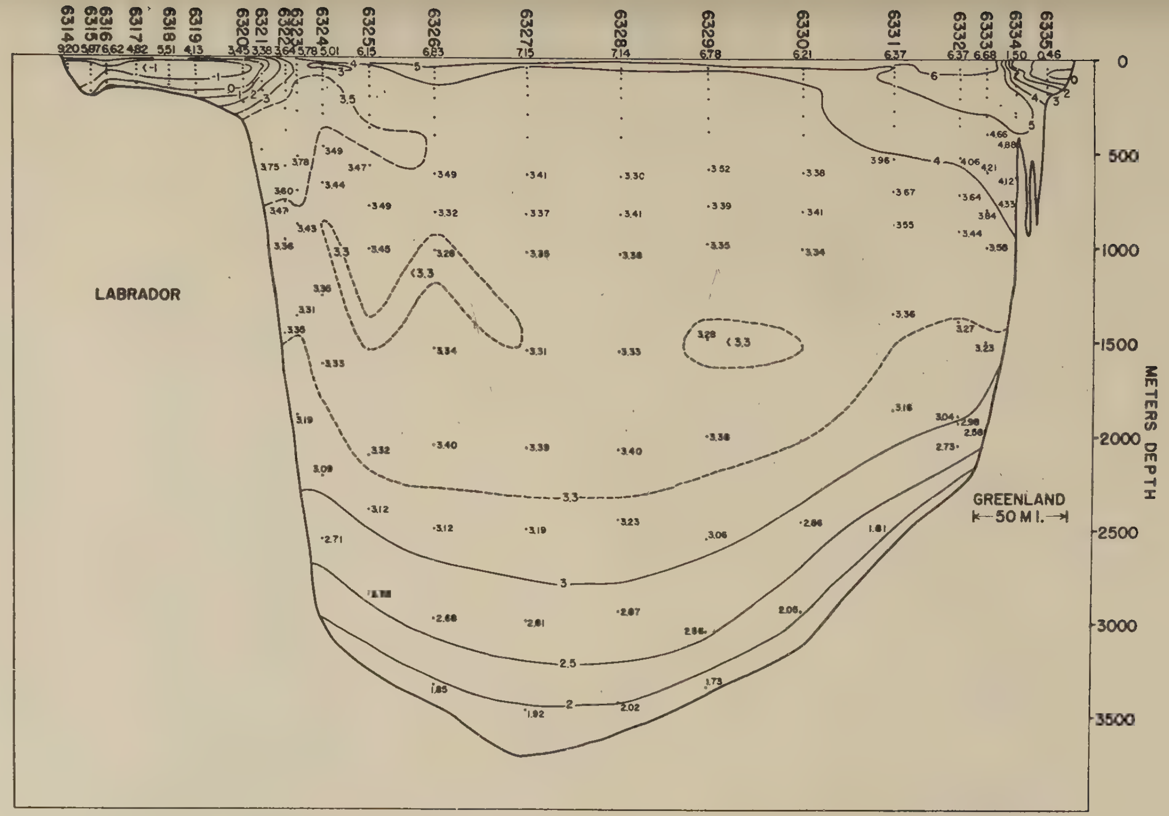

FIGURE 21.—Temperature distribution along section between South Wolf Island, Labrador, and Cape Farewell, Greenland, 15–20 July 1956.

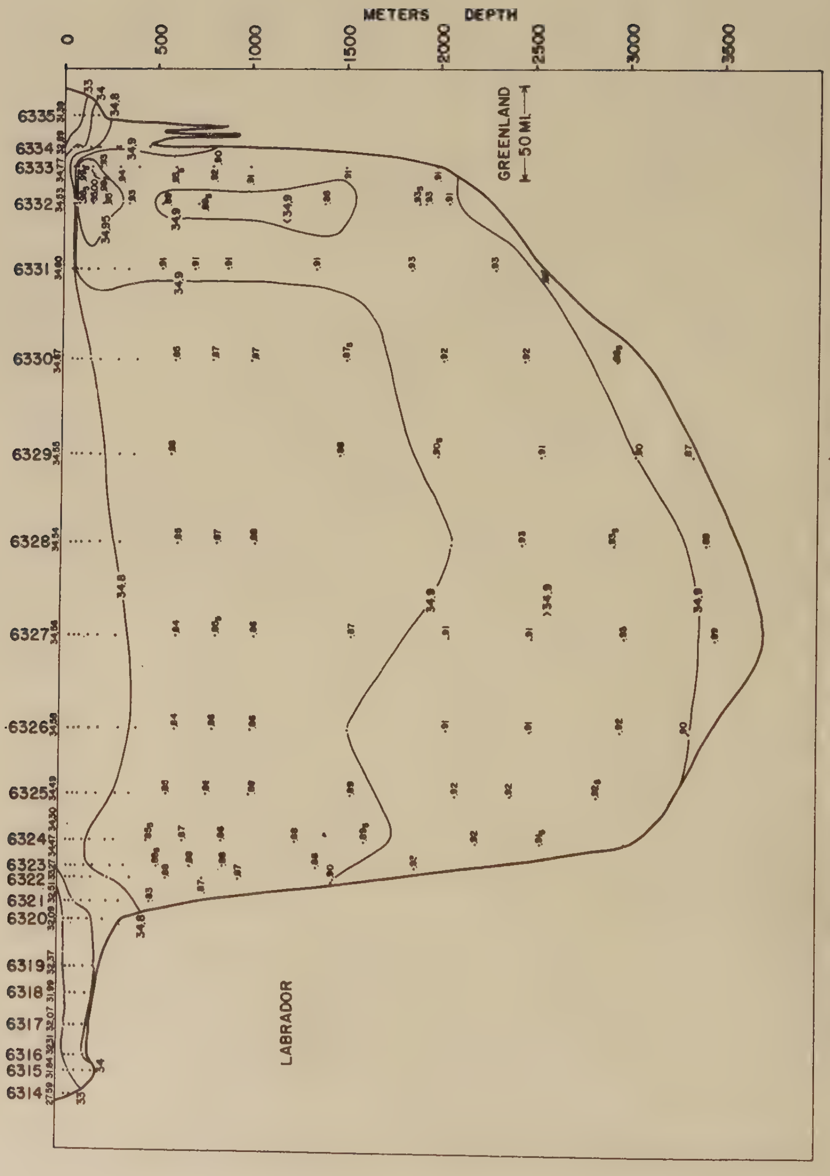

FIGURE 22.—Salinity distribution along section between South Wolf Island, Labrador, and Cape Farewell, Greenland, 15–20 July 1956.

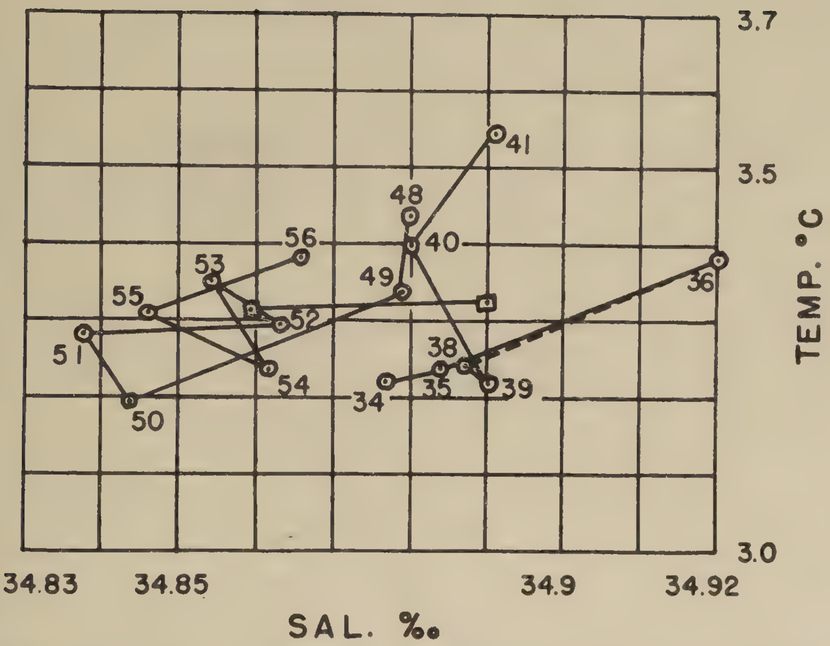

FIGURE 23.—Year to year variations in the temperature and salinity of the intermediate water of the Labrador Sea along the South Wolf Island–Cape Farewell section from summertime observations. For each year the average of all observed temperatures between 450 and 1750 meters from the central part of the section have been plotted against the average of the corresponding salinities and labeled with the last two digits of the year of observation. Solid lines connect the points for successive years except that since the section was not occupied in 1937 a broken line connects the points for 1936 and 1938. Squares indicate the means for the periods 1934–41 and 1948–56.

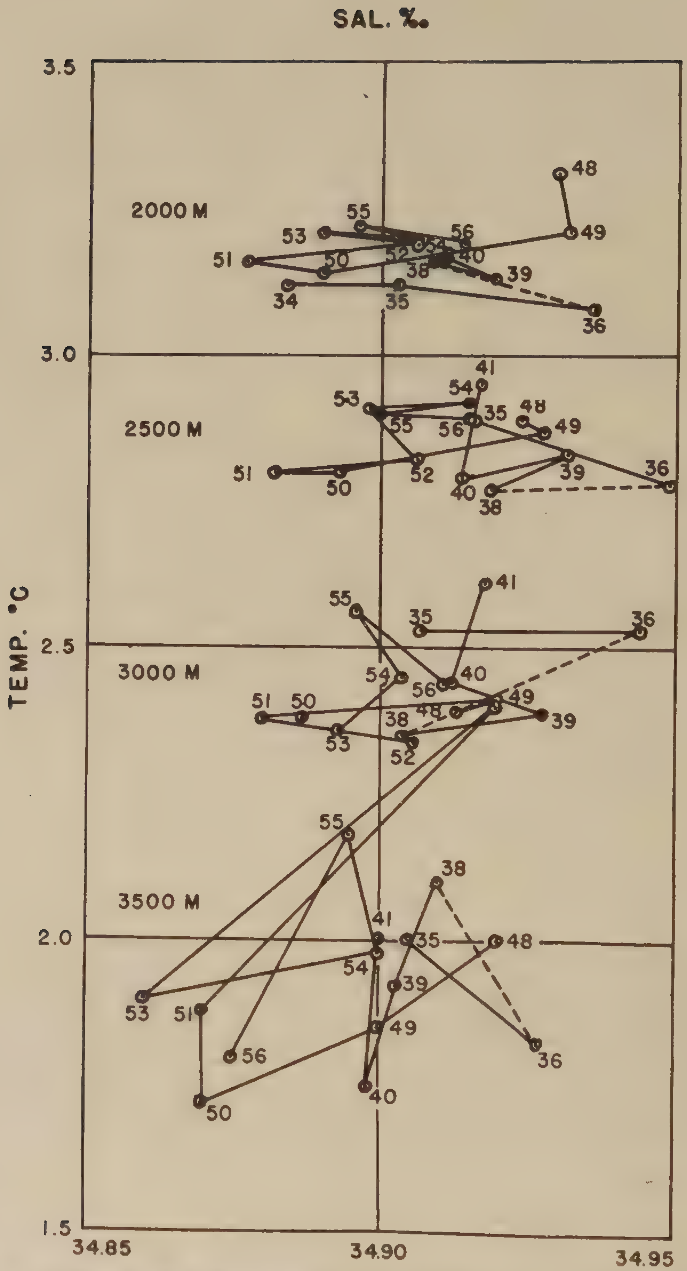

FIGURE 24.—Year to year variations in the temperature and salinity of the deep water of the Labrador Sea along the South Wolf Island–Cape Farewell section from summertime observations. For each year the average of all scaled values of temperature at and below 2000 meters have been plotted against the average of the corresponding scaled values of salinity and labeled with the last two digits of the year of observation.

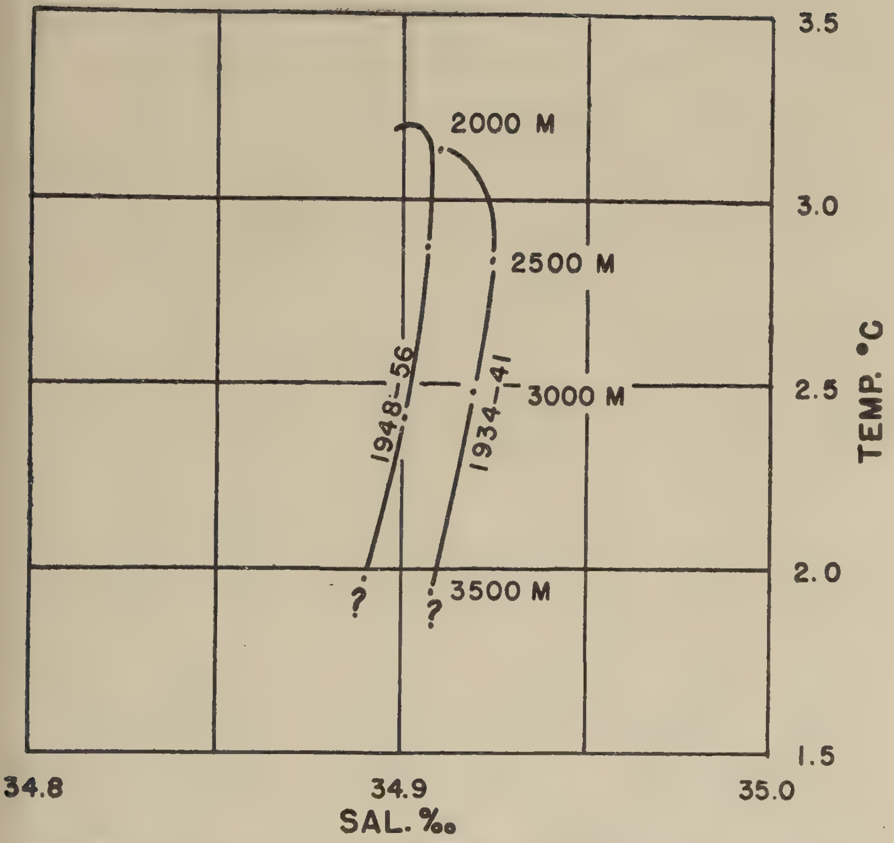

FIGURE 25.—Mean scaled values of temperature of the deep water of the Labrador Sea plotted against mean scaled values of corresponding salinity for the periods 1934–41 and 1948–56.

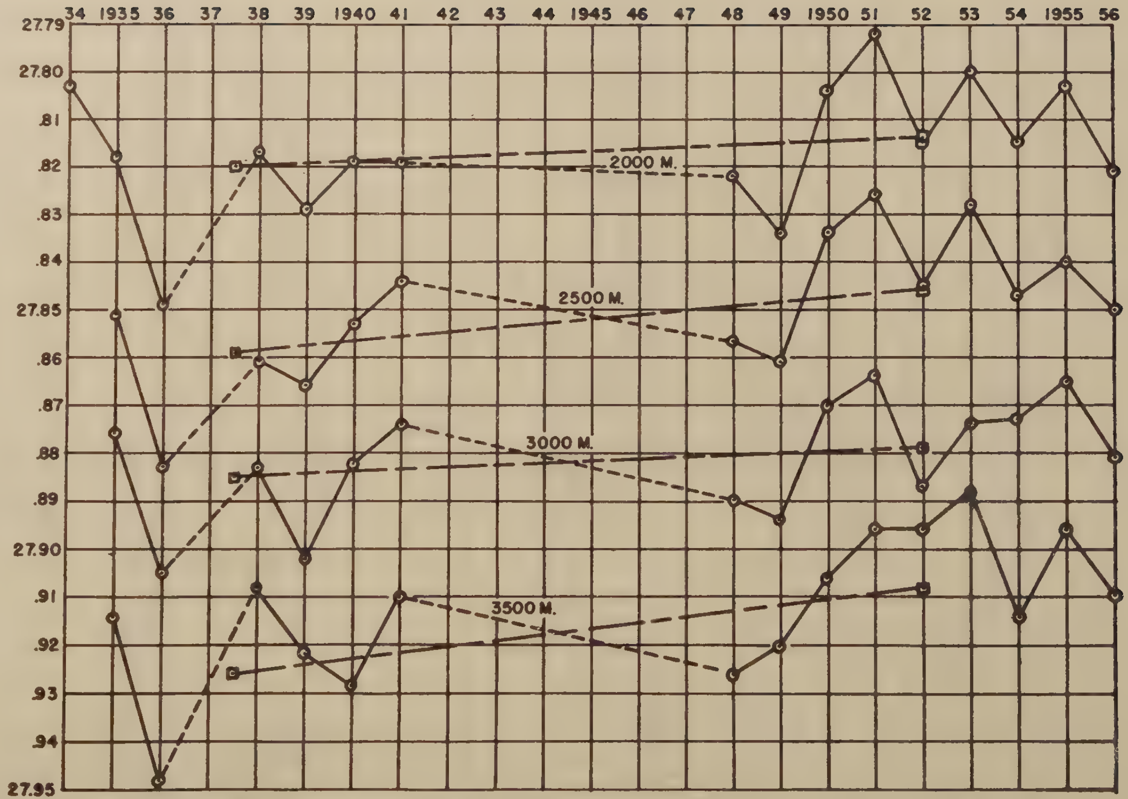

FIGURE 26.—Year to year variations in the density of the deep water of the Labrador Sea as represented by the value of σ_t corresponding to the temperature and salinities plotted in Figure 24.

The volume transport, mean temperature and resulting heat transport for all occupations of the sections across the Labrador Current off South Wolf Island and the West Greenland Current off Cape Farewell that have been considered in our discussions are listed in table 2. For the most part these measurements were made by the International Ice Patrol from the *Marion* in 1928, the *General Greene* 1931 to 1941 and the *Evergreen* 1948 to 1956. Two occupations of the Cape Farewell section, one by the *Godthaab* in 1928 and one by the *Meteor* in 1935, are included. For the section across the Labrador Current off South Wolf Island a tabulation of the minimum observed temperature is included and average values are presented. Averages are not listed for the West Greenland Current since there appears to be seasonal variations in the volume transport of the parent components (Irminger Current and East Greenland Current) having maximum rates of change in the summertime.

Figure 20 shows the dynamic topography in the vicinity of the section from South Wolf Island, Labrador, to Cape Farewell, Greenland found during the 1956 post season cruise. Figures 21 and 22 show the distribution of temperature and salinity along this section for the same occupation. In figure 21 the Labrador Current is to be seen with its characteristic temperature minimum over the shelf and its horizontal temperature gradient above the continental slope. The West Greenland Current also is recognizable from its characteristic cold inshore water and warm offshore band. In the intermediate water of the Labrador Sea the temperature minimum, which is considered to be a relic of the previous winter's cooling, was less pronounced and was warmer than usual. In figure 21 two small areas within which the temperature was less than 3.3 indicate the location of this minimum. In earlier bulletins of this series the different occupations of the section have been described as warm years or cold years according to the temperature found in the minimum and the cross sectional extent of the minimum. By this method the 1956 occupation would be classified as warm along with those of 1940, 41, 48, 49, 51, 52, and 53 while the cold years were 1934, 35, 36, 38, 39, 50, 54 and 55.

An attempt has been made to arrive at a more specific and numerical characterization of the intermediate water by taking the average of all temperatures observed between depths of 450 and 1,750 meters from all stations which lie offshore of the Labrador Current and the warm water of the West Greenland Current for each occupation. For 1956 this would include stations 6325–29. The averages of all the corresponding salinities for each occupation were also computed. These average temperatures have been plotted against their corresponding average salinities in figure 23. Each occupation of the section is thus characterized by a single T–S point. As the intermediate water is assumed to undergo an annual change the time of year should have some effect. In figure 23, however, no discrimination has been made as to date of occupation, although the actual dates of the occupations vary from June to August. There appears to be but little relationship between either temperature or salinity and the date of occupation within this summertime range. The mean date of the post war series of occupations is some 5½ days later than that of the pre war series. The mean T–S points for the periods 1934–41 and 1948–56 have been shown within squares and differ but little in temperature with the salinity lower in the later series.

A similar numerical analysis of the temperature and salinity of the deep water was attempted. Whereas in the intermediate water the remarkable uniformity permitted the grouping of all observations without regard to depth, in the deep water there is a sufficient vertical gradient, especially in temperature, to require a reduction to a common depth. All stations where the observations extended to a depth of 2,000 meters or more were considered, the individual station curves of vertical distribution of temperature and salinity being scaled for values at 2,000, 2,500, 3,000 and 3,500 meters. For each occupation all scaled values for each of these levels were averaged to get the mean temperatures and salinities plotted in figure 24. Near bottom along the section there is a characteristic tendency for the isotherms and isohalines to parallel the bottom. No adjustment has been made for these horizontal gradients. Because of the symmetry of the bottom and the spacing of the stations the shallower levels are less affected but the results in the deeper levels, especially the 3,500-meter level are somewhat erratic from the small number of data and the fortuitous spacing of stations with respect to the 3,500-meter isobath. The average temperatures for the periods 1934–41 and 1948–56, plotted against the corresponding average salinities in figure 25, show about the same salinity at 2,000 meters but for deeper levels show a lower salinity for the later period. In temperature the change is small with an increase at 2,000 meters, little change at 2,500 meters and a decrease at 3,000 meters. The small number of stations extending to 3,500 meters leaves this level doubtful.

The values of σ_t corresponding to average temperature and average salinity for individual occupations of the section are plotted against the year of occupation in figure 26. Again it must be kept in mind that the 3,500-meter level is doubtful because of the small number of data.

As shown in figure 22, the salinity maximum at depths of 150 to 200 meters off Cape Farwell had a value of 35.00°/$_{oo}$ in 1956. This characteristic warm high salinity water in the off-shore part of the West Greenland Current is normally contributed by the Irminger Current. In the 1930's this salinity maximum was remarkably constant at about 35.04°/$_{oo}$ but in 1949 it dropped to 34.97 and has not since attained its pre war value. In 1952, 1954 and 1956 there were indications of a partial return to the earlier situation, with the maximum values of 35.01, 35.00 and 35.00°/$_{oo}$ respectively. The lower salinity values of this maximum have been interpreted as indicating a failure of Irminger Current water to round Cape Farewell. The increase found in 1956 is considered to be a trend toward the restoration of conditions which existed during the 1930's and regarded as the normal situation.

This view is given support by the volume and heat transports of the West Greenland Current at this section. In bulletin 35 of this series normal seasonal variation relationships were published for the parent components (the East Greenland Current and the Irminger Current) based on assumptions that the mean temperature of the East Greenland Current component was constant at 3.2° and the mean temperature of the Irminger Current component was constant at 5.5° and that the seasonal variation in mean temperature of the resultant West Greenland Current was the result of seasonal variations in the volume transports of the parent components. From these normal seasonal variation curves the normal transports for the date of the 1956 occupation would be 2.88 and 1.65 for the Irminger Current and East Greenland Current components. These compare with actual transports of 2.86 and 4.46 respectively, indicating a normal contribution of the Irminger Current component and a contribution by the East Greenland Current about 2-2/3 normal. The total transport, mean temperature and heat transport of the West Greenland Current found in 1956 were 7.32, 4.10 and 30.01 respectively.

The net transport across the entire section from South Wolf Island, Labrador to Cape Farewell, Greenland, was northwestward about 2.54, which is of the same order of magnitude as the positive anomaly of the East Greenland Current contribution.

SUMMARY

1. The three dynamic topographic charts resulting from the season's current surveys have been discussed.
2. A more detailed analysis of the Labrador Current has been made based on the velocity profiles at 18 selected sections occupied during the 1956 season and post season cruises.

3. Mean curves representing the T–S relationship for Labrador Current water, mixed water and Atlantic Current water have been derived for the period 1948–56 and compared with similar curves for the period 1934–41 and the conditions found during 1956 have been compared with the means.

4. Tentative normal seasonal variation relationships have been presented for the volume transport, mean temperature and minimum observed temperature of the Labrador Current at sections F and G, located near the northeastern shoulder of the Grand Banks.

5. The temperature and salinity of the intermediate water of the Labrador Sea have been examined for each of the 16 occupations of the South Wolf Island-Cape Farewell section since 1934. While year to year variations have been large the average temperature for the period 1948–56 was the same as for the period 1934–41 but the salinity has been lower in the later period.

6. Examination of the deep water of the Labrador Sea for the same periods showed a slight warming and freshening at 2,000 meters, an isothermal freshening at 2,500 meters and a freshening accompanied by a cooling at 3,000 meters. The combined effects result in about the same decrease in density at each level.

The data collected in 1956 are tabulated below. The individual station headings give the station number, date, geographical position, depth of water and the dynamic height of the sea surface used in the construction of the dynamic topographic charts shown in fiures 12, 13, 14, 15 and 20. The depths of water are rough approximations, being the uncorrected sonic soundings based on a sounding velocity of 800 fathoms per second and containing an additional mechanical speed error of about 1/60. Where the depths of scaled values are enclosed in parentheses, the data are based on extrapolated vertical distribution curves of temperature or salinity or both. Asterisks apearing before observed temperatures indicate that these temperatures were determined from the depth of reversal and the corrected reading of an unprotected thermometer. The symbol σ_t signifies 1,000 (density–1) at atmospheric pressure and temperature t.

Table of Oceanographic Data

STATIONS OCCUPIED IN 1956

Station 6037; April 1; latitude 42°04′ N., longitude 51°00′ W. depth 3,017 m.; dynamic height 970.930.

Observed values			Scaled values			
Depth, meters	Temperature, ° C.	Salinity, °/₀₀	Depth, meters	Temperature, ° C.	Salinity, °/₀₀	σ_t
0	3.96	33.68	0	3.96	33.68	26.76
22	3.94	33.68	25	3.95	33.73	26.80
43	5.14	34.10	50	5.40	34.19	27.00
65	5.70	34.32	75	4.90	34.26	27.12
86	3.46	34.19	100	4.15	34.39	27.30
129	6.12	34.81	150	6.00	34.85	27.46
172	5.76	34.87	200	5.45	34.85	27.52
258	4.42	34.84	300	4.35	34.86	27.66
236	4.93	34.83	400	4.20	34.92	27.73
356	4.27	34.90	600	4.05	34.94	27.75
477	4.12	34.94	800	3.90	34.94	27.77
624	4.02	34.94	1,000	3.75	34.94	27.78
1,040	3.70	34.94				

Station 6038; April 2; latitude 41°56.5′ N., longitude 51°59′ W. depth 3,667 m.; dynamic height 971.151.

Observed values			Scaled values			
Depth, meters	Temperature, ° C.	Salinity, °/₀₀	Depth, meters	Temperature, ° C.	Salinity, °/₀₀	σ_t
0	13.75	35.75	0	13.75	35.75	26.84
25	13.78	35.76	25	13.78	35.76	26.84
50	13.82	35.76	50	13.82	35.76	26.83
75	13.78	35.78	75	13.78	35.78	26.85
100	13.72	35.77	100	13.72	35.77	26.86
150	13.78	35.77	150	13.78	35.77	26.84
200	13.45	35.75	200	13.45	35.75	26.90
300	10.41	35.46	300	10.00	35.34	27.23
295	9.50	35.23	400	7.30	35.08	27.46
433	6.64	35.02	600	4.50	34.88	27.65
564	4.73	34.89	800	3.90	34.88	27.72
716	4.00	34.88	1,000	3.75	34.90	27.75
1,116	3.64	34.91				

Station 6039; April 2; latitude 42°10.5′ N., longitude 51°15′ W. depth 3,072 m.; dynamic height 970.915.

Observed values			Scaled values			
Depth, meters	Temperature, ° C.	Salinity, °/₀₀	Depth, meters	Temperature, ° C.	Salinity, °/₀₀	σ_t
0	1.56	33.50	0	1.56	33.50	26.83
27	5.81	34.26	25	5.75	34.21	26.98
53	5.60	34.44	50	5.60	34.42	27.17
80	5.69	34.60	75	5.65	34.57	27.28
107	5.66	34.77	100	5.65	34.74	27.41
161	5.75	34.80	150	5.75	34.79	27.44
214	5.32	34.87	200	5.45	34.85	27.52
321	4.27	34.88	300	4.45	34.88	27.66
417	4.42	34.96	400	4.40	34.95	27.72
629	4.22	34.97	600	4.25	34.97	27.76
846	3.88	34.95	800	3.95	34.95	27.77
1,060	3.70	34.94	1,000	3.75	34.94	27.78
1,596	3.37	34.92				

Station 6040; April 2; latitude 42°44′ N., longitude 51°13′ W. depth 1,920 m.; dynamic height 971.012.

Observed values			Scaled values			
Depth, meters	Temperature, ° C.	Salinity, °/₀₀	Depth, meters	Temperature, ° C.	Salinity, °/₀₀	σ_t
0	0.42	33.32	0	0.42	33.32	26.75
25	0.35	33.33	25	0.35	33.33	26.76
49	0.30	33.34	50	0.30	33.34	26.77
74	0.21	33.48	75	0.20	33.48	26.89
98	0.31	33.57	100	0.35	33.58	26.96
148	1.33	34.08	150	1.40	34.09	27.31
197	2.01	34.35	200	2.05	34.35	27.47
295	2.47	34.42	300	2.50	34.43	27.49
372	2.85	34.58	400	3.00	34.63	27.61
551	3.56	34.80	600	3.60	34.81	27.70
726	3.61	34.83	800	3.60	34.84	27.72
917	3.61	34.85	1,000	3.60	34.85	27.73
1,412	3.57	34.86				

Station 6041; April 2; latitude 42°53′ N., longitude 50°51′ W. depth 1,042 m.; dynamic height 971.076.

Observed values			Scaled values			
Depth, meters	Temperature, ° C.	Salinity, °/₀₀	Depth, meters	Temperature, ° C.	Salinity, °/₀₀	σ_t
0	2.16	33.12	0	2.16	33.12	26.48
23	0.75	33.28	25	0.65	33.29	26.71
46	0.06	33.34	50	0.10	33.36	26.80
68	0.31	33.49	75	0.35	33.52	26.92
91	0.34	33.57	100	0.35	33.59	26.97
136	0.45	33.70	150	0.60	33.77	27.10
181	0.90	33.92	200	1.05	33.97	27.24
272	1.43	34.14	300	1.55	34.20	27.38
378	2.00	34.37	400	2.15	34.41	27.51
574	3.16	34.67	600	3.30	34.69	27.63
774	3.69	34.82	800	3.70	34.82	27.70
984	3.59	34.84	1,000	3.60	34.84	27.72

Station 6042; April 2; latitude 42°57′ N., longitude 50°47′ W. depth 258 m.; dynamic height 971.066.

Observed values			Scaled values			
Depth, meters	Temperature, ° C.	Salinity, °/₀₀	Depth, meters	Temperature, ° C.	Salinity, °/₀₀	σ_t
0	2.12	33.17	0	2.12	33.17	26.52
25	1.23	33.20	25	1.23	33.20	26.61
50	0.40	33.38	50	0.40	33.38	26.80
75	0.38	33.49	75	0.38	33.49	26.89
100	0.33	33.55	100	0.33	33.55	26.94
150	0.62	33.79	150	0.62	33.79	27.11
200	1.10	34.00	200	1.10	34.00	27.26
244	1.71	34.24				

Station 6043; April 2; latitude 43°01′ N., longitude 50°42′ W. depth 114 m.; dynamic height 971.065.

Observed values			Scaled values			
Depth, meters	Temperature, ° C.	Salinity, °/₀₀	Depth, meters	Temperature, ° C.	Salinity, °/₀₀	σ_t
0	2.45	32.99	0	2.45	32.99	26.35
26	1.69	33.06	25	1.75	33.06	26.46
51	0.62	33.30	50	0.65	33.29	26.71
77	0.38	33.46	75	0.40	33.45	26.86
103	0.55	33.65	100	0.50	33.62	26.99

Station 6044; April 2; latitude 43°05′ N., longitude 50°35′ W.; depth 91 m.; dynamic height 971.083.

Observed values			Scaled values			
Depth, meters	Temperature, ° C.	Salinity, °/₀₀	Depth, meters	Temperature, ° C.	Salinity, °/₀₀	σ_t
0	2.76	32.74	0	2.76	32.74	26.13
26	2.33	32.78	25	2.35	32.77	26.18
51	1.42	33.11	50	1.45	33.09	26.50
77	0.98	33.30	75	1.00	33.28	26.69

Station 6045; April 2; latitude 43°18.5′ N., longitude 50°17′ W.; depth 70 m.; dynamic height 971.091.

Observed values			Scaled values			
Depth, meters	Temperature, ° C.	Salinity, °/₀₀	Depth, meters	Temperature, ° C.	Salinity, °/₀₀	σ_t
0	2.73	32.66	0	2.73	32.66	26.06
28	2.47	32.68	25	2.50	32.67	26.09
55	1.56	33.00	50	1.70	32.94	26.37

Station 6046; April 2; latitude 43°04.5′ N., longitude 50°19′ W.; depth 78 m.; dynamic height 971.068.

Observed values			Scaled values			
Depth, meters	Temperature, ° C.	Salinity, °/₀₀	Depth, meters	Temperature, ° C.	Salinity, °/₀₀	σ_t
0	1.77	33.12	0	1.77	33.12	26.51
23	1.41	33.16	25	1.40	33.16	26.56
47	1.18	33.19	50	1.15	33.19	26.61
70	0.68	33.28	75	0.60	33.29	26.71

STATIONS OCCUPIED IN 1956—Continued

Station 6047; April 3; latitude 42°51′ N., longitude 50°22′ W.; depth 403 m.; dynamic height 971.010.

Observed values			Scaled values			
Depth, meters	Temperature, ° C.	Salinity, °/oo	Depth, meters	Temperature, ° C.	Salinity, °/oo	σt
0	0.94	33.24	0	0.94	33.24	26.66
25	0.19	33.41	25	0.19	33.41	26.84
49	0.14	33.54	50	0.15	33.54	26.94
74	0.33	33.65	75	0.35	33.65	27.02
99	0.58	33.78	100	0.60	33.78	27.10
148	0.95	34.02	150	1.00	34.04	27.29
197	1.87	34.29	200	1.90	34.30	27.44
296	2.71	34.55	300	2.70	34.56	27.58

Station 6048; April 3; latitude 42°40′ N., longitude 50°23′ W.; depth 1,756 m.; dynamic height 970.931.

Observed values			Scaled values			
Depth, meters	Temperature, ° C.	Salinity, °/oo	Depth, meters	Temperature, ° C.	Salinity, °/oo	σt
0	0.95	33.59	0	0.95	33.59	25.93
25	1.00	33.60	25	1.00	33.60	26.94
50	0.98	33.63	50	0.98	33.63	26.96
75	1.35	33.85	75	1.35	33.85	27.12
100	1.37	34.02	100	1.37	34.02	27.26
150	1.92	34.36	150	1.92	34.36	27.49
200	2.29	34.46	200	2.29	34.46	27.54
300	3.83	34.79	300	3.83	34.79	27.65
393	3.75	34.83	400	3.75	34.83	27.69
593	3.54	34.85	600	3.55	34.85	27.73
796	3.48	34.875	800	3.50	34.87	27.76
998	3.46	34.87	1,000	3.45	34.87	27.76
1,506	3.45	34.89				

Station 6049; April 3; latitude 42°17.5′ N., longitude 50°26′ W.; depth 2,926 m.; dynamic height 970.908.

Observed values			Scaled values			
Depth, meters	Temperature, ° C.	Salinity, °/oo	Depth, meters	Temperature, ° C.	Salinity, °/oo	σt
0	3.24	33.60	0	3.24	33.60	26.77
25	3.04	33.62	25	3.04	33.62	26.81
50	2.65	33.78	50	2.65	33.78	26.96
75	1.71	33.96	75	1.71	33.96	27.18
100	2.94	34.31	100	2.94	34.31	27.36
150	3.60	34.60	150	3.60	34.60	27.53
199	4.03	34.76	200	4.05	34.76	27.61
299	4.60	34.94	300	4.60	34.94	27.69
406	4.56	34.98	400	4.60	34.98	27.72
604	4.25	34.99	600	4.25	34.99	27.77
797	3.64	34.92	800	3.65	34.92	27.78
998	3.54	34.92	1,000	3.55	34.92	27.79
1,505	3.48	34.92				

Station 6050; April 3; latitude 41°50.5′ N., longitude 50°22′ W.; depth 3,749 m.; dynamic height 970.938.

Observed values			Scaled values			
Depth, meters	Temperature, ° C.	Salinity, °/oo	Depth, meters	Temperature, ° C.	Salinity, °/oo	σt
0	2.96	33.56	0	2.96	33.56	26.76
25	2.07	33.61	25	2.07	33.61	26.89
50	1.32	33.83	50	1.32	33.83	27.10
75	1.34	34.00	75	1.34	34.00	27.24
99	2.36	34.21	100	2.40	34.21	27.33
149	4.76	34.66	150	4.75	34.66	27.46
199	4.28	34.69	200	4.30	34.69	27.53
298	4.86	34.90	300	4.85	34.90	27.63
400	3.60	34.78	400	3.65	34.78	27.66
600	4.01	34.90	600	4.00	34.90	27.73
800	4.15	34.97	800	4.20	34.97	27.77
1,003	3.65	34.91	1,000	3.65	34.91	27.77
1,513	3.43	34.91				

Station 6051; April 3; latitude 41°25′ N., longitude 50°19 W.; depth 3,749 m.; dynamic height 971.160.

Observed values			Scaled values			
Depth, meters	Temperature, C.	Salinity, °/oo	Depth, meters	Temperature, ° C.	Salinity, °/oo	σt
0	13.12	35.635	0	13.12	35.635	26.88
25	13.00	35.62	25	13.00	35.62	26.89
50	12.97	35.62	50	12.97	35.62	26.89
75	------	35.62	75	12.90	35.62	26.91
100	12.53	35.52	100	12.53	35.52	26.91
150	8.80	34.82	150	8.80	34.82	27.03
200	9.60	34.97	200	9.60	34.97	27.02
300	10.39	35.31	300	10.39	35.31	27.15
378	8.56	35.12	400	8.10	35.08	27.34
569	5.22	34.90	600	5.00	34.90	27.62
760	4.35	34.92	800	4.20	34.91	27.72
955	3.62	34.87	1,000	3.65	34.88	27.74
1,453	3.81	34.95				

Station 6052; April 3; latitude 41°00′ N., longitude 50°15′ W.; depth 3,566 m.; dynamic height 971.255.

Observed values			Scaled values			
Depth, meters	Temperature, C.	Salinity, °/oo	Depth, meters	Temperature, ° C.	Salinity, °/oo	σt
0	14.88	35.88	0	14.88	35.88	26.69
27	14.87	35.88	25	14.85	35.88	26.70
53	14.61	35.83	50	14.65	35.84	26.71
80	13.83	35.73	75	13.95	35.74	26.78
106	13.63	35.73	100	13.65	35.73	26.84
160	13.64	35.74	150	13.65	35.74	26.85
213	12.24	35.43	200	12.55	35.51	26.90
319	11.69	35.45	300	11.80	35.45	27.00
356	7.91	34.73	400	6.05	34.56	27.22
532	3.75	34.40	600	4.25	34.61	27.47
709	*5.05	34.985	800	4.75	34.99	27.71
885	4.51	34.99	1,000	4.30	34.98	27.75
1,323	3.87	34.955				

Station 6053; April 4; latitude 41°58.5′ N., longitude 49°18′ W.; depth 2,926 m.; dynamic height 971.051.

Observed values			Scaled values			
Depth, meters	Temperature, C.	Salinity, °/oo	Depth, meters	Temperature, ° C.	Salinity, °/oo	σt
0	11.59	35.12	0	11.59	35.12	26.78
26	10.79	34.98	25	10.80	34.99	26.82
51	7.14	34.43	50	7.15	34.44	26.98
76	6.60	34.42	75	6.60	34.42	27.04
101	6.28	34.36	100	6.30	34.36	27.03
152	4.60	34.20	150	4.65	34.20	27.10
203	4.96	34.42	200	4.95	34.41	27.24
304	5.00	34.64	300	5.00	34.63	27.40
373	5.42	34.89	400	5.25	34.89	27.58
559	4.32	34.875	600	4.20	34.87	27.69
744	3.90	34.86	800	3.85	34.86	27.71
942	3.69	34.88	1,000	3.65	34.88	27.74
1,454	3.45	34.885				

Station 6054; April 4; latitude 41°33′ N., longitude 48°47′ W.; depth 3,274 m.; dynamic height 971.179.

Observed values			Scaled values			
Depth, meters	Temperature, C.	Salinity, °/oo	Depth, meters	Temperature, ° C.	Salinity, °/oo	σt
0	12.16	35.295	0	12.16	35.295	26.81
25	12.13	35.295	25	12.13	35.295	26.81
50	12.08	35.29	50	12.08	35.29	26.82
75	12.12	35.30	75	12.12	35.30	26.82
101	12.02	35.30	100	12.00	35.30	26.84
150	12.14	35.38	150	12.15	35.38	26.87
201	12.18	35.40	200	12.15	35.40	26.89
302	10.10	35.26	300	10.20	35.26	27.14
429	6.80	34.89	400	7.50	34.97	27.35
641	4.38	34.87	600	4.60	34.87	27.64
851	4.06	34.91	800	4.10	34.90	27.72
1,067	3.73	34.91	1,000	3.80	34.91	27.76
1,610	3.56	34.93				

Table of Oceanographic Data—Continued

STATIONS OCCUPIED IN 1956—Continued

Observed values			Scaled values			
Depth, meters	Temperature, ° C.	Salinity, °/°°	Depth, meters	Temperature, ° C.	Salinity, °/°°	σ_t
Station 6055; April 4; latitude 40°58.5′ N., longitude 48° 31′ W.; depth 3,255 m.; dynamic height 971.145.						
0	11.80	35.14	0	11.80	35.14	26.76
25	11.80	35.20	25	11.80	35.20	26.80
49	11.91	35.29	50	11.90	35.24	26.81
74	12.29	35.40	75	12.25	35.40	26.87
98	11.87	35.32	100	11.80	35.31	26.89
147	11.00	35.14	150	10.95	35.13	26.90
196	10.21	35.12	200	10.15	35.12	27.04
294	9.17	35.14	300	9.10	35.13	27.22
381	7.39	34.965	400	7.15	34.97	27.40
571	5.26	34.97	600	5.10	34.97	27.66
761	4.46	34.97	800	4.45	34.97	27.74
961	4.26	34.98	1,000	4.25	34.98	27.76
1,461	3.65	34.94				
Station 6056; April 4; latitude 41°35.5′ N., longitude 40°17′ W.; depth 4,298 m.; dynamic height 971.276.						
0	14.59	35.85	0	14.59	35.85	26.74
26	14.38	35.80	25	15.35	35.80	26.75
51	14.20	35.76	50	14.20	35.76	26.75
76	14.17	35.75	75	14.15	35.75	26.75
101	14.12	35.74	100	14.10	35.74	26.75
153	13.85	35.72	150	13.85	35.72	26.79
204	12.83	35.50	200	12.90	35.52	26.84
305	11.91	35.50	300	11.95	35.50	27.01
429	9.54	35.24	400	10.20	35.31	27.18
637	5.91	34.975	600	6.35	35.00	27.53
842	4.78	34.98	800	5.00	34.98	27.68
1,055	3.96	34.92	1,000	4.15	34.93	27.73
1,593	3.57	34.91				
Station 6057; April 5; latitude 41°58.5′ N., longitude 47°54′ W.; depth 3,768 m.; dynamic height 970.986.						
0	4.25	33.65	0	4.25	33.65	26.71
26	4.12	33.63	25	4.15	33.63	26.70
52	3.37	33.62	50	3.40	33.62	26.77
78	3.51	33.78	75	3.50	33.76	26.87
104	3.14	33.90	100	3.15	33.88	26.99
155	5.04	34.50	150	5.00	34.46	27.27
206	4.35	34.59	200	4.40	34.58	27.43
310	4.46	34.81	300	4.45	34.79	27.59
397	4.48	34.905	400	4.50	34.91	27.68
606	3.91	34.92	600	3.95	34.92	27.75
821	3.65	34.91	800	3.65	34.90	27.76
1,030	3.55	34.89	1,000	3.55	34.89	27.76
1,556	3.44	34.92				
Station 6058; April 5; latitude 42°21′ N., longitude 48°30′ W.; depth 3,383 m.; dynamic height 970.949.						
0	3.13	33.48	0	3.13	33.48	26.68
24	2.66	33.50	25	2.65	33.50	26.74
49	2.81	33.74	50	2.80	33.74	26.92
73	2.19	33.80	75	2.20	33.81	27.02
97	3.53	34.18	100	3.50	34.19	27.21
146	2.29	34.24	150	2.40	34.25	27.36
195	4.90	34.71	200	4.90	34.72	27.49
292	4.08	34.80	300	4.10	34.81	27.65
387	4.33	34.91	400	4.35	34.92	27.71
583	4.21	34.95	600	4.20	34.95	27.75
782	3.84	34.93	800	3.80	34.93	27.77
986	3.57	34.91	1,000	3.55	34.91	27.78
1,510	3.37	34.92				

Observed values			Scaled values			
Depth, meters	Temperature, ° C.	Salinity, °/°°	Depth, meters	Temperature, ° C.	Salinity, °/°°	σ_t
Station 6059; April 5; latitude 42°41′ N., longitude 49°10′ W.; depth 2,488 m.; dynamic height 970.890.						
0	3.15	33.64	0	3.15	33.64	26.81
24	2.68	33.81	25	2.65	33.81	26.99
49	2.05	33.92	50	2.05	33.93	27.13
73	2.44	34.19	75	2.45	34.21	27.32
98	2.82	34.37	100	2.85	34.38	27.42
147	3.43	34.62	150	3.45	34.62	27.56
195	3.99	34.77	200	4.05	34.78	27.62
293	4.22	34.88	300	4.20	34.88	27.69
393	4.05	34.91	400	4.05	34.91	27.73
588	3.75	34.91	600	3.75	34.91	27.76
782	3.50	34.90	800	3.50	34.90	27.78
981	3.42	34.88	1,000	3.40	34.885	27.78
1,483	3.34	34.90				
Station 6060; April 5; latitude 43°21′ N., longitude 48°53′ W.; depth 2,012 m.; dynamic height 970.886.						
0	3.80	33.80	0	3.80	33.80	26.87
25	1.97	33.99	25	1.97	33.99	27.19
50	2.25	34.14	50	2.25	34.14	27.28
75	2.53	34.33	75	2.53	34.33	27.41
99	2.70	34.40	100	2.70	34.40	27.45
149	2.98	34.52	150	3.00	34.52	27.53
199	3.47	34.64	200	3.50	34.64	27.57
298	3.78	34.84	300	3.80	34.84	27.70
401	3.63	34.86	400	3.65	34.86	27.73
601	3.48	34.865	600	3.50	34.86	27.75
801	3.42	34.87	800	3.45	34.87	27.76
1,003	3.39	34.88	1,000	3.40	34.88	27.77
1,510	3.38	34.89				
Station 6061; April 5; latitude 43°06′ N., longitude 48°09′ W.; depth 3,200 m.; dynamic height 970.927.						
0	4.40	33.75	0	4.40	33.75	26.77
25	4.31	33.76	25	4.31	33.76	26.79
50	4.14	33.82	50	4.14	33.82	26.85
75	3.36	33.92	75	3.36	33.92	27.01
100	3.58	34.26	100	3.58	34.26	27.26
150	4.94	34.63	150	4.94	34.63	27.40
200	5.11	34.81	200	5.11	34.81	27.54
300	4.79	34.93	300	4.79	34.93	27.66
385	4.26	34.99	400	4.25	34.99	27.77
518	3.99	34.95	600	4.00	34.95	27.77
781	3.85	34.95	800	3.85	34.95	27.78
980	3.68	34.93	1,000	3.65	34.93	27.78
1,484	3.39	34.925				
Station 6062; April 5; latitude 42°51′ N., longitude 47°32′ W.; depth 3,841 m.; dynamic height 970.953.						
0	4.44	33.68	0	4.44	33.68	26.71
23	4.26	33.68	25	4.25	33.68	26.73
47	4.24	33.72	50	4.25	33.73	26.77
70	4.28	33.79	75	4.20	33.82	26.85
93	3.34	33.93	100	3.35	34.00	27.08
140	3.50	34.41	150	3.55	34.46	27.42
186	3.93	34.64	200	4.10	34.69	27.55
279	4.41	34.86	300	4.40	34.88	27.66
387	4.34	34.92	400	4.30	34.92	27.71
579	4.01	34.92	600	4.00	34.92	27.75
770	3.77	34.915	800	3.80	34.92	27.77
967	3.79	34.94	1,000	3.80	34.94	27.78
1,468	3.51	34.93				

Table of Oceanographic Data—Continued

STATIONS OCCUPIED IN 1956—Continued

Station 6063; April 6; latitude 42°37′ N., longitude 46°55′ W.; depth 4,061 m.; dynamic height 971.199.

Observed values			Scaled values			
Depth, meters	Temperature, °C.	Salinity, °/₀₀	Depth, meters	Temperature, °C.	Salinity, °/₀₀	σt
0	14.30	35.77	0	14.30	35.77	26.74
25	14.35	35.78	25	14.35	35.78	26.74
52	14.37	35.79	50	14.40	35.79	26.73
77	14.15	35.74	75	14.15	35.75	26.75
103	13.33	35.595	100	13.40	35.61	26.80
154	12.72	35.50	150	12.75	35.51	26.86
206	11.67	35.33	200	11.80	35.35	26.92
309	9.61	35.11	300	9.80	35.14	27.11
393	6.91	34.82	400	6.80	34.82	27.33
586	5.10	34.90	600	5.05	34.90	27.61
778	4.27	34.93	800	4.25	34.93	27.72
974	4.02	34.935	1,000	4.00	34.93	27.75
1,468	3.62	34.925				

Station 6064; April 6; latitude 42°21′ N., longitude 46°13′ W.; depth 4,645 m.; dynamic height 971.485.

Observed values			Scaled values			
Depth, meters	Temperature, °C.	Salinity, °/₀₀	Depth, meters	Temperature, °C.	Salinity, °/₀₀	σt
0	15.46	36.05	0	15.46	36.05	26.70
23	15.45	36.055	25	15.45	36.06	26.70
47	15.43	36.06	50	15.40	36.06	26.71
70	15.34	36.08	75	15.30	36.08	26.75
93	15.30	36.08	100	15.25	36.08	26.76
140	15.21	36.08	150	15.20	36.08	26.77
186	15.22	36.09	200	15.20	36.09	26.79
279	15.13	36.105	300	15.15	36.11	26.81
351	15.11	36.11	400	14.55	35.99	26.85
544	11.76	35.50	600	10.55	35.32	27.13
749	7.41	35.045	800	6.85	35.05	27.50
952	5.75	35.10	1,000	5.50	35.09	27.70
1,485	3.82	34.935				

Station 6065; April 6; latitude 42°41.5′ N., longitude 45°52′ W.; depth 4,763 m.; dynamic height 971.500.

Observed values			Scaled values			
Depth, meters	Temperature, °C.	Salinity, °/₀₀	Depth, meters	Temperature, °C.	Salinity, °/₀₀	σt
0	14.95	36.11	0	14.95	36.11	26.86
24	15.08	36.10	25	15.05	36.10	26.82
48	15.07	36.11	50	15.05	36.11	26.83
72	15.10	36.105	75	15.10	36.11	26.82
96	15.11	36.105	100	15.10	36.11	26.82
145	15.10	36.11	150	15.10	36.11	26.82
193	15.10	36.12	200	15.10	36.12	26.83
289	15.09	36.12	300	15.10	36.12	26.83
370	15.01	36.11	400	14.80	36.07	26.87
565	12.24	35.60	600	11.55	35.50	27.08
768	8.27	35.15	800	7.80	35.12	27.42
978	5.83	35.065	1,000	5.70	35.06	27.66
1,533	4.18	35.02				

Station 6066; April 6; latitude 43°06′ N., longitude 45°26′ W.; depth 4,755 m.; dynamic height 971.509.

Observed values			Scaled values			
Depth, meters	Temperature, °C.	Salinity, °/₀₀	Depth, meters	Temperature, °C.	Salinity, °/₀₀	σt
0	15.07	36.08	0	15.07	36.08	26.80
26	15.08	36.08	25	15.05	36.08	26.80
52	15.08	36.09	50	15.05	36.09	26.82
78	15.10	36.10	75	15.05	36.09	26.82
103	15.07	36.09	100	15.05	36.09	26.82
156	15.09	36.09	150	15.10	36.09	26.81
208	15.11	36.09	200	15.10	36.09	26.81
311	15.12	36.10	300	15.10	36.10	26.82
318	15.13	36.10	400	14.45	35.94	26.84
496	13.11	35.69	600	11.15	35.42	27.10
689	9.48	35.24	800	7.60	35.08	27.41
881	6.51	35.02	1,000	5.50	34.97	27.61
1,393	3.84	34.91				

Station 6067; April 6; latitude 43°19′N., longitude 46°03′ W.; depth 4,755 m.; dynamic height 971.323.

Observed values			Scaled values			
Depth, meters	Temperature, °C.	Salinity, °/₀₀	Depth, meters	Temperature, °C.	Salinity, °/₀₀	σt
0	14.73	35.89	0	14.73	35.89	26.74
25	14.74	35.89	25	14.74	35.89	26.73
50	14.74	35.90	50	14.74	35.90	26.74
75	14.68	35.87	75	14.68	34.87	26.73
100	14.50	35.80	100	14.50	35.84	26.74
150	13.99	35.75	150	13.99	35.75	26.78
200	13.55	35.66	200	13.55	35.66	26.81
300	12.83	35.64	300	12.83	35.64	26.95
329	12.62	35.60	400	11.00	35.39	27.10
506	8.67	35.11	600	7.40	35.07	27.44
693	6.43	35.055	800	5.55	35.04	27.66
883	5.02	35.02	1,000	4.55	35.00	27.75
1,389	3.82	34.94				

Station 6068; April 7; latitude 43°27.5′ N., longitude 46°33′ W.; depth 4,481 m.; dynamic height 971.178.

Observed values			Scaled values			
Depth, meters	Temperature, °C.	Salinity, °/₀₀	Depth, meters	Temperature, °C.	Salinity, °/₀₀	σt
0	13.61	35.60	0	13.61	35.60	26.75
27	13.64	35.61	25	13.60	35.61	26.76
54	13.70	35.62	50	13.70	35.62	26.75
82	13.56	35.69	75	13.60	35.68	26.81
108	13.29	35.67	100	13.40	35.68	26.85
163	------	34.59	150	9.15	34.85	27.00
217	9.04	34.78	200	8.85	34.79	27.00
325	8.19	34.91	300	8.40	34.88	27.13
439	7.15	35.02	400	7.50	34.99	27.36
658	4.49	34.89	600	5.15	34.91	27.61
879	4.33	34.96	800	4.40	34.94	27.71
1,102	3.84	34.92	1,000	4.15	34.94	27.74
1;666	3.52	34.92				

Station 6069; April 7; latitude 43°37′ N., longitude 47°06 W.; depth 4,298 m.; dynamic height 971.024.

Observed values			Scaled values			
Depth, meters	Temperature, °C.	Salinity, °/₀₀	Depth, meters	Temperature, °C.	Salinity, °/₀₀	σt
0	4.60	33.86	0	4.60	33.86	26.84
25	4.77	33.89	25	4.77	33.89	26.84
50	6.19	34.23	50	6.19	34.23	26.94
75	8.22	34.69	75	8.22	34.69	27.02
100	8.53	34.78	100	8.53	34.78	27.04
149	8.54	34.86	150	8.55	34.86	27.10
199	6.06	34.635	200	6.05	34.64	27.28
299	4.68	34.64	300	4.70	34.64	27.44
399	4.58	34.84	400	4.55	34.84	27.62
601	4.03	34.915	600	4.05	34.91	27.73
805	3.79	34.905	800	3.80	34.90	27.75
1,012	3.69	34.91	1,000	3.70	34.91	27.77
1,540	3.42	34.90				

Station 6070; April 7; latitude 43°53′ N., longitude 48°00′ W.; depth 3,741 m.; dynamic height 971.052.

Observed values			Scaled values			
Depth, meters	Temperature, °C.	Salinity, °/₀₀	Depth, meters	Temperature, °C.	Salinity, °/₀₀	σt
0	9.44	35.00	0	9.44	35.00	27.07
26	9.44	35.00	25	9.45	35.00	27.06
52	9.42	35.00	50	9.40	35.00	27.07
78	9.37	34.99	75	9.35	34.99	27.07
103	9.39	34.99	100	9.35	34.99	27.07
156	9.44	35.01	150	9.40	35.01	27.08
208	9.59	35.06	200	9.55	35.05	27.08
311	7.95	35.04	300	8.20	35.04	27.29
366	5.67	34.88	400	5.35	34.89	27.56
553	4.62	34.96	600	4.50	34.96	27.72
745	4.17	34.945	800	4.10	34.95	27.76
943	3.92	34.95	1,000	3.85	34.95	27.78
1,459	3.49	34.91				

Station 6071; April 7; latitude 44°04′ N., longitude 48°37′ W.; depth 3,155 m.; dynamic height 970.919.

Observed values			Scaled values			
Depth, meters	Temperature, °C.	Salinity, ‰	Depth, meters	Temperature, °C.	Salinity, ‰	σt
0	3.52	33.88	0	3.52	33.88	26.95
26	3.51	33.88	25	3.50	33.88	26.96
52	3.23	33.92	50	3.25	33.91	27.01
78	2.93	34.08	75	2.95	34.05	27.15
103	3.10	34.20	100	3.10	34.18	27.24
156	2.84	34.48	150	2.85	34.47	27.50
208	3.83	34.625	200	3.75	34.61	27.52
311	3.86	34.82	300	3.85	34.80	27.66
400	3.76	34.86	400	3.75	34.86	27.72
601	3.51	34.87	600	3.50	34.87	27.76
804	3.45	34.875	800	3.45	34.87	27.76
1,011	3.41	34.885	1,000	3.40	34.88	27.77
1,536	3.37	34.90				

Station 6072; April 7; latitude 44°07.5′ N., longitude 48°51′ W.; depth 1,618 m.; dynamic height 970.873.

Observed values			Scaled values			
Depth, meters	Temperature, °C.	Salinity, ‰	Depth, meters	Temperature, °C.	Salinity, ‰	σt
0	2.29	33.88	0	2.29	33.88	27.07
25	1.56	34.14	25	1.56	34.14	27.33
50	2.05	34.38	50	2.05	34.38	27.49
76	2.24	34.47	75	2.20	34.47	27.56
101	3.02	34.60	100	3.00	34.60	27.59
151	2.76	34.58	150	2.75	34.58	27.59
201	2.73	34.60	200	2.75	34.60	27.61
302	3.66	34.78	300	3.65	34.78	27.66
396	3.75	34.87	400	3.75	34.87	27.73
596	3.70	34.86	600	3.70	34.86	27.73
798	3.58	34.88	800	3.60	34.88	27.75
1,004	3.48	34.88	1,000	3.50	34.88	27.76
1,528	3.45	34.88				

Station 6073; April 7; latitude 44°09.5′ N., longitude 48°58′ W.; depth 640 m.; dynamic height 970.942.

Observed values			Scaled values			
Depth, meters	Temperature, °C.	Salinity, ‰	Depth, meters	Temperature, °C.	Salinity, ‰	σt
0	3.77	33.95	0	3.77	33.95	26.99
25	3.65	33.96	25	3.65	33.96	27.01
50	3.32	33.94	50	3.32	33.94	27.03
74	1.30	34.00	75	1.30	34.00	27.24
99	1.36	34.22	100	1.35	34.22	27.42
148	2.24	34.42	150	2.25	34.42	27.51
198	2.41	34.48	200	2.40	34.48	27.54
297	2.84	34.56	300	2.85	34.56	27.57
356	2.93	34.62	400	3.15	34.67	27.63
499	3.52	34.76	(600)	3.60	34.82	27.71

Station 6074; April 7; latitude 44°11′ N., longitude 49°05′ W.; depth 155 m.; dynamic height 971.001.

Observed values			Scaled values			
Depth, meters	Temperature, °C.	Salinity, ‰	Depth, meters	Temperature, °C.	Salinity, ‰	σt
0	0.09	33.36	0	0.09	33.36	26.80
24	−0.29	33.34	25	−0.30	33.34	26.80
48	0.35	33.72	50	0.35	33.73	27.08
71	0.38	33.75	75	0.40	33.75	27.10
95	0.46	33.75	100	0.50	33.76	27.10
142	0.51	33.78	150	0.50	33.79	27.12

Station 6075; April 8; latitude 44°13.5′ N., longitude 49°13′ W.; depth 247 m.; dynamic height 971.033.

Observed values			Scaled values			
Depth, meters	Temperature, °C.	Salinity, ‰	Depth, meters	Temperature, °C.	Salinity, ‰	σt
0	0.47	33.24	0	0.47	33.24	26.69
25	0.46	33.25	25	0.46	33.25	26.69
50	0.44	33.26	50	0.44	33.26	26.70
75	0.30	33.28	75	0.30	33.28	26.73
100	0.09	33.315	100	0.09	33.315	26.76
150	0.06	33.31	150	0.06	33.31	26.76
			(200)	0.05	33.32	26.77

Station 6076; April 8; latitude 44°15.5′ N., longitude 49°22′ W.; depth 48 m.; dynamic height 971.032.

Observed values			Scaled values			
Depth, meters	Temperature, °C.	Salinity, ‰	Depth, meters	Temperature, °C.	Salinity, ‰	σt
0	0.74	33.30	0	0.74	33.30	26.71
25	0.56	33.27	25	0.56	33.27	26.70
40	0.51	33.28				

Station 6077; April 8; latitude 44°54′ N., longitude 49°24 W.; depth 82 m.; dynamic height 971.036.

Observed values			Scaled values			
Depth, meters	Temperature, °C.	Salinity, ‰	Depth, meters	Temperature, °C.	Salinity, ‰	σt
0	0.16	33.19	0	0.16	33.19	26.66
25	0.16	33.18	25	0.16	33.18	26.65
51	−0.14	33.26	50	−0.15	33.26	26.73
66	−0.14	33.26	(75)	−0.15	33.26	26.73

Station 6078; April 8; latitude 44°51.5′ N.,longitude 49°10′ W.; depth 88 m.; dynamic height 971.035.

Observed values			Scaled values			
Depth, meters	Temperature, °C.	Salinity, ‰	Depth, meters	Temperature, °C.	Salinity, ‰	σt
0	−0.02	33.18	0	−0.02	33.18	26.66
26	−0.05	33.18	25	−0.05	33.18	26.66
51	−0.27	33.28	50	−0.25	33.28	26.74
77	−0.27	33.31	75	−0.25	33.31	26.77

Station 6079; April 8; latitude 44°49.5′ N., longitude 48°58′ W.; depth 823 m.; dynamic height 971.008.

Observed values			Scaled values			
Depth, meters	Temperature, °C.	Salinity, ‰	Depth, meters	Temperature, °C.	Salinity, ‰	σt
0	−0.37	33.17	0	−0.37	33.17	26.66
21	−0.40	33.15	25	−0.40	33.18	26.68
43	−0.46	33.44	50	−0.35	33.56	26.98
64	0.20	33.68	75	0.30	33.70	27.06
86	0.34	33.71	100	0.40	33.73	27.08
128	0.53	33.79	150	0.65	33.88	27.18
171	0.79	33.98	200	1.15	34.10	27.33
257	1.82	34.30	300	2.15	34.39	27.49
338	2.39	34.47	400	2.90	34.60	27.60
500	3.57	34.77	(600)	3.60	34.82	27.71

Observed values			Scaled values			
Depth, meters	Temperature, °C.	Salinity, ‰	Depth, meters	Temperature, °C.	Salinity, ‰	σ_t
Station 6080; April 8; latitude 44°47.5′ N., longitude 48°44′ W.; depth 1,829 m.; dynamic height 970.897.						
0	3.84	33.98	0	3.84	33.98	27.01
23	3.83	33.98	25	3.85	33.98	27.01
46	3.73	34.07	50	3.70	34.11	27.13
69	3.70	34.32	75	3.70	34.35	27.32
92	3.78	34.44	100	3.85	34.48	27.41
138	4.48	34.68	150	4.60	34.72	27.52
185	4.76	34.82	200	4.75	34.83	27.59
277	4.29	34.87	300	4.20	34.88	27.69
388	4.03	34.90	400	4.00	34.90	27.73
582	3.81	34.90	600	3.80	34.90	27.75
777	3.71	34.915	800	3.70	34.91	27.77
975	3.49	34.89	1,000	3.50	34.89	27.77
1,477	3.36	34.91				
Station 6081; April 8; latitude 44°45′ N., longitude 48°30′ W.; depth 2,488 m.; dynamic height 970.910.						
0	3.98	34.01	0	3.98	34.01	27.02
25	3.97	34.01	25	3.97	34.01	27.02
50	3.98	34.02	50	3.98	34.02	27.03
74	3.80	34.06	75	3.80	34.06	27.08
99	3.64	34.24	100	3.65	34.25	27.25
148	4.80	34.70	150	4.80	34.70	27.48
198	4.53	34.78	200	4.50	34.78	27.57
297	4.22	34.88	300	4.20	34.88	27.69
340	3.90	34.86	400	3.85	34.88	27.72
519	3.84	34.92	600	3.80	34.92	27.77
705	3.70	34.91	800	3.55	34.90	27.77
891	3.49	34.89	1,000	3.45	34.90	27.78
1,375	3.38	34.91				
Station 6082; April 8; latitude 44°39′ N., longitude 47°54′ W.; depth 3,383 m.; dynamic height 970.909.						
0	3.57	33.97	0	3.57	33.97	27.03
25	3.58	33.97	25	3.58	33.97	27.03
49	3.22	34.04	50	3.20	34.04	27.12
74	2.86	34.13	75	2.85	34.13	27.22
99	2.57	34.27	100	2.55	34.27	27.37
147	3.17	34.46	150	3.20	34.47	27.47
196	4.45	34.78	200	4.50	34.79	27.58
295	4.65	34.925	300	4.65	34.92	27.68
331	------	34.91	400	4.40	34.91	27.69
507	4.03	34.93	600	3.90	34.93	27.76
689	3.80	34.93	800	3.75	34.93	27.77
877	3.70	34.93	1,000	3.65	34.93	27.78
1,371	3.46	34.92				
Station 6083; April 8; latitude 44°34′ N., longitude 47°21, W.; depth 3,841 m.; dynamic height 970.963.						
0	4.62	33.98	0	4.62	33.98	26.93
26	4.60	33.99	25	4.60	33.99	26.94
52	4.58	34.00	50	4.60	34.00	26.95
78	4.39	34.01	75	4.40	34.01	26.98
104	4.96	34.28	100	4.90	34.23	27.09
157	5.30	34.60	150	5.30	34.57	27.32
209	4.63	34.66	200	4.70	34.65	27.45
313	4.61	34.86	300	4.60	34.83	27.60
364	5.09	35.00	400	4.90	34.98	27.69
556	4.16	34.94	600	4.05	34.93	27.74
758	3.78	34.91	800	3.75	34.91	27.76
965	3.57	34.91	1,000	3.55	34.91	27.78
1,513	3.36	34.90				

Observed values			Scaled values			
Depth, meters	Temperature, °C.	Salinity, ‰	Depth, meters	Temperature, °C.	Salinity, ‰	σ_t
Station 6084; April 9; latitude 44°29′ N., longitude 46°42′ W.; depth 3,932 m.; dynamic height 970.992.						
0	6.88	34.31	0	6.88	34.31	26.92
23	7.33	34.38	25	7.30	34.38	26.91
46	7.05	34.40	50	7.00	34.40	26.97
69	6.67	34.44	75	6.75	34.46	27.05
93	7.14	34.60	100	7.05	34.60	27.12
138	6.61	34.54	150	6.70	34.60	27.16
185	7.16	34.82	200	6.85	34.81	27.31
278	4.91	34.76	300	4.95	34.79	27.53
381	5.08	34.95	400	5.05	34.95	27.65
574	4.45	34.975	600	4.40	34.97	27.74
772	4.08	34.97	800	4.05	34.96	27.77
976	3.73	34.935	1,000	3.70	34.93	27.78
1,504	3.45	34.925				
Station 6085; April 9; latitude 44°24′ N., longitude 46°02′ W.; depth 3,841 m.; dynamic height 971.009.						
0	5.65	34.04	0	5.65	34.04	26.86
27	6.24	34.17	25	6.20	34.16	26.89
53	6.81	34.36	50	6.75	34.34	26.95
80	6.65	34.35	75	6.70	34.36	26.98
106	5.34	34.25	100	5.70	34.27	27.04
160	8.55	34.92	150	8.10	34.81	27.13
214	4.21	34.40	200	5.30	34.53	27.28
320	4.02	34.68	300	4.05	34.62	27.50
420	4.86	34.925	400	4.80	34.90	27.64
628	4.32	34.96	600	4.45	34.96	27.73
835	3.62	34.89	800	3.70	34.90	27.76
1,047	3.72	34.92	1,000	3.70	34.91	27.77
1,585	3.40	34.92				
Station 6086; April 9; latitude 44°18.5′ N., longitude 45°15′ W.; depth 4,298 m.; dynamic height 971.093.						
0	9.82	34.90	0	9.82	34.90	26.93
22	9.76	34.88	25	9.75	34.88	26.92
44	9.68	34.865	50	9.65	34.87	26.93
66	9.64	34.87	75	9.60	34.86	26.93
88	9.53	-------	100	9.30	34.83	26.95
132	8.45	34.735	150	8.65	34.80	27.04
176	9.02	34.91	200	9.15	35.00	27.11
264	9.26	35.14	300	8.50	35.07	27.27
312	8.17	35.04	400	6.60	34.99	27.48
479	5.64	34.97	600	4.95	34.97	27.68
654	4.67	34.965	800	4.10	34.95	27.76
844	4.00	-------	1,000	3.85	34.94	27.77
1,360	3.55	34.91				
Station 6087; April 9; latitude 44°48.5′ N., longitude 45°13′ W.; depth 4,207 m.; dynamic height 971.031.						
0	5.27	33.92	0	5.27	33.92	26.81
29	5.94	34.08	25	5.80	34.04	26.84
58	8.86	34.70	50	8.05	34.54	26.92
87	5.44	34.17	75	7.00	34.40	26.97
115	9.07	34.90	100	7.20	34.44	26.97
173	9.42	35.09	150	9.40	35.04	27.10
231	7.15	34.90	200	8.35	35.00	27.24
346	5.27	34.85	300	5.75	34.86	27.50
412	5.07	34.905	400	5.10	34.89	27.59
626	4.50	34.98	600	4.55	34.98	27.73
845	3.93	34.94	800	4.05	34.95	27.76
1,066	3.43	34.88	1,000	3.55	34.89	27.76
1,632	3.31	34.895				

STATIONS OCCUPIED IN 1956—Continued

Station 6088; April 9; latitude 45°15.5′ N., longitude 45°15′ W.; depth 4,207 m.; dynamic height 970.919.

Observed values			Scaled values			
Depth, meters	Temperature, °C.	Salinity, ‰	Depth, meters	Temperature, °C.	Salinity, ‰	σ_t
0	4.26	34.08	0	4.26	34.08	27.05
25	3.97	34.14	25	3.97	34.14	27.13
50	3.80	34.16	50	3.80	34.16	27.16
76	3.61	34.24	75	3.60	34.24	27.24
101	3.32	34.25	100	3.30	34.25	27.28
151	3.59	34.41	150	3.55	34.41	27.38
202	5.36	34.83	200	5.30	34.82	27.52
303	4.71	34.90	300	4.75	34.90	27.64
402	3.96	34.88	400	4.00	34.88	27.71
602	4.13	34.95	600	4.10	34.95	27.76
802	3.89	34.94	800	3.90	34.94	27.77
1,003	3.64	34.92	1,000	3.65	34.92	27.78
1,508	3.31	34.90				

Station 6089; April 9; latitude 45°17.5′ N., longitude 46°01′ W.; depth 3,658 m.; dynamic height 970.918.

Observed values			Scaled values			
Depth, meters	Temperature, °C.	Salinity, ‰	Depth, meters	Temperature, °C.	Salinity, ‰	σ_t
0	4.43	34.10	0	4.43	34.10	27.04
25	4.24	34.10	25	4.24	34.10	27.07
49	3.57	34.07	50	3.55	34.07	27.12
74	3.27	34.10	75	3.30	34.10	27.16
98	2.73	34.14	100	2.75	34.14	27.24
147	4.44	34.56	150	4.40	34.56	27.42
196	3.54	34.54	200	3.55	34.55	27.49
294	5.01	34.95	300	5.00	34.95	27.66
314	4.92	34.955	400	4.55	34.96	27.72
467	4.33	34.965	600	4.00	34.94	27.76
618	3.95	34.94	800	3.60	34.91	27.78
793	3.63	34.91	1,000	3.50	34.90	27.78
1,269	3.32	34.89				

Station 6090; April 10; latitude 45°18.5′ N., longitude 46°42′ W.; depth 3,383 m.; dynamic height 971.025.

Observed values			Scaled values			
Depth, meters	Temperature, °C.	Salinity, ‰	Depth, meters	Temperature, °C.	Salinity, ‰	σ_t
0	5.53	34.00	0	5.53	34.00	26.84
24	5.52	34.02	25	5.50	34.03	26.86
49	5.68	34.09	50	5.70	34.09	26.89
73	5.76	34.16	75	5.85	34.20	26.96
97	9.24	34.96	100	9.00	34.93	27.08
145	5.04	34.50	150	5.00	34.50	27.30
194	4.84	34.58	200	4.85	34.59	27.39
291	5.01	34.86	300	4.90	34.85	27.59
320	4.75	34.86	400	4.80	34.88	27.62
479	4.70	34.98	600	4.45	34.88	27.66
639	4.34	34.98	800	3.95	34.84	27.68
817	3.90	34.94	1,000	3.65	34.82	27.70
1,295	3.32	34.89				

Station 6091; April 10; latitude 45°19.5′ N., longitude 47°27′ W.; depth 2,780 m.; dynamic height 970.971.

Observed values			Scaled values			
Depth, meters	Temperature, °C.	Salinity, ‰	Depth, meters	Temperature, °C.	Salinity, ‰	σ_t
0	4.65	33.81	0	4.65	33.81	26.79
25	4.55	33.805	25	4.55	33.805	26.79
49	4.91	34.04	50	4.90	34.05	26.96
74	4.83	34.17	75	4.80	34.17	27.06
98	4.39	34.21	100	4.40	34.22	27.15
147	5.73	34.60	150	5.70	34.60	27.29
196	4.54	34.60	200	4.55	34.60	27.31
294	5.02	34.90	300	5.00	34.91	27.63
375	4.83	34.95	400	4.75	34.95	27.68
562	4.25	34.95	600	4.15	34.95	27.75
748	3.90	34.94	800	3.85	34.94	27.77
942	3.69	34.925	1,000	3.65	34.92	27.78
1,442	3.41	34.915				

Station 6092; April 10; latitude 45°33′ N., longitude 47°48′ W.; depth 1,646 m.; dynamic height 970.930.

Observed values			Scaled values			
Depth, meters	Temperature, °C.	Salinity, ‰	Depth, meters	Temperature, °C.	Salinity, ‰	σ_t
0	4.26	33.89	0	4.26	33.89	26.89
23	4.29	34.06	25	4.25	34.06	27.04
46	3.89	34.03	50	3.85	34.03	27.05
69	3.83	34.07	75	3.80	34.09	27.10
92	3.81	34.16	100	3.90	34.23	27.20
138	4.53	34.54	150	4.15	34.56	27.44
184	3.34	34.59	200	3.20	34.59	27.56
276	2.87	34.61	300	3.00	34.63	27.61
313	3.08	34.65	400	3.50	34.79	27.69
481	3.65	34.87	600	3.50	34.86	27.75
656	3.50	34.86	800	3.45	34.87	27.76
835	3.45	34.87	1,000	3.45	34.87	27.76
1,311	3.38	34.885				

Station 6093; April 10; latitude 45°44′ N., longitude 48°05 W.; depth 630 m.; dynamic height 970.959.

Observed values			Scaled values			
Depth, meters	Temperature, °C.	Salinity, ‰	Depth, meters	Temperature, °C.	Salinity, ‰	σ_t
0	0.56	33.46	0	0.56	33.46	26.86
25	0.39	33.76	25	0.39	33.76	27.11
50	0.34	33.81	50	0.34	33.81	27.15
74	0.35	33.90	75	0.35	33.91	27.23
99	0.66	34.00	100	0.65	34.01	27.29
148	1.66	34.22	150	1.70	34.23	27.39
197	1.95	34.30	200	1.95	34.30	27.44
296	2.50	34.49	300	2.50	34.50	27.55
329	2.67	34.555	400	3.20	34.70	27.65
534	3.64	34.80	(600)	3.65	34.82	27.70

Station 6094; April 10; latitude 45°49′ N., longitude 48°13′ W.; depth 174 m.; dynamic height 971.011.

Observed values			Scaled values			
Depth, meters	Temperature, °C.	Salinity, ‰	Depth, meters	Temperature, °C.	Salinity, ‰	σ_t
0	−0.13	33.08	0	−0.13	33.08	26.58
25	−0.63	33.38	25	−0.63	33.38	26.84
50	−0.36	33.50	50	−0.36	33.50	26.93
75	0.12	33.63	75	0.12	33.63	27.01
101	0.05	33.68	100	0.05	33.68	27.06
151	0.06	33.72	150	0.05	33.72	27.10

Station 6095; April 10; latitude 45°52′ N., longitude 48°18′ W.; depth 112 m.; dynamic height 971.016.

Observed values			Scaled values			
Depth, meters	Temperature, °C.	Salinity, ‰	Depth, meters	Temperature, °C.	Salinity, ‰	σ_t
0	−0.11	33.02	0	−0.11	33.02	26.53
25	−0.73	33.22	25	−0.73	33.22	26.72
49	−0.46	33.38	50	−0.45	33.39	26.85
74	−0.13	33.60	75	−0.15	33.60	27.01
98	0.01	33.67	100	0.05	33.67	27.06

Station 6096; April 10; latitude 45°59.5′ N., longitude 48°29′ W.; depth 93 m.; dynamic height 971.026.

Observed values			Scaled values			
Depth, meters	Temperature, °C.	Salinity, ‰	Depth, meters	Temperature, °C.	Salinity, ‰	σ_t
0	0.09	33.06	0	0.09	33.06	26.56
26	−0.32	33.11	25	−0.30	33.11	26.61
52	−0.60	33.16	50	−0.60	33.15	26.66
78	−0.14	33.42	75	−0.25	33.38	26.83

Table of Oceanographic Data—Continued

STATIONS OCCUPIED IN 1956—Continued

Station 6097; April 10; latitude 46°08′ N., longitude 48°42′ W.; depth 73 m.; dynamic height 971.022.

Observed values			Scaled values			
Depth, meters	Temperature, ° C.	Salinity, ‰	Depth, meters	Temperature, ° C.	Salinity, ‰	σ_t
0	0.74	33.10	0	0.74	33.10	26.55
24	0.12	33.17	25	0.10	33.17	26.65
48	−0.32	33.19	50	−0.30	33.19	26.68
62	0.03	33.46				

Station 6098; April 10; latitude 46°17.5′ N., longitude 48°57′ W.; depth 69 m.; dynamic height 971.027.

Observed values			Scaled values			
Depth, meters	Temperature, ° C.	Salinity, ‰	Depth, meters	Temperature, ° C.	Salinity, ‰	σ_t
0	1.07	33.06	0	1.07	33.06	26.51
25	0.69	33.12	25	0.69	33.12	26.57
50	0.22	33.23	50	0.22	33.23	26.69

Station 6099; April 11; latitude 46°16.5′ N., longitude 48′31′ W.; depth 91 m.; dynamic height 971.024.

Observed values			Scaled values			
Depth, meters	Temperature, ° C.	Salinity, ‰	Depth, meters	Temperature, ° C.	Salinity, ‰	σ_t
0	0.71	33.14	0	0.71	33.14	26.59
25	0.31	33.23	25	0.31	33.23	26.69
51	0.17	33.24	50	0.20	33.24	26.70
76	−0.07	33.38	75	−0.05	33.38	26.82

Station 6100; April 11; latitude 46°14.5′ N., longitude 48°02′ W.; depth 128 m.; dynamic height 971.022.

Observed values			Scaled values			
Depth, meters	Temperature, ° C.	Salinity, ‰	Depth, meters	Temperature, ° C.	Salinity, ‰	σ_t
0	−0.45	32.99	0	−0.45	32.99	26.53
25	−0.84	33.08	25	−0.84	33.08	26.61
49	−1.04	33.30	50	−1.05	33.30	26.79
74	−0.62	33.32	75	−0.60	33.43	26.88
98	0.02	33.53	100	0.10	33.54	26.94

Station 6101; April 11; latitude 46°13′ N., longitude 47°44′ W.; depth 210 m.; dynamic height 971.047.

Observed values			Scaled values			
Depth, meters	Temperature, ° C.	Salinity, ‰	Depth, meters	Temperature, ° C.	Salinity, ‰	σ_t
0	−0.64	32.98	0	−0.64	32.98	26.53
25	−0.83	33.00	25	−0.83	33.00	26.55
50	−1.29	33.08	50	−1.29	33.08	26.62
75	−1.17	33.19	75	−1.17	33.19	26.71
100	−0.94	33.27	100	−0.94	33.27	26.77
150	0.21	33.58	150	0.21	33.58	26.97

Station 6102; April 11; latitude 46°12.5′ N., longitude 47°25′ W.; depth 677 m.; dynamic height 970.940.

Observed values			Scaled values			
Depth, meters	Temperature, ° C.	Salinity, ‰	Depth, meters	Temperature, ° C.	Salinity, ‰	σ_t
0	0.26	33.38	0	0.26	33.38	26.81
26	−0.13	33.64	25	−0.15	33.64	27.04
53	0.14	33.86	50	0.05	33.84	27.19
79	0.73	33.99	75	0.65	33.97	27.26
105	0.71	34.10	100	0.70	34.08	27.34
157	1.91	34.34	150	1.75	34.30	27.45
209	2.56	34.485	200	2.45	34.46	27.52
314	2.96	34.61	300	2.90	34.59	27.59
410	3.59	34.765	400	3.55	34.75	27.65
624	3.71	34.855	600	3.70	34.85	27.72

Station 6103; April 11; latitude 46°11′ N., longitude 47°10′ W.; depth 1,500 m.; dynamic height 970.880.

Observed values			Scaled values			
Depth, meters	Temperature, ° C.	Salinity, ‰	Depth, meters	Temperature, ° C.	Salinity, ‰	σ_t
0	2.24	34.20	0	2.24	34.20	27.33
25	2.05	34.19	25	2.05	34.19	27.34
49	1.72	34.27	50	1.70	34.27	27.43
74	2.09	34.38	75	2.10	34.38	27.48
98	2.15	34.42	100	2.15	34.42	27.52
147	2.52	34.52	150	2.55	34.53	27.57
196	2.99	34.62	200	3.00	34.63	27.61
294	3.33	34.70	300	3.35	34.71	27.64
393	3.79	34.84	400	3.80	34.84	27.70
590	3.71	34.87	600	3.70	34.87	27.74
789	3.55	34.875	800	3.55	34.87	27.75
989	3.43	34.87	1,000	3.45	34.87	27.76
1,439	3.40	34.88				

Station 6104; April 11; latitude 46°09′ N., longitude 46°39′ W.; depth 1,225 m.; dynamic height 970.870.

Observed values			Scaled values			
Depth, meters	Temperature, ° C.	Salinity, ‰	Depth, meters	Temperature, ° C.	Salinity, ‰	σ_t
0	3.15	34.06	0	3.15	34.06	27.14
25	2.42	34.24	25	2.42	34.24	27.35
50	1.58	34.20	50	1.58	34.20	27.38
75	2.51	34.39	75	2.51	34.39	27.46
100	4.79	34.75	100	4.79	34.75	27.52
150	2.94	34.56	150	2.94	34.56	27.56
200	3.36	34.70	200	3.36	34.70	27.63
300	4.71	34.965	300	4.71	34.965	27.70
403	4.00	34.90	400	4.00	34.90	27.73
602	3.57	34.88	600	3.55	34.88	27.75
800	3.47	34.88	800	3.45	34.88	27.76
1,002	3.42	34.88	1,000	3.45	34.88	27.76
1,209	3.42	34.88				

Station 6105; April 11; latitude 46°06′ N., longitude 45°59′ W.; depth 1,756 m.; dynamic height 970.881.

Observed values			Scaled values			
Depth, meters	Temperature, ° C.	Salinity, ‰	Depth, meters	Temperature, ° C.	Salinity, ‰	σ_t
0	4.09	34.19	0	4.09	34.19	27.15
24	3.78	34.21	25	3.75	34.21	27.21
49	3.62	34.24	50	3.65	34.24	27.24
73	3.56	34.31	75	3.55	34.31	27.30
97	3.45	34.39	100	3.45	34.40	27.38
146	3.79	34.60	150	3.80	34.61	27.52
195	3.63	34.74	200	3.65	34.75	27.64
292	3.66	34.845	300	3.70	34.85	27.72
391	3.61	34.86	400	3.60	34.86	27.74
585	3.61	34.875	600	3.60	34.87	27.75
778	3.45	34.875	800	3.45	34.88	27.76
974	3.40	34.885	1,000	3.40	34.88	27.77
1,468	3.31	34.89				

Station 6106; April 11; latitude 46°03.5′ N., longitude 45°20′ W.; depth 3,200 m.; dynamic height 970.916.

Observed values			Scaled values			
Depth, meters	Temperature, ° C.	Salinity, ‰	Depth, meters	Temperature, ° C.	Salinity, ‰	σ_t
0	4.73	34.16	0	4.73	34.16	27.06
22	5.29	34.37	25	5.25	34.36	27.16
43	4.13	34.285	50	3.90	34.27	27.24
65	3.70	34.25	75	3.65	34.25	27.25
87	3.66	34.28	100	3.95	34.40	27.34
129	5.28	34.625	150	5.00	34.62	27.40
172	4.66	34.62	200	4.50	34.66	27.48
259	4.33	34.78	300	4.25	34.82	27.64
378	4.01	34.86	400	3.95	34.87	27.71
564	3.72	34.885	600	3.65	34.88	27.74
749	3.50	34.885	800	3.50	34.89	27.77
942	3.55	34.90	1,000	3.55	34.90	27.77
1,430	3.48	34.92				

STATIONS OCCUPIED IN 1956—Continued

Station 6107; April 12; latitude 46°01.5′ N., longitude 44°47′ W.; depth 3,640 m.; dynamic height 970.988.

Observed values			Scaled values			
Depth, meters	Temperature, ° C.	Salinity, °/₀₀	Depth, meters	Temperature, ° C.	Salinity, °/₀₀	σ_t
0	5.73	33.71	0	5.73	33.71	26.59
26	6.02	34.055	25	6.00	34.05	26.82
52	6.66	34.36	50	6.55	34.34	26.98
78	6.96	34.455	75	6.95	34.45	27.01
105	6.86	34.58	100	6.90	34.56	27.11
156	3.36	34.30	150	3.55	34.32	27.31
208	4.16	34.55	200	4.00	34.50	27.41
313	4.91	34.87	300	4.90	34.84	27.58
412	4.79	34.90	400	4.80	34.90	27.64
616	4.45	34.96	600	4.50	34.96	27.72
819	4.19	34.96	800	4.20	34.96	27.76
1,026	3.68	34.91	1,000	3.75	34.92	27.77
1,547	3.31	34.88				

Station 6108; April 12; latitude 46°20′ N., longitude 44°50, W.; depth 1,500 m.; dynamic height 970.911.

Observed values			Scaled values			
Depth, meters	Temperature, ° C.	Salinity, °/₀₀	Depth, meters	Temperature, ° C.	Salinity, °/₀₀	σ_t
0	4.97	34.08	0	4.97	34.08	26.97
24	4.19	34.22	25	4.20	34.22	27.17
48	4.51	34.30	50	4.50	34.31	27.21
72	4.29	34.39	75	4.25	34.39	27.29
97	3.95	34.42	100	3.95	34.43	27.36
145	4.82	34.66	150	4.80	34.66	27.45
193	4.38	34.67	200	4.40	34.68	27.51
290	4.67	34.90	300	4.65	34.90	27.66
378	4.35	34.92	400	4.25	34.92	27.72
568	3.61	34.86	600	3.60	34.86	27.74
758	3.50	34.87	800	3.50	34.87	27.76
955	3.42	34.88	1,000	3.40	34.88	27.77
1,356	3.35	34.885				

Station 6109; April 12; latitude 46°28′ N., longitude 44°52′ W.; depth 631 m.; dynamic height 970.868.

Observed values			Scaled values			
Depth, meters	Temperature, ° C.	Salinity, °/₀₀	Depth, meters	Temperature, ° C.	Salinity, °/₀₀	σ_t
0	3.77	34.28	0	3.77	34.28	27.26
26	3.57	34.30	25	3.60	34.30	27.29
51	3.41	34.36	50	3.45	34.36	27.35
77	3.61	34.42	75	3.60	34.42	27.39
103	3.50	34.50	100	3.50	34.49	27.45
153	3.27	34.56	150	3.25	34.55	27.52
205	3.52	34.73	200	3.50	34.71	27.63
308	3.56	34.84	300	3.55	34.84	27.72
400	3.53	34.845	400	3.55	34.85	27.73
599	3.51	34.875	600	3.50	34.88	27.76

Station 6110; April 12; latitude 46°38′ N., longitude 44°57′ W.; depth 224 m.; dynamic height 970.879.

Observed values			Scaled values			
Depth, meters	Temperature, ° C.	Salinity, °/₀₀	Depth, meters	Temperature, ° C.	Salinity, °/₀₀	σ_t
0	3.67	34.16	0	3.67	34.16	27.17
26	3.41	34.19	25	3.40	34.19	27.22
51	3.32	34.20	50	3.35	34.20	27.23
77	3.13	34.23	75	3.15	34.23	27.27
102	3.05	34.28	100	3.05	34.27	27.32
153	3.18	34.465	150	3.15	34.45	27.45
204	3.53	34.80	200	3.50	34.79	27.69

Station 6111; April 12; latitude 46°47.5′ N., longitude 44°59′ W.; depth 187 m.; dynamic height 970.880.

Observed values			Scaled values			
Depth, meters	Temperature, ° C.	Salinity, °/₀₀	Depth, meters	Temperature, ° C.	Salinity, °/₀₀	σ_t
0	3.69	34.14	0	3.69	34.14	27.15
24	3.55	34.16	25	3.55	34.16	27.19
49	3.29	34.19	50	3.30	34.19	27.23
73	3.19	34.20	75	3.15	34.20	27.25
97	3.12	34.26	100	3.10	34.27	27.32
145	3.25	34.47	150	3.30	34.49	27.47

Station 6112; April 12; latitude 46°53.5′ N., longitude 45°02′ W.; depth 201 m.; dynamic height 970.880.

Observed values			Scaled values			
Depth, meters	Temperature, ° C.	Salinity, °/₀₀	Depth, meters	Temperature, ° C.	Salinity, °/₀₀	σ_t
0	3.69	34.15	0	3.69	34.15	27.16
25	3.68	34.15	25	3.68	34.15	27.16
50	3.36	34.19	50	3.36	34.19	27.22
75	3.09	34.23	75	3.09	34.23	27.28
100	3.10	34.305	100	3.10	34.305	27.34
149	3.30	34.50	150	3.30	34.51	27.49
189	3.83	34.71	(200)	3.90	34.76	27.63

Station 6113; April 12; latitude 46°52.5′. N., longitude 45°09′ W.; depth 224 m.; dynamic height 970.879.

Observed values			Scaled values			
Depth, meters	Temperature, ° C.	Salinity, °/₀₀	Depth, meters	Temperature, ° C.	Salinity, °/₀₀	σ_t
0	3.63	34.15	0	3.63	34.15	27.17
25	3.61	34.16	25	3.61	34.16	27.18
49	3.27	34.20	50	3.25	34.20	27.24
74	3.12	34.24	75	3.15	34.24	27.28
98	3.16	34.31	100	3.15	34.33	27.35
147	3.56	34.56	150	3.60	34.58	27.51
196	3.71	34.70	200	3.75	34.71	27.60

Station 6114; April 12; latitude 46°52′ N., longitude 45°51′ W.; depth 272 m.; dynamic height 970.862.

Observed values			Scaled values			
Depth, meters	Temperature, ° C.	Salinity, °/₀₀	Depth, meters	Temperature, ° C.	Salinity, °/₀₀	σ_t
0	3.96	34.13	0	3.96	34.13	27.12
25	3.30	34.21	25	3.30	34.21	27.25
49	3.12	34.305	50	3.10	34.31	27.35
74	3.53	34.45	75	3.55	34.45	27.41
99	3.18	34.48	100	3.20	34.49	27.48
148	4.39	34.77	150	4.40	34.77	27.58
198	3.69	34.79	200	3.70	34.79	27.67
257	3.65	34.84				

Station 6115; April 13; latitude 46°51.5′ N., longitude 46°07′ W.; depth 326 m.; dynamic height 970.878.

Observed values			Scaled values			
Depth, meters	Temperature, ° C.	Salinity, °/₀₀	Depth, meters	Temperature, ° C.	Salinity, °/₀₀	σ_t
0	3.53	34.16	0	3.53	34.16	27.19
25	3.50	34.17	25	3.50	34.17	27.20
51	3.19	34.21	50	3.20	34.21	27.26
76	3.11	34.22	75	3.10	34.22	27.18
101	3.14	34.31	100	3.15	34.31	27.34
152	3.82	34.59	150	3.80	34.57	27.49
203	3.63	34.78	200	3.65	34.78	27.66
304	3.60	34.84	300	3.60	34.84	27.72

Station 6116; April 13; latitude 46°51′ N., longitude 46°28′ W.; depth 659 m.; dynamic height 970.884.

Observed values			Scaled values			
Depth, meters	Temperature, °C.	Salinity, ‰	Depth, meters	Temperature, °C.	Salinity, ‰	σ_t
0	3.56	34.18	0	3.56	34.18	27.20
25	3.54	34.18	25	3.54	34.18	27.20
50	3.38	34.27	50	3.38	34.27	27.29
75	3.26	34.30	75	3.26	34.30	27.32
100	3.10	34.36	100	3.10	34.36	27.39
150	3.02	34.44	150	3.02	34.44	27.46
200	3.93	34.71	200	3.93	34.71	27.58
300	4.06	34.88	300	4.06	34.88	27.70
408	3.63	34.87	400	3.65	34.87	27.74
607	3.46	34.88	600	3.50	34.88	27.76

Station 6117; Apri 13; latitude 46°50.5′ N., longitude 46°46′ W; depth 1,216 m.; dynamic height 970.872.

Observed values			Scaled values			
Depth, meters	Temperature, °C.	Salinity, ‰	Depth, meters	Temperature, °C.	Salinity, ‰	σ_t
0	2.47	34.32	0	2.47	34.32	27.41
25	2.54	34.36	25	2.54	34.36	27.44
50	2.39	34.36	50	2,39	34.36	27.45
75	2.32	34.42	75	2.32	34.42	27.50
100	2.68	34.52	100	2.68	34.52	27.55
150	2.79	34.56	150	2.79	34.56	27.57
201	2.82	34.59	200	2.80	34.59	27.59
301	3.69	34.80	300	3.70	34.80	27.68
411	3.76	34.85	400	3.75	34.85	27.71
612	3.53	34.86	600	3.55	34.86	27.74
810	3.47	34.87	800	3.50	34.87	27.76
1,020	3.42	34.87	1,000	3.45	34.87	27.76

Station 6118; April 13; latitude 46°50′ N., longitude 47°04′ W.; depth 659 m.; dynamic height 970.933.

Observed values			Scaled values			
Depth, meters	Temperature, °C.	Salinity, ‰	Depth, meters	Temperature, °C.	Salinity, ‰	σ_t
0	0.48	33.79	0	0.48	33.79	27.12
25	0.62	33.83	25	0.62	33.83	27.14
51	0.43	33.95	50	0.45	33.95	27.25
76	0.55	34.035	75	0.55	34.03	27.31
101	0.98	34.15	100	0.95	34.14	27.37
152	2.10	34.39	150	2.10	34.38	27.48
203	2.13	34.445	200	2.15	34.44	27.53
304	2.90	34.59	300	2.85	34.58	27.58
401	3.39	34.71	400	3.40	34.71	27.64
600	3.75	34.84	600	3.75	34.84	27.70

Station 6119; April 13; latitude 46°50′ N. longitude 47°14′ W.; depth 332 m.; dynamic height 970.955.

Observed values			Scaled values			
Depth, meters	Temperature, °C.	Salinity, ‰	Depth, meters	Temperature, °C.	Salinity, ‰	σ_t
0	0.54	33.70	0	0.54	33.70	27.05
25	0.41	33.71	25	0.41	33.71	27.07
50	0.10	33.80	50	0.10	33.80	27.15
75	0.10	33.88	75	0.10	33.88	27.21
100	0.33	33.99	100	0.33	33.99	27.29
150	1.29	34.195	150	1.29	34.195	27.40
199	2.18	34.41	200	2.20	34.41	27.51
299	2.55	34.49	300	2.55	34.49	27.54

Station 6120; April 13; latitude 46°50′ N., longitude 47°29′ W.; depth 172 m.; dynamic height 971.029.

Observed values			Scaled values			
Depth, meters	Temperature, °C.	Salinity, ‰	Depth, meters	Temperature, °C.	Salinity, ‰	σ_t
0	−1.03	32.96	0	−1.03	32.96	26.52
25	−1.30	32.98	25	−1.30	32.98	26.54
50	−1.22	33.10	50	−1.22	33.10	26.64
75	−0.53	33.28	75	−0.53	33.28	26.76
99	0.21	33.53	100	0.20	33.54	26.94
149	0.31	33.67	150	0.35	33.67	27.04

Station 6121; April 13; latitude 46°49′ N., longitude 48°05′ W.; depth 110 m.; dynamic height 971.040.

Observed values			Scaled values			
Depth, meters	Temperature, °C.	Salinity, ‰	Depth, meters	Temperature, °C.	Salinity, ‰	σ_t
0	0.20	33.06	0	0.20	33.06	26.55
24	0.13	33.07	25	0.10	33.07	26.57
49	−0.27	33.10	50	−0.30	33.10	26.60
73	−0.36	33.12	75	−0.35	33.13	26.63
96	−0.13	33.30	100	−0.10	33.33	26.78

Station 6122; April 13; latitude 46°49′ N., longitude 48°36′ W.; depth 80 m.; dynamic height 971.038.

Observed values			Scaled values			
Depth, meters	Temperature, °C.	Salinity, ‰	Depth, meters	Temperature, °C.	Salinity, ‰	σ_t
0	0.74	33.13	0	0.74	33.13	26.58
24	0.70	33.14	25	0.70	33.14	26.59
49	0.54	33.14	50	0.50	33.14	26.60
68	0.20	33.20	75	0.10	33.22	26.69

Station 6123; May 19; latitude 43°38′ N., longitude 51°24′ W.; depth 88 m.; dynamic height 971.098.

Observed values			Scaled values			
Depth, meters	Temperature, °C.	Salinity, ‰	Depth, meters	Temperature, °C.	Salinity, ‰	σ_t
0	5.40	32.76	0	5.40	32.76	25.88
25	3.50	33.01	25	3.50	33.01	26.28
50	2.62	33.21	50	2.62	33.21	26.52
75	3.42	33.55	75	3.42	33.55	26.71

Station 6124; May 19; latitude 43°28′ N., longitude 51°39′ W.; depth 192 m.; dynamic height 971.096.

Observed values			Scaled values			
Depth, meters	Temperature, °C.	Salinity, ‰	Depth, meters	Temperature, °C.	Salinity, ‰	σ_t
0	5.74	32.64	0	5.74	32.64	25.75
25	3.04	33.06	25	3.04	33.06	26.35
50	0.24	33.07	50	0.24	33.07	26.56
75	2.67	33.57	75	2.67	33.57	26.80
99	2.46	33.77	100	2.45	33.78	26.97
149	1.94	33.98	150	1.95	33.98	27.18

STATIONS OCCUPIED IN 1956—Continued

Station 6125; May 19; latitude 43°24′ N., longitude 51°45′ W.; depth 969 m.; dynamic height 971.094.

Observed values			Scaled values			
Depth, meters	Temperature, °C.	Salinity, °/₀₀	Depth, meters	Temperature, °C.	Salinity, °/₀₀	σt
0	4.75	32.90	0	4.75	32.90	26.06
25	2.16	33.09	25	2.16	33.09	26.45
50	−0.18	33.16	50	−0.18	33.16	26.65
75	−0.14	33.40	75	−0.14	33.40	26.85
100	−0.07	33.51	100	−0.07	33.51	26.93
150	0.12	33.62	150	0.12	33.62	27.01
199	2.20	33.98	200	2.25	33.99	27.16
299	2.94	34.40	300	2.95	34.40	27.43
385	2.96	34.48	400	3.00	34.50	27.51
581	3.50	34.76	600	3.55	34.78	27.67
680	3.67	34.82	(800)	3.75	34.86	27.72

Station 6126; May 19; latitude 43°18′ N., longitude 51°56′ W.; depth 1,463 m.; dynamic height 971.055.

Observed values			Scaled values			
Depth, meters	Temperature, °C.	Salinity, °/₀₀	Depth, meters	Temperature, °C.	Salinity, °/₀₀	σt
0	3.40	32.96	0	3.40	32.96	26.24
25	0.09	33.02	25	0.09	33.02	26.53
50	−0.24	33.24	50	−0.24	33.24	26.72
75	−0.14	33.47	75	−0.14	33.47	26.90
101	−0.11	33.55	100	−0.10	33.55	26.96
151	1.35	33.90	150	1.35	33.89	27.15
201	2.16	34.08	200	2.15	34.07	27.24
302	4.76	34.60	300	4.75	34.60	27.41
405	2.86	34.58	400	2.90	34.58	27.58
604	3.67	34.82	600	3.65	34.82	27.70
802	3.61	34.86	800	3.60	34.86	27.74
1,002	3.68	34.90	1,000	3.70	34.90	27.76

Station 6127; May 19; latitude 43°06′ N., longitude 52°08′ W.; depth 2,468 m.; dynamic height 971.010.

Observed values			Scaled values			
Depth, meters	Temperature, °C.	Salinity, °/₀₀	Depth, meters	Temperature, °C.	Salinity, °/₀₀	σt
0	6.98	33.08	0	6.98	33.08	25.93
24	0.35	33.02	25	0.30	33.02	26.52
47	0.16	33.38	50	0.20	33.50	26.91
71	6.56	34.51	75	6.40	34.50	27.13
94	5.37	34.40	100	5.10	34.38	27.19
141	2.96	34.25	150	3.40	34.33	27.33
188	5.64	34.72	200	5.50	34.71	27.41
282	4.15	34.65	300	4.55	34.74	27.54
340	5.59	34.96	400	5.20	34.96	27.64
511	4.78	34.97	600	4.80	34.98	27.70
682	4.40	34.99	800	4.20	34.96	27.76
862	4.11	34.95	1,000	3.95	34.94	27.76
1,330	3.65	34.925				

Station 6128; May 19; latitude 42°49′ N., longitude 52°25′ W.; depth 3,237 m.; dynamic height 971.092.

Observed values			Scaled values			
Depth, meters	Temperature, °C.	Salinity, °/₀₀	Depth, meters	Temperature, °C.	Salinity, °/₀₀	σt
0	9.77	33.49	0	9.77	33.49	25.83
27	6.70	33.79	25	6.80	33.76	26.49
53	8.37	34.38	50	8.15	34.32	26.74
80	10.16	34.92	75	9.85	34.83	26.86
107	10.99	35.165	100	10.80	35.13	26.93
161	10.21	35.17	150	10.45	35.17	27.03
214	8.40	34.98	200	9.00	35.04	27.17
321	3.85	34.49	300	4.40	34.58	27.43
423	4.72	34.81	400	4.60	34.74	27.53
634	4.46	34.94	600	4.55	34.93	27.69
848	3.83	34.90	800	3.95	34.91	27.74
1,059	3.63	34.90	1,000	3.65	34.90	27.76
1,585	3.63	34.945				

Station 6129; May 19; latitude 42°33.5′ N., longitude 52°40′ W.; depth 3,841 m.; dynamic height 971.145.

Observed values			Scaled values			
Depth, meters	Temperature, °C.	Salinity, °/₀₀	Depth, meters	Temperature, °C.	Salinity, °/₀₀	σt
0	12.33	34.66	0	12.33	34.66	26.28
27	13.95	35.67	25	13.90	35.64	26.72
53	12.10	35.29	50	12.30	35.33	26.80
80	13.08	35.59	75	12.90	35.54	26.85
106	12.59	35.51	100	12.70	35.52	26.88
160	11.88	35.42	150	12.00	35.43	26.94
213	11.12	35.41	200	11.30	35.42	27.07
319	8.38	35.03	300	8.90	35.09	27.22
413	6.89	34.94	400	7.05	34.94	27.38
618	4.19	34.91	600	4.30	34.91	27.70
825	4.02	34.91	800	4.05	34.91	27.73
1,034	4.03	34.94	1,000	4.05	34.93	27.74
1,562	3.72	34.94				

Station 6130; May 19–20; latitude 42°21.5′ N., longitude 52°25′ W.; depth 3,841 m.; dynamic height 971.149.

Observed values			Scaled values			
Depth, meters	Temperature, °C.	Salinity, °/₀₀	Depth, meters	Temperature, °C.	Salinity, °/₀₀	σt
0	15.31	35.70	0	15.31	35.70	26.46
26	15.07	35.87	25	15.05	35.87	26.64
51	14.86	35.89	50	14.85	35.89	26.70
77	14.39	35.80	75	14.45	35.81	26.74
102	13.65	35.70	100	13.70	35.71	26.82
155	12.25	35.48	150	12.40	35.50	26.92
206	10.84	35.28	200	11.00	35.30	27.03
308	4.56	34.50	300	5.00	34.54	27.33
390	2.47	34.34	400	2.45	34.34	27.42
591	3.09	34.65	600	3.15	34.66	27.62
798	3.57	34.79	800	3.60	34.79	27.68
1,005	3.63	34.85	1,000	3.60	34.85	27.73
1,539	3.50	34.88				

Station 6131; May 20; latitude 42°02.5′ N., longitude 51°58′ W.; depth 3,841 m.; dynamic height 971.064.

Observed values			Scaled values			
Depth, meters	Temperature, °C.	Salinity, °/₀₀	Depth, meters	Temperature, °C.	Salinity, °/₀₀	σt
0	8.32	33.10	0	8.32	33.10	25.76
27	3.92	33.19	25	4.25	33.18	26.33
52	0.29	33.06	50	0.40	33.07	26.55
79	2.42	33.63	75	2.05	33.53	26.82
105	3.39	33.99	100	3.25	33.93	27.02
158	4.46	34.30	150	4.35	34.28	27.19
210	2.88	34.28	200	3.20	34.28	27.31
315	3.10	--------	300	3.10	34.42	27.44
372	3.12	34.57	400	3.15	34.63	27.59
559	4.12	34.86	600	4.15	34.88	27.69
749	4.21	34.94	800	4.15	34.94	27.74
948	3.86	34.92	1,000	3.80	34.92	27.77
1,463	3.74	34.95				

Station 6132; May 20; latitude 42°01′ N., longitude 51°01′ W.; depth 3,246 m.; dynamic height 970.941.

Observed values			Scaled values			
Depth, meters	Temperature, °C.	Salinity, °/₀₀	Depth, meters	Temperature, °C.	Salinity, °/₀₀	σt
0	6.82	33.29	0	6.82	33.29	26.12
24	4.78	33.30	25	4.70	33.30	26.37
49	2.07	33.86	50	2.05	33.87	27.09
73	3.48	34.26	75	3.45	34.26	27.27
98	2.64	34.30	100	2.65	34.31	27.39
147	4.93	34.73	150	5.05	34.75	27.49
195	6.47	35.08	200	6.45	35.08	27.57
293	5.31	35.01	300	5.15	35.00	27.68
349	4.19	34.88	400	4.00	34.87	27.71
527	3.79	34.87	600	3.75	34.87	27.73
708	3.64	34.88	800	3.60	34.88	27.75
897	3.51	34.88	1,000	3.50	34.89	27.77
1,389	3.42	34.90				

Table of Oceanographic Data—Continued

STATIONS OCCUPIED IN 1956—Continued

Station 6133; May 20; latitude 42°20.5′ N., longitude 51°27′ W.; depth 2,963 m.; dynamic height 971.016.

Observed values			Scaled values			
Depth, meters	Temperature, °C.	Salinity, ‰	Depth, meters	Temperature, °C.	Salinity, ‰	σ_t
0	7.81	33.11	0	7.81	33.11	25.84
27	3.69	33.26	25	4.00	33.23	26.40
52	4.73	33.76	50	4.65	33.71	26.72
79	4.97	34.28	75	4.95	34.22	27.09
105	4.66	34.28	100	4.70	34.28	27.16
158	5.64	34.60	150	5.45	34.55	27.28
210	6.40	34.88	200	6.30	34.84	27.41
315	5.14	34.88	300	5.30	34.88	27.56
408	5.47	35.01	400	5.45	35.00	27.64
611	4.09	34.90	600	4.15	34.90	27.71
814	4.16	34.96	800	4.15	34.96	27.76
1,023	3.96	34.945	1,000	4.00	34.95	27.77
1,550	3.57	34.92				

Station 6134; May 20; latitude 42°39.5′ N., longitude 51°00′ W.; depth 1,783 m.; dynamic height 971.123.

0	4.32	32.96	0	4.32	32.96	26.15
26	1.43	33.10	25	1.55	33.10	26.50
52	−0.13	33.24	50	−0.10	33.23	26.70
78	−0.29	33.40	75	−0.30	33.38	26.83
104	−0.25	33.45	100	−0.25	33.44	26.88
155	0.00	33.57	150	−0.05	33.56	26.97
208	0.41	33.75	200	0.35	33.72	27.08
312	1.81	34.22	300	1.60	34.17	27.36
414	2.96	34.61	400	2.85	34.56	27.57
617	3.83	34.82	600	3.80	34.82	27.69
819	3.71	34.86	800	3.75	34.86	27.72
1,027	3.56	34.86	1,000	3.55	34.86	27.74
1,552	3.47	34.89				

Station 6135; May 20; latitude 42°48′ N., longitude 50°50′ W.; depth 1,028 m.; dynamic height 971.102.

0	4.06	32.96	0	4.06	32.96	26.18
20	3.01	33.02	25	2.70	33.05	26.38
40	1.66	33.14	50	2.00	33.21	26.57
61	2.49	33.30	75	2.65	33.52	26.76
81	2.67	33.60	100	2.95	33.78	26.93
122	3.30	33.94	150	1.95	33.87	27.09
162	1.54	33.84	200	2.60	34.01	27.15
243	3.38	34.23	300	3.65	34.42	27.38
329	3.70	34.50	400	3.60	34.59	27.52
501	3.19	34.68	600	3.40	34.77	27.69
676	3.62	34.82	800	3.65	34.83	27.70
881	3.67	34.84	(1,000)	3.65	34.85	27.72

Station 6136; May 20; latitude 42°53′ N., longitude 50°44′ W.; depth 260 m.; dynamic height 971.090.

0	4.07	32.97	0	4.07	32.97	26.19
24	2.23	33.00	25	2.20	33.00	26.38
49	0.62	33.16	50	0.60	33.16	26.61
73	0.32	33.25	75	0.25	33.26	26.71
98	−0.19	33.41	100	−0.20	33.42	26.87
146	0.17	33.62	150	0.25	33.63	27.01
195	0.96	33.86	200	1.00	33.88	27.16
235	*1.33	34.06				

Station 6137; May 21; latitude 42°57.5′ N., longitude 50°40′ W.; depth 110 m.; dynamic height 971.086.

Observed values			Scaled values			
Depth, meters	Temperature, °C.	Salinity, ‰	Depth, meters	Temperature, °C.	Salinity, ‰	σ_t
0	5.14	32.88	0	5.14	32.88	26.00
26	1.44	33.12	25	1.60	33.11	26.51
51	0.12	33.24	50	0.15	33.23	26.69
77	−0.24	33.32	75	−0.25	33.31	26.77
102	0.03	33.41	100	−0.05	33.40	26.84

Station 6138; May 21; latitude 43°04′ N., longitude 50°31′ W.; depth 91 m.; dynamic height 971.100.

0	5.52	32.84	0	5.52	32.84	25.92
26	3.99	32.89	25	4.05	32.89	26.12
51	1.60	33.16	50	1.65	33.15	26.54
77	0.49	33.36	75	0.55	33.35	26.76

Station 6139; May 21; latitude 43°21′ N., longitude 50°13 W.; depth 60 m.; dynamic height 971.120.

0	6.39	32.58	0	6.39	32.58	25.62
26	3.63	32.77	25	3.65	32.76	26.06
52	3.63	32.77	50	3.65	32.77	26.07

Station 6140; May 21; latitude 42°58′ N., longitude 50°16′ W.; depth 93 m.; dynamic height 971.084.

0	5.66	32.86	0	5.66	32.86	25.92
26	1.09	33.12	25	1.20	33.11	26.54
52	0.60	33.26	50	0.65	33.26	26.69
78	0.36	33.29	75	0.40	33.29	26.72

Station 6141; May 21; latitude 42°47′ N., longitude 50°16′ W.; depth 357 m.; dynamic height 971.048.

0	2.67	32.94	0	2.67	32.94	26.29
24	0.53	32.97	25	0.50	32.97	26.46
47	−0.54	33.10	50	−0.55	33.13	26.64
71	−0.50	33.34	75	−0.40	33.38	26.84
94	0.16	33.55	100	0.25	33.59	26.98
141	0.65	33.84	150	0.75	33.89	27.19
188	1.30	34.10	200	1.50	34.16	27.36
			(300)	3.15	34.60	27.57

Station 6142; May 21; latitude 42°36′ N., longitude 50°17, W.; depth 1,829 m.; dynamic height 970.982.

0	2.58	32.92	0	2.58	32.92	26.28
26	0.96	33.00	25	0.95	33.00	26.47
52	2.04	33.47	50	1.95	33.43	26.74
78	2.47	33.68	75	2.45	33.65	26.88
104	1.55	33.95	100	1.65	33.90	27.13
155	2.16	34.28	150	2.15	34.26	27.39
207	2.17	34.41	200	2.15	34.40	27.50
311	2.69	34.57	300	2.65	34.55	27.58
418	3.45	34.75	400	3.35	34.72	27.65
625	4.01	34.92	600	4.00	34.91	27.74
829	3.67	34.90	800	3.70	34.90	27.76
1,035	3.52	34.91	1,000	3.55	34.91	27.78
1,553	3.45	34.905				

Table of Oceanographic Data—Continued

STATIONS OCCUPIED IN 1955—Continued

Station 6143; May 21; latitude 42°15′ N., longitude 50°18′ W.; depth 2,798 m.; dynamic height 970.995.

Observed values			Scaled values			
Depth, meters	Temperature, ° C.	Salinity, ‰	Depth, meters	Temperature, ° C.	Salinity, ‰	σ_t
0	10.12	33.90	0	10.12	33.90	26.09
24	11.83	35.09	25	11.80	35.10	26.73
47	11.71	35.25	50	11.60	35.24	26.87
71	10.75	35.18	75	10.55	35.16	27.00
95	9.88	35.08	100	9.80	35.08	27.06
141	9.06	35.11	150	8.80	35.10	27.25
188	7.75	35.06	200	7.50	35.05	27.40
283	*6.25	35.00	300	5.90	34.98	27.57
350	4.97	34.91	400	4.50	34.90	27.67
530	3.89	34.89	600	3.75	34.89	27.74
713	3.66	34.895	800	3.60	34.89	27.76
905	3.52	34.89	1,000	3.50	34.89	27.77
1,406	3.42	34.91				

Station 6144; May 21; latitude 41°53′ N., longitude 50°16′ W.; depth 3,566 m.; dynamic height 970.945.

Observed values			Scaled values			
Depth, meters	Temperature, ° C.	Salinity, ‰	Depth, meters	Temperature, ° C.	Salinity, ‰	σ_t
0	8.13	33.20	0	8.13	33.20	25.87
27	2.93	33.27	25	3.20	33.25	26.50
53	2.40	33.70	50	2.50	33.64	26.86
80	1.80	34.01	75	1.80	33.96	27.17
106	2.45	34.23	100	2.25	34.18	27.31
160	3.45	34.50	150	3.30	34.45	27.44
213	3.83	34.66	200	3.70	34.61	27.53
319	*5.12	35.05	300	4.90	35.01	27.72
426	5.31	35.08	400	5.20	35.08	27.72
637	4.64	35.04	600	4.80	35.05	27.76
847	4.07	34.98	800	4.15	34.99	27.78
1,060	3.77	34.955	1,000	3.85	34.96	27.79
1,594	3.48	34.94				

Station 6145; May 21; latitude 41°27.5′ N., longitude 50°18′ W.; depth 3,749 m.; dynamic height 970.944.

Observed values			Scaled values			
Depth, meters	Temperature, ° C.	Salinity, ‰	Depth, meters	Temperature, ° C.	Salinity, ‰	σ_t
0	8.09	33.10	0	8.09	33.10	25.79
24	2.90	33.19	25	2.85	33.21	26.50
48	2.57	33.72	50	2.50	33.77	26.97
72	2.34	34.12	75	2.30	34.12	27.27
96	1.88	34.16	100	1.90	34.16	27.33
144	1.96	34.31	150	2.05	34.34	27.46
192	3.52	34.60	200	3.60	34.63	27.55
288	4.46	34.86	300	4.55	34.88	27.65
391	4.95	35.01	400	4.95	35.01	27.71
587	4.20	34.96	600	4.15	34.96	27.76
786	3.87	34.94	800	3.85	34.94	27.77
988	3.79	34.94	1,000	3.80	34.94	27.78
1,506	3.56	34.955				

Station 6146; May 22; latitude 41°02.5′ N., longitude 50°17′ W.; depth 4,115 m.; dynamic height 971.099.

Observed values			Scaled values			
Depth, meters	Temperature, ° C.	Salinity, ‰	Depth, meters	Temperature, ° C.	Salinity, ‰	σ_t
0	12.80	33.94	0	12.80	33.94	25.63
24	7.67	33.85	25	7.65	33.85	26.44
47	7.25	33.90	50	7.25	33.90	26.53
188	7.81	34.86	75	7.35	34.00	26.60
281	6.47	34.74	100	7.50	34.16	26.71
286	5.46	34.78	150	7.75	34.57	27.00
406	3.72	34.70	200	7.65	34.85	27.23
511	4.63	34.91	300	5.65	34.75	27.42
648	4.15	34.90	400	3.75	34.70	27.59
1,005	3.93	34.96	600	4.35	34.90	27.69
			800	4.00	34.92	27.75
			1,000	3.95	34.96	27.78

Station 6147; May 22; latitude 42°01.5′ N., longitude 49°29′ W.; depth 2,926 m.; dynamic height 970.927.

Observed values			Scaled values			
Depth, meters	Temperature, ° C.	Salinity, ‰	Depth, meters	Temperature, ° C.	Salinity, ‰	σ_t
0	8.00	33.42	0	8.00	33.42	26.06
24	6.63	33.41	25	6.25	33.41	26.29
47	2.37	33.76	50	2.35	33.82	27.02
396	4.73	34.99	75	2.75	34.22	27.31
589	4.05	34.95	100	3.25	34.40	27.40
779	3.95	34.96	150	3.80	34.62	27.53
977	3.78	34.955	200	4.15	34.77	27.61
1,479	3.52	34.945	300	4.60	34.93	27.68
			400	4.75	34.99	27.71
			600	4.05	34.95	27.76
			800	3.90	34.96	27.79
			1,000	3.75	34.95	27.79

Station 6148; May 22; latitude 41°31.5′ N., longitude 48°57′ W.; depth 3,319 m.; dynamic height 971.005.

Observed values			Scaled values			
Depth, meters	Temperature, ° C.	Salinity, ‰	Depth, meters	Temperature, ° C.	Salinity, ‰	σ_t
0	10.76	33.43	0	10.76	33.43	25.61
25	6.84	33.67	25	6.84	33.67	26.42
50	9.14	34.42	50	9.14	34.42	26.66
76	10.04	35.04	75	10.05	35.04	26.99
101	9.36	35.06	100	9.35	35.06	27.13
150	7.20	34.72	150	7.18	34.72	27.19
200	4.22	34.50	200	4.21	34.50	27.39
301	4.55	34.82	300	4.55	34.82	27.61
355	5.95	35.11	400	5.80	35.11	27.69
520	5.17	35.08	600	4.70	35.04	27.76
679	4.40	35.01	800	4.15	34.98	27.77
858	4.06	34.97	1,000	3.90	34.96	27.79
1,321	3.59	34.94				

Station 6149; May 22; latitude 41°01′ N., longitude 48°31′ W.; depth 3,712 m.; dynamic height 971.061.

Observed values			Scaled values			
Depth, meters	Temperature, ° C.	Salinity, ‰	Depth, meters	Temperature, ° C.	Salinity, ‰	σ_t
0	11.53	33.52	0	11.53	33.52	25.55
26	5.45	33.30	25	5.50	33.30	26.28
51	6.62	33.81	50	6.55	33.80	26.56
77	10.02	34.89	75	9.90	34.80	26.83
103	9.90	34.94	100	9.95	34.94	26.93
153	5.27	34.30	150	5.55	34.33	27.10
205	3.27	34.26	200	3.35	34.26	27.28
308	3.86	34.62	300	3.80	34.59	27.50
424	4.45	34.87	400	4.35	34.83	27.63
634	4.66	34.99	600	4.65	34.98	27.72
844	4.05	34.95	800	4.15	34.96	27.76
1,059	3.98	34.98	1,000	4.00	34.97	27.78
1,605	3.48	34.94				

Station 6150; May 23; latitude 41°38′ N., longitude 47°12′ W.; depth 4,298 m.; dynamic height 971.350.

Observed values			Scaled values			
Depth, meters	Temperature, ° C.	Salinity, ‰	Depth, meters	Temperature, ° C.	Salinity, ‰	σ_t
0	18.37	36.10	0	18.37	36.10	26.04
25	17.36	36.16	25	17.36	36.16	26.33
50	17.06	36.24	50	17.06	36.24	26.47
75	16.66	36.24	75	16.66	36.24	26.56
100	16.17	36.15	100	16.17	36.15	26.61
150	15.12	35.95	150	15.12	35.95	26.70
199	13.74	35.66	200	13.70	35.66	26.78
299	13.09	35.66	300	13.05	35.66	26.91
398	11.07	35.39	400	11.05	35.38	27.07
595	6.82	35.00	600	6.70	35.00	27.48
791	4.88	34.99	800	4.85	34.99	27.70
990	4.66	35.02	1,000	4.65	35.02	27.76
1,486	3.63	34.94				

Table of Oceanographic Data—Continued

STATIONS OCCUPIED IN 1956—Continued

Station 6151; May 23; latitude 42°02′ N., longitude 47°46′ W.; depth 3,786 m.; dynamic height 971.269.

Observed values			Scaled values			
Depth, meters	Temperature, ° C.	Salinity, °/oo	Depth, meters	Temperature, ° C.	Salinity, °/oo	σ_t
0	17.51	35.62	0	17.51	35.62	25.89
26	16.03	36.02	25	16.05	36.02	26.54
52	15.32	35.89	50	15.35	35.90	26.60
78	15.17	35.94	75	15.20	35.94	26.67
104	14.27	35.78	100	14.35	35.80	26.75
155	13.82	35.74	150	13.85	35.74	26.81
206	13.35	35.69	200	13.40	35.69	26.86
310	11.68	35.45	300	11.80	35.47	27.01
409	9.53	35.24	400	9.70	35.26	27.22
610	6.24	35.03	600	6.35	35.04	27.56
807	4.48	34.945	800	4.50	34.95	27.71
1,011	4.05	34.95	1,000	4.05	34.95	27.76
1,524	3.79	34.97				

Station 6152; May 23; latitude 42°29.5′ N., longitude 48° 27′ W.; depth 3,219 m.; dynamic height 971.004.

Observed values			Scaled values			
Depth, meters	Temperature, ° C.	Salinity, °/oo	Depth, meters	Temperature, ° C.	Salinity, °/oo	σ_t
0	11.68	33.78	0	11.68	33.78	25.73
25	4.79	33.48	25	4.79	33.48	26.52
51	9.13	34.74	50	8.95	34.72	26.93
76	8.61	34.82	75	8.60	34.82	27.06
102	8.21	34.86	100	8.25	34.86	27.15
151	6.74	34.74	150	6.75	34.74	27.27
202	4.78	34.58	200	4.80	34.58	27.38
304	5.48	34.89	300	5.40	34.88	27.55
415	4.38	34.87	400	4.50	34.87	27.65
619	4.26	34.96	600	4.25	34.96	27.75
821	4.04	34.95	800	4.05	34.95	27.76
1,028	3.81	34.94	1,000	3.85	34.94	27.77
1,547	3.49	34.94				

Station 6153; May 23; latitude 42°41.5′ N., longitude 49°08′ W.; depth 2,378 m.; dynamic height 970.900.

Observed values			Scaled values			
Depth, meters	Temperature, ° C.	Salinity, °/oo	Depth, meters	Temperature, ° C.	Salinity, °/oo	σ_t
0	3.76	33.22	0	3.76	33.22	26.41
24	3.07	33.69	25	3.05	33.69	26.86
48	1.68	33.75	50	1.70	33.77	27.03
72	2.04	34.17	75	2.10	34.20	27.34
96	2.47	34.36	100	2.50	34.38	27.45
144	2.48	34.52	150	2.50	34.53	27.57
193	2.88	34.61	200	2.95	34.63	27.61
289	4.48	34.91	300	4.50	34.92	27.69
418	4.31	34.95	400	4.35	34.95	27.73
623	3.86	34.93	600	3.90	34.93	27.76
826	3.63	34.915	800	3.65	34.92	27.78
1,034	3.65	34.935	1,000	3.65	34.93	27.78
1,558	3.36	34.92				

Station 6154; May 24; latitude 43°26′ N., longitude 48°46′ W.; depth 2,012 m.; dynamic height 970.920.

Observed values			Scaled values			
Depth, meters	Temperature, ° C.	Salinity, °/oo	Depth, meters	Temperature, ° C.	Salinity, °/oo	σ_t
0	2.84	32.98	0	2.84	32.98	26.31
25	1.05	33.50	25	1.05	33.50	26.86
50	0.96	33.72	50	0.96	33.72	27.04
75	2.87	34.10	75	2.87	34.10	27.20
100	3.07	34.31	100	3.07	34.31	27.35
150	2.85	34.54	150	2.85	34.54	27.55
200	3.13	34.62	200	3.13	34.62	27.59
300	4.48	34.92	300	4.48	34.92	27.69
369	4.26	34.93	400	4.20	34.93	27.73
556	3.94	34.90	600	3.90	34.90	27.74
746	3.72	34.90	800	3.70	34.90	27.76
943	3.61	34.895	1,000	3.60	34.89	27.76
1,453	3.37	34.88				

Station 6155; May 24; latitude 43°13′ N., longitude 48°05′ W.; depth 3,383 m.; dynamic height 970.935.

Observed values			Scaled values			
Depth, meters	Temperature, ° C.	Salinity, °/oo	Depth, meters	Temperature, ° C.	Salinity, °/oo	σ_t
0	9.14	33.58	0	9.14	33.58	26.01
22	6.28	33.56	25	6.05	33.60	26.46
45	4.96	34.02	50	4.60	34.05	26.99
67	3.56	34.14	75	3.60	34.19	27.20
89	3.65	34.28	100	3.65	34.33	27.31
133	3.73	34.45	150	3.85	34.53	27.44
178	4.10	34.66	200	4.20	34.74	27.58
267	4.32	34.88	300	4.30	34.90	27.69
416	4.29	34.94	400	4.30	34.94	27.72
622	3.94	34.94	600	4.00	34.94	27.76
826	3.62	34.91	800	3.65	34.91	27.77
1,034	3.55	34.92	1,000	3.55	34.92	27.79
1,553	3.36	34.91				

Station 6156; May 24; latitude 43°02′ N., longitude 47°23′ W.; depth 3,658 m.; dynamic height 971.106.

Observed values			Scaled values			
Depth, meters	Temperature, ° C.	Salinity, °/oo	Depth, meters	Temperature, ° C.	Salinity, °/oo	σ_t
0	11.26	33.38	0	11.26	33.38	25.49
26	7.12	33.69	25	7.25	33.68	26.37
51	8.16	34.32	50	8.05	34.30	26.74
77	9.41	34.72	75	9.25	34.68	26.84
102	10.54	35.05	100	10.50	35.03	26.90
153	10.00	35.08	150	10.05	35.08	27.02
204	9.51	35.11	200	9.55	35.11	27.13
306	6.41	34.82	300	6.50	34.83	27.37
344	6.33	34.86	400	5.40	34.86	27.54
519	4.47	34.86	600	4.35	34.90	27.69
695	4.27	34.95	800	4.30	34.99	27.76
877	4.32	35.00	1,000	4.20	35.00	27.79
1,347	3.60	34.95				

Station 6157; May 24; latitude 42°31.5′ N., longitude 46°48′ W.; depth 4,152 m.; dynamic height 971.183.

Observed values			Scaled values			
Depth, meters	Temperature, ° C.	Salinity, °/oo	Depth, meters	Temperature, ° C.	Salinity, °/oo	σ_t
0	17.73	35.05	0	17.73	35.05	25.39
25	14.58	35.57	25	14.58	35.57	26.52
50	12.92	35.36	50	12.92	35.36	26.71
75	13.08	35.44	75	13.08	35.44	26.74
100	12.76	35.42	100	12.76	35.42	26.78
149	12.54	35.51	150	12.50	35.51	26.91
198	11.71	35.40	200	11.65	35.40	26.98
298	9.70	35.23	300	9.60	35.23	27.21
413	7.18	35.07	400	7.35	35.08	27.45
617	6.56	35.22	600	6.65	35.21	27.65
820	4.78	35.03	800	4.90	35.04	27.74
1,028	4.13	34.97	1,000	4.25	34.97	27.76
1,553	3.54	34.93				

Station 6158; May 24; latitude 42°19.5′ N., longitude 46°10′ W.; depth 4,572 m.; dynamic height 971.040.

Observed values			Scaled values			
Depth, meters	Temperature, ° C.	Salinity, °/oo	Depth, meters	Temperature, ° C.	Salinity, °/oo	σ_t
0	16.87	34.82	0	16.87	34.82	25.44
21	11.57	34.76	25	11.80	34.83	26.51
41	12.82	35.26	50	11.95	35.16	26.75
62	10.81	35.00	75	9.50	34.88	26.96
82	8.92	34.84	100	8.90	34.88	27.06
123	8.87	34.93	150	8.35	34.92	27.18
164	7.90	34.90	200	6.10	34.78	27.38
246	3.85	34.64	300	4.60	34.78	27.56
395	5.98	35.06	400	6.00	35.06	27.62
590	4.93	35.01	600	4.90	35.00	27.71
785	4.10	34.94	800	4.10	34.94	27.75
988	4.30	35.00	1,000	4.30	35.00	27.77
1,509	3.63	34.94				

Table of Oceanographic Data—Continued

STATIONS OCCUPIED IN 1956—Continued

Station 6159; May 25; latitude 42°45.5′ N., longitude 45°46′ W.; depth 4,663 m.; dynamic height 971.417.

Observed values			Scaled values			
Depth, meters	Temperature, ° C.	Salinity, ‰	Depth, meters	Temperature, ° C.	Salinity, ‰	σ_t
0	18.82	36.14	0	18.82	36.14	25.96
22	17.77	36.20	25	17.65	36.20	26.30
43	16.96	36.23	50	16.70	36.21	26.54
65	16.37	36.12	75	16.05	36.06	26.57
86	15.82	36.02	100	15.80	36.03	26.60
129	15.75	36.07	150	15.60	36.05	26.66
172	15.35	36.01	200	14.85	35.92	26.73
258	13.72	35.74	300	13.40	35.77	26.93
287	13.51	35.79	400	12.55	35.59	26.95
402	12.49	35.58	600	8.15	35.11	27.36
499	9.83	35.26	800	5.70	35.00	27.61
654	7.38	35.06	1,000	4.45	34.96	27.73
1,098	4.08	34.94				

Station 6160; May 25; latitude 43°10′ N., longitude 45°20′ W.; depth 4,663 m.; dynamic height 971.483.

Observed values			Scaled values			
Depth, meters	Temperature, ° C.	Salinity, ‰	Depth, meters	Temperature, ° C.	Salinity, ‰	σ_t
0	19.31	36.29	0	19.31	36.29	25.95
19	18.70	36.40	25	18.45	36.41	26.26
39	17.86	36.43	50	17.75	36.43	26.44
58	17.71	36.43	75	17.55	36.41	26.48
77	17.51	36.41	100	17.30	36.38	26.52
116	17.16	36.36	150	16.90	36.34	26.58
155	16.91	36.34	200	16.10	36.20	26.67
232	15.53	36.09	300	15.10	36.05	26.77
281	*15.34	36.095	400	13.60	35.78	26.89
411	13.44	35.75	600	9.25	35.22	27.27
532	11.05	35.45	800	5.30	34.92	27.60
681	7.21	34.94	1,000	4.10	34.91	27.73
1,079	3.94	34.91				

Station 6161; May 25; latitude 43°25.5′ N., longitude 45°52′ W.; depth 4,572 m.; dynamic height 971.369·

Observed values			Scaled values			
Depth, meters	Temperature, ° C.	Salinity, ‰	Depth, meters	Temperature, ° C.	Salinity, ‰	σ_t
0	17.37	35.80	0	17.37	35.80	26.06
28	15.37	35.84	25	15.60	35.83	26.50
56	15.05	35.75	50	15.05	35.76	26.56
85	15.43	36.04	75	15.35	35.93	26.63
112	15.34	36.04	100	15.40	36.04	26.70
169	14.63	35.96	150	14.85	35.99	26.79
225	13.86	35.78	200	14.20	35.86	26.82
337	12.76	35.60	300	13.15	35.65	26.88
422	11.45	35.45	400	11.85	35.50	27.02
631	6.41	34.92	600	7.15	34.98	27.40
837	4.91	34.96	800	5.00	34.95	27.66
1,053	4.79	35.04	1,000	4.80	35.02	27.74
1,606	3.71	34.96				

Station 6162; May 25; latitude 43°35.5′ N., longitude 46°27′ W.; depth 4,500 m.; dynamic height 971.306.

Observed values			Scaled values			
Depth, meters	Temperature, ° C.	Salinity, ‰	Depth, meters	Temperature, ° C.	Salinity, ‰	σ_t
0	17.69	36.02	0	17.69	36.02	26.15
24	17.12	35.98	25	17.05	35.98	26.27
47	15.20	35.90	50	15.20	35.90	26.64
70	15.20	35.95	75	15.10	35.94	26.69
93	14.80	35.86	100	14.80	35.86	26.69
141	14.84	35.90	150	14.65	35.88	26.74
188	13.96	35.78	200	13.70	35.74	26.84
413	9.73	35.19	300	11.85	35.46	26.99
614	6.25	34.94	400	10.00	35.21	27.14
813	5.05	35.095	600	6.40	34.94	27.47
1,021	4.65	35.04	800	5.10	35.09	27.75
1,550	3.60	34.94	1,000	4.65	35.04	27.77

Station 6163; May 25; latitude 43°37.5′ N., longitude 47°19′ W.; depth 4,115 m.; dynamic height 971.045.

Observed values			Scaled values			
Depth, meters	Temperature, ° C.	Salinity, ‰	Depth, meters	Temperature, ° C.	Salinity, ‰	σ_t
0	8.71	33.16	0	8.71	33.16	25.75
26	12.07	35.00	25	12.00	34.93	26.55
52	10.87	34.82	50	11.00	34.83	26.66
78	9.51	34.83	75	9.60	34.83	26.90
104	9.30	34.87	100	9.35	34.86	26.97
155	8.49	34.96	150	8.60	34.95	27.16
206	4.40	34.40	200	4.65	34.46	27.31
310	5.69	34.90	300	5.60	34.86	27.51
355	4.20	34.75	400	4.40	34.82	27.62
531	4.96	35.02	600	4.75	35.01	27.73
706	4.37	34.97	800	4.10	34.94	27.75
900	3.86	34.93	1,000	3.75	34.93	27.77
1,415	3.54	34.91				

Station 6164; May 25–26; latitude 43°50′ N., longitude 47°59′ W.; depth 3,841 m.; dynamic height 970.943.

Observed values			Scaled values			
Depth, meters	Temperature, ° C.	Salinity, ‰	Depth, meters	Temperature, ° C.	Salinity, ‰	σ_t
0	5.39	33.45	0	5.39	33.45	26.42
23	5.48	33.56	25	5.45	33.57	26.52
47	3.96	33.74	50	3.90	33.77	26.84
70	3.43	34.04	75	3.45	34.10	27.14
94	3.95	34.31	100	3.85	34.33	27.29
140	3.15	34.39	150	3.10	34.46	27.47
186	3.14	34.55	200	3.15	34.57	27.55
280	3.25	34.68	300	3.55	34.76	27.66
305	3.67	34.77	400	4.00	34.87	27.71
470	4.06	34.91	600	4.00	34.90	27.73
643	3.92	34.89	800	3.70	34.92	27.78
823	3.70	34.92	1,000	3.55	34.92	27,79
1,305	3.48	34.92				

Station 6165; May 26; latitude 43°58′ N., longitude 48°36′ W.; depth 3,109 m.; dynamic height 970.905.

Observed values			Scaled values			
Depth, meters	Temperature, ° C.	Salinity, ‰	Depth, meters	Temperature, ° C.	Salinity, ‰	σ_t
0	4.12	33.48	0	4.12	33.48	26.59
21	3.90	33.47	25	3.40	33.49	26.66
42	1.59	33.70	50	2.45	33.89	27.06
63	4.02	34.23	75	4.10	34.32	27.26
83	4.07	34.36	100	4.00	34.42	27.35
125	3.83	34.50	150	3.90	34.63	27.52
167	4.00	34.68	200	4.15	34.75	27.59
250	4.26	34.84	300	4.30	34.90	27.69
322	4.33	34.92	400	4.05	34.92	27.74
462	3.81	34.92	600	3.85	34.93	27.76
590	3.83	34.93	800	3.55	34.92	27.79
786	3.57	34.92	1,000	3.50	34.92	27.80
1,358	3.37	34.91				

Station 6166; May 26; latitude 44°04′ N., longitude 48°51′ W.; depth 1,646 m.; dynamic height 970.956.

Observed values			Scaled values			
Depth, meters	Temperature, ° C.	Salinity, ‰	Depth, meters	Temperature, ° C.	Salinity, ‰	σ_t
0	2.23	32.98	0	2.23	32.98	26.36
27	1.08	33.24	25	1.15	33.22	26.63
52	0.66	33.54	50	0.70	33.51	26.89
79	0.94	33.76	75	0.85	33.72	27.05
105	1.53	33.97	100	1.40	33.83	27.09
158	2.01	34.26	150	1.95	34.21	27.37
210	2.76	34.58	200	2.60	34.52	27.56
315	3.77	34.74	300	3.70	34.72	27.62
375	3.70	34.81	400	3.70	34.83	27.70
557	3.72	34.88	600	3.70	34.88	27.74
737	3.56	34.89	800	3.50	34.89	27.77
926	3.45	34.885	1,000	3.45	34.89	27.77
1,405	3.45	34.90				

Table of Oceanographic Data—Continued

STATIONS OCCUPIED IN 1956—Continued

Station 6167; May 26; latitude 44°06′ N., longitude 48°58′ W.; depth 835 m.; dynamic height 971.040.

Observed values: Depth, meters	Temperature, ° C.	Salinity, ‰	Scaled values: Depth, meters	Temperature, ° C.	Salinity, ‰	σ_t
0	1.26	32.90	0	1.26	32.90	26.36
25	−0.07	33.07	25	−0.07	33.07	26.57
50	−0.32	33.28	50	−0.32	33.28	26.75
75	−0.49	33.37	75	−0.49	33.37	26.83
101	−0.13	33.52	100	−0.15	33.51	26.94
151	1.28	33.97	150	1.30	33.96	27.21
201	1.57	34.18	200	1.55	34.18	27.36
302	2.10	34.38	300	2.10	34.38	27.48
388	2.33	34.44	400	2.40	34.45	27.52
583	3.49	34.79	600	3.55	34.82	27.71

Station 6168; May 26; latitude 44°08′ N., longitude 49°06′ W.; depth 162 m.; dynamic height 971.098.

Observed values: Depth, meters	Temperature, ° C.	Salinity, ‰	Scaled values: Depth, meters	Temperature, ° C.	Salinity, ‰	σ_t
0	2.86	33.02	0	2.86	33.02	26.34
25	2.74	33.02	25	2.74	33.02	26.35
49	−0.55	33.10	50	−0.60	33.10	26.61
74	−0.72	33.14	75	−0.70	33.14	26.66
98	−0.59	33.19	100	−0.60	33.19	26.69
147	0.26	33.61	150	0.30	33.65	27.02

Station 6169; May 26; latitude 44°10′ N., longitude 49°12′ W.; depth 56 m.; dynamic height 971.100.

Observed values: Depth, meters	Temperature, ° C.	Salinity, ‰	Scaled values: Depth, meters	Temperature, ° C.	Salinity, ‰	σ_t
0	3.43	33.04	0	3.43	33.04	26.30
26	2.62	33.08	25	2.65	33.08	26.41
42	0.87	33.09	(50)	0.20	33.09	26.57

Station 6170; May 26; latitude 44°11′N., longitude 49° 18′ W.; depth 46 m.; dynamic height 971.101.

Observed values: Depth, meters	Temperature, ° C.	Salinity, ‰	Scaled values: Depth, meters	Temperature, ° C.	Salinity, ‰	σ_t
0	3.91	33.05	0	3.91	33.05	26.26
24	3.55	33.06	25	3.45	33.06	26.31
34	1.97	33.10				

Station 6171; May 26; latitude 44°58′ N., longitude 49°18′ W.; depth 91 m.; dynamic height 971.098.

Observed values: Depth, meters	Temperature, ° C.	Salinity, ‰	Scaled values: Depth, meters	Temperature, ° C.	Salinity, ‰	σ_t
0	3.04	32.88	0	3.04	32.88	26.22
25	1.42	32.92	25	1.42	32.92	26.37
50	−0.55	33.04	50	−0.55	33.04	26.57
75	−0.62	33.20	75	−0.62	33.20	26.70

Station 6172; May 26; latitude 44°56.5′ N., longitude 49°05′ W.; depth 95 m.; dynamic height 971.094.

Observed values: Depth, meters	Temperature, ° C.	Salinity, ‰	Scaled values: Depth, meters	Temperature, ° C.	Salinity, ‰	σ_t
0	1.54	32.83	0	1.54	32.83	26.29
25	−0.10	32.98	25	−0.10	32.98	26.50
50	−0.77	33.07	50	−0.77	33.07	26.60
75	−0.93	33.14	75	−0.93	33.14	26.67

Station 6173; May 26; latitude 44°55′ N.; longitude 48°58′ W.; depth 686 m.; dynamic height 971.101.

Observed values: Depth, meters	Temperature, ° C.	Salinity, ‰	Scaled values: Depth, meters	Temperature, ° C.	Salinity, ‰	σ_t
0	1.22	32.81	0	1.22	32.81	26.31
22	0.36	32.89	25	0.20	32.90	26.42
43	−0.69	33.00	50	−0.85	33.03	26.57
64	−1.00	33.07	75	−1.05	33.08	26.62
86	−1.04	33.09	100	−1.00	33.11	26.64
129	−0.76	33.19	150	−0.35	33.36	26.81
173	0.08	33.58	200	0.55	33.75	27.09
259	1.34	34.10	300	2.00	34.34	27.46
341	2.58	34.54	400	2.85	34.61	27.61
537	3.15	34.72	(600)	3.20	34.75	27.69

Station 6174; May 27; latitude 44°53.5′ N., longitude 48°47′ W.; depth 1,170 m.; dynamic height 971.035.

Observed values: Depth, meters	Temperature, ° C.	Salinity, ‰	Scaled values: Depth, meters	Temperature, ° C.	Salinity, ‰	σ_t
0	1.31	32.92	0	1.31	32.92	26.38
27	0.62	33.14	25	0.65	33.13	26.59
53	0.13	33.32	50	0.20	33.29	26.73
80	−0.22	33.52	75	−0.20	33.48	26.91
105	0.08	33.66	100	0.00	33.63	27.02
159	0.77	33.86	150	0.65	33.83	27.14
212	1.27	34.06	200	1.15	34.01	27.26
317	2.25	34.44	300	2.10	34.39	27.49
317	2.22	34.46	400	2.90	34.64	27.63
480	3.41	34.76	600	3.70	34.84	27.71
647	3.74	34.86	800	3.75	34.88	27.73
835	3.72	34.88	(1,000)	3.70	34.89	27.75

Station 6175; May 27; latitude 44°50.5′ N., longitude 48°33′ W.; depth 1,829 m.; dynamic height 970.911.

Observed values: Depth, meters	Temperature, ° C.	Salinity, ‰	Scaled values: Depth, meters	Temperature, ° C.	Salinity, ‰	σ_t
0	2.76	33.26	0	2.76	33.26	26.54
26	2.73	33.37	25	2.75	33.37	26.63
51	1.47	33.96	50	1.50	33.94	27.18
77	1.82	34.12	75	1.80	34.10	27.29
102	2.28	34.29	100	2.25	34.27	27.39
152	2.28	34.42	150	2.30	34.41	27.50
203	2.56	34.57	200	2.55	34.56	27.60
305	3.47	34.76	300	3.45	34.75	27.66
418	3.69	34.86	400	3.70	34.85	27.72
627	3.67	34.90	600	3.70	34.90	27.76
837	3.60	34.88	800	3.60	34.89	27.76
1,054	3.61	-------	1,000	3.60	34.94	27.80
1,610	3.41	34.92				

Station 6176; May 27; latitude 44°45′ N., longitude 47°54′ W.; depth 3,182 m.; dynamic height 970.916.

Observed values: Depth, meters	Temperature, ° C.	Salinity, ‰	Scaled values: Depth, meters	Temperature, ° C.	Salinity, ‰	σ_t
0	6.71	33.76	0	6.71	33.76	26.51
17	6.63	33.77	25	6.15	33.85	26.65
33	5.49	33.94	50	4.30	34.10	27.06
50	4.30	34.09	75	4.40	34.35	27.25
100	4.47	34.57	100	4.50	34.57	27.41
133	4.58	34.64	150	4.60	34.70	27.50
199	4.63	34.87	200	4.65	34.87	27.64
379	4.51	34.94	300	4.60	34.92	27.68
574	4.08	34.95	400	4.45	34.94	27.71
773	3.82	34.93	600	4.05	34.95	27.76
980	3.65	34.93	800	3.80	34.93	27.77
1,511	3.42	34.91	1,000	3.65	34.93	27.78

STATIONS OCCUPIED IN 1956—Continued

Station 6177; May 27; latitude 44°38.5′ N., longitude 47°16′ W.; depth 3,658 m.; dynamic height 970.943.

Observed values			Scaled values			
Depth, meters	Temperature, ° C.	Salinity, °/oo	Depth, meters	Temperature, ° C.	Salinity, °/oo	σ_t
0	7.53	33.62	0	7.53	33.62	26.28
24	7.47	33.65	25	7.45	33.66	26.33
48	6.09	34.13	50	5.80	34.13	26.91
72	3.77	34.13	75	3.70	34.13	27.14
95	3.52	34.26	100	3.55	34.29	27.28
144	4.33	34.62	150	4.35	34.64	27.48
192	4.13	34.72	200	4.15	34.73	27.57
287	4.49	34.86	300	4.45	34.87	27.66
377	*4.24	34.93	400	4.20	34.93	27.73
568	4.08	34.945	600	4.05	34.94	27.75
762	3.78	34.93	800	3.75	34.93	27.77
968	3.70	34.93	1,000	3.70	34.93	27.78
1,511	3.43	34.92				

Station 6178; Mny 27; latitude 44°31.5′ N., longitude 46°37′ W; depth 3,841 m; dynamic height 970.974

Observed values			Scaled values			
Depth, meters	Temperature, ° C.	Salinity, °/oo	Depth, meters	Temperature, ° C.	Salinity, °/oo	σ_t
0	7.87	33.56	0	7.87	33.56	26.18
23	7.80	33.57	25	7.75	33.59	26.22
46	5.32	33.89	50	5.20	33.90	26.81
69	4.96	33.96	75	4.65	33.99	26.93
93	3.33	34.08	100	3.40	34.14	27.18
138	4.09	34.53	150	4.25	34.57	27.44
184	4.38	34.66	200	4.40	34.69	27.51
277	4.46	34.84	300	4.45	34.86	27.65
350	4.35	34.90	400	4.35	34.93	27.71
528	4.43	34.98	600	4.35	34.96	27.74
708	4.00	34.93	800	3.90	34.93	27.76
919	3.79	34.93	1,000	3.75	34.93	27.77
1,508	3.48	34.92				

Station 6179; May 28; latitude 44°25′ N., longitude 45′59° W.; depth 3,951 m.; dynamic height 970.980.

Observed values			Scaled values			
Depth, meters	Temperature, ° C.	Salinity, °/oo	Depth, meters	Temperature, ° C.	Salinity, °/oo	σ_t
0	7.79	33.62	0	7.79	33.62	26.25
25	7.75	33.61	25	7.75	33.61	26.24
49	4.38	33.77	50	4.25	33.77	26.80
73	3.29	33.96	75	3.25	33.97	27.06
97	3.33	34.14	100	3.25	34.16	27.21
147	5.33	34.63	150	5.25	34.63	27.37
196	4.42	34.62	200	4.40	34.62	27.46
293	4.45	34.82	300	4.45	34.83	27.62
402	4.53	34.93	400	4.50	34.93	27.69
599	4.22	34.95	600	4.20	34.95	27.75
795	3.86	34.93	800	3.85	34.93	27.76
1,002	3.73	34.925	1,000	3.75	34.92	27.77
1,534	3.46	34.92				

Station 6180; May 28; latitude 44°18.5′ N., longitude 45°20′ W.; depth 4,481 m.; dynamic height 971.015.

Observed values			Scaled values			
Depth, meters	Temperature, ° C.	Salinity, °/oo	Depth, meters	Temperature, ° C.	Salinity, °/oo	σ_t
0	8.90	33.99	0	8.90	33.99	26.36
21	9.04	34.01	25	8.65	34.03	26.43
42	7.33	34.16	50	7.30	34.26	26.82
63	7.30	34.46	75	6.65	34.39	27.00
84	6.23	34.32	100	6.50	34.41	27.04
126	6.98	34.58	150	5.55	34.46	27.20
168	4.62	34.37	200	4.45	34.45	27.32
252	4.27	34.61	300	4.10	34.67	27.54
320	*4.03	34.70	400	4.50	34.85	27.63
485	5.04	35.02	600	4.45	34.98	27.74
656	4.14	34.96	800	3.95	34.95	27.77
838	3.93	34.95	1,000	3.75	34.94	27.78
1,317	3.52	34.92				

Station 6181; May 28; latitude 44°49.5′ N., longitude 45°15′ W.; depth 4,207 m.; dynamic height 971.046.

Observed values			Scaled values			
Depth, meters	Temperature, ° C.	Salinity, °/oo	Depth, meters	Temperature, ° C.	Salinity, °/oo	σ_t
0	8.64	33.78	0	8.64	33.78	26.24
27	8.69	33.82	25	8.70	33.82	26.26
52	6.46	34.06	50	6.60	34.03	26.72
79	6.68	34.32	75	6.60	34.28	26.92
105	7.63	34.58	100	7.45	34.53	27.00
158	7.34	34.75	150	7.40	34.74	27.18
210	6.12	34.66	200	6.30	34.67	27.28
315	6.25	34.97	300	6.25	34.94	27.49
434	5.26	34.975	400	5.50	34.97	27.61
649	4.48	34.96	600	4.60	34.96	27.71
865	4.01	34.995	800	4.15	34.98	27.77
1,085	3.70	34.95	1,000	3.80	34.97	27.81
1,640	3.44	34.925				

Station 6182; May 28; latitude 45°21.5′ N., longitude 45°16′ W.; depth 4,262 m.; dynamic height 971.001.

Observed values			Scaled values			
Depth, meters	Temperature, ° C.	Salinity, °/oo	Depth, meters	Temperature, ° C.	Salinity, °/oo	σ_t
0	8.90	34.02	0	8.90	34.02	26.39
26	8.58	34.18	25	8.60	34.18	26.56
51	7.50	34.52	50	7.55	34.52	26.98
77	5.80	34.30	75	5.80	34.31	27.06
102	7.15	34.68	100	7.05	34.66	27.17
153	6.69	34.72	150	6.70	34.72	27.26
204	6.41	34.79	200	6.45	34.78	27.34
306	4.74	34.74	300	4.80	34.74	27.51
387	4.73	34.87	400	4.70	34.89	27.64
584	4.66	35.00	600	4.60	35.00	27.74
784	4.09	34.96	800	4.05	34.96	27.77
987	3.77	34.935	1,000	3.75	34.94	27.78
1,509	3.43	34.91				

Table of Oceanographic Data—Continued

STATIONS OCCUPIED IN 1956—Continued

Station 6183; May 28; latitude 45°23′ N., longitude 46°02′ W.; depth 3,521 m.; dynamic height 970.935.

Observed values			Scaled values			
Depth, meters	Temperature, ° C.	Salinity, ‰	Depth, meters	Temperature, ° C.	Salinity, ‰	σ_t
0	4.43	33.48	0	4.43	33.48	26.56
26	4.44	33.49	25	4.45	33.49	26.56
51	3.77	33.86	50	3.80	33.85	26.91
77	3.99	34.17	75	4.00	34.15	27.13
102	3.99	34.30	100	4.00	34.29	27.24
153	2.94	34.40	150	3.00	34.39	27.42
204	3.74	34.62	200	3.70	34.60	27.52
306	4.04	34.87	300	4.05	34.86	27.69
395	4.00	34.90	400	4.00	34.90	27.73
594	3.82	34.91	600	3.80	34.91	27.76
793	3.73	34.92	800	3.75	34.92	27.77
993	3.51	34.91	1,000	3.50	34.91	27.79
1,494	3.38	34.90				

Station 6184; May 28; latitude 45°24.5′ N., longitude 46°40′ W.; depth 3,292 m.; dynamic height 970.967.

Observed values			Scaled values			
Depth, meters	Temperature, ° C.	Salinity, ‰	Depth, meters	Temperature, ° C.	Salinity, ‰	σ_t
0	6.81	33.92	0	6.81	33.92	26.61
25	6.80	33.93	25	6.80	33.93	26.62
49	5.80	34.05	50	5.70	34.05	26.86
74	4.87	34.09	75	4.85	34.09	26.99
98	4.71	34.29	100	4.70	34.30	27.17
146	4.92	34.54	150	4.90	34.55	27.35
196	4.36	34.60	200	4.40	34.61	27.46
294	4.68	34.88	300	4.70	34.89	27.64
313	4.69	34.90	400	4.55	34.93	27.69
472	4.26	34.94	600	3.85	34.91	27.75
633	3.79	34.90	800	3.75	34.90	27.75
812	3.77	34.905	1,000	3.70	34.91	27.77
1,296	3.57	34.93				

Station 6185; May 29; latitude 45°24′ N., longitude 47°22′ W.; depth 2,743 m.; dynamic height 970.934.

Observed values			Scaled values			
Depth, meters	Temperature, ° C.	Salinity, ‰	Depth, meters	Temperature, ° C.	Salinity, ‰	σ_t
0	3.19	33.50	0	3.19	33.50	26.69
19	3.14	33.51	25	3.90	33.66	26.76
38	5.38	34.02	50	4.70	34.02	26.96
57	4.07	34.01	75	1.75	33.96	27.17
76	1.81	33.96	100	2.45	34.15	27.27
114	2.80	34.25	150	2.30	34.33	27.43
152	2.29	34.34	200	3.20	34.57	27.45
228	3.71	34.70	300	3.80	34.83	27.69
286	3.76	34.81	400	4.10	34.91	27.73
426	4.14	34.92	600	3.85	34.90	27.74
564	3.89	34.90	800	3.70	34.91	27.77
728	3.74	34.915	1,000	3.55	34.91	27.78
1,178	3.43	34.91				

Station 6186; May 29; latitude 45°37′ N., longitude 47°40′ W.; depth 1,417 m.; dynamic height 970.914.

Observed values			Scaled values			
Depth, meters	Temperature, ° C.	Salinity, ‰	Depth, meters	Temperature, ° C.	Salinity, ‰	σ_t
0	2.36	33.27	0	2.36	33.27	26.58
26	3.62	33.58	25	3.65	33.58	26.71
51	3.88	34.02	50	3.85	34.01	27.04
76	3.30	34.20	75	3.30	34.20	27.24
101	3.71	34.45	100	3.70	34.44	27.39
152	4.60	34.71	150	4.60	34.70	27.50
203	4.57	34.81	200	4.60	34.80	27.58
304	4.78	34.96	300	4.75	34.96	27.69
342	4.59	34.96	400	4.35	34.95	27.73
532	3.92	34.92	600	3.75	34.91	27.76
735	3.55	34.90	800	3.50	34.89	27.77
925	3.42	34.88	1,000	3.40	34.88	27.77
1,183	3.38	34.89				

Station 6187; May 29; latitude 45°45′ N., longitude 47°58′ W.; depth 640 m.; dynamic height 971.031.

Observed values			Scaled values			
Depth, meters	Temperature, ° C.	Salinity, ‰	Depth, meters	Temperature, ° C.	Salinity, ‰	σ_t
0	0.96	32.94	0	0.96	32.94	26.42
26	0.53	32.99	25	0.55	32.99	26.48
51	−0.25	33.24	50	−0.25	33.23	26.71
77	−0.77	33.37	75	−0.75	33.36	26.83
103	−0.23	33.58	100	−0.30	33.55	26.97
153	1.07	34.01	150	1.00	33.98	27.24
205	1.62	34.18	200	1.60	34.17	27.36
308	2.49	34.54	300	2.40	34.52	27.58
384	2.98	34.65	400	3.10	34.67	27.64
590	3.68	34.82	600	3.70	34.83	27.70

Station 6188; May 29; latitude 45°49.5′ N., longitude 48°07′ W.; depth 176 m.; dynamic height 971.057.

Observed values			Scaled values			
Depth, meters	Temperature, ° C.	Salinity, ‰	Depth, meters	Temperature, ° C.	Salinity, ‰	σ_t
0	0.26	32.91	0	0.26	32.91	26.43
24	0.04	32.92	25	0.05	32.92	26.45
48	−0.40	32.98	50	−0.50	33.00	26.54
72	−1.38	33.25	75	−1.35	33.29	26.79
96	−0.70	33.43	100	−0.65	33.44	26.90
145	−0.06	33.59	150	0.00	33.60	27.00

Station 6189; May 29; latitude 45°52.5′ N., longitude 48°14′ W.; depth 121 m.; dynamic height 971.069.

Observed values			Scaled values			
Depth, meters	Temperature, ° C.	Salinity, ‰	Depth, meters	Temperature, ° C.	Salinity, ‰	σ_t
0	1.31	32.83	0	1.31	32.83	26.31
25	1.02	32.85	25	1.02	32.85	26.35
49	0.13	32.97	50	0.10	32.98	26.50
74	−0.74	33.20	75	−0.75	33.20	26.71
98	−0.85	33.30	100	−0.85	33.31	26.79

Table of Oceanographic Data—Continued

STATIONS OCCUPIED IN 1956—Continued

Station 6190; May 29; latitude 45°59′ N., longitude 48°31′ W.; depth 93 m.; dynamic height 971.071.

Observed values			Scaled values			
Depth, meters	Temperature, °C.	Salinity, ‰	Depth, meters	Temperature, °C.	Salinity, ‰	σ_t
0	2.66	32.99	0	2.66	32.99	26.34
26	2.65	32.99	25	2.65	32.99	26.34
52	1.29	33.01	50	1.45	33.00	26.44
78	−0.39	33.26	75	−0.25	33.23	26.71

Station 6191; May 29; latitude 46°06′ N., longitude 48°42′ W.; depth 70 m.; dynamic height 971.071.

Observed values			Scaled values			
Depth, meters	Temperature, °C.	Salinity, ‰	Depth, meters	Temperature, °C.	Salinity, ‰	σ_t
0	2.34	33.00	0	2.34	33.00	26.37
28	2.32	33.01	25	2.35	33.01	26.38
56	1.50	33.01	50	1.70	33.01	26.43

Station 6192; May 29; latitude 46°17′ N., longitude 48°58′ W.; depth 68 m.; dynamic height 971.071.

Observed values			Scaled values			
Depth, meters	Temperature, °C.	Salinity, ‰	Depth, meters	Temperature, °C.	Salinity, ‰	σ_t
0	3.20	32.99	0	3.20	32.99	26.29
27	3.20	33.00	25	3.20	33.00	26.30
54	0.92	33.10	50	1.15	33.08	26.52

Station 6193; May 29; latitude 46°14.5′ N., longitude 48°34′ W.; depth 91 m.; dynamic height 971.071.

Observed values			Scaled values			
Depth, meters	Temperature, °C.	Salinity, ‰	Depth, meters	Temperature, °C.	Salinity, ‰	σ_t
0	2.65	33.00	0	2.65	33.00	26.35
25	2.66	33.02	25	2.66	33.02	26.36
50	1.90	33.02	50	1.90	33.02	26.42
75	0.19	33.21	75	0.19	33.21	26.68

Station 6194; May 29–30; latitude 46°12′ N., longitude 48°02′ W.; depth 114 m.; dynamic height 971.076.

Observed values			Scaled values			
Depth, meters	Temperature, °C.	Salinity, ‰	Depth, meters	Temperature, °C.	Salinity, ‰	σ_t
0	2.13	32.93	0	2.13	32.93	26.33
23	2.13	32.93	25	2.10	32.93	26.33
47	1.35	32.91	50	1.25	32.91	26.37
70	0.63	32.96	75	0.45	33.05	26.54
93	−0.29	33.39	(100)	−0.55	33.53	26.96

Station 6195; May 30; latitude 46°10.5′ N., longitude 47°43′ W.; depth 170 m.; dynamic height 971.090.

Observed values			Scaled values			
Depth, meters	Temperature, °C.	Salinity, ‰	Depth, meters	Temperature, °C.	Salinity, ‰	σ_t
0	0.61	32.80	0	0.61	32.80	26.33
25	0.25	32.83	25	0.25	32.83	26.37
50	−0.21	32.92	50	−0.21	32.92	26.46
74	−0.54	32.96	75	−0.55	32.96	26.50
99	−1.20	33.07	100	−1.20	33.08	26.62
148	−0.68	33.40	150	−0.65	33.42	26.89

Station 6196; May 30; latitude 46°10′ N., longitude 47°26′ W.; depth 695 m.; dynamic height 971.059.

Observed values			Scaled values			
Depth, meters	Temperature, °C.	Salinity, ‰	Depth, meters	Temperature, °C.	Salinity, ‰	σ_t
0	0.63	32.82	0	0.63	32.82	26.34
25	0.56	32.84	25	0.56	32.84	26.36
50	−0.64	33.00	50	−0.64	33.00	26.55
75	−1.26	33.13	75	−1.26	33.13	26.66
100	−1.38	33.20	100	−1.38	33.20	26.73
148	0.22	33.65	150	0.25	33.67	27.05
198	1.08	33.93	200	1.15	33.94	27.19
298	2.43	34.50	300	2.45	34.50	27.55
400	2.82	34.63	400	2.85	34.63	27.62
603	3.71	34.84	600	3.70	34.84	27.71

Station 6197; May 30; latitude 46°10′ N., longitude 47°08′ W.; depth 1,554 m.; dynamic height 970.902.

Observed values			Scaled values			
Depth, meters	Temperature, °C.	Salinity, ‰	Depth, meters	Temperature, °C.	Salinity, ‰	σ_t
0	2.35	33.21	0	2.35	33.21	26.54
25	3.35	33.71	25	3.35	33.71	26.85
50	2.48	33.99	50	2.48	33.99	27.14
75	3.56	34.30	75	3.56	34.30	27.29
101	3.25	-------	100	3.25	34.36	27.37
151	2.51	34.53	150	2.50	34.53	27.57
201	2.85	34.62	200	2.85	34.62	27.62
302	3.37	34.76	300	3.35	34.76	27.68
392	3.73	34.90	400	3.75	34.90	27.75
590	3.66	34.865	600	3.65	34.89	27.75
788	3.53	34.885	800	3.50	34.88	27.76
990	3.45	34.87	1,000	3.45	34.87	27.76
1,503	3.36	34.875				

Station 6198; May 30; latitude 46°09′ N., longitude 46°37′ W.; depth 512 m.; dynamic height 970.874.

Observed values			Scaled values			
Depth, meters	Temperature, °C.	Salinity, ‰	Depth, meters	Temperature, °C.	Salinity, ‰	σ_t
0	3.48	33.76	0	3.48	33.76	26.87
25	2.55	33.98	25	2.55	33.98	27.13
49	2.28	34.20	50	2.30	34.20	27.33
74	2.27	34.28	75	2.30	34.28	27.39
98	2.56	34.40	100	2.60	34.42	27.48
147	3.45	34.68	150	3.50	34.69	27.61
197	4.80	34.90	200	4.80	34.91	27.65
295	4.67	34.96	300	4.65	34.96	27.71
393	3.89	34.87	400	3.90	34.87	27.72
491	3.59	34.905				

Station 6199; May 30; latitude 46°05.5′ N., longitude 45°55′ W.; depth 1,646 m.; dynamic height 970.894.

Observed values			Scaled values			
Depth, meters	Temperature, °C.	Salinity, ‰	Depth, meters	Temperature, °C.	Salinity, ‰	σ_t
0	4.52	33.75	0	4.52	33.75	26.76
26	4.07	33.80	25	4.10	33.80	26.84
51	3.64	34.22	50	3.65	34.20	27.21
77	3.67	34.30	75	3.70	34.29	27.27
102	3.50	34.48	100	3.50	34.46	27.43
152	3.42	34.61	150	3.40	34.60	27.55
203	3.58	34.74	200	3.60	34.73	27.63
305	3.80	34.86	300	3.80	34.86	27.72
392	3.74	34.86	400	3.75	34.86	27.72
586	3.60	34.88	600	3.60	34.88	27.75
779	3.54	34.90	800	3.55	34.90	27.77
980	3.59	34.92	1,000	3.60	34.92	27.79
1,492	3.38	34.905				

Table of Oceanographic Data—Continued

STATIONS OCCUPIED IN 1956—Continued

Station 6200; May 30; latitude 46°01.5′ N., longitude 45°15′ W.; depth 3,292 m.; dynamic height 970.992.

Observed values			Scaled values			
Depth, meters	Temperature, ° C.	Salinity, °/₀₀	Depth, meters	Temperature, ° C.	Salinity, °/₀₀	σ_t
0	7.41	33.98	0	7.41	33.98	26.58
24	7.67	34.09	25	7.65	34.09	26.63
48	6.12	34.24	50	6.00	34.24	26.97
72	5.69	34.26	75	5.70	34.28	27.04
96	6.07	34.47	100	6.15	34.50	27.16
143	6.44	34.72	150	6.40	34.73	27.30
192	6.02	34.77	200	5.95	34.78	27.40
288	5.43	34.83	300	5.35	34.83	27.52
417	4.31	34.86	400	4.50	34.86	27.64
623	3.97	34.92	600	4.00	34.91	27.74
830	3.96	34.94	800	3.95	34.94	27.76
1,024	3.76	34.93	1,000	3.80	34.93	27.77
1,488	3.41	34.92				

Station 6201; May 30–31; latitude 46°01′ N., longitude 44°40′ W.; depth 3,475 m.; dynamic height 971.023.

Observed values			Scaled values			
Depth, meters	Temperature, ° C.	Salinity, °/₀₀	Depth, meters	Temperature, ° C.	Salinity, °/₀₀	σ_t
0	9.36	33.70	0	9.36	33.70	26.06
25	8.86	34.02	25	8.86	34.02	26.40
50	7.66	34.35	50	7.66	34.35	26.83
75	8.18	34.65	75	8.18	34.65	26.99
101	5.62	34.34	100	5.60	34.34	27.19
150	4.61	34.38	150	4.61	34.38	27.25
200	4.64	34.56	200	4.64	34.56	27.39
301	4.40	34.71	300	4.40	34.71	27.53
405	5.02	34.94	400	5.00	34.93	27.64
602	4.50	34.95	600	4.50	34.95	27.71
797	3.86	34.90	800	3.85	34.90	27.74
1,000	3.76	34.92	1,000	3.80	34.92	27.77
1,511	3.41	34.91				

Station 6202; May 31; latitude 46°22′ N., longitude 44°41′ W.; depth 1,390 m.; dynamic height 970.953.

Observed values			Scaled values			
Depth, meters	Temperature, ° C.	Salinity, °/₀₀	Depth, meters	Temperature, ° C.	Salinity, °/₀₀	σ_t
0	5.90	33.74	0	5.90	33.74	26.60
24	5.78	33.78	25	5.75	33.79	26.65
49	4.28	33.93	50	4.25	33.94	26.94
73	4.15	34.10	75	4.15	34.12	27.10
98	4.12	34.22	100	4.10	34.23	27.18
145	3.82	34.36	150	3.75	34.38	27.34
194	3.30	34.50	200	3.30	34.52	27.50
292	3.43	34.71	300	3.45	34.73	27.64
350	3.49	34.82	400	3.50	34.83	27.72
529	3.47	34.85	600	3.45	34.85	27.74
711	3.45	34.86	800	3.45	34.86	27.75
907	3.43	34.87	1,000	3.45	34.88	27.76
1,217	3.45	34.89				

Station 6203; May 31; latitude 46°28′ N., longitude 44°42′ W.; depth 421 m.; dynamic height 970.909.

Observed values			Scaled values			
Depth, meters	Temperature, ° C.	Salinity, °/₀₀	Depth, meters	Temperature, ° C.	Salinity, °/₀₀	σ_t
0	6.18	34.04	0	6.18	34.04	26.79
24	6.07	34.13	25	6.05	34.13	26.88
49	4.61	34.22	50	4.50	34.22	27.14
73	4.08	34.24	75	4.05	34.25	27.21
98	3.86	34.39	100	3.85	34.39	27.34
146	3.70	34.47	150	3.65	34.47	27.42
195	3.27	34.54	200	3.25	34.55	27.52
293	3.48	34.79	300	3.50	34.80	27.70
350	3.50	34.84	(400)	3.55	34.87	27.75

Station 6204; May 31; latitude 46°35′ N., longitude 44°41′ W.; depth 227 m.; dynamic height 970.881.

Observed values			Scaled values			
Depth, meters	Temperature, ° C.	Salinity, °/₀₀	Depth, meters	Temperature, ° C.	Salinity, °/₀₀	σ_t
0	5.70	34.14	0	5.70	34.14	26.93
23	5.46	34.20	25	5.40	34.20	27.01
46	4.46	34.30	50	4.25	34.32	27.24
69	3.86	34.42	75	3.85	34.43	27.37
92	3.81	34.45	100	3.80	34.46	27.40
138	3.28	34.50	150	3.30	34.53	27.50
184	3.34	34.66	(200)	3.40	34.73	27.65

Station 6205; May 31; latitude 46°40.5′ N., longitude 44°42′ W.; depth 172 m.; dynamic height 970.877.

Observed values			Scaled values			
Depth, meters	Temperature, ° C.	Salinity, °/₀₀	Depth, meters	Temperature, ° C.	Salinity, °/₀₀	σ_t
0	5.67	34.16	0	5.67	34.16	26.95
25	5.36	34.20	25	5.36	34.20	27.02
49	3.73	34.35	50	3.75	34.35	27.32
74	3.78	34.41	75	3.80	34.41	27.36
99	3.69	34.47	100	3.65	34.47	27.42
148	3.18	34.56	150	3.45	34.56	27.51

Station 6206; May 31; latitude 46°49.5′ N., longitude 44°43′ W.; depth 139 m.; dynamic height 970.890.

Observed values			Scaled values			
Depth, meters	Temperature, ° C.	Salinity, °/₀₀	Depth, meters	Temperature, ° C.	Salinity, °/₀₀	σ_t
0	5.76	34.12	0	5.76	34.12	26.91
24	5.42	34.16	25	5.40	34.16	26.98
49	5.20	34.19	50	5.15	34.19	27.03
73	3.82	34.37	75	3.80	34.38	27.33
98	3.53	34.39	100	3.50	34.39	27.37
127	3.33	34.44				

Station 6207; May 31; latitude 46°50.5′ N., longitude 44°54′ W.; depth 159 m.; dynamic height 970.897.

Observed values			Scaled values			
Depth, meters	Temperature, ° C.	Salinity, °/₀₀	Depth, meters	Temperature, ° C.	Salinity, °/₀₀	σ_t
0	5.97	34.12	0	5.97	34.12	26.88
26	5.81	34.11	25	5.80	34.11	26.90
52	4.00	34.20	50	4.05	34.19	27.16
78	3.80	34.28	75	3.85	34.27	27.25
104	3.66	34.35	100	3.70	34.34	27.31
157	3.37	34.41	150	3.40	34.40	27.39

Station 6208; May 31; latitude 46°50′ N., longitude 45°20′ W.; depth 224 m.; dynamic height 970.886.

Observed values			Scaled values			
Depth, meters	Temperature, ° C.	Salinity, °/₀₀	Depth, meters	Temperature, ° C.	Salinity, °/₀₀	σ_t
0	5.74	34.12	0	5.74	34.12	26.91
22	5.66	34.12	25	5.60	34.13	26.93
44	4.39	34.22	50	4.15	34.23	27.18
67	3.88	34.25	75	3.85	34.27	27.25
89	3.79	34.33	100	3.60	34.38	27.35
133	3.16	34.51	150	3.25	34.57	27.54
177	3.48	34.65	(200)	3.55	34.71	27.62

STATIONS OCCUPIED IN 1956—Continued

Station 6209; May 31; latitude 46°51′ N., longitude 45°42′ W.; depth 263 m.; dynamic height 970.875.

Observed values			Scaled values			
Depth, meters	Temperature, °C.	Salinity, ‰	Depth, meters	Temperature, °C.	Salinity, ‰	σ_t
0	5.55	34.15	0	5.55	34.15	26.96
24	5.45	34.15	25	5.45	34.15	26.97
46	3.96	34.24	50	3.90	34.25	27.22
70	3.82	34.30	75	3.75	34.32	27.29
93	3.42	34.42	100	3.40	34.45	27.43
140	3.34	34.58	150	3.40	34.62	27.57
187	3.58	34.77	200	3.60	34.79	27.68
222	3.58	34.82				

Station 6210; May 31; latitude 46°50.5′ N., longitude 45°59′ W.; depth 326 m.; dynamic height 970.896.

0	5.47	34.14	0	5.47	34.14	26.96
26	5.45	34.14	25	5.45	34.14	26.96
52	5.15	34.16	50	5.20	34.16	27.01
78	4.07	34.26	75	4.20	34.25	27.19
104	3.59	34.32	100	3.65	34.31	27.30
155	3.32	34.56	150	3.35	34.54	27.50
207	3.45	34.72	200	3.45	34.70	27.62
311	3.55	34.86	300	3.60	34.85	27.73

Station 6211; May 31; latitude 46°50′ N., longitude 46°24° W.; depth 657 m.; dynamic height 970.881.

0	3.90	33.74	0	3.90	33.74	26.82
25	3.89	33.77	25	3.89	33.77	26.84
50	2.52	34.08	50	2.52	34.08	27.21
75	2.93	34.32	75	2.93	34.32	27.37
100	2.91	34.47	100	2.91	34.47	27.49
150	3.05	34.60	150	3.05	34.60	27.58
200	3.59	34.74	200	3.59	34.74	27.64
300	3.92	34.89	300	3.92	34.89	27.72
412	3.49	34.88	400	3.55	34.88	27.75
618	3.49	34.90	600	3.50	34.90	27.78

Station 6212; May 31; latitude 46°48.5′ N., longitude 46°43′ W.; depth 1,225 m.; dynamic height 970.914.

0	2.07	33.26	0	2.07	33.26	26.60
25	2.32	33.44	25	2.32	33.44	26.72
49	2.18	33.78	50	2.15	33.80	27.02
74	1.16	34.06	75	1.15	34.07	27.31
98	2.28	34.24	100	2.35	34.26	27.37
147	3.10	34.51	150	3.10	34.52	27.52
197	2.97	34.61	200	3.00	34.62	27.61
295	3.17	34.73	300	3.20	34.74	27.68
365	3.76	34.85	400	3.75	24.87	27.73
553	3.60	34.88	600	3.55	34.88	27.75
745	3.50	34.85	800	3.50	34.86	27.75
1,051	3.42	34.88	1,000	3.45	34.87	27.76

Station 6213; June 1; latitude 46°47.5′ N., longitude 47°05′ W.; depth 640 m.; dynamic height 970.988.

Observed values			Scaled values			
Depth, meters	Temperature, °C.	Salinity, ‰	Depth, meters	Temperature, °C.	Salinity, ‰	σ_t
0	1.75	32.98	0	1.75	32.98	26.40
20	1.70	32.98	25	1.50	33.02	26.44
40	0.21	33.18	50	0.15	33.28	26.73
60	0.16	33.36	75	0.20	33.48	26.89
80	0.22	33.52	100	0.50	33.66	27.02
120	0.74	33.82	150	0.75	34.06	27.33
160	0.74	34.14	200	1.35	34.35	27.52
240	1.98	34.52	300	2.70	34.61	27.62
375	3.27	34.70	400	3.40	34.72	27.65
547	3.70	34.86	(600)	3.70	34.89	27.75

Station 6214; June 1; latitude 46°46.5′ N., longitude 47°13′ W.; depth 329 m.; dynamic height 971.018.

0	1.13	32.82	0	1.13	32.82	26.31
23	0.84	32.89	25	0.80	32.91	26.40
46	−0.07	33.23	50	−0.20	33.24	26.72
69	−0.40	33.28	75	−0.45	33.30	26.77
93	−0.47	33.49	100	−0.35	33.58	26.99
138	0.72	33.88	150	0.90	33.94	27.22
184	1.40	34.09	200	1.60	34.17	27.36
277	2.64	34.55	(300)	2.95	34.66	27.64

Station 6215; June 1; latitude 46°45′ N., longitude 47°30′ W.; depth 178 m.; dynamic height 971.089.

0	1.77	32.74	0	1.77	32.74	26.20
27	1.46	-------	25	1.50	32.74	26.22
53	0.99	32.77	50	1.05	32.76	26.27
80	0.14	32.82	75	0.35	32.81	26.35
106	−1.43	33.11	100	−1.20	33.05	26.60
160	*−0.62	33.47	(150)	−0.80	33.41	26.88

Station 6216; June 1; latitude 46°44′ N., longitude 48°05′ W.; depth 117 m.; dynamic height 971.064.

0	2.11	32.83	0	2.11	32.83	26.25
25	1.52	32.89	25	1.52	32.89	26.33
51	−0.68	33.04	50	−0.65	33.03	26.57
76	−0.76	33.27	75	−0.75	33.27	26.76
102	−0.50	33.32	100	−0.55	33.32	26.79

Station 6217; June 1; latitude 46°48′ N., longitude 48°43′ W.; depth 84 m.; dynamic height 971.065.

0	3.05	33.00	0	3.05	33.00	26.31
24	2.90	33.00	25	2.90	33.00	26.33
49	0.83	33.14	50	0.80	33.14	26.59
73	0.68	-------	75	0.65	33.27	26.70

Table of Oceanographic Data—Continued

STATIONS OCCUPIED IN 1956—Continued

Station 6218; June 12; latitude 47°11.5′ N., longitude 49°15′ W.; depth 96 m.; dynamic height 971.108.

Observed values			Scaled values			
Depth, meters	Temperature, ° C.	Salinity, °/₀₀	Depth, meters	Temperature, ° C.	Salinity, °/₀₀	σ_t
0	3.38	32.72	0	3.38	32.72	26.05
25	3.14	32.70	25	3.14	32.70	26.06
49	0.70	32.93	50	0.60	32.94	26.44
74	−0.51	33.15	75	−0.55	33.16	26.66

Station 6219; June 12; latitude 47°12′ N., longitude 48°40′ W.; depth 115 m.; dynamic height 971.108.

Observed values			Scaled values			
Depth, meters	Temperature, ° C.	Salinity, °/₀₀	Depth, meters	Temperature, ° C.	Salinity, °/₀₀	σ_t
0	3.61	32.66	0	3.61	32.66	25.99
26	2.53	32.82	25	2.55	32.82	26.21
51	0.55	32.88	50	0.60	32.88	26.39
77	−0.82	33.08	75	−0.80	33.07	26.60
103	−0.50	33.27	100	−0.55	33.25	26.74

Station 6220; June 12; latitude 47°13′ N., longitude 47°58′ W.; depth 169 m.; dynamic height 971.117.

Observed values			Scaled values			
Depth, meters	Temperature, ° C.	Salinity, °/₀₀	Depth, meters	Temperature, ° C.	Salinity, °/₀₀	σ_t
0	3.42	32.60	0	3.42	32.60	25.96
25	3.02	32.64	25	3.02	32.64	26.03
51	−0.16	32.90	50	−0.10	32.89	26.42
76	−1.42	32.98	75	−1.40	32.98	26.55
101	−1.27	33.16	100	−1.30	33.15	26.68
152	−0.32	33.38	150	−0.40	33.37	26.83

Station 6221; June 12; latitude 47°14′ N., longitude 47°40 W.; depth 216 m.; dynamic height 971.113.

Observed values			Scaled values			
Depth, meters	Temperature, ° C.	Salinity, °/₀₀	Depth, meters	Temperature, ° C.	Salinity, °/₀₀	σ_t
0	2.80	32.59	0	2.80	32.59	26.00
25	−1.41	32.86	25	−0.41	32.86	26.42
50	−1.36	33.01	50	−1.36	33.01	26.58
76	−1.47	33.06	75	−1.45	33.06	26.61
101	−1.52	33.06	100	−1.50	33.06	26.61
151	−1.43	33.12	150	−1.45	33.11	26.65
202	−0.29	33.49	200	−0.40	33.47	26.92

Station 6222; June 12–13; latitude 47°15.5′ N., longitude 47°07′ W.; depth 887 m.; dynamic height 971.012.

Observed values			Scaled values			
Depth, meters	Temperature, ° C.	Salinity, °/₀₀	Depth, meters	Temperature, ° C.	Salinity, °/₀₀	σ_t
0	3.08	32.86	0	3.08	32.86	26.20
25	0.90	33.06	25	0.90	33.06	26.51
51	−0.43	33.24	50	−0.40	33.23	26.72
76	−0.26	33.47	75	−0.30	33.46	26.90
102	0.39	33.70	100	0.35	33.68	27.04
152	1.60	34.14	150	1.55	34.12	27.32
203	1.94	34.32	200	1.90	34.31	27.45
305	2.75	34.58	300	2.70	34.57	27.59
390	3.01	34.66	400	3.05	34.67	27.64
591	3.65	34.80	600	3.65	34.80	27.68
797	3.59	34.83	800	3.60	34.83	27.71

Station 6223; June 13; latitude 47°17.5′ N., longitude 46°46′ W.; depth 1,188 m.; dynamic height 970.946.

Observed values			Scaled values			
Depth, meters	Temperature, ° C.	Salinity, °/₀₀	Depth, meters	Temperature, ° C.	Salinity, °/₀₀	σ_t
0	2.78	33.19	0	2.78	33.19	26.49
23	2.62	33.51	25	2.55	33.54	26.78
46	1.06	33.72	50	1.05	33.75	27.06
70	1.10	33.92	75	1.15	33.97	27.23
93	1.58	34.20	100	1.65	34.23	27.40
139	2.05	34.36	150	2.15	34.39	27.49
185	2.44	34.48	200	2.55	34.50	27.55
278	3.00	34.61	300	3.10	34.63	27.60
374	3.42	34.70	400	3.50	34.72	27.64
565	3.64	34.84	600	3.65	34.84	27.71
762	3.60	34.86	800	3.60	34.86	27.74
967	3.46	34.86	1,000	3.45	34.86	27.75

Station 6224; June 13; latitude 47°18′ N., longitude 46° 23 W.; depth 622 m.; dynamic height 970.900.

Observed values			Scaled values			
Depth, meters	Temperature, ° C.	Salinity, °/₀₀	Depth, meters	Temperature, ° C.	Salinity, °/₀₀	σ_t
0	4.61	33.52	0	4.61	33.52	26.57
24	4.17	33.79	25	4.15	33.80	26.83
48	3.27	34.09	50	3.15	34.10	27.17
73	1.63	34.20	75	1.65	34.20	27.38
97	1.77	34.26	100	1.80	34.27	27.43
144	2.85	34.52	150	2.90	34.53	27.54
193	3.18	34.63	200	3.20	34.64	27.60
290	3.92	34.855	300	3.90	34.86	27.71
400	3.85	-------	400	3.85	34.86	27.71
603	3.54	34.865	600	3.55	34.86	27.74

Station 6225; June 13; latitude 47°19.5′ N., longitude 45°52′ W.; depth 324 m.; dynamic height 970.900.

Observed values			Scaled values			
Depth, meters	Temperature, ° C.	Salinity, °/₀₀	Depth, meters	Temperature, ° C.	Salinity, °/₀₀	σ_t
0	5.02	33.57	0	5.02	33.57	26.56
25	4.52	33.75	25	4.52	33.75	26.76
49	3.36	34.15	50	3.35	34.16	27.20
74	3.85	34.34	75	3.85	34.35	27.31
99	4.59	34.60	100	4.60	34.60	27.42
148	3.31	34.57	150	3.35	34.57	27.53
197	3.64	34.69	200	3.65	34.70	27.60
296	3.73	34.84	300	3.75	34.84	27.70

Station 6226; June 13; latitude 47°20.5′ N., longitude 45°29′ W.; depth 261 m.; dynamic height 970.891.

Observed values			Scaled values			
Depth, meters	Temperature, ° C.	Salinity, °/₀₀	Depth, meters	Temperature, ° C.	Salinity, °/₀₀	σ_t
0	6.37	34.08	0	6.37	34.08	26.80
25	6.13	34.06	25	6.13	34.06	26.81
49	4.78	34.12	50	4.70	34.12	27.04
74	3.42	34.28	75	3.40	34.29	27.30
98	3.24	34.44	100	3.25	34.45	27.44
147	3.39	34.63	150	3.40	34.64	27.58
196	3.75	34.80	200	3.75	34.80	27.67
250	3.72	34.81				

STATIONS OCCUPIED IN 1956—Continued

Station 6227; June 13; latitude 47°21′ N., longitude 45°15′ W.; depth 224 m.; dynamic height 970.900.

Observed values			Scaled values			
Depth, meters	Temperature, °C.	Salinity, °/oo	Depth, meters	Temperature, °C.	Salinity, °/oo	σ_t
0	6.46	34.06	0	6.46	34.06	26.77
25	6.05	34.10	25	6.05	34.10	26.86
50	4.69	34.16	50	4.69	34.16	27.07
75	3.89	34.24	75	3.89	34.24	27.21
100	3.47	34.33	100	3.47	34.33	27.32
150	3.40	34.59	150	3.40	34.59	27.54
200	3.63	34.69	200	3.63	34.69	27.60

Station 6228; June 13; latitude 47°21.5′ N., longitude 45°01′ W.; depth 205 m.; dynamic height 970.898.

Observed values			Scaled values			
Depth, meters	Temperature, °C.	Salinity, °/oo	Depth, meters	Temperature, °C.	Salinity, °/oo	σ_t
0	6.84	34.08	0	6.84	34.08	26.74
24	5.78	34.10	25	5.70	34.10	26.90
48	4.70	34.13	50	4.55	34.13	27.05
73	3.51	34.23	75	3.45	34.24	27.25
97	3.29	34.37	100	3.25	34.38	27.38
145	3.20	34.54	150	3.20	34.55	27.53
184	3.50	34.64	(200)	3.65	34.68	27.58

Station 6229; June 13; latitude 47°24.5′ N., longitude 45°09′ W.; depth 224 m.; dynamic height 970.898.

Observed values			Scaled values			
Depth, meters	Temperature, °C.	Salinity, °/oo	Depth, meters	Temperature, °C.	Salinity, °/oo	σ_t
0	6.52	34.05	0	6.52	34.05	26.76
25	5.83	34.11	25	5.83	34.11	26.89
50	4.39	34.16	50	4.39	34.16	27.10
75	3.68	34.22	75	3.68	34.22	27.22
100	3.37	34.26	100	3.37	34.26	27.28
151	3.22	34.53	150	3.20	34.53	27.51
201	3.70	34.78	200	3.70	34.78	27.66

Station 6230; June 13; latitude 47°40.5′ N., longitude 45°44′ W.; depth 318 m.; dynamic height 970.901.

Observed values			Scaled values			
Depth, meters	Temperature, °C.	Salinity, °/oo	Depth, meters	Temperature, °C.	Salinity, °/oo	σ_t
0	5.88	33.75	0	5.88	33.75	26.60
25	5.30	33.91	25	5.30	33.91	26.80
50	4.51	34.13	50	4.51	34.13	27.06
75	3.80	34.23	75	3.80	34.23	27.21
100	3.42	34.36	100	3.42	34.36	27.35
150	3.20	34.58	150	3.20	34.58	27.55
200	3.84	34.78	200	3.84	34.78	27.64
300	3.69	34.84	300	3.69	34.84	27.71

Station 6231; June 13; latitude 47°44′ N., longitude 45°52 W.; depth 439 m.; dynamic height 970.897.

Observed values			Scaled values			
Depth, meters	Temperature, °C.	Salinity, °/oo	Depth, meters	Temperature, °C.	Salinity, °/oo	σ_t
0	5.26	33.58	0	5.26	33.58	26.54
25	4.61	33.78	25	4.61	33.78	26.77
50	3.77	34.23	50	3.77	34.23	27.22
75	3.52	34.35	75	3.52	34.35	27.34
100	3.31	34.40	100	3.31	34.40	27.40
150	3.23	34.59	150	3.23	34.59	27.56
200	3.96	34.75	200	3.96	34.75	27.61
300	3.88	34.84	300	3.88	34.84	27.69
400	3.56	34.86	400	3.56	34.86	27.74

Station 6232; June 13; latitude 47°51′ N., longitude 46°08′ W.; depth 1,064 m.; dynamic height 970.913.

Observed values			Scaled values			
Depth, meters	Temperature, °C.	Salinity, °/oo	Depth, meters	Temperature, °C.	Salinity, °/oo	σ_t
0	4.99	33.69	0	4.99	33.69	26.66
25	4.48	33.77	25	4.48	33.77	26.78
50	3.13	34.09	50	3.13	34.09	27.16
76	2.89	34.25	75	2.90	34.24	27.31
101	3.15	34.42	100	3.15	34.42	27.43
151	2.82	34.50	150	2.85	34.50	27.52
202	3.12	34.59	200	3.15	34.58	27.55
303	3.68	34.79	300	3.65	34.79	27.67
376	3.52	34.80	400	3.50	34.81	27.71
570	3.47	34.85	600	3.45	34.85	27.74
762	3.43	34.86	800	3.45	34.86	27.75
954	3.39	34.86	1,000	3.40	34.86	27.76

Station 6233; June 13–14; latitude 47°58′ N., longitude 46°21′ W.; depth 1,187 m.; dynamic height 970.925.

Observed values			Scaled values			
Depth, meters	Temperature, °C.	Salinity, °/oo	Depth, meters	Temperature, °C.	Salinity, °/oo	σ_t
0	4.00	33.34	0	4.00	33.34	26.49
25	3.88	33.67	25	3.88	33.67	26.77
51	1.91	33.89	50	1.95	33.88	27.09
76	2.11	34.28	75	2.10	34.27	27.40
101	2.12	34.40	100	2.15	34.40	27.50
152	2.52	34.52	150	2.50	34.52	27.57
203	2.77	-------	200	2.75	34.57	27.59
304	3.17	34.66	300	3.15	34.66	27.62
382	3.40	34.77	400	3.45	34.78	27.68
575	3.67	34.84	600	3.70	34.84	27.71
770	3.59	34.86	800	3.60	34.86	27.74
966	3.47	34.78	(1,000)	3.45	34.86	27.75

Station 6234; June 14; latitude 48°20′ N., longitude 45°55′ W.; depth 1,188 m.; dynamic height 970.876.

Observed values			Scaled values			
Depth, meters	Temperature, °C.	Salinity, °/oo	Depth, meters	Temperature, °C.	Salinity, °/oo	σ_t
0	4.69	33.86	0	4.69	33.86	26.83
25	4.48	34.02	25	4.48	34.02	26.98
50	2.39	34.25	50	2.39	34.25	27.36
75	2.09	34.38	75	2.09	34.38	27.49
100	2.38	34.46	100	2.38	34.46	27.53
150	2.77	34.59	150	2.77	34.59	27.60
200	3.14	34.70	200	3.14	34.70	27.65
300	3.39	34.79	300	3.39	34.79	27.70
404	3.62	34.85	400	3.65	34.85	27.72
607	3.62	34.87	600	3.65	34.87	27.74
813	3.48	34.86	800	3.50	34.87	27.76
1,020	3.40	34.88	1,000	3.40	34.88	27.77

Station 6235; June 14; latitude 48°38.5′ longitude 45°31′ W.; depth 1,171 m.; dynamic height 970.884.

Observed values			Scaled values			
Depth, meters	Temperature, °C.	Salinity, °/oo	Depth, meters	Temperature, °C.	Salinity, °/oo	σ_t
0	4.68	33.72	0	4.68	33.72	26.72
25	4.15	34.11	25	4.15	34.11	27.09
50	3.85	34.46	50	3.85	34.46	27.39
75	3.09	34.46	75	3.09	34.46	27.47
99	2.69	34.50	100	2.70	34.50	27.53
149	2.73	34.58	150	2.75	34.58	27.59
199	2.97	34.66	200	3.00	34.66	27.64
298	3.54	34.79	300	3.55	34.79	27.68
399	3.63	34.84	400	3.65	34.84	27.71
596	3.62	34.84	600	3.65	34.86	27.73
791	3.53	34.87	800	3.55	34.87	27.75
1,015	3.42	34.87	1,000	3.45	34.87	27.76

STATIONS OCCUPIED IN 1956—Continued

Station 6236; June 14; latitude 49°00.5′ N., longitude 45°03′ W.; depth 1,554 m.; dynamic height 970.891.

Observed values			Scaled values			
Depth, meters	Temperature, °C.	Salinity, ‰	Depth, meters	Temperature, °C.	Salinity, ‰	σt
0	4.51	33.80	0	4.51	33.80	26.80
24	4.12	33.93	25	4.05	33.94	26.96
48	2.35	34.20	50	2.35	34.22	27.34
72	2.26	34.32	75	2.25	34.33	27.43
96	2.19	34.37	100	2.20	34.38	27.48
144	2.75	34.55	150	2.80	34.56	27.57
193	3.06	34.67	200	3.10	34.68	27.64
289	3.44	34.78	300	3.45	34.79	27.69
371	3.53	34.84	400	3.55	34.84	27.72
556	3.59	34.83	600	3.60	34.85	27.73
740	3.52	34.83	800	3.50	34.85	27.74
932	3.42	34.85	1,000	3.40	34.85	27.75
1,427	3.27	34.89				

Station 6237; June 14; latitude 49°11′ N., longitude 45°39′ W.; depth 2,743 m.; dynamic height 970.875.

Observed values			Scaled values			
Depth, meters	Temperature, °C.	Salinity, ‰	Depth, meters	Temperature, °C.	Salinity, ‰	σt
0	6.49	34.50	0	6.49	34.50	27.11
26	5.70	34.49	25	5.70	34.49	27.21
53	5.05	34.48	50	5.10	34.48	27.27
79	4.56	34.55	75	4.65	34.54	27.37
105	3.99	34.59	100	4.10	34.58	27.46
157	3.24	34.65	150	3.30	34.64	27.59
210	3.10	34.68	200	3.15	34.68	27.63
315	3.24	34.73	300	3.20	34.72	27.67
404	3.41	34.825	400	3.45	34.82	27.72
605	3.51	34.82	600	3.50	34.87	27.76
804	3.51	34.88	800	3.50	34.88	27.76
1,010	3.40	34.87	1,000	3.40	34.87	27.77
1,533	3.17	34.88				

Station 6238; June 14; latitude 49°21′ N., longitude 46°18, W.; depth 3,109 m.; dynamic height 970.894.

Observed values			Scaled values			
Depth, meters	Temperature, °C.	Salinity, ‰	Depth, meters	Temperature, °C.	Salinity, ‰	σt
0	6.85	34.52	0	6.85	34.52	27.08
24	6.77	34.55	25	6.75	34.55	27.12
48	5.74	34.49	50	5.60	34.49	27.22
73	4.83	34.52	75	4.75	34.52	27.35
97	4.37	34.57	100	4.30	34.57	27.44
146	3.50	34.59	150	3.50	34.59	27.53
194	3.47	34.73	200	3.50	34.74	27.65
291	3.91	34.84	300	3.90	34.84	27.69
380	3.89	34.86	400	3.85	34.86	27.71
573	3.60	-------	600	3.60	34.84	27.72
766	3.53	34.86	800	3.50	34.86	27.75
966	3.44	34.85	1,000	3.45	34.86	27.75
1,482	3.31	34.86				

Station 6239; June 14; latitude 48°58.5′ N., longitude 46°40′ W.; depth 2,743 m.; dynamic height 970.925.

Observed values			Scaled values			
Depth, meters	Temperature, °C.	Salinity, ‰	Depth, meters	Temperature, °C.	Salinity, ‰	σt
0	6.85	34.48	0	6.85	34.48	27.05
26	6.43	34.50	25	6.45	34.50	27.12
53	6.12	34.51	50	6.15	34.51	27.17
79	5.59	34.51	75	5.70	34.51	27.23
105	4.73	34.49	100	4.90	34.49	27.30
157	3.58	34.53	150	3.65	34.52	27.46
210	4.18	34.78	200	4.05	34.74	27.59
315	3.40	34.77	300	3.50	34.76	27.67
410	3.65	34.81	400	3.65	34.81	27.69
615	3.59	34.82	600	3.60	34.82	27.71
821	3.46	34.83	800	3.45	34.83	27.72
1,028	3.43	34.86	1,000	3.45	34.85	27.74
1,549	3.32	34.88				

Station 6340; June 15; latitude 48°36.5′ N., longitude 47°02′ W.; depth 2,469 m.; dynamic height 970.864.

Observed values			Scaled values			
Depth, meters	Temperature, °C.	Salinity, ‰	Depth, meters	Temperature, °C.	Salinity, ‰	σt
0	6.58	34.51	0	6.58	34.51	27.11
25	6.09	34.52	25	6.09	34.52	27.18
50	5.76	34.51	50	5.76	34.51	27.22
75	4.77	34.54	75	4.77	34.54	27.36
100	3.94	34.57	100	3.94	34.57	27.47
150	3.54	34.69	150	3.54	34.69	27.60
201	3.54	34.80	200	3.55	34.80	27.69
301	3.55	34.83	300	3.55	34.83	27.71
402	3.48	34.85	400	3.50	34.85	27.74
600	3.48	34.88	600	3.50	34.88	27.76
795	3.42	34.89	800	3.45	34.89	27.77
995	3.36	34.88	1,000	3.35	34.88	27.77
1,499	3.32	34.89				

Station 6241; June 15; latitude 48°14.5′ N., longitude 47°19′ W.; depth 1,646 m.; dynamic height 970.877.

Observed values			Scaled values			
Depth, meters	Temperature, °C.	Salinity, ‰	Depth, meters	Temperature, °C.	Salinity, ‰	σt
0	3.80	33.43	0	3.80	33.43	26.58
23	2.96	33.65	25	3.00	33.70	26.87
45	3.47	34.35	50	3.60	34.39	27.36
68	3.97	34.50	75	3.65	34.49	27.43
90	2.69	34.47	100	2.80	34.51	27.53
135	3.24	34.69	150	3.25	34.71	27.65
180	3.23	34.74	200	3.25	34.75	27.68
270	3.35	34.78	300	3.45	34.80	27.70
321	3.45	34.82	400	3.50	34.85	27.74
486	3.53	34.86	600	3.55	34.86	27.74
655	3.55	34.86	800	3.50	34.88	27.76
832	3.48	34.88	1,000	3.45	34.88	27.76
1,294	3.37	34.89				

STATIONS OCCUPIED IN 1955—Continued

Station 6242; June 15; latitude 48°06.5′ N., longitude 47°26′ W.; depth 704 m.; dynamic height 970.941.

Observed values			Scaled values			
Depth, meters	Temperature, ° C.	Salinity, °/₀₀	Depth, meters	Temperature, ° C.	Salinity, °/₀₀	σ_t
0	3.72	33.32	0	3.72	33.32	26.49
24	2.10	33.46	25	2.05	33.46	26.77
49	1.58	33.67	50	1.55	33.68	26.97
73	0.91	33.94	75	0.95	33.95	27.22
97	1.36	34.12	100	1.40	34.13	27.34
146	2.06	34.35	150	2.10	34.36	27.47
194	2.42	34.50	200	2.45	34.51	27.56
291	3.00	34.66	300	3.05	34.67	27.64
421	3.25	34.76	400	3.25	34.75	27.68
632	3.53	34.83	600	3.50	34.82	27.72

Station 6243; June 15; latitude 47°49′ N., longitude 47°43′ W.; depth 318 m.; dynamic height 971.075.

Observed values			Scaled values			
Depth, meters	Temperature, ° C.	Salinity, °/₀₀	Depth, meters	Temperature, ° C.	Salinity, °/₀₀	σ_t
0	3.64	32.62	0	3.64	32.62	26.96
24	2.92	32.64	25	2.80	32.64	26.04
48	0.13	32.90	50	0.05	32.91	26.44
72	−0.65	33.05	75	−0.75	33.07	26.60
96	−1.14	33.19	100	−1.15	33.22	26.74
143	−0.03	33.65	150	0.20	33.72	27.09
190	1.41	34.05	200	1.50	34.10	27.31
286	2.28	34.40	(300)	2.40	34.44	27.51

Station 6244; June 15; latitude 47°46′ N., longitude 48°10′ W.; depth 260 m.; dynamic height 971.090.

Observed values			Scaled values			
Depth, meters	Temperature, ° C.	Salinity, °/₀₀	Depth, meters	Temperature, ° C.	Salinity, °/₀₀	σ_t
0	3.57	32.63	0	3.57	32.63	25.97
24	0.92	32.77	25	0.75	32.78	26.30
48	−1.42	-------	50	−1.40	32.94	26.52
72	−1.37	33.00	75	−1.35	33.01	26.58
96	−1.22	33.04	100	−1.20	33.06	26.61
144	−0.71	33.37	150	−0.50	33.43	26.88
192	1.10	34.01	200	1.15	34.03	27.27
249	1.49	34.16				

Station 6245; June 15; latitude 47°44′ N., longitude 48°28′ W.; depth 222 m.; dynamic height 971.099.

Observed values			Scaled values			
Depth, meters	Temperature, ° C.	Salinity, °/₀₀	Depth, meters	Temperature, ° C.	Salinity, °/₀₀	σ_t
0	3.70	32.55	0	3.70	32.55	25.90
25	1.99	32.67	25	1.99	32.67	26.13
49	−0.74	32.94	50	−0.80	32.94	26.50
74	−1.32	33.03	75	−1.30	33.03	26.58
98	−1.33	33.12	100	−1.35	33.13	26.67
147	−0.73	33.35	150	−0.65	33.37	26.84
196	1.00	33.92	200	1.15	33.96	27.22

Station 6246; June 15; latitude 47°40′ N., longitude 48°57′ W.; depth 178 m.; dynamic height 971.110.

Observed values			Scaled values			
Depth, meters	Temperature, ° C.	Salinity, °/₀₀	Depth, meters	Temperature, ° C.	Salinity, °/₀₀	σ_t
0	3.80	32.53	0	3.80	32.53	25.87
25	2.40	32.59	25	2.40	32.59	26.04
50	−0.19	32.80	50	−0.19	32.80	26.37
76	−1.09	33.02	75	−1.10	33.02	26.57
101	−0.90	33.18	100	−0.90	33.17	26.69
150	−0.40	33.41	150	−0.39	33.41	26.87

Station 6247; June 15; latitude 47°48.5′ N., longitude 48°49′ W.; depth 222 m.; dynamic height 971.101.

Observed values			Scaled values			
Depth, meters	Temperature, ° C.	Salinity, °/₀₀	Depth, meters	Temperature, ° C.	Salinity, °/₀₀	σ_t
0	3.72	32.66	0	3.72	32.66	25.98
26	1.89	32.64	25	2.00	32.64	26.11
52	−1.45	32.95	50	−1.30	32.92	26.50
78	−1.40	33.03	75	−1.40	33.02	26.58
103	−1.34	33.14	100	−1.35	33.12	26.66
154	−0.21	33.49	150	−0.30	33.46	26.90
206	1.07	33.93	200	0.95	33.88	27.16

Station 6248; June 15; latitude 47°59′ N., longitude 48°39 W.; depth 333 m.; dynamic height 971.019.

Observed values			Scaled values			
Depth, meters	Temperature, ° C.	Salinity, °/₀₀	Depth, meters	Temperature, ° C.	Salinity, °/₀₀	σ_t
0	3.49	32.86	0	3.49	32.86	26.15
22	2.69	33.12	25	2.55	33.13	26.45
45	1.85	33.23	50	1.65	33.23	26.60
67	0.87	33.23	75	0.70	33.37	26.77
90	0.46	33.68	100	0.60	33.83	27.14
135	1.87	34.23	150	1.95	34.26	27.41
179	2.06	34.32	200	2.15	34.35	27.46
269	2.38	34.44	(300)	2.50	34.47	27.53

Station 6249; June 15–16; latitude 48°04′ N., longitude 48°34′ W.; depth 677 m.; dynamic height 970.990.

Observed values			Scaled values			
Depth, meters	Temperature, ° C.	Salinity, °/₀₀	Depth, meters	Temperature, ° C.	Salinity, °/₀₀	σ_t
0	3.58	33.01	0	3.58	33.01	26.27
24	1.99	33.17	25	1.95	33.17	26.53
49	0.86	33.41	50	0.85	33.42	26.81
74	0.70	33.73	75	0.70	33.74	27.07
99	1.24	34.07	100	1.25	34.07	27.31
147	1.83	34.20	150	1.85	34.21	27.37
197	2.39	34.38	200	2.40	34.38	27.46
296	2.96	34.61	300	2.95	34.61	27.60
346	3.05	34.66	400	3.10	34.67	27.64
546	3.14	34.70	(600)	3.15	34.71	27.66

Table of Oceanographic Data—Continued

STATIONS OCCUPIED IN 1956—Continued

Observed values			Scaled values			
Depth, meters	Temperature, ° C.	Salinity, °/₀₀	Depth, meters	Temperature, ° C.	Salinity, °/₀₀	σ_t
Station 6250; June 16; latitude 48°08′ N., longitude 48°30, W.; depth 1,188 m.; dynamic height 970.950.						
0-------	3.35	33.32	0------	3.35	33.32	26.53
27------	2.78	33.54	25-----	2.85	33.52	26.74
53------	1.55	33.64	50-----	1.75	33.63	26.91
80------	1.22	33.93	75-----	1.25	33.86	27.13
106-----	1.55	34.19	100----	1.45	34.14	27.34
160-----	2.26	34.42	150----	2.15	34.38	27.48
213-----	2.61	34.54	200----	2.55	34.51	27.56
319-----	3.06	34.67	300----	3.00	34.65	27.63
434-----	3.43	34.77	400----	3.35	34.74	27.66
646-----	3.63	34.85	600----	3.60	34.84	27.72
864-----	3.57	34.87	800----	3.60	34.86	27.74
1,084---	3.51	34.88	1,000--	3.55	34.88	27.75
Station 6251; June 16; latitude 48°32.5′ N., longitude 48°04′ W.; depth 2,140 m.; dynamic height 970.876.						
0-------	4.53	33.84	0------	4.53	33.84	26.83
24------	5.50	34.32	25-----	5.45	34.33	27.11
49------	4.53	34.40	50-----	4.40	34.40	27.29
73------	3.33	34.48	75-----	3.30	34.48	27.46
98------	3.20	34.52	100----	3.20	34.52	27.51
147-----	3.23	34.68	150----	3.20	34.68	27.63
196-----	3.13	34.72	200----	3.15	34.72	27.67
294-----	3.46	34.80	300----	3.50	34.80	27.70
372-----	3.53	34.85	400----	3.50	34.85	27.74
561-----	3.38	34.84	600----	3.40	34.84	27.74
753-----	3.47	34.86	800----	3.45	34.86	27.75
949-----	3.41	34.885	1,000--	3.40	34.86	27.76
1,453---	3.31	34.895				
Station 6252; June 16; latitude 48°50′ N., longitude 47°56′ W.; depth 2,378 m.; dynamic height 970.888.						
0-------	5.49	34.08	0------	5.49	34.08	26.91
20------	6.05	34.48	25-----	6.00	34.48	27.16
41------	5.61	34.47	50-----	5.20	34.50	27.28
61------	4.75	34.54	75-----	4.50	34.55	27.40
82------	4.44	34.55	100----	4.05	34.56	27.45
123-----	3.60	34.57	150----	3.55	34.63	27.55
163-----	3.55	34.66	200----	3.45	34.71	27.63
245-----	3.39	34.77	300----	3.85	34.86	27.71
315-----	3.91	34.88	400----	3.65	34.86	27.73
479-----	3.43	34.84	600----	3.45	34.85	27.74
646-----	3.40	34.85	800----	3.50	34.85	27.74
819-----	3.47	34.85	1,000--	3.40	34.85	27.75
1,272---	3.35	34.86				

Observed values			Scaled values			
Depth, meters	Temperature, ° C.	Salinity, °/₀₀	Depth, meters	Temperature, ° C.	Salinity, °/₀₀	σ_t
Station 6253; June 16; latitude 49°13′ N., longitude 47°48′ W.; depth 2,469 m.; dynamic height 970.862.						
0-------	5.16	34.20	0------	5.16	34.20	27.04
26------	4.51	34.30	25-----	4.50	34.30	27.20
52------	2.90	34.44	50-----	2.90	34.43	27.46
77------	2.86	34.56	75-----	2.90	34.56	27.57
103-----	2.90	34.56	100----	2.90	34.56	27.57
154-----	3.04	34.68	150----	3.05	34.67	27.64
206-----	3.18	34.76	200----	3.15	34.75	27.69
309-----	3.35	34.82	300----	3.35	34.82	27.73
415-----	3.34	34.82	400----	3.35	34.82	27.73
620-----	3.32	34.82	600----	3.35	34.82	27.73
823-----	3.28	34.82	800----	3.30	34.82	27.74
1,030---	3.39	34.86	1,000--	3.40	34.85	27.75
1,550---	3.30	34.90				
Station 6254; June 16; latitude 49°39′ N., longitude 47°42′ W.; depth 2,652 m.; dynamic height 970.859.						
0-------	5.38	34.49	0------	5.38	34.49	27.25
25------	5.11	34.49	25-----	5.11	34.49	27.28
50------	4.25	34.50	50-----	4.25	34.50	27.38
75------	3.73	34.58	75-----	3.73	34.58	27.50
100-----	3.50	34.65	100----	3.50	34.65	27.58
150-----	3.40	34.73	150----	3.40	34.73	27.65
201-----	3.44	34.77	200----	3.45	34.77	27.68
301-----	3.38	34.81	300----	3.40	34.81	27.72
399-----	3.33	34.82	400----	3.35	34.82	27.73
596-----	3.29	34.83	600----	3.30	34.83	27.74
791-----	3.33	34.83	800----	3.35	34.84	27.74
991-----	3.35	34.87	1,000--	3.35	34.87	27.77
1,492---	3.28	34.915				
Station 6255; June 16; latitude 49°49.5′ N., longitude 48°20′ W.; depth 2,378 m.; dynamic height 970.865.						
0-------	5.51	34.55	0------	5.51	34.55	27.28
25------	5.17	34.55	25-----	5.17	34.55	27.32
51------	4.26	34.56	50-----	4.30	34.56	27.43
76------	3.82	34.63	75-----	3.85	34.63	27.52
101-----	3.53	34.66	100----	3.55	34.66	27.58
152-----	3.75	34.75	150----	3.75	34.74	27.62
203-----	3.54	34.78	200----	3.55	34.78	27.67
304-----	3.76	34.87	300----	3.75	34.87	27.73
380-----	3.50	34.84	400----	3.50	34.84	27.73
570-----	3.35	34.83	600----	3.35	34.83	27.73
761-----	3.30	34.82	800----	3.35	34.82	27.73
953-----	3.38	34.82	1,000--	3.35	34.82	27.73
1,436---	3.31	34.88				

Table of Oceanographic Data—Continued

STATIONS OCCUPIED IN 1956—Continued

Station 6256; June 16–17; latitude 50°01′ N., longitude 48°54′ W.; depth 2,012 m.; dynamic height 970.848.

Observed values			Scaled values			
Depth, meters	Temperature, °C.	Salinity, °/₀₀	Depth, meters	Temperature, °C.	Salinity, °/₀₀	σ_t
0	4.45	34.24	0	4.45	34.24	27.15
25	4.53	34.35	25	4.53	34.35	27.23
50	3.14	34.48	50	3.14	34.48	27.48
76	3.03	34.58	75	3.05	34.58	27.56
101	3.06	34.66	100	3.05	34.66	27.63
152	3.25	34.74	150	3.25	34.74	27.67
202	3.32	34.79	200	3.30	34.79	27.71
303	3.37	34.80	300	3.35	34.80	27.71
405	3.35	34.82	400	3.35	34.82	27.73
604	3.36	34.85	600	3.35	34.85	27.75
802	3.30	--------	800	3.35	34.86	27.76
1,003	3.36	34.87	1,000	3.35	34.87	27.77
1,511	3.30	--------				

Station 6257; June 17; latitude 49°37′ N., longitude 49°06′ W.; depth 1,774 m.; dynamic height 970.828.

Observed values			Scaled values			
Depth, meters	Temperature, °C.	Salinity, °/₀₀	Depth, meters	Temperature, °C.	Salinity, °/₀₀	σ_t
0	4.02	33.86	0	4.02	33.86	26.89
25	3.77	34.30	25	3.77	34.30	27.28
50	3.12	34.54	50	3.12	34.54	27.53
76	2.98	34.60	75	3.00	34.59	27.58
101	3.20	34.68	100	3.20	34.67	27.63
152	3.31	34.74	150	3.30	34.74	27.67
202	3.39	34.80	200	3.40	34.80	27.71
303	3.45	34.82	300	3.45	34.82	27.72
398	3.55	34.86	400	3.55	34.86	27.74
594	3.53	34.87	600	3.55	34.87	27.75
788	3.41	34.87	800	3.45	34.87	27.76
988	3.44	34.87	1,000	3.45	34.87	27.76
1,496	3.31	34.90				

Station 6258; June 17; latitude 49°13′ N., longitude 49°17′ W.; depth 1,646 m.; dynamic height 970.905.

Observed values			Scaled values			
Depth, meters	Temperature, °C.	Salinity, °/₀₀	Depth, meters	Temperature, °C.	Salinity, °/₀₀	σ_t
0	3.36	33.49	0	3.36	33.49	26.67
25	2.18	34.00	25	2.18	34.00	27.18
50	1.34	33.96	50	1.34	33.96	27.21
75	1.79	34.28	75	1.79	34.28	27.43
100	1.91	34.33	100	1.91	34.33	27.46
150	2.46	34.50	150	2.46	34.50	27.55
200	2.84	34.60	200	2.84	34.60	27.60
300	3.36	34.73	300	3.36	34.73	27.65
394	3.31	34.77	400	3.30	34.77	27.70
589	3.44	34.82	600	3.45	34.82	27.72
783	3.37	34.84	800	3.40	34.84	27.74
983	3.40	34.84	1,000	3.40	34.84	27.74
1,488	3.36	34.88				

Station 6259; June 17; latitude 48°44.5′ N., longitude 49°29′ W.; depth 1,170 m.; dynamic height 970.942.

Observed values			Scaled values			
Depth, meters	Temperature, °C.	Salinity, °/₀₀	Depth, meters	Temperature, °C.	Salinity, °/₀₀	σ_t
0	3.56	33.28	0	3.56	33.28	26.48
25	3.34	33.36	25	3.34	33.36	26.56
50	1.37	33.64	50	1.37	33.64	26.95
75	1.59	33.95	75	1.59	33.95	27.18
100	2.17	34.32	100	2.17	34.32	27.44
150	2.61	34.52	150	2.61	34.52	27.56
199	2.86	34.60	200	2.85	34.60	27.60
299	3.08	34.72	300	3.10	34.72	27.68
411	3.23	34.75	400	3.20	34.75	27.69
614	3.64	34.79	600	3.65	34.81	27.69
815	3.52	34.84	800	3.55	34.84	27.72
1,018	3.49	34.87	1,000	3.50	34.87	27.76

Station 6260; June 17; latitude 48°33.5′ N., longitude 49°33′ W.; depth 614 m.; dynamic height 970.985.

Observed values			Scaled values			
Depth, meters	Temperature, °C.	Salinity, °/₀₀	Depth, meters	Temperature, °C.	Salinity, °/₀₀	σ_t
0	3.57	32.84	0	3.57	32.84	26.14
25	1.20	33.04	25	1.20	33.04	26.48
50	−0.14	33.19	50	−0.14	33.19	26.68
75	0.05	33.55	75	0.05	33.55	26.96
100	0.87	33.92	100	0.87	33.92	27.21
150	1.64	34.23	150	1.64	34.23	27.40
201	2.36	34.42	200	2.35	34.42	27.50
301	2.91	34.60	300	2.90	34.60	27.60
398	3.12	34.72	400	3.15	34.72	27.67
600	3.19	34.77	600	3.20	34.77	27.71

Station 6261; June 17; latitude 48°14.5′ N., longitude 49°40′ W.; depth 224 m.; dynamic height 971.087.

Observed values			Scaled values			
Depth, meters	Temperature, °C.	Salinity, °/₀₀	Depth, meters	Temperature, °C.	Salinity, °/₀₀	σ_t
0	3.44	32.57	0	3.44	32.57	25.93
25	0.79	32.69	25	0.79	32.69	26.22
50	−1.31	32.98	50	−0.31	32.98	26.54
76	−1.35	33.08	75	−1.35	33.08	26.62
101	−1.38	33.11	100	−1.35	33.11	26.65
151	−0.36	33.46	150	−0.40	33.45	26.90
202	1.25	34.06	200	1.15	34.03	27.27

Station 6262; June 17; latitude 48°03.5′ N., longitude 49°45′ W.; depth 170 m.; dynamic height 971.093.

Observed values			Scaled values			
Depth, meters	Temperature, °C.	Salinity, °/₀₀	Depth, meters	Temperature, °C.	Salinity, °/₀₀	σ_t
0	3.88	32.57	0	3.88	32.57	25.89
25	1.74	32.69	25	1.74	32.69	26.16
50	−0.50	32.90	50	−0.50	32.90	26.45
75	−0.74	33.00	75	−0.74	33.00	26.55
100	−1.14	33.18	100	−1.14	33.18	26.70
150	−1.15	33.55	150	−0.15	33.55	26.97

Station 6263; June 17; latitude 47°48′ N., longitude 49°50′ W.; depth 115 m.; dynamic height 971.104.

Observed values			Scaled values			
Depth, meters	Temperature, °C.	Salinity, °/₀₀	Depth, meters	Temperature, °C.	Salinity, °/₀₀	σ_t
0	4.44	32.51	0	4.44	32.51	25.78
25	2.37	32.56	25	2.37	32.56	26.01
51	−0.28	32.82	50	−0.25	32.81	26.38
76	0.07	33.03	75	0.05	33.02	26.53
102	−0.42	33.24	100	−0.35	33.22	26.70

Station 6264; June 17; latitude 47°27′ N., longitude 49°58′ W.; depth 104 m.; dynamic height 971.102.

Observed values			Scaled values			
Depth, meters	Temperature, °C.	Salinity, °/₀₀	Depth, meters	Temperature, °C.	Salinity, °/₀₀	σ_t
0	5.15	32.72	0	5.15	32.72	25.87
25	3.43	32.77	25	3.43	32.77	26.09
50	1.80	32.93	50	1.80	32.93	26.35
75	0.64	33.10	75	0.64	33.10	26.56
100	−0.27	33.16	100	−0.27	33.16	26.65

Station 6265; June 18; latitude 47°37.5′ N., longitude 50°22′ W.; depth 115 m.; dynamic height 971.106.

Observed values			Scaled values			
Depth, meters	Temperature, °C.	Salinity, °/₀₀	Depth, meters	Temperature, °C.	Salinity, °/₀₀	σ_t
0	4.54	32.56	0	4.54	32.56	25.82
25	2.86	32.56	25	2.86	32.56	25.97
50	0.93	32.76	50	0.93	32.76	26.27
74	0.22	33.10	75	0.20	33.11	26.59
99	−0.18	33.21	100	−0.20	33.21	26.70

Table of Oceanographic Data—Continued

STATIONS OCCUPIED IN 1955—Continued

Station 6266; June 18; latitude 47°51.5′ N., longitude 50°52′ W.; depth 137 m.; dynamic height 971.111.

Observed values			Scaled values			
Depth, meters	Temperature, ° C.	Salinity, ‰	Depth, meters	Temperature, ° C.	Salinity, ‰	σ_t
0	4.49	32.35	0	4.49	32.35	25.66
25	2.65	32.51	25	2.65	32.51	25.95
51	0.26	32.77	50	0.35	32.76	26.30
76	−0.52	33.02	75	−0.50	33.00	26.54
102	−0.78	33.15	100	−0.75	33.14	26.66

Station 6267; June 18; latitude 47°53′ N., longitude 50°56′ W.; depth 148 m.; dynamic height 971.118.

Observed values			Scaled values			
Depth, meters	Temperature, ° C.	Salinity, ‰	Depth, meters	Temperature, ° C.	Salinity, ‰	σ_t
0	4.45	32.33	0	4.45	32.33	25.64
25	2.88	32.38	25	2.88	32.38	25.83
49	−0.30	32.71	50	−0.30	32.72	26.30
74	−0.92	32.90	75	−0.95	32.91	26.48
98	−1.21	33.06	100	−1.20	33.07	26.62
133	−0.61	33.24				

Station 6268; June 18; latitude 48°00.5′ N., longitude 51°14′ W.; depth 208 m.; dynamic height 971.123.

Observed values			Scaled values			
Depth, meters	Temperature, ° C.	Salinity, ‰	Depth, meters	Temperature, ° C.	Salinity, ‰	σ_t
0	4.72	32.18	0	4.72	32.18	25.49
26	0.91	32.48	25	1.05	32.47	26.04
52	−1.43	32.77	50	−1.30	32.75	26.36
78	−1.61	32.85	75	−1.60	32.84	26.44
105	−1.39	32.96	100	−1.45	32.94	26.52
156	−0.89	33.16	150	−0.95	33.14	26.67

Station 6269; June 18; latitude 48°07.5′ N., longitude 50°33′ W.; depth 199 m.; dynamic height 971.113.

Observed values			Scaled values			
Depth, meters	Temperature, ° C.	Salinity, ‰	Depth, meters	Temperature, ° C.	Salinity, ‰	σ_t
0	4.92	32.29	0	4.92	32.29	25.56
25	3.27	32.52	25	3.27	32.52	25.90
50	−0.63	32.87	50	−0.63	32.87	26.44
75	−1.21	33.01	75	−1.21	33.01	26.57
101	−1.40	33.02	100	−1.40	33.02	26.58
151	−0.79	33.30	150	−0.80	33.29	26.77

Station 6270; June 18; latitude 48°16′ N., longitude 51°53′ W.; depth 187 m.; dynamic height 971.113.

Observed values			Scaled values			
Depth, meters	Temperature, ° C.	Salinity, ‰	Depth, meters	Temperature, ° C.	Salinity, ‰	σ_t
0	4.25	32.47	0	4.25	32.47	25.77
25	1.62	32.64	25	1.62	32.64	26.13
50	−1.21	32.82	50	−1.21	32.82	26.42
75	−1.48	32.93	75	−1.48	32.93	26.51
100	−1.47	33.00	100	−1.47	33.00	26.57
150	−1.36	33.08	150	−1.36	33.08	26.63

Station 6271; June 18; latitude 48°24.5′ N., longitude 52°12′ W.; depth 196 m.; dynamic height 971.117.

Observed values			Scaled values			
Depth, meters	Temperature, ° C.	Salinity, ‰	Depth, meters	Temperature, ° C.	Salinity, ‰	σ_t
0	4.48	32.33	0	4.48	32.33	25.64
25	1.20	32.55	25	1.20	32.55	26.10
50	−0.96	32.80	50	−0.96	32.80	26.39
75	−1.49	32.90	75	−1.49	32.90	26.48
99	−1.45	32.96	100	−1.45	32.96	26.53
149	−1.39	33.06	150	−1.40	33.06	26.61
184	−1.20	33.13				

Station 6272; June 18; latitude 48°34.5′ N., longitude 52°36′ W.; depth 263 m.; dynamic height 971.104.

Observed values			Scaled values			
Depth, meters	Temperature, ° C.	Salinity, ‰	Depth, meters	Temperature, ° C.	Salinity, ‰	σ_t
0	4.46	32.31	0	4.46	32.31	25.63
23	2.53	32.50	25	2.25	32.53	26.00
47	−0.63	32.82	50	−0.80	32.84	26.42
70	−1.32	32.93	75	−1.30	32.95	26.52
94	−1.24	33.03	100	−1.25	33.05	26.60
140	−1.20	33.17	150	−1.10	33.24	26.75
187	−0.57	33.54	(200)	−0.35	33.64	27.04

Station 6273; June 18; latitude 48°38′ N., longitude 52°46′ W.; depth 224 m.; dynamic height 971.142.

Observed values			Scaled values			
Depth, meters	Temperature, ° C.	Salinity, ‰	Depth, meters	Temperature, ° C.	Salinity, ‰	σ_t
0	4.09	32.36	0	4.09	32.36	25.70
23	2.75	32.48	25	2.45	32.51	25.96
46	−1.16	32.78	50	−1.25	32.78	26.38
70	−1.42	32.80	75	−1.45	32.83	26.43
93	−1.50	32.98	100	−1.50	32.99	26.56
139	−1.43	33.04	150	−1.40	33.05	26.60

Station 6274; June 18; latitude 48°47′ N., longitude 52°47 W.; depth 135 m.; dynamic height 971.151.

Observed values			Scaled values			
Depth, meters	Temperature, ° C.	Salinity, ‰	Depth, meters	Temperature, ° C.	Salinity, ‰	σ_t
0	3.54	32.38	0	3.54	32.38	25.77
24	0.09	32.44	25	0.00	32.45	26.08
47	−1.12	32.66	50	−1.15	32.67	26.29
71	−1.19	32.76	75	−1.25	32.76	26.37
94	−1.30	32.76	100	−1.30	32.76	26.37

Station 6275; June 18; latitude 48°50′ N., longitude 52°39′ W.; depth 224 m.; dynamic height 971.152.

Observed values			Scaled values			
Depth, meters	Temperature, ° C.	Salinity, ‰	Depth, meters	Temperature, ° C.	Salinity, ‰	σ_t
0	4.21	32.33	0	4.21	32.33	25.67
23	−0.66	32.52	25	−0.80	32.54	26.18
46	−1.11	32.70	50	−1.15	32.71	26.32
70	−1.16	32.78	75	−1.20	32.79	26.39
92	−1.42	32.85	100	−1.45	32.85	26.44
139	−1.50	32.89	150	−1.50	32.93	26.51
185	−1.42	33.08	200	−1.40	33.14	26.68

Station 6276; June 18; latitude 48°55′ N., longitude 52°25′ W.; depth 341 m.; dynamic height 971.121.

Observed values			Scaled values			
Depth, meters	Temperature, ° C.	Salinity, ‰	Depth, meters	Temperature, ° C.	Salinity, ‰	σ_t
0	3.27	32.14	0	3.27	32.14	25.60
25	0.63	32.56	25	0.63	32.56	26.13
49	−1.18	32.72	50	−1.20	32.72	26.34
74	−1.47	32.80	75	−1.50	32.81	26.42
98	−1.56	32.96	100	−1.55	32.97	26.55
148	−1.38	33.14	150	−1.35	33.15	26.68
198	−0.77	33.48	200	−0.70	33.50	26.95
296	1.81	34.21	300	1.95	34.25	27.40

STATIONS OCCUPIED IN 1956—Continued

Station 6277; June 18; latitude 48°58′ N., longitude 52°12′ W.; depth 306 m.; dynamic height 971.151.

Observed values			Scaled values			
Depth, meters	Temperature, ° C.	Salinity, °/₀₀	Depth, meters	Temperature, ° C.	Salinity, °/₀₀	σ_t
0	3.58	32.10	0	3.58	32.10	25.54
24	0.13	32.56	25	0.05	32.58	26.18
49	−1.32	32.81	50	−1.35	32.82	26.42
73	−1.45	32.89	75	−1.50	32.89	26.47
98	−1.56	-------	100	−1.55	32.94	26.52
146	−1.48	33.01	150	−1.45	33.02	26.58
195	−1.27	33.06	200	−1.20	33.09	26.63
			(300)	2.10	34.19	27.33

Station 6278; June 18; latitude 49°01.5′ N., longitude 52°00′ W.; depth 302 m.; dynamic height 971.114.

Observed values			Scaled values			
Depth, meters	Temperature, ° C.	Salinity, °/₀₀	Depth, meters	Temperature, ° C.	Salinity, °/₀₀	σ_t
0	3.60	32.17	0	3.60	32.17	25.60
24	−1.15	32.81	25	−1.15	32.81	26.41
47	−1.32	32.89	50	−1.35	32.89	26.47
71	−1.45	32.92	75	−1.50	32.93	26.51
94	−1.56	32.98	100	−1.55	32.99	26.56
140	−1.49	33.04	150	−1.45	33.07	26.62
187	−1.16	33.28	200	−0.85	33.40	26.87
281	1.58	34.20	(300)	2.20	34.39	27.49

Station 6279; June 19; latitude 49°07′ N., longitude 51°40′ W.; depth 287 m.; dynamic height 971.108.

Observed values			Scaled values			
Depth, meters	Temperature, ° C.	Salinity, °/₀₀	Depth, meters	Temperature, ° C.	Salinity, °/₀₀	σ_t
0	3.66	32.[illegible]	0	3.66	32.07	25.52
25	0.59	32.56	25	0.59	32.56	26.13
51	−1.41	32.84	50	−1.35	32.83	26.42
76	−1.60	32.93	75	−1.60	32.93	26.51
101	−1.60	33.00	100	−1.60	32.99	26.56
151	−1.19	33.24	150	−1.20	33.23	26.74
201	−0.39	33.60	200	−0.40	33.59	27.01
284	1.66	34.25				

Station 6280; June 19; latitude 49°13′ N., longitude 51°18′ W.; depth 327 m.; dynamic height 971.050.

Observed values			Scaled values			
Depth, meters	Temperature, ° C.	Salinity, °/₀₀	Depth, meters	Temperature, ° C.	Salinity, °/₀₀	σ_t
0	2.59	32.07	0	2.59	32.07	25.61
26	−0.37	32.54	25	−0.30	32.52	26.14
51	−1.26	33.02	50	−1.25	33.01	26.57
77	−1.07	33.15	75	−1.10	33.13	26.66
102	−0.78	33.36	100	−0.80	33.33	26.81
154	0.15	33.79	150	0.05	33.76	27.13
205	1.44	34.13	200	1.30	34.10	27.32
307	2.49	34.48	300	2.45	34.46	27.52

Station 6281; June 19; latitude 49°29′ N., longitude 50°35′ W.; depth 339 m.; dynamic height 970.961.

Observed values			Scaled values			
Depth, meters	Temperature, ° C.	Salinity, °/₀₀	Depth, meters	Temperature, ° C.	Salinity, °/₀₀	σ_t
0	2.84	33.22	0	2.84	33.22	26.50
27	2.53	33.18	25	2.55	33.18	26.50
53	0.60	33.40	50	0.80	33.44	26.82
80	0.89	33.96	75	0.80	33.89	27.18
106	1.22	34.09	100	1.20	34.07	27.31
160	2.02	34.30	150	1.90	34.27	27.42
213	2.54	34.48	200	2.45	34.44	27.50
319	3.25	34.73	300	3.15	34.70	27.65

Station 6282; June 19; latitude 49°38′ N., longitude 50°03′ W.; depth 637 m.; dynamic height 970.898.

Observed values			Scaled values			
Depth, meters	Temperature, ° C.	Salinity, °/₀₀	Depth, meters	Temperature, ° C.	Salinity, °/₀₀	σ_t
0	3.51	33.66	0	3.51	33.66	26.79
23	3.46	33.68	25	3.45	33.75	26.86
46	3.53	34.47	50	3.45	34.46	27.43
69	3.07	34.42	75	3.10	34.48	27.48
92	3.13	34.66	100	3.10	34.66	27.63
137	3.11	34.67	150	3.10	34.67	27.64
184	3.10	34.67	200	3.10	34.68	27.64
276	3.25	34.73	300	3.25	34.72	27.66
356	3.25	34.72	400	3.30	34.74	27.67
548	3.33	34.78	600	3.35	34.79	27.70

Station 6283; June 19; latitude 49°47.5′ N., longitude 49°30′ W.; depth 1,335 m.; dynamic height 970.901.

Observed values			Scaled values			
Depth, meters	Temperature, ° C.	Salinity, °/₀₀	Depth, meters	Temperature, ° C.	Salinity, °/₀₀	σ_t
0	3.21	33.68	0	3.21	33.68	26.83
24	2.17	33.98	25	2.20	33.99	27.17
48	3.86	34.18	50	3.75	34.20	27.20
72	2.21	34.40	75	2.25	34.41	27.50
95	2.44	34.49	100	2.50	34.50	27.55
144	2.86	34.58	150	2.90	34.59	27.59
192	3.06	34.62	200	3.10	34.63	27.60
287	3.52	34.75	300	3.55	34.77	27.67
357	*3.51	34.83	400	3.60	34.83	27.71
535	3.66	34.835	600	3.60	34.83	27.71
714	3.37	34.80	800	3.45	34.82	27.72
914	3.53	34.86	1,000	3.50	34.86	27.75
1,202	3.42	34.86				

Station 6284; June 19; latitude 50°00.5′ N., longitude 49°02′ W.; depth 1,829 m.; dynamic height 970.853.

Observed values			Scaled values			
Depth, meters	Temperature, ° C.	Salinity, °/₀₀	Depth, meters	Temperature, ° C.	Salinity, °/₀₀	σ_t
0	4.56	34.39	0	4.56	34.39	27.26
20	4.39	34.37	25	4.25	34.40	27.30
39	2.99	34.54	50	3.00	34.58	27.57
59	3.02	34.61	75	3.25	34.71	27.65
78	3.26	34.72	100	3.30	34.74	27.67
117	3.32	34.76	150	3.45	34.79	27.69
156	3.43	34.80	200	3.40	34.80	27.71
234	3.35	34.80	300	3.35	34.80	27.71
412	3.32	34.80	400	3.35	34.80	27.71
596	3.32	34.80	600	3.35	34.80	27.71
768	3.30	34.84	800	3.35	34.84	27.74
970	3.37	34.86	1,000	3.35	34.86	27.76
1,496	3.31	34.86				

Station 6285; July 10; latitude 50°02.5′ N., longitude 48°54′ W.; depth 1,866 m.; dynamic height 970.851.

Observed values			Scaled values			
Depth, meters	Temperature, ° C.	Salinity, °/₀₀	Depth, meters	Temperature, ° C.	Salinity, °/₀₀	σ_t
0	7.83	34.43	0	7.83	34.43	26.87
22	4.55	34.43	25	4.55	34.44	27.30
45	4.82	34.56	50	4.75	34.57	27.39
67	4.39	34.61	75	4.20	34.62	27.49
90	3.72	34.65	100	3.60	34.66	27.58
134	3.39	34.73	150	3.40	34.75	27.67
179	3.38	34.78	200	3.40	34.80	27.71
269	3.49	34.84	300	3.45	34.84	27.73
318	3.40	34.84	400	3.40	34.85	27.75
478	3.37	34.86	600	3.35	34.86	27.76
638	3.31	34.855	800	3.35	34.87	27.77
812	3.32	34.87	1,000	3.35	34.88	27.77
1,275	3.33	-------				

Station 6286; July 11; latitude 49°49.5′ N., longitude 49°29′ W.; depth 1,390 m.; dynamic height 970.897.

Observed values			Scaled values			
Depth, meters	Temperature, °C.	Salinity, °/₀₀	Depth, meters	Temperature, °C.	Salinity, °/₀₀	σt
0	6.43	33.73	0	6.43	33.73	26.52
26	4.05	34.15	25	4.15	34.12	27.09
52	2.09	34.36	50	2.20	34.34	27.45
78	2.20	34.42	75	2.15	34.41	27.51
103	2.55	--------	100	2.50	34.48	27.53
156	2.88	34.66	150	2.85	34.64	27.63
207	3.09	34.71	200	3.05	34.70	27.66
310	3.38	34.775	300	3.35	34.77	27.69
415	3.42	34.79	400	3.45	34.79	27.69
621	3.42	34.79	600	3.45	34.79	27.69
827	3.41	34.86	800	3.45	34.85	27.74
1,040	3.40	34.875	1,000	3.40	34.87	27.77
1,350	3.37	34.88				

Station 6287; July 11; latitude 49°37.5′ N., longitude 50°02′ W.; depth 605 m.; dynamic height 970.900.

Observed values			Scaled values			
Depth, meters	Temperature, °C.	Salinity, °/₀₀	Depth, meters	Temperature, °C.	Salinity, °/₀₀	σt
0	5.03	33.02	0	5.03	33.02	26.13
23	3.50	33.93	25	3.35	33.98	27.06
46	2.26	34.42	50	2.25	34.44	27.52
69	2.49	34.49	75	2.50	34.50	27.55
92	2.65	34.53	100	2.75	34.54	27.56
137	3.07	34.59	150	3.10	34.60	27.58
183	3.18	34.63	200	3.20	34.65	27.61
275	3.18	34.72	300	3.20	34.73	27.67
297	3.19	34.73	400	3.30	34.77	27.70
495	3.34	34.79	(600)	3.35	34.81	27.72

Station 6288; July 11; latitude 49°28′ N., longitude 50°32′ W.; depth 351 m.; dynamic height 970.958.

Observed values			Scaled values			
Depth, meters	Temperature, °C.	Salinity, °/₀₀	Depth, meters	Temperature, °C.	Salinity, °/₀₀	σt
0	5.92	32.89	0	5.92	32.89	25.91
27	1.68	33.13	25	2.00	33.10	26.47
54	−0.22	33.48	50	−0.20	33.42	26.87
81	0.72	33.94	75	0.50	33.86	27.18
107	1.44	34.16	100	1.25	34.11	27.34
162	2.24	34.43	150	2.05	34.38	27.49
216	2.79	34.58	200	2.65	34.54	27.57
323	3.12	34.72	300	3.10	34.69	27.65

Station 6289; July 11; latitude 49°20′ N.; longitude 50°58′ W.; depth 333 m.; dynamic height 971.005.

Observed values			Scaled values			
Depth, meters	Temperature, °C.	Salinity, °/₀₀	Depth, meters	Temperature, °C.	Salinity, °/₀₀	σt
0	7.15	32.24	0	7.15	32.24	25.25
20	3.64	32.83	25	3.15	32.88	26.21
40	1.86	32.97	50	0.80	33.09	26.54
60	−0.11	33.29	75	−0.30	33.52	26.95
80	−0.32	33.61	100	0.40	33.86	27.19
120	1.13	34.05	150	1.70	34.20	27.37
160	1.83	34.25	200	2.30	34.39	27.48
240	2.67	34.50	(300)	3.00	34.63	27.61

Station 6290; July 11; latitude 49°10.5′ N., longitude 51°31′ W.; depth 322 m.; dynamic height 971.077.

Observed values			Scaled values			
Depth, meters	Temperature, °C.	Salinity, °/₀₀	Depth, meters	Temperature, °C.	Salinity, °/₀₀	σt
0	8.03	31.43	0	8.03	31.43	24.49
25	0.58	32.28	25	0.58	32.28	25.90
50	−1.11	32.79	50	−1.11	32.79	26.39
75	−1.10	33.03	75	−1.10	33.03	26.58
100	−0.67	33.34	100	−0.67	33.34	26.82
150	−0.28	33.73	150	−0.28	33.73	27.11
201	1.28	34.11	200	1.25	34.10	27.33
301	2.16	34.39	300	2.15	34.38	27.48

Station 6291; July 11; latitude 49°02′ N., longitude 51°53′ W.; depth 311 m.; dynamic height 971.134.

Observed values			Scaled values			
Depth, meters	Temperature, °C.	Salinity, °/₀₀	Depth, meters	Temperature, °C.	Salinity, °/₀₀	σt
0	8.97	31.33	0	8.97	31.33	24.28
25	3.62	32.31	25	3.62	32.31	25.71
50	−1.41	32.87	50	−1.41	32.87	26.46
75	−1.62	32.96	75	−1.62	32.96	26.54
99	−1.53	--------	100	−1.50	33.03	26.59
149	−1.28	33.18	150	−1.30	33.18	26.70
199	−0.33	33.57	200	−0.30	33.58	26.99
298	2.07	34.36	300	2.10	34.37	27.48

Station 6292; July 11; latitude 48°57.5′ N., longitude 52°06′ W.; depth 300 m.; dynamic height 971.138.

Observed values			Scaled values			
Depth, meters	Temperature, °C.	Salinity, °/₀₀	Depth, meters	Temperature, °C.	Salinity, °/₀₀	σt
0	7.98	31.51	0	7.98	31.51	24.57
24	3.17	32.19	25	3.00	32.21	25.69
49	−1.46	32.66	50	−1.50	32.68	26.31
73	−1.60	32.94	75	−1.60	32.95	26.53
98	−1.55	33.04	100	−1.55	33.05	26.61
147	−1.36	33.20	150	−1.35	33.21	26.74
196	−0.67	33.46	200	−0.55	33.49	26.93
284	1.79	34.22	(300)	2.20	34.36	27.47

Station 6293; July 11; latitude 48°50.5′ N., longitude 52°28′ W.; depth 375 m.; dynamic height 971.131.

Observed values			Scaled values			
Depth, meters	Temperature, °C.	Salinity, °/₀₀	Depth, meters	Temperature, °C.	Salinity, °/₀₀	σt
0	7.68	31.73	0	7.68	31.73	24.77
25	−0.51	32.45	25	−0.51	32.45	26.10
51	−1.42	32.86	50	−1.40	32.84	26.44
76	−1.60	32.92	75	−1.60	32.92	26.51
101	−1.54	33.00	100	−1.55	33.00	26.57
152	−1.40	33.16	150	−1.40	33.15	26.68
203	−0.98	33.43	200	−1.00	33.41	26.89
304	2.12	34.36	300	2.00	34.32	27.45

Station 6294; July 12; latitude 48°46.5′ N., longitude 52°43′ W.; depth 222 m.; dynamic height 971.144.

Observed values			Scaled values			
Depth, meters	Temperature, °C.	Salinity, °/₀₀	Depth, meters	Temperature, °C.	Salinity, °/₀₀	σt
0	8.26	31.88	0	8.26	31.88	24.82
25	1.79	32.40	25	1.79	32.40	25.93
50	−1.22	32.83	50	−1.22	32.83	26.42
75	−1.50	32.94	75	−1.50	32.94	26.52
100	−1.59	32.98	100	−1.59	32.98	26.55
150	−1.42	33.06	150	−1.42	33.06	26.61
200	−0.94	33.34	200	−0.94	33.34	26.83

STATIONS OCCUPIED IN 1956—Continued

Station 6295; July 12; latitude 48°45.5′ N., longitude 52°46′ W.; depth 155 m.; dynamic height 971.152.

Observed values			Scaled values			
Depth, meters	Temperature, ° C.	Salinity, °/oo	Depth, meters	Temperature, ° C.	Salinity, °/oo	σ_t
0	8.69	31.68	0	8.69	31.68	24.60
24	1.53	32.41	25	1.25	32.48	26.03
48	−1.37	32.84	50	−1.40	32.85	26.44
72	−1.51	32.91	75	−1.50	32.91	26.49
95	−1.51	32.92	100	−1.50	32.92	26.50
143	−1.39	32.94	150	−1.30	32.95	26.52

Station 6296; July 12; latitude 48°42.5′ N., longitude 52°58′ W.; depth 95 m.; dynamic height 971.178.

Observed values			Scaled values			
Depth, meters	Temperature, ° C.	Salinity, °/oo	Depth, meters	Temperature, ° C.	Salinity, °/oo	σ_t
0	9.80	31.52	0	9.80	31.52	24.30
22	3.46	32.15	25	2.85	32.22	25.70
44	−0.82	32.66	50	−0.90	32.66	26.28
66	−0.99	32.66	(75)	−1.00	32.66	26.28

Station 6297; July 12; latitude 48°36′ N., longitude 52°41′ W.; depth 272 m.; dynamic height 971.156.

Observed values			Scaled values			
Depth, meters	Temperature, ° C.	Salinity, °/oo	Depth, meters	Temperature, ° C.	Salinity, °/oo	σ_t
0	8.29	31.75	0	8.29	31.75	24.71
19	6.55	32.05	25	4.35	32.22	25.57
39	−0.04	32.62	50	−1.00	32.78	26.37
58	−1.48	32.83	75	−1.40	32.89	26.47
78	−1.41	32.90	100	−1.50	32.92	26.50
117	−1.57	32.94	150	−1.50	33.05	26.60
156	−1.46	33.08	200	−1.00	33.37	26.85
210	−0.88	33.44				

Station 6298; July 12; latitude 48°19′ N., longitude 52°05′ W.; depth 187 m.; dynamic height 971.144.

Observed values			Scaled values			
Depth, meters	Temperature, ° C.	Salinity, °/oo	Depth, meters	Temperature, ° C.	Salinity, °/oo	σ_t
0	7.58	31.91	0	7.58	31.91	24.93
25	2.01	32.41	25	2.01	32.41	25.93
50	−1.19	32.86	50	−1.19	32.86	26.45
75	−1.43	32.95	75	−1.43	32.95	26.52
100	−1.50	32.99	100	−1.50	32.99	26.56
150	−1.35	33.08	150	−1.35	33.08	26.63

Station 6299; July 12; latitude 48°11′ N., longitude 51°46′ W.; depth 187 m.; dynamic height 971.149.

Observed values			Scaled values			
Depth, meters	Temperature, ° C.	Salinity, °/oo	Depth, meters	Temperature, ° C.	Salinity, °/oo	σ_t
0	7.74	31.97	0	7.74	31.97	24.96
25	4.56	32.35	25	4.56	32.35	25.65
51	−1.10	32.88	50	−1.00	32.87	26.45
76	−1.36	32.94	75	−1.35	32.94	26.52
101	−1.48	33.01	100	−1.50	33.01	26.58
152	−1.33	33.11	150	−1.35	33.10	26.64

Station 6300; July 12; latitude 48°03′ N., longitude 51°25′ W.; depth 220 m.; dynamic height 971.130.

Observed values			Scaled values			
Depth, meters	Temperature, ° C.	Salinity, °/oo	Depth, meters	Temperature, ° C.	Salinity, °/oo	σ_t
0	6.92	32.18	0	6.92	32.18	25.23
25	4.13	32.50	25	4.13	32.50	25.81
50	−1.01	32.87	50	−1.01	32.87	26.45
75	−1.37	32.99	75	−1.37	32.99	26.56
100	−1.36	33.05	100	−1.36	33.05	26.60
149	−0.76	33.29	150	−0.75	33.29	26.77
199	−0.50	33.40	200	−0.50	33.40	26.86

Station 6301; July 12; latitude 47°51′ N., longitude 51°00′ W.; depth 157 m.; dynamic height 971.122.

Observed values			Scaled values			
Depth, meters	Temperature, ° C.	Salinity, °/oo	Depth, meters	Temperature, ° C.	Salinity, °/oo	σ_t
0	7.17	32.26	0	7.17	32.26	25.27
25	4.72	32.47	25	4.72	32.47	25.73
50	−0.55	32.85	50	−0.55	32.85	26.42
75	−1.14	32.98	75	−1.14	32.98	26.54
100	−1.17	33.10	100	−1.17	33.10	26.64
148	−0.62	33.29	150	−0.60	33.30	26.77

Station 6302; July 12; latitude 47°45.5′ N., longitude 50°48′ W.; depth 119 m.; dynamic height 971.131.

Observed values			Scaled values			
Depth, meters	Temperature, ° C.	Salinity, °/oo	Depth, meters	Temperature, ° C.	Salinity, °/oo	σ_t
0	7.17	32.43	0	7.17	32.43	25.40
24	4.74	32.45	25	4.45	32.45	25.74
49	−0.38	32.82	50	−0.50	32.82	26.39
73	−1.05	32.96	75	−1.05	32.97	26.53
97	−0.98	33.11	100	−0.95	33.13	26.66

Station 6303; July 12; latitude 47°38′ N., longitude 50°33 W.; depth 148 m.; dynamic height 971.131.

Observed values			Scaled values			
Depth, meters	Temperature, ° C.	Salinity, °/oo	Depth, meters	Temperature, ° C.	Salinity, °/oo	σ_t
0	6.84	32.35	0	6.84	32.35	25.38
24	6.16	32.41	25	5.65	32.44	25.60
48	−0.25	32.85	50	−0.40	32.86	26.42
72	−0.74	32.97	75	−0.75	33.00	26.55
96	−0.73	33.22	100	−0.70	33.22	26.72
139	−0.69	33.25				

Station 6304; July 12; latitude 47°31.5′ N., longitude 50°18′ W.; depth 183 m.; dynamic height 971.130.

Observed values			Scaled values			
Depth, meters	Temperature, ° C.	Salinity, °/oo	Depth, meters	Temperature, ° C.	Salinity, °/oo	σ_t
0	6.97	32.48	0	6.97	32.48	25.46
25	5.90	32.57	25	5.90	32.57	25.68
50	1.84	32.95	50	1.84	32.95	26.36
75	0.23	33.11	75	0.23	33.11	26.59
100	−0.24	33.20	100	−0.24	33.20	26.69

Station 6305; July 12; latitude 47°22′ N., longitude 50°00′ W.; depth 78 m.; dynamic height 971.124.

Observed values			Scaled values			
Depth, meters	Temperature, ° C.	Salinity, °/oo	Depth, meters	Temperature, ° C.	Salinity, °/oo	σ_t
0	7.57	32.60	0	7.57	32.60	25.48
24	5.98	32.72	25	5.80	32.74	25.81
48	1.01	33.03	50	0.85	33.04	26.51
72	0.09	33.09	75	0.05	33.10	26.59

Station 6306; July 12; latitude 47°40.5′ N., longitude 49°52′ W.; depth 121 m.; dynamic height 971.138.

Observed values			Scaled values			
Depth, meters	Temperature, ° C.	Salinity, °/oo	Depth, meters	Temperature, ° C.	Salinity, °/oo	σ_t
0	6.91	32.34	0	6.91	32.34	25.36
25	6.40	32.39	25	6.40	32.39	25.47
49	0.06	32.78	50	−0.05	32.80	26.36
74	−0.55	33.00	75	−0.55	33.01	26.55
98	−0.61	33.11	100	−0.60	33.12	26.63

STATIONS OCCUPIED IN 1956—Continued

Observed values			Scaled values			
Depth, meters	Temperature, ° C.	Salinity, ‰	Depth, meters	Temperature, ° C.	Salinity, ‰	σ_t
Station 6307; July 13; latitude 47°59′ longitude 49°43′ W.; depth 190 m.; dynamic height 971.127.						
0	6.06	32.03	0	6.06	32.03	25.23
25	4.59	32.09	25	4.59	32.09	25.43
50	−1.44	32.87	50	−1.44	32.87	26.46
75	−1.47	33.01	75	−1.47	33.01	26.58
100	−0.58	33.26	100	−0.58	33.26	26.74
150	0.01	33.64	150	0.01	33.64	27.03
Station 6308; July 13; latitude 48°10′ N., longitude 49°38′ W.; depth 224 m.; dynamic height 971.127.						
0	6.61	31.87	0	6.61	31.87	25.04
25	3.16	32.25	25	3.16	32.25	25.70
49	−1.36	32.87	50	−1.40	32.88	26.47
74	−1.44	33.00	75	−1.45	33.00	26.57
99	−1.29	33.12	100	−1.30	33.13	26.66
148	−0.70	33.44	150	−0.65	33.46	26.92
197	0.94	33.96	200	1.05	33.99	27.25
Station 6309; July 13; latitude 48°31′ N., longitude 49°28′ W.; depth 677 m.; dynamic height 971.006.						
0	6.63	32.15	0	6.63	32.15	25.25
20	5.66	32.81	25	4.90	32.91	26.05
41	2.21	33.15	50	0.80	33.30	26.71
61	0.07	33.50	75	0.25	33.72	27.09
81	0.39	33.81	100	1.00	34.08	27.32
122	1.96	34.31	150	2.45	34.45	27.51
163	2.60	34.50	200	2.80	34.57	27.58
244	3.07	34.62	300	3.05	34.66	27.63
296	2.94	34.67	400	3.15	34.70	27.65
452	3.18	34.71	(600)	3.25	34.75	27.68
Station 6310; July 13; latitude 48°36.5′ N., longitude 49°26′ W.; depth 1,069 m.; dynamic height 970.948.						
0	6.05	32.95	0	6.05	32.95	25.94
25	4.19	33.17	25	4.19	33.17	26.33
49	2.50	33.87	50	2.45	33.90	27.07
73	1.51	34.17	75	1.50	34.18	27.37
97	1.89	34.27	100	1.95	34.28	27.42
147	2.57	34.51	150	2.60	34.52	27.56
196	2.94	34.61	200	2.95	34.61	27.60
293	3.16	34.69	300	3.10	34.68	27.64
375	*3.15	34.72	400	3.25	34.74	27.67
561	3.39	34.80	600	3.45	34.81	27.71
745	3.47	34.85	800	3.50	34.86	27.75
951	3.43	34.86	1,000	3.45	34.86	27.75

Observed values			Scaled values			
Depth, meters	Temperature, ° C.	Salinity, ‰	Depth, meters	Temperature, ° C.	Salinity, ‰	σ_t
Station 6311; July 13; latitude 49°03.5′ N., longitude 49°16′ W.; depth 1,665 m.; dynamic height 970.868.						
0	7.06	33.59	0	7.06	33.59	26.32
25	7.03	34.25	25	7.03	34.25	26.85
50	4.39	34.55	50	4.39	34.55	27.41
76	3.84	34.63	75	3.85	34.63	27.52
101	3.56	34.67	100	3.55	34.67	27.59
151	3.35	34.76	150	3.35	34.76	27.68
202	3.45	34.78	200	3.45	34.78	27.68
303	3.47	34.84	300	3.50	34.84	27.73
405	3.47	34.86	400	3.45	34.86	27.75
604	3.36	34.86	600	3.40	34.86	27.76
801	3.38	34.87	800	3.40	34.87	27.77
1,002	3.36	34.88	1,000	3.35	34.88	27.77
1,508	3.33	34.92				
Station 6312; July 13; latitude 49°31′ N., longitude 49°08′ W.; depth 1,701 m.; dynamic height 970.863.						
0	7.72	33.73	0	7.72	33.73	26.34
25	5.25	34.39	25	5.25	34.39	27.18
49	4.60	34.54	50	4.55	34.54	27.38
74	3.70	34.60	75	3.70	34.60	27.52
99	3.58	34.71	100	3.55	34.71	27.62
148	3.50	34.77	150	3.50	34.77	27.68
197	3.43	34.78	200	3.45	34.78	27.68
296	3.43	34.82	300	3.45	34.82	27.72
369	3.48	34.85	400	3.45	34.85	27.74
556	3.41	34.86	600	3.40	34.86	27.76
743	3.34	34.85	800	3.35	34.87	27.77
936	3.36	34.87	1,000	3.35	34.87	27.77
1,430	3.32	34.89				
Station 6313; July 13; latitude 50°01′ N., longitude 49°01′ W.; depth 1,847 m.; dynamic height 970.874.						
0	8.65	34.38	0	8.65	34.38	26.71
25	7.73	34.43	25	7.73	34.43	26.89
50	4.62	34.55	50	4.62	34.55	27.38
75	3.89	34.60	75	3.89	34.60	27.50
101	3.47	34.65	100	3.45	34.65	27.58
151	3.37	34.75	150	3.35	34.75	27.67
201	3.42	34.80	200	3.40	34.80	27.71
302	3.46	34.82	300	3.45	34.82	27.72
399	3.46	34.84	400	3.45	34.84	27.73
593	3.40	34.84	600	3.40	34.84	27.74
782	3.32	34.85	800	3.35	34.85	27.75
983	3.36	34.89	1,000	3.35	34.89	27.78
1,493	3.32	34.91				
Station 6314; July 15; latitude 53°43′ N., longitude 55°48′ W.; depth 114 m.; dynamic height 1,454.941.						
0	9.20	27.59	0	9.20	27.59	21.34
25	−0.77	32.51	25	−0.77	32.51	26.15
50	−1.20	32.70	50	−1.20	32.70	26.32
74	−1.32	32.78	75	−1.30	32.78	26.38
99	−1.40	32.83	100	−1.40	32.83	26.43

STATIONS OCCUPIED IN 1956—Continued

Station 6315; July 15; latitude 53°51.5′ N., longitude 55°34′ W.; depth 214 m.; dynamic height 1,454.864.

Observed values Depth, meters	Temperature, °C.	Salinity, ‰	Scaled values Depth, meters	Temperature, °C.	Salinity, ‰	σ_t
0	5.97	31.84	0	5.97	31.84	25.09
25	−0.22	32.42	25	−0.22	32.42	26.06
50	−1.27	32.85	50	−1.27	32.85	26.44
75	−1.50	33.01	75	−1.50	33.01	26.58
100	−1.34	33.17	100	−1.34	33.17	26.70
150	−1.00	33.47	150	−1.00	33.47	26.94
190	−0.38	33.71	(200)	−0.20	33.77	27.15

Station 6316; July 15; latitude 53°56.5′ N., longitude 55°24′ W.; depth 169 m.; dynamic height 1,554.810.

Observed values Depth, meters	Temperature, °C.	Salinity, ‰	Scaled values Depth, meters	Temperature, °C.	Salinity, ‰	σ_t
0	6.62	32.31	0	6.62	32.31	25.38
25	1.13	32.74	25	1.13	32.74	26.25
50	−0.83	33.18	50	−0.83	33.18	26.69
75	−1.04	33.42	75	−1.04	33.42	26.90
99	−0.90	33.53	100	−0.90	33.53	26.98
149	0.74	34.01	150	0.80	34.02	27.29

Station 6317; July 15; latitude 54°08.5′ N., longitude 55°05′ W.; depth 172 m.; dynamic height 1,454.817.

Observed values Depth, meters	Temperature, °C.	Salinity, ‰	Scaled values Depth, meters	Temperature, °C.	Salinity, ‰	σ_t
0	4.82	32.07	0	4.82	32.07	25.40
24	−0.90	32.88	25	−0.95	32.89	26.46
49	−1.39	33.06	50	−1.40	33.07	26.62
73	−1.40	33.20	75	−1.40	33.21	26.74
97	−1.17	33.39	100	−1.10	33.41	26.89
145	0.07	33.85	(150)	0.20	33.89	27.22

Station 6318; July 15; latitude 54°17′ N., longitude 54°44′ W.; depth 192 m.; dynamic height 1,454.830.

Observed values Depth, meters	Temperature, °C.	Salinity, ‰	Scaled values Depth, meters	Temperature, °C.	Salinity, ‰	σ_t
0	5.51	31.99	0	5.51	31.99	25.26
26	−0.98	32.79	25	−0.70	32.78	26.37
51	−1.45	33.07	50	−1.45	33.06	26.61
77	−1.36	33.25	75	−1.35	33.23	26.75
102	−1.31	33.36	100	−1.30	33.35	26.84
154	−0.52	33.68	150	−0.60	33.65	27.06

Station 6319; July 15; latitude 54°30.5′ N., longitude 54°28′ W.; depth 227 m.; dynamic height 1,454.815.

Observed values Depth, meters	Temperature, °C.	Salinity, ‰	Scaled values Depth, meters	Temperature, °C.	Salinity, ‰	σ_t
0	4.13	32.37	0	4.13	32.37	25.71
25	−1.22	32.87	25	−1.22	32.87	26.46
49	−1.45	33.14	50	−1.45	33.15	26.68
74	−1.31	33.31	75	−1.30	33.31	25.81
98	−1.27	33.43	100	−1.25	33.44	26.92
147	−0.69	33.67	150	−0.65	33.68	27.09
196	0.38	33.96	200	0.45	33.98	27.27

Station 6320; July 15; latitude 54°46′ N., longitude 53°53′ W.; depth 338 m.; dynamic height 1,454.816.

Observed values Depth, meters	Temperature, °C.	Salinity, ‰	Scaled values Depth, meters	Temperature, °C.	Salinity, ‰	σ_t
0	3.45	32.09	0	3.45	32.09	25.55
20	−0.30	32.89	25	−0.45	32.95	26.50
40	−0.78	33.07	50	−1.15	33.09	26.63
61	−1.29	33.12	75	−1.25	33.18	26.70
80	−1.23	33.21	100	−0.95	33.32	26.81
121	−0.59	33.44	150	−0.25	33.69	27.08
162	−0.11	33.81	200	0.85	34.14	27.38
242	2.22	34.43	(300)	3.25	34.65	27.60

Station 6321; July 15; latitude 54°52′ N., longitude 53°41′ W.; depth 732 m.; dynamic height 1,454.740.

Observed values Depth, meters	Temperature, °C.	Salinity, ‰	Scaled values Depth, meters	Temperature, °C.	Salinity, ‰	σ_t
0	3.38	32.51	0	3.38	32.51	25.89
22	0.69	33.29	25	0.45	33.31	26.74
44	−0.18	33.47	50	−0.15	33.52	26.95
66	0.07	33.70	75	0.45	33.84	27.16
87	0.89	34.06	100	1.05	34.10	27.34
131	1.47	34.20	150	1.75	34.26	27.42
175	2.08	34.33	200	2.45	34.41	27.48
262	3.72	34.68	300	3.65	34.72	27.62
326	3.55	34.74	400	3.70	34.79	27.67
492	3.68	34.83	(600)	3.65	34.85	27.72

Station 6322; July 15; latitude 54°59′ W., longitude 53°22′ W.; depth 1,664 m.; dynamic height 1,454.650.

Observed values Depth, meters	Temperature, °C.	Salinity, ‰	Scaled values Depth, meters	Temperature, °C.	Salinity, ‰	σ_t
0	3.64	33.27	0	3.64	33.27	26.46
23	3.13	34.06	25	3.05	34.09	27.17
45	2.56	34.32	50	2.50	34.33	27.41
68	2.33	34.35	75	2.40	34.40	27.48
90	2.75	34.49	100	2.85	34.53	27.54
136	3.01	34.64	150	3.10	34.67	27.64
181	3.42	34.73	200	3.45	34.75	27.66
271	3.56	34.80	300	3.60	34.81	27.70
386	3.65	34.82	400	3.65	34.82	27.70
576	3.75	34.88	600	3.75	34.88	27.73
765	3.47	34.87	800	3.45	34.87	27.76
962	3.36	34.87	1,000	3.30	34.87	27.78
1,462	3.35	34.90	(1,500)	3.35	34.90	27.79

Station 6323; July 15; latitude 55°03.5′ N., longitude 53°14′ W.; depth 2,122 m.; dynamic height 1,454.608.

Observed values Depth, meters	Temperature, °C.	Salinity, ‰	Scaled values Depth, meters	Temperature, °C.	Salinity, ‰	σ_t
0	5.78	34.47	0	5.78	34.47	27.18
24	3.29	34.59	25	3.30	34.59	27.55
47	3.16	34.65	50	3.15	34.65	27.61
71	3.24	34.69	75	3.25	34.70	27.64
94	3.31	34.72	100	3.30	34.73	27.66
141	3.64	34.79	150	3.65	34.79	27.67
188	3.74	34.81	200	3.75	34.81	27.68
282	3.71	34.84	300	3.70	34.85	27.72
352	------	34.87	400	3.75	34.88	27.73
528	3.78	34.885	600	3.70	34.88	27.74
705	3.60	34.88	800	3.50	34.88	27.76
882	3.43	34.88	1,000	3.40	34.88	27.77
1,373	3.31	34.88	1,500	3.30	34.89	27.79
1,895	3.19	34.93	(2,000)	3.20	34.93	27.83

STATIONS OCCUPIED IN 1956—Continued

Station 6324; July 16; latitude 55°14′ N., longitude 52°59 W.; depth 3,005 m.; dynamic height 1,454.622.

Observed values			Scaled values			
Depth, meters	Temperature, ° C.	Salinity, ‰	Depth, meters	Temperature, ° C.	Salinity, ‰	σ_t
0	5.01	34.30	0	5.01	34.30	27.14
21	4.96	34.31	25	4.80	34.36	27.21
42	2.83	34.58	50	2.90	34.61	27.61
64	3.14	34.67	75	3.30	34.70	27.64
84	3.41	34.73	100	3.50	34.75	27.66
127	3.64	34.77	150	3.70	34.80	27.68
170	3.73	34.83	200	3.75	34.83	27.69
254	3.69	34.83	300	3.55	34.84	27.72
301	3.54	34.84	400	3.50	34.85	27.74
475	3.49	34.855	600	3.45	34.87	27.76
665	3.44	34.87	800	3.35	34.86	27.76
871	3.30	34.86	1,000	3.35	34.86	27.76
1,262	3.35	34.88	1,500	3.35	34.89	27.78
1,624	3.33	34.895	2,000	3.20	34.91	27.82
2,216	3.09	34.92	2,500	2.80	34.92	27.86
2,554	2.71	34.915	(3,000)	1.95	34.90	27.92

Station 6325; July 16; latitude 55°31.5′ N., longitude 52°29′ W.; depth 3,250 m.; dynamic height 1,454.630.

Observed values			Scaled values			
Depth, meters	Temperature, ° C.	Salinity, ‰	Depth, meters	Temperature, ° C.	Salinity, ‰	σ_t
0	6.15	34.49	0	6.15	34.49	27.15
26	6.07	34.52	25	6.05	34.51	27.18
50	3.43	34.64	50	3.45	34.64	27.57
76	3.14	34.67	75	3.15	34.67	27.63
100	3.24	34.70	100	3.25	34.70	27.64
151	3.44	34.75	150	3.45	34.75	27.66
202	3.39	34.75	200	3.40	34.75	27.67
302	3.37	34.81	300	3.40	34.81	27.72
374	3.55	34.85	400	3.55	34.85	27.73
576	3.47	34.85	600	3.45	34.85	27.74
789	3.49	34.86	800	3.50	34.86	27.75
1,013	3.45	34.88	1,000	3.45	34.88	27.76
1,550	3.30	34.89	1,500	3.30	34.89	27.79
2,105	3.32	34.92	2,000	3.30	34.92	27.82
2,398	3.12	34.92	2,500	3.00	34.92	27.85
2,850	2.58	34.925	(3,000)	2.35	34.92	27.90

Station 6326; July 16; latitude 55°55.5′ N., longitude 51°43′ W.; depth 3,438 m.; dynamic height 1,454.656.

Observed values			Scaled values			
Depth, meters	Temperature, ° C.	Salinity, ‰	Depth, meters	Temperature, ° C.	Salinity, ‰	σ_t
0	6.83	34.58	0	6.83	34.58	27.13
27	6.70	34.59	25	6.70	34.59	27.15
52	4.91	34.62	50	5.05	34.62	27.39
79	4.55	34.67	75	4.60	34.66	27.47
105	4.37	34.64	100	4.40	34.64	27.48
158	3.87	34.69	150	3.95	34.68	27.55
210	3.47	34.72	200	3.55	34.71	27.62
315	3.33	34.77	300	3.35	34.76	27.68
410	3.49	34.82	400	3.50	34.81	27.71
613	3.49	34.84	600	3.50	34.84	27.73
818	3.32	34.86	800	3.30	34.86	27.77
1,021	3.28	34.86	1,000	3.30	34.86	27.77
1,537	3.34	34.90	1,500	3.35	34.90	27.79
2,056	3.40	34.91	2,000	3.40	34.91	27.80
2,497	3.12	34.91	2,500	3.10	34.91	27.83
2,978	2.68	34.92	3,000	2.65	34.92	27.88
3,332	1.85	34.90				

Station 6327; July 17; latitude 56°28′ N., longitude 50°35′ W.; depth 3,712 m.; dynamic height 1,454.641.

Observed values			Scaled values			
Depth, meters	Temperature, ° C.	Salinity, ‰	Depth, meters	Temperature, ° C.	Salinity, ‰	σ_t
0	7.15	34.56	0	7.15	34.56	27.07
25	5.15	34.61	25	5.15	34.61	27.37
50	3.95	34.66	50	3.95	34.66	27.54
75	3.72	-------	75	3.72	34.68	27.58
100	3.55	34.69	100	3.55	34.69	27.60
148	3.38	34.66	150	3.40	34.66	27.60
198	3.39	34.76	200	3.40	34.76	27.68
298	3.33	34.78	300	3.35	34.78	27.69
414	*3.36	34.82	400	3.35	34.81	27.72
620	3.41	34.84	600	3.40	34.84	27.74
825	3.37	34.855	800	3.40	34.85	27.75
1,030	3.35	34.86	1,000	3.35	34.86	27.76
1,550	3.31	34.87	1,500	3.35	34.87	27.77
2,069	3.39	34.91	2,000	3.40	34.91	27.80
2,502	3.19	34.91	2,500	3.20	34.91	27.82
2,988	2.81	34.93	3,000	2.80	34.93	27.86
3,468	1.92	34.89	(3,500)	1.80	34.89	27.92

Station 6328; July 17; latitude 57°01.5′ N., longitude 49°27′ W.; depth 3,598 m.; dynamic height 1,454.617.

Observed values			Scaled values			
Depth, meters	Temperature, ° C.	Salinity, ‰	Depth, meters	Temperature, ° C.	Salinity, ‰	σ_t
0	7.14	34.54	0	7.14	34.54	27.06
26	4.75	34.62	25	4.80	34.62	27.42
52	4.30	34.63	50	4.35	34.63	27.47
78	3.65	34.67	75	3.70	34.66	27.57
104	3.48	34.70	100	3.50	34.69	27.61
155	3.36	34.72	150	3.35	34.74	27.66
208	3.45	34.78	200	3.45	34.77	27.68
312	3.38	34.81	300	3.40	34.81	27.72
416	3.41	34.845	400	4.40	34.84	27.74
623	3.30	34.85	600	3.30	34.85	27.76
830	3.41	34.87	800	3.40	34.87	27.77
1,035	3.38	34.88	1,000	3.40	34.88	27.77
1,556	3.33	-------	1,500	3.30	34.89	27.78
2,077	3.40	34.90	2,000	3.40	34.90	27.79
2,449	3.23	34.93	2,500	3.20	34.93	27.83
2,937	2.87	34.935	3,000	2.80	34.93	27.86
3,424	2.02	34.88	(3,500)	1.80	34.86	27.90

Station 6329; July 17; latitude 57°34.5′ N., longitude 48°26′ W.; depth 3,383 m.; dynamic height 1,454.607.

Observed values			Scaled values			
Depth, meters	Temperature, ° C.	Salinity, ‰	Depth, meters	Temperature, ° C.	Salinity, ‰	σ_t
0	6.78	34.55	0	6.78	34.55	27.11
26	5.25	34.65	25	5.30	34.64	27.37
52	4.39	34.71	50	4.45	34.71	27.53
78	3.79	34.735	75	3.85	34.73	27.60
104	3.60	34.725	100	3.60	34.73	27.63
155	3.58	34.76	150	3.60	34.76	27.66
207	3.61	34.785	200	3.60	34.78	27.67
311	3.44	34.83	300	3.45	34.83	27.72
388	3.39	34.84	400	3.40	34.84	27.74
583	3.52	34.88	600	3.50	34.88	27.76
780	3.39	-------	800	3.40	34.88	27.77
977	3.35	-------	1,000	3.35	34.88	27.77
1,485	3.28	34.88	1,500	3.30	34.88	27.78
2,003	3.38	34.905	2,000	3.40	34.91	27.80
2,549	3.06	34.91	2,500	3.10	34.91	27.83
3,047	2.56	34.90	3,000	2.60	34.90	27.86
3,347	1.73	34.87				

Table of Oceanographic Data—Continued

STATIONS OCCUPIED IN 1956—Continued

Station 6330; July 18; latitude 58°09′ N., longitude 47°16′ W.; depth 3,127 m.; dynamic height 1,454.627.

Observed values			Scaled values			
Depth, meters	Temperature, ° C.	Salinity, ‰	Depth, meters	Temperature, ° C.	Salinity, ‰	σ_t
0	6.21	34.67	0	6.21	34.67	27.29
25	6.20	34.67	25	6.20	34.67	27.29
50	4.72	34.71	50	4.72	34.71	27.50
75	4.58	34.71	75	4.58	34.71	27.51
101	4.29	34.74	100	4.30	34.74	27.57
151	3.92	34.80	150	3.90	34.80	27.66
201	3.81	34.82	200	3.80	34.82	27.69
302	3.84	34.845	300	3.85	34.85	27.70
402	3.51	34.84	400	3.50	34.84	27.73
604	3.38	34.85	600	3.40	34.85	27.75
806	3.41	34.87	800	3.40	34.87	27.77
1,008	3.34	34.87	1,000	3.35	34.87	27.77
1,516	3.30	34.875	1,500	3.30	34.88	27.78
2,027	3.30	34.92	2,000	3.30	34.92	27.82
2,459	2.86	34.92	2,500	2.80	34.92	27.86
2,941	2.05	34.885	(3,000)	1.95	34.88	27.90

Station 6331; July 18; latitude 58°41.5′ N., longitude 46°08′ W.; depth 2,563 m.; dynamic height 1,454.613.

Observed values			Scaled values			
Depth, meters	Temperature, ° C.	Salinity, ‰	Depth, meters	Temperature, ° C.	Salinity, ‰	σ_t
0	6.37	34.60	0	6.37	34.60	27.21
23	6.35	34.60	25	6.30	34.60	27.22
45	5.00	34.74	50	5.05	34.78	27.51
68	5.45	34.91	75	5.30	34.91	27.59
90	5.09	34.91	100	5.05	34.92	27.63
135	4.98	34.94	150	4.90	34.94	27.66
180	4.74	34.93	200	4.65	34.93	27.68
270	4.41	34.92	300	4.35	34.92	27.71
349	4.22	34.91	400	4.15	34.91	27.72
524	3.96	34.91	600	3.80	34.91	27.76
699	3.67	34.91	800	3.60	34.91	27.78
874	3.55	34.91	1,000	3.50	34.91	27.79
1,351	3.36	34.91	1,500	3.30	34.92	27.82
1,856	3.16	34.93	2,000	3.05	34.93	27.84
2,296	2.57	34.93	2,500	1.95	34.90	27.92
2,539	1.81	34.89				

Station 6332; July 19; latitude 59°04′ N., longitude 45°17′ W.; depth 2,195 m.; dynamic height 1,454.659.

Observed values			Scaled values			
Depth, meters	Temperature, ° C.	Salinity, ‰	Depth, meters	Temperature, ° C.	Salinity, ‰	σ_t
0	6.37	34.53	0	6.37	34.53	27.15
26	6.38	34.52	25	6.38	34.52	27.14
52	6.25	34.77	50	6.25	34.74	27.33
78	6.01	34.97	75	6.05	34.96	27.54
104	5.85	34.985	100	5.85	34.98	27.57
155	5.74	35.00	150	5.75	35.00	27.60
207	5.29	34.95	200	5.35	34.95	27.61
311	4.82	34.95	300	4.90	34.95	27.67
345	4.61	34.93	400	4.40	34.91	27.69
526	4.06	34.895	600	3.90	34.89	27.73
714	3.64	34.895	800	3.55	34.89	27.76
907	3.44	--------	1,000	3.40	34.89	27.78
1,390	3.29	34.88	1,500	3.25	34.89	27.79
1,892	3.04	34.935	2,000	2.85	34.92	27.86
1,924	2.98	34.93				
2,049	2.73	34.91				

Station 6333; July 19; latitude 59°13′ N., longitude 44°54′ W.; depth 2,012 m.; dynamic height 1,454.653.

Observed values			Scaled values			
Depth, meters	Temperature, ° C.	Salinity, ‰	Depth, meters	Temperature, ° C.	Salinity, ‰	σ_t
0	6.68	34.77	0	6.68	34.77	27.30
25	6.65	34.80	25	6.65	34.80	27.33
50	6.51	34.81	50	6.51	34.81	27.36
74	5.96	34.97	75	5.95	34.97	27.56
99	5.90	34.995	100	5.90	34.99	27.58
149	5.79	34.995	150	5.80	34.99	27.59
198	5.49	34.93	200	5.45	34.94	27.59
297	4.98	34.94	300	5.00	34.94	27.65
398	4.66	34.935	400	4.65	34.93	27.68
597	4.21	34.935	600	4.20	34.93	27.73
795	3.84	34.92	800	3.85	34.92	27.76
994	3.58	34.91	1,000	3.60	34.91	27.78
1,500	3.23	34.91	1,500	3.25	34.91	27.81
2,012	2.58	34.91	2,000	2.60	34.91	27.87

Station 6334; July 19; latitude 59°21′ N., longtiude 44°29′ W.; depth 1,097 m.; dynamic height 1,454.780.

Observed values			Scaled values			
Depth, meters	Temperature, ° C.	Salinity, ‰	Depth, meters	Temperature, ° C.	Salinity, ‰	σ_t
0	1.50	32.89	0	1.50	32.89	26.33
23	1.32	33.63	25	1.30	33.65	26.96
47	2.27	33.89	50	2.40	33.92	27.10
70	3.50	34.12	75	3.25	34.09	27.15
93	2.47	34.00	100	2.65	34.08	27.20
140	4.20	34.50	150	4.55	34.58	27.41
187	5.50	34.87	200	5.50	34.87	27.54
280	5.25	34.89	300	5.25	34.89	27.58
298	5.27	34.90	400	5.00	34.89	27.61
457	4.88	34.88	600	4.75	34.89	27.63
621	4.72	34.89	800	4.35	34.90	27.69
808	4.33	34.90	(1,000)	3.85	34.91	27.75

Station 6335; July 20; latitude 59°36′ N., longitude 44°14′ W.; depth 205 m.; dynamic height 1,454.936.

Observed values			Scaled values			
Depth, meters	Temperature, ° C.	Salinity, ‰	Depth, meters	Temperature, ° C.	Salinity, ‰	σ_t
0	0.46	31.39	0	0.46	31.39	25.20
25	0.34	31.61	25	0.34	31.61	25.38
50	0.22	31.91	50	0.22	31.91	25.63
75	0.00	32.53	75	0.00	32.53	26.14
100	0.25	33.09	100	0.25	33.09	26.57
149	2.70	34.21	150	2.70	34.21	27.30
178	3.07	34.37	(200)	3.30	34.48	27.46

* U. S. GOVERNMENT PRINTING OFFICE : 1958 O—473864

Contribution No. 900

Reprinted from LIMNOLOGY AND OCEANOGRAPHY
Vol. 3, No. 1, January, 1958
Printed in U.S.A.

The Effects of Winds on Water Levels on the New England Coast[1]

ARTHUR R. MILLER

Woods Hole Oceanographic Institution, Woods Hole, Mass.

ABSTRACT

Tidal records from Nantucket Sound, Cape Cod; Montauk, Long Island; and Portland, Maine, have been studied along with wind and barometric observations from each location. Results of this study show that departures from mean sea level due to wind may be resolved into two components. The first is a component which refers to symmetrical sinusoidal variation of sea level departure as a function of wind direction and applies to the outer coast and to the general level of Nantucket Sound in particular.

The second is an asymmetrical component which refers the responses of sea level at each observing station to local wind force, direction, fetch length, and local topography. Under different circumstances these components vary in relative importance in determining the local departure from mean sea level. In addition to wind direction and velocity, duration and size of wind field may determine whether one component is more important than the other.

The varying importance of each component probably governs the time-lag between peak winds and maximum sea level departures which will vary from several hours to as much as twenty hours.

INTRODUCTION

The coast of New England is subjected from time to time to extraordinarily high water, the scale of which is usually related to the intensity of storms. Most spectacular are the inundations that sometimes occur during hurricanes. The extra elevation of sea level over the normal tide during a hurricane may amount to as much as ten to fifteen feet (Redfield and Miller 1957). Elevations of this scale are uncommon and hence adequate data are rare. Related phenomena on a smaller scale but of greater frequency should provide data useful for a better understanding of unusually high waters. It is the purpose of this paper to explore the less spectacular but more frequent departures from mean sea level accompanying ordinary winter storms.

Where departures from normal water levels have been greater than the normal tide, common practice has been to identify these departures as storm surges. The term *surges* in this paper will refer to relatively short periods of excessive height occurring during passage of a storm. Apart from surging of water levels, another sea-level phenomenon accompanying a storm but of much longer duration is that of set-up (Miller 1957). The term *set-up* has been used to describe the total seaward slope of water surface from a shore line which is established and maintained by relatively steady winds.

These phenomena are difficult to separate analytically, one difficulty being the lack of firm distinction between definitions of surge and set-up. For this purpose the term set-up may be considered as slope of water surface developing *in situ* and surge as slope of water surface developing in *direction of propagation*. Since tidal observations are usually limited to the shoreline, measurements of slope are likewise limited. Consequently, with respect to a tide staff, the essential difference between the two phenomena is that surge is a rapid rise in water level with a duration of several hours or less, while set-up appears to be a relatively slow rise or fall of water level with durations of hours or days, depending on the persistence of winds and direction of winds.

---

[1] Contribution #900 from the Woods Hole Oceanographic Institution, Woods Hole, Massachusetts. This study was initiated with the aid of the Office of Naval Research, U. S. Navy. Further assistance was made available through the National Hurricane Research Project, U. S. Weather Bureau. The help of the U. S. Coast and Geodetic Survey and the U. S. Weather Bureau in providing data is gratefully acknowledged.

This paper attempts to describe the amount of set-up observed to accompany winds of various strengths and directions at several different positions on the New England coast. Observations from six tide gauging stations were used (Fig. 1). Four of these stations were situated about Nantucket Sound, the other two at Portland, Maine, and Montauk, Long Island. Montauk is more or less exposed to the open sea from the south, Portland from the east, while Nantucket Sound is exposed from the east, south, or west. In addition to the different exposures of the three regions, the tidal characteristics vary greatly both in time of high water and in tidal range. For instance, Woods Hole in Nantucket Sound has a mean range of less than two feet while Portland has a range greater than nine feet.

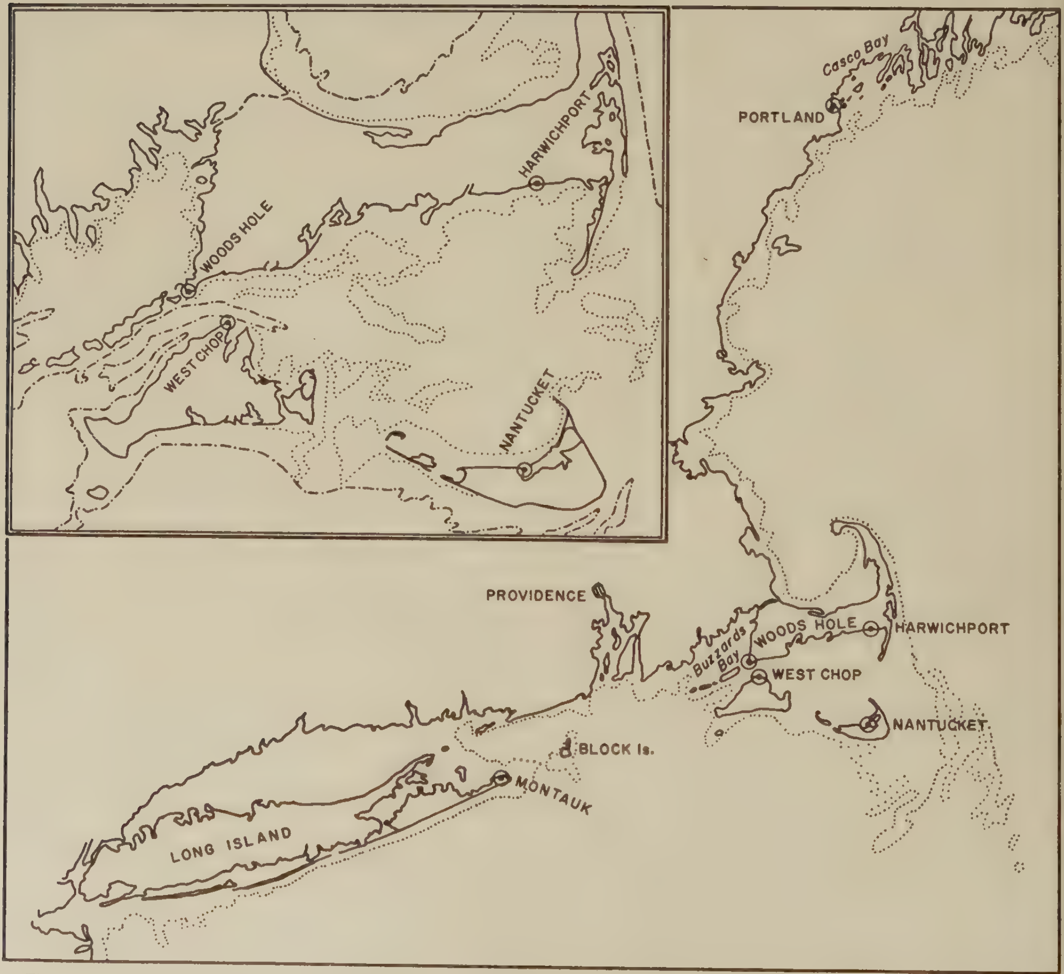

Fig. 1. Locations of tide gauges in New England and on Long Island. Insert is enlarged view showing Nantucket Sound area.

Within Nantucket Sound itself there is a difference of more than three hours between time of high water from one end to the other (Redfield 1953). The dissimilarity of the stations serves to emphasize those features within the analyzed data which are common to all six stations.

The tidal observations have been treated so that non-periodic effects are separated from the predictable periodic motions. The predicted tide if subtracted from the observations will give as a remainder the effects of non-periodic variation in barometric pressure, tangential stress of the wind, or other forces whatever they may be. These variations in sea level are referred to collectively as meteorological effect. Further refinement is obtained if the non-predictable periodic motion is eliminated by some means. The residue is called *non-tidal sea level.* Variations of non-tidal sea level are then assumed to be made of two parts: (1) *barometric effect,* and (2) set-up, attributed to the coastal effects of tangential wind stress on the sea surface.

The method for obtaining non-tidal sea level is the use of numerical filters to eliminate as much of the tidal "noise" from the data as possible, following the recommendations of Groves (1955). The advantage of the filtering system or weighted average over the subtraction of the predicted tide from observations is in this reduction of "noise" in the data and also, for the particular objectives of this study, the minimizing of short-duration oscillatory phenomena, such as long waves or surges. In fact, since the tidal curves about Nantucket Sound were not predictable in detail, the method of numerical filtering was the only suitable means to eliminate the tide. The specific filter used was that described by Doodson and Warburg (1941) to determine mean sea level for any hour (B 39 filter in Groves' tabulation).

NON-TIDAL SEA LEVEL

Nantucket Sound is a triangular area adjoining the southern shore of Cape Cod and separating the two islands, Martha's Vineyard and Nantucket, from the mainland (see insert in Fig. 1). The apex of this triangle which averages about 30 feet in depth funnels into a deeper channel-like area with average depth of 70 feet, called Vineyard Sound, which in turn is open to the ocean. The opening of the Sound to the east is partially closed to the ocean by land barriers extending from the Cape and Nantucket Island. Between the two islands there is an outlet to the ocean to the south, of lesser importance because of its limited depths.

Two of the gauging stations were in the eastern part of the Sound. To the north was the Harwichport gauge, and due south of Harwichport the Nantucket gauge. At the western end the two stations Woods Hole and West Chop were closer together. In spite of their closeness their tidal situations are different since Woods Hole is influenced in some degree by the passage entering into Buzzards Bay.

The tidal observations used were hourly heights obtained from October, 1953, to March, 1954. Figure 2 shows the results of numerical filtering of the data from Nantucket Sound, Montauk, and Portland for three representative storms. Each trace is referred to the monthly mean sea level of each station.

The concurrent non-tidal sea levels change in a very similar way at all of the six tide gauges. However, there were significant departures from this parallelism. For instance, during the northeast storm of November 7, the Montauk sea level rose to a height more than twice the height at Portland. There were periods when concurrent sea levels at Woods Hole or Nantucket differed appreciably from those at other stations. Frequently, there were times when no station differed from any other by more than a tenth of a foot. Thus, parallelism of non-tidal sea levels about New England is a loose, but real, generalization.

BAROMETRIC PRESSURE

In the passage of storms over the New England area there is usually a west to east motion. This motion is reflected in the barometric records. The relation is such that at times there will be parallelism in the pressure records among the stations similar

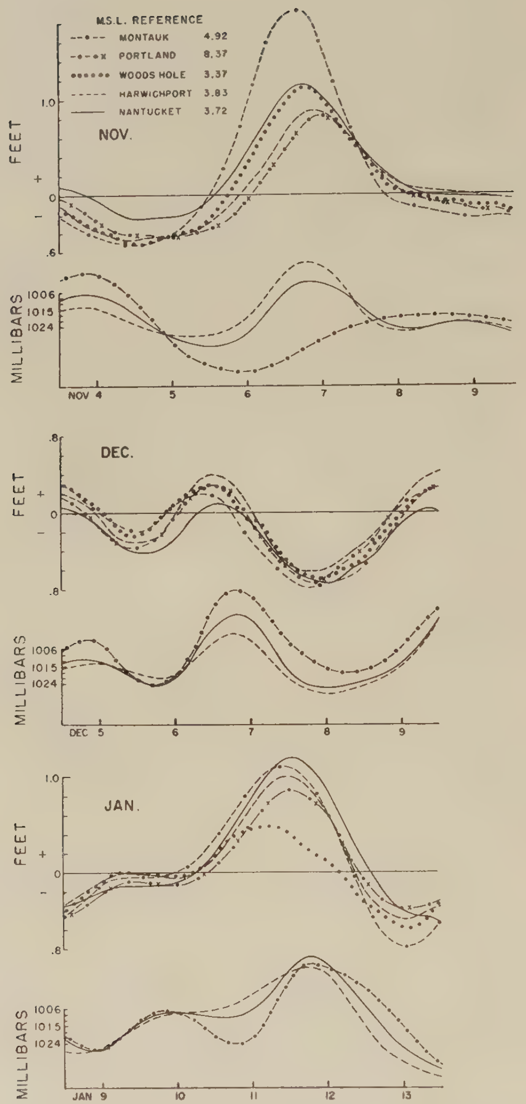

Fig. 2. Non-tidal sea levels during three storms with concurrent barometric pressures. The common datum for five stations is monthly mean sea level. Barometric pressures are shown for three general areas: Montauk - - - - -, Nantucket ———, Portland -·-·-·-·-.

to the sea level phenomena, or just as frequently the interrelations may be quite dissimilar. Whether the records are similar or not will depend on the size, speed, and geographical distribution of the pressure disturbance.

Barometric pressures are shown in Figure 2 below the non-tidal sea levels for all three localities. The vertical scale for pressure is inverted so that a rising curve represents a drop in pressure. As sea level rises and falls, an inverse correspondence of rise and fall of barometric pressure usually accompanies the sea level variation. The parallelism between the different locations is less close in the case of barometric pressure than in that of non-tidal sea levels.

In most cases where correspondence between the two types of curves was clear the fluctuation of sea level preceded the fluctuations of pressure, the precedence varying from six to twenty-four hours. The precedence of a sea level event before an event in pressure has not gone unnoticed. In cases of tropical hurricanes and other severe storms an abnormal rise of water levels is sometimes taken as a sign of an approaching storm (Cline 1926). The effect has been noticed in the Gulf of Mexico and along the east coast. The comparisons of sea level and pressure for the New England coast show that this is a regular phenomena.

BAROMETRIC CORRECTION

When there is an unequal distribution of pressure over a sea surface the level of the sea will rise under low pressure and fall under high pressure in an amount commensurate with the difference between the densities of air and water. The theoretical amount of rise of fall is approximately 1 foot for 30 millibars of pressure if equilibrium is established. Where pressure changes with time the response of sea level will be nearly immediate provided the volume of water involved can flow unimpeded (Doodson and Warburg 1941). It is not certain whether the latter condition is met in a restricted shallow sea such as Nantucket Sound.

Observations of sea level when other forces are at a minimum should indicate if the theoretical value is valid. Non-tidal sea levels for two stations, Harwichport and West Chop, were selected at periods when wind force was less than 15 knots and compared with barometric readings for the same time. While there was considerable scatter of values of sea level against pressure, as would be expected in such rough determinations, these values clustered linearly, and the results showed that theoretical relationship could be applied to the conditions at these stations.

With the pressure correction established empirically, the non-tidal sea levels were corrected for pressure. The sea levels resulting from the subtraction of the pressure fluctuations are shown in Figure 3 for the storms of December 7, September 2, and January 11. The subtraction of the pressure effect from the non-tidal sea levels altered the curves significantly—two feet in water level representing ranges of pressure up to 60 millibars as compared with ranges of non-tidal sea level up to three or four feet. The residue from this subtraction was assumed to be the variations of sea level resulting from wind set-up.

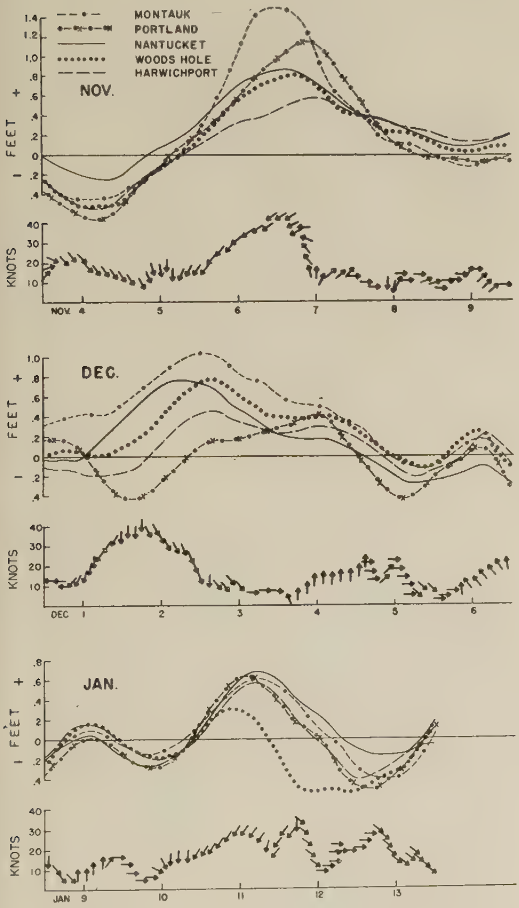

FIG. 3. Non-tidal sea levels corrected for effects of pressure. The common datum for five stations is monthly mean sea level. Observed winds at Nantucket are shown below each set of curves. Wind velocity is read on the knot scale opposite the arrow points.

WIND SET-UP

First attempts to relate the observed winds, examples of which are shown in Figure 3, to the observed set-up were wholly unsatisfactory. It was anticipated that the relation would be sinusoidal at each station, that is, rise and fall of sea level would be symmetrically responsive to some component of wind direction. At Atlantic City, sinusoidal symmetry was applicable in the correlation of set-up with geostrophic winds (Miller 1957). However, Atlantic City is part of a long, straight coastline. This is not the case with the New England coast where the coastline is broken by promontories, bays, and sounds.

Wind force acts on the sea surface as a frictional force on the skin layer; consequently, the velocity is maximal at the surface, decreasing with depth. If this motion is directed towards a coast, an elevation will result at the coastline which will continue to rise until the resulting slope of the surface is sufficient to balance the forces responsible for the motion. The development of elevation depends on transport of water to the coast; consequently, this phenomenon must follow the occurrence of winds giving rise to it. Also, an existing wind drift could conceivably resist casual wind shifts, since any change in the prevailing forces would have to be downwards before the general transport would be appreciably affected. The quality of steadiness of the wind, therefore, is important to the net amount of water being transported.

Non-tidal sea levels rise and fall aperiodically with time but fluctuate slowly enough to identify the time and height of each peak or trough. It was assumed that at each of these times of stationary sea level, a critical relation existed between the set-up and the wind force responsible for the fluctuation. Wind records from nearby weather stations were examined for the greatest velocity prior to the event of stationary sea level. The time, velocity, and direction were noted along with the time and height of set-up.

A time interval of less than 24 hours was considered to be a reasonable limit within which these comparisons were carried out. On a few occasions it was necessary to match sea level heights with early wind shifts where peak velocities were absent. The relation is not violated by the latter method since a peak velocity of some wind component is indicated by the shift of wind.

These selected heights of sea level were plotted on polar coordinates, where radial vectors corresponding to the direction and velocity of the wind were matched with the particular height. With the completion of the polar diagram, lines of equal height were drawn to fit the distribution of observations. During six months of observation full directional distribution of winds may be expected in New England, with some directions favored more than others. For the most part it was usually found that for a single wind direction there were a number of events to represent a full velocity spectrum up to 35 knots, and a linear relationship between set-up and wind was a reasonable description of the observations. With full directional distribution, very little interpolation was required for constructing the diagrams. The results of these diagrams were presumed to describe the sea level required to balance a given wind condition and to describe the characteristic conditions at the observing tide station.

The diagrams representing characteristic set-up for given winds are shown in Figure 4 for all 6 gauging stations. Lines of sea level are given in tenths of feet in terms of each local tide staff. The division between negative and positive set-up represents mean sea level at the station. This division was derived from the summation of all observations within the first 10-knot circle and also corresponds to the summation of the total monthly sea levels for the period of observation at each station. The diagrams are similar in general features but differ greatly from each other along critical wind directions. Nor do they show any features of symmetry except in the progressions in scale of set-up in adjoining compass directions. It is not clear from these diagrams how the scale of set-up is affected by local topography. They scarcely explain how a station, such as Harwichport, can exhibit a rise in sea level with the wind coming off the land.

THE SYMMETRICAL COMPONENT: THE GENERAL COASTAL COMPONENT

It is reasonable to assume that in a landlocked sea such as Nantucket Sound having free communication with the ocean a part of the set-up would result from a widespread change in the coastal non-tidal sea level induced by the general wind field over the off-lying ocean, and an additional part would result from the local winds and the topography surrounding each point of observation. This would account for the differences in the diagrams shown in Figure 4 and would explain the contradiction of wind blowing from the shore giving an increased sea level.

It was assumed that the observations from the four gauging stations about Nantucket Sound when averaged concurrently would represent the set-up as induced by wind on the offshore waters with the effect of local topography reduced to a minimum. The plot of the averaged sea levels from the four Nantucket Sound gauges over a polar wind diagram for Nantucket Sound (Fig. 5) showed that the greatest sea level rise was to be expected from ENE winds, the greatest negative set-up from WSW winds, and that minimum effects were to be expected from NNW and SSE winds. It also showed that both the positive and negative scale of set-up were equal in magnitude. The general characteristics of sea level for the Sound displayed symmetrical sinusoidal response to wind direction, in contrast to the skewness of sea level at the individual localities.

Aside from the above general characteristics for Nantucket Sound there were significant departures inconsistent in certain wind directions which are not shown in Figure 5. To explain these departures it was necessary to resort to weather maps rather than the locally observed winds at Nantucket. The inconsistencies fell into two groups: (1) light S–SW winds with time lags of 0–9 hours, and (2) strong NW–N winds with lags of 12–20 hours. In the

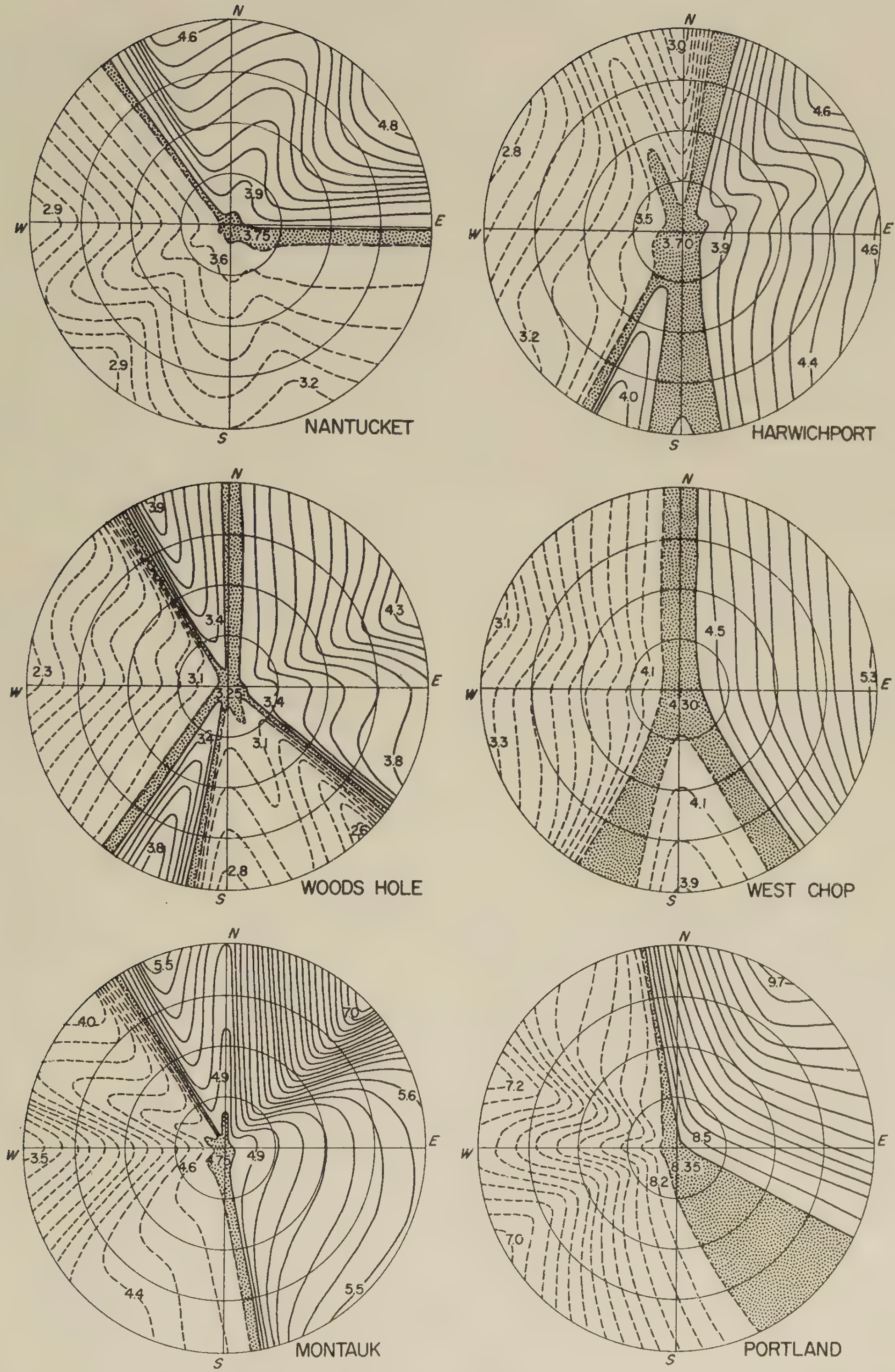

FIG. 4. Characteristic set-ups for six locations. Diagrams show set-up in terms of individual tide staffs for various wind vectors with speeds up to 40 knots. The concentric circles mark 10-knot intervals in wind speed. Shaded areas delineate neutral set-ups where winds have little or no effect on sea level. Dashed isopleths show negative set-ups and full isopleths positive set-ups, with intervals of 0.1 foot.

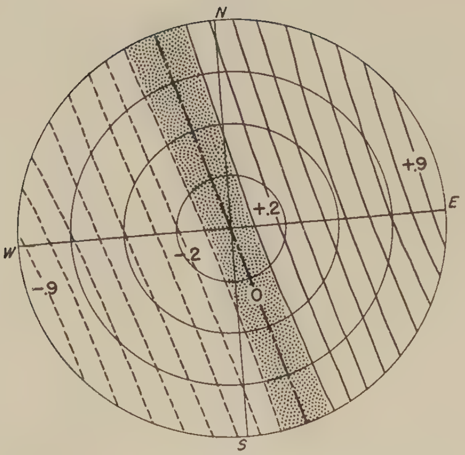

Fig. 5. Set-up for Nantucket Sound. Concentric circles mark intervals of 10 knots. Contour intervals are 0.1 foot.

first case, weather maps showed large high pressure systems over the area, with observed winds at Nantucket not necessarily representative of the larger wind field. In the second case, maps showed deep low pressure systems over Georges Bank and stronger NE winds to the east. It was evident here that dependence on local measured winds for data was limited to the extent in which they were representative of a broad wind field.

An earlier study (Miller 1957) making use of a wind field 300 miles in diameter showed that at Atlantic City, on an open coast without significant promontories or embayments, set-up varied sinusoidally with the direction of wind of a given velocity. This study also showed a quasi-linear relationship between the amount of set-up and increasing velocity of the geostrophic wind. The results of the present analysis for Nantucket Sound indicate a similar sinusoidal variation of sea level and a scale of set-up velocity corresponding to the Atlantic City values.

It was not practicable to determine the general coastal set-up for Montauk or Portland with the data at hand, but it was instructive to apply the generalizations of Atlantic City and Nantucket Sound to both locations. By properly orienting the Atlantic City scale to the coastlines about Montauk and Portland so that maximum general coastal set-ups would be indicated by winds 40° from the normal to the coastline, relations of local set-up were deduced which were consistent with those found about Nantucket Sound.

THE ASYMMETRICAL COMPONENT: THE LOCAL COMPONENT

The contribution of local wind and topography to the set-up observed at the different gauging stations was obtained by subtracting the symmetrical effects attributed to the Sound as a whole from the actual observations. This simple operation gave results for local set-ups which appeared to be systematic and commensurate with the local fetches. Diagrams of local set-up for each of the six tide-gauging stations are shown in Figure 6.

It is instructive to compare the local values of set-up with the open water exposures of each tide gauge (see Fig. 1). Harwichport and Nantucket tide gauges were more or less protected by land barriers from local wind effect except from the southwest for Harwichport and northwest to north for Nantucket. Local set-up showed that Harwichport was vulnerable to excessive sea level from the SSW and Nantucket was vulnerable from the NNW. Lowest local levels were indicated with N winds at Harwichport and SE winds at Nantucket. Other wind directions showed a minimum effect on local level, which was probably due to the limited fetch in these directions. It was apparent that the derived local set-ups agreed qualitatively with the available fetches of each locality.

West Chop and Woods Hole presented modified patterns of local set-up which were more complex than those at the eastern end of the Sound since neither station can be considered a terminus for water transport. Their fetch characteristics from the Sound are mixed with the available fetches in Vineyard Sound and Buzzards Bay.

There were two maxima for positive local set-up in Woods Hole: one from SSW, the Vineyard Sound, and the other from NNW, Buzzards Bay. There were also two maxima for negative set-up: one for SE winds apparently blowing Buzzards Bay water away from Woods Hole, and the other for NW winds affecting Nantucket Sound. In

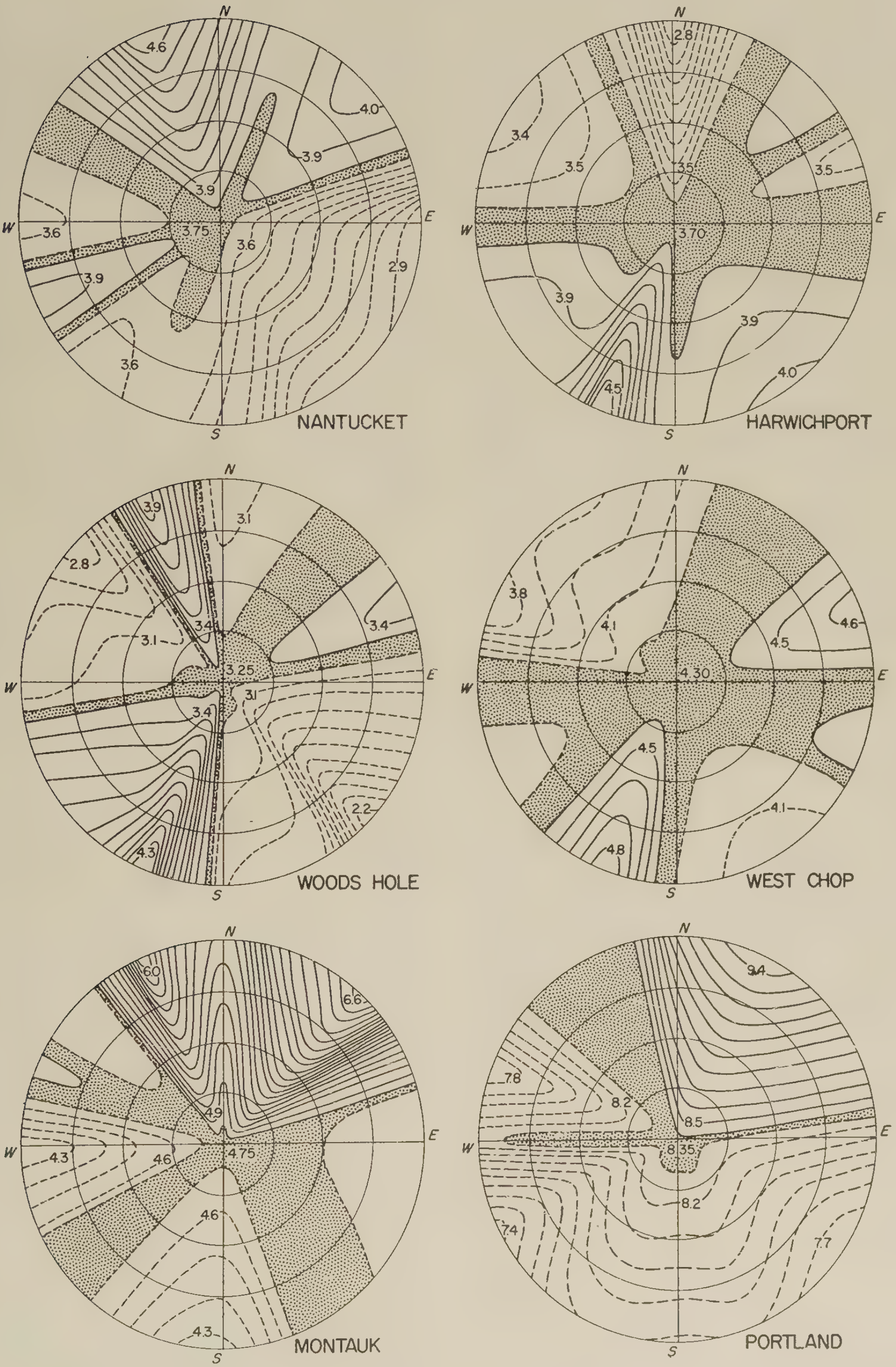

Fig. 6. Local set-ups for six locations, general coastal effects having been removed. Diagrams denote the contribution to total set-up provided by local environment of individual stations and local winds. Concentric circles mark intervals of 10 knots. Contour intervals are 0.1 foot.

contrast to Woods Hole, West Chop local levels appear to be lowered or unaffected by wind from most quarters. Only SSW winds from Vineyard Sound produce appreciable positive set-up. It is possible that the lack of sea level response to wind in the West Chop area is made up for in the acceleration of tidal currents which are notably strong here.

Observations of set-up at Portland and Montauk were matched with appropriate wind observations. The characteristics thus obtained were assumed to be made up of two parts—general coastal effect and local effect. Diagrams of characteristic set-up are shown in Figure 4. It is curious that Portland at the southern end of Casco Bay which itself is exposed to the southeast is least affected with southeast winds. Assuming general coastal set-up to be similar in scale to that at Atlantic City and Nantucket Sound, the Atlantic City scale was oriented to give maximum coastal set-up with winds from 100°, or 40° to the right of normal to the general coastline orientation (050°–230°). Subtraction of the assumed coastal set-up from the observations gave a diagram of local set-up which was reasonable in respect to the local fetch about Portland (Fig. 1 and 6). Portland, at the southern end of box-like Casco Bay, is directly exposed to a NE fetch of the bay itself. A number of islands tend to limit the available fetch in other directions. Local set-up showed maximum positive set-up in the NNE direction and other elevations above mean sea level confined to the NE quadrant. Maximum negative set-up occurred with WSW and WNW winds; all southerly winds tended to lower the local sea level.

The nearest wind data available for Montauk were observations from Block Island. However, Block Island observations lacked continuity. Comparison of Block Island winds with Providence winds, records of which were available for 24 hours a day, showed that Providence was a reasonable substitute. The Montauk tide gauge is exposed to the north on the Montauk peninsula. Characteristic set-ups showed that southerly winds were least effective in raising or lowering sea level. The Atlantic City scale was oriented for a coastline bearing 070°–250° and subtracted from the characteristic set-up. The local set-ups (Fig. 6) derived from this manipulation, showed that maximum positive set-up could be expected with winds from the NE. This corresponds to a line of fetch between Point Judith, Rhode Island, and Montauk. A secondary maximum developed along a line of fetch between New London, Connecticut, and Montauk with NNW winds. The scale of maximum positive set-up was considerably greater than at the other five stations. In contrast, negative set-up was much smaller in scale. Maximum negative set-up occurred with west winds; southerly and easterly winds lowered local sea level only a small amount.

TIME-LAG

The empirical means by which characteristic set-ups were obtained by matching observations of stationary non-tidal sea level with prior winds define the time-lags for each station. However, it is difficult to generalize time lags for particular conditions and localities beyond the following. Statistically a lag of five or six hours between observed peak winds and maximum sea levels applies to the New England Coast. Time lags may vary from one to twenty hours apparently dependent on whether general coastal set-up or local set-up is dominant. This is understandable from the point of view where set-up consists of accumulated wind drift, the greater lag representing drift from greater distance. For instance, time-lags for Woods Hole maxima originating apparently from movement of Buzzards Bay water vary from 2 to 6 hours, while other maxima from Vineyard Sound and Nantucket Sound vary from 5 to 9 hours. These amounts of time-lag are barely more than estimates since the observations show considerable variance.

DISCUSSION

It is clear from the diagrams of characteristic set-up and local set-up that the phenomenon of rise and fall of sea level in response to wind forces is a complex one stemming from local and distant causes. It should not be inferred that these diagrams are complete and finite, since they depend on statistical evaluation for each point of the compass. The nature, duration, and gradient of the winds are such as to indicate that even a statistically correct diagram may not be justifiable for singular events, since it is not known whether the local factors or distant factors will dominate. The interplay of these factors suggests that it would be difficult to generalize for a large area, although that generalization may hold when distant factors prevail.

The storm of November 7, 1953, serves to illustrate to some extent the dominance of one factor over another and the reinforcement or opposition of these factors. Local set-up diagrams were used to obtain the equilibrium condition of local sea level with wind, and the Atlantic City scale (Fig. 5) was used to obtain the general coastal effect. The same observed winds were applied for both the offshore and local equilibria. The results are shown in Figure 7 with the measured non-tidal sea level, barometric effect removed, superimposed over the supposed equilibrium heights. The magnitude of each curve is given in terms of the local tide staff.

It is seen that for Montauk and Portland the local set-up dominated the sea level condition with minor reinforcement from the offshore effects. In contrast, Harwichport and Nantucket were dominated by the offshore factors. Local wind effect served to reinforce or oppose the offshore set-up in a minor fashion. Woods Hole and West Chop were similarly dominated, although it is not clear why West Chop sea level rose in advance of the two conditions of equilibrium with the wind.

FETCH LENGTH AND TOPOGRAPHY

When maximum positive set-up is reached for a given wind velocity and that set-up is representative of the local deformation of the sea surface, equilibrium is assumed between the tangential forces of the wind and sea level. It is necessary to assume, also, that total transport due to wind drift is zero, otherwise the set-up is not truly maximal. It does not follow that the same conditions will hold for maximum negative set-up.

Proudman (1953), in discussing an inclined wind drift in which total transport is zero, introduces a relation where

$$\frac{gh \sin \theta}{u_a^2} = 3.0 \times 10^{-6} \frac{q+3}{q+2}$$

which has bounds of

$$3.0 \times 10^{-6} < \frac{gh \sin \theta}{u_a^2} < 4.5 \times 10^{-6}.$$

Sin θ is the inclination of the sea surface for a given distance or fetch, u_a^2 is the square of the wind force, g the acceleration of gravity, and h is the average depth.

ζ, the amount of set-up, divided by some distance, F, will approximate sin θ provided some fetch length is found corresponding to the total length of deformation. Then

$$3.0 \times 10^{-6} < \frac{g\zeta}{u_a^2} \cdot \frac{h}{F} < 4.5 \times 10^{-6}$$

When the depth-to-fetch ratio is constant, ζ will depend on u_a^2 if equilibrium obtains.

The ratio of depth over fetch sets the theoretical limits of set-up for given velocities of wind. Figure 8 demonstrates the relation between maximum set-up, ζ, and fetch ratio, h/F, for wind velocity of 30 knots. Set-up is given in feet and the fetch ratio is given in feet to nautical miles. The two curves give the limits set by the Proudman function and the circles represent the maximum set-ups indicated by the local set-up diagrams. The large open circle represents the minimum fetch ratio for maximum coastal set-up at Montauk if the path of fetch is taken normal to the general coastline.

The Portland fetch ratio was taken along the length of Casco Bay whose bearing was 15° off the wind direction giving maximum positive set-up. Figure 8 shows Portland set-up for 30 knots of wind and a fetch ratio of 2.3, within the theoretical bounds.

For West Chop the fetch length was rotated 15° from the maximum wind to comply with channel direction of Vineyard

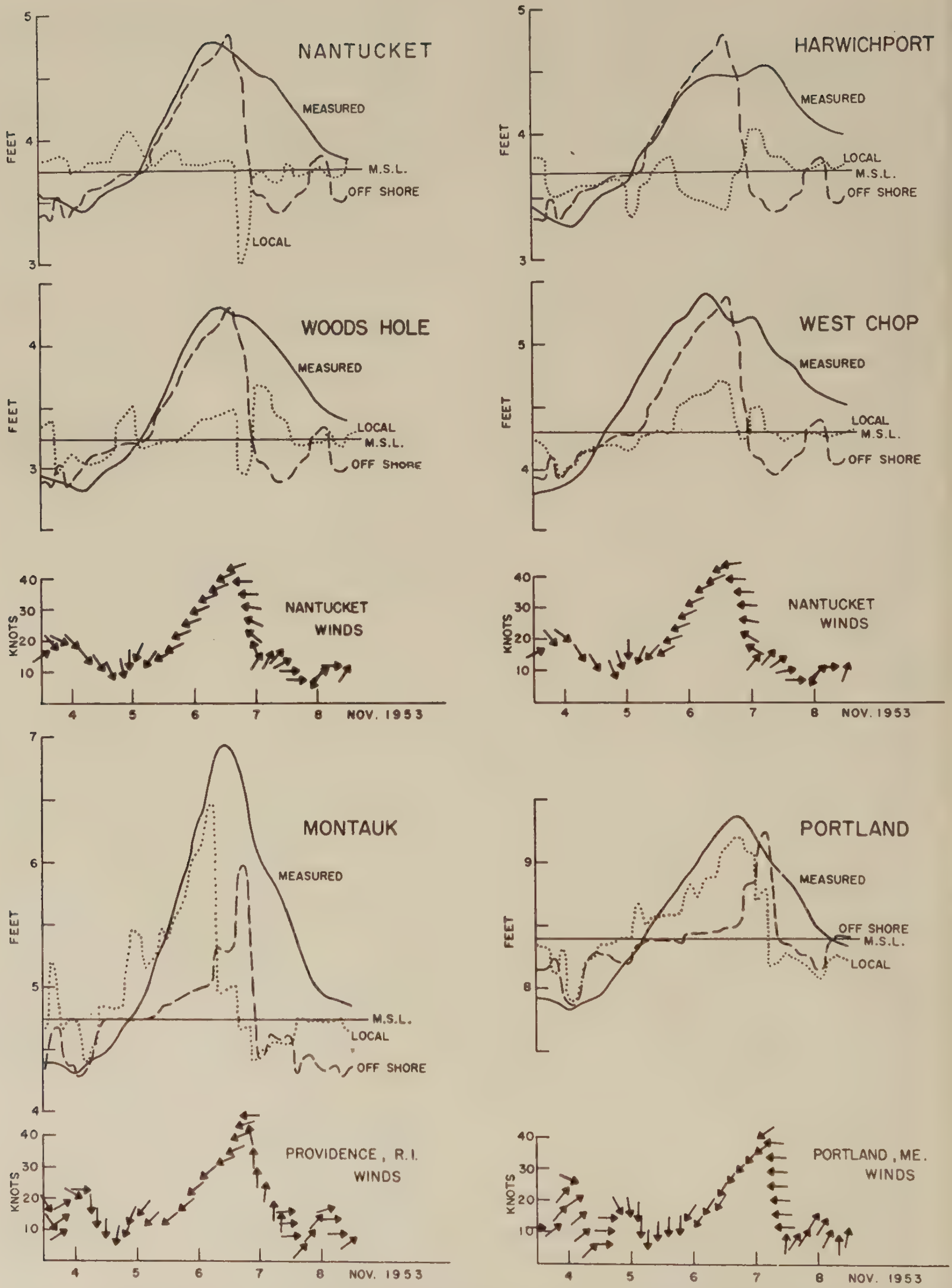

Fig. 7. Comparison of contribution of coastal and local set-ups to the measured non-tidal sea levels for six localities during severe storm of November 7, 1953. Height is given in terms of the tide staff at each locality. Observed winds are shown for each area.

Sound; this was necessary in order to give the wind a water surface to work on. Maximum set-up and a fetch ratio of 5.8 on a much lower scale than Portland, shows a value, for 30 knots of wind, of 0.4 feet, agreeing with the theoretical limit.

The paths of fetch for Portland and West Chop giving maximum local set-up were forced by geographical circumstance into clockwise rotation from the direction of wind. In contrast to the 40° deviation of maximum *coastal* set-up to the right of effective winds, this suggests that the shallower and more limited fetches of local set-up require an angular deviation of approximately 15°. Paths of fetch for the four other stations were taken, allowing for this angular deviation.

Maximum set-up for Woods Hole is greatest with either SSW winds or NNW winds. The first is similar to West Chop with winds piling up water from Vineyard Sound. The second maximum arises from Buzzards Bay. When the path of fetch is rotated from the NNW direction, the fetch runs parallel to the western shoreline of Cape Cod with a depth-to-fetch ratio of 2.1. For 30 knots of wind local set-up is 0.8 feet. The theoretical limits are 0.7 and 1.0 feet.

Maximum local set-up for Montauk arises with NE winds. Angular rotation of path of fetch greatly extends fetch length into the head of Buzzards Bay. The long fetch and shallowness of the Bay give a small ratio of 1.1 and theoretical limits of set-up of 1.1 to 1.8 feet for 30 knots of wind. Local set-up given by the Montauk diagram is 1.6 feet.

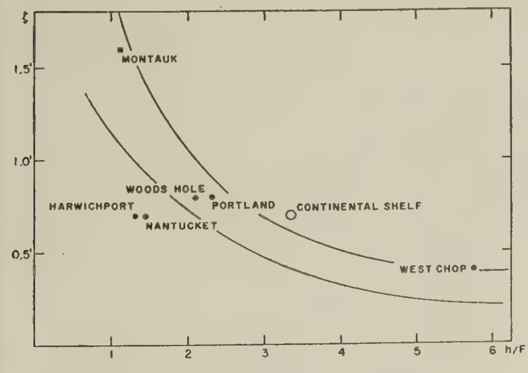

FIG. 8. Set-up as a function of depth-to-fetch ratio. Curves define limits set by Proudman's relation for winds with velocities of 30 knots. Coordinates of the circles are determined from maximum positive set-ups for 30-knot winds and fetches approximately 15° to the right of the wind direction. The units of *h/F* are feet to nautical miles.

Harwichport and Nantucket set-ups for 30 knot winds do not fall within the theoretical limits. The depth-to-fetch ratios for Harwichport and Nantucket are 1.3 and 1.4 respectively. These are minimum ratios. The path of fetch for Harwichport extends through Muskeget Channel between the islands. If the fetch were taken beyond Nantucket Sound, the deeper water and increasing fetch would increase the ratio. With a shorter fetch the average depth and fetch ratio would also increase, since the shoals of Muskeget Channel would be eliminated from the fetch length. A shorter fetch for Nantucket would increase its ratio also for similar reasons; its fetch may not be lengthened because of the mainland. No alternative numbers are given; however, with fetches five miles shorter than those taken both ratios increase to 2.0 or greater.

On the whole, the maximum local set-ups for all six stations appear to be in agreement with theoretical values if the paths of fetch are based on an approximate 15° deviation to the right of the wind. The fetch for coastal set-up is more obscure, but a ratio which reaches a minimum at the edge of the continental shelf approaches the value of 3 when the path is taken normal to the shelf.

SUMMARY

By adopting a uniform scale for coastal set-up requiring a net transport of water 40° to the right of the wind, an angle of 15° to 20° net drift to the right of wind was developed for local set-up where fetches were limited by local topography. Local effects were separated from distant effects by assuming a sinusoidal or symmetrical variation in the amount of coastal set-up with direction of winds. When the characteristic set-ups for locations about the New England coast were obtained empirically, local set-up characteristics were derived by removing the effects of coastal set-up from the data. The local set-ups were asymmetrical with the direction of wind, being largely governed by effects of local topography and immediate fetches available. The time-lag between maximum wind and maximum set-up associated with that wind varied between one and 14 hours. A statistical lag of five to six hours is usual for the New England coast; however, actual time-lags are difficult to determine because of the duality of set-up.

REFERENCES

Cline, I. M. 1926. Tropical cyclones. MacMillan, New York. 301 pp.

Doodson, A. T., and H. D. Warburg. 1941. Admiralty manual of tides. His Majesty's Stationery Office, London. 270 pp.

Groves, Gordon W. 1955. Numerical filters for discrimination against tidal periodicities. Trans. Amer. Geophys. Union, **36**(6): 1073–1084.

Miller, Arthur R. 1957. The effect of steady winds on sea level at Atlantic City. Meteor. Monogr., **2**, No. 10: In press.

Proudman, J. 1953. Dynamical oceanography. Wiley, New York. 409 pp.

Redfield, A. C. 1953. Interference phenomena in the tides of the Woods Hole region. J. Mar. Res., **12**(1): 121–140.

Redfield, A. C., and A. R. Miller. 1957. Water levels accompanying Atlantic Coast hurricanes. Meteor. Monogr., **2**, No. 10: In press.

Contribution No. 906

Reprinted from LIMNOLOGY AND OCEANOGRAPHY
Vol. 3, No. 3, July, 1958
Printed in U.S.A.

Primary Production of Continental Shelf Waters off New York[1]

JOHN H. RYTHER AND CHARLES S. YENTSCH

Woods Hole Oceanographic Institution, Woods Hole, Mass.

ABSTRACT

The chlorophyll-radiation method of measuring primary production, described earlier by the authors, was employed on six oceanographic cruises during 1956–7, each occupying 25 stations across the continental shelf off New York. The relationship photosynthesis/hour (opt. light): chlorophyll *a*, using the oxygen production method, was found to agree with that determined earlier from culture and harbor water experiments, despite wide variations of temperature, nutrients, and the abundance of phytoplankton. The same ratio, with photosynthesis measured by C^{14} uptake, was extremely variable and usually lower than that obtained by oxygen-production photosynthesis values.

Estimates of daily production beneath a square meter of sea surface by the chlorophyll-radiation method and *in situ* C^{14} values agreed within reasonable limits in 75% of the measurements; for the remainder of the times the C^{14} values were consistently lower.

Daily production throughout the year ranged roughly from 0.20 to 1.00 g carbon/m²/day within the whole area studied. Estimated annual production decreased in a seaward direction from 160 g carbon/m²/year in the shallow coastal waters to 100 g carbon/m²/year on the continental slope. These values are intermediate between Riley's estimates for Long Island Sound and the Sargasso Sea.

INTRODUCTION

The authors have recently described a method of estimating the rate of primary production by phytoplankton from measurements of chlorophyll, light penetration, and incident radiation (Ryther and Yentsch 1957). During the past year we have investigated this method further and have employed it routinely, whenever possible in conjunction with the C^{14} and "light and dark bottle" oxygen techniques. These studies were carried out as part of an investigation of the plankton ecology of the continental shelf region off New York. The measurements of productivity in themselves represent a minor part of the total effort of this investigation. They are presented here primarily to demonstrate the use and to some extent the reliability of the above-mentioned new technique throughout a period of a year and in waters where production varies widely both seasonally and geographically.

CRUISE PLAN AND METHODS

Productivity measurements have been made at 25 stations in the continental shelf area off New York. These stations are arranged in a triangle, two sides of which constitute sections across the shelf in depths of water ranging from about 50 to 2000 meters. The inshore end of one section is opposite Montauk Point, Long Island; that of the other is near Barnegat Lightship off the New Jersey coast. The third leg of the triangle connects these inshore stations and is laid out closely parallel to and slightly inside the 50-meter contour. The location of these stations is shown in Figure 1.

At each station of 100 meters or more of depth water samples were collected with a plastic-lined sampler from depths of 0, 10, 25, 50, 75, and 100 meters. At stations of less depth, samples were collected from 0, 10, and 20 meters and thereafter at 20-meter intervals to the bottom. Normally two-liter samples from each depth were millipore filtered and subsequently analyzed for plant

---

[1] Contribution No. 906 from the Woods Hole Oceanographic Institution. These studies were carried out under Contract AT(30-1)-1918 with the U. S. Atomic Energy Commission and with the partial support of Research Grants G-3234 and G-2650 from the National Science Foundation. The authors wish to acknowledge the help provided by E. M. Hulburt, G. C. McLeod, W. H. Sutcliffe, D. W. Menzel in the field, Mrs. R. W. Kahler in the laboratory analyses, and B. H. Ketchum in reviewing this manuscript.

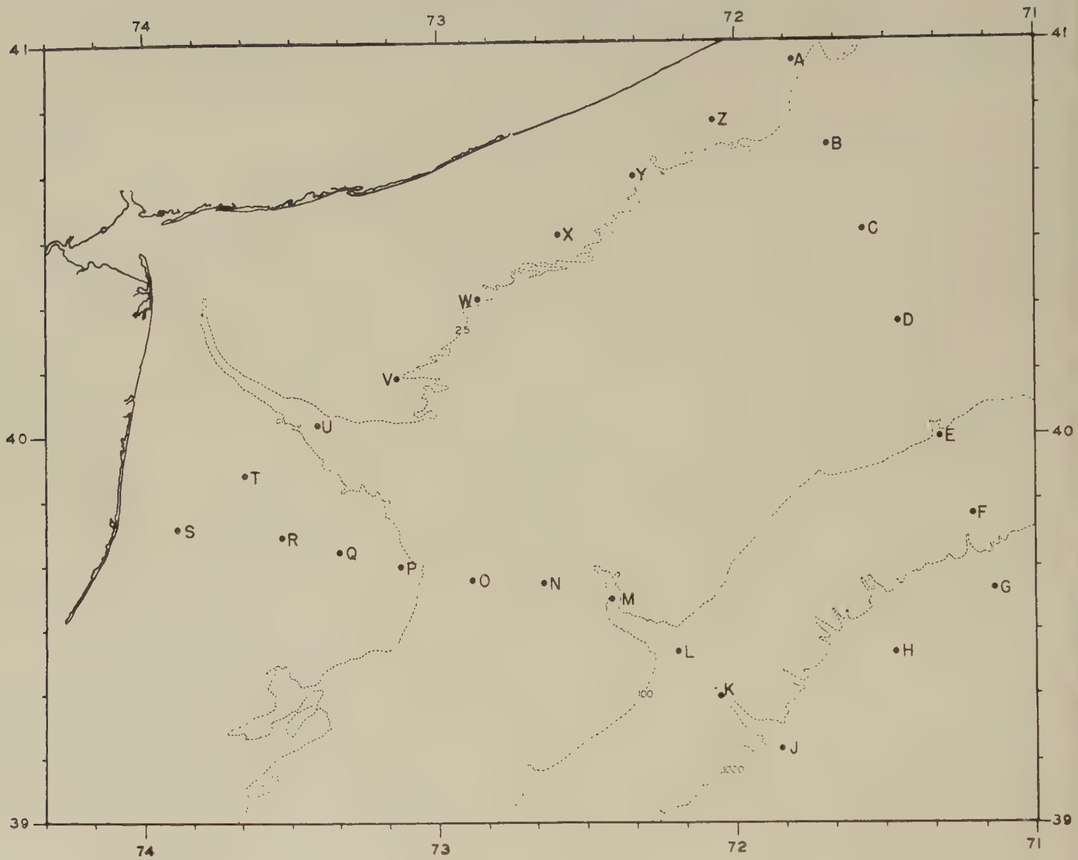

FIG. 1. The continental shelf area off Long Island and New Jersey showing station locations. Depth contours in fathoms.

pigments according to the method of Richards with Thompson (1952) as modified by Creitz and Richards (1955). When phytoplankton was scarce, two casts were made and 4 to 5 liters of water were filtered.

Water from the 10-meter sample was dispensed into two transparent and two darkened bottles, one of each receiving approximately 3 μcuries of $C^{14}O_3^=$. All four bottles were then placed in an incubator cooled with running sea water and illuminated with ten 15-watt fluorescent lamps, which provided a light intensity incident to the bottles of 1500 foot-candles.

The samples containing C^{14} were removed after 12 hours, filtered, and productivity calculated according to the method of Steemann Nielsen (1952) except that the dark uptake of C^{14} was routinely subtracted from that observed in the light and no correction was made for respiration.

The other pair of light and dark bottles was removed from the incubator after 24 hours, their oxygen concentration determined by the Winkler method, and photosynthesis (expressed as carbon fixed) calculated from the difference between them, using an assimilatory quotient (O_2/CO_2) of 1.25 (see Ryther 1956a).

During each cruise *in situ* C^{14} measurements were also made, weather permitting, at one shallow station (<50 meters), one deep station (>1000 meters), and one station of intermediate depth.

For these measurements light and dark bottles with $C^{14}O_3^=$ added were filled with the water samples taken from each depth to 100 m or to the bottom. These were then fastened to a wire, suspended at the depths from which the samples were taken, and exposed to natural illumination, usually from sunrise to noon, occasionally from noon to sunset or from sunrise to sunset. The samples were processed, and productivity was calculated in the same way as for the incubator-exposed C^{14} samples.

Light penetration was measured at each station occupied during daylight with a submarine photometer. The mean extinction coefficient of daylight was calculated over the depth to which 1% of the surface light penetrated. Where direct photometry could not be employed due to unfavorable weather or limitation of time, secchi disc readings were converted to values for extinction coefficient using the relationship

$$k = \frac{1.7}{\text{Secchi disc}}$$

as proposed by Poole and Atkins (1929), which was consistent with our measurements where both methods were employed. Extinction coefficients for stations occupied at night were estimated by interpolation between stations where measurements could be made in daylight.

The daily rate of primary production ($mgC/m^3/day$) was calculated for five depths from chlorophyll *a*, light penetration, and incident radiation using the equations given by Ryther and Yentsch (1957). This was done for every cruise and at every station. These values, and those obtained from *in situ* C^{14} measurements, were plotted against depth and graphically integrated to give daily production on an areal (square meter) basis.

Normally radiation values used in these calculations were taken from Kimball's (1928) tables, so that production is expressed in terms of average or normal radiation for the area studied and the particular time of year in question. However, at those stations and times when *in situ* C^{14} experiments were conducted simultaneously, in order that the two methods could be compared, production was calculated from radiation values which were actually measured using either a recording Epply Pyrheliometer or a G. E. Radiation Meter.

The measurements which will be presented in this paper were made during six cruises in the months of September, December, February, March, May, and July, and will thus give a rough picture of the annual cycle of primary production in these coastal waters.

THE RELATIONSHIP BETWEEN PHOTOSYNTHESIS AND CHLOROPHYLL *a*

In the earlier studies already referred to the relationship between photosynthesis at optimum light intensity and chlorophyll *a* was determined using natural plankton populations from the Woods Hole region and cultures of marine phytoplankton. The results of these experiments and some values from the literature were used to calculate a mean value of 3.7 grams carbon assimilated per hour per gram of chlorophyll *a*.

Figure 2A shows the ratio of photosynthesis per hour at optimum light and chlorophyll *a* as determined from the 10-meter samples collected at each station during the six continental shelf cruises. The open circles represent values obtained by the "light and dark bottle" oxygen method; the closed circles are values obtained by C^{14} uptake. The data are plotted as a log function so that both high and low ratios will appear equally weighted on the graph. There is still some bias in favor of high ratios obtained by the oxygen method, however, since with large positive differences between light and dark bottles, one cannot distinguish between experimental error and high photosynthesis, and the data are therefore included, while negative differences (more oxygen in the dark than in the light bottles) were recognizable as experimental error and discarded. The absence from the graph of values obtained by the oxygen method indicates either that such measurements were not attempted (*i.e.*, during the first two cruises) or that significant results were not obtained.

The line drawn through Figure 2A represents the 3.7 ratio obtained in the earlier experiments described above. The points

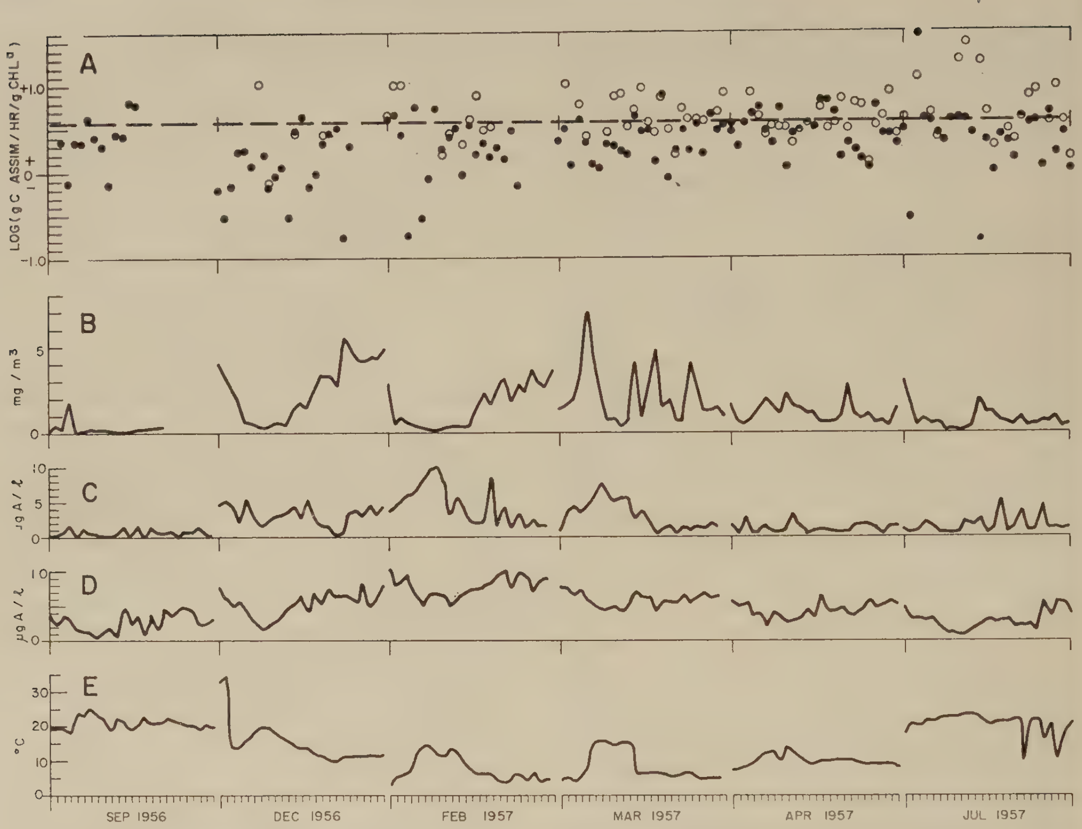

FIG. 2. Biological, chemical, and physical properties of water from 10 meters depth shown for all stations occupied during six continental shelf cruises. Station data presented for each cruise in alphabetical order (A–Z) as stations were occupied. (*A*) Log ratio photosynthesis/hour (optimum light): chlorophyll *a*. Open circles, oxygen method; filled circles, C^{14} method. (*B*) Chlorophyll *a* concentration. (*C*) Available nitrogen ($NH^+ + NO_2^- + NO_3^-$). (*D*) Phosphate. (*E*) Temperature.

obtained by the oxygen method appear to be distributed rather evenly about this line despite their high degree of scatter. This is more obvious if one looks at the frequency distribution of the ratios in Figure 3A, which shows a decided peak of values ranging from 3.0 to 4.0 and a normal distribution of ratios about this mode.

In our earlier report, we acknowledged that the value 3.7 was no more than the mean of some highly variable data, and that there was little reason to assume that it would be constant under all conditions. The data presented here certainly show no less variability. However, there is no obvious effect of environmental conditions upon the ratio despite rather wide variations in the abundance of phytoplankton (*i.e.*, chlorophyll *a*), the concentration of available nitrogen and phosphorus, and temperature (Figure 2B, C, D, and E). This is a hopeful indication that most of the scatter of our observations is due to experimental error. Unless this error is systematic in nature, the mean would appear to assume greater reliability than we had originally hoped for.

The values obtained by the C^{14} method are obviously scattered for the most part below the 3.7 line, as emphasized again by their frequency distribution (Fig. 3B.). Furthermore they show no obvious normal distribution about a mean, as do the oxygen values, but appear to be almost equally spread between values of 1.0 and 4.0, and with a considerable number below 1.0. A similar variability in the relationship between chlorophyll *a* and C^{14} uptake has been reported by Holmes *et al.* (1957), Holmes

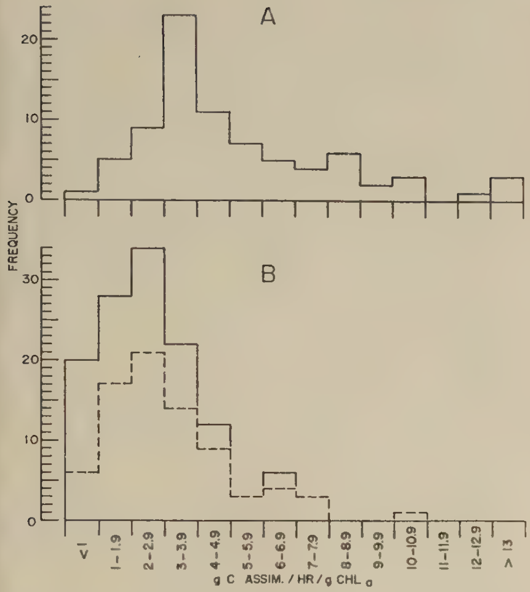

FIG. 3. Frequency distribution of the ratio photosynthesis per hour (opt. light): chlorophyll *a* for values given in Figure 2A. (*A*) Oxygen method. (*B*) C^{14} method. Broken line in (*B*) represents those C^{14} values which were obtained simultaneously with the oxygen method values shown in (*A*).

(in press), Doty (unpublished data), Currie (in press), and others. We have interpreted this fact on the basis of our contention that the ratio photosynthesis: respiration in marine phytoplankton is not constant (Ryther 1954; Ketchum *et al.*, in press). If this is true and C^{14} uptake, uncorrected for respiration, is a measure of net photosynthesis (Ryther 1954, 1956a, 1956b), then the ratio of C^{14} uptake: chlorophyll should not be constant and should fall below 3.7 by an amount equivalent to respiration. The fact that these ratios are quite variable and are, for the most part, less than 3.7 is consistent with this hypothesis. There is some indication that the highest C^{14}: chlorophyll ratios existed during the spring when they closely approached the 3.7 value, indicating that net and gross production (at optimum light conditions) were almost equal. At that time of the year the standing crop of phytoplankton and its *in situ* rate of production were also highest as will be shown in the following section.

THE COMPARISON BETWEEN *in situ* C^{14} MEASUREMENTS AND PRODUCTION CALCULATED FROM CHLOROPHYLL AND RADIATION

Figure 4 shows the values for production integrated over the euphotic zone and expressed in grams carbon/m²/day for all stations and for the six cruises between September 1956 and July 1957. The clear bar graphs are values calculated from chlorophyll and radiation. The dark bars are the

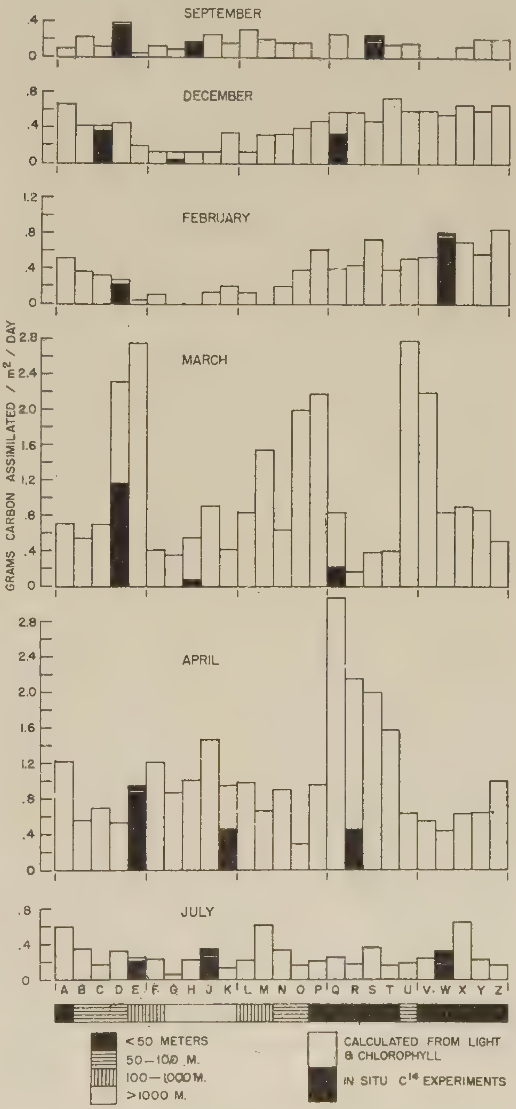

FIG. 4. *In situ* primary production measured by C^{14} method and/or calculated from chlorophyll, radiation, and light penetration for all stations occupied during six cruises.

in situ C^{14} measurements. For each cruise the data are presented chronologically in the order in which the stations were occupied (*i.e.*, A–Z). No attempt has been made here to depict seasonal or geographical variations, which will be discussed in the following section, but this complete presentation of data will illustrate the magnitude and range of production, its relation to water depth, and its variability from station to station. However, the main purpose of the figure is to show the comparison between values calculated by the chlorophyll and the *in situ* C^{14} methods.

Of the 17 pairs of data obtained by the two methods, five agree within 10% and all but four differ by less than two-fold. Since the chlorophyll and C^{14} methods measure gross and net production respectively, some difference between them is to be expected. It is true that where there is a big discrepancy, the C^{14} method consistently gave the lower values. But the cases in which the two methods agree and disagree do not seem to be in accord with other evidence. In July and September, when the water was thermally stratified, nutrients low, and the crop of phytoplankton at its minimum, the greatest discrepancy between net and gross production might be expected. At those times the C^{14} and chlorophyll methods gave comparable results, with the former often the higher. On the other hand, during the spring flowering net and gross production should be nearly equal; yet in March and April when production was highest, the greatest discrepancy between the two methods was observed. We do not yet understand this apparent inconsistency, which may result from some systematic error in either method. It is virtually certain that such errors exist, in sampling and technique as well as in the assumptions upon which the calculations are based. Until these are eliminated, or at least assessed, there can be little significance attached to differences between values obtained by the two methods.

SEASONAL AND GEOGRAPHICAL VARIABILITY OF PRIMARY PRODUCTION

It is difficult to construct a picture of the annual cycle of primary production with data obtained from six cruises. However, the times of these cruises were chosen so as to coincide with the periods of most rapid change or greatest contrast in biological activity. To the extent that these were wise choices, some idea may be had of the seasonal trend and annual range of production. Similarly, geographical variability may be examined within the area studied, which again was chosen for its contrasting features particularly with respect to water depth.

These temporal and spatial trends are somewhat obscured by the high degree of variability of data from one station to the next during any one cruise (see Fig. 4). Judging from the variability of other chemical and biological parameters (Fig. 2), there is reason to assume that this erratic distribution actually exists, though it may be exaggerated by experimental error. The resulting rather confusing picture may be improved by averaging the results from several geographically similar stations. This was done for five shallow, inshore stations (A, S, U, W, Y), five stations of intermediate depth (B, C, D, O, N), and five stations of greater than 1000 meters depth (F, G, H, J, K). Productivity data used in this discussion are limited to measurements obtained by the chlorophyll method. The results are illustrated in Figure 5.

It may be seen that the annual range of production does not differ appreciably between the inshore and offshore locations, 0.20–0.85 g carbon/m²/day for the former and 0.10–1.10 g carbon/m²/day for the latter. It is interesting to compare these values with Riley's most recent estimates of production in Long Island Sound (Riley 1956) which, when converted to carbon assimilation by the method used above, indicate a range of 0.23–1.70 g carbon/m²/day for 1952–3 and 0.24–1.51 g carbon/m²/day for 1953–4. His calculations are based upon *in situ* chemical changes in the water column over periods of several weeks, and such long-term averages obscure extremes which may persist for a few days only. On the other hand, there is no reason to assume that the six continental shelf cruises (comprising in all about one month out of the year) would

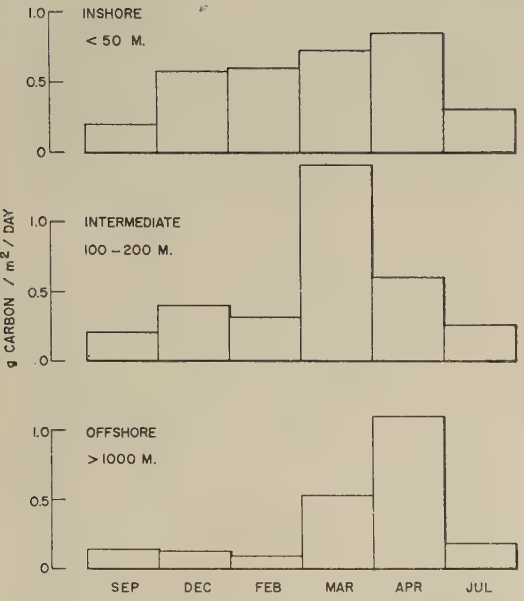

FIG. 5. Mean daily primary production beneath a square meter of sea surface at five shallow, five intermediate, and five deep stations for each of six cruises.

coincide exactly with the period of maximum and minimum production, even though they were chosen with this object in view. Thus we may tentatively conclude that the annual range of production is about the same from Long Island Sound across the adjacent continental shelf to the slope waters. Extending the comparison to truly oceanic conditions, we may again refer to Riley (1957) who has recently made new estimates of primary production in the north central Sargasso Sea. His values for gross production range from 0.09 to 0.89 g carbon/m^2/day, again strikingly similar to the range observed in the other regions discussed above.

This similarity in the annual range of production is not surprising, for it simply illustrates the fact that throughout the oceans enrichment processes exist, at times of sufficient magnitude that nutrient concentrations do not limit photosynthesis, at other times so weakly developed that organic production is probably largely dependent upon regeneration of nutrients within the euphotic layer. This, of course, does not imply that total annual production is comparable in these different parts of the sea. It is rather obvious from Figure 5 that this value is higher in the inshore area than in the shelf or slope waters, due to the persistence of relatively high production in the shallow waters throughout the winter and spring in contrast to the spring flowerings of greater magnitude but of briefer duration which occurred in the deeper waters.

The fact that the onset of the spring flowering in temperate latitudes is earlier in shallow and later in deep waters, and the explanation for this phenomenon, has been dealt with by Sverdrup (1953), Riley (1957), and others and need not be discussed in detail here. In brief it involves the interrelationship between the depths of the euphotic and mixed layers (*i.e.*, Sverdrup's critical depth) which determines the average light intensity to which the phytoplankton community is exposed. Since shallow coastal waters are mixed to the bottom in wintertime, the average light intensity within the water column is inversely proportional to its depth, and in sufficiently shallow waters the average plant cell within the water column receives adequate light for production throughout the year. In such places the plants have access to the nutrients dissolved within the entire water column and regenerated from the bottom, photosynthesis is limited by light only, and production can persist at a moderately high level throughout the winter and spring, and until thermal stratification imposes a barrier between the illuminated plants in the upper water and the reservoir of nutrients in the deep water and the bottom. Following the development of the thermocline there may be a brief period of high production, since the average cell above the thermocline is now exposed to much greater radiation. But the limited supply of nutrients in these surface waters is then quickly exhausted, and photosynthesis is reduced to a low level throughout the summer and until cooling and mixing processes again destroy the thermocline.

In contrast to the situation described above, the offshore waters are mixed in winter to a depth of 200 m or more, and the average plant cell within this water column does not receive sufficient light to grow. Here production exists at a low level throughout the winter and until thermal stratification retains the cells in the upper water layer. There then follows the classical spring flowering which may be of greater magnitude than that occurring in the shallow waters (see Fig. 5), since the nutrients have not been depleted by growth during the winter. As in the shallow water this activity rapidly exhausts the supply of nutrients from the surface waters, and low summer production ensues, perhaps punctuated by minor flowerings resulting from the temporary breakdown of the thermocline through local storm action, as described by Riley (1957).

Thus daily photosynthesis in the open sea may equal or exceed that of shallow coastal waters, but high levels of production in offshore waters cannot be sustained over long periods, as they may be inshore, unless there exist mechanisms such as upwelling for the continued enrichment of the surface waters. Except in these cases the annual production of the oceans must be considerably lower than that of shallow coastal waters 50 meters or less in depth.

As mentioned earlier, no accurate calculation of annual production may be made from six scattered points. But a rough and rather subjective estimate (obtained by drawing a smooth annual curve through the points) is of some interest, particularly when compared with Riley's values for Long Island Sound and the Sargasso Sea. For the sake of consistency, the latter have been recalculated from Riley's data using an assimilatory quotient of 1.25 in converting from oxygen changes to carbon fixation. The results, presented in Table 1, show that annual production decreases in a seaward direction, as discussed above, the variation across the continental shelf being relatively small and the values for that region being intermediate between those for Long Island Sound and the Sargasso Sea.

TABLE 1. *Annual rate of carbon fixation, in grams per square meter of sea surface*

	Total depth (meters)	gC/m²/yr
Long Island Sound	25	380
Continental Shelf	25–50	160
	50–1000	135
	1000–2000	100
North Central Sargasso Sea	>5000	78

REFERENCES

CREITZ, G. I., AND F. A. RICHARDS. 1955. The estimation and characterization of plankton populations by pigment analyses. III. A note on the use of "millipore" membrane filters in the estimation of plankton pigments. J. Mar. Res., **14**: 211–216.

CURRIE, R. I. (in press). Some observations on organic production in the North-East Atlantic. Rapp. Proc. Verb. Cons. Internat. Explor. Mer.

HOLMES, R. W. (in press). Surface chlorophyll *a*, surface primary production, and zooplankton volumes in the North-Eastern Pacific Ocean. Rapp. Proc. Verb. Cons. Internat. Explor. Mer.

HOLMES, R. W., M. B. SCHAEFER, AND B. M. SHIMADA. 1957. Primary production, chlorophyll and zooplankton volumes in the tropical eastern Pacific Ocean. Bull. Inter-Amer. Trop. Tuna Comm., **2**: 129–169.

KETCHUM, B. H., J. H. RYTHER, C. S. YENTSCH, AND N. CORWIN. (in press). Productivity in relation to nutrients. Rapp. Proc. Verb. Cons. Internat. Explor. Mer.

KIMBALL, H. H. 1928. Amount of solar radiation that reaches the surface of the earth on the land and on the sea, and the methods by which it is measured. Mon. Weath. Rev., **56**: 393–398.

POOLE, H. H., AND W. G. R. ATKINS. 1929. Photoelectric measurements of submarine illumination throughout the year. J. Mar. Biol. Assoc. U. K., **16**: 297–324.

RICHARDS, F. A., with T. G. THOMPSON. 1952. The estimation and characterization of plankton populations by pigment analyses. II. A spectrophotometric method for the estimation of plankton pigments. J. Mar. Res., **11**: 156–172.

RILEY, G. A. 1956. Oceanography of Long Island Sound, 1952–1954. IX. Production and utilization of organic matter. Bull. Bingham Oceanogr. Coll., **15**: 324–334.

———. 1957. Phytoplankton of the north central Sargasso Sea. Limnol. Oceanogr., **2**: 252–270.

RYTHER, J. H. 1954. The ratio of photosynthesis to respiration in marine plankton algae and its effect upon the measurement of productivity. Deep-Sea Res., **2**: 134–139.

———. 1956a. The measurement of primary production. Limnol. Oceanogr., **1**: 72–84.

———. 1956b. Interrelation between photosynthesis and respiration in the marine flagellate, *Dunaliella euchlora*. Nature, **178:** 861–862.

Ryther, J. H., and C. S. Yentsch. 1957. The estimation of phytoplankton production in the ocean from chlorophyll and light data. Limnol. Oceanogr., **2:** 281–286.

Steemann Nielsen, E. 1952. The use of radioactive carbon (C^{14}) for measuring organic production in the sea. J. Cons. Internat. Explor. Mer, **18:** 117–140.

Sverdrup, H. U. 1953. On conditions for the vernal blooming of phytoplankton. J. Cons. Internat. Explor. Mer, **18:** 287–295.

Contribution No. 915

VOL. 15, NO. 4 JOURNAL OF METEOROLOGY AUGUST 1958

ON THE STRUCTURE AND MAINTENANCE OF THE MATURE HURRICANE EYE

By Joanne S. Malkus

Woods Hole Oceanographic Institution[1]

(Original manuscript received 14 June 1957; revised manuscript received 24 March 1958)

ABSTRACT

An attempt is made to derive the significant features of a mature hurricane eye in terms of a simplified model of the physical processes undergone by the air composing it. In particular, a quantitative relation is prescribed among the fields of motion, temperature, and humidity on the basis of assumptions concerning the exchange of mass and momentum between the eye and its surrounding cloud bands.

The basic assumptions are that eye air mixes with the cloud wall on its descent; the latter is maintained by lower level outflow caused by unbalanced centrifugal and Coriolis forces, resulting from the incorporation into the eye of high cloud-wall momentum. Joint entrainment and angular momentum calculations for two hypothetical cases of stationary hurricanes of differing intensity show qualitative agreement in major features with existing incomplete observations and delineate a computational framework for real cases when available. Modifications of eye structure in moving storms are finally considered.

1. Introduction

The important role played by the eye in a tropical storm has recently been emphasized by Riehl (1956). He has demonstrated that the phenomenally low pressures (950 to 890 mb) in hurricane centers are not achievable by any possible lifting of the lowest air in the convective systems of the rain areas. He has further pointed out that since most tropical storms are associated with little or no disturbance above 100 mb the low central pressures must come from a very warm eye which slopes outward aloft over the rain area. The eye soundings available to date indicate that adequately high temperatures are indeed found in eyes, the warming being particularly pronounced in the middle and upper troposphere.

It is, therefore, of considerable importance to study the structure and maintenance of the eye and to attempt to discover the manner in which the warming is produced. It has been suggested that descending motion occurs in hurricane centers, but neither the amount of the descent nor the origin of the descending air has been established. In addition to its great warmth and low pressure, the eye has several other mysterious features, the most striking being the weak winds within it, despite the raging cyclonic gales in the convective wall only a few kilometers away.

The purpose of this work is to construct a model in which the eye air comes largely from the convective wall at high levels, descends with some exchange of properties through the mid-troposphere, and undergoes strong divergence and outflow in the lowest kilometer or so. It is first shown that a typical eye temperature and humidity sounding is obtainable by such descent, mixing and evaporation of liquid water. Then an angular momentum budget is made. In the model, eye air begins descent from high levels where cyclonic angular momentum is weak; it acquires angular momentum from the adjacent cloud wall as it descends and arrives at 800 to 900 mb with supergradient cyclonic speeds. Outflow near the surface results from excessive centrifugal and Coriolis accelerations, which give rise to low-level divergence of the order of 10^{-4} sec^{-1}. It is hypothesized that this low-level divergence, produced by the importation of cyclonic angular momentum into the sinking eye air, is responsible for the continued maintenance of the forced descent which is then calculable. If it is assumed that the outflow from eye to surrounding rain band occurs mainly in the lowest kilometer, the descent rate averages about 10 to 15 cm per sec at about 1 km above the surface, which decreases upward in a manner estimable from the calculated mass fluxes. The spreading of the air outward in the lowest kilometer, plus some destruction of angular momentum by surface friction, results in very low average wind velocities in the eye and a sharp gradient in wind at the eye wall. In the final section, modifications in eye structure in a storm moving in a tropical current with vertical shear are considered.

The model evolved here shows qualitatively the significant eye-like features in temperature, humidity, and momentum structure. It relates these fields quantitatively in a self-consistent and physically plausible manner. Beyond this, observations available to test the results are still incomplete. Those used here were primarily an eye radiosonde made at Tampa, Florida

---

[1] Contribution No. 915 from the Woods Hole Oceanographic Institution.

(Riehl, 1948), a summary of eye dropsondes (Jordan, 1957), aircraft and drop soundings from an exceptionally deep Pacific typhoon (Simpson, 1952), and some recent unpublished data gathered by the National Hurricane Research Project. The work here suggests several critical observational tests which should be made and outlines a method of utilizing future measurements to determine the origin of eye air.

2. Temperature and humidity structure

We shall now determine whether a characteristic eye sounding may be produced by descent, entrainment from the eye-wall cloud band, and evaporation of liquid water. The sounding for the convective wall is taken as curve B in fig. 1. This sounding is arrived at by moist adiabatic lifting of subcloud air which has been isothermally (at 26.0C) expanded to 960 mb and had moisture added up to 19 g per kg. This should be a good approximation to the air structure in the active cloud band around the eye wall of a 960 to 970 mb hurricane (Riehl, 1956; Palmén and Riehl, 1957). Curves T and H, fig. 1, give the mean West Indies sounding for September (after Jordan, 1957a) and the mean hurricane-rain-area sounding (after Schacht, 1947), respectively.

The assessment of the eye-air origin is done in the manner of a standard entrainment calculation, as modified by Malkus (1955) for a downdraft. As the air descends in the eye we calculate what fraction of environment air must be mixed with descending air in each height interval to give eye properties, close to those observed at the next lower level. Evaporation of liquid water is hypothesized below the freezing level or about 450 mb. Evaporation gives rise to cooling at a rate of about 2.5C per g per kg evaporated. This will be found important in slowing down the warming rates above and beyond the slowing by mixing. Accumulating radar evidence confirms the occurrence of this process which will be discussed later in relation to the water budget of the storm.

The calculation is carried out as follows: at 100 mb, a downward flux of mean tropical (curve T, fig. 1) substratospheric air is started, arbitrarily called M g per sec (to be evaluated later). At 150 mb we calculate the amount of mixing (with curve B) required to give eye properties after dry adiabatic descent. It is found that one part convective wall air to two parts descending air is about right, or that $\Delta M/M = 0.5$. This process is continued down to 350 mb, where it becomes more plausible for the entrained cloud band air to be 2/3 undilute B and 1/3 mean hurricane rain area H. This is in agreement with work on large convective clouds (Malkus and Ronne, 1954; Riehl and Malkus, 1958) which suggests that undilute cloud cores are surrounded by more dilute cloud matter of increasing width at lower levels.

Curve E in fig. 1 shows the resulting eye sounding and table 1 summarizes the entrainment calculation. Actual eye soundings are shown in table 2 for comparison. One of the few extending to great heights is reproduced in table 2A and was discussed by Riehl (1948). Noteworthy features duplicated by the calculated results are (1) pronounced warmth confined mainly above 700 mb, and (2) high stability up to 400 mb, above which height the lapse rate becomes steep. The humidities reported by the radiosonde were high and Riehl discarded them as excessive. We see by comparison with table 1 that such humidities are extremely plausible if the eye air comes largely from the convective wall, as in the model. Furthermore, the recent eye dropsondes from 500 mb (Jordan, 1957) show average humidities closely similar to these for hurricanes of moderate strength. Jordan's mean eye

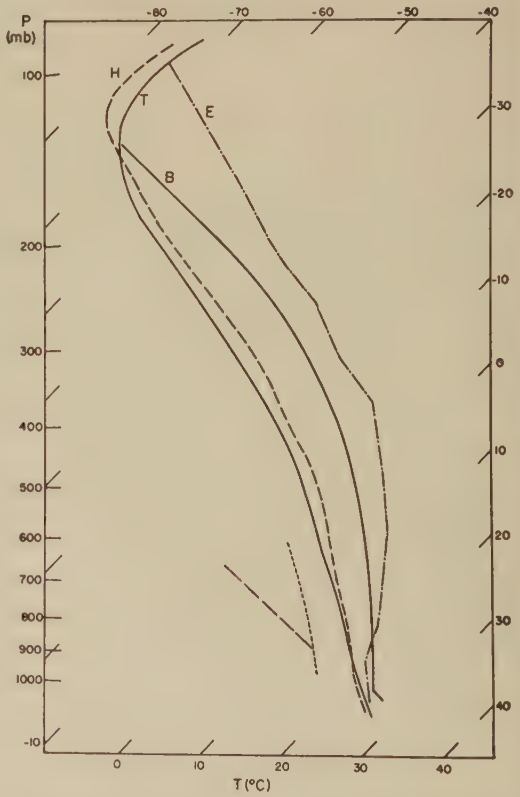

FIG. 1. Tephigram showing T: mean September sounding for the West Indies area, after Jordan (1957a); H: mean hurricane rain sounding, after Schacht (1947); B: sounding obtained by moist adiabatic ascent of subcloud air after isothermal (26.0C) expansion to 960 mb with addition of moisture to 19 g per kg and dry adiabatic ascent to saturation. Used as convective wall sounding for eye calculation for moderate hurricane; E: calculated sounding for moderate hurricane eye (see table 1). The short dashed line gives the slope of dry adiabats. The short dotted line indicates moist adiabat.

sounding for the moderate strength hurricane appears in table 2B.

The calculated eye sounding closely resembles the Tampa eye at upper levels and falls somewhere between the Tampa eye and Jordan's mean moderate eye below 600 mb. In it the eye environment is chosen as more H and less B on descent, becoming totally H at and below 800 mb. Beginning at 450 mb, evaporation is introduced in the amounts indicated while it is assumed to be negligible or small above the freezing level. The entrained cloud-band air can easily supply the water evaporated if the B cloud matter has close to adiabatic liquid or solid water content and the H cloudy air has a water content about half of that. However, we find that 2/3 of the water introduced into the eye model comes in above 500 mb, while nearly all evaporation takes place lower down. The plausibility of this distribution is examined from the standpoint of cloud physics in Section VI on mechanisms.

The downward mass flux in the model (table 1) is the largest at 850 mb ($\approx$1200 m elevation) because we hypothesize divergence and outflow from the eye below that. The entrainment calculation says that 98 per cent of the eye air descending at 850 mb has come from the cloud bands around the eye, about 50 per cent of it from above 500 mb. The 50-mb increments of mass ΔM (units relative to 100 mb) are large between 200 and 500 mb and below 700 mb and rather smaller in between. It should be noted that we could have obtained an equally plausible eye sounding by using less evaporation and more mixing in mid-levels, but this combination will later be precluded for any realistic hurricane model by angular momentum requirements. The qualitative reality of the height distribution of entrainment in table 1 is therefore suggested. In the real hurricane eye, we suppose the high rate of introduction of cloud matter aloft to be due to the spreading of anvils and cloud tops and the low-level secondary maximum to result from intense turbulent mixing and intermittent cloud penetrations due to relative motion between eye and cloud bands which will be considered later.

The rigid test of the entrainment hypothesis for the origin of eye air lies, however, in whether it can lead to a reasonable angular momentum structure.

Table 1. Eye sounding calculated by entrainment method.

P (mb)	T (°C)	rh (%)	*q* (g/kg)	Environment composition	Vertical mass flux (gm/sec relative to 100 mb)	ΔM	Entrainment rate $\frac{1}{M}\frac{dM}{dz}\cdot 10^6(\text{cm}^{-1})$	Evaporation gm/kg
100	−73.9	20	.002	100%B	1	0.5	0.2	
150	−55.0	20	0.03	100%B	1.5	1.05	0.4	
200	−41.0	20	0.1	100%B	2.55	1.25	0.3	
250	−28.0	20	0.3	100%B	3.8	2.3	0.5	
300	−19.5	25	0.7	100%B	6.1	1.8	0.3	
350	−10.0	24	1.2	2/3B, 1/3H	7.9	4.8	0.6	
400	− 4.6	31	2.1	2/3B, 1/3H	12.7	9.4	0.8	
450	0	40	3.4	2/3B, 1/3H	22.1	6.2	0.4	1.1
500	3.7	53	5.3	2/3B, 1/3H	28.3	1.8	0.1	1.6
550	7.2	62	7.1	2/3B, 1/3H	30.1	2.1	0.1	2.1
600	9.9	73	9.5	2/3B, 1/3H	32.2	1.5	0.1	1.7
650	12.3	82	11.4	2/3B, 1/3H	33.7	1.2	0.1	1.6
700	14.4	87	13.0	2/3B, 1/3H	34.9	4.2	0.2	1.0
750	16.8	88	14.2	2/3B, 1/3H	39.1	4.7	0.2	1.5
800	18.1	96	15.8	100%H	43.8	4.4	0.2	1.0
850	19.5	97	16.5	100%H	48.2	3.9	0.2	0.7
900	22.0	91	17.1		31.6*		0	1.1
970 (sfc)	25.3	87	18.3					

* Reduced due to lateral divergence. See text.

Table 2. Observed hurricane-eye soundings.

A. Tampa case (1 radiosonde)				B. Jordan average moderate (20 dropsondes)			
P (mb)	T (°C)	rh (%)	*q* (g/kg)	P (mb)	T (°C)	rh (%)	*q* (g/kg)
100	−73.9						
200	−41.0						
300	−19.5	23	0.6				
400	− 4.6	30	2.1				
500	3.7	53	5.3	500	− 0.4	70	5.1
600	10.2	73	9.7	600	8.7	72	8.6
700	15.1	86	13.4	700	14.4	83	12.5
800	17.8	93	15.3	800	19.0	89	15.4
900	20.0	93	15.4	900	22.9	91	17.7
966 (sfc)	23.2	97	18.3	~975 (sfc)	25.7	90	18.9

3. Angular momentum budget of the eye

One of the most amazing features of hurricane eyes is their weak surface winds. Any proper theory of eye dynamics must attempt to explain this phenomenon, and any theory of eye air origin must be consistent with it. An apparent obstacle to the acceptance of the entrainment idea has been the high cyclonic angular momenta which must be introduced into the eye if cloud-band air enters it in significant quantity. The present model suggests that high-level origin of much of the air (where the cyclonic circulation is weaker) coupled with destruction by friction and spreading laterally at low levels can produce a near-calm surface eye.

This contention is now backed by a quantitative angular momentum budget. We begin by considering the laws governing the angular momentum of a hypothetical steady-state, symmetrical hurricane. The absolute angular momentum of any ring of air a distance r from the hurricane axis may be altered in only two ways: one, by exchange with surrounding rings (mixing); and two, by destruction due to surface friction. Relative angular momentum is altered by change of distance from the axis.

We shall now inquire how the tangential linear velocity v_θ in its eye is distributed, altered by mixing, friction, and change of radius. The basic idea is that the air aloft which starts to descend in the eye has little or no relative angular momentum at first and acquires cyclonic angular momentum by mixing; these cyclonic velocities can be balanced by small and plausible pressure gradients down to about 1 km where they become supergradient and the air is flung outward again into the convective wall. In dealing with a symmetrical case, we are forced to ignore the marked observed streakiness in the real tangential velocity field of a hurricane and to treat our v_θ as an average around the storm. We also lose any contribution to momentum produced by pressure torques, which probably would prove disastrous in consideration of the dynamics of the rain area, which is the energy-providing region of the storm. It seems, however, that the basic dynamics of the eye are not obscured by the averaging process, as further exposition of this model will show.

First, we shall consider air just within the eye wall, say at a radius from the center of $r = 30$ km. We shall assume it descends with little change in radius down to 1.2 km (850 mb) above the sea, where it spreads out rapidly. The reasons for this will be enlarged upon later. The air just within the eye at $r = 30$ km is mixing with air in the convective band at roughly $r \approx 30$ km also in the amounts calculated in table 1. Since the radius is assumed to change little down to 1.2 km, we may consider only relative momentum per unit mass for the moment. Table 3 shows angular momentum calculation in terms of v_θ, the tangential velocity component ($v_\theta r$ = relative angular momentum per unit mass). The v_θ velocities in the new air incorporated into the eye are given in the column marked "Environment v_θ." This is taken as zero at 100 mb for the twofold reason that many hurricane circulations have nearly or entirely vanished by that level and also we began our descent there with air of undisturbed tropical properties. No complete series of upper level eye wall velocity data exists, much less an average tabulation over many hurricanes; therefore, the remaining values in the "Environment v_θ" column were chosen somewhat arbitrarily. They are at least consistent with the three observed levels (1500, 15,000, and 35,000 ft) of a single moderate storm, namely Carrie, 1957. Down to 500 mb the momentum calculation is straightforward, momentum being introduced to the eye in each interval in proportion to the introduced mass flux. From 500 mb down we call upon the destruction of momentum by friction, in the amounts listed in the fifth column from the left. It may be noted that our frictional destruction equals or exceeds the introduction by entrainment in the low levels of the eye, and we may well enquire whether such a stress distribution is at all realistic. The descent rate in the eye is estimated in the next section and for convenience is entered in column 3. From the time required to descend from one level to the next lower, we estimate the frictional force per unit mass required to produce the Δv_θ and from that the corresponding $\partial \tau_{\theta z}/\partial z$ or rate of upward decay of tangential shearing stress, entered in column 4. There is no way of checking these figures observationally except by noting that the highest values found here are about seven times those measured in the undisturbed trade (Charnock, Francis, and Sheppard, 1956; Bunker 1955) and about 1/3 those calculated (Palmén and Riehl, 1957) for the inner hurricane rain area. Finally we introduced in the lowest 1200 m the amount of radial spreading estimated in the next section (actually all these calculations had to be carried out simultaneously) and arrive at the low-level v_θ values for the eye of 10 m per sec (cyclonic positive) at 900 mb and about 2.7 m per sec at the surface. For the latter calculations it was necessary to consider absolute angular momentum, namely

$$v_{\theta u} r_u + \frac{f}{2} r_u^2 - \text{momentum destroyed by friction} = v_{\theta L} r + \frac{f}{2} r_L^2,$$

where the subscripts u and L denote the upper and lower level, respectively, and f is the Coriolis parameter.

Plausible ranges in friction, mixing, and spreading would give considerable range in eye rim v_θ without even considering the streakiness in v_θ in the convective ring. Thus, the values in the last column in table 3 and their height distribution should not be taken literally but may be expected to vary widely in the average from one storm to the next and in both time and space for a single storm. The point of the calculation described here is rather to make plausible a mechanism for the maintenance of the angular momentum budget of the eye and to set up a framework to be used on actual storm data when available. If the basic features of this model are sound, we would expect a downward increase on cyclonic rotation in the eye to the level where friction and spreading become important; this might well be higher than in the case considered here and observations of middle and low cloud drifts in real situations could be used together with v_θ profiles in the wall to determine the upper limit of frictional and divergence effects.

4. Divergence, vertical motion, and eye maintenance

The radial equation of motion for a steady-state, cylindrically symmetrical hurricane is

$$v_r \frac{\partial v_r}{\partial r} = f v_\theta + \frac{v_\theta^2}{r} - \frac{1}{p}\frac{\partial p}{\partial r} + \frac{1}{p}\frac{\partial \tau_{rz}}{\partial z}, \qquad (1)$$

where r and v_r are positive outward, $r = 0$ at the center, v_θ is positive for cyclonic wind, and the remaining symbols have their standard meanings.

If we can estimate $v_r \, \partial v_r/\partial r$, we can estimate the divergence and descent rates. The forthcoming calculations are based on the following approximate modelling of the eye: down to 850 mb where outflow is assumed to begin $v_r \, \partial v_r/\partial r \approx 0$ and we may calculate the pressure gradients required to keep our previously calculated v_θ's in balance (if we can say something about radial stress distribution). Below 850 mb we hypothesize that the cyclonic speeds are too large to be balanced by the pressure gradients so that excessive centrifugal and Coriolis forces (primarily the former) cause the descending air to be flung outward again into the rain area, maintaining the forced descent.

We begin by estimating $v_r \, \partial v_r/\partial r$ at the surface, assuming that $\partial p/\partial r$ vanishes there. We take $\partial \tau_{rz}/\partial z$ in roughly the same ratio to $\partial \tau_{\theta z}/\partial z$ ($\sim$40%) as found by Riehl and Palmén (1957) and calculate from equation (1) as follows:

$$v_r \frac{\partial v_r}{\partial r} = 0.5 \times 10^{-4} \times 2.7 \times 10^2 + \frac{(2.7)^2 \times 10^4}{3.10^6} - 10^3 \times 0.31 \times 10^{-4} = 0.7 \times 10^{-2}.$$

In the extreme case considered where $\partial p/\partial r$ at the surface vanishes, any wind is supergradient and will undergo outward acceleration (this is even true of an anticyclonic wind due to the predominance of the centrifugal over the Coriolis term). However, friction will reduce (but cannot reverse) the outward acceleration and if it were much larger than the value used would render it vanishingly small.

Since the height distribution of shearing stress inside a real hurricane eye is not known, we shall not attempt to refine this calculation further but will merely compute the divergence and descent consequent if $v_r \, \partial v_r/\partial r \approx 0.7 \times 10^{-2}$ throughout the lowest 1.2 km.

Since $v_r = 0$ at $r = 0$ we find that

$$v_r \text{ (m/sec)} = (0.13r)^{\frac{1}{2}}, \qquad (2)$$

where r is in kilometers. We obtain maximum outflow rate of about 2 m per sec at the outer edge of a 30 km eye. This is less than 20 per cent of the mean radial inflow from outside into the rain area side of the convective wall and is therefore not implausible. It is envisaged that in nature this outflow is not steady but occurs in fits and starts, as does the average eye v_θ which may oscillate from +2–4 m per sec to −1 or 2 m per sec. Temporary and local intrusions of much higher velocities accompanying cloud penetrations (discussed later) can be common. The oscillations in average v_θ and v_r (which are both of the same order of magnitude) can give the light and very variable wind conditions characteristic of hurricane eyes. It thus would be very difficult by spot observations to assess the small average flow within an eye and its average stress distribution.

The divergence within the theoretical eye comes out of the order of 10^{-4} sec^{-1} and we may estimate the descent rate at 1.2 km (where it is a maximum) using an integrated form of the continuity equation. Equating the downflux at 1.2 km to the efflux through the cylindrical walls we obtain

$$\rho \pi r^2 \bar{w} = \rho (2\pi) r h v_r \qquad (3)$$

and $\bar{w}$ at 850 mb comes out −16 cm/sec. The remaining upper w's in table 3 were calculated from this by ratios of descending mass flux and that at 900 mb was calculated by first subtracting the efflux between 850 and 900 mb. While a descent rate of 16 cm per sec may seem large, it is actually little more than the values found observationally in the subsidence ring around a small heated island and insignificantly small compared to the convective downdrafts associated with an ordinary cumulonimbus. It is not envisaged as being uniform across a real eye, but to be concentrated primarily between cloud regions which may, in fact, show weak ascent (Jordan, 1952). The maximum downward flux across the entire eye (and we have chosen a large eye) is only about 1 to 10 per cent of the upward flux in the eye wall (the range depending

Table 3. Angular-momentum calculation for the eye rim.

P mb	Environment v_θ m/sec	w cm/sec	Friction $\partial\tau_{\theta z}/\partial z\cdot 10^4$ dyne/cm³	Effect of friction Δv_θ m/sec	Effect of entrainment Δv_θ m/sec	Effect of spreading Δr km	Effect of spreading Δv_θ m/sec	Final eye rim v_θ m/sec
100	0	0.3		0	1.7			0
150	5	0.5		0	3.4			1.7
200	10	0.9		0	2.6			5.1
250	12.5	1.3		0	2.8			7.5
300	15.0	2.0		0	1.7			10.3
350	17.5	3.0		0	2.0			12.0
400	20.0	4.0		0	3.5			14.0
450	22.5	7.0		0	1.5			17.5
500	25.0	9.0	0.11	−1.3	0.5			19.0
550	27.5	10.0	0.22	−2.3	0.9			18.2
600	30.0	10.0	0.28	−2.2	0.8			16.8
650	32.5	11.0	0.35	−2.2	0.7			15.4
700	35.0	11.0	0.55	−3.2	2.9			13.9
750	37.5	13.0	0.65	−3.2	3.2			13.6
800	40.0	14.0	0.70	−2.7	3.0			13.6
850	42.5	16.0	0.70	−2.8	2.8	4	−1.9	13.8
900	52.0	10.0	0.70	−4.8	0	5	−0.8	10.0
970	52.0	0						~2.7

on the width and strength of the convective updrafts in the wall) and *at most* less than 1 per cent of the upflux in the whole rain area choosing conservative values of convergence and size of rain area.

Since $v_r\Delta t \sim \Delta r$, the amount of radial spreading, and $\bar{w}\Delta t \sim h$, equation (3) enables us to estimate that the total radial spreading from 850 mb to outflow is roughly one-half of the initial radius of the air at 850 mb. This was used in calculating the loss of relative momentum due to spreading appearing in table 3.

The average vertical velocities calculated tell us that the eye air will require different lengths of time to traverse the eye downward, depending on the level where it entered. For example, about 25 per cent of the air descending at 850 mb has entered the eye at 400 mb or above and requires about a day, on the average, to descend from there and flow out. Thus radiational heat losses may be important in the thermal budget of the eye and these have so far been ignored. If the eye lost heat by radiation at 2C per day, it would require 20 per cent less than the calculated evaporation to keep the temperature of the descending air the same as those of table 1. Such refinements are hardly worthwhile until many more observations are available.

5. Pressure-temperature relations and an eye-core calculation

Table 4 shows the radial pressure gradients at the eye rim necessary to make a self-consistent model. They were calculated from equation (1) and the v_θ's of table 3 assuming $v_r\partial v_r/\partial r \sim 0$ above 850 mb and 0.7×10^{-2} below and were adjusted in the low levels to give a plausible upward decay of $\partial\tau_{rz}/\partial z$ from 0.31×10^{-4} dynes per cm³ at the surface to zero at 650 mb. The fourth column expresses them in terms of D (altimeter correction) variations in 10 mi for comparison with the results of the National Research Project. Observations at the one level that penetrated the eye of Carrie 1957 shows at least the same order magnitude. Further checks will require eye penetration at several levels.

We may now investigate conditions in the more central portions of an eye and inquire how the thermal, water, and momentum budgets are to be maintained there. Let us consider, for example, $r = 15$ km. We first calculate the radial pressure gradients there assuming $1/\rho\,\partial p/\partial r$ goes to zero at $r = 0$ (symmetrical eye). Thus at 15 km, gradients are roughly half those at 30 km and these values are tabulated in column 2 of table 5. We next compute v_θ in the eye core assuming no acceleration down to 850 mb and $v_r\partial v_r/\partial r = 0.7 \times 10^{-2}$ below. We take both components of eye-core friction to be roughly one-half of those at the rim, since diminution of stress in the quieter center seems in-

Table 4. Pressure gradients at eye rim.

(No radial accelerations down to 850 mb; $v_r\dfrac{\partial v_r}{\partial r}$~$0.7\times 10^{-2}$ below)

P mb	v_θ m/sec	$\frac{1}{\rho}\frac{\partial p}{\partial r}\cdot 10^2$ cm/sec²	ΔD/10 miles ft	$\partial\tau_{rz}/\partial z\cdot 10^4$ dynes/cm³
100	0	0	0	0
150	1.7	2	1	0
200	5.1	11	6	0
250	7.5	25	13	0
300	10.3	41	22	0
350	12.0	54	29	0
400	14.0	72	39	0
450	17.5	111	60	0
500	19.0	130	70	0
550	18.2	119	64	0
600	16.8	102	55	0
650	15.4	87	47	0
700	13.9	70	38	0.10
750	13.6	67	36	0.10
800	13.5	66	36	0.20
850	13.7	66	36	0.20
900	10.0	35	19	0.23
970	~2.7	0	0	0.31

Table 5. Eye-core calculation.

P mb	$\frac{1}{\rho}\frac{\partial p}{\partial r}\cdot 10^2$ cm/sec^2	v_θ m/sec	T °C	Environment (of core)	ΔM/M	q g/kg	rh %	Evaporation g/kg	Friction Δv_θ m/sec	r_0 km
100	0	0	−73.9			.002	20			
150	1	0.9	−54.9	100%B	.47	0.03	20			27.5
200	6	2.6	−40.9	100%B	.64	0.1	20			22.5
250	12	3.7	−27.8	100%B	.40	0.3	20			20.0
300	20	5.1	−19.2	100%B	.60	0.6	20			18.0
350	27	6.0	− 9.8	100%B	.40	1.0	20			18.0
400	36	7.0	− 4.2	100%B	.84	2.1	30			17.0
450	55	8.7	1.4	1/2B, 1/2E	.55	3.3	35	0.2		17.5
500	65	9.5	3.7	100%E	.29	4.5	45	1.2		17.5
550	60	9.1	6.6	100%E	.29	6.7	60	1.3	−0.7	17.0
600	51	8.4	9.3	100%E	.22	8.0	65	1.3	−1.1	17.0
650	43	7.7	11.7	100%E	.20	10.1	76	1.0	−1.1	18.0
700	35	7.0	13.9	100%E	.17	11.7	80	1.2	−1.1	18.0
750	33	6.8	16.9	100%E	.35	12.9	81	0.7	−1.6	20.0
800	33	6.8	18.2	100%E	.60	15.3	93	1.0	−1.6	20.0
850	33	6.9	19.5	100%E	.30	16.1	95	0.9	−1.6	19.0
900	17	5.1	21.0	100%E	.30	17.0	97	0.5	−1.6	21.0
970	0	2.2	24.3	100%E	.30	18.2	94	0.9	−2.4	24.0

evitable. The resulting v_θ distribution appears in column 3 of table 5.

We may next inquire whether reasonable temperature gradients across the eye could exist to support these pressure gradients and arrive at an eye-core temperature sounding. If we assume vanishing disturbance at 100 mb and no eye radial pressure gradient at the ground, it follows from hydrostatic considerations that the eye core must be warmer than the rim aloft and slightly cooler in the low levels. A detailed calculation of the resulting eye-core temperatures gives the results in column 4. We see that nowhere need the eye-core temperature depart from that at the rim by more than 1.4C to maintain the necessary pressure gradients. Thus it should matter little in what part of an eye a temperature sounding is taken.

A more important question to ask is how can an eye core acquire this thermal and momentum structure? With what air, if any, does it mix on descent? We first tried an entrainment calculation for the eye core similar to that of table 1, but this time assuming the environment tabulated in table 5. It was possible to obtain the eye core sounding with the humidities given in table 5 with roughly the same entrainment rates used for the rim and 25 per cent reduced evaporation. We chose the environment of undilute cloud matter B above 400 mb because we envisage anvil penetrations well across the eye at upper levels (see Section VI). If this cloudy air has adiabatic water content and if some liquid water remains in the eye-rim air E (curve E, fig. 1) introduced into the core, the water budget in the core will balance nicely. Note that both core and rim soundings show near saturation humidities from 800 to 900 mb so that variable weak convergence fields (due perhaps to uneven roughness or heating from below) could easily account for the fluctuating low-level cloudiness so common in many eyes (Simpson, 1952).

The remaining question concerns the eye-core-momentum budget and whether the entrainment and momentum requirements are mutually consistent. It is not possible to make a precise angular-momentum calculation for the eye core, but we can determine what mean radius the incorporated air must have come from to give us the tabulated distribution of the eye core v_θ. These values of r_0, the mean radius of origin of the air entrained into the eye core, are presented in the last column of table 5. This computation was done similarly to that of table 3 except that v_θ was given and r_0 was the unknown. The resulting r_0's are consistent with the postulates of the model, since the air can have come in a long way aloft, while a "mixing length" of only 2 to 3 km (cumulus scale) is permitted in mid-levels. At low levels a rather long exchange length is again permitted due to the high rate of momentum destruction by friction (given in the next to last column assuming $\partial \tau_{\theta z}/\partial z$ is about one half that at the eye rim).

6. Mechanisms and water budget

Nothing has been said yet about the possible slope outward of real eye walls with height, which many workers believe is important in producing low pressures in the inner rain area. We note from the model calculation summarized in table 3, in fact, that no air from a radial distance greater than the minimum (ground) eye radial extent, in our case 30 km, descended throughout the eye, but rather the descending ring was assumed to maintain a more or less constant radius of this size all the way down from 100 to 850 mb. This seems to be required by angular momentum considerations. If any air much outward of 30 km flowed regularly inward, the excessive cyclonic rotation acquired would be so great that it would be rapidly flung out again. No pressure gradients appear available in real cases to balance such forces at great heights nor are any mechanisms at hand to destroy the cyclonic momentum. We are thus forced to conclude that air sinking along sloping eye walls at great heights and distances from the storm center only descends short intervals before being again ejected and incorporated into the cloud band.

To understand the slope of eye walls, we must look to the dynamics of the cloud band itself. The writer believes it important to regard this band as a convective phenomenon with fluctuations and repeating life cycle which only on an average that is long compared to the life of its elements resembles the textbook vortex. It is suggested here that the average outward slope arises for the same reason that trade cumuli, on the average, slant backwards—*i.e.*, negative shear in the radial flow component. The asymmetry in eye-wall slope introduced by a shearing basic current (discussed in Section VIII) supports this view.

When individual cumulonimbi shoot up, they at first grow nearly vertically and only acquire the pronounced backslant as the updraft gradually decays. When a cumulonimbus tower hits the tropopause or an upper tropospheric stable layer, anvils of tens of kilometers extent in all directions appear, caused by the forced outward spreading of the rising air as it strikes a "lid." Time-lapse pictures (see Malkus and Ronne, 1954) show that, although the spreading is greatest in the direction of the shear, they also spread considerably in the opposite direction, often opposing a strong wind. Langmuir[2] has proposed this lateral spreading of cloud matter as an important moisture transfer mechanism in the undisturbed trade, and here we suggest its relevance to tropical storms. When the cumulonimbi composing the eye wall reach up to great heights (limit ~150 mb where curve B, fig. 1, runs out of buoyancy) they do so roughly vertically at first, and by anvil-spreading inject moist air in bursts into the upper eye. The average pronounced outward slope of the eye wall occurs because the growth stage of any cumuliform cloud is negligibly short compared to the dissipation stage, so that most tropical cumulus appear with a strong slant in the direction of the wind shear. This sequence of cloud events showed up very clearly in a beautiful series of aircraft time-lapse films taken by the National Hurricane Research Project in the eye of Hurricane Greta, 1956.

We may now consider the evaporation process and water budget in more detail. We hypothesize that when anvils and cumulonimbus streamers are injected into the eye at great heights (up to about 40,000 ft depending on where the undilute wall air runs out of buoyancy) the cloudy air mixes with the air already there in roughly the calculated proportions and begins descent, aided by local negative buoyancy and well fortified with ice particles which evaporate on the way down. Workers in cloud physics (see, for example, Ludlam and Saunders, 1956) tell us that the large ice particles characteristic of cirrus anvils evaporate only very slowly and thus we have neglected evaporation as small above the freezing level and only introduced it in significant amounts below the melting height, or about 450 to 500 mb. Although the average descent rates calculated here for eye air imply that some of the air entering at great heights would require more than a day to reach low levels, the ice particles would presumably descend much faster after leaving their supporting updraft. If the ice particles are only 100 μ in radius they would descend from 400 to 850 mb in about 3 hr, permitting most of the water entering the eye aloft to reach middle and lower levels before entirely evaporating, as the model requires. We note further that pressure increment for pressure increment, the needed rates per unit mass in the eye of table 1 are comparable to condensation rates in wet adiabatic ascent. Therefore we may conclude that the water consumption in an eye stands roughly in the ratio to the production in the rain area as do the respective vertical mass fluxes. We mentioned earlier that the total eye descent came out about 1 to 10 per cent of the upflux in the eye-wall cloud band and conservatively lower than 1 per cent of estimated upflux in the whole rain area. Thus the water budget of the model eye is quite reasonable.

Confirmation in real cases of this high-level injection and evaporation process has occurred since the original evolution of this model. A series of beautiful radar eye photographs by Atlas (Kessler, 1957) made in Edna, 1954, show the anvil penetration and subsequent sinking and evaporation. Furthermore, Kessler's analysis using eye soundings together with the radar evidence demonstrates rather conclusively that the evaporation was vital in achieving the observed eye humidities which are inexplicable by any other mechanism. The writer has also seen the same process at work in the aircraft radar pictures made at 35,000 ft crossing the eye of Carrie, 1957.

Concerning the water entering the eye below 500 mb (masswise about 1/3 of the total in table 1), we envisage a mechanism more similar to normal convective entrainment, since at low levels large cumulonimbi become wider and are accompanied by outrider clouds which may penetrate into the eye. In a current with strong vertical shear, this effect may be greatly enhanced as we shall describe in Section VIII. Reduced entrainment and water introduction in mid-levels could be a result of two causes: (1) the restricted

---

[2] During a Woods Hole lecture series, 1956.

"mixing length" at those levels due to angular momentum constraints (see table 5); and (2) the fact that air motion through normal cumuli is minimum at midlevels, with stronger mixing near cloud base and efflux near the tops (see Malkus, 1954).

Since we have hypothesized evaporation as a brake on hurricane-eye warmth, we may well ask what would happen were upper cloud injection inhibited and the brake weakened. Could this be a contributory link producing an unusually deep warm eye? This possibility is considered in the next section.

7. Very warm eyes; Typhoon Marge, 1951

The hurricane eye penetrated by the Tampa radiosonde (table 2A) had a central pressure of 966 mb; it is well known that the deepest hurricanes on record have central pressures as low as 890 mb and thus must have much warmer eyes. By differentials from the hydrostatic equation we find for tropical storm conditions that

$$dp_c \approx 7d\bar{T}_v,$$

where p_c is the central surface pressure and $\bar{T}_v$ is the mean virtual temperature of the central column from the surface to 100 mb, no disturbance being assumed above that level. Therefore, an extreme hurricane eye must average nearly 11C warmer than the moderate eyes discussed.

There are two ways that an eye may be much warmer and still mix with the wall at about the same rate to satisfy angular momentum requirements. The first is to evaporate less water and the second is to have a warmer convective band. Trial calculations like that of table 1 were undertaken using each mechanism separately. First we altered evaporation alone, reducing it by about 40 per cent. The surface pressure is reduced only to about 913 mb, although the resulting sounding has a warmer, more marked "eye" character than that of fig. 1. The warmer convective band possibility was next considered alone. If subcloud air is expanded isothermally to 890 mb (at 26C) and picks up moisture to saturation (24.5 g per kg), which seems extreme, the resulting moist adiabatic ascent may be used as a wall sounding. Taking the same rates of mixing and evaporation used in table 1, we obtain a central pressure of about 912 mb, which is still not extreme.

It would appear that some combination of the above effects is required to obtain a record low. We successfully produce one in table 6 by using an environment wall B′ (isothermal expansion at 26C to 920 mb; moisture content 21.8 g per kg, ascent shown in curve B′, fig. 2). Evaporation is reduced by 1/3 from table 1 and while the overall entrainment from the wall is closely comparable, we reduce it by about 1/2 above 450 mb, supposing reduced cloud injections. The resulting theoretical eye sounding of table 6 appears as curve E′ of fig. 2. A pressure-height calculation assuming an undisturbed atmosphere above 100 mb gives a central surface pressure of 889 mb. Note the extreme stabilities throughout the low troposphere, the strong lapse rate aloft, and the much lower relative humidities than those of the moderate eyes. Fortunately, sounding and pressure data are available for one real extreme hurricane, namely Typhoon Marge, 1951 (Simpson, 1952), whose temperature and (dropsonde) humidities are repeated in the last two columns of table 6. These are almost identical with those of the theoretical eye except for high humidities in the lowest levels. These probably arose from spume and increased sea surface evaporation which was not considered in the calculation. In this penetration of Marge's eye the central pressure was about 895 mb, so that her upper structure must have resembled that calculated fairly closely.

It is interesting to speculate about the causes of the extremely warm eye. It is possible that a warmer convective rain band is not a cause but partly a

Table 6. Hypothetical eye sounding for extreme hurricane and comparison with typhoon Marge, 1951.

P mb	T °C	*q* g/kg	rh %	Environment	ΔM/M	Evaporation g/kg	Marge T °C	Marge rh (dropsonde) %
100	−73.9	negligible		100%B′	0.25			
150	−51.1	negligible		100%B′	0.35			
200	−34.0	0.1	10	100%B′	0.25			
250	−20.3	0.4	13	100%B′	0.30			
300	− 9.5	1.0	17	100%B′	0.15			
350	− 0.4	1.5	14	2/3B′, 1/3H	0.30			
400	6.0	2.2	15	2/3B′, 1/3H	0.35			
450	10.2	3.6	20	2/3B′, 1/3H	0.15			
500	16.4	4.2	18	2/3B′, 1/3H	.065	0.8	16.6	M
550	20.0	5.3	20	2/3B′, 1/3H	.071	1.0	20.2	28
600	23.1	6.7	22	2/3B′, 1/3H	.048	1.0	23.5	28
650	26.1	7.9	23	2/3B′, 1/3H	.17	1.4	26.0	35
700	26.0	10.0	32	2/3B′, 1/3H	.20	0.8	27.0	40
750	27.0	11.4	38	2/3B′, 1/3H	.25	1.3	27.0	60
800	26.0	13.3	50	100%H	.20	1.4	24.0	79
850	25.2	14.5	60		0	1.2	23.0	96
890 (sfc)	26.4	15.7	65				27.0	92

consequence of the low central pressure, following Palmén and Riehl's (1957) reasoning concerning pick-up heat from the sea under strong winds. Thus it may be that reduced evaporation is critical and if so we must enquire what could inhibit the water supply to the eye by about 30 to 40 per cent, or the major fraction of that entering the moderate eye at upper levels. The evidence points to reduced cloud injections, especially since we had to reduce upper-level entrainment in table 6 to produce a record eye. Reduced anvil penetrations could occur if outflow aloft in the rain area were much stronger than normal, particularly in the early life of the storm. This fits in with Riehl's (1948a) ideas about hurricane formation, which he contends is most explosively intense when a high-level disturbance is superposed on the developing storm and throws air out of it aloft. This upper outflow accelerates the pressure drop (thus indirectly the warming in the convective band) and, according to this reasoning, might also inhibit the cloud-band moisture supply to the storm, thus giving a warmer eye. This can be a self-accelerative growth process.

Some qualitative confirming evidence arises from recent aircraft studies: these soundings (Jordan, 1957) indicate that the low-humidity eyes are associated with the deeper storms. Inspection of eye photographs suggests also that the deeper eyes are visually better-defined and more cloud-free than the weaker ones, this being particularly true of Marge, whose eye was absolutely clear above 9000 ft and whose convective wall sharply terminated at 35,000 ft. Eye cloudiness in weaker storms is the rule and not the exception (Simpson, 1954, 1956).

In this connection, it is tempting to speculate about man-made interference with tropical storms. If inhibition of high-level water supply is an important factor in producing extremely warm eyes, one is led to inquire whether artificial introduction of water might not be able to cool the core and thus inhibit the storm. The amount of water needed to saturate an eye is, to be sure, greatly in excess of what could be carried in by aircraft, but does not vastly exceed the amount of sea water raised by an underwater explosion of an atomic bomb. The Bikini lagoon test raised about a thousand billion grams; evaporation of one hundred times this much water could saturate the eye of a typhoon like Marge (table 6). Unfortunately, cooling of this air to its wet-bulb temperature would only raise the central pressure in the eye from 890 mb to about 930 mb, which is still in the intense-storm range. Saturating the eye of a more moderate hurricane like that of table 1 (which has higher original humidity) could raise the central pressure by 10–12 mb at most. Thus introduction of water into the eye does not appear to be a promising possibility for hurricane modification.

8. Eyes of storms moving in a tropical current with shear

In utilizing observations to model moving hurricanes, we must distinguish between the motion of the low-pressure center, the motion of the eye as visible on radar (*i.e.*, the motion of precipitating cloud bands), and the motion of the air in the eye. It is possible that all of these may be different.

We note that on examining figs. 1 and 2 that the pronounced warmth of the eye occurs mainly above 700 mb, and thus the contribution to low surface pressures must come mainly from the eye column between 700 and 100 mb. A pressure-height calculation readily confirms this, showing the eye D value decreases by less than 10 per cent below 700 mb. We further note from table 1 that 23 per cent of the air in the eye of the model moderate hurricane at 700 mb

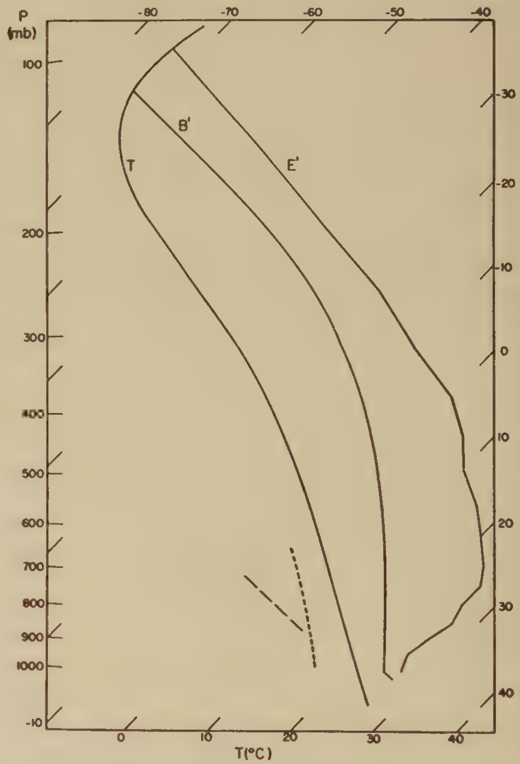

FIG. 2. Tephigram showing T: mean September sounding for the West Indies area, after Jordan (1957a); B′: sounding obtained by moist adiabatic ascent of subcloud air after isothermal (26.0C) expansion to 920 mb, with addition of moisture to 21.8 g per kg and dry adiabatic ascent to saturation. Used as convective wall sounding for eye calculation for extreme hurricane (Section VII); E′: calculated eye sounding for extreme hurricane (889 mb) tabulated in table 6. Very similar to observed sounding in typhoon Marge, 1951 (Simpson, 1952). The short dashed line gives slope of dry adiabats. The short dotted line indicates moist adiabats.

has come from 350 mb or above. Although considerable variation from storm to storm is possible, it seems that in real cases a significant fraction of the air reaching 700 mb must come from great heights to balance the thermal and momentum budgets jointly. This enables us to derive an upper limit for the relative horizontal motion between eye air and low-pressure center. Using the descent rates of table 1, we find it takes approximately one day for air originally in the eye at 350 mb to descend to 700 mb. If air enters the eye at one rim at 350 mb, it may translate through the eye (maintaining constant distance from the center) and just leave at 700 mb from the opposite rim if its translation speed differs by 1 m per sec from that of the low center. The only way that the eye (low-pressure center) could be translating at a vastly different speed from the air within it is to form on one side and die on the other, but this is precluded unless the descent rates are 5 to 10 times greater than those we have calculated. If the descent was multiplied by five, for example, air entering at 350 mb could have a linear speed differing by 5 m per sec from the speed of the low center and still remain in the eye down to 700 mb. Descent-rates this large seem implausible from the viewpoint of the overall budgets of the storm. The outflow of eye air into the rainband would approach 5 to 10 m per sec and the water consumption by the eye would become a significant fraction of that produced in the rain area. We thus predict that the average eye wind above 700 mb differs little (1 to 2 m per sec) from the translation speed of the low center, and that if a mass of neutral density balloons were introduced into the eye at 350 mb a fraction of them at least would remain in the eye for a major part of a day, leaving at 700 mb or below. This prediction is limited in application to steady-state mature storms still in tropical regions.

Below about 700 mb, since the computed descent-rates are much greater, it is possible for the air in the eye to move at a different speed from the eye itself (again defined as the low-pressure center). For this to take place, the lower eye must grow on one side and die on the other or, better said, new cloud bands must form on one side and old ones die on the other so that the center propagates at a different speed from the air within it. According to the calculations in Section IV, the air from 700 to 900 mb in the eye descends at a rate of the order of 10 cm per sec so that its descent time from 700 mb to outflow is roughly five hours. In this time it could move at 3 to 5 m per sec relative to the eye and just cross from one wall to the other following an approximately elliptical path and maintaining the distance from the axis required by angular momentum considerations.

We have suggested that 97 per cent of the air in the eye at 700 mb comes originally from the cloud bands. The translation speed of the low center, which we predict differs little from that of the eye air above 700 mb, should therefore be governed by the linear momentum introduced into the eye from the cloud bands. Thus if there is a mechanism for "steering" the storm, it occurs by the introduction of momentum

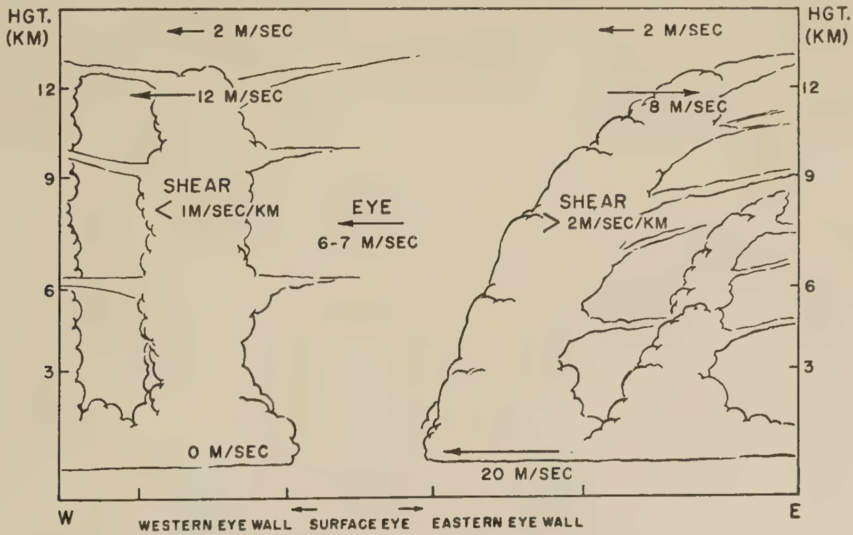

Fig. 3. Schematic illustration of asymmetry in eye structure when tropical easterly current has pronounced negative shear. The velocities given by the arrows illustrate a hypothetical set of winds (coordinates fixed to ground) resulting when a storm circulation with inflow at low levels and outflow aloft is superposed on a trade current of 10 m per sec at the ground decreasing to 2 m per sec in the stratosphere.

into the eye from the cloud bands. How the storm is steered should depend, if this model holds up, upon two factors: first, what the linear momentum in the cloud band is; and second, what portions of the cloud bands are drawn on by the eye.

We shall illustrate by one crude example in which the "steering level" fortuitously comes out to be about 500 mb. Suppose that we have an undisturbed easterly current with strong negative shear, its speed decreasing from 10 m per sec at the surface to 2 m per sec at 100 mb. This is not atypical of the trades in the wet season and would give an easterly speed of 6 to 7 m per sec at 500 mb. Now superimpose this flow upon a storm with radial inflow at low levels and outflow at high levels such that, in coordinates fixed to the ground, the east-west profile of the storm resembles the sketch in fig. 3. From previous work on tropical cumuli (Malkus, 1952, 1954; Malkus and Ronne, 1954) we would expect to find the eastern eye wall showing a much more pronounced backslant than the western wall. Furthermore, since cumuli grow on the upshear side and dissipate on the downshear side, we would expect most of the inflow from cloud band to eye to occur from the western wall. If the upper eye is getting about 75 per cent of its air from the western cloud band and only 25 per cent from the eastern, it will translate about 6 to 7 m per sec toward the west. This should be closely the rate of propagation of the warm core and thus of the surface low pressure center. It fortuitously turns out to be close to the speed of the undisturbed 500 mb easterlies. Although this work suggests that the "steering level" depends on a number of complex factors and may vary widely from storm to storm (or even within the life of a single storm), at least it points to a mechanism governing it and a way to compute it once more about the cloud bands and their interaction with the surroundings is known.

In order to carry on to low levels of the same storm, we recall that entrainment into the eye was calculated to be small between 500 and 700 mb but below 700 mb the eye received again nearly 2/3 the mass that it already had. If it received this entirely from the western cloud bands, it would suffer a braking effect and the air descending in the eye would translate westward at only 3 to 4 m per sec. The outflow from the eye then takes place primarily on the eastern side and probably would begin somewhat higher than in the symmetrical storm.

The motion of the cloud-free space called the "radar eye" would now only *average* 6 to 7 m per sec at low levels and presumably would do so by formation of new cloud matter at the western edge of the eastern band and dissipation at the eastern edge of the western band. We may expect the *propagation speed* of the cloud bands (as distinct from the motions of individual radar clouds) to be controlled by the motion of the warm core. This determines, by controlling the pressure field, the boundary between the rain-area inflow and the eye outflow and thus the line of convergence between these; this is the place where new clouds would be forming at all times. Individual cloud bands may move at much different speeds, however, and instantaneously the radar clouds may have a horizontal velocity quite different from the motion of the low-pressure center and *should not* be used in determining the motion of the storm. Clouds may intrude into the eye, which at low levels may seem to disappear and reform or even jump as old cloud bands die and new ones form.

Thus, this work suggests the following:

1. Under conditions of strong shear in the basic current, the average low-level winds in the hurricane eye may differ significantly from the motion of the low-pressure center, although they should rarely differ by more than 3 to 4 m per sec.
2. The propagation speed of the cloud bands should be the same as the speed of the low-pressure center although the motion of individual clouds and cloud groups may be quite different and should not be used to infer storm motion.
3. At upper levels the average translation speed of the eye air should be closely (within 1 to 2 m per sec) that of the motion of the low-pressure center.
4. The horizontal motion of the low-pressure center has considerable inertia against sudden changes since only about 20 per cent of its air is being replaced every six hours, while the radar eye is much more ephemeral and may change its apparent velocity every hour or so (the lifetime of an individual cumulonimbus) by meters per second and may twist and turn, and even disappear and reappear elsewhere.

All of these predictions may be tested observationally.

9. Concluding remarks

This work suggests the importance of the convective structure of tropical storms in their maintenance and motions, and outlines a calculation framework for utilizing future observations to test the physical ideas. The actual values of the parameters may vary widely from storm to storm and the criterion lies, therefore, in whether they obey the predicted relation to each other in selected cases, although the number of physical constraints should not permit orders-of-magnitude differences from the values used herein. If the broad outlines of the model prove justifiable, it may be extended in the future to discuss eye formation and the role of the convective rainbands in initiation and maintenance of the storm.

Acknowledgments—This work was supported by the U. S. Weather Bureau's National Hurricane Research Project, which has also generously made available its excellent hurricane data and the constant assistance, advice, and criticism of its staff members.

The writer is particularly grateful to Mr. Robert Simpson for his encouragement from the outset, and to Dr. N. E. LaSeur and Dr. C. L. Jordan of Florida State University. The problem was originally formulated in discussions with them and has been aided all along the way by their contributions.

REFERENCES

Bunker, A. F., 1955: Turbulence and shearing stresses measured over the North Atlantic Ocean by an airplane-acceleration technique. *J. Meteor.*, **12**, 445–455.

Charnock, H., J. R. D. Francis, and P. A. Sheppard, 1956: An investigation of wind structure in the trades: Anegada 1953. *Phil. Trans.*, **249**, 179–234.

Jordan, C. L., 1952: On the low-level structure of the typhoon eye. *J. Meteor.*, **9**, 285–290.

——, 1957: *Mean soundings for the hurricane eye.* Natl. Hurricane Res. Proj. Rep. No. 13, U. S. Wea. Bur., 10 pp.

——, 1957a: *A mean atmosphere for the West Indies area.* Nat. Hurricane Res. Proj. Rep. No. 6, U. S. Wea. Bur., 17 pp.

Kessler, E., 1957: *Eye region of Hurricane Edna,* 1954. *J. Meteor.*, **15**, 264–270.

Ludlam, F. H., and P. M. Saunders, 1956: Shower formation in large cumulus. *Tellus*, **8**, 424–442.

Malkus, J. S., 1952: Recent advances in the study of convective clouds and their interaction with the environment. *Tellus*, **2**, 71–78.

——, 1954: Some results of a trade cumulus cloud investigation. *J. Meteor.*, **11**, 220–237.

——, 1955: On the formation and structure of downdrafts in cumulus clouds. *J. Meteor.*, **12**, 350–354.

——, and C. Ronne, 1954: On the structure of some cumulonimbus clouds which penetrated the high tropical troposphere. *Tellus*, **6**, 351–366.

Palmén, E., and H. Riehl, 1957: Budget of angular momentum and energy in tropical cyclones. *J. Meteor.*, **14**, 150–159.

Riehl, H., 1948: A radiosonde observation in the eye of a hurricane. *Quart. J. r. meteor. Soc.*, **74**, 194–196.

——, 1948a: On the formation of typhoons. *J. Meteor.*, **5**, 247–264.

——, 1956: *Formation of hurricanes.* Unpublished lecture notes, Woods Hole Ocean. Inst. and Univ. of Chicago.

——, and J. Malkus, 1958: *Unpublished manuscript on the equatorial trough zone.* In press.

Schacht, E. J., 1947: A mean hurricane sounding for the Caribbean area. *Bull. Amer. meteor. Soc.*, **27**, 324–327.

Simpson, R. H., 1952: Exploring the eye of typhoon Marge, 1951. *Bull. Amer. meteor. Soc.*, **33**, 286–298.

——, 1954: Structure of an immature hurricane. *Bull. Amer. meteor. Soc.* **35**, 225–350.

——, 1956: *Some aspects of tropical cyclone structure.* Tropical Cyclone Symposium Pap. No. 8, Brisbane, Dec. 1956, 19 pp.

Contribution No. 920

Särtryck ur Tellus nr 3, 1958

The Release of Latent Heat in Tropical Storms Due to the Fall-Out of Sea-Salt Particles

By A. H. WOODCOCK

Woods Hole Oceanographic Institution[1], Woods Hole, Massachusetts

(Manuscript received August 12, 1957 revised April 1, 1958)

Abstract

Observations of atmospheric sea salt in a hurricane are used to estimate the weight of salt in the clear air at cloud levels. These quantities are then used to determine the rate of release of heat in the moist air layers below, due to condensation on this salt as it falls from the relatively dry air at higher levels. This rate is found adequate to alter significantly the distribution of heat and water vapor in the cloud-layer air and to explain much of the observed potential temperature increase in the lower air converging upon the central regions of hurricanes.

1. Introduction

In meteorology computations involving the release of latent heat of vaporization of water assume that no significant amount of condensation occurs in the atmosphere until the relative humidity reaches 100 per cent. In fact the assumption of dry-adiabatic conditions in well-mixed sub-saturated air below cloud base is sometimes used as a basis for judging the probable accuracy of temperature measurements made in this air (JORDAN, 1952). In air containing certain quantities of hygroscopic particles, this assumption is probably not valid. The author has shown that condensation on sea salt particles in ascending air can bring about a significant release of latent heat in the sub-cloud layer at relative humidities less than 100 per cent (WOODCOCK, 1950).

The previous attempt to use measurements of sea-salt particles to estimate the role of the salt in the release of latent heat in the sub-cloud layer was not very conclusive. This was due primarily to uncertainty about the maximum amounts of salt to be expected in storms at sea, and to a failure to realize that salt falling from higher levels might also be important. Recently developed techniques (WOODCOCK, 1950a, 1952) (WOODCOCK and SPENCER, 1957), designed to sample the larger salt particles, have shown the presence in strong winds of particles having a weight of nearly 10^{-6} grams. These measurements have also shown that the glass slide technique averages quantities of salt, in one to ten kilometer sampling lengths over the sea, which may vary by a factor of two to ten within these lengths. Thus for this and other reasons (see section 8), one need not regard the averaged hurricane data used here as limiting quantities, since they result from application of the older glass-slide sampling

---

[1] Contribution No. 920 of the Woods Hole Oceanographic Institution. Work supported by the Office of Naval Research, under contract Nonr-798(00) (NR-082-124).

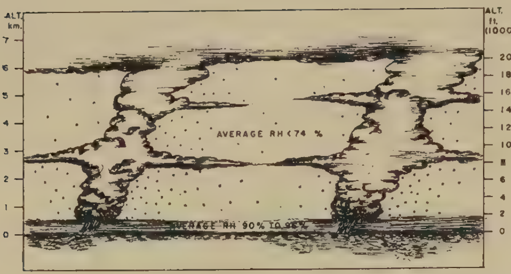

Fig. 1. Diagram illustrating the idea of the fall-out of large salt particles associated with clouds. This figure is intended to represent a cross-section normal to two cloud lines. It is assumed that the average relative humidity in the clear air at cloud levels above 5,000 feet is less than 74 per cent.

technique. No new measurements have thus far been made in these storms using the new techniques, but for present purposes the earlier observations are useful.

The current interest in expanding our knowledge of tropical storms and the improved facilities for doing so caused the author to hazard a second attempt to show that the quantity of airborne sea-salt is important in these storms. The primary purpose of the present paper is to discuss the role of salt which is carried upward by the clouds, in subsequently altering the distribution of heat and water vapor as it falls back towards the sea. It is hoped that hurricane-research aircraft will be able to test some of the conclusions of this study through direct measurements.

Byers (1944, p. 432) and Riehl (1951 and 1954) have discussed the near-isothermal expansion of the sub-cloud air flowing in towards the central low-pressure areas of tropical cyclones. Riehl emphasized the basic role of this phenomenon in altering the stability of the atmosphere in the central areas of hurricanes (Riehl, 1954, p. 313—316). Both of the above authors assumed that the sensible heat required to compensate for the adiabatic cooling as the pressure falls in the converging air (roughly 1° C per 10 mb of pressure decrease), is derived from the greatly agitated sea surface waters.

The following sections of this paper are intended to show that a large part of this heat can come from latent heat released by condensation of water vapor on salt particles. It is pictured that these particles, which are produced by bursting bubbles at the sea surface (Blanchard, Woodcock, 1957) (Kientzler et al., 1954) are carried up in the clouds, are distributed laterally by shear and turbulence and fall into or are mixed into the relatively clear air between the clouds. Here the particles will alter the vapor and heat distributions as they fall in and out of layers of air having different relative humidities on their way down towards the sub-cloud layer, as suggested by Figure 1. In falling from an area where the RH averages < 74 per cent, to one in which the average RH is 90 per cent or 96 per cent, condensation releases heat at a rate which is sufficient to account for the observed warming of the air flowing into tropical cyclones, if one assumes a salt fall-out of a certain average intensity over the whole area of the observed isothermal expansion.

2. Preliminary description of the model proposed

The purpose here is the initial clarification of the primary problem, which is to demonstrate that the transport of salt between the sea, the sub-cloud and cloud layers can result in a sensible heating of the sub-cloud air through the release of latent heat.

The spray particles entering the atmosphere from the sea can be divided, for present purposes, into two groups: 1), those particles which fall back into the sea without being carried out of the sub-cloud air, and 2), those which return to the sea after ascending in clouds and falling through relatively dry regions of the cloud-layer atmosphere.

Group one particles will produce a net cooling of the sub-cloud air due to evaporation. The amount of this cooling will be directly related to the difference in the salinity of the droplets which are ejected into the air from the bubbles in the sea and their salinity upon falling from the air and re-entering the sea. The relative humidity over spray droplets of sea water is about 98 %. Since surface-air relative humidities of 90 % and 96 % are assumed in the discussion below, the spray droplets will evaporate to some extent (see Fig. 2) before returning to the sea. Thus evaporation from these group one spray particles will tend to stabilize thermally the lower part of the sub-cloud layer, which

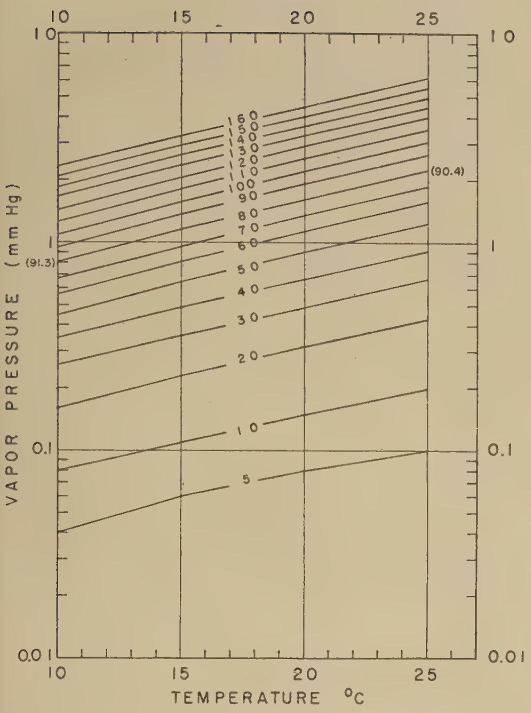

Fig. 2. Vapor pressure lowering over concentrated sea water at various temperatures and salt concentrations. Concentrations represent chloride in parts per thousand, by weight. (From Arons and Kientzler, 1954).

contains the dryest air in this usually well-mixed section of the trade-wind or hurricane atmospheres (Bunker et al. 1949) (Riehl, 1954). The sensible heat required for this evaporation is assumed to come from the sea surface.

Group two particles are carried upwards into the clouds through the sub-cloud layer. They are assumed to enter cloud base having a salinity equal to that existing when they were ejected from the sea (i.e. equilibrium at RH 98 %). From the time of their production to the time when they enter cloud base, this group of particles could thus cause no net change in the total heat of the sub-cloud air. After being carried upwards to various altitudes in the clouds, the particles are mixed or fall into the dryer inter-cloud air and eventually fall back into the sub-cloud layer as relatively dry salt particles. The heat required to vaporize the water from the group-two particles is thus derived from high in the cloud-layer air. The quantity of latent heat released in the sub-cloud layer by condensation as these particles re-enter the layer, will be inversely proportional to their salinity as they subsequently fall into the sea or re-enter the clouds. In this cycle of vertical motions group-two particles will cool the cloud layer air and will warm the sub-cloud air, adding to the instability of each.

With the above model in mind, the author will now try to show that the range of increase of potential temperature observed in converging lower air in hurricanes may be computed, at least in part, from the quantities of salt found in these storms.

3. Sea salt in lower air

During the tropical storm which passed near Miami, Florida on September 22, 1949, the author made measurements of the average weight and number of the salt particles of certain size ranges present at an altitude of 40 meters above the sea at Hillsboro Lighthouse (Woodcock, 1950). Fig. 3, curve 12, shows the number and size of the salt particles found, presented as a cumulative-number distribution curve. For comparison other observations are shown which were made from aircraft at cloud levels in trade-wind

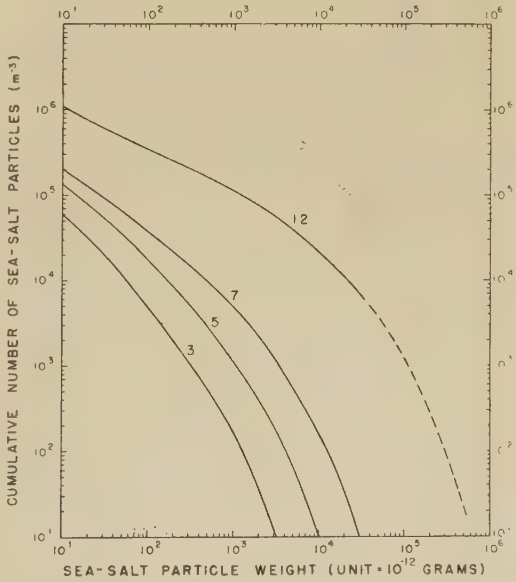

Fig. 3. Cumulative number distribution curves for averaged observations during wind forces 3, 5, 7 and 12.

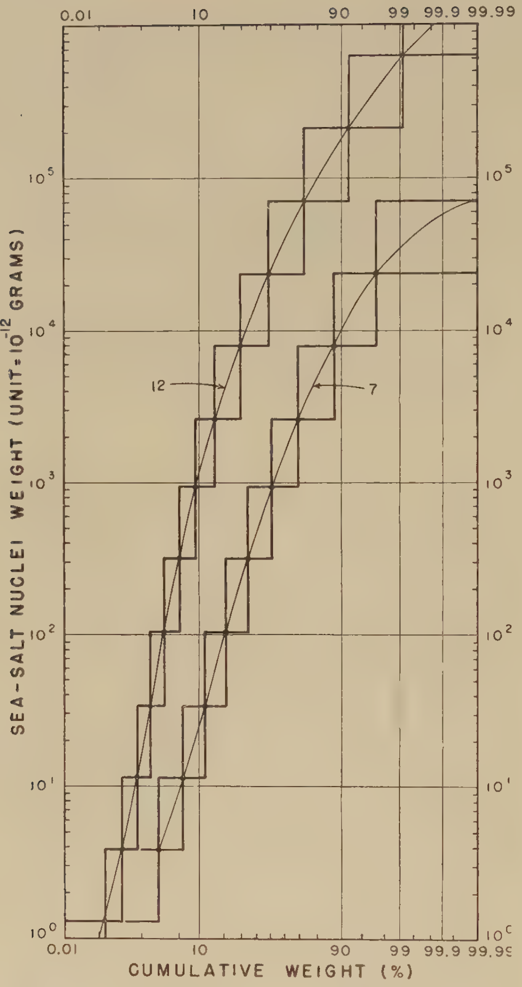

Fig. 4. Averaged cumulative per cent weight distribution of sea salt particles. Curve 12 represents hurricane conditions, and is taken from the measurements averaged in curve 12 of Figure 3. Curve 7 represents the averaged force 7 wind data given on line 7 of Figure 3. The rectangular areas are interpreted as follows: the range between 8,000 and 24,000 $\mu\mu$ gram particles (curve 12) contains about 20 per cent of the total weight in all of the particles measured. The curved lines are drawn through the points which represent the weight limits of each weight range. (See text for further discussion.)

areas under more moderate wind conditions. The broken portion of curve 12 is a reasonable extrapolation, based upon the author's wide experience in salt-aerosol sampling.[1]

The cumulative number distribution curve, which was originally derived from thirty-one size range measurements, was divided into fourteen weight ranges in accordance with the convenient size steps of the Porton eyepiece graticule (May, 1945). The product of the total number in each weight range and the median-number weight, approximates the weight of salt in each range. The ratios of these individual weights to their sum were used to derive the cumulative per cent weight distribution values shown on Figure 4. The sum of weights of sea salt represented by the force 12 curves on Figures 3 and 4 is 1.2 mg m^{-3}. As a test of the accuracy of this weight estimate, a further division of each of these fourteen steps into five, making a total of seventy size ranges, increased this value by only 0.1 mg m^{-3}. Thus curve 12 of Figure 4 is, for present purposes, a close approximation of the total salt represented by curve 12 of Fig. 3.

On Table I, column 1 shows the particle weights represented by curve 12 of Figure 3, divided into 20 weight range categories. Each of these weight ranges contains about 5 per cent of the total mass of sea salt present in all of the particles. The particle weights were taken from curve 12, Figures 3 and 4 as follows: Note on curve 12, Figure 4, that the salt particles in the weight range of about 320 to 1,200 $\mu\mu$ grams contain about 5 per cent of the total salt. In this weight range the cumulative number distribution curve (on Figure 3) crosses the mid-point of this selected 5 per cent interval at the nuclei weight of about 600 $\mu\mu$ grams. This and other similarly derived nuclei weights are shown in column 1 of Table I. Columns 2, 3 and 4 of Table I give the radii and the rates of fall of these nuclei as relatively dry salt particles.

Amounts of salt near cloud-base altitudes have been found to be about the same as those a few hundred feet over the sea surface, under a wide range of wind conditions. On the assumption that a similar mixing of

---

[1] The hurricane samples were unfortunately taken prior to the development by the author of the "multi-strip sampling" technique (Woodcock, 1952). This sampling method which utilizes the low sampling efficiency of wide slides or "ribbons" (Langmuir, 1945), makes it possible to selectively sample the large sparsely distributed nuclei, despite the presence in the air of great numbers of the small nuclei. See the discussion section of this paper for further remarks about salt in hurricane winds.

TABLE 1

The sea-salt particle distribution represented by curve 12, Figure 3, divided into 20 equal weight categories. The nuclei weights given in column 1 are those of the median number particle and are used to compute the distribution of salt and condensed water at severals levels in the atmosphere. Inital weight of salt in each 5 % interval is 60 μ gms m^{-3}. See the text for more information.

Sea-salt nuclei as crystalline particles near sea surface				Sea-salt nuclei as droplets upon arrival at cloud base				
Weight 10^{-12} g	Radius μ	Fall Rate cm sec^{-1}	Amount of salt falling μgms.m^{-2} sec^{-1}	Radius μ	Fall Rate cm. sec^{-1}	Amount of salt & water falling μ gms.m^{-2} sec^{-1}		Wt. of salt in each size range μgms. m^{-3}
						salt	water	
1	2	3	4	5	6	7	8	9
50	1.8	0.084	0.05	9	1.0	0.6	36	60.5
600	4.0	0.42	0.25	17	3.5	2.2	74	61.9
1,750	5.8	0.86	0.52	22	5.8	3.7	90	63.0
3,200	7.0	1.27	0.76	26	8.0	5.2	113	64.5
4,800	8.0	1.63	0.98	29	9.7	6.3	128	65.4
7,100	9.2	2.15	1.29	32	11.4	7.5	137	66.0
9,900	10.2	2.72	1.63	35	13.4	9.0	147	66.8
13,100	11.2	3.25	1.95	37	15.0	10.2	155	68.2
16,700	12.2	3.85	2.31	40	17	11.8	170	69.5
21,800	13.3	4.50	2.70	42	19	13.4	177	70.7
28,000	14.5	5.45	3.27	45	22	15.6	196	72.3
36,000	15.7	6.40	3.84	48	24	17.7	210	73.9
44,000	16.8	7.30	4.38	51	26	20.0	224	75.6
54,000	18.0	8.40	5.04	54	29	22.4	244	77.4
68,000	19.4	9.70	5.82	57	32	25.4	257	79.5
88,000	21.2	11.6	6.9	61	36	29.9	293	83.0
114,000	23.1	13.8	8.3	65	40	33.8	307	85.6
152,000	25.4	16.7	10.0	70	44	39.2	331	89.0
223,000	29.0	22.0	13.2	77	50	46.7	345	93.5
410,000	35.4	33.0	19.8	90	63	68.5	441	108.7
			93.0			379.1	4,075	1,495.0

aerosols exists in hurricanes, the quantity of salt derived above can be used to estimate amounts carried upwards by clouds.

4. Transport of salt by ascending clouds

Using a reasonable average rate of rise of air in the cumulus clouds of 4 m sec^{-1} (MALKUS) and a weight of salt at cloud base altitudes of 1.2 mg m^{-3}, the estimated ascent of salt is 4.8 mg m^{-2} sec^{-1}.

What proportion of a storm area contains such actively growing cumuli? Wexler found in a study of numerous radar (PPI) scope photographs of hurricane spiral rain bands, that the width of these bands was about the same as the width of the spacing between them (WEXLER, 1947). If these rain bands roughly delineate the size of the areas of major ascent of moist cloud air, one might estimate that the areas of ascent are about the same size as the areas between.

It seems excessive to suppose however that one-half of a storm area contains actively ascending cloud material. A more conservative ratio of active cloud area to relatively clear inter-cloud area of one to ten is tentatively used. Sea salt ascending in the clouds at a rate of 4.8 mg m^{-2} sec^{-1} will, on this assumption, be sufficient to produce an average fall over ten square meters of 0.48 mg m^{-2} sec^{-1}.

What proportion of this salt is subtracted from the cloud layer air, by the various rain mechanisms (MIYAKE, SUGUIRA, 1950) (WOODCOCK, 1952) (WOODCOCK, BLANCHARD, 1955) which cause the salt particles to be carried back to the sea in solution in the falling raindrops? Miyake and Suguira (1954) have shown that the rate of precipitation of chloride during the passage of typhoon "Kitty" in Japan ranged

TABLE 2

Rates of fall of sea salt in hurricane at equilibrium concentration at different relative humidities.* Quantities of salt taken from Table I, column 1 and from Figure 4.

Wt. of sea salt in particles 10^{-12} g	RH 90 %			RH 96 %			RH 98 %		
	Particle radii μ	Particle fall rate cm sec^{-1}	Sea salt falling μ gms m^{-2} sec^{-1}	Particle radii μ	Particle fall rate cm sec^{-1}	Sea salt falling μ gms m^{-2} sec^{-1}	Particle radii μ	Particle fall rate cm sec^{-1}	Sea salt falling μ gms m^{-2} sec^{-1}
50	4.2	0.3	0.2	5.3	0.4	0.2	7.0	0.6	0.4
600	9.6	1.3	0.8	12.1	1.9	1.1	15.8	3.0	1.8
1,750	13.6	2.5	1.5	17.4	3.9	2.3	22.6	6.0	3.6
3,200	16.7	3.7	2.2	21.2	5.7	3.4	27.7	8.8	5.3
4,800	19.0	4.8	2.9	24.3	7.4	4.4	31.8	11.3	6.8
7,100	21.7	6.1	3.7	27.6	9.3	5.6	36.2	14.5	8.7
9,900	24.2	7.6	4.6	31.0	11.5	6.9	40.5	17.8	10.7
13,100	26.6	9.0	5.4	34.0	13.6	8.2	44.5	21.0	12.6
16,700	28.8	10.4	6.2	37.0	15.0	9.0	48.3	24.5	14.7
21,800	31.5	12.4	7.4	40.0	18.2	10.9	52.5	28.5	17.1
28,000	34.2	14.5	8.7	44.0	21.5	12.9	57.5	32.7	19.6
36,000	37.2	17.0	10.2	47.5	25.0	15.0	62.5	37.0	22.2
44,000	39.8	18.8	11.3	51.0	28.5	17.1	66.6	41.0	24.6
54,000	42.6	21.6	12.9	54.5	31.7	19.0	72.0	46.0	27.6
68,000	46.1	25.0	15.0	59.0	36.0	21.6	77.5	51.0	30.6
88,000	50.2	29.0	17.4	64.0	40.0	24.0	84.0	57.5	34.4
114,000	54.7	33.0	19.8	69.8	46.0	27.6	92.0	65.0	39.0
152,000	60.3	39.0	23.4	76.5	53.0	31.8	102.0	74.5	44.7
223,000	68.5	46.5	27.9	87.5	63.0	37.8	113.0	84.0	50.4
410,000	83.9	62.0	37.2	110.0	84.0	50.4	140.0	108.0	65.0
			217.7			308.2			439.8

* It is assumed here that the amount of salt is constant as the RH is varied. The original data (Woodcock, 1950, p. 398) are inadequate to test this assumption. Sampled amounts of salt differed by a factor of 2.4, while the RH varied from 82 % to 91 %. These RH values are thought to be too low however, due to the necessity to expose the thermometers inside the lighthouse enclosure (with several windows open). Thermometers exposed outside were immediately coated with a briny film, thus making the readings uncertain.

from about 0.003 to 0.08 mg m^{-2} sec^{-1}, with an average of about .02. This range of values agrees very well with one estimated from the average rainfall in moving storms (Riehl, 1954, p. 295) and from the chloride concentration in typhoon and hurricane rains (Miyake, Suguira, 1954) (Harrison, Williams, 1897).

Thus the estimated fall-out of chloride transported up in the clouds (about 0.27 mg m^{-2} sec^{-1}) exceeds by a factor of more than ten the average observed rate of chloride fall in rains.

If, for the moment, one assumes that within the storm area sufficient salt has been carried up in the clouds to establish a steady state, then the average fall of briny particles through the relatively clear inter-cloud air (S_f) is simply derived as follows:

$$S_f = \frac{S_a - S_r}{10} \qquad (1)$$

where S_f = sea salt falling (mg m^{-2} sec^{-1})
S_a = sea salt ascending in clouds (4.8 mg m^{-2} sec^{-1})
S_r = sea salt carried down in rains (0.04 mg m^{-2} sec^{-1})

Using equation (1) it is found that a fall-out of salt aerosols from the inter-cloud air of about 0.44 mg m^{-2} sec^{-1} should occur. (It will be noted that this quantity is very similar to the fall of salt computed on Table 2 from the observed values. This similarity is presumably due to a realistic choice of variables in estimating fall-out from the inter-cloud air.)

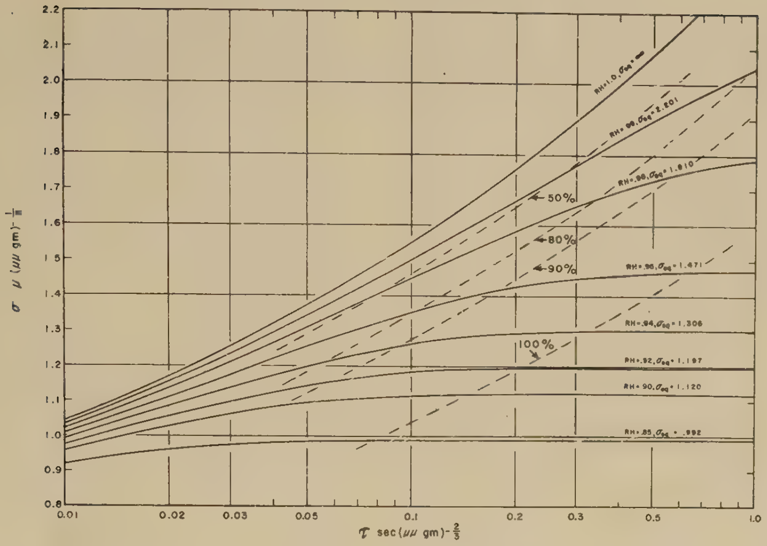

Fig. 5. Sea-salt particle-growth curves at various fractional humidities and a temperature of 25 C. Multiplication of τ by the cube root of nucleus mass, and of σ by the nucleus mass raised to the 2/3 power, converts coordinates to droplet radius in microns and time in seconds (from KEITH and ARONS, 1954). The dashed lines have been added by the present author to estimate the time required to establish various fractions of the equilibrium volume of the droplets.

When the salt particles fall from the relatively dry inter-cloud air into the moist sub-cloud air, condensation occurs and heat is released.

5. Heating of unsatured sub-cloud air by condensation on falling salt

The amount of water which will condense (W_L) as the falling salt particles enter the moist air, is computed from the equation

$$W_L = S_f \frac{1}{c} \qquad (2)$$

where W_L is expressed as mg m^{-2} sec^{-1}

S_f = weight of salt falling (mg m^{-2} sec^{-1})

c = concentration of sea salt in particles by weight fraction (from ARONS and KIENTZLER, 1954).

Utilizing the relationships given in equation (2) and the salt fall-out, the weights of condensed water were computed. The heating of the air resulting from this condensation was then derived as follows:

$$T = m_L / C_p \qquad (3)$$

where T = temperature change (°C gm^{-1} sec^{-1})

m = weight of water condensed (gms gm^{-1} sec^{-1})

L = latent heat of vaporization of water (585 cal gm^{-1})

C_p = specific heat of moist air (0.245 cal gm^{-1})

Assuming that 0.44 mg m^{-2} sec^{-1} of sea salt are falling from an air layer having a RH of < 74 per cent,[1] into regions where the RH is 90, 96 and 98 per cent, equation (2) is used to derive the amount of water condensed. In so doing the data on Figure 2 are used. It is found that water is condensed at a rate of 12.6 mg m^{-2} sec^{-1}, if the moist layer RH is 98 per cent, 5.9 mg m^{-2} sec^{-1} if it is 96 per cent and 2.9 mg m^{-2} sec^{-1}, if it is 90 per cent. This assumes that a steady state exists and that condensation on all particles proceeds to a state of vapor pressure equilibrium in the moist air. In the time required to fall 200 meters, most of these particles will reach more than 90 % of their equilibrium size at these relative humidities (see Fig. 5; GUNN and KINZER, 1949; and Stoke's law).

---

[1] In a recent series of temperature soundings by the Woods Hole Oceanographic Institution aircraft (August 1956), the relative humidity in the clear air above 5,500 feet was 72 per cent or less in several locations in the West Indian region. It is supposed that it is the more or less normal trade-wind air and clouds of this time of year which are drawn into tropical cyclones (see discussion of this point by Wexler, 1947).

The computed heating of the moist layer of air resulting from the above amounts of condensed water, utilizing equation (3), is shown in Table 3 below. The degree of this heating in any given mass of air depends of course upon the average relative humidity there. The air-layer depths selected for tabulation[1] lie in the range of those reported for the sub-cloud layer in tropical storms. It is this layer which contains most of the air spirally converging upon the rain-area. The extent to which the assumed relative humidities of this air are realistic is uncertain. Similar high values have however been reported and utilized in other hurricane studies (see TANNEHILL, 1943, Fig. 10; SIMPSON, 1947, and RIEHL, 1954, Fig. 11–29).

Riehl has indicated the potential temperature as a function of surface pressure in hurricanes (RIEHL, 1954, p. 287). It is concluded from his study of available data that the average pressure drop is about 50 mb, and that the average amount of sensible heating of the converging air is about 4° C.

Using Hughes' Figure 8 (HUGHES, 1952), which shows the average trajectories and rates of convergence of surface air to a point within 0.5° latitude (30 nautical miles) of the moving storm center, it is estimated that the heating of this air occurs in from 12 to 22 hours, with an average of about 18 hours. In other words 4° C is the approximate temperature increase in the air within the range of time required for it to move into the 0.5° latitude point from a distance of 240 nautical miles out from the center. On Table 3 it can be seen that the latent heat released due to condensation upon salt particles produces temperature increases which range from about 0.5 to 9 °C, depending upon the time used, the average relative humidity of the sub-cloud layer and the thickness of this layer. It is assumed of course that the high relative humidities are maintained by evaporation from the sea surface. As a rough first approximation, the similarity of this range of heating computed from the salt fall-out, to the range given in Riehl's study (see RIEHL, 1954, p. 287), encourages further work in this direction.

6. Effects of salt fall-out from undiluted aerosols

The fall-out of salt into the moist lower air from the cloud layer will not, of course, be in a steady state, since the clouds which transport most of the salt are so unsteady (KESSLER) (SIMPSON). In order to estimate the average heating effects of this salt fall upon the sub-cloud layer as a whole, it was necessary in the previous section to assume a steady state and a ten times dilution of the salt transported by the clouds. It is of interest to consider some effects, of shorter duration, which might arise in areas where the aerosol population might remain undiluted. In order to do this it becomes necessary to estimate the aerosol concentrations to be expected in inter-cloud areas near active cloud systems.

Below it will be shown that condensational growth of the salt nuclei in ascent to cloud base and within the clouds will result in a "compression" of their spacial distribution.

TABLE 3

Computed air temperature increases, in layers of various vertical thickness, due to condensation on falling salt

Height of layer Meters	Air temperature increase in 18 hours (°C)		
	RH 90	RH 96	RH 98
200	1.0	2.9	9.4
400	0.5	1.5	4.7

---

[1] A cubic meter of air is assumed to weigh one kilogram. No corrections have been made in this paper for pressure effects upon particle distributions or fall rates, since the condensation processes discussed are thought to occur largely at low altitudes.

The largest increase in concentration occurs as the nuclei fall from the clouds into relatively dry inter-cloud air. The cloud and its local environment thus become an area of concentration of salt.

a) *Ascent of salt-laden air to cloud base.* Columns 5 through 9, Table I, show the changes which occur as a result of the lifting of air from near the surface up to cloud base.

The radii in column 5 are taken from the sea-salt nuclei growth measurements of Kieth and Arons, and they represent the sizes of the salt particles of column 1 at cloud base, assuming dry adiabatic ascent at a rate of one meter per second (see Figure 6).[1] The rates of fall of individual particles, which are given in column 6, are taken directly from Stoke's law and, for the larger particles, from the measurements of GUNN and KINZER (1949). The amounts of sea salt which are falling, are given in column 7, and are the product of the fall rate (column 6) and the quantity of salt in the size ranges concerned (column 9). The amounts of water falling are a product of the amounts of salt falling (column 7) and their concentration, expressed as grams per gram. (These rates of fall of salt and water represent fall relative to the air.) Finally, column 9, which indicates an increased amount of salt in the air, is a product of the initial amount of salt passing unit area per second and the quantity one over the rate of ascent of the air minus the rate of fall of the particles.

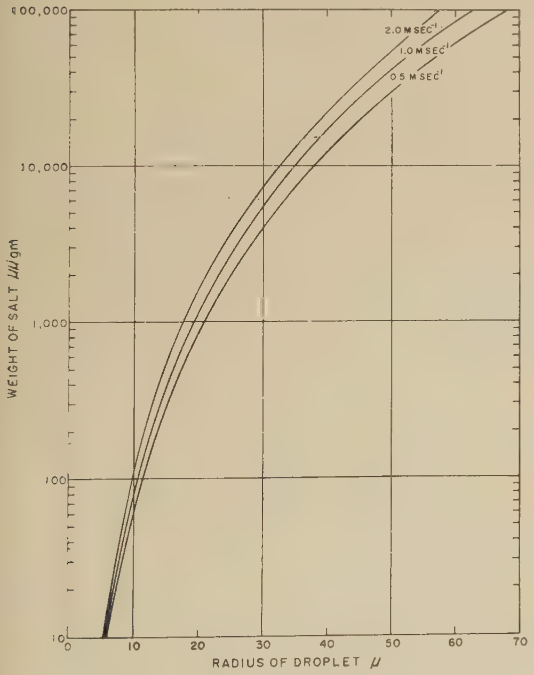

Fig. 6. Calculated radius of sea-salt droplets at cloud base (RH 100 per cent), as a function of nucleus mass and rate (taken from KEITH and ARONS, 1954).

More definitely expressed, this relationship becomes:

$$W = w' \frac{1}{v-u} \tag{4}$$

where W = wt. of sea salt m^{-3} of air

w' = wt. of sea salt crossing each m^{-2} per second (μ gms)

v = rate of ascent of air (m sec^{-1}), and

u = rate of fall of the particles (m sec^{-1}).

In each case w' is fixed, in any column of air ascending at a steady rate, by the initial quantity of salt of each size range in the air as it rises from near the sea surface, by the fall rate of the particles and by the rate of rise of the air. This means that within an ascending column of air the weight of salt passing each square meter of horizontal surface, which is fixed in reference to the ground, is constant. It is assumed here that there is a horizontal homogeneity in the salt aerosol population.

Thus it seems, from the results in column 9, that the adiabatic ascent of moist air containing salt particles, will cause a concentration or a compression of the particle distribution. This compression is due to the condensational growth of the particles and to their consequent increased fall rate (in Table I, compare columns 2 and 3 to columns 5 and 6). It can be seen in equation (4) that the changing relationships between the rates of rise of the air and of the particles, alter the salt particle concentration.

An increase in the amount of salt with increasing altitude in the sub-cloud layer of the trade-wind atmosphere was first reported

---

[1] The conditions assumed in deriving the droplet sizes given in Figure 6, are not strictly applicable to the present case. However the error, in computed particle size at cloud base, which results from these differences in conditions is not significant here.

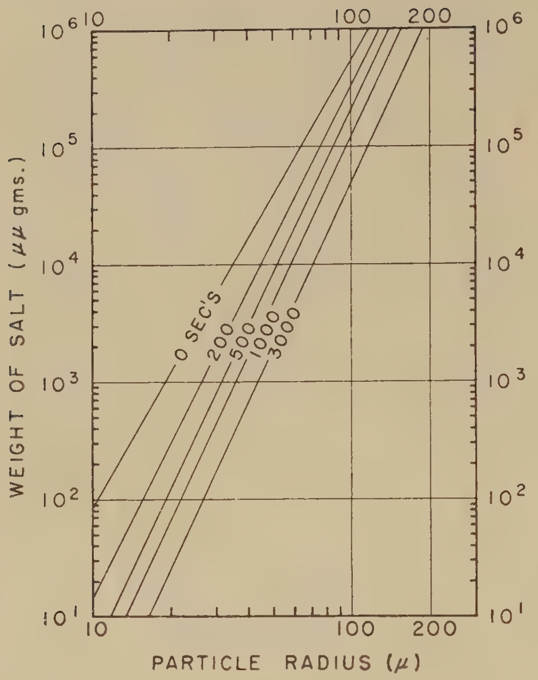

Fig. 7. Sizes of salt particles after given times in cloud:—including growth in coming to cloud base at 1 m/sec rise. (From KEITH and ARONS, 1954, see text).

by LODGE (1955) and has been subsequently occasionally observed by the author while making nuclei measurements for other purposes. These observations are not adequate to be used here as a test for the computed increase in salt with altitude. Such test measurements are planned in the future, using the recently developed airborne flame photometer (WOODCOCK, SPENCER, 1957) in conjunction with the glass-slide sampling method (WOODCOCK, 1952).

(b) *Ascent of salt-laden air in cumuli.* In the trade-wind areas the cumulus clouds are the major mechanism bringing about the transport of surface air from near cloud base altitudes upwards into the cloud layer (MALKUS, 1956) (RIEHL et al., 1951). We now assume that the clouds serve a similar role in the lower air spiraling into hurricanes, and determine the change in salt particle size and concentration as the air rises in these clouds and into the inter-cloud regions.

Figure 7 shows the radii of the various weights of sea-salt particles as a function of time of exposure in cloud air, assuming a relative humidity in the cloud of 100 per cent. These growth rates were derived for the author by C. H. Kieth, and are based upon his experimental determination of the condensation on sea-salt nuclei (KIETH, ARONS, 1954).

In Table 4, the droplet radii shown in column 2 are taken from the 1,000 second curve of Figure 7. At the rate of ascent assumed, this is about the time required for an air parcel to rise from cloud base to the top of a cloud of medium vertical development. Equation (4) is again applied to the different conditions in the cloud, in order to determine the additional "compression" of the particle distribution due to the changed relative motions. In this case, however, W is determined by the quantity of salt in the air at cloud base and by the increased values for particle fall rate and rate of rise of the air in the cloud. The sums of the quantities in column 6 of Table 4, show that the calculated amount of salt per unit volume of air has again been increased by ascent in the cloud, as it was in ascending in the sub-cloud layer. Comparison of columns 4 and 5 of this table to columns 4, 7 and 8 of Table I, show that there has also been a marked increase in the rates of fall of salt and water with reference to the ascending air.

(c) *Fall-out of salt particles from cloud into clear air.* As the large salt-containing droplets in the cloud (column 2, Table 4) fall or are mixed into the clear environmental air, evaporation occurs and the resulting alteration of particle settling rate again compresses the distribution. This compression is derived as follows:

$$W' = W_c \frac{U}{U'} \qquad (5)$$

where W' = wt. of sea salt in the clear air (μ gms m^{-3}) after evaporation to equilibrium has occurred

W_c = wt. of sea salt in cloud (column 6, Table 4) in μ gms m^{-3}

U = particle fall rate as droplet in cloud (column 3, Table 4), in cm sec^{-1}

U' = particle fall rate after evaporation to equilibrium in clear air, in cm sec^{-1}

TABLE 4

Alterations in the distribution of the salt particles represented by curve 12 figure 3, upon ascent in a cumulus cloud and upon falling out of the cloud into clear inter-cloud air.

Sea-salt nuclei as cloud droplets after 1000 seconds in cloud; R. H. 100 %; rise rate 4 m sec^{-1}						Droplets fall into clear air at cloud levels where R. H. < 74 % and evaporate to a crystal state		
Weight of sea-salt particles 10^{-12} g	Cloud droplet radius μ	Cloud droplet fall rate cm sec^{-1}	Amounts of salt and water falling μ gms. m^{-2} sec^{-2}		Wt. of salt in each size range μgms. m^{-3}	Salt particle radius μ	Particle fall rate cm. sec^{-1}	Wt. of salt in each size range μ gms. m^{-3}
			salt	water				
1	2	3	4	5	6	7	8	9
50	19	4.4	2.7	1,545	61	1.8	0.084	2,980
600	32	11.6	7.3	1,663	63	4.0	0.42	1,710
1,750	40	17.5	11.4	1,739	65	5.8	0.86	1,320
3,200	45	22.0	14.7	1,775	67	7.0	1.27	1,130
4,800	50	25.5	17.4	1,823	68	8.9	1.63	1,075
7,100	54	29.5	20.5	1,869	70	9.2	2.15	925
9,900	58	33.0	23.2	1,887	71	10.2	2.72	863
13,100	62	36.5	26.5	1,983	72	11.2	3.25	825
16,700	65	39.5	29.2	1,981	74	12.2	3.85	770
21,800	68	42	31,5	1,868	75	13.3	4.50	685
28,000	72	46	35.4	1,935	77	14.5	5.5	656
36,000	76	50	39.5	1,980	79	15.7	6.4	618
44,000	80	54	44.2	2,106	82	16.8	7.3	600
54,000	83	57	47.9	2,077	84	18.0	8.4	577
68,000	88	61	53.0	2,177	87	19.4	9.7	546
88,000	92	65	58.5	2,111	90	21.2	11.6	508
114,000	98	70	68.8	1,921	93	23.1	13.8	465
152,000	104	76	74.5	2,225	98	25.4	16.7	440
223,000	113	84	87.4	2,273	104	29.0	22.0	398
410,000	128	97	117.3	2,403	121	35.4	33.0	362
			811	39,341*	1,602			17,453

* This fall rate, expressed in more familiar terms, is about 0.04 mm hr^{-1}, which is near the minimum measured within trade-wind orographic clouds (BLANCHARD, 1953).

Column 9 of Table 4 shows that a "compression" of salt concentration of about one order of magnitude would result if evaporation to a crystalline state in the clear air occurred with a continuous source of cloud particles allowing the establishment of a steady-state condition. The total rate of fall of salt in the clear air is the same as that in the cloud, for the product of the fall rate and the salt concentration, columns 8 and 9 of Table 4, can be seen to equal the values in column 4. In other words the conservation of mass principle is assumed to apply here, so that the number of particles falling into the top of a given column of air in a certain time interval must equal the number falling out at the bottom of this column in the same interval.

Thus the ascent of salt-laden air from near the sea surface to cloud base altitudes, its ascent in cumulus clouds and its final passage into the clear cloud-level air, tend in each case to increase the quantity of salt in the air.

As previously mentioned, an increase of salt with altitude is sometimes observed in the sub-cloud layer. Recent use of an air-borne flame photometer in trade-wind clouds has indicated that the average salt (sodium) content of these clouds is sometimes higher than the average salt content of the air below cloud base (WOODCOCK, SPENCER, 1957). No data are available however on the nuclei present in the clear air at cloud levels at times or at places where an inter-cloud increase in salt might have been encountered. Observations aimed specifically at exploration of the salt nuclei gradients in the lower trade-wind atmosphere during storms are needed to test the above calculated gradients.

The computed and observed increase with altitude in the amount of salt particles in the air encourages some calculations concerning the possible effects of these particles in altering the distribution of water vapor and temperature as they fall, in undiluted concentration, from the higher levels towards the sea. For convenience in making the calculations of salt fall-out in inter-cloud air, it is assumed that the ascent of new masses or bubbles (Scorer, Ludlam, 1953) of cloud materials is frequent enough to produce a relatively steady source of the larger salt particles, which supply the greatest amount of falling salt (see column 4, Table 4). With a markedly transient cloud source of the falling particles, the wide range of fall speeds present among these larger particles (see column 8, Table 4) would soon cause a diminishing concentration in the clear air as the larger particles fell away from the smaller.

Of course the droplet population of a significant volume of a cumulus cloud is not likely to have been exposed to saturated conditions for exactly 1,000 seconds as was assumed in Table 4. However, for the rate of rise assumed here, exposure times in ascending air parcels of about 500 to perhaps 1,500 seconds seems reasonable for the clouds concerned. On Figure 7 and Table 4 it can be seen that this range of exposure duration is not sufficient to cause droplet size differences, for any given particle weight, which would markedly alter the particle-concentration effects discussed here. The important requirements are that droplets of the approximate sizes given be present in the clouds and that they form on salt particles having weights approximating those given. No reference to measurements of the droplet size distribution of marine cumuli in tropical storms has been found in the literature. However, Squire's results in Australian and Hawaiian maritime clouds during moderate winds (Squires, Gillespie, 1952) (Squires, Warner, 1957) are consistent with the computed drop size distributions given here. The effects of coalescence of droplets upon size distribution and in increasing rates of fall were not considered above. Introduction of these complicating effects would serve only to increase salt fall-out, which for present purposes is shown to be adequate.

The purpose of the above computations of the compression effects of ascent and growth upon salt particle concentration was to show, in the section to follow the local heating effects of fall-out of salt from areas of undiluted aerosol concentration. In estimating these effects in the sub-cloud layer as a whole, it will be remembered that, in section 5 above, a dilution of the cloud-borne salt by a factor of ten was assumed.

(d) *Altered vapor and temperature distribution in cloud layer.* When the particles fall from the cloud into the inter-cloud air having a relative humidity less than 74 %, evaporation to relative dryness will occur. The diminishing droplet size causes a sharp reduction in rate of fall of individual particles (see column 8, Table 4). However, the great increase in the salt concentration in the air, shown in column 9, will cause the total rate of fall of salt m^{-2} sec^{-1} in each weight range to remain the same as it was in the cloud – note for instance that the product of the fall rate and the weight of salt in each size range (columns 8 and 9 of Table 4) is equal to the quantities in column 4. The sum of these quantities can be seen to be 811 μ grams of sea salt falling per square meter per second.

If, in falling towards the sea, this mass of salt moves out of the dry air (RH $<$ 75 per cent) and into a layer where the RH is 90 per cent, condensation will occur on the particles, heat will be released and water will be carried downward. Upon subsequently falling out of the moist layer and into a dry

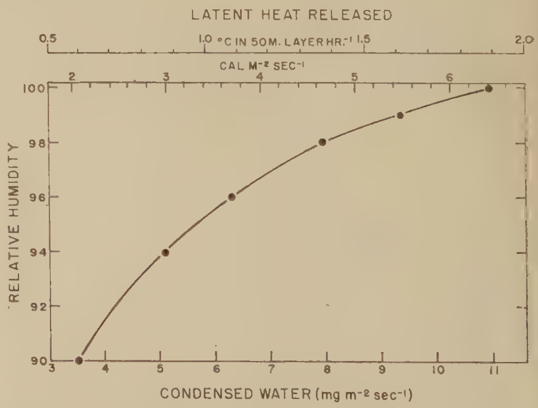

Fig. 8. Condensation and heating in moist layer of air of 50 m depth, during initial 100 seconds after entry into layer of salt particles falling from dry air. (See text for more information.)

TABLE 5

Amounts of water condensed on salt particles 100 seconds after they fall into saturated air from dry air (RH < 74 %).

Sea-salt particle weight 10^{-12} g	Total amounts of salt falling μ gms m^{-2} sec^{-1}	Particle radius after 100 seconds μ	Particle fall rates after 100 seconds cm sec^{-1}	Amount of water falling after 100 seconds μ gms m^{-2} sec^{-1}
50	2.7	12.5	2.1	440
600	7.3	21.5	6.0	492
1,750	11.4	26.5	9.0	491
3,200	14.7	30.0	11.5	503
4,800	17.4	33.0	13.5	526
7,100	20.5	36.0	15.8	542
9,900	23.2	38.5	17.8	539
13,100	26.5	41.0	20.0	569
16,700	29.2	42.5	21.3	539
21,800	31.5	45.0	23.8	517
28,000	35.4	47.0	25.5	521
36,000	39.5	50	28.7	541
44,000	44.2	52	31.0	559
54,000	47.9	55	33.7	572
68,000	53.0	58	36.4	585
88,000	58.5	61	39.0	579
114,000	68.8	64	42.0	596
152,000	74.5	69	47.0	592
223,000	87.4	75	53.5	598
410,000	117.3	86	64.0	641
	811			10,942

layer, evaporation will occur, the dry layer will be cooled and water vapor added. Thus the passage of salt-bearing particles down through the atmosphere will act to warm and dry the moist layers and to cool and moisten the dry layers. The heat released and the water transported by this process is estimated as follows.

The particles represented by column 4, Table 4, upon falling from dry air into saturated air, will cause condensation of about 11 mg of water m^{-2} sec^{-1} during the first one hundred seconds of their fall through the moist air. This quantity was derived as shown in Table 5, using the information given in Figure 5. Other quantities were obtained in this manner for unsaturated air layers. The results are given in Figure 8.

Since the condensation in the first one hundred seconds will occur in an air layer of about 50 meters of vertical thickness, or less (see fall rates, Table 5), we can estimate the average heating of this layer. Using equation (3), it is found that the condensation rates given on the lower scale of Figure 8 will heat 50 kg of air by the amounts given on the upper scale. This range of rates of release of latent heat is equivalent to the wet-adiabatic lifting of the lower air at 3 to 10 cm sec^{-1}.

Thus fall-out of undiluted aerosols can produce greater amounts of local heating than those estimated for the sub-cloud layer as a whole (Table 3). It is suggested that this heating may be an important factor in the production of instability, especially in those cases where moist parcels of air are trapped by overlying layers of stable air.

Thus a significant transport of water and release of heat can occur at relative humidities of 100 per cent and less as sea-salt aerosols fall through layers of air of different relative humidities. Of course the actual amount of water condensed would be somewhat less, due to the slow lowering of the relative humidity of a moist layer, of specific vertical extent, as water is removed and latent heat released. It is supposed that such lowering of the relative humidity is, in many cases, reduced or prevented by ascent due to the heating of the air.

It may be useful to point out a further effect of the fall-out of salt particles through the moist air of the cloud layer. Their tendency to establish vapor pressure equilibrium at each level should act to equalize the relative water vapor distribution. A trend towards constancy of relative humidity would result from the fact that in air over sea-salt solutions of constant salinity, the relative humidity changes very little with temperature. Note on Figure 2 for instance, that the relative humidity over a sea-salt solution, which is 80 ‰ chloride, is 91.3 % at ten degrees and 90.4 % at twenty-five degrees. Particles falling through air layers of differing relative humidity will add water to the relatively dry levels and subtract water from the relatively moist levels. The trend will always be towards a more constant droplet salinity and hence a more constant relative humidity. To what extent this effect is traceable in the trade-wind or tropical-storm atmosphere is as yet unknown.

7. Accuracy of measurement of salt particles

The isopiestic method (Glasstone, 1940) for measuring the weights of salts in solution in small droplets is considered sufficiently accurate as applied to the problems discussed here. Figure 9 shows several test comparisons of weights of chloride measured by titration, using a microburette to measure the silver nitrate solution, and by the isopiestic method (Woodcock, 1950) (Woodcock, Gifford, 1949). The error of the titration was less than plus or minus 10 per cent. Twomey (1954) has recently demonstrated the close correspondence of the individual salt particle sizes determined isopiestically and by the chemically sensitized film method of Seely (1952). It should be noted that experimental application of the isopiestic method above a relative humidity of about 90 per cent apparently introduces an error which becomes increasingly significant as 100 per cent is approached (Crozier, 1954).

8. Discussion

In evaluating and expanding upon the foregoing explanation for the relatively constant temperature of the surface air in hurricanes, consideration of the following questions seems useful at this time.

a) Will the fall speed of the salt particles in the inter-cloud air be sufficient to bring them down to the sub-cloud air before they are carried out of the storm area by radial winds?

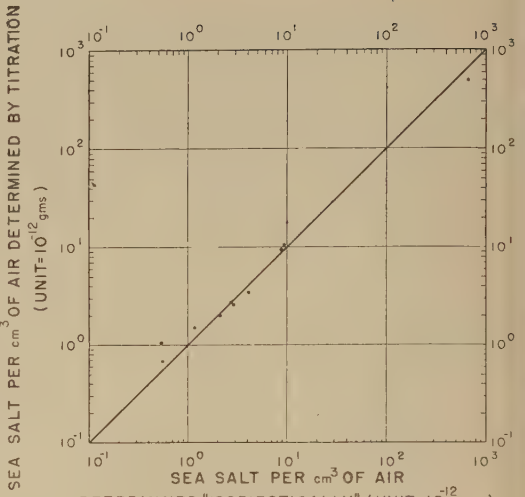

Fig. 9. The quantities of airborne salt collected by impingement on one mm wide strips and measured directly by precipitation with silver nitrate and indirectly by the equal pressure method.

The data on Table 1 show that the particles which contribute most to the salt fall-out, descend as crystalline nuclei (RH < 74 %) at rates of several hundreds to one thousand meters per hour. They will soon fall back from the inter-cloud to the sub-cloud layers, if they are not carried up into the regions of rapid out-flow at high levels. This conclusion is based upon Riehl's evidence (1954, p. 303) that the radial wind speeds at intermediate altitudes are low, and vacillate between inflow and outflow. At the upper levels high outflow rates will probably carry the particles far out from their areas of origin. The question of the role of the fall-out of these dispersed particles in the release of heat in moist peripheral regions of storms, such as those in the lower atmosphere in advance of Edna and Ione (Kessler, 1957), will be investigated in a later study.

b) Are observed rates of radial inflow of surface air adequate to replace the ascending air required to transport the salt up in clouds?

In section 2 of this paper it was simply assumed that cumulus clouds in a hurricane carry aloft sufficient surface air and aerosols to maintain a certain average or "steady state" salt fall through the inter-cloud area. This assumption seems questionable however, if it is supposed that there is no interchange of air between the cloud and sub-cloud layers, and that each mass of rising air in the clouds is replaced by an equal mass of converging sub-cloud air. This question is elaborated in the following discussion.

Converging sub-cloud air in tropical storms is thought to equal in mass the air which ascends in the cumuli and which eventually flows radially outwards at higher levels (RIEHL, 1954). Observations of radially converging lower air, which might be compared to the above estimates of the amounts of ascending air needed to carry the load of salt aerosols, are not available for individual storms. However, in Hughes' study (HUGHES, 1952) of the pattern of low level winds (at about 1,000 feet) in Pacific tropical cyclones, averaged radial inflow was derived for 28 storms. From this inflow averaged ascent over the whole storm area of from 1 to 12 cm sec^{-1} is derived, the greater and more rapid part of the ascent being in or near the central "rain area". In the present study of the role of salt particles in the release of latent heat, the best estimates of the range of rates of ascent of air required to carry a sufficient salt load lie between 10 and 100 cm sec^{-1}. This range of rates is computed, assuming that the salt load of the sub-cloud air varies from the average of my own measurements to a maximum which is about equal to the highest values reported in the literature (about 10 mg m^{-3}, RAU, 1956). Thus an overlap of the range of rates of ascent derived from Hughes' measurements, and the range of rates of ascent required to carry the salt load occurs, but a wide disparity in average magnitude exists.

It appears improbable from the above estimates that the radial inflow of the lower air is sufficient to carry the salt load required in the present study. A mass of ascending air several times that of the recorded average inflowing air is required. The question remains open however, for recent evidence indicates that the earlier observations of radial inflow are too low, and also that a considerable interchange of air between the cloud and sub-cloud layers occurs which is part of the normal growth mechanism of trade-wind cumulus clouds (MALKUS). This latter evidence shows that a part of the air ascending in cumuli can be regarded as "cyclic air", and that it is incorrect to assume that the amount of radially converging air necessarily equals the amount ascending in the cumuli.

c) Is it necessary to regard the amounts of salt observed in one hurricane as an upper limit of quantities to be expected in these storms? This problem is especially pertinent here, since the present study reveals somewhat marginal heating effects from salt amounts taken from available data.

The experience of sampling atmospheric salt particles under a wide range of conditions has convinced the author that the amount of salt represented by curve 12 of Figure 3 should not be considered an upper limiting quantity. The hurricane-aerosol data used here, which are the only available data, were obtained at a time when most of the storm was over land. The sampling position was the top of Hillsboro Lighthouse, on the Florida east coast, at Pompano. At the time of sampling, September 22, 1948, 2330, E.S.T. (WOODCOCK, 1950), the storm center or "eye" was over inland Florida, and the air from which the samples were taken had only recently passed from over land about 30 miles south of the station (see surface winds, Miami to Key West, N.W.R.C., Ashville, N.C.). Since the salt aerosol load of the air is a function of the fetch over the sea, as well as of wind force (WOODCOCK, 1954), this recent passage of the air from over land would result in a relatively low salt content when compared to this content if the entire cyclone had been over the sea. The author has little doubt that the salt load of the lower air in severe wind storms at sea commonly exceeds the amounts given here by a factor of ten or more. Such amounts would of course result in proportional increases in the heating of the sub-cloud air in the model proposed. However, the above hurricane sample serves the purpose here, which is to demonstrate that observed quantities of salt nuclei, upon ascent in clouds, will alter the distribution of water vapor and temperature as they fall back towards the sea. The magnitudes of these effects are certainly large enough to satisfy a first-approximation study.

It is perhaps not a coincidence that the weights of salt required to bring about the release of latent heat discussed here, add little to the air density. The maximum quantity of airborne sea salt considered (i.e. about 10 mg m^{-3}) will produce a density increase, at ordinary surface pressures, about equal to the increase caused by a temperature decrease of 0.01 C in the usual air temperature range.

9. Conclusions and Recommendations

A mature hurricane at sea is a gigantic salt-aerosol generating and distributing mechanism. Fall-out from the aerosols carried aloft in the storm clouds, may liberate significant amounts of latent heat in the moist lower layers of the atmosphere. Thus the vast self-generated salt cloud in the atmosphere of these storms should be seriously considered as one of the properties influencing their stability. In the model proposed a moist lower layer and a relatively dry inter-cloud layer of air is required.

It is recommended that many measurements of the size distribution of sea-salt particles be made in the relatively clear air in various parts of tropical (and extra-tropical) marine cyclones. If these measurements reveal a salt fall-out of several milligrams per square meter per second into the air converging upon a storm center, the effects of this salt in adding to the internal temperature gradient become apparent. Riehl shows for instance (Riehl, 1954, p. 313—316) that the isothermal expansion of the converging sub-cloud air, results in temperature excesses of several degrees as this air ascends in the "rain area" of hurricanes.

Acknowledgments

The author is especially grateful for the critical efforts of Dr. Arnold Arons, which resulted in a clarifying and unifying revision of the original form of this paper. He is also indebted to his associate, Mr. D. C. Blanchard and to Mr. W. V. Kielhorn for helpful suggestions.

REFERENCES

Arons, A. B., and Kientzler, C. F., 1954: Vapor pressure of sea-salt solutions. Trans. Amer. Geophys. Union, **35**, 722—728.

Blanchard, D. C., 1953: Raindrop size-distribution in Hawaiian rains. Jour. Met., **10**, 457—473.

Blanchard, D. C., and Woodcock, A. H., 1957: Bubble formation and modification in the sea and its meteorological significance. Tellus, **9**, 145—158.

Bunker, A. J., Haurwitz, B., Malkus, J. S., and Stommel. 1949: Vertical distribution of temperature and humidity over the Caribbean Sea. Pap. Phys. Oceanogr. and Meteor., **XI**, No. 1, pp. 1—82.

Byers, H. R., 1944: General Mereorology, McGraw-Hill, New York.

Crozier, W. D., 1954: Errors in the "isopiestic" method for measuring masses of salt particles. Science, **120**, 840—841.

Glasstone, Samuel, 1940: Text-book of physical chemistry. D. Van Nostrand Co., Inc., New York, 1289 pp.

Gunn, R., and Kinzer, G, D., 1949: The terminal velocity of fall of water droplets in stagnant air. J. Meteor., **6**, 243—248.

Harrison, J. B., and Williams, John, 1897: The proportions of chlorine and nitrogen as nitric acid and as ammonia in certain tropical rainwaters. J. Amer. Chem. Soc., **19**, 1—9.

Hughes, L. A., 1952: On the low-level wind structure of tropical storms. Jour. Meteor., **9**, 422—428.

Jordan, C. L., 1952: On the low-level structure of the typhoon eye. Jour. Meteor., **9**, 285—290.

Kessler, Edwin III, 1957: Outer precipitation bands of hurricanes Edna and Ione. Bull. Amer. Met. Soc., **38**, 335—346.

Kientzler, C. F., et al., 1954: Photographic investigations of the projection of droplets by bubbles bursting at a water surface. Tellus, **6**, 1—7.

Kieth, C. H., and Arons, A. B., 1954: The growth of sea-salt particles by condensation of atmospheric water vapor. J. Meteor., **11**, 173—184.

Langmuir, I., and, Blodgett, K. B., 1945: A mathematical investigation of water droplet trajectories. Gen. Elec. Res. Lab. Rep., A.T.S.C. contract W-38-038-Ac-9131, 1—47.

Lodge, J. P., 1955: A study of sea-salt particles over Puerto Rico. J. Meteor., **12**, 493—499.

Malkus, Joanne Starr, 1956: On the maintenance of the Trade-Winds. Tellus, **8**, 335—350.

— Personal communication.

May, K. R., 1945: The Cascade Impactor: An instrument for sampling coarse aerosols. Jour. Sci. Inst., **22**, 187—195.

Miyake, Y., and Suguira, Y., 1950: The mechanism of the dissolution of the atmospheric chlorides into rain water. Pap. Meteor. Geophys., **I**, 222—226.

Miyake, Y., and Suguira, Y., 1954: Chemical studies of rain water accompanied by a typhoon. Geophys. Mag. Tokyo, **26**, 29—34.

Rau, Walter, 1956: Bestimmung der Grösse und Häufigkeit der chloridteilchen im maritimen Aerosol. Meteor. Rund., **9**, 210—214.

Riehl, H., Yeh, T. C., Malkus, J. S., and Laseur, N. E., 1951: The north-east trade of the Pacific Ocean. Q. Jour. Roy. Met. Soc., **LXVII**, 598—626.

Riehl, H., 1951: Aerology of tropical storms, Compendium of Meteorology, 902—913, Amer. Meteor. Soc., Boston, Mass.

— 1954: Tropical Meteorology, McGraw-Hill, New York.

Scorer, R. S., and Ludlam, F. H., 1953: Bubble theory of penetrative convection. Quart. J. Roy. Met. Soc., **79**, 94—103.

Seely, B. K., 1952: Detection of micron and submicron chloride particles. Analyt. Chem., **24**. 576—579.

Simpson, R. H., 1947: A note in the movement and structure of the Florida hurricane of October 1946. Mon. Wea. Rev., **75**, 53—58.

— Personal communication.

Squires, P., and Gillespie, C. A., 1952: A cloud droplet sampler for use on aircraft. Quart. J. Roy. Met. Soc., **78**, 387—393.

Squires, P., and Warner, J., 1957: Some measurements in the orographic cloud of the Island of Hawaii and in trade wind cumuli Tellus, **9**, 475—494.

Tannehill, I. R., 1943: Hurricanes. Princeton University Press, Princeton, New Jersey.

Twomey, S., 1954: The composition of hygroscopic particles in the atmosphere. J. Meteor. **11**, 334—338.

Wexler, Harry, 1947: Structure of hurricanes as determined by radar. Annals N.Y. Acad. Sci., **XLVII**; Art. 8, 821—844.

Woodcock, A. H., 1950: Sea salt in a tropical storm. J. Meteor., **7**, 397—401.

— 1954: Airborne sea salt as a function of altitude and wind force. J. Meteor., **10**, 362—371.

— 1952: Atmospheric salt particles and raindrops. Jour. Meteor., **9**, 200—212.

Woodcock, A. H., and Spencer, A. T., 1957: An airborne flame photometer and its use in the scanning of marine atmospheres for sea salt particles. J. Meteor., **14**, 437—447.

Woodcock, A. H., and Gifford, Mary M., 1949: Sampling atmospheric sea-salt nuclei over the ocean. J. Marine Research, **8**, 177—197.

Woodcock, A. H., and Blanchard, D. C., 1955: Tests of the salt-nuclei hypothesis of rain formation. Tellus, **7**, 437—448.

Woodcock, A. H., 1950 a: Impact deposition of atmospheric sea salts on a test plate. Proc. Am. Soc. Testing Mats., **50**, 1151—1166.

PRINTED IN SWEDEN
ESSELTE, STHLM 58

Contribution No. 923

PERSPECTIVES IN MARINE BIOLOGY

EDITED BY

A. A. BUZZATI-TRAVERSO

THE INADEQUACY OF EXPERIMENT IN MARINE BIOLOGY*

ALFRED C. REDFIELD
Oceanographic Institution
Woods Hole, Massachusetts

A SYMPOSIUM

HELD AT SCRIPPS INSTITUTION OF OCEANOGRAPHY
UNIVERSITY OF CALIFORNIA
MARCH 24–APRIL 2, 1956

1958
UNIVERSITY OF CALIFORNIA PRESS
BERKELEY AND LOS ANGELES

---

*Contribution No. 923 from the Woods Hole Oceanographic Institution.

THE INADEQUACY OF EXPERIMENT IN MARINE BIOLOGY*

ALFRED C. REDFIELD
Oceanographic Institution
Woods Hole, Massachusetts

I do not wish to give the impression that I am opposed to experiment in an absolute sense—as one might be against sin. Rather, I will deal with something analogous to temptation—with the question of how far one should go in an alluring direction in choosing a line of conduct. By inadequate I mean not sufficient for the purpose at hand. I intend to discuss how sufficient the experimental method is for the solution of the problems of marine biology.

We will agree, I think, that the problem must dictate the methods to be employed for its solution, not the reverse, and experiment is merely one of a number of methods for obtaining information. Some subjects, such as atomic physics, grow almost wholly by experiment; others, like astronomy, develop by reasoning about direct observations of natural events. Astronomy leans heavily on physical experiment, however, in deriving the principles by which observation is interpreted.

I believe that in the United States the progress of marine biology was retarded for fifty years by the introduction of experimental methods into biology. The leaders who came to Woods Hole in the last decades of the nineteenth century were excellent naturalists interested in exploring the life in the sea. At the turn of the century, almost to a man, these leaders became preoccupied with more general problems—the mechanistic conception of life, the physiology of morphogenesis, and genetics—for which experimentation promised the answers. It may be that in the long run marine biology will prove to have been benefited by this diversion of interest. For the time being, however, interest in marine biology per se languished.

For example, few objects have been subject to such intense experimental investigation by biologists as the sea-urchin egg. Yet recently, when concern developed for the dwindling supply of this experimental material near Woods Hole, it was discovered that almost nothing was known of the biology of Arbacia between the time when the pluteus died in the finger bowl and when ripe adults were delivered to the laboratory by the collecting crew. Dr. Allee once informed me that the lack of attention being given at Woods Hole to life in the sea led Frank R. Lillie to initiate the establishment of the Oceanographic Institution.

---

*Contribution No. 923 from the Woods Hole Oceanographic Institution.

My argument depends upon a distinction between observation and experiment, a distinction that is not always obvious. When I note that ice is forming on the surface of the sea I make an observation; similarly, when I take the temperature of the water in which the ice is forming or measure its chlorinity by chemical titration. These observations depend, of course, on experimental procedures that have been employed to justify the use of the thermometer and the chloride titration and to calibrate the instruments. If I bring sea water into the laboratory and determine its freezing point under varied conditions of salinity I am making observations under controlled conditions that combine to be an experiment. The results may be used to interpret the observations of nature—but always at the risk that some considerations, such as supercooling, have been overlooked which may invalidate the conclusions. For example, it can be argued from the experimental determination of the freezing point of the blood of fish that these organisms cannot live at temperatures below about -0.6° C. Yet fish live abundantly at temperatures as low as -1.8° C. in the Arctic Ocean. This paradox was only resolved when observation in nature led to an experimental investigation of the conditions under which supercooling may exist both in sea water and in blood (Scholander et al., 1957).

Experiments are essentially observations made under conditions rigged so as to answer particular questions. They may be rigged to give yes or no answers as where one determines whether an organism moves toward or away from some source of stimulation. More generally they attempt to relate behavior quantitatively to one or more variables in the situation, all other variables supposedly being kept under control. In this sense, experiments are always unnatural, and subject to the question: how adequate are the results when applied to the situations in nature? Experiment is an application of the Socratic method to natural events. The experimenter asks the questions; nature is expected to give the answers. The success of the Socratic method depends on the wisdom of Socrates. It presumes a clear concept of the nature of the problem by the questioner. When nature is expected to give the answers it requires the availability of appropriate operational procedures to decipher her reply.

Many years ago Galileo was in a position to ask good questions about the motion of falling bodies which could be answered by available techniques for measuring space and time. The number of teeth in a horse's mouth could be learned by simple observation as soon as counting was invented, but probably was not asked until someone noticed the general uniformities in mammalian morphology. Today physiology and genetics invite inquiry into the very numbering of the hairs of one's head. The question, how many angels can stand on the point of a pin, remains unanswered because of the deplorable lack of fundamental knowledge of angelic physics. Are we in a much better position today to design experiments to explain the fluctuations in marine populations, the migrations of fishes, or the successions of phytoplankton with the seasons?

In the most general way, what science does is to construct models of nature. These may be concrete physical structures that imitate some chosen part of physical reality. More frequently they are mathematical expressions defining the relations of selected variables and constants. Graphs are convenient presentations of restricted parts of these mathematical models, or may merely replicate the relations between large numbers of simple observations—as in maps and charts. Anatomical drawings are models of a limited part of the organic world at some fixed stage in its cycle. Verbal descriptions are less tangible models, subject to the uncertain use of semantics and logic.

The value of these models lies in the fact that they may be duplicated and thus become the common property of all persons interested, in a way direct observations of nature never can. They arrange the phenomena of nature in an orderly way, and are themselves subject to manipulation according to accepted roles, so that many relationships may be deduced from the model itself, which are not immediately obvious from the observation of nature. No model deals with more than a fragment of nature, yet it is inherent in the philosophy of science that each shall be not only consistent internally but shall be consistent with all other models that represent nature correctly. The models interlock and overlap.

The part played by observation, experiment, and inference in the construction of models of nature may be clarified by a consideration of how a physical model is developed—say a hydraulic model of tidal behavior in an estuary. One must start from an adequate number of observations to define the problem—in this instance with a chart of the basin and information on the tides in the off-lying sea. From the chart data a small-scale model of the basin is constructed; the tide is reproduced by a mechanical device operating on the part of the model replicating the off-lying sea. The correctness of the behavior of the model must then be verified by comparison with observations on the tides and currents at selected points within the basin. If the verification is satisfactory it may be inferred that the model represents correctly the motions of the water at other points within the basin. The model can then be employed to examine many questions, such as the water levels that might result from unusual perturbations of sea level as the result of storms, the accumulation of pollutants, or the distribution of the pelagic larvae of marine organisms spawned at some spot.

More often than not the behavior of the model will not be verified satisfactorily at the first trial because certain factors have been left out of account, deliberately or by inadvertence. In scaling down the model, surface forces become exaggerated in relative importance. This may be overcome by reducing the vertical scale less than the horizontal. The time scale of the tidal rhythm must also be reduced as the model becomes smaller.

The sophisticated model-builder can infer the correct scaling factors for time, depth, and extent from the mathematical models provided by hydrodynamics, which in turn arose from observation, experiment, and inference. At present he cannot deal theoretically with the resistance caused by the roughness of the bottom. This difficulty must be met empirically by roughening the bottom of the model in one way or another until by trial and error the verification of the model is satisfactory.

In another type of hydraulic model roughness is dealt with by experiment. In towing-tank experiments designed to determine the power required to drive ships, the wave-making resistance of a given hull form may be correctly estimated from the forces required to tow a model ship at various speeds. A substantial part of the total resistance is due, however, to the friction of the ship's bottom in moving through the water. This factor cannot be deduced in a satisfactory way from the behavior of the model. Instead direct resort is made to experiment by towing steel plates, coated to duplicate the actual roughness of the ship's bottom, at varied speeds in a towing tank. From the experimental results the frictional resistance of the ship is computed and added to the wave-making resistance estimated from the towed model to give the final value for the required power. Verification is made by the actual performance of the ship at sea.

In a general sense the whole procedure employed in making these models is experimental—the question being to see how closely the construction based on selected considerations will duplicate the phenomena of nature. In the more restricted sense in which I use the term—that experiment is a systematic set of observations designed to relate the behavior of certain variables in the situation as a whole—experiment is only a part of the whole procedure. Substantial information must be available about the natural prototype before the construction of a model can be attempted. Direct resort to observation of natural phenomena must be taken again to verify whether the results of experiment and reasoning built into the model do indeed reproduce these phenomena correctly.

The limitation of the experimental method as an aid in developing effective models of nature arises from the uncertainty that the experimental results on selected variables can be applied correctly to interpreting the situation as a whole. In this point, Dr. Warren Weaver made some pertinent remarks in his recent presidential address to the American Association for the Advancement of Science (Weaver, 1955):

> What made possible the great success that the physical sciences have experienced, particularly during the last century and a half? The explanation appears to be rather simple. Physical nature first of all, seems to be on the whole very loosely coupled. That is to say excellently workable approximations result from studying physical nature bit by bit, two or three variables at a time, and treating these bits as isolated. Furthermore, a large number of the broadly applicable laws are, to useful approximation, linear, if not directly in the relevant variables, then in nothing worse than their second time derivatives. And finally, a large fraction of physical phenomena (meteorology is sometimes an important exception) exhibit stability: perturbations tend to fade out, and the great consequences do not result from very small causes.
>
> These three extremely convenient characteristics of physical nature bring it about that vast ranges of phenomena can be satisfactorily handled by linear algebraic or differential equations, often involving only one or two dependent variables; they also make the handling safe in the sense that small errors are unlikely to propagate, go wild, and prove disastrous. Animate nature, on the other hand, presents highly complex and highly coupled systems—these are, in fact, dominant characteristics of what we call organisms. It takes a lot of variables to describe a man, or for that matter a virus; and you cannot often usefully study these variables two at a time.

> Animate nature also exhibits very confusing instabilities, as students of history, the stock market, or genetics are well aware.

Certain experimental physiologists of the past generation were acutely aware of the difficulties that the highly coupled character of biological systems introduced into their mechanistic analyses. The problem was discussed by Jacques Loeb (1916) in The Organism as a Whole. In the preface to his book on respiration, J. S. Haldane (1922) wrote:

> About the middle of the last century the younger physiologists . . . set about the investigate living organisms piece by piece, precisely as they would investigate the working of a complex mechanism. This method seemed to them to promise success, and was popularized by such masters of clear and forceful expression as Huxley. It is still the orthodox method of physiology, but the old confidence in it has steadily diminished in proportion as exact experimental investigation has shown that the various activities of a living organism cannot be interpreted in isolation from one another, since organic regulation dominates them. The keynote of this book is the organic regulation of breathing and its associated phenomena.
>
> * * * *
>
> I hope that the book may contribute toward establishing human physiology in its rightful place, which has been usurped too long by experiments on fragments of frogs and other animals, or on the mere superficial physical and chemical aspects of bodily activity.
>
> * * * *
>
> The leaders of the mechanistic movement of last century got rid of vitalism, but in doing so got rid of life itself. The bondage of biology to the physical sciences has lasted more than half a century. It is now time for biology to take her rightful place as an exact independent science; to speak her own language and not that of other sciences.

I do not follow Haldane in his antagonism to the mechanistic approach to biological problems, and he clearly had no reservations regarding the effectiveness of the experimental method as such. His revolt was essentially against the limitations inherent in experiment when applied in isolation to a fragment of a highly coupled system, as a means of discovering the properties of the organism as a whole.

We may now ask what we mean by marine biology, and in what sense it is entitled to "a rightful place" as an "independent science" with a language of its own.

The justification, as I see it, is that a rich and varied fauna and flora are found in an unique environment, and that the properties of this environment have impressed special characteristics on its inhabitants and their behavior. That the sea is extensive, continuous, and relatively uniform and its inhabitants appear to have played a significant part in the origin and evolution of life merely adds to the importance of marine biology when considered as an independent discipline. Independent is not quite the right word, because there are many overlapping relations, both in phenomena and conception, between life in the sea and elsewhere. More precisely it is convenient to consider marine biology as a separate discipline within the realm of science.

From this viewpoint marine biology is primarily ecological; its objective is to develop effective models, and ultimately a single consistent model, of life in the sea. It aims to understand a unique ecological system that exists in an environment having special properties. Its materials are the interrelations of organism to environment, and organism to organism. It is concerned with the position of the organism as a whole in populations as a whole and in the environment as a whole. Its task is synthetic even more than analytic. For its purposes it needs to know how organisms behave and what they require. It can afford, at least for the time being, to leave the analysis of the internal mechanisms, which permit them to behave as they do, to those who are building models of the more general properties of living matter.

The construction of an effective model requires a substantial knowledge of the prototype. The first task of marine biology was to discover and describe what manner of plants and animals exist in the sea. The result has been to reveal the most varied array of animal forms to be found on earth. So far as the larger forms are concerned, this search seems to have reached the point of diminishing returns. New species may still be had for a dime a dozen, but it is rare that a new discovery alters our general conceptions greatly. The chief problem here is one of conservation rather than development. The line of advance in taxonomic knowledge is held by a perilously thin force of specialists. The grim reaper could easily deprive us of the ability to know what organisms we are talking about. The state of affairs is quite different so far as microörganisms are concerned. Marine bacteriology is only in its beginning, whereas the nannoplankton still resist investigation.

If we can take some satisfaction in our acquaintance with the kinds of the larger animals and plants to be found in the sea, what can be said of our knowledge of their life histories and behavior? I have already mentioned the lamentable ignorance that exists concerning the common sea urchin at Woods Hole. Except for a few commercially important species and a scattering of text-book examples among the others, almost no precise information exists on the details of the life of marine organisms. We do not even know how to sample certain populations effectively. A tremendous range of phenomena still awaits simple observation. The comparative physiologist is a valued ally of the marine biologist in this quarter, particularly in determining the relations between the organism and the environment. His contribution will, of course, lean heavily on the experimental procedure.

The most general problem of marine biology is to understand the distribution and abundance of life in the sea. The approach to this problem must be primarily statistical through the development of significant relationships between large quantities of observations on biological and physical events, occurring often in widely scattered places. Classical examples of investigations of this sort are Johannes Schmidt's studies on the natural history of the eel and Hjort's work on the year classes of the herring, both strictly statistical. The present-day problem of productivity is another case in point. This problem depends in its conception on general ideas concerning the nature of the photosynthetic process, gained through experiments made originally on land plants. The primary observations are the determination of rates of carbon assimilation made by procedures that are experimental only in the same sense that the measurement of temperature with a thermometer is experimental. The solution of the problem will follow only when large numbers of such observations are related statistically to other information, such as the light intensity, the motion of water, and its chemical content, over widely distributed areas of the sea.

The nature of marine biology is such that, like other sciences, it can profit from the experimental approach, both in defining its problems and in elaborating the details of its solutions. However, the greater need at the moment is more knowledge of the phenomena to be explained. If this need is to be met, greater encouragement should be given to young men motivated by the curiosity of the naturalist. The instincts, interests, and capabilities of such men are frequently quite different from those who excel in the so-called exact sciences. The future naturalists, however, require a different and better education than they have frequently enjoyed in the past. They need enough acquaintance with the exact sciences to toughen their wits, and to overcome the inferiority they frequently feel in the face of those who can juggle the equations. Equally, they need better acquaintance with the whole gamut of the earth sciences, because life in the sea cannot be understood without understanding the sea itself and what makes it what it is.

It is the ability to provide this sort of training, and to conduct the work for which training is offered, that gives the Scripps Institution of Oceanography and other similar institutions an unique opportunity to advance the discipline of marine biology.

REFERENCES

Haldane, J. S.
1922. Respiration. New Haven, Conn., Yale Univ. Press, 427 pp.
Loeb, J.
1916. The organism as a whole. New York, Putnam, 379 pp.
Scholander, P. F., L. van Dam, J. W. Kanwisher, H. T. Hammel, and M. S. Gordon
1957. Supercooling and osmoregulation in arctic fish. J. Cellular and Comparative Physiology. 49:5-24.
Weaver, W.
1955. Science and people. Science. 122:1255-1259.

DISCUSSION

D. I. Arnon

I cannot believe that there is serious disagreement today among biologists about the necessity of both the experimental laboratory approach and the "naturalist" approach in understanding nature. In evaluating the contributions and the excesses of the laboratory method in biology, we must keep in mind that there is a "physiology" and a "pathology" of the experimental method. It would be unwise to invoke examples of the pathology of the experimental method in discussing its immense contribution to biology.

I can think of no more striking example to illustrate the inadequacy of the observational approach, unaided by laboratory experiment, in understanding nature, than in the matter of photosynthesis. The most brilliant observer cannot deduce from observing green plants in nature that there are busy chemical laboratories transforming light into chemical energy. The best that Aristotle could deduce from observing green leaves on a warm day is that they provide shade for the slender parts of the plant against the full force of the sun. It was not until the green plant was taken to the laboratory and placed under artificial conditions that the key chemical reaction of the universe, on which all life on this planet depends, was discovered.

There is one other point I would like to stress. Marine biology, like agriculture, depends on application of fundamental concepts of biology to a special environment. If marine biology is not to become only an applied science it is essential that it not only draw on the accumulated "capital" of fundamental knowledge in biology, amassed by experimental techniques in other areas, but it also contribute its share of basic research to biology. Only by conscious planning and encouragement can fundamental research acquire and maintain its share of support in an institution that, like a marine station, a medical school, or an agricultural experiment station, can always be expected to have a number of immediately relevant, practical, or clinical problems to explore. With reference to medical schools and agricultural stations, it is interesting to note that the greatest progress in clinical and field applications has been made by those institutions that maintained the most generous program of basic experimental research. I believe that this lesson is not without significance for those who are responsible for guiding the growth of marine stations.

A. C. Hardy

First I must say how much in sympathy I am with Dr. Redfield's outlook; I wholeheartedly agree with him on the importance of observations in the field. Since, however, he has spoken of the inadequacy of experiment I feel a word or two should be said about the inadequacy of observation. Nearly all our observations have to be indirect ones employing various capturing devices and instruments working in a world we cannot see. The validity of our methods of observation must first be tested by experiment before they are put into use; yet this is rarely done. So often it is formed after a long and expensive survey of the distribution of plankton or young fish, that the data so collected are almost useless because the animals being surveyed display a marked patchiness, a vertical migration, or an avoidance of surface nets in the daytime. The use of nets in the sea is really an experiment, an experiment to see if the net, by being used in a certain way, and at certain intervals of time and space, can fix an adequate series of samples which will represent the actual distribution of the animals concerned in nature. The adequacy of such experiments, and the observations they produce, must be tested by controls. Only when the control experiments of repeated sampling fix consistent results can we be satisfied that our observations are adequate.

A. D. Hasler

Limnology and oceanography on this continent find common ground in the American Society of Limnology and Oceanography. However, there is too little common ground for extended contact and mutual approach to similar problems. I propose, therefore, a compromise between the two notions debated here. In the northern part of the midwest of North America are many thousands of small lakes where it is possible to conduct small-scale oceanographic experiments or large-scale limnological experiments—a hydrobiological laboratory. I propose that natural research areas be set aside where small lakes are available for experiments. We have made a small approach to experimental lake ecology. A natural constriction in a lake (hourglass shape) enabled us to construct an experimental and control unit by bulldozing a barrier across the constriction. This lake was acid, low in calcium, and the water brown in color. To the lake on one side of the barrier was added $CA(OH)_2$; the other lake was untreated. Here an experimental situation was made available for study of biological, chemical, and physical processes where one factor was experimentally altered. If such areas were accessible to aquatic ecologists many marine biological experiments could be conducted in the field. At the moment this extension of laboratory procedure seems farfetched. If it has merit, however, procedures should be set in motion now for forming natural lake areas for future experimental use.

A. A. Buzzati-Traverso

Unfortunately I cannot subscribe to the statements of Dr. Redfield concerning the inadequacy of experiment in marine biology. I do not believe that the progress of marine biology was retarded for fifteen years by the introduction of experimental methods in biology. What happened was that many leading biologists working at Woods Hole were interested in some fundamental aspects of life activity that could be studied on marine forms. They were not interested in problems of marine biology or in the life of marine organisms per se. If marine biologists, that is, those biologists whose primary interests are the ones just outlined, had devoted more attention to experimental procedures I am sure that by now we would have a better understanding of life in the ocean. In the history of biology there has been a case that, I believe, can be cited as parallel to the one under discussion. After the publication of Charles Darwin's work on the origin of species there was a large number of papers that appeared on the paleontology and the comparative morphology of plants and animals. This was, and is, a very important contribution, which established evolution as a fact rather than as a theory. Later, however, the interest in evolutionary studies languished because further additions along these lines did not change basically our views on the matter. It was only when the experimental approach was introduced to evolutionary studies, thanks to the development of genetics, that this area became again very productive and is today one of the most flourishing in the field of biology. It is my belief that a similar series of events has taken place in marine biology. For many decades a lot of very important observational data have been collected on the distribution of marine forms; taxonomic and zoögeographical studies of great significance thus became available. Although there certainly still are very many gaps to be filled in at present, due to the vastness of the ocean, it is necessary to concentrate now at the experimental level in the laboratory, if we wish to understand the relationships between these organisms and between the organisms and their environment. Only when we have acquired sufficient knowledge about the nutrition, the physiology, and the genetics of several marine forms, will we be ready to return to the field with a different outlook, certainly much more productive than the current one. It is a problem of strategy of research. Obviously, we are interested in explaining nature, but for this aim we have to alternate the observation of natural phenomena with the analysis of experiments that we can devise. At one time one method is more profitable than the other, and at another time the positions are reversed. It is my belief that at this time, in 1956, the experimental approach is needed more than the observational one in marine biology.

A. C. Redfield

This discussion reminds me of a time when I was looking into the scattering of light by fluids and was disturbed to find how little experimental evidence was presented for the theoretical discussions. It was explained to me that this was to be expected since the theoretical physicist looks down his nose at the experimentalist as his "yes man"—and vice versa. I hope this state of affairs will not develop in marine biology.

In building a house the services of an architect, carpenter, mason, electrician, and plumber are all required. Would it not be presumptuous if the plumber were to claim that his contribution was the most fundamental, even though it has recently added more to the convenience of modern living than the others, and has become a source of national pride? The architect, who sees the matter as a whole, will tell you that the first step is to find out what the owner wants—to define the problem.

Marine biology can develop fully only if it employs all means of discovery at its disposal: observation, comparison, correlation, and experiment. It will develop soundly only if it is led by men whose primary interest is in what goes on in the sea, men who have an insight into what procedures can most profitably be employed in solving the problems nature presents.

Contribution No. 928

Reprinted from LIMNOLOGY AND OCEANOGRAPHY
Vol. 3, No. 1, January, 1958
Printed in U.S.A

The Rate of Development of *Balanus balanoides* (L.) Larvae[1]

H. BARNES AND MARGARET BARNES

The Marine Station, Millport, Scotland, and the Woods Hole Oceanographic Institution

ABSTRACT

Experiments are described on the rate of transition of State I to State II *B. balanoides* larvae at a series of temperatures. A value of 2.2 was found for Q_{10} between 1° and 18° C. The data regarding the length of the planktonic phase over the area of distribution are reviewed and new data also given. There is little indication of a high correlation with temperature. The discrepancy may be accounted for by acclimation, but it is suggested that the quality and quantity of food should be considered as interacting with and perhaps compensating for the effect of temperature.

Balanus balanoides (L.) is widely distributed over the arctic-boreal regions; the conditions of its environment, therefore, differ widely, and information regarding rate processes at any stage of the life cycle is clearly of importance in any interpretation of the ecology of the species. Plankton collections at a number of places have given some information regarding the rate of development of the free living larval stages, but there is no recorded experimental work. While such work on the late larval stages involves all the difficulties associated with the culture and maintenance of marine planktonic organisms, the Stage I to Stage II transition may be easily studied. Ripe embryos, teased out from the egg lamellae present in the mantle cavity of the adult readily hatch into Stage I nauplii and soon pass into Stage II nauplii.

MATERIAL AND METHODS

A number of lamellae of the same apparent degree of ripeness were teased out into sea water contained in a petri dish; the liberated Stage I nauplii accumulate on the lighter side of the dish and may be easily pipetted off. Since the rate of transition from Stage I to II changes during the season (under constant experimental conditions) presumably according to the ripeness of the lamellae, all the following experiments were run on a single batch of nauplii after the techniques had been tested in a series of preliminary experiments.

Small samples of active nauplii were pipetted into large test tubes containing 5 ml sea water, brought to and subsequently maintained at constant temperature in water baths; experiments were run at 1.0, 5.5, 6.1, and 18.5°C. Some 40–50 such tubes were set up at each temperature. All the tubes were held in the multiple arms of a single mechanical shaker and gently agitated throughout the experiments, since the preliminary experiments had shown that without gentle shaking the rate of transition is reduced and the results are very erratic. This may be due to the fact that without agitation the nauplii were often crowded together and tended to be less active in the relatively small volume of water used. Whether the lower rate of transition in the absence of gentle agitation is the result of less activity *per se* or whether it is perhaps due to the greater ease of ecdysis among actively swimming animals is unknown. From time to time formalin in the usual strength was added to three replicate tubes at each temperature, the appropriate intervals being selected on the basis of earlier experiments. The number of Stage I and Stage II nauplii were subsequently counted under a low power binocular microscope. From the results the mean percentage of larvae that had moulted to Stage II at any time (corrected for viability by expressing as percentage of ultimate numbers of Stage II) was plotted against the time, and from the smoothed curves the rate of transition, that is, time of half change, was calculated.

---

[1] Contribution No. 928 from the Woods Hole Oceanographic Institution. One of us (H. B.) wishes to acknowledge the receipt of a Research Fellowship from the Institution and leave of absence granted by the Council of the Scottish Marine Biological Association. We wish to thank Dr. B. H. Ketchum for his advice, Mr. H. Turner, Jr., for facilities during the experiments, and Mr. D. Bumpus for information regarding temperatures.

RESULTS

These are shown in Figure 1 in which the reciprocal of the time of half change (relative rate of transition) is plotted on a logarithmic scale against temperature. The two are linearly related over the whole range with a Q_{10} of about 2.2. Such a value might have been anticipated for an arctic-boreal species at the range of temperatures of the normal habitat, namely 0–8°C for the planktonic phase (see Scholander *et al.* 1953). However, it is a little surprising that no falling off in the value of Q_{10} is apparent at the higher temperatures—higher than those at which the larvae are normally found but not higher than those to which the adult is subjected in the southern parts of its distribution. This may indicate that the larvae are completely viable up to 18°C and that up to this limit temperature effects on the larval stage do not limit the distribution of the species. However, the Stage I to II transition takes place rapidly; the later stages which take much longer in development may not be viable at the higher temperatures.

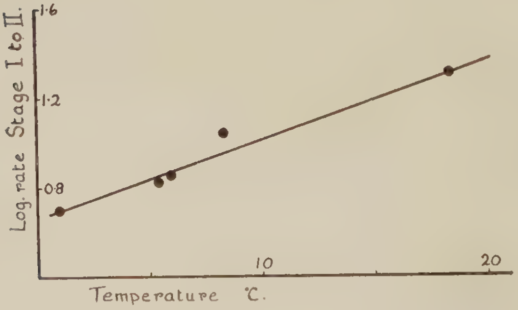

FIG. 1. The effect of temperature on the Stage I to II transition. Animals were kept in filtered sea water and gently agitated.

COMPARISON WITH PLANKTONIC DATA

The results may be compared with what is known of the length of planktonic life under natural conditions. When sampling problems are taken into account, even with collections taken at short intervals, it is difficult to estimate with any accuracy the length of individual stages—usually a matter of only a few days. We may consider the planktonic life up to the cypris; the cypris stage may be variable and estimates based on the settlement dates are even more crude.

There is satisfactory data from the Firth of Clyde (Scotland). Pyefinch (1948) making hauls every three days during the spring months estimated the time for development up to the cypris stage was 32 days in 1944 and 30 days in 1947. We have confirmed these results taking daily hauls with the Hardy plankton indicator; the estimates are the same whether first appearances or peak values are used. The mean sea-surface temperature for this region during the month of March when the larval population is developing is about 7°C (Barnes 1955). Although there is a considerable amount of data on the general biology of *B. balanoides* both round the coast of Britain and Northern France, there are no further reports on plankton collections which allow satisfactory estimates of the larval life to be made.

Again, although there is much literature on the plankton of the Norwegian coast, little attention has so far been paid to the cirripede larvae. However, through the courtesy of Dr. F. K. Wiborg, we have been able to examine plankton hauls taken in the Lofoten area. For the present purpose the hauls were taken too infrequently, but the best estimate using the results from all the stations is some 27–30 days at a temperature of 3–4°C. Runnström (1924–25) while stressing that there may be some variability from year to year gives a plankton life of 30 days for the waters near Bergen at a temperature of 4°C. He also states that in Liverpool Harbour nauplii appeared on February 22 and cyprids on April 6, a period of 43 days.

TABLE 1. *Rate of development of planktonic phase of* B. balanoides

Place	Days	Sea surface temperature °C
Ungava Bay (Canada)	48	1
Halifax Harbour (Canada)	40	1–2
Woods Hole (U. S. A.)	21	6.6
Newport (Rhode Is., U. S. A.)	33	1.0
Millport (Scotland)	32	7.0
Bergen (Norway)	30	4.3
Lofoten (Norway)	27–30	3.0

Bousfield (1952–53) has given much information on *B. balanoides* around the Canadian coast, but the plankton data cover only Halifax Harbour. Weekly samples during the spring of 1952 indicated the first appearance of nauplii on February 26 and Stage VI on April 4; cyprids were settling on the shore by April 10, so that a period of 40 days may be taken as the best estimate for Stage I–VI. During this period ice was observed in the harbor, and Bousfield states that the surface temperatures were less than 3°C. Data by Banks (1955) for Halifax Inner Harbour indicates that 1–2°C is a better estimate for the temperature, a value substantiated by those for Eastport, Maine (U. S. Coast and Geodetic Survey 1955).

We have been able, through the courtesy of Dr. M. J. Dunbar, to examine plankton hauls taken by the Eastern Canadian Arctic Investigations in the Ungava Bay Region. In 1949, Stage II nauplii were first taken on June 4 and cyprids on August 11, which is a period of 48 days for development.

Fish (1925) found in plankton collected at Woods Hole that nauplii first appeared during December and cyprids in February. However, we have recently examined biweekly collections taken by Dr. C. S. Rao at Woods Hole, and while confirming the occurrence of nauplii on December 6 found they were followed by cyprids 21 days later. The mean sea surface temperature at this time was 6.6°C. It would seem that due to conditions pertaining at the time of Fish's collections his nauplii did not give rise to viable cyprids (see Barnes 1956). Fish also records that he observed large quantities of early stage nauplii on January 30 somewhat further to the south at Newport (Rhode Island), and that these were followed by abundant cyprids on March 4, 33 days later; the temperature may be taken as similar to that at Woods Hole for February, namely 1.0°C (U. S. Coast and Geodetic Survey 1955). The data discussed above are collected together in Table 1.

DISCUSSION

It is evident from Table 1 that while at some of the colder places the period of larval development is somewhat longer, there is no regular relation with temperature. In most cases a period of about 30 days is required whatever the temperature. The results stand, therefore, in marked contrast to the effect of temperature on the Stage I to II transition as determined experimentally. It is realised that there is some doubt about feeding in Stage I and that the absolute rates of the different stages may vary; one might expect nevertheless the value of Q_{10} to be similar for all stages. It is possible that acclimation is responsible for the roughly constant period of development, but in this connection it must be noted that the temperature during the later stages of embryonic development varies widely; for example the adults have been buried under the ice in the Canadian Arctic, while at Woods Hole the temperature falls only from 15° in October to 11°C in November. Acclimation to habitat conditions has been shown to be a common feature among poikilothermous animals (Bullock 1955) and has been suggested for a number of planktotrophic larvae by Thorson (1946); the comparisons are, however, largely interspecific.

On the other hand the availability of the right kind of food has been shown to be of fundamental importance in the development of planktonic larvae with high metabolic rates, and it is suggested that this factor may interact with and compensate for temperature effects.

REFERENCES

BANKS, R. E. 1955. Seasonal changes in the water temperature of Halifax Harbour and Bedford Basin. Naval Research Department, Nova Scotia, U/P Section IV, Research Note 55/1.

BARNES, H. 1955. Climatological and salinity data for Millport, Scotland. Glasgow Nat., **17**: 193–204.

———. 1956. *Balanus balanoides* (L.) in the Firth of Clyde: the development and annual variation of the larval population, and the causative factors. J. Anim. Ecol., **25**: 72–84.

BOUSFIELD, E. L. 1952–3. The distribution and spawning seasons of barnacles on the Atlantic coast of Canada. Ann. Rept. Nat. Mus. Canad. 1952–3, Bull. **132**: 112–154.

BULLOCK, T. H. 1955. Compensation for temperature in the metabolism and activity of poikilotherms. Biol. Rev., **30**: 311–342.

FISH, D. J. 1925. Seasonal distribution of the plankton of the Woods Hole region. Bull. U. S. Bur. Fish., **41**: 91–179.

PYEFINCH, K. A. 1948. Notes on the biology of cirripeds. J. Mar. Biol. Ass. U. K., **27**: 464–503.

RUNNSTRÖM, S. 1924–25. On the biology and development of *Balanus balanoides* (Linné). Bergen Mus. Aarbok, Nr. 5, 1–46.

SCHOLANDER, P. F., W. FLAGG, V. WALTERS, AND L. IRVING. 1953. Climatic adaptation in arctic and tropical poikilotherms. Physiol. Zoöl., **26**: 67–92.

THORSON, G. 1946. Reproduction and larval development of Danish marine bottom invertebrates. Medd. Komm. for Havundersøg., Kbh., serie Plankton, **4**: 1–523.

U. S. COAST AND GEODETIC SURVEY. 1955. Surface water temperatures at tide stations. Atlantic Coast, North and South America. U. S. C. & G. S., Spec. Publ. No. 278. 5th Edition.

Contribution No. 930

JOURNAL OF METEOROLOGY
APRIL 1958 VOLUME 15 SHORTER CONTRIBUTIONS 230 - 231

"DISTER": A DISPLACEMENT SEQUENCE STEREOSCOPE

By William S. von Arx

Woods Hole Oceanographic Institution[1]

(Manuscript received 25 September 1957)

When motion pictures of clouds or ground features are made at right angles to the line of flight of an airplane, a stereobase is generated between successive exposures which is equal in length to the product of the velocity of the airplane and the interval of time between successive exposures. As these photographs are projected in the usual way the point of view changes with time and progresses along the line of flight without binocular stereopsis. But when a suitable rotating shutter or polarizing chopper is synchronized with the projector it becomes possible to view one frame with one eye and the next frame with the other to reveal the impression of depth; provided the order in which the two eyes perceive successive frames is the same as the direction of flight and the rate of projection is greater than ten frames per second so that *persistence of vision* will permit the successive images to be fused stereoscopically.

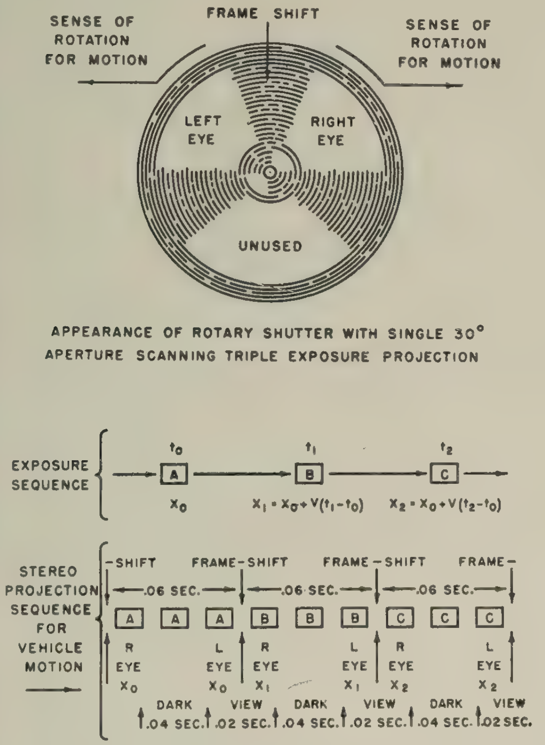

FIG. 1. Schematic representation of the method by which aerial motion pictures of clouds may be studied stereoscopically.

If the interval between successive exposures from the aircraft is a second or more, the stereobase then exceeds the length of the aircraft and the binocular stereoscopic effect is so strong that the form and difference in range of clouds and ground features perhaps ten miles distant can be perceived independently of other clues such as geometrical and aerial perspective, super-position and relative parallax. At this exposure rate some cloud development is also perceptible, especially in active cumulus towers.

The simplest equipment used to reveal the stereoscopic information available in such films consists of a rotary shutter, coupled through a flexible shaft to an extension of the shutter shaft of a (Kodak Analyst) motion-picture projector. The rotary shutter has a diameter about equal to twice the interpupilary distance of the observer and contains a single transparent sector about 30 deg in angular width. The stereoscopic viewing shutter rotates once per frame and the phase of rotation is adjusted so that the transparent sector is between the eyes (the opaque portions blocking both) when the projector is shifting frames. The sense of rotation must permit the clear sector to progress with the sense of motion of the vehicle so that the trailing eye sees the last presentation of the first frame and the leading eye sees the first presentation of the next successive frame. Then after a brief interval of darkness, the frame just seen by the leading eye is re-exposed to the trailing eye and the next succeeding frame exposed to the leading eye, and so on at a rate sufficiently rapid that flicker is suppressed. This sequence of events is shown schematically in the accompanying figure.

Nearly the same effects can be obtained by substituting for the flexible shaft and shutter, a disc of polarizing material rotating just in front of the projection lens. Most projectors chop the image of each frame three times to reduce flicker. Therefore each of the three successive presentations of each frame on the screen is polarized at an angle 120 deg different from its neighbors. Alternation of views between the right and left eyes can be obtained by setting analysers in a pair of spectacle frames at the proper extinction angles to permit the first and last presentation of each frame to be viewed separately by each eye. This has the advantage that several persons can see the displacement sequence stereopsis at the same time, but with somewhat less striking effect since the extinction is not wholly complete. To reduce flicker both eyes can be permitted to see the intermediate exposure without stereopsis.

The useful base for conspicuous stereopsis lies between 0.5 and 20 per cent of the range. At air speeds of from 100 to 300 kn a time lapse of 1 sec between successive exposures will reveal the three-dimensional forms of clouds from about 0.2 to 5, and 0.6 to 15 mi away respectively and the spatial relationships of cloud groups beyond stereoscopic range can be sensed through their bluer color, diminishing parallax and occasional superposition.

---

[1] Contribution No. 930 from Woods Hole Oceanographic Institution.

Contribution No. 931

SYNOPTIC PHOTOGRAPHY*

By William S. von Arx

Woods Hole Oceanographic Institution, Woods Hole, Massachusetts

In a programme of field observations it is interesting to know the relationship of the site of each measurement to the environment as a whole. When conditions are changing, the time of measurement relative to the life cycle of a natural process may be as significant as the relative position. While suitably detailed synoptic mapping can provide this information, the means are not always available to gather the necessary data point by point. In cases where the natural process is visible or related to visible changes, a photographic synopsis can be helpful.

Since many natural changes occur slowly and the view from ships and high-flying aircraft evolves at a leisurely pace, time-lapse photography has been used to bring rates of change within the scope of human appreciation. In a similar way it is difficult to see the structure of natural occurrences which are so extensive that the observer is embedded within them or unable to move far enough away to view things whole. In these instances wide-field photographic systems and associated stereoscopic viewing techniques have served to bring the breadth and depth of the visible environment within the compass of the human eye.

Recently a few optical systems have been developed empirically but along quantitative lines, which have proved useful in detailed field investigations from fixed ground stations, and from moving ships and aircraft. The optical systems for synoptic photography are adaptations of well-known principles or designs. As yet they lack the critical definition to which modern lens designs have made us accustomed. But at this cost they minimize the problem of providing uniform illumination over very wide angles of view and offer a number of desirable possibilities in the distortion of shapes and angles to make measurements of these quantities more convenient.

LIMITATIONS OF CONVENTIONAL LENSES

The conventional camera lens, like a pin-hole, admits light from each point on the object and allows it to fall on the sensitive surface without deviation.

---

* *Contribution No. 931 from the Woods Hole Oceanographic Institution.*

The words ' synoptic photography ' are intended to embrace those optical and photographic operations which permit fields of view approaching and exceeding one hemisphere to be recorded on a single film with a single click of the shutter. One would like to add that this process may be repeated over and over so as to record the motion as well as the space relationships of objects in the field of view at intervals suitable for analytical study.

The focusing effect of conventional lenses is used to increase the amount of light admitted, but the pin-hole-like geometry of the image is carefully unchanged. This geometry is identical with a fixed view through a window frame. Were the image to be inscribed on the glass and removed, its natural aspect could be restored only when the eye is returned to the original centre of perspective. To extend the total angle of the field of view to 180° the centre of perspective would have to coincide with the plane of projection, and this would have to be infinite in size, rendering fields in excess of 180° physically impossible. Moreover the light reaching the extremities of the image is dimmed as the obliquity of the aperture increases and since the image scale increases as well, the combined result is that the image brightness falls off with the fourth power of the cosine of the angle of obliquity.

It is well known that all these difficulties can be reduced by bending the rays before they enter the aperture stop of the optical system. The simple ‘ fish eye ’ camera described by R. W. Wood (1934), the remarkable whole-sky lens designed by Robin Hill (1924) and some modern lenses employ such bending and resulting image distortion. The problem remains to bend the incoming rays of light enough to permit a very broad field of view to be recorded by an ordinary motion picture camera, and produce an image which is directly intelligible, as in Fig. 1, and at the same time capable of restoration to natural dimensions with standard projection equipment.

THE NATURAL OBJECT SPACE

The choice of an unconventional image geometry useful in synoptic photography is guided by two basic considerations: (1) the symmetry of visual range, and (2) the properties of mirrors and lenses.

To the observer embedded in the atmosphere the visual range varies with altitude and is cut short by cloud layers and the earth or sea surface, but tends to have radial symmetry around a vertical axis. From the ground the apparent vault of the sky tends to retain this radial symmetry but to depart strongly from the hemisphere ideal. For physical study, however, it is convenient to disregard this physiological impression however strong it may be. Within the volume of the sea or in a very hazy atmosphere the visual range is nearly spherically symmetrical. Thus it seems appropriate, as a useful first approximation in most naturally hazy conditions, to regard the object space as spherical in preference to the customary plane which conventional lenses are designed to record without distortion.

The means by which a spherical surface can be represented on a flat plane have been studied exhaustively by cartographers. The crux of their problem is that a sphere is non-developable; that is to say, a spherical shell cannot be flattened without tearing, folding or deforming the surface in some manner. Eliminating the tearing and folding operations as optically unsuitable, there is left the group of perspective projections of the sphere and some of the simpler non-perspective projections. The gnomonic, stereographic and orthographic perspective projections of a sphere can be managed with refracting optics

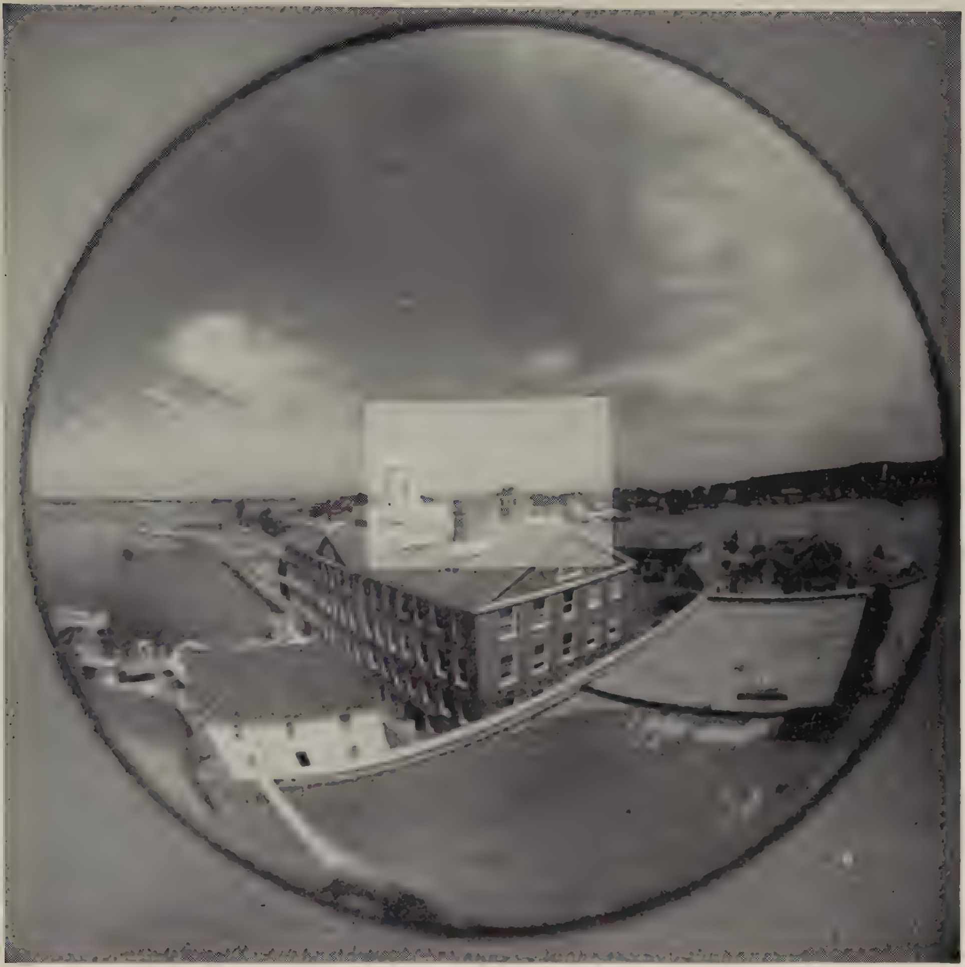

Fig. 1. A 176° field of view in orthographic projection compared with the field of a 15 mm. f.1 motion picture objective

(von Arx 1953). The equidistant projection (among several others) can be effected with reflecting optics.

PERSPECTIVE PROJECTIONS OF A SPHERE

Cartographically the perspective projections are produced (as shown in Fig. 2) by passing rays through a spherical surface and onward to a tangent plane: from the centre of the sphere in the gnomonic case, from the antipode of the point of tangency in the stereographic case, and from infinitely far above the antipode in the orthographic case.

The ordinary camera employs the gnomonic projection. In this system all great circles are represented as straight lines, but small circles become hyperbolas and the scale of projection increases markedly with distance from the point of tangency.

In the stereographic projection all circles, great and small, are represented by arcs of various circles. Moreover, circles which cross at right angles remain orthogonal in projection. The scale of projection increases with distance from the point of tangency but not as drastically as in the gnomonic case.

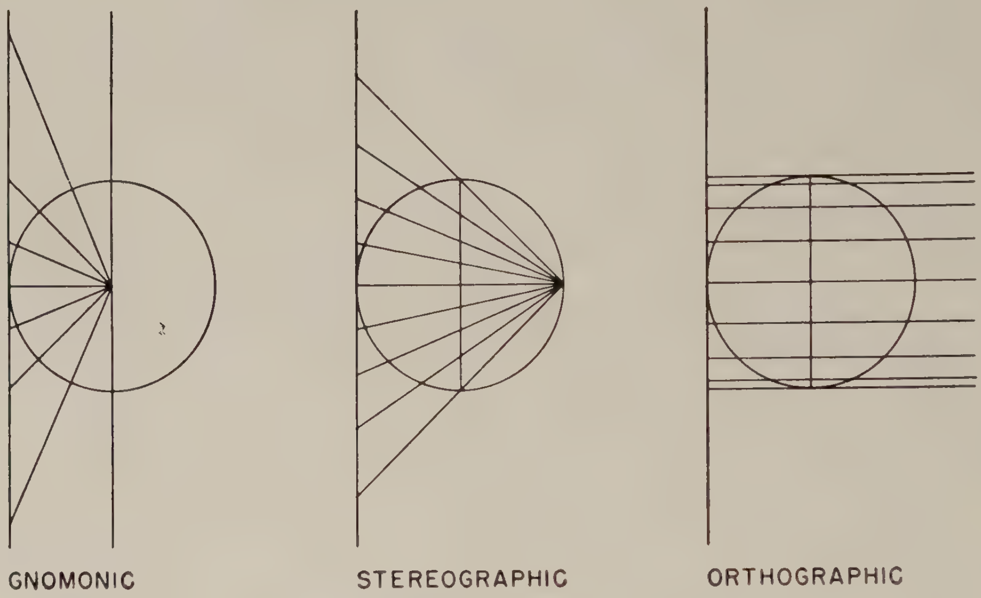

Fig. 2. Principles of the perspective projections

The orthographic projection represents small circles as straight lines and great circles as ellipses of different eccentricity. The radial scale of the projection diminishes with increasing angular distance from the point of tangency, reaching the vanishing point as this angle approaches 90°.

Of this group of possibilities, the orthographic projection, while limited to one hemisphere, has advantages for recording events in spherical spaces since it can be restored to spherical shape by other means than projecting the photographic image backward through the optical train (although this can always be done). Instead it is possible to project an orthographic image with standard motion picture projectors on the exterior of a small spherical transmission screen from the centre of curvature of which all the shapes and angles of the original object space are very nearly restored to normal. In this way an image can be subjected to angular measurement with a miniature theodolite fixed at the centre of curvature of the screen. The orthographic image is also intelligible when projected on a flat screen since it gives the impression of a sphere viewed from a distance. When the 180° camera is rotated around a vertical axis to cover the whole environment and the horizon cuts through the centre of the field, the vertical dimensions of objects do not change as they traverse the field of view. The lateral compression of the image is identical to the foreshortening of shapes on a spinning globe and therefore rationalized almost intuitively.

REFRACTING SYSTEM

The principle of the refracting system for synoptic photography can be demonstrated by looking backward through a wide field telescope or binocular. Here one will see a small, uniformly bright image of the view beyond, in which all angles are condensed and gradients of contrast are heightened. The formation of this miniature image does not involve aperture stops or appreciable changes in focal length with increasing obliquity of the angle (θ) of view. Thus the ($\cos^4\theta$) loss of light occurs only at the iris of the eye or camera diaphragm, where the total angle subtended by the small image can be less than 10 or 12 degrees, with the result that the illumination is tolerably uniform. The small image lies at infinity because the objective lens acts as a collimator. Therefore the image can be photographed with an ordinary camera focused for infinity, and with the same exposure as would be correct were the telescope removed.

The field of this miniature view can be widened by placing the curved side of a short focus plano-convex lens against the eyepiece, or by placing an equally strong plano-concave lens a little distance ahead of the eyepoint. As the air gap is changed between either of these auxiliary lenses and the eyepiece, the distortion of the image will be seen to change and the field of view to open and close. If the flat surface of either type of auxiliary lens does not limit the field of view it is possible to adjust the air space so that the image has the properties of an orthographic projection of a sphere and the field of view will approach 180°.

If the front surface of the negative auxiliary lens is slightly curved toward the object space a stereographic projection can be obtained by suitable adjustment of the air gap and the field of view opened beyond one hemisphere. The curvatures of the auxiliary lenses depend upon the quality of the eyepiece and the degree of residual spherical aberration present at the eyepoint.

Since the last war a high quality telescope has become available (the M-71H gunsight) which is equipped with an eyepiece having a 65° field. This field can be expanded by placing ahead of the eyepiece a block of low dispersion glass 65 mm in diameter, having a deep curve in the order of minus 12 mm radius on one side and a polished flat on the other, to accept rays at angles up to grazing incidence and bend them into the 65° cone of acceptance above the eyepoint of the eyepiece. When this type of lens is placed approximately 60 mm ahead of the eyepiece and a 16 mm motion picture camera fitted with a 50 mm focal length objective is placed at the telescope objective, the field of view can approach 180° with acceptably little lateral chromatic aberration and internal reflection. When the field lens is moved to within 40 mm of the eyepiece the full film frame will be utilized but the field of view reduced to 100° by 150°.

The air gap between the eyepiece and the auxiliary lens required to form an orthographic image is most easily determined empirically. The first nodal point of the optical train is placed at the centre of curvature of a transparent globe bearing the usual array of latitude and longitude circles as shown in Fig. 3*a*. Visual inspection of the final image on a ground glass screen at the focal plane of the camera will show what air space is required to render the latitude circles straight and parallel and the longitude circles spaced apart at the equator by $R \sin\theta$, where R is the radius of the image and θ is measured from optical axis of the lens system. If both the objective lens and erecting system in the telescope are left in place, the image is upright and can be placed at infinity by adjusting the focusing spiral on the eyepiece.

While this image may seem to appear sharply focused to the eye, the photographic results may be disappointing if the diaphragm opening is larger than 5 mm. This discrepancy is caused by the marked curvature of the image surface and by spherical aberration in the field compressor. These damaging effects can be reduced to acceptable levels (*a*) by adding a field flattener at the site of the first real image, (*b*) stopping down the camera lens, or (*c*) by using camera lenses of very short focal length to increase the depth of field.

Under full daylight conditions, as in Fig. 3*b*, large stops are not needed since even the slower colour films can be exposed successfully at f/8 when the single frame shutter speed of the camera is in the neighbourhood of 1/30 second. Moreover high shutter speeds are not necessary because the effective focal length of the optical train is so short (less than 3 mm) that the system is almost immune to vibration. Even in aircraft the effects of engine vibration and landing shock can generally be neglected.

A compound optical system such as this contains several real images. The largest of these is located immediately behind the eyepiece near the position of the telescope graticule. If the graticule is removed and a slot cut through in its place, it becomes possible to insert transparent plastic slips bearing written notes to be photographed in sharp focus and with proper exposure at appropriate places in the film record (the image is inverted at this point so that the notes, written with china marking pencil on celluloid or lucite slips, must also be inverted to appear upright on the finished film).

These refracting systems are well adapted to aircraft in that only the first glass surface need be exposed to the external air blast, and the length is relatively great (about thirty inches over-all) so that the camera is easily accessible in the fuselage even though the optical train is mounted in the nose or tail cone. When the system is trained straight ahead there is little relative motion of the image except in the foreground. At airspeeds near 150 knots and altitudes above 2,000 ft, a time lapse interval of even one second permits the relative motion in the foreground to appear smooth upon projection. With the system trained on either beam under the same flight conditions, the range of apparently smooth motion is removed beyond three-quarters of a mile.

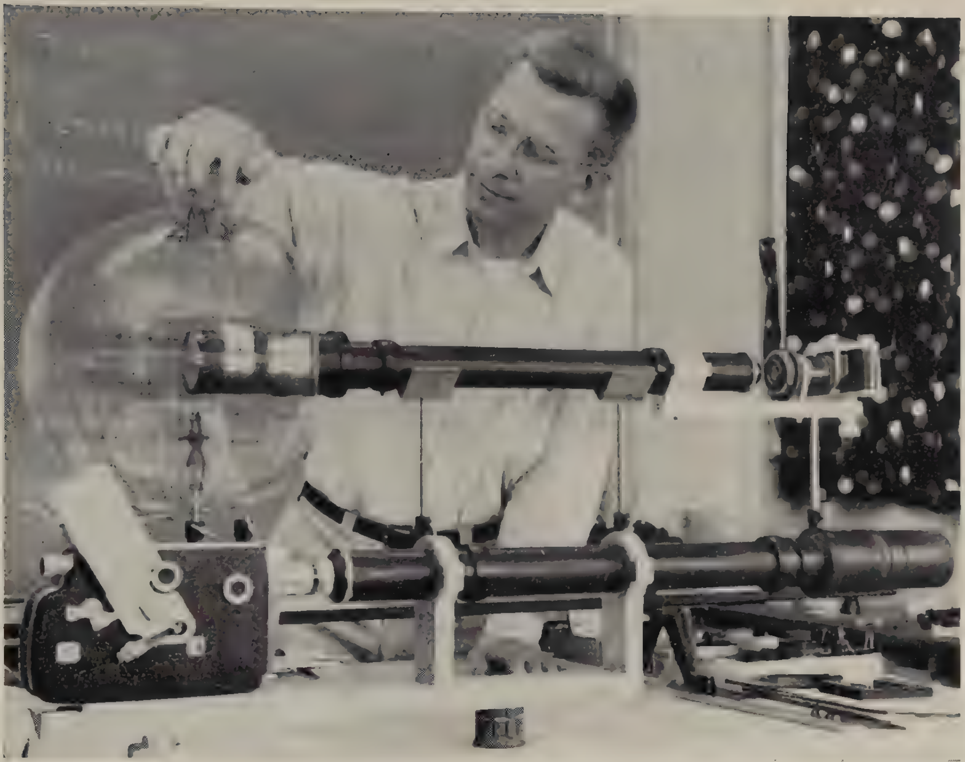

Fig. 3*a*. Foreground, a 176° orthographic aircraft camera. Background, the optical train of a similar camera mounted with the entrance pupil centered in a transparent sphere bearing co-ordinate markings for tests of the orthography of the final image

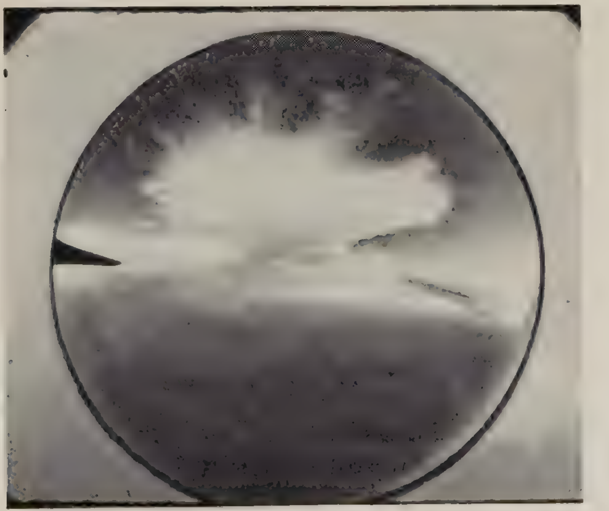

Fig. 3*b*. One frame from a filmstrip taken with the 176° orthographic camera, shown in Fig. 3*a*, mounted in the baggage compartment of a DC-3 aircraft. (Note that the field includes the walkway on the wing inboard of the port engine nacelle and the inner termination of the stabilizer de-icing boot)

STEREOSCOPIC EFFECTS

When the system is trained at right angles to the path of motion each successive exposure is displaced laterally to form a succession of stereoscopic pairs. It is possible to view the finished films stereoscopically as they run through a standard projector if this is fitted with a suitably synchronized auxiliary shutter or polarizing chopper. Such a device, dubbed *Dister* (von Arx 1957), permits each eye to see each stereoscopic pair of frames independently, in the proper order, and rapidly enough for persistence of vision to permit fusion of the two images.

If the interval between successive exposures from the aircraft is a second or more, the stereobase then exceeds the length of the aircraft and the binocular stereoscopic effect itself is so great that the form and difference in range of clouds and ground features several miles away can be perceived independently of other clues such as geometrical and aerial perspective, superposition and relative parallax. At this exposure rate some cloud development is also perceptible, especially in active cumulus towers.

The stereoscopic viewing equipment may consist of a rotary shutter with a single clear sector (about 30° wide), coupled in proper phase through a flexible shaft to an extension of the shutter shaft of a standard motion picture projector. The stereo shutter rotates once per frame and the phase is adjusted so that the transparent sector is between the eyes (the opaque portions blocking both) while the projector is shifting frames. When the sense of rotation permits the clear sector to progress with the sense of motion as the vehicle, the trailing eye sees the last of the first frame and the leading eye sees the first of the next successive frame in sufficiently rapid sequence for stereoscopic fusion to occur.

Nearly the same effects can be obtained by substituting for the flexible shaft and shutter a disc of polarizing material rotating just in front of the projection lens. Alternation of views between the right and left eyes can be obtained by setting analysers in a pair of spectacle frames at the proper extinction angles to permit the first and last presentation of each frame to be viewed separately by each eye. By this means several persons can see the displacement sequence stereopsis at the same time, but with somewhat less striking effect since the extinction is not wholly complete.

The useful base for conspicuous stereopsis lies between 0·5 and 20 per cent of the range. At air speeds of from 100 to 300 knots a time lapse of 1 second will reveal the three-dimensional forms of clouds from about 5 to 15 miles away respectively and the spatial relationships of cloud groups beyond stereoscopic range can be sensed through their bluer colour, diminishing parallax and occasional superposition.

TIME-LAPSE TRIGGERING MECHANISMS

Various mechanisms have been built which trigger spring driven cameras at regular intervals for time-lapse photography, but there are advantages in driving the shutter slowly or rewinding the spring between exposures so that an entire roll of film can be exposed without interruption. A simple mechanism of the first type has been built for the Bolex camera and of the latter type for the Kodak-100 camera. Each has different properties but both have served reliably in aircraft and the latter on shipboard as well.

The time-lapse mechanism for the Bolex camera was designed by F. C. Ronne and A. T. Spencer to do away with the spring drive, which on a Bolex can be decoupled with the lever provided on the camera body. The motor-drive shaft, also provided, can be coupled to a battery-powered permanent magnet D.C. motor running at a rate which will turn the shutter and advance the film once each second. The shutter aperture is masked down to 14 degrees and the rotation rate monitored by stop watch from time to time so that exposure is controlled with the lens diaphragm setting alone.

The time-lapse mechanism for the Kodak-100 camera, designed by M. P. Howland, Jr., consists of a scotch yoke designed to trigger the single frame lever on the up-stroke and rewind the mainspring on the down-stroke. By this means the spring cannot be wound unless some tension was lost in making an exposure during the previous half cycle. The exposure interval remains 1/25 second regardless of the time-lapse interval which, in turn, can be altered some 20 or 30 per cent by changing the voltage across the permanent magnet D.C. motor, or by interchanging motor gears when larger alterations are required.

In either of these systems the shutter can be arranged to remain open throughout the time-lapse interval and closed only while the film is being advanced. This has applications to night-time photography of clouds in moonlight, and of aurorae. The large camera aperture required for adequate exposure does, however, press the refracting optical train below the limits of useful resolving power. Reflecting optics perform better at high relative aperture.

REFLECTING SYSTEMS

When the field of view is expanded by reflectors it is almost inevitable that the camera photographs itself, but the field can be so wide that the camera image is relatively small. Henyey and Greenstein (1945) have produced a reflecting system with a concave spherical mirror which yields critically sharp definition over 140° field. To expand the field of view beyond this angle it is necessary to employ convex reflectors which sacrifice critical definition (Figs. 4*a*, *b*).

A number of investigators, notably Deppermann (1949), Baumbach (1953), and Georgi (1957) have examined the problem of reflection optics from the standpoint of the kind of projection produced in the finished photograph. It is acknowledged that beyond one hemisphere a convex spherical surface is unsuitable because it produces too much compression at the edges of the field, and that for physical analysis something approximating an equidistant projection is desirable because of the ease with which position measurements can be made on prints or projected pictures.

Figs. 5 and 6 show the difference in rate of increase of the field of view for convex spherical and paraboloidal reflectors as recorded by a conventional

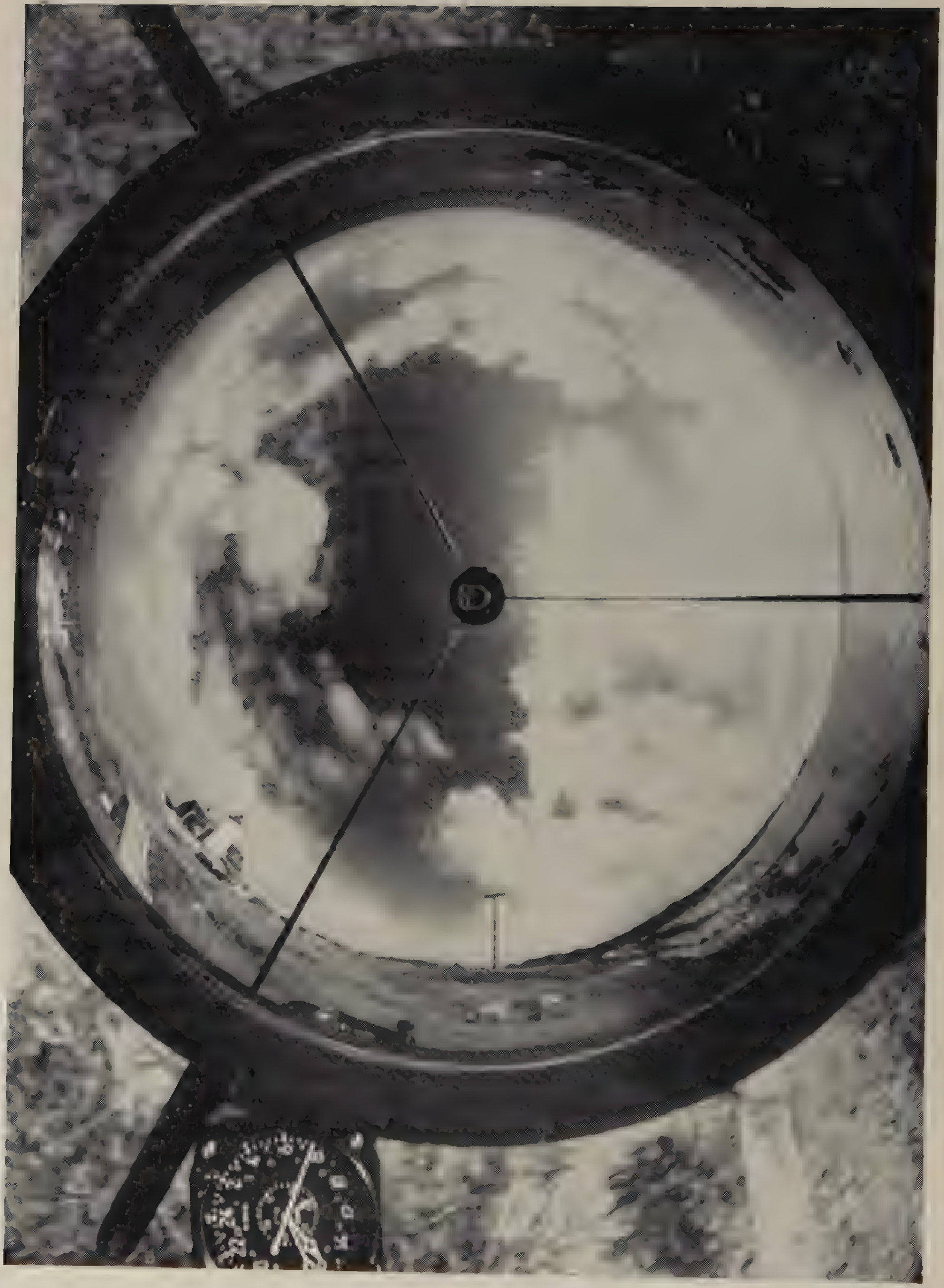

Fig. 4a. Vertical exposure through 240° total angle taken with a 35 mm camera mounted 8 focal lengths above the vertex of a 16-inch paraboloidal reflector

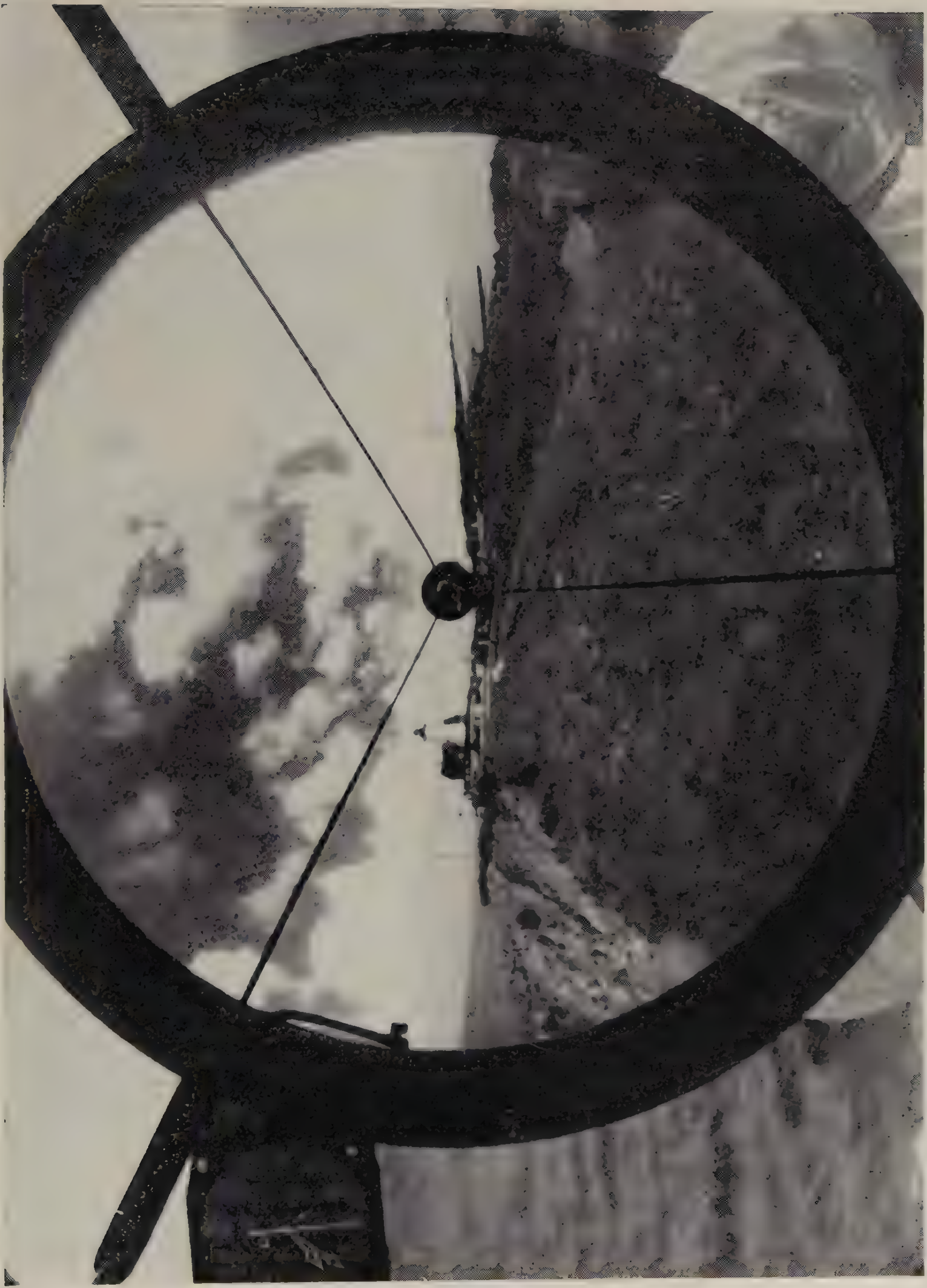

Fig. 4*b*. Horizontal exposure through 240° taken near the same point

camera situated at various distances from the vertex of the paraboloid and from the centre of curvature of the sphere. In these graphs a straight line through the origin represents the equidistant projection. One can see by inspection of the curves for the spherical mirror that in no case is even roughly equidistant image geometry maintained over a half-field in excess of 90°. However, the paraboloidal reflector is capable of approximately equidistant projection when

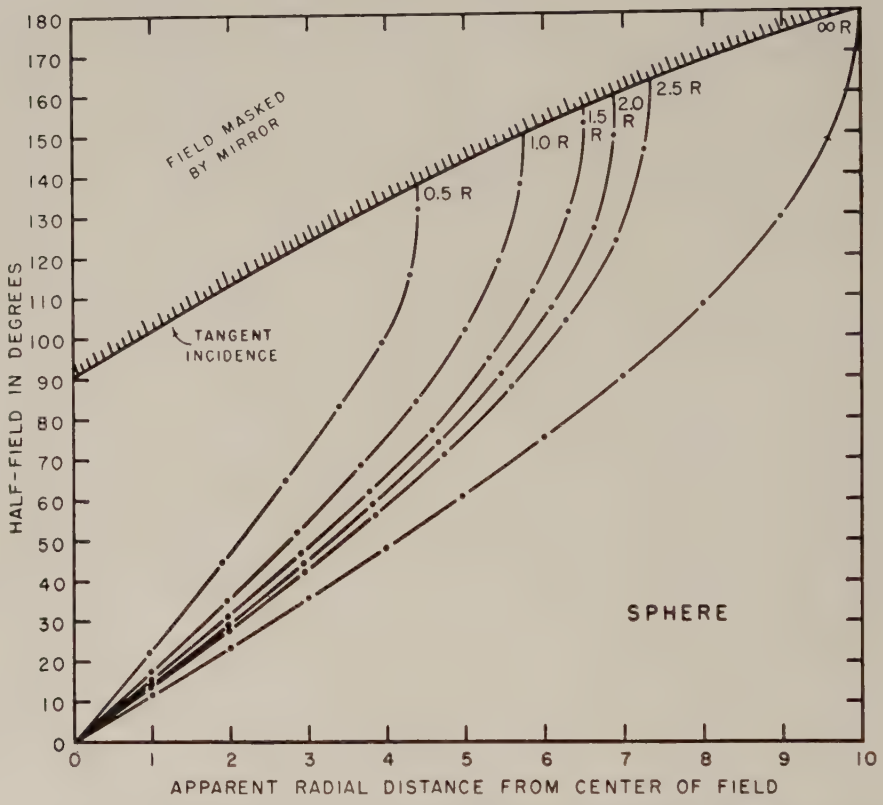

Fig. 5. Curves showing the field of view as a function of the radial distance from the centre of the image obtained with a conventional camera at various distances above the centre of curvature of a convex spherical reflector. In this graph the equidistant projection is represented by a straight line through the origin

the camera is mounted a distance 4 to 8 focal lengths above the vertex of the reflecting surface. This provides a field of approximately 150° either side of the central camera image. A total field approaching 300° should be possible, except for the failure of inexpensive commercial grade paraboloidal surfaces to match the mathematical ideal at their outer extremities. A practical upper limit for commercial surfaces therefore is probably in the neighbourhood of 240°. When the field is thus limited it becomes possible to use second surface reflectors which tend to produce ghost images under high contrast lighting

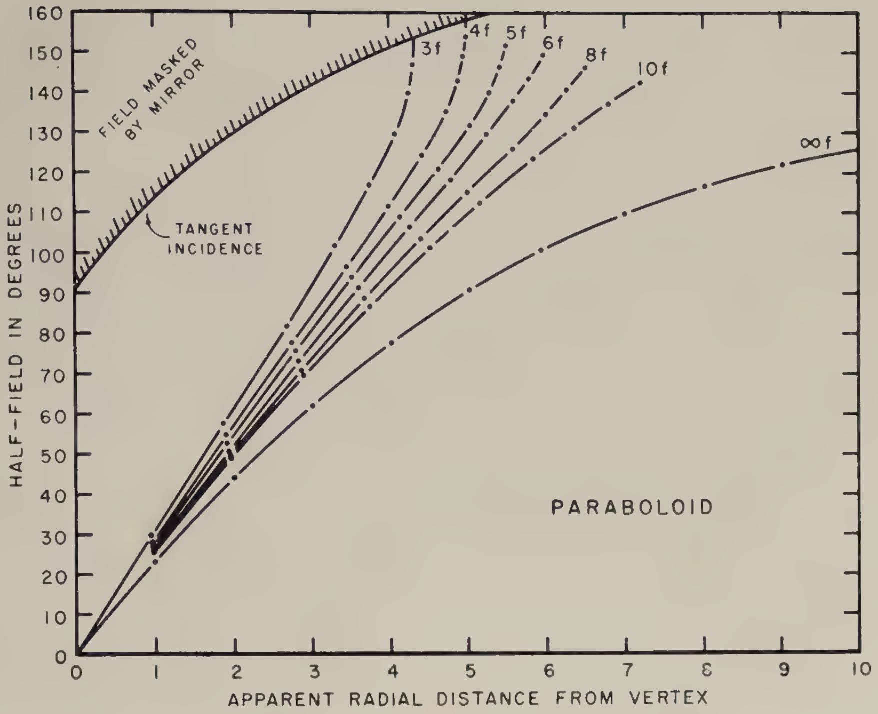

Fig. 6. Curves showing the field of view as a function of the radial distance from the centre of the image obtained with a conventional camera at various distances above the vertex of a convex paraboloidal reflector. A straight line through the origin of this graph corresponds to the equidistant projection

conditions but permit regular cleaning and minimize the corrosive influence of salt spray in a marine atmosphere.

With the extreme angle of the field of view provided by reflecting optics, time-lapse motion pictures of the whole sky can be made at a slower rate than is ordinarily required for narrow field cameras. It is found for example that a repetition rate of 4 frames/min is adequate to record the motions of all but the very lowest clouds as an intelligible representation of the cloud structures occurring during the course of the day. At this rate something less than 100 ft of film is consumed in a day and this can be projected at 16 frames per second in a little over four minutes. Greater economy of film can be managed by increasing the exposure interval to one frame per minute which produces an intelligible record of high clouds but a somewhat jumpy representation of the cloud motions at low levels. However, this rate lends itself to night-time photography of clouds and aurorae when the shutter is set to remain open between film shift cycles.

THE PHYSIOLOGICAL SKY

The vault of the sky is assumed to be spherical for the purposes of physical analysis, but physiologically it departs strongly from the appearance of a spherical dome. The physiological vault has properties of shape which depend on cloud height and visual range. In general, elevation angles near the horizon tend to be over-estimated at the expense of those near the zenith so that the moon appears to be larger at the horizon than at the zenith, and the same physiological effect applies to the sun, constellations and clouds. Neuberger (1951) has tabulated the discrepancy of physical and physiological elevation angles as follows:

Apparent elevation angle	0°	15°	30°	45°	60°	75°	90°
True elevation angle	0°	7°	14°	25°	39°	60°	90°

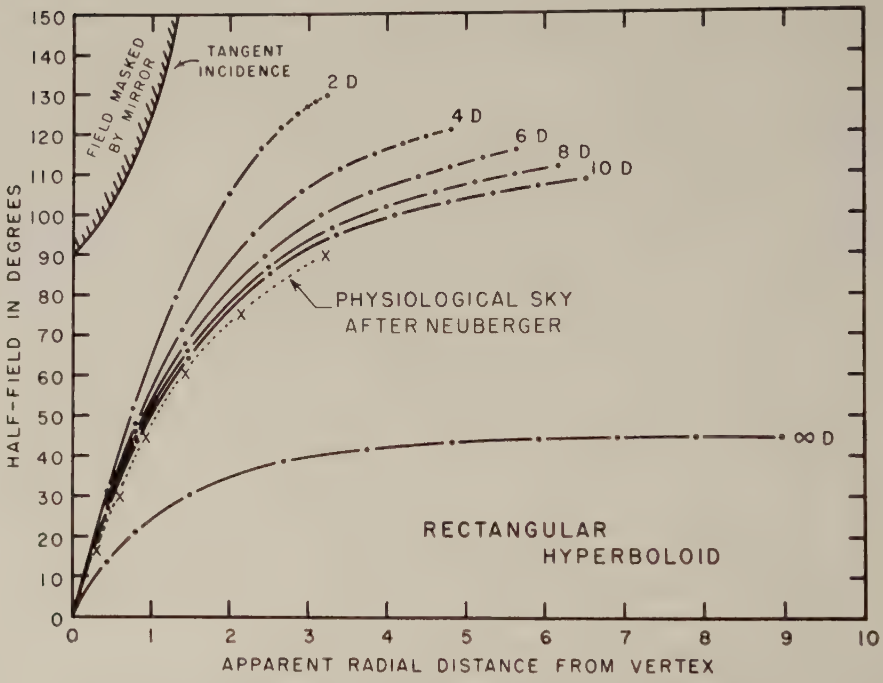

Fig. 7. Curves showing the field of view as a function of the radial distance from the centre of the image obtained with a conventional camera at various distances above the vertex of a convex rectangular hyperboloid, compared with the corresponding function for the 'physiological sky' as defined by Neuberger (1951)

Thus, for an appraisal of sky conditions under physiologically familiar circumstances, a whole-sky camera should distort the field of view by exaggerating the low elevation angles. A number of projective geometries have been studied in which conics of revolution have been combined with the gnomonic properties of ordinary camera images. Of the conics examined the rectangular hyperboloid most nearly approximates the physiological impression of the vault of the sky when, as indicated in Fig. 7, the camera is placed some $10D$ from the vertex, where D is the distance from the vertex to the co-ordinate origin of the curve. This result has not been subjected to experimental test.

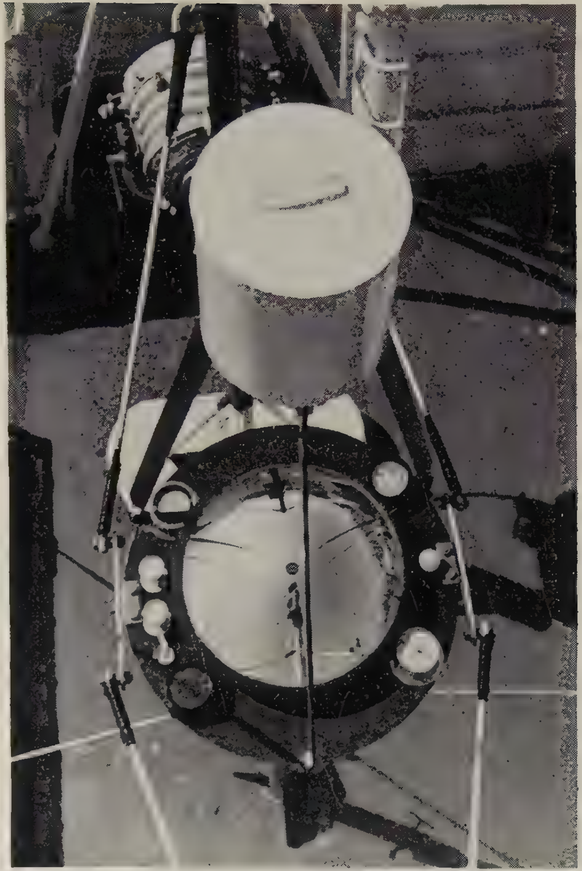

Fig. 8*a*. The 'Weather Aspect Recorder' mounted on a ship's bridge. It is seen from above, with the camera housing and the instruments clustered around the main mirror

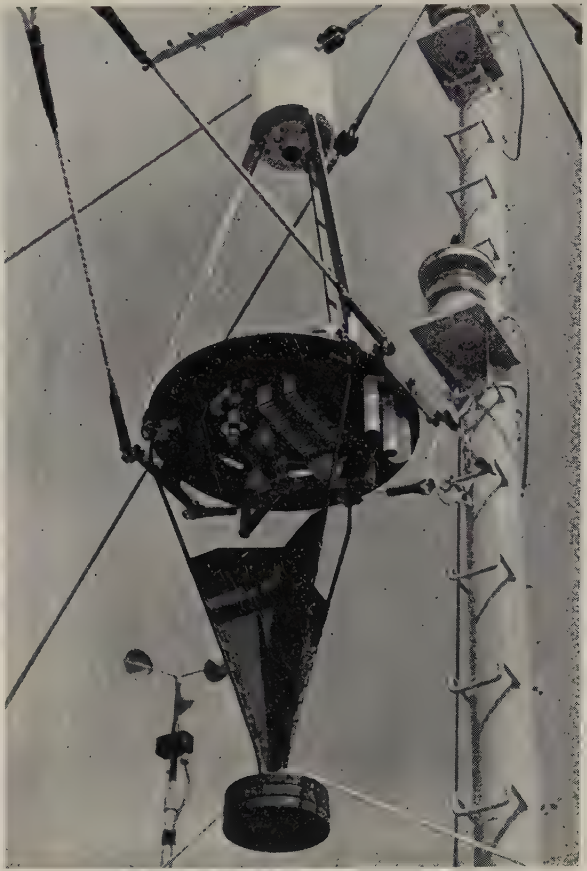

Fig. 8*b*. The same instrument seen from below, showing the anemometer cups, battery for the camera trigger and sail to balance the wind load on the camera housing

Parabolic reflectors have been used to some extent. One system of this kind (Figs. 8*a*, *b*, *c*) consists of a 3·75 inch focal length glass searchlight reflector 16 inches in diameter silvered and coated on the concave side as a second surface mirror mounted some thirty inches (8 focal lengths) beneath a Kodak-100 motion picture camera fitted with a 15 mm cine objective. This instrument has been mounted on shipboard, in a hammock-like cradle to remove most of the effects of roll, to record through 240° the aspect of the whole sky and sea surface once each minute. A magnetic compass and meteorological instruments of several kinds are mounted around the mirror where they are recorded in the corners of each frame. This arrangement has been used to provide a photographic log of the daylight weather and sea state conditions.

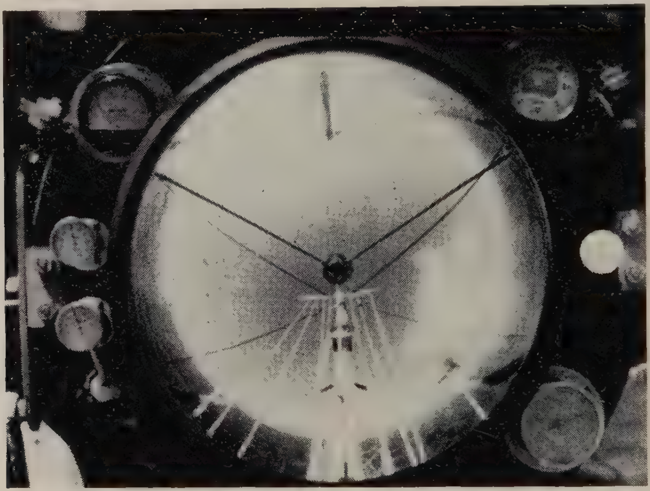

Fig. 8*c*. One frame of a record obtained with the ' Weather Aspect Recorder ' at sea near Puerto Rico

While such reflectors are achromatic, they tend to produce strong curvature of field. As in the case of the refracting systems the effects of field curvature on final definition can be reduced with a field flattener or by admitting only a small pencil of light through the camera lens. If the focal length of this lens is short the relative aperture may be very high for a pencil of given diameter, but the final image may then be so small that the grain in the emulsion becomes the limiting factor in definition. More recently some compound reflecting systems have been devised to surmount this difficulty with a reflecting field flattener which, at the same time, serves to adapt the reflecting type of optics to aircraft and other exposed installations.

The compound system shown in Fig. 9*a* consists of two reflectors ahead of the camera; a convex paraboloidal primary 16 inches in diameter with 3·75 in. focal length and a convex spherical secondary 4 inches diameter and 14 inches radius of curvature mounted 7·0 inches above the vertex of the paraboloid.

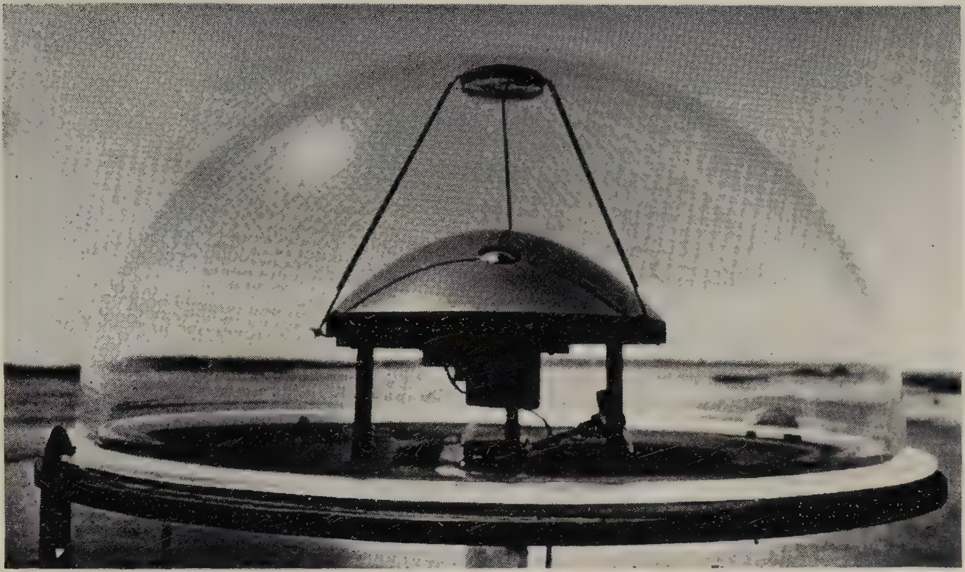

Fig. 9*a*. The compound reflecting system. The secondary mirror is supported by three struts rooted in the primary mirror support, but can be attached directly to the plexi-glass blister. The blister 36-inches in diameter is large enough to shelter a number of ground station instruments as well as to shield the optics against wind vibration

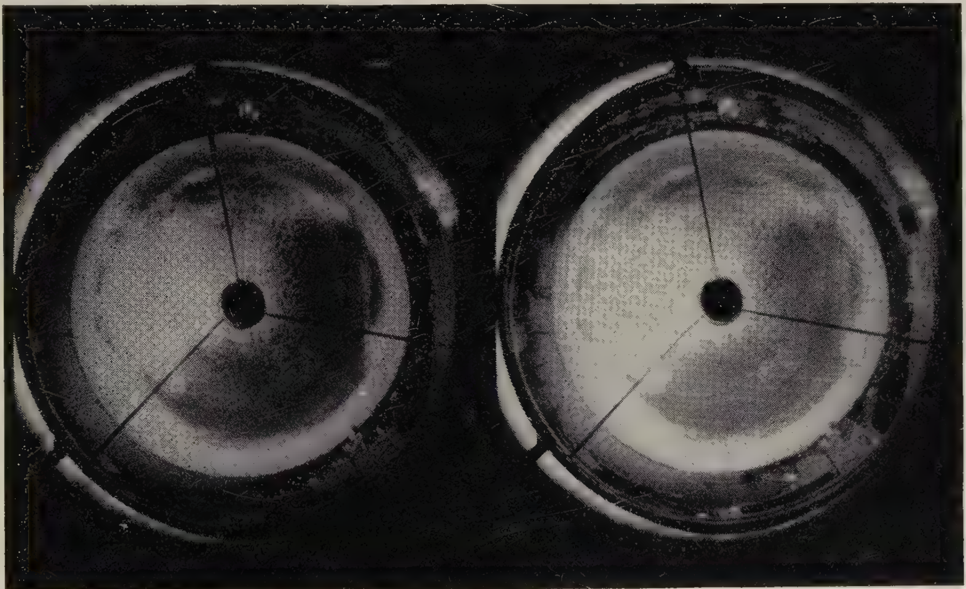

Fig. 9*b*. Portion of a test film made with the equipment shown in Fig 9*a*. The camera below the primary mirror is pointed straight up, but far enough below the hole in the vertex of the primary mirror to mask out the direct view of the sky surrounding the secondary reflector

The curvature of field produced by the primary mirror is nearly cancelled by that of the secondary. This permits the image to be in sharp focus over a much wider angle than is the case with a single reflector, and a larger entrance pupil to be tolerated at the camera. The vertex of the primary is perforated so that a time-lapse camera with an objective of 15 mm focal length can be mounted below the primary mirror with a full view of the secondary. The obstruction due to the secondary mirror is less than 1 per cent of the area of the field. The system covers 270° in nearly equidistant projection.

By these means the camera can be mounted inboard in aircraft or shielded by the primary mirror against weather. The system can also be housed under a spherical plexi-glas blister without serious interference due to internal reflections. If the secondary is made oversize, there is room in the blister and in the photographic frame for the dials of accessory instruments to be included in the field of view. These instruments can face outward and thus be illuminated by the ambient light to ensure properly balanced exposure. This compound design can take many forms and has potentialities as an airborne system, as a weather-tight whole-sky recorder for ground and shipboard stations, and perhaps also as a free-flooding camera or radiance collector for photographic measurements of light penetration into the sea.

CONCLUSION

Wide-field time-lapse systems of these kinds have been developed in response to specific needs in the laboratory to photograph large rotating models of the oceans and atmosphere under limited head room, in aircraft to record the points of entry into cumulus clouds to study the relation of vertical motion and liquid water content measurements to the visible column of cloud droplets, at ground stations to record cloud motions over heated islands, and from shipboard to provide a log of the daylight cloud cover, surface weather, and sea and swell conditions encountered day by day. There are other applications for the present systems, as well as many possible improvements and modifications for specific needs. It is hoped this account of a few preliminary efforts may be of some help to those facing related observational problems.

ACKNOWLEDGMENTS

The author would like to thank the Office of Naval Research, U.S. Navy, the Hurricane Program of the U.S. Weather Bureau, and the Jet Stream Analysis group of the Geophysics Research Directorate, U.S. Air Force for the support they have given these experiments. He would also like to thank Dr. Joanne S. Malkus and Mr. F. C. Ronne for testing some of the optical trains in tropical latitudes.

REFERENCES

Baumbach, S.	1953	Ein Winkeltreuer Wolkenspiegel nach J. Georgi. *Tech. Mitt. d. Instrumentenw. d. Deut. Wetterd. No. 26*
Deppermann, C. E.	1949	An Improved Mirror for Photography of the Whole Sky. *Bull. Am. Meteor. Soc.*, **30** (8), pp. 282–285
Georgi, J.	1957	The Photographic Sky Mirror. *Weather*, **12**, pp. 149–153

HENYEY, L. G. and GREENSTEIN, J. L. 1945 Miscellaneous Optical Designs. *OSRD Rept. No. 4505.* Yerkes Optical Bureau. University of Chicago, pp. 53

HILL, ROBIN 1924 A Lens for Whole Sky Photographs. *Quart. J. Roy. Met. Soc.*, **50**, pp. 227–235

NEUBERGER, H. 1951 *Introduction to Physical Meteorology*, Pennsylvania State College, State College, Pa., pp. 266

VON ARX, W. S. 1953 Cartographic Principles Applied to Wide Field Photography. *Photographic Engineering*, 4(2), pp. 60–73

1957 'DISTER'; A Displacement Sequence Stereoscope. *Bull. Am. Meteor. Soc.* (in press)

WOOD, R. W. 1934 *Physical Optics.* 3rd ed. Macmillan, New York, pp. 67, 68

PRINTED BY HEADLEY BROTHERS LTD 109 KINGSWAY LONDON WC2 AND ASHFORD KENT

Contribution No. 932

Bulletin of the Museum of Comparative Zoology
AT HARVARD COLLEGE
Vol. 119, No. 2

FOUR NEW RAJIDS FROM THE GULF OF MEXICO

By Henry B. Bigelow and William C. Schroeder
Museum of Comparative Zoology and
Woods Hole Oceanographic Institution

CAMBRIDGE, MASS., U.S.A.
PRINTED FOR THE MUSEUM
July, 1958

No. 2 — *Four New Rajids from the Gulf of Mexico*[1]

By Henry B. Bigelow and William C. Schroeder

Museum of Comparative Zoology and
Woods Hole Oceanographic Institution

Recent otter trawling operations of the U. S. Fish and Wildlife Service vessel "Oregon" in the Gulf of Mexico have yielded four new species of batoids, three of them falling in the genus *Raja* and one in *Cruriraja*. These, added to about a dozen new species of elasmobranchs described from the Gulf during the past seven years, and records of others previously unknown from the western Atlantic, emphasize the richness of the Gulf fauna. We are indebted to Stewart Springer and Harvey R. Bullis, Jr. of the U. S. Fish and Wildlife Service for the opportunity of describing these species. Drawings are by Eugene N. Fischer.

RAJA OREGONI sp. nov.

Figures 1, 2

Study Material. Mature male, 1440 mm in total length, holotype, U. S. Nat. Mus. No. 156710, and an immature male 1069 mm in total length, paratype, M. C. Z. No. 39617, both from the northern part of the Gulf of Mexico, the holotype from Lat. 29°10′N, Long. 88°13′W, in 205 fathoms, "Oregon" station 1247, the paratype from Lat. 28°32′N, Long. 86°20′W, in 260 fathoms, "Oregon" station 1277.

Distinctive Characters. The combination of features distinctive for *oregoni* among hard-nosed skates of the genus *Raja* are: anterior contour of disc deeply concave, with narrowly projecting snout, of the shape pictured in Figure 1; upper surface of pectorals without conspicuous markings of any sort; disc, rearward of the spiracles, without any large thorns, its midbelt bare even of prickles; tail with three rows of large close-set thorns extending to base of first dorsal fin; lower surface with pore openings in head region marked conspicuously with black dots.

---

[1] Contribution No. 932 from The Woods Hole Oceanographic Institution.

Comparison with previously known species. It is only with species sharing the diagnostic features listed in the preceding section that comparison seems called for, a limitation welcome because about 110 recognizably distinct species of the genus *Raja* have been named already from one part of the oceans or another (Bigelow and Schroeder 1953, p. 147).

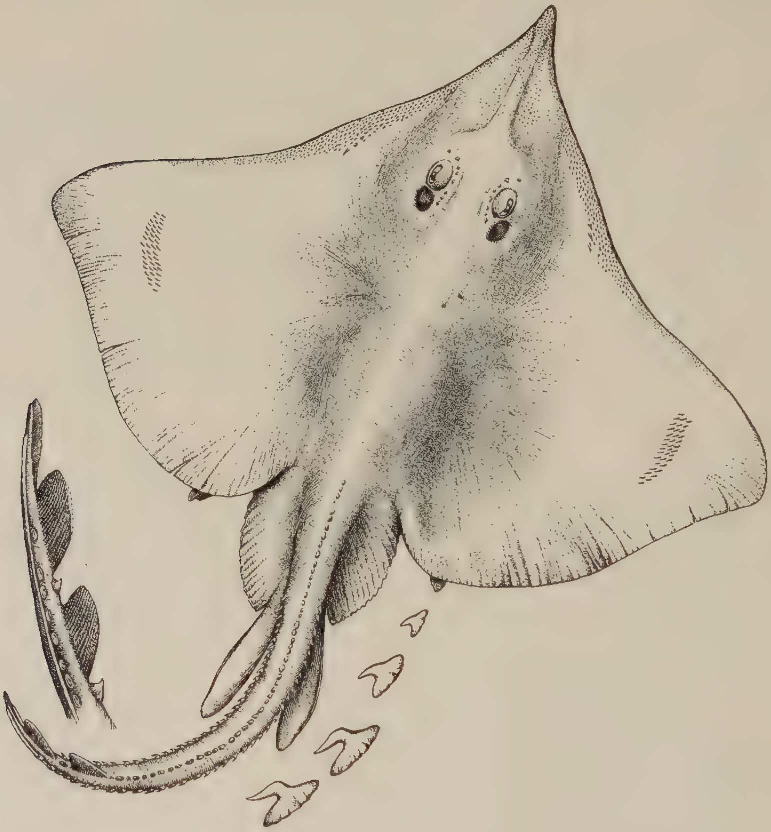

Figure 1. *Raja oregoni*, dorsal view of type, mature male 1440 mm long; end of tail showing dorsal fins and caudal fin about x 0.2; tail thorns from mid row about x 1.

Among the skates known from the North Atlantic (including the Gulf of Mexico) *oregoni* most nearly resembles *laevis* Mitchill 1817, the common barn-door skate of the northeastern American coast and its eastern Atlantic representative, *batis* Linnaeus 1758. But the thorns on the tail of *oregoni* are much larger than on *laevis* or on *batis,* closer set, and with those on the lateral rows

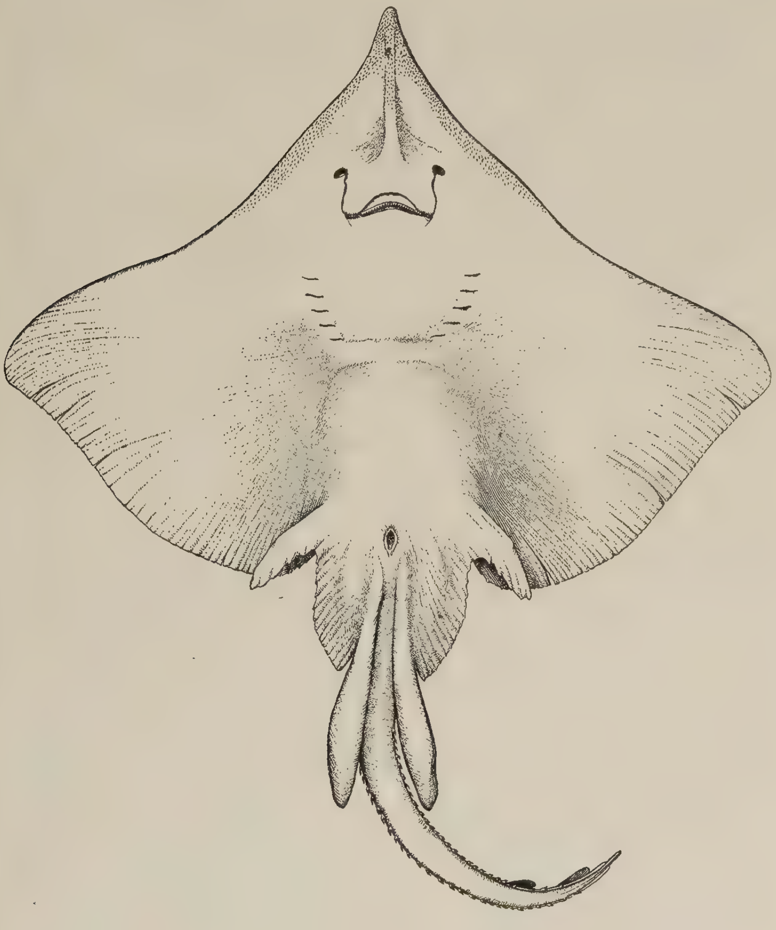

Figure 2. *Raja oregoni,* ventral view of specimen shown in Figure 1.

along the rear half of the tail directed rearward in very characteristic shape (Fig. 1). Other differences are that the snout is noticeably longer in *oregoni* (length anterior to orbits about 4 times as great as the distance between orbits) than in either *laevis* or *batis* (2.4-3 times) in males of about equal size; that the rostral cartilage is narrower and that the black pore markings of the ventral surface are restricted to the area anterior to the abdominal region whereas in *laevis* and in *batis* they are present on the rearward part of the disc as well.

The only other western North Atalntic skates that *oregoni* resembles at all closely in general appearance, combined with thorn pattern, are *R. olseni* Bigelow and Schroeder 1951 and *R. teevani* Bigelow and Schroeder 1951 but there is no danger of confusing it with either of these. Conspicuous respects in which it differs from *olseni* are in a shorter interspace between first and second dorsal fins, with only 1 thorn (3-6 thorns in *olseni*); in a larger number (31 to 48) of thorns in the mid-row on tail (only 13-26 in *olseni*) with the lateral rows closely and regularly spaced (irregularly and widely spaced in *olseni*). Other differences of perhaps equal significance taxonomically, though less noticeable, are that in *oregoni* the expanded outer-posterior margin of the nostrils is smooth edged (fringed in *olseni*, Bigelow and Schroeder 1951, fig. 2B; 1953, fig. 54 α B), that the upper surface of the snout, with the outer-anterior edge of the pectorals, is prickly (smooth in *olseni*), that the nuchal region is naked in *oregoni* but is armed with a strong thorn in large specimens of *olseni*[1] (not, however, on the juveniles). On the other hand, no trace is to be seen on the upper surface of *oregoni* of the white dots marking the pores that are a conspicuous feature of *olseni*, nor has the latter any dark dots on the under surface as is the case in *oregoni*.

Oregoni resembles *teevani* closely in anterior contour of its disc but differs in having 3 rows of prominent thorns on the tail (one row on *teevani*), by having a tail which narrows posteriorly as is usual among skates (on *teevani* the posterior half of tail is as wide or wider than the anterior), and by having a space, occupied by a thorn, between its dorsals (dorsals are confluent on *teevani*), and *teevani* lacks dark pores on the under surface.

---

[1] Specimens at hand include a nearly mature male *olseni* 510 mm long recently collected by "Oregon" in the Gulf of Mexico at Station 1514.

Oregoni is set apart, by the combination of characters classed above as "diagnostic," from all hard-nosed skates yet known

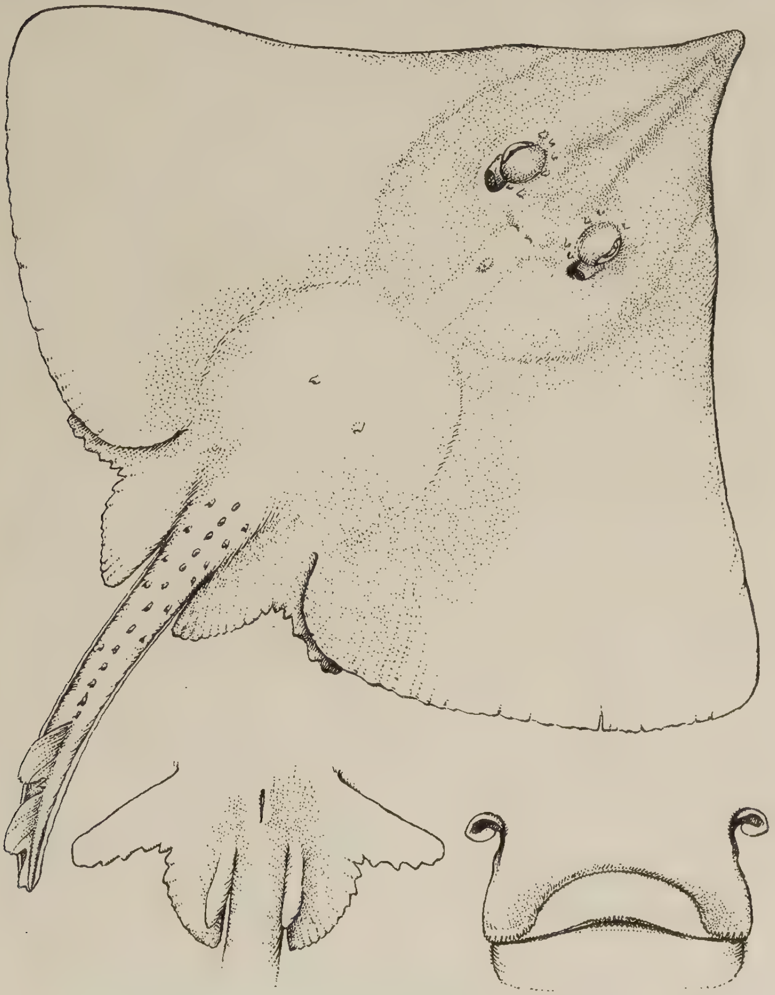

Figure 3. *Raja flavirostris,* immature male 374 mm long, "William Scoresby" station 79, from Lat. 51°01′30″S, Long. 64°59′30″W, in British Museum (Natural History); pelvic fins about x 0.4; mouth, nostrils and nasal curtain about x 0.8.

from the east coast of South America, or from the Magellanic region, with the exception of *R. flavirostris* Philippi 1892 the recorded range of which extends from Argentine and Patagonian waters to Chile. And it differs sharply from half grown and larger *flavirostris*[1] in a conspicuously longer tail (46-50 per cent of total length contrasted with 41.8-42.5 per cent in the half-grown *flavirostris* with which we have compared it; in lacking the large nuchal thorn that is characteristic of *flavirostris;* also in the greater size, more regular spacing, and shape of the thorns in the lateral rows on the tail (cf. Fig. 1 with Fig. 3 of *flavirostris*).

The only skates known from European or tropical west African waters, and from southern Africa, with which *oregoni* shares an outer anterior contour of the shape pictured in Figure 1, combined with a disc that is wholly bare of thorns posterior to the spiracles, but a tail that is armed with 3 regular rows (one median and two laterals) of close-set thorns, are: *Raja batis* Linnaeus 1758, *R. alba* Lacépède 1803 (including *R. marginata* Lacépède 1803, partly grown specimens and some adults), and *R. miraletus* Linnaeus 1758 (some specimens). And it is marked off from all of these by characters that cannot reasonably be credited to variation (whether individual or regional) or explained away on the basis either of sex or of the stage of growth of the particular specimens that have served as the bases for published accounts. Thus it differs from *batis* in the same respects in which it differs from *laevis* of the North American coast (p. 00), and this also applies to the skate that has been reported as *batis* from South Africa (Thompson 1914, p. 156; Barnard 1925, p. 70; Smith 1949, p. 66) though available information regarding the latter is scanty. And while it resembles *alba* of European waters and the skate that has been reported under that name in southern African waters from Walfish Bay on the west around the Cape to Natal on the east, first by von Bonde and Swart (1924, p. 5) both as *alba* and as *stabuliforis*

---

[1] We are indebted to the British Museum for the loan of three *flavirostris*, a male 374 mm long, a female 353 mm, and a juvenile male of 180 mm, from the series reported upon and pictured by Norman 1937, p. 13, fig. 4.

Garman 1913, next as *marginata* (Barnard 1925, pp. 63, 65), and more recently as *alba* by Smith (1949, p. 66), the skin of the tail of *oregoni* is naked between the thorns (described as ''strongly spinulose'' for *alba* by Clark, 1926, p. 48), as well as over the inner-posterior parts of the disc as a whole while it is more or less prickly on adults of *alba.* Further, the mid-row of thorns on its tail does not extend forward on to the disc as it does in *alba,* when adult, and the black pore markings characteristic of the lower surface of *oregoni* (Fig. 4) are not present on *alba.* Again, *oregoni* resembles *R. miraletus* in its pointed snout, smoothness of posterior part of disc and presence of 3 rows of thorns on the tail. But its outer anterior contour is much more deeply concave than that of *miraletus;* it lacks the 2 nuchal thorns characteristic of the latter; the number of thorns in each of the rows along is tail is much greater, there being about 50 in the median row on the male pictured in Figure 1, contrasted with 14 pictured by Rey for an adult male of *miraletus* 402 mm long, and 25 recorded by him for a female, not counting those between the dorsal fins (Rey, 1928, p. 573, pl. 13, fig. 2). Also, the interspace between the two dorsals is noticeably shorter in *oregoni* than in *miraletus;* and while black pore marks are present on the lower surface of *oregoni,* they are lacking on *miraletus.* And *oregoni* is much the larger growing member of the pair, it being unlikely that *miraletus* grows longer than about 500 mm, nor does *oregoni* show any signs of the large, light-blue centered eye spots, one of which marks the upper surface of each pectoral of *miraletus.*

It is interesting, in passing, that in the presence of the black pore markings on its lower surface *oregoni* parallels not only *batis,* but also *oxyrhynchus* Linnaeus 1758 (including *macrorhynchus* Bonaparte 1832-41) among European species. But there is no question of specific unity in this case, the snout of *oregoni* being less narrowly pointed than that of *oxyrhynchus* with the outer anterior contour of the disc much less deeply concave; the 3 rows of large tail thorns of *oregoni,* so conspicuous a feature of the adult male, being represented on the adult male *oxyrhynchus* by a single median row of about 8 to 12 thorns; the two dorsal fins separated by an interspace with a thorn in *oregoni* being confluent at the base, or nearly so, in *oxyrhynchus;* and the black pore marks on the lower surface, which are confined

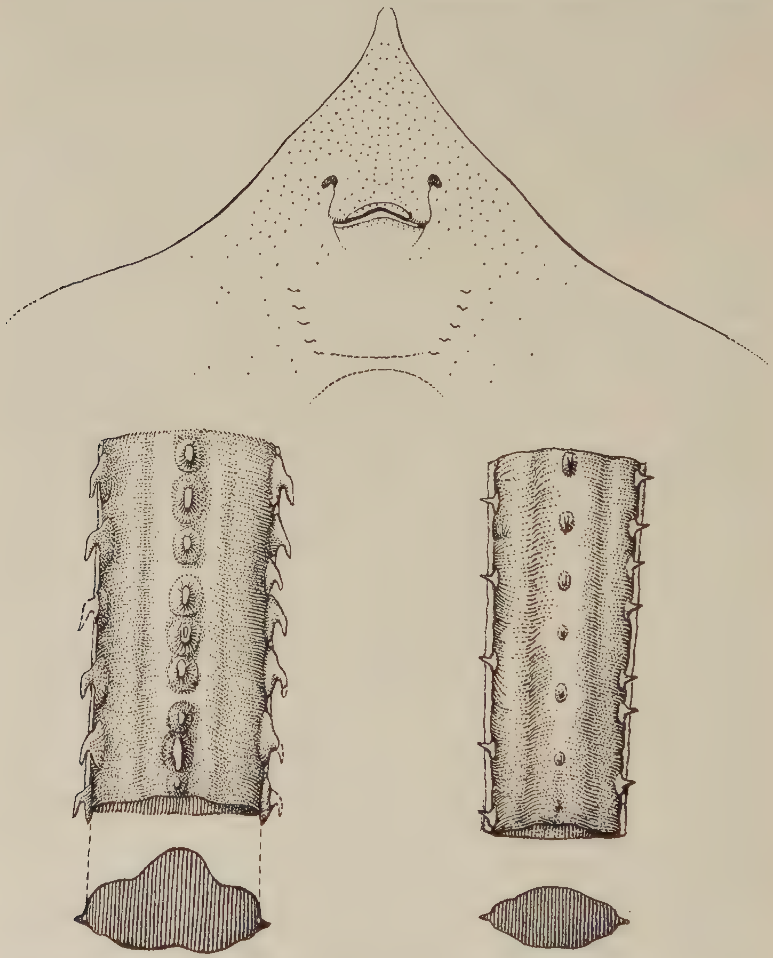

Figure 4. *Raja oregoni*, ventral view of head to show dark mucous pores, about x 0.1. *Lower left*, section of tail from 8th to 16th thorns in mid row, from first dorsal fin, about x 0.5, same specimen as in Figure 1. *Lower right*, *Raja laevis*, section of tail from 3rd to 9th thorns in mid row, from first dorsal fin, about x 0.5, a male 1185 mm long from off Nantucket, Massachusetts.

mostly to the head region in *oregoni* being distributed over the abdominal region as well in *oxyrhynchus.*

In its concave outer anterior outlines, with narrow snout, and in the black dots marking the lower surface of its head, *oregoni* most nearly resembles *R. rhina* Jordan and Gilbert 1880 among skates of the west coast of North America. But it differs from *rhina* in lacking the nuchal spine or spines that characterize *rhina,* as well as in the orderly arrangement of the thorns on its tail which on *rhina* are usually arranged irregularly with the rows interrupted. Furthermore, the mid zone of disc from the scapular region on to the tail is smooth on *oregoni* but has a band of small thorns with stellate bases on *rhina.*

Similarly, the narrowness of its ''nose'' combined with its lack of thorns anywhere on the disc rearward from the spiracles, contrasted with the presence of 3 rows of thorns along the tail, marks off *oregoni* among hard-nosed skates known from the Pacific coast of Central and South America, except *flavirostris* which was originally described from Chile. Respects in which it differs from *flavirostris* are summarized above.

Among the dozen or so narrow-nosed species of *Raja* that have been reported, with adequate published accounts, from the Indo-West Pacific region, three only are described, with a fourth pictured, as with the openings of the pores black-marked on the lower surface, and *oregoni* cannot be identified with any one of these. Thus *oregoni* lacks a nuchal thorn which is present and conspicuous in *australis* Macleay 1884 from Australia and Tasmania and the 3 rows of thorns on the tail of *oregoni* are longer and more regular than in *australis.* While *oregoni* lacks a nuchal thorn and the tail thorns are arranged in regular rows, *tobae* Tanaka 1916 from Japan has 2 thorns on the nuchal region and its 3 rows of tail thorns are irregular. *Oregoni,* lacking thorns along the midline of disc, differs from *porosa* Günther 1874, from the north Chinese coast, which has 3 or 4 conspicuous thorns in that area, and the 3 rows of thorns on the tail of *oregoni* distinguish it from *gudgeri* Whitley 1940, from Western Australia, which has but a single row as well as a much longer snout.

Neither can *oregoni* be referred to any of the other Indo-West Pacific species that it resembles at all closely in the anterior contour of its disc, for no known member of this group parallels *oregoni* in the presence of three regular rows of large close-set thorns extending from the base of the tail rearward as far as the first dorsal fin, but combined with a total lack both of thorns and of prickles on the mid belt of the disc posterior to the spiracles. While it agrees with *macracauda* Ishiyama 1955 from Japan in shape of snout and disc and also in presence of dark pores below,[1] it differs from *macracauda* in having 3 rows of thorns on the tail (only 1 row in *macracauda*).

Description of holotype. Proportional dimensions in per cent of total length:[2]

Disc. — Extreme breadth 69.8; length 53.2.

Snout length. — In front of orbits 17.4; in front of mouth 18.5.

Orbits. — Horizontal diameter 2.8; distance between 4.5.

Spiracles. — Length 2.1; distance between 6.4.

Mouth. — Breadth 8.0.

Exposed nostrils. — Distance between inner ends 8.3.

Gill openings. — Length, 1st 1.4; 3rd 1.8; 5th 1.2; distance between inner ends, 1st 13.8; 5th 8.1.

First dorsal fin. — Vertical height 1.5; length of base 3.6.

Second dorsal fin. — Vertical height (damaged); length of base 3.8.

Pelvics. — Anterior margin 10.9.

Distance. — From tip of snout to center of cloaca 50.0; from center of cloaca to 1st dorsal 37.2; to tip of tail 50.0; from rear end of 2nd dorsal base to tip of tail 4.2.

Interspace between. — 1st and 2nd dorsals 1.3.

Disc nearly 1.4 times as broad as long, maximum angle in front of spiracles about 72°; anterior margins sinuous, being rather strongly concave from tip of snout to opposite orbits where they are slightly convex, hence again concave, this second concavity culminating about three-fifths the distance between tip of snout and outer corners of disc which are sharply rounded; posterior margins about straight near outer corner, then gently rounded, as is inner margin. Axis of greatest breadth about 72 per cent back from tip of snout to axils of pectorals. Tail with a narrow lateral fold, low down on each side, beginning almost imperceptibly beyond level of tips of pelvics by a distance equal to about twice the interorbital width, widening posteriorly and continuing almost to extreme tip of tail being much the widest opposite dorsals and caudal membrane; length of tail from center of cloaca to origin of first dorsal fin 0.75 times as great, and to its tip equal to distance from center of cloaca to tip of snout.

---

[1] Two young specimens examined by us, through the kindness of Dr. Ishiyama.

[2] The measurements from which the proportional dimensions have been calculated were taken on a horizontal line between perpendiculars at given points (see Bigelow and Schroeder 1953, fig. 1 and p. 4).

A row of 7 or 8 small thorns along inner margin of each orbit, ending about opposite middle of spiracle. End of snout covered with coarse prickles; smaller prickles over rostral process, on translucent areas in front of orbits and in space between orbits. A band of small thorns and coarse prickles extends along edge of disc beginning rearward from tip of snout by a distance about equal to that between spiracles, and ending a little in advance of alar thorns, being coarsest in the area opposite and a little posterior to the spiracles. No thorns in the scapular region. A median row of about 48 thorns beginning on tail opposite axils of pectorals and extending to first dorsal fin, of unequal sizes, some with points directed obliquely rearward, others with points broken or worn; a row of thorns low down on each side of the median row, beginning a little in advance of tips of pelvics and ending opposite second dorsal fin, 31 on the left and 34 on the right, those with points still intact directed rearward parallel, or nearly so, to axis of tail; 1 thorn between dorsals. Alar thorns prominent, in two to four rather regular rows, 43 on left side of disc, 38 on right, rest of body, pelvics and tail smooth, including dorsal fins and skin over eyes. A short row of 9 or 10 mucous pores in nuchal region on each side, parallel to midline, at a distance from it equal to about two-thirds length of orbit, the pores not ringed with dark as conspicuously as on *garricki*. Lower surface with prickles in front of and aside the mouth, densest toward end of snout and along margins of disc where they extend rearward about one-half the distance toward outer angle of pectoral; a few minute prickles scattered on disc between mouth and fifth pair of gill openings; rest of lower surface naked.

Snout in front of orbits 6 times as long as orbit, its length in front of mouth 2.2 times as great as distance between exposed nostrils. Distance between orbits about 1.6 times as great as length of orbit. Orbit 1.3 times as long as spiracle. Nasal curtain fringed; expanded posterior (outer) margin of nostrils smooth, without fringes. Upper and lower jaws strongly arched centrally. Teeth $\frac{36}{33}$, more nearly in longitudinal rows than in quincunx, with circular or ovate base, those in upper jaw in median sector of mouth with a prominent narrow upright cusp, the adjacent teeth pointing very slightly toward corner of mouth where the cusps become low triangular; lower teeth similar.

Distance between first gill openings 1.7 times as great as between exposed nostrils; between fifth openings 0.97 times; first gill openings 1.2 times as long as fifth and about 0.2 as long as breadth of mouth. First and second dorsals similar in size and perhaps in shape (second dorsal damaged). Interspace between dorsals 0.36 times as long as base of first dorsal. Second dorsal confluent with caudal membrane. Caudal membrane base equal to first dorsal base. Pelvics deeply concave, strongly scalloped along anterior side of excavation, moderately so rearward; anterior margin 0.74 times as long as distance from its own origin to rear tip of pelvic; anterior lobe slender, including four radial cartilages besides the first stout one; posterior lobe moderately convex, with a narrowly rounded tip, extending 0.36 times the distance from axil of pectorals toward first dorsal. Claspers reaching beyond tips of pelvics by a distance equal to seven-tenths the distance from front of orbits toward tip of snout.

Color. Upper surface brownish, without spots or other markings. Lower surface pale bluish-gray on disc, pelvics and claspers; tail pale brown; scattered black pores anterior to abdominal region, most numerous around mouth and in front of level of mouth to near tip of snout.

The other known specimen of this species, an immature male 1069 mm long, differs in the following respects. The disc is about 1.3 times as broad as long; maximum angle in front of spiracles 70°; axis of greatest breadth 70 per cent back from tip of snout toward axils of pectorals. The tail is relatively shorter, the distance from center of cloaca to its tip being 0.85 times the distance from center of cloaca to tip of snout. Because of the relatively shorter tail on the immature male, the snout is longer relative to total length (21.5 per cent to eye and 23.2 per cent to mouth opening, compared with only 17.4 and 18.5 per cent, respectively, for the mature male), the disc proportionately wider, and longer (76.5 per cent and 57.2 per cent, compared with 69.8 and 53.2 per cent, respectively, for the larger male). There are 5 small thorns along inner margin of each orbit and 1 or 2 immediately in front of orbit; fewer prickles on end of snout; and the anterior edge of the disc is smooth. The median row of thorns on tail numbers 31, the side rows 24 on the left and 22 on the right, these latter ending opposite first dorsal fin and there is no thorn between the dorsals. On the lower surface the prickles along the margins of disc extend rearward about three-fifths the distance toward outer angle of pectoral. The snout in front of orbits is 7 times as long as orbit, its length in front of mouth 2.5 times as great as distance between exposed nostrils. The jaws are less strongly arched and there are $\frac{38}{34}$ teeth, with low triangular cusps, only those near outer corners being slightly oblique.

The second dorsal, which is undamaged on this specimen, is similar to the first in shape but with a slightly shorter base and the interspace between the dorsals is relatively shorter, being about 0.14 times as long as the base of first dorsal. The anterior margin of the pelvic is almost as long as the distance from its own origin to rear tip of pelvic and the posterior lobe extends 0.31 times the distance from the axils of pectorals toward first dorsal. The claspers fail to reach the tips of the pelvics by a distance equal to length of fifth gill opening.

Known only from the offing of Cape San Blas, Florida, in 205-260 fathoms. Named in recognition of the fishery explorations of U. S. Fish and Wildlife Service vessel ''Oregon'' in the Gulf of Mexico and the Caribbean Sea.

RAJA GARRICKI sp. nov.

Figures 5, 6, 7

Study Material. Mature male, 975 mm in total length, holotype, U. S. Nat. Mus. No. 156711, and another male 1019 mm in total length, paratype, M. C. Z. No. 39616, both from the northern part of the Gulf of Mexico, Lat. 28°32′N, Long. 86°20′W, in 260 fathoms, ''Oregon'' station 1277.

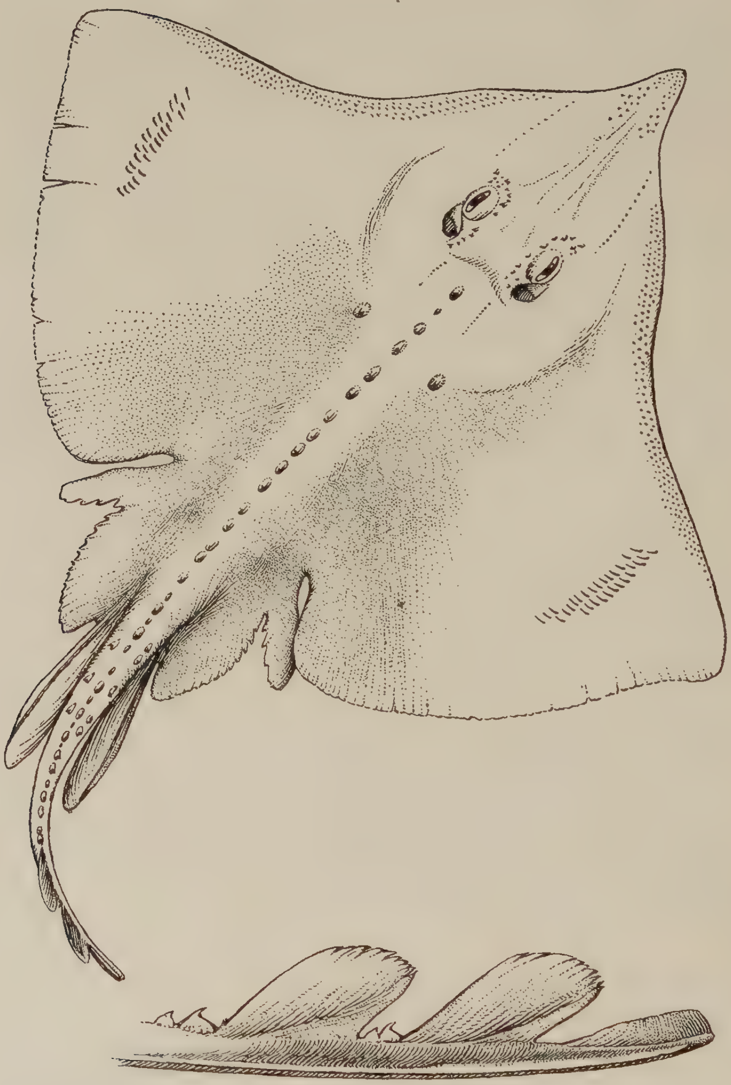

Figure 5. *Raja garricki,* dorsal view of type, mature male 975 mm long; end of tail showing dorsal fins and caudal fin, about x 0.5.

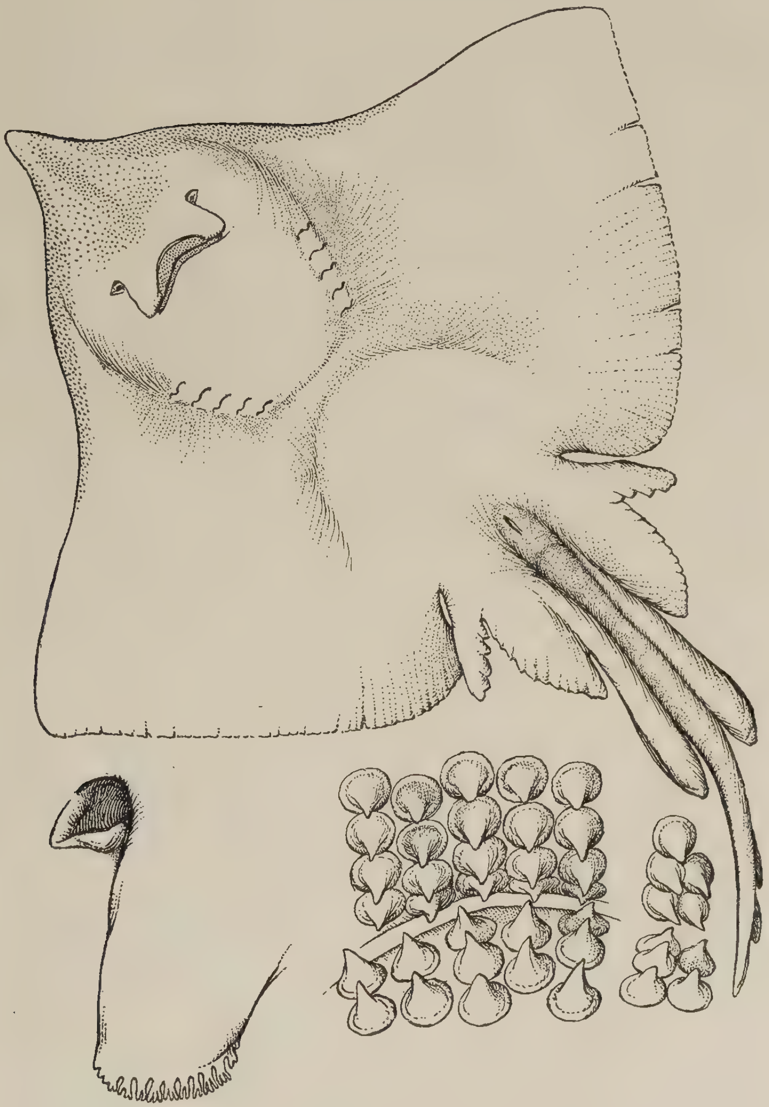

Figure 6. *Raja garricki*, ventral view of specimen shown in Figure 5; right hand nostril and nasal curtain, about x 1; upper and lower teeth from center and from near outer part of jaws, about x 2.4.

Distinctive Characters. Characters in combination which distinguish *garricki* from other species of the genus *Raja* are: margins of disc anterior to outer angles of pectorals sinuous (at least in the males, the female has not been seen); snout pointed (Fig. 5); disc with a single row of large thorns along the midbelt extending from the nuchal region to the first dorsal fin, with an interrupted row on either side on the tail; a single large scapular thorn on each side of the midrow; lower surface with dark mucous pores anterior to the abdominal region (Fig. 7).

Comparison with previously known species. The only western Atlantic skates with a disc somewhat the shape of *garricki* and with dark pores on the under surface are *laevis, oregoni, flavirostris, platana* Günther 1880 and *agassizi* Müller and Henle 1841. But *garricki* differs from all of these (excepting some specimens of *agassizi*) by having a continuous row of thorns along the mid-line of disc and tail, extending from the nuchal region to the dorsals whereas the midrow of thorns on the above mentioned species does not extend much, if any, forward beyond the axils of the pectorals. And *garricki* may be distinguished from *agassizi* by the position of its first dorsal which originates much nearer to tip of tail than to tips of pelvics (nearer pelvics than tip of tail on *agassizi*) and by a dorsal fin interspace much shorter than base of either first or second dorsal. Also, the dark pores on the under surface of *garricki* are much more conspicuous and more numerous than on *agassizi.*

In the eastern Atlantic, including southern Africa, only *batis* and *oxyrhynchus* have a narrow snout together with dark pores below, and both of these lack the thorns along the midline of the disc that are present on *garricki.*

Garricki falls with *rhina* and *flavirostris* of the eastern Pacific in general shape of disc and in the presence of dark pores below. But *garricki* differs in spination from *rhina* by having scapular thorns and a single row of midline thorns on the disc but no additional small thorns in the midzone. *Flavirostris* has one nuchal thorn but no other midline thorns on disc.

Garricki somewhat resembles *lemprieri* Richardson 1844-48, *porosa* Günther 1874, and *australis* Macleay 1884 in the Indo-Australian region in having a narrow snout and dark pores

(Munro 1956, p. 15) on the lower surface but its row of thorns along the midzone of disc sets it apart from these species which lack thorns in this area and from *gudgeri* Whitley 1940 which has but a very short row along the middle of the back as well as a very long and narrow snout resembling that of *oxyrhynchus*. *Garricki* closely resembles *macracauda* Ishiyama 1955 from Japan in shape of disc and in having dark pores below but, except for 2 nuchals, *macracauda* lacks thorns along the midline of disc and has no scapular thorns.

Description of holotype. Proportional dimensions in per cent of total length:

Disc. — Extreme breadth 78.3; length 59.0.

Snout length. — In front of orbits 18.3; in front of mouth 19.0.

Orbits. — Horizontal diameter 3.5; distance between 5.4.

Spiracles. — Length 3.1; distance between 6.9.

Mouth. — Breadth 8.5.

Exposed nostrils. — Distance between inner ends 9.1.

Gill openings — Length, 1st 1.5; 3rd 1.8; 5th 1.5; distance between inner ends, 1st 15.7; 5th 9.4.

First dorsal fin. — Vertical height 2.8; length of base 4.0.

Second dorsal fin. — Vertical height 2.6; length of base 3.7.

Pelvics. — Anterior margin 10.6.

Distance. — From tip of snout to center of cloaca 55.4; from center of cloaca to 1st dorsal 30.7, to tip of tail 44.6; from rear end of 2nd dorsal base to tip of tail 5.0.

Interspace between. — 1st and 2nd dorsals 1.2.

Disc about 1.3 times as broad as long, maximum angle in front of spiracles about 78°; anterior margins weakly concave just posterior to tip of snout, thence slightly convex followed by a stronger concavity culminating about midway between tip of snout and outer corners which are sharply rounded; posterior margins at first about straight from outer corner, then gently rounded, as is inner margin. Axis of greatest breadth about 62 per cent of distance back from tip of snout toward axils of pectorals. Tail with a narrow lateral fold, low down on each side, beginning abruptly in advance of tips of pelvics by a distance equal to about three-fourths the interorbital width and continuing almost to extreme tip of tail, widest opposite dorsals and caudal membrane; length of tail from center of cloaca to origin of first dorsal fin 0.56 times as great, and to its tip 0.80 times as great, as distance from center of cloaca to tip of snout.

A patch of 11 small thorns immediately in front of left orbit and 7 in front of right followed by a row of 7 or 8 larger thorns along inner margins of orbits ending slightly posterior to rear margins of spiracles. End of snout densely covered with small thorns and prickles extending rearward over rostral process in diminishing numbers; a band of small thorns and prickles extends along edge of disc from tip of snout to about opposite foremost alar thorns, narrow near end of snout, then widening and the prickles coarsening half way from snout to opposite orbits, again smaller rearward. A single stout thorn on each side of median row in scapular region; a median row of prominent thorns from nuchal region to first dorsal fin, of which 4 are in the nuchal-scapular area, the second of these being very small, followed by 32 thorns of which 7 are anterior to pectoral axil and 25 on tail, these latter somewhat closer together and more uneven in size; a row of 3 large thorns aside the median row on left side of the mid-tail region and 5 on the right side, unevenly spaced; 2 prominent thorns between dorsal fins. All the thorns on body and tail that have retained their sharp points are directed obliquely rearward. Alar thorns prominent, in two to three irregular rows, 26 on left side of disc, 30 on right; rest of body, pelvics and tail smooth as is space between orbits and skin over eyes; first and second dorsals with a few scattered prickles.

A short longitudinal row of 11 dark pigmented mucous pores on the right side of first nuchal thorn and of 8 on the left side, at a distance from the midline about two-thirds as great as diameter of orbit. The presence of mucous pores, in a conspicuous pattern in this region, has thus far been found only on *Raja fyllae* Lütken 1887, *laevis* and in the new species *oregoni* and *clarkii* among skates known from the western North Atlantic. (See Bigelow and Schroeder, 1954, p. 57.)

Lower surface with prickles in front of and aside the mouth, most dense toward end of snout and along margins of disc where they extend rearward about three-fifths the distance toward outer angle of pectoral; a few exceedingly small widely scattered prickles over parts of the scapular and abdominal regions and on pelvics; rest of lower surface naked.

Snout in front of orbits 5.2 times as long as orbit, its length in front of mouth 2.1 times as great as distance between exposed nostrils. Distance between orbits about 1.6 as great as length of orbit. Orbit 1.1 as long as spiracle. Nasal curtain fringed; expanded posterior (outer) margins of nostrils smooth, without fringes. Upper and lower jaws strongly arched centrally. Teeth $\frac{35}{35}$ more nearly in quincunx arrangement than in longitudinal rows, with circular or ovate base, those in upper jaw in median sector of mouth with a prominent upright cusp, the adjacent teeth with cusps pointing toward corner of mouth, those near corners of mouth with flattened crowns; lower teeth similar but median teeth with cusps at slight angle, which increases outwardly.

Distance between first gill openings 1.7 times as great as between exposed nostrils; between fifth openings 1.0 times; first gill openings 1.1 times as long as fifth and about 0.2 as long as breadth of mouth. First and second dorsals similar in size and shape. Interspace between dorsals 0.33 as long as base of first dorsal. Caudal membrane base equal to that of first dorsal. Pelvics deeply concave, strongly scalloped along anterior side of excavation, moderately so rearward; anterior margin 0.58 as long as distance from its own origin to rear tip of pelvic; anterior lobe slender, including four radial cartilages beside the first stout one; posterior lobe moderately convex, with a narrowly rounded tip, extending about one-half the distance from axil of pectorals toward first dorsal. Claspers reaching beyond tips of pelvics by a distance equal to seven-tenths the distance from front of orbits toward tip of snout.

Rostral cartilage firm, extending nearly to tip of snout. Anterior pectoral rays reaching about three-sevenths the distance from front of orbits toward tip of snout.

Color. Upper surface plain brownish without spots or other markings. Lower surface pale bluish dusky on disc, pelvics and claspers, tail tending more to pale brownish. Scattered black pores anterior to abdominal region, most numerous around mouth and in front of level of mouth to near tip of snout. (Fig. 7.)

The other known specimen of this species, a male 1019 mm long, differs as follows: maximum angle of disc in front of spiracles 74°, axis of greatest breadth about 67 percent of distance back from tip of snout toward axils of pectorals; length of tail from center of cloaca to origin of first dorsal fin is 0.53 times as great and to its tip 0.78 times as great as from center of cloaca to tip of snout. There is a patch of 8 small thorns along anterior edge of each orbit; fewer prickles over rostral process which is naked toward orbits; 5 thorns in the mid row in the nuchal-scapular area, followed by 41 thorns to first dorsal, of which 8 are anterior to pectoral axils and 33 are on tail; a row of 5 unevenly spaced large thorns on left side of tail aside the median row, 2 on right; 31 alar thorns on left and 33 on right side of disc. The mucous pores in nuchal region are in a series of 9 on each side. On the lower surface the prickles along the anterior margin of disc extend less than halfway toward outer angle of pectoral.

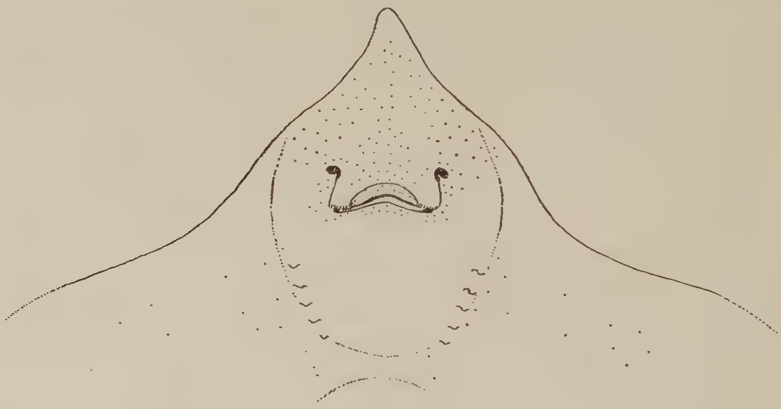

Figure 7. *Raja garricki,* ventral view of head to show dark mucous pores, about x 0.1.

Known only from the offing of Cape San Blas, Florida, in 260 fathoms. Named for Dr. J. A. F. Garrick of Victoria University College, Wellington, in recognition of his work on elasmobranchs of New Zealand.

RAJA CLARKII sp. nov.

Figures 8, 9

Study Material. Immature male, 665 mm in total length, holotype, U. S. Nat. Mus. No. 156712, another male 580 mm long, and a female 747 mm long, paratypes, M. C. Z. No. 39618, all from the northern part of the Gulf of Mexico, Lat. 28°32′N, Long. 86°20′W, in 260 fathoms, "Oregon" station 1277.

Diagnostic Features. The presence of 1 to 3 pairs of prominent white roundish or barlike markings on the upper surface of disc in combination with a broad snout and a band of formidable and very sharp thorns which extend along the lower surface from the tip of snout almost to the extreme outer margin of pectorals sets off *clarkii* from all other known members of the Rajidae.

Description of holotype. Proportional dimensions in per cent of total length:

Disc. — Extreme breadth 68.7; length 55.0.

Snout length. — In front of orbits 14.2; in front of mouth 15.3.

Orbits. — Horizontal diameter 3.2; distance between 3.6.

Spiracles. — Length 3.3; distance between 6.0.

Mouth. — Breadth 8.7.

Exposed nostrils. — Distance between inner ends 4.5.

Gill openings. — Length, 1st 1.2; 3rd 1.6; 5th 1.3; distance between inner ends, 1st 14.9; 5th 8.9.

First dorsal fin. — Vertical height 1.7; length of base 4.3.

Second dorsal fin. — Vertical height 1.7; length of base 4.3.

Pelvics. — Anterior margin 11.7.

Distance. — From tip of snout to center of cloaca 53.4; from center of cloaca to 1st dorsal 34.6; to tip of tail 46.6; from rear end of 2nd dorsal to tip of tail 3.2.

Interspace between. — 1st and 2nd dorsals 0.6.

Disc about 1.25 times as broad as long; outline of snout as in Figure 8; anterior margin rather strongly convex in front of orbits, thence concave with outer corners broadly rounded; posterior and inner margins gently rounded. Axis of greatest breadth about 70 per cent of distance back from tip of snout

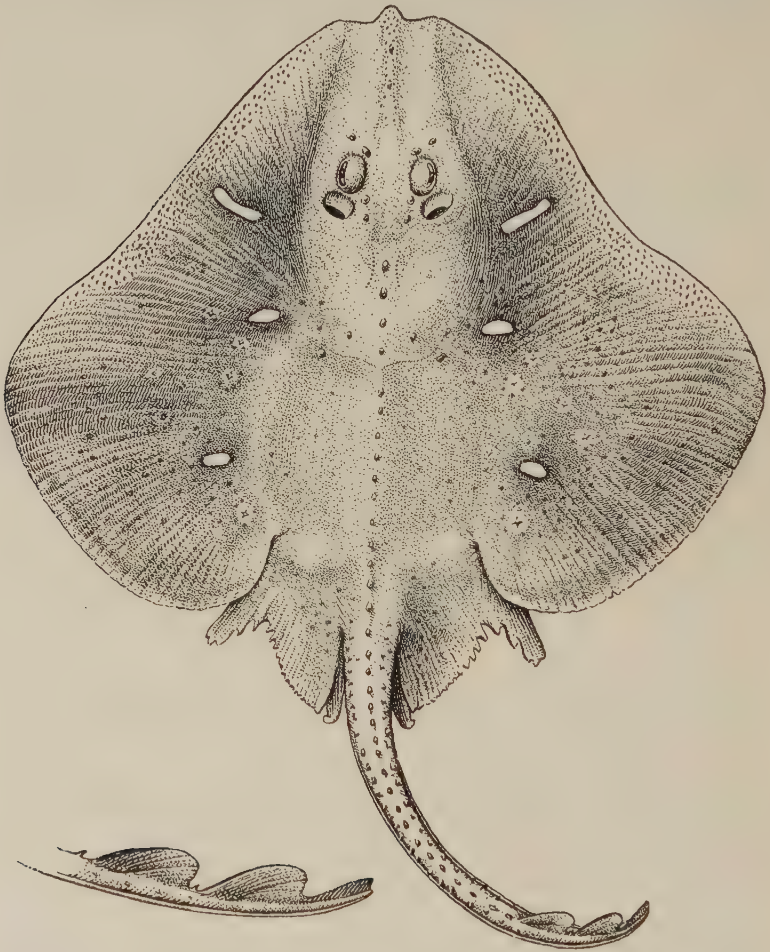

Figure 8. *Raja clarkii,* dorsal view of type, immature male 665 mm long; end of tail showing dorsal fins and caudal fin, about x 0.5.

to axils of pectorals. Tail with a narrow lateral fold, low down on each side, beginning just beyond tips of pelvics and continuing almost to extreme tip of tail, widening posteriorly, widest opposite dorsals; length of tail from center of cloaca to origin of first dorsal fin 0.65 times as great and to its tip 0.87 times as great as distance from center of cloaca to tip of snout.

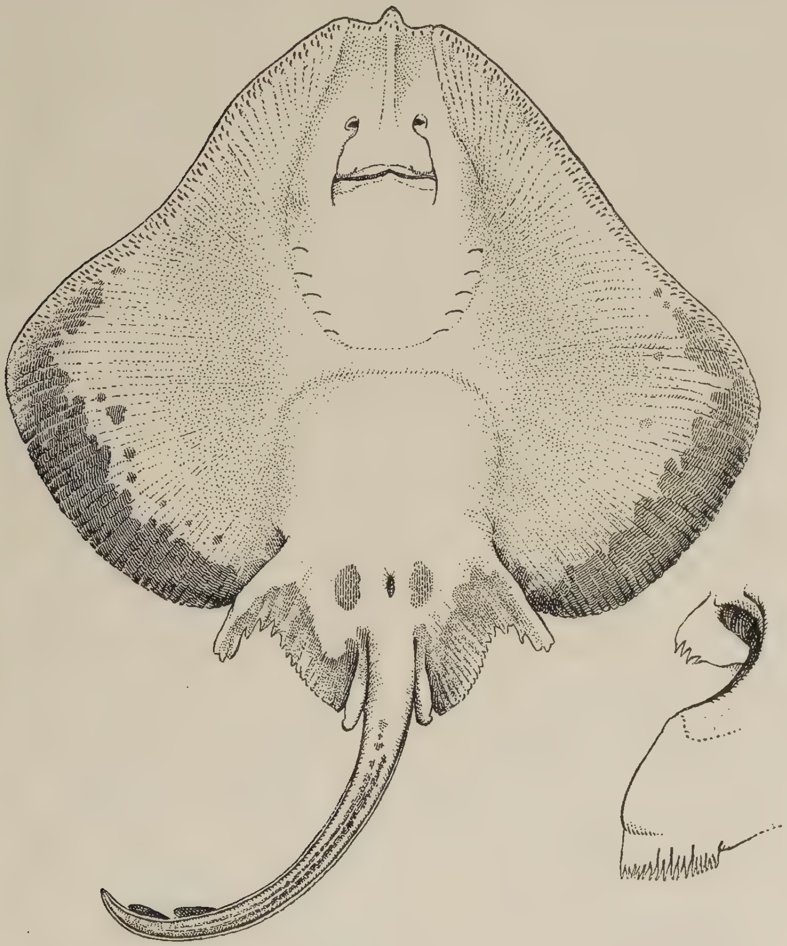

Figure 9. *Raja clarkii,* ventral view of specimen shown in Figure 8; right-hand nostril and nasal curtain, about x 1.1.

A small thorn in advance of each orbit by a distance of about ⅓ orbit's diameter; a larger thorn immediately next to inner anterior edge of orbit, with one at posterior end of orbit and another smaller one inward toward median line, this last opposite rear end of spiracle. Snout and disc in front of orbits and space between orbits with small thorns, many with stellate bases, and with prickles; two stouter thorns over rostral process, located 27 and 47 per cent, respectively, in the distance from tip of snout toward orbits; a band of small thorns extends along edge of disc from near tip of snout to about opposite scapular region. A triangular patch of three thorns on each side of median row in scapular region; a median row of 34 thorns from nuchal region to first dorsal, of which 4 are in the nuchal-scapular area, followed by 7 anterior to pectoral axils and by 23 on tail, all of these of about equal size and equally spaced; a row of thorns on each side of the median row beginning about opposite axils of pelvics and continuing to opposite first dorsal, many with sharp hooked points directed rearward; 1 thorn between dorsals. Alar thorns not yet exposed; rest of disc with scattered prickles, very sparse in some areas and mostly minute; also small thorns and prickles on tail in addition to the three prominent rows, mostly low down, from near axils of pelvics nearly to tip of tail; pelvics smooth; dorsals with an occasional prickle. A longitudinal row of 12 dark ringed mucous pores on right side and 13 on left outward from first nuchal thorn by a distance about one-third the diameter of orbit.

Lower surface with prickles along rostral process out to tip of snout with a few scattered over translucent area in front of nostrils; also a band of strong, very sharp thorns all of about the same size, curving inward or obliquely rearward, extending from near end of snout almost to outer angle of pectoral, in a band about 0.4 times as wide as distance between orbits, these characters in combination being a striking feature of this species; rest of lower surface smooth.

Snout in front of orbits 4.4 times as long as orbit, its length in front of mouth 3.4 times as great as distance between exposed nostrils. Distance between orbits about 1.1 as great as length of orbit. Orbit about the same length as spiracle. Nasal curtain fringed; expanded posterior (outer) margins of nostrils with a few fringes. Upper and lower jaws moderately arched. Teeth $\frac{63}{61}$, in part in longitudinal rows and in part more or less in quincunx, with rounded base and triangular cusp, inclined toward corners of mouth.

Distance between first gill openings 3.3 times as great as distance between exposed nostrils; between fifth openings 2.0 times; first gill openings about as long as fifth and about 0.14 as long as breadth of mouth. First and second dorsals similar in size and shape. Interspace between dorsals 0.14 as long as base of first dorsal. Caudal membrane with base a little shorter than that of first dorsal base. Pelvics deeply concave, strongly scalloped along anterior side of excavation, moderately so rearward; anterior margin 0.78 as long as distance from its own origin to rear tip of pelvic; anterior lobe slender, including four radial cartilages besides the first stout one; posterior lobe moderately convex, with a narrowly rounded tip, extending a little less than half the distance from axils of pectorals toward first dorsal. Claspers reaching beyond tips of pelvics by a distance equal to less than half diameter of orbit.

Rostral cartilage firm, extending nearly to tip of snout. Anterior pectoral rays reaching anterior edge of disc but falling short of end of rostral cartilage which continues into snout protuberance.

Color. Upper surface pale brown with darker punctulations scattered over disc, pelvics and more or less of tail. Three pairs of prominent white markings on disc, of which one pair is opposite spiracles, bar-like, somewhat curved, and a little longer than interorbital space; a second pair about half as long and opposite scapular region and a little closer together than first pair; a third pair about size of second pair, in line with first pair and opposite eighth thorn from nape in median series. Lower surface white with a wide irregular grayish band along posterior and inner margins, extending from a little in advance of outer angles to axils of pectorals and along rear margin of pelvics; also a pair of grayish spots opposite cloaca and a few small ones here and there on disc, with some gray markings on tail and on claspers.

The other two known specimens of this species, a male 580 mm long and a female of 747 mm agree very closely with the holotype in proportional dimensions and in the formidable band of sharp thorns on the under surface along the anterior margin of the disc. The chief differences are as follows. They have a disc 1.2 times as wide as long, and 65.3 and 65.0 per cent, respectively, of the total length of the specimens, as compared with 1.25 times as wide and 68.7 per cent as long as the holotype, while the length of tail from center of cloaca to origin of dorsal fin is 0.69 times as great and to its tip 0.90 times as great as distance from center of cloaca to tip of snout on both specimens as compared with 0.65 and 0.87 times, respectively, on the holotype. The two thorns over the rostral process on the 580 mm male are located 34 and 58 per cent in the distance from tip of snout to orbits while the 747 mm female has three such thorns located 23, 44, and 60 per cent in this distance. There are 40 thorns in the median row on the 580 mm male of which 28 are posterior to the pectoral axil, and there are 38 thorns on the 747 mm female of which 27 are posterior. The mucous pores number 9 on one side and 11 on the other on the smallest skate and 14 on each side of the largest which also has more numerous prickles on lower surface over the translucent area in front of nostrils than on the other two specimens. The tooth count of the 580 mm male is $\frac{61}{59}$, and of the 747 mm female $\frac{60}{60}$.

The upper surface of the female has the three pairs of prominent white markings of about the same relative size and location as on the holotype but below there are no gray spots in the cloacal region while there is an oval gray spot on each side of the rostral process near its tip. The small male has only one pair of white spots above, opposite the spiracles, roundish, and about half the size of the orbit.

Known only from the northern part of the Gulf of Mexico, Lat. 28°32′N, Long. 86°20′W, in 260 fathoms. Named for Robert S. Clark in recognition of his revision of European skates and rays.

Cruriraja rugosa sp. nov.

Figures 10, 11

Study Material. Immature male, 367 mm in total length, holotype, U. S. Nat. Mus. No. 156713 from the northeastern part of the

Gulf of Mexico, in 200-300 fathoms, trawled by the "Oregon," station number not known.

Distinctive Characters. Cruriraja rugosa differs from all other known members of its genus in that the under side of its tail is covered with minute prickles, this area being smooth in all other species.

Comparison with previously known species. From other western Atlantic species it differs as follows: from *atlantis* Bigelow and Schroeder 1948, by the short space between its dorsals, equal to about one-fourth the length of first dorsal base (about 2½ times the dorsal base on *atlantis*); from *poeyi* Bigelow and Schroeder 1948, by its prickles on disc, the presence of two nuchal thorns and of a single row of thorns on the midline of tail (disc without prickles, no nuchal thorns, midline row of thorns on tail divides into two rows posteriorly on *poeyi*). It differs from the two species of *Cruriraja* known from South Africa, as follows: from *parmomaculata* (von Bonde and Swart 1924, p. 9, pl. 21, fig. 2) in having a wide space lacking thorns along the midline of disc between the 2 nuchal thorns and axils of pectorals, by lacking scapular thorns, and by its plain coloration (*parmomaculata,* described from a young specimen 181 mm in total length, has a continuous row of thorns from the nuchal region to the first dorsal, 1 scapular thorn on each side and 14-18 blackish brown spots of varying size on the disc). *Rugosa* with its widely interrupted row of thorns along the midline of back, its lack of thorns in the scapular region and the rounded rear margins of its dorsal fins may be readily distinguished from *durbanensis* (von Bonde and Swart 1924, p. 11, pl. 22, fig. 1) which has an uninterrupted row of thorns along the midline of back from nape of first dorsal on a male 232 mm long, 2 scapular thorns on each shoulder and dorsal fins which are pointed posteriorly; and on a female 311 mm long the midrow of thorns ends about halfway along tail, leaving a wide thornless space before first dorsal.

Description of holotype. Proportional dimensions in per cent of total length:

Disc. — Extreme breadth 59.4; length 46.0.

Snout length. — In front of orbits 12.0; in front of mouth 15.0.

Orbits. — Horizontal diameter 4.5; distance between 2.8.

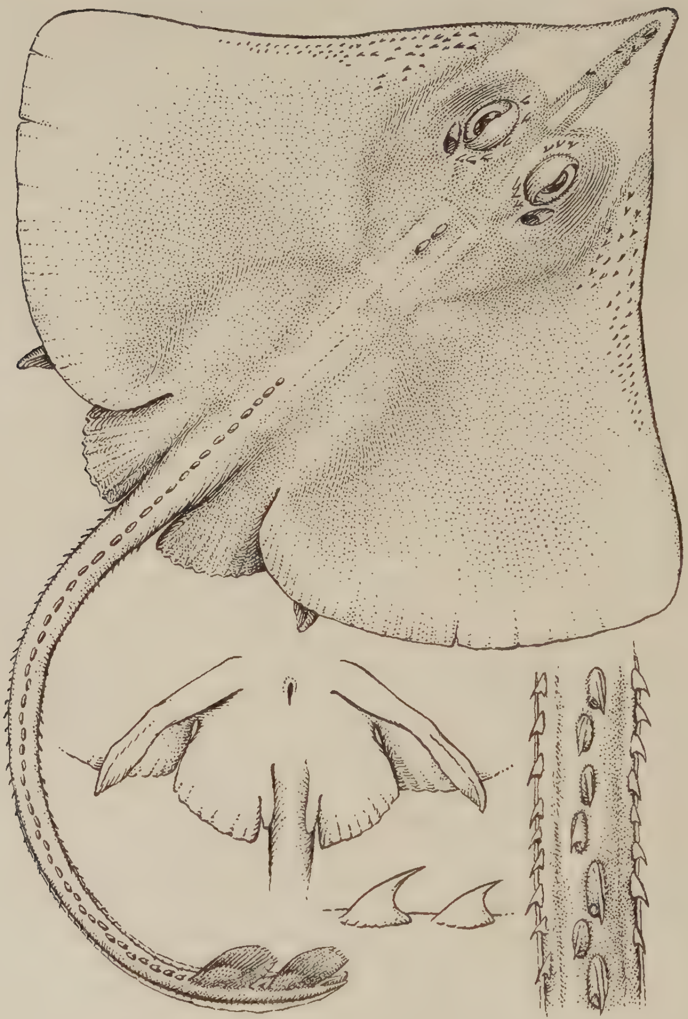

Figure 10. *Cruriraja rugosa*, type, immature male 367 mm long; pelvic fins about x 0.5; section of tail about x 2; first 2 thorns in front of dorsal fin about x 3.

Spiracles. — Length 2.2; distance between 6.5.

Mouth. — Breadth 6.3.

Exposed nostrils. — Distance between inner ends 5.5.

Gill openings. — Length, 1st 1.5; 3rd 1.5; 5th 1.2.

First dorsal fin. — Vertical height 2.7; length of base 4.5.

Second dorsal fin. — Vertical height 2.6; length of base 3.3.

Pelvics. — Length of limb 15.0.

Distance. — From tip of snout to center of cloaca 40.6; from center of cloaca to 1st dorsal 48.0; to tip of tail 59.4; from rear end of 2nd dorsal base to tip of tail 2.5.

Interspace between. — 1st and 2nd dorsals 1.1.

Disc about 1.3 times as broad as long, maximum angle in front of spiracles about 87°; anterior margins from snout to outer corners of pectorals slightly sinuous, the corners abruptly rounded; posterior and inner margins gently rounded. Axis of greatest breadth about 70 per cent of distance back from tip of snout to axils of pectorals. Tail with a lateral fold, low down on each side beginning about 55 per cent of the distance from straight. Teeth $\frac{43}{42}$, arranged in quincunx, with ovate base and axils of pelvics toward tip of tail, very narrow anteriorly but widening considerably on approaching tip of tail; length of tail from center of cloaca to origin of first dorsal 1.2 times as great and to its tip 1.45 times as great as distance from center of cloaca to tip of snout.

Inner margin of left orbit with 6 thorns, 2 of which are anterior, 1 midway and 3 posterior; right orbit with 3 anterior and 3 posterior thorns, the last two in each case being opposite the spiracles. A staggered row of 4 thorns on anterior part of rostral process followed by a pair of rostral thorns a little more than half the distance from tip of snout toward a line connecting anterior margins of orbits; a band of sharp, backward pointing thorns along margins of disc, beginning opposite anterior edge of orbits and ending about opposite scapular region, the thorns decreasing in size and the band narrowing posteriorly. Two prominent nuchal thorns followed by a naked area and then by a midrow of 47 thorns beginning about 1½ eye's diameter in advance of axils of pectorals and continuing uninterrupted to first dorsal fin, becoming staggered posteriorly, but in a single row; an additional row of smaller thorns each side of the midrow, low down on tail, beginning about opposite tips of pelvics and extending nearly to first dorsal where it merges with a band of prickles; all the tail thorns pointing strongly rearward; a single thorn between dorsals. Upper surface of disc (including skin over eyes) covered with minute prickles except along posterior margins and on extreme tip of snout; pelvics naked; tail prickly, everywhere except along the midzone; dorsals densely prickly. Lower surface of disc entirely smooth, but tail covered with minute prickles from about opposite tips of pelvics to opposite origin of second dorsal.

Snout in front of orbits 2.8 times as long as orbit, its length in front of mouth about 2.7 times as great as distance between exposed nostrils. Distance between orbits 0.65 times as great as length of orbit. Orbit twice as long as spiracle. Nasal curtain with a very short, blunt fringe, expanded outer margins of nostrils smooth, without fringes. Upper and lower jaws nearly short triangular cusp.

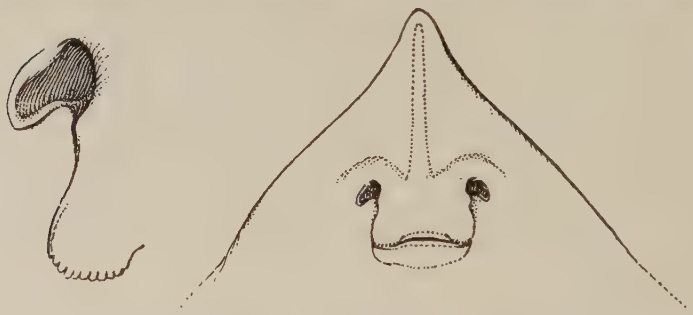

Figure 11. *Cruriraja rugosa,* ventral view of head, about x 0.5; right-hand nostril and nasal curtain, about x 2.

Distance between first gill openings twice as great as distance between exposed nostrils; between fifth openings about 1.2 times; first to fourth gill openings about 1.3 times as long as fifth and about 0.25 as long as breadth of mouth. First and second dorsals similar in shape the first slightly the larger. Interspace between dorsals 0.25 times as long as base of first dorsal. Caudal fin very small. Anterior division of pelvics long and slender reaching beyond tips of posterior lobe when pulled back; posterior lobe with 12 rays, quadrate, the rear margin gently rounded and faintly scalloped, the tips reaching but little beyond rear margin of disc. Claspers failing to reach tips of pelvics by a distance equal to half the diameter of eye.

Rostral cartilage firm, narrow, extending nearly to tip of snout. Anterior pectoral rays reaching 22 per cent the distance from front of orbits toward tip of snout.

Color. Upper surface of disc brownish with a bluish tinge, without spots or other markings; tail pale brownish; dorsal brownish with a pale area basally. Below pale bluish on disc, the tail pale brown.

Known only from a single specimen, an immature male 367 mm long, trawled in 200-300 fathoms in the northeastern part of the Gulf of Mexico.

REFERENCES

BARNARD, K. H.

1925. A monograph of the fishes of South Africa. Part I. Ann. S. African Mus., vol. 21, part 1, pp. 1-418, 18 figs.

BIGELOW, H. B. AND W. C. SCHROEDER

1948. New genera and species of batoid fishes. Jour. Mar. Res., vol. 7, no. 3, pp. 543-566, 9 figs.

1951. Three new skates and a new chimaerid fish from the Gulf of Mexico. Jour. Washington Acad. Sci., vol. 41, no. 12, pp. 383-392, 4 figs.

1953. Fishes of the western North Atlantic. Mem. Sears Found. Mar. Res., no. 1, part 2, x + 588 pp., 127 figs.

1954. Deep water elasmobranchs and chimaeroids from the northwestern Atlantic Slope. Bull. Mus. Comp. Zool., vol. 112, no. 2, pp. 37-87.

BONAPARTE, CHARLES LUCIEN

1832-1841. Iconografia della fauna Italica . . ., vol. 3, Pesci, 78 pls. (not numbered) and accompanying text (pages not numbered). For dates of publication see Salvadori, Boll. R. univ. Mus. Zool. Anat. Comp., Turin, vol. 3, no. 48, 1888.

CLARK, R. S.

1926. Rays and skates — Sci. Invest. Fisher. Board Scotland, 1926, no. 1, 66 pp., atlas, 36 pls.

GARMAN, SAMUEL

1913. The Plagiostomia (sharks, skates and rays). Mem. Mus. Comp. Zool., vol. 36, xiii + 515 pp., and atlas, 75 pls.

GÜNTHER, ALBERT

1874. Third notice of a collection of fishes recently obtained by Mr. Swinhoe in China, Ann. Mag. Nat. Hist., ser. 4, vol. 13, pp. 154-159.

1880. Report on the shore fishes — "Challenger" Rept. Zool., vol. 1, part 6, 82 pp., 32 pls.

ISHIYAMA, REIZO

1955. Studies on the rays and skates belonging to the family Rajidae, found in Japan and adjacent regions. Jour. Shimonoseki College of Fisheries, vol. 4, no. 1, pp. 43-51.

JORDAN, D. S. AND C. H. GILBERT

1880. Description of a new species of ray, *Raia rhina,* from the coast of California. Proc. U. S. Nat. Mus., vol. 3, pp. 251-253.

LACÉPÈDE, B. G. E.

1803. Histoire Naturelle Poissons, vol. 11, 399 pp., 3 pls.

LINNAEUS, C.

1758. Systema Naturae, 10th ed., Holmiae, vol. 1, 824 pp.

LÜTKEN, C. F.

1887. Korte Bidrag til Nordisk ichthyographi. 4. Vidensk. Medd. naturh. Foren. Copenhagen, pp. 1-4, pl. 1.

MACLEAY, WILLIAM

1884. Some results of trawl fishing outside Port Jackson. Proc. Linn. Soc. N. S. Wales, vol. 8, pp. 457-462.

MITCHILL, S. L.

1817. Memoir on ichthyology — Amer. Monthly Mag. Crit. Rev., vol. 2, pp. 321-328.

MÜLLER, JOHANNES AND F. G. J. HENLE

1841. Systematische Beschreibung der Plagiostomen. Berlin, xxii + 200 pp., 60 pls.

MUNRO, IAN S. R.

1956. Handbook of Australian fishes. *In:* Fisheries Newsletter, vol. 15, no. 9, 32 pp. Canberra.

NORMAN, J. R.

1937. Coast fishes. Part II. The Patagonian region. Discovery Reports, vol. 16, pp. 1-150, pls. 1-5.

PHILIPPI, R. A.

1892. Algunos pecos de Chile. An. Mus. Nac. Chile, sec. 1, Zool., 16 pp., 6 pls.

REY, LUIS LOZANO

1928. Fauna Iberica. Peces, vol. 1, 690 pp., 20 pls. Inst. Nac. Ciencias, Madrid.

RICHARDSON, JOHN

1844. Zoology . . . . H. M. S. ''Erebus'' and ''Terror'', part 7, Fishes.
1848. 139 pp., 60 pls. London.

SMITH, J. L. B.

1949. The sea fishes of southern Africa, 550 pp., 1232 figs., 103 pls. Central News Agency, S. Africa.

TANAKA, S.

1916. A new species of Japanese fish. (In Japanese.) Dobwts. Zool., Tokyo, vol. 28, pp. 313-314.

THOMPSON, W. W.

1914. Catalogue of fishes of the Cape Province. Mar. Biol. Report, Prov. Cape of Good Hope, no. 2, pp. 132-167.

VON BONDE, C. AND D. B. SWART

1924. The Platosomia (skates and rays) collected by the S. S. ''Pickle''. Rep. 3, Fish. Mar. Biol. Surv., S. Africa (1922), Spec. Rept. 5, 22 pp., pls. 20-23.

WHITLEY, G. P.

1940. The fishes of Australia. Part I. Royal Zool. Soc. New South Wales, 280 pp.

Contribution No. 933

On the Transient Response of a β-plane Ocean*

G. VERONIS**

1. Introduction

In addition to inertio-gravity waves two mechanisms exist in the ocean for the propagation of large scale disturbances. The first is that of horizontal divergence which occurs together with a change in the free surface height. (This mechanism is necessary also for the generation of inertio-gravity waves). The second mechanism is due to the variation of the coriolis parameter—the so-called β-effect. The transient nature of the latter mechanism can be seen from the following example.

Suppose that a rotationally symmetric (cyclonic) wind begins to blow over the water surface. Locally the ocean will respond in such a way as to come to equilibrium with the stress acting on the surface. Initially, therefore, the sea surface will assume a rotationally symmetric slope with the low point in the center. With non-uniform rotation the water in the northern part of the region will travel slower than the water in the southern section. Water will converge in the eastern part and diverge in the region west of the center. Hence, an additional re-distribution of mass is necessary to bring the system to equilibrium. The system is unsteady because the non-uniformity of rotation requires a finite time to manifest itself.

It is the purpose of this paper to investigate the effects of the above mechanisms for the case of an ocean which is rotating non-uniformly and which is subjected to a localized wind stress. The analysis is carried out on the β-plane (as introduced by ROSSBY (1939), i.e., the coriolis force is considered to be a linear function of latitude when differentiated but it is taken to be constant when undifferentiated. Inertio-gravity waves are neglected and attention is directed toward the quasi-geostrophic response only. The last restriction is made for both mathematical and physical simplicity. VERONIS and STOMMEL (1956)* have shown that inertio-gravity waves are unimportant in the energetics of the system when the time scale is longer than a half-pendulum day.

In the present paper as in previous ones the ocean is assumed to be infinite in the horizontal, i.e., no lateral boundaries are included. Such a restriction limits the validity of the analysis to a time scale comparable to that which is required for a barotropic ROSSBY wave to reflect from a boundary and interact with other waves. The difficulties which are encountered when boundaries are included are realized very quickly when one attempts to solve the problem of a bounded, frictionless, β-plane ocean, subjected to a wind stress which is zonally uniform and varies sinusoidally in latitude and in time. If the period of the wind stress variation is large, the assumed width of the ocean becomes critical. The reason for this critical dependence on the exact width of the ocean is that barotropic ROSSBY waves have a period of a few days for systems of oceanic scale and resonance occurs for any systems which allows an integral number of ROSSBY wave periods to occur for each period of the wind stress. The difficuly is clearly a mathematical one and is partly due to the fact that friction is neglected. However, since friction is probably not important in the dispersion of large scale disturbances from a localized wind stress, it will be neglected here along with boundary effects.

Finally, a note must be added about the value of the present investigation. Although general analytical solutions to arbitrary forcing functions are often desirable, the useful-

---

* Received Jan. 13, 1958. Contribution no. 933 from the Woods Hole Oceanographic Institution.

** Woods Hole Oceanographic Institution.

* Hereafter referred to as AVS.

ness of such solutions are determined by the facility with which they can be applied to actual situations. Unfortunately, the mathematical complexity of the present solution renders it practically useless. One must impose severe restrictions on the system to derive even a qualitative result. Perhaps the principal justification for presenting this study is that several other investigators have expressed an interest in pursuing a similar course. The horrendous computational problem which faces them is given in the final solution.

2. Mathematical model

Consider an infinite two-layer ocean of finite depth and initially at respect with respect to a rotating coordinate system. At time t=0 a wind stress begins to act on the surface. The linear equations governing the surface height, thermocline and vertically averaged velocities in each layer can be derived from the equations of motion and continuity for a fluid in a rotating system. It suffices here to consider a one-layer system. The extention to a two-layer fluid is given in AVS and will not be reproduced, since the final numerical results here are restricted to a barotropic system. Thus

$$\frac{\partial u}{\partial t}-fv=-g\frac{\partial \eta}{\partial x}+\frac{\tau_x}{D} \qquad (1)$$

$$\frac{\partial v}{\partial t}+fu=-g\frac{\partial \eta}{\partial x}+\frac{\tau_y}{D} \qquad (2)$$

$$\frac{\partial \eta}{\partial t}+D\left(\frac{\partial u}{\partial x}+\frac{\partial v}{\partial y}\right)=0 \qquad (3)$$

where $\boldsymbol{\tau}=(\tau_x, \tau_z)$ is the wind stress vector, D is the depth, η is the free surface deviation, f is the coriolis term and the remaining variables have their usual meanings.

Cross-differentiating (1) and (2) to eliminate η yields the vorticity equation

$$\frac{\partial \zeta}{\partial t}+f\left(\frac{\partial u}{\partial x}+\frac{\partial v}{\partial y}\right)+\beta v=\frac{1}{D}\mathrm{curl}_z\,\boldsymbol{\tau} \qquad (4)$$

where $\zeta=\frac{\partial v}{\partial x}-\frac{\partial u}{\partial y}$ is the vorticity, and $\beta=\partial f/\partial y=\text{constant}$.

To study the geostrophic response of the ocean one may now make the geostrophic approximation, viz.,

$$-fv=-g\frac{\partial \eta}{\partial x} \qquad (5)$$

$$fu=-g\frac{\partial \eta}{\partial y} \qquad (6)$$

then from (3), (4), (5), (6)

$$\frac{\partial}{\partial t}\nabla^2\eta-\frac{1}{\lambda^2}\frac{\partial \eta}{\partial t}-\frac{\beta}{f}\frac{\partial^2 \eta}{\partial t\partial y}+\beta\frac{\partial \eta}{\partial x}=\frac{1}{f\lambda^2}\mathrm{curl}_z\,\tau \qquad (7)$$

where $\lambda^2=gD/f^2$ and f is now assumed constant.

If the x and y scales are comparable, then the term $\frac{B}{f}\frac{\partial^2\eta}{\partial t\partial y}$ may be neglected since for geostrophic response the time scale is assumed to be much longer than a half-pendulum day. Thus, $\frac{\partial \eta}{\partial x}\gg\frac{1}{f}\frac{\partial^2\eta}{\partial t\partial y}$, and

$$\frac{\partial}{\partial t}\nabla^2\eta-\frac{1}{\lambda^2}\frac{\partial \eta}{\partial t}+\beta\frac{\partial \eta}{\partial x}=\frac{1}{f\lambda^2}\mathrm{curl}_z\,\tau \qquad (8)$$

The boundary conditions are

$$\eta=0 \qquad x=y=\infty,\ \text{all } t \qquad (9)$$
$$\eta=0 \qquad \text{everywhere at } t=0$$

3. Solution

The response of the ocean will be determined for a wind stress distribution given by a tweak, i.e., the curl of the wind stress is assumed to act at a point and at one instant of time. Mathematically,

$$\mathrm{Curl}_z\,\boldsymbol{\tau}=W\delta(\xi,\zeta,\tau) \qquad (10)$$

where W is the amplitude of $\mathrm{curl}_z\,\boldsymbol{\tau}$ and $\delta(\xi,\zeta,\tau)$ is the dirac delta given by

$$\delta(\xi,\zeta,\tau)=\infty \qquad \xi=0,\ \zeta=0,\ \tau=0 \qquad (11)$$
$$=0 \qquad \text{elsewhere}$$

The dirac delta can be used to generate more general solutions. Thus from the following property of δ

$$\int_{-\infty}^{\infty}\delta(\xi)\phi(x-\xi)\,d\xi=\phi(x) \qquad (12)$$

it is clear that once the solution for η is known for δ, a general solution for η may be derived by writing the general wind curl distribution as

$$\int_{-\infty}^{\infty}\int_{-\infty}^{\infty}\int_{-\infty}^{\infty}\delta,(\xi,\zeta,\tau)\ \mathrm{curl}_z\boldsymbol{\tau}(x-\xi,\ y-\zeta,t-\tau)\,d\xi d\zeta d\tau \qquad (13)$$

and the final solution as

$$\eta(x,y,t)=\int_{-\infty}^{\infty}\int_{-\infty}^{\infty}\int_{-\infty}^{\infty}\eta_\delta(x',y'\,t')\ \mathrm{curl}_z\boldsymbol{\tau}(x-x',y-y',t-t')\,dx'dy'dt' \qquad (14)$$

where $\eta_\delta(x',y',t')$ is the solution for $\mathrm{curl}_z\boldsymbol{\tau}=\delta(\xi,\zeta,\tau)$

One can derive the solution η_δ by taking a LAPLACE transform with respect to time and solving the resultant equation by either a GREEN's function method or by FOURIER transforms. The mathematical problem then reduces to inverting the expression

$$\bar{\eta}=-\frac{We^{-x\beta/2p}}{2pf\lambda^2}K_0\left[r\sqrt{\left(\frac{\beta}{2p}\right)^2+\frac{1}{\lambda^2}}\right] \qquad (15)$$

where $r=\sqrt{x^2+y^2}$, is the LAPLACE transform variable and K_0 is the BESSEL function of the second kind. Thus it is necessary to find

$$\eta=\frac{1}{2\pi i}\int_{\gamma-i\infty}^{\gamma+i\infty}\bar{\eta}e^{pt}dp \qquad (16)$$

BASSET's integral representation of the K_0 function

$$K_0(r\alpha)=\int_0^\infty\frac{\cos ru}{\sqrt{u^2+\alpha^2}}du,\quad r>0,$$

$$|\arg x|<\pi/2$$

Hence,

$$K_0\left[r\sqrt{\left(\frac{\beta}{2p}\right)^2+\frac{1}{\lambda^2}}\right]=\int_0^\infty\frac{\cos ru}{\sqrt{u^2+1/\lambda^2}\sqrt{p^2+\frac{\beta^2}{4(u^2+1/\lambda^2)}}}du \qquad (17)$$

If (17) be substituted into (16) and the integral signs are interchanged (the latter operation can be proved to be admissable in the present case) and if the following LAPLACE inversions are employed;

$$\text{for}\quad a>0,\quad 1-e^{a/p}\sim\left(\frac{a}{t}\right)^{1/2}J_1(2\sqrt{at})$$

$$\text{for}\quad a<0,\quad 1-e^{a/p}\sim-\left(\frac{a}{t}\right)^{1/2}I_1(2\sqrt{at})$$

$$\frac{1}{(p^2+\gamma^2)^{1/2}}\sim J_0(\gamma t)$$

one finds that

$$\eta=\frac{W}{2\pi f\lambda^2}\int_0^\infty\frac{\cos ru}{\sqrt{u^2+1/\lambda^2}}\int_0^t\left(\frac{x\beta}{2t}\right)^{1/2}J_1\left(2\sqrt{\frac{x\beta\tau}{2}}\right)J_0\left[\frac{\beta(t-\tau)}{\sqrt{u^2+1/\lambda^2}}\right]d\tau du \qquad (18)$$

$$-\frac{W}{2\pi f\lambda^2}\int_0^\infty\frac{\cos ru J_0\left(\frac{\beta t}{2\sqrt{u^2+1/\lambda^2}}\right)}{\sqrt{u^2+1/\lambda^2}}du$$

for $x>0$

For $x<0$, $-J_1$. must replace J_1.

Expression (18) represents η_δ in equation (14). Thus a general solution for the geostrophic response of the sea surface to an arbitrary wind stress distribution is obtained.

For $\beta=0$, (18) reduces to

$$\eta=-\frac{W}{2\pi f\lambda^2}K_0\left(\frac{r}{\lambda}\right),\quad t>0 \qquad (19)$$

which can also be derived by neglecting β originally.

The other variables for both upper and lower layers may be found from (5) and (6) and from the expressions given in AVS for the baroclinic mode.

4. Quasi-non-divergent flow

Expression (18) presents one with a rather severe computational task. Hence, an approximate solution for quasi-non-divergent flow (very large λ^2) is given below. Numerical values can be computed relatively simple for the latter solution.

If the scale length of the disturbances is L, say, and if $\frac{\lambda}{L}\gg 1$, then the divergence is small and one can derive an approximate solution by neglecting the term $\frac{1}{\lambda^2}$ in the radical in (18) or by neglecting the divergence $\left(\text{i.e., the term } \frac{1}{\lambda^2}\frac{\partial\eta}{\partial t}\right)$ in (8) and solving the resultant problem. Then,

$$\eta=-\frac{W}{2\pi f\lambda^2}\int_0^t\frac{2K_0(2\sqrt{r\beta\tau})\cos\sqrt{2(x+r)\beta(t-\tau)}\,d\tau}{\sqrt{\tau(t-\tau)}}$$

A convenient method for evaluating from (20) is given by THOMPSON (1952). Let $\tau=t\sin^2\phi$, $\alpha=\beta rt$, $\gamma=\cos\frac{\theta}{2}$, $x=r\cos\theta$.

Then

$$\eta=-\frac{W}{2\pi f\lambda^2}\int_0^\infty \frac{J_0(2\alpha\sqrt{\gamma^2+z^2})}{\sqrt{1+z^2}}dz \qquad (21)$$

The integral for η may be shown to satisfy

$$\frac{\partial^2\eta}{\partial\alpha\delta\gamma}+4\alpha\gamma\eta=0 \qquad (22)$$

The partial differential equation (22) can be evaluated numerically provided values of η are known along an $\alpha=$constant and a $\gamma=$constant line in the α,γ plane. The sevalues can be computed directly from (21).

5. Results

Before the numerical results are presented, a few facts about the approximate solution should be noted.

The first of the two mechanisms listed in the introduction, i.e., horizontal divergence, is absent in the approximate solution. The essential effect of horizontal divergence is to bring about a re-distribution of mass in this model in response to the imposed distribution of wind stress. Therefore, the re-distribution takes place instantaneously. Thus the mechanism for the removal* of water from the origin is not included.

Also, the influence function $W\delta(\xi,\zeta,\tau)$ is used here as the total wind stress instead of as the auxiliary function for the more general wind stress distribution. Hence, for the particular storm considered, the entire influence of the storm is concentrated at one point in space and at one instant of time. Clearly, the numerical results have only a qualitative significance and even the latter must be restricted to regions removed from the point of application of the wind stress and to times well after the wind stress is applied.

The amplitude W in (10) thus contains the entire effect of the storm on the ocean. A wind system of solid rotation acting for a period of one day and over a region of 500 km. radius is assumed. The velocity at the outer edge of the system is chosen to be 30 m/sec. The transverse wind stress component, τ_θ, (there is no radial component here) can be computed from

$$\tau_\theta=\kappa\rho v^2_\theta$$

where $\rho=$density of air, $\kappa=2.3\times10^{-3}$ and v_θ is the transverse wind velocity. From the above values

$$W=2\pi\times10^{12}\ \mathrm{m^3/sec}$$

With

$$f=10^{-4}\ \mathrm{sec^{-1}},\quad \lambda^2=4\times10^{12}\ \mathrm{m^2}$$

one can compute the magnitunde of η.

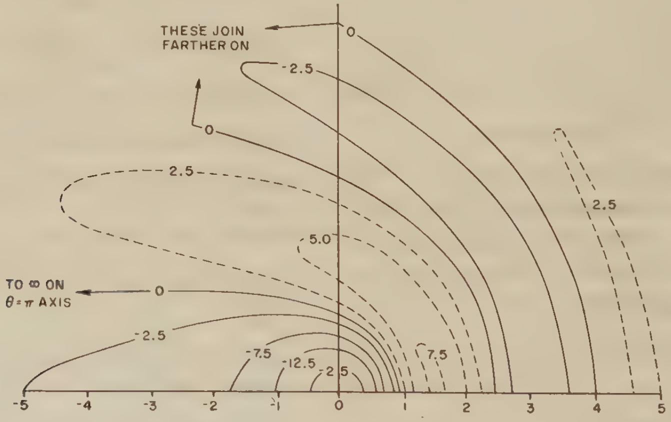

Fig. 1. Contour heights (in cm.) of surface deviation from its equilibrium value. Distances along any radial line are measured in units of $\sqrt{\beta rt}$. Graph is symmetric about the X axis.

---

* The total stress curl is assumed positive here. In general, the integrated value of the curl will vanish and the water will simply be re-distributed rather than removed from the system.

Figure 1 shows both the time and space distribution of η. Proceeding along a radial line indicates the change of the surface heights at either (a) a point in space as time increases or (b) an instant of time with increasing distance from the origin. The effect of β is indicated by the a symmetry in the eastwest direction. For constant f the contour lines would be symmetrical about the origin. The large negative values of η near the origin reflect of an imposed positive vorticity.

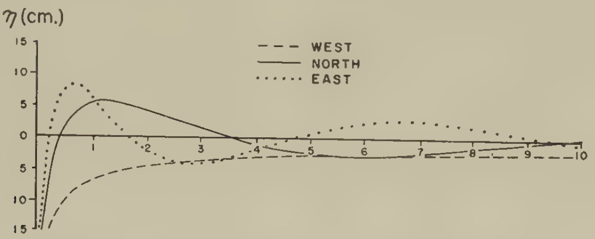

Fig. 2. η at a distance of 2000 km from tweak as a functipn of t.

In figure 2 the surface height is plotted as a function of time for points 2000 kms. from the tweak and at points to the east, north and west of the disturbance. The origin reflects the unrealistic nature of the disturbance. To the east and north there are wave crests (after the initial depression) and to the west there is a single trough. Then the qualitative picture described in the introduction is borne out here. There is an additional effect of the east-west asymmetry which does not enter the simple picture given previously but which must enter into the re-distribution of mass.

The waves of shortest period (approximately five days) occur due east of the tweak and the periods become longer as the direction is rotated about the origin from east to west. The waves are not waves in the simple Fourier sense since there is some dispersion. It is interesting to note that the relative amplitude of each wave decreases slowly with time. To the east of the tweak the height of the second peak is still one third that of the first and it occurs six days later. For points closer to the origin the wave "periods" would be shorter.

Acknowledgement. The author wishes to express his gratitude to Henry Stommel for several discussions on aspects of this problem.

References

ROSSBY, C.G., 1939:
"Relation between variations in the intensity of the zonal circulation of the atmosphere and the displacements of of semi-permanent centers of action." J. Mar. Res., **2**, No. 1., 38–55.

THOMPSON, P.D., 1952:
"Notes on the theory of large-scale disturbances in atmospheric flow with applications to numerical weather prediction." Geophysical Research Papers, No. 16. Geophysics Research Division, Air Force Cambridge Research Center. 106 pp.

VERONIS, G. and Henry STOMMEL, 1956:
"The action of variable stresses on a stratified ocean." J. Mar. Res., **15**, No. 1, 43-75.

Contribution No. 934

Deep-Sea Research, 1958, Vol. 5, pp. 62 to 71. Pergamon Press Ltd., London

An airborne radiation thermometer

WILLIAM S. RICHARDSON and CHARLES H. WILKINS

(*Received* 23 *September* 1957)

Abstract—An airborne radiation thermometer for use in measuring sea surface temperatures from aircraft is described. Infra-red radiation from the water surface is compared to the radiation from a black body at known temperature within the instrument. The sensitivity is about 0·01°C. Errors attending such measurents are discussed, and several applications to oceanographic research are cited.

INTRODUCTION

THE determination of the surface temperature of solids or liquids by measuring the radiation emitted from them is generally called radiation pyrometry, and optical pyrometers for the measurement of high temperatures have been in use for many years. Such a device measures the difference between the radiation from the surface and the back radiation from the detecting element (generally a thermocouple). As long as the surface temperature is high compared to the ambient temperature, reasonable fluctuations in ambient temperature do not cause serious errors in such a measurement. However, to measure the temperature of a target at or near ambient temperature it is necessary to provide elaborate compensation or to use a chopped system in which the detector " looks " alternately at the target and a known temperature, comparing the two. This technique was first used in oceanography by STOMMEL and his co-workers (1953) who developed a most useful if somewhat insensitive instrument for measuring ocean surface temperatures from aircraft. The instrument described in this paper is an outgrowth of this work.

It is well known that the hemispherically radiated energy (E) from a unit area of a surface at temperature T is:

$$E = e\sigma T^4 \tag{1}$$

where e is the emissivity of the surface and σ is the Stefan–Boltzmann constant. This energy originates from a layer in the surface of thickness sufficient to give total absorption, and in the case of water at the wave lengths of interest this thickness is about 0·01 mm. Liquid water is very nearly a black body for all wave lengths beyond 1 μ in the infra-red and for the purposes of this paper we will assume $e = 1$.

The spectral distribution of the energy from such a surface is governed by the Planck distribution law and for 300°K is shown in Fig. 1. The shaded sections indicate regions of the spectrum where the energy is lost, at any reasonable distance from the target, due to absorption by water–vapour or carbon dioxide in the air path. The effect of this absorption and of emission by these substances will be discussed below. As can be seen in the figure the energy is peaked at about 10 μ in the infra-red and is transmitted primarily by a " window " in the atmosphere between 8 μ and 12 μ.

If the detector has an active area A and a responsivity R (volts output per watt of radiant energy input) and is used in an optical system of focal length f and diameter D, then the electrical signal developed from the target area on the sea will be S where:

$$S = \frac{D^2 AR\tau_1 \tau_2 \sigma T_W^4}{4\pi^2 f^2} = KT_W^4 \tag{2}$$

where τ_1 is the fractional transmission of the optical system, τ_2 is the same for the atmosphere, and T_W indicates surface water temperature. If the optical system is

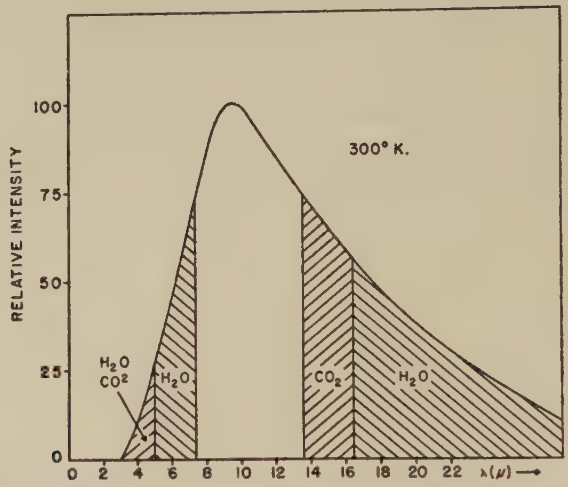

Fig. 1. The spectral distribution of energy from a 300°K black body.

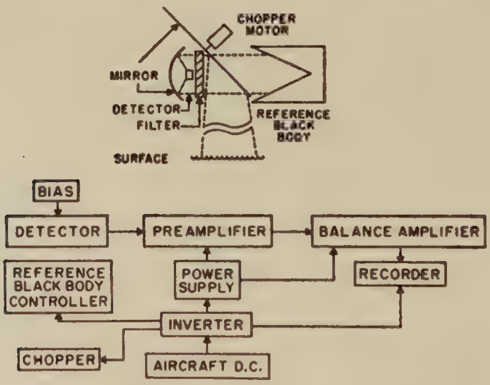
CHOPPER MOTOR
MIRROR
DETECTOR
FILTER
REFERENCE BLACK BODY
SURFACE
BIAS
DETECTOR
PREAMPLIFIER
BALANCE AMPLIFIER
REFERENCE BLACK BODY CONTROLLER
POWER SUPPLY
RECORDER
INVERTER
CHOPPER
AIRCRAFT D.C.

Fig. 2. Block diagram of the Radiometer.

chopped at frequency ν so that the detector sees a reference black body at temperture T_R (alternating with T_W) then the electrical signal will be AC at frequency ν with amplitude S' and:

$$S' = K(T_R^4 - T_W^4) = 4KT_R^3 \, \Delta T \tag{3}$$

where $\Delta T = T_W - T_R$. The last approximation holds only if τ_2 is the same in both paths and for ΔT small compared to the fixed T_R. In this case the a.c. signal amplitude is a linear function of the difference between the ocean and reference temperatures.

In general the instrument consists of a detector, an optical system, the reference black body, amplifiers and a recorder. A block diagram is shown in Fig. 2, and each component is discussed in a following section.

THE OPTICAL SYSTEM

Normally mirror optics are used in this type of system although lenses of silver chloride or arsenic trisulphide glass are also useful. In this particular instrument a first-surfaced aluminized spherical mirror of 3 in. diameter and $1\frac{1}{2}$ in. focal length is used as the focussing member. The mirror chopper is first-surfaced aluminized Plexiglas 12 in. in diameter and cut in the form of two 90° sectors with 90° openings between. This is rotated by a synchronous motor at 300 rev/min to give a chopping frequency of 10 c/s. Filters to help isolate the 8 μ to 12 μ band can be added but the cost in energy loss is quite high. Any filter must, of course, be put between the detector and the chopper so that its emission does not contribute to the a.c. signal.

THE DETECTOR

This instrument uses a thermistor bolometer as a detector (Wormser, 1953). Thermocouples and other types of bolometers have also been used, but the rigid mounting of the thermistor flakes seems to provide better performance in aircraft than other units of comparable cost and sensitivity. (The Golay cell used by Stommel (1953) was very sensitive, but very microphonic in the aircraft). The detector consists of a thin flake of thermistor material 2 mm × 2 mm, blackened, and exposed to the radiation through a silver sulphide coated silver chloride window. This coating is opaque to radiation of wavelengths shorter than 2 μ and acts as a filter opening up between 2 μ and 5 μ in the infra-red; its transmission is shown in Fig. 3. An additional matched flake within the detector capsule is hidden from the radiation and provides DC balance with changing ambient temperature. The two flakes are connected as two arms of a bridge biased to ± 180 V/d.c. with small dry batteries. Since the flake resistances are about 3 MΩ the battery drain is not large, but carefully selected batteries must be used to eliminate noise at this level.

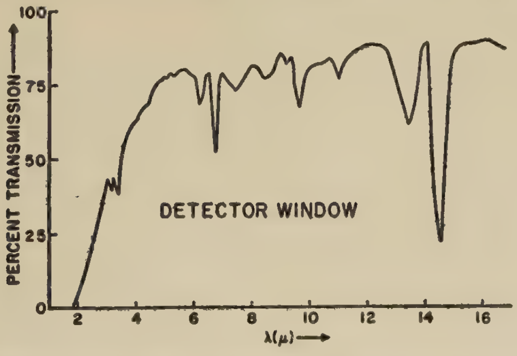

Fig. 3. Spectral transmission of the detector window. All other optical components are non-selective.

The size of the detector flake is dictated by cost and availability. The 2 mm × 2 mm size when used with the above mirror provides a target area on the sea surface of about 50 ft × 50 ft at 1000 ft altitude (and in proportion at other altitudes).

THE AMPLIFIERS AND RECORDERS

The signal which arises from the detector bridge when radiation falling on the flake changes its temperature and resistance is a 10 c/s AC voltage which is amplified by the pre-amplifier shown in Fig. 4. The detector and bias connections are also shown. This unit is a commercial one (WORMSER, 1953) manufactured for use with the detector. It has a voltage gain of 5000 and a passband (3 dB down) from 5 to 250 c/s.

The pre-amplifier filaments are run on 12 V/d.c. transformed, rectified and strongly filtered from 115 V/d.c. The *B* voltage is supplied by a rectifier supply, glo-tube regulated at 250 V/d.c. and strongly filtered. A tap from one of the glow-tubes provides 105 V/d.c. for the balance amplifier described below.

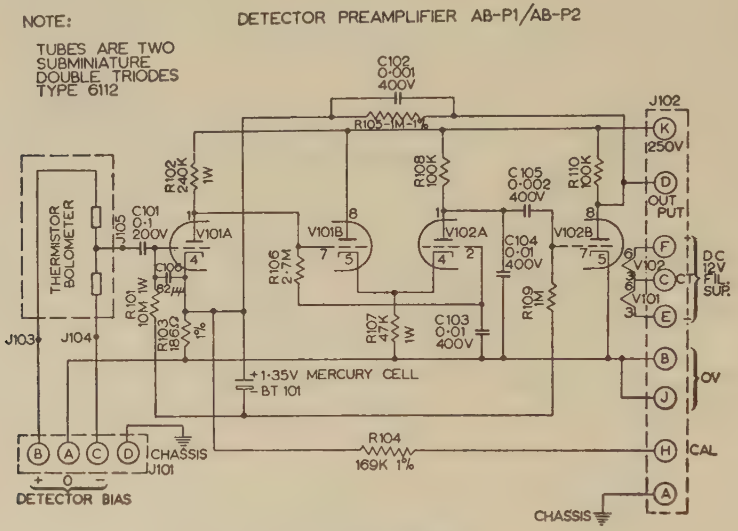
NOTE:
TUBES ARE TWO SUBMINIATURE DOUBLE TRIODES TYPE 6112
DETECTOR PREAMPLIFIER AB-P1/AB-P2
C102 0·001 400V
R105-1M-1%
J102
K
250V
D
OUT PUT
F
V102
C
CT
V101
E
DC 12V FIL. SUP.
B
J
OV
H
CAL
A
CHASSIS
THERMISTOR BOLOMETER
J105
C101 0·1 200V
V101A
R102 240K 1W
C106 82μμ
R101 10M 1W
R103 1863 1%
R106 2·7M
V101B
R107 47K 1W
R108 100K
V102A
C103 0·01 400V
C105 0·002 400V
C104 0·01 400V
R109 1M
R110 100K
V102B
+1·35V MERCURY CELL BT 101
R104 169K 1%
J103
J104
B
A
C
D
CHASSIS
J101
+ 0 −
DETECTOR BIAS

Fig. 4. Preamplifier.

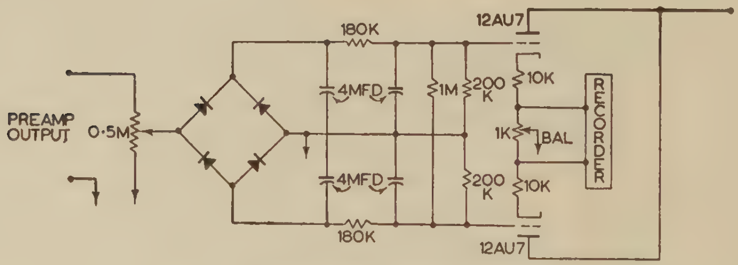
180K
12AU7
PREAMP OUTPUT
0·5M
4MFD
4MFD
1M
200 K
10K
1K
BAL
200 K
10K
RECORDER
180K
12AU7

Fig. 5. Rectifier and balance amplifier.

The a.c. signal from the pre-amplifier is divided by a potentiometer for gain control and rectified by a full-wave silicon diode bridge. The d.c. output of this bridge is then filtered to remove the chopping frequency and passed to a balanced cathode follower circuit as shown in Fig. 5. The output of this balance circuit drives the recorder.

The recorder may be any commerical unit of either the self-balancing poteniometer or d.c. amplifier-recorder type. For most purposes a sensitivity of the order of 50 mV full-scale in the recorder eliminates the need for additional d.c. amplification after the pre-amplifier.

THE REFERENCE BLACK BODY

The choice of the form of reference black body is dictated by convenience and the exactness required in the reference temperature. A water surface may be used and this provides very simple reference for laboratory work. It is somewhat inconvenient for work in the aircraft. In the latter case some type of thermostated blackened cone is

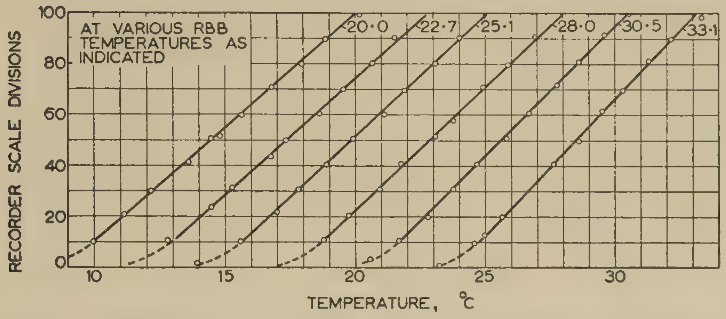

Fig. 6. Calibration curves for various reference black body temperatures.

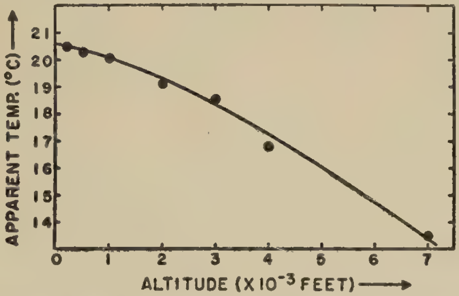

Fig. 7. Apparent temperature of Gulf Stream water off Cape Hatteras on December 20, 1956, as a function of flight altitude.

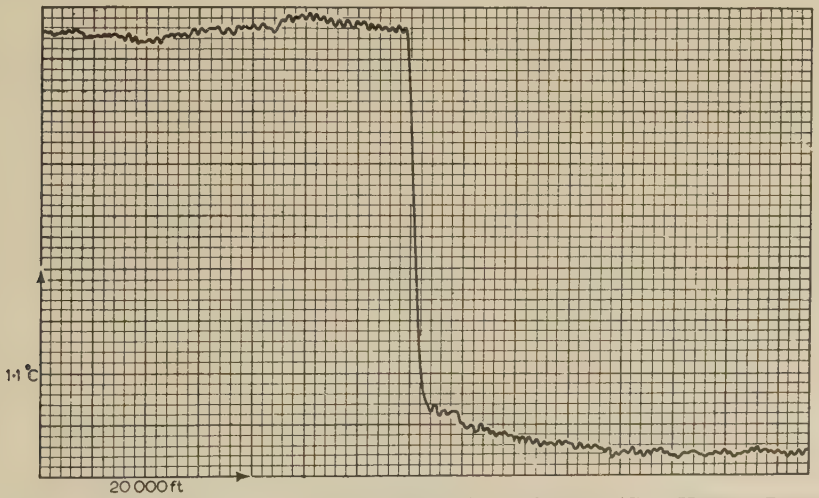

Fig. 8. Typical signal obtained on crossing the edge of the Gulf Stream (Cape Hatteras December 20, 1956; altitude 1000ft). The higher frequency oscillations were the result of a temporary instrumental difficulty.

generally used. This should have a base (open end) somewhat larger than the diameter of the focusing element and an apex angle of less than 30°. Two forms of this have been used successfully with this equipment. The first is a thin walled brass cone wrapped with heating wire on the outside and having a small bead thermistor at its apex. The thermistor senses the cone temperature and controls it by means of a simple electronic proportional controller which feeds power to the heater windings. This arrangement will hold the cone temperature to about ± 0·1° around the set temperature. A similar form of reference black body consists of a box with the thin-walled cone in one face. The box is oil-filled and thermostated with the same type of proportional controller. The oil is stirred and its temperature is measured with another thermistor which is part of a Wheatstone bridge, the output of which is fed to one channel of a two-channel recorder. The other channel of the recorder is used for the radiometer signal so the ocean temperature signal and the reference temperature signal are recorded side by side. The oil bath is controlled to about ± 0·02° around the set temperature, and any fluctuations in it (which will also be fluctuations in the radiometer signal) are immediately apparent. An open oil bath of much smaller volume and similarly stirred and thermostated has been used recently. The optical system " looks " at it by means of a 45° mirror. This has proved to be the most satisfactory method to date, and the calibrations shown in Fig. 6 and the records in Fig. 8 were obtained with it.

The use of a null system in which the reference temperature is rapdily changed to follow the sea temperature to keep the detector output null would be desirable. However, no black body has yet been made tht can be controlled fast enough to keep up with the rapid fluctuations in ocean temperature which are often encountered. The reference temperature may be set close to the average of the temperatures encountered and the small fluctuations above and below this level recorded. This requires some type of phase detection to tell whether the signal corresponds to hotter or colder than the reference.

Of course, all of the reference black bodies described above will only operate above the aircraft ambient temperature. For lower ocean temperatures an ice bath may be used as the reference.

OPERATION AND CALIBRATION

With the mirror chopper stopped, no signal appears at the recorder and the balance control in the cathode follower balance circuit is used to zero the recorder at the desired point on the scale. The gain is then set up to give the desired sensitivity as observed when the instrument looks at a pan of water and the water temperature is varied. When this gain is roughly set to the desired level a more careful calibration is made and then the chopper stopped. A reproducable calibration signal consisting of a small 60 c/s a.c. voltage or a 10 c/s signal obtained from chopping a light and photocell with the mirror is then fed into the pre-amplifier and the deflection noted. This signal is then used whenever it is desired to reset the gain control to reproduce the sensitivity setting at which the calibration was made. The actual temperature of the reference black body is determined by adjusting the water pan temperature to null the signal (as observed on an oscilloscope). A typical calibration curve is shown in Fig. 6. This procedure is repeated at any reference temperature which it may be desirable to use in the field.

ERRORS

The instrument is subject to a variety of errors which it is well to bear in mind. If the instrument is used off null as described above the signal amplitude is roughly proportional to the detector bias voltage. Thus the calibration will change as these batteries run down. Generally the batteries become noticeably noisy before their voltage falls very low, but the calibrations must be rechecked periodically (once a month or so) to check for decaying bias voltage.

The other errors which interfere with absolute temperature measurements in flight are associated with the atmosphere and the reflection of solar radiation from the sea surface. When the aircraft is banked sharply into the sun's glitter path (on a clear day with medium sun angles) a signal is observed corresponding to an apparent temperature increase of about 1°C. These signals arise from reflected radiation in the visible and very near infra-red portion of the spectrum passing the detector window filter. It is easily demonstrated that there is not sufficient long wave length solar radiation in the nominal pass band of the filter to account for the signals. This interference disappears at normal incidence and is not ordinarily troublesome.

Absorption of part of the radiation emitted by the sea surface by atmospheric water-vapour and carbon dioxide is a more serious problem. Water-vapour shows strong absorption between 5 μ and 7 μ and carbon dioxide has a strong band from 14 μ to 16 μ; the wings of these bands delineate the ends of the 8 μ to 12 μ " window." The molecules emit radiation at the air temperature in the regions where they absorb radiation from the sea surface. These effects are difficult to compute. For the present we must be satisfied with empirical comparisons between the radiation thermometer and contact water temperature measurements. As a typical case we may consider a clear day with the humidities normally encountered in sub-tropical (tradewind) areas. When flown at 1500 ft the instrument is generally in error by about 1°C, with a proportionally less error as the altitude decreases. Equally large errors may be expected in areas where the water-vapour content is less but the difference in air–sea temperature is larger. Fig. 7 shows the apparent temperature at a fixed location in the Gulf Stream off Cape Hatteras as a function of altitude, up to 7000 ft. A quantitative empirical approach to the problem of atmospheric transmission and emission will be the subject of a later paper.

The observed random noise on the recorder corresponds to about 0·02°C. This agrees well with the figure calculated from equation 2 estimating τ_1 and τ_2 both equal to 0·5 and taking the manufacturers' values for R (200 V/W) and the observed equivalent noise input of 2 μV as the minimum detectable signal. The electronic circuit is very stable with respect to drift, but slow variations in the reference black body temperature will cause a correspondingly slow drift in the temperature record. This is eliminated in the two-channel recording system mentioned above. It must, of course, be borne in mind that this sensitivity (0·02°C) to gradients in the ocean surface deteriorates as the atmospheric absorption increases. Thus it is possible to detect a large thermal gradient such as that occurring at the edge of the Gulf Stream from several thousand feet, but the apparent amplitude of the change decreases with altitude. For general survey work and tracking the edge of the Gulf Stream (VON ARX and RICHARDSON, 1953; VON ARX, BUMPUS and RICHARDSON, 1955) it is customary to fly at 1000-1500 ft and accept the attendant errors. It is then possible to make a low pass with the aircraft to obtain a more exact absolute temperature at any particular place.

APPLICATION OF THE INSTRUMENT

Use of an airborne radiation thermometer in tracking the edge of the Gulf Stream has been described elsewhere (Von Arx and Richardson, 1953; Von Arx, Bumpus and Richardson, 1955). A typical record of the temperature gradient across the edge is shown in Fig. 8. The instrument has been used to detect small changes in the surface temperature which occur in the trade wind areas (Malkus, 1957) (Fig. 10).

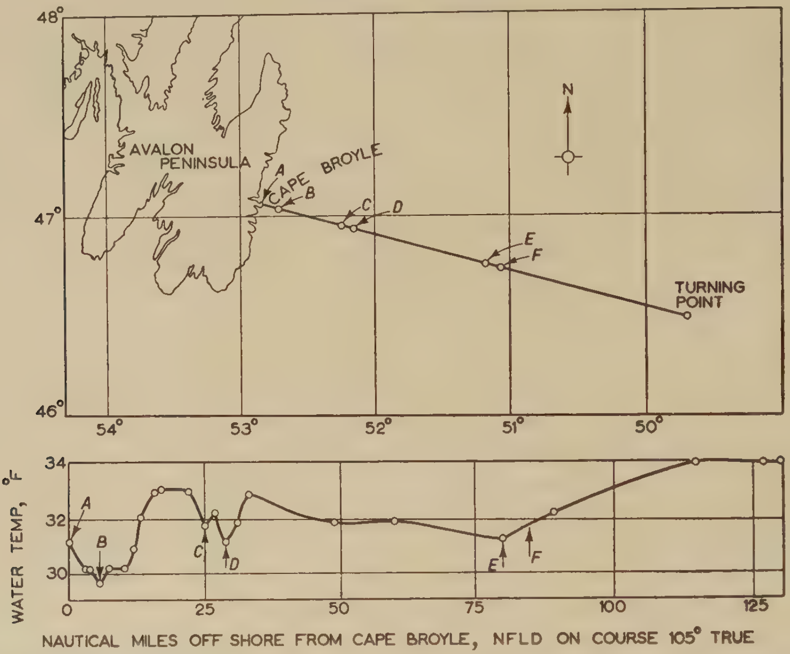

Fig. 9. Surface temperature measurements on a course inbound to the Avalon Peninsula of Newfoundland showing two bands of cold water near the Coast.

There are a variety of oceanographic and limnological problems where surface temperatures provide a good indication of the processes which are occurring. The aircraft by virtue of its speed and its ability to reach normally inaccessible places is often the only vehicle which may be used. Also the high speed provides a degree of synopticity which is not achievable with ships. Figs. 8, 9 and 10 show some typical results.

Acknowledgements—The authors are indebted to the United States Navy Bureau of Aeronautics (Contract No. NOas 55-401-c) and Office of Naval Research (Contract No. Nonr-1367(00)) for support of various phases of this work. Suggestions from and assistance by our colleagues at the Woods Hole Oceanographic Institution are also gratefully acknowledged.

Woods Hole Oceanographic Institution. Contribution No. 934.
from the Woods Hole Oceanographic Institution.

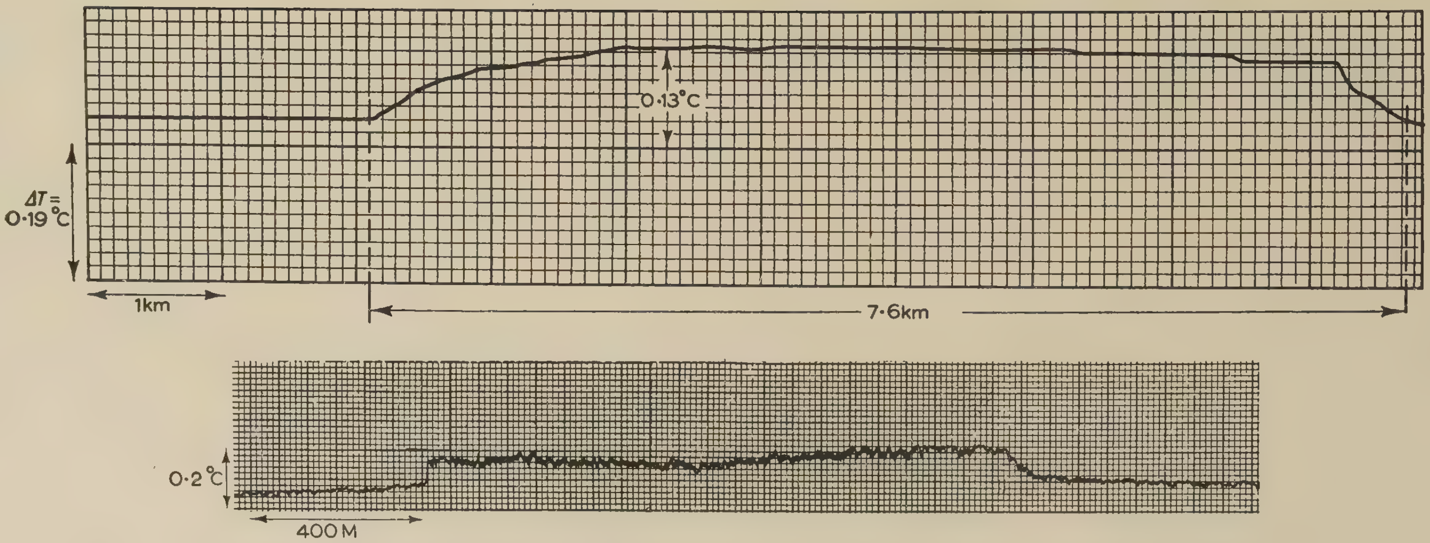

Fig. 10. The upper record is a warm patch north of Jamaica in April, 1956. The lower trace is a similar patch recorded by a contact thermometer on the R/V *Atlantis* in the same area on the same day.

REFERENCES

MALKUS J. S. (1957) Trade Cumulus cloud groups: some observations suggesting a mechanism of their origin. *Tellus* **9**, 33-44.

STOMMEL H. *et al.* (1953) Rapid Aerial survey of gulf stream with camera and radiation thermometer. *Science* **117**, 339-640.

VON ARX W. S. and RICHARDSON W. S. (1953). *The Surface Outcrop of the Gulf Stream Front.* Woods Hole Oceanographic Institution Technical Report, Ref. 53-24 (Unpublished Manuscript).

VON ARX, W. S., BUMPUS D. F. and RICHARDSON W. S. (1955) On the Fine-structure of the Gulf Stream Front. *Deep-Sea Res.* **3**, 46-65.

WORMSER E. M. (1953) Properties of thermistor infra-red detectors, *J. Opt. Soc., Amer.* **43**, 15-21. (These units and their associated pre-amplifiers were manufactured by the Barnes Engineering Co., Stanford, Conn. Similar units are manufactured by Servo Corporation of America, New Hyde Park, New York).

Printed in Great Britain by The Salisbury Press Ltd., Publicity House, Wilton Road, Salisbury, Wilts. (9597)

Contribution No. 935

Reprinted from THE JOURNAL OF GENERAL MICROBIOLOGY
Vol. 18, No. 2, April 1958

(*All rights reserved*) PRINTED IN GREAT BRITAIN

LEWIN, J. C., LEWIN, R. A. & PHILPOTT, D. E. (1958). *J. gen. Microbiol.* 18, 418–426

Observations on *Phaeodactylum tricornutum*

BY JOYCE C. LEWIN, R. A. LEWIN AND D. E. PHILPOTT

Woods Hole Oceanographic Institution and Marine Biological Laboratory, Woods Hole, Mass., U.S.A.

SUMMARY: *Phaeodactylum tricornutum* Bohlin was isolated from a marine tank at Woods Hole, Mass., U.S.A. It appeared to be identical with the Plymouth strain of '*Nitzschia closterium* forma *minutissima*'. Cells were of two characteristic types, oval and fusiform, each of which remained constant for many cell divisions in clonal culture. Triradiate cells arose rarely as atypical forms of the fusiform variety. Oval cells could arise as endospores within a fusiform cell. The transition from oval to fusiform was also studied, but details of the life cycle remain to be worked out. Electron micrographs showed the fusiform cells to be devoid of any organized siliceous structure, in agreement with previous observations. However, the oval cells were seen to possess a silica valve of a pennate diatom type, resembling those of the genus *Cymbella*. Only one valve was present on each cell, the remainder of the cell wall being unsilicified. The valve was $6{\cdot}2\,\mu$. long, was equipped with a raphe, and was perforated by pores arranged in 60 striae. Oval and fusiform cells both contained approximately the same amount of silica (0·4–0·5 % dry weight). In each case, most of this silica could be recovered as a particulate fraction resistant to digestion in hot nitric acid. The silica obtained from oval cells was in the form of diatom valves, whereas that from fusiform cells consisted of irregular particles clearly not derived from broken silica walls.

Mucilaginous capsular material, soluble in hot water, represented 16 % of the dry weight of oval cells; it was absent from fusiform cells. Acid hydrolysis and paper chromatography indicated xylose, mannose, fucose, and galactose as components of the capsule.

Allen & Nelson (1910) isolated a small marine organism, which they referred to as '*Nitzschia closterium* W. Sm. forma *minutissima*'; unfortunately they did not publish any formal description or illustration of it. The fusiform cells resembled in shape those of the diatom *N. closterium* (Ehrenberg) W. Sm., but the dimensions were smaller. Cultures of this smaller organism isolated by Allen & Nelson (1910) have been maintained at Plymouth Marine Laboratory, Devon, England, and distributed to laboratories around the world. Since it grows rapidly in a wide range of temperature and illumination and in many different nutrient media, much of the fundamental work published on marine diatoms has been carried out with this strain. In addition, it has been extensively used as food for raising a variety of marine animals. Some unusual features exhibited by this organism have prompted further studies to elucidate its nature and affinities.

Barker (1935) observed that a contaminated culture of the Plymouth strain, which had been maintained at the Hopkins Marine Station in California for several years, contained spindle-shaped cells, oval-shaped cells, and cells shaped like three-pointed stars. In the course of isolating bacteria-free cultures, he observed a tendency for the spindle-shaped cells to become less numerous on successive transfers to fresh agar while the number of oval cells increased. When grown in liquid media, on the other hand, a gradual reversion to spindle-shaped cells occurred. Triradiate cells were only rarely observed. Barker confirmed that these various cell forms all belonged to a genetically pure line. In 1942 Wilson & Lucas reported that triradiate forms of this organism arose independently in cultures maintained in Plymouth and in Hull. In a detailed illustrated account of this unusual organism, Wilson (1946) reported the presence of fusiform, triradiate and cruciform cells, and observed that both fusiform and triradiate cells sometimes gave rise to ovals. The ovals so formed either divided to produce more ovals or grew two or three arms to form fusiform or triradiate cells, respectively. Unlike the other cell types, the oval cells tended to produce mucilaginous capsules. Wilson did not observe auxospores, and stated that they were therefore not necessary for the elongation of the cells. The cell walls were so weakly silicified that he could not distinguish the valve markings characteristic of the Nitzschioideae. He considered the triradiate form to be identical with an organism of doubtful affinities, *Phaeodactylum tricornutum* Bohlin, 1897. Electron micrographs of fusiform and triradiate cells of the Plymouth strain showed no evidence of a characteristic diatom structure in the walls (Hendey, 1954; Bourrelly & Dragesco, 1955). In the material examined by these workers there were evidently few or no oval forms present, since these were not illustrated. In the course of physiological studies of the factors responsible for the changes of form of this organism, we prepared electron micrographs of oval as well as of fusiform cells. It immediately became apparent that *P. tricornutum* is an even more unusual and interesting organism than we had hitherto suspected. The structure of the walls of oval cells, as well as chemical and physiological differences between oval and fusiform cells, are described in this paper.

METHODS

In September 1956, we observed fusiform cells of *Phaeodactylum tricornutum* in a large outdoor tank behind the Woods Hole Oceanographic Institution, containing sea water enriched with a commercial fertilizer. By serial streaking of the cells on enriched sea-water agar plates we isolated the organism in bacteria-free culture. We also obtained from Dr M. Droop (Marine Station, Millport, Scotland) two other pure cultures of *P. tricornutum* for comparison: Millport No. 14, isolated by Droop in 1951 from a rock pool on the island of Segelskär, off the south coast of Finland, and Millport No. 15, the Plymouth strain. When the Woods Hole strain and the two European strains were grown in separate samples of the same batch of medium, they appeared identical. For the studies reported in this paper we used only the Woods Hole strain.

Two basal culture media were used:

(1) Enriched sea water, which consisted of nine volumes of sea water to one volume of a supplementary mineral solution; the final concentrations of added minerals were $Ca(NO_3)_2.4H_2O$, 0·01 %; K_2HPO_4, 0·002 %; 0·5 p.p.m. Fe; 0·3 p.p.m. Zn; 0·1 p.p.m. each of B, Co, Cu, Mn, Mo; $Na_2SiO_3.9H_2O$ to give a

Si concentration of 5 p.p.m. In some cases Tryptone (Difco) was added at a concentration of 0·1 %.

(2) Artificial sea water, which consisted of NaCl, 2·0 %; $Ca(NO_3)_2.4H_2O$, 0·05 %; K_2HPO_4, 0·01 %; $MgSO_4.7H_2O$, 0·01 %; trace elements and silicate as in (1). For solid media, agar was employed at a concentration of 1·0 % (w/v). The cultures were constantly illuminated with white fluorescent lights (300 f.c.) and maintained at 21°. Aeration of liquid mass cultures was provided by a slow passage of air filtered through sterile cotton wool.

Samples of dry organisms were analyzed for major constitutents as follows: (1) Micro-Kjeldahl N determinations ($\times 6{\cdot}25 =$ protein); (2) total ash and total silica; (3) silica in valves after digestion with hot concentrated nitric acid. In addition 100 mg. samples of dry organisms were extracted by: (1) successive methanol extractions; (2) cold dilute hydrochloric acid, pH 3; (3) water at 100°. Ash and silica were determined in the cell residues remaining after these extractions. The methanol extracts (1) were pooled, the solvent removed by evaporation, and the solid residue, comprising various pigments and lipids, was dried in a vacuum desiccator and weighed. The cold aqueous extract (2) contained inorganic salts and soluble carbohydrates including leucosin. Free and combined hexoses were determined quantitatively by the anthrone reaction and were expressed as glucose equivalents. Two successive water extractions at 100° (3) removed the capsular material from the cells. The extracts were concentrated to 5 ml. and poured into 15 ml. ethanol. The flocculum which formed was removed by centrifugation, washed, dried and weighed.

Paper chromatographic analysis of the capsular material was carried out as follows. A sample of the dried material (5 mg.) was heated in a sealed tube with 1·0 ml. of 0·7 % H_2SO_4 for 6 hr. at 105°. The hydrolysate was neutralized with $BaCO_3$, and the supernatant fluid evaporated to dryness and redissolved in one drop of water. This extract was chromatographed on paper for 16 hr. together with reference sugars, using either of two separate solvent mixtures: (*a*) butanol:H_2O:acetic (4:1:1), or (*b*) phenol:H_2O (4:1) in ammonia vapour. The chromatograms were dried, sprayed with 1 % (w/v) aniline phthalate, and developed for 5 min. at 100°.

Silicon determinations were carried out as follows. Material such as acid-cleaned valves, or the ash from dried cells or extracted cell residues, was fused with excess sodium carbonate in platinum crucibles. The flux was dissolved in water, and the silicon in solution was determined colorimetrically by the ammonium molybdate reaction (Lewin, 1954).

In preparing material for electron microscope observations we used whole cells, walls from cells burst by rapid transfer into distilled water, and silica valves prepared by digesting the cells with hot concentrated nitric acid. An R.C.A. Model EMU electron microscope was used.

RESULTS

Character of colonies on an agar surface

The colonies of *Phaeodactylum tricornutum* which formed from cells streaked on agar were mainly of two different types. Those composed of fusiform cells were dark brown, rounded, with smooth margins, and showed a satiny iridescence due to the parallel alignment of the cells. Colonies of oval cells were more diffuse, with irregular edges where individual cells migrated over the surrounding agar, and of a lighter shade of brown since the cells were separated from one another by colourless mucilaginous capsules. These two types of colonies could be readily distinguished with a binocular dissecting microscope, and, after growth for 2 or 3 weeks, even with the naked eye. It was possible also to recognize colonies, initially comprising only fusiform cells, but later giving rise to oval cells, which began to spread over the agar from one or more sites at the edge of the colony. The fact that oval cells could creep over a surface in this fashion, as do many species of pennate diatoms, suggested that cells of this type might possess a raphe, as do all motile diatoms.

Observations on the life cycle

Wilson (1946) attempted to follow the life cycle of his organism by examination of cells from liquid cultures. In cultures originating from oval cells, he noted that cells with short arms appeared, and that the average length of the arms increased in successive transfers. Although normally such cells bore two arms, he occasionally observed the origin of triradiate or other variant forms. We followed the development of individual cells on agar by drawing them at daily intervals, and observed:

(*a*) Oval cells divided to form oval cells (confirming Wilson's observations).

(*b*) Fusiform cells divided to form fusiform cells of similar length and form (confirming Wilson's observations).

(*c*) Inflated fusiform cells, approximately 25μ. long, produced a pair of ovals (cf. Wilson, Fig. 2) by division of the protoplasm within the central enlarged region of the cell. These oval cells sometimes divided again and were ultimately released by rupture of the parent wall. This observation did not bear out Wilson's supposition that oval cells arose from fusiform cells by unequal division.

Liquid and agar cultures also occasionally contained spherical auxospores, naked vacuolate protoplasts 6–12μ. in diameter, which were usually attached to an empty wall of a fusiform cell. All our attempts to follow the fate of individual auxospores on agar have so far proved unsuccessful.

Among 64 subclones which originated from single colonies on agar and were grown in liquid medium, one was found in which the cells were initially all triradiate. Since this form was believed to be atypical, the following experiment was carried out. The culture was allowed to age until abundant oval cells had been produced. It was then streaked on agar, and after 10 days 100 colonies of oval cells were isolated and transferred into liquid medium 1. When examined after 28 days, these cultures contained only oval cells.

Transfers were then made into medium 1 + Tryptone, which had been found to promote the production of armed cells. Ten days later all the cultures had produced abundant fusiform cells. Since no triradiate forms were seen, this form evidently does not persist beyond the intermediate stage of the oval cells. This confirms observations by Wilson (1946) and by Droop (Hendey, 1954), and supports the view that triradiates are not a normal stage of the life cycle. These studies are being continued with a view to determining what factors may be responsible for the changes in cell form and whether a sexual cycle may be involved.

Cell walls

The oval cells of *Phaeodactylum tricornutum* are approximately 8μ. long and 3μ. wide; the fusiform cells extend to a length of 35μ. Intact oval and fusiform cells, and cell membranes of both cell types prepared by bursting the cells in distilled water, were examined with the electron microscope. No perforated valves were seen on any of the intact fusiform cells (Pl. 1, figs. 1, 2), nor on the fusiform membranes (Pl. 1, figs. 3, 4), confirming the observations of Hendey (1954) and of Bourrelly & Dragesco (1955). However, the oval cells were seen to possess a valve of opaque material, presumably silica, of a typical pennate diatom structure (Pl. 2, figs. 5, 7). This valve was more clearly distinguishable in preparations of cell membranes freed from other cell material, and appeared as a silicified area on one side (Pl. 2, figs. 6, 8).

A typical diatom cell regularly possesses a silica frustule, composed of two valves and connecting bands, which completely encloses it in a silica shell. In both cell types of *Phaeodactylum tricornutum* the cell membranes appeared to be composed of a pair of overlapping parts, most readily perceived at the ends of cells seen in side view (Pl. 1, fig. 2 and Pl. 2, fig. 9). These evidently correspond to the epitheca and hypotheca of a typical diatom. The unsilicified portions of the cell membranes were transparent to the electron beam, pliable and structureless, except for faint indications of a fibrous nature. A unique feature of the oval cells of *P. tricornutum* was the presence of only one valve covering only part of the cell surface (Pl. 2, fig. 9). This was the case in over 90 % of the cells examined; in the remainder, for one reason or another, no valve could be seen.

When oval cells were digested with nitric acid, the cell contents and membranes disappeared and only the valves remained, thereby confirming their siliceous nature. The 'cleaned' valves were *c.* $6{\cdot}2\mu$. long by $1{\cdot}6\mu$. wide, with a raphe, a central and polar nodules, and 60 rows of pores or striae (equivalent to 95 in 10μ.). The apical axis of the valve was slightly curved producing a shape characteristic of the genus *Cymbella* (Pl. 2, fig. 10). Identical silica valves were also found in the two Phaeodactylum strains sent to us by Droop. Though the valve markings of the strain used here are so fine that it would be impossible to distinguish them with a light microscope, we considered that the valves themselves should be detectable without recourse to electron microscopy. Once we knew what to look for, we extracted the pigment from some oval cells with methanol, stained the cells with toluidine blue, and mounted them in Hyrax. When we examined them under oil immersion we could make out in some cells the dark line of the axial area on the surface.

Chemical analyses of fusiform and oval cells

By inoculating tubes of liquid medium with oval and with fusiform cells from selected colonies of *Phaeodactylum tricornutum* on agar, clones of the two cell forms were isolated. Mass cultures of each were grown in 2 l. Erlenmeyer flasks under conditions of constant temperature, light, and aeration. After incubation for 16 days, aeration was stopped. The oval cells, which grew as clumps, settled within a few minutes to the bottom of the flask, whereas the fusiform cells remained in suspension for some hours. The cells were concentrated and separated by centrifugation. The fusiform cells packed to form a smooth pasty mass, occupying only half the volume taken up by the gelatinous mass of oval cells. Microscopic examination revealed among the fusiform cells less than 1 % of ovals. The yields from 1·5 l. culture medium in one experiment are summarized in Table 1.

Table 1. *Yield of* Phaeodactylum tricornutum *from* 1·5 *l. of culture medium*

	Oval cells	Fusiform cells
Packed cell volume (ml.)	5·8	2·7
Total number of cells	$2{\cdot}15 \times 10^{10}$	$2{\cdot}17 \times 10^{10}$
Dry weight (mg.)	431	439

Table 2. *Chemical composition of oval and fusiform cells of* Phaeodactylum tricornutum

	Organisms	
	Oval	Fusiform
	% of dry wt.*	
Lipid	24	34
Protein	34	41
Carbohydrate		
Soluble in cold dilute acid	3	2
Soluble in hot water, precipitated with ethanol (capsular material)	16	0
Miscellaneous		
Soluble in cold dilute acid (not carbohydrate, not ash)	10	10
Soluble in hot water, not precipitated with ethanol	3	2
Ash	13	12
Total	103	101

* Averages of 2–3 determinations

The cells were analyzed as described on p. 420 (Methods), and the results shown in Table 2. Approximately 16 % of the dry weight of oval cells consisted of a mucilaginous material, soluble in hot water, and corresponding to the cell capsules which stain metachromatically with toluidine blue. Paper chromatograms of the hydrolysate of this substance indicated the presence of xylose, mannose, fucose and galactose. A mucilaginous fraction was not present in the fusiform cells, which lacked capsules, but which contained higher percentages of lipid and protein than the ovals.

Silica determinations were carried out on samples of dried cells of each type which had been rinsed with cold dilute acid, washed, dried and ashed. Both oval and fusiform cells contained approximately the same amount of silica (0·4–0·5 % of dry weight). This was unexpected, since no silica walls have ever been observed in the fusiform cells. Separate samples of oval and fusiform cells were digested with hot concentrated nitric acid. After this treatment, a small amount of white flocculent material remained floating on the surface of the nitric acid in each case. No silica valves were present in this flocculum. In the case of the oval cells, there also always remained a white precipitated deposit, which proved on chemical analysis to contain most of the cell silica (0·3–0·4 % of dry weight), and which consisted of diatom valves as revealed by the electron microscope. In two out of four analyses of fusiform cells, a white precipitate was also obtained after nitric acid digestion. This likewise proved to contain most of the cell silica (0·3–0·4 % of dry weight), but when examined with the electron microscope it appeared to be composed only of structureless debris, comprising irregular particles of various sizes, plainly not derived from silica walls.

DISCUSSION

It seems to be the opinion of most workers who have studied *Phaeodactylum tricornutum* that the oval and the fusiform cells are the typical prevalent stages in the life cycle. With prolonged cultivation on an agar surface the oval cells predominate, apparently being favoured since they have some ability to spread over the agar surface. Barker (1935) and Droop (see Hendey, 1954) have observed the transition to a predominance of oval cells on solid media. On the other hand, on prolonged cultivation in a liquid culture the fusiform cells predominate. Apparently they are at an advantage since in an actively growing culture they are more buoyant, whereas the oval cells tend to associate in clumps and sink to the bottom. Both Barker and Droop have reported a tendency for the formation of fusiform cells in liquid culture.

The triradiate cells have been the only form hitherto readily recognizable in samples of littoral water from nature. This is evidently because the fusiform cells might be mistaken for shortened *Nitzschia closterium*, and the ovals cells, when noticed at all, would be classified as minute, unidentifiable pennate diatoms. Triradiate forms originate rarely in the laboratory, but under certain conditions, as in static cultures, such cells may be favoured by selection, perhaps because of a decreased rate of sinking, and may overgrow the other forms. In addition to triradiates, cruciform cells (Wilson, 1946), curved cells, and other abnormal forms have occasionally been observed. When such a morphological abnormality arises, it reproduces clonally, forming daughter cells of the same shape as the parent cell, since cell division takes place in a longitudinal plane. The cell membrane is evidently inelastic enough to maintain its characteristic shape through successive cell divisions. However, variants of this sort tend to persist only until they produce oval cells, since these in due course typically give rise to normal fusiform cells.

Some data on the chemical composition of '*Nitzschia closterium* forma *minutissima*' have been reported by previous workers. Bidwell, Krotkov & Reed (1952) analyzed for free and bound sugars in cells of the triradiate variety. They found approximately 0·3 mg. ethanol-soluble sugars (glucose, fructose, sucrose) in 10^{10} cells. According to our calculations these free sugars would represent approximately 0·15 % of the dry weight. These workers also reported 6·4 mg. carbohydrate from the ethanol-insoluble residue, which we estimate would represent approximately 3·2 % of the dry weight. After acid hydrolysis, glucose, representing 2·5 % of the dry weight, was found to be the main constituent of this fraction. This glucose most probably came from leucosin, a water-soluble polymer of glucose characteristic of the Chrysophyta and reported from *Phaeodactylum tricornutum* by Parke (Hendey, 1954). In our analyses, leucosin could account for the 2–3 % of soluble carbohydrate in the cold dilute acid extract, a value in agreement with that calculated from the data of Bidwell, Krotkov & Reed (1952). Probably there were few or no oval cells in the material analyzed by these workers, since they did not report insoluble polysaccharide sheaths. Ketchum & Redfield (1949), using an empirical formula, calculated the proportions of protein, carbohydrate and lipid in the same organism, based on the R value (degree of reduction) and on the percent protein Their figures indicated 42 % protein, 25 % lipid, 33 % carbohydrate in the organic fraction, and an ash residue representing 19·5 % of the dry weight. Expressed on the same bases, our values were, respectively, 39, 28, 22 and 13 % for ovals, and 47, 39, 2 and 12 % for fusiform cells.

Harvey (1955) reported that about 1 % of the dry weight of the *Phaeodactylum tricornutum* he examined was silica. In the present study, the washed cells of both forms of our *P. tricornutum* were found to contain approximately 0·4 % silica on a dry-weight basis. This is present in the oval cells largely as silica valves. It is not known in what chemical condition the silica exists in the fusiform cells, since no recognizable structures remained after digestion with concentrated nitric acid. In comparison with other diatoms, Phaeodactylum is very weakly silicified, and enough silicon dissolves from Pyrex glass vessels in alkaline culture media to fulfil its meagre requirements. Harvey (1955) reported that heavy crops of *P. tricornutum* were produced in enriched sea water in hard-glass vessels without added silicate or silica sol, and we observed no difference in the rate of growth of oval or fusiform cells in artificial sea-water media, whether silicon was added or not. Analyses and physiological studies of this organism have been extensively quoted as representative of the diatoms. Present evidence seems to indicate that *P. tricornutum* is a most atypical diatom; its taxonomic position will be discussed in the following paper (Lewin, 1958).

Contribution No. 935 from the Woods Hole Oceanographic Institution, Woods Hole, Massachusetts. These studies were supported by Contract NR 163–392

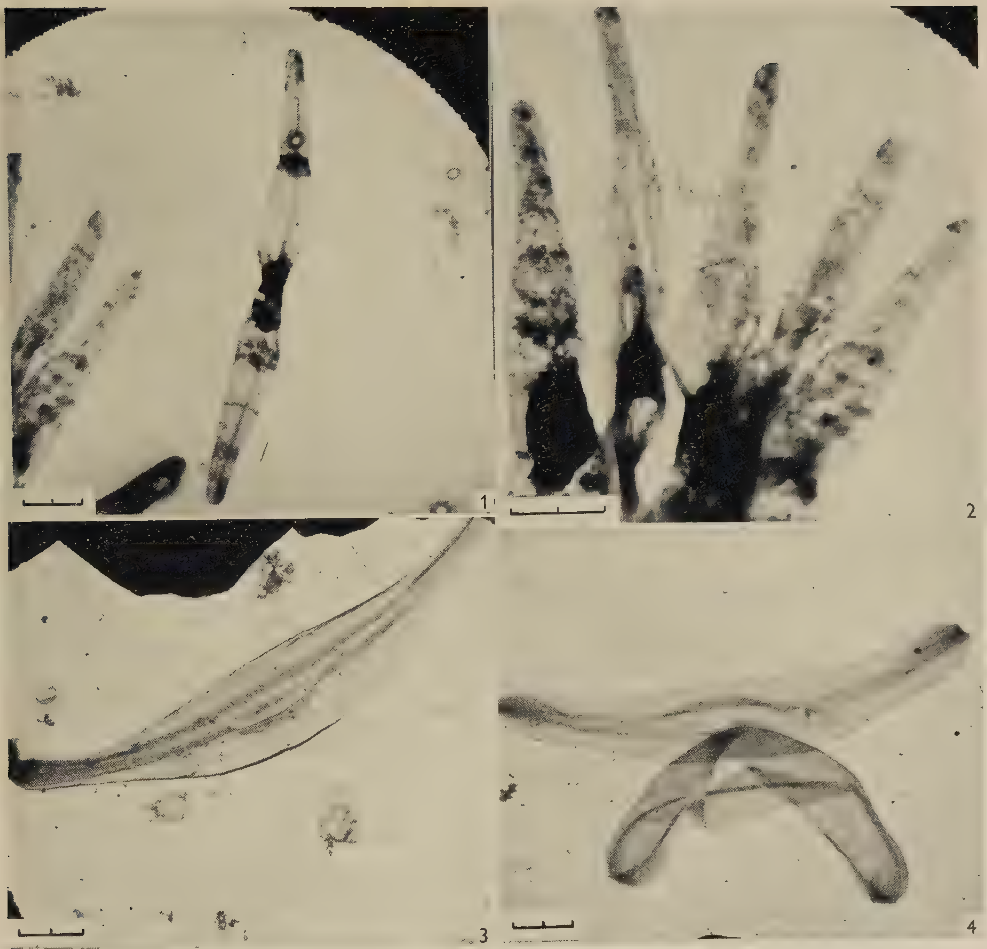

J. C. Lewin, R. A. Lewin and D. E. Philpott—*Phaeodactylum tricornutum.*
Plate 1

(*Facing p.* 426)

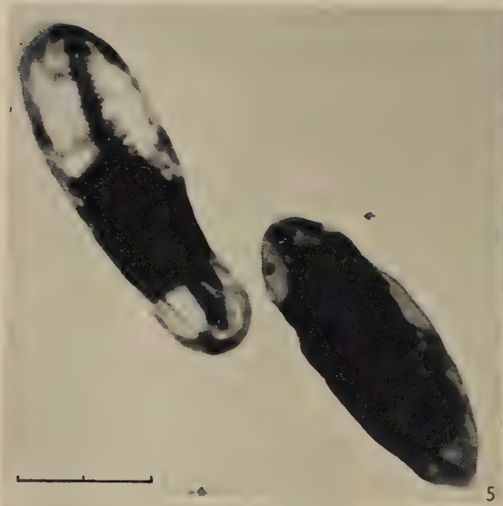

5

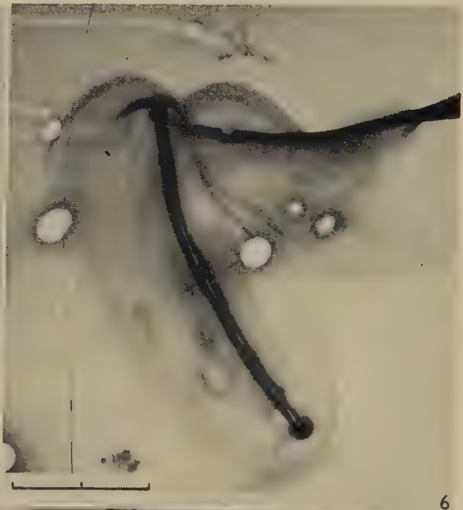

6

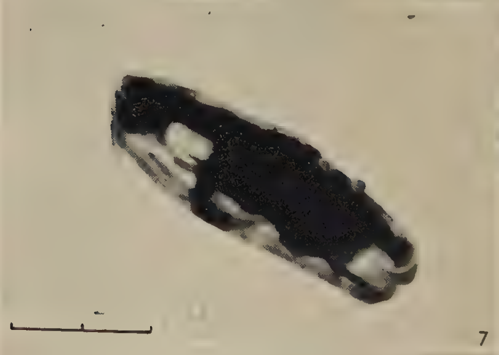

7

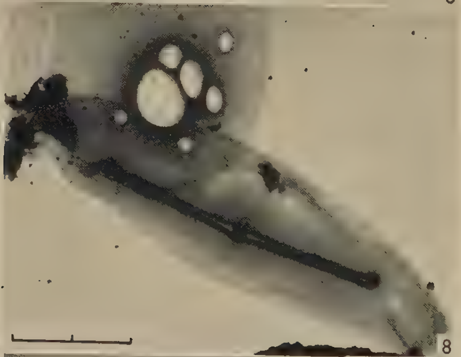

8

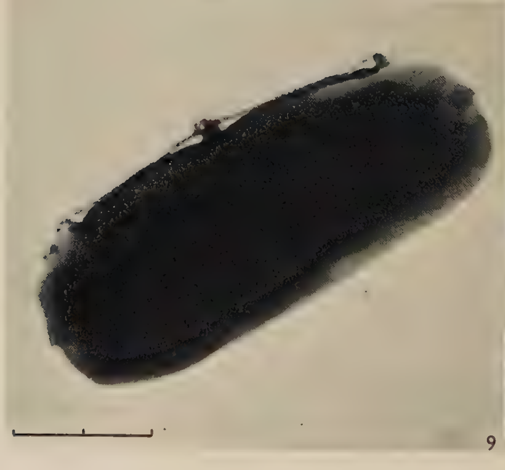

9

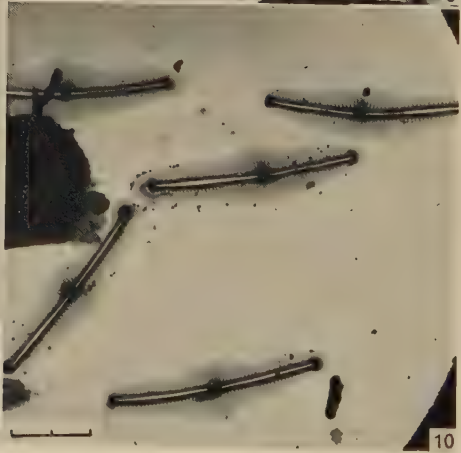

10

J. C. LEWIN, R. A. LEWIN AND D. E. PHILPOTT—*PHAEODACTYLUM TRICORNUTUM.*
PLATE 2

between the Biology Branch, Office of Naval Research, and the Woods Hole Oceanographic Institution. The authors are grateful to Dr N. I. Hendey, Dr H. Bold, and Dr W. R. Taylor for their comments on the manuscript.

REFERENCES

ALLEN, E. J. & NELSON, E. W. (1910). On the artificial culture of marine plankton organisms. *J. mar. biol. Ass. U.K.* **8**, 421.

BARKER, H. A. (1935). Photosynthesis in diatoms. *Arch. Mikrobiol.* **6**, 141.

BIDWELL, R. G. S., KROTKOV, G. & REED, G. B. (1952). Paper chromatography of sugars in plants. *Canad. J. Bot.* **30**, 291.

BOHLIN, K. (1897). Zur Morphologie und Biologie einzelliger Algen. *Öfvers Vetensk-Akad. Förh., Stockh.* **54**, 507.

BOURRELLY, P. & DRAGESCO, J. (1955). Contribution à la connaissance d'une algue rarissime '*Phaeodactylum tricornutum*' Bohlin. *Bull. Micr. Appl.* (2) **5**, 41.

HARVEY, H. W. (1955). *The Chemistry and Fertility of Sea Waters.* Cambridge University Press.

HENDEY, N. I. (1954). Note on the Plymouth 'Nitzschia' culture. *J. mar. biol. Ass. U.K.* **33**, 335.

KETCHUM, B. H. & REDFIELD, A. C. (1949). Some physical and chemical characteristics of algae grown in mass culture. *J. cell. comp. Physiol.* **33**, 281.

LEWIN, J. C. (1954). Silicon metabolism in diatoms. I. Evidence for the role of reduced sulfur compounds in silicon utilization. *J. gen. Physiol.* **37**, 589.

LEWIN, J. C. (1958). The taxonomic position of *Phaeodactylum tricornutum. J. gen. Microbiol.* **18**, 427.

WILSON, D. P. (1946). The triradiate and other forms of *Nitzschia closterium* (Ehrenberg) Wm. Smith forma *minutissima* of Allen and Nelson. *J. mar. biol. Ass. U.K.* **26**, 235.

WILSON, D. P. & LUCAS, C. E. (1942). Nitzschia cultures at Hull and at Plymouth. *Nature, Lond.* **149**, 331.

EXPLANATION OF PLATES

PLATE 1

Electron micrographs of *Phaeodactylum tricornutum*. Each scale line represents 2 μ.

Fig. 1. Fusiform cell.
Fig. 2. Fusiform cells.
Fig. 3. Membrane from fusiform cell.
Fig. 4. Membranes from fusiform cells.

PLATE 2

Electron micrographs. Each scale line represents 2 μ.

Fig. 5. Oval cells.
Fig. 6. Membranes from oval cells.
Fig. 7. Oval cell.
Fig. 8. Membrane from oval cell.
Fig. 9. Oval cell, side view.
Fig. 10. Silica valves of oval cells.

(*Received* 18 *October* 1957)

Contribution No. 936

Reprinted from THE JOURNAL OF GENERAL MICROBIOLOGY
Vol. 18, No. 2, April 1958
(*All rights reserved*)
PRINTED IN GREAT BRITAIN

LEWIN, J. C. (1958). *J. gen. Microbiol.* 18, 427–432

The Taxonomic Position of *Phaeodactylum tricornutum*

BY JOYCE C. LEWIN

Woods Hole Oceanographic Institution, Woods Hole, Mass., U.S.A.

SUMMARY: A revised taxonomic description of *Phaeodactylum tricornutum* Bohlin is presented, with special emphasis on the details of the silica valve, a structure hitherto unobserved. The features distinguishing *P. tricornutum* from *Nitzschia closterium* (Ehr.) W. Sm., with which it has frequently been confused, are summarized. In view of the unique characters of *P. tricornutum*, it is proposed to establish within the Bacillariales a new suborder, the Phaeodactylineae, to which *Phaeodactylum* is assigned as the only known genus.

In 1897 Bohlin described a new genus of unicellular algae, *Phaeodactylum*, with a single species, *P. tricornutum*. The organism was stellate with three narrow arms, possessed yellow-brown chromatophores and was weakly silicified. On the basis of the chemical nature of the cells and their characteristic plane of division, parallel with that of the arms, Bohlin considered that *P. tricornutum* was closely related to the diatoms. Wilson (1946), in a study of the various cell forms of '*Nitzschia closterium* W. Sm. forma *minutissima*', recognized the triradiate form of this organism as identical with *P. tricornutum* Bohlin. Since Hendey (1954) found no evidence for siliceous structures in the cell walls of this organism, he felt that it could not be classed as a diatom, and the presence of leucosin, as shown by Parke (recorded by Hendey, 1954), suggested to him a possible relationship to the Chrysophyceae. On the basis of the absence of movement, the absence of a raphe, and the absence of siliceous structure, Bourrelly & Dragesco (1955) also concluded that *P. tricornutum* could not be regarded as a diatom, but was a 'primitive Chrysococcalian'. Since the oval cells of *P. tricornutum* have now been shown to possess a silica valve (Lewin, Lewin & Philpott, 1958), it seems necessary to describe the organism more precisely on this basis, and to assign it to an appropriate taxonomic position. Though the specific epithet *tricornutum* might appear inappropriate, having been based on an atypical form, it has to be retained according to the rules of the International Code of Botanical Nomenclature (Lanjouw *et al.* 1956).

NEW DESCRIPTION

The emended description of the species is as follows:

Phaeodactylum tricornutum Bohlin emend.

Unicellular, normally with one parietal brown chromatophore in central region. Two typical forms of cells. (*a*) Ovate, 8 μ. long × 3 μ. wide, one silica valve per cell. Cells may be slowly motile, or immobile in mucilaginous clumps. (*b*) Fusiform, up to 25–35 μ. long, with two more or less blunt, slightly bent arms.

Silica wall absent. Non-motile. Rarely variants occur (triradiate, cruciform, lunate, etc.) which tend to persist in clones.

Valve weakly silicified, with a thin ragged margin; 6·2μ. long by 1·6μ. wide. Girdle bands absent. Valve flat, linear lanceolate, slightly curved, symmetrical about the transapical plane (as in *Cymbella* spp.); one edge convex, the other more or less straight with a median bulge. Ends broadly rounded but not capitate. Raphe slightly curved. Central area small, frequently with a pore on the side of the bulge. Striae approximately 60 (equivalent to 95 in 10μ.), mostly transverse but radiating in region of bulge. Puncta 2–6 per stria. (These details are revealed by electron microscopy. Under the light microscope it is just possible to detect the axial area, but no other features of the valve can be distinguished.)

CLASSIFICATION

Phaeodactylum tricornutum should undoubtedly be assigned to the Chrysophyta, since the cells possess golden-brown chromatophores, store leucosin and oil, and develop a silica wall at certain stages. The genus exhibits sufficient diatom characteristics to justify its inclusion within the class Bacillariophyceae. Among these features are the following: vegetative division longitudinal (usually not by formation of endospores), silica valve of a pennate diatom type, gliding movement of the oval cells, and auxospore formation.

The taxonomic position of *Phaeodactylum tricornutum* within the Bacillariophyceae is not readily apparent. Since the valve structure so closely resembles that of *Cymbella* spp. it might seem desirable to place the genus within the family Cymbellaceae. On the other hand, each oval cell possesses only one valve, and this feature distinguishes *P. tricornutum* from diatoms of all existing suborders. It is felt that this character, and the total absence of a siliceous wall from cells of the fusiform phase, provide sufficient justification for the formation of a new suborder. In the same way, various members of the Achnanthaceae, although their raphidate valves indicate close affinities to certain genera of the Biraphidineae, have been set apart as a separate suborder, the Monoraphidineae, on the basis of possessing dissimilar valves. It is therefore proposed that a new suborder, the Phaeodactylineae, be established. The taxonomic position of *P. tricornutum* would then be as follows:

Phylum	Chrysophyta
Class	Bacillariophyceae
Order	Bacillariales (Hendey, 1937)
Suborder	Phaeodactylineae (nov.subord.). Unlike all other diatoms hitherto described, the cells do not possess more than one silicified valve, which, when present, only partially covers the cell. **Cellulae valva unica, cellulam partim tegenti, instructae, vel nudae.**
Family	Phaeodactylaceae (nov.fam.). **Characteribus subordinis Phaeodactylineae.** The only family of the suborder.

Genus	Phaeodactylum (Bohlin, 1897). The only genus. Cells existing in two typical forms: motile oval cells which possess a silica valve, and non-motile fusiform cells lacking a silica valve.
Species	*P. tricornutum.* The only known species. (Description p. 427.)

Clarification of the distinctions between Phaeodactylum tricornutum *Bohlin and* Nitzschia closterium (*Ehr.*) *W. Sm.*

Over the past fifty years the organism known as '*Nitzschia closterium* forma *minutissima*' has been widely used in investigations of various aspects of physiology and biochemistry of diatoms and for studies of marine plankton. It is obvious now that a most atypical diatom was selected. *Phaeodactylum tricornutum* is apparently not even a normal component of marine phytoplankton, since it has usually been reported from intertidal rock-pools or sea-water tanks. It therefore seems unjustifiable to extend conclusions drawn from studies with this alga to diatoms in general or to phytoplankton. As a further complication, physiologists using the Plymouth strain often dropped the designation 'forma *minutissima*', and referred to it in publications simply as '*N. closterium*'. Since a true *N. closterium* exists, which is very different from *P. tricornutum* (see Table 1), it is often difficult to be sure which of the two organisms was being studied. As far as can be determined, the Plymouth strain of '*N. closterium* f. *minutissima*' was the subject of investigation in the following papers: Ahmad (1930); Barker (1935); Bidwell, Krotkov & Reed (1952); Chu (1946*a*, *b*); Clarke & Mazur (1941); Dutton &

Table 1. *Comparative features of* Nitzschia closterium (*Ehr.*) *W. Sm. and* Phaeodactylum tricornutum *Bohlin*

	N. closterium	*P. tricornutum*	
		Fusiform cells	Oval cells
Length	25–100 μ. (Cupp, 1943)	Up to 25–35 μ.	8 μ.
Motility	Actively motile	Non-motile	Slowly motile
Silica wall	Two valves with irregular markings. Multiple, fraying intercalary bands (see Pl. 1, figs. 2 & 4)	None (see Pl. 1, fig. 1).	Single valve of *Cymbella type.* No girdles or intercalary bands (see Pl. 1, fig. 3)
Form of colonies	Spreading rapidly over surface in reticulate pattern with fimbriate margin	Rounded, margin entire	Spreading for short distances, margin irregular
Growth in liquid media	Cells settle and grow in mucilaginous masses	Cells separate, tend to remain suspended	Cells settle and grow in small mucilaginous clumps
Heterotrophic growth (in darkness on 0·5 %, w/v, glucose)	Yes (3 isolates tested) (Lewin, unpublished)	No (3 isolates tested)	

Manning (1941); Dutton, Manning & Duggar (1943); French (1955); Harvey (1933, 1937, 1953*a*, *b*); Hutner (1948); Jameson, Drummond & Coward (1922); Ketchum (1939*a*, *b*); Ketchum, Lillick & Redfield (1949); Ketchum & Redfield (1938, 1949); King & Davidson (1933); Leigh-Clare (1927); Levring (1945); Lovern (1936); Lucas (1936); Pace (1941); Peach & Drummond (1924); Spencer (1952, 1954); Stanbury (1931); Strain & Manning (1942); Waksman, Stokes & Butler (1937); Villeret (1955); von Brand, Rakestraw & Renn (1937, 1939); von Brand & Rakestraw (1940); ZoBell (1935). In 1954, Ryther isolated another strain of *P. tricornutum* from the Great South Bay, Long Island, N.Y., which likewise was referred to as '*N. closterium*' in the following papers: Ryther (1954, 1956*a*, *b*); Ryther & Vaccaro (1954). Riley (1943) obtained a crude culture of '*N. closterium*' from a tank containing sea water from Long Island Sound enriched with commercial fertilizer. The cells had the same dimensions as *P. tricornutum* and, as in *P. tricornutum*, dense cultures could be grown without added silicate. Unfortunately, since the culture has been lost, it is no longer possible to determine its identity. The information contained in all of the papers listed above, with the possible exception of Riley (1943), should in the future be considered as relating to *P. tricornutum*.

Contribution No. 936 from the Woods Hole Oceanographic Institution, Woods Hole, Massachusetts. These studies were supported by Contract NR-163–392 between the Biology Branch, Office of Naval Research, and the Woods Hole Oceanographic Institution. The author is indebted to Mr N. I. Hendey (Admiralty Materials Laboratory), Mr R. Ross (British Museum), Dr G. Papenfuss (University of California), Dr P. Conger (Smithsonian Institution, Washington), Dr W. R. Taylor (University of Michigan), and Dr H. Bold (University of Texas) for valuable guidance with problems of taxonomy. The electron micrographs were taken in collaboration with Mr D. E. Philpott, Marine Biological Laboratory, Woods Hole, Mass.

REFERENCES

AHMAD, B. (1930). Observations on a diatom (*Nitzschia closterium* W. Sm.) as a source of vitamin A. *Biochem. J.* **24**, 860.

BARKER, H. A. (1935). Photosynthesis in diatoms. *Arch. Mikrobiol.* **6**, 141.

BIDWELL, R. G. S., KROTKOV, G. & REED, G. B. (1952). Paper chromatography of sugars in plants. *Canad. J. Bot.* **30**, 291.

BOHLIN, K. (1897). Zur Morphologie und Biologie einzelliger Algen. *Öfvers. Vetensk-Akad. Förh., Stockh.* **54**, 507.

BOURRELLY, P. & DRAGESCO, J. (1955). Contribution à la conaissance d'une algue rarissime '*Phaeodactylum tricornutum*' Bohlin. *Bull. Micr. Appl.* (2), **5**, 41.

BRAND, T. VON & RAKESTRAW, N. W. (1940). Decomposition and regeneration of nitrogenous organic matter in sea water. III. Influence of temperature and source and condition of water. *Biol. Bull., Woods Hole*, **79**, 231.

BRAND, T. VON, RAKESTRAW, N. W. & RENN, C. E. (1937). The experimental decomposition and regeneration of nitrogenous organic matter in sea water. *Biol Bull., Woods Hole*, **72**, 165.

BRAND, T. VON, RAKESTRAW, N. W. & RENN, C. E. (1939). Further experiments on the decomposition and regeneration of nitrogenous organic matter in sea water. *Biol. Bull., Woods Hole*, **77**, 285.

Chu, S. P. (1946*a*). The utilization of organic phosphorus by phytoplankton. *J. mar. biol. Ass. U.K.* **26**, 285.

Chu, S. P. (1946*b*). Note on the technique of making bacteria-free cultures of marine diatoms. *J. mar. biol. Ass. U.K.* **26**, 296.

Clarke, H. T. & Mazur, A. (1941). The lipids of diatoms. *J. biol. Chem.* **141**, 283.

Cupp, E. E. (1943). Marine plankton diatoms of the west coast of North America. *Bull. Scripps Instn Oceanogr.* **5**, (1) 1.

Dutton, H. J. & Manning, W. M. (1941). Evidence for carotinoid-sensitized photosynthesis in the diatom *Nitzschia closterium*. *Amer. J. Bot.* **28**, 516.

Dutton, H. J., Manning, W. M. & Duggar, B. M. (1943). Chlorophyll fluorescence and energy transfer in the diatom *Nitzschia closterium*. *J. phys. Chem.* **47**, 308.

French, C. S. (1955). Fluorescence spectrophotometry of photosynthetic pigments. In *The Luminescence of Biological Systems*, pp. 51–74. Editor Frank H. Johnson. Washington, D.C.: A.A.A.S.

Harvey, H. W. (1933). On the rate of diatom growth. *J. mar. biol. Ass. U.K.* **19**, 253.

Harvey, H. W. (1937). The supply of iron to diatoms. *J. mar. biol. Ass. U.K.* **22**, 205.

Harvey, H. W. (1953*a*). Synthesis of organic nitrogen and chlorophyll by *Nitzschia closterium*. *J. mar. biol. Ass. U.K.* **31**, 477.

Harvey, H. W. (1953*b*). Note on the absorption of organic phosphorus compounds by *Nitzschia closterium* in the dark. *J. mar. biol. Ass. U.K.* **31**, 475.

Hendey, N. I. (1937). The plankton diatoms of the Southern Seas. '*Discovery*' *Rep.* **16**, 151.

Hendey, N. I. (1954). Note on the Plymouth '*Nitzschia*' culture. *J. mar. biol. Ass. U.K.* **33**, 335.

Hutner, S. H. (1948). Essentiality of constituents of sea water for growth of a marine diatom (*N. closterium*). *Trans. N.Y. Acad. Sci.* **10**, 136.

Jameson, H. L., Drummond, J. C. & Coward, K. H. (1922). Synthesis of vitamin A by a marine diatom (*Nitzschia closterium* W. Sm.) growing in pure culture. *Biochem. J.* **16**, 482.

Ketchum, B. H. (1939*a*). The absorption of phosphate and nitrate by illuminated cultures of *Nitzschia closterium*. *Amer. J. Bot.* **26**, 399.

Ketchum, B. H. (1939*b*). The development and restoration of deficiencies in the phosphorus and nitrogen composition of unicellular plants. *J. cell. comp. Physiol.* **13**, 373.

Ketchum, B. H., Lillick, L. & Redfield, A. C. (1949). The growth and optimum yields of unicellular algae in mass culture. *J. cell. comp. Physiol.* **33**, 267.

Ketchum, B. H. & Redfield, A. C. (1938). A method for maintaining a continuous supply of marine diatoms by culture. *Biol. Bull., Woods Hole*, **75**, 165.

Ketchum, B. H. & Redfield, A. C. (1949). Some physical and chemical characteristics of algae growth in mass culture. *J. cell. comp. Physiol.* **33**, 281.

King, E. J. & Davidson, V. (1933). IV. Relation of silica to the growth of phytoplankton. *Biochem. J.* **27**, 1015.

Lanjouw, J. *et al.*, editors (1956). *International Code of Botanical Nomenclature.* Utrecht, Netherlands.

Leigh-Clare, J. L. (1927). A search for vitamin D in the diatom *Nitzschia closterium* (W. Sm.). *Biochem. J.* **21**, 368.

Levring, T. (1945). Some culture experiments with marine plankton diatoms. *Göteborgs VetenskSamh. Handl.* F. 6, Ser. B, **3**, no. 12, 1.

Lewin, J. C., Lewin, R. A. & Philpott, D. E. (1958). Observations on *Phaeodactylum tricornutum*. *J. gen. Microbiol.* **18**, 418.

Lovern, J. A. (1936). Fat metabolism in fishes. IX. The fats of some aquatic plants. *Biochem. J.* **30**, 387.

Lucas, C. E. (1936). On certain inter-relations between phytoplankton and zooplankton under experimental conditions. *J. Cons. int. Explor. Mer*, **11**, 343.

Pace, N. (1941). Pigments of the marine diatom *Nitzschia closterium*. *J. biol. Chem.* **140**, 483.

Peach, E. A. & Drummond, J. C. (1924). On the culture of the marine diatom *Nitzschia closterium* (f.) *minutissima* in artificial sea water. *Biochem. J.* **18**, 464.

Riley, G. A. (1943). Physiological aspects of spring diatom flowerings. *Bull. Bingham oceanogr. Coll.* **8**, (Art. 4), 1.

Ryther, J. H. (1954). The ecology of phytoplankton blooms in Moriches Bay and Great South Bay, Long Island, New York. *Biol. Bull., Woods Hole*, **106**, 198.

Ryther, J. H. (1956*a*). Photosynthesis in the ocean as a function of light intensity. *Limnol. and Oceanogr.* **1**, 61.

Ryther, J. H. (1956*b*). The measurement of primary production. *Limnol. and Oceanogr.* **1**, 72.

Ryther, J. H. & Vaccaro, R. F. (1954). A comparison of the oxygen and C^{14} methods of measuring marine photosynthesis. *J. Cons. int. Explor. Mer*, **20**, 25.

Spencer, C. P. (1952). On the use of antibiotics for isolating bacteria-free cultures of marine phytoplankton organisms. *J. mar. biol. Ass. U.K.* **31**, 97.

Spencer, C. P. (1954). Studies on the culture of a marine diatom. *J. mar. biol. Ass. U.K.* **33**, 265.

Stanbury, F. A. (1931). The effect of light of different intensities, reduced selectively and non-selectively, upon the rate of growth of *Nitzschia closterium*. *J. mar. biol. Ass. U.K.* **17**, 633.

Strain, H. H. & Manning, W. M. (1942). Chlorofucine (chlorophyll γ), a green pigment of diatoms and brown algae. *J. biol. Chem.* **144**, 625.

Villeret, S. (1955). Sur la présence des enzymes des uréïdes glyoxyliques chez les algues d'eau douce. *C.R. Acad. Sci., Paris*, **241**, 90.

Waksman, S. A., Stokes, J. L. & Butler, M. R. (1937). Relation of bacteria to diatoms in sea water. *J. mar. biol. Ass. U.K.* **23**, 359.

Wilson, D. P. (1946). The triradiate and other forms of *Nitzschia closterium* (Ehrenberg) Wm. Smith, forma *minutissima* of Allen and Nelson. *J. mar. biol. Ass. U.K.* **26**, 235.

ZoBell, C. E. (1935) The assimilation of ammonium nitrogen by *Nitzschia closterium* and other marine phytoplankton. *Proc. nat. Acad. Sci., Wash.* **21**, 517.

EXPLANATION OF PLATE

Electron micrographs. Each scale line represents 2μ.

Fig. 1. Fusiform cells of *Phaeodactylum tricornutum* Bohlin.
Fig. 2. Silica wall of *Nitzschia closterium* (Ehr.) W. Sm.
Fig. 3. Silica walls of oval cells of *P. tricornutum*.
Fig. 4. Enlarged portion of silica wall of *N. closterium*.

(*Received* 18 *October* 1957)

Journal of General Microbiology, Vol. 18, No. 2

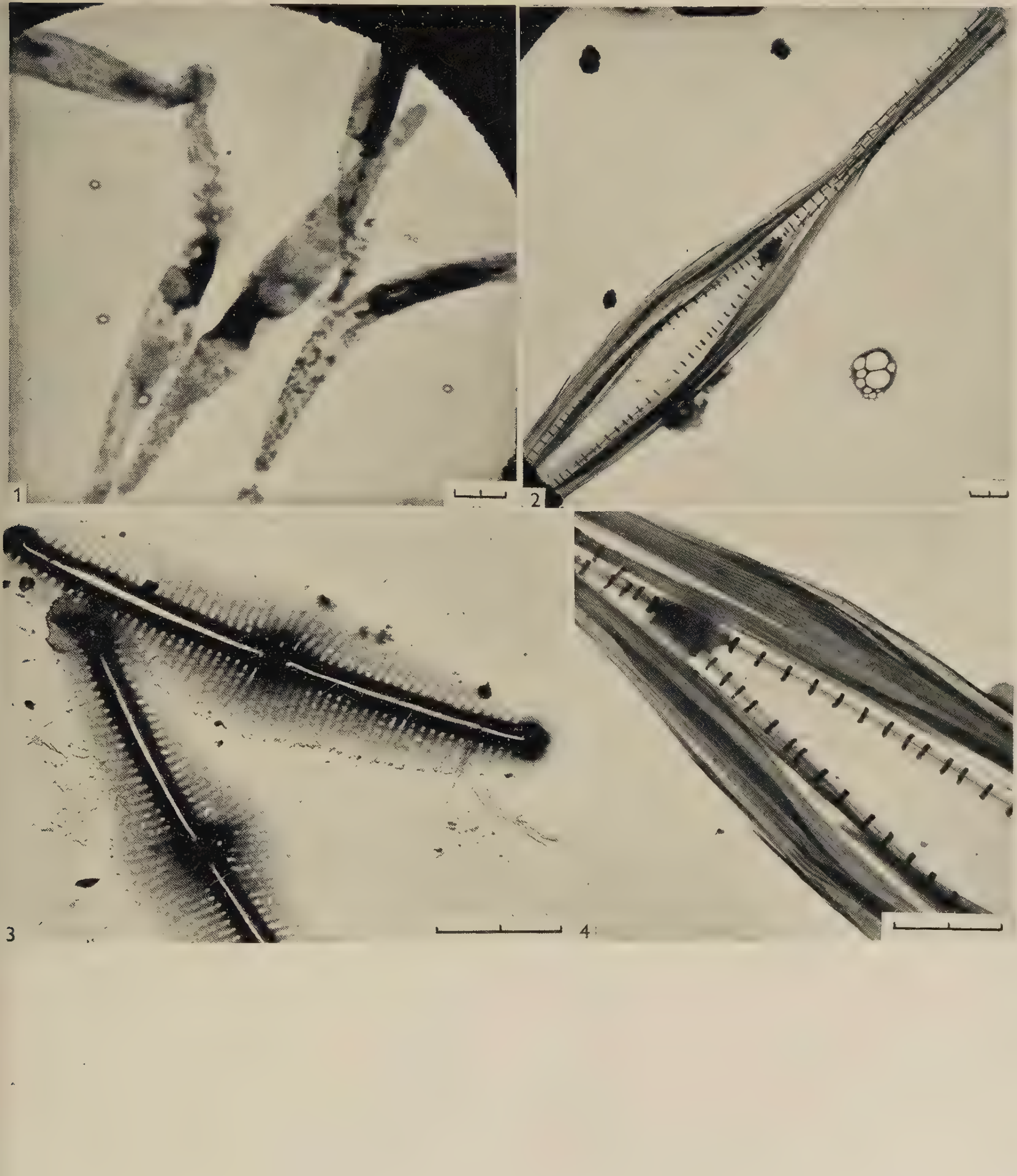

J. C. LEWIN—THE TAXONOMY OF *PHAEODACTYLUM TRICORNUTUM*. PLATE 1

(*Facing p.* 432)

Contribution No. 938

THE NAUTILUS

Vol. 72 JULY, 1958 No. 1

THE EFFECT OF NUTRITION ON THE COLOR OF THE CALLUS OF POLINICES DUPLICATUS

By HARRY J. TURNER, JR.[1]

Color patterns of the shells of mollusks are occasionally included in descriptions of a species. However the use of color patterns as a diagnostic specific character must be considered with caution because of the variability that may occur within a given species. As an example, the beach clam, *Donax variabilis,* displays a wide variety of colors and patterns. Similarly the carnivorous gastropod, *Purpura* (= *Thais*) *lapillus,* may be plain or banded depending on the diet (Moore, 1935). Specimens subsisting on a diet of *Mytilus* tend to have broad dark bands while those feeding on *Balanus* display either plain colors or only faint markings. A shift from a *Mytilus* to a *Balanus* diet alters the deposition of the darker pigments so that banding of the new shell is either faint or absent.

The predaceous moon snail, *Polinices duplicatus,* is distinguished from other members of the genus by the presence of a prominent callus that partially obscures the umbilicus. Say (1858) in his original description of the species reported the callus to be dark brown and this character has been repeated in various manuals of conchology (Minor, 1950, Abbott, 1955). Recently the author discovered a population of *P. duplicatus* at Duxbury, Massachusetts, in which a very high percentage of the specimens possessed calluses that were pearly white with faint pink margins at the lines of contact with the main bodies of the shells. A collection of 315 specimens taken from this locality contained 256 individuals with white calluses, fairly evenly divided between the two sexes. The live weights of the individual specimens of the collection ranged from one to 27 grams and the 59 snails with the brown callus were scattered at random throughout the range. In a similar collection taken from Barnstable Harbor,

---

[1] Contribution Number 938 from the Woods Hole Oceanographic Institution.

Massachusetts, 388 out of 479 specimens had the typical brown callus. The question arose as to whether the variation in color was due to some environmental influence or to a genetic difference. Serious consideration was given to placing the kind with the white callus in a separate subgenus.

The environments of the two localities were similar in many respects. Both were flats of fine compact sand near the low tide mark and there was little difference in temperature and salinity. The flat at Duxbury, however, was heavily populated with a recent set of soft clams, *Mya arenaria,* which the snails were consuming in large numbers while the Barnstable flat contained no *Mya* at all. The only significant food supply in the latter locality was a dense population of the tiny duck clam *Gemma gemma* which appeared to be utilized only by the smallest snails although an occasional specimen could be found feeding on a mud snail *Nassa* or a razor clam, *Ensis.*

The marked difference in the food supply in the two localities suggested that the color variation of the callus of *P. duplicatus* might be due to nutrition rather than a genetic difference. To test this possibility, five snails, each with a dark brown callus and weighing approximately one gram, were placed in a box of sand supplied with a continuous stream of salt water from the laboratory seawater system. One hundred soft clams, *Mya arenaria,* were added for food. As a control, five additional snails, each with a brown callus, were placed in a similar box of sand but no food was added.

The experiment was run for 35 days. The snails in the first box drilled and consumed 83 clams and gained a little over two grams in weight on the average. In every case the callus had turned pearly white with only the faintest tinge of pink at the margin. Each snail had secreted enough shell to advance the leading edge of the lower whorl slightly more than 180 degrees. The snails that had not been supplied with clams neither advanced the leading edges of their shells nor gained weight and the calluses remained dark brown.

It is clear that the large number of specimens of *P. duplicatus* with white calluses in the Duxbury population resulted from the abundant supply of *M. arenaria* as food. Similarly the preponderance of snails with brown calluses at Barnstable was due to a scarcity of suitable food. Apparently also, the typical condition as described applies to specimens which are poorly nourished.

References

Abbott, R. T. 1954. American sea shells, p. 186, D. Van Nostrand Company, New York.

Minor, R. W. 1950. Field book of seashore life. p. 624, Van Rees Press, New York.

Moore, H. B. 1936. The biology of *Purpura Lapillus*. I. Shell variation in relation to environment. Jour. Mar. Bio. Ass'n. U. K., V. 21, N. 1, pp. 61-89.

Say, Thomas. 1858. The complete writings of Thomas Say on the conchology of the United States. Edited by W. G. Binney, pp. 85-86.

Contribution No. 939

Särtryck ur Tellus nr 2, 1958

Some Examples of Stationary Planetary Flow Patterns in Bounded Basins[1]

By HENRY STOMMEL, A. B. ARONS and A. J. FALLER
Woods Hole Oceanographic Institution, Massachusetts

(Manuscript received August 22, 1957)

Abstract

A simple regime of fluid flow is defined. This regime can occur in a homogeneous layer of fluid (i) of uniform depth on a rotating sphere and bounded by meridional barriers (ii) of uniform depth on a betaplane and bounded by barriers running north-south (iii) of radially non-uniform depth on a rotating plane and bounded by radial barriers. The essential elements defining the regime are: (a) the flow in the whole layer is steady and geostrophic except and only (b) at the western boundary where a narrow, intense western boundary current is permitted to depart markedly from geostrophy, and (c) the system, which would otherwise be at rest, is driven by a distribution of sources and sinks of fluid (this includes driving agents such as the wind, which can be expressed in terms of source and sink distributions).

Predictions concerning patterns of flow have been deduced from the defined regime and verified experimentally on a rotating model of type (iii). Certain results obtained were by no means intuitively obvious from *a priori* considerations.

Introduction

It is generally recognized that the specific results obtained in theoretical hydrodynamics are not achieved deductively from the general hydrodynamical equations, but on the contrary, are derived deductively only from very much simplified fluid models (or, to say the same thing, an abbreviated set of equations). For example, there is a large range of problems where the so-called perfect fluid idealization proves an adequate representation of what is observed; another range in which laminar viscous flow is adequate. Hydraulic engineers have invented even simpler sets of equations to describe gradually varied flow and flow in transitions. The justification for applying such simplified equations to any particular set of problems is largely *a posteriori;* that is, we judge the reasonableness of the simplified regime of fluid flow by its results.

In meteorology and oceanography there is a constant search for such simple regimes. As an example from meteorology, Rossby's recognition of the essential dynamical elements of the long waves in the westerlies has led to formulation of a barotropic regime of atmospheric flow—and a simple set of equations—which meteorologists hope may describe major features of the atmospheric circulation and perhaps even be useful for prediction. In oceanography there has gradually emerged a conception of a regime of fluid flow which seems to be peculiarly applicable to large scale stationary oceanic flow patterns (for a summary see STOMMEL, 1957). This regime can occur in a homogeneous layer of fluid (i) of uniform depth on a rotating sphere and bounded by meridional barriers (ii) of uniform depth on a beta-plane and bounded by barriers running north-south (iii) of radially non-uniform depth on a rotating plane and bounded by radial barriers. The essential elements which define this simplified regime are: (a) the flow in the whole layer is steady and geostrophic except and only

---

[1] Contribution No. 939 of the Woods Hole Oceanographic Institution.

(b) at the western boundary where a narrow, intense western boundary current is permitted to depart markedly from geostrophy; and moreover, (c) this system, which would otherwise be at rest, is driven by a distribution of sources and sinks of fluid (various driving agents such as the wind can be expressed in terms of source and sink distributions, so this is no real restriction).

Although our main interest in this regime of planetary flow is in its possible applicability to oceanic circulation, we felt that some of its implications were so bizarre and contrary to intuition that it would be reassuring if they could be partially tested by model experiments. Thus, the model experiments are not meant as »scale models» of what perhaps occurs in the real ocean. We conceive of them as being tests of the internal consistency of the conceptual elements (a, b, c) which define the regime. The notion that such a regime can exist is mainly built on plausibility arguments. The elements which make up the regime are susceptible to quantitative mathematical description; hence, given the distribution of sources and sinks, the circulation pattern can be deduced. If, in comparing the predicted circulation pattern with that observed in a model experiment with a rotating basin, a large discrepancy should arise, it would suggest, among other things, that there were hidden inconsistencies or contradictions in the formulation of the regime. On the other hand, if the experiments with the basin verify the predictions, especially for flow patterns which do not seem intuitively obvious, the belief that such a simple regime might be applicable to the ocean is strengthened, although of course not confirmed. One then, however, feels encouraged to undertake the labor involved in constructing theoretical models and pursuing their implications, the ultimate validation lying in agreement between predictions of the theory and observable phenomena in the ocean.

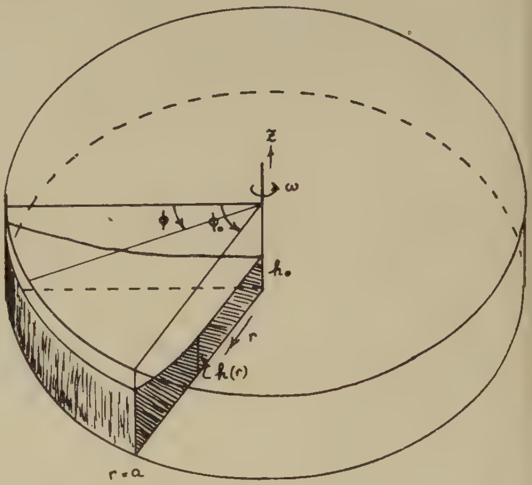

Fig. 1. Schematic diagram of rotating sector showing notation used in theoretical formulation.

A priori predictions for a particular rotating model

The model used in this work was a pie-shaped sector of a rotating basin of fluid (Fig. 1). The bottom of the basin is level. The free surface is a paraboloidal cylinder with axis vertical, concave upward. The undisturbed depth varies radially from a minimum at the center to a maximum at the rim. The top is covered with a sheet of glass to prevent the air in the room from exerting a stress on the water surface. After the basin has been rotating for some time the fluid in the sector is completely at rest with respect to the basin. In a geometrical configuration of this kind it is clear that any radial component of geostrophic flow is horizontally divergent due to the radial variation in depth of the fluid. A radially outward (inward) component of flow in the interior can therefore only occur if there is a local source (sink) of water. Components of geostrophic flow along circles of constant radius are permissible without divergence, except where blocked by radial barriers.

Before we had carried out any mathematical analysis or experimental work we could see that our regime led qualitatively to some rather remarkable deductions. For example, consider the circulation induced by a point source ⊕ and sink ⊖ of equal intensity placed near to the eastern boundary of the sector (the absolute sense of rotation of the basin in Fig. 2, as viewed from above is counterclockwise, as in the northern hemisphere on the earth) at different radii. Since there are no distributed sources or sinks over the remainder of the basin, all radial geostrophic flow is prohibited in the interior. We deduce that the only permissible circulation pattern, according to the rules of the regime, is one in which zonal geostrophic flow

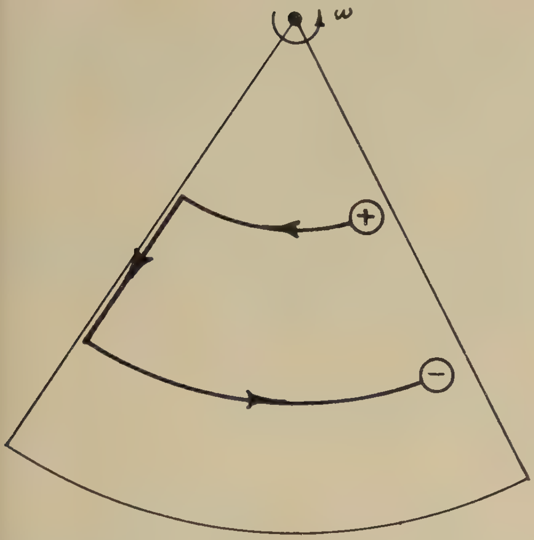

Fig. 2. Diagram of circulation induced in rotating sector by source ⊕ and sink ⊖ positioned as shown.

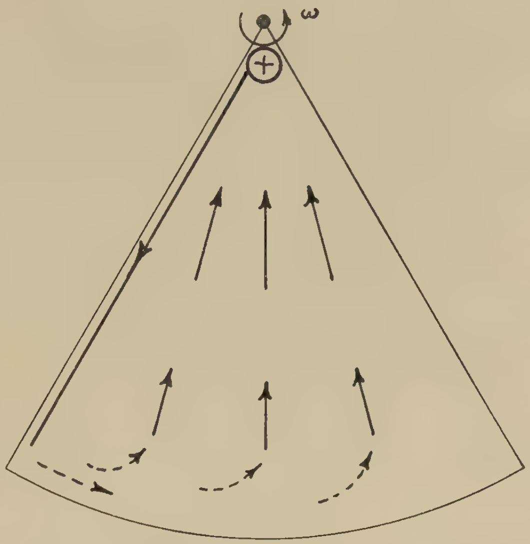

Fig. 3. Sketch of flow pattern expected with source ⊕ at apex of sector, surface of fluid rising uniformly. (Dashed arrows are sketched in to indicate portions of flow not given by elementary theory but evidently required by continuity.)

extends from the source to the western boundary, thence down the western boundary in a narrow, intense boundary current to the radius of the sink, and thence, in another zonal geostrophic flow to the sink. This flow pattern is very circuitous as compared to what occurs in the absence of rotation and non-uniform depth. It was the first flow pattern which we attempted to verify by an actual experiment.

From the point of view of our interest in the eventual application of the regime to oceanic circulation patterns it was desirable to make some deductions and experiments involving distributed sources and sinks. It is easy to obtain a uniform sink (source) over the whole fluid surface by allowing the tank slowly to fill up (empty), thus producing an overall rise (drop) of the free equilibrium surface. As an example, consider the flow pattern induced by an isolated source at the apex of the sector (Fig. 3). Since there is no point sink provided, the free surface rises uniformly—the equivalent of a uniformly distributed sink over the entire sector. Hence, qualitatively, one would expect an inward directed radial component of geostrophic velocity everywhere in the sector, connected to the source by a western boundary current, as sketched in Fig. 3. This is indeed rather surprising: the basin fills up from the rim, although water is added at the apex. But a quantitative analysis (see below) reveals even more surprising features. When the sector is allowed to fill up from an isolated source at the western edge of the rim (Fig. 4), the interior geostrophic flow is again toward the center, but the mathematical development indicates

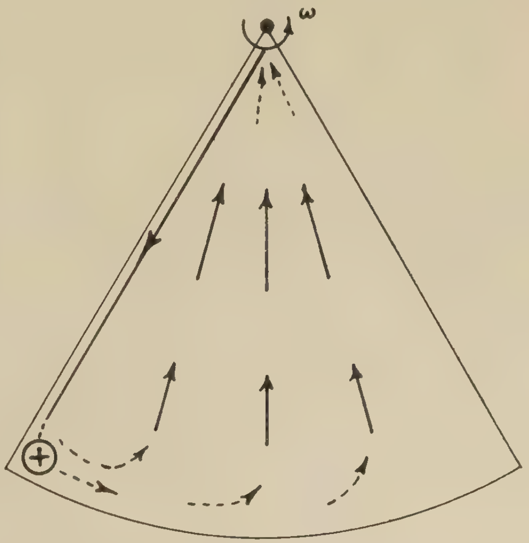

Fig. 4. Sketch of flow pattern expected with source ⊕ at western edge of rim, surface of fluid rising uniformly.

that the interior radial geostrophic transport is so large that it feeds. at the apex, a narrow western boundary current which flows *toward* the source. Such a flow pattern (Fig. 4) is far from being intuitively obvious, but is clearly verified by experiment.

Mathematical analysis

A system of cylindrical coordinates is adopted with notation defined in Fig. 1. The radial pressure gradient associated with the paraboloidal shape of the free surface balances the centripetal acceleration term. We take

$$h = h_0\left(1 + l\frac{r^2}{a^2}\right) \qquad (1)$$

$$\text{where } l = \frac{\omega^2 a^2}{2gh_0};$$

h denotes the height of the unpertubed paraboloidal surface. Assuming hydrostatic equilibrium in the vertical direction and denoting by ζ the vertical displacement associated with steady geostrophic flow, the equations of motion (neglecting inertial terms) take the form

$$2\omega v_\varphi = g\frac{\partial \zeta}{\partial r} \qquad (2)$$

$$-2\omega v_r = \frac{g}{r}\frac{\partial \zeta}{\partial \varphi} \qquad (3)$$

Neglecting ζ relative to h, the equation of continuity is

$$\frac{\partial}{\partial r}(hrv_r) + \frac{\partial}{\partial \varphi}(hv_\varphi) = -r\dot{\zeta} \qquad (4)$$

$$\text{where } \dot{\zeta} = \frac{\partial \zeta}{\partial t}$$

Equations (1) throught (4) determine the "interior solution" for the regime we are describing.

Carrying out the differentiation in equation (4)

$$rv_r\frac{dh}{dr} + h\left[\frac{\partial(rv_r)}{\partial r} + \frac{\partial v_\varphi}{\partial \varphi}\right] = -r\dot{\zeta} \qquad (5)$$

Cross differentiation and addition of (2) and (3) shows the second term of (5) to be zero. Obtaining $\frac{dh}{dr}$ from (1) and solving for v_r, we have:

$$v_r = -\frac{\dot{\zeta}a^2}{2h_0 lr} \qquad (6)$$

Thus the interior geostrophic flow which arises when a source adds water to the basin, producing a positive $\dot{\zeta}$, is northerly directed and has no φ component.

$$\left[\frac{\partial v_\varphi}{\partial \varphi} = -\frac{\partial(rv_r)}{\partial r} = 0, \text{ and } v_\varphi = 0 \text{ at eastern edge.}\right]$$

If sources S (rate of addition of volume) are assumed to produce a uniform vertical rise of the surface throughout the basin, geometrical requirements give the relation:

$$\dot{\zeta} = -\frac{2S}{\varphi_0 a^2}, \qquad (7)$$

and equation (6) becomes

$$v_r = -\frac{S}{\varphi_0 h_0 lr} \qquad (8)$$

Consider the water budget of the shaded sector defined by $r = r$ in Fig. 5. T_I represents the transport into the sector by the interior geostrophic flow; T_v represents the vertical transport associated with $\dot{\zeta}$; S_0 denotes the source transport; and T_w denotes the western boundary transport. We have postulated the existence of T_w as one of the elements of the regime, and we solve for it on the basis of the mass conservation requirement:

$$T_w + T_I + S_0 + T_v = 0 \qquad (9)$$

The ambiguity implied in the term T_w should be carefully noted. This is *not* a dyna-

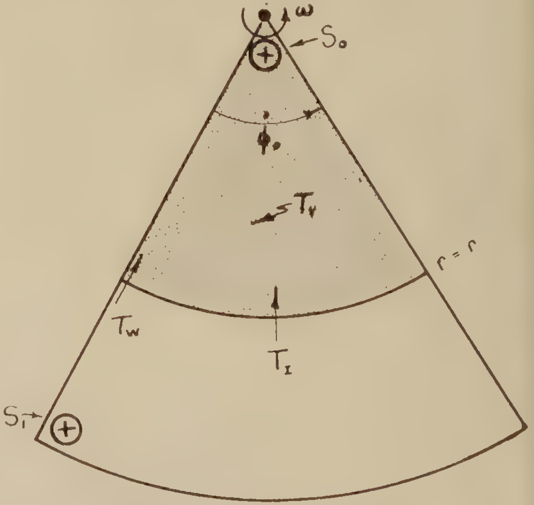

Fig. 5. Notation for analyzing water budget of the shaded sector $T_w + T_I + T_v + S_0 = 0$

mical solution; T_w is simply postulated as a *net* transport. There is nothing in the definition of the regime which precludes more than one stream at the western boundary or meandering of any kind. The net transport may be the result of a single current, of parallel currents in opposite directions, or some other combination.

From equations (7), (8) and the geometry of the system:

$$T_I = -hr\varphi_0 v_r = \frac{S}{l}\left(1+\frac{lr^2}{a^2}\right) \qquad (10)$$

$$T_v = -\frac{\varphi_0 r^2}{2}\dot{\zeta} = -S\frac{r^2}{a^2} \qquad (11)$$

Solving for T_w:

$$T_w = -\frac{S}{l}\left(1+\frac{lr^2}{a^2}\right) - S_0 + \frac{Sr^2}{a^2} = -S_0 - \frac{S}{l} \qquad (12)$$

where, for the general case depicted in Fig. 5,

$$S = S_0 + S_1$$

We can now interpret the results for T_w for various specific cases:

Case 1. S_0 positive, $S_1 = 0$. (Fig. 3).
For this case equation (12) becomes:

$$T_w = -S_0\left(1+\frac{1}{l}\right) \qquad (13)$$

The mathematical analysis of the postulated regime thus predicts a southerly transport at the western boundary of the model. The transport is *larger* than the input of the source at the apex by the amount S_0/l, l being the parameter characterizing the slope of the equilibrium paraboloidal surface. If the angular velocity ω is such that $h(a) = 2h_0$, $l = 1$, and the total boundary transport is *twice* the transport of the source. The transport is independent of r and the boundary current must therefore flow undiminished to the outer rim of the basin, turn to the eastward at the outer rim, and from that region feed the north-bound interior geostrophic flow. Part of the boundary current (the amount S_0/l) represents a *recirculation flow* of water originally in the basin.

Case 2. $S_0 = 0$, S_1 positive (Fig. 4).
For this case equation (12) becomes:

$$T_w = -\frac{S_1}{l} \qquad (14)$$

This predicts a flow pattern essentially similar to that of Case 1, but the result is even more surprising. If $l = 1$, the regime requires a *southerly* boundary current with a transport *equal to that at the source* in the southwest corner! (The same result, of course, is obtained regardless of the position of S_1 along the outer boundary.)

Case 3. $S_0 = -xS_1$, S positive. (i.e. a fraction x of the input is drained off at the apex of the model.)

For this case equation (12) becomes:

$$T_w = \frac{S_1}{l}\Big[x(l+1) - 1\Big] \qquad (15)$$

In this situation the ambiguity as to the detailed nature of T_w is well dramatized. T_w is only a *net* transport. Thus equation (15) might be interpreted as describing a southerly transport of magnitude $\frac{S_1}{l}$ paralleling a northerly transport $\frac{S_1 x}{l}(l+1)$, or as a single transport either north or south (changing direction when $x = \frac{1}{l+1}$), or as some other combination leading to the same *net* T_w.

Order of magnitude of approximations in the theory

Numerical values for flow, rotation, and basin geometry are given in a later section. Utilizing the numerical data, it can be shown that:

$$\frac{\zeta \text{ max.}}{h} \sim 10^{-4}$$

and that the fractional transport neglected by dropping ζ from the equation for T_I is also of the order of 10^{-4}.

If the sector is cut off at some small radius $r = a_0$ instead of extending to a sharp apex at $r = 0$, equation (12) becomes, to first order terms:

$$T_w = -S_0 - \frac{S}{l} - S\frac{a_0^2}{a^2}\left(1+\frac{1}{l}\right) \qquad (16)$$

The contribution of the third term on the right hand side is of the order of 10% when a_0/a is about 0.2.

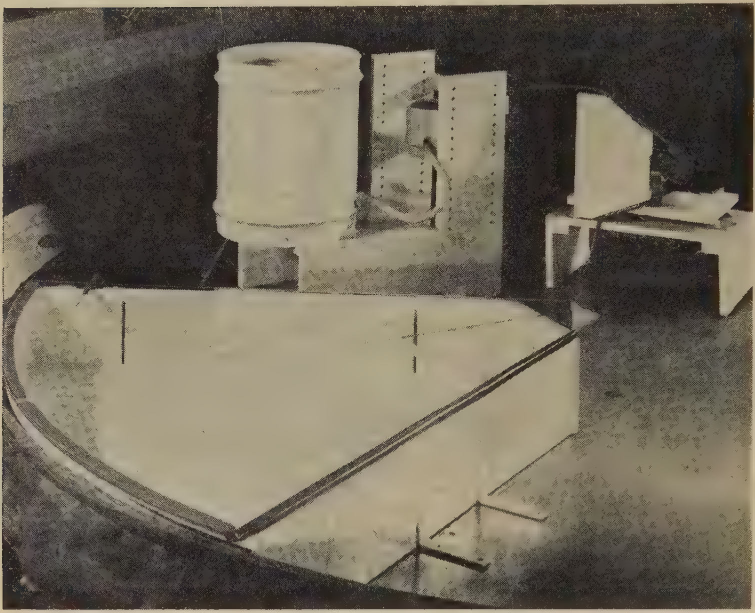

Fig. 6. A photograph of the rotating tank showing the 60° sector with 1/4-inch slots at various positions in the walls for the introduction or extraction of mass. When not in use the slots are sealed with tape. The glass cover prevents wind stress on the free surface of the water. A controlled flow rate is obtained by adjusting the level of the small can (with an overflow) into which water is pumped continuously. A constant head of water is thereby maintained in the large can containing the dyed source water.

The Laboratory Experiments

To check and demonstrate the principles of the foregoing theory and quantitative notions concerning the flow in a simple laboratory model, the 7-ft. diameter rotating tank previously employed for oceanographic models (VON ARX, 1952) was used. For these studies a truncated sector of 60° width (Fig. 6) was isolated by wooden partitions with several vertical slots in the walls for the introduction or extraction of mass. An alternate source was direct injection of the fluid through a vertical glass tube at any desired point in the interior of the sector.

The rate of in flow of mass was an important consideration and was adjusted so that the Rossby number for the western boundary current was of the same order of magnitude as that for the Gulf Stream system. Similar values of the Rossby number (defined by $R_0 = v/\omega R = = .001$ where v is a representative velocity and ωR is the tangential speed of rotation) are obtained when the circulations have approximately the same degree of geostrophy. The ratio of depth at the rim to that at the center (h_a/h_0) was set at approximately 2 in all cases, a value corresponding to $l = 1$ in the theoretical discussion. Other significant parameters were $\omega = 1.05$ sec.$^{-1}$, $a = 100$ cm., and $\bar{h} = 8$ cm.

Fig. 7 shows a sequence of photographs of an experiment which corresponded approximately to the situation of Fig. 2. Dyed water entered through the slot at the upper right and showed the path followed by the water in migrating zonally across the tank, down the western boundary, and zonally across the tank to the exit slot at the eastern wall of the sector. The flow was not as simple as that of the idealized diagram primarily because only 5/6 S_0 passed through the exit slot and 1/6 S_0 was used to raise the level of water in the sector. By the preceding theoretical arguments, there should have been a slow radially inward (poleward) flow over the interior of the tank and this was manifest in the poleward spread of dye from both of the zonal currents. In addition to the southward flowing western boundary current of strength S_0, the theory also predicts an additional component of 1/6 S_0 which is required by continuity and is associated with the distributed sink of 1/6 S_0. This "recirculation" was not made up of source water and must have been drawn from the interior of the basin. We interpret the thin streak of clear water (Figs. 8b, c) between the primary current near the western wall and the poleward flowing mass in the interior as evidence for the "recirculation" flow.

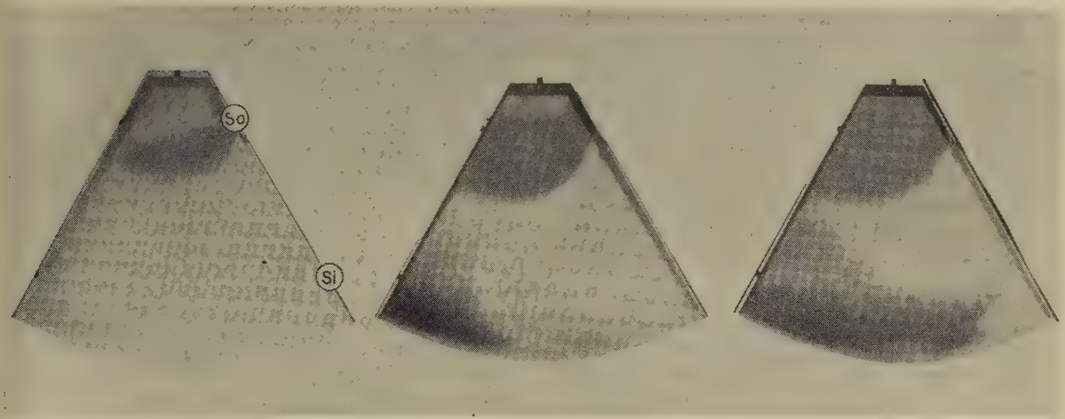

Fig. 7. Photographs at 20, 80, and 220 minutes after the introduction of dye, showing the path followed by the source water ($S_0 = 50$ cc./min.) in flowing from a slot in the eastern wall near the apex to the sink ($S_1 = 5/6\ S_0$) in the same wall near the rim (corresponding to Fig. 2).

Fig. 8 illustrates the circulation with the source at the apex of the sector and with no external sink, i.e., with a uniform rise of the water level in the tank (a uniformly distributed sink). (Compare with Fig. 3 and Case 1. of the mathematical analysis.) In accord with the theory, the interior of the basin filled from the rim and continuity was maintained by an intense western current S_0 from the source, which was augmented by a recirculation (theoretically of strength S_0 for $l = 1$) from the interior water. Evidence for this recirculation is the clear streak in Figs. 8b, c which penetrates toward the rim into the dyed fluid near the western wall. By evaluating the volume of fluid-containing dye, the transport of the total western boundary current has been determined for comparison with the source strength. The data of Table I show that: a) at 20 minutes the dyed fluid was composed almost entirely of source water, b) at 60 minutes the dyed fluid occupied twice the total volume of the input, which implies mixing with an equal volume of clear water (presumably that from the recirculated component of the boundary current), and c) at 125 minutes the dyed volume was less than twice that of the source input, a fact which is consistent with the decrease in the factor l as the mean depth of the fluid ($\bar{h}$) gradually increased. These results are in rough agreement with the quantitative predictions of the theory.

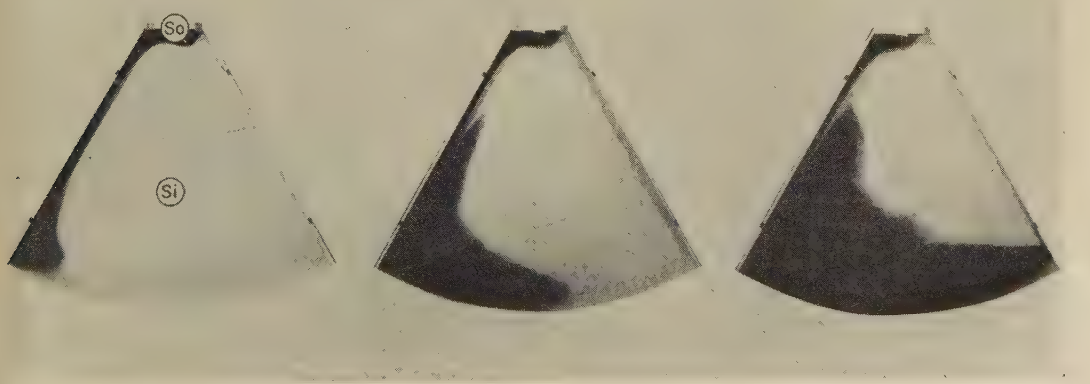

Fig. 8. Photographs at 20, 60, and 80 minutes with $S_0 = 120$ cc./min. The source was at the apex and there was no external sink (corresponding to Fig. 3).

Table 1. Data for the experiment corresponding to Fig. 8.

Elapsed time (minutes)	20	60	125
Volume with dye (liters)	1.9	14.6	27.4
Total input from source	2.4	7.2	15.0
Mean depth (h), (cm)	7.7	8.2	10.3

The situations discussed in Cases 2. and 3. of the analysis are illustrated by Figures 9 and 10. In each case the dyed mass was injected through a vertical glass tube in the southwestern corner. In Fig. 9, with a sink of equal strength at the apex, the greater part of the source mass passed smoothly out through the sink as a western boundary current, except for protuberances caused by inertial oscillations in the tank. (These were the product of slight periodic variations of the rotation rate due to uneven wearing of the driving belt.)

By eliminating the external sink at the apex and allowing the surface to rise slowly (a uniformly distributed sink) as in Fig. 10, we have a situation corresponding to Fig. 4 and to Case 2. of the analysis. Figs. 10b and 10c (three minutes apart) show the rapid southward flowing boundary stream by means of permanganate dye from crystals that were introduced through slits in the glass cover. The intrusion of clear water into the colored mass near the source indicates that the southward flowing current mixed with the source mass, and the

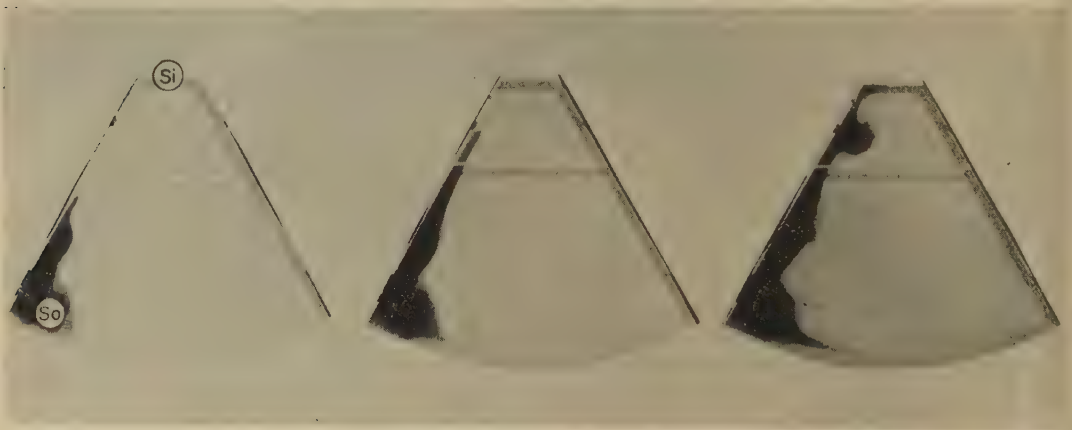

Fig. 9. Photographs at 5, 10, and 20 minutes with $S_0 = 100$ cc./min. The dyed fluid was injected through a vertical glass tube in the southwest corner of the tank and the sink was at the apex.

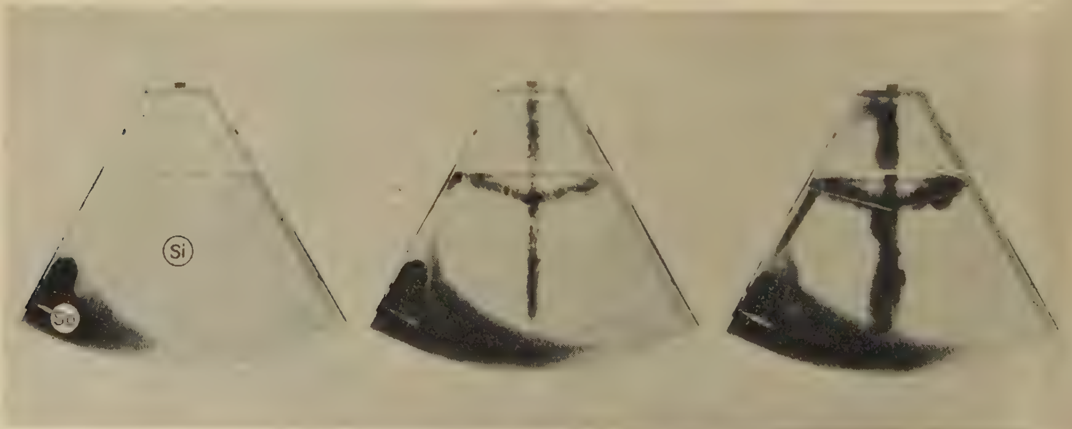

Fig. 10. Photographs at 15, 32, and 35 minutes with $S_0 = 100$ cc./min. This experiment corresponded to fig. 4 and was identical to that of Fig. 9 except that the external sink at the apex was eliminated. Potassium permanganate dye from crystals introduced through slits in the glass cover showed the southward flowing western boundary current.

mixture gradually spread across the tank near the rim. (The anomalous apparent southward flow of permanganate dye in the interior (Fig. 10c) was due to the dense concentration of heavy dye near the botton and antitriptic outward flow toward surfaces of lower "geopotential". The bottom surface of the model was not an equipotential surface, and the introduction of density gradients destroys the simple interpretation of the simulation of the "β" effect by a radial variation of depth.)

REFERENCES

STOMMEL, HENRY, 1957: A survey of ocean current theory. *Deep-Sea Research* 4, pp. 149-184.

VON ARX W. S., 1952: A laboratory study of the wind-driven ocean circulation. *Tellus*, 4, pp. 311—318.

PRINTED IN SWEDEN
ESSELTE, STHLM 58

Contribution No. 940

Reprinted from LIMNOLOGY AND OCEANOGRAPHY
Vol. 3, No. 3, July, 1958
Printed in U.S.A.

Benthic Studies in Buzzards Bay. I. Animal-Sediment Relationships[1]

HOWARD L. SANDERS

Woods Hole Oceanographic Institution, Woods Hole, Mass.

ABSTRACT

During October and November 1955 a bottom faunal study was undertaken at 19 localities in Buzzards Bay, Massachusetts. The number of animals ranged from 1,064 to 12,576/m² with a mean number of 4,430. In comparison with certain other areas these numbers appeared small and seemed to be due to the relatively low concentrations of chemical nutrients and modest primary production of the region. Two faunal assemblages were recognized: one, present in the muddy sediments and dominated by the lamellibranch *Nucula proxima* and the polychaete *Nephthys incisa* was essentially the same community described from Long Island Sound; the other, restricted to the sandier sediments and characterized by species of the amphipod genus *Ampelisca*. The two primary feeding types, the filter-feeders and the deposit-feeders, numerically dominated in the sand and mud sediments, respectively. The distribution of certain dominant deposit-feeders in Long Island Sound and Buzzards Bay was poorly correlated with the silt-clay fraction of the sediment. However, when clay alone was used, a much better agreement was obtained. It was suggested that clay is probably the most valid criterion for the distribution of deposit-feeders. The distribution of infaunal filter-feeders seemed related to the degree of sorting and the median grain size of the sediment, with largest populations present in well-sorted fine sand. The hydrodynamic implications of this distribution are discussed.

INTRODUCTION

A quantitative benthic survey was undertaken in Buzzards Bay, Massachusetts, during October and November of 1955. Four survey stations (Fig. 1: H, J, P, and R) were selected as being representative of different widespread sediment and faunal assemblages. They were subjected to intensive monthly sampling over a twelve-month period (February 1956–February 1957) with the purposes of measuring some of the dynamic properties of benthic communities such as growth, mortality, and organic turnover of the more important species components; of obtaining additional data on animal-sediment relationships; and of defining the niches of the numerically abundant species. This paper is concerned with animal-sediment relationships.

Buzzards Bay is a somewhat elongate body of water approximately 46 kilometers in length and about 19.5 kilometers wide at its greatest diameter. It opens to the sea at the south, and along part of the eastern boundary there is appreciable water exchange with Vineyard Sound through the channels that separate the Elizabeth Islands. There is also some water exchange with Cape Cod Bay by means of the Cape Cod Canal (not shown in Fig. 1).

The Bay, as a whole, is relatively shallow, averaging only 11 meters in depth. Bottom temperatures vary from a maximum of approximately 22°C in summer to about 2°C in winter, while salinity values range from 29.5 to 32.5‰.

The locations and depths of the nineteen stations included in this study are shown in Figure 1.

---

[1] Contribution No. 940 from the Woods Hole Oceanographic Institution. This research was supported by National Science Foundation Grant G-2101.

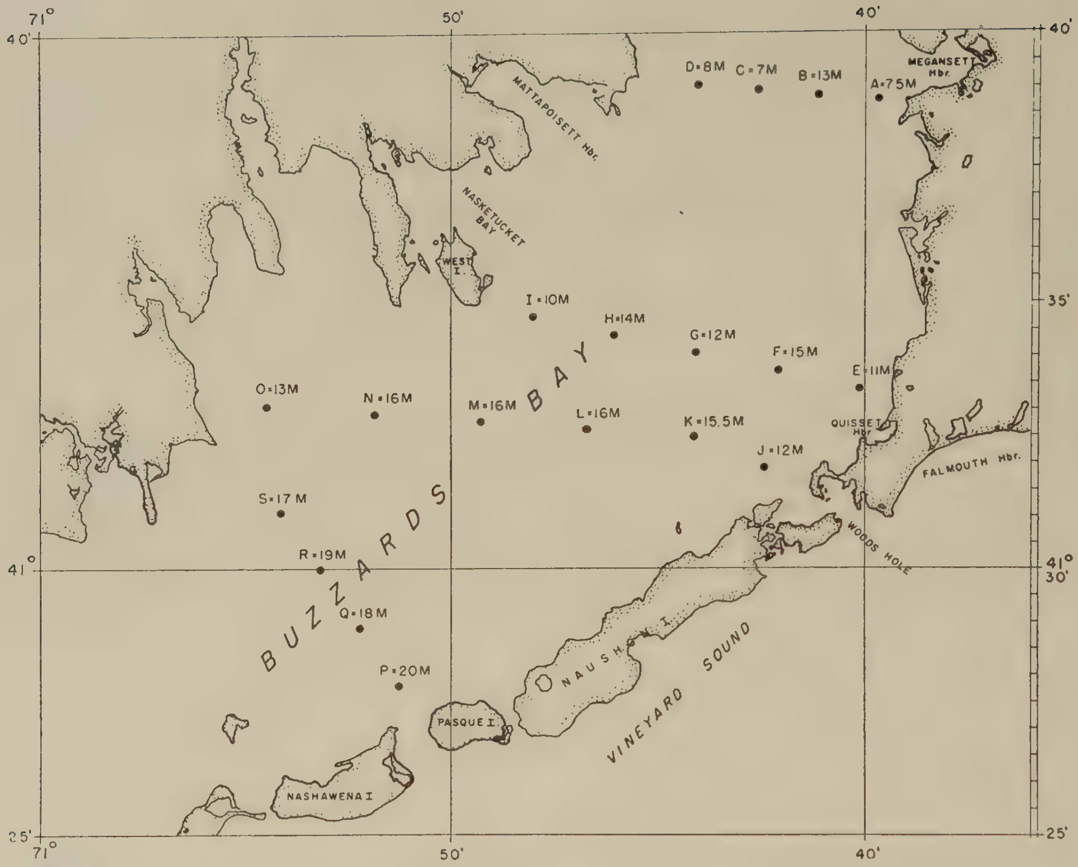
71°
50'
40'
40'
40'
35'
41°
41° 30'
25'
25'
71°
50'
40'
D=8M
C=7M
B=13M
A=75M
MEGANSETT Hbr.
MATTAPOISETT Hbr.
NASKETUCKET BAY
WEST I.
I=10M
H=14M
G=12M
F=15M
E=11M
O=13M
N=16M
M=16M
L=16M
K=15.5M
QUISSET Hbr.
J=12M
FALMOUTH Hbr.
S=17M
R=19M
WOODS HOLE
Q=18M
P=20M
BUZZARDS BAY
NAUSHON I.
VINEYARD SOUND
PASQUE I.
NASHAWENA I

FIG. 1. Map of Buzzards Bay showing the locations and depths of the stations represented in the survey.

METHODS

Samples were obtained with a Forster anchor dredge that was modified by welding the entire frame into a single unit. The apparatus was calibrated to dig to the depth of 7.6 cm, and a small-meshed burlap bag attached to the frame retained the sediment. A small portion of the sediment was saved for sediment analysis, and the volume of the remainder was measured before washing the contents through a sieve of 0.5 mm aperture. The animals retained on the screen were carefully picked out alive in the laboratory and preserved in formalin.

A graded series of sieves was used to divide the sands and gravels into seven size categories. The five silt fractions and the clays were determined by pipetting (Soil Survey Staff 1951). The silt components consisted predominantly of feldspar and some quartz, and the absence of clay particle aggregates indicated that the dispersing agent, sodium hexametaphosphate, was effective. The clay fraction, analyzed by Dr. Ivan Milne of the Gulf Research Development Company, consisted predominantly of illite and chlorite. Montmorillonite, kaolonite, feldspar, and quartz were also detected. The results of the mechanical analyses are given in Table 1. Silt-clay percentages, median grain sizes, and sorting coefficients are given in Table 2. The sorting value was obtained by dividing the variation between the 20 and 80 percentiles by two.

FAUNAL ANALYSES

The numbers present at each station are given in Table 2. The mean number of organisms at all the stations is 4,430/m²,

TABLE 1. *The particle size analysis by per cent weight of the 19 stations included in the Buzzards Bay survey*

Station	Gravel		Sand					Silt					Clay
	(8.0–4.0 mm)	(3.9–2.0 mm)	(1.9–1.0 mm)	(0.9–0.5 mm)	(0.49–0.25 mm)	(0.24–0.125 mm)	(0.124–0.062 mm)	(61–31 μ)	(30–16 μ)	(15–8 μ)	(7–4 μ)	(3–2 μ)	(>2μ)
A	2.04	4.76	14.63	53.74	20.48	2.58	0.74	←		0.99			→
B	0.29	0.46	4.98	23.14	44.20	17.16	3.76	←		5.82			→
C	1.41	1.62	5.46	31.30	48.32	8.85	0.35	←		3.00			→
D	0.14	0.20	1.86	14.52	43.40	33.70	2.06	←		4.02			→
E	—	0.27	5.16	35.06	49.30	7.62	0.28	←		2.20			→
F	—	—	0.06	0.30	1.43	2.62	4.37	10.66	18.38	20.35	12.57	9.85	19.55
G	—	0.07	1.73	13.66	34.19	32.96	2.13	1.05	3.18	3.00	2.47	1.12	4.19
H	—	0.21	3.49	26.70	46.05	13.40	2.33	0.92	0.78	1.05	1.86	0.97	2.42
I	3.34	3.58	8.99	19.92	30.16	21.85	4.48	2.09	0.93	0.93	1.07	0.42	2.20
J	—	0.06	0.43	3.47	7.39	7.11	15.65	14.35	11.53	8.69	10.33	6.41	14.28
K	—	—	—	—	0.10	0.21	1.78	10.75	16.93	22.23	22.23	8.00	17.47
L	—	—	0.05	0.12	0.27	1.67	4.21	23.50	14.13	13.52	13.73	10.05	19.10
M	—	—	—	0.04	0.23	0.93	5.45	11.96	18.63	17.67	16.51	9.52	18.70
N	—	0.06	1.24	9.18	40.48	42.18	2.30	0.89	0.18	0.53	—	0.71	2.21
O	1.09	1.16	1.25	1.29	2.24	3.37	15.99	16.45	15.17	14.26	10.79	4.20	12.57
P	—	0.06	0.04	0.32	12.50	78.05	4.04	0.79	0.54	1.58	1.20	0.52	0.38
Q	—	—	0.06	0.45	0.68	5.96	20.87	13.62	14.53	13.05	12.72	6.62	11.40
R	—	0.20	0.12	0.28	0.84	1.36	5.27	17.23	20.09	16.87	7.19	12.22	18.18
S	1.24	0.19	1.23	4.27	12.57	19.43	10.04	9.87	11.72	6.47	8.51	2.90	11.59

TABLE 2. *The values of certain geological and ecological factors measured in the survey*

Station	Silt-clay percentage	Clay percentage	Sorting coefficient (mm)	Median grain size (mm)	No. Animals /m²	Epifauna		Filter-feeding infauna				Deposit-feeding infauna			
						No./m²	% of total	No./m²	% of total	No. dominant spp. /m²*	% of total filter-feeders	No./m²	% of total	No. dominant spp. /m²**	% of total deposit-feeders
A	0.99		0.67	0.68	1629	745	45.73	295	33.27	124	42.03	233	26.35	0	0.00
E	1.79		0.48	0.45	2259	115	5.09	980	45.71	837	85.41	227	10.59	213	93.84
C	3.00		0.50	0.44	3305	450	13.62	1841	64.48	1765	95.87	363	12.71	0	0.00
D	3.81		0.31	0.31	3283	191	5.82	2371	76.68	2007	84.65	321	10.38	136	42.37
N	4.40		0.30	0.26	5859	125	2.13	4648	81.06	3945	84.22	687	11.97	30	4.37
P	5.00		0.10	0.18	12576	5290	42.06	5185	62.91	3114	60.06	3084	34.72	941	30.51
B	5.32		0.45	0.37	2619	179	6.83	1761	72.17	1452	82.45	258	10.57	189	73.26
I	6.68		0.70	0.38	4379	437	9.98	2575	65.32	2186	84.79	426	10.81	315	73.94
H	6.90		0.45	0.37	5519	179	3.24	3227	60.43	2855	88.49	1539	28.82	448	29.10
G	13.29	4.19	0.34	0.26	3061	33	0.11	1497	49.44	739	49.37	1423	46.99	1004	73.37
					44489			24380	$\bar{x}=64.87$	19024	$\bar{x}=78.03$	8561	$\bar{x}=22.79$	3316	$\bar{x}=38.73$
S	43.64	11.59	0.26	0.04	4319	267	6.18	1362	23.61	1002	73.51	1845	45.53	1578	85.58
J	59.42	12.35	0.089	0.03	5455	447	8.19	2072	41.29	1238	59.75	2836	56.52	2272	80.11
Q	63.00	11.40	0.080	0.023	3211	57	1.78	620	19.31	55	8.87	2391	74.46	1955	81.76
O	67.14	12.52	0.079	0.023	4462	0	0.00	405	9.08	0	0.00	3892	87.23	3758	96.56
R	81.19	18.18	0.038	0.013	6068	126	2.08	125	2.10	0	0.00	5545	93.32	4527	81.61
M	83.95	18.70	0.029	0.010	5934	146	2.46	104	1.80	62	59.62	5632	97.30	5173	91.85
F	85.47	19.45	0.029	0.010	1187	0	0.00	41	3.45	8	19.51	1049	88.37	737	70.26
L	86.23	19.10	0.042	0.012	7982	182	2.30	377	4.87	109	28.91	7089	91.52	6114	86.25
K	93.36	17.45	0.020	0.015	1064	18	1.69	215	20.55	106	49.30	742	70.94	673	90.70
					39628			5321	$\bar{x}=13.81$	2580	$\bar{x}=48.49$	26787	$\bar{x}=78.35$	26787	$\bar{x}=86.35$

* *Ampelisca spinipes, A. macrocephala, Byblis serrata, Cerastoderma pinnulatum.*

** *Tellina tenera, Nephthys incisa, Nucula proxima, Turbonilla* sp., *Retusa caniculata, Cylichna orzya, Nerinides* sp.

with a range of from 1,064 at Station K to 12,516 at Station P.

Buzzards Bay has numerically smaller benthic populations than some other areas. This is shown in the following table.

Location	No. of stations	Range	Mean	Screen mesh size
Buzzards Bay (present study)	19	1,064–12,576	4,430	0.5
Loch Craiglin, Scotland (Raymont 1949)	5	5,409–19,065	14,275	1.0
English Channel (Mare 1942)	1		2,356	1.0
Long Island Sound (Sanders 1956)	8	5,566–46,404	16,446	1.0

The Buzzards Bay-Woods Hole environment can be compared with Long Island Sound (Riley 1955, Sanders 1956) in regard to at least a limited number of factors. Chlorophyll readings (Yentsch, unpublished) and phosphorus concentrations (Crowin, unpublished) have been collected from the dock of the Woods Hole Oceanographic Institution. From the nature of the local current system it is apparent that such samples are fairly typical of the water present in the surrounding regions, and the values measured, therefore, can be applied directly to Buzzards Bay. The mean depth of Long Island Sound is 20 meters and of Buzzards Bay 11 meters. Yet Long Island Sound exceeds Buzzards Bay in winter maximum phosphorus, average chlorophyll/m^3, and mean benthic population by factors of 2.5, 3.5, and 3.6, respectively. It seems obvious that since the depth is not markedly different in these two areas, the very much larger bottom population present in Long Island Sound is the result of the larger phytoplankton population, its major source of food.

BENTHIC COMMUNITIES IN BUZZARDS BAY

One of the main objectives of this paper is to delimit the level-bottom animal communities present in Buzzards Bay. To facilitate this end, the distribution by num-

TABLE 3. *The numbers and proportion of 8 species of animals commonly associated with sandy sediments in Buzzards Bay*

Station	1		2		3		4		5		6		7		8	
	No.	%	No.	%	No.	%	No.	%	No.	%	No.	%	No.	%	No.	%
A	124	7.61	—	—	—	—	—	—	—	—	62	3.81	15	0.92	78	4.79
E	14	0.62	57	2.52	28	1.24	738	32.67	14	0.62	419	18.55	85	3.76	114	5.05
C	1715	51.89	50	1.51	—	—	—	—	—	—	275	8.32	75	2.27	25	0.76
D	1628	49.59	322	9.81	57	1.74	—	—	136	4.14	336	10.23	64	1.95	14	0.43
N	98	1.67	833	14.22	2720	46.42	294	5.02	6	0.10	74	1.26	270	4.61	25	0.48
P	566	7.77* 4.50**	849	11.65 6.75	1520	20.89 12.09	179	2.41 1.42	92	1.26 0.73	238	3.27 1.89	209	2.87 1.66	—	—
B	1306	49.87	129	4.93	17	0.65	—	—	189	7.22	258	9.85	266	10.16	34	1.30
I	928	21.20	91	2.08	22	0.50	1145	26.14	229	5.23	22	0.50	480	10.96	437	9.98
H	471	8.53	90	1.63	—	—	1394	25.26	362	6.56	36	0.65	615	11.14	326	5.91
G	439	14.34	54	1.76	11	0.30	—	—	268	8.76	32	1 05	64	2.09	—	—
	7289	$\bar{x}=18.59$	2475	$\bar{x}=6.31$	4375	$\bar{x}=11.16$	3750	$\bar{x}=9.39$	1296	$\bar{x}=3.29$	1752	$\bar{x}=4.47$	2143	$\bar{x}=5.47$	1053	$\bar{x}=2.69$
S	639	14.80	303	7.02	60	1.39	—	—	218	5.05	36	0.83	36	0.83	72	1.67
J	455	8.34	—	—	—	—	789	14.46	—	—	—	—	—	—	55	1.01
Q	—	—	—	—	—	—	55	1.71	—	—	—	—	11	0.34	11	0.34
O	—	—	—	—	—	—	—	—	—	—	—	—	—	—	—	—
R	—	—	—	—	—	—	—	—	—	—	—	—	—	—	204	3.36
M	10	0.17	—	—	—	—	52	0.87	—	—	—	—	—	—	42	0.71
F	8	0.63	—	—	—	—	—	—	—	—	—	—	—	—	—	—
L	36	0.45	—	—	—	—	73	0.92	—	—	—	—	—	—	182	2.30
K	9	0.85	—	—	—	—	97	9.12	—	—	—	—	—	—	36	3.38
	1157	$\bar{x}=2.92$	303		60		1066	$\bar{x}=2.69$	218		36		47		602	$\bar{x}=1.52$

1. *Ampelisca spinipes*
2. *Ampelisca macrocephala*
3. *Byblis serrata*
4. *Cerastoderma pinnulatum*
5. *Tellina tenera*
6. *Nephthys bucera*
7. *Glycera americana*
8. *Lumbrinereis tenuis*

* Percent of infauna.

** Percent of total fauna.

ber of the abundant species is arranged according to the increasing silt and clay content of the sediment (see Tables 3 and 4. Since Station P alone carried a numerically significant epifaunal population, it was necessary to designate for that station in Table 3 both an infaunal and total faunal column.) Certain of these dominant species are wholly or largely limited to sediments with small amounts of silts and clays (*Ampelisca spinipes*, *A. macrocephala*, *Byblis serrata*, *Tellina tenera*, *Nephthys bucera*, and *Glycera* sp.), while others (*Nucula proxima*, *Nephthys incisa*, *Nerinides* sp., *Retusa caniculata*, and *Cylichna orzya*) are largely confined to soils with large concentrations of silts and clays. Other animals such as *Ninöe nigripes*, *Lumbrinereis* sp., and, less strikingly, *Unciola irrorata*, are more widely distributed.

It seems possible from this distribution that two faunal assemblages can be recognized, one found in sediments with low concentrations of fine particles and represented in the survey by Stations A, E, C, D, N, P, B, I, H, and G, the other in sediments with large concentrations of silts and clays and represented by Stations S, J, Q, O, R, M, F, L, and K. Certain stations in the middle of the soil spectrum show transitions from one assemblage to the other; for example, Station G contained appreciable numbers of *Nephthys incisa*, while *Tellina tenera* and *Ampelisca macrocephala* were abundant at Stations S and J.

It is usual to describe benthic communities after the manner of Petersen (1913) by combining the names of two of the characteristic species. Such dominant species should both be numerous and belong to different taxonomic units.

The soft-bottom association is essentially the same as the *Nephthys incisa-Yoldia limatula* community described from Long Island Sound (Sanders 1956). The common representatives in Buzzards Bay are listed below. The percentage composition is given only

TABLE 4. *The numbers and proportion of 8 species of animals commonly associated with muddy sediments in Buzzards Bay*

Station	1		2		3		4		5		6		7		8	
	No.	%	No.	%	No.	%	No.	%	No.	%	No.	%	No.	%	No.	%
A	—	—	—	—	—	—	—	—	—	—	—	—	—	—	31	1.09
E	—	—	—	—	—	—	—	—	—	—	—	—	24	1.06	—	—
C	—	—	—	—	—	—	—	—	—	—	—	—	—	—	138	4.18
D	—	—	—	—	—	—	—	—	—	—	—	—	—	—	50	1.52
N	—	—	24	0.41	—	—	—	—	—	—	—	—	25	0.43	123	2.10
P	—	—	—	—	—	—	—	—	—	—	15	0.21	641	*5.10 **8.80	224	3.35 1.78
B	—	—	—	—	—	—	—	—	—	—	—	—	—	—	9	0.31
I	10	0.23	—	—	—	—	—	—	—	—	44	1.00	32	0.73	33	0.75
H	16	0.29	16	0.29	—	—	—	—	54	0.98	—	—	326	5.91	18	0.33
G	755	24.67	10	0.33	—	—	—	—	11	0.36	—	—	117	3.82	21	0.69
	781	$\bar{x}=1.99$	50						65		59		1165	$\bar{x}=2.97$	647	$\bar{x}=1.65$
S	603	13.96	121	2.80	—	—	579	13.41	169	3.91	96	2.22	591	13.68	169	3.91
J	418	7.66	73	1.34	1218	22.33	36	0.66	218	4.00	91	1.67	127	2.33	273	5.00
Q	739	23.01	320	9.97	254	7.91	56	1.74	255	5.71	387	12.05	88	2.74	55	1.71
O	349	7.82	70	1.57	2162	48.45	28	0.63	698	15.64	251	5.63	147	3.29	237	5.31
R	869	14.32	3306	54.48	—	—	374	6.16	159	2.62	193	3.18	68	1.12	—	—
M	1385	23.34	2040	34.38	—	—	1145	19.30	312	5.26	291	4.90	52	0.88	—	—
F	445	35.88	49	3.86	16	1.26	65	5.13	146	10.51	16	1.26	—	—	—	—
L	1642	20.71	3378	42.61	—	—	389	4.91	304	3.83	401	5.06	97	1.22	—	—
K	340	31.95	88	8.27	—	—	45	4.23	116	10.90	80	7.52	27	2.54	—	—
	6790	$\bar{x}=17.13$	9445	$\bar{x}=23.83$	3650	$\bar{x}=9.21$	2717	$\bar{x}=6.85$	2377	$\bar{x}=6.00$	1806	$\bar{x}=4.56$	1197	$\bar{x}=3.01$	734	$\bar{x}=1.85$

1. *Nephthys incisa*
2. *Nucula proxima*
3. *Turbonilla* sp.
4. *Nerinides* sp.
5. *Retusa caniculata*
6. *Cylichna orzya*
7. *Ninöe nigripes*
8. *Unciola irrorata*

* Percent of infauna.
** Percent of total fauna.

for those species comprising more than one per cent of the population.

	% composition
Polychaeta	
Nephthys incisa	17.13
Nerinides sp.	6.85
Ninöe nigripes	3.01
Lumbrinereis tenuis	1.52
Tharyx acutus	1.08
Exogone dispar	
Lumbrinereis hebes	
Aricidea sp.	
Scolelipedes sp.	
Maldanopsis elongata	
Melinna cristata	
Crustacea	
Ampelisca spinipes	2.92
Unciola irrorata	1.85
Hutchinsoniella macracantha	
Edotea montosa	
Lamellibranchia	
Nucula proxima	23.83
Cerastoderma pinnulatum	2.69
Pitar morrhuana	2.55
Yoldia limatula	
Gastropoda	
Turbonilla sp.	9.21
Retusa caniculata	6.00
Cylichna orzya	4.56
Nassarius triviattatus	
Bela turricola	
Enteropneusta	
Dolichoglossus kowalevskii	
Tunicata	
Molgula complanata?	

The two most common forms are *Nephthys incisa* and *Nucula proxima*, comprising 17.13 and 23.83 % of the population by number. Since *Yoldia limatula* makes a much less significant numerical contribution in Buzzards Bay, it is proposed that *Nucula proxima* replace it as a characterizing dominant. The upper salinity associated with this community in Long Island Sound was 29.2, in Buzzards Bay 32‰. The other environmental conditions associated with this community have been described elsewhere (Sanders 1956)

The predominantly sand assemblage is clearly characterized by three closely related species of amphipods, *Ampelisca spinipes*, *A. macrocephala*, and *Byblis serrata* which together constitute over 36 % of the community. The remaining really abundant species in this association is the lamellibranch, *Cerastoderma pinnulatum*, which comprised more than 10 % of the population at the time of sampling. However, because this organism is an annual, being present in markedly reduced numbers or even absent during a significant fraction of the year, it is a poor characterizing species. It therefore seems reasonable to designate this sand bottom association as the *Ampelisca* spp. community, which in Buzzards Bay is found in sediments containing less than 35-45 % silt-clay. The common representatives are listed below. The per cent composition is given only for those species comprising more than one per cent of the population.

	% composition	
Polychaeta		
Glycera americana	5.47	
Nephthys bucera	4.47	
Ninöe nigripes	2.97	
Lumbrinereis tenuis	2.69	
Nephthys incisa	1.99	
Sthenelais boa		
Pholöe minuta		
Eteone lacta		
Phyllodoce arenae		
Paraspionosyllis longicirrata		
Podarke obscura		
Nereis zonata		
Diopatra cuprea		
Haploscolopos fragilis		
Pista sp.		
Polycirrus eximus		
Ampharete arctica		
Scalibregma inflatum		
Crustacea		
Ampelisca spinipes	18.59	
Byblis serrata	11.31	
Ampelisca macrocephala	6.31	
Unciola irrorata	1.65	
Oxyurostylis smithi		
Paraphoxus spinosus		
Phoxocephalus holbölli		
Leptocheirus pingius		
Cerapus tubularis		
Corophium spp.		
Ptilanthura tenuis		
Edotea montosa		
Stenothöe sp.		
Batea secunda		epifauna
Erichthonius brasiliensis		
Aeginella longicornis		
Crago septemspinosus		
Pagurus annulipes		
Neopanope texana		
Lamellibranchia		
Cerastoderma pinnulatum	10.17	
Tellina tenera	3.29	
Nucula delphinodonta		
Pandora gouldiana		
Lyonsia hyalina		
Laevocardium mortoni		
Ensis directus		
Gastropoda		
Natica pusilla		
Nassarius triviattatus		
Crepidula plana		epifauna
Mitrella lunata		
Anachis avara		
Tunicata		
Molgula complanata?	1.85	

The same community with most of the same species represented also occurs in the sandy sediments of Long Island Sound where the *Ampelisca* species comprised about 32 % of the fauna. Since too few stations of this type were present in the survey (Stations 1, 4, and Charles Island), the writer did not feel justified in naming the association in Long Island Sound. In view of the faunal analyses in Buzzards Bay, however, it seems apparent that the infauna of the sandy sediments of Long Island Sound also belongs to the *Ampelisca* spp. community. Evidence for the presence of similar communities elsewhere can be found in the studies of Miyadi (1940), who observed that an *Ampelisca* species was a common organism in the sandy sediments of Tanabe-wan and Osaka-wan, two somewhat enclosed Japanese Bays.

Certain differences exist in the species composition of the ampeliscids in the Long Island Sound and Buzzards Bay regions. *Ampelisca macrocephala* and *Byblis serrata* are largely absent from the region investigated in the central Long Island Sound area. Instead, two sibling species, designated tentatively by the writer as *Ampelisca A* and *B*, comprise the dominant ampeliscid species of the region. Both forms appear identical morphologically, differing only in size, the former being approximately three times as heavy as the latter. There is little overlap in the distribution of the species, with *Ampelisca A* present in sediments with relatively less silt and clay. Probably both forms have been lumped together and included in the species *Ampelisca spinipes*. (Taxonomic difficulties involved in the genus *Ampelisca* have been discussed in detail by Reid 1951.)

There is some indication that *Ampelisca spinipes* in Buzzards Bay may be composed of the same two components, although there appears to be more overlap in the distributions which tend to blur size differences. To test this contention, size-frequency distributions of the *Ampelisca spinipes* representatives were constructed for the nine samples having adequate numbers of this form. The mean length of the largest 20% in each of the four stations having the least silt-clay content was appreciably larger than any of the remaining five stations. Converting length to dry weight (Sanders 1956) the average dry weight equivalent of the largest 20% of the population at the four stations with less silt-clay was approximately 2.8 times as large as the mean dry weight equivalent of the other five stations. These data at least imply that both

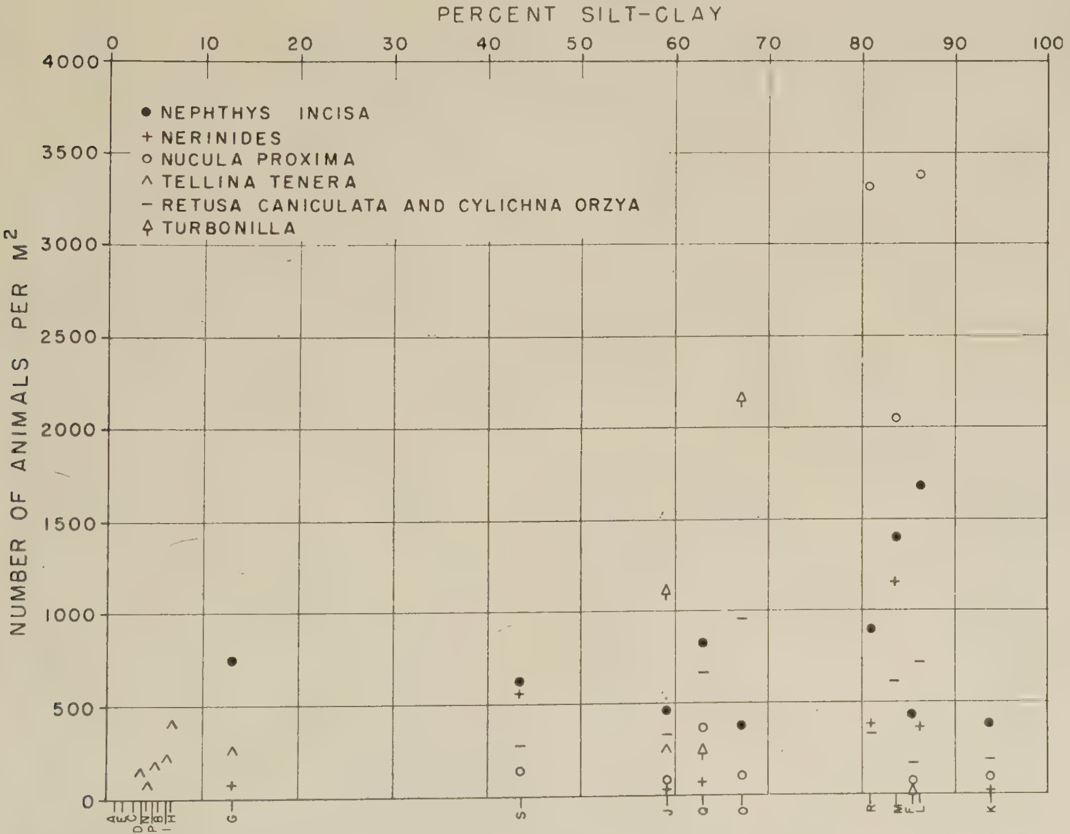

FIG. 2. Relationship of number to sediment composition for seven common deposit-feeders in Buzzards Bay.

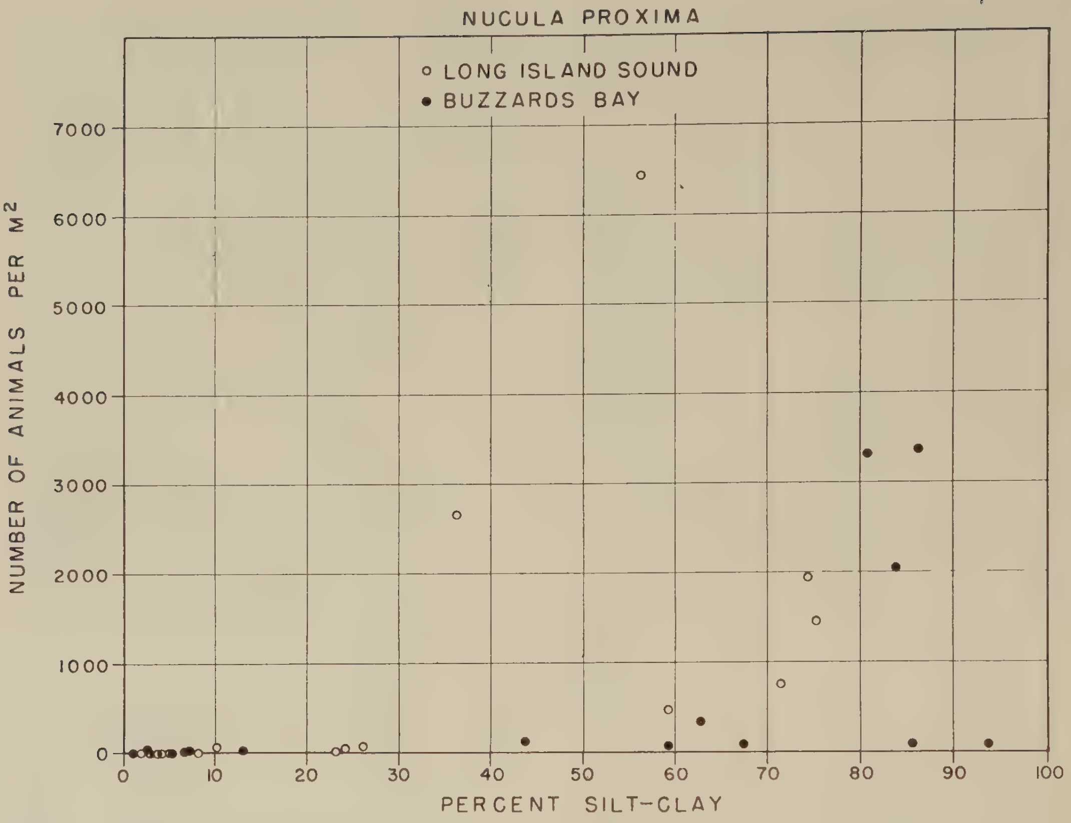

FIG. 3a. Relationship of the number of *Nucula proxima* to the silt-clay component of the sediment in Long Island Sound and Buzzards Bay.

Ampelisca A and *B* may be present in Buzzards Bay.

Stickney and Stringer (1957) describe an *Ampelisca* community in Greenwich Bay, Rhode Island. Their association is present in mud or mud and some sand, with a number of stations carrying more than 10,000 individuals of *Ampelisca spinipes* to the square meter. In contrast, *Ampelisca spinipes* appears to be restricted to the sandy sediments in Buzzards Bay (see Table 3) and Long Island Sound. Other components of Stickney and Stringer's community, *i.e.*, *Nucula proxima*, *Retusa* (Tornatina) *caniculata*, and *Pitar morrhuana* are important constituents of the *Nephthys incisa-Nucula proxima* community in Buzzards Bay (Table 4).

From observations in the laboratory Enequist (1949) defines the ampeliscid type of feeding in which the animals "do not ingest their food chiefly during burrowing but by sucking together tripton with the aid of the current set up by the pleopods and by scraping off or whirling up the surface detritus with the antennae." Since the ampeliscids in Long Island Sound and Buzzards Bay are largely limited to the sandy sediments, it is obvious that they must obtain their food predominantly from suspended matter in the water. *Ampelisca macrocephala* in Greenwich Bay inhabits a similar environment and thus probably feeds in the same manner. However, regarding the extremely abundant *Ampelisca spinipes*, Stickney and Stringer (1957) state, "The digestive tracts of *Ampelisca spinipes* were found to contain large amounts of both mineral and organic detritus suggesting that these species feed upon bottom deposits." This observation, together with the fact that the animal is most abundant in the softer deposits, indicates that in Greenwich Bay, *Ampelisca spinipes* obtains its food largely from settled detritus secondarily suspended by the animal's activity. Conceivably, *Ampelisca spinipes* of Greenwich Bay may be the same animal as *Ampelisca B* in Long Island Sound, since the latter form is found in finer sediments than *Ampelisca A*. Finally, it should be noted that the *Ampelisca* community of Greenwich Bay is replaced in Long Island Sound and Buzzards Bay by the *Nephthys incisa-Nucula proxima* community, which has an extremely small ampeliscid component.

ANIMAL-SEDIMENT RELATIONSHIPS

The primary consumers, *i.e.*, herbivores and detritus feeders, usually comprise 80–99% by number of the benthic faunal in Buzzards Bay. The filter-feeders or animals that obtain their food from suspended matter make up the majority of the fauna in the sandy sediments, while the deposit-feeders living on organic matter in or on the bottom dominate the fauna in the finer sediments. In the *Ampelisca* spp. community the filter-feeders comprise almost two-thirds of the population by number, while over 80% of the fauna of the *Nephthys incisa-Nucula proxima* community are deposit-feeders. The sand sediment, where the *Ampelisca* spp. community is found, reflects the more pronounced current activity in such environments which in turn brings more potential food to the filter-feeding organisms than would weaker currents. Conversely, over mud bottoms, the feeble currents allow organic matter to settle out, thus providing an adequate source of nutrition for large numbers of deposit-feeders.

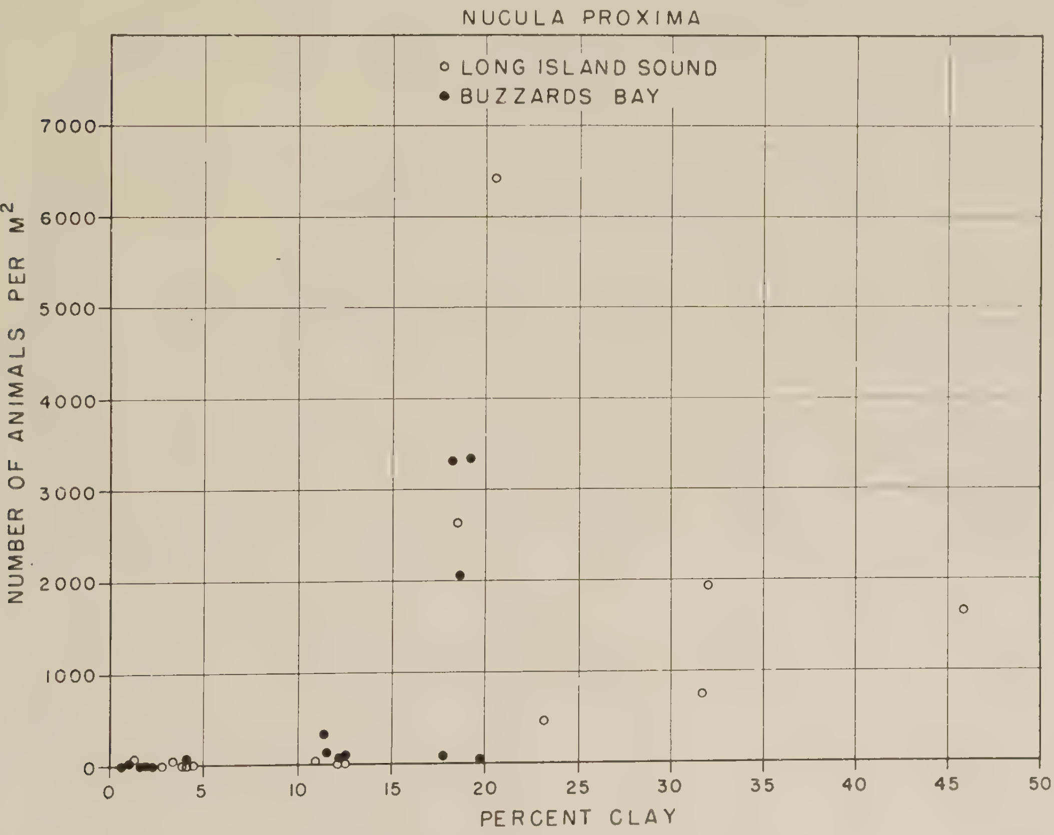

FIG. 3b. Relationship of the number of *Nucula proxima* to the clay component of the sediment in Long Island Sound and Buzzards Bay.

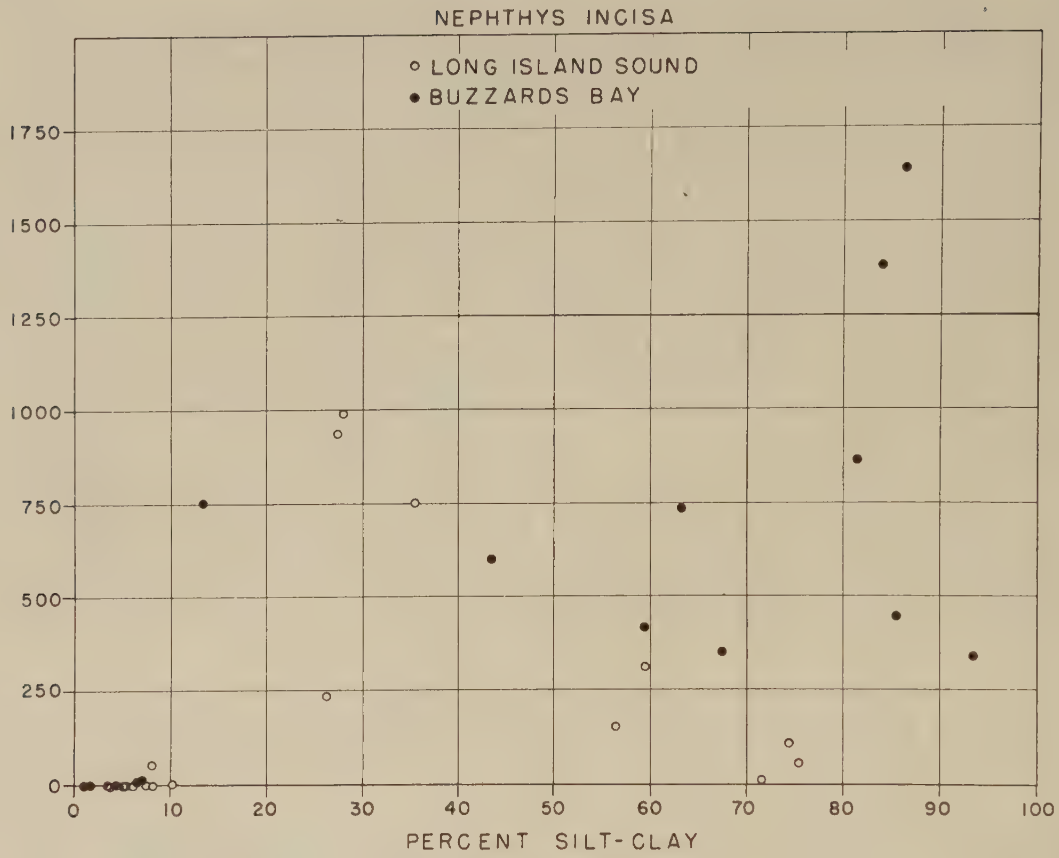

FIG. 4a. Relationship of the number of *Nephthys incisa* to the silt-clay component of the sediment in Long Island Sound and Buzzards Bay.

Within each feeding type a few species are numerically dominant. In the *Ampelisca* spp. community four species comprise 78% of the filter-feeders, and in the *Nephthys incisa-Nucula proxima* community seven forms constitute over 86% of the deposit-feeding fauna (see Table 2). Figure 2 shows the distribution of seven of these deposit-feeders plotted against the silt-clay content of the sediment. A summation of the percentages of filter-feeders and deposit-feeders gives the total for the primary consumers.

It should be noted that one of the included dominant deposit-feeders is a species of the pyramidellid genus *Turbonilla*. All pyramidellid gastropods are believed to be highly specific ectoparasites whose hosts are usually sedentary polychaetes, molluscs, and coelenterates (Fretter and Graham 1949). Yet it is impossible to conceive that the particular species under consideration could possibly have a parasitic mode of life because of its great abundance relative to the animals that might serve as hosts.

Turbonilla is the numerically dominant species of Stations J and O, comprising 22.3 and 48.5%, respectively, of the total population. At Station Q it constitutes 7.9% of the fauna. The only associated animals that might conceivably be abundant enough to serve as possible hosts in this environment are *Nephthys* and *Nucula*. One should expect excellent agreement in a host-parasite relationship, and yet there exists a poor correlation between the distribution patterns of *Turbonilla* and the postulated hosts (Fig. 2). Furthermore, many thousands of living *Nephthys* and *Nucula* have been observed by this writer without finding any indication of a pyramidellid parasite. The actively burrowing habit of *Nephthys* makes that animal an unlikely host, and it is unreasonable to suppose that the diminutive *Nucula* could serve as a suitable host for the larger and often more numerous *Turbonilla*. It is much more likely that this particular species of *Turbonilla* is not an ectoparasite but a deposit-feeder, using its buccal pump to draw in the extremely soft, organically-rich superficial sediment.

The distribution of deposit-feeders in Buzzards Bay and Long Island Sound

Realizing that the distribution of any species in nature is the result of a complex of environmental factors, a unifactorial analysis gives, at best, only a moderately good correlation. For example, the relationship between the distribution of certain deposit-feeding species and the fine fractions of the sediment can be modified in sediments of very high concentrations of these con-constituents by the reduction of oxygen.

The numerically abundant species of deposit-feeders are essentially the same in both of these regions, yet the greatest concentration in Buzzards Bay occurs in sediments with an appreciably higher fraction of silts and clays than in Long Island Sound, although the points are too few to demonstrate this statistically. Figure 3a shows the relationship between the silt-clay composition of the sediments and the numbers of *Nucula proxima*, the most abundant deposit-feeder in both regions. The Long Island Sound samples reveal high numerical values at from 35 to 60% silt-clay, while in Buzzards Bay the highest values are found between 80 to 87%, with low numbers in the region of Long Island Sound maximum.

The differences in distribution between the two areas are much more pronounced than that indicated in Figure 3a. Sediment

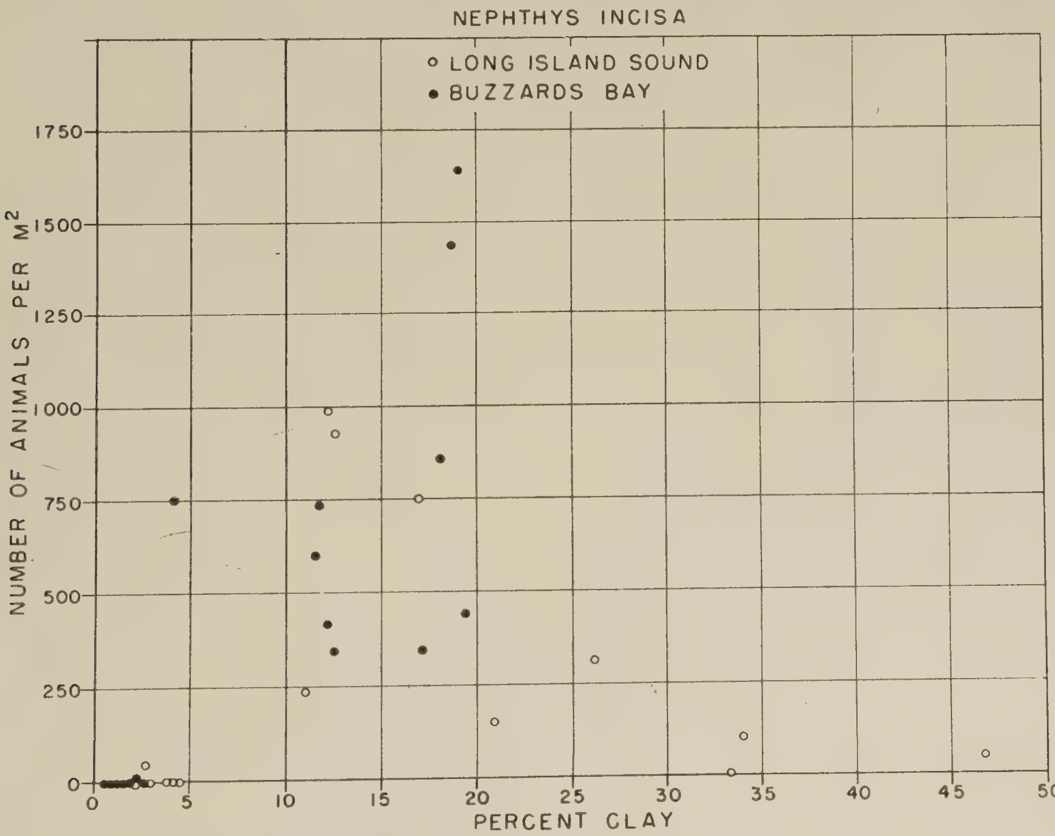

FIG. 4b. Relationship of the number of *Nephthys incisa* to the clay component of the sediment in Long Island Sound and Buzzards Bay.

analyses were not performed on all samples taken in the Long Island Sound study, particularly in regard to a number of samples from Stations 2, 7, and 8. However, the sediments that were analyzed (Sanders 1956) indicate that probably all samples from these stations had a silt-clay content that varied between 25 and 60 %. The number of *Nucula*/m² that were present in the samples not included in Figure 3a are given below. These help to confirm the existence of maximum populations in intermediate silt-clay percentages.

Station 7	September 9, 1953	9,050
	February 3, 1954	4,600
	September 10, 1954	1,200
Station 8	August 1, 1953	4,100
	February 3, 1954	8,000
	July 23, 1954	10,000
Station 2	February 5, 1954	5,450

Essentially the same distributional pattern can be demonstrated for the next most abundant deposit-feeder, *Nephthys incisa* (Fig. 4a) except that the degree of difference in distribution is even more marked. Like *Nucula, Nephthys* in Buzzards Bay is found in largest numbers in 80 to 87 % silt-clay, although the polychaete is abundant over a wider sediment range than *Nucula*. By contrast, in Long Island Sound the largest populations of *Nephthys* are encountered in sediments of from 22 to 40 % silt-clay, while in sediments of more than 70 % silt-clay only small numbers are present.

Why should there be an apparent regional difference in the distribution patterns of *Nephthys* and *Nucula*? A closer scrutiny of the silt-clay fraction of the sediment in these two areas gives a clue. What is immediately evident is that the clay component of this fraction is much larger in the Long Island Sound samples, averaging 48.3 % with a range of from 37.8 to 61.2 %. On the other hand, in Buzzards Bay the clays average only 21.4 % of the silt-clay fraction with a minimum of 18.1 and a maximum of 26.9 %.

Much better agreement is obtained regarding the distribution of *Nucula* and *Nephthys* in Long Island Sound and Buzzards Bay if the number of animals is plotted against only the clay percentage (Figs. 3b and 4b). The Long Island Sound data show that the largest populations of *Nucula* are found between 16 and 22 % clay, and that appreciable numbers are present in sediments with greater clay concentrations. In Buzzards Bay almost the same sediment range, 16 to 19 % clay, representing some of the stations with the largest clay fractions, support the biggest populations of *Nucula*.

There is also excellent agreement in the distribution of *Nephthys* in Long Island Sound and Buzzards Bay (Fig. 4b). With the single exception of Station G with about 4 % clay, the largest populations seem to be confined to sediments with 10 to 20 % clay in both areas. At higher and particularly lower concentrations of clay the numbers of *Nephthys* rapidly diminish.

The data strongly suggest that clay is the most valid sediment correlate for the distribution of deposit-feeding organisms. Clays are much smaller than the silt particles and therefore have a relatively much larger surface area to bind organic matter, the source of food for deposit-feeders. Larger detrital components also tend to accumulate here due to the feeble currents. On the other hand, large concentrations of organic matter may reduce the oxygen content in the sediments and can ultimately limit the environment for deposit-feeders. It is no wonder that the clay fraction seems well correlated with the distribution of deposit-feeding animals.

The distribution of filter-feeding animals in Long Island Sound and Buzzards Bay

The analyses of the samples in both regions demonstrate that the filter-feeders are the dominant feeding type in the sandy sediments, yet it is not entirely evident that the silt-clay concentration alone can explain their distribution pattern (see Table 2). The distribution of filter-feeders may be controlled by the hydrodynamic processes which determine the sediment character rather than directly by the sediment. In the following theoretical speculations three processes need to be considered: the turbulence of water flow, the settling velocities of particles, and the transport of particles. The current necessary to convert the laminar flow over the bottom into turbulent flow is dependent on two factors which are inversely related, the size of the grain protruding into the flow and the velocity of the current. This is shown as the roughness velocity in Figure 5 (Inman 1949). The larger the sediment particles the smaller the velocity necessary to convert a hydrodynamically smooth bottom to one that is hydrodynamically rough. The settling velocity of sediment particles is given by Stokes' Law for grains less than 0.18 mm diameter, and the relationship between particle size and velocity is linear. Particles larger than 0.18 mm fall more slowly than Stokes' Law might predict, because the turbulence created by the falling object becomes a factor (see Fig. 5). The velocity necessary to cause a particle to move along the bottom (threshold velocity, Fig. 5) is minimal for grain sizes of 0.18 mm. Smaller sizes act as a hydrodynamically smooth bottom, and the drag becomes distributed equally rather than on exposed individual particles. It is a point of some interest that the roughness velocity, settling velocity, and threshold velocity are the same for grains of 0.18. Thus sand grains of this size are most easily moved.

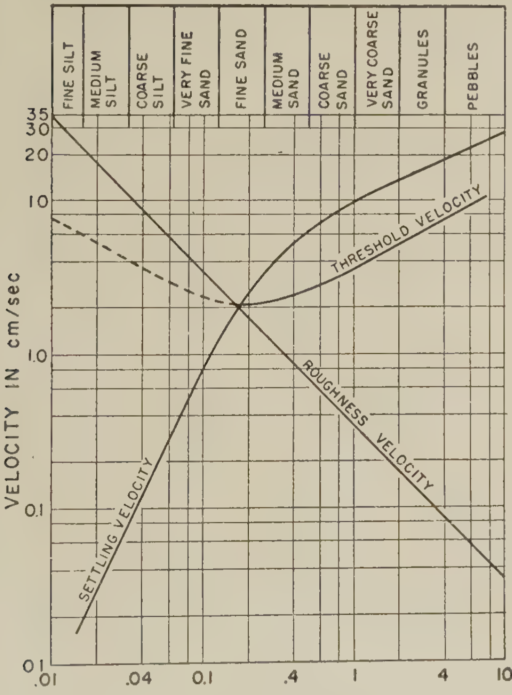

Fig. 5. Relation of grain diameter to settling velocity, threshold velocity, and roughness velocity. Modified from Inman (1949).

Since both finer and coarser sediments are more difficult to move, bottom sediments in the act of transport become better sorted as the diameter approaches 0.18 mm. This has been observed in the sediment studies for Cape Cod Bay (Hough 1942), Barataria Bay (Krumbein and Aberdeen 1937), and the Red Sea (Shakri and Higazy 1944).

The sediment analyses in Buzzards Bay agree with the above findings. By far the best sorted sample, Station P, had a median grain size that was precisely 0.18 mm (see Table 2). This station supports the largest total population and the largest number of filter-feeders. The probability is small that this is mere chance. This observation finds further support in the fact that the next largest number of filter-feeders were present at Station N where the sediment was relatively well sorted and median grain size of 0.26 deviated less from 0.18 mm than at any of the other stations. It therefore appears that two sediment criteria, a median grain size in the fine sands and a well-sorted sample, may be correlated with large populations of infaunal filter-feeders.

The Long Island Sound sediment data were reinterpreted from this point of view. These samples as a rule were much more poorly sorted than the Buzzards Bay series. The Charles Island sample of October 23, 1953, had a much larger population of filter-feeders than any of the other stations from which complete sediment analyses could be obtained. Within Long Island Sound the sediment at this station was the best sorted and had a median grain size of 0.15 mm. Thus the Long Island Sound data confirm the Buzzards Bay observations.

Since these results indicate a possible relationship between infaunal filter-feeders and a well-sorted, fine grain, it is pertinent to define the characteristics of such an environment. Because these sediment particles are precisely the sizes most easily moved, their presence in large concentrations is indicative of little active sediment transport. Such an environment is stable, which is an obvious advantage to organisms that live on and in the sediments.

As particle sizes become larger than 0.18 mm, the material will slide or roll over the bottom rather than go into suspension, because the roughness velocity is less than the threshold and settling velocities (see Fig. 5). Infaunal filter-feeders must maintain connection with the sediment surface in order to feed, and the shifting of the sand particles tend to make the maintenance of this connection precarious. The stations that best typify these conditions in Buzzards Bay (A and E) support very modest populations of infaunal filter-feeders.

Sediments that predominantly consist of silts and clays support meager numbers of filter-feeders for an entirely different reason. These sediments reflect the feeble currents present which allow the fine particles, including the organic matter, to settle out. There is therefore a smaller amount of organic matter in suspension to supply food for the filter-feeders. Most of the stations with fine sediments (Q, O, R, M, F, L and K) support small populations of filter-feeders.

What can be deduced about the well-sorted fine sands? For reasons previously stated, it must be a stable environment. Furthermore, the extremely good sorting indicates that the intensity of the current over the bottom during a tidal cycle must be remarkably constant, probably deviating only slightly from a velocity of two centimeters per second. Finally, currents of this intensity must be adequate to support the large populations of filter-feeders found in such sediments.

REFERENCES

Enequist, P. 1949. Studies on the soft-bottom amphipods of the Skagerak. Zool. Bidr. Uppsala, **28**: 297–492.

Fretter, V., and A. Graham. 1949. The structure and mode of life of the Pyramidellidae, parasitic opistobranchs. J. Mar. Biol. Ass. U. K., **28**: 493–532.

Hough, J. L. 1942. Sediments of Cape Cod Bay, Mass. J. Sed. Pet., **12**(1): 10–30.

Inman, D. I. 1949. Sorting of sediments in the light of fluid mechanics. J. Sed. Pet., **19**(2): 51–70.

Krumbein, W. C., and E. Aberdeen. 1937. The sediments of Barataria Bay. J. Sed. Pet., **7**(1): 3–17.

Mare, M. F. 1942. A study of a marine benthic community with special reference to the microorganisms. J. Mar. Biol. Ass. U. K., **25**: 517–554.

Miyadi, D. 1940. Marine benthic communities of the Osaka-wan. J. Oceanogr., **12**(2): 371–385.

Petersen, C. G. J. 1913. Valuation of the sea. II. The animal communities of the sea bottom and their importance for marine zoogeography. Rep. Danish Biol. Sta., **21**: 110 pp.

Raymont, J. E. G. 1949. Further observations on changes in the bottom fauna of a fertilized sea loch. J. Mar. Biol. Ass. U. K., **28**(1): 9–19.

Reid, D. M. 1951. Report on the Amphipoda (Gammaridae and Caprellidae) of the coast of tropical West Africa. Atlantide Rept. No. 2. Sci. Res. Danish Exped. to trop. West Africa, 1945–1946: 189–291.

Riley, G. A. 1955. Review of the oceanography of Long Island Sound. Deep-Sea Res., Suppl. to Vol. **3**: 224–238.

Sanders, H. L. 1956. Oceanography of Long Island Sound, 1952–1954. X. Biology of marine bottom communities. Bull. Bingham Oceanogr. Coll., **15**: 345–414.

Shukri, N. M., and R. A. Higazy. 1944. Mechanical analyses of some bottom deposits of the northern Red Sea. J. Sed. Pet., **14**(2): 43–69.

Soil Survey Staff. 1951. Soil Survey Manual, U. S. Dept. Agr. Handbook No. **18**: 1–503.

Stickney, A. P., and L. D. Stringer. 1957. A study of the invertebrate bottom fauna of Greenwich Bay, Rhode Island. Ecology, **38**(1): 111–122.

Contribution No. 942

DISTRIBUTION OF THE ATLANTIC BIGEYE TUNA, *THUNNUS OBESUS*, IN THE WESTERN NORTH ATLANTIC AND THE CARIBBEAN SEA.—Although the Atlantic bigeye tuna, *Thunnus obesus* (Lowe), was first taken from west of the Azores as recently as 1955 (Bullis and Mather, 1956, Amer. Mus. Novitates, No. 1765: 2), it is now apparent that the species is widely distributed in the western north Atlantic and probably in the Caribbean, also (Table I, Fig. 1).

page 238

In the Caribbean Sea, the species occurs off the islands of Hispaniola, Puerto Rico, and St. Croix, and probably off Venezuela. In addition to the captures in the former area mentioned by Bullis and Mather (*loc. cit.*) a 180 lb. individual was taken off Ponce, Puerto Rico, in the spring of 1955. This was reported by Rolf Juhl of Ponce to Donald S. Erdman, who sent the information to us. Fernandez-Yepez and Santaella (Soc. Venez. Act. Submar., 1956, Publ. Ocas., Bol. No. 1: 23 pp.) mentioned the capture of several tunas, mostly 80–110 kg., off the Venezuelan island of Margarita. These were listed as bluefin tuna, *T. thynnus* (Linnaeus), but the measurements and photograph of a 145 cm. individual resemble *T. obesus* much more closely than *T. thynnus*. Specifically, the diameter of the eye, the length of the pectoral fin, and the depth of body are all notably greater than the corresponding dimensions of an average western Atlantic bluefin of this size. Also, while nearly all the bluefins recorded from southern waters have weighed over 250 lbs., or less than 5 lbs., most of these Venezuelan tunas in question weighed from 175 to 245 lbs. It therefore seems likely that at least a large percentage of the fish from Venezuelan waters reported by these authors and other observers as bluefin tuna were actually *T. obesus*.

Recently the species has been identified among the catches of sport fishermen off Miami, Florida, and Ocean City, Maryland. Four caught off Miami and reported to us by Al Pflueger, taxidermist, and by Dr. C. Richard Robins and Prof. Luis R. Rivas of the University of Miami, were large individuals (123–68 lbs.). We have been informed, however, that 15 to 50 lb. Atlantic bigeyes are sometimes taken in considerable numbers off Ocean City. In 1954, for example, as many as 30 per day were said to have

TABLE I

RECORDS OF ATLANTIC BIGEYE TUNA

No.	Locality	Date	Number Taken	Size	Vessel or observer	Source
1	Margarita Isl., Venezuela		Several	Mostly 80–110 kg.	M/V BOSO MARU	Fernandez-Yepez and Santaella (1956)
2	Ponce, Puerto Rico & St. Croix, V. I.	Winter, 1955	Few		M/V SANTO ANTONINO, Capt. Archie Cross	Bullis & Mather (1956)
3	Ponce, Puerto Rico	Spring, 1955	1	180 lbs.	Rolf Juhl	Donald S. Erdman
4	Alta Vela Isl., Dominican Rep.	IV-21-'55	2	150 cm. 152 cm.	M/V OREGON	Bullis & Mather (1956)
5	Miami, Fla.	X-20-'55	2	140 cm. 123 lbs.	Charter boat, CHIEF	Al Pflueger L. R. Rivas
6	Miami, Fla.	XI-'56	1	160.0 cm. 168 lbs.	Charter boat?	C. R. Robins Al Pflueger
6A	Miami, Fla.	XI-11-'56	1	148.2 cm. 137 lbs.	Charter boat?	L. R. Rivas
7	29°42′N 77°12′W	X-19-'57	1	75 cm. 22 lbs.	M/V DELAWARE	J. L. Squire
8	31°16′N 77°12′W	X-18-'57	1	Head only	M/V DELAWARE	J. L. Squire
9	33°55′N 75°13′W	X-16-'57	1	138 cm. 135 lbs.	M/V DELAWARE	J. L. Squire
10	Ocean City, Md.	IX-4-'57	1	66 cm.	Yt. JOHNNY, J. Englesby	F. J. Mather, III
11	Ocean City, Md.	IX-6-'57	2	18 lbs.	Charter boats or yachts	Milton L. Dennis
12	Ocean City, Md.	IX-7-'57 IX-15-'57	3	16 lbs.	Charter boats or yachts	Milton L. Dennis
13	37°45′N 71°49′W	X-8-'57	1	136 cm. 120 lbs.	M/V DELAWARE	R. H. Gibbs, Jr
14	38°12′N 70°00′W	X-4-'57	1	172 cm.	M/V DELAWARE	R. H. Gibbs, Jr.
15	42°18′N 64°02′W	IX-10-'57	1	125 cm.	M/V DELAWARE	R. H. Gibbs, Jr.
16	Bermuda Isl.		1–2		L. S. Mowbray	Louis S. Mowbray (1956)

been taken by individual sportfishing boats in July. In other years they were most abundant in September. This information was received from Col. Milton L. Dennis of Ocean City, who said that he had reported this previously, but that his identification of the fish had been questioned. The fish taken September 4, 1957 was pointed out by Col. Dennis to one of us (Mather) as a bigeye tuna, and a thorough examination showed that his identification was correct. Col. Dennis was also familiar with the very similar blackfin tuna, *T. atlanticus*, and the bluefin tuna, both of which occur in this locality. Frank Stick of Kitty Hawk, North Carolina, has told us of the capture of some *T. obesus* by sport fishermen off Cape Hatteras.

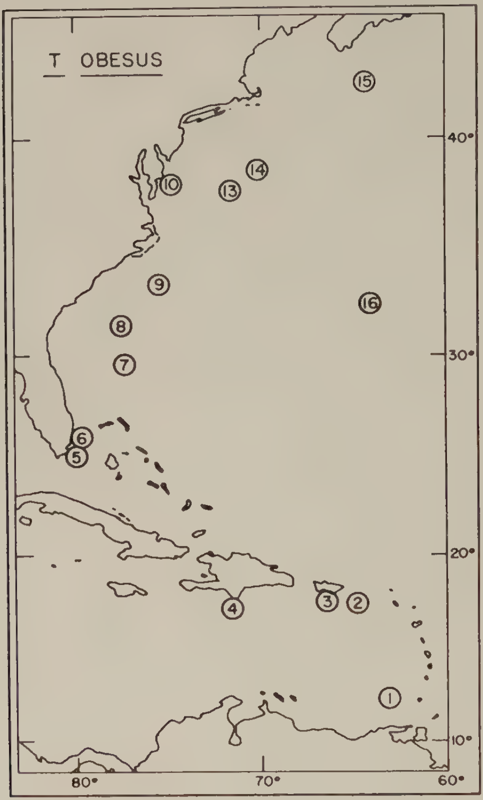

Figure 1. Locations of catches recorded in Table 1. Stations 11 and 12 are the same as 10.

The U. S. Fish and Wildlife Service M/V Delaware, in September and October 1957, took six bigeyes at long-line stations spaced along a zone from 25 to 140 miles outside the hundred fathom curve, extending from 42°18′N. latitude (off Browns Bank) to 29°42′N (off St. Augustine, Florida). One of us (Gibbs) was on the Delaware through the kind invitation of James L. Squire, of the U. S. Fish and Wildlife Service, and examined three of these individuals. The catch off Browns Bank is the northernmost record of the species for the western Atlantic.

It is notable that, with the exception of the reported "run" off Ocean City in July, 1954, all of the records from off the U. S. coast were in the months of September, October or November. Additional long-line fishing in deep water and a closer check on landings of sport fishermen should determine whether the species is definitely seasonal in the region.

According to Louis S. Mowbray ("The Gamefishes of Bermuda," paper presented at International Gamefish Conference, International Oceanographic Foundation, Nassua, 1956: 8 pp.), one or two bigeye tuna have been definitely identified at Bermuda. He suggests that others may have been mistaken for the blackfin tuna, *T. atlanticus*, which is abundant there. Thus it is likely that the range of the western Atlantic individuals is continuous with that of those taken commercially off the Azores, Madeira, the Canary Islands, and the west coast of Africa.—Frank J. Mather, III, and Robert H. Gibbs, Jr., *Woods Hole Oceanographic Institution, Woods Hole, Massachusetts*. Contribution No. 942. Work supported by a grant from the National Science Foundation.

page 239

Contribution No. 943

Reprinted from
Journal of Fluid Mechanics, Vol. 4, Part 3, p. 225, July 1958

Finite amplitude cellular convection

By W. V. R. MALKUS and G. VERONIS
Woods Hole Oceanographic Institution, Woods Hole, Massachusetts

(*Received* 22 *November* 1957)

Summary

When a layer of fluid is heated uniformly from below and cooled from above, a cellular regime of steady convection is set up at values of the Rayleigh number exceeding a critical value. A method is presented here to determine the form and amplitude of this convection. The non-linear equations describing the fields of motion and temperature are expanded in a sequence of inhomogeneous linear equations dependent upon the solutions of the linear stability problem. We find that there are an infinite number of steady-state finite amplitude solutions (having different horizontal plan-forms) which formally satisfy these equations. A criterion for 'relative stability' is deduced which selects as the realized solution that one which has the maximum mean-square temperature gradient. Particular conclusions are that for a large Prandtl number the amplitude of the convection is determined primarily by the distortion of the distribution of mean temperature and only secondarily by the self-distortion of the disturbance, and that when the Prandtl number is less than unity self-distortion plays the dominant role in amplitude determination. The initial heat transport due to convection depends linearly on the Rayleigh number; the heat transport at higher Rayleigh numbers departs only slightly from this linear dependence. Square horizontal plan-forms are preferred to hexagonal plan-forms in ordinary fluids with symmetric boundary conditions. The proposed finite amplitude method is applicable to any model of shear flow or convection with a soluble stability problem.

Introduction

This is a study of the non-linear advective processes which determine the form and amplitude of cellular convection. We shall pose our problem as a formal extension of the conventional linearized stability theory. One purpose is to advance a bit closer to the formidable problem of the onset of turbulence.

Linearized stability theory determines those conditions of a known steady field of flow which first permit the growth of an infinitesimal disturbance. The amplitude of the preferred disturbance or class of preferred disturbances is found from the theory to grow exponentially in time for values of the external parameters in excess of a critical value.

In actuality such disturbances do not grow exponentially without limit, but by advecting heat and momentum they alter their own form and the distribution of their energy sources to achieve a finite equilibrium amplitude. How does this amplitude depend on the external parameters? How much heat and momentum are advected? What distortion of the form of the disturbance occurs at various amplitudes? What determines the preferred state of motion when the stability problem is degenerate, i.e. when more than one solution is possible at the point of instability? Under what conditions does this finite disturbance itself become unstable? Is the new field a similar cellular disturbance or has it the form of an aperiodic 'turbulent' motion?

We have chosen to investigate the steady-state, finite-amplitude, vertical convection of heat for several reasons. It is perhaps the simplest manifestation of non-linear advection in fluids, both geometrically and in the equipment needed for controlled experiments. The stability problem has been exactly solved in terms of trigonometric and hyperbolic functions (Rayleigh 1916; Pellew & Southwell 1940). Some detailed experimental data on the heat transport due to the convection at and beyond the point of instability exist (Malkus 1954a) to compare with theoretical deductions.

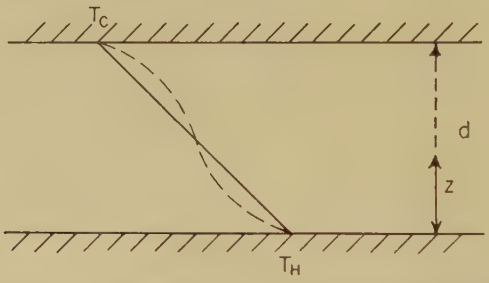

Figure 1. Geometry of the convection problem.

The physical situation to be studied is shown schematically in figure 1. The fluid is contained between two extensive horizontal conducting surfaces distance d apart. The upper surface is held at the temperature T_C and the lower surface at the higher temperature T_H. In the absence of motion the temperature distribution in the fluid is determined solely by the thermal conductivity and is indicated by the heavy line connecting T_H and T_C. In 1916 Lord Rayleigh deduced the criterion for marginal stability in such a fluid layer. This criterion involves what has come to be called the Rayleigh number

$$\lambda \equiv \frac{\alpha g}{\kappa\nu}\beta_m d^4$$

where α is the linear coefficient of expansion of the fluid, g is the magnitude of the gravitational acceleration, $\beta_m = (T_H - T_C)/d$ is the mean negative temperature gradient, κ is the thermometric conductivity and ν the kinematic viscosity of the fluid. When λ exceeds a critical value convection occurs as a regular cellular pattern. The theory does not distinguish between rectangular, triangular or hexagonal horizontal plan-forms for these cells. All could occur at the same value of λ with identical exponential growth rates. Another undetermined quantity in the linear theory is the sign of vertical motion in the centre of the hexagons.

The observations recorded in the earlier experimental paper (Malkus 1954a) establish that for values of λ up to ten times the critical value λ_c a steady cellular convection exists in the fluid. The heat transport due to this convection shows a remarkably linear increase from zero at the critical λ to a value greater than that due to the conduction alone at $\lambda = 10\lambda_c$. This is the range of λ to be studied in this paper.

At $\lambda \doteqdot 10\lambda_c$ a new instability occurs in the fluid producing disordered aperiodic motions, quasi-cellular in appearance. This has been interpreted as the onset of some type of turbulence. However, the heat transport once again increases linearly with λ, but with a steeper slope than in the cellular region. Further discrete changes which steepen the slope of the heat transport curve appear at higher values of λ and appear to be associated with further instabilities. Each transition leads to a more intense and apparently more disordered field of motion. A preliminary statistical study of the convection at these high values of λ has been made in an earlier paper (Malkus 1954b). Several results of the present study of cellular convection which relate to the aperiodic convection at large λ will be discussed in the conclusion.

The dashed curve connecting T_C and T_H in figure 1 is an example of the distribution of horizontally-averaged temperature when cellular convection occurs. The boundary conditions prevent convective heat transport at the boundaries. Hence the additional heat transport is permitted by increased mean temperature gradients at the boundary and decreased gradients in the mid-regions of the fluid. One task we now undertake is to determine the magnitude and shape of this distortion of the mean temperature field.

In the first section we describe the iterative method of solution for the finite amplitude fields of temperature and velocity. This is followed by a detailed treatment of the simplest case, that of two-dimensional convection (roll cell) for free surface boundary conditions. We were able to carry this analysis to 'sixth order' and investigate many of the 'distortions' of the initial convective disturbance. In § 3 we study the first finite amplitude effects of cellular convection with rectangular and hexagonal plan-forms (three-dimensional cells). Up to this point a multiply-infinite set of steady-state finite amplitude solutions has been generated, and we turn to the problem of their stability. The 'relative stability' argument of § 4 resolves the indeterminancy of the steady-state equations by providing a criterion which selects the realizable solutions. In § 5 we discuss the finite amplitude solutions when the fluid has rigid boundaries and in conclusion describe certain approximation techniques to extend the useful range of the formal analysis.

1. Basic equations and the method of solution

The equations which have been used by past authors to investigate convective instability are attributed to Boussinesq (1903, p. 173). They are based on the assumptions that the viscosity and thermal conductivity of the fluid can be treated as constants and that variations in the initial density field are important only in the buoyancy-force term in the equations of motion. Jeffreys (1930) has shown that the resulting disturbance equation is valid in compressible fluids if the temperature gradient minus the adiabatic lapse rate is used rather than the actual temperature gradient and if the total variations in density in the fluid are very small compared to the mean density. In liquids these equations for the local conservation of heat, momentum, and mass respectively are

$$(\partial/\partial t-\kappa\nabla^2)\mathbf{T} = -\mathbf{V}.\nabla\mathbf{T}, \tag{1.1}$$

$$(\partial/\partial t-\nu\nabla^2)\mathbf{V} = -\mathbf{V}.\nabla\mathbf{V}-\nabla\tilde{P}/\rho_0+\gamma(\mathbf{T}-\mathbf{T}_0)\mathbf{k}, \tag{1.2}$$

$$\nabla.\mathbf{V} = 0, \tag{1.3}$$

where $\mathbf{V}$ is the vector velocity of the fluid, $\mathbf{T}$ is the actual temperature, $\mathbf{T}_0$ is a standard temperature and ρ_0 a standard density. $\tilde{P} = P-gz$ where P is the pressure, $\gamma = \alpha g$, and $\mathbf{k}$ is a unit vector in the z-direction. The non-linear advective terms $\mathbf{V}.\nabla\mathbf{T}$ and $\mathbf{V}.\nabla\mathbf{V}$ are to be retained in this analysis and are the principal objects of interest. However, in applying these equations to finite amplitude processes it must be borne in mind that the maximum density fluctuation from the mean must be small. Several interesting geophysical and astrophysical applications of this work require reappraisal of the assumptions and the inclusion of additional terms in the equations.

To clarify the role of the non-linear terms they will be divided into terms which are finite when averaged over a horizontal plane and which therefore modify the average field, and into terms of zero average.

Denoting an average over a horizontal plane by a bar above the quantity, the heat flux equation (1.1) becomes

$$\frac{\partial\bar{\mathbf{T}}}{\partial t}+\frac{\partial}{\partial z}(\kappa\beta) = -\frac{\partial}{\partial z}(\overline{WT}) \tag{1.4}$$

where $\beta = -\partial\bar{\mathbf{T}}/\partial z$, $T = \mathbf{T}-\bar{\mathbf{T}}$, and W is the vertical component of $\mathbf{V}$. Using (1.4), (1.1) may be rewritten as

$$(\partial/\partial t-\kappa\nabla^2)T = \beta W-h, \tag{1.5}$$

where $h = \mathbf{V}.\nabla T-\partial(\overline{WT})/\partial z, \qquad \bar{h} = 0.$

From (1.2) and (1.5) two useful relations can be generated which describe the gross energetics of any flow. Multiplying (1.5) by $\gamma T/\beta_m$, (1.2) by $\mathbf{V}$, and averaging the resulting equations over the entire fluid, one obtains

$$\frac{1}{2}\frac{\gamma}{\beta_m}\frac{\partial}{\partial t}(\overline{T^2})_m = \gamma\left(\frac{\beta}{\beta_m}\overline{WT}\right)_m-\frac{\gamma\kappa}{\beta_m}(\overline{\nabla T.\nabla T})_m, \tag{1.6}$$

and

$$\frac{1}{2}\frac{\partial}{\partial t}(\overline{\mathbf{V}.\mathbf{V}})_m = \gamma(\overline{WT})_m-\nu(\overline{\nabla V_i.\nabla V_i})_m, \tag{1.7}$$

where the subscript m denotes the mean value over a vertical line joining the two horizontal boundaries, and V_i denotes the i-component of the velocity. The averages over the triple-product terms generated by the zero average non-linear terms and the average over the work term $\mathbf{V}.\nabla P$ must all vanish since they represent conservative advections within the fluid system (implying that $(\overline{A\mathbf{V}.\nabla A})_m = 0$ when $\nabla.\mathbf{V} = 0$ and A is any fluctuating scalar field).

Equation (1.7) is the 'power integral' of the motion. It states that the time rate of change of kinetic energy per unit mass is equal to the rate of release of potential energy by the convection minus the rate of dissipation of kinetic energy by the viscous stresses. Equation (1.6) has been written as a 'power integral' to parallel (1.7). However (1.6) is more correctly interpreted as either the balance equation for the mean square of fluctuations of the internal energy, or, equivalently, as an entropy balance equation. The particular value of these non-linear integral statements is in the determination of amplitude when the form of the motion is known or adequately approximated (e.g. Meksyn & Stuart 1951). We shall consider them later in this paper.

Since we will pivot our analysis about the linearized stability problem, it is convenient to eliminate all but one of the dependent variables appearing as linear terms in (1.2), (1.3) and (1.5). Therefore, we cross differentiate to remove the pressure and the linear terms involving the two horizontal velocity components U and V in (1.2) and (1.3). The resulting relation between W and T (plus non-linear terms) is

$$(\partial/\partial t - \nu\nabla^2)\nabla^2 W = \gamma\nabla_1^2 T + L(\mathbf{M}), \tag{1.8}$$

where
$$L(\mathbf{M}) \equiv \frac{\partial^2 M_x}{\partial x \partial z} + \frac{\partial^2 M_y}{\partial y \partial z} - \nabla_1^2 M_z,$$

$$M_x = \mathbf{V}.\nabla U, \qquad M_y = \mathbf{V}.\nabla V, \qquad M_z = \mathbf{V}.\nabla W,$$

and
$$\nabla_1^2 \equiv \partial^2/\partial x^2 + \partial^2/\partial y^2.$$

The two equations which relate the linear components U and V to W are

$$\left(\frac{\partial}{\partial t} - \nu\nabla^2\right)\left(\nabla_1^2 U + \frac{\partial^2 W}{\partial x \partial z}\right) = -\frac{\partial^2 M_x}{\partial y^2} + \frac{\partial^2 M_y}{\partial x \partial y}, \tag{1.9}$$

$$\left(\frac{\partial}{\partial t} - \nu\nabla^2\right)\left(\nabla_1^2 V + \frac{\partial^2 W}{\partial y \partial z}\right) = \frac{\partial^2 M_x}{\partial x \partial y} - \frac{\partial^2 M_y}{\partial x^2}. \tag{1.10}$$

The linear parts of (1.8), (1.9) and (1.10) are just those found in the analysis of convective instability. Cross differentiating (1.8) and (1.5) produces the usual sixth-order equation in the one 'linear' variable W:

$$\left(\frac{\partial}{\partial t} - \kappa\nabla^2\right)\left(\frac{\partial}{\partial t} - \nu\nabla^2\right)\nabla^2 W - \gamma\beta\nabla_1^2 W = -\gamma\nabla_1^2 h + \left(\frac{\partial}{\partial t} - \kappa\nabla^2\right)L(\mathbf{M}). \tag{1.11}$$

All terms on the right of (1.11) are non-linear terms with zero average. On the left are linear terms except for the important horizontal-average temperature gradient which depends upon $\overline{WT}$. To establish this latter relation we first note that the time-independent integral of (1.4) for fixed boundary temperatures is

$$\kappa\beta + \overline{WT} = H = \kappa\beta_m + (\overline{WT})_m, \tag{1.12}$$

where H is the constant heat flux between the horizontal surfaces due to both conduction ($\kappa\beta$) and convection ($\overline{WT}$). Then from the general integral of (1.4) one may write

$$\frac{\beta}{\beta_m} = 1 + \frac{1}{\kappa\beta_m}\left\{(\overline{WT})_m - \overline{WT} + G\left(\frac{\partial \overline{WT}}{\partial t}\right)\right\}, \tag{1.13}$$

where G is that part of β which vanishes when the time variations of $\overline{WT}$ vanish. G is perhaps important in the study of the onset of the aperiodic 'turbulent' convection, but since it will soon disappear from this problem its explicit form need not be given here.

At this point it is of value to non-dimensionalize the physical quantities appearing in the equations. This will simplify the mathematical manipulations and produce the pertinent physical parameters in the problem. Let

$$\mathbf{V} \equiv (\kappa/d)\mathbf{V}', \quad T \equiv (\nu\kappa/\gamma d^3)T', \quad (x,y,z) \equiv d(x',y',z'), \quad t \equiv (d^2/\kappa)t'. \tag{1.14}$$

Having made this change all primes will now be dropped. *In the remainder of this work all unprimed quantities are non-dimensional unless it is otherwise stated.* Using (1.13) and (1.14), equations (1.6), (1.8) and (1.11) become

$$\tfrac{1}{2}\partial(\overline{T^2})_m/\partial t = \lambda(\overline{WT})_m + \{(\overline{WT})_m^2 - (\overline{WT^2})_m + (\overline{WTG})_m\} - (\overline{\nabla T . \nabla T})_m \tag{1.15}$$

$$(\sigma^{-1}\,\partial/\partial t - \nabla^2)\nabla^2 W = \nabla_1^2\, T + \sigma^{-1} L(\mathbf{M}) \tag{1.16}$$

$$\begin{aligned}(\partial/\partial t - \nabla^2)(\sigma^{-1}\,\partial/\partial t - \nabla^2)\nabla^2 W - \lambda\nabla_1^2\, W - \{(\overline{WT})_m - \overline{WT} + G\}\nabla_1^2\, W \\ = -\nabla_1^2 h + \sigma^{-1}(\partial/\partial t - \nabla^2)L(\mathbf{M})\end{aligned} \tag{1.17}$$

where $\sigma \equiv \nu/\kappa$ is the Prandtl number, and λ is the previously defined Rayleigh number. The non-dimensional forms of equations (1.9) and (1.10) will be used later in the analysis but are not needed immediately.

In the usual studies of disturbances of the state of steady conduction, one seeks solutions of the form

$$\left.\begin{aligned} W &= \epsilon W_0 + \epsilon^2 W_1 + \epsilon^3 W_2 + \ldots, \\ T &= \epsilon T_0 + \epsilon^2 T_1 + \epsilon^3 T_2 + \ldots, \end{aligned}\right\} \tag{1.18}$$

with similar expansions for the other variables, where ϵ is a constant parameter. It is then required that expressions (1.18) satisfy the complete equations of motion for all values of ϵ less than some maximum ϵ. The coefficients of each power of ϵ generated by substituting the expressions (1.18) into the equations of motion must vanish individually and the resulting series for each of the variables must converge if relations (1.18) are to represent a satisfactory solution to the problem. Stability theory is concerned with the solutions of the first-order equation only. For first-order solutions to be complete one must require that ϵ be proportional to the amplitude of the disturbance and that this amplitude be infinitesimal. In this finite amplitude study we will find that a similar identification of ϵ and amplitude is necessary if (1.18) is to represent a solution*.

An important point in this expansion remains to be discussed. When the actual forms for the W_i and T_i are substituted into (1.15), one finds an explicit relation between ϵ and λ. Thus

$$\lambda = \lambda_0 + \epsilon\lambda_1 + \epsilon^2\lambda_2 + \ldots, \tag{1.19}$$

where the numbers λ_i are integrals of functions of W_i and T_i. Such a relation between the amplitude and the physical parameter is to be expected. One might have preferred the amplitude to be given as a power series in λ since λ is actually the variable which can be controlled. However, (1.19) is a natural consequence of the expansion (1.18). Explicit determination of the λ_i is discussed in the following paragraphs.

The sequence of linear inhomogeneous equations in powers of ϵ generated by inserting equations (1.18) and (1.19) into equation (1.17) is

$$\left.\begin{aligned}
\mathscr{L}(W_0) &\equiv (\partial/\partial t - \nabla^2)(\sigma^{-1}\,\partial/\partial t - \nabla^2)\nabla^2 W_0 - \lambda_0 \nabla_1^2\, W_0 = 0,\\
\mathscr{L}(W_1) &= \lambda_1\, \nabla_1^2\, W_0 - \nabla_1^2 h_{00} + \sigma^{-1}(\partial/\partial t - \nabla^2)L_{00},\\
\mathscr{L}(W_2) &= \lambda_1\, \nabla_1^2 W_1 + \lambda_2\, \nabla_1^2 W_0 + \{(\overline{W_0\, T_0})_m - \overline{W_0\, T_0} + G_{00}\}\nabla_1^2\, W_0 - \\
&\qquad - \nabla_1^2(h_{01} + h_{10}) + \sigma^{-1}(\partial/\partial t - \nabla^2)(L_{01} + L_{10}),\\
\mathscr{L}(W_i) &= \sum_0^{n-1} \lambda_{i-n} \nabla_1^2\, W_n + \sum_{n+l=0}^{i-2} \{(\overline{W_n T_l})_m - \overline{W_n T_l} + G_{nl}\}\nabla_1^2\, W_{i-(n+l+2)} + \\
&\qquad + \sum_{n=0}^{i-1} \{-\nabla_1^2\, h_{n,i-(n+1)} + \sigma^{-1}[\partial/\partial t - \nabla^2] L_{n,i-(n+1)},
\end{aligned}\right\} \tag{1.20}$$

where the subscripts n, l on the non-linear terms h, L and G mean that W_n or $\mathbf{V}_n$ and T_l are to be substituted for W or $\mathbf{V}$ and T in these terms. The T_i can be determined from the W_i by the auxiliary equations derived from (1.16)

$$\left.\begin{aligned}
\nabla_1^2\, T_0 &= (\sigma^{-1}\,\partial/\partial t - \nabla^2) W_0,\\
\nabla_1^2\, T_i &= (\sigma^{-1}\,\partial/\partial t - \nabla^2)\nabla^2 W_i - \sigma^{-1} \sum_0^{i-1} L_{n,i-(n+1)},
\end{aligned}\right\} \tag{1.21}$$

with similar expansions for U_i and V_i. Each of the W_i must satisfy the boundary conditions for the vertical velocity, each of the T_i the boundary conditions for the temperature fluctuations. The various boundary conditions of the problem will be discussed in the next section.

The first of equations (1.20) is the classical Rayleigh stability equation, and $\mathscr{L}$ can be termed the linear constant-coefficient Rayleigh operator. Assume tentatively that it is solved for W_0 (normalized) and λ_0, and that from the auxiliary equations T_0, U_0, V_0 are also known. The second of equations (1.20) is a linear inhomogeneous equation for W_1. The inhomogeneous terms depend on the known forms of W_0, T_0, U_0, V_0 and the unknown

* V. S. Sorokin (1954) attempted to solve the second order equations by assuming that $\epsilon \sim (\surd\lambda - \surd\lambda_0)^{1/2}$. His neglect of the important terms containing β/β_m in the basic equations prevented him from obtaining any quantitative finite-amplitude results.

number λ_1. The solution of this equation for W_1 will be the sum of a homogeneous solution plus the particular integral generated by these inhomogeneous terms. Three difficulties arise at this point. (1) The part of the homogeneous term which has the form of W_0 will produce a secular (non-periodic) response in the particular integral—a solution which has no physical counterpart; (2) that part of the homogeneous term which satisfies the boundary conditions will contain an arbitrary constant; (3) a part of the inhomogeneous term may satisfy $\mathscr{L}(W) = 0$ but not the boundary conditions (i.e. it will differ from W_0) and will also give rise to a secular response. The last occurs nowhere in our analysis because the inhomogeneous terms themselves always satisfy the boundary condition. The first two complications require that a method be adopted which resolves the indeterminacy and which makes the ϵ-equations a soluble iterative sequence.

We have found only one such method*. It is to require (1) that the λ_i be evaluated so as to eliminate the 'resonant' inhomogeneous terms, for example

$$\lambda_1(\overline{W_0\,\nabla_1^2\,W_0})_m = (\overline{W_0\,\nabla_1^2\,h_{00}})_m - \sigma^{-1}\{\overline{W_0(\partial/\partial t - \nabla^2)L_{00}}\}_m, \qquad (1.22)$$

and (2) that $(\overline{W_0 W})_m = \epsilon$, i.e. that ϵ be proportional to the amplitude of that part of W which has the form W_0. Then from (1.18) all W_i ($i > 0$) must be orthogonal to W_0, though not necessarily orthogonal to each other. The latter requirement removes the arbitrary constants of the homogeneous parts of the W_i equations.

To eliminate the resonant terms in the second-order equation, we must have

$$\begin{aligned}\lambda_2(\overline{W_0\nabla_1^2 W_0})_m^{-1} = {} & -\lambda_1(\overline{W_0\,\nabla_1^2\,W_1})_m - \\ & -\{\overline{W_0[(\overline{W_0\,T_0})_m - \overline{W_0\,T_0} + G_{00}]\nabla_1^2\,W_0}\}_m + \\ & + [\overline{W_0\,\nabla_1^2(h_{01}+h_{10})}]_m - \sigma^{-1}[\overline{W_0(\partial/\partial t - \nabla^2)(L_{01}+L_{10})}]_m.\end{aligned} \qquad (1.23)$$

Higher λ_i generated from (1.20) by the first requirement above are

$$\begin{aligned}\lambda_i = (\overline{W_0\,\nabla_1^2\,W_0})_m^{-1}\Big\{ & -\sum_{n=0}^{i-1}\lambda_{i-(n+1)}(\overline{W_0\,\nabla_1^2\,W_n})_m + (\overline{W_0\,\nabla_1^2\,h_{n,i-n+1}})_m - \\ & -\sigma^{-1}[\overline{W_0(\partial/\partial t - \nabla^2)L_{n,i-(n+1)}}]_m - \\ & -\sum_{n+l=0}^{i-2}[\overline{\{(\overline{W_n\,T_l})_m - \overline{W_n\,T_l} + G_{nl}\}W_0\,\nabla_1^2\,W_{i-(n+l+2)}}]_m\Big\}.\end{aligned} \qquad (1.24)$$

A formal technique for determining the amplitude and distortion of a disturbance as a function of the external parameters is now complete. Can one determine the range of λ in which a series solution terminated after a term ϵ^i is a good approximation to the whole series for W? The best we can do to test the validity of a limited solution is to compare the amplitude of W_i to ϵ, the amplitude of W_0. If this ratio exceeds 0·1, for example, we can be fairly sure that an additional function W_{i+1} must be computed to keep errors in distortion below 10%. However, the important energy and heat transport terms are proportional to products of W and T. Hence the error in these terms will be much smaller than the error of W and T themselves. Examples of determination of the errors in limited solutions are given in the following section.

---

* Recently we have learned that an analogous method was proposed by Lindstedt (1883) to obviate similar difficulties which arise in problems of celestial mechanics.

The proposed technique cannot answer all the explicit questions raised in the Introduction. If a solution to the stability problem, W_0, is independent of time, then none of the equations (1.20) can lead to time dependence. If there are many solutions to the stability problem, then the equations (1.20) give as many answers. To determine which of these answers is realized in an experiment we must separately investigate their 'relative stability'.

Therefore, we do not present this technique as a unique statement of the finite amplitude problem. Several alternative approaches which also answer some but not all of our questions are discussed in the Conclusion.

The following section discusses the consequences of this ϵ-expansion with generating functions based on the simplest solution of the Rayleigh problem.

2. ANALYSIS FOR THE TWO-DIMENSIONAL CASE WITH FREE SURFACES

The first step in a determination of the effects of finite amplitude in equation (1.20) is the resolution of the stability problem. Pellew & Southwell (1940) have made a most comprehensive study, which will be only briefly outlined here. They investigate the first of equations (1.20), $\mathscr{L}(W_0) = 0$, to determine W_0 and λ_0 for three different sets of boundary conditions on the velocities. In every case the boundaries are perfect heat conductors, that is, the fluctuation temperature vanishes there. The conditions at a free boundary are

$$W = \partial^2 W/\partial z^2 = T = 0, \tag{2.1}$$

and are a consequence of the divergence relation (1.3) when the boundary cannot support a stress. The conditions at a rigid boundary are

$$W = \partial W/\partial z = T = 0, \tag{2.2}$$

and are a consequence of the divergence relation when all velocity components must vanish at the boundary.

The assumption made in solving the Rayleigh problem is that the field of motion is separable, i.e.

$$\left.\begin{aligned} W_0 &= \phi(x,y)F(z)G(t), \\ \text{and}\qquad \nabla_1^2\phi(x,y) &= -\alpha^2\pi^2\phi(x,y), \end{aligned}\right\} \tag{2.3}$$

where the separation parameter α is the effective wave-number of the disturbance in the horizontal plane. (In what follows we treat $\phi(x,y)$ as a normalized function.) Pellew & Southwell have shown that this assumption is justified only if the horizontal plan-form of the motion consists of regular 'close-packed cells' at whose lateral boundaries the normal derivatives of the temperature and velocity fluctuations vanish. The plan-forms which satisfy these requirements are the two-dimensional 'roll', the general rectangle, the equilateral triangle and the hexagon. Hence a characteristic value λ_0 will have associated with it an infinite number of possible characteristic functions, all with the same α. Pellew & Southwell correctly suggest that this degeneracy in the first-order theory is removed by 'higher-order' effects, though they were apparently under the impression that the hexagonal plan-form was the preferred motion in all experiments.

Another important contribution of Pellew & Southwell to this first-order problem is their proof that all oscillatory solutions decay. Hence maintained convection is initiated as a steady motion and "limiting conditions of stability are in fact obtained when all time variations (in $\mathscr{L}(W_0) = 0$) are made zero".

Therefore, with the use of (2.3), the equation $\mathscr{L}(W_0) = 0$ becomes

$$(\partial^2/\partial z^2 - \alpha^2\pi^2)^3 W_0 + \lambda_0 \alpha^2\pi^2 W_0 = 0, \tag{2.4}$$

which is a linear sixth-order equation with constant coefficients. Its general solution is

$$W_0 = \phi(x,y) \sum_{i=1}^{3} (A_i \cosh 2\mu_i z + B_i \sinh 2\mu_i z), \tag{2.5}$$

where A_i and B_i are arbitrary constants and

$$4\mu_i^2 \equiv \alpha^2\pi^2\{1 - (\lambda_0/\alpha^2\pi^2)^{1/3}\omega_i\}, \tag{2.6}$$

where the ω_i are the three cube-roots of unity.

Application of the conditions for two free boundaries to (2.5) and (2.6) generates the characteristic functions

$$W_0 = A\phi(x,y)\sin n\pi z, \tag{2.7}$$

where n is an arbitrary integer, and the characteristic values are

$$\lambda_{0n} = \pi^4(n^2+\alpha^2)^3/\alpha^2. \tag{2.8}$$

The lowest value of λ_{0n} is $27\pi^4/4$, and it occurs for $\alpha^2 = \frac{1}{2}$ and $n = 1$. The case $n = 1$ is our primary concern, since, before the modes corresponding to higher values of n can occur, the mode corresponding to $n = 1$ has grown to finite amplitude, markedly altering the basic temperature field.

For two rigid boundaries the characteristic function becomes

$$W_0 = \phi(x,y) \sum_{1}^{3} A_i \cosh 2\mu_i(z - \tfrac{1}{2}), \tag{2.9}$$

where $2z = \pm 1$ at the boundaries and where A_2 and A_3 are related to A_1 by the conditions

$$\sum_{1}^{3} A_i \cosh \mu_i = 0, \qquad \sum_{1}^{3} \mu_i A_i \sinh \mu_i = 0. \tag{2.10}$$

The μ_i are found from (2.6) once λ_0 and α are known. The relation between λ_0 and α has been determined numerically by Pellew & Southwell (1940, p. 377). The lowest value of λ_0 is 1707·8 for $\alpha^2 = 3{\cdot}13/\pi$.

For one rigid and one free boundary the first characteristic function is the second, or 'odd' mode of (2.9) with $2z = 1$ at the rigid boundary and $2z = 0$ at the free boundary. Pellew & Southwell found the minimum eigenvalue to be $\lambda_0 = 1100{\cdot}65$ for $\alpha^2 = 2{\cdot}68/\pi$.

The primary conclusion drawn from the first-order equations is that for $\lambda < \lambda_0$ all infinitesimal disturbances to the purely conductive state decay in time. What will be the equilibrium amplitude of the preferred disturbances for $\lambda \geqslant \lambda_0$?

Finite amplitude solution for rolls

In the remainder of this section we will study the solutions generated by (1.20) for the very simplest case, that of the two-dimensional roll with two free boundaries. Many, but not all, of the properties of the other solutions to this problem are exhibited in this case. However, it must be borne in mind that neither the two free boundaries nor the roll can be realized in practice.

A complete solution to the first-order equations for strip plan-form and two free boundaries is

$$\left.\begin{aligned} W_0 &= 2\cos\pi\alpha x \sin\pi z, \\ T_0 &= (1+\alpha^2)^2(2\pi^2/\alpha^2)\cos\pi\alpha x\sin\pi z, \\ U_0 &= -(2/\alpha)\sin\pi\alpha x\cos\pi z, \qquad V_0 = 0, \\ \lambda_0 &= \pi^4(1+\alpha^2)^3/\alpha^2, \end{aligned}\right\} \tag{2.11}$$

from (1.20), (1.21), (1.9), (1·10) and (2.1).

As noted previously the lowest value of λ_0 is $27\pi^4/4$ and occurs when $\alpha^2 = \frac{1}{2}$. Before solving the second-order equation for W_1, the quantities h_{00}, L_{00} and λ_1 must be determined from (2.11). Now

$$h_{00} \equiv \mathbf{V}_0 . \nabla T_0 - \frac{\partial}{\partial z}(\overline{W_0 T_0}) = \frac{4\pi^2(1+\alpha^2)^2}{\alpha^2}\left[\tfrac{1}{2}\pi\sin 2\pi z - \frac{\partial}{\partial z}(\tfrac{1}{2}\sin^2\pi z)\right] = 0,$$

independently of the choice of α. Also

$$L_{00} \equiv \frac{\partial^2}{\partial x \partial z}(\mathbf{V}_0 . \nabla U_0) + \frac{\partial^2}{\partial y \partial z}(\mathbf{V}_0 . \nabla V_0) - \nabla_1^2 \mathbf{V}_0 . \nabla W_0 = 0.$$

Hence from (1.22) $\lambda_1 = 0$. We shall find that $\lambda_1 = 0$ for all symmetric solutions to the first-order equations. However, the conclusion that $h_{00} = L_{00} = 0$ is true only for rolls and only with two free boundaries. This fortuitous vanishing of all zero-average advection by the first-order solutions leads to $\mathscr{L}(W_1) = 0$; hence $W_1 = U_1 = T_1 = 0$ from (1.20) and (1.21). Therefore $h_{01} = h_{10} = L_{01} = L_{10} = 0$, and the third-order equation of (1.20) becomes

$$\mathscr{L}(W_2) = \lambda_2 \nabla_1^2 W_0 + \{(\overline{W_0 T_0})_m - \overline{W_0 T_0}\}\nabla_1^2 W_0, \tag{2.12}$$

where λ_2 is given by

$$\lambda_2(\overline{W_0 \nabla_1^2 W_0})_m = -[\{(\overline{W_0 T_0})_m - \overline{W_0 T_0}\}\overline{W_0 \nabla_1^2 W_0}]_m \tag{2.13}$$

from (1.23). From (2.11) and (2.13)

$$\lambda_2 = \tfrac{1}{2}\pi^2(1+\alpha^2)^2/\alpha^2. \tag{2.14}$$

Therefore (2.12) becomes

$$\nabla^6 W_2 - \lambda_0 \nabla_1^2 W_2 = -\pi^4(1+\alpha^2)^2 \cos \pi\alpha x \sin 3\pi z. \qquad (2.15)$$

Before investigating the distortions of the roll form generated by (2.15), the implications of our first finite-amplitude results, equation (2.14), will be studied. From (1.19), (1.18) and (2.11), to this third-order approximation, $\epsilon^2 = (\lambda - \lambda_0)/\lambda_2$ and

$$(\overline{WT})_m = \epsilon^2(\overline{W_0 T_0})_m = 2(\lambda - \lambda_0). \qquad (2.16)$$

Also, from (1.13) in its non-dimensional form,

$$\beta/\beta_m = 1 + 2(1 - \lambda_0/\lambda)\cos 2\pi z. \qquad (2.17)$$

In (2.17) the distortion of the mean temperature gradient β/β_m is determined by products of zero-order functions only and requires that for $\lambda > 2\lambda_0$ the gradient should become negative in the mid-regions of the fluid. Equation (2.16) asserts a linear relation between the convective heat transport and λ. (Note that this relation is independent of σ.) That the observed heat transport shows just such a linear relation from λ_0 to the second transition at $10\lambda_0$ suggests that this third approximation provides an adequate description of the field of motion throughout the entire range of steady convection. However, this is not the case as we shall now establish by the investigation of higher order terms.

λ_4-*approximation*

The solution of (2.15) for W_2 is

$$W_2 = C_W \cos \pi\alpha x \sin 3\pi z, \qquad (2.18)$$

where

$$C_W = \frac{\pi^2(1+\alpha^2)^2}{\pi^4(3^2+\alpha^2)^3 - \lambda_0 \alpha^2}.$$

Hence from (1.21) and (1.9)

$$T_2 = C_T \cos \pi\alpha x \sin 3\pi z, \quad U_2 = -(3/\alpha) C_W \sin \pi\alpha x \cos 3\pi z, \qquad (2.19)$$

where

$$C_T = (\pi/\alpha)^2 (3^2+\alpha^2)^2 C_W.$$

Therefore the first distortion of a finite-amplitude roll does not affect the horizontal plan-form, but only the vertical structure. The addition of the term $\sin 3\pi z$ to the first-order solution increases the amplitude of W and T near the boundaries in keeping with the increased gradients near the boundaries (see equation (2.17)).

This rather straightforward iterative analysis will now be extended to determine λ_3, λ_4, λ_5 and λ_6 and the accompanying W_i, T_i, U_i.

From (2.11) and (2.19) one finds that

$$\nabla_1^2(h_{02} + h_{20}) = C_1(\alpha)\cos 2\pi\alpha x(2\sin 2\pi z + \sin 4\pi z)$$

and $$\sigma^{-1}\nabla^2(L_{02} + L_{20}) = \sigma^{-1} C_2(\alpha) \cos 2\pi\alpha x (2 \sin 2\pi z + 3 \sin 4\pi z). \qquad (2.20)$$

Since W_0 is orthogonal to the expressions (2.20), and since $\overline{W_0 T_1} = \overline{W_1 T_0} = 0$, then $\lambda_3 = 0$. Therefore

$$\mathscr{L}(W_3) = \cos 2\pi\alpha x[C_3(\alpha,\sigma)\sin 2\pi z + C_4(\alpha,\sigma)\sin 4\pi z]. \tag{2.21}$$

W_3 and T_3 are of the same form as $\mathscr{L}(W_3)$, but with different coefficients $C(\alpha,\sigma)$, and

$$U_3 = \sin 2\pi\alpha x[C_5(\alpha,\sigma)\cos 2\pi z + C_6(\alpha,\sigma)\cos 4\pi z].$$

In order to determine λ_4 one must construct h_{03}, h_{30}, L_{03} and L_{30} from (2.11) and (2.21). This leads to

$$\begin{aligned}\nabla_1^2(h_{03}+h_{30}) &= \cos \pi\alpha x(D_1 \sin 3\pi z + D_2 \sin 5\pi z) + \\ &\quad + \cos 3\pi\alpha x(D_3 \sin \pi z + D_4 \sin 3\pi z + D_5 \sin 5\pi z),\end{aligned} \tag{2.22}$$

with an identical form for $\nabla^2(L_{03}+L_{30})$ differing only in the coefficients $D(\alpha,\sigma)$. Therefore

$$[\overline{W_0\, \nabla_1^2(h_{03}+h_{30})}]_m = [\overline{W_0\, \nabla^2(L_{03}+L_{30})}]_m = 0 \tag{2.23}$$

and

$$\begin{aligned}\lambda_4 &= \frac{[(\overline{W_0\, T_2} + \overline{W_2\, T_0})\overline{W_0\, \nabla_1^2\, W_0}]_m + (\overline{W_0\, T_0}\; \overline{W_0\, \nabla_1^2\, W_2})_m}{(\overline{W_0\, \nabla_1^2\, W_0})_m} \\ &= -\tfrac{1}{4}C_T + 2\pi^2(1+\alpha^2)^2\alpha^{-2}\, C_W.\end{aligned} \tag{2.24}$$

Since λ_4 is an integral of zero-order and second-order functions only, it is not dependent upon σ. Hence, to the fifth order, σ does not influence the amplitude of the convection. Indeed the largest part of the σ-dependent inhomogeneous term in the equation for W_4, namely, $\sigma^{-1}\nabla^2(L_{03}+L_{30})$, is smaller than the corresponding term in $\nabla_1^2(h_{03}+h_{30})$ by a factor $\alpha^2/[2\pi^2(1+\alpha)^2\sigma]$, $\doteqdot 10^{-2}/\sigma$. Hence in the determination of W_4 and λ_6 these higher-order momentum advection terms will be neglected.

λ_6-approximation

Proceeding as above one finds that

$$\begin{aligned}W_4 &= \cos \pi\alpha(E_1 \sin 3\pi z + E_2 \sin 5\pi z) + \\ &\quad + \cos 3\pi\alpha(E_3 \sin \pi z + E_4 \sin 3\pi z + E_5 \sin 5\pi z),\end{aligned} \tag{2.25}$$

with a similar form for T_4 where $E = E(\alpha,\sigma)$.

As for previous λ_i with odd i, $\lambda_5 = 0$ since $\overline{W_0\, W_3} = \overline{W_0\, T_3} = \overline{W_3\, T_0} = 0$ and $[\overline{W_2(h_{20}+h_{02})}]_m = 0$. Therefore

$$\begin{aligned}\lambda_6 = (\overline{W_0\nabla_1^2 W_0})_m^{-1}\{&(\overline{W_0 T_4} + \overline{W_4 T_0})(W_0\nabla_1^2\, W_0) + (\overline{W_2 T_0} + \overline{W_0 T_2})\overline{W_0\nabla_1^2\, W_2} + \\ &+ \overline{W_0 T_0}\; \overline{W_0\nabla_1^2\, W_4} - (\alpha/\pi)^2(1+\alpha^2)^{-2}[T_2\nabla_1^2(h_{03}+h_{30}) + \\ &+ T_3\nabla_1^2(h_{02}+h_{20})]\}_m,\end{aligned} \tag{2.26}$$

where use has been made of the facts that $(\overline{Th})_m = 0$ and $T_0 = N_0\, W_0$ in order to simplify the last term.

Here for the first time the Prandtl number can have an effect upon amplitude, since the coefficients in W_3 and W_4 are functions of σ.

We are now able to investigate the ranges of λ in which these various solutions W_2, W_3, W_4 first become significant contributors to the field of motion.

For the initially unstable disturbance $\lambda_0 = 27\pi^4/4$ and $\alpha^2 = \frac{1}{2}$ and from (2.14), (2.18), (2.19) and (2.24) $\lambda_2 = 9\pi^2/4$ and $\lambda_4 = -0{\cdot}1248 \doteqdot -\frac{1}{8}$. Then, to this λ_4-approximation, from (1.19)

$$\epsilon^2 = \frac{1}{2}\left\{-\frac{\lambda_2}{\lambda_4} + \left[\left(\frac{\lambda_2}{\lambda_4}\right)^2 + 4\frac{(\lambda-\lambda_0)}{\lambda_4}\right]^{1/2}\right\}. \tag{2.27}$$

Equation (2.27) tells one that ϵ^2 becomes imaginary when

$$\lambda - \lambda_0 = -\tfrac{1}{4}\lambda_2^2/\lambda_4 \doteqdot 1{\cdot}5\lambda_0. \tag{2.28}$$

Hence the range of λ in which this λ_4-approximation is valid is certainly less than $1{\cdot}5\lambda_0$, while the range in which the previous λ_2-approximation is valid must be smaller still. When $\lambda-\lambda_0 = 1{\cdot}5\lambda_0$, $\epsilon^2 = -\frac{1}{2}\lambda_2/\lambda_4 = 2(\lambda-\lambda_0)/\lambda_2$ from (2.27) and (2.28), and ϵ^2 is twice as great as the amplitude predicted in (2.16) for the λ_2-approximation. Therefore the hope that the λ_2-approximation would be valid throughout the laminar convection range is unjustified. It is now clear that the distortion of the initial disturbance must play a significant part in determining the observed heat transport.

The λ_6-computation from (2.26) though tedious, has proved of considerable value in explaining both the observed relation between λ and $(\overline{WT})_m$ and the nature of the ϵ-expansion. Since λ_6 is a function of σ, the various coefficients, $C(\alpha,\sigma)$, $D(\alpha,\sigma)$, $E(\alpha,\sigma)$, entering into it have been computed for $\alpha^2 = \frac{1}{2}$ at three values of σ. For $\sigma = 0{\cdot}8$, a value appropriate for a gas, $\lambda_6 = 2{\cdot}31\times10^{-3}$. For $\sigma = 8$, a value appropriate for water, $\lambda_6 = 2{\cdot}30\times10^{-3}$. For $\sigma=\infty$, $\lambda_6 = 2{\cdot}29\times10^{-3}$. It would be necessary to include the small neglected σ-term in W_4 in order to decide whether the effect of σ on heat transport is just very small or whether it vanishes completely. We will return to the effects of σ in the following section. Here we will study amplitudes and distortions when $\lambda_6 = 2{\cdot}30\times10^{-3}$ corresponding to the value of σ for water.

In order to determine ϵ as a function of λ, to the λ_6-approximation, from (1.19) one must solve the cubic equation

$$(\epsilon^2)^3\lambda_6 + (\epsilon^2)^2\lambda_4 + \epsilon^2\lambda_2 + \lambda_0 - \lambda = 0, \tag{2.29}$$

for $\lambda_0 = 27\pi^4/4$, $\lambda_2 = 9\pi^2/4$, $\lambda_4 = -\frac{1}{8}$, $\lambda_6 = 2{\cdot}30\times10^{-3}$. The heat transport to this same approximation is

$$\begin{aligned}(\overline{WT})_m &= \epsilon^2(\overline{W_0\,T_0})_m[1+\epsilon^4(\overline{W_2\,T_2})_m/(\overline{W_0T_0})_m] \\ &= \epsilon^2(\overline{W_0\,T_0})_m(1+7{\cdot}15\times10^{-7}\epsilon^4)\end{aligned} \tag{2.30}$$

from (1.18), (2.18) and (2.19). In figure 2 we have plotted the total heat transport, divided by its value at λ_0 against λ/λ_0 for the λ_6-approximation, for the λ_4-approximation from (2.27), and for the λ_2-approximation from (2.16). The two additional curves labelled α^2 and λ_6 (*ZANL*) will be discussed shortly.

Effects of λ_6 and zero-average non-linear terms

Perhaps the most interesting aspect of the curve for λ_6 is that it has brought the heat transport back very nearly to the λ_2-curve in the range $\lambda_0 \leqslant \lambda \leqslant 3\lambda_0$. This alternating character of the various approximations to λ makes the observed linear relation between heat transport and λ more understandable. One can anticipate that the λ_8-curve, like the λ_4-curve, will diverge to the right at some λ greater than $3\lambda_0$, while the λ_{10}-curve, like the λ_6-curve, will be more nearly parallel to that for λ_2. This alternation also suggests that a more satisfactory formulation of our problem should be sought permitting an expansion $\lambda = \lambda(\epsilon)$ in some monotonic sequence.

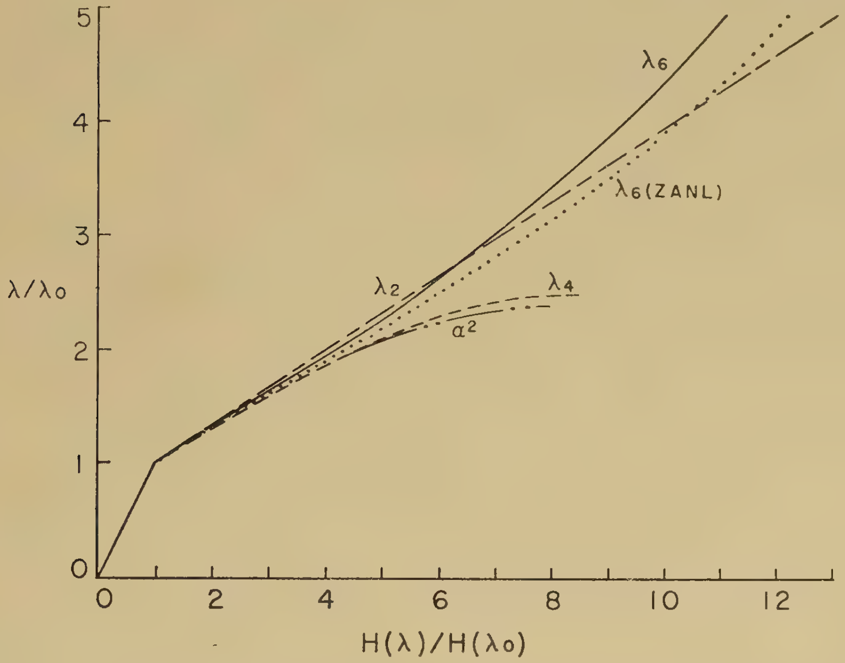

Figure 2. Heat transport *vs* Rayleigh number for the second, fourth and sixth approximations, for the fourth approximation with variable α^2, and for the sixth approximation without zero-average non-linear terms.

The percentage error of the λ_6-curve at various λ can be estimated by comparing the magnitude of the various terms in the expansion of $\overline{WT}$ (or equivalently of β/β_m). From (1.18), (1.13), and the preceding equations for W_i and T_i,

$$\begin{aligned}\overline{WT} &= \epsilon^2\{\overline{W_0 T_0} + \epsilon^2(\overline{W_0 T_2} + \overline{W_2 T_0}) + \epsilon^4(\overline{W_0 T_4} + \overline{W_2 T_2} + \overline{W_4 T_0}) + \ldots\} \\ &= \epsilon^2(\overline{W_0 T_0})_m\{2\sin^2 \pi z + \epsilon^2(1{\cdot}098 \times 10^{-2})\sin \pi z \sin 3\pi z + \\ &\qquad + \epsilon^4[1{\cdot}43 \times 10^{-6} \sin^2 3\pi z - 2{\cdot}22 \times 10^{-5} \sin \pi z \sin 3\pi z + \\ &\qquad\qquad + 2{\cdot}38 \times 10^{-5} \sin \pi z \sin 5\pi z\}. \qquad (2.31)\end{aligned}$$

Therefore

$$\frac{\beta}{\beta_m} = 1+\frac{(\overline{WT})_m-\overline{WT}}{\lambda}$$

$$= 1+\epsilon^2(\overline{W_0\,T_0})_m\lambda^{-1}\{(1-5{\cdot}49\times10^{-3}\epsilon^2+1{\cdot}11\times10^{-5}\epsilon^4)\cos 2\pi z+$$

$$+(5{\cdot}49\times10^{-3}\epsilon^2-2{\cdot}3\times10^{-5}\epsilon^4)\cos 4\pi z+1{\cdot}26\times10^{-5}\epsilon^4\cos 6\pi z+\ldots\}. \tag{2.32}$$

For $\lambda = 3\lambda_0$, equation (2.29) has the root $\epsilon^2 = 57{\cdot}7$, whence

$$\beta/\beta_m = 1+1{\cdot}301[0{\cdot}801\cos 2\pi z+0{\cdot}160\cos 4\pi z+0{\cdot}041\cos 6\pi z+\ldots], \tag{2.33}$$

suggesting that at this value of λ the error due to neglected terms is less than 2%. This error is of course much smaller at smaller λ, but will rise rapidly for $\lambda > 3\lambda_0$.

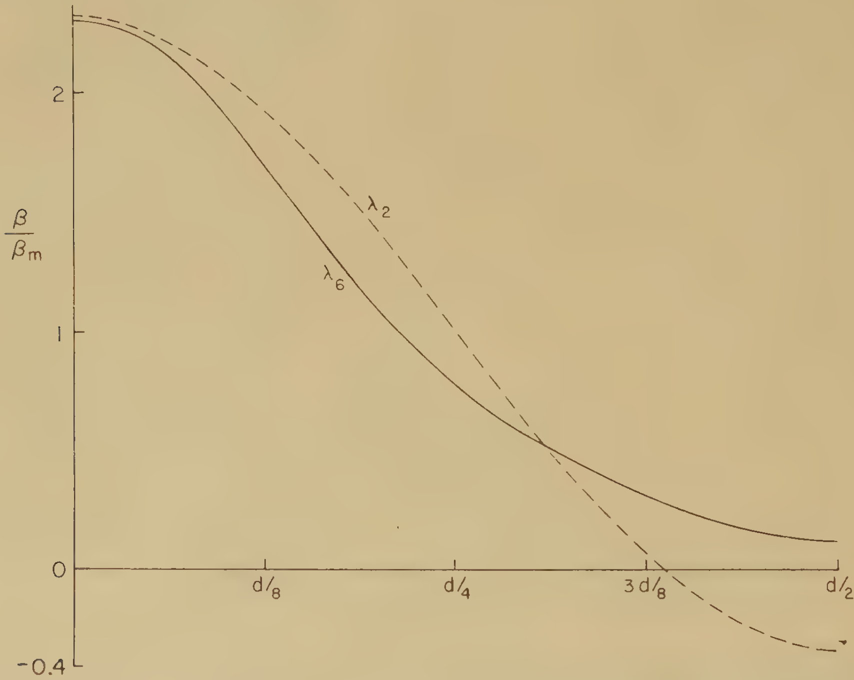

Figure 3. Comparison of the mean temperature gradients predicted by the second and sixth approximations for free rolls at $\lambda = 3\lambda_0$.

An interesting consequence of relation (2.32) is depicted in figure 3. The curves β/β_m for λ_2 from (2.17) and for λ_6 from (2.33) at $\lambda = 3\lambda_0$ are drawn from a boundary to the middle of the fluid. Despite the negligible change in heat transport (given by the gradients at the boundary), the distortion of the finite amplitude disturbance has prevented the gradient from becoming negative. This is probably a property of the convection at all λ, but no general proof that $\beta/\beta_m \geqslant 0$ has yet been found.

Another matter of some interest is the effect of the zero-average non-linear terms h and $L(\mathbf{M})$ on the transport of heat. One can easily recompute

λ_2, λ_4, and λ_6, neglecting h and $L(\mathbf{M})$, and compare the resulting transport with that found in (2.29) and (2.30). From (2.13) and (2.24) it is seen that λ_2 and λ_4 are unchanged. However, a redetermination of W_4 and T_4 leads to $\lambda_6 = 1{\cdot}44 \times 10^{-3}$ from (2.26). A new solution of the cubic (2.29) with this value of λ_6 determines the heat transport curve labelled $\lambda_6(ZANL)$ in figure 2. One concludes that, to this approximation, neglect of the zero-average non-linear terms increases the amplitude of the predicted heat transport.

Amplitude effects on the horizontal wave-number

Up to this point in the calculations we have considered only the growth process of the free roll when $\alpha^2 = \frac{1}{2}$, its optimum value for a lowest λ_0. However, it is improbable that the distortions of the growing disturbance are not accompanied by a change in the basic horizontal wave-number. Indeed the expressions for λ_0, λ_2, and λ_4 (see (2.11), (2.14) and (2.24)) have been written as explicit functions of α^2 so that we may investigate the effects of changing α on the heat transport.

We have as yet no criterion to select the physically realized finite amplitude solution from the manifold of steady solutions permitted by the equations. In first-order theory the criterion is to find the lowest value of λ_0, for this disturbance is the 'first' to grow. But for λ greater than this lowest λ_0 a variety of disturbances of different α^2 could grow, each corresponding to different $\lambda > \lambda_{\text{min}}$. In a following section we shall establish a 'relative stability' criterion to select the realized solution. Here, we shall investigate one extreme, namely, that solution which leads to the maximum heat transport.

To the λ_2-approximation the heat transport is a maximum for minimum λ_0, i.e. at $\alpha^2 = \frac{1}{2}$, for all λ. However from (1.19), (2.14) and (2.24), to the λ_4-approximation,

$$(\overline{WT})_m = \lambda_2\left\{-\frac{\lambda_2}{\lambda_4} - \left[\left(\frac{\lambda_2}{\lambda_4}\right)^2 - \frac{4(\lambda-\lambda_0)}{\lambda_4}\right]^{1/2}\right\}, \tag{2.34}$$

where

$$\lambda_0 = \frac{\pi^4(1+\alpha^2)^3}{\alpha^2}, \quad \lambda_2 = \frac{\pi^2(1+\alpha^2)^2}{2\alpha^2}, \quad \lambda_4 = -\frac{(1+\alpha^2)^2}{4\alpha^2}\,\frac{(3^2+\alpha^2)^2+2(1+\alpha^2)^2}{(3^2+\alpha^2)^3-(1+\alpha^2)^3}.$$

We seek that $\alpha^2 = \alpha^2(\lambda)$ which leads to a maximum $(\overline{WT})_m$. From (2.34) this extreme relation is

$$\frac{\partial}{\partial\alpha^2}(\overline{WT})_m = 0 = \frac{\partial K}{\partial\alpha^2} - \frac{2K}{2(\lambda-\lambda_0)-(\overline{WT})_m}\,\frac{\partial\lambda_0}{\partial\alpha^2}, \tag{2.35}$$

where $K \equiv \lambda_2^2/|\lambda_4|$. An explicit solution for α^2 first will be sought for λ close to $(\lambda_0)_{\text{min}}$ where α^2 will be close to $\frac{1}{2}$. We let $\alpha^2 = \frac{1}{2}+\Delta$; then

$$K = 6\lambda_c(1 - a\Delta + b\Delta^2 + \ldots) \tag{2.36}$$

and

$$\lambda_0 = \lambda_c(1+\tfrac{4}{3}\Delta^2+\ldots),$$

where $\lambda_c \equiv (\lambda_0)_{\min}$, $a \doteqdot 0{\cdot}621$ and $b \doteqdot 1{\cdot}782$ from (2.34). Hence

$$(\overline{WT})_m = 6\lambda_c[1-(1-\tfrac{2}{3}x)^{1/2}+A\Delta-B\Delta^2+\ldots], \tag{2.37}$$

where

$$A = a\left\{\frac{1-\frac{1}{3}x}{(1-\frac{2}{3}x)^{1/2}}-1\right\}, \qquad x \equiv \frac{\lambda-\lambda_c}{\lambda},$$

$$B = \frac{b+\frac{1}{2}a^2+\frac{4}{9}-\frac{1}{3}bx}{(1-\frac{2}{3}x)^{1/2}} - \frac{a^2}{2}\,\frac{(1-\frac{1}{3}x)^2}{(1-\frac{2}{3}x)^{3/2}} - b.$$

Then equation (2.35) for the extreme α^2 yields

$$\Delta = A/2B; \tag{2.38}$$

at $\lambda = 2\lambda_c$ for example, $\Delta \doteqdot 0{\cdot}0591$ and

$$(\overline{WT})_m|_{\alpha^2=\frac{1}{2}+\Delta} = 1{\cdot}00672(\overline{WT})_m|_{\alpha^2=\frac{1}{2}}.$$

Hence, for this extreme solution, α^2 does change appreciably even in the limited range of λ in which the λ_4-approximation gives an adequate description of the motion. However, the change in heat transport is quite negligible and tells one that this change in α^2 plays an unimportant role in the energetics of our probem.

Though certainly beyond the useful limit of the λ_4-approximation, the 'end point' of the λ_4-curve has been computed as a function of α^2 to complete the extreme $(\overline{WT})_m$-curve labelled (α^2) in figure 2. At this end point

$$\lambda = \tfrac{1}{4}\lambda_2/|\lambda_4| + \lambda_0 \equiv \lambda_{\text{imag}},$$

and

$$(\overline{WT})_m|_{\lambda=\lambda_{\text{imag}}} = 4(\lambda_{\text{imag}}-\lambda_0). \tag{2.39}$$

Hence, from (2.35) for the extreme $(\overline{WT})_m$ as a function of α^2, we have, using the values of λ_{imag} and $(\overline{WT})_m$ in (2.39),

$$\partial K/\partial\alpha^2 + 4\,\partial\lambda_0/\partial\alpha^2 = 0. \tag{2.40}$$

It is seen that this condition for maximum heat transport at the end point is identical with the condition for minimum λ_{imag} from (2.39). A plot of λ_{imag} against α^2, using λ_0, λ_2, and λ_4 from (2.34), leads to the (λ, H)-point given in figure 2. The value of α^2 at this minimum λ_{imag} is 27/40.

We have now progressed about as far as is practicable in the ϵ-sequence for the simplest of the solutions to the Rayleigh problem. The two important properties of the non-linear terms which control the amplitude of the steady disturbance have been exhibited. These are the distortion of the disturbance from its initial form and the distortion by the disturbance of the mean temperature field. This latter plays the dominant role in amplitude determination for the free rolls. In the following section we shall establish the relative importance of these two effects for the general rectangle and the hexagon.

3. ANALYSIS FOR THE THREE-DIMENSIONAL CELLULAR MOTION

The greater complexity of the general rectangle and hexagon plan-forms prohibits an analysis as extended as that for the rolls. However, the non-vanishing of the first zero-average advection terms causes even the λ_2-approximation for these plan-forms to exhibit many of the properties found for the roll-cell in the λ_6-approximation.

General rectangle

We start this analysis with the general rectangular cell with two free boundaries. A complete solution to the first-order equations is

$$\left.\begin{aligned} W_0 &= 2\sqrt{2}\cos\pi lx\cos\pi my\sin\pi z, \\ T_0 &= N_0 2\sqrt{2}\cos\pi lx\cos\pi my\sin\pi z, \\ U_0 &= -2\sqrt{2}l\alpha^{-2}\sin\pi lx\cos\pi my\cos\pi z, \\ V_0 &= -2\sqrt{2}m\alpha^{-2}\cos\pi lx\sin\pi my\cos\pi z, \end{aligned}\right\} \tag{3.1}$$

$$\lambda_0 = \pi^4(1+\alpha^2)^3/\alpha^2, \qquad N_0 \equiv \pi^2(1+\alpha^2)^2/\alpha^2, \qquad l^2+m^2 = \alpha^2.$$

From (1.5), (1.8) and (3.1),

$$\left.\begin{aligned} \nabla_1^2 h_{00} &= -8\pi^3 N_0\alpha^{-2}m^2l^2\{\cos 2\pi lx+\cos 2\pi my\}\sin 2\pi z, \\ L_{00} &= 8\pi^3 l^2m^2\alpha^{-4}(1+\alpha^2)[\cos 2\pi lx+\cos 2\pi my]\sin 2\pi z. \end{aligned}\right\} \tag{3.2}$$

Hence $\lambda_1 = 0$ as before and, from (1.20),

$$\mathscr{L}(W_1) = \frac{8\pi^3m^2l^2N_0}{\alpha^2}\left[\left\{1+\frac{4}{\sigma}\frac{(1+l^2)}{(1+\alpha^2)}\right\}\cos 2\pi lx + \right.$$
$$\left. + \left\{1+\frac{4}{\sigma}\frac{(1+m^2)}{(1+\alpha^2)}\right\}\cos 2\pi my\right]\sin 2\pi z. \tag{3.3}$$

The solution of (3.3) is

$$W_1 = (C_{lm}\cos 2\pi lx + C_{ml}\cos 2\pi my)\sin 2\pi z, \tag{3.4}$$

where

$$C_{lm} = -\frac{8\pi^3\alpha^{-2}m^2l^2N_0\{1+4\sigma^{-1}(1+l^2)/(1+\alpha^2)\}}{64\pi^6(1+l^2)^3-4\pi^2l^2\lambda_0}, \qquad C_{lm}(m,l) = C_{ml}.$$

From (1.21) and (3.4)

$$T_1 = (D_{lm}\cos 2\pi lx + D_{ml}\cos 2\pi my)\sin 2\pi z, \tag{3.5}$$

where

$$D_{lm} = \frac{\lambda_0 C_{lm} - 2\pi N_0 m^2\alpha^{-2}}{4\pi^2(1+l^2)}, \qquad D_{lm}(m,l) = D_{ml}.$$

From (1.9) and (1.10) expanded for U_1 and V_1,

$$\partial(M_x)_{00}/\partial y - \partial(M_y)_{00}/\partial x = 0,$$

so that

$$\left.\begin{aligned} U_1 &= -(C_{lm}/l)\sin 2\pi lx\cos 2\pi z, \\ V_1 &= -(C_{ml}/m)\sin 2\pi my\cos 2\pi z. \end{aligned}\right\} \tag{3.6}$$

To determine the first finite amplitude results for the general rectangle we must construct λ_2 from (1.23). Here

$$\lambda_2 = \{\overline{W_0\nabla_1^2W_0}[\overline{W_0T_0}-\overline{W_0T_0}]_m + \overline{W_0\nabla_1^2(h_{01}+h_{10})} +$$
$$+\sigma^{-1}\overline{W_0\nabla^2(L_{01}+L_{10})}\}_m/(\overline{W_0\nabla_1^2W_0})_m, \tag{3.7}$$

while from (3.1), (3.5) and (3.6) the lengthy forms of h_{ij} and L_{ij} lead to

$$\frac{[\overline{W_0\nabla_1^2(h_{01}+h_{10})}_m]}{(\overline{W_0\nabla_1^2W_0})_m} = -\frac{\pi^2}{2\alpha^2}(m^2D_{lm}+l^2D_{ml}) \equiv \tfrac{1}{2}N_0D(\sigma,l,m) \tag{3.8}$$

and

$$\frac{[\overline{W_0\nabla^2(L_{01}+L_{10})}]_m}{(\overline{W_0\nabla_1^2W_0})_m} = -\frac{N_0\pi}{2\alpha^2}(m^2C_{lm}+l^2C_{ml}) \equiv \tfrac{1}{2}N_0C(\sigma,l,m).$$

Therefore

$$\lambda_2 = \lambda_2(\sigma,m,l) = \tfrac{1}{2}N_0(1+D+C/\sigma), \tag{3.9}$$

and from (1.18) and (1.19) this first effect of ϵ on heat transport is

$$(\overline{WT})_m = \text{function of } (\sigma,l,m) = \frac{2(\lambda-\lambda_0)}{1+D+C/\sigma}. \tag{3.10}$$

For the special case of a square cell $l^2 = m^2 = \frac{1}{2}\alpha^2$; from (3.4), (3.5) and (3.8)

$$1+D+C/\sigma = 1+\frac{8x^2}{(1+\alpha^2)(32x^3-1)}\left\{1+\frac{1}{4x^2\sigma}+\frac{1}{2x\sigma^2}\right\}, \tag{3.11}$$

where $$x \equiv (1+\tfrac{1}{2}\alpha^2)/(1+\alpha^2).$$

For the 'limiting rectangle' $l \to 0$, $m^2 \to \alpha^2$, we have

$$1+D+C/\sigma = 1+\tfrac{1}{2}; \tag{3.12}$$

that is, $W_1 = U_1 = V_1 = 0$, from (3.4) and (3.6), but

$$T_1 = -(N_0/2\pi)\cos 2\pi lx \sin 2\pi z$$

from (3.5).

Figure 4 is a plot of $\frac{1}{2}(\overline{WT})_m/(\lambda-\lambda_0)$ as given by equation (3.10), for values of l/m between these two extremes, with $\alpha^2 = \frac{1}{2}$, and for several values of σ. The dependence of $(\overline{WT})_m$ on α^2 will be discussed shortly.

Finite amplitude effects

Perhaps the most important aspect of these finite amplitude effects is that the heat transport for the limiting rectangle does not coincide with that for the roll. Neither rolls nor long rectangles can satisfy the (distant) lateral boundary conditions in real convection. However, a long rectangle is certainly the more realistic limiting form to compare with squares and hexagons.

A second aspect of this initial amplitude convection is that squares transport more heat than any other rectangle when $\sigma \geqslant 0{\cdot}8$*. Most gases have a value of σ very close to this critical value and may exhibit a far less decided choice of plan-form than liquids. However there is some evidence that these strong effects of σ on heat transport disappear at large Rayleigh numbers (Malkus 1954 a).

As for the roll plan-form, one expects that the value of α^2 can change as the rectangle grows in amplitude. We investigate this effect for the case of the square and, again arbitrarily, seek that value of α^2 which leads to a maximum value of $(\overline{WT})_m$ at $\lambda \geqslant (\lambda_0)_{\min} = \lambda_c$. From (3.10) and (3.11),

---

* When $\sigma \ll 1$ (cf. $\sigma \doteqdot 1/40$ for mercury), the radius of convergence of the $\lambda = \lambda(\epsilon, \sigma^{-1})$ series which we have evolved is very small. In such a case it is better to non-dimensionalize $\mathbf{V}$ by writing $\mathbf{V} = \delta\mathbf{V}'/d$ and obtain the series $\lambda = \lambda(\epsilon, \sigma)$.

$$(\overline{WT})_m = 2(\lambda-\lambda_0)\left\{1+\frac{8x^2}{(1+\alpha^2)(32x^3-1)}\left(1+\frac{1}{4x^3\sigma}+\frac{1}{2x\sigma^2}\right)\right\}^{-1}. \qquad (3.13)$$

For values of λ near λ_0, α^2 will be near $\frac{1}{2}$. We write $\Delta \equiv \alpha^2 - \frac{1}{2}$, whence

$$\lambda_0 = \lambda_c(1+4\Delta^2/3+\ldots),$$

$$x = \tfrac{5}{6}(1-4\Delta/15+8\Delta^2/45+\ldots),$$

$$(\overline{WT})_m = \frac{2(\lambda-\lambda_c)}{F}\,\frac{[1-4\lambda_c\Delta^2/3(\lambda-\lambda_c)+\ldots]}{(1-c\Delta+d\Delta^2+\ldots)}, \qquad (3.14)$$

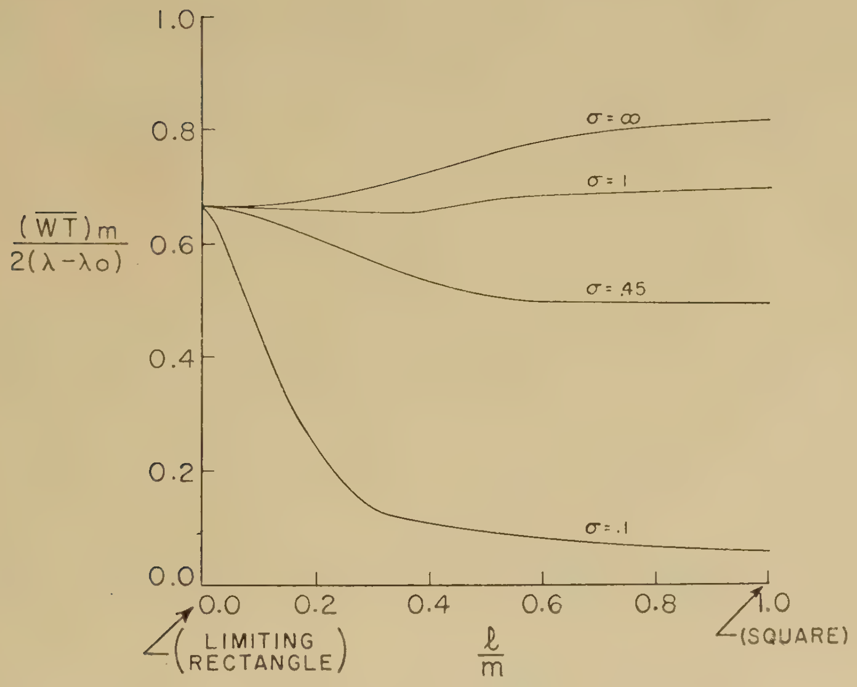

Figure 4. Heat transport for the general rectangle with $\alpha^2 = \frac{1}{2}$ at several values of σ.

where

$$F \equiv 1+\frac{100}{473}\left(1+\frac{9}{25\sigma}+\frac{3}{5\sigma^2}\right),$$

$$c \equiv \frac{100}{473F}(0{\cdot}7124+0{\cdot}0645\sigma^{-1}+0{\cdot}2674\sigma^{-2}),$$

$$d = \frac{100}{473F}(0{\cdot}7800+0{\cdot}0927\sigma^{-1}+0{\cdot}2900\sigma^{-2}).$$

Therefore $\partial(\overline{WT})_m/\partial\Delta = 0$, when the optimum value of Δ is

$$\Delta_{\text{opt}} = \frac{\lambda_c}{\lambda-\lambda_c}\,\tfrac{1}{2}c\left\{\frac{4}{3}+\frac{\lambda_c}{\lambda-\lambda_c}(d-c^2)\right\}^{-1}$$

and
$$[(\overline{WT})_m]_{\text{opt}} = 2(\lambda-\lambda_c)(1+\tfrac{1}{2}c\Delta_{\text{opt}})/F. \tag{3.15}$$

For $\sigma = \infty$, $c \doteqdot 0{\cdot}1245$ and $d \doteqdot 0{\cdot}1362$. When $\lambda = 2\lambda_c$, $\Delta_{\text{opt}} = 0{\cdot}0428$ and
$$[(\overline{WT})_m]_{\text{opt}}/(\overline{WT})_m|_{\alpha^2=\frac{1}{2}} = 1{\cdot}00267.$$

For $\sigma = 1$, $c \doteqdot 0{\cdot}1561$ and $d \doteqdot 0{\cdot}1589$. When $\lambda = 2\lambda_c$, $\Delta_{\text{opt}} = 0{\cdot}0532$ and the above displayed ratio is 1·00415. Hence, for those values of σ for which the square cell transports the most heat, this transport is only negligibly increased by an optimization of α^2. However this optimization causes a 10% increase in α^2 for $\lambda = 2\lambda_0$.

The optimum α^2 equals $\frac{1}{2}$ for the limiting rectangle since from (3.12) λ_2 is independent of α^2.

The range of λ in which these λ_2-approximations for the general rectangular cell are useful is apparently even more restricted than it was for rolls, i.e. $\lambda_c \leqslant \lambda < 2\lambda_c$. This was established by the extremely tedious computation of λ_4 for the square with $\alpha^2 = \frac{1}{2}$. It was found that here $\lambda_4 \doteqdot 0{\cdot}185$, indicating that corrections due to λ_4 become important for $\lambda-\lambda_c > 0{\cdot}5\lambda_c$.

λ_2 *for hexagons*

Before attempting further interpretation of these results we will investigate the initial finite amplitude convection of the hexagonal plan-form. Past experimental literature gives one the impression that Rayleigh-like convection is realized only as hexagons. However these observations of plan-form were made with rigid bottom and free top boundaries. The one experimental study of plan-form made with symmetric boundary conditions will be discussed shortly.

The complete solution to the first-order problem for a hexagonal plan-form and two free boundaries was first given by Christopherson (1940), and is as follows

$$\left.\begin{aligned}
W_0 &= \frac{2}{\sqrt{3}}\left\{2\cos\frac{2\pi x}{\sqrt{3}L}\cos\frac{2\pi y}{3L}+\cos\frac{4\pi y}{3L}\right\}\sin\pi z \equiv \frac{2}{\sqrt{3}}\,\phi_1\sin\pi z\\
T_0 &= (2/\sqrt{3})N_0\phi_1\sin\pi z,\\
U_0 &= -\frac{2}{\alpha}\sin\frac{2\pi x}{\sqrt{3}L}\cos\frac{2\pi y}{3L}\cos\pi z,\\
V_0 &= -\frac{2}{\sqrt{3}\alpha}\left\{\cos\frac{2\pi x}{\sqrt{3}L}\sin\frac{2\pi y}{3L}+\sin\frac{4\pi y}{3L}\right\}\cos\pi z,\\
\lambda_0 &= \pi^4(1+\alpha^2)^3/\alpha^2, \qquad N_0 = \pi^2(1+\alpha^2)^2/\alpha^2,
\end{aligned}\right\} \tag{3.16}$$

where $L = 4/3\alpha$ is the non-dimensional length of one side of the hexagon. Averages over the hexagon can be taken over the region $0 \leqslant x \leqslant \sqrt{3}L/2$ and $0 \leqslant y \leqslant L/2$, which covers one-twelfth of the plan-form and is the smallest symmetric segment.

Possible variations of α^2 from its initial value $\alpha^2 = \frac{1}{2}$ have played such a small role in the initial heat transport of the general rectangle that we simplify the following analysis by choosing $\alpha^2 = \frac{1}{2}$ from the start. Then from (1.5), (1.8) and (3.16),

$$\left.\begin{aligned} \nabla_1^2 h_{00} &= -\tfrac{1}{2}\pi^3 N_0(\phi_1+\phi_2)\sin 2\pi z \\ L_{00} &= (3\pi^2/2)(\phi_1+\phi_2)\sin 2\pi z, \end{aligned}\right\} \tag{3.17}$$

where

$$\phi_2 \equiv 2\cos\frac{2\pi x}{\sqrt{3}L}\cos\frac{2\pi y}{L} + \cos\frac{4\pi x}{\sqrt{3}L}, \qquad \overline{\phi_1\phi_2} = 0, \qquad \nabla_1^2\phi_2 = -(3\pi^2/2)\phi_2.$$

Here, for the first time in our study, h_{00} and L_{00} have a horizontal dependence which is not orthogonal to the plan-form of W_0. This unusual property of the hexagonal solutions will be important in the case of one rigid and one free boundary, where due to the asymmetry the z-dependence of h_{00} and L_{00} and the z-dependence of W_0 are not orthogonal. However in this case of two free boundaries $\lambda_1 = 0$, since $(\sin\pi z\sin 2\pi z)_m = 0$. Therefore, from (1.20),

$$\mathscr{L}(W_1) = \tfrac{1}{2}\pi^3 N_0[(1+3/\sigma)\phi_1 + (1+11/3\sigma)\phi_2]\sin 2\pi z, \tag{3.18}$$

with the solution

$$W_1 = -(9\sqrt{3}/4\pi)(C_1\phi_1 + C_2\phi_2)\sin 2\pi z, \tag{3.19}$$

where

$$C_1 = \frac{1+3/\sigma}{729/4-\lambda c/\pi^4}, \qquad C_2 = \frac{1+11/3\sigma}{1331/4-3\lambda c/\pi^4}.$$

From (1.21) and (3.18), we have

$$T_1 = -\frac{\pi}{2\sqrt{3}}\left[3\left(\frac{729}{4}C_1 - \frac{3}{\sigma}\right)\phi_1 + \frac{9}{11}\left(\frac{1331}{4}C_2 - \frac{11}{3\sigma}\right)\phi_2\right]\sin 2\pi z. \tag{3.20}$$

The comparison of W_1 and T_1 for the hexagon with W_1 and T_1 for the general rectangle assures one that the σ-dependence of these initial finite amplitude distortions is similar. Therefore, a determination of the hexagon λ_2 for $\sigma \to \infty$ will permit an adequate comparison of hexagonal and general rectangle initial heat transports. Consequently the computation of λ_2 from (3.7) is considerably simplified, for we need not compute L_{01} and L_{10}. Then

$$[\overline{W_0\nabla_1^2(h_{01}+h_{10})}]_m = -(\alpha^2\pi^2/N_0)[\overline{T_0(h_{01}+h_{10})}]_m \tag{3.21}$$

from (3.16). Now $(\overline{Th})_m = 0$ in general, and therefore

$$(\overline{T_0 h_{00}})_m = 0, \qquad [\overline{T_1 h_{00} + T_0(h_{01}+h_{10})}]_m = 0, \quad \text{etc.}; \tag{3.22}$$

hence

$$[\overline{W_0\nabla_1^2(h_{01}+h_{10})}]_m = (\alpha^2\pi^2/N_0)(\overline{T_1 h_{00}})_m.$$

From (3.22), (3.21) and (3.18),

$$(\overline{T_1 h_{00}})_m = -\frac{27}{8}\pi^4\left\{\frac{729}{4}C_1 - \frac{3}{\sigma} + \frac{1}{11}\left(\frac{1331}{4}C_2 - \frac{11}{3\sigma}\right)\right\} \equiv -\frac{27}{8}\pi^4 C. \tag{3.23}$$

Then from (3.7), (3.23) and (3.16) for $\sigma = \infty$,

$$\lambda_2 = \tfrac{1}{2}N_0 - (\overline{T_1 h_{00}})_m = \tfrac{1}{2}N_0\{1+\tfrac{1}{3}(C)_{\sigma=\infty}\} = (9\pi^2/4)(1{\cdot}379).$$

The initial finite amplitude heat transport for the hexagon from (1.8), (1.19), and λ_2 above is $(\overline{WT})_m = 1{\cdot}45(\lambda-\lambda_0)$. In figure 4 we see that this heat transport is smaller than that due to the square and larger than that due to the limiting rectangle.

Mixed horizontal plan-form

There is yet another class of solutions to the first-order equations which may grow to finite amplitude, viz. the class of all possible linear combinations of the individual plan-forms. We will consider only the single case of a square (S) and a general rectangle (G). The first-order solution will be

$$W_0 = \surd 2(\phi_S + r\phi_G)(1+r^2)^{-1/2}\sin\pi z \equiv \surd 2\phi\sin\pi z, \tag{3.24}$$

where

$$\phi_S = 2\cos(\pi\alpha x/\surd 2)\cos(\pi\alpha y/\surd 2), \qquad \overline{\phi^2} = 1,$$
$$\phi_G = 2\cos\pi l x\cos\pi m y, \qquad l^2+m^2 = \alpha^2,$$

and $0 \leqslant r \leqslant \infty$ is a free parameter determining the fractional contribution of ϕ_G to the total plan-form. In the case $\alpha^2 = \frac{1}{2}$, $\sigma = \infty$, we can quickly determine λ_2 by the method used for the hexagon (see equation (3.23)). From (3.24),

$$\begin{aligned} h_{00} = \pi N_0(1+r^2)^{-1}\{&h_{00}(S)+r^2h_{00}(G)+ \\ &+2r(1\mp l\mp m)\cos(\tfrac{1}{2}\pm l)\pi x\cos(\tfrac{1}{2}\pm m)\pi y\sin 2\pi z\}. \end{aligned} \tag{3.25}$$

Hence

$$\begin{aligned} W_1 = (1+r^2)^{-1}\{&W_1(S)+r^2W_1(G)+ \\ &+(2rB/\pi^3)(4+A)^{-2}\cos(\tfrac{1}{2}\pm l)\pi x\cos(\tfrac{1}{2}\pm m)\pi y\sin 2\pi z\} \end{aligned} \tag{3.26}$$

and

$$T_1 = (1+r^2)^{-1}\{T_1(S)+r^2T_1(G)-(2rB/\pi)\cos(\tfrac{1}{2}\pm l)\pi x\cos(\tfrac{1}{2}\pm m)\pi y\sin 2\pi z\}$$

where

$$A = (\tfrac{1}{2}\pm l)^2+(\tfrac{1}{2}\pm m)^2, \quad B = N_0(1\mp l\mp m)(4+A)^2/[(4+A)^3-\lambda c A/\pi^4].$$

Then

$$(\overline{T_1 h_{00}})_m = (1+r^2)^{-2}\{(\overline{T_1 h_{00}})_m(S)+r^4(\overline{T_1 h_{00}})_m(G)-\tfrac{1}{2}r^2N_0B(1\mp l\mp m)\}. \tag{3.27}$$

Finally, from (3.24), (3.9) and (3.27)

$$\lambda_2 = (1+r^2)^{-2}\{\lambda_2(S)+2r^2\lambda_2(I)+r^4\lambda_2(G)\}, \tag{3.28}$$

where

$$\lambda_2(I) \equiv \tfrac{1}{2}N_0+\tfrac{1}{4}B(1\mp l\mp m).$$

Hence λ_2 has an extremum with respect to r at

$$(r^2)_{\text{opt}} = [\lambda_2(S)-\lambda_2(I)]/[\lambda_2(G)-\lambda_2(I)],$$

where

$$(\lambda_2)_{\text{opt}} = [\lambda_2(S)\lambda_2(G)-\lambda_2^2(I)]/[\lambda_2(S)+\lambda_2(G)-2\lambda_2(I)]. \tag{3.29}$$

This extreme is a maximum if $2\lambda_2(G)\lambda_2(I) \geqslant \lambda_2^2(I)+\lambda_2^2(G)$. Comparison of (3.9) for $\lambda_2(G)$ with $\sigma = \infty$, $\alpha^2 = \frac{1}{2}$, and (3.28) for $\lambda_2(I)$ establishes that this inequality is true for all values of $l = (\frac{1}{2} - m^2)^{1/2}$. We recall that an increase in λ_2 decreases the heat transport. Therefore, as one might have anticipated, this mixture of first-order plan-forms reduces the initial finite amplitude heat transport.

Before a formal attempt is made to determine the physically realized solution from the vast degenerate set we have constructed, a relevant experimental study will be discussed. In 1935 Schmidt & Milverton made optical observations of the spacing of convecting cells between two rigid boundaries. Shining a collimated beam of light horizontally through water ($\sigma = 8$) they detected a spatial oscillation in intensity due to the density variations in each cell. The patterns obtained by rotating the beam through 180° in the horizontal contain one maximum in the spacing of the light fringes in the case of limiting rectangles, two maxima for squares, and three maxima for hexagons. At these maxima, from the initial $\alpha^2 = 3{\cdot}13/\pi$ (appropriate to the case of two rigid boundaries) the ratio of horizontal extent of each cell to the vertical spacing of the boundaries will be 2 for squares and limiting rectangles and 1·8 for hexagons. Schmidt & Milverton do not record any rotation of their beam to determine uniquely the plan-form. However, the average ratio of horizontal fringe spacing to cell height in their experiment was 2·1. They believed that they were observing squares. We can tentatively conclude that these cells were either squares or limiting rectangles, but not hexagons.

The qualitative aspects of our heat transport computations for various plan-forms will most probably be preserved in going from the symmetric case of two free boundaries to the symmetric case of two rigid boundaries. For two free boundaries we found that the square transports more heat, the limiting rectangle less heat than the hexagon. Hence one anticipates that heat transport is a selective factor in establishing the observed flow from the many solutions.

4. A ‘ RELATIVE STABILITY ’ CRITERION

When seeking a realizable steady-state solution to the equations of motion one must verify not only that the solution formally satisfies the time-independent equations but also that it is stable against all infinitesimal disturbances which satisfy the boundary conditions. If it is not stable then surely there is at least one other solution to the equations. This other solution may not be a steady one in the local sense, but for fixed boundary conditions is must be statistically steady; that is, integrals of moments of this solution over the entire field will be independent of time.

The general problem of the stability of a known solution $\mathbf{v}$ and $\mathbf{T}$ can be immensely complicated. For example, years of labour have been devoted to simple two-dimensional shear flow (the Orr–Sommerfeld problem) and no exact solution has yet been found. Hence it is improbable that we could formally determine the stability of finite amplitude solutions even if we knew them exactly.

Fortunately the answer to a simpler question will suffice here. We will assume that we know the complete set of steady and statistically steady solutions to the equations of motion. Then any experimentally realized solution is contained in this set. We ask, are any of these solutions stable against those infinitesimal disturbances that have the form of the other solutions? If there is an affirmative answer for just one of these solutions, we will have determined the realized solution. If there are several solutions which are 'relatively stable', then either these solutions can be realized separately (i.e. they are metastable) or a broader class of infinitesimal disturbances must be considered to remove the remaining indeterminancy.

In formulating such a question we have hoped that a detailed knowledge of the individual solutions and their interactions would not be required to answer it. Indeed we seek some simple integral property of the solutions which will single out the stable one.

From (1.1), (1.2) and (1.3) in dimensional form, the equations of an arbitrary disturbance $\mathbf{v}'$, T' on the field $\mathbf{v}, \mathbf{T}$ are

$$(\partial/\partial t-\kappa\nabla^2)T' = -\mathbf{v}\,.\,\nabla T'-\mathbf{v}'\,.\,\nabla\mathbf{T}-\mathbf{v}'\,.\,\nabla T', \tag{4.1}$$

$$(\partial/\partial t-\nu\nabla^2)\mathbf{v}' = -\mathbf{v}\,.\,\nabla\mathbf{v}'-\mathbf{v}'\,.\,\nabla\mathbf{v}-\mathbf{v}'\,.\,\nabla\mathbf{v}'-\nabla\widetilde{P}'/\rho_m+\gamma T'\mathbf{k}, \tag{4.2}$$

and

$$\nabla\,.\,\mathbf{v}' = 0. \tag{4.3}$$

These are the general equations which determine the stability of $\mathbf{v}, \mathbf{T}$. We first construct the disturbance power integrals (see (1.6) and (1.7)),

$$(\gamma/2\beta_m)\partial(\overline{T'^2})_m/\partial t = (\gamma/\beta_m)[\kappa(\overline{T'\nabla^2T'})_m+(\overline{W'T'\beta})_m-(\overline{T'\mathbf{v}'\,.\,\nabla T})_m] \tag{4.4}$$

and

$$\tfrac{1}{2}\,\partial(\overline{\mathbf{v}'\,.\,\mathbf{v}'})_m/\partial t = \nu(\overline{\mathbf{v}'\,.\,\nabla^2\mathbf{v}'})_m+\gamma(\overline{W'T'})_m-(\overline{\mathbf{v}'\,.\,\mathbf{v}'\,.\,\nabla\mathbf{v}})_m, \tag{4.5}$$

where $\mathbf{T}$ has been replaced by $\overline{\mathbf{T}}+T$ and $\beta = -\partial\overline{\mathbf{T}}/\partial z$. If $\mathbf{v}$ and $\mathbf{T}$ are stable to the disturbance $\mathbf{v}'$, T', the right-hand sides of (4.4) and (4.5) will be negative. One may interpret (4.4) as the equation for the balance of entropy* associated with the disturbance T'. Equation (4.5) is the equation for the balance of kinetic energy of the disturbance $\mathbf{v}'$. The first term on the right-hand side of (4.4) is proportional to the loss of entropy by thermal diffusion; the second is proportional to the gain of entropy through interaction with the initial mean temperature gradient β; and the third is proportional to the gain or loss of entropy through interaction with the initial field of temperature fluctuation. In (4.5) the first term is the loss of kinetic energy of the fluctuation $\mathbf{v}'$ by viscosity, the second is the production of kinetic energy by convection and the last is the gain or loss of kinetic energy through interaction with the initial velocity field.

We will now restrict the class of disturbances to be considered to those which have the form of steady or statistically steady solutions to the basic equations; that is,

---

* In this irreversible process of steady convection we regard 'entropy' as proportional to and as a shorthand for the mean square of the local fluctuations of internal energy. We prescribe no (thermodynamic) role for this 'entropy' which cannot be deduced from the basic disturbance equation (4.1).

$$\mathbf{v}' = A\mathbf{v}_1, \qquad T' = BT_1 \tag{4.6}$$

where A and B are arbitrary amplitudes and $\mathbf{v}_1$, T_1 are correct solutions. Then from (4.4), (4.5) and (4.6),

$$\frac{\partial B}{\partial t} = -I_1 B + I_2 A, \qquad \frac{\partial A}{\partial t} = -I_3 A + I_4 B, \tag{4.7}$$

where

$$I_1 \equiv -\kappa(\overline{T_1 \nabla^2 T_1})_m / (\overline{T_1^2})_m, \qquad I_2 \equiv [(\overline{W_1 T_1}\beta)_m - f_T]/(\overline{T_1^2})_m,$$
$$f_T \equiv (\overline{\mathbf{v}_1 T_1 . \nabla T})_m, \qquad I_3 \equiv -[\nu(\overline{\mathbf{v}_1 . \nabla^2 \mathbf{v}_1})_m + f_v]/(\overline{\mathbf{v}_1 . \mathbf{v}_1})_m,$$
$$f_v \equiv (\overline{\mathbf{v}_1 . \mathbf{v}_1 . \nabla \mathbf{v}})_m, \qquad I_4 \equiv \gamma(\overline{W_1 T_1})_m / (\overline{\mathbf{v}_1 . \mathbf{v}_1})_m.$$

The solution of (4.7) will decay with time if

$$[\tfrac{1}{4}(I_1+I_3)^2 - (I_1 I_3 - I_2 I_4)]^{1/2} - \tfrac{1}{2}(I_1+I_3) < 0. \tag{4.8}$$

But (I_1+I_3) contains the two large positive-definite diffusive dissipation terms and is invariably positive. Therefore decay will occur if

$$I_1 I_3 > I_2 I_4. \tag{4.9}$$

Since $\mathbf{v}_1$, T_1 are solutions,

$$\left.\begin{aligned} \kappa(\overline{T_1 \nabla^2 T_1})_m + (\overline{W_1 T_1}\beta_1)_m &= 0, \\ \nu(\overline{\mathbf{v}_1 . \nabla^2 \mathbf{v}_1})_m + \gamma(\overline{W_1 T_1})_m &= 0. \end{aligned}\right\} \tag{4.10}$$

With the use of (4.10) the stability criterion (4.9) becomes

$$[\overline{W_1 T_1}(\beta_1 - \beta)]_m + f_T + f_v(\overline{W_1 T_1}\beta_1)_m / \gamma(\overline{W_1 T_1})_m > 0. \tag{4.11}$$

The basic equations for $\mathbf{v}_1$, T_1 allow the triple product integrals f_v and f_T to be expressed as double product integrals, that is,

$$\left.\begin{aligned} f_T = (\overline{\mathbf{v}_1 . T_1 \nabla T})_m &\equiv -(\overline{T\mathbf{v}_1 . \nabla T_1})_m \\ &= [\overline{T(\partial T_1/\partial t - \kappa \nabla^2 T_1 - W_1 \beta_1)}]_m, \\ f_v = (\overline{\mathbf{v} . \partial \mathbf{v}_1/\partial t} &- \nu\overline{\mathbf{v} . \nabla^2 \mathbf{v}_1} - \gamma \overline{W T_1})_m. \end{aligned}\right\} \tag{4.12}$$

All the double product terms of (4.12) vanish in horizontal integration if the field $\mathbf{v}, T$ is developed from a fundamental periodic function orthogonal to the fundamental function of $\mathbf{v}_1$, T_1. This is the case for all different solutions which can be generated by the iterative method of the previous sections (for $\lambda < 2^4\lambda_0$). Hence in our problem f_v and f_T vanish. To determine from (4.11) which of the many solutions is stable we must find that solution for which $[\overline{W_i T_i}(\beta_i - \beta)]_m > 0$, where the index i ranges over all solutions but the one considered. A physical interpretation of this conclusion is that the stable solution will produce more entropy per unit time from the mean temperature field of any other solution than it does from its own mean field.

The stability criterion can be further simplified and given another physical interpretation. Since $H = \kappa\beta + \overline{WT}$ for all solutions, then

$$[\overline{W_i T_i}(\beta_i - \beta)]_m = \kappa(\beta\beta_i - \beta_i^2)_m > 0. \tag{4.13}$$

Condition (4.13) is not satisfied if $(\beta_i^2)_m \geqslant (\beta^2)_m$, for on applying Schwarz's inequality we have $(\beta_i^2)_m^2 \geqslant (\beta^2)_m(\beta_i^2)_m \geqslant (\beta\beta_i)_m^2$. Therefore a necessary condition for stability is that

$$(\beta^2)_m > (\beta_i^2)_m, \tag{4.14}$$

that is, the stable solution has a greater mean-square gradient than any other solution. If there is only one such solution, the criterion (4.14) uniquely resolves the formal degeneracy. If several solutions have the same maximum $(\beta^2)_m$, they are either metastable or a larger class of infinitesimal disturbances must be considered to decide which is realized.

Yet another physical meaning can be given to the maximum $(\beta^2)_m$ criterion. From (4.10),

$$\frac{\beta^2}{\beta_m^2} - 1 = \left(\frac{\overline{WT}}{\kappa\beta_m}\right)_m - \left(\frac{\beta\overline{WT}}{\kappa\beta_m^2}\right)_m = \frac{1}{\gamma\kappa\beta_m}\left\{\nu(-\overline{\mathbf{v}\,.\,\nabla^2\mathbf{v}})_m - \frac{\gamma\kappa}{\beta_m}(-\overline{T\nabla^2 T})_m\right\}, \tag{4.15}$$

which states that for the stable solution the rate of dissipation of kinetic energy minus a quantity proportional to the rate of increase of entropy by thermal diffusion is a maximum. Equation (4.15) may also be written

$$(\beta^2/\beta_m^2)_m - 1 = N_2F,$$

where $$N \equiv (\overline{WT})_m/\kappa\beta_m, \qquad F \equiv (\overline{WT}^2)_m/(\overline{WT})_m^2 - 1, \tag{4.16}$$

The quantity N depends only upon the amplitude of the convective heat transport. The quantity F depends only upon the z form of the heat transport. But all the solutions for λ_2 found in § 3 have identical z forms for $\overline{WT}$. Therefore the only stable solution found in § 3 is the one of maximum convective heat transport. For $\sigma \geqslant 1$ this solution is the square.

A summary of our conclusions on relative stability is as follows.

(*a*) Maximum heat transport is the stability criterion for all symmetric λ_2 solutions.

(*b*) Maximum $(\beta^2)_m$ is the stability criterion for all solutions generated by the iteration of orthogonal linear forms (which includes all in this paper).

(*c*) Equation (4.11) is the most general stability criterion for vertical convection.

It is of some interest to relate the total potential energy of the convecting fluid to these stability conditions. In general the potential energy is $V = g\rho z$. Hence

$$(\overline{V})_m = \frac{g}{d}\int_{d/2}^{d/2} z\bar{\rho}\,dz = \frac{g}{d}\int_{d/2}^{d/2} z\int_0^z \frac{\partial\bar{\rho}}{\partial z'}\,dz'\,dz, \tag{4.17}$$

where z is now measured from the mid-point of a symmetric convective field. From our density–temperature relation

$$\partial\bar{\rho}/\partial z' = \rho_0\,\alpha\beta, \tag{4.18}$$

so that

$$(\overline{V})_m = \frac{\gamma\rho_0\,d^2\beta_m}{12}\left[1 - \left\{\frac{6}{d^3}\int_{d/2}^{d/2} z^2\,\frac{\beta}{\beta_m}\,dz - \frac{1}{2}\right\}\right]. \tag{4.19}$$

The expression within curly brackets is zero when $\beta = \beta_m$ and approaches unity as β approaches zero in all but the boundary regions. In steady convection

$$\beta/\beta_m \doteq 1 + [(\overline{WT})_m - \overline{WT}]/\kappa\beta_m,$$

so that

$$(\overline{V})_m = \frac{\gamma\rho_0 d^3\beta_m}{12}\left[1 - \frac{(\overline{WT})_m}{2\kappa\beta_m}\left\{1 - \frac{3}{d}\int_{-d/2}^{d/2} \frac{z^2}{d^2}\frac{\overline{WT}}{(\overline{WT})_m}\,dz\right\}\right]. \tag{4.20}$$

In comparing two solutions of identical form, i.e. with identical values of $\overline{WT}/(\overline{WT})_m$, equation (4.20) asserts that the one of maximum heat transport will produce a minimum $(\overline{V})_m$. This conclusion is in keeping with the stability condition for λ_2 deduced from (4.16). However, the general condition for relative stability is not the requirement that the total potential energy be a minimum though such a relation might have been supposed from considerations based on equilibrium mechanics.

5. EXTENSION TO RIGID SURFACE BOUNDARY CONDITIONS

In this final section we will discuss the determination of finite amplitude effects for two rigid boundaries and for one rigid and one free boundary. We can hardly expect the rigid boundaries to modify the qualitative properties of the free boundary convection, for the important physical processes and the symmetry remain unaltered. We can expect quantitative changes due to the additional constraint on motion near the boundary. However, the asymmetry introduced by the rigid–free boundaries can modify the dependence of initial growth on λ and, as experiments bear out, can lead to hexagons as the preferred plan-form. We shall find that the significant qualitative effects of these boundary conditions can be deduced without the final lengthy numerical computation for the λ_i.

The complexity of these computations is perhaps the best measure of the limitations of the finite amplitude method studied in this paper. In conclusion we will turn from them to discuss alternative methods for determining finite amplitude effects.

Rigid boundary analysis

Proceeding just as in the simpler case, one writes the first-order solution for two rigid boundaries, as given by equations (2.9), (2.10) and (1.21), as

$$\left.\begin{aligned} W_0 &= \sum_1^3 A_i \cosh 2\mu_i z\,\phi(x,y) \equiv W\phi, \\ T_0 &= a^{-2}\sum_1^3 (4\mu_i^2 - a^2)A_i \cosh 2\mu_i z\,\phi(x,y) \equiv t\phi, \end{aligned}\right\} \tag{5.1}$$

where z is now measured from the mid-point, $-\frac{1}{2} \leqslant z \leqslant \frac{1}{2}$, $a^2 = \alpha^2\pi^2$, A_i/A_1 and μ_i are the complex numbers determined by Pellew & Southwell, A_1 is chosen to normalize W_0, and ϕ is the normalized plan-form. In general

$$-\nabla_1^2 h_{00} = 2[-(\nabla_1^2\phi^2)W\,\partial t/\partial z + (-\nabla_1^2\psi)t\,\partial W/\partial z], \tag{5.2}$$

$$L_{00} = 8\left\{(\phi^2-\psi^2)\left(\frac{\partial W}{\partial z}\frac{\partial^2 W}{\partial z^2} - W\frac{\partial^3 W}{\partial z^3}\right) + \Gamma^2\left(\frac{\partial W}{\partial z}\frac{\partial^2 W}{\partial z^2} - a^2 W\frac{\partial W}{\partial z}\right)\right\}, \tag{5.3}$$

where

$$\psi \equiv a^{-2}\left[\left(\frac{\partial\phi}{\partial x}\right)^2 + \left(\frac{\partial\phi}{\partial y}\right)^2\right], \qquad \Gamma^2 \equiv 4a^{-4}\left[\left(\frac{\partial^2\phi}{\partial x\partial y}\right)^2 - \frac{\partial^2\phi}{\partial x^2}\frac{\partial^2\phi}{\partial y^2}\right].$$

Therefore

$$-\nabla_1^2 h_{00} = a^{-2}\sum_{i=1}^{3}\sum_{j=-3}^{3} A_i A_j \mu_i[(-\nabla_1^2\phi)(4\mu_i^2-a^2)^2 + (-\nabla_1^2\psi)(4\mu_j^2-a^2)^2] \times \\ \times \sinh 2(\mu_i+\mu_j)z,$$

and

$$L_{00} = 4\sum_{i=1}^{3}\sum_{j=-3}^{3} A_i A_j \mu_i[(\phi^2-\psi^2)(\mu_j^2-\mu_i^2) + \Gamma^2(4\mu_j^2-a^2)]\sinh 2(\mu_i+\mu_j)z, \tag{5.4}$$

where $\mu_j \equiv -\mu_{-j}$, $A_j \equiv A_{-j}$, $A_0 \equiv 0$. Hence, due to symmetry alone, $\lambda_1 = 0$, because $[\cosh 2\mu_i z \sinh 2(\mu_i+\mu_j)z]_m = 0$. We let

$$W_1 = \tfrac{1}{2}\sum_{ij}\sum_{k} P_{kij}\sinh 2(\mu_i+\mu_j)z, \tag{5.5}$$

where $-\nabla_1^2 P_{kij} = a_k^2 P_{kij}$. Then from (1.20) for W_1,

$$[\{4(\mu_i+\mu_j)^2 - a_k^2\}^3 + a_k^2\lambda_0]P_{kij} \\ = 2A_i A_j \alpha^{-2}\mu_i\{(-\nabla_1^2\phi^2)(4\mu_i^2-a^2)^2 + (-\nabla_1^2\psi^2)(4\mu_j^2-a^2)^2 + \\ + 4a^2\sigma^{-1}[-\nabla_1^2(\phi^2-\psi^2) - 4(\mu_i+\mu_j)^2(\phi^2-\psi^2)](\mu_i^2-\mu_j^2) + \\ + a^2\sigma^{-1}[-\nabla_1^2\Gamma^2 - 4(\mu_i+\mu_j)^2\Gamma^2](4\mu_i^2-a^2)\}_k. \tag{5.6}$$

As we saw in § 3, k sums over the three orthogonal functions $\cos 2\pi lx$, $\cos 2\pi my$ and $\cos 2\pi lx \cos 2\pi my$ generated in h_{00} and L_{00} by the general rectangle, and over the two orthogonal functions ϕ_1 and ϕ_2 of (3.18) for the hexagon. The T_1 determined by this W_1 is written

$$T_1 = \tfrac{1}{2}\sum_{ij}\sum_{k} G_{kij}\sinh 2(\mu_i+\mu_j)z \tag{5.7}$$

where

$$a_k^2 G_{kij} = P_{kij}\{4(\mu_i+\mu_j)^2 - a_k^2\}^2 + 2\sigma^{-1}A_i A_j \mu_i\{4(\phi^2-\psi^2)(\mu_i^2-\mu_j^2) + \\ + \Gamma^2(4\mu_i^2-a^2)\}_k.$$

Recall that

$$\lambda_2 = (\overline{W_0\nabla_1^2 W_0})_m^{-1}\{[\overline{W_0 T_0} - (\overline{W_0 T_0})_m]\overline{W_0\nabla_1^2 W_0} + \overline{W_0\nabla_1^2(h_{01}+h_{10})} + \\ + \sigma^{-1}\overline{W_0\nabla^2(L_{01}+L_{10})}\}_m, \tag{5.8}$$

showing that the first finite amplitude results depend upon both the initial disturbance and the first distortion of this disturbance W_1, T_1, U_1, and V_1. The only computationally difficult term in λ_2 due to the (W_0, T_0)-field alone is

$$(\overline{W_0 T_0}\,\overline{W_0\nabla_1^2 W_0})_m = -\frac{1}{8}\sum_{\substack{i,r=1\\ i,s=-3}}^{3} A_i A_j A_r A_s(4\mu_3^2-a^2)^2 \times \\ \times\left[\frac{\sinh(\mu_i+\mu_j+\mu_r+\mu_s)}{\mu_i+\mu_j+\mu_r+\mu_s} + \frac{\sinh(\mu_i+\mu_j-\mu_r-\mu_s)}{\mu_i+\mu_j-\mu_r-\mu_s}\right] \tag{5.9}$$

which is the sum of 324 complex numbers. But the last two terms in λ_2 caused by the distortion introduce 1944 additional complex numbers. The task of computing the numbers involved in (5.9) for several plan-forms can hardly be justified at this time. However, these numbers determine our only finite amplitude result rigorously applicable to a realizable experiment and could be used to check the physical validity of the formalism.

Analysis for one rigid–one free boundary

The case of one rigid and one free boundary leads to the first-order solution

$$W_0 = \sum_{1}^{3} A_i \sinh 2\mu_i z, \tag{5.10}$$

where $0 \leqslant z \leqslant \frac{1}{2}$ and A_i/A_1 and μ_i are known complex numbers as before. Comparing (5.11) and (5.1), we see that $\nabla_1^2 h_{00} + \sigma^{-1}\nabla^2 L_{00}$ must be identical in form to (5.4), with the change that the index i runs from -3 to 3 while the index j runs from 1 to 3. Hence

$$\begin{aligned}(W_0 \nabla_1^2 W_0)_m \lambda_1 &= [\overline{W_0(\nabla_1^2 h_{00} + \sigma^{-1}\nabla^2 L_{00})}]_m \\ &= -a^{-2} \sum_{\substack{r,j=1 \\ i=-3}}^{3} A_r A_i A_j \mu_i \left[\sum_k \overline{P'_{kij}\phi}\right] \times \\ &\qquad\qquad \times [\sinh 2\mu_r z \sinh 2(\mu_i+\mu_j)z]_m \end{aligned} \tag{5.11}$$

where

$$\begin{aligned} P'_{kij} = \{&[(4\mu_i^2 - a^2)^2(-\nabla_1^2\phi^2) + (4\mu_j^2 - a^2)^2(-\nabla_1^2\psi^2)] - \\ &- 4a^2\sigma^{-1}(\mu_j^2 - \mu_i^2)[\nabla_1^2(\phi^2 - \psi^2) + 4(\mu_i+\mu_j)^2(\phi^2-\psi^2)] - \\ &- a^2\sigma^{-1}(4\mu_i^2 - a^2)[\nabla_1^2\Gamma^2 + 4(\mu_i+\mu_j)^2\Gamma^2]\}_k. \end{aligned} \tag{5.12}$$

In contrast with previous computations of λ_1, the z-function average $[\sinh 2\mu_r z \sinh 2(\mu_i+\mu_j)z]_m$ is not zero, while, as was noted in § 3, $\overline{P'_{kij}\phi}$ will not vanish for hexagons. Therefore a finite λ_1 exists for hexagons with one rigid and one free boundary. Similarly $(\overline{W_0 T_1} + \overline{W_1 T_0})_m$ will not vanish and must be included in the heat transport. We will not proceed further with this particular evaluation of λ_1 and $(\overline{W_0 T_1} + \overline{W_1 T_0})_m$ but will enquire into the qualitative consequences of their existence.

First-order theory is indeterminate with respect to the sign of the motion in the centre of hexagons. It could be either up or down. In contrast the sign of the amplitude of a rectangle is not a true degeneracy, since a change of sign leads to no observable change in the field of motion. The conclusion that λ_1 is not zero uniquely removes this degeneracy in the hexagon, for λ_1 determines the sign of the amplitude ϵ. From (1.19), $\epsilon = (\lambda - \lambda_0)/\lambda_1$ for the initial convection, and hence if λ_1 is positive ϵ is positive and the motion is up in the hexagon centre, whereas if λ_1 is negative ϵ is negative and the motion is down. We have estimated λ_1 by graphical methods for $\sigma = 8$ and find that $\lambda_1 \doteqdot 9{\cdot}5$. Hence the motion is up in the centre of hexagons as is observed.

One must now determine under what conditions the finite amplitude hexagon is preferred to the square or rectangle in the case of one rigid and one free boundary. To the λ_2-approximation,

$$\epsilon^2\lambda_2+\epsilon\lambda_1-(\lambda-\lambda_0)=0;$$

hence

$$\epsilon=(\lambda_1/2\lambda_2)[\{1+4\lambda_2(\lambda-\lambda_0)/\lambda_1\}^{1/2}-1], \tag{5.13}$$

where the second root is discarded since it does not vanish when $\lambda=\lambda_0$. The corresponding heat transport from (5.13) is

$$(\overline{WT})_m \doteqdot [(\lambda-\lambda_0)/\lambda_2-\epsilon\lambda_1/\lambda_2][(\overline{W_0\,T_0})_m+\epsilon(\overline{W_0\,T_1}+\overline{W_1\,T_0})_m], \tag{5.14}$$

where we have kept all terms in $(\overline{WT})_m$ necessary in the determination of λ_2. Equation (5.14) asserts that the heat transport will be less than that due to λ_2 alone for values of $(\lambda-\lambda_0)$ close to zero. However if $\lambda_1(\overline{W_0\,T_1}+\overline{W_1\,T_0})_m^{-1}$ ($=Q$ say) is positive the heat transport will exceed the value appropriate to λ_2 when

$$\lambda-\lambda_0 \geqslant |\lambda_1|(\overline{W_0\,T_0})_m^{1/2}(Q/\lambda_2)^{1/2}+(\overline{W_0\,T_0})_m\,Q. \tag{5.15}$$

Since the value of λ_2 for hexagons and the value of λ_2 for squares will be comparable (certainly within a factor of two), then hexagons can become the preferred disturbance if $\lambda_1(\overline{W_0\,T_1}+\overline{W_1\,T_0})_m^{-1}$ is positive and if the critical value of $(\lambda-\lambda_0)$ as given by (5.15) is small enough so that (5.14) is still valid. We have not yet determined the magnitude of $(\overline{W_0T_1}+\overline{W_1T_0})_m$ but a graphical method of integration assures us that its sign is positive. Hence we conclude that hexagons will not appear as the initial instability with one rigid and one free boundary, but will appear for some finite $(\lambda-\lambda_0)$ with positive vertical velocity in their centres. There is some experimental evidence to support this conclusion. Benard (1901) describes the initial appearance of convection due to cooling a fluid from above as "a disordered cellular regime" which becomes a steady field of hexagons after the cooling has continued a short time.

Amplitude determination by integral techniques

The lengthy task of computation needed to determine finite amplitude effects for realistic boundary conditions encouraged us to consider less exact methods. Stuart (1958) describes the use of power integrals to determine the amplitude of any disturbance whose form is assumed to be a good approximation to a correct solution. Stuart's study was concerned with finite amplitude processes in shearing flow, but he has discussed with us the application of this method to thermal convection. We will briefly outline our impressions of the virtues and limitations of the thermal power integrals as tools for finite amplitude study. In particular, we will compute the heat transport for the case of two rigid boundaries which can be compared with the experimental results.

In the steady state the kinetic power integral (1.7) is a homogeneous relation between the amplitudes and forms of $\mathbf{v}$ and T. If $\mathbf{v}=A\mathbf{v}'$ and

$T = BT'$, where T' and the W' component of $\mathbf{v}'$ are normalized, then (1.7) in non-dimensional form may be written

$$B/A = \nu(-\overline{\mathbf{v}' . \nabla^2\mathbf{v}'})_m/\gamma(\overline{W'T'})_m. \tag{5.16}$$

On the other hand the thermal power integral equation (1.6) is an inhomogeneous relation since β/β_m from (1.13) also contains the amplitude. Equations (1.6) and (1.13) may be written

$$AB = (\lambda - \lambda_S)/S, \tag{5.17}$$

where

$$S = (\overline{W'T'})_m \left\{ \frac{(\overline{W'T'^2})_m}{(\overline{W'T'})_m^2} - 1 \right\}, \qquad \lambda_S = \frac{B}{A} \frac{(-\overline{T'\nabla^2 T'})_m}{(\overline{W'T'})_m}.$$

Equation (5.17) for the convective heat transport is like the observed linear relation between heat transport and λ, since S and λ_S will be constants for any particular form of $\mathbf{v}'$ and T'. If we use the form of the initial Rayleigh instability of the case of two free boundaries for $\mathbf{v}'$ and T', then from (2.7),

$$(\overline{W'T'})_m = 1, \qquad S = \tfrac{1}{2}, \qquad \lambda_S = \lambda_0,$$

and

$$AB = 2(\lambda - \lambda_0), \tag{5.18}$$

independent of the plan-form of the initial disturbance. Equation (5.18) is identical with our results for λ_2 in the case of roll cells with free boundaries. This is understandable, for the free roll is the one case in which U_1, V_1, W_1, T_1 distortions and σ effects did not influence initial growth. Since distortions and σ effects uniformly tend to reduce amplitude we may hope that this use of the power integral sets an upper limit on heat transport.

Other inhomogeneous integral relations may be deduced from the heat equation which lead to different but lower values of the heat transport at the same λ and for the same choice of $\mathbf{v}'$, T'. For example we may write the non-dimensional heat equation from equations (1.5) and (1.13) as

$$\lambda W = h + [\overline{WT} - (\overline{WT})_m]W - \nabla^2 T \equiv L. \tag{5.19}$$

Then squaring both sides and averaging we obtain the inhomogeneous relation

$$\lambda^2 = (\overline{L^2})_m/(\overline{W^2})_m, \tag{5.20}$$

which must be satisfied by any correct solution to the problem. If we again use the form of the initial Rayleigh instability for the case of two free boundaries for $\mathbf{v}'$ and T', but for simplicity use the roll plan-form (since (5.20) depends upon plan-form), then

$$AB = (2\lambda^2 - \lambda_0^2)^{1/2} - \lambda_0. \tag{5.21}$$

Thus we have derived a different law for heat transport from that given by the power integral. In general, equation (5.21) yields a lower heat transport for given λ than does (5.18). Only for $\lambda \doteq \lambda_0$ do the two formulae agree since it is only at infinitesimal AB that this choice of $\mathbf{v}'$ and T' is a correct solution. In spite of this difficulty, the power-integral heat transports seem to bear too remarkable a resemblance to the observations to be fortuitous, as we will now show by a computation of the Rayleigh function for rigid boundaries paralleling (5.18).

Pellew & Southwell have proposed an approximate solution to the first-order characteristic functions (for rigid boundaries) which is easier to work with than the correct solution,

$$W' = N^{1/2}[\sin n\pi z + P\cosh \pi(z-\tfrac{1}{2}) + Q\pi(z-\tfrac{1}{2})\sinh \pi(z-\tfrac{1}{2})]\phi, \quad (5.22)$$

and

$$T' = \surd 2\phi \sin \pi z,$$

where ϕ is the normalized plan-form, $N^{1/2}$ is a normalizing constant, $P = 0{\cdot}4921$ and $Q = 0{\cdot}3416$ are constants chosen to satisfy boundary conditions. Using this form and relation (1.21) to fix B/A, equation (5.17) leads to $\lambda_S = 1713{\cdot}7$, $S = 1/1{\cdot}51$, and

$$AB = 1{\cdot}51(\lambda - 1713{\cdot}7). \quad (5.23)$$

The correct value of λ_S for the infinitesimal disturbance is 1707·8, indicating that (5.22) is an adequate approximation to the correct infinitesimal solution. The heat transport law (5.23) is in such good agreement with the observations reported in table 1 that one is tempted to extend this use of the power integrals beyond the range of steady convection. As discussed in the Introduction, a second instability occurs at $\lambda \doteqdot 18\,000$, leading to aperiodic convection and an abrupt change to a new linear law of heat transport. In all, five or six transitions appear in the data up to $\lambda \doteqdot 10^6$, where 'fully turbulent' conditions seem finally to be achieved. If, as suggested by the success of the power integral, self-distortion of a disturbance is not very important, then perhaps the interaction between several different disturbances plays a small role in the determination of heat transport. To test this possibility we can determine the total heat transport which would result from the independent growth of first, second and higher Rayleigh-like modes of instability. That is,

Transition	λ Theoretical	λ Experimental	S_i^{-1} Theoretical	AB/λ Theoretical	AB/λ Experimental
1	1 708	1 700 ± 80	1·51	0	0
2	17 600	18 000 ± 1 000	1·72	1·37	1·3 ± 0·1
3	61 000	55 000 ± 4 500	1·83	2·63	2·3 ± 0·1
4	170 000	170 000 ± 15 000	$1{\cdot}9^-$	4·29	3·4 ± 0·1
5	411 000	425 000 ± 20 000	$1{\cdot}9^+$	6·87	4·5 ± 0·1
6	855 000	860 000 ± 30 000	2·0	8·52	5·7 ± 0·1

Table 1. Convective heat transport at the experimental transitions computed from equation (5.24).

$$AB = \sum_1^{\infty} (\lambda - \lambda_{S_i})/S_i, \quad (5.24)$$

where the S_i determine the slope of the growth curve for the mode i and λ_{S_i} is the value of λ for instability for that mode. Equation (5.24) has the form of the observed heat transport up to $\lambda \doteqdot 10^6$. The values of the S_i and λ_{S_i} have been computed in the same way as S and λ_S of (5.23) with the approximate functions of Pellew & Southwell for each instability. The results are tabulated in table 1 and compared with observations in water made by Malkus (1954a). In dimensional form AB/λ is the ratio of the convective heat transport to the heat transport in the absence of convection. For large values of λ, S_i^{-1} approaches its free surface value and has been set equal to this value for λ greater than 800 000. Equation (5.24) agrees quite well with experiment at the end of the steady convective range, but by $\lambda \doteqdot 55\,000$ at the end of the first aperiodic range there is an error of approximately 15%. This percentage error continues to increase with λ through all observable transitions. Equation (5.24) cannot be correct in the range of λ beyond observable transitions since it leads to an incorrect gross dependence of heat transport on λ (giving $AB/\lambda \sim \lambda^{1/4}$ instead of the observed variation as $\lambda^{1/3}$). However it is rather remarkable that (5.24) works as well as it does. This suggests to us the possibility that aperiodicity permits the several disturbances to be more or less independent which certainly could not be the case if they were steady superimposed motions. The quasi-independence due to the aperiodicity could permit a greater release of potential energy and hence lead to a more stable field of motion than any other. Such thoughts are of course only speculation and a formal theory for the onset of thermal turbulence has yet to be found.

6. CONCLUDING REMARKS

To summarise the conclusions: the initial finite amplitude convection is determined primarily by the distortion of the mean temperature field, secondarily by the self-distortion of the disturbance; the number of formal steady-state solutions increases with increase of Rayleigh number beyond the critical value; however this degeneracy is removed if there is only one finite amplitude solution which has a greater mean-square temperature gradient than any other solution. More particular conclusions are that: square plan-forms are preferred to hexagonal plan-forms in ordinary fluids with symmetric boundary conditions; the initial stages of convection are markedly altered in a fluid of small Prandtl number; the effect of distortion of the disturbance on the thermal field prevents the mean gradient of the temperature from changing sign in the mid-regions of the fluid; the zero-average non-linear terms reduce the amplitude of the disturbance; the preferred horizontal wave-number increases with increasing Rayleigh number.

The approach to finite amplitude processes given above is applicable to those convection and shear flow studies with adequately solved stability problems. The method can determine those conditions which permit a steady finite amplitude disturbance to occur before the appearance of the infinitesimal disturbance. Hence it is a tool to extend the study by Meksyn & Stuart (1952) of the onset of disturbances in channel shear flow. The method is of particular value in the resolution of explicit or hidden degeneracies in a stability theory. Hidden degeneracies exist when there are velocity-dependent forces other than advection which play no role in the criterion for instability. This occurs for example in the study of geomagnetism. There one wishes to determine when an electrically conductive fluid heated from below will select a joint magneto-convective state of motion rather than a pure convective state.

However, beyond the initial finite amplitude effects the technique we have described here can become prohibitively tedious. In addition the ϵ-sequence will fail to describe the preferred field of motion after a second instability has occurred, though this sequence may still converge to a set of formal steady-state solutions. We continue to search for an adequate descriptive framework which can include the second instability and in particular can deal with aperiodicity.

This study bears a relation to two previous works on fully developed turbulence. A paper on turbulent convection (Malkus 1954b) and a paper on turbulent shear flow (Malkus 1956) were based on the assumption that the most stable field of flow would be that one which released the maximum amount of potential energy per unit time. The section of this paper on relative stability suggests that a maximum mean-square temperature gradient (equation (4.14)) is the more appropriate stability criterion. The only qualitative prediction of the earlier works which appears to be altered by this change is the structure of the boundary regions and this causes a reduction in the turbulent transports. These modifications will be discussed in a following paper.

It was our good fortune that Dr J. T. Stuart was visiting the United States during the preparation of this paper. We wish to acknowledge many fruitful discussions of our common problem with him.

The work was performed under the auspices of the Office of Naval Research and is Contribution No. 943 from the Woods Hole Oceanographic Institution.

REFERENCES

BENARD, M. 1901 *Ann. Chim. Phys.* **23**, 62.

BOUSSINESQ, J. 1903 *Theorie Analytique de la Chaleur*, vol. 2. Paris: Gauthier-Villars.

CHRISTOPHERSON, D. G. 1940 *Quart. J. Math.* **11**, 63.

JEFFREYS, H. 1930 *Proc. Camb. Phil. Soc.* **26**, 170.

LINDSTEDT, A. 1883 *Mem. Acad. Imp. Sci. St. Petersburg* **31**, no. 4.

MALKUS, W. V. R. 1954a *Proc. Roy. Soc.* A, **225**, 185.

MALKUS, W. V. R. 1954b *Proc. Roy. Soc.* A, **225**, 196.

MALKUS, W. V. R. 1956 *J. Fluid Mech.* **1**, 521.

MEKSYN, D. & STUART, J. T. 1951 *Proc. Roy. Soc.* A, **108**, 517.

PELLEW, A. & SOUTHWELL, R. V. 1940 *Proc. Roy. Soc.* A, **176**, 312.

RAYLEIGH, LORD 1916 *Phil. Mag.* (6), **32**, 529

SCHMIDT, R. J. & MILVERTON, S. W. 1935 *Proc. Roy. Soc.* A, **152**, 586.

SOROKIN, V. S. 1954 *Prikl. Mat. i Mekh.* **18**, 197.

STUART, J. T. 1958 *J. Fluid Mech.* **4**, 1.

Contribution No. 944

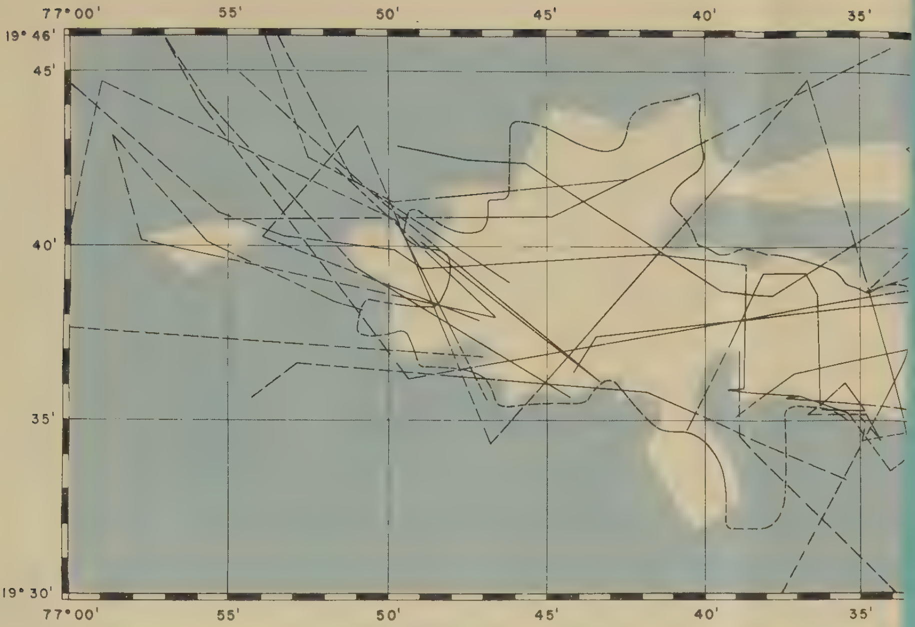
77°00'
55'
50'
45'
40'
35'
19°46'
45'
40'
35'
19°30'

A. Navigational tracks of soundings over the deep plain
Solid tracks (smooth bottom) and dashed tracks (m

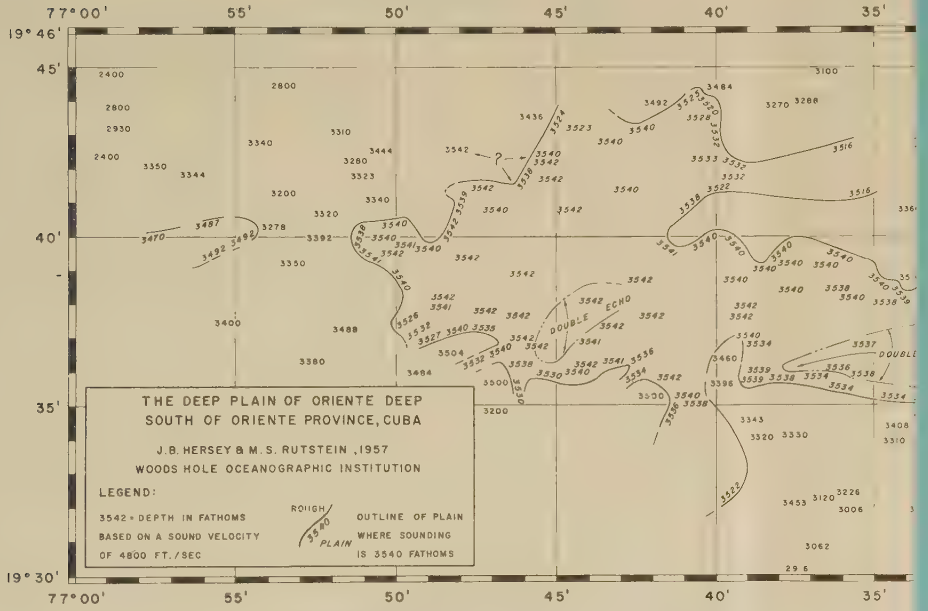
77°00'
55'
50'
45'
40'
35'
19°46'
45'
40'
35'
19°30'
DOUBLE ECHO
THE DEEP PLAIN OF ORIENTE DEEP
SOUTH OF ORIENTE PROVINCE, CUBA
J.B. HERSEY & M.S. RUTSTEIN, 1957
WOODS HOLE OCEANOGRAPHIC INSTITUTION
LEGEND:
3542 = DEPTH IN FATHOMS
BASED ON A SOUND VELOCITY
OF 4800 FT./SEC
ROUGH
3540
PLAIN
OUTLINE OF PLAIN
WHERE SOUNDING
IS 3540 FATHOMS

B. Bathymetric chart of the deep plain of the Oriente D
feet per second sound velocity. Deep-plain sounding
ings (upright) over surrounding mountainous ter
shown as a solid line (good control) or a dashed li
sub-bottom echoes were recorded are surrounded b

NAVIGATIONAL TRACKS OF SOUNDIN
DEEP PLAIN OF OR

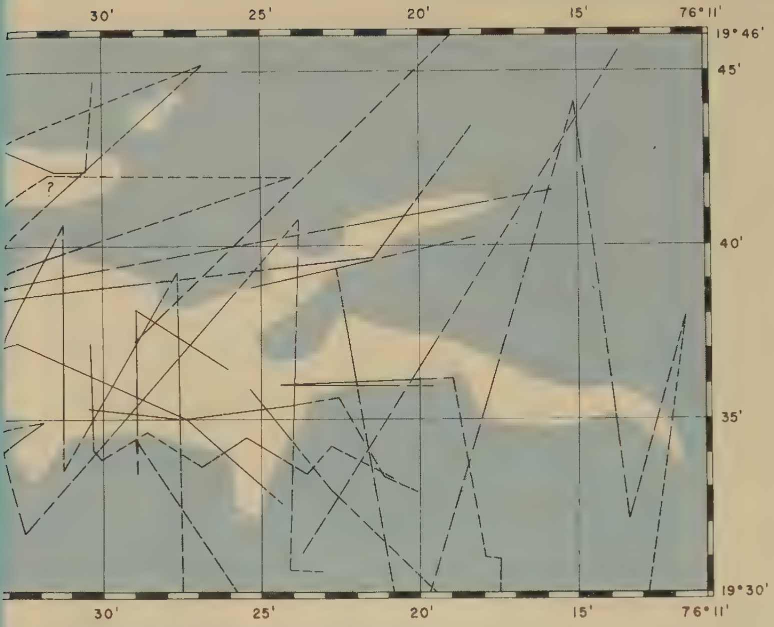
30'
25'
20'
15'
76° 11'
19° 46'
45'
40'
35'
19° 30'
?

of Oriente Deep. White area is the deep plain.
ountainous terrain) indicate the control.

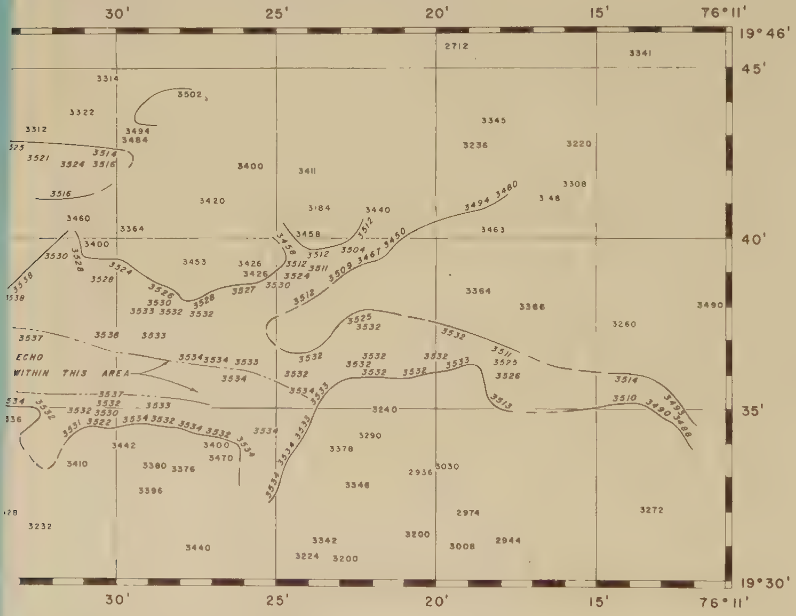
30'
25'
20'
15'
76° 11'
19° 46'
45'
40'
35'
19° 30'
ECHO
WITHIN THIS AREA

eep. Soundings are in fathoms based on 4800
s (slanted) are separated from selected sound-
rain by the observed edge of the deep plain
ne (poor control). Areas of deep plain where
y coded dashed lines.

GS AND BATHYMETRIC CHART,
IENTE DEEP

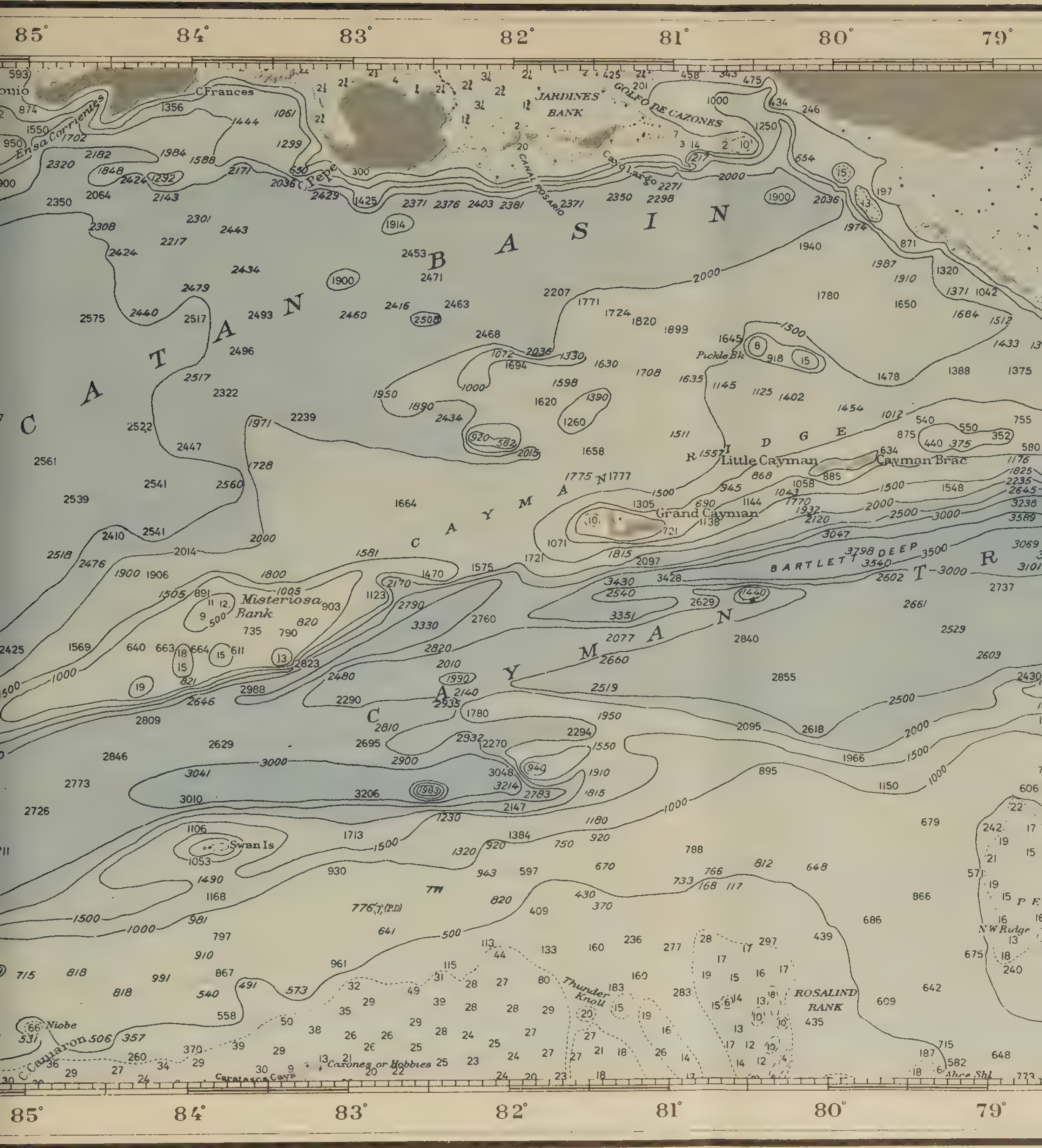
85°
84°
83°
82°
81°
80°
79°
C Frances
Ensa Corrientes
JARDINES BANK
GOLFO DE CAZONES
CANAL ROSARIO
Cayo Largo
Pepe
YUCATAN BASIN
Pickle Bk
CAYMAN RIDGE
Little Cayman
Cayman Brac
Grand Cayman
BARTLETT DEEP
CAYMAN TRENCH
Misteriosa Bank
Swan Is
Niobe
C Camaron
Caratasca Cays
Cayones or Hobbies
Thunder Knoll
ROSALIND BANK
N W Ridge
Alice Shl

MAP OF PORTION OF CARIBBEAN SEA

A portion of H.O. chart 5487 showing location of Oriente Deep

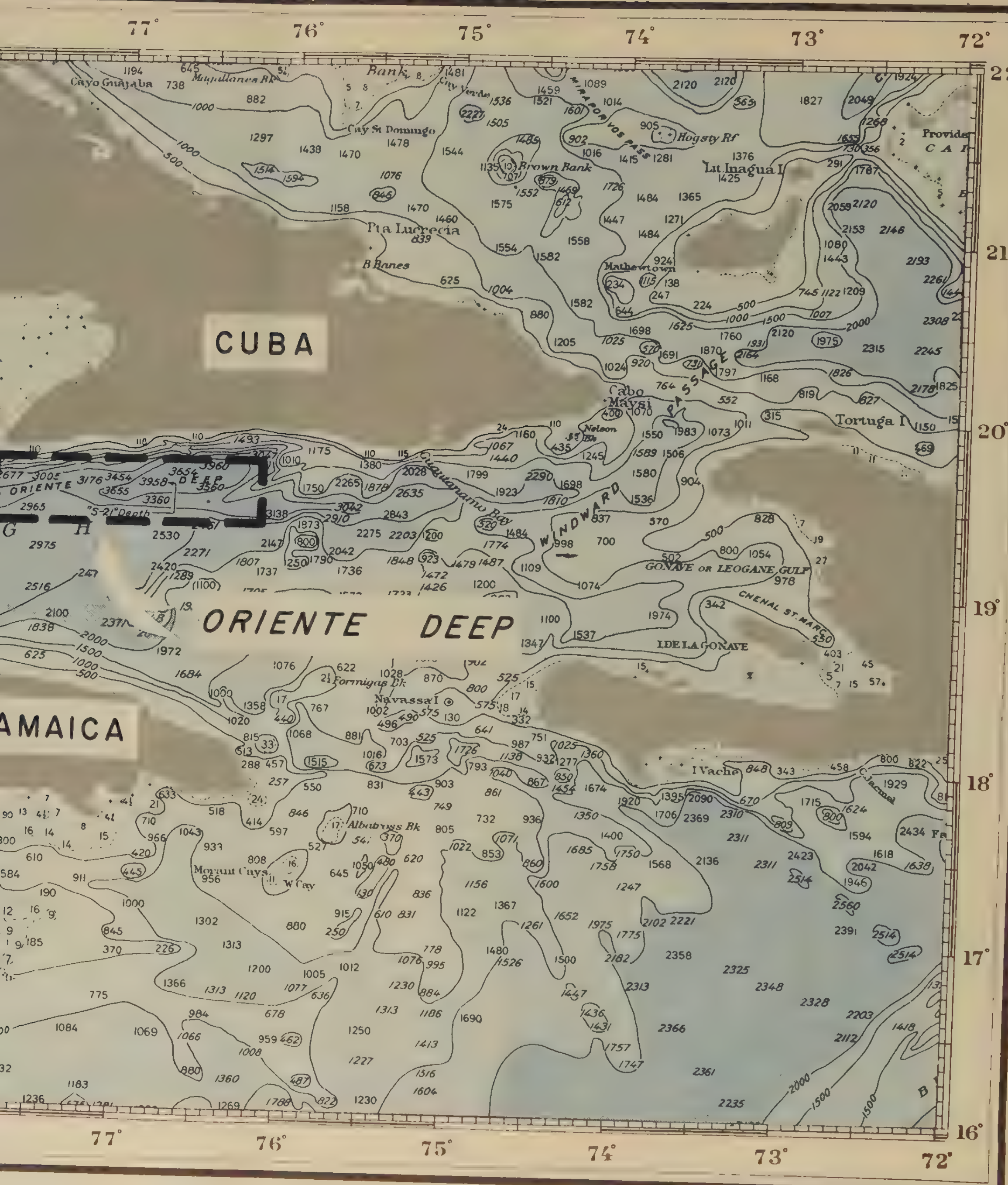
77°
76°
75°
74°
73°
72°
22°
21°
20°
19°
18°
17°
16°
CUBA
AMAICA
ORIENTE DEEP
ORIENTE DEEP
"S-21" Depth
Cayo Guajaba
Magallanes Bk
Bank
Cay Verde
Cay St Domingo
Pta Lucrecia
B Banes
Brown Bank
Hogsty Rf
Lit Inagua I
Mathewtown
Providence
CAI
MIRAPOR VOS PASS
PASSAGE
WINDWARD
Cabo Maysi
Nelson Bk
Tortuga I
Guantanamo Bay
GONAVE OR LEOGANE GULF
CHENAL ST. MARC
I DE LA GONAVE
Formigas Bk
Navassa I
I Vache
C Jacmel
Albatross Bk
Morant Cays
W Cay
1000
500
2000
1500

BULLETIN OF THE GEOLOGICAL SOCIETY OF AMERICA
VOL. 69, PP. 1297-1304, 2 FIGS, 5 PLS. OCTOBER 1958

RECONNAISSANCE SURVEY OF ORIENTE DEEP (CARIBBEAN SEA) WITH A PRECISION ECHO SOUNDER

BY J. B. HERSEY AND MILTON S. RUTSTEIN

ABSTRACT

The submarine slope of the southern coast of Cuba is steep and rugged south of Sierra Maestra, Oriente Province; the average slope in one locality between depths of 1000 and 2000 fathoms is 31°. Two major reversals in slope, at about 2000 fathoms and 2800 fathoms, are taken as evidence of fault zones. Below 2800 fathoms the topography is mountainous in an area parallel to the coast and about 15 miles wide; local relief is several hundred fathoms, but the area deepens to its center where there is a nearly flat plain 3–5 miles wide and about 25 miles long, which also parallels the coast. The plain slopes gradually westward from 3530 to 3542 fathoms with local northward slopes (depths are based on sound velocity of 4800 feet per second); it is the deepest known part of Oriente Deep. The plain is surrounded by hills and intervening gorges which have relatively smooth bottoms grading down to it. Details of the topographic relations indicate that the plain is underlain by unconsolidated sediment brought in by turbidity currents flowing down the gorges. Recent coring in a similar near-by plain supports this view. Seismic evidence, though meager, suggests that the sediment is 1200–1500 feet thick.

CONTENTS

TEXT

Page
Introduction 1297
Acknowledgments 1298
Methods 1298
  Navigation 1298
  Soundings 1298
Observations 1298
Discussion 1300
Geological interpretation 1302
Summary and conclusions 1303
References cited 1303

ILLUSTRATIONS

Figure Page
1. Average vertical-sound velocity 1299
2. Relative positions of an arbitrary location after adjustment of celestial navigation . . 1299

Plate Facing page
1. Map of portion of Caribbean Sea 1297

Following page
2. Slope from 1000 fathoms off Cuba to deep plain of Oriente Deep 1300
3. High-resolution sounding on the flat bottom, taken over western portion of deep plain 1300
4. Cross-sectional profiles of southeastern gorge 1300
5. Divide between northeastern and southeastern gorges near east end of deep plain 1300

Facing page
6. Navigational tracks of soundings and bathymetric chart, deep plain of Oriente Deep 1304

INTRODUCTION

The Oriente Deep lies 15–20 miles south of the southern coast of Oriente Province, Cuba, and is part of the Bartlett or Cayman trough, a deep trench extending from the northwestern tip of the island of Hispaniola more than 1000 miles westward and southward, where it gradually shoals in the Gulf of Honduras. The Bartlett Deep to the west and the Oriente Deep are the deepest parts of this trench (Pl. 1).

During March and April 1956, scientists on the ATLANTIS and BEAR, research ships of the Woods Hole Oceanographic Institution, carried out oceanographic investigations in the Cayman Sea south of Cuba. Depth profiles were recorded across the Oriente Deep with echo sounders fitted with the precision graphic recorders described by Knott and Hersey (1956). On several occasions, especially during the night, when the ships were not otherwise engaged, we were able to make more detailed bathymetric studies there. Although the bathymetric studies had to be subordinated to the other work, we learned much about the geological characteristics of this deep which could be found out only with the aid of depth soundings precise to at least a part in 3000. We also gained experience in using precisely measured depth profiles both as an aid to navigating the ship at sea and for checking the results of other navigational data after the cruise.

ACKNOWLEDGMENTS

The soundings on which this study is based were the work of all the scientists aboard ATLANTIS and BEAR, and the navigational control is the work of the ships' officers. We gratefully acknowledge their considerable contribution to this study. Mr. Charles Innis prepared the figures. We are indebted to the U. S. Hydrographic Office for permission to use a portion of their chart HO-5487 as Plate 1. The cruise during which the soundings were taken was supported under Contract Nonr-1367 with the Office of Naval Research.

METHODS

Navigation

In this area such modern electronic aids to navigation as Loran were not available; the tracks of the ship were determined by celestial navigation and dead reckoning. We could make use of cross bearings on mountain peaks on the southern coast of Cuba, but inasmuch as most of the sounding was done at night this method of position fixing was of little use. We might have made long sounding lines starting at known shore points and returning to the coast for closure, but too much time would have been consumed in making observations over a terrain too rugged to map in meaningful detail. From previous visits to the area we knew that the bottom of the Oriente Deep was flat. Hence we elected to study in more detail the shape of the flat area and its relation to the surrounding rugged topography. Since we were generally out of sight of landmarks, the precision of the navigation was by no means comparable to that of the soundings. From the traverses made under the most favorable weather, and when star fixes, sun lines, and dead reckoning agreed well with each other, we outlined the main features of the shape of the flat portion of the deep. On other traverses for which the position control from these data gave results obviously inconsistent with the soundings, we found that in most instances corrections to dead-reckoning data could be applied by noting the times of crossing the edges of the flat area. By thus adjusting the poorer traverses a consistent picture could be mapped. There remain many uncertainties in detail, but we believe that the broad outline is accurate within about 1–1.5 miles.

Soundings

Both ships were fitted with an Edo UQN-1B echo sounder and an 18-inch Woods Hole precision graphic recorder (Knott and Hersey, 1956), which were operated routinely on the 400-, 500-, or 1000-fathom scale. Occasionally, while lying to over the flat area BEAR recorded at considerably higher resolution (25- and 50-fathom scales). Time was recorded by interrupting the depth scale every 5 minutes by an electric clock powered by the precision 60 cps power source. Other data such as course and speed of the ship were written on the recorder chart as well as in the deck log.

The power sources generally operated at about 1 part in 3000–5000 less than 60 cps but held a much more nearly constant rate, which was monitored continuously by recording a break-circuit chronometer on the record. All depth scales could be read to a fathom in depth whenever the beginning of the echo was clear. Since this was uniformly the case where the bottom was flat, the echo travel times there are accurate to the equivalent of a fathom in depth at 3000–5000 fathoms. The soundings shown on Plate 6*B* are based on a sound velocity of 4800 feet per second (in conformity with United States custom over the past 10 years), which is considerably too low in this area. We did not take adequate deep hydrographic data to compute an accurate average velocity; approximate average velocity as a function of depth is given in Figure 1 from Matthew's tables (1939) for this area. Although the possibility should not be discounted, significant variation is unlikely in average vertical velocity over an area as small as the Oriente Deep. We assume that small differences in echo travel time are true indicators of differences in depth.

OBSERVATIONS

The adjusted traverses of both ships are shown in Plate 6*A*. The track for each period when soundings were taken was plotted on transparent plastic drafting film with appropriate geographic co-ordinates. Ship tracks over the flat areas (solid lines) are distinguished from those showing relief (dashed lines). Those tracks judged to be based on the best navigation were superimposed on one another. From these the general outline of the flat bottom of the deep could be traced. Other tracks for which there were several crossings of the edge of the plain were adjusted for best fit by eye by moving their plot over those already established to a best fit with edges of the plain. This procedure adjusts the celestial navigation but not the dead reckoning. Parts of other tracks did not fit the outlines of the flat areas because they indicated that the flat portion was too wide or too narrow. Usually this resulted from not making due allowance for headwinds or cross winds in the original dead reckoning. By adjusting either speed or course made good on these latter tracks over the part for which the position of the plain was already well established, the whole track became much more consistent with the previously established picture. The soundings (Pl. 6*B*) show that the flat portion slopes to the west and in places to the north as well, thus providing approximate position control by its depth pattern. The position control for a few of the traverses was so poor that only by adjusting their soundings to fit could their position be adjusted. In all cases but two this sort of adjustment also made the edges of the flat portion fit satisfactorily. Such adjustments can be influenced by prejudice, but we believe that the cross check provided by comparing both the horizontal extent and depth of the flat area effectively minimizes this danger. Furthermore most of the adjustments were small. The distribution of simple translation adjustments is shown in Figure 2 as a plot of the positions of an arbitrary location before and after adjustment. The center of the diagram is the location before adjustment, and the black dots indicate individual translations. Eight tracks required no adjustment.

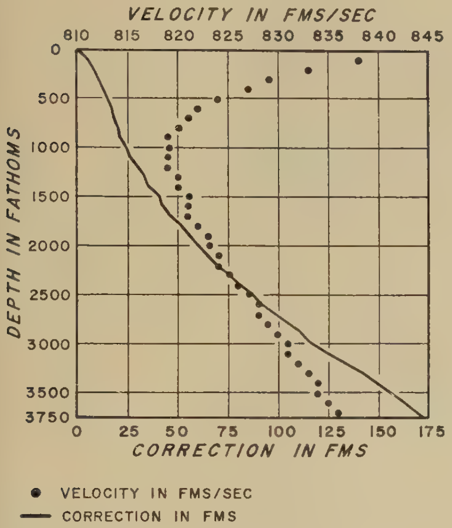

FIGURE 1.—AVERAGE VERTICAL-SOUND VELOCITY After Matthews (1939)

The soundings and the outline of the flat portion of the deep are shown in Plate 6*B*; selected soundings over the surrounding relief are also indicated, but there are far too few soundings over the rough topography to make any but the broadest generalizations about it. In addition to the traverses made to delineate the flat portion a few traverses were made while the ships were en route to or from ports on the southern coast of Cuba. From these is gained a general impression of topography between the island and the deep (Pl. 2). While the ships were lying to over the flat portion a number of high-resolution recordings (50-fathom scale) were made, some of which showed pronounced multiple echoes; unlike multiples often seen over rough terrain, these are unlikely to be side echoes and probably represent penetration into the bottom (Pl. 3). Twice the two ships travelled in company from port; echo soundings were recorded, and frequent radar ranges and bearings were taken between the ships. This operation was intended to extend the usefulness of the single traverse by correlating soundings at the two ships. The records are similar and show qualitatively similar terrain, but the terrain is too rugged to allow detailed correlation of the records taken from ships more than a mile apart. Over the flat portion of the deep the soundings from the two

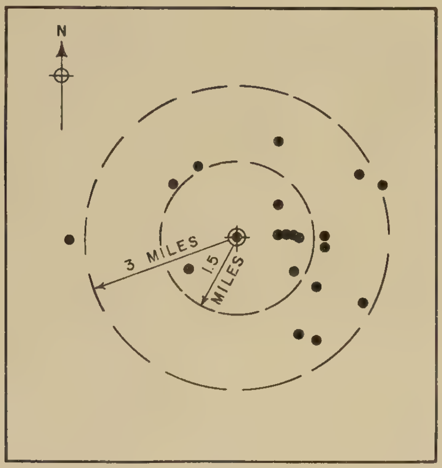

FIGURE 2.—RELATIVE POSITIONS OF AN ARBITRARY LOCATION AFTER ADJUSTMENT OF CELESTIAL NAVIGATION

ships agreed (within 1 fathom); however, once established, this could not aid us further in studying the shape of the deep, since it was seldom possible to survey in company there.

DISCUSSION

The southern coast of Oriente Province, Cuba, trends approximately east-west. Oriente Deep extends parallel to the coast along its western half as far east as Santiago. Farther east the deep terminates in shoaler water. Even the grossest features of the submarine topography are complicated, and the island slope north of Oriente Deep is steep (Pls. 1, 2). There are similar features on other crossings several miles apart. All indicate the steep slope to about 2000 fathoms, then a slight reversal and another somewhat less steep slope to about 2800 fathoms, another reversal, and a still more gradual slope down to the plain. The grade from 2800 fathoms to the plain is irregular and in places mountainous, showing local relief of several hundred fathoms. To the south of the plain there is a zone at least 3–5 miles wide where the topography is similarly complicated.

The flat portion of the deep follows the same trend as the coast line and is about 25 miles long and 3–5 miles wide. The sounding lines across the plain indicate that it is as smooth as the echo sounder (3.5 miles away!) is able to determine even when operated on a very high-resolution scale (Pl. 3). Over a considerable part of the plain the returning echo on a high-resolution scale is complex, as in Plate 3. The more or less regular undulation in depth of all the echo sequences is due to the motion of the ship in the surface waves, but the multiple echoes clearly recorded persist with nearly the same, or at least comparable, spacing over a wide area (Pl. 6*B*). We believe that the second group of echoes were reflected from a horizon below the bottom, which occurs widely in the part of the deep where the relief is least. If it is sediment, as we believe it to be, its sound velocity is unlikely to exceed that in the water by much, so that the thickness of sediment to the deeper horizon is about 30 feet. Since a 12-kc sound pulse penetrated the bottom here, the first layer of sediment is probably exceedingly porous; even in shallow water high-frequency sound will not penetrate far into sediments other than unconsolidated silts and muds. A review of several shallow-water studies on sediment penetration by sound is given by Smith and Nichols (1953).

The soundings on the plain deepen from east to west from about 3530 to 3542 fathoms in about 20 miles. In the central portion soundings deepen from about 3534 on the south to 3540 fathoms on the north in 3 miles. In so short a distance in this area the average vertical velocity for soundings probably would not vary appreciably; thus it is reasonable to assume that these slopes are as small as indicated. This is further evidence of a fine, porous sediment.

In Plate 6*B* the soundings shown paralleling the edge of the plain are those obtained just within the flat area where traverses crossed its boundary. The soundings shown well out on the plain are either at places where the ship changed course or where a significant change in grade occurred. The sounding lines across the plain show little evidence of undulations even as large as a fathom. However, soundings around the edge show two types of change from rough to flat topography. In one, the depth at the edge is as great as it is farther out on the plain; in the other varying smooth grades are always shoaler at the edge than farther out. Most of these gentle grades appear to be at the mouths of gorges in the surrounding hills; this suggests that these gorges are the supply ducts for sediments that have filled the bottom of the deep. In Plate 6*A* is shown a long sinuous track around the western half of the plain. Here the ship was zig-zagged back and forth across the edge of the flat area in order to cross a number of these shoaler fans. We had no opportunity to explore them in detail, but in the northern central portion a gorge was found trending eastward and gradually shoaling. Farther to the east it deepens irregularly. On the eastern end of the plain, two gorges trend away and shoal gradually to the east. The northern gorge is smooth at its western end where it grades onto the plain, but farther east two sounding lines suggest that its bottom becomes rougher as it shoals. The southerly gorge was surveyed in somewhat more detail (Pl. 6*B*); five sounding

PLATE 2.—SLOPE FROM 1000 FATHOMS OFF CUBA TO DEEP PLAIN OF ORIENTE DEEP

Soundings taken from the offing of Santiago de Cuba to the eastern portion of the deep plain

PLATE 3.—HIGH-RESOLUTION SOUNDING ON THE FLAT BOTTOM, TAKEN OVER WESTERN PORTION OF DEEP PLAIN

Recordings show multiple echoes probably indicating sound penetration of bottom sediments.

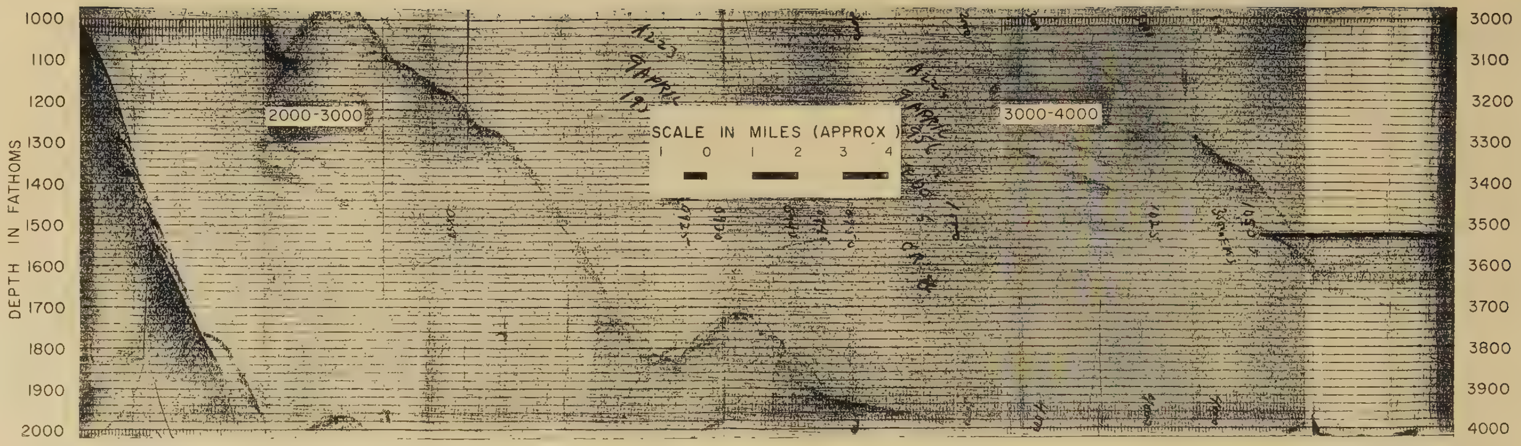

SLOPE FROM 1000 FATHOMS OFF CUBA TO DEEP PLAIN OF ORIENTE DEEP

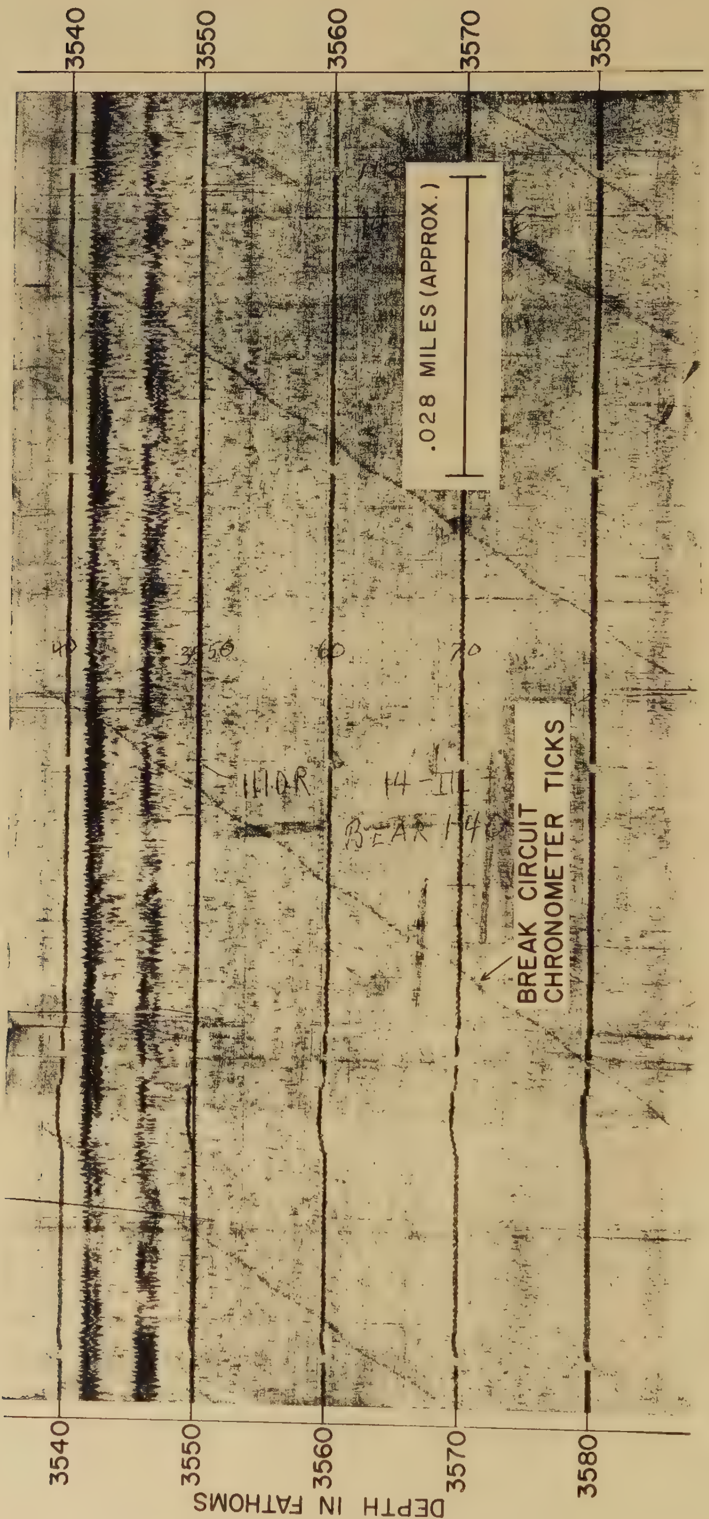

HIGH-RESOLUTION SOUNDING ON THE FLAT BOTTOM, TAKEN OVER WESTERN PORTION OF DEEP PLAIN

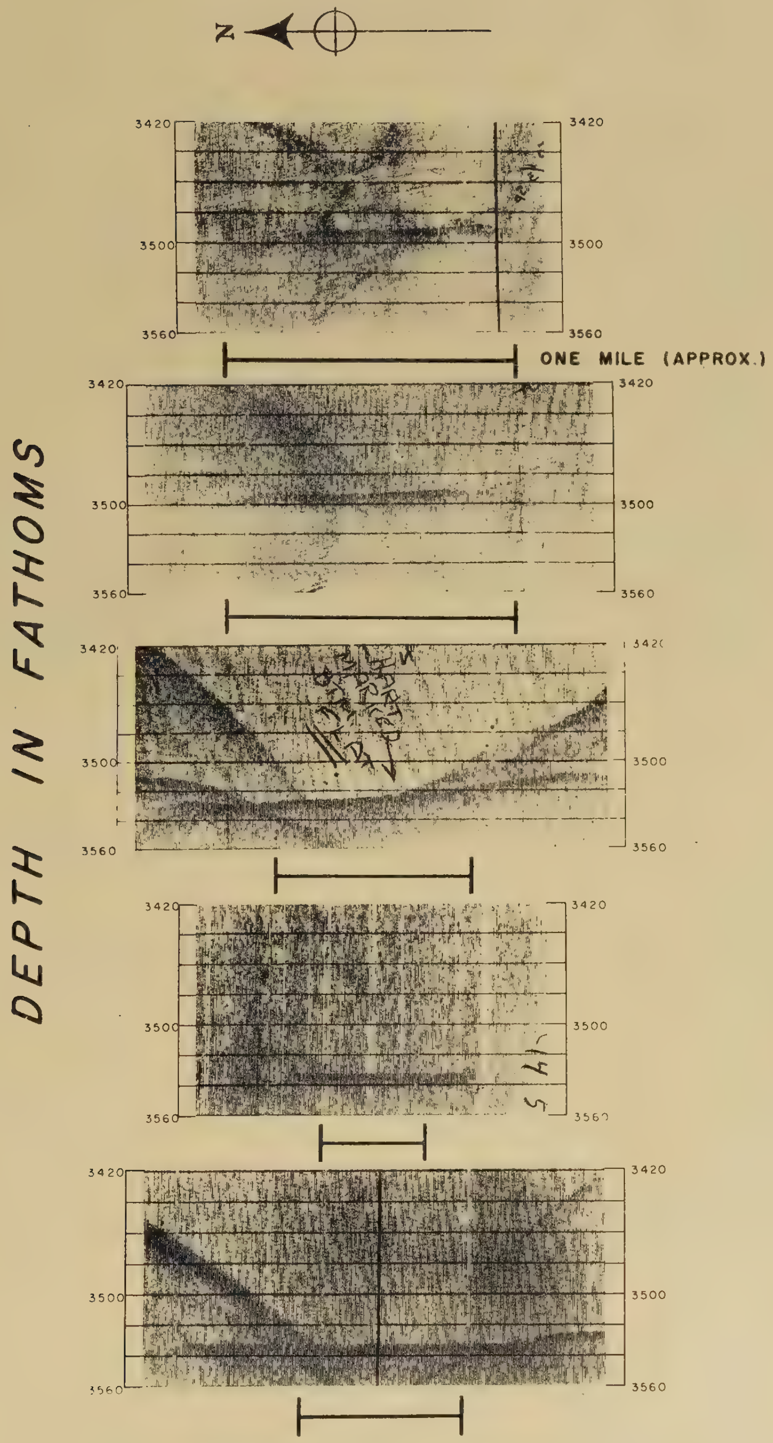

CROSS-SECTIONAL PROFILES OF SOUTHEASTERN GORGE

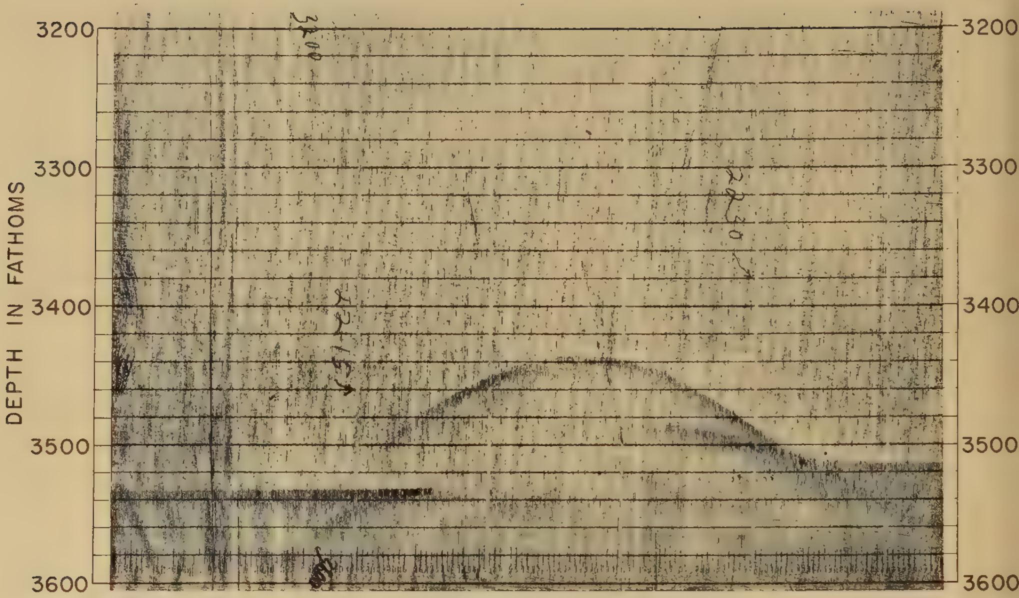

FIGURE 1

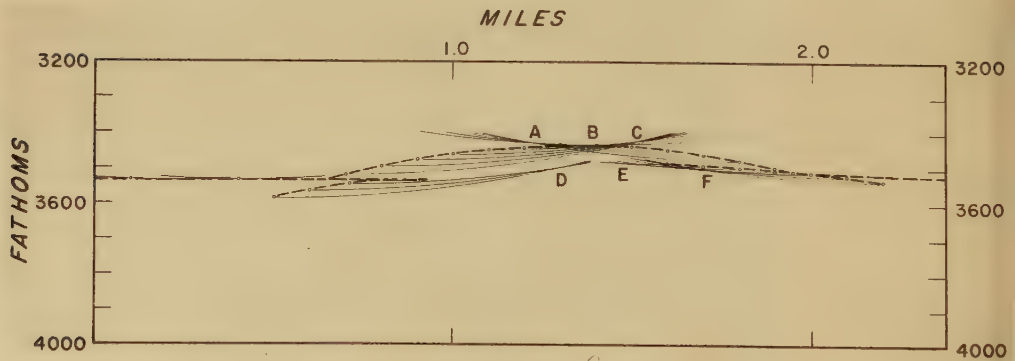

FIGURE 2

DIVIDE BETWEEN NORTHEASTERN AND SOUTHEASTERN GORGES NEAR EAST END OF DEEP PLAIN

Horizontal scales are identical, and figures are aligned.

lines across it are shown in Plate 4. These are arranged from east to west (top to bottom), and the traverses are printed with the northern edge always at the left regardless of the original direction of the traverse. Most of the traverses show pronounced crescent-shaped side-echo sequences from the surrounding rough topography; the smoother bottom of the gorge is shown as a short gently sloping echo sequence. In the upper reaches of the gorge the smooth bottom slopes to the north, but farther west the northerly slope lessens until near its mouth the bottom of the gorge is flat.

Most of the echoes from the smooth bottom of the gorge are somewhat stronger than the side echoes. On one traverse of Plate 4 the noise from the ship recorded by the echo sounder was so great that it obscured nearly all side echoes. Noise interference is a problem in most deep echo sounding; noise intensity depends directly on ship's speed. The worst offender on our ships is the propeller; its rhythmic beat produces the nearly regular pattern of noise evident on all these echograms. This noise never obscured echoes on the flat area but frequently made continuous depth recording underway impossible over the rough topography. This accounts in part for our sketchy knowledge of the topography surrounding the flat. The crescent-shaped echo sequences in the rough topography are almost certainly weaker because the reflected sound is scattered by single highlights rather than reflected from a broad surface such as the flat area.

The echo sequences recorded by an echo sounder do not record faithfully the details of the bottom profile under the ship's track. Echoes may be received from a scattering surface on a rough bottom before and after the ship passes over it, thus producing crescent-shaped echo sequences like those in Plate 5. Such a scattering surface may be laterally displaced from the ship's track, and with present echo-sounding techniques there is no easy way of determining how far it is displaced. Nevertheless if the chip has proceeded on a steady course over such highlights it is possible in some cases to learn more about their shape and size than is obvious from the record. The techniques of this sort of analysis have been discussed by several authors (*e.g.*, Pinke, 1938). Probably the simplest technique is to choose a sounding track perpendicular to the apparent depth contours constructed from the original records. Then on a one-to-one cross section of the traverse, swing a series of circular arcs scaled to the indicated soundings from centers corresponding to the position of the ship for each sounding. The envelope formed by the successive arcs from a given echo sequence may be taken as the approximate profile of the corresponding reflecting surface. Such a profile is not necessarily in the vertical plane under the ship's track, and there may be other complications over complex topography that make the interpretation uncertain. Nevertheless the method gives a more nearly accurate profile than the graphic record and should be applied wherever more clearly defined bottom shapes are needed. As an example, the profile in Figure 1 of Plate 5 was taken across the divide between the two easternmost gorges feeding the flat area. The difference in level of the two smooth portions of the profile indicates that the gorges are separated by the rougher topography. In Figure 2 of Plate 5 the results of an arc-swing analysis are shown. The dashed lines show the recorded soundings scaled to the same vertical scale as the horizontal scale of Figure 1 of Plate 5. The envelopes of the arcs form the closest approximation to actual bottom profiles available from the data. The principal crescent translates to an envelope (*A*-*B*-*C*) slightly concave upward, whereas the others form a highlight at *D* and a sloping "surface" *E*-*F*. The flat profiles, of course, translate to flat profiles. This sample illustrates how different from the form of the sounding record the profile may be and suggests that the rough terrain is characterized by abrupt changes in level, which further suggest that the rough terrain is formed of complexly fractured rock. This interpretation appears the most reasonable of all possibilities because of the generally rugged character of the deep.

PLATE 4.—CROSS-SECTIONAL PROFILES OF SOUTHEASTERN GORGE

Sounding profiles were taken at different speeds over the bottom as indicated by distance scales.

PLATE 5.—DIVIDE BETWEEN NORTHEASTERN AND SOUTHEASTERN GORGES NEAR EAST END OF DEEP PLAIN

Horizontal scales are identical, and figures are aligned.

Figure 1.—Uncorrected profile

Figure 2.—Profile corrected by arc-swinging analysis and with vertical exaggeration removed

GEOLOGICAL INTERPRETATION

The structure of the Bartlett Trough has been inferred largely from its bathymetry and what is known of the structure of Cuba, Jamaica, Hispaniola, and smaller islands in its vicinity. The dimensions of the trough are so great compared with these adjacent islands, and the topography of the trough seems to follow such a unified pattern, that its tectonic history must be related to that of the Caribbean as a whole; interpretations of local structure must be consistent with this fact. Hess (1938) proposed that the trough was part of a more extensive region of differential horizontal movement in which the central Caribbean moves eastward relative to Cuba. Meyerhoff (1954) discussed Caribbean structures in relation to a tectonic hypothesis in which major horizontal couples are proposed as the principal forces acting on the region. Butterlin (1956) reviewed the several principal hypotheses about the tectonics of the Caribbean region and pointed out the differences of opinion about, for example, Cenozoic tectonics in Oriente Province, adjacent to the trough. Students of this region do not agree about structures associated with the southern coast line of Oriente Province; some follow Taber (1931) in regarding the post-early Miocene history as one of subsidence of the trough accompanied by normal faulting; others (Woodring, 1928; Lewis and Straczek, 1955) favor folding and high-angle thrust faulting. All agree that the Bartlett Trough was formed essentially as today by mid-Miocene time and that changes in elevation of the whole region accompanied by faulting have continued to the present.

When combined with other geological and geophysical data about the trough the present study should help to evaluate the several points of view. The topography of the island slope was not studied in detail, but the crossings made indicate interruptions in the slope (Pl. 2). This sounding line was taken about 45° to the general slope. The 16-degree slope along the track from 1000 to 2000 fathoms may be taken as a slope of about 31°, a rather high submarine slope to persist for a mile in depth. The crescent-form echo sequences at the break in slope indicate at least a local reversal in the slope. If a fault zone is associated with this slope, it could be the principal fault zone of vertical movement between the Sierra Maestra and Oriente Deep. A similar fault zone that continues to the second clear reversal at 2800 fathoms might be identified from the beginning of the next steep slope at 2300 fathoms. H. A. Meyerhoff (Personal communication) observed Miocene sediments dipping steeply southward at the coast west of Santiago, which suggests that the slopes just discussed may be bedding-plane slopes. This interpretation further suggests that the Oriente Deep is part of a geosynclinorium, rather than a trough bounded by normal faulting. Pronounced crescent-form echo sequences can be seen from 1000 to 2000 fathoms superimposed on more diffuse sequences (Pl. 2). The diffuse echo sequence indicates fine-scale roughness, whereas the crescent sequences probably come from marked prominences. Sounding lines parallel to the coast show sudden irregular changes in depth. Hence, the slope is probably deeply cut and may be locally talus-covered. Meyerhoff (Personal communication) found transverse faults which "... cut out the Miocene in places, bringing the more complex structures of the Sierra Maestra to the water's edge. Almost invariably these transverse faults have been excavated into deep valleys, and drowned water gaps cut the Mid-Tertiary hogback at subregular intervals." Our data are not adequate to correlate submarine topography with these deep valleys, but such correlation may well obtain. The territory between the slope reversal at 2800 fathoms and the southern limits of the area surveyed has irregular topography and considerable relief (*e.g.*, 400 fathoms in 2 miles within 3–4 miles of the plain), which deepens toward the plain from all sides. We believe that this region is a zone of rock complexly fractured by the same tectonic activity that caused the major faulting and subsidence. The irregular topography of the deep appears to be mountainous rather than smoothly undulating. More bathymetric detail will probably show that this rugged area extends great distances along the Bartlett Trough.

We have suggested that the deep plain is sedimentary, and that the sediment was supplied possibly by density currents flowing down the gorges on all sides. B. C. Heezen (Personal communication) recently took a core 5.5 m long in a similar deep plain south of Guantanamo Bay. His findings strengthen this hypothesis: alternate layers of sand and red clay each about 10 cm thick were found; the topmost layer was sand, and the sand became progressively coarser deeper in the core; at 3 m shell fragments and beach pebbles were found, and, at 5 m, wood. The grades in the gorges are enough greater than those on the plain to suggest that sediments there are somewhat coarser than on the plain; in one gorge at least (the northern one at the eastern end) rather coarse material or rougher terrain is indicated by the echograms. These gorges appear similar to those bordering the Cul-de-Sac area in southeastern Hispaniola, as described by R. R. Shrock (Personal communication). There a broad valley, partly below sea level, has been uplifted after submergence below the sea (for a more detailed description *see* Butterlin, 1956). The valley floor is flat and covered by a fine sedimentary blanket, in places a fine calcareous ooze. The bordering gorges are cut in limestone cliffs and have smooth bottoms which grade down to the valley floor and are gravel-covered. The qualitative similarity of these two areas suggests that the materials forming them may be similar. For example, the sediment indicated by the multiple bottom echo discussed above may be similar to the calcareous ooze in the vicinity of salt-water lakes in the Cul-de-Sac. However, we know little about the immediate local area other than the facts developed above. A thorough seismic study of the Cayman sea area is needed to reveal the broad structural relations; underwater photography, bottom coring (especially in the deep plain), and continued sounding studies over a much broader area are needed to extend our knowledge of the recent history of the trough.

Although the results presented here are not enough to give full descriptions of the structures, it is reasonable to speculate about the sedimentation taking place in the modern Oriente Deep. The large flat area outlined in Plate 6*B* and the smaller one imperfectly outlined to the west of it appear to be recent sediment having its source in landslides initiated by local seismic activity and probably carried to the greatest available depths by turbidity currents that flow down gorges such as those charted. This type of activity probably has been going on since the subsidence of the Bartlett Trough began. The sediments appear to be ponding in places determined by preexisting topography. The gradual downward trend of rough terrain from all sides into the deep suggests this, but there are probably continuing rock movements in the trough which modify its development in detail. Although no systematic seismic studies of this region have been completed a very few seismic-reflection observations have been made that show a prominent M-type reflection of the sort described by Hersey and Ewing (1949). If this reflection comes from the first solid rock beneath these sediments, its delay of about 0.5 second after the bottom reflection implies a sediment thickness of the order of at least 1200–1500 feet, depending on the compressional wave velocity in the sediments. Test of this deduction will have to await a more systematic seismic study of the area.

SUMMARY AND CONCLUSIONS

(1) The deep submarine slope off the southern coast of Cuba south of Sierra Maestra is about 31°; it is deeply cut and probably has local talus slopes.

(2) The two principal reversals in slope are at about 2000 fathoms and 2800 fathoms. These may be principal fault zones. Their east-west extent may be only a few miles.

(3) Below 2800 fathoms rugged topography dominates an area about 15 miles wide north-south, and local relief is several hundred fathoms.

(4) The rugged topography deepens gradually to the center of Oriente Deep where there is a nearly flat plain 3–5 miles wide and roughly 25 miles long.

(5) The flat area is bounded by hills and gorges. The gorges have relatively smooth bottoms in their lower reaches which grade onto the flat. These relationships suggest that the plain is underlain by sediment supplied from the surrounding gorges. A core taken recently in a near-by flat area by B. C. Heezen on R/V VEMA of Columbia University contains graded sand and clay.

(6) In one part of the plain the character of the multiple bottom echo suggests strongly that secondary echoes come from a subsurface horizon about 30 feet below. Such bottom penetration of 12 kc sound further suggests that the bottom material is a very porous unconsolidated sediment.

(7) Seismic-reflection observations over the plain suggest that the underlying sediment may be about 1200–1500 feet thick.

REFERENCES CITED

Butterlin, J., 1956, La constitution géologique et la structure des Antilles: Centre Natl. de la Recherche Sci., 453 p.

Hersey, J. B., and Ewing, W. M., 1949, Seismic reflections from beneath the ocean floor: Am. Geophys. Union Trans., v. 30, p. 5–14

Hess, H. H., 1938, Gravity anomalies and island arc structures with particular reference to the

West Indies: Am. Philos. Soc. Proc., v. 79, p. 71–96

Knott, S. T., and Hersey, J. B., 1956, Interpretation of high resolution echo-sounding techniques and their use in bathymetry, marine geophysics, and biology: Deep-Sea Research, v. 4, p. 36–44

Lewis, E., and Straczek, J. A., 1955, Geology of south-central Oriente, Cuba: U.S. Geol. Survey Bull. 975-D, 336 p.

Matthews, D. J., 1939, Tables of the velocity of sound in pure water and sea water for use in echo-sounding and sound ranging: London, Hydrog. Dept., Admiralty, 87 p.

Myerhoff, H. A., 1954, Antillean tectonics: N. Y. Acad. Sci. Trans., Ser. II, v. 16, p. 149–155

Pinke, F., 1938, Accurate determination of depth and bottom configuration: Congress Internat. de Geographie, C. R. Travaux de la Sec. II-b, p. 111–134

Smith, W. O., and Nichols, H. B., 1953, Mapping water-saturated sediments by sonic methods: Sci. Monthly, v. 77, p. 36–41

Taber, S., 1931, The structure of the Sierra Maestra near Santiago de Cuba: Jour. Geology, v. 39, p. 532–557

Woodring, W. P., 1928, Tectonic features of the Caribbean region: Third Pan-Pacific Sci. Cong. Proc., Tokyo, 1926, p. 401–431

WOODS HOLE OCEANOGRAPHIC INSTITUTION, WOODS HOLE, MASS.

MANUSCRIPT RECEIVED BY THE SECRETARY OF THE SOCIETY, DECEMBER 23, 1957

WOODS HOLE OCEANOGRAPHIC INSTITUTION CONTRIBUTION NO. 944

Contribution No. 945

An Optical Method for the Measurement of Surface Waves in the Laboratory*

ALAN J. FALLER

Abstract—The heights of surface waves in a laboratory experiment may be observed by variations in the absorption of light as it passes vertically through the fluid. With uniform illumination through the glass bottom of a tank the optical path length through a black dye solution may be recorded photographically from above the tank and the heights of surface waves may be measured from the film density. A linear relation between film density and wave height is possible if the 'straight-line' region of a film blackening curve is used and if the dye has a sufficiently constant absorption coefficient in the band of significant wave lengths. Optimum results are obtained by using as strong a concentration of dye as the intensity of illumination permits and by selecting a film with maximum contrast. In a simple experiment it was found possible to measure variations of the height of the free surface of the fluid to an accuracy approaching one per cent of the total depth, but significantly greater precision may be possible by using more elaborate apparatus.

Introduction—In a large variety of laboratory experiments involving gravity waves both at the free surface of a fluid and at the interface between two fluids it is desirable to have precise measurements of the wave structure; for example the waves produced by or which interact with towed ship models, waves created by the action of wind stress, or internal gravity waves which may exist in stratified models of oceans, rivers, or lakes.

This particular study was motivated by a desire to measure the height of the interface of two fluids in a two-layer atmospheric model developed by *Fultz* [1952] at the University of Chicago. In this model it is possible to represent the polar dome of cold air and the wave cyclones that occur along frontal surfaces in the atmosphere. The precise details of the generation of these waves at the interface of the two fluids are adequately described in the above reference and are not significant to the particular technique developed here.

The essence of the optical method by which these waves were to be measured was to provide a glass bottom in the circular tank, and to illuminate the fluids uniformly from below, so as to photograph the variations of optical density from above. In this technique the resultant film density could be calibrated as a function of the vertical thickness of the dyed fluid (either the lower or upper fluid), and the detailed shape of the interface of the two fluids could be determined from analysis of the film density pattern with a microdensitometer.

In an attempt to reproduce this model and to measure the depth of the interface, optical difficulties were encountered which rendered the method impractical for this particular experiment. Because of the necessarily small difference in the specific gravities of the two fluids (adjusted to a difference of 0.005), a colloidal suspension of water droplets was produced in the mixture of chlorobenzene and toluene (water being the less dense fluid and the mixture the more dense). In addition a detergent was required to reduce the interfacial tension between the two fluids and the problem was complicated by a precipitate from the detergent. The optical technique seemed to have more general applicability, however, and was developed further for the measurement of surface waves on water.

THEORY

The relation of film density to depth of liquid—In the following discussion it will be assumed that there is sufficient illumination to work in the 'straight-line' portion of a film response curve, that is, where the film density D is linearly related to the logarithm of exposure [see for example *Neblette*, 1938, or other texts on photographic theory]

$$D = C_0 \log (\text{exposure}) + C_1$$

In terms of film and illumination characteristics this statement becomes

$$D = \gamma \log \int C_2 \, P_{0\lambda} \, S_\lambda \, e^{-k\lambda^2 t} \, d\lambda + C_1 \qquad (1)$$

where γ is the slope of the film response curve; C_1 includes the base density of the film and the inertia of the emulsion; S_λ is the sensitivity of the film to radiation of wave length λ; $P_{0\lambda}$ is the relative illuminating power per unit wave length

---

* Contribution No. 945 from the Woods Hole Oceanographic Institution.

incident on the bottom of the wave tank; C_2 accounts for losses by reflection at the interfaces of air, glass, and water; k_λ is the absorption coefficient per unit wave length; t is the duration of the exposure; and z is the geometric path length in the dyed fluid. If k_λ equals a constant $\bar{k}$, (1) may be written in the form

$$D = -\gamma \bar{k} z \log e + \gamma \log t + \gamma \log \cdot \int C_2 P_{0\lambda} S_\lambda \, d\lambda + C_1 \qquad (2)$$

For constant values of $P_{0\lambda}$, S_λ, C_2, t, and C_1 (that is, constant experimental conditions) we deduce the following linear relation between D and z

$$D = -(\gamma \log e)\bar{k} z + C \qquad (3)$$

which may be differentiated to obtain

$$\frac{\partial D}{\partial z} = -\gamma(\log e)\,\bar{k} \qquad (4)$$

From the above it is clear that the maximum sensitivity of density change to depth change exists for maximum values of γ and $\bar{k}$ and that it is desirable to use as high a concentration of dye as possible and a film which may be developed to high contrast.

It is important to note that appreciable changes in the value of $\bar{k}$ may require unreasonably large changes in the intensity of illumination required to produce the same film illumination P. Suppose the dye concentration is doubled and x is the factor by which P_0 must be increased to produce the same value of P. Then

$$P = P_0 e^{-\bar{k}z} = (xP_0)e^{-2\bar{k}z}$$

$$x = e^{+\bar{k}z} = P_0/P$$

In a particular example described below $P_0/P = 48$; therefore the illumination would have to be increased by this factor to double the sensitivity by increasing the dye concentration. Greater variations may be had through variation of the film contrast.

Errors caused by refraction and internal reflection—Because a ray path through the dye solution passes obliquely and with varying angles through the air-fluid interface there are inherent errors due to refraction and internal reflection. To simplify the discussion it will be assumed that the camera is sufficiently far from the water surface that the effect of the viewing angle of the camera may be neglected.

A simple consideration of the refraction due to the slope of waves using Snell's Law shows that for a wave slope of angle i the percentage error in the total depth of the fluid is as given in Table 1. The significance of these errors depends upon the accuracy required and the amplitude of the waves with respect to the total depth of fluid, but it is apparent that for many problems this error may be small enough to be neglected. If it should be necessary to apply a correction for refraction, the approximate wave slopes could first be determined and the correction applied as a second order effect. However it would also be necessary to consider the viewing angle of the camera if this angle deviated appreciably from the normal.

TABLE 1 – *Refraction errors at an air-water interface*

i	error
°	pct
10	0.1
20	0.3
30	1.0
40	1.9
50	3.4

A computation of the reduction in light intensity caused by the variation of internal reflection with angle of incidence from Fresnel's formulas showed that this effect is generally small compared to the refraction effect and may be neglected in all cases except for extremely steep waves. In a two-layer model, errors caused by refraction and internal reflection would be negligible because large incident angles would occur only at the interface of the two fluids where the difference between indices of refraction would be much smaller than at an air-water boundary.

An alternate method of conducting experiments would be to illuminate from above and to photograph from below so that the path length through the fluid would not depend upon refraction at the disturbed air-fluid interface. Most experimental arrangements, however, would not permit the use of a camera at a sufficient distance beneath the apparatus.

Errors caused by inaccurate exposure time and uneven illumination—From (2) it is apparent that a change in the duration of exposure t would not affect $\partial D/\partial z$ and would only add a constant density correction to the entire film. Such an error would be easily recognized in the average density, and the correction could be determined by assuming that the average depth of water was the same over the observed area with and without waves. Of course it is necessary to use a sufficiently rapid exposure that the waves to be observed do not move a significant fraction of their wave length in the exposure interval. For the example discussed below the speed of gravity waves would have been approximately 50 cm/sec and in the exposure interval of 1/200 sec the waves would have moved only 0.25 cm compared to an observed wave length of 13 cm.

Errors produced by uneven illumination from below may be determined by a 'null' experiment, that is, no waves. It is again evident from (2) that $\partial D/\partial z$ is independent of $P_{0\lambda}$ and the additive correction to D is a function of position alone. In the experimental example below this correction was applied by graphical subtraction of the 'null' contours from the wave contours.

Note that these simple corrections are possible only when the exposures remain in the 'straight-line' portion of the film-response curve.

A Simple Experiment

An apparatus was constructed (Fig. 1) to test the utility of the method. A symmetrical wave pattern was generated in a circular tank (with a plate glass bottom) by tapping one side of the tank sharply so as to generate waves of equal amplitude but opposite phase on opposite sides of the tank. Uniform diffuse illumination was approximated by five equally-spaced photofloods shining on a white background. Although the illumination appeared uniform to the eye, the film, developed to extreme contrast and analyzed with a microdensitometer, showed marked variations in density from 0.82 at the center to 0.50 near the rim with some minor irregularities. The camera, a Ciroflex Model *D*, was mounted 38 inches above the water surface to obtain the maximum image size.

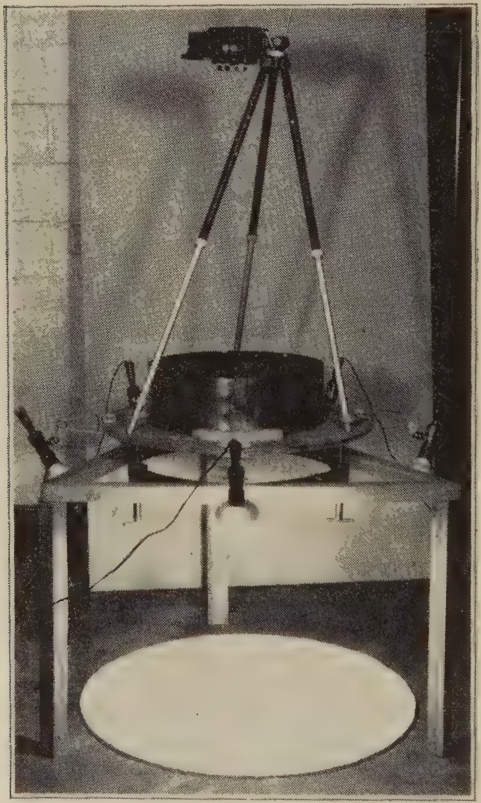

Fig. 1 – The experimental apparatus showing the circular tank with a glass bottom, illuminated from below and photographed from above

A means for calibrating the relationship of depth to density of the film was provided by the three leveling screws which supported the platform, tank, and tripod. By raising one of the supporting screws a linear variation of depth of fluid could be produced over any desired range from one side of the tank to the other.

Several black dyes were tested for spectral dependence of the absorption coefficient, and it was shown that for the conditions of the experiment (spectral film sensitivity, dye concentration and illumination spectra) water-soluble black nigrosine was sufficiently close to a uniformly black dye that the entire visible spectrum could be used with the assumption k_λ was equal to a constant.

The conditions of the experiment were as follows:

Dye concentration, water-soluble black nigrosine, 0.043 g/L.
Depth of solution, 1 inch
Diameter of tank, 18 inches
Relative illumination as measured by a GE DW68 exposure meter: before adding dye, 620; after adding dye, 13
Optical density of solution, 1.68; $\bar{k} = 4.03$ in^{-1}
Verichrome orthochromatic film developed 15 min at 23°C in D-19 developer
Duration of exposure, 1/200 sec
Lens aperture, f/5.6

The microdensitometer used for the analysis consisted of a microscope with a constant light source and a stop of 40 μ diameter. Light transmitted through this area of the film was received by a photocell and the output was displayed on the meter of an Ansco Color densitometer. Because of film granularity the meter fluctuated erratically by ± 0.05 as the film was transported continously across the optical system. For the wave analysis 1400 observations on a grid interval of 1 mm (image diameter 42 mm) were obtained.

Three photographs of the 'null' experiment were analyzed to obtain the illumination correction and to estimate variations of the shutter speed. The average film density was 0.70 and the difference between the lightest and the darkest points was 0.09. Measurements with the tank tilted from $z = 0.75$ on one side to $z = 1.25$ at the other gave a value of $\partial D/\partial z = -2.80$ in^{-1}. From (2) the approximate shutter speed variation may be determined

$$\frac{\partial D}{\partial t} = \frac{\gamma \log e}{t} = -\frac{1}{\bar{k}t}\frac{\partial D}{\partial z}$$

or for small finite differences

$$\Delta D = -(\Delta t/\bar{k}t)\Delta D/\Delta z$$

For the range of densities of 0.09 for the three trials the range of shutter speeds was 13.5 pct. A value of $\gamma = 1.6$ may also be obtained from the above value for $\partial D/\partial z$ uzing $\bar{k} = 4.03$ in^{-1} as determined approximately from exposure meter measurements. Much higher values of γ and greater sensitivity could be obtained by the selection of a special high contrast film.

Figure 2 is an analyzed wave pattern superimposed on a print of the wave photograph, the waves having been generated by tapping one side of the tank sharply. Contour heights are in terms of inches with a maximum variation from the average of ±0.1 in. The contour intervals are not quite constant because the contours were analyzed

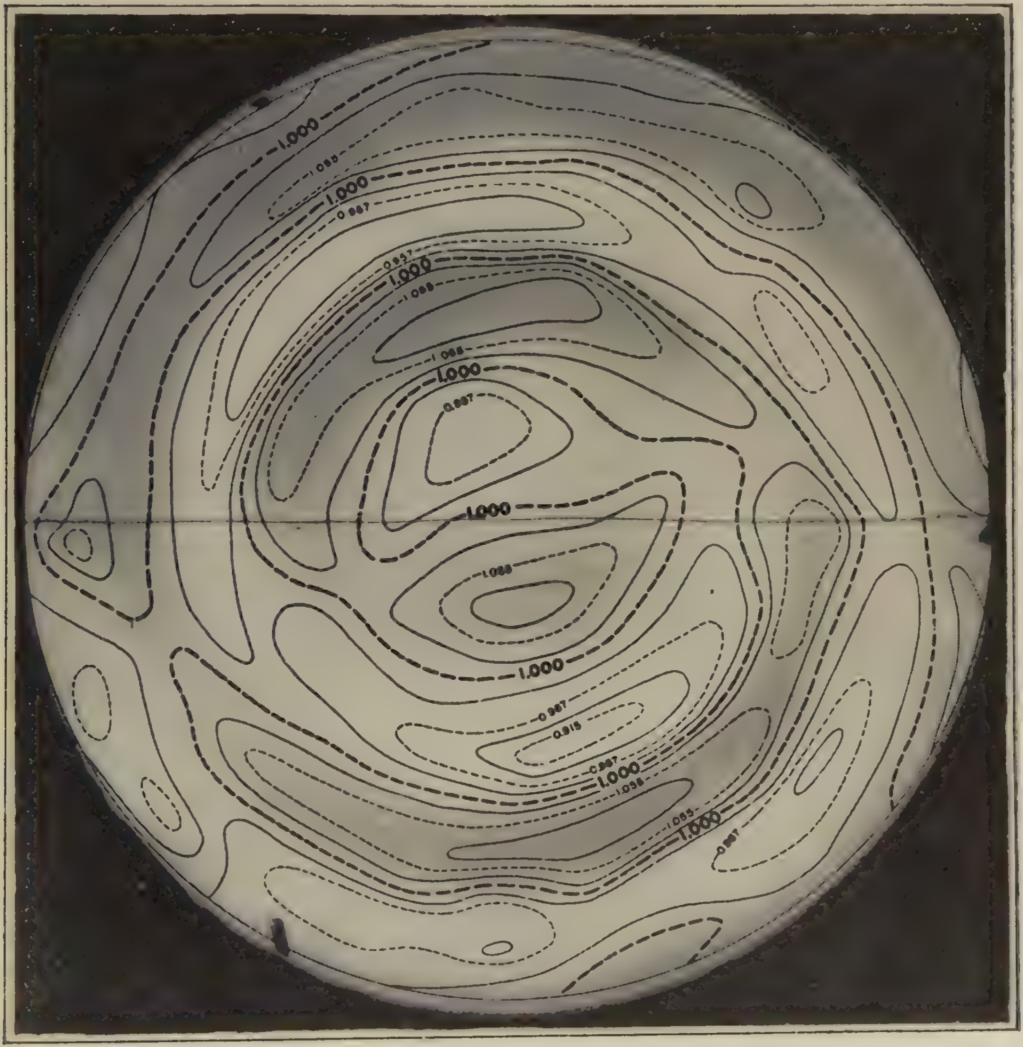

FIG. 2 - A microdensitometer contour analysis of waves superimposed upon the wave photograph; the contour interval is approximately 0.05 inch

on the basis of density and because the curve of the relationship of depth to density was not quite linear in this range of densities (approaching the toe of the film response curve).

The effect of the uneven illumination has been corrected in the contours by graphical subtraction of the 'null' density pattern from the pattern with waves. This effect is apparent in the print densities, however, which become darker (for the same contour height) nearer the rim. (Some error also is introduced in the superposition of the two patterns.) Small-scale irregularities are attributed to granularity of the film which led to erratic individual density values some of which have been smoothed out in the analysis. In defense of the method it should be added that no reference was made to the print of the wave pattern until the countour analysis had been completed.

CONCLUSIONS AND RECOMMENDATIONS

This optical method is suitable for obtaining the three-dimensional structure of a water surface, and rapid sequence photography can extend the technique to time variations. A complete record is obtained which may be analyzed selectively at a later date. Analysis of a large number of films could be accomplished by an automatic scanning device which could smooth fine-scale irregularities of the film and could apply a predetermined illumination correction automatically. Such a scanning system could be designed to produce the wave profile or spectrum along any particular direction.

Another technique for the analysis of the contours of constant density from a film is that developed by *O'Brien* and *Stewart* [1938]. By making successive positive and negative prints on Eastman Kodak Kodalith film an overall γ of 40 or more was obtained in which case a line of constant density appeared as a sharp boundary between black and white areas on the final negative. Different contours were selected by varying the exposure on the final positive Kodalith transparency. The principal difficulty in application to wave analysis would be the production of sufficiently uniform illumination that variations from this source would not contribute to significant density variations.

It is the author's opinion that by selecting a more suitable film, by producing more uniform illumination, and by smoothing of film irregularities an accuracy of better than one per cent of the total depth could readily be obtained, and that greater precision is possible under ideal conditions. Regardless of the accuracy of the method, a wave pattern photograph is obtained that is readily interpreted qualitatively.

Acknowledgment—The research reported in this paper was supported by the Office of Naval Research under Contract Nonr-1831(00)(NT 083–107), and was submitted in partial fulfillment of the requirements for the course Special Problems in Optics under the supervision of Arthur C. Hardy at the Massachusetts Institute of Technology.

REFERENCES

FULTZ, DAVE, On the possibility of experimental models of the polar-front wave. *J. Met.* **9**, 379–384, 1952.

NEBLETTE, C. B., *Photography, its principles and practice*, 3d. ed., van Nostrand, New York, 590 pp., 1938.

O'BRIEN, B., AND H. S. STEWART, Production of isodensity contours of a photographic negative (abstract), *J. Opt. Soc. Amer.* **28**, 50, 1938.

Woods Hole Oceanographic Institution, Woods Hole, Massachusetts

(Communicated manuscript received January 22, 1958; open for formal discussion until January 1, 1959.)

Contribution No. 946

EXTRAIT

Rapp. et Proc.-Verb. Vol. 144, 1958
Cons. Internat. Explor. de la Mer

D. ENVIRONMENTAL CONDITIONS FOR PRIMARY PRODUCTION

D. 1.

Productivity in Relation to Nutrients[1])

By Bostwick H. Ketchum, John H. Ryther, Charles S. Yentsch, *and* Nathaniel Corwin
Woods Hole Oceanographic Institution

Introduction

Brandt (1899, 1902) first suggested that phytoplankton production must be dependent upon the supplies of nitrate and phosphate in natural waters. Proof of this relationship, and of the virtually complete removal of these elements from the water, required more accurate analytical methods than were available at that time. Since the early 1920's however, studies extending from the coast of Norway and the English Channel to the Antipodes have established the interrelationship between these nutrients and the growth of phytoplankton[2]).

The correlation between productivity and nutrients is most clearly demonstrated in moderate to high latitudes where a definite annual sequence of plant production occurs. During the winter season, when phytoplankton growth is at a minimum, vertical mixing, which is greatest at this time, produces a nearly uniform distribution of plant nutrients. As a result of the spring bloom these nutrients are rapidly depleted to low values which persist throughout the summer and much of the autumn. Nathansohn (1906) first pointed out that the stability of the water column, associated with the vernal warming of the surface waters, was intimately correlated with plankton production. Opposing effects of stability are recognized. In a well mixed water column the rate at which nutrients are transferred from the deep richer waters to the surface is maximal, but the plant cells may be carried below the illuminated zone, thus reducing the net production and growth of the population. On the other hand, in a stable water column, the phytoplankton are retained in the illuminated zone, where they can quickly exhaust the nutrients, since the rate of supply is decreased in proportion to the increased stability (Atkins, 1924, 1925; Braarud & Klem, 1931; Braarud, Gaarder, & Grøntved, 1955; Gran & Braarud, 1935; Hart, 1934; Riley, 1942; Sverdrup, 1953, 1955).

Direct estimates of productivity have been made from the removal of nutrients from the water (Atkins, 1923; Cooper, 1938; Kreps & Verjbinskaya, 1930, 1932). The maximum quantity of total phosphorus in the water column in winter has been used as an index of fertility (Russell, 1935; Cooper, 1938; Harvey, 1948, 1950; Armstrong & Harvey, 1950). It should be emphasized, however, that such estimates are minimal unless regeneration *in situ* and the return of nutrients to surface waters by mixing are also evaluated. For example, the data of Redfield, Smith, and Ketchum (1937) indicate that only about 2 % of the total phosphorus cycle between May and November was reflected by changes in the quantity of inorganic phosphorus in the euphotic zone, whereas about 73 % was supplied by vertical mixing and about 25 % by regeneration (Ketchum, 1947). In his excellent evaluation of plant production from changes in phosphate, Steele (1956) shows that only about 18 % of the summer production can be attributed to changes of phosphate in the euphotic zone and 82 % is contributed by vertical mixing. These values do not include the effects of regeneration, which he calculates would increase the original estimate by one quarter to one third. Even in the shallow waters (20 metres) of Long Island Sound, Riley's (1956) estimate of gross production (470 g.C/m^2./year) would require ten times the total amount of phosphorus in the water at its maximum concentration (Riley & Conover, 1956). Thus, although the total phosphorus of a water column may be a qualitative index of relative fertility, especially where the water is shallow enough so that the euphotic zone extends nearly to the bottom, the rates of supply of nutrients by mixing and regeneration account for the major part of the nutrient cycle and of plant production.

---

[1]) Contribution No. 946 from the Woods Hole Oceanographic Institution. This work was supported in part by funds from the Atomic Energy Commission under Contract AT (30-1)—1918, and by research grants from the National Science Foundation.

[2]) See, for example: Atkins (1923, 1926, 1926 a); Braarud & Føyn (1931); Cooper (1933); Dankin & Colefax (1935); Gran (1931); Harvey (1926, 1928); Harvey, *et al.* (1935); Hart (1934); Hentschel & Wattenberg (1930); Kalle (1937); Kreps & Verjbinskaya (1930, 1932); Marshall & Orr (1928); Matudaira (1939, 1942); Redfield (1934); Riley, *et al.* (1949).

We need much better information concerning the rate of recycling and reuse of nutrients by the phytoplankton. This is particularly true of oceanic conditions in semi-tropical and tropical waters where repeated observations throughout the year may show little or no change in nutrient concentrations. Plant production in such waters may be entirely dependent upon and limited by the processes of regeneration and vertical diffusion of essential nutrients. In the surface tropical waters of the Atlantic 90 % of the total dissolved phosphorus may be present in organic combination (Ketchum, Corwin, & Keen, 1955). We do not know whether these organic compounds can be used directly by the phytoplankton, nor how rapidly they are decomposed.

Not only is the variation in nutrient concentration in the sea correlated with the growth of phytoplankton, but the various elements change in a related way, and the ratios of change ($\Delta O_2 : \Delta CO_2 : \Delta P : \Delta N$) in the water are similar to the ratios found in the plankton population (Harvey, 1926; Redfield, 1934; Cooper, 1937; Fleming, 1940). These ratios, though less precise than the combining ratios of chemistry, have had a similar stimulating effect on the study of plankton ecology. They have, however, at times been misused, since some have assumed that the ratio of concentration in the sea is similar to the ratio of change, and that the measurement of one element, generally phosphorus since the analytical procedure is the simplest, can be substituted for a more complete study of nutrients. Cooper (1937, 1938) pointed out that the ratio of concentration of nitrate and phosphate departs markedly from a "normal" ratio of 15:1 (by atoms) and that the anomaly is greatest in confined seas, such as the Mediterranean. In the tropical Atlantic we have observed values as great as 60 atoms of nitrogen to one of phosphorus directly below the euphotic zone. Riley and Conover (1956) found an N:P ratio during the winter maxima of about 8:1, about half the value which might be expected for oceanic waters. Furthermore after the spring phytoplankton flowering, the nitrate nitrogen was reduced to negligible quantities, although there was still about 0·5 μg.at./l. of inorganic phosphorus. Our studies in Woods Hole and in coastal waters have yielded similar results, indicating that nitrogen is the serious limiting factor in these waters.

Anomalous N:P ratios may determine the species which dominate a population even when neither element is limiting in the classical Liebig sense. Thus Ryther (1954) showed that an unusually low N:P ratio favoured the growth of *Nannochloris* and of *Stichococcus* which dominated the population of Great South Bay where such N:P ratios were common during the summer.

The foregoing discussion indicates the hopelessness of understanding the mineral nutrition of phytoplankton by determining only one element, unless it has been firmly established that the element is the limiting factor. Even then variations in the ratio may modify the dominance of species. No doubt, determinations of phosphorus and nitrogen, with or without silicate analyses, will also prove inadequate in many cases. Harvey (1947) has shown that manganese may limit growth of cultures. Hutner and Provasoli (1953) and Droop (1955) have demonstrated the need for vitamin B_{12}, and Lucas (1949, 1955) has emphasized the importance of ectocrines, as yet not chemically identified, in controlling plankton production.

Although we have emphasized so far the constancy of the chemical composition of plankton in relation to the essential nutrients, it has been repeatedly demonstrated that cultures of phytoplankton organisms can be grown which accumulate excesses of essential elements or which develop deficiencies which can be so drastic as to completely stop the growth of the population (Ketchum, 1939, 1939a; Ketchum & Redfield, 1949; Rodhe, 1948). Ryther, 1954, has shown that in such nutrient deficient cultures the rate of photosynthesis is reduced until it becomes just sufficient to balance the loss by respiration. In other words, although gross photosynthesis is still carried on by the population there is no net production of new organic matter, a condition which indeed must exist if further growth of the population is stopped by the nutrient deficiency.

There is little or no direct evidence, based upon chemical analyses, that populations in the sea are deficient in composition. Harris and Riley (1956) found that the phytoplankton population in Long Island Sound has a "normal" N:P ratio of about 16·7:1, even though the ratio of concentration in the water was 8:1 or less. However, it is difficult to conceive of the populations which grow in the impoverished Sargasso Sea as being anything other than deficient in these essential elements. We have far too few analyses of the composition of natural populations, and most of these analyses have been made using collections from coastal waters and particularly at times when the population was high, making collecting easy. Dr. John H. Ryther has studied the effects of adding nutrients to surface Caribbean water. Some previously unpublished data, given in Table 1, show that the addition of nitrate and phosphate to natural sea water may considerably increase both gross and net production, but more importantly the addition eliminated the large discrepancy between the ^{14}C and oxygen determination of photosynthesis. This is expressed as the net:gross photosynthesis ratio which is discussed below. In several such experiments addition of phosphate or

Table 1

Effect of enrichment on photosynthesis of natural populations. Surface water exposed for 3 days to natural light in running sea water on deck

(Location 16°40′ N., 65°05′ W.)

Conditions	Type of measurement	Photosynthesis g. C/m³./day	Net: Gross
No enrichment	^{14}C	0·0018	
	O_2	0·0125	0·14
P + N enriched[1]) ...	^{14}C	0·11	
	O_2	0·135	0·82

[1]) 100 μg. at./l. of NO_3'-N, 6·6 μg. at./l. PO_4'''-P.

of nitrate or of both increased photosynthesis, indicating that it was limited by deficiencies of these elements. In some, these additions made no change in low photosynthesis rates, indicating that some other essential nutrient may have been limiting.

In the natural environment and especially in impoverished areas, it is the rate of supply of nutrients through regeneration and physical processes of mixing which can determine how rapidly the population can photosynthesize. When the rate of supply is low the population may always be limited by a deficiency of the element and the net photosynthesis may be always a small fraction of the gross photosynthesis, most of which is required to balance the respiratory needs of the phytoplankton themselves.

This lengthy introduction may imply to some that the relationship between essential nutrients and productivity in the sea is well understood. Such is far from the case. An enumeration of problems may serve to indicate those areas in which additional information is drastically needed.

1. How frequently do the nutrients recycle during the annual production of the phytoplankton population?
2. What is the rate of regeneration of essential nutrients as a result of the decomposition of organic matter? How does this rate vary with temperature, with the concentration of organic matter, with the concentration of bacteria, and with the type of organic matter?
3. What proportion of the phytoplankton production is consumed by the zooplankton population, and how much of the nutrients are excreted by the zooplankton in a form directly usable by the phytoplankton population?
4. What proportion of the organic material produced in the surface waters falls into the deep sea? If, as has been suggested, most of the organic matter decomposes *in situ* and practically all of the remainder decomposes before the organisms and detritus sink to a thousand metres, what is the source of nutrition of the population of organisms living at greater depths?
5. Is the succession of species which dominate populations in the natural environment related to their inorganic nutrition? to temperature? to organic substances promoting or inhibiting growth?
6. How variable is the chemical composition of phytoplankton collected under different conditions in the ocean? Are the phytoplankton which grow in nutrient deficient areas such as the Sargasso Sea comparable with or different from those collected in coastal regions?
7. If nutrient deficient phytoplankton are produced in the sea is their ability to photosynthesize reduced until it barely balances their respiratory needs, as can happen in laboratory cultures?

These questions remain partially or completely unanswered. For many of them we have some estimates, for others there is virtually no answer known.

Investigations in progress

Studies are being conducted in many laboratories throughout the world which may, in time, solve these problems, and answer other questions which are as yet poorly defined. Some preliminary results of an intensive study of coastal plankton populations which is being conducted at the Woods Hole Oceanographic Institution are presented here. This is done, not in the hope of giving any final answers to these questions, but rather for the purpose of outlining the method of attack and of elaborating the questions which we feel are essential to solve.

The observational programme has been planned to include stations in various depths of water ranging from 25 to 1,500 fathoms (see Figure 1). This plan was adopted since the variables which control plankton production may be different in inshore and offshore waters. The programme includes measurements of productivity; of the standing crop of phytoplankton by direct counts and by chlorophyll analyses; of zooplankton by quantitative tows; of nutrient concentrations; of light penetration; and of hydrographic conditions determined by the temperature and salinity of the water. The programme was initiated in September, 1956.

It has become abundantly clear that there is a need for a definition of the physiological state of the phytoplankton organisms in the sea. By microscopic examination one can qualitatively state whether or not cells look healthy, but an independent, quantitative evaluation seems essential before we can fully understand the diverse responses of populations to environmental conditions. Some of our attempts to evaluate various indications of the physiological state of the populations will be discussed.

Net and gross photosynthesis

Photosynthesis measurements have been made by both the carbon-14 and the dark and light bottle oxygen method at all stations on our coastal cruises. A sample of water, obtained in a plastic sampling bottle (VAN DORN, 1956) from a depth of 10 metres,

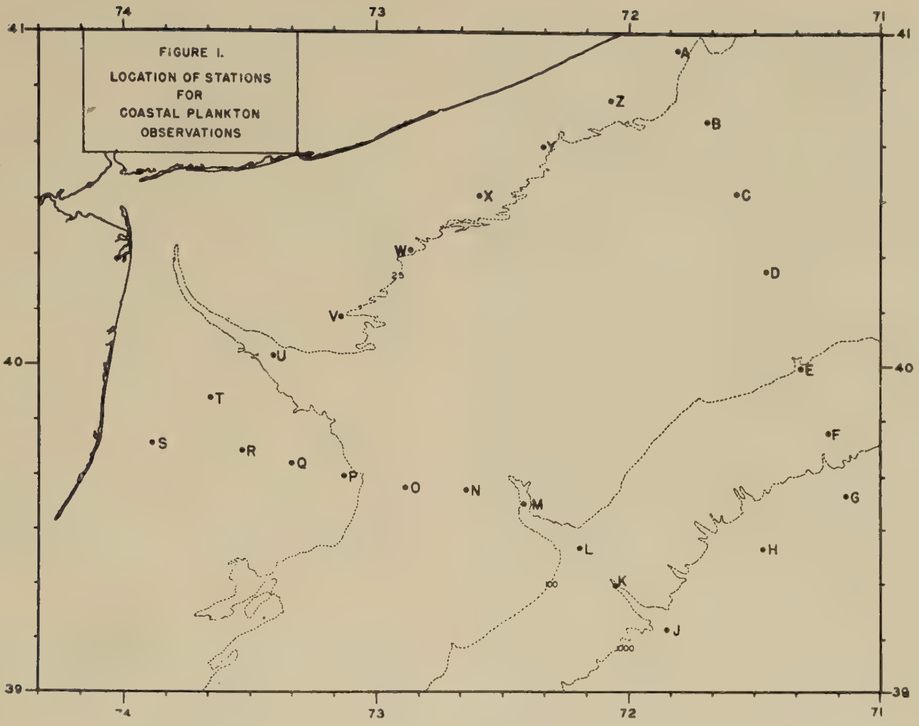
FIGURE I.
LOCATION OF STATIONS FOR COASTAL PLANKTON OBSERVATIONS
74
73
72
71
41
40
39
A
B
C
D
E
F
G
H
J
K
L
M
N
O
P
Q
R
S
T
U
V
W
X
Y
Z

Figure 1. Location of stations for coastal plankton observations.

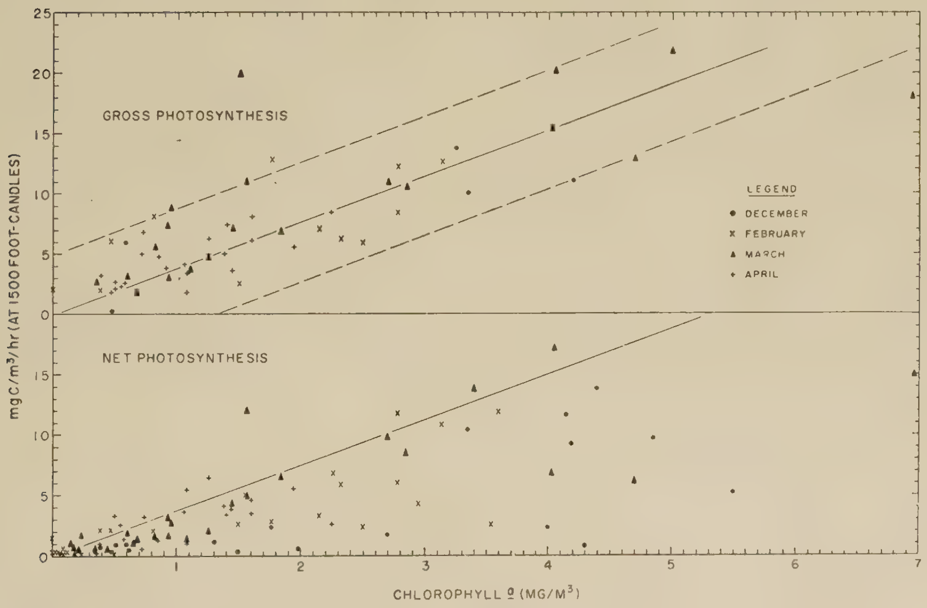

Figure 2. Gross and net photosynthesis at 1500 foot candles related to the chlorophyll *a* concentration. Gross photosynthesis was determined by dark and light oxygen bottle experiments. The envelope corresponds to an oxygen titration difference of ± 0·05 ml/l. Net photosynthesis was determined by carbon-14 assimilation experiments, uncorrected for respiration.

is dispensed into a series of 150 ml. glass stoppered bottles, placed in a tank of flowing sea water in the laboratory on the ship and exposed to an illumination of 1,500 foot candles. The carbon-14 bottles are ordinarily removed after a period of twelve hours whereas the dark and light oxygen bottles remain for a period of 24 hours of illumination. The difference between the oxygen content of the dark and light bottle is taken as gross photosynthesis, and is corrected to the carbon equivalent using an assimilatory quotient (O_2/CO_2) of 1.25. The assimilation of carbon-14, which is not corrected for respiration as suggested by Steemann Nielsen (1952), is taken as the net photosynthesis of the population (cf. Ryther, 1954).

The values thus far observed have been plotted as a function of chlorophyll *a* in Figure 2. Ryther and Yentsch (1957) concluded that gross photosynthesis is closely related to the concentration of chlorophyll *a* and suggest, as an assimilation factor, 3·7 g. of carbon per hour per gramme chlorophyll *a* at optimum light intensity. This correlation line is indicated on the two parts of Figure 2. In general the oxygen measureurements scatter at random about this correlation line with considerable individual deviations. Many of the carbon-14 points also approximate this correlation line, but a large proportion are substantially low.

The ratio of net to gross photosynthesis at optimum light intensity may be useful as an indication of the physiological state of the population. This ratio should, in a healthy population, be approximately 0·9 to 0·95 if respiration is 5 to 10 % of total photosynthesis. If, however, the plankton population is not capable of increasing for any reason, the net photosynthesis should be negligibly small and the ratio should approach zero. The mean total gross photosynthesis, and the net photosynthesis, as measured by ^{14}C fixation, for observations at various times of year are shown in Figure 3 (Ryther, unpublished). Five offshore stations—in depths greater than 500 fathoms—and five inshore stations—in depths less than 25 fathoms—were averaged to give these results. Total photosynthesis at the offshore stations ranged from 0·6 to 1·7 mg.C/m³./hr., and the ratio of net to gross photosynthesis ranged from 0·35 to 0·60. At the inshore stations the gross photosynthesis ranged from 0·6 to 13·3 mg.C/m³./hr. The net:gross photosynthesis ratio was 0·9 or more in September and February, indicating healthy growing populations, although the total photosynthesis at these two times was quite different. In December and March, although the rates of total photosynthesis were large, the net: gross photosynthesis ratio was only 0·40 and 0·50.

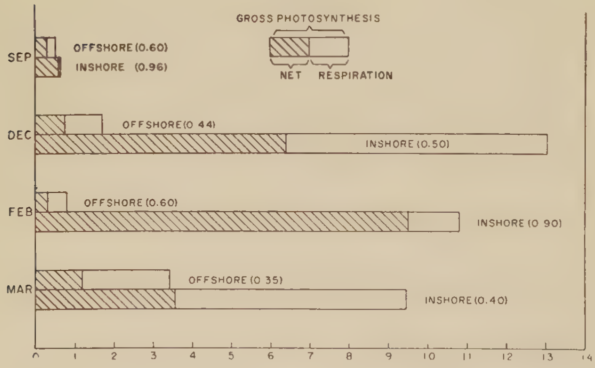

Figure 3. Comparison of net and gross photosynthesis for inshore and offshore (> 500 fm) stations on various surveys. The figures in parentheses are ratios of net: gross photosynthesis.

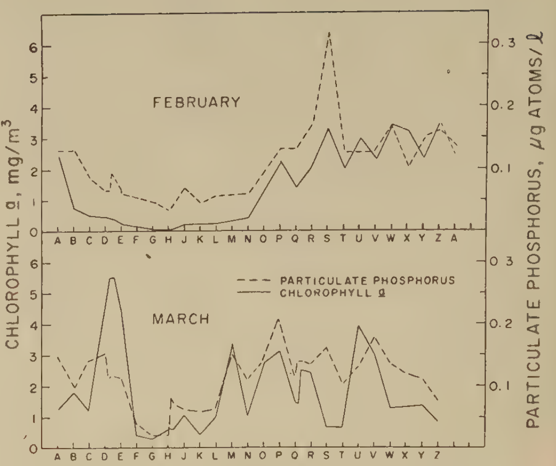

Figure 4. Quantities of particulate phosphorus and of chlorophyll *a* in the euphotic zone at the stations shown in Figure 1 during February and March 1957.

It seems clear that there are differences in the physiological state of the phytoplankton organisms in the natural environment. We cannot as yet tie these variations in the net:gross photosynthesis ratio with nutrient deficiencies, but this seems to be an almost certain contributing factor especially when one considers that the offshore stations which are typically deficient in nutrients are also typically low in the net:gross photosynthesis ratio. The data in Table 1 indicate that the addition of nutrients to oceanic populations can not only increase the rate of photosynthesis, but can also increase the ratio of net to gross photosynthesis.

Variations in phytoplankton chlorophyll

As mentioned above, our observations suggest that the chlorophyll content is an index of potential gross photosynthesis at optimum light intensity. However, the chlorophyll content of a natural population varies, not only because of changes in the size of the population, but for other reasons as well. Recent observations indicate that the chlorophyll content of populations, both natural and in cultures, undergoes large diurnal variations. Doty and Oguri (1957) described

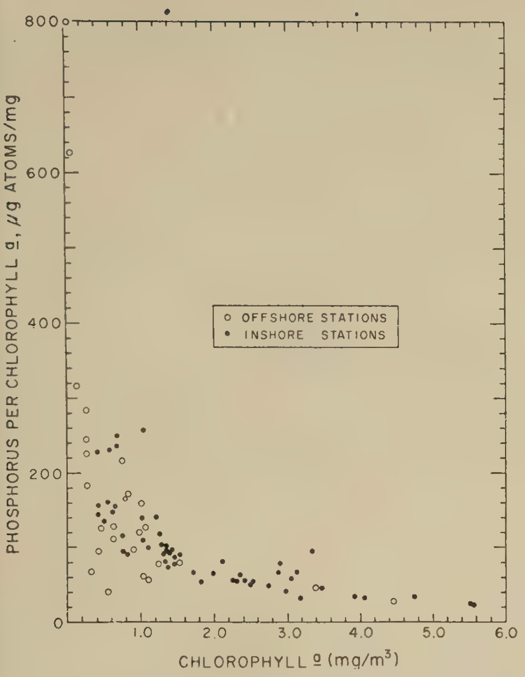

Figure 5. The variation of the ratio of particulate phosphorus per chlorophyll *a* as a function of the chlorophyll *a* content of the water.

a nearly 6-fold variation in the rate of ^{14}C fixation of samples taken from the Pacific depending upon the time of day the sample was collected. YENTSCH and RYTHER (1957) have confirmed the diurnal variation in ^{14}C fixation, though their changes were smaller, and show that the variation is closely associated with similar variations in the chlorophyll content of the population.

The mid-day decrease in chlorophyll is the result of the well-known photooxidation of this pigment (RABINOWITCH, 1945), but changes in chlorophyll content of cells may also be related to nutrient deficiencies. It seems clear, therefore, that chlorophyll alone is an inadequate measure of the standing crop of phytoplankton, though YENTSCH and RYTHER (1957) show that in spite of the diurnal variations it may still be a good index for the maximum gross photosynthesis under optimum light conditions.

Phosphorus : Chlorophyll relationship

It was thought that the ratio of phosphorus to chlorophyll might offer promise of more consistency. Since the nitrogen:phosphorus ratio in these waters is low, phosphorus is probably not directly limiting the population growth. The nitrogen:chlorophyll ratio might, therefore, be more significant, but we have not yet determined particulate nitrogen on large numbers of samples. That the particulate phosphorus and chlorophyll content of the water vary in similar ways is shown by the results of the February and March cruises in Figure 4.

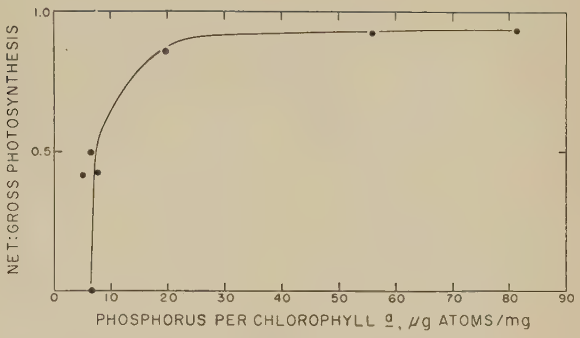

Figure 6. The ratio of net : gross photosynthesis as a function of cellular phosphorus per chlorophyll *a* in a phosphorus deficient culture of *Dunaliella euchlora*.

The particulate phosphorus in the water is partly contained in plant cells, partly in organic detritus and partly adsorbed on living and dead organic particles and on silts and clays in suspension in the water. To minimize the physically adsorbed phosphorus our samples are acidified (1 ml. conc. HCl to about 200 ml. of sea water: pH = 1·3) before filtration. A large number of comparisons between acidified and unacidified samples shows that as much as 30 % of the particulate phosphorus may be released by the addition of this amount of acid. Some of the phosphorus released may be extracted from the cell sap of the phytoplankton, but the acidification is not drastic enough to release organically bound phosphorus.

Pursuing the general concept that the chemical composition of plankton organisms is more constant than the environment, one might expect that, in the plant cell, the ratio of phosphorus to chlorophyll would be constant. In cultures of *Phaeodactylum tricornutum* (*Nitzschia closterium* forma *minnutissima*) and of *Dunaliella euchlora* containing adequate phosphorus, this seems to the nearly true, since we have measured ratios ranging from 40—80 μg.at. P/mg. chlorophyll *a*. The relationship observed in natural waters, however, is much more complex, as shown in Figure 5 where the ratio of particulate phosphorus to chlorophyll is compared to the chlorophyll content of the water. At high chlorophyll concentrations the ratio lies between 20 and 40 μg.at. P/mg. Chl. *a*, but at low chlorophyll concentrations the importance of the detrital phosphorus becomes predominant, and the ratio becomes very large. For equal amounts of chlorophyll *a*, the offshore waters, identified by the open circles in Figure 5, appear to contain less particulate phosphorus than the inshore waters. This might be expected since the offshore waters contain lower inorganic nutrient concentrations and less particulate mtater of all kinds. The offshore waters at times, however, have lower chlorophyll concentrations than have ever been observed in the inshore waters. These

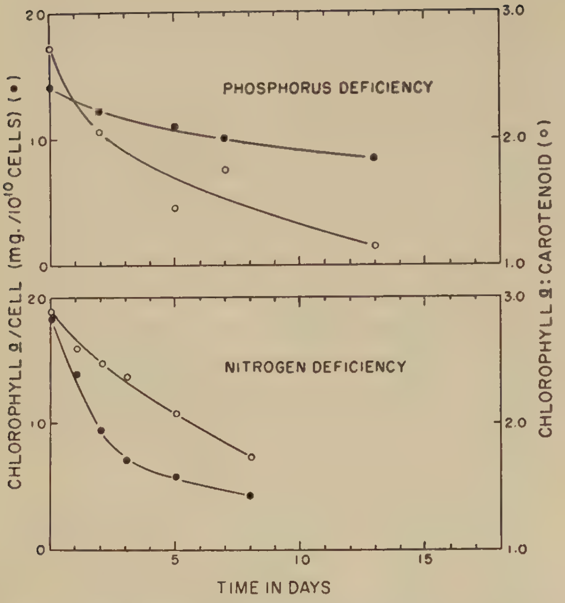

Figure 7. The change in chlorophyll *a* per cell and in the ratio chlorophyll *a*: carotenoid in cultures of *Dunaliella euchlora* deficient in phosphorus or in nitrogen.

have the highest ratios of particulate phosphorus to chlorophyll.

The high ratios of phosphorus to chlorophyll observed at low chlorophyll concentrations suggests that the pigment is quickly decomposed as the cells die, but the phosphorus remains bound, for some time afterwards, to the organic detrital material.

In cultures, the development of a deficiency in phosphorus is related to a decrease in the net:gross photosynthesis ratio as is shown in Figure 6, (cf. RYTHER, 1954). In this experiment with *Dunaliella euchlora*, this ratio dropped sharply when the phosphorus per chlorophyll *a* in the cells fell below about 25 μg.at./mg. It is interesting and suggestive that this is about the lowest ratio which has been observed in the natural populations. It seems probable that the phosphorus:chlorophyll ratio could be a useful index of the physiological state of natural populations if we could separate detrital from plant phosphorus. Unfortunately we do not yet know how this can be done.

Chlorophyll : Carotenoid relationships

It has long been known that deficiencies, particularly of nitrogen and of iron, lead to chlorotic cells. In a culture chlorosis can be readily detected by eye or expressed as the chlorophyll per cell. In the natural environment, however, very different sizes of cells and the different numbers of chloroplasts in various species make it impossible to state from chlorophyll measurements and cell counts alone whether the population is chlorotic or not.

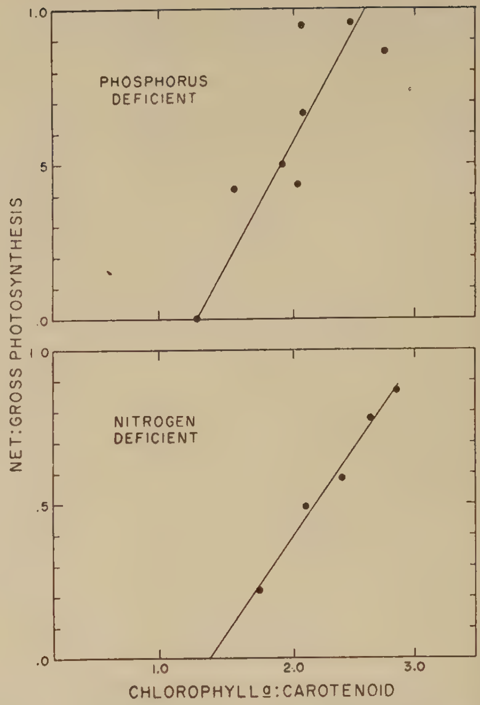

Figure 8. The ratio of net : gross photosynthesis in relation to the chlorophyll *a*: carotenoid ratio in cultures of *Dunaliella euchlora* deficient in phosphorus or in nitrogen.

C. S. YENTSCH (unpublished) has observed that the diurnal changes in chlorophyll, described above, are accompanied by comparable, but smaller, changes in the plant carotenoids. The chlorophyll *a*:carotenoid ratio, therefore is more constant than the chlorophyll concentration. However, wide variations in this ratio are observed under different conditions in the sea. In culture experiments, nutrient deficiencies can be shown to produce similar variations. Such a ratio may, therefore, be an index of chlorosis of the natural population.

The decrease of the chlorophyll content of the cells, and of the chlorophyll:carotenoid ratio in cultures of *Dunaliella euchlora* after various times of growth in a medium deficient in phosphorus or nitrogen are shown in Figure 7 (YENTSCH, unpublished). The nitrogen deficiency has a greater effect on the chlorophyll per cell but a smaller effect on the chlorophyll:carotenoid ratio than was observed with the phosphorus deficiency. The ratio of pigments may not, therefore, be a precise measure of chlorosis, but a low ratio would suggest a chlorotic, unhealthy population.

In these same experiments net and gross photosynthesis measurements were made from dark and light oxygen bottle experiments at an illumination of 1,500 foot candles. The ratio of net:gross photosynthesis is related to the chlorophyll:carotenoid ratios in these cultures in Figure 8 (RYTHER &

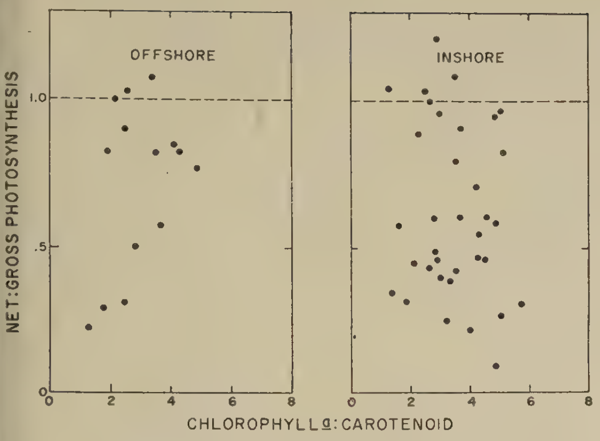

Figure 9. The ratio of net: gross photosynthesis compared to the ratio of chlorophyll *a*: carotenoid in natural populations in the sea.

YENTSCH, unpublished). As the nutrient deficiency develops the ratio of net to gross photosynthesis decreases.

The relationship seems much more consistent in the nitrogen experiment, which, perhaps should be expected, since chlorophyll synthesis is more directly associated with nitrogen metabolism. A value of zero for the net: gross ratio would correspond to a nutrient induced compensation point. The results on the cultures indicates that chlorophyll: carotenoid ratios slightly greater than unity correspond to the nutrient deficiency which prevents net photosynthesis. We have observed populations in the sea in which this pigment ratio approaches unity.

Lest we end on too optimistic a note, however, it must be said that the ratio of net: gross photosynthesis is not clearly related to the chlorophyll: carotenoid ratio in the natural environment. These ratios, observed on samples collected at 10 metres of depth at stations during the December, February, March, and April surveys, are compared in Figure 9. In the offshore waters (depths greater than 500 fm.) some indication of a correlation may be present, though the spread of points is much greater than was observed in the culture experiments. In the inshore waters there is no correlation between these two ratios. The population in the offshore waters may be nutrient limited, and this may lead to the fair correlation in this area, but the evidence is certainly unconvincing as yet. No explanation for the numerous low net: gross photosynthesis ratios in the inshore waters which may occur even at high pigment ratios is known.

References

ARMSTRONG, F. A. J., & HARVEY, H. W., 1950. "The cycle of phosphorus in the waters of the English Channel". J. Mar. Biol. Assoc. U.K., **29**: 145—62.

ATKINS, W. R. G., 1923. "Phosphate content of sea water in relation to growth of algal plankton". J. Mar. Biol. Assoc. U.K., **13**: 119—50, 700—20.

— 1924. "On the vertical mixing of sea water and its importance for the algal plankton". Ibid., **13** (2): 319—24.

— 1925. "On the thermal stratification of sea water and its importance for the algal plankton". Ibid., **13** (3): 693—99.

— 1926. "The phosphate content of sea water in relation to the growth of the algal plankton. Part III." Ibid., **14**: 447—67.

— 1926 a. "A quantitative consideration of some factors concerned in plant growth in water. II. Some chemical factors". J. du Cons., **1**: 197—226.

BRAARUD, T., & FØYN, B., 1931. "Beiträge zur Kenntnis des Stoffwechsels im Meere". Avh. Norske Vidensk.-Akad. Oslo, I, Mat.-Nat. Klasse, **14**: 1—24.

BRAARUD, T., & KLEM, A., 1931. "Hydrographical and chemical investigations in the coastal waters off Møre and in the Romsdalsfjord." Hvalrådets Skr., **1**: 1—88.

BRAARUD, T., GAARDER, R. K., & GRØNTVED, J., 1953. "The phytoplankton of the North Sea and adjacent waters in May 1948." Rapp. et Proc.-Verb., **133.**

BRANDT, K., 1899. "Über den Stoffwechsel im Meere". Wiss. Meeresunters., Abt. Kiel, **4**: 213—30.

— 1902. "Über den Stoffwechsel im Meere". Ibid., **6**: 23—79.

COOPER, L. H. N., 1933. "Chemical constituents of biological importance in the English Channel, November 1930—January 1932. Parts I and II". J. Mar. Biol. Assoc. U.K., **18**: 677—753.

— 1937. "On the ratio of nitrogen to phosphorus in the sea". Ibid., **22**: 177—82.

— 1938. "Redefinition of the anomaly of the nitrate-phosphate ratio". Ibid., **23**: 179.

— 1938. "Phosphate in the English Channel 1933—38, with a comparison with earlier years, 1916 and 1923—32". Ibid., **23**: 181—95.

DAKIN, W. J., & COLEFAX, A. N., 1935. "Observations on the seasonal changes in temperature, salinity, phosphates, and nitrate nitrogen and oxygen of the ocean waters on the continental shelf off New South Wales and the relation to plankton production". Proc. Linn. Soc., N.S.W., **60**: 303—14.

DOTY, M. S., & OGURI, M., 1957. "Evidence for a photosynthetic daily periodicity". Limnol. and Oceanogr., **2**: 37—40.

DROOP, M. R., 1955. "A suggested method for the assay of vitamin B_{12} in sea water". J. Mar. Biol. Assoc. U.K., **34**: 435—40.

FLEMING, R. H., 1940. "The composition of plankton and units for reporting populations and production". Proc. 6th, Pac. Sci. Congr., 1939, **3**: 535—40.

GRAN, H. H., 1931. "On the conditions for the production of plankton in the sea". Rapp. Proc.-Verb., **75**: 37—46.

GRAN, H. H., & BRAARUD, T., 1935. "A quantitative study of the phytoplankton in the Bay of Fundy and the Gulf of Maine (including observations on hydrography, chemistry and turbidity)." J. Biol. Bd. Canada, **1** (5): 279—467.

HARRIS, E., & RILEY, G. A., 1956. "Oceanography of Long Island Sound, 1952—1954. VIII. Chemical composition of the plankton". Bull. Bingham Oceanogr. Coll., **15**: 315—23.

Hart, T. J., 1934. "On the phytoplankton of the southwest Atlantic and the Bellingshausen Sea". Discovery Rep., **8**: 3—268.

Harvey, H. W., 1926. "Nitrate in the sea". J. Mar. Biol. Assoc. U.K., **14**: 71—88.

— 1928. "Biological chemistry and physics of sea water". Univ. Press, Cambridge.

— 1939. "Substances controlling the growth of a diatom". J. Mar. Biol. Assoc. U.K., **23**: 499—520.

— 1947. "Manganese and the growth of phytoplankton". Ibid., **26**: 562—79.

— 1948. "The estimation of phosphate and of total phosphorus in sea waters". Ibid., **27** (2): 337—59.

— 1950. "On the production of living matter in the sea off Plymouth". Ibid., **29**: 97—137.

Harvey, H. W., Cooper, L. H. N., Lebour, M. V., & Russell, F. S., 1935. "Plankton production and its control." J. Mar. Biol. Assoc. U.K., **20** (2): 407—42.

Hentschel, E., & Wattenberg, H., 1930. "Plankton und Phosphat in der Oberflächenschicht des südatlantischen Ozeans". Ann. Hydr. u. Marit. Meteorol., **58**: 273—77.

Huthner, S. H., & Provasoli, L., 1953. "A pigmented marine diatom requiring vitamin B_{12} and uracil". News Bull. Phycol. Soc. Amer., **6**: 7—8.

Kalle, K., 1937. "Nährstoff-Untersuchungen als hydrographisches Hilfsmittel zur Unterscheidung von Wasserkörpern". Ann. Hydr. u. Marit. Meteorol., **65**: 1—18.

Ketchum, B. H., 1939. "The absorption of phosphate and nitrate by illuminated cultures of *Nitzchia closterium*." Amer. Journ. Bot., **26** (6): 399—407.

— 1939 a. "The development and restoration of deficiencies in the phosphorus and nitrogen composition of unicellular plants". Journ. Cell. & Comp. Physiol., **13** (3): 373—81.

— 1947. "The biochemical relations between marine organisms and their environment". Ecol. Monogr., **17**: 309—15.

Ketchum, B. H., & Redfield, A. C., 1949. "Some physical and chemical characteristics of algae grown in mass culture." Journ. Cell. & Comp. Physiol., **33** (3): 281—300.

Ketchum, B. H., Corwin, N., & Keen, D. J., 1955. "The significance of organic phosphorus determinations in ocean waters". Deep Sea-Res., **2**: 172—81.

Kreps, E., & Verjbinskaya, N., 1930. "Seasonal changes in the phosphate and nitrate content and in hydrogen ion concentration in the Barents Sea". J. du Cons., **5**: 329—46.

— — 1932. "The consumption of nutrient salts in the Barents Sea". Ibid., **7**: 25—45.

Lucas, C. E., 1949. "External metabolites and ecological adaptation". Symposia Soc. Exper. Biol., III, Growth, 336—56.

— 1955. "External metabolites in the sea". Suppl. Deep-Sea Res., **3**: 139—48.

Marshall, S. M., & Orr, A. P., 1928. "The photosynthesis of diatom cultures in the sea". J. Mar. Biol. Assoc. U.K., **15**: 321—60.

Matudaira, T., 1939. "The physiological property of sea water considered from the effect upon the growth of diatom, with special reference to its vertical and seasonal changes". Bull. Japan. Soc. Sci. Fish., **8** (4): 187—93.

— 1942. "On inorganic sulphides as a growth-promoting ingredient for diatom". Proc. Imp. Acad. Tokyo, **18** (2): 107—16.

Nathansohn, A., 1906. "Über die Bedeutung vertikaler Wasserbewegungen für die Produktion des Planktons im Meer". Abh. Sachs. Ges. Wiss., **29** (5): 359—441.

Rabinowitch, E. I., 1945. "Photosynthesis". I and II, Intersci. Publ. Inc., New York.

Redfield, A. C., 1934. "On the proportions of organic derivatives in sea water and their relation to the composition of plankton". James Johnstone Memorial Vol., Univ. of Liverpool, 176—92.

Redfield, A. C., Smith, H. P., & Ketchum, B. H., 1937. "The cycle of organic phosphorus in the Gulf of Maine". Biol. Bull., **73** (3): 421—43.

Riley, G. A., 1952. "The relationship of vertical turbulence and spring diatom flowerings". J. Mar. Res., **5**: 67—87.

— 1956. "Oceanography of Long Island Sound 1952—1954. IX. Production and utilization of organic matter". Bull. Bingham Oceanogr. Coll., **15**: 324—44.

Riley, G. A., & Conover, S. M., 1956. "Oceanography of Long Island Sound, 1952—1954. III. Chemical Oceanography". Bull. Bingham Oceanogr., Coll., **15**: 47—61.

Riley, G. A., Stommel, H., & Bumpus, D. F., 1949. "Quantitative ecology of the plankton of the western north Atlantic". Bull. Bingham Oceanogr. Coll., **12** (3): 1—169.

Rodhe, W., 1948. "Environmental requirements of fresh water plankton algae". Symbolae Botanicae Upsalienses, **10** (1): 149.

Russell, F. S., 1935. "The seasonal abundance of young fish in offshore waters of the Plymouth area". J. Mar. Biol. Assoc. U.K., **20**: 147—74.

Ryther, J. H., 1954. "The ecology of phytoplankton blooms in Moriches Bay and Great South Bay, Long Island, New York". Biol. Bull., **106** (2): 198—209.

— 1954. "The ratio of photosynthesis to respiration in marine plankton algae and its effect upon the measurement of productivity". Deep-Sea Res., **2**: 134—39.

Ryther, J. H., & Yentsch, C. S., 1957. "The estimation of phytoplankton production in the ocean from chlorophyll and light data". Limnol. & Oceanogr., **2** (3).

Steele, John H., 1956. "Plant production on the Fladen Ground". J. Mar. Biol. Assoc. U.K., **35**: 1—33.

Steemann Nielsen, E., 1952. "The use of radio-active carbon (C^{14}) for measuring organic production in the sea". J. du Cons., **18** (2): 117—40.

Sverdrup, H. U., 1953. "On conditions for the vernal blooming of phytoplankton". J. du Cons., **18**: 287—95.

— 1955. "The place of physical oceanography in oceanographic research." J. Mar. Res., **14**: 287—94.

van Dorn, W. G., 1956. "Large-volume sampler". Trans. American Geophys. Union, **37** (6): 682—84.

Yentsch, C. S., & Ryther, J. H., 1957. "Short-term variations in phytoplankton chlorophyll and their significance". Limnol. & Oceanogr., **2** (2): 140—42.

BIANCO LUNO A/S, KBH.

Contribution No. 949

FURTHER OBSERVATIONS ON SELF-FERTILIZATION IN CHTHAMALUS SP.[1]

There is little doubt that obligatory cross-fertilization is common throughout the operculate species of barnacles, but contrary to a previous view (Crisp, 1950) is has been shown recently that some species although normally cross-fertilizing may, in the absence of contiguous individuals, self-fertilize (Barnes and Crisp, 1956). This has been shown to be the case in *Chthamalus stellatus, Balanus perforatus* and *Verruca stroemia* the first two being intertidal and the third largely a sublittoral species. In the case of *Chthamalus stellatus* self-fertilization, although apparently less efficient than cross-fertilization appears to produce viable nauplii; clearly there is a survival value in self-fertilization particularly evident in *Chthamalus stellatus* where isolated individuals occur high up the shore.

During the course of ecological work along the American coasts the opportunity has been taken of examining other species of *Chthamalus* for evidence of self-fertilization. It was not possible to follow the development of broods throughout a season but samples of the species were taken in a restricted area as opportunity arose.

In each case twenty well grown contiguous individuals were taken and twenty individuals separated by at least 5 cm.; the state of the ovary and embryos were recorded. The places of collection and species concerned are listed below.

East Coast: (a) Rocky Beach, Woods Hole, Mass., *C. fragilis* Darwin. West Coast: (b) Will Rogers Beach, Santa Monica, California, *C. fissus* Darwin; (c) Big Rock, Malibou Beach California, *C. fissus;* (d) Charleston, Coos Bay, Oregon, *C. dalli Pilsbry;* (e) Anacortes, Washington, *C. dalli;* (f) San Juan, Outer coast, Washington, *C. dalli.*

The results are given in Table I which shows the percentage of the animals with their gonads in various states of development.

It is evident that in all three species at all the places investigated isolated individuals bear ripe embryonic masses. These appeared to be normal and in all cases (except Woods Hole where pickled material was examined) were capable of giving active and apparently viable nauplii. There is again evidence that self-fertilization is delayed beyond the time at which cross-fertilization would have occurred.

TABLE I. Comparision of separate (sep.) and contiguous (con.) individuals, *Chthamalus* sp.

Place	Date	CONDITION (%)							
		Empty or unfertilized		Early stage embryos		Limbed embryos present		Eyed nauplii present	
		Sep.	Con.	Sep.	Con.	Sep.	Con.	Sep.	Con.
(a)	1/7/57	45	35	20	35	5	15	30	15
(b)	11/4/57	100	100	0	0	0	0	0	0
	3/6/57	50	35	0	0	40	35	10	30
	17/6/57	35	25	35	5	15	55	15	15
(c)	3/6/57	95	85	0	0	0	5	5	10
(d)	29/6/57	30	25	25	45	5	10	40	20
(e)	3/7/57	75	90	15	5	0	0	10	5
(f)	2/8/57	75	45	15	50	0	0	10	5

It would seem that facultative self-fertilization is common in the genus perhaps extending to all species.

REFERENCES

Barnes, H. and D. J. Crisp. 1956. Evidence of self-fertilization in certain species of barnacles. J. Mar. biol. Ass. U. K., **35,** 631-639.

Crisp, D. J. 1950. Breeding and distribution in *Chthamalus stellatus.* Nature, Lond., **166,** 311 only.

H. BARNES AND MARGARET BARNES[2]

THE MARINE STATION, MILLPORT, SCOTLAND;
OCEANOGRAPHIC INSTITUTE, WOODS HOLE;
DEPARTMENT OF ZOOLOGY, UNIVERSITY OF CALIFORNIA, LOS ANGELES;
THE FRIDAY HARBOR LAROBATORIES, UNIVERSITY OF WASHINGTON, SEATTLE

---

[1] Contribution No. 949 from the Woods Hole Oceanographic Institution.

[2] One of us (H.B.) wishes to acknowledge the receipt of a Research Fellowship from the Oceanographic Institute, Woods Hole; support from the National Science Foundation (Grant No. G 3235, Prof. T. H. Bullock) and the Office of Naval Research (Contract No. NR 165/142, Dr. D. L. Ray); and leave of absence granted by the Council of the Scottish Marine Biological Association.

Reprinted from *Ecology,* Vol. 39, No. 3, July, 1958

Contribution No. 951

The Journal of the Oceanographical
Society of Japan. Vol. 14, No. 2, June 1958

A Theory of Vertical Structure of Density in the Ocean*

Takashi ICHIYE**

1. Introduction

In the cradle age of oceanography the thermohaline circulation was considered as the primary cause of oceanic circulation, but recent success in wind driven circulation theory caused this notion to be neglected until certain studies of the deep sea circulation have been done by STOMMEL (1955, 1957) and one of his results—existence of a deep counter current under the Gulf Stream—was indeed verified by an observation (SWALLOW and WORTHINGTON, 1957). In fact this sort of circulation is a principal part of deep sea circulation, and yet analytical discussion of the problem seems to be prohibitive, since the problem is essentially non-linear. In this respect Stommel is also a pioneer who discusssed a solution of a non-linear problem about the mechanism of thermocline retaining an advective term in heat transfer equation (STOMMEL, 1957b), although LINEYKIN (1955) and STOMMEL & VERONIS (1957) worked on theoretical models of thermocirculation based on linearized equations. This paper treats the similar problem to Stommel's non-linear theory from different approach and the author considers that it is somewhat worthwhile to be printed in this journal, since in Japan this problem seems to be novel.

2. Fundamental equations

As equations of motion we consider the following system.

$$-f\rho v=-\frac{\partial p}{\partial x}+A\rho\frac{\partial^2 u}{\partial z^2} \qquad (1)$$

$$f\rho u=-\frac{\partial p}{\partial y}+A\rho\frac{\partial^2 v}{\partial z^2} \qquad (2)$$

$$g\rho=-\frac{\partial p}{\partial z} \qquad (3)$$

where f is Coriolis' coefficient and A is vertical eddy viscosity. The equation of continuity is

$$\frac{\partial \rho u}{\partial x}+\frac{\partial \rho v}{\partial y}+\frac{\partial \rho w}{\partial z}=0 \qquad (4)$$

Differentiating (1) and (2) with z and substituting (3) we have

$$-f\frac{\partial \rho v}{\partial z}=g\frac{\partial \rho}{\partial x}+\frac{\partial}{\partial z}\left(A\rho\frac{\partial^2 u}{\partial z^2}\right) \qquad (5)$$

$$f\frac{\partial \rho u}{\partial z}=g\frac{\partial \rho}{\partial y}+\frac{\partial}{\partial z}\left(A\rho\frac{\partial^2 v}{\partial z^2}\right) \qquad (6)$$

Cross-differentiating (5) and (6) and substituting (4) we have

$$-f\frac{\partial^2}{\partial z^2}(\rho w)+\beta\frac{\partial \rho v}{\partial z}$$
$$=\frac{\partial}{\partial z}\left\{\frac{\partial}{\partial x}\left(A\rho\frac{\partial^2 v}{\partial z^2}\right)-\frac{\partial}{\partial y}\left(A\rho\frac{\partial^2 u}{\partial z^2}\right)\right\} \qquad (7)$$

As an equation of mass flux we take

$$u\frac{\partial \rho}{\partial x}+v\frac{\partial \rho}{\partial y}+w\frac{\partial \rho}{\partial z}=K\frac{\partial^2 \rho}{\partial z^2} \qquad (8)$$

When we assume the geostrophic relation for horizontal velocity which is quite plausible for deep sea current, equations (7) and (8) become very simple. For from (5) and (6) we have

$$\rho v\fallingdotseq-\frac{g}{f}\int_{z_0}^{z}\frac{\partial \rho}{\partial x}dz,\quad \rho u\fallingdotseq\frac{g}{f}\int_{z_0}^{z}\frac{\partial \rho}{\partial y}dz \qquad (9)$$

where z_0 is a reference level where horizontal velocity vanishes. Putting into the equation (8) we can see easily that the first two terms in the left hand side vanish when

$$\frac{\partial \rho}{\partial x}\int_{z_0}^{z}\frac{\partial \rho}{\partial y}dz-\frac{\partial \rho}{\partial y}\int_{z_0}^{z}\frac{\partial \rho}{\partial x}dz=0 \qquad (10)$$

General expression for ρ which satisfies this condition is very difficult to get, but when ρ is expressed by

$$\rho=\rho_1(x,y)\rho_2(z)+\rho_3(z)+\rho_4(x,y) \qquad (11)$$

the condition (10) is satisfied for arbitrary functions ρ_1, ρ_2 and ρ_3 and for function ρ_4 satisfying

---

* Received February 20, 1958. Woods Hole Oceanographic Institution Contribution No. 951

** Oceanographical Section, Japan Meteorological Agency. Now at Woods Hole Oceanographic Institution, Woods Hole, Mass.

tween the surface and bottom is 5, or when we take the bottom value of $\sigma_t=28$, then its surface value is 23.

The results of numerical computation are shown in fig. 1, where vertical density distribution computed by the formula (26) or (27) is shown for different values of s ranging from -10^3 to 10^3. When s has a large positive value, conspicuous thermocline develops very near the surface, whereas for a large negative value of s upper homogeneous layer extends down to the great depth. As the absolute value of s decreasing, the density distribution approaches to that of linear change with the depth. Such density distribution is closely associated with the structure of vertical current which is expressed by

$$W/k=\epsilon''/\epsilon' \doteqdot \frac{s}{2}(Z-Z^2)+\varphi_m(z) \qquad (34)$$

where $\varphi_m(Z)$ is the correction term, and for the positive value of s the vertical current is upwards and for negative s, it is downwards. In other words, upwards motion brings the water of deeper layer near the surface, so that the thermocline develops near the surface (for $s>0$), and downwards motion brings the surface water to deeper layer (for $s<0$). Since the sign of s is determined only by that of α, the density field increasing eastwards ($\alpha>0$) produces the upwards motion ($s>0$). On the other hand, small absolute value of s indicates that the mixing effect is more predominant than that of advection, which results in the linear distribution of density and small amount of vertical velocity.

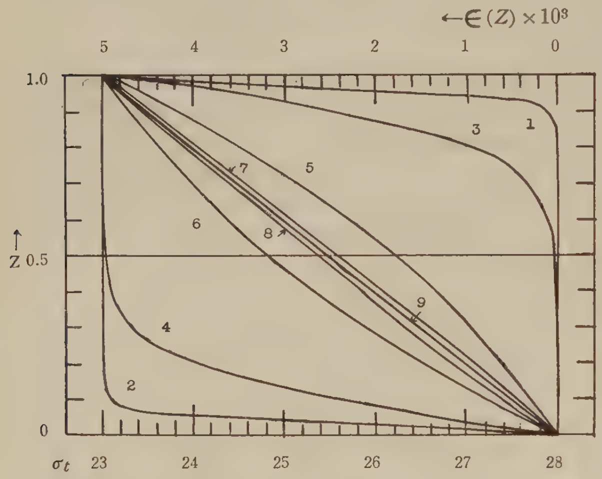

Fig. 1 Profiles of density for non-viscous ocean.
Curves 1, $s=10^3$; 2, $s=-10^3$; 3, $s=10^2$; 4, $s=-10^2$; 5, $s=10$; 6, $s=-10$; 7, $s=1$; 8, $s=-1$; 9, $s=0$

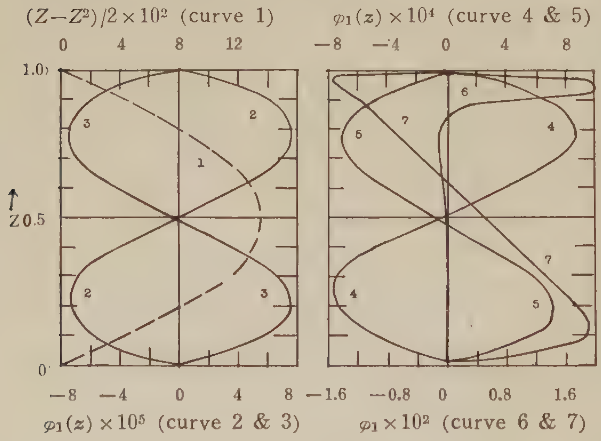

Fig. 2 The main term (broken line $(Z-Z^2)/2$) and correction term $\varphi_1(Z)$ in the equation (31)
Curve 1, $=(Z-Z^2)/2$; 2, $s=1$; 3, $s=-1$; 4, $s=10$; 5, $s=-10$; 6, $s=10^3$; 7, $s=-10^3$

The curves shown in fig. 1 are based on

the first approximation, and in fact the correction term is so small that higher order of the approximation is almost the same as the first approximation. The correction term is computed for $s=\pm1$, ±10 from the equation (33) and for $\pm10^3$ by numerical integration. The result is shown in fig. 2, where the distribution of the main term $\frac{s}{2}(Z-Z^2)$ is also shown. We can see from these curves that correction term is quite small compared with the main term, for example the maximum of the correction term is about 7×10^{-4} of that of the main term for $s=\pm1$ and about 2×10^{-4} for $s=\pm10^3$. Therefore we cannot distinguish the second approximation from the first by the scale of the charts here used.

5. Solution of viscous model

When the vertical eddy viscosity is considered, the equation (15) is transformed to the ordinary differential equation about z by assuming $\sigma=e^{\alpha X+\delta Y}F(Z)$ and the result is

$$sF+\frac{d^2}{dZ^2}\left(\frac{FF'}{F}\right)=rF' \tag{35}$$

where

$$r=a(\alpha^2+\delta^2-l\delta)/mk=Agz_0^2(\alpha^2+\delta^2-l\delta)/Kx_0^2f^2$$

Similarly to the process in non-viscous case, we introduce the function $\in(Z)$ and integrate the equation (35) under boundary conditions that $W=0$ at $Z=0,1$ and $\in(1)=\varepsilon$ then we obtain

$$(1-\in)(\in''/\in')=s(Z-Z^2)/2+\phi(Z)-r(\in-\varepsilon Z) \tag{36}$$

where $\phi(Z)$ is the same function as defined by (28).

The equation (36) is also not integrable analytically, but we can obtain the approximate solution by iteration method, when $r\varepsilon$ is of the same order of magnitude as s or less. For this purpose we start from the solution for $\in(z)$ obtained in the previous section and then integrate the next equation successively

$$\in''_m/\in'_m=s(Z-Z^2)/2+\varphi_{m-1}(Z)-r(\in_{m-1}-\varepsilon Z) \tag{37}$$

As numerical examples, we consider the case of $s=\pm10^2$ and density distributions computed by the equation (37) are shown for $r=\pm2\times10^2$ and $\pm2\times10^3$ in fig. 3A. In this example the second approximation is almost the same as the first one (fig. 3B). When r is negative, the effect of additive term with r is to make the density distribution approach to the linear decrease with the depth, whereas when it is positive, the effect is the same as that of increasing absolute value of s. In the actual ocean, the term of $\beta\delta$ is predominent in the coefficient $\alpha^2+\delta^2-l\delta$ of r, since $l\doteqdot0.4$ and also the density generally increases northwards, δ is considered as positive, so that r is usually negative. As a result, the effect of vertical eddy viscosity produces the density distribution of more thoroughly mixed state.

When $|r\varepsilon|\gg|s|$, this procedure of iteration becomes poor in convergence and we had

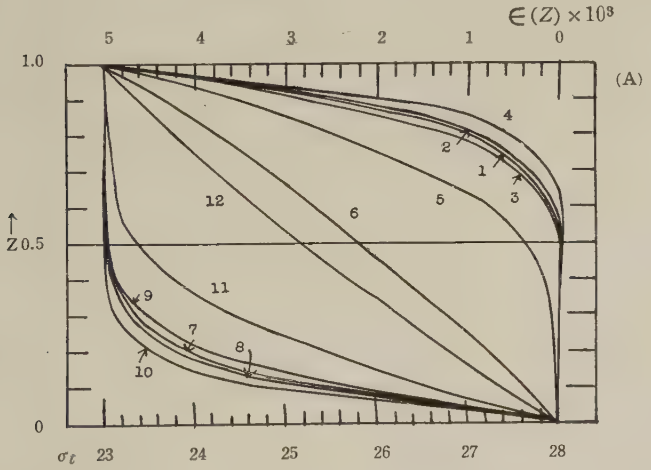

Fig. 3A Profiles of density for viscous ocean
$s=10^2$ from curve 1 to 6, $s=-10^2$ from 7 to 12. Curve 1, $r=0$; 2, $r=2\times10^2$; 3, $r=-2\times10^2$; 4, $r=2\times10^3$; 5, $r=-2\times10^3$; 6, $r=-5\times10^4$. Curve 7, $r=0$; 8, $r=2\times10^2$; 9, $r=-2\times10^2$; 10, $r=2=10^3$; 11, $r=-2\times10^3$; 12, $r=-5\times10^4$

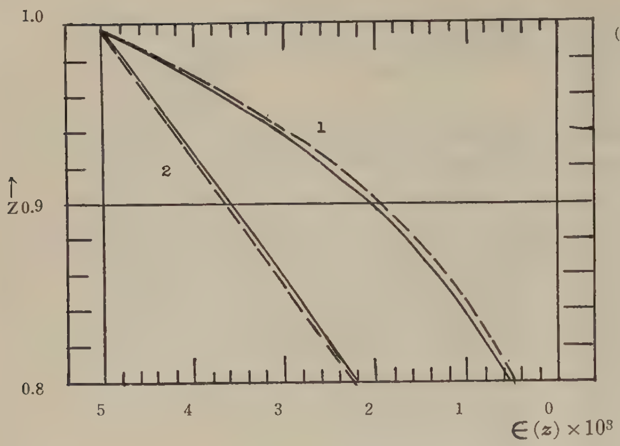

(B) Fig 3B Profiles of density for viscous ocean near the surface given by the first (broken line) and the second approximation (solid line).
Curve 1, $r=2\times10^3$; 2, $r=-2\times10^3$, both $s=10^2$.

better resort to the method of expanding $\in(Z)$ in series of powers of $1/r$ such as

$$\in=\xi_0++\xi_1 r^{-1}+\xi_2 r^{-2}+\cdots\cdots$$

where

$$\xi_0=\varepsilon Z+s(Z-Z^2)/2r+\varphi_1(Z)/r$$

Then the equation (36) becomes

$$\xi_0''+\xi_1''r^{-1}+\xi_2''r^{-2}+\cdots\cdots$$
$$=-(\xi_1+\xi_2 r^{-1}+\cdots\cdots)(\xi_0'+\xi_1'r^{-1}+\cdots\cdots)$$

and the coefficients $\xi_1, \xi_2\cdots\cdots$ are determined by equating the term of same power of $1/r$. The first two terms are given by

$$\xi_1=\frac{c_2}{(c_1-c_2Z)},\quad \xi_2=-\frac{3c_2^3}{(c_1-cZ_2)^4},$$

where $c_1=\varepsilon+s/2r$, $c_2=s/r$

In fig. 3, the results of computation by this method are shown by taking $s=\pm10^2$ and $r=-5\times10^4$. They indicate that the increase of absolute value of r produces the density distribution more close to the linear change about the depth, which is considered as well-mixed state. This is plausible, since we can see easily that $\in=\varepsilon Z$ is the solution of (36) under the boundary conditions considered here, as $|r|$ becomes infinitive.

6. Concluding remarks

It is rather amazing that the density structure has very simple profiles as shown in fig. 1 and 3. So far as the geostrophic assumption for horizontal velocity is valid, the simplified equation of mass flux (12) is considered as sufficiently exact, because the density distributions obtained both in section 4 and 5 satisfy the relation (11). On the other hand, the solutions shown here are very crude, particularly those in section 5, so that in order to discuss fine structure of density we should obtain more analytically rigorous solution, and this is especially true when $r\varepsilon$ is of the same order of magnitude as s, because somewhat more complicate density profiles may be encountered in such range of parameters, although in such case they are, as a whole, represented by a linear curve.

Acknowledgement: The author wishes his thanks to Mr. Henry STOMMEL, Dr. George VERONIS and Dr. Willem MALKUS who have stimulated his interest about convective circulation.

References

LINEYKIN, P. C., 1955;
"On the determination of the thickness of the baroclinic layer in the sea." Doklady SSSR Akad. Nauk, **101**
STOMMEL, H., 1956;
"On the determination of the depth of no meridional motion." Deep Sea Res. **3** (2)
STOMMEL, H. 1957a;
"A survey of ocean current theory." Deep Sea Res. **4** (3)
STOMMEL, H. 1957b;
"Reflections on the mechanism of the main thermocline." (Unpublished manuscript)
STOMMEL, H. and G. VERONIS, 1957;
"Steady convective motion in a horizontal layer of fluid heated uniformly from above and cooled non-uniformly from below." Tellus **9** (3)
WORTHINGTON, L. V. and J.C. SWALLOW, 1957;
"Measurements of deep currents in the Western North Atlantic." Nature **179** pp 1183–1184

Contribution No. 952

TSUNAMI WAVES

what are known about them—

how we have studied them.

Takashi Ichiye*

Oceanographic Section, Japan Meteorological Agency, Tokyo.

AS IS WELL KNOWN to many people in the world, Japan is quite rich in experiences of earthquakes. There are various kinds damage caused by earthquakes, and one of the st important phenomena accompanying them *unami* or destructive sea waves, which in some es cause more serious damage than an earthke itself. Originally the world *tsu* means a t, harbour or a small bay in Japanese and *nami* ans a wave. The combination of *tsu* and *nami* icates the characteristic features of long waves erated by a sudden movement of the ocean tom, since such waves become very conspicuous en they approach the coast and enter into a t or bay (Darbyshire and Ishiguro, 1957).

As shown by the fact that the word tsunami now widely used in foreign countries as a term ining long waves with a period longer than that swells and shorter than that of tidal waves, an seems to be most vulnerable to the attack such waves, because submarine earthquakes ur quite frequently off the coast of Japan along elt forming the so-called Circum Pacific Earthke Belt and moreover bottom topography and stal configuration near Japan are especially ourable for development of such waves, as stated er.

In this brief note is described the nature of the ves caused by a deformation of the ocean bottom y, with reference to many facts experienced l observed in Japan and also a summary is en of the studies about them carried out recently Japan, although some people have used this m tsunami as a word generally defining long ves including those originated by meteorological ses such as storm surges.

In this respect there is an interesting story ich illustrates the property of tsunami. In the dal age of Japan about 300 years ago, there a custom that a feudal lord of a Northern province sent cods which were caught for the first time in a year to the Shogunate in Tokyo as a present. In order to catch cods as good and abundant as possible, this lord dispatched some young officials to supervise fishing and he gave a prize to an official who brought the most splendid catch.

One year in 1611 two men sent to one village for this business fell in love with a beautiful girl of the village chief. But one of them lost his suit as happens in many cases, and on the night when the wedding between the other man and the girl was celebrated he desperately went off to the sea to fish with fishermen. That night he caught an extraordinarily large catch, so he and the fishermen came back in the morning to the village. Then they found that the whole village had been washed away during the night by a tsunami, including the newly married couple. Further, other fishing ports in this district were also severely damaged and in that year there was no catch of cods from the coast except that of this man, who was accordingly honoured and promoted by his lord.

The moralistic lesson of this story is such that the proverb says "fortune and misfortune are two buckets in a well". However, from a scientific point of view, it suggests two interesting facts related to tsunami. One is that there is often abnormal catch of fishes before an occurrence of a submarine earthquake, and this fact is not fully explained scientifically but some biologists suggest that change in the earth current or some microseisms before an earthquake may stimulate fishes. The other important property of tsunami indicated in this story is that the waves usually become noticeable as they approach the coast so that in the open sea they are not recognized even on board a small fishing boat.

---

raduated at Tokyo University, Geophysical Institute in 1944. Entered into Kobe Marine Observatory in 1945. Got a degree D. Sc. from Tokyo University in 1952. Moved to oceanographic section of Central Meteorological Observatory of Tokyo in 55. Came to Woods Hole Oceanographic Institution in January, 1957 under sponsorship of The Rockefeller Foundation, enging in study of physical oceanography, especially about the problem of oceanic circulation and estuarine or coastal phenomena.

1. The tsunamis experienced in Japan in the past

The historical age of Japan began about two thousand years ago, and according to "Earthquake Records of Japan" (Nippon Jishin Shiryo) which is based on old documents and official history books of Japan, about 80 tsunamis occurred along the coast of Japan during the historical age to the present, the oldest of which was in A.D. 684. By use of the data given in the records, the distributions of tsunamis which attacked the coast of Japan are shown in Fig. 1, where each tsunami is classified in five scales according to its magnitude (the smallest tsunami of "O" scale is not shown in order to avoid too complicated a figure) and the frequency of occurrence of each class is indicated by different symbols along the coast. Further, the centres of tsunamis determined either by seismographs or by mareograms are indicated by black symbols and those estimated from historical records of damage caused by tsunamis as well as earthquake are shown with white symbols.

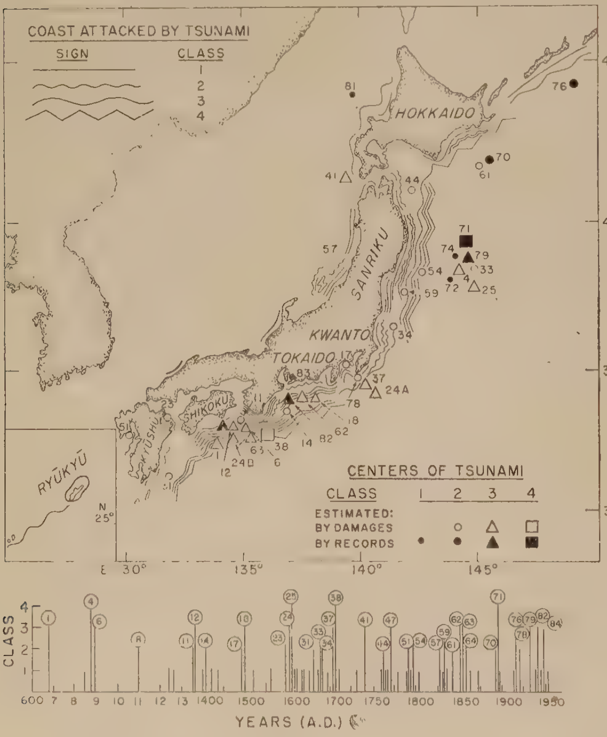

Fig. 1.

Special (upper chart) and chronological (lower chart) distribution of tsunami near Japan.

The figure clearly shows that tsunamis attacked the Pacific coast of Japan most frequently among which the Northern coast (off Sanriku district) and the Southern coast (off Takaido district and Shikoku island) are most notable. Next to them the coast of Hokkaido, Kanto district, Kurile island and Okinawa islands were also noted. On the o
hand it is quite remarkable that tsunamis
relatively rare and their magnitude is also gene
small along the Japan sea coast and this is du
the condition that earthquakes in this region w
forms the so-called Outer Seismic Belt of Japan
usually local and occur either very close to the c
or entirely on land thus they do not cause a l
tsunami.

The lower part of Fig. 1 shows the chronolog
distribution of tsunamis based on the same dat
the Records, where numbers attached correspon
those of centres in the upper chart, and it sugg
that the occurrence of tsunami in the past is
distributed arbitrarily but forms three groups,
is, from A.D. 680 to 900, from 1360 to 1600,
from 1700 to the present, and these periods co
pond naturally to the most active periods of ea
quakes in Japan.

We should mention something about the cl
fication of tsunamis shown in this figure.
classfication is done originally according to
maximum wave height of each tsunami, where
scale 4 gives the severest tsunami with wave hei
more than 30m, scale 3 gives the height of 1
20m, scale 2 gives the heights from 4 to 6m, sca
gives the value of about 2m, and the weakest s
O means waves of about 1 m.

Such classification can be also associated
the total energy of tsunami (R. Takahashi, 1
since the heights of these waves are closely rel
with the total energy. When we assume that
tsunami propagate with a velocity of long w
$\sqrt{gh}$, then the total energy emitted from the so
region is given by

$$E = \pi \rho g \, V R \Sigma A^2 T$$

where ρ is the density of water, R is the dist
from the source, A amplitude, T the half perio
each tsunami wave and summation must be t
with respect to all wave trains that occur in
tsunami. Further, when we compare the total en
thus computed with the scale number M in
tsunami, we can find empirically the relation
tween them such as

$$E = E_0 \cdot 10^{0{\cdot}6M} \, erg$$

where $E_0 = 2{\cdot}5 \times 10^{21}$. As an example of estima
of the total energy, we consider the tsunami of
which attacked the Northern coast of Japan.
this tsunami the value of A at the 200m dep
estimated as 5m by use of the data of mareog
and Green's formula for the change of the a
tude with the depth and the period $2T$ is abou
min. and the number of main half waves is
so that we obtain $E = 1{\cdot}6 \times 10^{23} erg$ which am
to about 10^{-3} of the total energy of seismic w
estimated by H. Kawasumi (1951).

ich estimation of the energy is very crude nature, but some ideas about the order of itude of tsunami may be obtained from the es computed.

Causes of tsunami

ome tsunamis in the past were caused by sion of volcanoes or by a landslide, and the famous example of the former is the explosion rakatoa in 1883, which sent destructive waves ver the world. As an example of the latter we nention the tsunami of scale 3 in 1792 that ked the North-western corner of Kyushu and ed the death of 1,200 people, but the tsunamis ed by such effects are usually local and very l in their magnitude. The most frequent and rtant causes of large scale tsunamis are the en deformation of ocean bottom accompanying marine earthquake.

t is still not well known about the movement he ocean bottom due to an earthquake, since no ct measurement or observation has been carried However, we can estimate the vertical disement of the sea bottom by comparing the ding before and after an earthquake and also nation of horizontal extension of source region ossible, as stated later. Further, from the obation of formation of land dislocation on land ase of an earthquake we can expect that the d of such bottom motion is ranged from several nds to several minutes.

As for estimation of the vertical displacement ea bottom, the present stage of our knowledge is from satisfactory, and no reliable estimation has done about the ocean bottom distant from the t. There are many reasons which make it diffi- to get enough knowledge of vertical displacet, one of which is that the accuracy of sounding ocean is not enough to get the precise values essary for such estimation, since such movement ht be several meters at the largest. Especially exact bottom topography near Japan has been wn only recently, so that the estimation of the imum uprise of the sea bottom in the midst of ami Bay, which is considered to be close to the entre, from the comparison of soundings carried before and after the great earthquake in Kanto rict in 1923 is somewhat doubtful, though this s such an enormous value of about 17m.

However, the recent measurement of the verl displacement carried out in case of the earthke on January 13 of 1945 is quite reliable and give information about the movement of the bottom caused by an earthquake. This result own in Fig. 2*a*, which gives the maximum up- of the bottom of about 1·3m though this earthquake is relatively small $M_K=4$* and the accompanying tsunami has only scale 1.

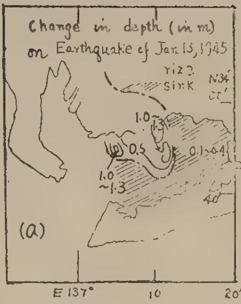

Fig. 2(*a*).
Example of bottom deformation caused by an earthquake.

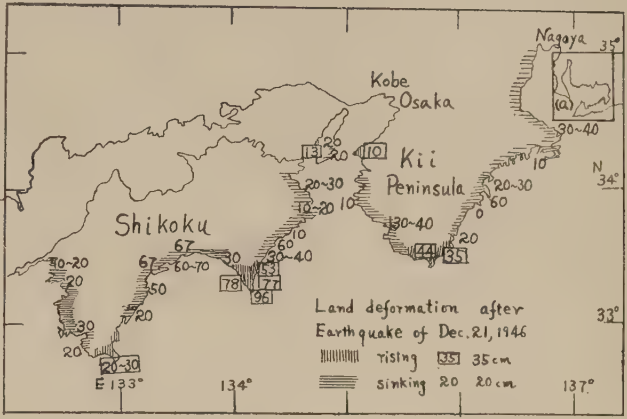

Fig. 2(*b*).
Example of land deformation caused by an earthquake (area surrounded with rectangle corresponds to the region of Fig. 2*a*.)

Further, as for the displacement of land measured on land in case of an earthquake much data has been available since about fifty years ago, and here may be mentioned one recent example which gives the result of precise levelling and other measurements carried out after the earthquake in 1946 which caused severe tsunami along the Southern coast of Japan. In Fig. 2*b*, is shown the distribution of the vertical motion along the coast, which gives the maximum uprise of Cape Muroto of about lm to the maximum sinking of about 0·6 to 0·7m on the Southern coast of Shikoku and the Eastern coast af Kii Peninsula. Therefore, it seems to be reasonable to consider that a displacement of bottom of about one meter or more occurred in the source region which was located to the South of this coast.

---

* M_K is the Japanese magnitude of earthquake, which is related to Gutenberg's magnitude as $M=4{\cdot}85+0{\cdot}5M_K$. The earthquake which caused the tsunami of March 3, 1933 has $M_K=8{\cdot}3$, that of December 21, 1946 has $M_K=6{\cdot}5$.

3. Mareograms of tsunamis—estimation of extension of a source

As the first step to obtain an idea of tsunami here is shown the mareograms recorded in cases of the severest tsunamis which attcked Japan in recent years. In Fig. 3 those obtained at the tsunami on March 3, 1933 off the Northern coast of Japan are shown, with the location of each tidal station. In Fig. 4 the similar records of the tsunami on December 21, 1946 are shown. Although these two tsunamis are different in location where they were generated and propagated, it is remarkable that the mareograms indicate some common characteristic features. When closely examined, they are recognized to consist of three parts, the initial movement *I*, main waves *M* and secondary oscillation *S*, as indicated in each curve. From the curves, we can see that the initial movement of the sea water caused by tsunami is usually associated with the sudden fall of surface, although at some stations a slight rise of sea level preceded the abrupt fall, which agrees well with many visual observations of people who had met a tsunami as they said that after a shock of earthquake they went to the coast and they saw the sea water retreated from the coast at first, then a large wave came. The main waves are considered as the principal part of tsunami which seems to be less influenced by
topographic effects, and therefore they have la
amplitudes and consist of several wave t
continuing several hours. The largest ampli
or especially maximum elevation of sea su
which is most important for the estimatio
damage occurs not always at the first wave bu
later wave trains. The period of the main w
is ranged from several minutes to more than
hour and even for the same tsunami it is some
different at each station, which is due to the e
of the topography on the propagation of the wa
as stated later, since the tsunami generally pa
through the continental shelf and also is affe
by the coastal configuration.

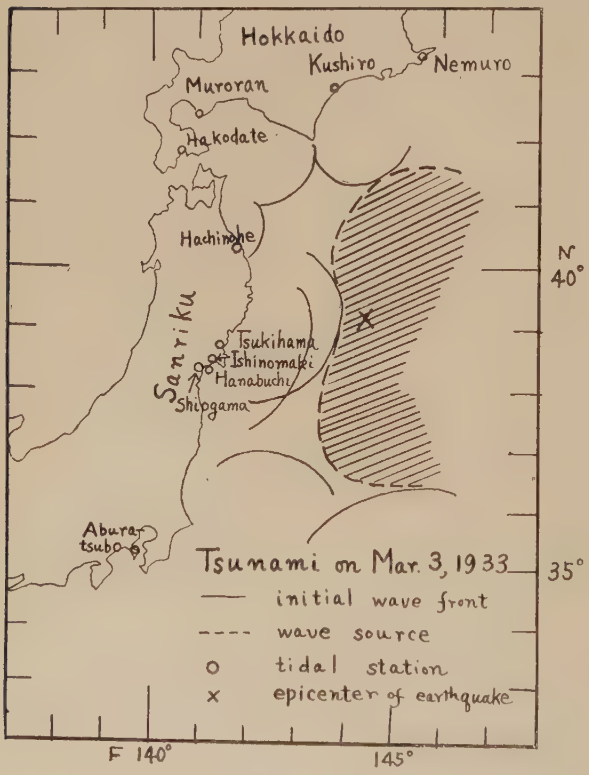

Fig. 3(*a*).
Mareograms of tsunami on March 3, 1933.

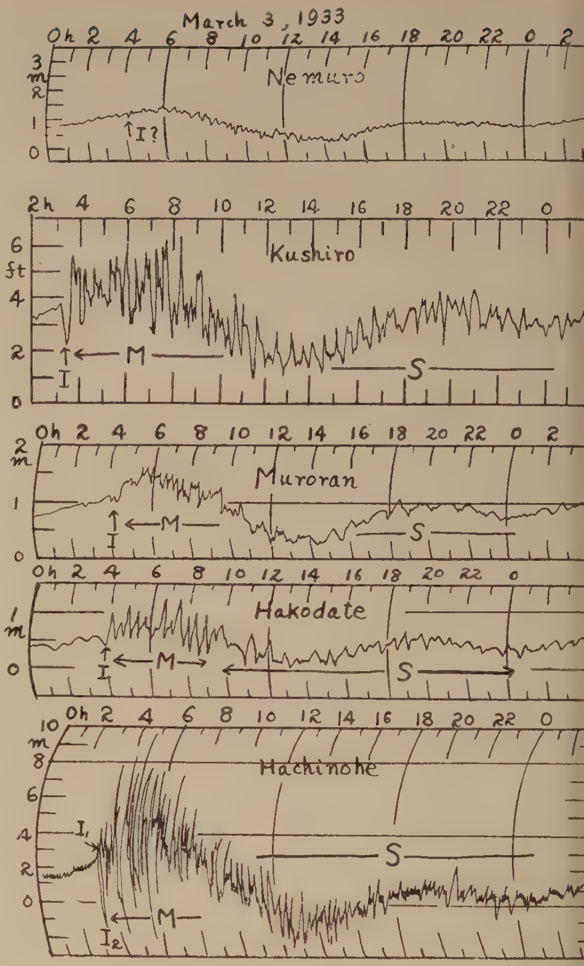

Fig. 3(*b*).

The secondary oscillation is caused by the
and forth motion of bay or shelf water afte
incident main waves have passed away or
been reflected from the coast, since these inci
waves are not totally reflected. However
mareograms the difference between the
waves and this part is usually not so clear, ex
at some stations where the period of secon
oscillation is quite different from that of the

es, (in 1933 tsunami, at Hakodate and Hono-
, in 1946 tsunami, at Sakai and Hososhima).

We can use these mareograms to determine the
ension of a source region. When we make travel
rt assuming the point source of tsunami as an
entre of the earthquake determined with seis-
grams, by use of the formula for a propagating
ed of long waves, we often find that the
puted time of arrival of tsunami is much earlier
n the observed one, and this indicates that the
e front of tsunami does not coincide with the
entre of an earthquake in its beginning. There-
, instead, we assume that each tidal station
responds to a source of waves and make a travel
rt for each station from the beginning of the
thquake shown with seismographs to the arrival
tsunami shown with a mareogram, then we
ain many arcs corresponding to the wave front
er a travel time for each station, which are
icated in Figs. 3*a* and 4*a* as "initial wave front".
envelope of these arcs may be considered as
ource region. In the two tsunamis such region
a quite large area, the diameter of which has
nost the same order of length as wave length of
tsunami. Thus we can consider that the tsunami is caused by a deformation of very large bottom area, within which the epicentre of the earthquake causing such deformation is usually located.

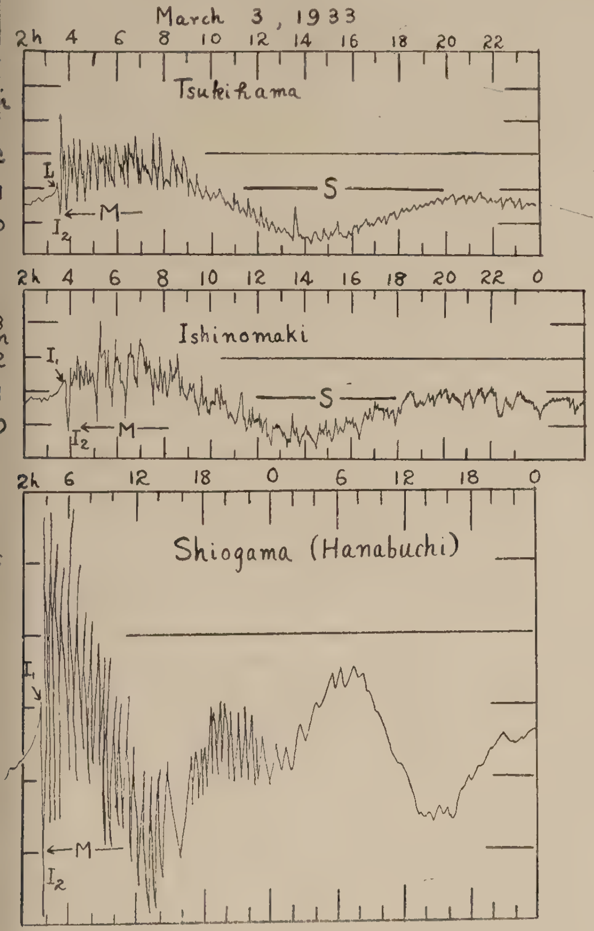

Fig. 3(*c*).

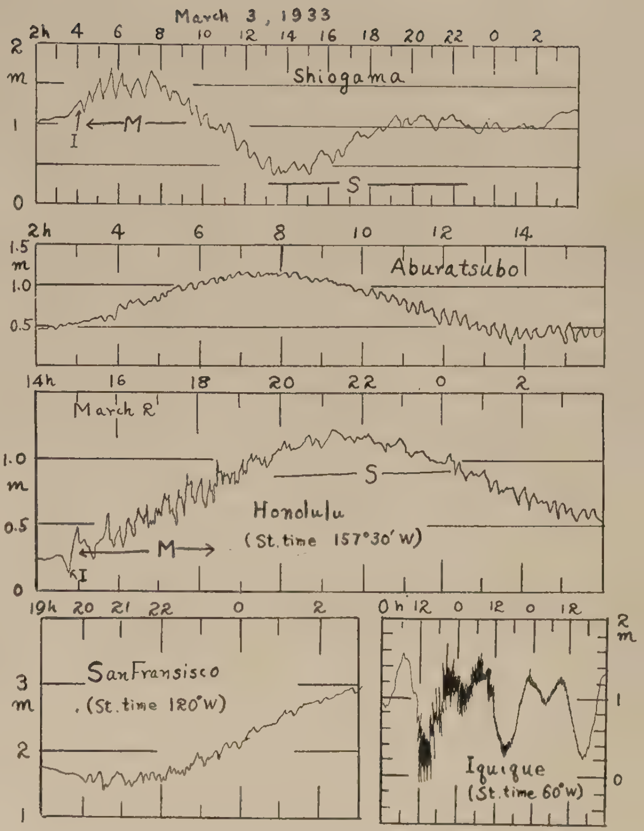

Fig. 3(*d*).

The area of such source seems to be proportional to the scale of tsunami and energy of earthquake, for we have the following table which indicates the radius of belt area of respective earthquakes scale of tsunami, and the diameter of the source region as determined by the stated method. (Omote, 1947).

TABLE 1

Date	1933 III,3	1936 XI,3	1939 V,1	1940 VIII,2	1944 XII,7	1946 XII,21
Radius of felt area (km)	920	440	410	495	570	760
Scale	3	0	0	1	3	3
Diameter of source (km)	600	90	50	210	130	350

4. Model experiment on the generation of tsunami

We have already some ideas about the movement of the sea bottom which causes a tsunami

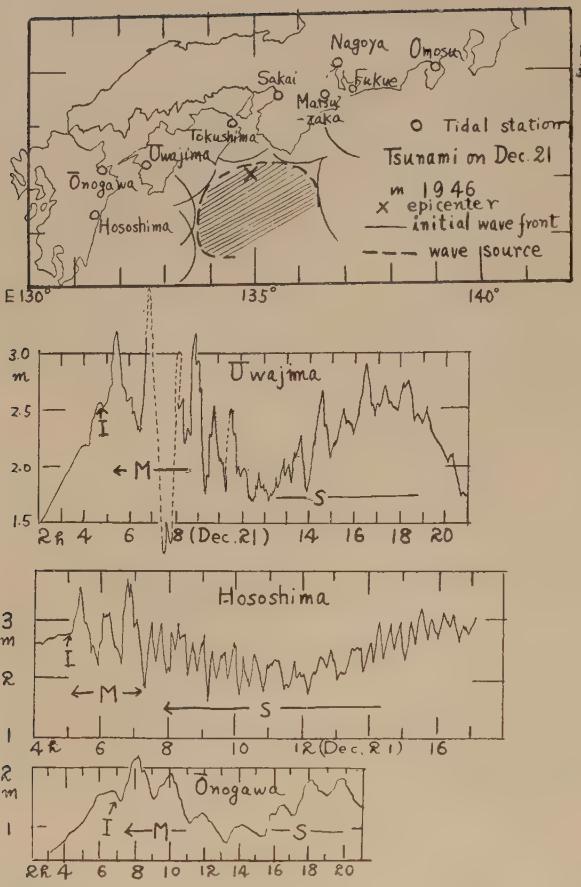

Fig. 4(*a*).

Mareograms of tsunami on December 21, 1946.

but it is still not so easy to obtain quantitative relationships between the mode of bottom motion and deformation of sea surface. As a preliminary procedure to get such knowledge, some model experiments were carried out (Takahashi, 1934), though they are not so conclusive and therefore it is highly desirable to repeat such kinds of experiments, especially by use of electronic techniques recently developed so remarkably.

The results of his experiments are shown in Figs. 5*a* to *c*, where the equipment is schematically shown in Fig. 5*b*, in which V is a tank of 8 × 4 feet with one foot depth, and P is a piston of 10 cm. diameter which is moved by a spring F, whose speed is regulated with some device B. The deformation of water surface is photographed by camera K by use of the beam coming from S. In Fig. 5*a* the change of surface profiles with time is shown for up and downward motion of the piston, where H is the depth of the water in the tank, S the distance of stroke of the piston and T is an interval from the beginning to the end of the motion of the piston.

As shown in the right hand side of Fig. 5*a*, when the piston is moved upwards the surface of the water just above the piston heaps up into a c
Then as this cone becomes higher, its base spre
When a certain height is reached, the peak
in, leaving an elevated circular bank of wate
the margin. The water just above the piston
in further to such an extent that it becom
truncated cone with a hollow in the middle. T
the water begins to heap again, and the w
process is repeated, only with the cone lower t
the initial one.

The relationships between the motion of
piston and that of the water surface are illustra
in Fig. 4*c*, where the maximum height of a cone
or its non-dimensional form η_0/H is plotted
function of $\frac{S}{H}$ and $\sqrt{\frac{g}{H}}\cdot T$. These curves sug
that generally larger value of S and smaller T, t
is, a larger speed of piston produces larger am
tude but for a certain value of T there is s
optimum value in S for maximum η_0.

5. Theoretical researches on the generation of tsunami

The mechanism of the generation of tsunam
rather simple, as far as the qualitative expla
tion is concerned. However, the quantita
relationships between the motion of the bot

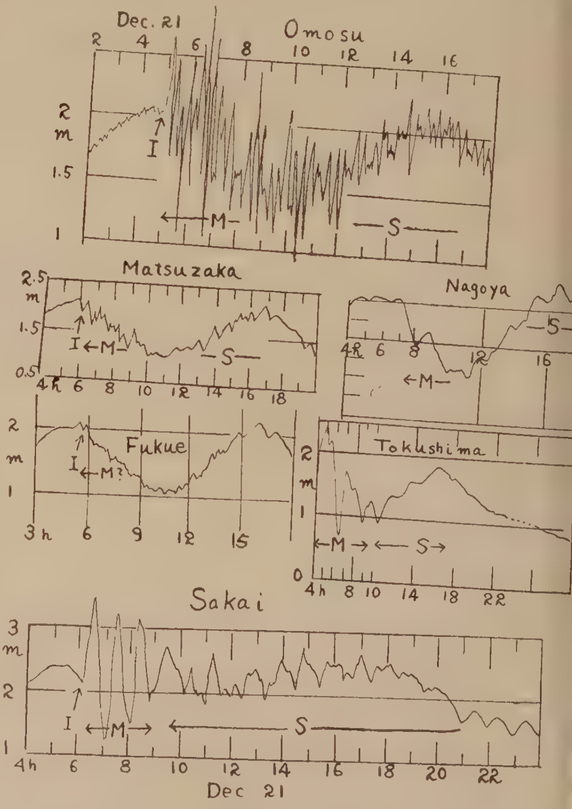

Fig. 4(*b*).

l water surface are quite difficult and the nplete hydrodynamical treatment seems to be yet given, owing to difficulties of mathematical ocesses involved. Many Japanese physicists re treated the problem based on various lrodynamical models since 1915, though satistory theory does not appear yet.

These studies are basically to solve the Laplan under some boundary conditions and here we olain the process briefly. When we assume that whole motion of water is potential flow and put the velocity potential Φ, then it satisfies

$$\delta^2\Phi/\delta x^2+\delta^2\Phi/\delta y^2+\delta^2\Phi/\delta z^2=0 \qquad (6\cdot1)$$

ere we take x and y as horizontal coordinates l z vertical one. Then Φ should also satisfy the undary condition at the surface such as

$$\delta^2\Phi/\delta t^2 + g.\delta\Phi/\delta z=0$$

(dynamic condition) (6·2)

d $\delta\zeta/\delta t^2= -\delta\Phi/\delta z$

(kinematic condition) (6·3)

ere t is time, g the gravity constant and ζ is the face elevation. Further, when we assume the ttom velocity is given by f (x, y, t) then at the ttom

$$\delta\Phi/\delta z=f\ (x, y, t) \qquad (6\cdot4)$$

Generally the surface elevation is expressed by mbinations of the type of Fourier integrals.

$$\zeta\sim\int\int_{-\infty}^{\infty} F\ (x, y, m, n)\ expi\ (\sqrt{gk \tanh kh}t \pm mx+ny)\ dm\ dn \qquad (6\cdot5)$$

where the function F is determined by the given function f, h is the depth of water, and also $k^2=m^2+n^2$.

The exact evaluation of the integral is quite difficult, so that heretofore some simplification has been applied. Generally, the wave length of tsunami is much larger than the depth of the sea, so the function F is assumed to have larger value for smaller portion of k, therefore in the integral we might put $\sqrt{gk \tanh kh} = k\sqrt{gh}$ because the contribution from integrand for smaller values of k is largest. This assumption simplifies the valuation of the integral which gives the waves propagating with the speed of long waves and especially for one dimensional case without changing wave forms. Some of the results of such computation are shown in Fig. 5d, where d (1) and d(2) are waves caused by one dimensional source, which have the wave profile exactly the same as the shock at the bottom and also the wave with equal profile propagates to both directions from the source.

The waves caused by two dimensional source are shown in Figs. d(3) and d(4), where in d(3) the bottom motion is the same as that of the circular piston which moves upward at a uniform speed during a certain interval (Takahashi, 1943, 1946, 1947) and in d(4) the motion of bottom is more continuous both in space and time, that is, the function $f(x, y, t)$ of bottom speed is given by $exp(-r^2/a^2-t^2/b^2)$ with numerical value of b=40 sec. and also r is the distance from the centre of the source (Nakamura, 1953). These two models in two dimensional source give almost similar wave

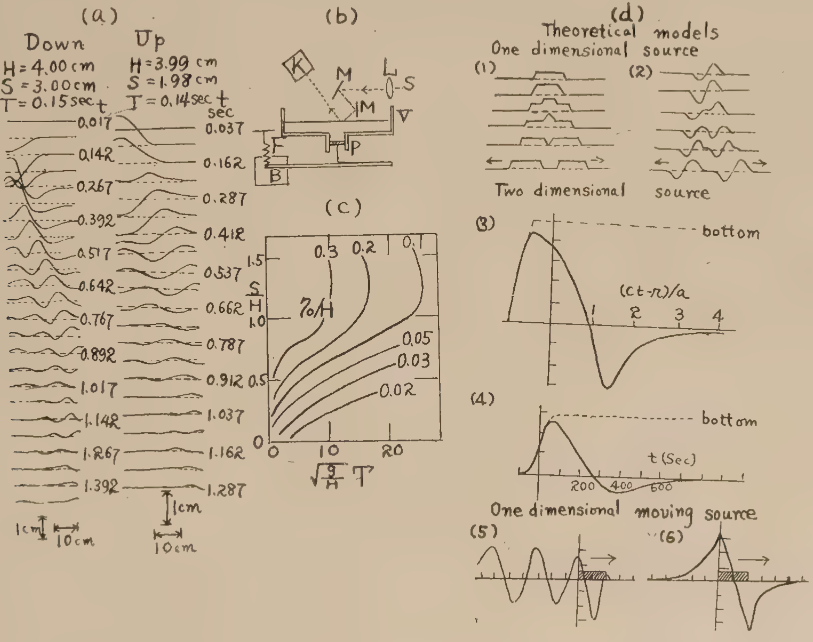
(a)
Down
Up
H=4.00cm
S=3.00cm
T=0.15sec
H=3.99 cm
S=1.98cm
T=0.14sec
t
t sec
0.017
0.142
0.267
0.392
0.517
0.642
0.767
0.892
1.017
1.142
1.267
1.392
0.037
0.162
0.287
0.412
0.537
0.662
0.787
0.912
1.037
1.162
1.287
1cm
10cm
1cm
10cm
(b)
K
M
L
S
M
V
F
P
B
(c)
1.5
S/H
1.0
0.5
0
0.3
0.2
0.1
η/H
0.05
0.03
0.02
0
10
20
$\sqrt{\frac{g}{H}}T$
(d)
Theoretical models
One dimensional source
(1)
(2)
Two dimensional source
(3)
bottom
(ct-r)/a
1
2
3
4
(4)
bottom
t (Sec)
200
400
600
One dimensional moving source
(5)
(6)

Fig. 5.

Experimental and theoretical studies about generation of tsunami.

profile, though the form of function $f(x, y, t)$ is quite different and the characteristic features of waves propagating in two dimensions, are such that the profile shows one ridge and one trough though the movement of the bottom has only an upward component as shown with broken lines and also that amplitude of the waves decreases as proportional to $1/\sqrt{r}$ owing to the effect of dispersion in diverging waves. (Lamb, pp.298–301).

Although these models based on long wave assumption give characteristic pictures of tsunamis, particularly concerning the main portion moving with the velocity of long waves, they fail to explain complete features. For example, the actual tsunamis consist of many trains, which is not explained from these models. However, when we take into account two types of models which are not simplified under the assumption of long waves, we can obtain waves consisting of trains.

One of such models is the forced waves caused by a source moving with a constant speed C. Mathematically such waves are considered as those caused from the contribution of the integrand $F(x, k)$ in ζ^* which has an infinitely large value near k_0 satisfying the relation $C=\sqrt{g \tanh k_0 h/k_0}$ and the computed wave profiles for $\frac{C}{\sqrt{gh}}=0{\cdot}5$ and $2{\cdot}0$ are shown in Fig. $d(5)$ and 6 respectively (Ichiye, 1950). They show that a source moving more slowly than the speed of long waves $\sqrt{gh}$ causes wave trains with almost the same order of wave length as the dimension of the source (which is shown as a shaded block), whereas that moving faster than $\sqrt{gh}$ produces only one trough and one ridge. Further, in this model the amplitude of waves becomes very large for the speed $C=\sqrt{gh}$ owing to resonance, where the wave profile has an intermediate form between the above two cases, when a frictional effect is taken into account. Of course, such mechanism of moving source is not always applied to all tsunamis, but some tsunamis may have been generated by such source, as suggested by the deformation of sea bottom having the progressing type which was detected by seismographs or other evidence.

Another model is in itself the same as those of $d(1)$ to $d(4)$, but we abandon the assumption of long waves in the evaluation of the integral (6·5). In such model, the integral for ζ cannot be expressed analytically, and we have to compute the integral numerically. In Fig. 6 we show one result of such calculation, where we take a source of one dimension with the half length $R=40$ km which moves upwards with a constant speed during a time

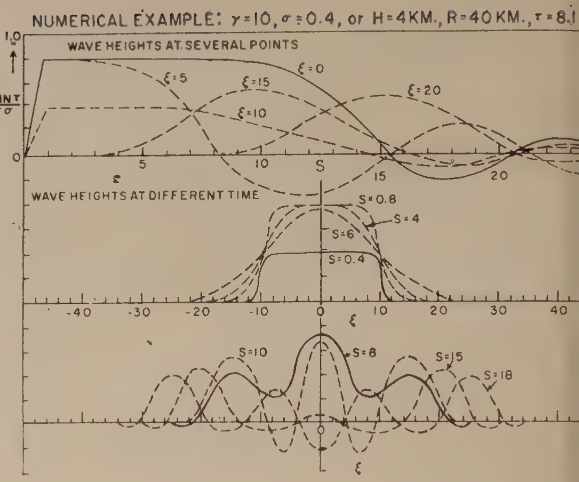

Fig. 6.

A result of numerical computation of an integral of surf elevation caused by one dimensional bottom shock. (put the depth $H=4$km, length of source $2R=80$ duration of bottom shock) $\tau=8{\cdot}1$ sec., and we take n dimensional numbers $r=R/H$, $\delta=\tau\sqrt{g/H}$, $x/H=$ $\sigma(t/\tau+1)=S$, where x is the distance from an origin t is time since the beginning of bottom motion.

interval of $\tau=8{\cdot}1$ sec. in a sea of depth $h=4$ (Inchiye and Hidaka, 1957). The wave profiles several points are shown in the upper part those at different stages are shown in the lo part, the latter of which corresponds to those $5d(1)$. Though the movement of the source is same in this model and that of Fig. $5d(1)$ the files obtained are quite different, first because surface profile changes from an initial form sim to the bottom motion and secondly that the wa have many trains in this model, as time proce after the end of the motion of the bottom, whic due to dispersion of waves, where in this model take into account all components of waves hav different wave length. When we compare Fi with the result of model experiment in Fig $5a$, can see that the present model gives more c agreement to the experimental result than of Fig. $5d(1)$.

6. Propagation of tsunamis

The tsunami propagate with a speed of waves, that is $\sqrt{gh}$ and therefore the refract phenomenon occurs when they travel in the se a variable depth. This effect is particularly portant off the Northern coast of Japan, w many tsunamis in the past attacked the co In Fig. $7a$, we show conventional refract diagram, which is drawn for the waves genera in the source corresponding to tsunami in and solid lines are the orthogonals to the fronts shown with broken lines, where the hei of tsunamis inversely proportional to the dista between neighbouring orthogonals. These cu clearly indicate that the tsunami generated rthern Japan converge towards the coast of nriku district, because the Japan trench running nost parallel to the coast has an effect like a nverging lense for tsunami waves. One reason at the Sanriku district was often attacked by vere tsunami in the past as shown in Fig. 1 is plained by such effect of convergence of the ergy of tsunami.

---

* Here we consider one dimensional case in (6·5), where $n=o$, $k=m$.

The tsunamis are also affected with the reflec- n where the change of depth is abrupt as well at the coast. On the other hand, even when e depth is variable, tsunamis propagate without lection where its change is gradual and in such se the amplitude varies proportional to $b^{-\frac{1}{2}}h^{-\frac{1}{4}}$ or cording to Green's law, where b is the width of canal if the waves proceed in a canal. (Lamb, . 273–275). Actually, the tsunamis are partially flected when they propagate in a sea with a riable depth and the larger the wave length, the re the reflection.

In order to explain this condition more quantitavely, we consider the waves propagating from the gion with uniform depth h_1, into the region with through the portion of variable depth, and we t the amplitude of incident, reflected and ansmitted waves as A, B and E, respectively. hen B/A or E/A is dependent on frequency or ave length of incident waves for a certain ometrical configuration of the transient part. hen the wave length or period of incident waves ecomes infinite, perfect reflection occurs and we ve

$$/A\to 2\sqrt{h_1}/(\sqrt{h_1}+\sqrt{h_2}),\quad B/A\to(\sqrt{h_1}-h_2)/(\sqrt{h_1}+\sqrt{h_2})$$

On the other hand, when it decreases, there is reflection and

$$E/A\to(h_1/h_2)^{\frac{1}{4}},\quad B/A\to 0$$

chiye, 1951).

Moreover, in a transient part the effect of iction might become more conspicuous, because e change of depth causes more turbulence than a sea with uniform depth. The attenuation of e amplitude of tsunami which pass through ch transient part is expressed by (Ichiye, 1949)

$$exp\,\{-\tau o(k+4\nu\pi^2\sigma^2/ghm)\},\quad \tau o=\int\frac{dx}{\sqrt{gh}}$$

here k is a coefficient of a friction which is sumed as proportional to the velocity and ν is a rizontal eddy viscosity, τo is a travel time of e waves in a transient part, the mean depth of hich is hm and σ is the frequency of the incident aves. The schematical forms of E/A as a function frequency or wave length is shown in Fig. 7b, th or without friction, where the sinusoidal part the curves is due to the effect of proper cillation in a transient region and we can see that the effect of friction diminishes the amplitude of shorter waves.

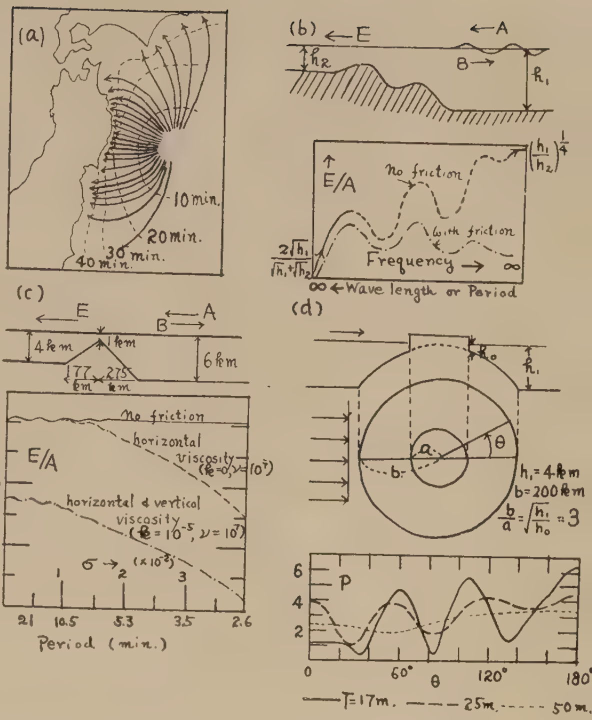

Fig. 7.

Some properties of tsunami waves propagating in a sea of variable depth.

The effect of reflection is especially important when the tsunamis propagate into a continental shelf where theratio $h_2/h_1<1$. Presumably tsunamis in the initial stage consist of waves of various wave length. However, when they approach the coast, the longer waves are reflected and shorter waves are attenuated by friction at the continental shelf, so that there should exist optimum wave length which arrives at the coast after passing through a shelf. On the other hand, when the depth changes very gradually and yet the distance of portion with variable depth is long, the effect of friction predominates over that of reflection, so that the shorter waves are more dissipated, thus tsunami waves at a distant station from the source have usually longer periods than those in the neighbourhood of the source as seen in mareograms of tsunami in 1933 shown in Fig. 3.

Further, when we look back at Fig. 1 we can see that tsunamis generated off the Northern coast of Japan usually did not attack the Southern coast and vice versa. One reason has been explained as an effect of refraction as stated above, and another is certainly considered as an effect of Bonin-Mariana ridge which is located between these two regions. In Fig. 7c the amplitude ratio E/A of transmitted and incident waves is computed as a function of periods of incident waves, assuming the waves proceed from the Northern sea to the South passing through the ridge consisting of two straight lines, as shown in the figure. We can see the noticeable effect of friction because without friction this ratio is almost constant and larger than one, whereas it decreases quite remarkably even for a moderate value of friction constant $k=10^{-5}$ and eddy viscosity $v=10^7$ (c.g.s.).

In some islands located in the midst of the ocean, such as Hawaii, heights of tsunami become quite remarkable even for waves of distant origin (Shepard *et al*, 1950). This phenomenon is usually considered as an effect of diffraction of tsunami by an island. However, this is not exactly true, because wave length of tsunamis is much longer than a dimension of an island, so that the existence of the island does not much affect the waves, if the island is surrounded by a sea of constant depth. On the other hand, such island is usually surrounded by a slope of varying depth which has much larger diameter than the island and when the waves approach such region oscillation of water in the slope is excited, so that when the diameter of slope has a comparative order of magnitude such forced oscillation becomes very conspicuous owing to some sort of resonance. (Homma, 1952). The theoretical result based on this model is shown in Fig. *7d*, where we assume a circular island of a radius a surrounded by a slope of a depth given by $h=h_0(r/a)^2$. When we put the amplitude ratio of the waves along the island and the incident ones P, this is a function of an angle measured from the rear of the island and also of the period of incident waves T. We can see that the waves of shorter periods show larger maximum amplitude and also that they have more variable height distribution along the coast, whereas those with long period have almost uniform height which is smaller than the maximum height in the shorter waves. In these curves the wave lengths for $T=17$, 25 and 50 min are about 200, 300 and 600 km, respectively and $b=200$ km, so that for the shortest waves such resonance phenomenon is most conspicuous. If we do not take into account the slope, the height distribution along the coast for the same island becomes more uniform and the height itself becomes smaller than in this model.

Since tsunami propagate with velocity of long waves, we can predict their travel time when we know the depth of ocean. This principle was applied for the tsunami traversing the Pacific Ocean by Bache already in 1886 (Dietrich, 1957). However, in earlier days the depth of contour of the Pacific Ocean was not so exactly known and also the distance between the source of tsunami and tidal stations was not correctly measured and some authors (Miyabe, 1934), suggest that the computed travel time is shorter than the observed one. However, when we use a stereographic map satisfying the condition that the projected cir
remains as a circle and apply the Hugen's meth
to compute the travel time (Hirono, 1952); th
the error in the distance due to the distortion o
map can be avoided and better agreement
achieved as shown in the next table which is bas
on the data in 1933-tsunami.

TABLE 3

Travel time to	Honolulu		SanFransisco		SantaMonica		Iqui
	h	m	h	m	h	m	h
Observed	7	32	10	22	10	50	21
Miyabe's comp.	7	8	9	30	10	11	
Hirono's comp.	7	32	10	12	11	06	21

7. One example of the distribution of height of tsunami along the coast

Before proceeding to detailed discussion abo
dynamics of tsunamis near a coast we show t
distribution of their heights along the Northe
coast of Japan, based on the measurements at t
tsunami in 1933, about which many descriptic
have been given already in this report. Tl
tsunami was smaller in its scale than that in 18
which was generated almost at the same pla
that is, off Northern Japan, and yet the maximu
height reached 20 to 30 meters as shown in Fig.

These charts indicate that the maximum wa
height of 10 to 30 meters were experienced alo
the coast shown in sub-charts (*d*) and (*e*). Furth
detailed examination of these distribution cha
suggests that the height is much influenced
coastal configuration. For example, in a sub-ch
(*a*) we can see that the height to the East of Ca
Erimo which is located in the middle of the ch
is about 4 to 9 m, whereas it is only 2 to 5 m
the West. Generally speaking, the height is larg
at the portion exposed directly to the open se
particularly at the tip of capes or projection, exce
in some bays shown in the sub-chart (*e*).

As seen from these charts, the coast of Northe
Honshu is quite rich in small bays, and it is o
Lias type. As stated later, when the long wav
enter into a bay, the oscillation of water in t
bay is excited and when the incident waves
also oscillatory type, there occurs the phenomen
of resonance, if the period of the waves and th
of the proper oscillation of the bay coincide.
Fig. 9*a*, we show the frequency distributions of t
period of proper oscillation in bays on the Sanri
coast which is computed from the formula $4l\sqrt{gh}$
where l is the length of a bay, h_m the mean dep

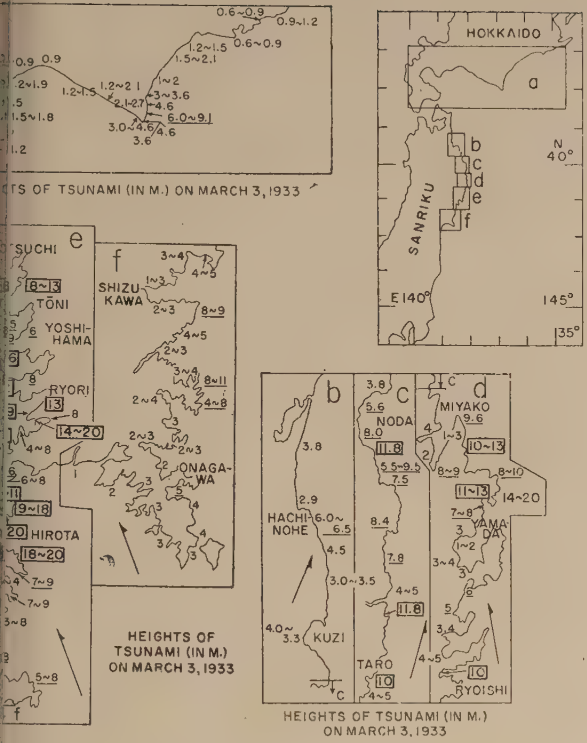

Fig. 8.

Heights of tsunami (in M.) of March 3, 1933 along the coast of Northern Japan.

d in a (1) only larger bays are counted whereas (2) all bays in the district are included. We can e that the predominant period of larger bays in is district is between 20 to 25 min, and that of e whole bays is between 5 and 10 min. On the her hand, the period of tsunami in the generated ea or after the passage of continental shelf is also nsidered to be between 10 to 30 minutes, so that can conclude that one reason of severe tsunamis this district may be, as a whole, due to the sonance of the water in bays to the incident ves, though individually the period of each bay ght be different from the incident waves.

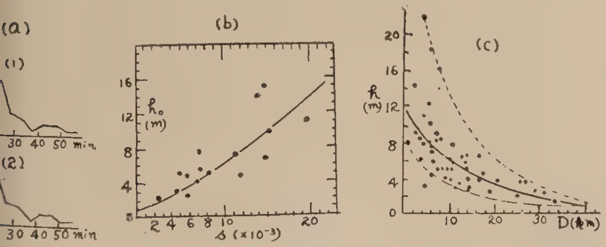

Fig. 9.

Frequency distributions of periods of oscillation in bays (*a*) and relationships between heights of tsunami and bottom slope (*b* and *c*).

The bottom topography near the considered gion is not shown in these charts, but there are some relationships between the height of the tsunami and the bottom configuration, which is shown in Fig. 9*b* and *c*. The height of the tsunami within a bay was more or less modified by the configuration of the bay, so that it is better to consider the height at the mouth of the bay. In Fig. 9*b* such height for all bays h_0 is plotted against the slope of the bottom outside each bay and we can see that these points indicate the relationship

$$h_0 = 1{\cdot}0 + 2{,}500\, S^{1.35}$$

where h_0 is in meters and S is a slope. (Matsuo, 1934) In Fig. 9*c*, the height on the open coast h which seems to be more representative for the tsunami on the coast than h_0 is plotted against the distance D (in km) from the coast to the 100m depth contour, and these points seem to be represented by a curve

$$h = 12{\cdot}3e^{-0.067D}$$

(Yamaguchi, 1934). Both relationships indicate that the height becomes larger as increasing bottom slope. This fact might be explained also by the theory of the propagation of long waves in a variable depth, which is discussed in the last section, because when the slope is small, the waves travel in a shallow sea for a long time and the bottom friction diminishes the amplitude conspicuously, whereas when the slope becomes steeper they arrive at the coast without much influence from the bottom friction and then at the coast they are reflected, so that the height there increases rapidly.

8. Behaviour of tsunami near the coast

Here we explain the behaviour of tsunami when they approach the coast. After being generated in the midst of ocean, they enter into a continental shelf before arriving at the coast. Some part of the waves are reflected at the continental slope as stated in section 7, and the transmitted waves have their amplitude increased and their length diminished since the former is proportional to $h^{-\frac{1}{4}}$ and the latter to $h^{\frac{1}{2}}$, so that the steepness of the waves also increases.

When the incident waves are of solitary wave, there occurs a secondary oscillation in the shelf with a period of $To = 4L/\sqrt{gh}$, where L is the length and h is the depth of the shelf, and this oscillation is similar to that in a bay with the same length and depth. On the other hand, if the incident waves are of oscillatory type, the oscillation in the shelf shows resonance phenomenon, its amplitude $\dot{E}$ being extremely large when the period of T of incident waves coincide with T_0 or its integral fraction, with the maximum resonance at $T = T_0$, that is, for the longest period of the proper oscillation (Fig. 10*a*).

After passing through the shelf, these waves have their amplitude increased and length diminished more and more, as approaching the coast or entering into a bay, and sometimes they roll and break as a surf and in many cases where the wave height is not so large they flood the land gradually.

The height of tsunami in a bay is closely associated with a configuration of the bay and usually in a deep bay of V-shape or U-shape which is open to the ocean directly the height reaches maximum value. On the other hand, in a long bay with more shallow depth or a bay of complicated contour the height is much diminished owing to the bottom friction and reflection by the lateral boundaries Fig. 10*a*.

The distribution of the height within a bay also is much influenced with the configuration, and from the examples in the tsunami of 1933 we can classify three groups as shown in Fig. 10*b*, where we plot the height measured along the side of a bay against

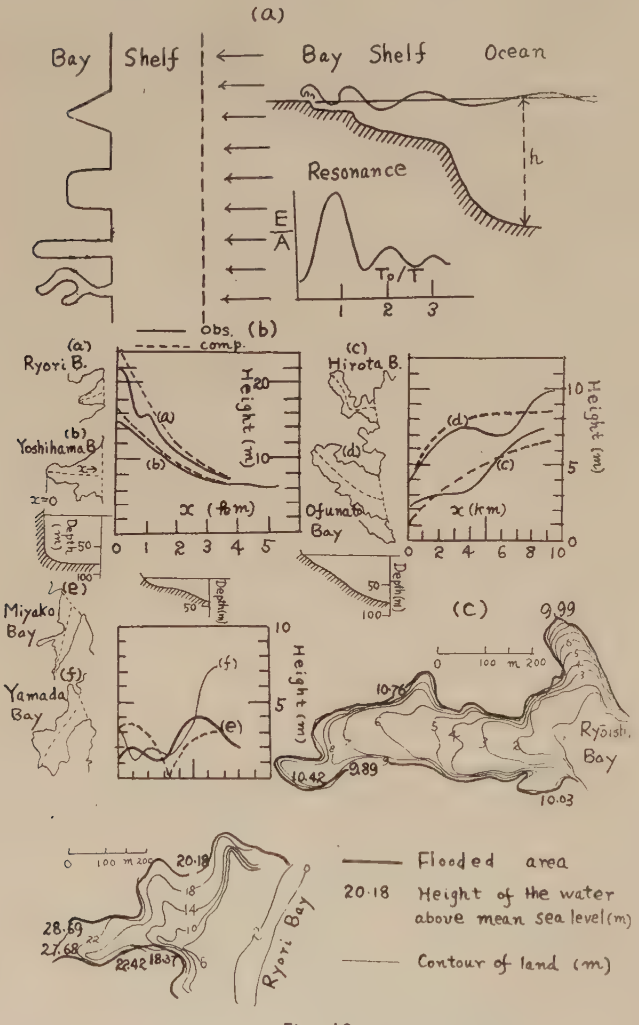
(a)
Bay
Shelf
Bay
Shelf
Ocean
Resonance
h
E/A
T_0/T
1
2
3
obs.
comp.
(b)
(a) Ryori B.
(b) Yoshihama B.
x=0
Depth
50
100
Height (m)
20
10
(a)
(b)
x (km)
0 1 2 3 4 5
(c) Hirota B.
(d)
Ofunato Bay
(d)
(c)
10
5
0
x (km)
0 2 4 6 8 10
Height (m)
Depth (m)
50
100
(e) Miyako Bay
(f) Yamada Bay
(f)
(e)
10
5
Height (m)
(c)
9.99
0 100 m 200
10.76
Ryōishi Bay
10.42
9.89
10.03
0 100 m 200
20.18
18
14
10
28.69
27.68
22
22.42
18.37
6
Ryori Bay
Flooded area
20.18 Height of the water above mean sea level (m)
Contour of land (m)

Fig. 10.

Behaviour of tsunami near a coast.

the distance along the central line from the en the bay, and the shape of each bay and de distribution of it are also shown. The first gr bays *a* and *b* shows that the maximum heigh attained at the end, which is also highest it among the three groups. The second group bay and *d* has a maximum value at the mouth. In third group bays *e* and *f*, which has the lowest v among the three, the minimum height is foun the midst of a bay.

As a dynamical explanation of such differe we can suggest that the bays belonging to the group are relatively short in length with V U-shape and not only is the mean depth larger t other groups but also the deep sea continues to end of the bay, so that the waves coming from mouth can proceed to the end without reflection dissipation at the bottom. On the other hand, bays of the second group are relatively long and coast line is more complicated, with decrea depth towards the end, the mean depth itself b more shallow than the first group. Therefore such bays the waves are dissipated by the bot friction which becomes more effective near the of the bay or they are partially reflected by a ping bottom or curved boundary, so that the am tude decreases towards the end. The bays of third group are similar in their configuration the depth is much smaller and also more or complicated in the boundary. In such bays, period of the proper oscillation increases owin small depth, so that it becomes larger than tha the incident waves. In such cases there appea nodal line in the midst of the bay, which seems correspond to the minimum height and also effect of bottom friction diminishes the he generally.

When we assume that the incident waves at mouth as a sine wave such as $e^{i\sigma t}$ and consider depth h and breadth b of a bay are expressed power law of the distance x from the end such a

$$h=h_0\xi^m,\ b=b_0\xi^n,\ \xi=x/l \qquad ($$

where l is the length of the bay, then we obtain distribution of amplitude of the waves in a given by

$$E\sim\xi^{\alpha}\,[J_p(\beta\xi^{\gamma})\,\{Y_p(\beta)+KY_{p+1}(\beta)\}$$

$$-Y_p(\beta\xi^{\gamma})\,\{J_p(p)+KJ_{p+1}(\beta)\}]$$

where J and Y are Bessel Function of the first the second kind and $a=(1-m-n)/2$, $\gamma=1-$

$$p=\frac{a}{r}$$

$$\beta=l\sigma/\sqrt{gh_0},\ \ K=\kappa\sqrt{gh_0}/\sigma$$

in which κ is the ratio of frictional coefficien the bottom friction at the end to horizontal viscosity where the flux of water U is put t

portional to $-\delta U/\delta x$, or $\kappa U= -\delta U/\delta x$, so that
has a dimension of a length, and $\kappa=\infty$ corres-
ds to the case of complete reflection at the end
reas $\kappa=o$ corresponds to the case of no boundary
he end or the free passage of the waves there.
iye, 1952). For a bay of given geometrical
figuration, we obtain the amplitude distribution
(9·2) similar to that of group 1 for $\kappa=\infty$ or
plete reflection at the end and that similar to
group 2 for the intermediate value of κ ($\kappa=o$
s the vanishing height at the end) and also
n β exceeds a certain critical value, then there
ears a nodal line as in the group 3. In Fig. 10b
computed distribution of the amplitude is also
wn for each group, where we take $m=o$ and $n=\frac{1}{2}$
group 1 and put $K=\infty$ whereas we put $m=1$ and
$\frac{1}{2}$ for the group 2 and 3, by taking the constants
h as h_0, b_0 determined from the actual geometri-
configuration of each bay and also putting
$=0{\cdot}1$. These curves agree with the observed
ribution at least qualitatively, therefore we can
clude the dynamical explanation stated above,
re the difference between group 2 and 3 is only
to the condition that in the former the value
β is below the critical value, whereas in the
er it exceeds the one, or since this quantity is
portional to the ratio of the period of proper
illation of the bay T_0 to that of the incident
es T, so that this means that the period T_0
omes larger due to the decrease of $\sqrt{gh_0}$.

When tsunami finally arrive at the shore, there
ur two kinds of phenomena, according to steep-
s of the front as stated above. When the
pness is very large, the front proceeds as if it
e a vertical wall of water and then it rolls and
aks as surf at the place where the depth is
ost the same as the height. On the other hand,
n the steepness is smaller, the tsunami just
rflows a land because the sea level rises above
mean position. In Fig. 10c we show these two
mples from the data in the tsunami of 1933,
re the upper chart corresponds to the latter
e and the flooded area by tsunami almost coin-
e with the contour-lines, whereas the lower chart
resenting the former case indicates that the
er reached higher and higher as it advanced.

After overflowing on land, tsunami flows in the
e manner as river water, so that it flows towards
direction where the resistance is least, that is,
re the slope is least and also the ground is
raulically most smooth, or there may be no
ldings, trees or other obstruction. In such
ourable places, the current gains its velocity
re than 1 m/sec, so that it causes much severe
nage to buildings even when the height itself
small and only a few meters. (Ishimote and
giwara, 1934, Ichiye 1949).

Concluding remarks

This article is aimed to show a synthetic review
the researches of tsunami carried out in Japan,
so that data and facts about tsunami are limited only to those obtained in Japan. However, it seems to be quite necessary to include the whole results of the studies in the world, especially in the United States, in order to give complete descriptions of the phenomenon of tsunami. The author hopes to fulfil such requirement in the future, so that he can make up the incompleteness of this article.

In conclusion, some remarks are added about how to develop knowledge about the dynamical properties of tsunami.

(1) The dynamics of the generation of tsunami are not yet fully understood, owing to the mathematical difficulties accompanying the problem. These difficulties may be solved in two directions. One is the model experiment in a tank and another is a high speed computer, both of which are much developed in recent years.

(2) The motion of sea bottom due to the earthquake should be measured with some instruments. This problem seems to be very important not only in the dynamics of tsunami but also for seismology and geology.

(3) In order to know the response of sea surface to bottom motion, actual record of tsunami which is not perturbed by bottom topography and coast should be obtained. For this purpose, recording instruments should be installed at small Islands in the midst of the ocean.

(4) We need to know the motion of water near the bottom as tsunami is passing, because the effect of bottom friction is very important when it proceeds in the sea where the depth is variable, as stated before, and yet we are now very poor in knowledge about the effect of friction on long waves or how such waves cause turbulence, when they travel in a shallow sea.

(5) After tsunami approches the coast, height distributions are much affected by coast or bottom topography, so that the height is sometimes quite different at places which are located very close to each other. It should be explained that the tsunami near the coast behaves not only as a wave but also as a current. Such problems might be solved also with model experiment and by solving hydrodynamic equations of non-linear type, since in this region curvatures of the flow, friction and effect of finite amplitude become more important.

Acknowledgement

This report is based on the manuscript of a lecture given at Woods Hole Oceanographic Institution. The author expresses his hearty thanks to Dr. C.O.D. Iselin, D. R. Ketchum, Dr. J. Hersey and other people of the Institution for much useful advice and encouragement.

Literature

Darbyshire, J. and Ishiguro S, 1957 : *Tsunami Nature*, Vol. 180, No. 4577.

Dietrich, G., 1957 : *Alligemeine Meereskunde*, pp. 326-327, Berlin.

Hirono, T., and Hisamoto, S., 1952 : A method of drawing the wave front of tsunami on a chart, *Geophys. Mag.*, Vol. 2.3.

Homma, H., 1950 : On the behaviour of seismic sea waves around a circular island, *Geophys. Mag.* 21.

Hydrographic Office, Japan, 1948 : Report on the Nankai Earthquake in 1946. *Hydrogr. Bull.*

Ibid, 1948 : Report of the Mikawa Earthquake in 1945. (Change of sea bottom in Mikawa Bay). *Ibid.*

Ichiye, T., 1948 : Tsunami as an overflow on land (in Japanese), *Umi to Sora* 25.

1949 : On the theory of tsunami (in Japanese) *Umi to Sora*, 27,3.

1950 : On the generation of tsunami. *Oceanogr. Mag.* 2, 3.

1950*b* : On the wave caused by the disturbance travelling at the bottom (1). *Mem. Kobe. Mar. Obs.* 8.

1951*a* : On the oscillation in a continental shelf or bay. *Mem. Kobe. Mar. Obs.* 9.

1951*b* : On the propagation of long waves, *ibid.*

1952 : On the amplitude of tsunami in a bay. *Ibid*, 10.

Ichiye, T., and Hidaka K., 1957 : On the generation of tsunami caused by the impulsive motion of a sea bottom. *Jour. Oceanog. Soc., Japan* (to be published).

Ishimoto, M., and Hagiwara T., 1934 : The tsunami considered as a phenomenon of sea water overflowing the land. *Bull. Earthq. Res. Inst. Suppl. Vol.*

Kawasumi, H., 1951 : Measure of earthquake danger and expectancy of maximum intensity throughout Japan as inferred from seismic activity in historical times. *Bull.* *E*
Res. Inst. 29.

Lamb. H., 1932 : *Hydrodynamics*. Cambridge.

Matsuo, H., 1934 : Estimation of energy of tsunam
protection of coasts. *Bull. Earthq. Inst. Suppl. Vol.*

Miyabe, N., 1934 : An investigation of the Sanriku ts
based on Mareogram data. *Bull. Earthq. Res. Inst. Supp*

Nakamura, K., 1953 : On the waves caused by the
mation of the bottom. *Science Rep. Tohoku Univ. Ge*
5, No. 3.

Nasu, N., 1934 : Heights of tsunami and damages to
tures. *Bull. Earthq. Res. Inst. Suppl. Vol.*

Omote, S., 1947 : On the central area of seismic sea
Bull. Earth. Res. Inst.

Shepard, F. P., MacDonald G. A., and Cox, D. C.,
The tsunami of April 1, 1946. *Bull. Scripps. Inst.* 5.

Takahashi, R., 1934 : A model experiment on the mech
of seismic sea wave generation. *Bull. Earthq. Res.*
Suppl. Vol.

1942, 1946, and 1947 : On seismic sea waves caus
deformations of the sea bottom. *Bull Earthq. Res.*
20, 23 and 25 (in Japanese).

1943 : Transmission and reflection of tsunami
at sea ridges and continental shelves. *Bull. Earthq*
Inst. 21.

1950 : On estimation of further tsunami damage the Pacific coast of Japan. *Bull. Earthq. Res. Inst.* 29.

Yamaguchi, S., 1934 : Abnormally high waves or tsu
Bull. Earthq. Res. Suppl. Vol.

Yoshida, K., 1948 : On the partial reflection of long w
Geophys. Note 31.

1950 : On the estimation of reflection coefficier
tidewaves, tsunami and swell. *Geophys.* Note 3, 14

Reprinted from
THE PORT ENGINEER
Vol. VII, No. I

Woods Hole Oceanographic Institution.
Contribution No. 952

Contribution No. 953

Deep-Sea Research, 1958, Vol. 5, pp. 80 to 82. Pergamon Press Ltd., London

LETTER TO THE EDITORS

The abyssal circulation

(*Received* 18 *February*, 1958)

IN my survey of the theories of ocean currents (*Deep-Sea Res.*, 1957, 4, 149-184) several schematic interpretations of ocean circulatory patterns are presented. In this letter I wish to show how, using the same principles, it is possible to sketch in broad outline the flow pattern for the abyssal circulation of the world ocean.

It seems likely that the low temperature of deep waters in the world ocean is maintained in the face of downward diffusion of heat from the warm surface layers by a very slow upward component of velocity in the deep water. An adequate theory of the thermocline would, presumably, deduce this upward velocity as a function of surface heating, turbulence parameters, etc. We might regard the thermocline as a " pumping mechanism " which slowly draws up deep water and hence actually determines the rate of flow of the abyssal circulation. An estimate of the maximum upward component of velocity under the thermocline, $w_{\max}$, is given in terms of the depth of the thermocline, z_t, by the equation.

$$w_{\max} = \frac{\sqrt{2}}{4} \frac{\beta g \alpha l}{f^2} z^2{}_t \, \theta_0.$$

This equation is obtained from a very primitive model* of convection on a beta-plane and contains neither the turbulence parameter nor the artificial basic stability explicity. Both enter implicitly, of course, through the very structure of the model ; both are basically objectionable, are introduced to circumvent our lack of physical knowledge about turbulence and our inability to handle the non-

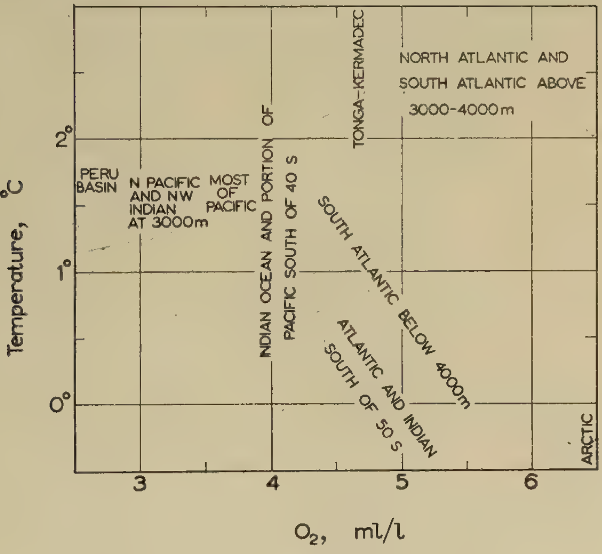

Fig. 1.

---

*HENRY STOMMEL and GEORGE VERONIS (1957) *Tellus* 9, 401-407, to which the reader is referred for definitions of quantities : the above relation being derived by substituting $Gz_t = 1$ into equation (20).

linearity of the energy equation respectively. Consequently our conclusions are limited, at best, to order of magnitude considerations. If we take as representative oceanic averages

$$\beta = 2 \times 10^{-13}\ \mathrm{cm}^{-1}\ \mathrm{sec}^{-1}$$

$$g = 10^{3}\ \mathrm{cm\ sec}^{-2}$$

$$\alpha = 2 \times 10^{-4}\ {}^{\circ}\mathrm{C}^{-1}$$

$$\theta_0 = 10^{\circ}\mathrm{C}$$

$$f = 10^{-4}\ \mathrm{sec}^{-1}$$

$$l = 5 \times 10^{-9}\ \mathrm{cm}^{-1}$$

$$z_t = 2 \cdot 10^{4}\ \mathrm{cm}$$

we find that $w_{\max}$ is of the order of 3×10^{-5} cm sec^{-1}. Since the area of the ocean at 2000 m is about 3×10^{14} m^2, the total upward flux of water across the 2,000 m level over the entire world ocean is of the order 90×10^6 m^3 sec^{-1}, about twice the maximum estimated by analysis of hydrographic data. The slow upward flow over most of the ocean must be compensated for somewhere by downward flowing sources of deep water. I envisage these deep-water sources as occurring in very limited areas of weak gravitational stability where the thermocline " springs a leak." The location of these sources is apparently very sensitive to climatic factors ; we determine it by consideration of the distribution of dissolved oxygen in the ocean below 3,000 m (Fig. 1). Evidently the two sources are in the North Atlantic, and in the Weddell Sea (heavy black circles in Fig. 2); there is no source in the Arctic regions of the Pacific Ocean. The simple beta-plane convective model also assures us that the wind has no effect on the water below 2,000 m. Therefore, we have a distributed " sink " more or less over the entire ocean below 2,000 m acting on the water below ; and two point " sources." To complete the picture of the thermal circulation in the ocean we must connect the distributed sink

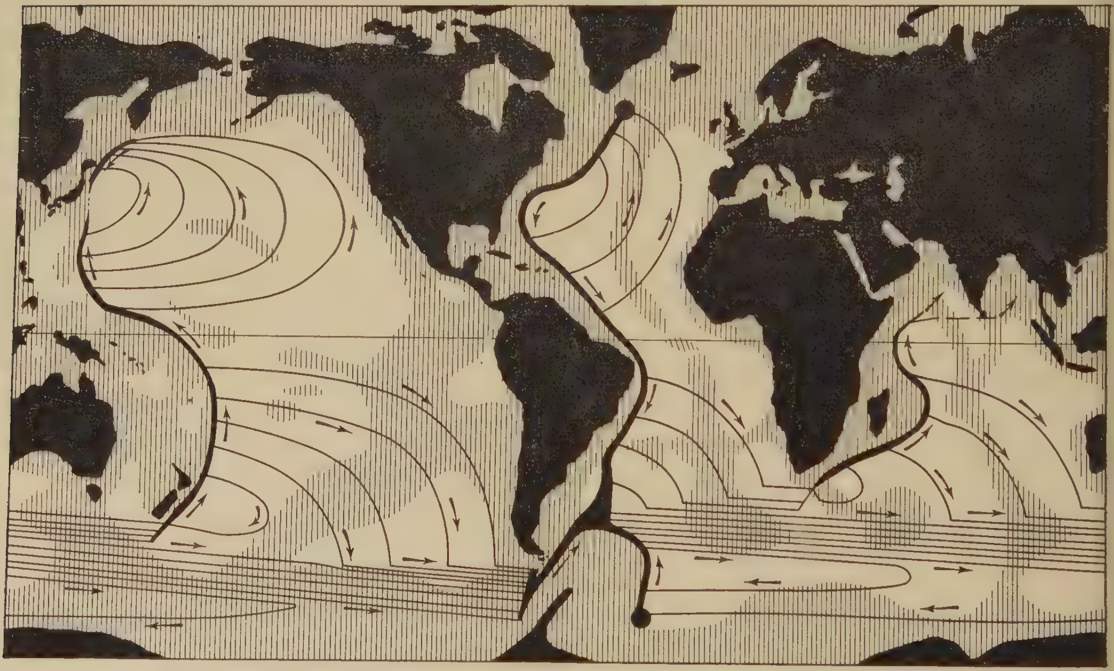

Fig. 2.

to the sources in a way consistent with the dynamics of the fluid on a beta-plane or rotating sphere.

The streamlines in Fig. 2 are sketched following the modified form of Goldsbrough's method for the rotating sphere as described in my survey article. Because of the distributed " sink " the flow below 2,000 m is everywhere horizontally convergent, hence the meridional component of velocity below 2,000 m must everywhere in the interior of the ocean be directed away from the equator ($\beta v = -f \operatorname{div}_h \vec{v}$): except at the equator itself where it must vanish. Having fixed the meridional component and vertical component, the zonal component is determined by the continuity equation working westward from the eastern coasts. At the western coasts intense boundary currents are introduced as necessary to connect with the sources. The chief ambiguity is how much water to admit through Drake Passage ; the Antarctic Circumpolar Current Transport is fixed however. Summarizing the features of flow deduced in Fig. 2 : If the two sources each have strength 20 ($\times 10^6$ m^3/sec), then the western boundary currents are : western North Atlantic, 24 southward ; western South Indian, 14 northward ; western South Pacific, 30 northward ; western North Pacific, less than 10, directed toward 30°N. latitude circle. The zonal transport of the Antarctic Circumpolar Current (below 2,000 m) is 50 across 55°S. latitude circle. In the interior of all oceans at mid-latitudes below 2,000 m the mean meridional component of velocity is of the order of 0·03 cm sec^{-1}. The value of $w_{\max}$ is $1{\cdot}5 \times 10^{-5}$ cm sec^{-1}.

The above presentation is in the nature of a *tour-de-force.* One cannot pretend that it describes the the abyssal circulation accurately in detail.

Woods Hole, Mass., U.S.A. HENRY STOMMEL

Contribution No. 953 *from The Woods Hole Oceanographic Institution.*

Printed in Great Britain by The Salisbury Press Ltd., Publicity House, Wilton Road, Salisbury, Wilts. (9601)

Contribution No. 955

[Reprinted from THE JOURNAL OF GENERAL PHYSIOLOGY, November 20, 1958,
Vol. 42, No. 2, pp. 243–250]
Printed in U.S.A.

DELAYED LIGHT ACTION SPECTRA OF SEVERAL ALGAE IN VISIBLE AND ULTRAVIOLET LIGHT*, ‡

BY G. C. McLEOD

(*From The Biological Laboratories, Harvard University, Cambridge, and The Woods Hole Oceanographic Institution, Woods Hole*)

(Received for publication, February 24, 1958)

ABSTRACT

Action spectra for delayed light production by several algae were determined from 250 to 750 mμ incident light.

In the visible portion of the spectrum the action spectra resemble those reported by previous workers for photosynthesis and light emission. Blue-green algae had a maximum at 620 mμ, red algae at 550 mμ, whereas green and brown algae have action spectra corresponding to chlorophyll and carotenoid absorption.

In the ultraviolet portion of the spectrum delayed light is emitted by algae down to 250 mμ incident light.

The action spectra of the different algae are not alike in the ultraviolet portion of the spectrum.

This indicates that pigments other than chlorophyll must be sensitizing or shielding the algae in the ultraviolet region.

INTRODUCTION

Strehler and Arnold (10) showed that after a period of illumination, light was given out by plants for as long as 2 minutes, with a very low intensity. The action spectrum of the production of the delayed light was shown to be the same as the action spectrum of photosynthesis in both algae and higher plants (10). Later experiments demonstrated that the emission spectrum of the delayed light is the same as the fluorescent spectrum of chlorophyll in the living plant, and that it was chlorophyll which emitted the delayed light (1).

In the present experiments, the production of delayed light by several marine and fresh water algae was used to determine the action spectrum from 250 to 750 mμ.

Materials and Methods

The fresh water algae were from the culture collection of Dr. William Arnold of Oak Ridge, Tennessee. The blue-green alga, *Anacystis nidulans*, was grown in the

---

* Work sponsored by the National Science Foundation, Grant No. G-2510.

‡ Contribution No. 955 from The Woods Hole Oceanographic Institution.

Gerloff *et al.* (6) Chu No. 10 medium. The red alga, *Porphyridium cruentum,* was grown in the Punnett and Chambers adaptation of R. H. Swain's medium. Both of these species were grown at 20°C. and illuminated with daylight type fluorescent tubes. A green alga, *Chlorella pyrenoidosa* (Emerson's strain), was grown in Knop's solution at 20°C. under red fluorescent tubes with 5 per cent carbon dioxide in air.

The following marine algae were obtained from the culture collection of Dr. John H. Ryther of The Woods Hole Oceanographic Institution: a green alga, *Dunaliella euchlora*; a chrysophyte, *Monochrysis sp.*; and, two diatoms, *Phaeodactylum tricornutum* and *Coscinodiscus sp.* All marine algae were grown in an enriched sea water medium at 20°C., with 5 per cent carbon dioxide in air, and illuminated with red fluorescent tubes.

TABLE I

Transmission of Standard and Modified Knop's Medium between 225 and 460 mμ

mμ	Standard Knop's medium	Modified Knop's medium (minus Fe salt, 0.0001 per cent)
460	95.3	99.6
400		
375	88.8	99.2
350	75.5	99.2
325	56.0	94.5
300	37.2	82.0
275	22.8	91.8
250	19.0	77.1
225	24.5	

(1 cm. cell, Beckman DU spectrophotometer)

Cells were centrifuged out of the culture medium and transferred, after washing, to Knop's medium minus the iron salt. The modified Knop's medium was made up with 2.5 per cent NaCl for the marine algae. Table I gives the transmission of standard and modified Knop's medium in the ultraviolet portion of the spectrum. The action spectrum was made with a suspension transmitting 85 to 95 per cent of the light from 250 to 750 mμ.

Optical Methods

Since the method of measuring delayed light production has already been adequately described (1, 2, 10), only the modifications in equipment are described here

Light from a 2 kilowatt xenon high pressure arc lamp operated from a Miller D.C. arc welder was focussed on the entrance slit of a Hilger monochromator which has apertures of $f_{1.9}$ and f_6. The intensity of illumination was controlled with an iris diaphragm. The relative light intensity was determined with an Eppley thermopile connected to a low resistance galvanometer.

Cells were pumped from a darkened container through black rubber tubing making two 180° bends, into a square quartz tube (3.5 mm. O.D.) held vertically in a light-tight aluminum case against the exit slit of the monochromator. The thermopile was mounted directly in back of the quartz tube. From the square quartz tube the cell suspension flowed through black rubber tubing, in the dark, to a flat spiral of glass tubing held in a light-tight aluminum case in front of a photomultiplier which measured the intensity of the delayed light. From the flat spiral of glass tubing the cell suspension flowed to a Maisch metering pump, and back into the darkened flask.

Delayed light was measured using between 0.13 and 0.18 mm.^{3} of cells per cc. The flow rate of the cell suspension was 36 cc. per second; the velocity, 120 cm. per second. The intensity of the emitted light was measured by the photomultiplier approximately 0.2 second after excitation. The action spectra were made at about one-quarter of the saturating light for each algal species.

The photomultiplier (No. 6217, S 10 response) was mounted inside a metal tube which ran horizontally through a metal tank. The tank was insulated and packed with dry ice to reduce the dark current. The voltage on the photomultiplier was 850 volts. Current from the photomultiplier was measured with a vibrating reed electrometer. The collecting anode was connected to the input of the reed by a 10^8 ohm resistor, and to ground through a 0.0005 microfarad condenser with a high resistance. The reed input was connected to the feed-back lead through a 10^{11} ohm resistor.

Experiments were made with the shutter alternately open for 1 minute and then closed for 1 minute. During the time that the shutter was closed the wave length drum was changed to the next setting, and the entrance and exit slits of the monochromator were adjusted to give a 50 A dispersion at each wave length. The simple experiment of stopping the pump and getting no signal from the cell suspension shows that the light is delayed light and not fluorescence. It also shows that there is no light scattering down the suspension and into the measuring cell.

RESULTS

Figs. 1 through 7 give separate determinations of the delayed light action spectrum of several algae. Collection of this data was started at a wave length of 440 mμ, taking the even multiples of ten down to 250 mμ, up on the odd multiples to 750 mμ, and then back to 440 mμ on the even ones. This was done to minimize any effects of changes in the cell suspension that might take place in the 1½ to 2 hours of the run. Curves showing the data can be compared with one another and with those published for the delayed light action spectrum of *Chlorella* (10) and of the blue-green and red algae (2).

In Figs. 1 through 7 the ordinate is the relative effectiveness per incident quantum in producing the delayed light. The intensity of the emitted light was divided by the galvanometer readings to give an initial slope. The initial slope at each wave length setting divided by the wave length gave the relative values in quanta. These values were plotted as a function of wave length at 10 mμ intervals from 250 to 750 mμ.

DISCUSSION

The action spectrum for the blue-green alga, *Anacystis nidulans* (Fig. 1), shows a broad band at 620 mμ, and a smaller band at 400 mμ. In the visible

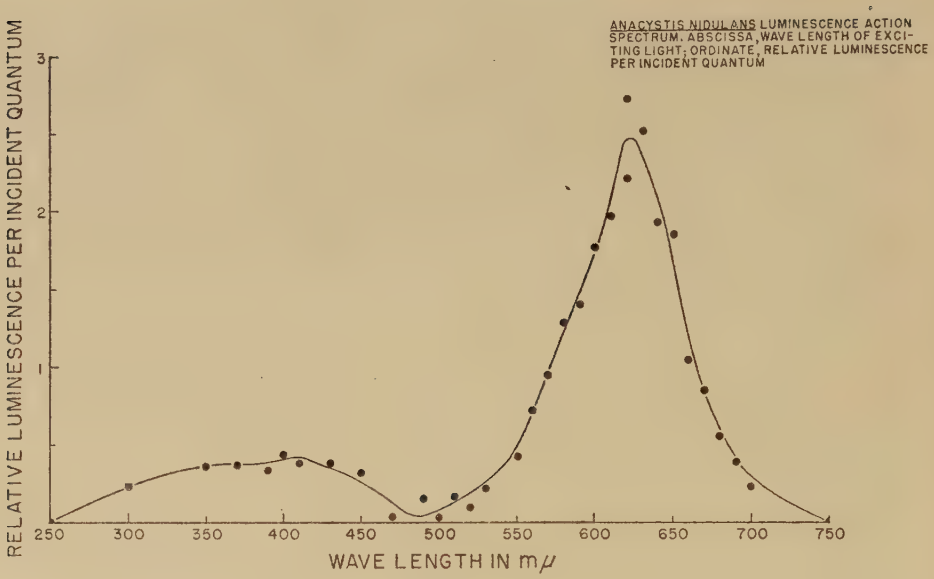

ANACYSTIS NIDULANS LUMINESCENCE ACTION SPECTRUM. ABSCISSA, WAVE LENGTH OF EXCITING LIGHT; ORDINATE, RELATIVE LUMINESCENCE PER INCIDENT QUANTUM

Fig. 1

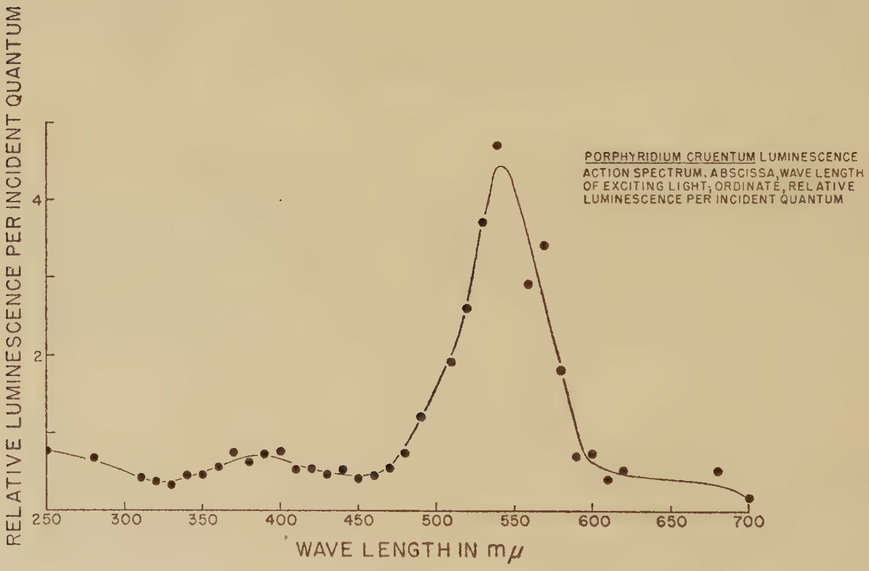

PORPHYRIDIUM CRUENTUM LUMINESCENCE ACTION SPECTRUM. ABSCISSA, WAVE LENGTH OF EXCITING LIGHT; ORDINATE, RELATIVE LUMINESCENCE PER INCIDENT QUANTUM

Fig. 2

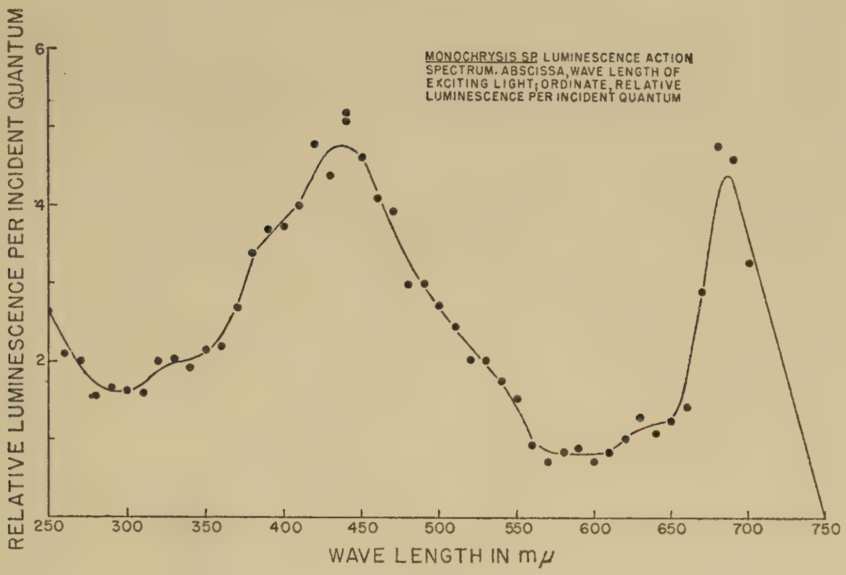
MONOCHRYSIS SP. LUMINESCENCE ACTION SPECTRUM. ABSCISSA, WAVE LENGTH OF EXCITING LIGHT; ORDINATE, RELATIVE LUMINESCENCE PER INCIDENT QUANTUM
RELATIVE LUMINESCENCE PER INCIDENT QUANTUM
6
4
2
250
300
350
400
450
500
550
600
650
700
750
WAVE LENGTH IN mμ

Fig. 3

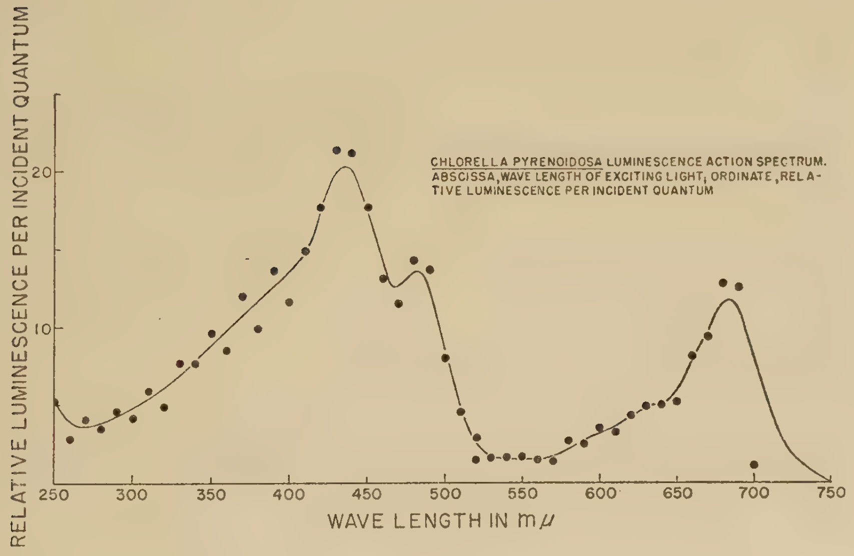
CHLORELLA PYRENOIDOSA LUMINESCENCE ACTION SPECTRUM. ABSCISSA, WAVE LENGTH OF EXCITING LIGHT; ORDINATE, RELATIVE LUMINESCENCE PER INCIDENT QUANTUM
RELATIVE LUMINESCENCE PER INCIDENT QUANTUM
20
10
250
300
350
400
450
500
550
600
650
700
750
WAVE LENGTH IN mμ

Fig. 4

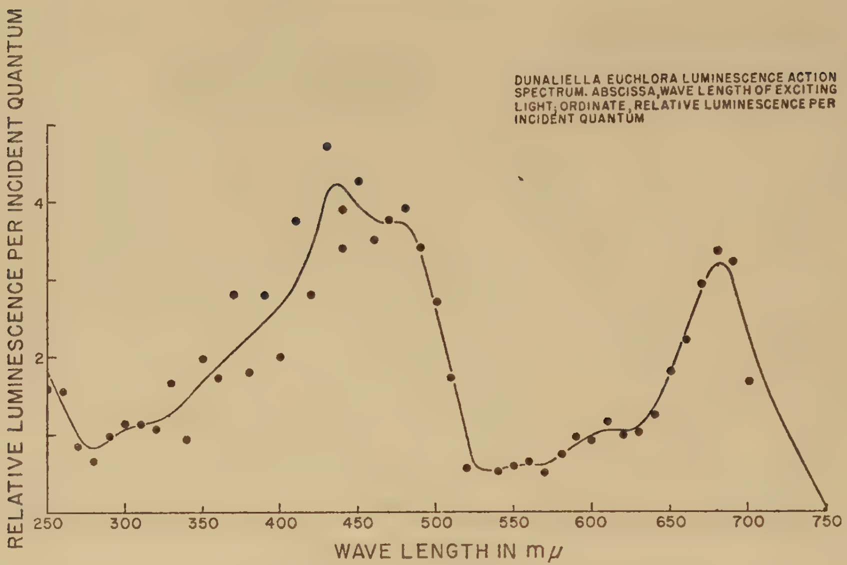

DUNALIELLA EUCHLORA LUMINESCENCE ACTION SPECTRUM. ABSCISSA, WAVE LENGTH OF EXCITING LIGHT; ORDINATE, RELATIVE LUMINESCENCE PER INCIDENT QUANTUM

Fig. 5

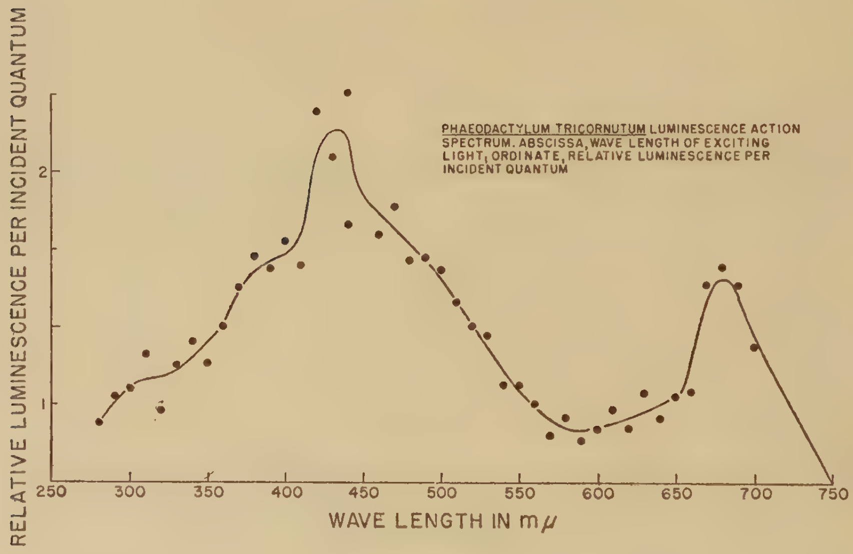

PHAEODACTYLUM TRICORNUTUM LUMINESCENCE ACTION SPECTRUM. ABSCISSA, WAVE LENGTH OF EXCITING LIGHT, ORDINATE, RELATIVE LUMINESCENCE PER INCIDENT QUANTUM

Fig. 6

part of the spectrum the curves agree with the action spectrum for photosynthesis and chlorophyll fluorescence in blue-green algae described by Duysens (3) and Haxo and Blinks (8), but not with the action spectrum for photosynthesis in the blue-green algae, *Chroococcus*, given by Emerson and Lewis (5) in which the chlorophyll is fully active.

The action spectrum for the red alga, *Porphyridium cruentum*, is given in Fig. 2. The action spectrum for the delayed light production shows a peak at 550 mμ, a flat shoulder between 600 mμ and 660 mμ, and a fall to zero at 700 mμ. In the ultraviolet part of the spectrum there is a flat shoulder between 360 and 400 mμ, and an increase at 250 mμ.

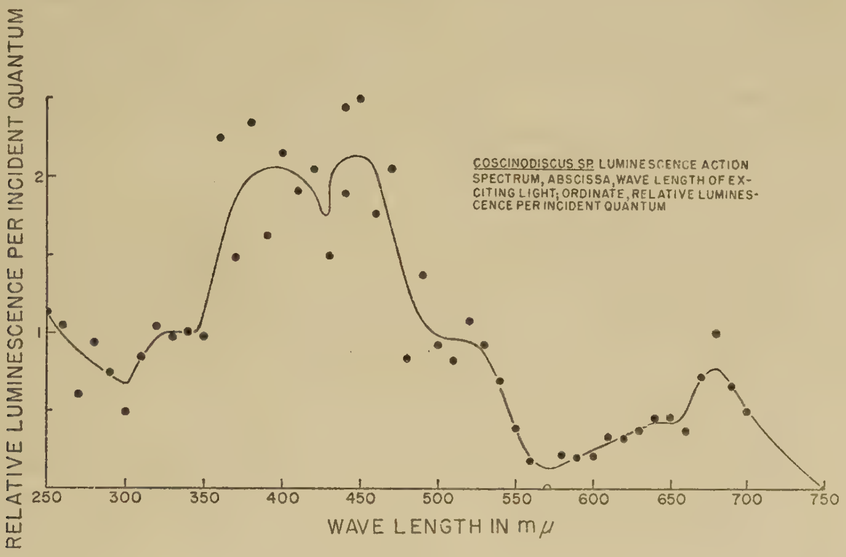

FIG. 7

In both the blue-green and red algae, the action spectra are those of the accessory pigments. The low yield in the region in which chlorophyll *a* is mainly absorbing demonstrates that the path of energy transfer, as Duysens (4) suggests, is from phycoerythrin *via* phycocyanin to chlorophyll *a*.

Figs. 3 through 5 show delayed light action spectra for fresh water and marine green and golden green algae with peaks at 680 mμ and 440 mμ. In the ultraviolet part of the spectrum there is a gentle shoulder from 440 mμ down to 280 mμ, and a rise at 250 mμ.

The action spectra for two diatoms (Figs. 6 and 7) demonstrate the broad band of fucoxanthin absorption and the 680 mμ peak of chlorophyll absorption.

The action spectra in the visible part of the spectrum for algae have been discussed by previous workers. In the ultraviolet part of the spectrum the action spectra indicate that the pigments are still active. That plants can photosynthesize in this region has already been suggested (9), and Harris and Zscheile (7) showed that the chlorophylls have several minor absorption peaks in the spectral region 280 to 380 mμ. The increase at 250 mμ may be an experimental quirk, but it is tempting to think of a protein absorption of the light energy in this part of the spectrum.

I wish to thank Dr. Alexander Hollaender for making possible my visit to the Oak Ridge National Laboratory. I am deeply indebted to Dr. William Arnold of Oak Ridge for permitting the use of all the apparatus in these measurements and for his kind interest, cooperation, and most helpful suggestions in all phases of the work. Thanks are also due to Mrs. Helen Sherwood of Oak Ridge, for her help in making the determinations. Finally, I wish to thank Dr. John H. Ryther of the Woods Hole Oceanographic Institution whose continual enthusiasm helped make this project possible.

BIBLIOGRAPHY

1. Arnold, W., and Davidson, J. B., The identity of the fluorescent and delayed emission spectra in *Chlorella*, *J. Gen. Physiol.*, 1954, **37,** 677.
2. Arnold, W., and Thompson, J., Delayed light production by blue-green algae red algae, and purple bacteria, *J. Gen. Physiol.*, 1956, **39,** 311.
3. Duysens, L. M. N., Transfer of light energy with pigment systems present in photosynthesizing cells, *Nature*, 1951, **168,** 518.
4. Duysens, L. M. N., Transfer of excitation energy in photosynthesis, Doctoral Dissertation, 1952.
5. Emerson, R., and Lewis, C. M., The photosynthetic efficiency of phycocyanin in *Chroococcus*, and the problem of carotenoid participation in photosynthesis, *J. Gen. Physiol.*, 1942, **25,** 579.
6. Gerloff, G. C., Fitzgerald, G. P., and Skoog, F., The isolation, purification, and culture of blue-green algae, *Am. J. Bot.*, 1950, **37,** 216.
7. Harris, D. G., and Zscheile, F. P., Effect of solvent upon absorption spectra of chlorophylls A and B: their ultraviolet absorption spectra in ether solution, *Bot. Gaz.*, 1943, **104,** 515.
8. Haxo, F. T., and Blinks, L. R., Photosynthetic action spectra of marine algae, *J. Gen. Physiol.*, 1950, **33,** 389.
9. Levring, T., Submarine daylight and the photosynthesis of marine algae, *Göteborgs K. Vetenskaps- och Vitterhets-Samhäll. Handl.*, 1947, **5,** 1.
10. Strehler, B. L., and Arnold, W., Light production by green plants, *J. Gen. Physiol.*, 1951, **34,** 809.

Contribution No. 957

Reprinted from BIOLOGICAL BULLETIN, Vol. 114, No. 3, pp. 357–374, June, 1958
Printed in U. S. A.

THE ACOUSTICAL BEHAVIOR OF SOME FISHES IN THE BIMINI AREA[1, 2]

JAMES M. MOULTON

Bowdoin College, Brunswick, Maine

While many kinds of marine organisms are recognized as sound sources, it is not clear in most cases under what conditions the species concerned became sonic in nature, nor what patterns of behavior the sounds normally accompany. Spontaneous sound production, by many fishes known to produce sounds, tends to become partially or completely suppressed in captivity (Dobrin, 1947; Fish, 1948; Moulton, 1956b); one must frequently resort to artificial stimuli such as handling or electric shock (Fish, 1954; Fish *et al.*, 1952) to elicit any sound for study. Failure of free fishes to respond consistently to man-made sounds introduced into the water (Moulton and Backus, 1955) has aroused considerable interest, evident in writings since the time of Aristotle, in the role that the sounds of fishes themselves play in nature.

In order to obtain further information on the production of fish sounds and their significance to fish behavior, the period from 13 June to 13 August 1956 was spent at the Lerner Marine Laboratory of the American Museum of Natural History on North Bimini, Bahama Islands. A glass-panelled power boat and the clarity of the water facilitated extensive observation of near-shore fishes during underwater listening, and well-stocked fish pens provided opportunity for close observation of such fishes in a reasonably natural environment. Recordings of marine sounds, accompanied by notes on simultaneous observations, have been compared with recordings made in the laboratory from carefully identified specimens. The identity of certain sounds recorded at sea and in the laboratory has been determined by this aural comparison and by the study of vibragrams made at the Woods Hole Oceanographic Institution.

The fishes most frequently heard along the western edge of the Great Bahama Bank in the Bimini area, the Nassau grouper, *Epinephalus striatus* (Bloch), and the squirrelfish, *Holocentrus ascensionis* (Osbeck), are inhabitants of relatively shallow water. That sightings of the Nassau grouper and squirrelfish occurred only in areas where incidence of their calling was high, and that these species were generally observed in areas where their sounds were recorded, indicates a value of underwater listening in studying the distributions, even limited ones, of some sound-producing species.

Listening equipment used in the investigation consisted of an AX-58-C Rochelle salt hydrophone and a Woods Hole Suitcase amplifier; an undesignated Rochelle

---

[1] Contribution No. 957 from the Woods Hole Oceanographic Institution.

[2] The work was performed at the Lerner Marine Laboratory of the American Museum of Natural History and at the Woods Hole Oceanographic Institution, under grants of the Institution and of the Bowdoin College Faculty Research Fund established by the Class of 1928. Preparation for publication has been facilitated by Research Grant NSF-G4403 of the National Science Foundation.

TABLE I

Fishes making no sounds or only chewing sounds during the Bimini study

Family	Species	Comment
Acanthyridae	*Acanthus coeruleus*	1 specimen
Antennariidae	*Histrio histrio*	1 specimen
Apogonidae	*Apogon maculatus*	1 specimen
Balistidae	*Canthidermis sabaco*	Several individuals
Belonidae	*Strongylura marinus*	1 specimen
Chaetodontidae	*Chaetodon striatus*	1 specimen
	Pomacanthus paru	A 4″ specimen
Clupeidae	*Jenkinsia lamprotaenia*	Large school and individual specimens
Echeneididae	*Phtheirichthyes lineatus*	2 specimens
Fierasferidae	*Carapus affinis*	1 specimen
Gerridae	Unidentified majarra	Several specimens
Gobiidae	*Bathygobius soporator*	Feeding sounds recorded from a group. Male known to call in the breeding season (Tavolga, 1956).
Haemulidae	*Haemulon album*	Several specimens
	Haemulon parra	Several specimens
Labridae	*Halichoeres radiatus*	Feeding sounds recorded
Lutianidae	*Lutianus griseus*	1 specimen
Malacanthidae	*Malacanthus plumeri*	1 specimen
Mullidae	*Upeneus maculatus*	Feeding sounds recorded
Ogocephalidae	*Ogocephalus radiatus*	1 specimen
	Ogcocephalus vespertilio	1 specimen
Orectolobidae	*Ginglymostoma cirratum*	1 specimen
Pristidae	*Pristis pectinatus*	1 specimen
Rachycentridae	*Rachycentron canadus*	1 specimen
Scorpaenidae	*Scorpaena plumeri*	1 specimen
Serranidae	*Promicrops itaiara*	1 specimen
Sparidae	*Calamus providens*	1 specimen
Sphyraenidae	*Sphyraena barracuda*	1 specimen

salt hydrophone and a modified Heathkit amplifier Model A-7C, or an Ekotape microphone Model 205. Recordings were made at 7½ and 3¾ in./sec. on the Ekotape tape recorder and selected recordings have been analyzed on a vibration frequency analyzer, the Kay Vibralyzer. Sound-generating equipment used during the investigation consisted of a Hewlett-Packard audio oscillator Model LAJ or the Ekotape tape recorder, a Craftsman C550 amplifier, and a QBG transducer. All observations at sea were made in calm weather from the 30-foot motor launch RESEARCH of the Lerner Marine Laboratory, between 0800 and 1400 hours from 9 July to 12 August. Suitcase amplifier settings varied from $0 + 14 - 20$ to $0 + 10 - 5$. During work at sea, the hydrophone was suspended just above the bottom, or so that it cleared the bottom in the shoalest water in the listening area at drift stations.

Forty species of fishes, distributed among 29 families, were studied at Bimini

(Tables I and II). The stimuli used in eliciting sound in the laboratory were those of handling, capture in a net or feeding, or a combination of these. All sounds reported were recorded from isolated, submerged specimens, except the pectoral fin drumming and tooth stridulation of individual triggerfishes (Balistidae) which were not heard while the fish were being handled under water. All other sounds described were produced in air as well as under water, except the snap of the demoiselle, *Pomacentrus leucosticus* (Mueller and Troschel), which was recorded only from submerged specimens.

The species which produced no detectable sounds other than those of chewing

TABLE II

Characteristics of fish sounds recorded at Bimini

Family	Species	Vibration frequency analysis
Balistidae	*Balistes vetula* in air at microphone	Sound: Toothplate stridulation Duration: .12 sec./stridulation Frequency span: 0 to above 8 kc. Predominant intensities: .7–1.8 kc., 2.1–3.8 kc.
	Melichthys piceus in air at microphone	Sound: Toothplate stridulation Duration: .06 to .1 sec./stridulation Freq. span: 0 to above 8 kc. Pred. int.: 1.2 to 2.3 kc.
	B. vetula in air at microphone	Sound: Pectoral fin-drumming Duration: .03 sec./pulse Freq. span: 0 to 5.8 kc. Pred. int.: 1 to 1.7 kc.
	M. piceus in air at microphone	Sound: Pectoral fin-drumming Duration: .02 to .04 sec./pulse Freq. span: 0 to above 8 kc. Pred. int.: .7 to 2.2 kc.
	Feeding of a mixed group of the two spp. at AX-58-C hydrophone	Freq. span: 0 to above 8 kc. Pred. int.; .6 to 2.9 kc.
Carangidae	*Caranx hippos* hand-held in aquarium at hydrophone	Sound: Stridulation, pharyngeal teeth Duration: .06 sec./stridulation Freq. span: 0 to above 8 kc. Pred. int.: .3 to 1.2 kc., 1.7 to 3.3 kc.
Chaetodontidae	*Angelichthyes ciliaris* in cement tank at AX-58-C hydrophone	Sound: Grunt, single or repeated Duration: .06 to .1 sec./grunt Freq. span: 0 to 1.1 kc. Pred. int.: Below .5 kc.
	Pomacanthus arcuatus W. of Turtle Rocks at AX-58-C hydrophone	Sound: Grunt or moan-like sound Duration: .04 to .2 sec. Freq. span: 0 to 1.5 kc. Pred. int.: Below .5 kc.

TABLE II—*Continued*

Family	Species	Vibration frequency analysis
Diodontidae	*Diodon hystrix* hand-held in aquarium at hydrophone	Sound: Toothplate stridulation Duration: .09 sec./stridulation Freq. span: 0 to 8 kc. Pred. int.: 2.5 to 5.5 kc., with narrow intensity bands at 3, 4.3 and 5 kc.
Haemulidae	*Haemulon sciurus* hand-held in aquarium at hydrophone	Sound: Stridulation, pharyngeal teeth Duration: .02 to .1 sec./stridulation Freq. span: 0 to above 8 kc. Pred. int.: 1.5 to 4 kc.
Holocentridae	*Holocentrus ascensionis* in aquarium (Fig. 10) and at Turtle Rocks (Fig. 12); AX-58-C hydrophone	Sound: Thump-like single, or volleyed Duration: .04 to .1 sec./thump Freq. span: 0 to above 4 kc. Pred. int.: Below 1 kc.
Pomacentridae	*Pomacentrus leucostictus* in aquarium; male pursuing others of species at hydrophone	Sound: Single or repeated snaps Duration: .02 sec./snap Freq. span: 0 to 1.5 kc. Pred. int.: 0 to .8 kc.
Serranidae	*Epinephalus adsencionis* in cement tank at AX-58-C hydrophone	Sound: Vibrant grunt, single or repeated Duration: .04 to .1 sec./grunt Freq. span: 0 to .9 kc. Pred. int.: 0 to .3 kc.
	Epinephalus striatus in live car at AX-58-C hydrophone	Sound: Vibrant grunt, single or repeated Duration: .1 to .2 sec./grunt Freq. span: 0 to 2 kc. Pred. int.: 0 to .4 kc.
Tetradontidae	*Spheroides spengleri* hand-held in aquarium at hydrophone	Sound: Toothplate stridulation Duration: .07 sec./stridulation Freq. span: 0 to above 8 kc. Pred. int.: 1.3 to 3 kc.

are shown in Table I. Twelve species producing other-than-chewing sounds are listed in Table II, together with data derived from vibration frequency analysis. Of this latter group, only three species were identified as sources of sounds recorded during listening at sea—squirrelfish, Nassau grouper and black angelfish, *Pomacanthus arcuatus* (Linnaeus), all of which use the air bladder in sound production.

No individual free fishes were identified at sea as sources of stridulatory noises. Vibration frequency analysis of these latter sounds from recordings made at sea is rendered somewhat difficult by a broad band of sound with predominant intensities between 2 and 6 kc., which is characteristic of warmer seas, and which has generally been ascribed to snapping shrimp. It is not unlikely, however, that sounds created by the teeth of reef fishes (Table II—feeding of balistids) may contribute to this sound band, which on vibration frequency analysis tends to obscure upper frequency ranges of various sounds clearly discernible below the 2-kc level.

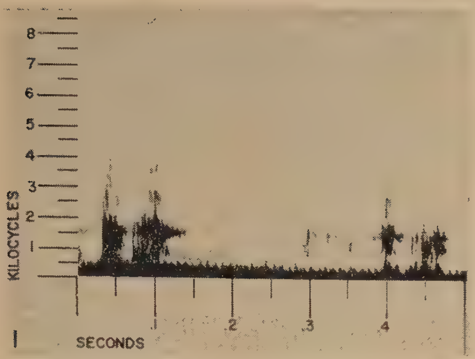

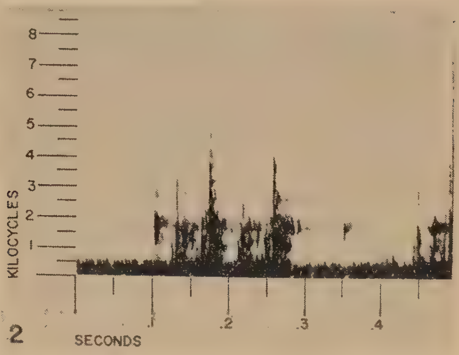

Figure 1. The pectoral fin-drum of *Balistes vetula* in air.
Figure 2. The pectoral fin-drum of *Melichthys piceus* in air.

Sound Production and Behavior of Bimini Fishes

In the following account, each family of which sound-producing representatives were studied at Bimini, is dealt with from the points of view of the sounds produced and the correlated behavior. Initial references are to earlier descriptions dealing with sound production in the families concerned.

Balistidae (Bridge, 1910, pp. 357, 361; Fish, 1948, pp. 15–19, 1954, pp. 62–65; Schultz and Stern, 1948, p. 132). The queen triggerfish, *Balistes vetula* L., and the black triggerfish, *Melichthys piceus* (Poey), each possesses above the base of the pectoral fin a thin membrane lying lateral to the air bladder and covered by scales larger and more plate-like than those elsewhere on the body (Figs. 3, 4), a characteristic of these genera of the Balistidae (Evermann and Marsh, 1900). Males and females removed from the water and handled, frequently elevated and rapidly fluttered the pectoral fins against this region, as described by Schultz and Stern (1948), resulting in the production of a throbbing sound (Table II; Figs. 1, 2). Bridge (1910, p. 357) attributes a throbbing sound primarily to movements of the pectoral girdle.

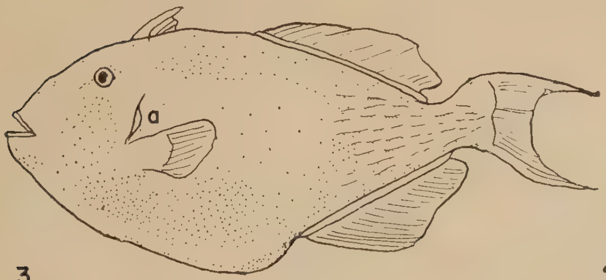

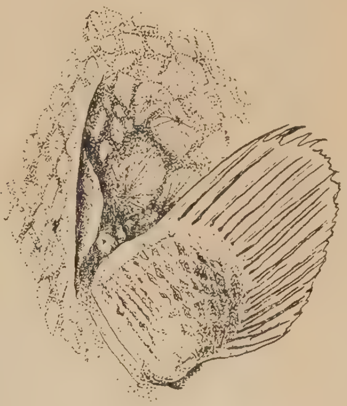

Figure 3. Outline of *M. piceus* showing (a) position of drumming membrane posterior to the gill opening. × 3.
Figure 4. Detail of the drumming membrane of *M. piceus*. × 2.5.

Differentiation of the "drumming membrane" is not apparent externally in the ocean triggerfish (*Canthidermis sabaco* Poey), nor does this species during handling move the pectoral fins to the drumming position. Similarly, the toothplate stridulation readily demonstrated by the queen and black triggerfishes (Table II; Figs. 5, 6) during handling out of water was not performed by the several ocean triggerfish studied.

While tooth stridulation and pectoral fin drumming were not heard from isolated triggerfishes handled underwater, recordings made during the feeding about the hydrophone of a captive population of queen and black triggerfishes showed predominant intensities of accompanying sounds between .6 and 2.9 kc. (Table II), which essentially spans the frequency ranges of predominant intensities obtained during tooth stridulation by these species in air. It was not possible to ascribe any specific sounds recorded at sea to triggerfishes, although their feeding activity probably contributed to background sounds recorded. They are common in the area studied.

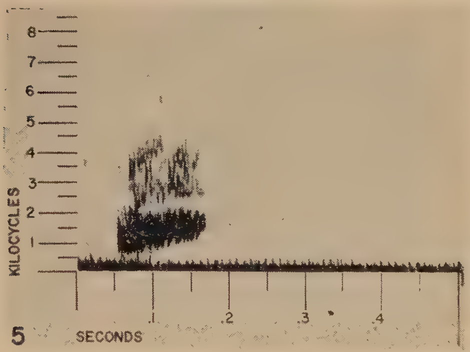

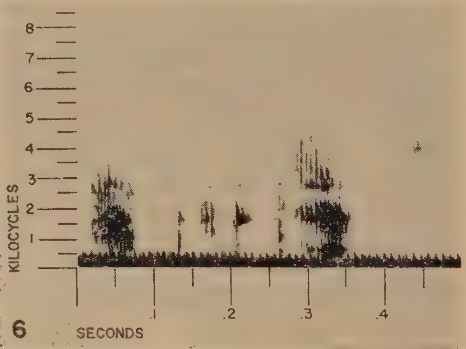

FIGURE 5. Tooth stridulation of *B. vetula* in air.
FIGURE 6. Tooth stridulation of *M. piceus* in air.

Carangidae (Bridge, 1910, p. 363; Fish, 1948, pp. 25–30). The pharyngeal tooth stridulation of *Caranx hippos* (Linnaeus) was recorded in a laboratory aquarium during handling of a 3.5-inch individual (Table II; Fig. 7). The sound recorded was not identified in any recording made at sea. Similar sound production in a related species, *Caranx crysos* (Mitchill), has been described by Fish (1954), but the thump she describes as occurring during shock was not heard during handling of the small specimen, nor was any detectable sound recorded from adult carangids swimming around and past the hydrophone at sea. A local fisherman related the stridulatory sound to "rattling of the ear bones" and asserted that a hooked specimen making this noise attracts other individuals of the species.

Chaetodontidae (Bridge, 1910, p. 361). The vibrant deep grunts of the queen, *Angelichthyes ciliaris* (Linnaeus), and black, *Pomacanthus arcuatus* (L.), angelfishes (Table II) are not easily distinguished from those of the serranids with which they may occur. Vibration frequency analysis shows (Fig. 8) a tendency for highest frequencies of the angelfish grunts to be located in the middle of the call, whereas serranid grunts tend to be initiated with high frequency spikes. Each may vary in the direction of the other, however, and since serranids and angelfishes tend to occur in similar areas, the sounds of the two may be confused. Field and laboratory observations indicated that serranids are far more prolific in call production under ordinary circumstances than are the angelfishes.

Under laboratory conditions, both queen and black angelfishes produce the grunt during feeding on bits of conch, and when startled to quickened swimming by an observer. The deeply recessed air bladder, as seen in the black angelfish, bears no intrinsic muscles, and sound production is due to the contraction of axial musculature adjacent to the air bladder. Each quick motion of a black angelfish nibbling at the hydrophone at sea resulted in a brief grunt, although more leisurely swimming of both species in laboratory tanks was not accompanied by sound production. Handling of black angelfish under water brings forth brief grunts of low intensity, coinciding with body muscle contractions. Uniquely among species studied, the black angelfish, usually in pairs, readily approached and butted against the hydrophone at sea.

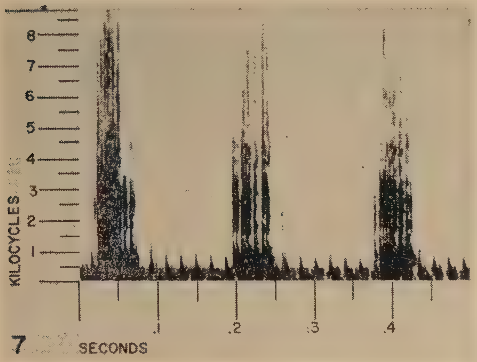

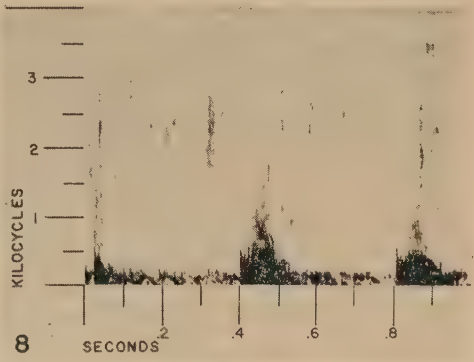

FIGURE 7. Pharyngeal tooth-stridulation of *Caranx hippos* in aquarium.

FIGURE 8. A short and two longer calls of *Pomacanthus arcuatus* west of Turtle Rocks, the latter during approach of another *P. arcuatus*. Snapping shrimp in background.

The deeply recessed position of the air bladder brings it into intimate association with surrounding peritoneum, and to the latter attach many of the axial muscle fibers heavily surrounding the slender ribs. These attached fibers appear to maintain a tension on the wall of the air bladder; cutting of the fibers creates a resonance within the bladder, and results in its partial collapse.

The maximum duration of angelfish grunts obtained during this investigation occurred west of Turtle Rocks on 10 July (Fig. 8), when an adult black angelfish examining the hydrophone and butting gently at its rubber case suddenly gave vent to prolonged, rather moan-like sounds, each of .2-sec. duration, and swam toward an approaching fish of the same species. The two fish faced each other for a few moments, after which both came quietly to the hydrophone and finally swam off together. The interpretation of a recognition signal in the prolonged grunts was rather difficult to avoid, for prior to production of the longer grunts, the first fish produced shorter, sharper sounds during its examination of the hydrophone. On another occasion, 12 July in the same area, sounds similar to the shorter grunts

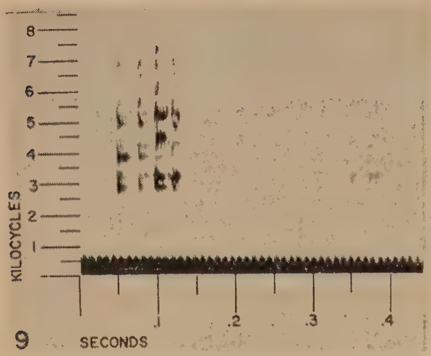

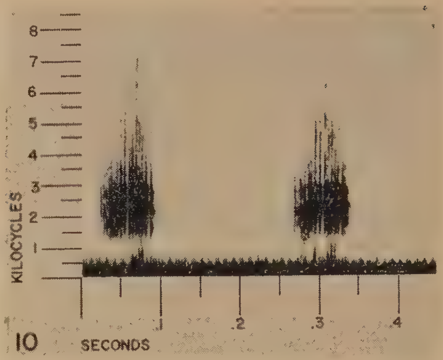

FIGURE 9. Toothplate stridulation of *Diodon hystrix* in aquarium.
FIGURE 10. Toothplate stridulation of *Spheroides spengleri* in aquarium.

were recorded as a pair of black angelfishes butted several times against a pair of cowfish, *Lactophrys tricornis* (L.), approximately 6 feet from the hydrophone.

No sounds were recorded from the single species of butterflyfish studied, *Chaetodon striatus* L., nor were sounds recorded from an immature specimen (4-inch, total length) of the French angelfish, *Pomacanthus paru* (Bloch).

Diodontidae, Tetradontidae (Fish, 1948, 1954; Burkenroad, 1931). The porcupinefish, *Diodon hystrix* L., and the puffer, *Spheroides spengleri* (Bloch), were so similar in acoustical behavior as to merit a single discussion (Table II). Both produce sound during and after inflation by stridulation of the toothplates, the sound being of a klaxon-like variety (Figs. 9, 10). Only feeding sounds were recorded from undisturbed individuals. Frequencies of greatest intensities are similar in chewing and stridulation noises, although these levels vary between the two species (Table II.) and may be expected to vary with size. Only a single individual of each was recorded at Bimini. Observations on these species and on the common puffer, *Spheroides maculatus* (Bloch and Schneider) of the Woods Hole area suggest that the stridulatory sound is more readily elicited from smaller individuals than from full-grown animals.

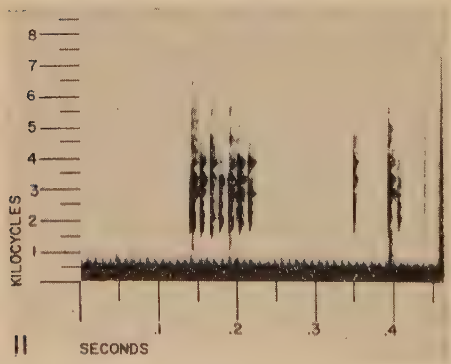

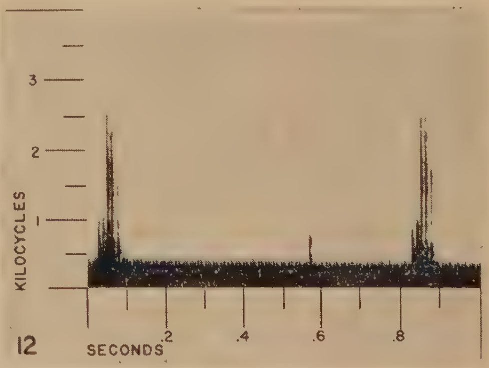

FIGURE 11. Pharyngeal tooth stridulation of *Haemulon sciurus* in aquarium.
FIGURE 12. Single thump-like sounds of *Holocentrus ascensionis* in cement tank.

Haemulidae (Burkenroad, 1930, 1931; Fish, 1948, pp. 63–66; Schultz and Stern, 1948, p. 131). Although the fishes called grunts are notoriously noisy species of warmer marine waters, due to the rasping stridulation of the pharyngeal teeth, observations at Bimini indicated that not all species of the Haemulidae are equally important sound producers (Tables I and II). The haemulid rasp was not identified in any recordings made at sea; it was heard only from hand-held specimens of the blue-striped (Table II; Fig. 11) and yellow grunts, *Haemulon sciurus* (Shaw) and *H. flavolineatum* (Desmarest), respectively; no recordings of the latter were obtained. The observations of Burkenroad (1930) which related the sounds of *Haemulon* to movements of the pharyngeal teeth were confirmed, with the exception that the association between the dorsal pharyngeal teeth and the anterior end of the air bladder seems more important in resonating the rasping sound than does the varying relation between the air bladder and the lower pharyngeal teeth. The opercula are somewhat extended during sound production. Rubbing together of dissected pharyngeal toothplates produces a much fainter sound than that produced by the living fish.

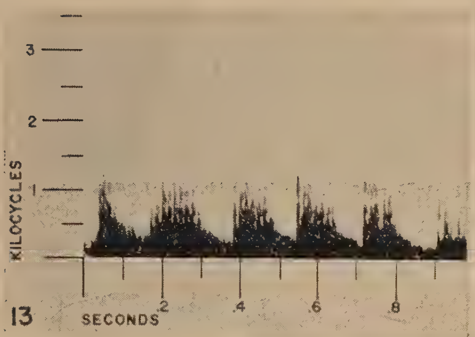

13

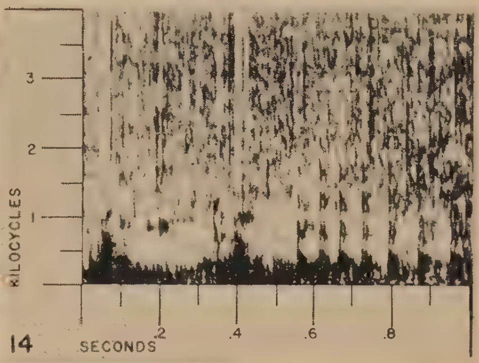

14

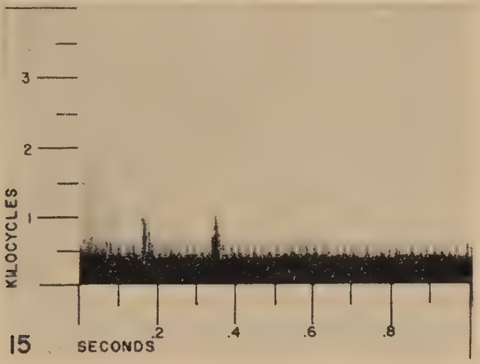

15

FIGURE 13. Grunts of *Epinephalus striatus* in cement tank.

FIGURE 14. Two *E. striatus* grunts (left) and a volley of thump-like sounds of *H. ascensionis* west of Turtle Rocks. Snapping shrimp in background.

FIGURE 15. Snaps of male *Pomacentrus leucostictus* in aquarium.

Holocentridae (Fish, 1948). Sound production by the squirrelfish, *Holo-*

centrus ascensionis, said to have derived its name from its chattering call (D. de Sylva, personal communication), is characteristic of the western edge of the Great Bahama Bank (Table II; Fig. 12, 14). It was recorded only along, and mainly to the west of, the island and rock chain extending from North Bimini south to South Cat Cay (Tables III and IV; Fig. 16). In rocky areas of the bottom along a relatively narrow area probably extending not far below the limits of visibility from the surface, squirrelfish are characteristically found in the daytime each hovering near a depression approximately large enough to receive a single fish. Generally living in higher parts of ledges than the grouper, an occasional squirrelfish inhabits a rocky fissure with *E. striatus.* Collection of squirrelfish in traps up to a mile east of Turtle Rocks and occasional sightings in deeper reaches east of the Bimini-Cat Cay chain indicated that the species may move beyond its more common daytime habitat along the outer face of the Bank. Holocentrids are mainly nocturnal in their habits (Barbour, 1905, p.119; Randall, 1955, pp. 33, 38) and at night their local distribution may be considerably more dispersed than during the daytime, although the species considered here is said to return to the same hole each day (Ray and Ciampi, 1956, p. 207).

TABLE III

Grouper and squirrelfish sound production along the western edge of the Great Bahama Bank in the Bimini area

Recording station	Duration of recording	Calls/minute		
		Grouper	Squirrelfish	Both
1) At 15 fa. depth W of Moselle Shoal, drifting N	13 min.	.08	0	.08
2) At 25 fa. depth SW of (1), drifting N	18 min.	.4	0	.4
3) W of gap between Round and Turtle Rocks	6 min.	1.0	5.2	6.2
4) W of Turtle Rocks	5 min.	.2	7.2	7.4
5) W of Turtle Rocks	11.5 min.	.8	6.3	7.1
6) W of Turtle Rocks	45 min.	1.9	9.5	11.4
7) W of Turtle Rocks, drifting SE	14 min.	.6	3.4	4.0
8) W of Triangle Rocks, drifting NE	10 min.	1.3	3.3	4.6
9) West of Triangle Rocks	13 min.	1.7	3.2	4.9
10) W of gap between Piquet and Triangle Rocks	15 min.	2.5	8.6	11.1
11) W of Piquet Rocks	12 min.	2.4	4.1	6.5

Average number of calls/minute (11 stations):

Grouper	1.2
Squirrelfish	4.6
Both	5.8

Squirrelfish sounds are produced by contractions of body wall musculature against the rather firm-walled air bladder which is closely associated with the rib cage. The first three ribs are expanded, flattened and thinned dorsally, and are intimately associated with the air bladder wall; more posterior ribs are easily separated from the bladder. Physiological stimulation indicated that the musculature chiefly responsible for sound production was that attaching to the dorsal portions of the first three ribs, which appear to serve as drumheads. The structure of the air bladder, and its close relationship with the auditory region of the skull, have been described by Nelson (1955).

The thump-like sounds of squirrelfish may be repeated singly at irregular intervals or produced in rapid volleys; they are more sharply peaked on vibration frequency analysis than are the sounds of angelfish and grouper. When produced by startled or handled squirrelfish, the sounds are volleyed in bursts of 4 to 20. Singly-produced sounds are of longer duration than those produced in volleys; these singly-produced sounds are not dissimilar to the ear from the sounds of Nassau grouper, although they cover a greater frequency span than do those of the grouper when both are recorded at the hydrophone.

TABLE IV

Grouper and squirrelfish sound production over the Great Bahama Bank in the Bimini Area

Recording station	Duration of recording	Calls/minute		
		Grouper	Squirrelfish	Both
1) On Moselle Shoal	23 min.	.04	.06	.1
2) Over wreck ENE of North Rock	27 min.	.4	0	.4
3) At North Rock, E side	27.5 min.	.04	.2	.2
4) At Crossing Rocks, W side	37.5 min.	.1	1.0	1.1
5) In Bimini Harbor entrance, drift to N	6.5 min.	0	.6	.6
6) 50′ off S. Bimini, W side	13 min.	.7	.2	.9
7) At Round Rock, W side	8 min.	1.0	0	1.0
8) At Round Rock, E side	9 min.	.3	0	.3
9) On line between Turtle and Round Rocks, drift NW	10 min.	.9	1.9	2.8
10) Same station	30 min.	1.4	1.8	3.2
11) North end of Turtle Rocks, E side	4 min.	0	0	0
12) Same station	3 min.	0	0	0
13) On line between Triangle and Turtle Rocks, drift NE	12 min.	.4	2.2	2.6
14) Concrete shipwreck, E of Turtle Rocks	9 min.	0	0	0
15) Triangle Rocks, E side	11 min.	0	.6	.6
16) Dollar Harbor	5.5 min.	0	0	0
17) Wedge Rocks, NE side	8 min.	.8	1.4	2.2

Average number of calls/minute (17 stations):

Grouper	.3
Squirrelfish	.5
Both	.8

Undisturbed squirrelfish confined in laboratory aquaria and outdoor tanks remained silent during listening periods of up to three hours; confined specimens produced sounds only when handled, fed or startled. Quickened swimming during feeding was characterized by sound production of a considerably lower intensity than that produced during handling of the fish. Sudden startling of confined squirrelfish generally resulted in volleys of sound production.

At sea, squirrelfish were sometimes heard when no individuals were sighted, but the acoustical behavior of the species was characteristic when specimens were approached by the suspended hydrophone at drift stations. This behavior included

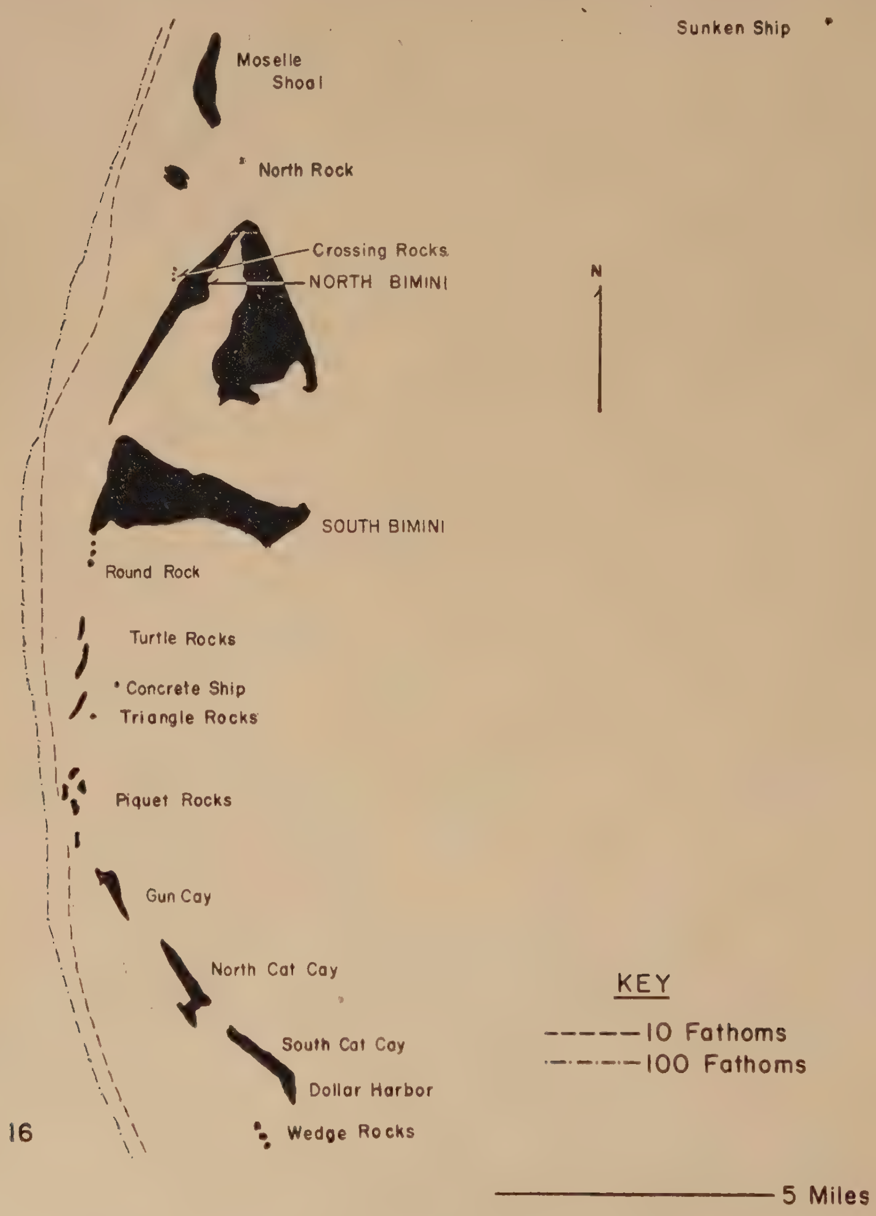
Sunken Ship
Moselle Shoal
North Rock
Crossing Rocks
NORTH BIMINI
N
SOUTH BIMINI
Round Rock
Turtle Rocks
Concrete Ship
Triangle Rocks
Piquet Rocks
Gun Cay
North Cat Cay
KEY
10 Fathoms
100 Fathoms
South Cat Cay
Dollar Harbor
16
Wedge Rocks
5 Miles

FIGURE 16. The Bimini area from Moselle Shoal to South Cat Cay.

erection of the spiny fins, adjustment of position so that an eye was directed toward the approaching hydrophone, movement toward a rocky depression near which the fish hovered, and production of the call in volleys of 3 to 20 individual pulses. The continuing approach of the hydrophone resulted in the fish's moving into its rocky shelter.

Pomacentridae (Fish, 1948, pp. 59–63). The sharp but rather faint knocks or snaps produced probably only by males of the demoiselle, *Pomacentrus leucostictus* (Mueller and Troschel), were recorded when a given individual suddenly dashed from cover to pursue other individuals approaching its place of concealment (Table II; Fig. 15). These were heard on several occasions. The behavior was similar to that of a sciaenid, *Corvina nigra* (Bloch) described by Dijkgraaf from Naples (1947).

Serranidae (Fish, 1954, pp. 36–44). The air bladder of the Nassau grouper, *Epinephalus striatus,* is thin-walled and lacks intrinsic muscles, yet this species equals the squirrelfish in its importance as a source of marine sound in the Bimini area (Table II; Figs. 13, 14). Contractions of body wall musculature appear to be responsible for the sound production, while the unusually heavy peritoneum stretched over the air bladder and adjacent organs apparently acts as the sounding board. Appropriate stimulation of opened fishes brought about some sound production, even after deflation of the air bladder. The strong contractions of body wall musculature accompanying production of the call are visible externally, and are easily elicited by startling or handling the fish in laboratory tanks. Sounds similar to those produced on alarm, but of a somewhat lower intensity, are produced during quickened swimming accompanying feeding.

Like the squirrelfish, the Nassau grouper inhabits the underwater ledges west of the Bimini-Cat Cay chain of rocks and island (Fig. 16). Its distribution is broader from east to west than that of the squirrelfish, since it was sighted where rocky fissures occurred in an otherwise sandy bottom in the Bimini lagoon, and it was seen and recorded in a shipwreck approximately 11 miles northeast of North Bimini Island on the Great Bahama Bank (Station 2, Table IV; Fig. 16). Unidentified sounds thought to originate from serranids were recorded at depths exceeding 15 fathoms west of North Bimini Island (Stations 1 and 2, Table III), from which depths serranids have been obtained at Bimini (Scholander *et al.,* 1951; Scholander and van Dam, 1954).

The Nassau grouper tends to be more secretive in its habits than the squirrelfish, ordinarily lying deeper in rocky fissures or well beneath overhanging ledges on the outer faces of which squirrelfish are more frequently seen. In acoustical behavior, the two are similar. As the suspended hydrophone approaches a grouper, the fins are erected and the fish retreats to cover, accompanying the retreat with the characteristic vibrant grunts. Like the call of the squirrelfish, that of the grouper was sometimes heard when no individual was sighted. The call is a characteristic marine sound of the area immediately west of the Bimini-Cat Cay chain.

The sound of the rock hind, *Epinephalus adsencionis* (Osbeck) (Table II), while of markedly lower intensity than that of the Nassau grouper, is produced under similar circumstances in laboratory tanks and is of similar characteristics. It was never specifically recognized during recording at sea. No sounds whatever were recorded from a captive *Promicrops itaiara* (Lichtenstein) weighing in the neighborhood of 300 pounds, although the fish on one occasion very nearly swallowed the hydrophone.

Distribution of Grouper and Squirrelfish Sounds in the Bimini Area

The distribution of squirrelfish and Nassau grouper in the Bimini area has been summarized above. Determination of this distribution was based on both visual and aural observations. The sounds of these species were selected to explore the possibility of determining the distribution of sonic species by aural means alone.

The total area of observation extended approximately 20 miles along the northwest edge of the Great Bahama Bank (Fig. 16), from Moselle Shoal on the north to Wedge Rocks on the south, and in an east-west direction from the location of a sunken freighter on the Great Bahama Bank (25° 49′ N, 79° 7′ W) 10.7 miles on a heading of 75 degrees from the northern tip of the Bimini Islands, to a station over an approximate depth of 150 feet southwest of Moselle Shoal. Recordings were made at 28 stations (Tables III and IV), all but two (Stations 1 and 2, Table III) being approximately on or within the 6-fathom line to permit observation of fishes during recording. Table III includes those stations, fixed and drift, at which recordings began on or were wholly confined to the edge of the Great Bahama Bank, to the west of the Bimini-Cat Cay chain; Table IV includes those stations located further in upon the Bank, in most cases immediately to the east of the Bimini-Cat Cay chain. The stations are in each case listed in order from north to south, and are referable to Chart No. 1854 of the United States Hydrographic Office, and to U. S. Coast and Geodetic Survey Chart No. 1112.

While not each call ascribed to either grouper or squirrelfish in Tables III and IV has been analyzed by vibration frequency analysis, a broad sample of recordings made at sea has been thus treated, and the results have indicated that the interpretations of recordings upon which Tables III and IV are based are correct. In erecting Tables III and IV, a rapid volley of either grouper or squirrelfish sounds has been characterized as a single call. Closely consecutive calls of the same species but of different individuals are usually interpretable as such on the basis of intensity differences, due to the origins' being at different distances from the hydrophone.

It will be noted in Table III that, although squirrelfish calls were lacking in the deepest stations recorded (1 and 2), along the sloping edge of the Bank they predominated over grouper calls by a factor of nearly 4. Moving of the listening station from the slope side of the Bimini-Cat Cay chain immediately to the Bank side (Table IV) resulted in an abrupt drop in incidence of calling by both species, but particularly by the squirrelfish. On the Bank itself, where squirrelfish were much less frequently sighted, their calls predominated over grouper calls by a factor of less than 2. The calling of these two species together was over 7 times as frequent along the edge of the Bank as to the east of its edge (Tables III and IV). The difference in incidence of calling between slope and Bank sides of the Bimini-Cat Cay chain is exemplified especially by comparison of Table III, Stations 4, 5 and 6, with Table IV, Stations 9, 10, 11 and 12. Short moves of the listening station resulted in marked differences in the incidence of underwater biological sounds.

Although not indicated by the data presented in Tables III and IV, observations at drift stations (Table III, Stations 7 and 8; Table IV, Stations 9 and 13) indicated that as the hydrophone moved over alternately sandy and rocky bottom, the incidence of calling rose markedly as the boat moved over underwater ledges and fell over the sandy stretches; the incidence of calling thus provided an indication as to the type of bottom beneath the boat, and correlated with sightings of grouper and squirrelfish.

Other Underwater Sounds of the Bimini Area

Sounds most frequently heard during the underwater listening in the Bimini area, other than those described, are (1) the snapping and crackling characteristic of tropical seas, generally attributed to snapping shrimp, but actually indistinguishable by methods commonly employed from the sounds of some stomatopods (Johnson, *et al.*, 1947; Moulton, 1957); (2) a rattling sound like that produced by the spiny lobster, *Panulirus argus* (Moulton, 1957); and (3) another unidentified rattling sound with its predominant frequencies lying between .5 and 1.3 kc., each pulse being of .02 second duration, and repeated at intervals of approximately .12 second in volleys of varying length. In addition to these, a distinctive series of sounds was recorded twice the same day (12 July 1956 at Stations 6 and 9, Table IV). At Station 6, the sound was a buzz-like whine singly produced; at Station 9, the same sound was preceded by a number of sharp metallic raps and was followed by a number of brief chirps of somewhat lower frequency than the raps. The metallic raps were so similar to the sound of pounding on a steel hull that two observers, prone at the glass panels, concluded a vessel to be bearing down on the listening post. Since the listening boat was quiet except for water noise along the hull, and since no other boats were within view to the horizon, it is assumed that the sounds were of biological origin, but the source is unknown. They do not correspond with known cetacean sounds (Mr. William Schevill, personal communication).

Discussion

The behavior of the Nassau grouper and squirrelfish in the Bimini area furnishes a marked exception to the generalization (Fish, 1954, p. 7) that fishes in the field are silenced by strange contacts. Both of these species were obviously stimulated to active sound production by approach of the boat and suspended hydrophone at drift stations over shallow waters. The spiny fin erection and movement toward concealment of these species upon approach of the hydrophone were strongly suggestive that the sounds described are related to self-protection, a probability further suggested by production of the same sounds during handling of these fishes. Although some fishes may use echo-location (Griffin, 1955), there is no evidence at present of its being involved in the cases under discussion. Circumstances surrounding production of grouper and squirrelfish calls, as observed at Bimini, were similar to those that surround production of sea robin grunts (Moulton, 1956b). While the grunts are readily produced during handling by most specimens of the sea robins common at Woods Hole, *Prionotus evolans* (L.) and *P. carolinus* (L.), the grunts are also produced by sea robins contained together in live cars and living on the bottom. Sea robin grunts are not, however, so easily stimulated by startling as are the sounds of Nassau grouper and squirrelfish which readily produced sounds recorded at sea after periods of confinement of two weeks in laboratory aquaria.

The squirrelfish is the most significant producer of underwater sound among fishes in the Bimini area, and if the 20-mile extent of the Bank area studied may be considered typical of the whole, of the edges of the Great Bahama Bank generally. In view of this significance, Fish's (1948, p. 44) estimate of the sonic importance of the Holocentridae as "probably none" must be rejected. Since holocentrids are of wide distribution in tropical and sub-tropical waters, it seems probable that their sonic importance extends to other waters than those of the Bimini area.

The acoustical behavior of the angelfishes (Chaetodontidae) has not been hitherto adequately described, but there can be little doubt that the behavior of the single specimen recorded at Turtle Rocks on 10 July furnished evidence of a call accompanying recognition behavior in this species. The black angelfish which is most common of the angelfishes in the Bimini area, has a tendency to examine underwater objects (hydrophone, swimming cowfishes), such examination being accompanied by sounds of briefer duration than those proposed as a part of recognition behavior. The black angelfish is usually observed in pairs during July and August at Bimini. It seems likely that chaetodontids may contribute to underwater sound in other tropical and sub-tropical areas, although they are not discussed among sound-producing fishes of the Pacific by Fish (1948).

Further evidence of the tendency of captive fishes to become silent unless disturbed was provided by all species studied during the summer of 1956. The only species to produce sound spontaneously in laboratory aquaria during listening periods of up to three hours, other than those produced during feeding and being startled, was the small pomacentrid, *Pomacentrus leucostictus*, probably a male, as it pursued other individuals encroaching on its hiding place.

As is the case along the northeastern coast of the United States where the most significant fish producers of underwater sound which have been identified (sciaenids, triglids, and batrachoidids) are fishes using, rather than skeletal stridulatory mechanisms, muscles in close association with the air bladder (Tower, 1908; Fish, 1954; Moulton, 1956b), a holocentrid, a serranid and a chaetodontid are the most frequently calling fishes of the area immediately about the Bimini-Cat Cay chain. Of the former, however, both sea robins and toadfish produce sounds with muscles intrinsic to the air bladder, while all three of the most important calling fishes of the Bimini area use muscles extrinsic to the air bladder in producing their sounds.

The structural specializations and behavioral patterns of the sound producing species studied at Bimini have provided further striking evidence of the significance of sound in the biology of the species concerned, and the consistent incorporation of sound production into behavioral patterns observed in the clear water about Bimini (Nassau grouper, squirrelfish, angelfish) strengthens a conclusion that sound is of significance to the species concerned. Yet, as has repeatedly been affirmed, clear evidence of effectiveness of the sounds concerned in modifying the movements of fishes in nature is still lacking, although Tavolga (1956) has observed the females of a goby to demonstrate increased activity during sound production by the male in breeding. The sounds of all calling species studied at Bimini are produced by both sexes, except for the snaps of *Pomacentrus leucostictus.*

Experiments of playing into the water artificial sounds and recordings of natural sounds such as those that have elsewhere modified fish behavior (Moulton, 1956a, 1956b; Tavolga, 1956) had no notable effect in the Bimini area. During all listening at sea in the Bimini area, all during daylight, sound production was prolific or rare, depending on the distribution of the species concerned and not on alternating periods of quiet and of sound production which seem to characterize production of the staccato call of sea robins at Woods Hole (Moulton, 1956b). Therefore, these experiments are not reported in detail. The Nassau grouper and squirrelfish were never observed in areas where their calls were not heard at Bimini.

The most characteristic component of background noise in the Bimini area is the "crackle" so characteristic of warmer seas, and which has generally been ascribed to snapping shrimp (Johnson *et al.,* 1947). By the analysis methods used, this noise in the Bimini area presents components cumulatively spanning the frequency range examined (up to 8 kc.). The invertebrates largely responsible are a common stomatopod (*Gonodactylus oerstedi*) and several kinds of snapping shrimps, including *Alpheus armatus* and *Synalpheus* spp. (Johnson *et al.,* 1947; Pearse, 1950; Moulton, 1957). The sound spectra obtained during this study from recordings of feeding and of stridulation sounds of various fishes indicate that in regions where producers of such sounds are numerous, they may contribute extensively to the spectrum of underwater sounds generally attributed to invertebrate sound producers.

I am much indebted to Dr. R. H. Backus for constructive criticism of the manuscript of this paper. I am also indebted to Mr. Donald de Sylva for assistance in identification of several of the fishes studied, and to Mr. E. R. Powell for assistance with the illustrations. Use of the generous facilities of the Lerner Marine Laboratory of the American Museum of Natural History is gratefully acknowledged.

SUMMARY

1. On the basis of observations and recordings at sea and in the laboratory, the acoustical behavior of 13 species of Bahamian fishes is described, and their sounds are defined. Twenty-six species producing no calls in the course of this study are specified.

2. The most important sound-producers among fishes of the Bimini area are the squirrelfish, *Holocentrus ascensionis,* and the Nassau grouper, *Epinephalus striatus.* Their characteristic sounds may be anticipated when these species encounter a strange object at sea, and probably generally during the daytime along the edges of the Great Bahama Bank.

3. A single observation has indicated that calling is a component of recognition behavior in the black angelfish, *Pomacanthus arcuatus.* The families Chaetodontidae and Holocentridae should be added to lists of fish families containing calling members.

4. The usefulness of underwater listening in studying the distribution of some calling fishes has been demonstrated in the cases of the squirrelfish and Nassau grouper.

LITERATURE CITED

Barbour, T., 1905. Notes on Bermudian fishes. *Bull. Mus. Comp. Zool.*, **46**: 109–134.

Bridge, T. W., 1910. Fishes. Cambridge Natural History, **7**: 139–537. Macmillan and Co., Ltd., London.

Burkenroad, M. D., 1930. Sound production in the *Haemulidae*. Copeia, 1930, No. 1: 17–18.

Burkenroad, M. D., 1931. Notes on the sound producing marine fishes of Louisiana. Copeia, 1931, No. 1: 20–28.

Dijkgraaf, S., 1947. Ein Töne erzeugender Fisch im Neapler Aquarium. *Experientia*, **3**: 493.

Dobrin, M. B., 1947. Measurements of underwater noise produced by marine life. *Science*, **128** (**105** N.S.): 19–23.

Evermann, B. W., and M. C. Marsh, 1900. The fishes of Porto Rico. *Bull. U. S. Fish Comm. for 1900:* 1–350.

Fish, M. P., 1948. Sonic fishes of the Pacific. ONR Contr. N6 ori-195, T.O. 1, Tech. Report No. 2.

Fish, M. P., 1954. The character and significance of sound production among fishes of the western North Atlantic. *Bull. Bingham Oceanographic Collection*, **14**; Art. 3: 1–109.

Fish, M. P., A. S. Kelsey, Jr. and W. H. Mowbray, 1952. Studies on the production of underwater sound by North Atlantic coastal fishes. *J. Mar. Res.*, **11**: 180–193.

Griffin, D. R., 1955. Hearing and acoustic orientation in marine animals. Papers Mar. Biol. and Oceanogr., Deep-Sea Research, suppl. to Vol. 3, pp. 406–417.

Johnson, M. W., F. A. Everest and R. W. Young, 1947. The role of snapping shrimp (Crangon and Synalpheus) in the production of underwater noise in the sea. *Biol. Bull.*, **93**: 122–138.

Moulton, J. M., 1956a. The movements of menhaden and butterfish in a sound field. *Anat. Rec.*, **125**: 592.

Moulton, J. M., 1956b. Influencing the calling of sea robins (*Prionotus* spp.) with sound. *Biol. Bull.*, **111**: 393–398.

Moulton, J. M., 1957. Sound production in the spiny lobster *Panulirus argus* (Latreille). *Biol. Bull.*, **113**: 286–295.

Moulton, J. M., and R. H. Backus, 1955. Annotated references concerning the effects of man-made sounds on the movements of fishes. Fisheries Circ. No. 17, Dep't of Sea and Shore Fisheries, Augusta, Maine.

Nelson, E. M., 1955. The morphology of the swim bladder and auditory bulla in the *Holocentridae*. *Fieldiana: Zoology*, **37**: 121–130.

Pearse, A. S., 1950. Notes on the inhabitants of certain sponges at Bimini. *Ecology*, **31**: 149–151.

Randall, J. E., 1955. Fishes of the Gilbert Islands. Atoll Research Bull., No. 47, Pacific Science Board, Natl. Acad. of Sci., National Research Council, Washington.

Ray, C., and E. Ciampi, 1956. The Underwater Guide to Marine Life. A. S. Barnes and Co., New York.

Scholander, P. F., C. L. Claff, C. T. Teng and V. Walters, 1951. Nitrogen tension in the swimbladder of marine fishes in relation to the depth. *Biol. Bull.*, **101**: 178–193.

Scholander, P. F., and L. van Dam, 1954. Secretion of gases against high pressures in the swimbladder of deep sea fishes. I. Oxygen dissociation in blood. *Biol. Bull.*, **107**: 247–259.

Schultz, L. P., and E. M. Stern, 1948. The Ways of Fishes. D. Van Nostrand Co., Inc., New York.

Tavolga, W. N., 1956. Visual, chemical and sound stimuli as cues in the sex discriminatory behavior of the gobiid fish *Bathygobius soporator*. *Zoologica*, **41**, Part 2: 49–64.

Tower, R. W., 1908. The production of sound in the drum-fishes, the sea-robin and the toadfish. *Annals N. Y. Acad. Sci.*, **18**: 149–180.

Contribution No. 958

Reprinted for private circulation from
THE JOURNAL OF GEOLOGY
Vol. 66, No. 4, July 1958
PRINTED IN U.S.A.

A MODEL RELATING DYNAMICS AND SEDIMENT PATTERN IN EQUILIBRIUM IN THE REGION OF SHOALING WAVES, BREAKER ZONE, AND FORESHORE[1]

ROBERT L. MILLER AND JOHN M. ZEIGLER
University of Chicago and Woods Hole Oceanographic Institution

ABSTRACT

A theoretical model is presented for the expected patterns of sediment size and sorting in the region of shoaling wave, breaker, and beach foreshore. This model is based on theoretical considerations and published experimental results and is intended to hold for the above-mentioned dynamic zones in a state of equilibrium. Comparison with detailed observations in three natural situations and with published sediment size and sorting patterns appears to give good agreement with the model. The implication is that such generalized patterns may serve in the recognition of departures from equilibrium and change in general environment in the study of contemporary sediments and possibly in the recognition of dynamic environments in ancient rocks.

INTRODUCTION

The interpretation and prediction of contemporary sediment patterns on beach and near-shore areas have attracted the attention of a number of investigators. In the present study we focus attention on that portion which extends from the breaker zone to the top of the foreshore and seaward to a depth not exceeding 2 fathoms. Our purpose is to combine published theoretical and experimental work in such a way as to formulate or predict sediment patterns by using variables representing the water movements and the sediment size and degree of sorting. The predicted patterns are then compared with observed sediment patterns collected by us in various field locations and with published areal sediment patterns.

No attempt is made to cover thoroughly the extensive literature on this subject. Pertinent papers are referred to in the text.

We take the point of view that the beach and surf region can be subdivided into several zones which are characterized by dynamics peculiar to that zone, with resulting cut and fill leading to typical sorting and size patterns. The area of interest will be limited to a narrow band along the shore which has as its landward margin the well-defined upper limit of wave swash on the foreshore. The outer margin is seaward of the breaker zone at low tide. In all cases, the area limits fixed for sampling purposes at low tide remain the same, but the proportions of the zone change as the tide rises or falls, and the breaker line migrates in a shoreward or seaward direction.

The region in which the breakers form is surely an important one in sedimentary processes. Not only does it migrate with the tides from day to day, but it also migrates across the land with passage of time, as sea level changes. Clearly the great energy concentrated in this narrow band and its margins both seaward and landward is of primary importance in forming the final sediment pattern of all within its range. Although the band is narrow at any one time, its migrations with tide and long-term sea-level changes must leave its effect as the dominant process on an areally important proportion of the sedimentary record. The long-range purpose of this initial study is to ascertain to what extent and in how fine a detail certain sediment size and sorting patterns in ancient rocks can be recognized as typical of the breaker zone and its margins in contemporary sediments.

Figure 1 shows the dynamic zones which we feel characterize the surf region. The "step" as a topographic feature which appears when conditions are favorable is a distinct break in slope just under the average wave crest at the point of plunge. The zones will be discussed in some detail in the main body of the paper. In brief, Zone W is characterized by shoaling wave dynamics; Zone B, just at the breaking wave and including the step when present, is characterized by turbulence; and Zone S, the beach foreshore up to the limit of swash, is characterized by sheet flow, first up and then down the foreshore.

---

[1] Woods Hole Oceanographic Institution Contribution No. 958. Manuscript received February 13, 1958.

It is important to understand the distribution and application of the great energy concentrated in this narrow band. Those who study ancient environments by interpreting the sediment pattern of ancient rocks are well aware that the land-sea interface moved across a considerable part of inundated portions of continents as the sea encroached farther and farther inland. Sometimes the interface was marked by beaches which moved with the rise or fall of sea level, became buried and preserved (Thompson, 1937), or were destroyed. Workers with ancient rocks have immediate use for ideas or techniques which will aid in interpreting past environments and the effects of marine inundation. Certainly, one of the long-range purposes of this study is to ascertain to what extent and in how fine detail certain sediment size and sorting patterns in ancient rocks can be recognized as typical of modern environments—in this particular case the surf zone and beach foreshore.

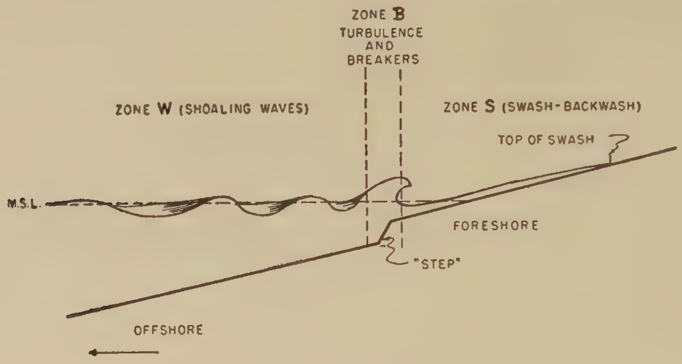

Fig. 1.—The dynamic zones

FIELD METHODS

In those field studies made by us and referred to in this paper, the following properties were measured.

Median sediment diamter (mm.)	Md.
Degree of sorting[2]	$D.S. = \frac{P_{80} - P_{20}}{P_{50}}$
Wave height	H
Wave length	L
Wave period	P
Still-water depth	S.W.D.
Still-water level	S.W.L.
Average velocity of backwash on foreshore	$\bar{V}_{max}$
Slope of foreshore	S
Average depth of flow of backwash . . .	t_d
Local topography of near-shore and beach foreshore	

Other variables were also measured in the course of the study but are not directly used in the present study.

---

[2] The measure of sorting used in this paper differs from those customarily employed, in that the effect of size is removed from the measure of the "spread" of the frequency distribution by dividing by the median or 50th percentile. In an earlier paper (Miller and Olson, 1955) the coefficient of variation = standard deviation ÷ mean was applied for a similar purpose. The present measurement is simpler to compute and appears to serve equally well. The term "sorting" means different things to different people. To us, a handful of pebbles of roughly the same size class is as "well sorted" as a handful of sand grains in a single size class.

Clearly the standard deviation will faithfully reflect the size units and therefore will not be a useful measure for our purposes. For full discussion of various aspects of this problem see Doeglas, 1946; Inman, 1949.

Wave length was measured directly, using a tape to measure from crest to crest. The number of waves passing the tide gauge per minute was called *wave period*.

Wave height was recorded by observing the height of successive troughs and crests with respect to still-water level on a marked tide gauge. The tide gauge itself consisted of a plastic pipe forced into the bottom (fig. 2). A small hole in the pipe below water surface acted as a damping mechanism, permitting only small fluctuations of still-water level in the pipe. A Ping-Pong ball floating inside marked the still-water level.

All these measurements were made in a defined study area; therefore, there is a distribution-in-space aspect which is especially important in the sediment (and the cut-and-fill measurements) (see Inman and Rusnak, 1956). Time also is an important factor. It is obvious that all the afore-mentioned variables change with time; hence a number of repeated measurements were taken during each hour at Falmouth Beach and during each 2-hour period at Highland Light Beach over a full tidal cycle in each case (see fig. 2*a*).

The field procedure at Falmouth Beach will be described briefly. A portion of beach 75 feet long and 36 feet wide was selected. This area covered the zone of upwash, zone of breaking waves, and seaward of the breaking waves (fig. 1). Thirty-six sample stations were established within the area (fig. 3). The stations were marked by iron rods pushed into the sand. Sediment samples were taken in half-pint containers once each hour at each station for 11 consecutive hours.

A considerable problem was encountered in reducing the relatively large amount of data to a usable form. We chose to describe the sediment in terms of median and sorting values contoured over the study area (e.g.

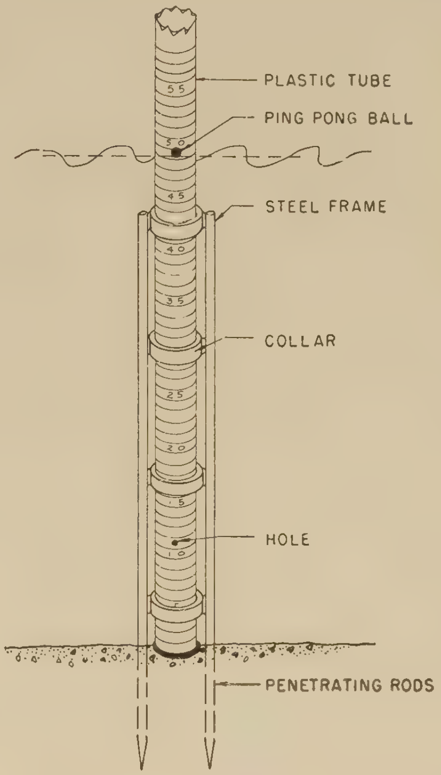

FIG. 2.—Still-water level gauge

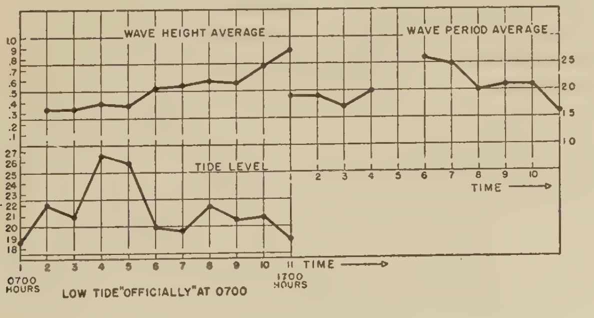

FIG. 2*a*—Falmouth study, 1956

fig. 9). The median and sorting values are not contoured directly; rather, a surface of best fit is passed through all of the sample points. This gives a pattern free of local irregularities in sediment size and degree of sorting. The technique for fitting surfaces to sedimentary data is described by Miller (1956); in this particular study the computations involved in fitting surfaces to our data were done by the high-speed computer AVIDAC, at Argonne Laboratories in Chicago, and by IBM.

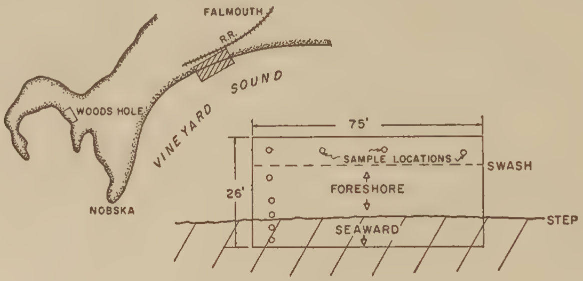

FIG. 3.—Location sketch of Falmouth Beach

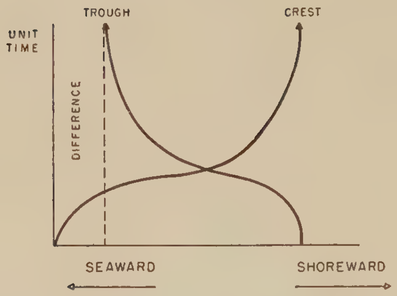

FIG. 4.—Directional movement of sediment particle under crest and trough in shoaling wave.

An alternative to using trend maps for analysis of the areal size and sorting distribution is the application of the analysis of variance as described in Krumbein (1953) and Krumbein and Miller (1953).

SHOALING WAVES (ZONE W)

A hypothesis relating the dimensions (length and internal-wave velocity) of shoaling waves to the movement of sediment was proposed by P. Cornaglia and described briefly in a speech by Münch-Peterson (1950). Cornaglia states in his proposal that, because crest velocity is greater than trough velocity in shallow water, the force moving a sediment particle will act to move the particle in the direction that the crests are moving, a distance proportional to the difference between crest and trough velocities. Figure 4 illustrates his theory. Cornaglia then states that the difference between trough and crest velocity becomes less as the water depth increases until there is not enough difference to move the particle a net distance in either direction. Meanwhile the influence of gravity becomes increasingly important in pulling sediment particles downslope—seaward. Somewhere, according to Cornaglia, all of these forces are equal, and each sediment particle has a "null point" where net movement along a line normal to the wave direction is zero—the particle simply moves back and forth. Seaward of this point the net movement is seaward, and landward of this point the movement is landward. If a lot of different sizes are present, only one size is at its "null point"; the larger sizes move downslope (seaward) and the finer sizes in the direction of the crests. It follows, therefore, that, for given slopes and given wave characteristics, each particle has a "null point" where net movement of that particle is zero.

Münch-Peterson (1950) holds that the above-described theory is not valid, in that the influence of gravity relative to wave pressure is too small to be considered important, no matter what the bottom slope is. Ippen and Eagleson (1955) point out that Cornaglia's hypothesis has not gained recognition in the United States. Scott (1954) describes equilibrium conditions for various grain sizes, as observed through an interesting series of wave-tank experiments.

Careful laboratory observations on single sedimentary particles in a wave tank by Ippen and Eagleson (1955), however, appear to verify at least a part of Cornaglia's hypothesis. For a fixed slope of 1:15, the existence of "null points" and zones of forward movement were recorded in this study, for several combinations of wave height and length ratios, with single particles varying in size and specific gravity. Seaward movement was also noted, but to a much less degree. They concluded that net sediment transport is dependent on the balance between transportation shoreward due to wave action and transportation seaward due to gravity. They further conclude that "a special 'null point' or zone of zero net sediment size on the given beach under a given incident wave . . . confirming the existence of the so-called Cornaglia 'neutral line.' For the plane fixed beach of 1:15 slope employed, and a range of incident wave steepness of $0.01 \leq H/L \leq 0.08$, the null point appears independent of the sediment diameter to roughness diameter ratio, D/K, and of boundary layer effects and may be given by the following relation:

$$\left(\frac{H}{d}\right)^2\left(\frac{L}{H}\right)\left(\frac{C}{w}\right)=11.6\,.$$

"This equation holds, provided that fluid velocities are greater than that required for the incipient motion of the particle being considered. H, C, and L are *local* wave characteristics, and w is the fall velocity of the sediment particle under consideration. The constant 11.6 is valid only for a slope of 1:15 and must be presumed to vary with a function of the slope for the general case."

The present writers have applied the hypothesis to Zone W, the region of shoaling waves (see fig. 1). The equation given above was solved for depth for a given sediment particle size under the wave conditions observed at Falmouth beach (fig. 2*a*). Contour maps of the "neutral lines" were then made to scale on transparent paper so that they could be laid over the sediment size and sediment sorting, for comparisons. The following describes in detail the way in which the null point or neutral line maps were constructed:

1. Ippen and Eagleson's empirical equation,

$$\left(\frac{H}{d}\right)^2\left(\frac{L}{H}\right)\left(\frac{C}{w}\right)=11.6\,,$$

was rearranged into a suitable and dimensionally correct form:

$$\frac{HLC}{d^2}(0.0865)=w \qquad (1\mathrm{W})$$

where

H = wave height,
L = wave length,
C = wave celerity,
d = still-water depth,
w = terminal fall velocity of the sediment particle.

2. Wave celerity varies as a function of L, H, and d. If the effect of H (wave height) is neglected, an equation due to Airy (1842) may be used, where

$$C^2=\frac{gL}{2\pi}\tanh\frac{2\pi d}{L}\,. \qquad (2\mathrm{W})$$

3. H and L values characteristic of a given period of time were made available by averaging field observations taken over the time period. Thus for a time period, equation (1W) was solved for w, given (1) various values of d, (2) C values corresponding to d (eq. [2W]), and (3) fixed H and L.

4. The resulting terminal fall velocities were then transposed to grain diameters by the use of a nomogram devised by Rouse (1937).

Figure 5*a* shows the relationship between grain size and still-water depth for Cornaglia's null points. Curves were constructed for four separate hour periods during the 12-

hour tidal-cycle study at Falmouth Beach. From these curves still-water depths corresponding to the range of median grain diameters found at Falmouth were used to construct the contour maps of figure 6, *a–c*. Figure 5*b* shows curves for larger wave height and wave length.

The null-point maps are on the same scale as the maps of sediment size and sediment sorting. In this way, comparisons of several of the variables at corresponding times may be conveniently made. In figure 6, *a*, the null points contoured were for time T approximately at low tide. The observed median sediment size ranges for T indicates a minimum median contour of 0.5 contour interval. We therefore computed null points for median sizes ranging from 0.5 to 4.0 mm. The dotted lines show where S.W.L. intersects the beach at about the middle of hour T_1. The small circles indicate the sampling points, and the double circles the position of the tide gauge. The observed median values are given at each

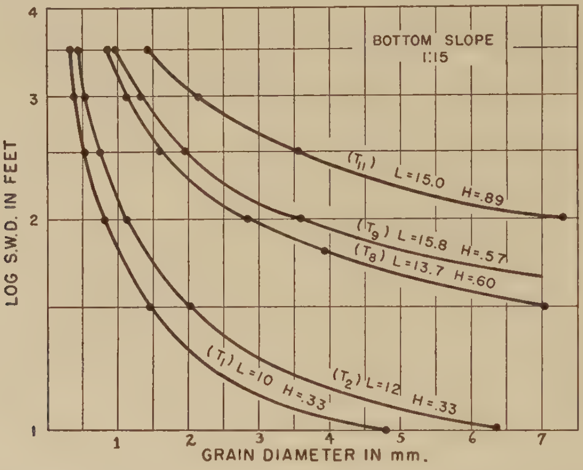

FIG. 5*a*.—Prediction in terms of SWD of position of null point for grain size with given H, L, and transforming wave celerity (for several tidal stages at Falmouth).

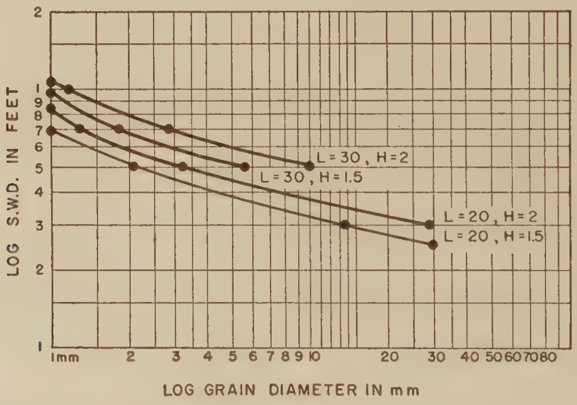

FIG. 5*b*.—Prediction of null-point–SWD relation for an extended range of wave H, L. The legitimacy of extrapolation here is questionable. Note that, for wave height of 1.5 feet and wave length of 20 feet, small pebbles of 13.5 mm. in diameter begin net shoreward movement in SWD of just less than 3 feet.

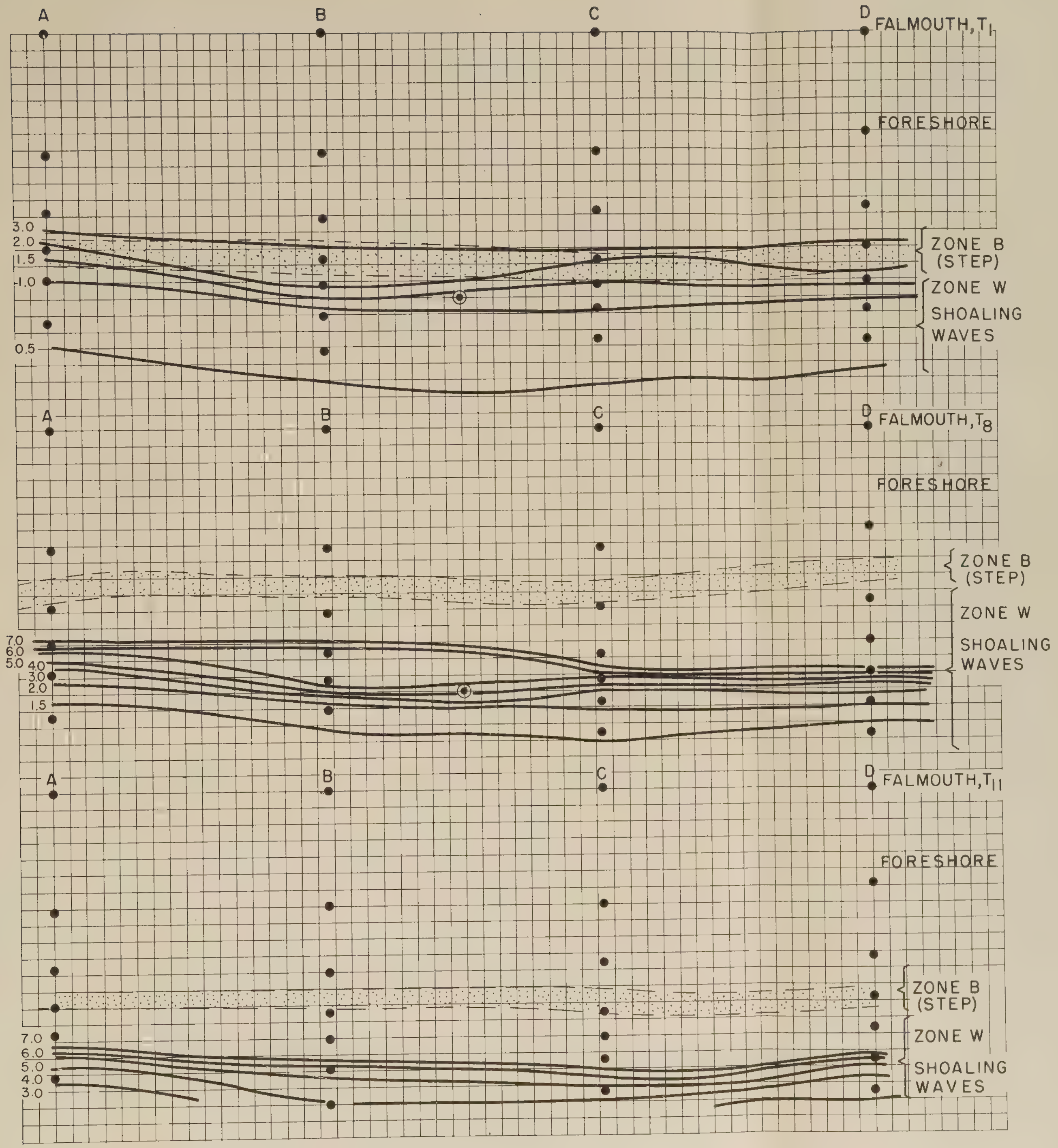

FIG. 6.—Computed position of null points (*neutral lines*) for 0.5–3.0-mm. grain size for three tidal stages at Falmouth in accord with the wave height, wave length, and SWD at those particular times.

of the sample points for comparison with the contours for null points.

Let us now examine the combined theories to see what we would expect if they are correct. We shall use two models: Model I, no seaward motion under gravity; Model II, both landward and seaward motion.

MODEL I, FIGURE 7

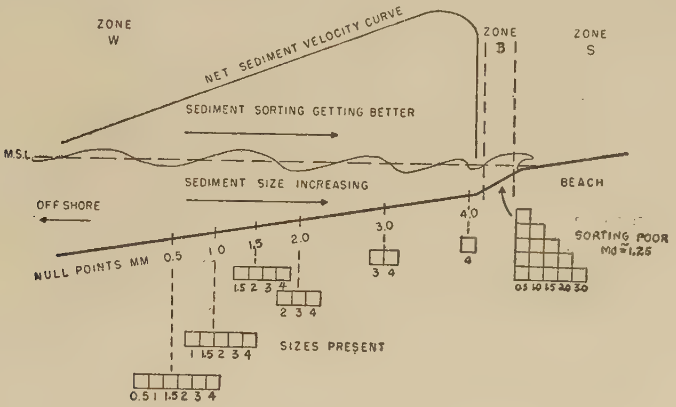

FIG. 7.—Model I

We may conveniently start with a hypothetical situation in which there is a wide range of sizes, well mixed so that there is an equal proportion of each size everywhere within Zone W. If wave action is then begun, the various sizes will be sorted in accord with their various null points. Let us suppose for illustration that there are five arbitrary size classes numbered 1 through 5. We shall hold beach slope and wave length and height constant. Then there will be five null points on a traverse normal to the beach, so spaced that the finest is seaward and the largest nearest land. As the waves begin to transport the material, everything finer than the value at the null point will move toward shore, accelerating until maximum velocity is reached just seaward of the plunge point. Just shoreward of the plunge point, the velocity of the sediment drops to zero. We refer here to net sediment velocity in a shoreward direction for convenience, even though the particles actually may move in a forward-backward path, with a net forward movement. Our expectation under this model is that the median sediment size will increase regularly toward the shore and, at a given null point, will be greater than, or equal to, that null-point value. The sorting will become better by regular degrees toward the shore.

Shoreward of the largest null point and where the net sediment velocity curve drops to zero, the accumulated mass of sediment in transport is abruptly deposited, to be once again put into motion in a different manner in Zone B. The sorting at this point should be poor, and in our illustrative model the median should exceed 2.0.

The expected accumulation of sediment medians at the boundary between Zones W and B is also shown in figure 7.

This model utilizes the region of oscillation for a given particle size with shoreward net movement on the land side but does not consider seaward movement on the seaward side of the null point.

MODEL II, FIGURE 8

Suppose we also take into consideration that on the seaward side of the null point all larger sediment particles will move offshore. Figure 8 then illustrates what our expectation would be for the hypothetical situation where the distribution of sediment sizes is initially homogeneous.

1. As before, sediment Md. size increases toward the shore, with the Md. size corresponding exactly to null-point values.
2. Sorting is uniformly excellent, with one size class at each null point.
3. The accumulation at Zone B drawn from seaward in Zone W will have the same appearance as in Model I with low Md. value and poor sorting.
4. There will be a seaward accumulation but less well defined, with an Md. value coarse, and poor sorting.

Before testing the agreement of the models with natural conditions at Falmouth Beach, we shall list a series of factors which should be kept in mind when figures 9–11 are examined.

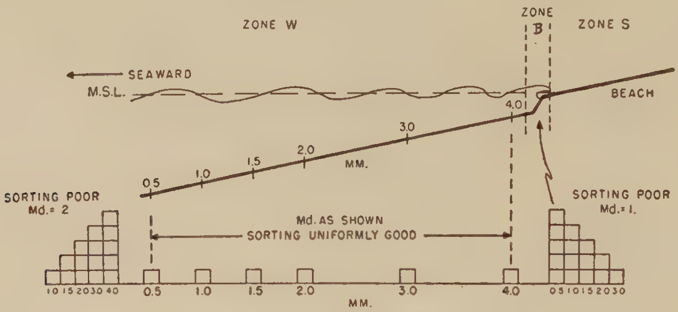

Fig. 8.—Model II

(1) The neutral line contour maps are based on an equation which is for a slope of 1:15. Falmouth Beach has a slope of 1:10 (This changes the constant in eq. [1W]).

(2) In addition, the equation is based on a perfectly plane beach. Local irregularities in the bottom slope established before the 12-hour study by markedly different wave conditions should not be expected to be completely erased.

(3) It is appropriate to consider the three zones defined in this paper as a "palimpsest" in which the patterns left by previous tides and changing wave conditions are only partially erased and show through the pattern put down at the time of study. This is particularly applicable to Zone W.

(4) The Falmouth Beach sampling grid was chosen sufficiently small on a traverse parallel to the beach so as to minimize the effect of longshore or littoral movement. In this way we effectively deal only with movements of wave and current orthogonal to the beach.

(5) No allowance for effect of wave period has been made.

We shall now turn to a comparison of the theoretical neutral lines with median size and sorting trend maps for several time stages during a single tidal cycle, as observed at Falmouth Beach.

Figure 9 facilitates a comparison of the expected position of the calculated neutral lines with observed size and sorting, for tidal period T_1 (low tide) in the form of a trend map (see fig. 6, *a*). We focus attention on Zone W (shoaling-wave zone).

1. The trend-map median size contours are consistently higher in value on a traverse toward the beach than the calculated neutral-line contours. This fits either Model I or Model II.
2. There is a tendency for median size to increase toward the margin of Zone B (the breaker zone). This fits both Model I and Model II.
3. Sorting clearly improves shoreward in the trend map. This fits only Model I.

Figure 10, showing the trend map for tidal period T_8 (falling tide), appears to reverse the picture. In Zone W, median size decreases strongly toward the new position of Zone B. No clear-cut interpretation is possible for the sorting trend map.

However, at T_{11}, 1 hour before low tide,

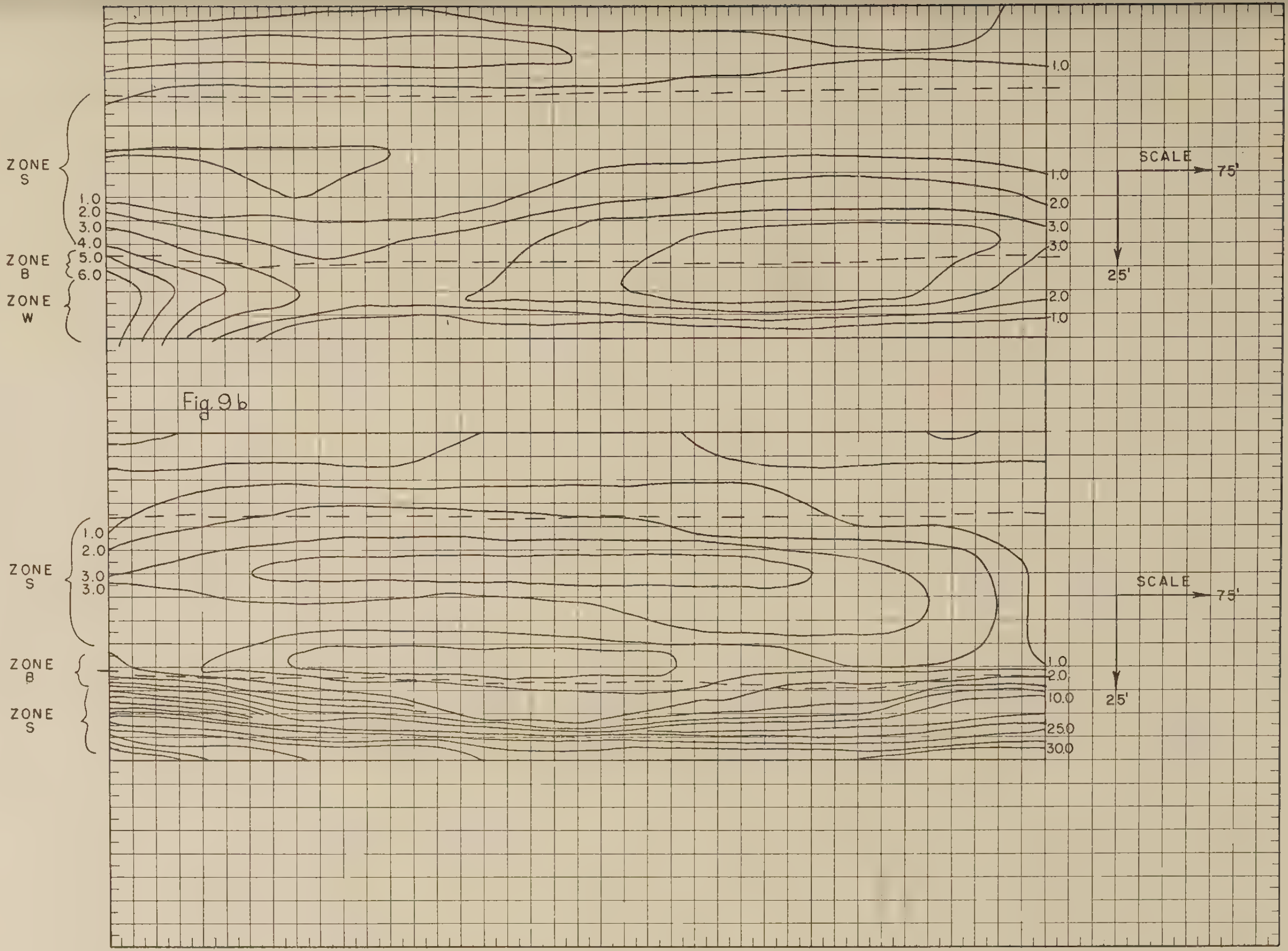
ZONE S
ZONE B
ZONE W
1.0
2.0
3.0
4.0
5.0
6.0
1.0
1.0
2.0
3.0
3.0
2.0
1.0
SCALE
75'
25'
Fig 9 b
a
ZONE S
ZONE B
ZONE S
1.0
2.0
3.0
3.0
1.0
2.0
10.0
25.0
30.0
SCALE
75'
25'

FIG. 9.—*a*, Median size trend map of T_1 Falmouth. Contour intervals = 1.0 mm. *b*, Sorting trend map of T_1 Falmouth. Contour interval = 1.0 mm.

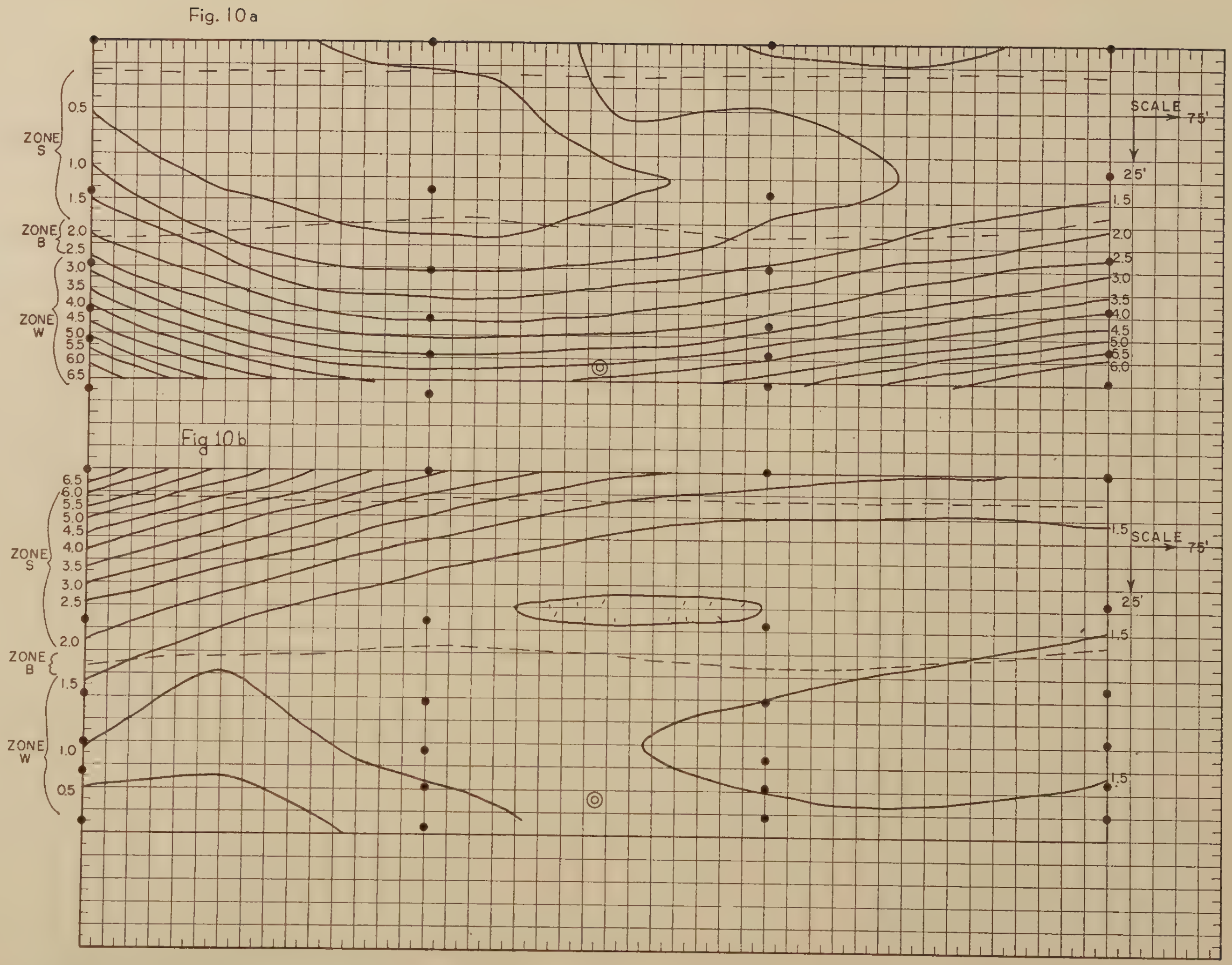
Fig. 10a
ZONE S
ZONE B
ZONE W
0.5
1.0
1.5
2.0
2.5
3.0
3.5
4.0
4.5
5.0
5.5
6.0
6.5
SCALE
75'
25'
Fig 10b
ZONE S
ZONE B
ZONE W

FIG. 10.—*a*, Median size trend map of T_8 Falmouth. Contour interval = 0.5 mm. *b*, Sorting trend map of T_8 Falmouth. Contour interval = 0.5 mm. *b*, Sorting trend map of T_8 Falmouth. Contour interval = 0.5 mm.

at the end of the tidal cycle studied, figure 11 appears to show that the pattern has reverted, at least in part, to that of tidal period T_1, the previous low tide. During this tidal cycle, wave height and length have increased, with the result that the neutral-line contours (fig. 6, *c*) are greater than the trend-map contours for median size. Whether or not a significant lag in the process is required to bring the expected into agreement with observed, we cannot say. Nevertheless, part of Zone W shows once again improvement in sorting toward Zone B, and similarly an increase, locally at least, in median size.

It seems striking to us that the combination of changing sea-state and tidal effect did not succeed in changing the basic pattern established at T_1 and returned to at T_{11}. There may be here a response to some underlying stability within this region. Clearly, repeated studies of this kind will be needed.

We now examine several other places. The trend map for Highland Beach on Cape Cod, taken at low tide, figure 12, shows the expected increase of median size toward the shore. Sorting also improves as expected, but a strong non-orthogonal component appears, so that the contours do not parallel the beach. It is possible that the near-shore littoral-current effect was not canceled out here, even though the length of traverse along the beach was only 75 feet.

The trend map for Indiana Dunes State Park beach on Lake Michigan shows the expected improvement of sorting in a shoreward direction, but the median-size trend map shows the expected increase in median size toward the shore in only one portion of Zone W (fig. 13).

Model I appears to be favored over Model II by the trend maps. We conclude, therefore, that the sand moved in accordance with a modified form of Cornaglia's theory and that, in the very shoal waters where our experiment was conducted, gravity played very little part in moving materials offshore. The above discussion is based on the initial assumption of a uniform distribution for the sediment. In the conclusions we shall take up the implications for Zone W when the initial distribution is symmetrical and also when it is polymodal. These two alternatives will give more realistic models. We felt that the uniform distribution would serve better as a first approximation.

A note on tidal effect.—The tidal effect is negligible in the Lake Michigan study. In the case of the Falmouth and Highland regions, we feel that low tide presents a pattern which is returned to in each successive low tide. Space does not permit the addition of eleven more trend maps. However, the following describes the pattern changes observed on an hourly basis through a full tidal cycle at Falmouth. The description is from a total of eleven trend maps completed for each of the hourly periods of the tidal cycle.

1. Low tide: as shown in figure 9. As the tide rises, the pattern established at low tide remains unchanged, but a new step is formed during the third hour, about 5 feet in a shoreward direction from the original step. Ripple marks are scattered through the interval between old and new steps.
2. High tide: the old step and the original Zone W pattern is now almost erased and does not show at all on the smoothed-surface trend map but can be seen clearly on contouring the original data. A series of incipient "steps" where tide and wave were long enough in a "steady state" are scattered from the original step to the high-tide breaker zone.
3. Falling tide: see, for example, figure 10. The pattern appears to be reversed. However, just at the next hour, the upper pattern of figure 8 is erased, and the original low-tide pattern begins to emerge until we reach the last period of the cycle (fig. 11).

At Highland, the trend maps were computed for every 4-hour interval in the tidal cycle. Once again, the low-tide pattern weakens as new steps are formed temporarily with the rising tide, and the low-tide pattern becomes dominant with the recurrence of low tide.

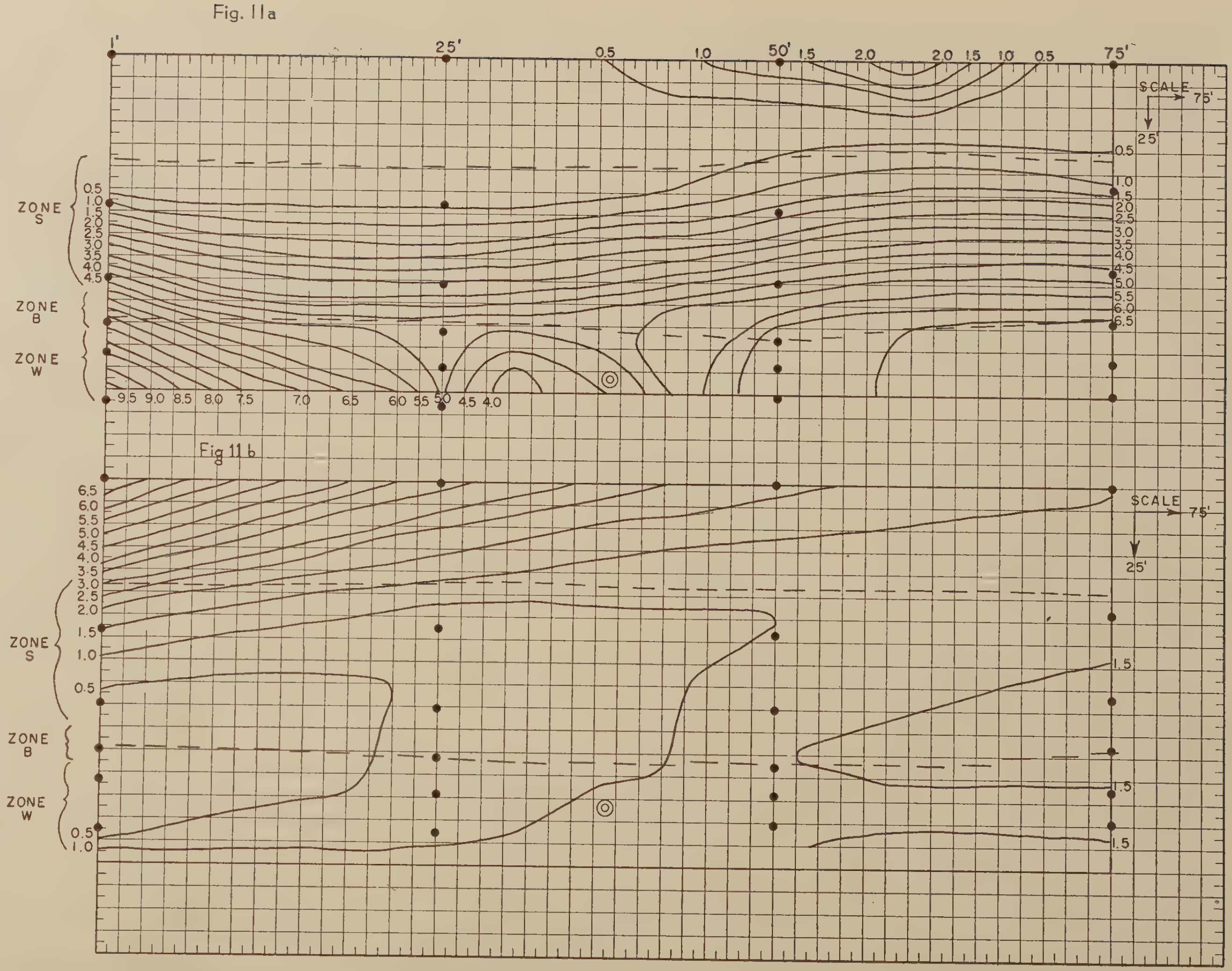
Fig. 11a
1'
25'
50'
75'
0.5
1.0
1.5
2.0
SCALE
75'
25'
ZONE S
ZONE B
ZONE W
0.5
1.0
1.5
2.0
2.5
3.0
3.5
4.0
4.5
5.0
5.5
6.0
6.5
7.0
7.5
8.0
8.5
9.0
9.5
Fig 11 b
ZONE S
ZONE B
ZONE W
6.5
6.0
5.5
5.0
4.5
4.0
3.5
3.0
2.5
2.0
1.5
1.0
0.5
SCALE
75'
25'

FIG. 11.—*a*, Median size trend map of T_{11} Falmouth. Contour interval = 0.5 mm. *b*, Sorting trend map of T_{11} Falmouth. Contour interval 0.5 mm.

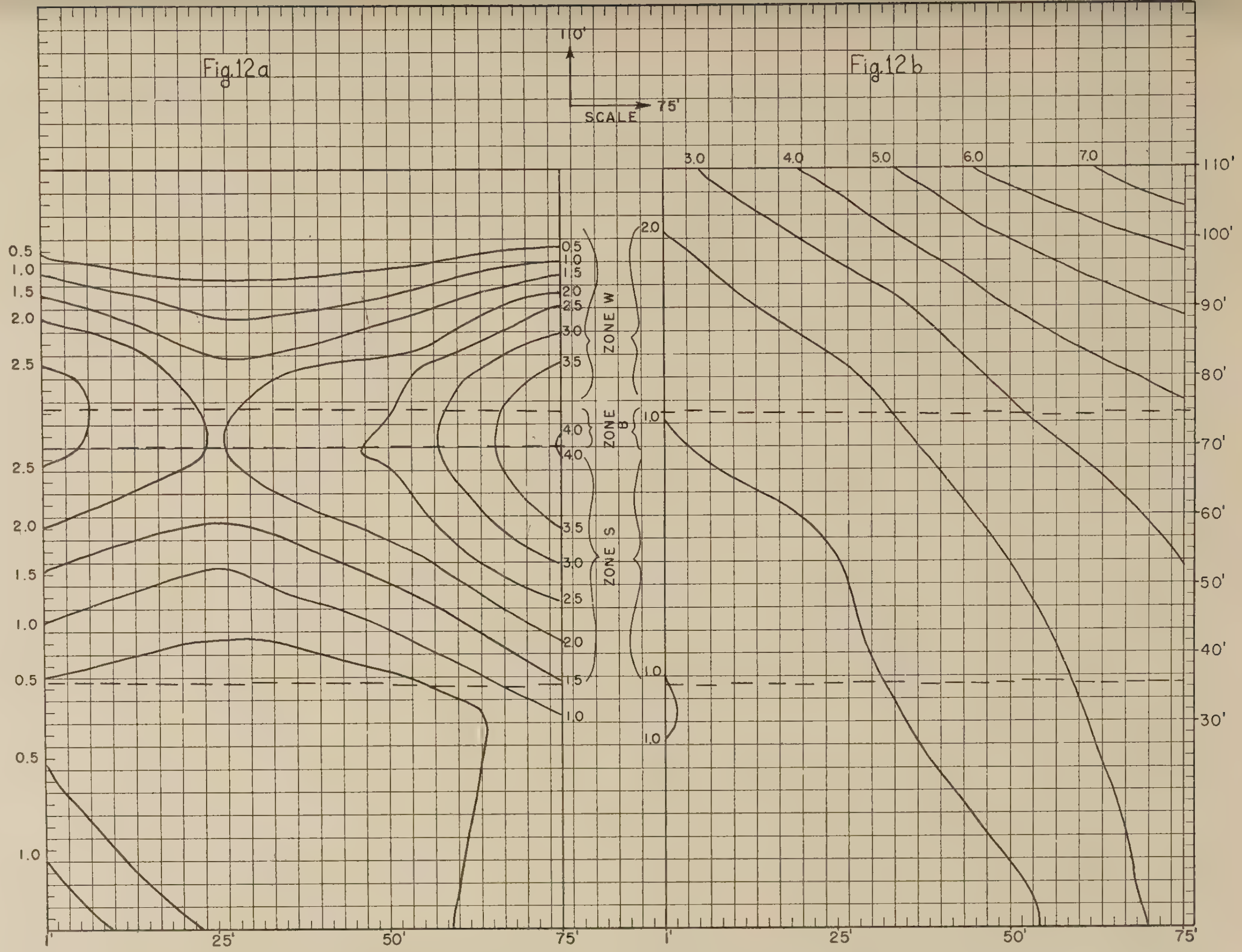

FIG. 12.—*a*, Median size trend map of Highland (low tide). Contour interval = 0.5 mm. *b*, Sorting trend map Highland (low tide). Contour interval = 1.0 mm.

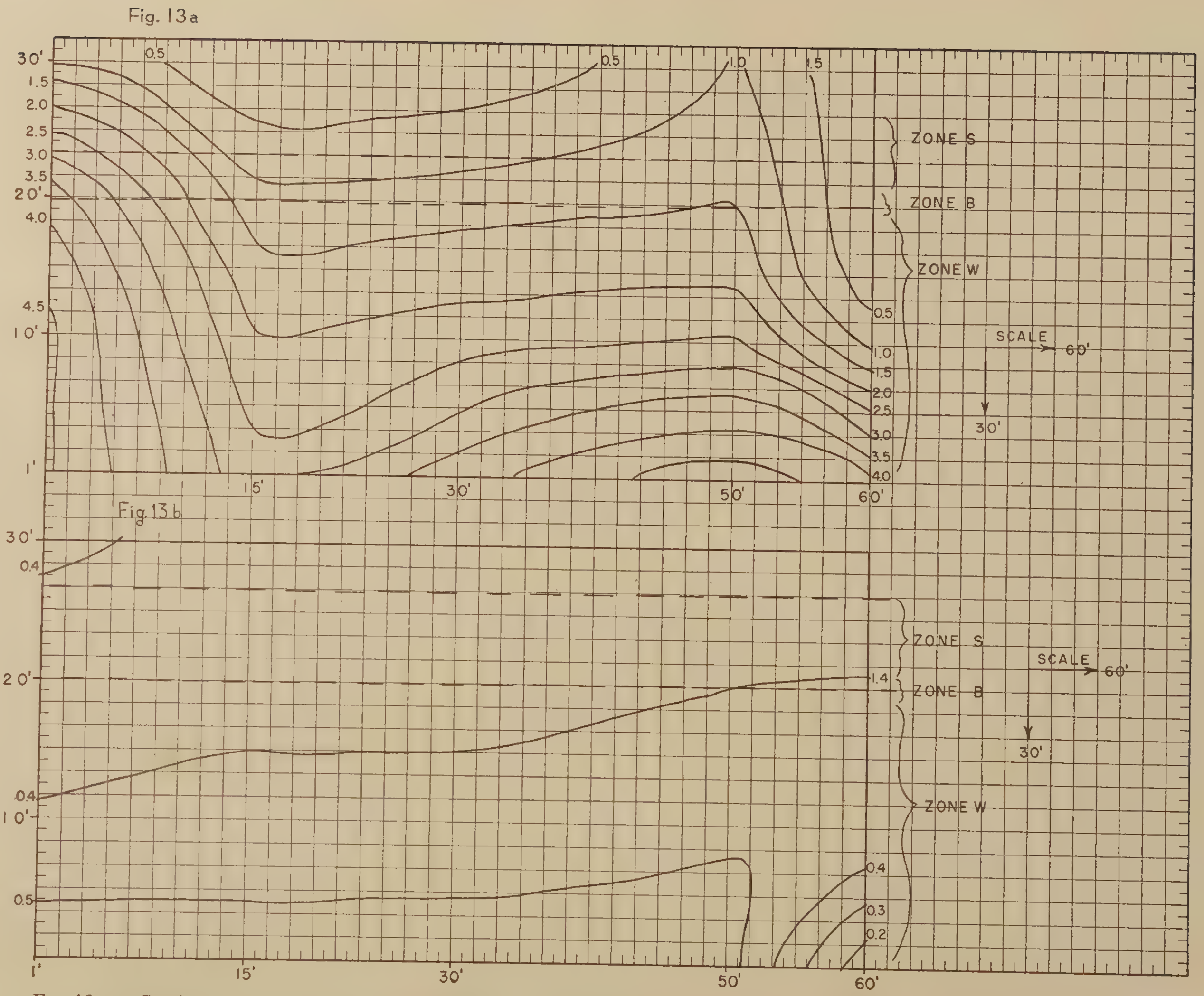
Fig. 13a
30'
1.5
2.0
2.5
3.0
3.5
20'
4.0
4.5
10'
1'
0.5
0.5
1.0
1.5
ZONE S
ZONE B
ZONE W
0.5
1.0
1.5
2.0
2.5
3.0
3.5
4.0
SCALE
60'
30'
15'
30'
50'
60'
Fig. 13b
30'
0.4
20'
0.4
10'
0.5
1.4
ZONE S
ZONE B
ZONE W
SCALE
60'
30'
0.4
0.3
0.2
1'
15'
30'
50'
60'

FIG. 13.—*a*, Sorting trend map of a Lake Michigan beach. Contour interval = 0.5 mm. *b*, Median size trend map of a Lake Michigan beach. Contour interval = 0.10 mm.

BREAKER ZONE (ZONE B)

Zone B is the region in which the forward net sediment velocity of Zone W drops to zero. It is where the breaking wave is met at its base by the returning backwash of a previous wave. The point of collision of the breaker and the swash, in our opinion is characterized by a turbulent region in which the net movement is vertically upward, so that a sorting action occurs. Although the returning swash does not always catch the base of the next wave just at the point of plunging, it does so a majority of the time. The flow characteristics of the backwash are a function of the slope of the foreshore, the size of wave creating the parent swash, and the size of sediment on the foreshore. Just as the incoming breaker deposits its load, it is met by the returning backwash, also carrying an accumulation of sediment. If the slope of the foreshore is sufficiently steep, a moderately well-sorted, relatively coarse "step" may be built in this turbulent zone.

The sediment which builds the "step" is derived in part from the load abruptly deposited by the incoming wave at this point. Thus the slope of the bottom in the near-offshore is also important (see discussion in the section on "Shoaling Waves" [Zone W]). The remainder of the sediment is carried down the foreshore slope by the backwash from the previous wave.

In the way described above, a grading or sorting action occurs in the vertical direction within the breaking wave over Zone B. The finer material does not settle out so rapidly as the coarse material, and the finest is probably carried forward onto the foreshore. We should, under these circumstances, expect the coarsest material to be concentrated at the step, whereas finer material should be found on both the seaward and the landward sides. In the specific terms of the sediment parameters dealt with in this paper, our expectation under the above mechanism is as follows:

1. Size. See figure 14.
2. Degree of sorting. This is difficult to specify. A sorting action occurs in all three zones. In Zone W, due to the action of shoaling waves on the bottom; in Zone S under the turbulent sheet flow downslope on the foreshore; and, finally, the above-described vertical movement in Zone B. Although less fine material is expected to remain in Zone B under the swirling turbulent motion, fine material may or may not be trapped with the coarser material as it settles out. This would greatly affect the numerical value of any measurement of degree of sorting.

Table 2 shows median size and degree of sorting for a traverse of samples collected across the breaker zone at a number of localities and under varying surf conditions. The sample points were arranged as shown in figure 15, so that the first sample was taken just inside Zone W; the second sample was taken on the slope of the topographic step in Zone B; the third sample at the crest of the step in Zone B; and the fourth sample midway between the upper margin of swash on the foreshore and sample point 3.

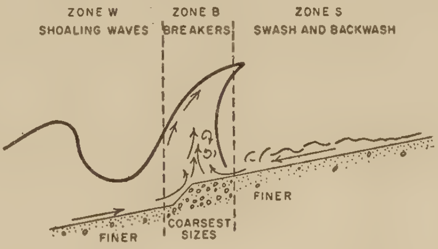

FIG. 14.—Mechanism for sediment pattern in the breaker zone (zone B). Arrows indicate net sediment movements at the moment the wave breaks.

Inspection of the table indicates that sediment samples taken at points 2 and 3 in the breaker zone have consistently larger medians than either sample point 1 in Zone W or sample point 4 in Zone S. The field evidence, within the limits of our data, thus supports the previous discussion regarding the expected size distribution across Zone B. This does not, of course, support the *uniqueness* of our hypothesis.

The data on degree of sorting seem to fall into two categories. The value of the sorting coefficients of the sample points in Zone B are either both higher or both lower than the sample in Zone W or Zone S. As suggested earlier, we are not, under the present relatively crude model, able to advance consistent expectations for degree of sorting in Zone B.

Further field data, bearing on the above discussion, were collected by sampling the wave itself. This was done in Zone B by using a series of cups fastened to a rod. Just as the wave is on the point of breaking, the rod is held vertically so that the cups sampled a vertical series of points through the wave (see fig. 16).

A single horizontal set of samples was caught by the same device at a later time as the wave plunged down on the foreshore (see fig. 16). The results as given in table 1 are not to be considered quantitatively accurate,[3] but should be of some interest.

Inspection of table 1 shows that the largest volume of sediment is found at the sample points nearest the bottom of the wave. The largest sizes are also found at the lower sample points, with one exception—in the vertical traverses. In two of the three vertical traverses, the sorting is poorest near the bottom. It is tempting to attribute the discrepancies to the failure of the sampling device. However, it is evident that further study is needed.

TABLE 1

Sample	Md. (Mm.)	Sorting	Weight (Gm.)	Location
Vertical traverse:				
1...........	0.38	1.39	46.19	Nauset, 1
2...........	.34	0.85	49.67	
3...........	.25	0.92	11.87	
1...........	.41	1.32	22.78	Nauset, 2
2...........	.35	0.77	7.87	
3...........	.30	0.90	1.07	
1...........	.26	0.79	15.88	Nauset, 3
2...........	.34	0.76	7.97	
3...........	.30	0.83	2.90	
*Horizontal traverse:**				
1...........	.34	0.71	23.48	
2...........	.33	0.79	74.68	
3...........	0.33	0.79	38.88	

* Average of three sets of samples.

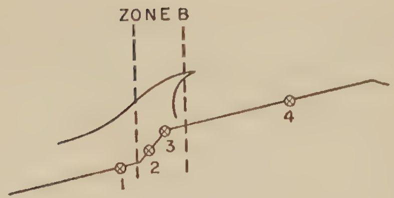

FIG. 15.—Location of sample points for study of size distribution across zone *B*.

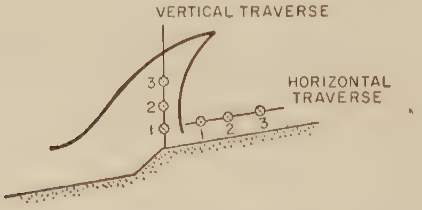

FIG. 16.—Location of sampling points for sediment carried within the breaking wave. Sample cups about 1 foot apart. Horizontal traverse about 6 inches above foreshore.

Some question arose as to whether the breaker itself deposited sediment on the foreshore. A suggestive bit of data is found in the averaged horizontal traverse of table 1. Note that median size and degrees of sorting are about the same in the several sampling points. The weight column indicates that, at least for that particular sequence of waves, a measurable quantity of sediment was carried across the breaker zone and deposited on the foreshore.

---

[3] Effort was made to prevent the cup from disgorging part of its catch by downcurving the rear portion to create an eddying motion to the sediment-laden water. However, we do not, at this stage, know how much of the total catch was immediately lost.

The data of the vertical traverses within the limits of the small sample lend further credence to the hypothesis advanced earlier regarding the mechanism of water versus sediment within the breaker and the heaviest suspension to be lowest also.

In summary, this section presents a hypothesis for the mechanism in the breaker zone which results in the sediment pattern consistently observed at this place in nature. The field evidence presented in this section supports the hypothesis of net vertical movement in the base of the turbulent breaker, with a secondary sorting action on the material thrown into suspension. It is clear, however, that the hypothesis presented is qualitative and is only one possible explanation.

TABLE 2

LOCATION	MEDIAN SIZE (MM.) Sample Point 1	2	3	4	DEGREE OF SORTING (MM.) 1	2	3	4
Nobska Beach.....	0.33	0.88	0.44	0.29	4.12	4.35	1.61	0.93
Falmouth.........	4.60	4.90	5.20	1.09	0.83	0.37	0.31	1.04
Sippewissett.......	0.11	0.36	0.11	0.11	0.26	2.20	1.72	0.24
M. B. L. Beach.....	0.69	1.09	0.72	0.48	1.00	0.82	0.60	1.12
Old Silver Beach...	0.24	0.72	0.70	0.68	3.38	0.56	0.60	0.68
Sandwich.........	1.84	3.60	9.60	5.40	1.93	2.75	1.19	0.96
Green Harbor.....	0.43	0.42	0.76	0.24	2.99	2.45	5.12	0.98
Poponesset........	0.74	0.81	0.66	0.68	0.97	1.59	0.76	0.84

FORESHORE (ZONE S)

In this section we shall put together our field observation and field measurements of velocity of flow with published experimental observations, to form a model for the sediment pattern of the foreshore. This model will be used to express our expectation of sediment size and sediment sorting. The model is then applied to several beaches in which the following information is available: (1) slope of foreshore, (2) average depth of backwash, (3) average velocity at surface of backwash, and (4) an estimate of the velocity gradient from top of swash to the lower end of the backwash return.

We proceed to work out a sediment pattern for a given beach in terms of the model. This pattern is then compared with the sediment patterns actually found at that beach.

THE MODEL

The model consists of the following elements:

1. *An assumption as to the sorting or size pattern left just after a given upwash or swash has passed over the foreshore.*—Consider that a given wave breaks and carries up the foreshore a load of sediment in suspension as well as by rolling or saltation. The sediment load is derived partly from the lower part of the foreshore and partly from material carried in the breaker itself. As the velocity of the upwash approaches zero, the load is dropped along the way, presumably with the coarsest material first, and the finest carried upslope. Certainly the mechanism of erosion and subsequent deposition of the upwash is not so simple. A detailed discussion of the complexities of backwash from a qualitative viewpoint is given in Demarest (1947). In the present discussion however, we are not concerned with presenting a detailed mechanism for erosion and deposition during the upwash. We wish merely to establish a pattern of sediment size and sorting after the upwash has passed over the foreshore, an as arbitrary starting point. The subsequent backwash and its effect on this initial distribution will then be discussed in some detail, from the working part of the model. Field samples of the foreshore sediment are collected just after the backwash when the foreshore is

momentarily free of water. We shall therefore assume that, just prior to the backwash, the following sediment pattern is found: graded size, with the finest nearest the top of the foreshore. Graded sorting, with the best sorting near the top of the foreshore.

2. *Consideration of the velocity required to start a grain of a given size moving downslope under the backwash.*—A relation between turbulent flow and initiation of sediment movement on a rough bottom has been experimentally determined by Ippen and Verma (1953). In their paper, v_e is defined to be the "edge velocity" at the upper edge of a sediment particle resting on a rough bottom (see fig. 17) where conditions of fully turbulent, uniform, steady flow are present. Then, for v_e just large enough to initiate movement in a given size of particle, the following is empirically established:

$$\bar{V}_e = 0.12w\left[S^{1/2}\frac{d}{K_e}(S_s - 1)\right]^{-0.3}, \quad (18)$$

where w = terminal fall velocity for given grain size, d = grain diameter, S_s = specific gravity of grain, S = slope of the energy gradient, and K_e = effective hydraulic roughness length. In actual computation we took S_s to be 2.67 for quartz, S to be equivalent to the average slope of the sediment-water interface on the foreshore, and K_e to be 2.5 × K where K is the average grain diameter of the bottom. This last was based on inspection of the relation between K and K_e as given in table 1 of Ippen and Verma.

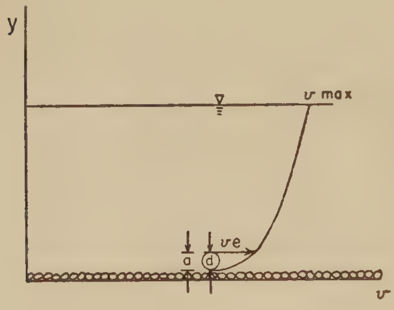

FIG. 17.—Definition sketch giving notation for velocity profile in the turbulent backwash. (Based in part on a figure in Ippen and Verma, 1953.)

3. *Velocity distribution on the foreshore.*—Velocity at the surface is measured on both backwash and upwash by timing a float, such as a Ping-Pong ball, over a measured distance. The traverses were normal to the breaker zone and so arranged that the upper end was well below the top of the swash and the lower end well above the breaker line. By timing the float over the measured distance for repeated trials, an average maximum (surface) velocity for upwash and for backwash was recorded.

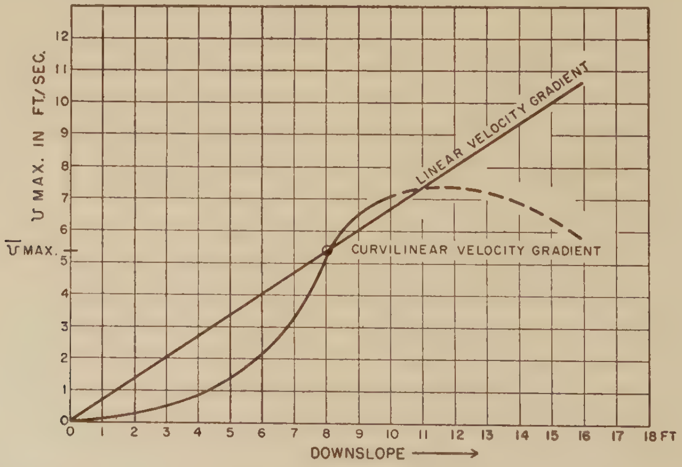

FIG. 18.—Postulated surface velocity gradients for backwash based on data from Nauset Beach, Cape Cod, Massachusetts.

We may, for simplicity, assume that the gradient for the surface velocity of the backwash is linear, starting at the top of the swash and proceeding to a maximum at the lower end of the traverse. Then the recorded average surface velocity forms the mid-point value of the traverse (see fig. 18). Since the velocity is usually at a maximum when a profile from sediment interface to free surface at the top is considered, the surface velocity will henceforth be referred to as the maximum velocity, $v_{\max}$.

At Nauset Beach on Cape Cod, Massachusetts, the velocity was measured over a traverse, and an average was determined to be 5.32 ft/sec. Then, for zero velocity at the top of the traverse and 5.32 ft/sec at 8 feet downslope, we have the linear equation $v_{\max} = 0.665x$. Field observations tend to indicate that a more realistic $v_{\max}$ gradient would not be linear but would take the general form shown in figure 18, where the dimensions are once again based on the Nauset Beach study.

The postulated drop in the velocity curve at the upper end of figure 18 is thought to be due to the accumulated sediment load entrained in the backwash, and subsequently the velocity is abruptly checked when backwash strikes the next oncoming wave or the "dead" water at the foot of the foreshore. It should be emphasized at this point that accurate measurements of flow characteristics on swash or backwash under field conditions is a very difficult problem. Adaptation of Pitot tube devices, for example, have thus far proved unsuccessful because of almost immediate clogging of the orifice with sand. The shallowness of the flow renders standard current meters inoperable, e.g., Price-Gurley or Ekman.

4. *Computation of theoretical contours of size and sorting distribution on the foreshore.*—For a given grain size we compute the edge velocity necessary to initiate movement in the direction of flow. This direction will be downslope under the backwash. We use the relation as given in equation (1S) of section 2 above. Then, for the resulting v_e, we compute the surface velocity $v_{\max}$, by using a logarithmic equation due to Krey (1927) as cited in Rouse (1938):

$$V = V_{\max}\left\{\frac{\log(1 + y/a)}{\log(1 + t_d/a)}\right\}, \quad (2S)$$

where y = variable distance from the bottom, t_d = total depth of flow, and a = a very small distance between boundary and reference axis. The notation is illustrated in figure 17. By taking y equivalent to grain diameter and a equivalent to y, the equation takes the following convenient form:

$$V_{\max} = \bar{V}_e\left\{\frac{\log(1 + t_d/a)}{\log 2}\right\}. \quad (3S)$$

The $V_{\max}$ computed[4] for a given grain size is now translated into specific field conditions, either by referring to the straight-line first approximation for the velocity gradient or, graphically, by using the more realistic postulated curvilinear velocity gradient. For example, in the Nauset Beach study, previously referred to, the following data are available for a selected grain diameter:

Selected grain diameter	d = 1 mm. = 0.0033 feet
Average surface velocity of backwash	$V_{\max}$, 5.34 ft/sec
Average grain size on foreshore	K = 1 mm. = 0.0033 feet
Specific gravity of quartz . . .	S_s = 2.67
Slope of foreshore	S = 0.10
Effective hydraulic roughness length	K_e = 2.5K = 0.0082
Terminal fall velocity for 1 mm.	w = 0.496 ft/sec
Length of traverse	16 feet
Depth of flow	t_d = 0.2 feet

Then $\bar{V}_e$ = 0.0992 ft/sec from equation (1S) and $v_{\max}$ = 0.587 ft/sec.

---

[4] We also tried the Prandtl form of the Von Karman velocity-deficiency equation for fully turbulent uniform steady flow, as cited in Bakmeteff (1936), where, in our present notation,

$$\frac{V_e - V_{\max}}{\sqrt{gdS}} = \frac{1}{k}\left(\frac{d}{t_d}\right), \qquad k = 0.4\,.$$

We found, however, that, within the range of our field data, the lower end of the velocity profile did not include our very small values for d, the distance from sediment interface to the top of the sediment particle. It thus was not possible to use the equation for extrapolation from $V_{\max}$ to V_e.

Referring to figure 18, we find that, for the linear velocity gradient, the 1-mm. grain size begins to move downslope at approximately 0.9 feet from the upper end of the traverse. If we use the postulated curvilinear velocity gradient, we find that the 1-mm. grain size begins to move downslope at approximately 3.2 feet from the top of the traverse. Table 3 presents the expected distance downslope that various grain sizes will begin to move under observed field conditions at Nauset and Highland Light Beaches, both on Cape Cod, Massachusetts.

We now return to the expected sediment pattern left by the upwash and construct an expected or theoretical sediment distribution on the foreshore for a given beach at a given time. We consider that the sediment distribution over the foreshore just after the upwash consists of graded size, with the finest near the top of the foreshore, and graded sorting, with the best sorted near the top of the foreshore. Under these circumstances, we may expect a zone near the upper end of the foreshore to show rapid increase in size on a traverse downslope and a rapid improvement in sorting. Continuing downslope, we expect a regular continued rise in median size, but poor sorting with irregular contour pattern. The above conclusions are arrived at by the following reasoning. Everything is put into motion under backwash within, let us say, the upper 10 per cent of the foreshore. However, as the backwash passes over successively lower portions of the foreshore, it is passing over an increasingly coarse bottom. Large particles put into motion higher in the traverse come to rest downslope as the velocity gradient passes its maximum. Still larger sizes in the lower foreshore are not appreciably moved at all. Finer sizes put into motion near the top of the foreshore are carried under the turbulent flow and trapped in an irregular manner between interstices or in eddies around larger particles; thus we expect a band near the top of the foreshore of graded small sizes, increasing rapidly downslopes followed by a regular coarsening of the sizes, to the edge of the breaker zone. We also expect good sorting, improving downslope, in the band of small sizes at the top of the foreshore. Below this band we expect poor sorting, irregularly distributed in contours over the lower 80–90 per cent of the foreshore within the sediment size and foreshore-slope ranges of this study (see fig. 19).

TABLE 3*

Distance Downslope at Which Given Grain Size Begins To Move under Backwash

Nauset		Highland Light	
Grain Size (Mm.)	Distance Downslope (Feet)	Grain Size (Mm.)	Distance Downslope (Feet)
0.5	2.7	0.5	1.5
1.0	3.2	1.0	2.0
2.0	3.6	2.0	2.5
3.0	3.6	3.0	2.6
Av. breaker height	1.5 feet	Av. breaker height	3.2 feet
Av. slope of foreshore	6° approx.	Av. slope of foreshore	13° approx.
Av. surface velocity for backwash	5.34 ft/sec	Av. surface velocity for backwash	6.13 ft/sec

* The velocity measurements are of the same order of magnitude as observed by Demarest (1947), who found average velocity for the backwash to be about 6 ft/sec for slopes from 9° to 13°.

If the tide rises, the well-sorted band of finer material is continually erased or covered and appears higher on the beach, while the major active portion takes over a larger portion of the foreshore.

As the tide falls, the well-sorted band of finer material increases in width, reaching a maximum at low tide. This last is shown in the Highland Light trend maps (fig. 12). Comparison of the theoretical or expected sedimented pattern for size and sorting on the foreshore is now made with trend maps for various beaches based on sediment samples collected in the field. We shall first consider the Falmouth Beach tidal trend maps (figs. 9, 10, 11). The median size contours for tide stages T_1 and T_{11} increase downslope. This is in good agreement with our model. The sorting contours decrease downslope, as expected, for T_8 and T_{11} but are reversed for time T_8. The Highland Light trend maps show agreement for both size and sorting contours, with the expected contours. The Lake Michigan beach trend map (fig. 13) for sorting shows agreement with the model.

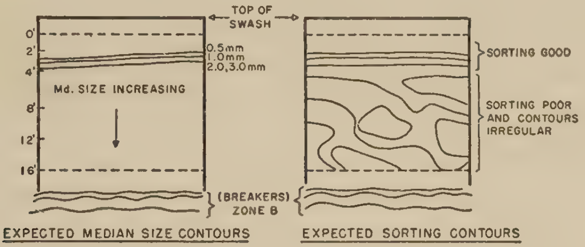

FIG. 19.—Plan view of foreshore, showing expected pattern of contours of median size and sorting of sediment.

In no case are contours concentrated toward the upper end of the foreshore as predicted by the model. Inspection of the trend maps and comparison, for example, with the calculated position of contours for Highland Light in table 3 indicated that agreement is not sensitive enough to warrant direct comparison of computed contour maps with the trend maps.

We feel, however, that the agreement between model and sediment patterns actually observed on various beach foreshores is sufficiently strong to suggest that some progress has been made toward relating foreshore sediment patterns in nature with the dynamics that created these patterns.

Published work appears to support the expectation of increase in size and down the foreshore toward the breaker zone.

Bascom (1951) describes the variation in median size of sediment on a traverse which includes the foreshore. Based on observations of a number of beaches on the Pacific Coast, he finds that there is a marked gradation in median size of sediment, from coarsest at the breaker line to successively finer up the slope of the foreshore up to, but not including, the crest of the berm. This is also in agreement with the observations of Evans (1939) on the foreshore of a Lake Michigan beach, near White Lake Harbor.

Krumbein (1938*a*) analyzed a short stretch of foreshore on Waverly Beach, Lake Michigan, by a grid of sampling points. Local irregularities tend partly to obscure the trend, but examination of a contour map made by the present writers, based on the Md. size data given by Krumbein, is quite suggestive of a general trend toward larger Md. size toward the plunge line and finer sizes near the crest of the berm (see fig. 20). The writers have also constructed a size-free sorting map from Krumbein data using $\sigma_\phi/\text{Md.}_\phi$ (see fig. 20).

In another study of areal variation by Krumbein (1938*b*) an irregularly spaced distribution of points was used in sampling about 1,000 feet along a beach at Little Sister Bay, Wisconsin. This beach is exceptionally coarse, ranging from pebble sizes to cobbles. Because of the large sizes relative to the local competency of waves to move the sediment, ice-shove patterns were apparently preserved in part through the summers. Our present study is definitely limited at the upper size ranges to particles which are small enough to be at least occasionally

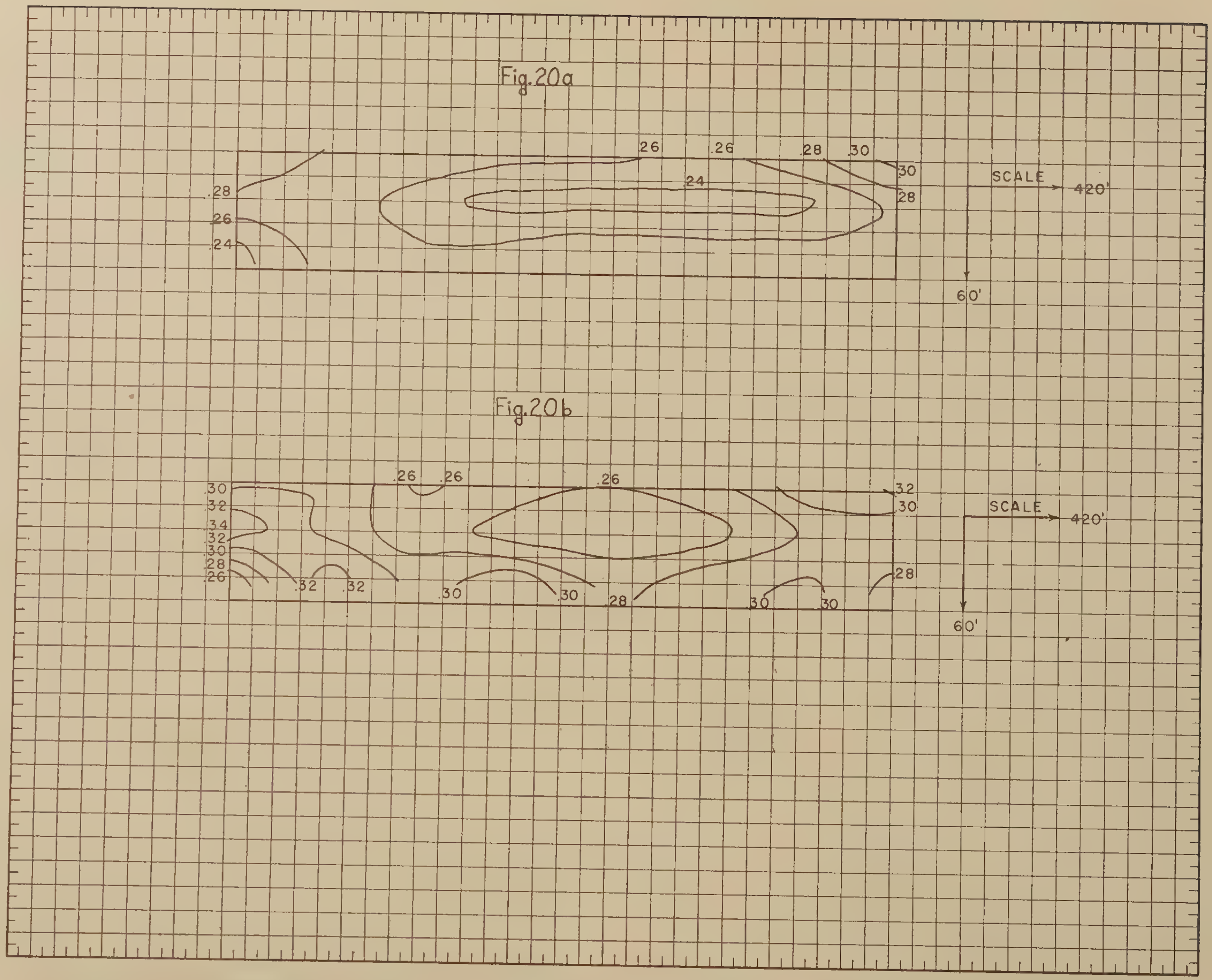
Fig. 20a
.26
.26
.28
30
30
28
.28
26
.24
24
SCALE
420'
60'
Fig. 20b
.26
.26
.26
.32
.30
.30
.32
.34
.32
.30
.28
.26
.32
.32
.30
.30
.28
.30
30
28
SCALE
420'
60'

FIG. 20.—*a*, Map of median size of Lake Michigan, near Michigan City, Indiana (data from Krumbein, 1938*a*), Waverly Beach. Contour interval = 0.02 mm. *b*, Map of sorting σ_ϕ/M_ϕ at Lake Michigan (data from Krumbein, 1938*a*) near Michigan City, Indiana, Waverly Beach. Contour interval = 0.02 mm.

moved by local waves and swash. Although geometric mean size shows a tendency to increase toward the surf zone, in Krumbein's study no clear pattern emerges for sorting expressed as $\sigma_\phi/\text{Md.}_\phi$. It is evident that further work is required to find the upper and lower size limits for the prediction equations and mechanisms discussed in the present paper.

SUMMARY

Essentially this paper represents an effort to establish a pattern of sediment size and sorting free of local fluctuation and representative of foreshore and near-shore in a state of equilibrium. The region is divided into three dynamic zones: Zone W that of shoaling waves landward of near-shore bars; Zone B, the breaker zone; and Zone S, the swash-backwash zone. Each zone is treated separately. Published hypotheses and experimental investigations, which included the properties we could also measure in the field, were combined by us into model form, representing a proposed mechanism and a resulting sediment pattern. The model was then compared with trend maps of several field locations in which very local fluctuations were removed. By substituting observed values for the parameters of the model, a detailed comparison was made in the case of Falmouth Beach and near-shore. Highland Beach and Lake Michigan Beach were compared with the model in a less detailed way. And, finally, Waverly Beach, representing unadjusted field data, was compared with the model for the foreshore zone.

In this way three levels of comparisons were made: first, where both wave and current data and a trend map were available; second, trend map only available; and, third, field data only. Agreement of model with the natural cases, although tempered by the information available, was still sufficiently good to warrant publication.

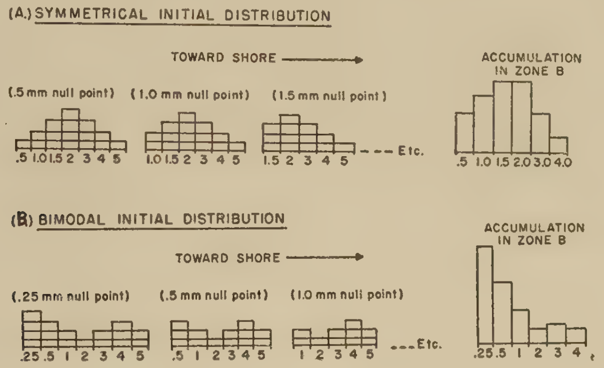

FIG. 21.—Expected displacement of sediment under Model I for a symmetrical initial distribution and bimodel initial distribution.

DISCUSSION

An immediate extension of the earlier discussion of Zone W is to consider the implications of two initial frequency distributions of sediment size which are closer to reality than that of the uniform distribution.

A. *Initial symmetrical frequency distribution, as an approximation to the normal distribution.*—A simplified frequency distribution using unit per cent by weight with a median of 2.0 mm. serves as a representative of the large class of approximately normal or mederately skewed distributions found in nature. As in the earlier discussion, assume that this initial distribution is distributed over the near-shore region under discussion and that wave motion subsequently begins and continues until a stable pattern is established. Figure 21, *a*, illustrates the initial distribution, the changes as successive null points are passed in a shoreward direction, and the nature of the distribution dropped in Zone B. We apply dynamic Model I (discounting seaward movement for the sizes under consideration). As in the simpler model using a uniform distribution, the same trends are evident. The median sizes increase in a shoreward direction, and the sorting improves in a shoreward direction. The most notable differences seem to be (1) the rate at which the sorting and median sizes change in the shoreward direction (this alters the relative position of the individual contour lines but not the basic pattern) and (2) the nature of the accumulation finally dumped at the "step" in Zone B.

(a) TREND MAP FOR MEDIAN SEDIMENT SIZE

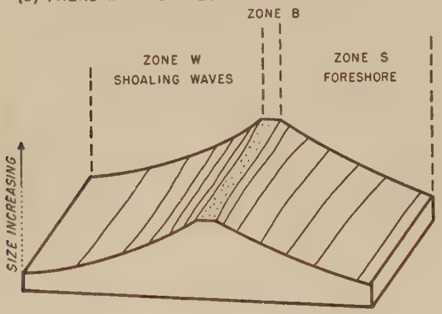

(b) TREND MAP SURFACE FOR SORTING

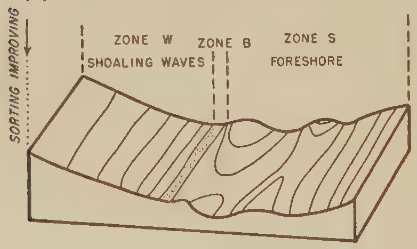

Fig. 22.—Postulated trend maps for nearshore breaker zone and foreshore in equilibrium with wave and current dynamics.

B. *Initial bimodal frequency distribution, representing the general form of certain glacial deposits.*—Figure 21, *b*, illustrates the inital distribution, the changes corresponding to successive null points in shoreward direction, and the form of the final accumulation dumped in Zone B. Interpretation is similar to that of the symmetrical distribution.

The underlying sediment pattern in the near-shore–foreshore region under consideration appears to us to be composed in part of the following factors: (1) the nature of the initial sediment distribution, including the range of sizes, as well as the relative amounts in the various size classes; (2) the availability and kind of sediment being brought in both from the seaward side of the shore line, e.g., by littoral drift, and from the landward side, e.g., by wind, storm, abnormally high tides, and slope wash (see, e.g., Inman and Chamberlin, 1955); (3) the nature of the local wave and current system in an average sense, discounting the temporary effect of violent storms, on the one hand, and abnormally quiescent periods, on the other; and (4) the nature of removal of sediment, e.g., along the shore. If the last three factors are considered to represent averaged conditions in a stable situation, we may consider this region to be an open system in equilibrium over a period of time. It should be possible to characterize such a situation in terms of an underlying pattern of median size and sorting of sediment from which extremely local variation has been removed.

Our investigations have led us to propose the following composite trend map as a model, figure 22, representing the near-shore–foreshore region in a state of equilibrium, as discussed above. Departures from this equilibrium state—e.g., a wasting or building beach—should be reflected in departures of the trend map from this composite model.

Further work along the lines of the present investigation appears to be worth doing. An extension in scope to include the phenomena of bars and an extension seaward beyond the region of shoaling waves are planned for the future. The relation of current and tide and waves in the larger sense, as discussed by Scruton (1955 and especially 1956) and by Van Andel (1954), must then be taken into account.

ACKNOWLEDGMENTS.—Our thanks for illuminating discussions are due to Dr. C. Carver and Dr. A. C. Redfield, of the Woods Hole Oceanographic Institution. We are indebted to C. Hayes, B. Gill, F. Fuglister, G. Hampsen, and J. Helwig for their aid on this project. Without their enthusiastic support this study could not have been reported. Finally, we are greatly indebted to S. Zawadski, of the Argonne Laboratories, A.E.C., for patient guidance and hours of work on the high-speed computer, AVIDAC. This work was carried out under ONR-Geography Branch (Contract No. Nonr-1254(00))(NR-388-018).

REFERENCES CITED

AIRY, G. B., 1842, On waves and tides, p. 289: London, Encyclopaeddia Metropolitan.

BAKMETEFF, B. Z., 1935, The mechanics of turbulent flow: Princeton, N.J., Princeton Univ. Press.

BASCOM, W. H., 1951, The relationship between sand size and beach face slope: Trans. Am. Geophys. Union. v. 32, no. 6. p. 866–874.

DEMAREST, D. F., 1947, Rhomboid ripple marks and beach slope: Jour. Sed. Petrology v. 17, no. 1, p. 18–22.

DOEGLAS, D. J., 1946, Interpretation of the results of mechanical analyses: Jour. Sed. Petrology, v. 16, p. 19–40.

EVANS, O. F., 1939, Sorting and transportation of material in the swash and backwash: Jour. Sed. Petrology, v. 9, no. 1, p. 28–31.

INMAN, D. L., 1949, Sorting of sediments in the light of fluid dynamics: Jour. Sed. Petrology, v. 19, no. 2, p. 51–70.

INMAN, D. L., and CHAMBERLIN, T. K., 1955, Particle size distribution in near-shore sediments: S.E.P.M. Special Bull. no. 3, p. 106–127.

INMAN, D. L., and RUSNAK, G., 1956, Changes in sand level on the beach and shelf at La Jolla, California: Beach Erosion Board, Tech. Mem. 82.

IPPEN, A. T., and EAGLESON, P., 1955, A study of sediment sorting by waves shoaling on a plane beach: M.I.T. Hydrodynamics Lab. Technol. Rept. no. 18.

IPPEN, A. T., and VERMA, R. P., 1953, The motion of discrete particles along the bed of a turbulent stream: Proc., Minn. Internat. Hydraulic Convention, Minneapolis, Minn.

KRUMBEIN, W. C., 1938*a*, Local areal variation of beach sands: Geol. Soc. America Bull., v. 49, p. 653–658.

——— 1938*b*, Beach environment in Little Sister Bay, Wisconsin: *ibid.*, p. 629–652.

——— 1953, Statistical designs for sampling beach sand: Trans. Am. Geophys. Union, v. 34, no. 6, p. 857–867.

KRUMBEIN, W. C., and MILLER, R. L., 1953, Design of experiments for statistical analysis of geological data: Jour. Geology, v. 61, no. 6, p. 510–522.

MILLER, R. L., 1956, Trend surfaces. 1. the relation of sediment size parameters to current-wave systems and physiography: Jour. Geology, v. 64, no. 5, p. 425–446.

MILLER, R. L., and OLSON, E. C., 1955, The statistical stability of quantitative properties as a fundamental criterion for the study of environments: Jour. Geology, v. 63, no. 4, p. 376–387.

MÜNCH-PETERSON, 1950, Münch Petersen's littoral drift formula: Bull. Beach Erosion Board, v. 4, no. 4, p. 1–31.

——— 1937, Monogram for the settling velocity of spheres, p. 57–64: Rept. Comm. Sed. 1926–37, Nat. Research Council. Div. Geology and Geography, Washington, D.C.

ROUSE, H., 1938, Fluid mechanics for hydraulic engineers: New York, McGraw-Hill Book Co.

SCOTT, T., 1954, Sand movement by waves: Beach Erosion Board Tech. Memo 48.

SCRUTON, P. C., 1955, Sediments of the eastern Mississippi delta: S.E.P.M. Spec. Pub. no. 3, p. 21–50.

——— 1956, Oceanography of Mississippi Delta sedimentary environments: Bull. A.A.P.G., v. 40, no. 12, p. 2864–2952.

THOMPSON, W. O., 1937, Original structures of beaches, bars, and dunes: Geol. Soc. America Bull., v 48, p. 723–752.

VAN ANDEL, T. J., and POSTMA, H., 1954, Recent sediments of the Gulf of Paria, v. I: Amsterdam, North Holland Pub. Co.

Contribution No. 959

PHYSICAL OCEANOGRAPHY OF THE GRAND BANKS REGION AND THE LABRADOR SEA IN 1957[1]

By Floyd M. Soule and R. M. Morse

(U. S. Coast Guard)

For the 1957 field work the USCGC *Evergreen* was again designated as the oceanographic vessel of the International Ice Patrol. The *Evergreen* is a 180-foot tender-class cutter and descriptions of the arrangement of facilities for oceanographic work will be found in earlier bulletins of this series. No significant changes were made, either in the laboratory or deck gear or in such vessel characteristics as affect the oceanographic work.

At the beginning of the season, while en route from Woods Hole, Mass., to Argentia, Newfoundland, the *Evergreen* was diverted from her oceanographic assignment to surface vessel ice patrol duties until 3 April on which date she proceeded to begin the first current survey of the 1957 season. This survey covered the waters over and immediately seaward of the southern and eastern slopes of the Grand Banks from about longitude 52° W. on the southern slope to the latitude of Flemish Cap on the eastern slope. The work of collection of data began on the southwestern slope of the banks on the early morning of 4 April and progressed eastward around the Tail of the Banks and thence northward along the eastern slope. Except for being hove to for 23½ hours in heavy weather between the second and third stations of the survey and again for 2¼ hours on 14 April the work of collection of data progressed without major interruption and was completed on the morning of 18 April. The *Evergreen* then proceeded to Argentia, arriving there at mid-day on 19 April.

A second survey was made with the *Evergreen* leaving St. John's, Newfoundland, on 29 April. The area covered by this survey was similar to that covered by the first survey and with work progressing in the same direction. The work of collection of data began on the early morning of 1 May and again the only interruption to the work of collection of data occurred near the beginning of the survey, this time for 4½ hours on the morning of 2 May. The final station of the survey was completed on the early morning of 12 May and the *Evergreen* proceeded to Argentia, arriving there the following morning.

Extract from U. S. Coast Guard Bulletin No. 43
Pages 81 - 131. Reprinted as Contribution No. 959
in the Collected Reprints of the Woods Hole Oceanographic Institution.

Diversion of the *Evergreen* for surface vessel ice patrols prevented any further oceanographic work during the 1957 season. A postseason cruise, comprising 53 stations, made during late July, however, consisted of occupations of the Bonavista triangle 22–25 July and the section across the Labrador Sea from South Wolf Island, Labrador, to Cape Farewell, Greenland, 26–29 July. Thus in 1957, a total 237 stations were occupied, 96 during the first survey, 88 during the second survey, 30 in the occupation of the Bonavista triangle and 23 on the Labrador Sea section. The oceanographic work was under the supervision of Oceanographer Floyd M. Soule who was assisted by Lt. R. M. Morse. During the two surveys made during the season Lt. John E. Murray also assisted. Other assistants in the observational work were Francis N. Brown, yeoman first class; Elwood C. Gray, aerographer's mate first class; Lewis M. Lawday, aerographer's mate second class; Hugh R. McCartney, Jr., aerographer's mate second class; and Herbert A. Ashmore, aerographer's mate third class.

Temperature and salinity measurements were made at each of the 237 stations. At the 23 stations along the Labrador Sea section the observations extended from the surface to as near bottom as was practicable. At the other 214 stations the observations extended from the surface to about 1,500 meters where the depth of water permitted. The intended depth of observations, in meters, were 0, 25, 50, 75, 100, 150, 200, 300, 400, 600, 800, 1,000 and thence by 500-meter intervals.

A sample of old water taken from a part of an ice berg located well away from the original surface of the berg and away from old crevasse lines, was collected for subsequent determination of tritium concentration.

Temperatures were measured with deep sea reversing thermometers. Most of the thermometers used were of Richter & Wiese manufacture but a small percentage were made by Negretti & Zambra, G. M. Manufacturing Co., and Kahl Scientific Inst. Corp. The depths of observation were based on unprotected reversing thermometers made by Richter & Wiese and by Kahl. As a control on the performance of the individual thermometers and a guide in determining when and which thermometers were in need of thermal manipulation for the removal of gas particles to their small bulbs, a program of intercomparison of protected thermometers was carried out as in previous years. The individual thermometers used in pairs were periodically shifted so that each thermometer eventually was paired with several other thermometers. From a total of 1957 comparisons, the probable difference between the corrected reading of a pair of protected thermometers was 0.011° C. Since many of the thermometers used had recent laboratory comparisons with thermometers tested by the National Bureau of Standards, and as in most cases the temperatures are the mean of the corrected readings of a pair of thermometers, it is considered that the observed temperatures listed in the table of oceanographic data have a probable error of about ±0.01° C.

Routine salinity measurements, as in previous years, were made with a Wenner salinity bridge. Prior to the beginning of the 1957 season the bridge was cleaned and the calibration curve redetermined. For this purpose several composite samples of actual sea water collected during the 1956 field work and well distributed over the range of salinities encountered in the Grand Banks region and the Labrador Sea were measured on the Wenner bridge and by silver nitrate titration. Assuming that, over the range of salinity involved, the relationship between conductivity and salinity has the form

$$C = C' (K + LS)$$

where C is the conductivity corresponding to any salinity S and C' is the conductivity corresponding to salinity S', and K and L are constants, the calibration curve of the bridge has the form

$$S = \frac{a}{b + m} - c$$

where S is the salinity, m is the reading of the X-dials of the bridge at balance and a, b, and c are constants.

The constant b was measured electrically and mean values of a and c were determined from the measurements of the several samples by bridge and titration. The resulting calibration curve was found to be

$$S = \frac{9817.725}{200.2 + m} - 4.2534$$

This method permits the arbitrary selection of a single point on the calibration curve. This point was so selected as to bring the salinity of Copenhagen normal sea water and the salinity of the deep water near the middle of the range of the bridge, a salinity of 35 °/₀₀ corresponding to a dial reading of 49.911.

As the calibration curve, determined in this manner, is defined by the silver nitrate titration of the several samples used, the accuracy of the measurement of salinities by the bridge is no better than the accuracy of the silver nitrate titrations used in the calibration. The precision with which the salinities may be measured with the bridge is better, however, and is considered to be about 0.005 °/₀₀.

Water from an oil-sealed carboy of sea water was used as a working standard for the routine measurements. At least twice during each run samples of Copenhagen normal sea water were measured as unknowns. These measurements indicated corrections of less than .005 °/₀₀ except for stations 6504 through 6519 for which a correction of +.01 °/₀₀ was indicated and applied. Copenhagen water of the batch P_{22} was used as the reference standard and a series of measurements were also made to compare the conductivity-salinity relationship of the batch P_{22} with that of batch P_{23} to permit a subsequent shift to the latter as a future reference standard.

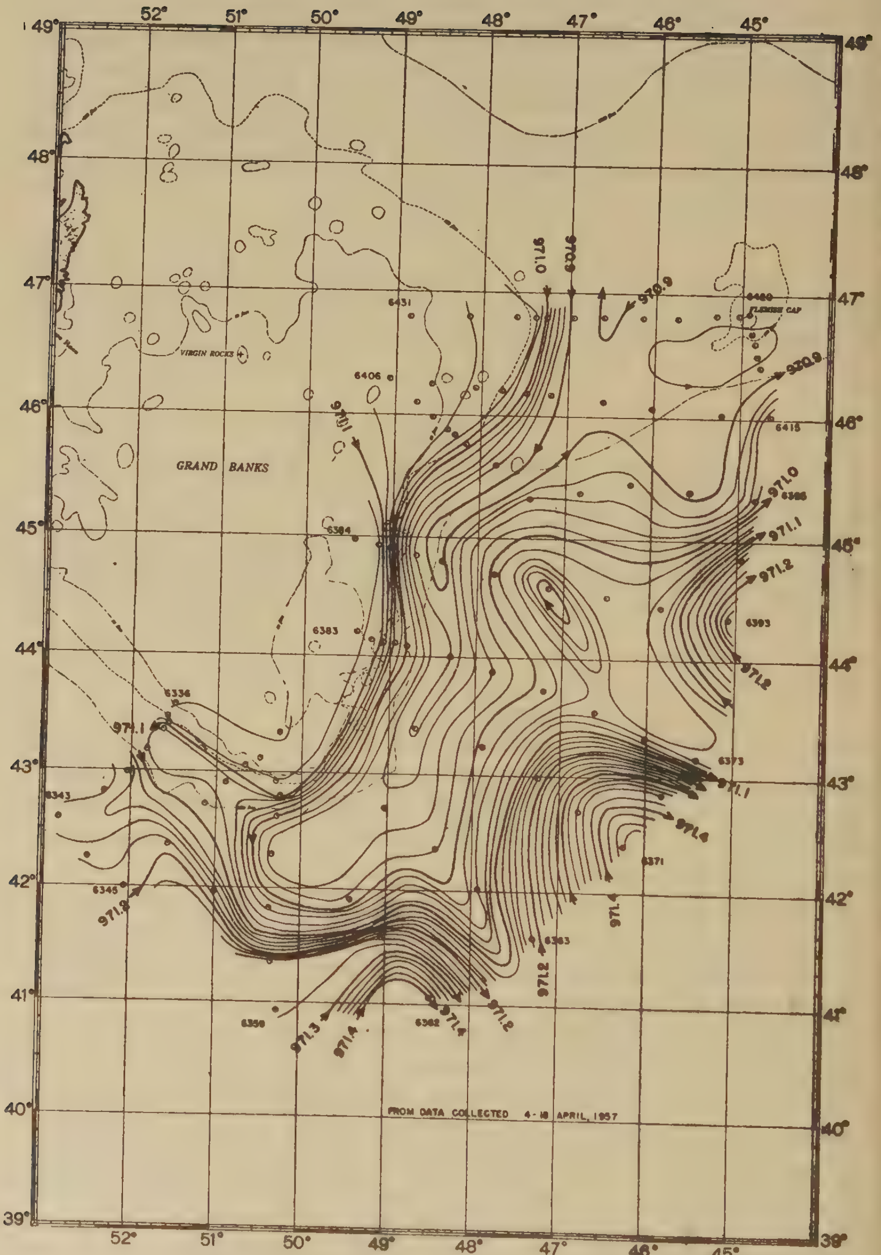
52°
51°
50°
49°
48°
47°
46°
45°
49°
48°
47°
46°
45°
44°
43°
42°
41°
40°
39°
VIRGIN ROCKS
GRAND BANKS
FLEMISH CAP
6431
6406
6384
6383
6336
6343
6345
6350
6362
6363
6371
6373
6393
6386
6415
6420
971.0
970.9
970.9
970.9
971.0
971.0
971.1
971.2
971.2
971.1
971.4
971.4
971.2
971.2
971.4
971.4
971.3
971.2
971.1
FROM DATA COLLECTED 4-18 APRIL, 1957

FIGURE 19.—Dynamic topography of the sea surface relative to the 1000-decibar surface from data collected 4–18 April 1957. Oceanographic station positions are indicated and the station numbers given at turning points.

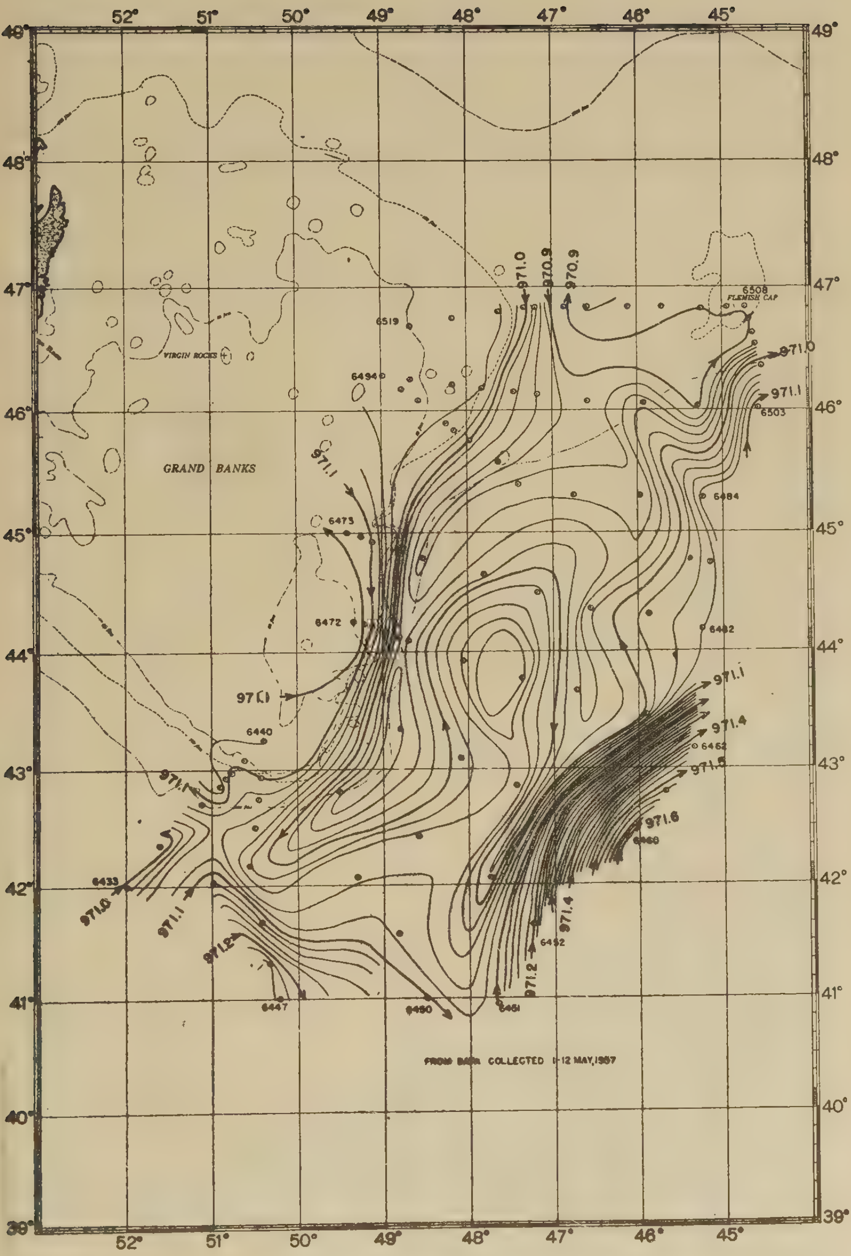
52°
51°
50°
49°
48°
47°
46°
45°
49°
48°
47°
46°
45°
44°
43°
42°
41°
40°
39°
971.0
970.9
970.9
6508
FLEMISH CAP
6519
VIRGIN ROCKS
6494
971.0
971.1
6503
GRAND BANKS
971.1
6484
6475
6472
6482
971.1
971.0
6440
971.4
6462
971.5
971.1
971.6
6468
6433
971.0
971.1
971.2
971.4
6452
971.2
6447
6450
6451
FROM DATA COLLECTED 1-12 MAY,1957

FIGURE 20.—Dynamic topography of the sea surface relative to the 1000-decibar surface from data collected 1–12 May 1957. Oceanographic station positions are indicated and the station numbers given at turning points.

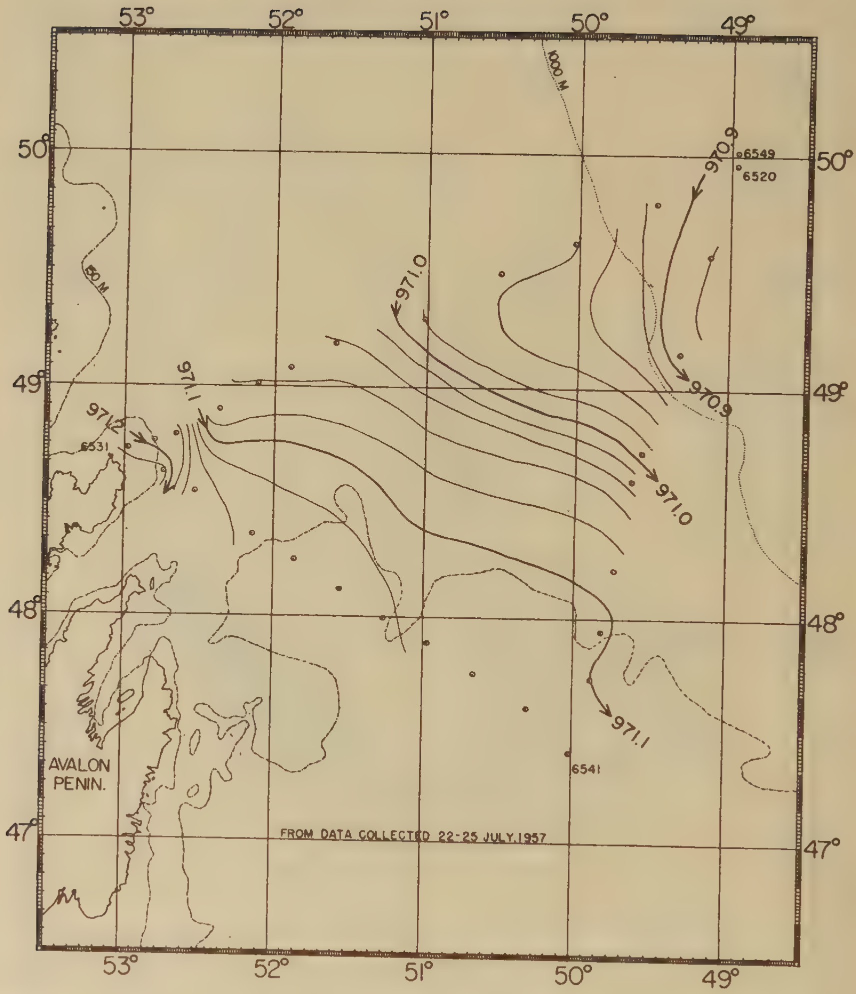
53°
52°
51°
50°
49°
50°
49°
48°
47°
1000 M
150 M
970.9
6549
6520
971.0
971.1
971.2
6531
970.9
971.0
971.1
6541
AVALON PENIN.
FROM DATA COLLECTED 22-25 JULY, 1957

FIGURE 21.—Dynamic topography of the sea surface relative to the 1000-decibar surface from data collected 22–25 July 1957. Oceanographic station positions are indicated and the station numbers given at turning points.

Figures 19, 20, and 21 shown in chronological sequence the dynamic topography found during the two surveys of the Grand Banks region and the postseason occupation of the Bonavista triangle. In the April survey, figure 19, the Labrador Current entering the northern edge of the surveyed area was about normal as to speed and location. Additions of water from the Grand Banks between 45° N. and 46° N. served to increase the effective width of the current from 45° N. to the Tail of the Banks. At the Tail of the Banks the Grand Banks water followed the bottom contours to the westward but the major portion of the Labrador Current continued southward beyond the 42d parallel and thence curved eastward to about 48°30′ W. paralleling the outer edge of the Atlantic Current. At about 48°30′ W. these swifter moving waters curved to the southeastward beyond the limits of the survey between 47° and 48° W. where a pool of colder water filled the concave portion of a meander of the Atlantic Current to the right. Beyond the meander the margin of the Atlantic Current pushed northward between about 46° W. and 47° W. The clockwise eddy centered near 44°30′ N. 47°00′ W. contained warm water derived from this Atlantic Current salient.

It will be noted that while the dynamic heights in the low valley between the Labrador Current and the Atlantic Current were about normal and those on the Grand Banks were slightly above normal those in the highest part of the Atlantic Current covered by the survey were some 10 or 15 dynamic centimeters below normal. The Atlantic Current margins in the area surveyed had a relatively thin layer of Atlantic Current water under which there was a layer of anomalous mixed water inclined downward to the southeast. While this anomalous mixed water had a characteristic temperature salinity relationship it appeared to be a mixture of the usual mixed water and Atlantic Current water. Its upper surface sloped from about 300 meters at station 6369 to about 1,000 meters at station 6371. The under surface of this anomalous mixed water was similarly inclined downward in a seaward direction over the usual mixed water. In the vicinity of Flemish Cap the water was Labrador Current water from its T–S characteristics, whereas usually at least the southeastern part of Flemish Cap is occupied by mixed water. Here, between stations 6417 to 6415, there again is indication of a downward seaward inclination, this time with the usual mixed water between Labrador Current water and Atlantic Current water. These are considered indications that prior to this survey an unusually large amount of Labrador Current water was brought into the area and that vigorous wind stirring took place. Further confirmation is offered by the observations which showed the characteristic temperature minimum of the Labrador Current near 75 meters to have been almost completely wiped out and the minimum temperatures about a half degree warmer than normal.

The observations made during the second survey indicated a continuation of this mixing at subsurface levels but with some recovery of the Labrador Current temperature minimum and the area in which undiluted Labrador Current water was found more nearly normal. The reestablished temperature minimum in the Labrador Current was shallower than normal and, except in the northernmost sections, warmer than normal. Figure 20 shows the highest dynamic heights of the Atlantic Current in the surveyed area to have returned to about normal values.

A cold water pool with counterclockwise circulation and partly detached from the Labrador Current lay westward of 51° W. south of the Tail of the Banks. The clockwise eddy found in the first survey near 44°30′N. 47°00′ W. was still present in the second survey somewhat southwestward of its previous position and connected by a warm salty ridge to the Atlantic Current water in the southern part of the surveyed area. This was accompanied by a cold fresh valley extending southward from the 45th parallel to the southern limits of the chart between the ridge and the Atlantic Current to the eastward. This is the reverse of the usual relative positions of a pair of meanders which develop a counterclockwise intertwining as the pattern decays and moves with a translation parallel to the Atlantic Current.

Figure 21 shows the dynamic topography found at the Bonavista triangle during the postseason cruise. In any comparison of the situation shown here with the topography farther south shown in figures 19 and 20 it should be kept in mind that figure 20 was the result of a survey conducted 1 to 12 May whereas the Bonavista triangle was occupied 22 to 25 July. Our only information as to changes which might have taken place in the current pattern in the Grand Banks area is from berg drifts and these indicate that the current pattern in the western half of the area surveyed in May remained remarkably steady and as shown in figure 20 through June and July.

There are two features of the dynamic topography shown in figure 21 that are especially worthy of note. One is the exceptionally high dynamic heights found near the Cape Bonavista corner and the other is the comparatively small distance from Cape Bonavista to the eastern edge of the water following the western branch of the Labrador Current. The low densities of the inshore stations which produced the large dynamic heights were largely the result of low salinity. In terms of berg movements, the division between eastern and western branches of the Labrador Current meant that any bergs crossing the 49th parallel eastward of about 52°30′ W. would follow the eastern branch. Because of the absence of opportunity to make any dynamic topographic surveys of the northeastern slope of the Grand Banks during the 1957 season the significance of this unusually far westward division point cannot be assessed.

As implied above in the discussion of figures 19 and 20 the temperature-salinity relationships found at each station of the two surveys made in 1957 were examined.

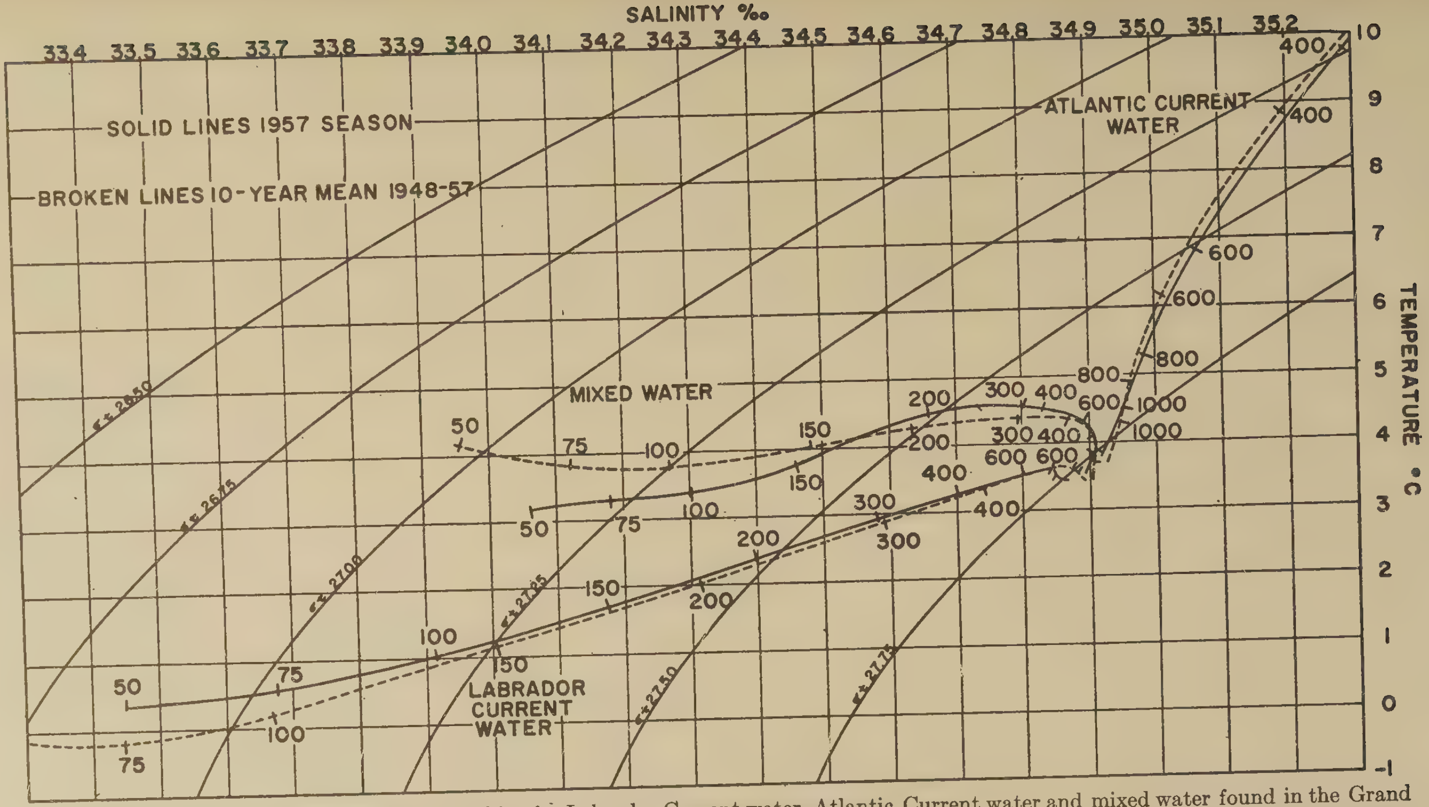

FIGURE 22.—Temperature-salinity relationships for Labrador Current water, Atlantic Current water and mixed water found in the Grand Banks region. Solid lines show conditions found during 1957 and broken lines represent the 10-year means for the period 1948–57. An approximate depth scale in meters is given.

From their T–S characteristic relationships the Labrador Current water and the Atlantic Current water found in the Grand Banks region are water masses. Usually also in this region these water masses mix in a sufficiently constant proportion so that the mixed water can be regarded as a virtual water mass. The mean T–S relationships for these three water masses for the 10-year period 1948–57 are shown in figure 22 in comparison with the conditions found in 1957. The 10-year means are shown as broken lines and the 1957 conditions are represented by solid lines.

The typical mixed water found in the Grand Banks region is not always present. In some years the proportion of the parent water masses producing the mixed water is variable and the resulting mixed water follows no definite pattern of characteristic T–S relationship. Also occasionally a group of stations will be found to have a consistent pattern differing from the typical mixed water. In 1957, as mentioned above in the discussion of figures 19 and 20, such a group of stations was found to have a T–S pattern which indicated a mixture of the usual mixed water with Atlantic Current water. These observations have been excluded in computing the average T–S values for the mixed water as shown in figure 22.

The presence of mixed water as a virtual water mass in the Grand Banks region raises questions as to what happens to this mixed water after it is formed. One possibility was that the mixed water formed in the Grand Banks region might supply the intermediate water of the Labrador Sea. The T–S characteristics of the water were examined at the bulk of the stations taken 1951 through 1956 and located in the northward-moving water north of Flemish Cap. No surveys extended into this area in 1948, 1949, 1950, and 1957, so that the 88 stations examined represent all of the postwar observations in the area in question. The resulting individual station curves showed some grouping in the mixed water but more scatter than in the mixed water of the Grand Banks region. The T–S curves fell principally between the Grand Banks curves for Labrador Current water and mixed water with a few stations on the Atlantic Current side of Grand Banks mixed water. The interpretation is that some of the mixed water formed in the Grand Banks region moves northward of Flemish Cap mixing in varying proportions with Labrador Current water in the more northern area and that some sinking and seaward spreading of the mixed water goes on in both areas.

To determine the spread of individual station curves from the 1957 characteristic T–S curves an ellipse was constructed for each level for each water mass using probable differences of individual temperatures and salinities from their average values as the semiaxes of the ellipses. The ellipses for a given level for the three water masses were separate from each other except that at 800 meters the mixed-water ellipse was tangent to that for Atlantic Current water, and at 1,500 meters the mixed-water ellipse slightly overlapped those for Labrador Current water and Atlantic Current water.

The curves in figure 22 representing the conditions found in 1957 indicate that the Labrador Current water was denser than average down to about 300 meters and lighter than average below this level. The salinity was the determining factor and counteracted a slight opposite effect of temperature anomalies. In the mixed water the 1957 observations showed denser than average water down to a depth of about 200 meters and lighter than average below that depth. Here both temperature and salinity anomalies combined to produce the density anomalies. In the Atlantic Current water densities down to about 200 meters were close to average and below that level were lighter than average, with the higher than average temperatures outweighing the effect of slightly greater than average salinities.

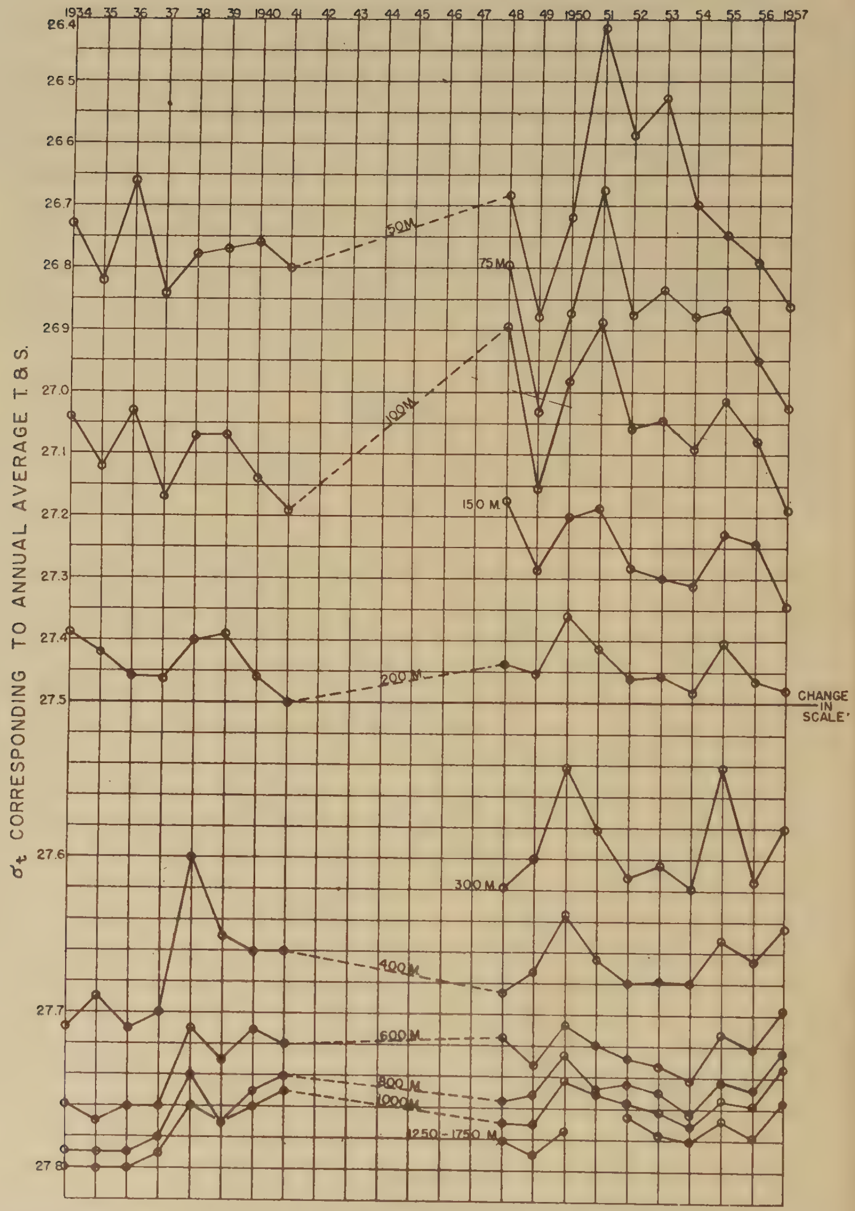

FIGURE 23.—Year-to-year fluctuations in density of the Labrador Current water found in the Grand Banks region at selected levels 1934–41 and 1948–57. The plotted points represent values of σ_t corresponding to the average temperature and average salinity for the particular year and level.

As the T–S characteristics found in the Grand Banks region fluctuate slightly from year to year figure 23 has been prepared to show the amount of this fluctuation as it affects the density at the different levels in the Labrador Current water. The densities shown are the values of σ_t corresponding to the average temperature and average salinity for the particular level and year. It is of interest to note the degree of fluctuation within the 10-year period 1948–57 used for the normal curve shown in figure 22. Similar yearly averages for some of the levels are available for the 8-year period 1934–41 and are also shown in figure 23 to show the changes which have occurred over the longer period. Thus it appears that in recent years the Labrador Current water has been increasing in density in the upper 200 meters and decreasing in density at levels below that. The net effect of these density changes on the average dynamic height of the 50-decibar surface relative to the 1,000-decibar surface shows no consistent trend.

The position of the steep horizontal temperature gradient at the sea surface which occurs near the outer margins of the Atlantic Current in the Grand Banks region is of great practical importance in determining the southern limits of berg drifts. This steep gradient is called the cold wall. Since it is not always vertical and since we are concerned with its location in a layer whose thickness is commensurate with the draft of an iceberg, in studies of its fluctuations its position has been taken as the horizontal projection of the line along which water of 34.95 °/₀₀ salinity corresponds to a temperature of 6° C. The position of the cold wall has been delineated thus for each survey which has included this area. To enable the numerical expression of its position, or its retreat from or advance toward the Grand Banks, the area between it and certain fixed rhumb lines has been used. These rhumb lines are the 45th parallel from the cold wall westward to the 49th meridian, the 49th meridian from 45° N. to 43° N. and a line from 43° N. 49° W. through 42° N. 47° W. extended to the cold wall.

It is presumed that the position of the cold wall is determined by the relative strengths of the Labrador Current and the Atlantic Current. For each survey for which the position of the cold wall can be delineated, the salinity, temperature and velocity distributions, as well as the volume and heat transports are available for the Labrador Current entering the area from the northward past the 45th parallel. Using what are believed to be realistic values of average velocity distribution, it has been further assumed that each million cubic meters per second of volume transport of the Labrador Current entering the area will require a sea surface area of 10,000 sq. kilometers. The area between the cold wall and the rhumb lines has therefore been reduced by such a proportionate amount to give a remaining adjusted area, A, whose size, it was expected, would be related to forces associated with the North Atlantic eddy and consequently with the Atlantic Current which makes up the outer margin of the eddy in the Grand Banks sector.

It was further assumed that the difference in sea level between Bermuda and Charleston, S. C., is related to the volume transport of the North Atlantic eddy and consequently to the forces determining the position of the periphery of the Atlantic Current in the Grand Banks sector. While the difference in sea level between Bermuda and Charleston is not directly measurable the fluctuations in the difference are available from the fluctuations at each station. Since it was anticipated that a weak North Atlantic eddy would result in a retreat of the cold wall and therefore an increase in the adjusted area A the sea level variable used was the sea level at Charleston minus the departure from average sea level at Bermuda. A very good correlation existed between this variable and the adjusted area A in the Grand Banks sector 13½ months later as checked by 27 surveys made during the period 1934–41.

With the resumption of oceanographic work in 1948 no agreement could be found between the adjusted area A predicted from the tide-gage readings at Bermuda and Charleston and the adjusted area A found during surveys of the area. In 1952 it was realized that the time lag no longer was the 13½ months found during the prewar surveys but about 11½ months. Using this time lag for the postwar surveys a new relationship was computed as

$$A = 6.97(H - 5.07) + 1.67$$

where A is the adjusted area in units of 10,000 sq. km and H is sea level at Charleston minus the Bermuda departure from an average of 4.16 expressed in feet. This gave a poor correlation. For example, during the first survey of 1957 the predicted adjusted area A was +0.55 whereas that actually found was +4.12. The predicted adjusted area A for the second survey was +5.22 as compared with an actual adjusted area of +6.02.

Changes have taken place in the sea level at Charleston and at Bermuda. The mean sea level at Charleston for the decade 1947–56 was 5.32 ft. instead of the 5.07 prewar mean. Mean sea level at Bermuda for this postwar decade was 4.33 ft. instead of the 4.16 which had been used in the past. The mean annual variation curve of sea level at Charleston minus the departure of sea level from the mean of 4.33 at Bermuda for this decade shows three maxima and three minima. From 1948 to 1957 there were 20 surveys made which included the position of the cold wall, seven during the month from mid-March to mid-April, six during the month from mid-April to mid-May, six during the month from mid-May to mid-June and one in the second half of June. The mean dates show a maximum near the April-May group. As this maximum could be related to any of the three maxima or any of the three minima in the sea level curve, each of the years during which more than one survey was made was examined as to consistency of sign of the change in adjusted area with the different time lags representing correlations with the different maxima and minima of the sea level curve. In none of the time lags was the sign consistent, the best being a time lag of 11.4 months where there were eight cases of positive sign and two negative. It must therefore be concluded that the very good correlation between the position of the cold wall as determined during the 27 prewar surveys and the Charleston-Bermuda tide-gage data was fortuitous and not real, and we must find other means of predicting the position of the cold wall.

In the more detailed examination of the circulation in the upper 1,000 meters with respect to the fluctuations in the Labrador Current particularly, certain sections have been occupied as frequently as operational considerations permit. Tentative normal seasonal variation relationships have been derived for some of these sections where the number of occupations has been sufficient and the distribution of the dates of the occupations has been satisfactory.. Of these there were occupations of sections F, T, U, and W during the two 1957 surveys, and the component sections of the Bonavista triangle (NW, SW, SE) during the postseason cruise. An additional section across the Labrador Current off South Wolf Island, Labrador, repeated during the 1957 postseason cruise, has usually been occupied at about the same time of year and for this section average values, rather than normal seasonal variations have been used for comparison. The location of the section F is from the Grand Banks to Flemish Cap at the parallel of 46°45′ N. Section T runs southeasterly from about 46°20′ N. 49°00′ W. Section U runs easterly from the Grand Banks near the 45th parallel. Section W runs south from the Grand Banks along the meridian of 50°15′ W.

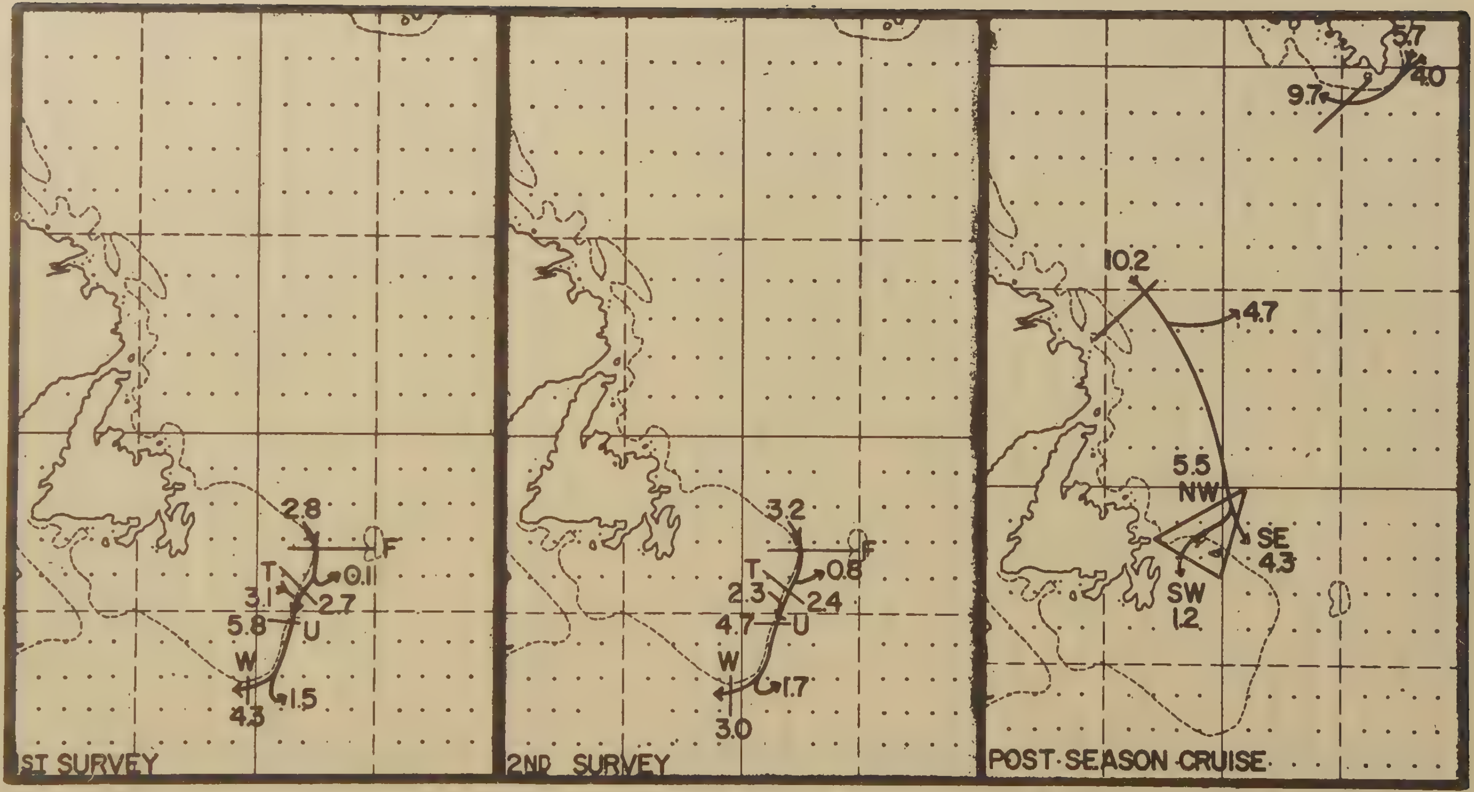
1ST SURVEY
2.8
T
3.1
2.7
0.11
F
5.8
U
W
4.3
1.5
2ND SURVEY
3.2
T
2.3
2.4
0.8
F
4.7
U
W
3.0
1.7
POST·SEASON CRUISE
5.7
4.0
9.7
10.2
4.7
5.5
NW
SE
4.3
SW
1.2

FIGURE 24.—Schematic representation of circulation deduced from sections occupied during 1957. Numerals indicate volume transport in units of cu.m/sec $\times 10^{-6}$

During the two surveys and postseason cruise of 1957 there were 12 occupations of such sections across the Labrador Current. Table 1 gives the volume transport, mean temperature, minimum observed temperature and heat transport found during these occupations and lists the corresponding seasonal normal values for comparison. Both in the table and in the text, volume transport is expressed in millions of cubic meters per second, mean temperature and minimum observed temperature are given in degrees centigrade and heat transport is given in millions of cubic meter degrees centigrade per second.

Table 1.—Summary of velocity sections across Labrador Current occupied in 1957

Section	Volume transport			Mean temperature			Minimum observed temperature			Heat transport		
	1957	Normal	Anomaly	1957	Normal	Anomaly	1957	Normal	Anomaly	1957	Normal	Anomaly
First survey:												
F	2.84	2.75	+0.09	0.52	1.58	−1.06	−1.19	−1.26	+0.07	1.46	4.34	−2.88
T	2.68	3.37	−1.69	0.79	1.94	−1.15	−0.83	−1.40	+0.57	2.11	6.54	−4.43
U	5.83	5.26	+0.57	1.04	1.56	−0.52	−1.10	−1.20	+0.10	6.07	8.21	−2.14
W	4.31	4.23	+0.08	1.05	2.12	−1.07	−0.68	−0.53	−0.15	4.51	8.97	−4.46
Second survey:												
F	3.17	2.93	+0.24	1.54	1.79	−0.25	−1.62	−1.29	−0.33	4.88	5.24	−0.36
T	2.35	3.30	−0.95	2.02	1.80	+0.22	−1.23	−1.40	+0.17	4.76	5.94	−1.18
U	4.69	4.63	+0.06	1.35	2.15	−0.80	−1.50	−1.19	−0.31	6.32	9.95	−3.63
W	3.02	4.15	−1.13	2.04	2.82	−0.78	−0.66	−0.60	−0.06	6.16	11.70	−5.54
Postseason:												
NW	5.15	4.17	+0.98	1.99	1.49	+0.50	−1.62	−1.59	−0.03	10.23	6.21	+4.02
SW	1.29	0.66	+0.63	−0.37	0.20	−0.57	−1.66	−1.65	−0.01	−0.47	0.13	−0.60
SE	4.53	3.38	+1.15	2.94	2.07	+0.87	−1.33	−1.60	+0.27	13.31	7.00	+6.31
S. Wolf Is.	10.22	4.99	+5.23	2.96	2.48	+0.48	−1.70	−1.50	−0.20	30.26	12.38	+17.88

Figure 24 shows a schematic representation of the volume transports given in Table 1. In both the first and second surveys there was some loss of volume transport between sections F and T whereas there is normally some increase because of a contribution off the Grand Banks from the northwest between these sections. In 1957 apparently the contribution off the banks was larger than normal but occurred farther south between sections T and U resulting in about normal or somewhat larger than normal volume transports at sections F and U and subnormal volume transports at section T. At section W the volume transport was normal during the first survey but dropped off during the second survey instead of holding steady as is normal.

The mean temperature of the Labrador Current was decidedly below normal at each of the four sections during the first survey even though the minimum observed temperatures were normal or warmer than normal. By the time of the second survey, however, the mean temperature had warmed up at the two northern sections, but the two southern sections were still about 0.8° colder than normal. The minimum observed temperatures were lower during the second survey (except at section W) with a restoration of a more nearly normal profile of the Labrador Current.

The preponderance of negative anomalies of mean temperature made its effect felt in heat transport where the anomalies are all negative for both surveys. The occupation of the Bonavista triangle during the postseason cruise was not very satisfactory from the standpoint of equating horizontal inflow past the northwest side to outflow past the southwest and southeast sides. Thus the volume transport into the triangle was found to be 5.15, whereas the sum of the outflow past the other sides was 5.82. The volume transport anomalies were positive at all three sides. The mean temperatures were above normal at the two sides where the greatest transports exist and below normal along the southwest side. The resulting heat transport was hence correspondingly greater than normal with the above mentioned discrepancy of inflow and outflow being repeated and giving the inflowing heat at 10.23 and the outflowing heat at 12.84 for an average positive anomaly of 4.86. The minimum observed temperatures were near normal at the northwest and southwest sides and about a quarter of a degree above normal at the southeast side.

Farther north, off South Wolf Island, Labrador, the volume transport of the Labrador Current was found to be 10.22 which is some two times the average value for the 20 occupations of this section. The mean temperature was about a half degree warmer than average and the minimum observed temperature of −1.70 was near the coldest recorded for the 20 occupations (−1.72 in 1940 and −1.70 in 1949) and 0.2° colder than average. Because of the large volume transport and high mean temperature the positive anomaly of heat transport was very large. As the South Wolf Island section was occupied only a few days after the occupation of the Bonavista triangle and the volume transport found was about twice that past the Bonavista triangle a volume transport of 4.7 has been indicated in figure 24 as moving off to the eastward between the South Wolf Island section and Bonavista.[2]

At the Greenland end of the section across the Labrador Sea the West Greenland Current off Cape Farewell was also found to be unusually vigorous with a volume transport of 9.74 which is more than twice its seasonal normal of 4.41. Although the mean temperature of 4.15 was about three quarters of a degree below the seasonal normal of 4.89 the resulting heat transport of 40.39 was very large compared to its normal value of 21.56. If the mean temperatures of the East Greenland Current and Irminger Current components of the West Greenland Current are taken as constant at 3.2 and 5.5 respectively the computed volume transports of the components may be derived as 5.73 for the East Greenland Current component for a positive anomaly of 4.56 and 4.01 for the Irminger Current component for a positive anomaly of 0.77. As the mean temperatures have been assumed constant the anomalies of heat transport are proportional to those of volume transport and are computed as 14.60 and 4.23 respectively.

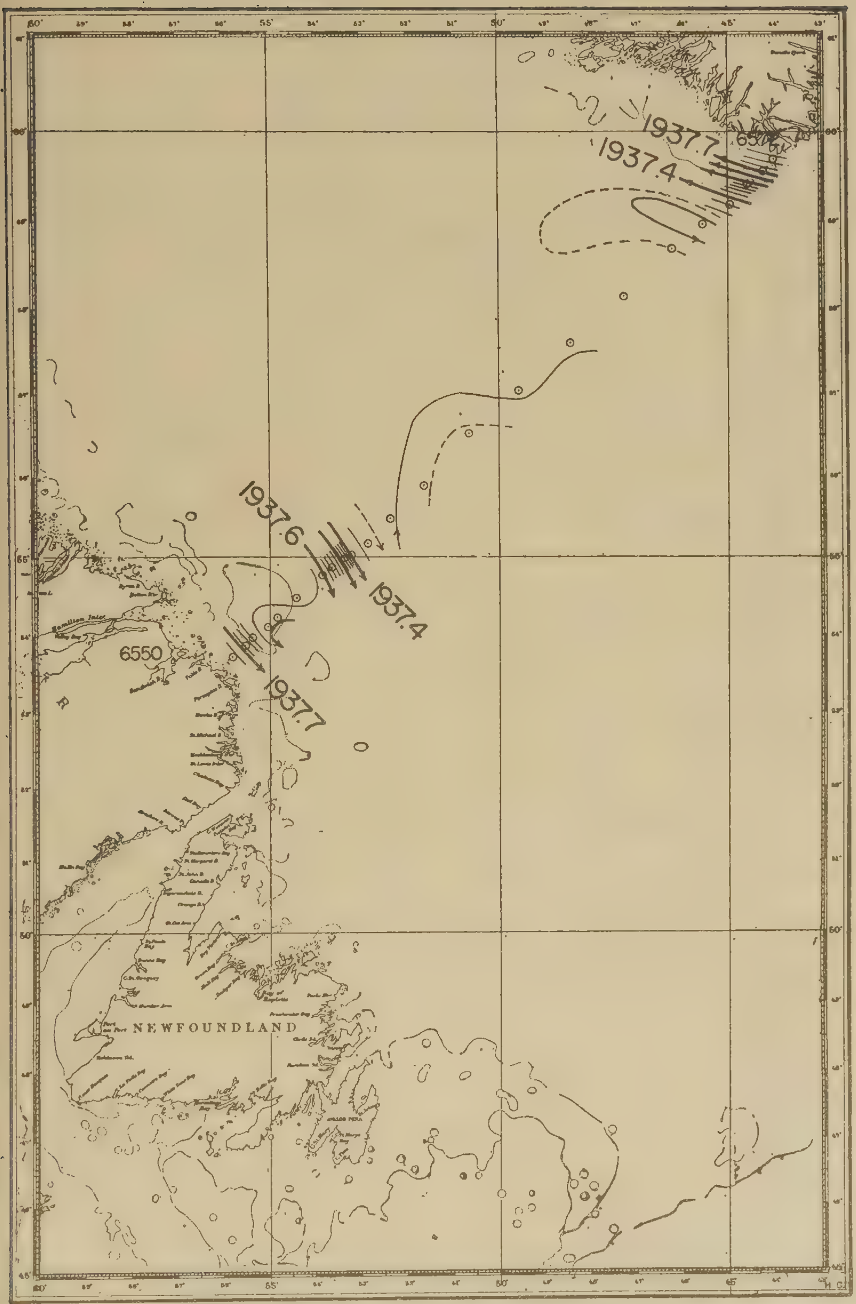
1937.7
1937.4
1937.6
1937.4
6550
1937.7
Hamilton Inlet
NEWFOUNDLAND
60°
55°
50°
45°

FIGURE 25.—Dynamic topography of the sea surface relative to the 2000-decibar surface from data collected 26–29 July 1957. Oceanographic station positions are indicated by circles.

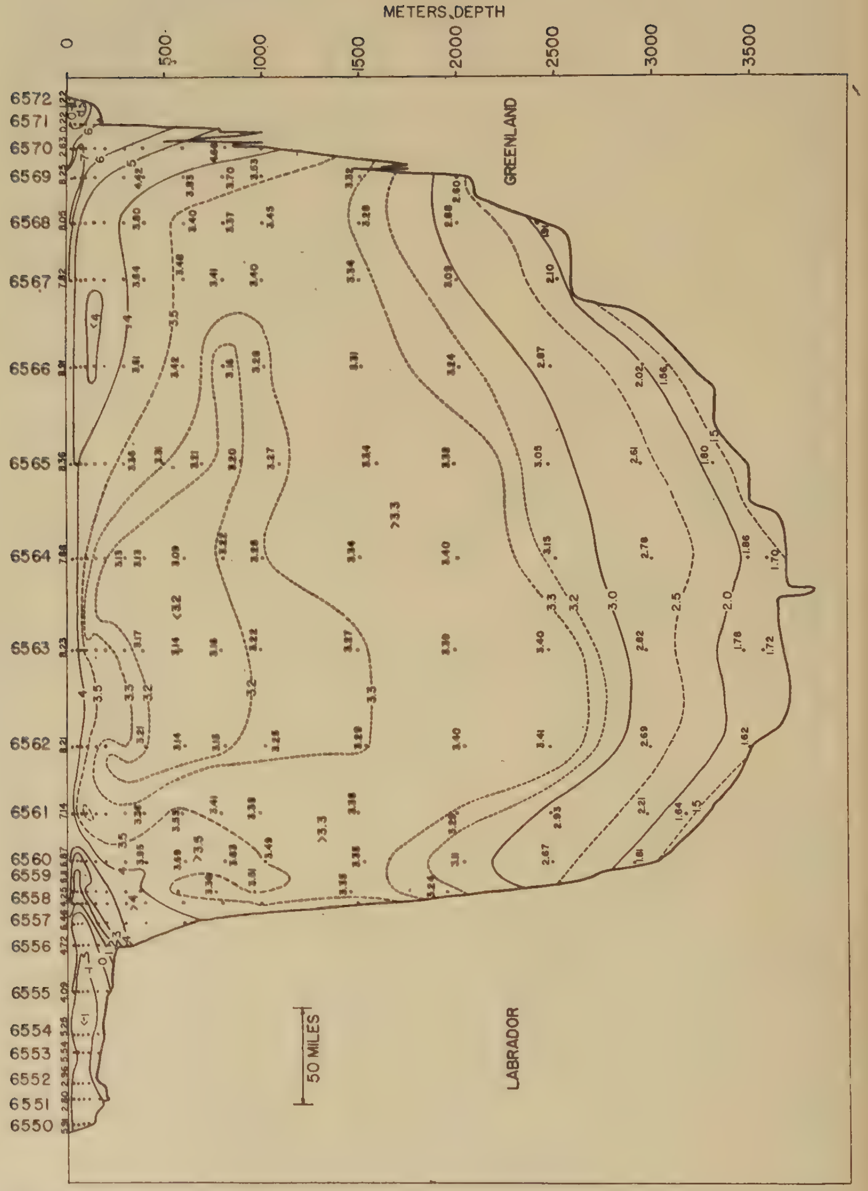

FIGURE 26.—Temperature distribution along section between South Wolf Island, Labrador and Cape Farewell, Greenland 26–29 July 1957.

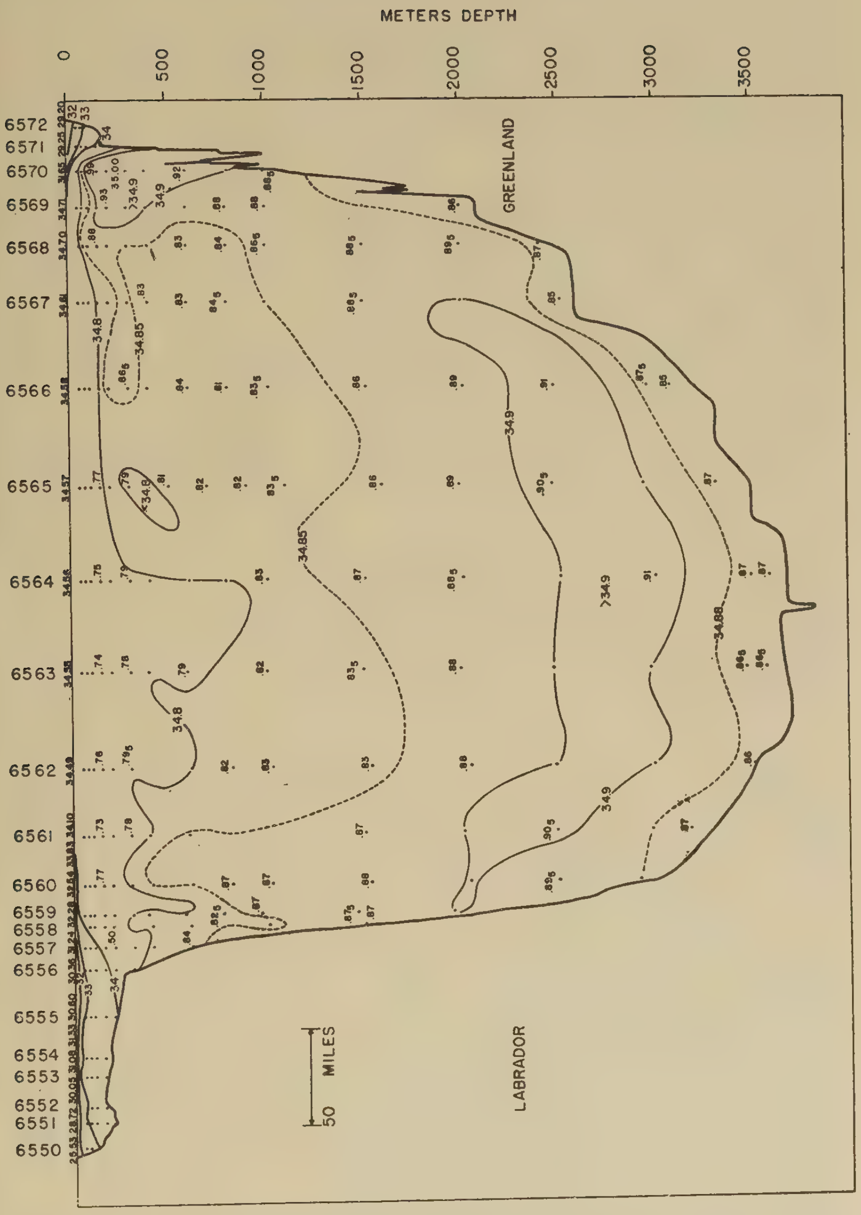

FIGURE 27.—Salinity distribution along section between South Wolf Island, Labrador and Cape Farewell, Greenland 26–29 July 1957.

Figures 25, 26, and 27 show respectively, the dynamic topography in the vicinity of the section across the Labrador Sea from South Wolf Island, Labrador to Cape Farewell, Greenland, and the temperature and salinity distributions along that section. The temperature and salinity distribution and the indications of the GEK have been considered along with the dynamic heights at the stations, in the construction of figure 25 which, of course, must remain an estimate away from the line of the section.

In figure 26 showing the temperature distribution along the section from South Wolf Island, Labrador to Cape Farewell, Greenland, one of the most interesting features is, as usual, the temperature minimum of the intermediate water in the central part of the section with the temperature maximum immediately below it. The minimum is considered to be a relic of the previous winter's cooling. In 1957 this minimum was cold and the temperature of 3.09° at station 6564 is 0.02° colder than any observation in the series of occupations from 1934 to 1941 and 1948 to 1957 (the previous low of 3.11° was observed in 1952). The northeastern end of the temperature minimum is narrowed in depth by the warmer water of the offshore portion of the West Greenland Current which returns eastward between stations 6566 and 6568. This eastward-returning flow explains the exceptionally wide band of warm water which might otherwise be misinterpreted as a broad band of the Irminger Current component of the West Greenland Current. The surface flow pattern is shown in figure 25.

The Irminger Current contribution to the West Greenland Current is shown more clearly by the salinity maximum near the Cape Farewell end of figure 27. As indicated in this figure the maximum salinity observed here was 35.00°/₀₀. This again is below the prewar values of the maximum which, in the 1930s was consistently about 35.04°/₀₀.

The motionless surface along this section does not lie at a uniform depth. It is at a deeper level than it is beneath the Labrador Current in the Grand Banks region and usually between 1,500 and 2,500 meters. The selection of a single level as reference for showing the dynamic topography of the entire section is then a compromise and its selection is materially assisted by studying the shape of the surfaces of equal potential density. These surfaces intersecting the Labrador Sea section occupied in 1957 indicated the most nearly motionless single level was at about 2,000 meters. The dynamic heights for this section therefore have been referred to the 2,000-decibar surface. The net volume transport across the section above this reference surface was computed to be 1.36 × 10^6 cu. m/sec net southeasterly.

---

[2] While the volume transport for the Bonavista triangle has been based on a reference surface of 1,000 decibars and the 2,000-decibar surface has been used for the South Wolf Island section about 90 percent of the transport at the latter section takes place above the 1,000-decibar surface which still leaves some 9.0 × 10^6 cu m/sec off South Wolf Island compared with 5.5 past the Bonavista triangle.

In bulletin number 42 of this series average temperatures were plotted against average salinities for the intermediate water and for the deep water at 2,000, 2,500, 3,000 and 3,500 meters for each occupation of this section. For purposes of comparison similar values for the 1957 occupation of the section are given below:

1957 averages	T	S
Intermediate water	3.22	34.82_{8} (stations 6562–6565)
2,000 meters	3.18	34.88_{7}
2,500 meters	2.95	34.89_{4}
3,000 meters	2.35	34.89_{1}
3,500 meters	1.75	34.86_{5}

Thus the intermediate water was near the cold limit of the group of occupations 1934–41 and 1948–57 and the salinity was lower than any other year of the group. In the deep water both temperature and salinity were close to these values for the 1953 occupation at 2,000, 2,500 and 3,000 meters and near the cold and low salinity limits of the group at 3,500 meters. The values of σ_t corresponding to these average temperatures and average salinities were smaller than found in 1956 at all levels. This continues the trend of the last two decades toward lighter water.

SUMMARY

1. The two dynamic topographic charts resulting from the season's current surveys and the dynamic topography found at the Bonavista triangle during the postseason cruise have been discussed with respect to surface circulation.

2. Temperature-salinity relationships of the Labrador Current water, Atlantic Current water and mixed water, found in the Grand Banks region during 1957, have been compared with mean T–S curves for the period 1948–57. The continuation of the trend of the last few years to increasing salinity in the upper 200 meters in the Labrador Current and freshening of the water below that level has been noted.

3. Year to year changes in density of the Labrador Current water have been noted for the periods 1934–41 and 1948–57.

4. The apparent relation between the position of the cold wall in the Grand Banks sector and sea level differences at Bermuda and Charleston were further investigated in the light of more recent data, and it was concluded that the correlation found in prewar years was fortuitous.

5. A more detailed analysis of the circulation in the upper 1,000 meters has been made on the basis of volume and heat transports and mean and minimum observed temperatures at 12 selected sections across the Labrador Current occupied during the 1957 season and postseason surveys.

6. The exceptionally vigorous circulation on both the Labrador and Greenland sides of the Labrador Sea in 1957 has been noted.

7. The temperature and salinity of the intermediate and deep waters of the Labrador Sea in 1957 have been examined and compared with averages for the groups of occupations during 1934–41 and 1948–57. The 1957 observations showed the intermediate water to have a salinity below any of the prior occupations and a temperature near the previous cold limit, and the deep water to be near average at 2,000, 2,500 and 3,000 meters, and near the cold- and low-salinity limits at 3,500 meters.

TABLE OF OCEANOGRAPHIC DATA

The data collected in 1957 are tabulated below. The individual station headings give the station number, date, geographical position, depth of water and dynamic height of the sea surface used in the construction of the dynamic topographic charts shown in figures 19, 20, 21 and 25. The depths of water are rough approximations, being the uncorrected sonic soundings based on a sounding velocity of 800 fathoms per second and containing an additional mechanical speed error of about 1/60. Where the depths of scaled values are enclosed in parenthesis, the data are based on extrapolated vertical distribution curves of temperature or salinity or both. Asterisks appearing before observed temperatures indicate that these temperatures were determined from the depth of reversal and the corrected reading of an unprotected thermometer. The symbol σ_t signifies 1,000 (density -1) at atmospheric pressure and temperature t.

Station 6336; 4 April; 43°35′ N., 51°30′ W.; depth 93 m.; dynamic height 971.142.

Observed values			Scaled values			
Depth, meters	Temperature, °C.	Salinity, ‰	Depth, meters	Temperature, °C.	Salinity, ‰	σ_t
0	1.77	32.60	0	1.77	32.60	26.10
28	1.77	32.60	25	1.75	32.60	26.10
55	1.44	32.80	50	1.55	32.75	26.22
84	0.63	33.44	75	0.90	33.25	26.66

Station 6337; 4 April; 43°29′ N., 51°35′ W.; depth 178 m.; dynamic height 971.139.

Observed values			Scaled values			
Depth, meters	Temperature, °C.	Salinity, ‰	Depth, meters	Temperature, °C.	Salinity, ‰	σ_t
0	1.28	32.65	0	1.28	32.65	26.16
26	1.29	32.65	25	1.30	32.65	26.16
53	1.02	32.70	50	1.10	32.69	26.20
80	−0.35	33.31	75	−0.20	33.24	26.72
107	1.25	33.68	100	0.95	33.61	26.95
159	1.75	33.90	150	1.70	33.88	27.11

Station 6338; 5 April; 43°25′ N., 51°34′ W.; depth 310 m.; dynamic height 971.114.

Observed values			Scaled values			
Depth, meters	Temperature, °C.	Salinity, ‰	Depth, meters	Temperature, °C.	Salinity, ‰	σ_t
0	0.70	32.77	0	0.70	32.77	26.29
26	0.71	32.77	25	0.70	32.77	26.29
50	0.27	33.06	50	0.27	33.06	26.55
76	1.48	33.48	75	1.45	33.47	26.81
101	4.69	34.07	100	4.65	34.06	26.99
152	4.34	34.12	150	4.35	34.12	27.07
202	3.97	34.23	200	4.00	34.23	27.19
303	2.98	34.32	300	3.00	34.32	27.37

Station 6339; 5 April; 43°21.5′ N., 51°38′ W.; depth 622 m.; dynamic height 971.078.

Observed values			Scaled values			
Depth, meters	Temperature, °C.	Salinity, ‰	Depth, meters	Temperature, °C.	Salinity, ‰	σ_t
0	0.69	32.81	0	0.69	32.81	26.33
24	0.69	32.81	25	0.70	32.81	26.33
47	0.67	32.83	50	0.75	32.85	26.36
70	1.34	33.38	75	2.10	33.55	26.83
93	------	34.07	100	5.10	34.07	26.95
140	3.98	34.06	150	3.70	34.03	27.06
187	2.62	33.88	200	2.70	33.95	27.09
280	3.28	34.40	300	3.35	34.50	27.47
501	3.51	34.54	(400)	3.45	34.79	27.69
514	3.49	34.71	(600)	3.50	34.83	27.72

Station 6340; 5 April; 43°11′ N., 51°48′ W.; depth 1,646 m.; dynamic height 971.081.

Observed values			Scaled values			
Depth, meters	Temperature, °C.	Salinity, ‰	Depth, meters	Temperature, °C.	Salinity, ‰	σ_t
0	0.77	32.82	0	0.77	32.82	26.33
24	0.78	32.82	25	0.80	32.82	26.33
47	0.78	32.84	50	1.10	32.97	26.43
70	4.98	33.88	75	5.80	34.09	26.88
93	------	34.87	100	9.85	34.86	26.89
140	8.70	34.76	150	8.70	34.79	27.02
187	8.68	34.92	200	8.55	34.92	27.15
280	6.89	34.87	300	6.00	34.85	27.46
416	3.06	34.74	400	3.20	34.74	27.68
624	3.93	34.86	600	3.90	34.85	27.70
834	3.93	34.87	800	3.95	34.87	27.71
1,048	3.72	34.84	1,000	3.75	34.85	27.71
1,580	3.44	34.82				

Station 6341; 5 April; 43°00′ N., 52°03′ W.; depth 2,652 m.; dynamic height 971.152.

Observed values			Scaled values			
Depth, meters	Temperature, °C.	Salinity, ‰	Depth, meters	Temperature, °C.	Salinity, ‰	σ_t
0	2.15	32.98	0	2.15	32.98	26.37
25	2.95	32.99	25	2.95	32.99	26.31
49	9.55	34.57	50	9.55	34.66	26.78
74	10.52	33.04	75	10.50	35.04	26.91
98	9.64	34.94	100	9.60	34.92	26.98
148	6.48	34.44	150	6.45	34.43	27.06
198	6.23	34.40	200	6.25	34.40	27.07
296	6.25	34.65	300	6.25	34.66	27.27
361	6.67	34.89	400	6.15	34.86	27.44
550	4.03	34.75	600	4.10	34.78	27.62
747	4.38	34.89	800	4.45	34.91	27.69
937	4.49	------	1,000	4.45	34.92	27.70
1,417	4.34	34.92				

Station 6342; 5 April; 42°49.5′ N., 52°20′ W.; depth 3,155 m.; dynamic height 971.166.

Observed values			Scaled values			
Depth, meters	Temperature, °C.	Salinity, ‰	Depth, meters	Temperature, °C.	Salinity, ‰	σ_t
0	4.30	33.54	0	4.30	33.54	26.62
25	6.63	34.08	25	6.63	34.08	26.76
50	10.89	35.07	50	10.89	35.07	26.87
75	11.12	35.17	75	11.12	35.17	26.91
100	11.19	35.17	100	11.19	35.17	26.89
150	11.20	35.17	150	11.20	35.17	26.89
200	11.88	35.36	200	11.88	35.36	26.91
300	8.85	35.09	300	8.85	35.09	27.23
417	4.53	34.60	400	5.15	34.66	27.41
633	4.37	34.905	600	4.90	34.87	27.61
856	4.31	34.925	800	4.35	34.92	27.71
1,067	3.84	34.89	1,000	4.00	34.90	27.73
1,590	3.71	34.91				

Station 6343; 5 April; 42°35.5′ N., 52°50′ W.; depth 3,841 m.; dynamic height 971.145.

Observed values			Scaled values			
Depth, meters	Temperature, °C.	Salinity, ‰	Depth, meters	Temperature, °C.	Salinity, ‰	σ_t
0	10.64	35.05	0	10.64	35.05	26.90
25	10.66	35.05	25	10.66	35.05	26.89
50	10.70	35.05	50	10.70	35.05	26.89
75	10.70	35.06	75	10.70	35.06	26.90
100	10.91	35.11	100	10.91	35.11	26.90
150	11.22	35.20	150	11.22	35.20	26.91
200	7.78	34.61	200	7.78	34.61	27.02
300	6.86	34.74	300	6.86	34.74	27.25
339	5.48	34.86	400	5.55	34.69	27.38
496	5.62	34.92	600	5.30	34.98	27.64
647	5.13	34.99	800	4.80	35.00	27.72
825	4.77	35.00	1,000	4.45	34.99	27.75
1,297	3.96	34.955				

Station 6344; 6 April; 42°15.5′ N., 52°30′ W.; depth 4,070 m.; dynamic height 971.174.

Observed values			Scaled values			
Depth, meters	Temperature, °C.	Salinity, ‰	Depth, meters	Temperature, °C.	Salinity, ‰	σ_t
0	6.41	34.00	0	6.41	34.00	26.73
21	6.42	34.00	25	6.50	34.01	26.73
42	7.09	34.14	50	7.80	34.32	26.79
64	9.19	34.67	75	9.50	34.75	26.86
85	9.81	34.81	100	10.20	34.92	26.88
127	10.81	35.13	150	8.20	34.69	27.02
169	5.90	34.31	200	5.00	34.18	27.04
254	4.43	34.10	300	4.85	34.23	27.10
392	5.68	34.58	400	5.65	34.60	27.30
594	4.83	34.88	600	4.90	34.89	27.62
801	4.63	34.975	800	4.65	34.98	27.72
1,005	4.21	34.955	1,000	4.25	34.95	27.74
1,522	3.66	34.92				

STATIONS OCCUPIED IN 1957—Continued

Station 6345; 6 April; 42°00.5′ N., 52°04′ W.; depth 4,115 m.; dynamic height 971.188.

Observed values			Scaled values			
Depth, meters	Temperature, °C.	Salinity, ‰	Depth, meters	Temperature, °C.	Salinity, ‰	σ_t
0	11.81	35.33	0	11.80	35.33	26.90
27	11.81	35.32	25	11.80	35.22	26.90
53	11.83	35.33	50	11.85	35.33	26.89
80	11.84	35.325	75	11.85	35.33	26.89
106	11.84	35.33	100	11.85	35.33	26.89
160	11.86	35.33	150	11.85	35.33	26.89
214	11.85	35.33	200	11.85	35.33	26.89
320	9.61	35.18	300	10.05	35.22	27.13
413	7.63	35.01	400	7.95	35.03	27.32
622	5.32	34.975	600	5.45	34.98	27.62
834	4.60	34.98	800	4.70	34.98	27.71
1,045	4.21	34.96	1,000	4.30	34.96	27.74
1,576	3.68	34.935				

Station 6346; 6 April; 41°57.5′ N., 51°01′ W.; depth 3,338 m.; dynamic height 971.173.

Observed values			Scaled values			
Depth, meters	Temperature, °C.	Salinity, ‰	Depth, meters	Temperature, °C.	Salinity, ‰	σ_t
0	5.95	33.86	0	5.95	33.80	26.64
27	6.05	33.85	25	6.00	33.84	26.66
53	10.13	34.90	50	9.50	34.79	26.89
80	11.83	35.32	75	11.65	35.27	26.89
106	11.99	35.35	100	12.00	35.35	26.88
159	11.61	35.245	150	11.63	35.27	26.89
212	11.65	34.34	200	11.65	35.33	26.93
318	8.75	35.11	300	9.55	35.17	27.18
358	6.52	34.79	400	5.05	34.64	27.40
542	2.75	34.54	600	3.35	34.65	27.59
732	4.74	34.935	800	4.75	34.99	27.71
925	4.65	35.01	1,000	4.50	35.00	27.75
1,425	3.78	34.895				

Station 6347; 6 April; 42°22.5′ N., 51°33′ W.; depth 3,110 m.; dynamic height 971.197.

Observed values			Scaled values			
Depth, meters	Temperature, °C.	Salinity, ‰	Depth, meters	Temperature, °C.	Salinity, ‰	σ_t
0	4.71	33.49	0	4.70	33.49	26.53
27	11.03	35.13	25	10.45	35.00	26.89
53	12.05	35.385	50	12.00	35.37	26.90
80	12.18	35.42	75	12.15	35.41	26.90
106	12.23	35.425	100	12.20	35.43	26.90
160	12.26	35.425	150	12.25	35.43	26.89
212	11.99	35.37	200	12.10	35.39	26.89
318	10.31	35.27	300	10.65	35.29	27.08
383	8.49	35.10	400	8.15	35.08	27.33
576	5.69	34.97	600	5.55	34.97	27.61
772	4.78	34.99	800	4.70	34.98	27.71
974	3.86	34.89	1,000	3.80	34.89	27.74
1,492	3.69	34.91				

Station 6348; 6 April; 42°43′ N., 51°08′ W.; depth 1,920 m.; dynamic height 971.093.

Observed values			Scaled values			
Depth, meters	Temperature, °C.	Salinity, ‰	Depth, meters	Temperature, °C.	Salinity, ‰	σ_t
0	−0.39	33.20	0	−0.39	33.20	26.70
26	−0.66	33.22	25	−0.65	33.22	26.72
51	−0.66	33.23	50	−0.65	33.23	26.73
77	−0.59	33.24	75	−0.60	33.24	26.73
103	0.03	33.29	100	−0.05	33.28	26.74
153	0.30	33.58	150	0.25	33.56	26.96
204	0.92	33.985	200	0.90	33.95	27.23
307	2.06	34.28	300	2.00	34.26	27.40
335	2.38	34.38	400	2.90	34.52	27.54
503	3.37	34.68	600	3.60	34.76	27.66
672	3.75	34.80	800	3.85	34.84	27.69
847	3.87	34.85	1,000	3.80	34.85	27.71
1,295	3.56	34.85				

Station 6349; 7 April; 42°54.5′ N., 50°54′ W.; depth 1,060 m.; dynamic height 971.074.

Observed values			Scaled values			
Depth, meters	Temperature, °C.	Salinity, ‰	Depth, meters	Temperature, °C.	Salinity, ‰	σ_t
0	0.42	32.89	0	0.42	32.89	26.40
25	0.41	32.89	25	0.41	32.89	26.40
50	0.00	33.12	50	0.00	33.12	26.61
76	−0.09	33.15	75	−0.10	33.16	26.64
101	−0.43	33.40	100	−0.40	33.39	26.85
150	0.50	33.82	150	0.50	33.82	27.15
200	1.27	33.97	200	1.30	33.97	27.22
301	3.13	34.44	300	3.15	34.44	27.44
358	------	-------	(400)	3.60	34.72	27.63
			(600)	3.75	34.83	27.69
			(800)	3.75	34.84	27.70
			(1,000)	3.70	34.85	27.72

Station 6350; 7 April; 43°03′ N., 50°39′ W.; depth 183 m.; dynamic height 971.125.

Observed values			Scaled values			
Depth, meters	Temperature, °C.	Salinity, ‰	Depth, meters	Temperature, °C.	Salinity, ‰	σ_t
0	0.63	32.81	0	0.63	32.81	26.34
26	0.63	32.81	25	0.63	32.81	26.34
52	−0.39	33.17	50	−0.30	33.14	26.64
78	−0.58	33.26	75	−0.55	33.25	26.74
105	−0.31	33.42	100	−0.40	33.39	26.85
156	0.30	33.55	150	0.25	33.53	26.93
191	0.39	33.70	(200)	0.40	33.74	27.09

Station 6351; 7 April; 43°07.5′ N., 50°31′ W.; depth 89 m.; dynamic height 971.129.

Observed values			Scaled values			
Depth, meters	Temperature, °C.	Salinity, ‰	Depth, meters	Temperature, °C.	Salinity, ‰	σ_t
0	0.45	32.865	0	0.45	32.865	26.38
25	0.44	32.86	25	0.44	32.86	26.38
50	0.41	32.87	50	0.41	32.87	26.39
75	−0.22	33.34	75	−0.22	33.34	26.80

Station 6352; 7 April; 43°20.5′ N., 50°16′ W.; depth 64 m.; dynamic height 971.148.

Observed values			Scaled values			
Depth, meters	Temperature, °C.	Salinity, ‰	Depth, meters	Temperature, °C.	Salinity, ‰	σ_t
0	0.78	32.68	0	0.78	32.68	26.22
26	0.73	32.69	25	0.75	32.69	26.22
52	0.72	32.70	50	0.70	32.70	26.23

Station 6353; 7 April; 42°56′ N., 50°17′ W.; depth 89 m.; dynamic height 971.122.

Observed values			Scaled values			
Depth, meters	Temperature, °C.	Salinity, ‰	Depth, meters	Temperature, °C.	Salinity, ‰	σ_t
0	0.04	33.06	0	0.04	33.06	26.56
23	0.01	33.06	25	0.00	33.06	26.56
45	0.00	33.065	50	0.00	33.07	26.57
68	−0.26	33.24	(75)	−0.35	33.29	26.75

Station 6354; 7 April; 42°48′ N., 50°15′ W.; depth 320 m.; dynamic height 971.105.

Observed values			Scaled values			
Depth, meters	Temperature, °C.	Salinity, ‰	Depth, meters	Temperature, °C.	Salinity, ‰	σ_t
0	−0.48	33.18	0	−0.48	33.18	26.68
24	−0.47	33.175	25	−0.45	33.18	26.68
48	−0.50	33.205	50	−0.50	33.22	26.71
71	−0.62	33.36	75	−0.65	33.37	26.84
95	−0.64	33.42	100	−0.65	33.43	26.89
142	−0.38	33.51	150	−0.30	33.53	26.95
190	0.10	33.66	200	0.20	33.69	27.06
285	1.39	33.97	(300)	1.60	34.02	27.24

TABLE OF OCEANOGRAPHIC DATA—Continued

STATIONS OCCUPIED IN 1957—Continued

Observed values			Scaled values			
Depth, meters	Temperature, °C.	Salinity, °/oo	Depth, meters	Temperature, °C.	Salinity, °/oo	σ_t
Station 6355; 7 April; 42°37.5′ N., 50°17′ W.; depth 1,829 m.; dynamic height 971.007.						
0	−0.62	33.21	0	−0.62	33.21	26.71
25	−0.68	33.21	25	−0.68	33.21	26.72
49	−0.65	33.24	50	−0.65	33.25	26.75
74	0.04	33.59	75	0.05	33.60	27.00
98	0.49	33.80	100	0.50	33.83	27.15
148	1.36	34.12	150	1.40	34.13	27.34
196	1.88	34.27	200	1.90	34.28	27.42
294	2.34	34.42	300	2.40	34.44	27.51
333	2.90	34.595	400	3.10	34.66	27.63
501	3.35	34.73	600	3.60	34.80	27.69
673	3.69	34.84	800	3.70	34.84	27.71
851	3.68	34.845	1,000	3.65	34.85	27.72
1,310	3.61	34.855				
Station 6356; 7 April; 42°18′ N., 50°21′ W.; depth 2,898 m.; dynamic height 970.945.						
0	0.88	33.54	0	0.88	33.54	26.90
27	0.96	33.63	25	0.95	33.62	26.96
52	1.37	33.845	50	1.30	33.83	27.10
79	1.89	--------	75	1.85	34.03	27.22
104	1.92	34.215	100	1.90	34.19	27.35
157	2.43	34.40	150	2.35	34.38	27.46
210	2.58	34.50	200	2.55	34.48	27.53
314	3.17	34.65	300	3.05	34.63	27.60
408	4.17	34.835	400	4.10	34.82	27.66
609	3.79	34.85	600	3.80	34.85	27.71
808	3.65	34.865	800	3.65	34.86	27.73
1,019	3.58	34.87	1,000	3.60	34.87	27.75
1,566	3.45	34.875				
Station 6357; 7–8 April; 41°50′ N., 50°22′ W.; depth 3,749 m.; dynamic height 971.035.						
0	−0.09	33.16	0	−0.09	33.16	26.64
27	−0.28	33.16	25	−0.25	33.16	26.65
53	−0.44	33.35	50	−0.40	33.32	26.79
80	−0.30	33.35	75	−0.35	33.49	26.92
106	−0.16	33.62	100	−0.20	33.60	27.01
160	0.79	33.87	150	0.55	33.82	27.15
214	4.23	34.49	200	3.45	34.34	27.33
320	3.59	34.65	300	3.65	34.63	27.54
404	3.68	34.74	400	3.65	34.74	27.63
605	3.74	34.81	600	3.75	34.81	27.68
808	3.72	34.845	800	3.75	34.84	27.70
1,013	3.63	34.85	1,000	3.65	34.85	27.72
1,534	3.55	34.865				
Station 6358; 8 April; 41°20.5′ N., 50°20′ W.; depth 3,749 m.; dynamic height 971.268.						
0	14.09	35.83	0	14.09	35.83	26.83
26	14.10	35.825	25	14.10	35.83	26.82
51	14.12	35.825	50	14.10	35.83	26.82
77	14.13	35.83	75	14.10	35.83	26.82
103	14.15	35.835	100	14.15	35.83	26.81
153	14.19	35.855	150	14.20	35.85	26.82
205	14.10	35.835	200	14.10	35.84	26.83
308	12.14	35.55	300	12.35	35.57	26.98
414	9.46	35.19	400	9.80	35.24	27.19
622	4.83	34.78	600	5.10	34.79	27.52
832	5.03	35.00	800	5.00	34.98	27.68
1,036	4.45	34.96	1,000	4.55	34.97	27.73
1,541	3.70	34.91				

Observed values			Scaled values			
Depth, meters	Temperature, °C.	Salinity, °/oo	Depth, meters	Temperature, °C.	Salinity, °/oo	σ_t
Station 6359; 8 April; 40°55.5′ N., 50°15′ W.; depth 3,660 m.; dynamic height 971.275.						
0	13.84	35.77	0	13.84	35.77	26.83
25	13.83	35.745	25	13.83	35.745	26.82
49	13.81	35.74	50	13.80	35.74	26.82
74	13.79	35.74	75	13.80	35.74	26.82
98	13.03	35.76	100	13.80	35.76	26.83
148	13.83	35.755	150	13.80	35.75	26.82
196	13.68	35.725	200	13.60	35.72	26.85
294	11.10	35.25	300	10.75	35.19	26.99
303	10.42	35.14	400	8.80	35.09	26.99
472	7.74	35.06	600	6.15	34.95	27.51
654	5.62	34.895	(800)	4.95	34.90	27.62
	5.67	35.00	(1,000)	4.50	34.91	27.68
817	4.73	34.95				
Station 6360; 8 April; 41°55′ N., 49°25′ W.; depth 3,200 m.; dynamic height 970.985.						
0	1.47	33.36	0	1.47	33.36	26.72
28	1.21	33.43	25	1.25	33.42	26.78
54	1.12	33.55	50	1.15	33.53	26.87
82	1.90	33.95	75	1.65	33.86	27.10
109	2.27	34.09	100	2.15	34.05	27.22
163	6.15	34.78	150	5.05	34.64	27.40
217	4.26	34.57	200	4.85	34.62	27.42
325	3.51	34.66	300	3.55	34.63	27.55
420	4.76	34.90	400	4.55	34.86	27.64
631	4.84	35.02	600	4.85	35.02	27.73
844	4.18	34.95	800	4.35	34.96	27.74
1,058	3.94	34.935	1,000	4.00	34.94	27.76
1,593	3.63	34.93				
Station 6361; 8 April; 41°34.5′ N., 49°03′ W.; depth 3,292 m.; dynamic height 971.243.						
0	14.05	35.84	0	14.05	35.84	26.84
25	14.06	35.835	25	14.06	35.835	26.84
50	14.06	35.835	50	14.06	35.835	26.84
74	14.05	35.83	75	14.05	35.83	26.83
99	14.03	35.83	100	14.05	35.83	26.83
148	14.07	35.8 5	150	14.05	35.83	26.83
198	14.09	35.845	200	14.10	35.84	26.83
297	11.67	35.48	300	11.60	35.46	27.04
411	8.63	35.08	400	8.95	35.11	27.24
622	5.80	34.98	600	5.95	34.98	27.56
835	4.76	34.975	800	4.90	34.97	27.69
1,051	4.22	34.95	1,000	4.35	34.95	27.73
1,598	3.70	34.93				
Station 6362; 9 April; 41°03′ N., 48°28′ W.; depth 3,567 m.; dynamic height 971.407.						
0	14.62	35.935	0	14.62	35.935	26.80
26	14.64	35.94	25	14.65	35.94	26.79
52	14.65	35.935	50	14.65	35.93	26.78
78	14.64	35.935	75	14.65	35.93	26.78
104	14.64	35.93	100	14.60	35.93	26.79
155	14.63	35.93	150	14.60	35.93	26.79
206	14.60	35.925	200	14.60	35.925	26.79
310	14.54	35.91	300	14.55	35.91	26.79
384	13.01	35.59	400	12.65	35.55	26.90
568	8.76	35.15	600	8.15	35.08	27.33
749	5.05	34.79	800	5.00	34.84	27.57
942	4.83	34.98	1,000	4.75	34.98	27.70
1,436	4.01	34.96				

TABLE OF OCEANOGRAPHIC DATA—Continued
STATIONS OCCUPIED IN 1957—Continued

Station 6363; 9 April; 41°35.5′ N., 47°18′ W.; depth 4,298 m.; dynamic height 971.176.

Observed values			Scaled values			
Depth, meters	Temperature, °C.	Salinity, °/oo	Depth, meters	Temperature, °C.	Salinity, °/oo	σ_t
0	14.32	35.82	0	14.32	35.82	26.77
26	14.37	35.835	25	14.35	35.83	26.77
52	14.35	35.84	50	14.35	35.84	26.78
78	14.31	35.82	75	14.30	35.83	26.78
104	13.74	35.72	100	13.80	35.74	26.82
155	12.93	35.56	150	12.95	35.58	26.87
206	11.96	35.48	200	12.10	35.49	26.97
310	9.54	35.20	300	9.70	35.23	27.20
417	5.52	34.68	400	6.05	34.75	27.37
606	4.99	34.91	600	5.00	34.91	27.63
794	4.58	34.95	800	4.55	34.95	27.71
996	4.21	34.94	1,000	4.20	34.94	27.74
1,521	3.72	34.925				

Station 6364; 9 April; 42°01.5′ N., 47°56′ W.; depth 3,703 m.; dynamic height 971.036.

Observed values			Scaled values			
Depth, meters	Temperature, °C.	Salinity, °/oo	Depth, meters	Temperature, °C.	Salinity, °/oo	σ_t
0	9.14	34.60	0	9.14	34.60	26.80
26	8.71	34.60	25	8.70	34.60	26.87
52	8.15	34.56	50	8.20	34.57	26.93
78	6.94	34.37	75	6.95	34.38	26.95
104	8.84	34.815	100	8.50	34.78	27.04
155	5.98	34.515	150	6.05	34.53	27.19
207	6.14	34.65	200	6.10	34.63	27.26
311	6.28	35.05	300	6.30	35.02	27.55
433	5.69	35.00	400	5.95	35.01	27.59
661	4.31	34.91	600	4.55	34.93	27.69
897	4.21	34.95	800	4.25	34.93	27.72
1,122	3.90	34.93	1,000	4.10	34.94	27.75
1,684	3.51	34.87				

Station 6365; 9 April; 42°21.5′ N., 48°26′ W.; depth 3,010 m.; dynamic height 970.980.

Observed values			Scaled values			
Depth, meters	Temperature, °C.	Salinity, °/oo	Depth, meters	Temperature, °C.	Salinity, °/oo	σ_t
0	4.36	33.80	0	4.36	33.80	26.81
25	4.29	33.85	25	4.29	33.85	26.86
50	4.15	33.85	50	4.15	33.85	26.87
75	3.46	33.91	75	3.46	33.91	26.99
100	4.09	34.28	100	4.09	34.28	27.23
149	4.66	34.53	150	4.65	34.54	27.37
199	4.39	34.61	200	4.40	34.61	27.46
299	4.21	34.73	300	4.20	34.73	27.57
335	4.38	34.805	400	4.55	34.89	27.66
512	4.66	34.96	600	4.55	34.96	27.72
694	4.32	34.95	800	4.15	34.94	27.74
881	4.02	34.935	1,000	3.90	34.92	27.76
1,373	3.53	34.89				

Station 6366; 9 April; 42°42.5′ N., 49°02′ W.; depth 2,236 m.; dynamic height 970.947.

Observed values			Scaled values			
Depth, meters	Temperature, °C.	Salinity, °/oo	Depth, meters	Temperature, °C.	Salinity, °/oo	σ_t
0	1.57	33.71	0	1.57	33.71	26.99
26	1.49	33.78	25	1.50	33.78	27.05
52	1.47	33.88	50	1.45	33.87	27.13
78	2.16	34.14	75	2.05	34.11	27.28
104	2.85	34.24	100	2.75	34.23	27.31
155	3.91	34.50	150	3.80	34.47	27.41
207	4.94	34.80	200	4.90	34.78	27.53
311	4.96	34.905	300	4.95	34.90	27.62
405	4.85	34.94	400	4.85	34.94	27.66
607	4.27	34.94	600	4.30	34.94	27.72
811	3.82	34.89	800	3.85	34.89	27.73
1,019	3.61	34.88	1,000	3.65	34.88	27.74
1,546	3.51	34.895				

Station 6367; 10 April; 43°23.5′ N., 48°41′ W.; depth 1,829 m.; dynamic height 970.916.

Observed values			Scaled values			
Depth, meters	Temperature, °C.	Salinity, °/oo	Depth, meters	Temperature, °C.	Salinity, °/oo	σ_t
0	0.12	33.34	0	0.12	33.34	26.79
23	0.12	33.39	25	0.20	33.42	26.85
45	1.16	33.94	50	1.35	34.04	27.27
68	2.04	34.27	75	2.35	34.32	27.42
91	2.80	34.415	100	2.80	34.43	27.46
137	2.75	34.50	150	2.80	34.52	27.54
182	2.97	34.58	200	3.05	34.60	27.58
273	3.31	--------	300	3.35	34.71	27.64
419	3.48	34.785	400	3.50	34.77	27.68
630	3.63	34.85	600	3.60	34.84	27.72
845	3.59	34.87	800	3.60	34.87	27.75
1,060	3.45	34.86	1,000	3.50	34.86	27.75
1,603	3.40	34.87				

Station 6368; 10 April; 43°14.5′ N., 47°54′ W.; depth 3,246 m.; dynamic height 971.009.

Observed values			Scaled values			
Depth, meters	Temperature, °C.	Salinity, °/oo	Depth, meters	Temperature, °C.	Salinity, °/oo	σ_t
0	4.66	33.91	0	4.66	33.91	26.87
24	5.45	34.07	25	5.45	34.07	26.91
48	8.83	34.76	50	8.85	34.76	26.98
72	8.98	34.80	75	8.95	34.80	26.99
96	8.94	34.83	100	8.90	34.82	27.01
144	2.88	34.125	150	3.00	34.15	27.23
193	4.85	34.53	200	4.85	34.54	27.35
289	4.07	34.635	300	4.40	34.71	27.53
310	4.63	34.765	400	4.95	34.92	27.64
468	5.02	34.98	600	4.60	34.95	27.70
629	4.49	34.945	800	4.10	34.92	27.74
801	4.07	34.92	1,000	3.80	34.90	27.75
1,260	3.48	34.88				

Station 6369; 10 April; 42°59′ N., 47°15′ W.; depth 3,200 m.; dynamic height 971.166.

Observed values			Scaled values			
Depth, meters	Temperature, °C.	Salinity, °/oo	Depth, meters	Temperature, °C.	Salinity, °/oo	σ_t
0	14.03	35.765	0	14.03	35.765	26.79
25	14.06	35.76	25	14.06	35.76	26.78
52	14.02	35.76	50	14.00	35.76	26.79
77	13.81	35.73	75	13.80	35.73	26.81
103	13.19	35.59	100	13.25	35.61	26.83
154	12.20	35.41	150	12.25	35.43	26.89
205	11.15	35.23	200	11.30	35.25	26.94
308	6.87	34.73	300	7.00	34.76	27.25
459	6.03	34.915	400	6.25	34.84	27.41
692	5.28	35.035	600	5.60	35.01	27.63
926	4.43	34.97	800	4.85	35.01	27.72
1,157	4.09	34.94	1,000	4.30	34.95	27.73
1,738	3.57	34.91				

Station 6370; 10 April; 42°41′ N., 46°47′ W.; depth 3,978 m.; dynamic height 971.347.

Observed values			Scaled values			
Depth, meters	Temperature, °C.	Salinity, °/oo	Depth, meters	Temperature, °C.	Salinity, °/oo	σ_t
2	14.93	36.035	0	14.92	36.035	26.81
27	14.94	36.035	25	14.95	36.03	26.80
52	14.92	36.03	50	14.95	36.03	26.80
77	14.89	36.015	75	14.90	36.02	26.80
103	14.84	36.01	100	14.85	36.01	26.81
152	14.78	35.995	150	14.80	35.99	26.80
202	14.77	35.99	200	14.80	35.99	26.80
303	13.69	35.77	300	13.75	35.78	26.86
461	10.07	35.25	400	11.50	35.45	27.05
709	6.43	35.01	600	7.60	35.07	27.41
968	4.13	34.93	800	5.50	34.97	27.61
1,198	4.45	34.98	1,000	4.15	34.94	27.74
1,747	3.62	34.905				

TABLE OF OCEANOGRAPHIC DATA—Continued

STATIONS OCCUPIED IN 1957—Continued

Station 6371; 10 April; 42°24.5′ N., 46°15′ W.; depth 4,572 m.; dynamic height 971.458.

Observed values			Scaled values			
Depth, meters	Temperature, °C.	Salinity, °/oo	Depth, meters	Temperature, °C.	Salinity, °/oo	σt
0	14.86	36.04	0	14.86	36.04	26.83
23	14.90	36.04	25	14.90	36.04	26.82
47	14.91	36.04	50	14.90	36.04	26.82
71	14.93	36.05	75	14.95	36.05	26.82
95	14.97	36.07	100	14.95	36.07	26.83
142	14.97	36.07	150	14.95	36.07	26.83
189	14.97	36.07	200	14.95	36.07	26.83
284	14.97	36.075	300	14.90	36.06	26.83
393	13.91	35.805	400	13.80	35.79	26.85
592	10.22	35.265	600	10.05	35.25	27.16
794	6.84	35.03	800	6.70	35.02	26.50
999	4.71	34.905	1,000	4.70	34.90	27.65
1,521	4.12	34.95				

Station 6372; 11 April; 42°51′ N., 45°48′ W.; depth 4,663 m.; dynamic height 971.366.

Observed values			Scaled values			
Depth, meters	Temperature, °C.	Salinity, °/oo	Depth, meters	Temperature, °C.	Salinity, °/oo	σt
0	15.31	36.05	0	15.31	36.05	26.73
26	15.39	36.05	25	15.35	36.05	26.72
51	15.38	36.05	50	15.40	36.05	26.71
77	15.42	36.05	75	15.40	36.05	26.71
102	15.42	36.065	100	15.40	36.06	26.72
153	15.44	36.06	150	15.45	36.06	26.71
204	15.02	35.97	200	15.10	35.98	26.72
306	13.38	35.70	300	13.50	35.71	26.86
406	11.65	35.47	400	11.75	35.49	27.03
601	5.76	34.715	600	5.75	34.72	27.39
791	5.29	34.98	800	5.30	34.98	27.64
990	4.77	35.00	1,000	4.75	35.00	27.72
1,490	3.63	34.89				

Station 6373; 11 April; 43°10′ N., 45°26′ W.; depth 4,663 m.; dynamic height 971.049.

Observed values			Scaled values			
Depth, meters	Temperature, °C.	Salinity, °/oo	Depth, meters	Temperature, °C.	Salinity, °/oo	σt
0	7.67	34.66	0	7.67	34.66	27.08
26	8.71	34.89	25	8.65	34.89	27.10
52	9.00	34.965	50	9.00	34.96	27.11
78	9.03	34.97	75	9.00	34.97	27.12
103	9.02	34.97	100	9.00	34.97	27.12
156	8.08	34.82	150	8.20	34.84	27.14
207	6.60	34.65	200	6.80	34.67	27.21
310	5.51	34.76	300	5.55	34.75	27.43
357	5.31	34.78	400	5.15	34.80	27.52
528	4.70	34.875	600	4.60	34.91	27.67
694	4.55	34.94	800	4.40	34.94	27.71
881	4.23	34.94	1,000	4.05	34.93	27.74
1,370	3.51	34.895				

Station 6374; 11 April; 43°20′ N., 46°01′ W.; depth 4,663 m.; dynamic height 971.067.

Observed values			Scaled values			
Depth, meters	Temperature, °C.	Salinity, °/oo	Depth, meters	Temperature, °C.	Salinity, °/oo	σt
0	4.52	33.95	0	4.52	33.95	26.92
23	4.41	33.96	25	4.40	33.97	26.95
47	4.38	34.045	50	4.45	34.06	27.01
70	5.79	34.29	75	6.30	34.37	27.04
93	8.24	34.76	100	8.40	34.81	27.08
139	8.99	34.95	150	8.75	34.93	27.12
186	7.62	34.77	200	7.30	34.75	27.20
279	5.76	34.73	300	5.70	34.74	27.40
348	5.51	34.79	400	5.35	34.84	27.53
516	4.98	34.92	600	4.80	34.91	27.65
681	4.61	34.945	800	4.40	34.94	27.71
867	4.27	34.94	1,000	4.10	34.94	27.75
1,360	3.59	34.90				

Station 6375; 11 April; 43°32.5′ N., 46°37′ W.; depth 4,481 m.; dynamic height 971.050.

Observed values			Scaled values			
Depth, meters	Temperature, °C.	Salinity, °/oo	Depth, meters	Temperature, °C.	Salinity, °/oo	σt
0	9.62	34.91	0	9.62	34.91	26.97
18	9.34	34.875	25	9.20	34.85	26.99
35	9.02	34.79	50	8.05	34.66	27.02
53	7.85	34.63	75	7.25	34.50	27.01
70	7.26	34.515	100	7.20	34.50	27.02
105	7.20	34.50	150	6.00	34.40	27.10
140	6.19	34.395	200	5.35	34.49	27.25
210	5.28	34.51	300	4.90	34.65	27.43
434	4.68	34.81	400	4.70	34.78	27.55
651	4.47	34.92	600	4.50	34.91	27.68
866	4.18	34.93	800	4.30	34.93	27.71
1,082	3.92	34.81	1,000	4.00	34.92	27.75

Station 6376; 11 April; 43°43′ N., 47°12′ W.; depth 4,253 m.; dynamic height 971.011.

Observed values			Scaled values			
Depth, meters	Temperature, °C.	Salinity, °/oo	Depth, meters	Temperature, °C.	Salinity, °/oo	σt
0	4.54	33.885	0	4.54	33.885	26.86
27	4.81	33.98	25	4.80	33.97	26.91
53	4.79	34.16	50	4.80	34.13	27.03
80	7.56	34.67	75	7.15	34.58	27.08
106	7.00	34.66	100	7.15	34.67	27.16
160	3.92	34.32	150	4.45	34.38	27.26
214	4.59	34.55	200	4.40	34.49	27.36
320	4.67	34.73	300	4.65	34.70	27.50
418	4.55	34.83	400	4.55	34.81	27.60
628	4.26	34.90	600	4.30	34.90	27.69
837	3.94	34.89	800	4.00	34.89	27.72
1,052	3.64	34.88	1,000	3.70	34.88	27.74
1,600	3.45	34.875				

Station 6377; 12 April; 43°52.5′ N., 47°48′ W.; depth 3,887 m.; dynamic height 970.961.

Observed values			Scaled values			
Depth, meters	Temperature, °C.	Salinity, °/oo	Depth, meters	Temperature, °C.	Salinity, °/oo	σt
0	4.62	33.92	0	4.62	33.92	26.88
25	4.70	33.96	25	4.70	33.96	26.91
51	4.45	34.07	50	4.45	34.06	27.01
76	3.95	34.20	75	4.00	34.19	27.16
102	2.96	34.18	100	3.00	34.18	27.25
152	3.49	34.45	150	3.45	34.44	27.41
204	5.03	33.96	200	3.70	34.57	27.50
306	4.87	34.39	300	4.00	34.72	27.59
400	4.13	34.825	400	4.15	34.83	27.65
602	4.29	34.93	600	4.30	34.93	27.71
806	3.88	34.91	800	3.90	34.91	27.75
1,010	3.76	34.91	1,000	3.75	34.91	27.76
1,529	3.47	34.90				

Station 6378; 12 April; 44°00.5′ N., 48°18′ W.; depth 3,383 m.; dynamic height 970.922.

Observed values			Scaled values			
Depth, meters	Temperature, °C.	Salinity, °/oo	Depth, meters	Temperature, °C.	Salinity, °/oo	σt
0	2.73	34.01	0	2.73	34.01	27.14
22	2.73	34.005	25	2.75	34.01	27.14
45	2.61	34.01	50	2.55	34.01	27.16
68	2.46	34.00	75	2.40	34.01	27.17
91	2.26	34.075	100	2.40	34.14	27.27
136	3.05	34.46	150	3.35	34.53	27.49
181	3.71	34.63	200	3.85	34.70	27.58
272	4.08	34.81	300	4.10	34.83	27.66
368	4.08	34.86	400	4.05	34.86	27.69
556	3.80	34.87	600	3.75	34.87	27.73
747	3.70	34.885	800	3.70	34.88	27.74
943	3.57	34.88	1,000	3.55	34.88	27.75
1,450	3.38	34.885				

TABLE OF OCEANOGRAPHIC DATA—Continued

STATIONS OCCUPIED IN 1957—Continued

Station 6379; 12 April; 44°05.5′ N., 48°48′ W.; depth 1,646 m.; dynamic height 971.000.

Observed values			Scaled values			
Depth, meters	Temperature, °C.	Salinity, °/oo	Depth, meters	Temperature, °C.	Salinity, °/oo	σt
0	−0.67	33.16	0	−0.67	33.16	26.67
25	−0.69	33.165	25	−0.69	33.165	26.68
49	−0.53	33.32	50	−0.50	33.33	26.80
74	−0.09	33.59	75	−0.05	33.60	27.00
98	0.35	35.72	100	0.40	33.74	27.09
148	1.30	34.09	150	1.30	34.10	27.32
198	2.09	34.295	200	2.10	34.30	27.42
296	2.78	34.55	300	3.00	34.63	27.61
286	3.08	34.665	400	3.35	34.74	27.66
433	3.43	34.765	600	3.55	34.79	27.68
586	3.52	34.79	800	3.65	34.83	27.70
752	3.64	34.83	1,000	3.60	34.85	27.73
1,194	3.57	34.855				

Station 6380; 12 April; 44°06.5′ N., 48°57′ W.; depth 650 m.; dynamic height 971.031.

Observed values			Scaled values			
Depth, meters	Temperature, °C.	Salinity, °/oo	Depth, meters	Temperature, °C.	Salinity, °/oo	σt
0	−0.66	33.16	0	−0.66	33.16	26.67
24	−0.68	33.17	25	−0.70	33.17	26.68
47	−0.60	33.445	50	−0.60	33.48	26.92
70	−0.23	33.575	75	−0.20	33.59	27.00
93	0.02	33.635	100	0.10	33.68	27.05
140	1.04	33.99	150	1.15	34.07	27.31
187	1.66	34.24	200	1.70	34.26	27.42
281	1.90	34.325	300	1.95	34.35	27.48
484	2.81	34.59	(400)	2.35	34.47	27.54
			(600)	3.50	34.75	27.66

Station 6381; 12 April; 44°07′ N., 49°05′ W.; depth 165 m.; dynamic height 971.090.

Observed values			Scaled values			
Depth, meters	Temperature, °C.	Salinity, °/oo	Depth, meters	Temperature, °C.	Salinity, °/oo	σt
0	−0.23	33.135	0	−0.23	33.135	26.63
23	−0.66	33.15	25	−0.70	33.15	26.66
46	−0.84	33.22	50	−0.85	33.23	26.73
69	−0.80	33.26	75	−0.75	33.27	26.76
93	−0.72	33.30	100	−0.65	33.33	26.81
138	−0.22	33.515	(150)	−0.10	33.58	26.98

Station 6382; 12 April; 44°09′ N., 49°13′ W.; depth 104 m.; dynamic height 971.118.

Observed values			Scaled values			
Depth, meters	Temperature, °C.	Salinity, °/oo	Depth, meters	Temperature, °C.	Salinity, °/oo	σt
0	−0.07	33.16	0	−0.07	33.16	26.64
23	−0.16	33.15	25	−0.15	33.15	26.64
47	−0.22	33.14	50	−0.25	33.14	26.64
70	−0.42	33.17	75	−0.45	33.18	26.68

Station 6383; 12 April; 44°12.5′ N., 49°23′ W.; depth 50 m.; dynamic height 971.121.

Observed values			Scaled values			
Depth, meters	Temperature, °C.	Salinity, °/oo	Depth, meters	Temperature, °C.	Salinity, °/oo	σt
0	0.05	33.115	0	0.05	33.115	26.60
25	0.00	33.12	25	0.00	33.12	26.61
41	−0.04	33.11	(50)	−0.10	33.11	26.60

Station 6384; 12 April; 44°58.5′ N., 49°26′ W.; depth 62 m.; dynamic height 971.126.

Observed values			Scaled values			
Depth, meters	Temperature, °C.	Salinity, °/oo	Depth, meters	Temperature, °C.	Salinity, °/oo	σt
0	−0.42	33.09	0	−0.42	33.09	26.60
25	−0.42	33.085	25	−0.42	33.085	26.60
51	−0.67	33.11	50	−0.65	33.11	26.63

Station 6385; 12 April; 44°55.5′ N., 49°10′ W.; depth 179 m.; dynamic height 971.123.

Observed values			Scaled values			
Depth, meters	Temperature, °C.	Salinity, °/oo	Depth, meters	Temperature, °C.	Salinity, °/oo	σt
0	−0.47	33.015	0	−0.47	33.015	26.55
25	−0.47	33.02	25	−0.47	33.02	26.55
51	−0.90	33.10	50	−0.90	33.09	26.62
76	−0.94	33.12	75	−0.95	33.12	26.65
101	−0.98	33.18	100	−1.00	33.17	26.69
151	0.09	33.65	150	0.05	33.64	27.03

Station 6386; 12 April; 44°54′ N., 49°01′ W.; depth 640 m.; dynamic height 971.054.

Observed values			Scaled values			
Depth, meters	Temperature, °C.	Salinity, °/oo	Depth, meters	Temperature, °C.	Salinity, °/oo	σt
0	−0.81	33.02	0	−0.81	33.02	26.56
24	−0.80	33.02	25	−0.80	33.02	26.56
48	−1.10	33.20	50	−1.10	33.21	26.73
72	−0.68	33.42	75	−0.60	33.44	26.89
96	0.06	33.65	100	0.10	33.68	27.05
143	0.72	33.885	150	0.75	33.90	27.20
190	0.94	33.97	200	1.00	34.00	27.26
286	1.81	34.29	300	1.90	34.31	27.45
328	2.00	34.35	400	2.35	34.44	27.51
523	3.00	34.64	(600)	3.40	34.76	27.68

Station 6387; 13 April; 44°51′ N., 48°43′ W.; depth 1,829 m.; dynamic height 970.913.

Observed values			Scaled values			
Depth, meters	Temperature, °C.	Salinity, °/oo	Depth, meters	Temperature, °C.	Salinity, °/oo	σt
0	−0.11	33.41	0	−0.11	33.41	26.85
17	−0.07	33.42	25	−0.05	33.48	26.90
33	0.02	33.59	50	1.10	33.93	27.20
50	1.13	33.93	75	1.55	34.09	27.29
67	1.41	34.04	100	2.10	34.26	27.39
101	2.15	34.27	150	2.80	34.54	27.55
134	2.72	34.50	200	2.95	34.64	27.62
201	2.98	34.64	300	3.45	34.77	27.68
242	3.33	34.72	400	3.50	34.80	27.70
339	3.49	34.78	600	3.60	34.84	27.72
420	3.50	34.80	800	3.55	34.86	27.74
528	3.59	34.825	(1,000)	3.55	34.87	27.75
798	3.55	34.86				

Station 6388; 13 April; 44°48′ N., 48°25′ W.; depth 2,469 m.; dynamic height 970.898.

Observed values			Scaled values			
Depth, meters	Temperature, °C.	Salinity, °/oo	Depth, meters	Temperature, °C.	Salinity, °/oo	σt
0	0.80	33.57	0	0.80	33.57	26.93
28	1.16	33.78	25	1.10	33.76	27.06
55	2.12	34.20	50	2.00	33.99	27.18
82	2.80	34.39	75	2.65	34.35	27.42
109	2.56	34.445	100	2.65	34.43	27.48
165	3.09	34.575	150	2.95	34.53	27.53
219	4.05	34.77	200	3.65	34.71	27.61
328	4.07	34.85	300	4.05	34.84	27.67
406	3.99	34.87	400	4.00	34.87	27.71
616	3.78	34.89	600	3.80	34.89	27.74
832	3.48	34.86	800	3.45	34.86	27.75
1,048	3.43	34.87	1,000	3.45	34.87	27.76
1,590	3.39	34.885				

TABLE OF OCEANOGRAPHIC DATA—Continued

STATIONS OCCUPIED IN 1957—Continued

Station 6389; 13 April; 44°41′ N., 47°48′ W.; depth 3,429 m.; dynamic height 971.014.

Observed values			Scaled values			
Depth, meters	Temperature, °C.	Salinity, °/oo	Depth, meters	Temperature, °C.	Salinity, °/oo	σ_t
0	5.19	34.15	0	5.19	34.15	27.00
22	5.11	34.135	25	5.10	34.14	27.00
46	5.01	34.22	50	5.50	34.28	27.06
68	7.40	34.65	75	7.85	34.79	27.15
91	8.35	34.96	100	8.30	34.94	27.20
136	7.84	34.84	150	7.50	34.81	27.22
182	6.77	34.77	200	6.50	34.77	27.33
273	5.68	34.83	300	5.40	34.82	27.51
338	5.08	34.80	400	4.90	34.83	27.57
564	4.54	34.91	600	4.50	34.92	27.69
829	4.25	34.94	800	4.30	34.94	27.72
1,018	3.67	34.885	1,000	3.70	34.89	27.75
1,459	3.44	34.88				

Station 6390; 13 April; 44°35′ N., 47°10′ W.; depth 3,841 m.; dynamic height 971.152.

Observed values			Scaled values			
Depth, meters	Temperature, °C.	Salinity, °/oo	Depth, meters	Temperature, °C.	Salinity, °/oo	σ_t
0	10.11	35.19	0	10.11	35.19	27.10
26	10.05	35.18	25	10.05	35.18	27.10
50	10.09	35.18	50	10.10	35.18	27.09
76	10.01	35.17	75	10.00	35.17	27.11
101	9.92	35.155	100	9.95	35.16	27.11
152	9.37	35.07	150	9.35	35.07	27.14
202	8.84	34.96	200	8.85	34.96	27.13
303	8.66	34.975	300	8.65	34.98	27.17
371	8.48	34.95	400	8.00	34.93	27.24
561	5.14	34.82	600	4.95	34.82	27.56
755	4.47	34.915	800	4.45	34.93	27.70
958	4.43	34.97	1,000	4.40	34.96	27.73
1,493	3.49	34.88				

Station 6391; 13 April; 44°31′ N., 46°30′ W.; depth 3,841 m.; dynamic height 971.036.

Observed values			Scaled values			
Depth, meters	Temperature, °C.	Salinity, °/oo	Depth, meters	Temperature, °C.	Salinity, °/oo	σ_t
0	8.64	34.86	0	8.64	34.86	27.08
26	8.44	34.83	25	8.45	34.83	27.09
52	7.94	34.73	50	8.00	34.76	27.11
78	7.44	34.67	75	7.45	34.67	27.12
104	7.53	34.685	100	7.55	34.685	27.11
155	5.86	34.455	150	5.45	34.47	27.16
208	5.96	34.60	200	5.95	34.57	27.24
312	5.92	34.78	300	5.90	34.77	27.41
402	4.89	34.78	400	4.90	34.78	27.53
609	4.30	34.89	600	4.30	34.89	27.68
818	4.20	34.94	800	4.20	34.94	27.74
1,023	3.91	34.92	1,000	3.95	34.92	27.75
1,535	3.46	34.895				

Station 6392; 13 April; 44°26.5′ N., 45°52′ W.; depth 4,024 m.; dynamic height 971.041.

Observed values			Scaled values			
Depth, meters	Temperature, °C.	Salinity, °/oo	Depth, meters	Temperature, °C.	Salinity, °/oo	σ_t
0	13.01	35.71	0	13.01	35.71	26.96
25	12.93	35.69	25	12.93	35.69	26.96
50	10.38	35.115	50	10.38	35.115	27.00
75	8.37	34.79	75	8.37	34.79	27.07
100	8.13	34.80	100	8.13	34.80	27.11
150	5.47	34.385	150	5.47	34.385	27.16
201	5.14	34.485	200	5.15	34.48	27.26
301	5.13	34.68	300	5.15	34.68	27.42
458	5.46	34.97	400	5.35	34.87	27.55
688	4.43	34.94	600	4.85	34.95	27.67
919	4.01	34.93	800	4.20	34.94	27.74
1,147	3.45	34.86	1,000	3.80	34.91	27.76
1,715	3.40	34.89				

Station 6393; 13 April; 44°21.5′ N., 45°04′ W.; depth 4,253 m.; dynamic height 971.253.

Observed values			Scaled values			
Depth, meters	Temperature, °C.	Salinity, °/oo	Depth, meters	Temperature, °C.	Salinity, °/oo	σ_t
0	14.43	35.90	0	14.43	35.90	26.81
27	14.53	35.90	25	14.50	35.90	26.79
53	14.52	35.895	50	14.50	35.90	26.79
81	14.50	35.89	75	14.50	35.89	26.78
107	13.74	35.71	100	13.95	35.76	26.79
161	12.99	35.61	150	13.15	35.63	26.86
205	10.18	35.02	200	10.45	35.08	26.95
321	10.67	35.22	300	10.60	35.19	27.01
450	8.49	35.10	400	9.35	35.15	27.20
671	5.09	34.91	600	6.05	34.95	27.53
890	4.60	34.96	800	4.70	34.94	27.68
1,111	4.31	34.965	1,000	4.45	34.96	27.73
1,664	3.56	34.90				

Station 6394; 14 April; 44°51′ N., 44°57′ W.; depth 4,481 m.; dynamic height 971.154.

Observed values			Scaled values			
Depth, meters	Temperature, °C.	Salinity, °/oo	Depth, meters	Temperature, °C.	Salinity, °/oo	σ_t
0	10.99	--------	0	10.99	34.92	26.73
25	10.73	--------	25	10.73	34.89	26.76
51	10.35	34.885	50	10.35	34.85	26.79
76	10.33	34.85	75	10.30	34.85	26.80
101	10.01	34.89	100	10.00	34.89	26.88
151	9.84	34.835	150	9.85	34.83	26.86
202	8.69	34.69	200	8.75	34.69	26.93
303	7.66	34.85	300	7.70	34.85	27.22
324	5.58	34.665	400	5.50	34.77	27.46
490	5.39	34.90	600	5.00	34.94	27.65
660	4.77	34.95	800	4.50	34.95	27.71
839	4.39	34.945	1,000	4.10	34.92	27.74
1,310	3.53	34.88				

Station 6395; 14 April; 45°21.5′ N., 44°48′ W.; depth 4,481 m.; dynamic height 970.977.

Observed values			Scaled values			
Depth, meters	Temperature, °C.	Salinity, °/oo	Depth, meters	Temperature, °C.	Salinity, °/oo	σ_t
0	4.38	34.26	0	4.38	34.26	27.18
23	4.19	34.25	25	4.15	34.25	27.20
45	3.99	34.235	50	3.95	34.23	27.20
68	3.86	34.23	75	3.90	34.25	27.22
91	4.10	34.33	100	4.50	34.42	27.30
137	6.40	34.75	150	6.20	34.74	27.34
182	5.75	34.72	200	5.65	34.73	27.40
273	5.16	34.78	300	4.80	34.76	27.53
318	4.57	34.75	400	3.85	34.74	27.61
489	3.29	34.735	600	3.35	34.76	27.68
670	3.39	34.79	800	3.55	34.83	27.71
851	3.59	34.84	1,000	3.55	34.85	27.73
1,328	3.44	34.86				

Station 6396; 14 April; 45°23.5′ N., 45°33′ W.; depth 3,841 m.; dynamic height 970.890.

Observed values			Scaled values			
Depth, meters	Temperature, °C.	Salinity, °/oo	Depth, meters	Temperature, °C.	Salinity, °/oo	σ_t
0	3.86	34.35	0	3.86	34.35	27.31
25	------	34.38	25	3.75	34.38	27.33
50	3.55	34.38	50	3.55	34.38	27.35
75	3.14	34.415	75	3.14	34.415	27.42
100	3.01	34.45	100	3.01	34.45	27.47
150	3.07	34.50	150	3.07	34.50	27.50
200	3.21	34.63	200	3.21	34.63	27.59
300	3.31	34.74	300	3.31	34.74	27.67
397	3.48	34.79	400	3.50	34.79	27.69
583	3.62	34.845	600	3.60	34.85	27.73
760	3.53	34.86	800	3.50	34.86	27.75
955	3.42	34.86	1,000	3.40	34.86	27.76
1,449	3.33	34.87				

TABLE OF OCEANOGRAPHIC DATA—Continued

STATIONS OCCUPIED IN 1957—Continued

Observed values			Scaled values			
Depth, meters	Temperature, °C.	Salinity, °/₀₀	Depth, meters	Temperature, °C.	Salinity, °/₀₀	σt
Station 6397; 14 April; 45°27.5′ N., 46°14′ W.; depth 3,475 m.; dynamic height 970.935.						
0	3.62	34.22	0	3.62	34.22	27.23
27	3.59	34.215	25	3.60	34.22	27.23
54	3.47	34.215	50	3.50	34.22	27.24
82	3.07	34.22	75	3.15	34.22	27.27
109	2.93	34.25	100	2.95	34.24	27.30
162	3.43	34.38	150	3.25	34.34	27.35
217	3.95	34.62	200	3.75	34.55	27.47
326	4.71	34.87	300	4.65	34.83	27.60
399	4.46	34.915	400	4.45	34.91	27.69
601	4.12	34.91	600	4.10	34.91	27.73
805	3.67	34.87	800	3.70	34.87	27.74
1,010	3.46	34.86	1,000	3.45	34.86	27.75
1,529	3.43	34.88				
Station 6398; 14–15 April; 45°23′ N., 46°50′ W.; depth 3,200 m.; dynamic height 970.930.						
0	2.71	34.01	0	2.71	34.01	27.14
26	3.08	34.05	25	3.05	34.04	27.13
52	3.68	34.18	50	3.65	34.17	27.19
78	3.11	34.17	75	3.15	34.17	27.23
103	4.05	34.40	100	3.95	34.37	27.32
156	4.58	34.645	150	4.55	34.63	27.45
207	4.90	34.78	200	4.85	34.76	27.52
310	4.71	34.88	300	4.75	34.87	27.62
407	4.40	34.90	400	4.45	34.90	27.68
616	3.78	34.875	600	3.80	34.88	27.73
828	3.60	34.87	800	3.65	34.87	27.74
1,042	3.47	34.87	1,000	3.50	34.87	27.76
1,586	3.44	34.89				
Station 6399; 15 April; 45°20′ N., 47°24′ W.; depth 2,926 m.; dynamic height 970.947.						
0	3.24	34.085	0	3.24	34.085	27.15
26	3.22	34.08	25	3.20	34.08	27.15
53	3.18	34.185	50	3.20	34.08	27.15
79	2.96	34.09	75	3.00	34.09	27.18
105	3.47	34.08	100	3.35	34.17	27.21
157	2.60	34.21	150	2.65	34.20	27.30
210	3.97	34.59	200	3.75	34.53	27.45
315	4.14	34.85	300	4.30	34.83	27.64
420	4.43	34.92	400	4.45	34.91	27.69
629	3.90	34.89	600	4.00	34.89	27.72
840	3.65	34.88	800	3.70	34.88	27.74
1,050	3.51	34.87	1,000	3.55	34.87	27.75
1,575	3.45	34.89				
Station 6400; 15 April; 45°35′ N., 47°50′ W.; depth 1,737 m.; dynamic height 970.921.						
0	0.83	33.67	0	0.83	33.67	27.01
21	0.99	33.74	25	1.05	33.76	27.07
43	1.41	33.89	50	1.50	33.93	27.17
64	1.61	34.02	75	1.95	34.12	27.30
86	2.51	34.22	100	2.75	34.30	27.37
128	3.08	34.42	150	3.25	34.49	27.47
170	3.35	34.54	200	3.50	34.62	27.56
256	3.76	34.76	300	3.90	34.79	27.65
289	3.89	34.79	400	3.85	34.82	27.68
445	3.79	34.835	600	3.65	34.85	27.72
612	3.64	34.85	800	3.50	34.86	27.75
792	3.52	34.86	1,000	3.50	34.87	27.76
1,286	3.42	34.87				
Station 6401; 15 April; 45°45.5′ N., 48°10′ W.; depth 622 m.; dynamic height 971.008.						
0	−0.73	33.07	0	−0.73	33.07	26.60
26	−0.74	33.07	25	−0.75	33.07	26.60
51	−0.73	33.16	50	−0.75	33.15	26.66
77	0.06	33.66	75	−0.05	33.63	27.02
102	0.85	33.88	100	0.75	33.86	27.17
152	1.01	33.98	150	1.00	33.97	27.24
203	1.26	34.07	200	1.25	34.06	27.30
305	2.54	34.525	300	2.50	34.50	27.55
365	2.92	34.635	400	3.05	34.67	27.64
568	3.36	34.77	(600)	3.40	34.78	27.69
Station 6402; 15 April; 45°50.5′ N., 48°18′ W.; depth 169 m.; dynamic height 971.050.						
0	−0.68	33.185	0	−0.68	33.185	26.70
25	−0.74	33.19	25	−0.74	33.19	26.70
51	−0.83	33.235	50	−0.80	33.23	26.73
76	−0.41	33.51	75	−0.45	33.49	26.93
101	−0.12	33.61	100	−0.15	33.61	27.02
151	−0.08	33.62	150	−0.05	33.62	27.02
Station 6403; 15 April; 45°53′ N., 48°23′ W.; depth 114 m.; dynamic height 971.055.						
0	−0.65	33.015	0	−0.65	33.015	26.56
25	−0.69	33.09	25	−0.69	33.09	26.61
50	−0.83	33.38	50	−0.83	33.38	26.85
74	−0.68	33.44	75	−0.65	33.44	26.90
99	−0.56	33.47	100	−0.55	33.47	26.92
Station 6404; 15 April; 45°59′ N., 48°33′ W.; depth 89 m.; dynamic height 971.072.						
0	−0.67	32.995	0	−0.67	32.995	26.55
25	−0.72	33.00	25	−0.72	33.00	26.55
50	−0.80	33.015	50	−0.80	33.015	26.56
75	−0.33	-------	(75)	−0.33	33.15	26.64
Station 6405; 15 April; 46°06.5′ N., 48°45′ W.; depth 82 m.; dynamic height 971.074.						
0	−0.53	33.00	0	−0.53	33.00	26.54
26	−0.53	33.01	25	−0.55	33.01	26.55
53	−0.57	33.01	50	−0.55	33.01	26.55
74	−0.80	33.09	75	−0.80	33.09	26.61
Station 6406; 15 April; 46°18′ N., 49°04′ W.; depth 70 m.; dynamic height 971.074.						
0	−0.45	32.975	0	−0.45	32.975	26.52
26	−0.47	32.98	25	−0.45	32.98	26.52
52	−0.51	32.99	50	−0.50	32.99	26.53

STATIONS OCCUPIED IN 1957—Continued

Station 6407; 15 April; 46°16′ N., 48°34′ W.; depth 91 m.; dynamic height 971.070.

Observed values			Scaled values			
Depth, meters	Temperature, °C.	Salinity, °/oo	Depth, meters	Temperature, °C.	Salinity, °/oo	σ_t
0	−0.65	32.965	0	−0.65	32.965	26.52
27	−0.65	32.96	25	−0.65	32.96	26.51
53	−0.70	32.96	50	−0.70	32.96	26.51
80	−0.96	33.11	75	−0.90	33.08	26.61

Station 6408; 16 April; 46°14′ N., 48°03′ W.; depth 115 m.; dynamic height 971.058.

Observed values			Scaled values			
Depth, meters	Temperature, °C.	Salinity, °/oo	Depth, meters	Temperature, °C.	Salinity, °/oo	σ_t
0	−0.78	32.99	0	−0.78	32.99	26.54
25	−0.82	33.00	25	−0.82	33.00	26.55
50	−0.99	33.04	50	−0.99	33.04	26.58
75	−1.17	33.275	75	−1.17	33.275	26.78
100	−0.94	-------	(100)	−0.94	33.56	27.01

Station 6409; 16 April; 46°13′ N., 47°46′ W.; depth 169 m.; dynamic height 971.051.

Observed values			Scaled values			
Depth, meters	Temperature, °C.	Salinity, °/oo	Depth, meters	Temperature, °C.	Salinity, °/oo	σ_t
0	−0.80	33.10	0	−0.80	33.10	26.62
26	−0.77	33.11	25	−0.75	33.11	26.63
53	−1.02	33.26	50	−1.00	33.23	26.74
79	−0.87	33.42	75	−0.90	33.39	26.87
105	−0.46	33.53	100	−0.55	33.51	26.95
157	0.39	33.78	150	0.35	33.74	27.09

Station 6410; 16 April; 46°11.5′ N., 47°28′ W.; depth 677 m.; dynamic height 970.987.

Observed values			Scaled values			
Depth, meters	Temperature, °C.	Salinity, °/oo	Depth, meters	Temperature, °C.	Salinity, °/oo	σ_t
0	−0.50	33.33	0	−0.50	33.33	26.80
25	−0.51	33.36	25	−0.51	33.36	26.82
49	−0.47	33.41	50	−0.45	33.41	26.87
74	0.32	33.775	75	0.35	33.79	27.13
98	0.78	33.935	100	0.80	33.94	27.22
147	1.21	34.09	150	1.25	34.10	27.33
196	1.67	34.24	200	1.70	34.25	27.41
294	2.37	34.46	300	2.40	34.47	27.54
380	2.65	34.55	400	2.75	34.57	27.59
579	3.49	34.81	(600)	3.55	34.83	27.71

Station 6411; 16 April; 46°10.5′ N., 47°11′ W.; depth 1,463 m.; dynamic height 970.902.

Observed values			Scaled values			
Depth, meters	Temperature, °C.	Salinity, °/oo	Depth, meters	Temperature, °C.	Salinity, °/oo	σ_t
0	0.84	33.80	0	0.84	33.80	27.11
27	0.90	33.81	25	0.90	33.81	27.12
53	1.33	34.13	50	1.30	34.09	27.31
81	1.68	34.28	75	1.60	34.25	27.42
107	1.94	34.36	100	1.90	34.33	27.46
161	2.40	34.48	150	2.30	34.45	27.53
215	2.89	34.61	200	2.75	34.37	27.59
322	3.38	34.74	300	3.30	34.72	27.66
397	3.54	34.79	400	3.55	34.79	27.68
605	3.63	34.85	600	3.65	34.85	27.72
820	3.49	34.85	800	3.50	34.86	27.75
1,034	3.42	34.865	1,000	3.45	34.86	27.75
1,376	3.36	34.88				

Station 6412; 16 April; 46°08′ N., 46°36′ W.; depth 732 m.; dynamic height 970.894.

Observed values			Scaled values			
Depth, meters	Temperature, °C.	Salinity, °/oo	Depth, meters	Temperature, °C.	Salinity, °/oo	σ_t
0	2.11	34.14	0	2.11	34.14	27.29
25	2.09	34.16	25	2.09	34.16	27.31
50	2.10	34.22	50	2.10	34.22	27.36
75	2.15	34.305	75	2.15	34.305	27.42
100	2.18	34.33	100	2.18	34.33	27.44
150	2.68	34.48	150	2.68	34.48	27.51
200	3.14	34.63	200	3.14	34.63	27.59
300	3.48	34.755	300	3.48	34.755	27.66
402	3.73	34.835	400	3.75	34.83	27.69
604	3.67	34.86	600	3.70	34.86	27.73

Station 6413; 16 April; 46°05′ N., 46°00′ W.; depth 1,829 m.; dynamic height 970.888.

Observed values			Scaled values			
Depth, meters	Temperature, °C.	Salinity, °/oo	Depth, meters	Temperature, °C.	Salinity, °/oo	σ_t
0	2.31	34.165	0	2.31	34.165	27.30
25	2.31	34.195	25	2.31	34.195	27.33
50	2.38	34.21	50	2.38	34.21	27.33
76	2.41	34.34	75	2.40	34.34	27.43
101	2.54	34.365	100	2.55	34.36	27.44
151	2.68	34.53	150	2.70	34.53	27.55
202	2.91	34.60	200	2.90	34.60	27.60
303	3.90	34.82	300	3.90	34.82	27.68
400	3.87	34.85	400	3.88	34.85	27.70
600	3.64	34.86	600	3.64	34.86	27.73
800	3.48	34.86	800	3.49	34.86	27.75
1,000	3.44	34.86	1,000	3.44	34.86	27.75
1,499	3.38	34.87				

Station 6414; 16 April; 46°02′ N., 45°12′ W.; depth 3,383 m.; dynamic height 970.884.

Observed values			Scaled values			
Depth, meters	Temperature, °C.	Salinity, °/oo	Depth, meters	Temperature, °C.	Salinity, °/oo	σ_t
0	3.77	34.47	0	3.77	34.47	27.41
24	3.73	34.49	25	3.75	34.49	27.42
48	3.63	34.54	50	3.65	34.54	27.47
72	3.64	34.555	75	3.65	34.56	27.49
96	3.54	34.61	100	3.55	34.61	27.54
143	3.42	34.635	150	3.45	34.64	27.57
190	3.50	34.69	200	3.50	34.70	27.62
286	3.35	34.73	300	3.40	34.74	27.66
302	3.40	34.74	400	3.40	34.77	27.69
469	3.51	34.80	600	3.65	34.84	27.71
649	3.67	34.85	800	3.55	34.85	27.73
831	3.53	34.85	1,000	3.50	34.86	27.75
1,320	3.37	34.87				

Station 6415; 17 April; 46°01′ N., 44°38′ W.; depth 3,842 m.; dynamic height 970.989.

Observed values			Scaled values			
Depth, meters	Temperature, °C.	Salinity, °/oo	Depth, meters	Temperature, °C.	Salinity, °/oo	σ_t
0	7.05	34.625	0	7.05	34.625	27.14
18	7.28	34.62	25	7.30	34.62	27.10
36	7.24	34.62	50	7.05	34.60	27.12
54	6.91	34.58	75	6.40	34.53	27.15
71	6.47	34.535	100	6.00	34.52	27.20
107	5.91	34.515	150	6.15	34.64	27.27
143	6.19	34.62	200	5.85	34.73	27.37
214	5.72	34.745	300	4.65	34.75	27.54
323	4.39	34.75	400	4.05	34.77	27.62
497	3.84	34.81	600	4.00	34.86	27.70
680	4.09	34.89	800	3.90	34.88	27.72
873	3.80	34.88	1,000	3.75	34.88	27.73
1,395	3.56	34.89				

TABLE OF OCEANOGRAPHIC DATA—Continued

STATIONS OCCUPIED IN 1957—Continued

Station 6416; 17 April; 46°25′ N., 44°47′ W.; depth 1,554 m.; dynamic height 970.892.

Observed values			Scaled values			
Depth, meters	Temperature, °C.	Salinity, °/oo	Depth, meters	Temperature, °C.	Salinity, °/oo	σ_t
0	4.20	34.36	0	4.20	34.36	27.28
26	4.36	34.38	25	4.40	34.38	27.27
52	4.33	34.495	50	4.35	34.48	27.35
78	4.74	34.65	75	4.70	34.64	27.44
103	4.50	34.66	100	4.50	34.65	27.47
156	4.16	34.70	150	4.20	34.69	27.54
208	4.36	34.81	200	4.35	34.80	27.61
311	4.00	34.825	300	4.05	34.82	27.66
418	3.63	34.82	400	3.70	34.82	27.70
630	3.58	34.85	600	3.60	34.85	27.73
846	3.50	34.85	800	3.50	34.85	27.74
1,055	3.43	34.86	1,000	3.45	34.86	27.75
1,520	3.43	34.865				

Station 6417; 17 April; 46°30′ N., 44°48′ W.; depth 457 m.; dynamic height 970.874.

Observed values			Scaled values			
Depth, meters	Temperature, °C.	Salinity, °/oo	Depth, meters	Temperature, °C.	Salinity, °/oo	σ_t
0	4.50	34.585	0	4.50	34.585	27.42
27	4.54	34.595	25	4.55	34.59	27.42
54	4.86	34.67	50	4.85	34.67	27.46
81	4.48	34.67	75	4.60	34.67	27.48
108	3.83	34.645	100	4.00	34.65	27.53
163	3.64	34.70	150	3.70	34.68	27.58
216	3.55	34.73	200	3.55	34.72	27.63
324	3.68	34.80	300	3.65	34.78	27.66
436	3.59	34.84	400	3.65	34.83	27.70

Station 6418; 17 April; 46°36′ N., 44°50′ W.; depth 220 m.; dynamic height 970.877.

Observed values			Scaled values			
Depth, meters	Temperature, °C.	Salinity, °/oo	Depth, meters	Temperature, °C.	Salinity, °/oo	σ_t
0	2.98	34.42	0	2.98	34.42	27.43
26	2.98	34.42	25	3.00	34.42	27.45
52	3.00	34.43	50	3.00	34.43	27.45
78	2.96	34.45	75	2.95	34.44	27.46
104	2.91	34.505	100	2.90	34.49	27.51
156	3.03	34.57	150	3.00	34.56	27.56
208	3.29	34.67	200	3.25	34.65	27.60

Station 6419; 17 April; 46°41.5′ N., 44°53′ W.; depth 169 m.; dynamic height 970.877.

Observed values			Scaled values			
Depth, meters	Temperature, °C.	Salinity, °/oo	Depth, meters	Temperature, °C.	Salinity, °/oo	σ_t
0	3.00	34.42	0	3.00	34.42	27.45
27	2.99	34.405	25	3.00	34.42	27.44
53	3.00	34.42	50	3.00	34.42	27.45
80	2.98	34.435	75	3.00	34.43	27.45
107	2.91	34.47	100	2.90	34.46	27.49
159	3.03	34.605	150	3.00	34.58	27.57

Station 6420; 17 April; 46°50.5′ N., 44°56′ W.; depth 146 m.; dynamic height 970.883.

Observed values			Scaled values			
Depth, meters	Temperature, °C.	Salinity, °/oo	Depth, meters	Temperature, °C.	Salinity, °/oo	σ_t
0	2.98	34.38	0	2.98	34.38	27.41
25	2.97	34.37	25	2.97	34.37	27.41
49	2.95	34.375	50	2.95	34.38	27.41
74	2.94	34.39	75	2.95	34.39	27.42
99	2.80	34.435	100	2.80	34.44	27.47
133	2.89	34.485				

Station 6421; 17 April; 46°50.5′ N., 45°02′ W.; depth 169 m.; dynamic height 970.883.

Observed values			Scaled values			
Depth, meters	Temperature, °C.	Salinity, °/oo	Depth, meters	Temperature, °C.	Salinity, °/oo	σ_t
0	3.02	34.37	0	3.02	34.37	27.40
25	3.03	34.385	25	3.03	34.385	27.41
49	2.98	34.39	50	3.00	34.39	27.42
74	2.86	34.42	75	2.85	34.42	27.46
99	2.81	34.43	100	2.80	34.43	27.46
			(150)	3.00	34.50	27.51

Station 6422; 17 April; 46°49.5′ N., 45°18′ W.; depth 220 m.; dynamic height 970.881.

Observed values			Scaled values			
Depth, meters	Temperature, °C.	Salinity, °/oo	Depth, meters	Temperature, °C.	Salinity, °/oo	σ_t
0	3.01	34.37	0	3.01	34.37	27.40
25	2.98	34.38	25	2.98	34.38	27.41
49	2.98	34.38	50	3.00	34.38	27.41
74	2.94	34.39	75	2.95	34.39	27.42
98	2.82	34.435	100	2.85	34.44	27.47
147	2.99	34.58	150	3.00	34.58	27.57
196	3.28	34.67	200	3.30	34.67	27.62

Station 6423; 17 April; 46°48.5′ N., 45°44′ W.; depth 258 m.; dynamic height 970.890.

Observed values			Scaled values			
Depth, meters	Temperature, °C.	Salinity, °/oo	Depth, meters	Temperature, °C.	Salinity, °/oo	σ_t
0	2.83	34.35	0	2.83	34.35	27.40
24	2.82	34.34	25	2.80	34.34	27.40
48	2.78	34.35	50	2.80	34.35	27.41
72	2.80	34.355	75	2.80	34.36	27.42
96	2.81	34.365	100	2.80	34.37	27.43
143	2.82	34.40	150	2.85	34.42	27.46
191	3.18	34.58	200	3.25	34.61	27.57
239	3.64	34.74				

Station 6424; 17 April; 46°48.5′ N., 46°08′ W.; depth 320 m.; dynamic height 970.882.

Observed values			Scaled values			
Depth, meters	Temperature, °C.	Salinity, °/oo	Depth, meters	Temperature, °C.	Salinity, °/oo	σ_t
0	2.86	34.33	0	2.86	34.33	27.38
25	2.76	34.34	25	2.76	34.34	27.40
50	2.83	34.36	50	2.83	34.36	27.41
74	2.84	34.375	75	2.85	34.38	27.42
99	2.82	34.40	100	2.80	34.40	27.44
148	3.19	34.57	150	3.20	34.58	27.55
198	3.44	34.70	200	3.45	34.70	27.62
297	3.58	34.84	300	3.60	34.84	27.72

Station 6425; 17 April; 46°48.5′ N., 46°36′ W.; depth 677 m.; dynamic height 970.905.

Observed values			Scaled values			
Depth, meters	Temperature, °C.	Salinity, °/oo	Depth, meters	Temperature, °C.	Salinity, °/oo	σ_t
0	1.42	33.99	0	1.42	33.99	27.22
25	1.38	33.985	25	1.38	33.985	27.22
49	1.29	33.985	50	1.30	33.99	27.23
74	1.50	34.16	75	1.50	34.17	27.37
98	1.80	34.30	100	1.85	34.32	27.46
146	2.37	34.47	150	2.40	34.48	27.54
196	2.74	34.565	200	2.75	34.57	27.59
294	3.24	34.725	300	3.25	34.73	27.66
397	3.44	34.79	400	3.45	34.79	27.69
610	3.54	34.845	600	3.55	34.83	27.71

TABLE OF OCEANOGRAPHIC DATA—Continued

STATIONS OCCUPIED IN 1957—Continued

Station 6426; 17 April; 46°48.5′ N., 46°57′ W.; depth 1,243 m.; dynamic height 970.885.

Observed values			Scaled values			
Depth, meters	Temperature, °C.	Salinity, °/oo	Depth, meters	Temperature, °C.	Salinity, °/oo	σ_t
0	1.70	34.13	0	1.70	34.13	27.31
23	1.74	34.145	25	1.75	34.15	27.33
46	1.64	34.15	50	1.65	34.15	27.34
69	1.69	34.18	75	1.70	34.19	27.36
92	1.73	34.30	100	1.85	34.34	27.47
138	2.85	34.59	150	2.95	34.61	27.60
184	3.06	34.65	200	3.10	34.67	27.64
276	3.20	34.72	300	3.20	34.74	27.68
305	3.21	34.75	400	3.20	34.75	27.69
476	3.11	34.75	600	3.50	34.82	27.72
661	3.66	34.85	800	3.55	34.86	27.74
859	3.50	34.86	1,000	3.45	34.86	27.75
994	3.44	34.86				

Station 6427; 17 April; 46°48.5′ N., 47°15′ W.; depth 622 m.; dynamic height 970.986.

Observed values			Scaled values			
Depth, meters	Temperature, °C.	Salinity, °/oo	Depth, meters	Temperature, °C.	Salinity, °/oo	σ_t
0	−0.86	33.15	0	−0.86	33.15	26.66
22	−0.80	33.27	25	−0.80	33.28	26.76
44	−0.81	33.33	50	−0.75	33.38	26.85
66	−0.53	33.53	75	−0.40	33.59	27.01
87	−0.15	33.655	100	0.10	33.75	27.11
131	0.86	33.98	150	1.05	34.04	27.29
175	1.29	34.12	200	1.60	34.21	27.39
262	2.43	34.48	300	2.65	34.55	27.58
280	2.50	34.52	400	3.05	34.67	27.64
454	3.14	34.72	(600)	3.25	34.81	27.73

Station 6428; 18 April; 46°48′ N., 47°23′ W.; depth 312 m.; dynamic height 971.039.

Observed values			Scaled values			
Depth, meters	Temperature, °C.	Salinity, °/oo	Depth, meters	Temperature, °C.	Salinity, °/oo	σ_t
0	−1.03	33.10	0	−1.03	33.10	26.63
24	−1.10	33.12	25	−1.10	33.12	26.65
47	−1.19	33.24	50	−1.20	33.25	26.76
71	−1.12	33.36	75	−1.05	33.37	26.85
95	−0.78	33.46	100	−0.65	33.49	26.94
142	0.50	33.81	150	0.65	33.85	27.16
189	1.16	34.00	200	1.25	34.02	27.27
284	1.56	34.145	(300)	1.60	34.16	27.35

Station 6429; 18 April; 46°48′ N., 47°37′ W.; depth 169 m.; dynamic height 971.035.

Observed values			Scaled values			
Depth, meters	Temperature, °C.	Salinity, °/oo	Depth, meters	Temperature, °C.	Salinity, °/oo	σ_t
0	−0.80	33.21	0	−0.80	33.21	26.72
23	−0.82	33.22	25	−0.85	33.22	26.72
47	−1.05	33.27	50	−1.05	33.29	26.78
69	−0.91	33.39	75	−0.85	33.42	26.89
93	−0.57	33.52	100	−0.45	33.56	26.99
140	------	-------	(150)	0.45	33.84	27.16

Station 6430; 18 April; 46°48.5′ N., 48°10′ W.; depth 117 m.; dynamic height 971.060.

Observed values			Scaled values			
Depth, meters	Temperature, °C.	Salinity, °/oo	Depth, meters	Temperature, °C.	Salinity, °/oo	σ_t
0	−0.74	33.005	0	−0.74	33.005	26.55
25	−0.75	33.01	25	−0.75	33.01	26.56
49	−0.95	33.035	50	−0.95	33.04	26.58
73	−1.10	33.18	75	−1.10	33.19	26.71
97	−1.04	33.30	100	−1.05	33.32	26.81

Station 6431; 18 April; 46°48.5′ N., 48°50′ W.; depth 89 m.; dynamic height 971.076.

Observed values			Scaled values			
Depth, meters	Temperature, °C.	Salinity, °/oo	Depth, meters	Temperature, °C.	Salinity, °/oo	σ_t
0	−0.73	32.91	0	−0.73	32.91	26.47
27	−0.73	32.915	25	−0.75	32.91	26.47
54	−0.75	32.92	50	−0.75	32.92	26.48
82	−0.77	32.92	75	−0.75	32.92	26.48

Station 6432; 1 May; 42°02.5′ N., 50°58′ W.; depth 3,292 m.; dynamic height 971.120.

Observed values			Scaled values			
Depth, meters	Temperature, °C.	Salinity, °/oo	Depth, meters	Temperature, °C.	Salinity, °/oo	σ_t
0	14.68	36.09	0	14.68	36.09	26.90
24	10.10	-------	25	10.10	34.95	26.92
49	10.52	-------	50	10.60	35.05	26.90
73	12.00	35.40	75	12.00	35.40	26.92
97	11.92	-------	100	11.95	35.39	26.92
146	12.39	-------	150	12.35	35.54	26.96
195	11.56	35.43	200	11.40	35.42	27.05
292	8.55	35.155	300	8.40	35.14	27.34
340	7.78	35.05	400	6.80	34.99	27.46
510	5.23	34.92	600	4.85	34.93	27.65
679	4.72	34.95	800	4.30	34.93	27.71
854	4.17	34.915	1,000	4.05	34.91	27.73
1,300	3.74	34.91				

Station 6433; 1 May; 41°59′ N., 52°00′ W.; depth 4,024 m.; dynamic height 971.010.

Observed values			Scaled values			
Depth, meters	Temperature, °C.	Salinity, °/oo	Depth, meters	Temperature, °C.	Salinity, °/oo	σ_t
0	1.68	33.34	0	1.68	33.34	26.69
25	−0.04	33.38	25	−0.04	33.38	26.75
49	0.07	33.34	50	0.10	33.35	26.79
73	0.85	33.62	75	0.85	33.65	26.99
97	1.79	33.95	100	1.80	33.96	27.17
147	1.52	34.13	150	1.50	34.14	27.34
196	1.74	34.24	200	1.75	34.25	27.41
293	2.69	34.49	300	2.75	34.50	27.53
387	2.96	34.59	400	3.05	34.60	27.58
602	4.63	34.945	600	4.65	34.94	27.69
833	4.39	34.965	800	4.45	34.97	27.74
1,044	4.03	34.93	1,000	4.10	34.94	27.75
1,576	3.68	34.92				

Station 6434; 1 May; 42°21′ N., 51°36′ W.; depth 3,338 m.; dynamic height 970.975.

Observed values			Scaled values			
Depth, meters	Temperature, °C.	Salinity, °/oo	Depth, meters	Temperature, °C.	Salinity, °/oo	σ_t
0	0.68	33.28	0	0.68	33.28	26.70
24	0.63	33.39	25	0.60	33.39	26.79
48	0.07	33.50	50	0.10	33.51	26.92
72	1.25	33.88	75	1.25	33.90	27.16
96	1.23	34.00	100	1.25	34.02	27.27
143	1.68	34.19	150	1.70	34.21	27.38
191	2.07	34.33	200	2.15	34.35	27.46
287	2.90	34.58	300	2.95	34.60	27.59
363	3.16	34.675	400	3.30	34.71	27.65
550	3.86	34.845	600	3.85	34.85	27.70
742	3.69	34.845	800	3.70	34.85	27.72
937	3.72	34.865	1,000	3.70	34.87	27.74
1,439	3.64	34.89				

TABLE OF OCEANOGRAPHIC DATA—Continued
STATIONS OCCUPIED IN 1957—Continued

Observed values			Scaled values			
Depth, meters	Temperature, °C.	Salinity, °/oo	Depth, meters	Temperature, °C.	Salinity, °/oo	σt
Station 6435; 1 May; 42°42′ N., 51°07′ W.; depth 2,286 m.; dynamic height 971.092.						
0	0.90	33.28	0	0.90	33.28	26.69
24	−0.53	33.36	25	−0.55	33.36	26.82
47	−0.42	33.46	50	−0.40	33.46	26.91
71	−0.26	33.50	75	−0.25	33.51	26.94
95	−0.17	33.56	100	−0.15	33.57	26.99
142	0.29	33.72	150	0.40	33.76	27.11
189	0.76	33.89	200	0.85	33.93	27.21
284	1.49	34.15	300	1.55	34.17	27.36
372	*1.72	34.215	400	1.95	34.27	27.42
560	3.27	34.66	600	3.50	34.70	27.62
748	3.81	34.81	800	3.80	34.83	27.69
941	3.82	34.845	1,000	3.80	34.85	27.71
1,436	3.61	34.86				
Station 6436; 1 May; 42°52′ N., 50°54′ W.; depth 1,005 m.; dynamic height 971.135.						
0	0.18	33.20	0	0.18	33.20	26.67
23	0.05	33.21	25	0.00	33.21	26.69
46	−0.43	33.26	50	−0.45	33.28	26.76
69	−0.48	33.38	75	−0.43	33.40	26.86
92	−0.36	33.48	100	−0.30	33.50	26.93
138	−0.04	33.61	150	0.00	33.63	27.02
185	0.16	33.69	200	0.20	33.71	27.08
277	0.61	33.83	300	0.75	33.88	27.18
388	1.45	34.14	400	1.55	34.17	27.36
601	3.49	34.72	600	3.50	34.72	27.64
782	3.66	34.82	800	3.65	34.82	27.70
956	3.63	34.84	1,000	3.65	34.84	27.71
Station 6437; 1 May; 42°55′ N., 50°50′ W.; depth 403 m.; dynamic height 971.101.						
0	0.38	33.22	0	0.38	33.22	26.67
24	0.07	33.23	25	0.05	33.23	26.70
47	−0.10	33.24	50	−0.15	33.24	26.72
71	−0.43	33.26	75	−0.45	33.27	26.75
94	−0.48	33.33	100	−0.45	33.35	26.81
142	−0.17	33.49	150	−0.15	33.51	26.94
187	0.03	33.62	200	0.15	33.67	27.05
283	1.07	33.99	300	1.35	34.07	27.30
374	2.69	34.475	400	3.10	34.63	27.60
Station 6438; 1 May; 42°58.5′ N., 50°46′ W.; depth 146 m.; dynamic height 971.097.						
0	0.44	33.11	0	0.44	33.11	26.58
15	0.32	33.12	25	0.25	33.14	26.62
40	0.12	33.17	50	−0.05	33.19	26.67
65	−0.35	33.22	75	−0.35	33.23	26.71
90	−0.35	33.25	100	−0.35	33.27	26.74
130	−0.37	33.36				
Station 6439; 1–2 May 1957; 43°05′ N., 50°37′ W.; depth 89 m.; dynamic height 971.103.						
0	1.08	33.03	0	1.08	33.03	26.48
26	0.93	33.035	25	0.95	33.03	26.49
52	0.45	33.08	50	0.50	33.07	26.54
78	−0.29	33.29	75	−0.25	33.25	26.73

Observed values			Scaled values			
Depth, meters	Temperature, °C.	Salinity, °/oo	Depth, meters	Temperature, °C.	Salinity, °/oo	σt
Station 6440; 2 May; 43°15′ N., 50°23′ W.; depth 71 m.; dynamic height 971.120.						
0	1.57	32.755	0	1.57	32.755	26.22
25	1.47	32.765	25	1.47	32.765	26.24
50	0.58	32.92	50	0.58	32.92	26.42
Station 6441; 2 May; 42°57′ N., 50°25′ W.; depth 89 m.; dynamic height 971.102.						
0	0.49	33.105	0	0.49	33.105	26.56
26	0.46	33.11	25	0.45	33.11	26.58
51	0.35	33.11	50	0.35	33.11	26.58
77	−0.13	33.17	75	−0.10	33.17	26.65
Station 6442; 2 May; 42°45′ N., 50°27′ W.; depth 329 m.; dynamic height 971.076.						
0	−0.25	33.20	0	−0.25	33.20	26.69
15	−0.31	33.20	25	−0.45	33.21	26.71
31	−0.48	33.22	50	−0.65	33.23	26.73
47	−0.66	33.22	75	−0.65	33.26	26.75
63	−0.65	33.25	100	−0.60	33.31	26.78
94	−0.60	33.30	150	−0.55	33.60	27.02
125	−0.61	33.37	(200)	−0.25	34.22	27.51
188	−0.32	34.10	(300)	0.90	34.66	27.80
Station 6443; 2 May; 42°30.5′ N., 50°30′ W.; depth 1,280 m.; dynamic height 971.057.						
0	−0.17	33.22	0	−0.17	33.22	26.70
27	−0.16	33.255	25	−0.15	33.22	26.70
52	0.08	33.275	50	0.05	33.26	26.72
79	2.77	33.78	75	2.50	33.75	26.95
104	1.71	33.815	100	1.90	33.81	27.05
158	1.00	33.93	150	1.05	33.91	27.19
210	1.57	34.03	200	1.45	34.01	27.24
314	2.03	34.36	300	2.00	34.32	27.45
325	2.24	34.42	400	2.60	34.57	27.60
489	3.17	34.69	600	3.30	34.73	27.66
654	3.32	34.74	800	3.40	34.75	27.67
863	3.41	34.75	1,000	3.50	34.76	27.67
1,092	3.57	34.775				
Station 6444; 2 May; 42°10.5′ N., 50°33′ W.; depth 2,743 m.; dynamic height 971.024.						
0	1.87	33.705	0	1.87	33.705	26.96
27	1.50	33.70	25	1.50	33.70	26.99
53	1.52	33.705	50	1.50	33.70	26.99
80	1.01	33.695	75	1.10	33.70	27.01
106	0.96	33.73	100	0.95	33.72	27.04
160	1.75	34.01	150	1.55	33.96	27.19
213	2.62	34.12	200	2.45	34.09	27.22
319	3.31	34.48	300	3.25	34.41	27.41
418	3.33	34.75	400	3.35	34.71	27.64
627	3.45	34.79	600	3.45	34.79	27.69
837	3.59	34.84	800	3.60	34.83	27.71
1,048	3.57	34.85	1,000	3.55	34.85	27.73
1,576	3.47	34.87				

STATIONS OCCUPIED IN 1957—Continued

Station 6445; 2 May; 41°40.5′ N., 50°25′ W.; depth 3,749 m.; dynamic height 971.125.

Observed values			Scaled values			
Depth, meters	Temperature, °C.	Salinity, °/oo	Depth, meters	Temperature, °C.	Salinity, °/oo	σ_t
0	11.70	35.27	0	11.70	35.27	26.88
25	11.81	35.28	25	11.81	35.28	26.86
50	11.95	35.32	50	11.95	35.32	26.87
75	12.13	35.375	75	12.13	35.375	26.88
100	12.08	35.38	100	12.08	35.38	26.88
148	12.32	35.41	150	12.30	35.41	26.87
198	12.12	35.49	200	12.10	35.49	26.97
298	8.54	35.10	300	8.50	35.10	27.29
327	7.67	35.065	400	5.55	34.89	27.54
493	3.76	34.70	600	3.55	34.74	27.64
661	3.52	34.765	800	3.70	34.82	27.70
837	3.73	34.83	1,000	3.65	34.85	27.72
1,299	3.55	34.855				

Station 6446; 2 May; 41°19′ N., 50°20′ W.; depth 3,475 m.; dynamic height 971.245.

Observed values			Scaled values			
Depth, meters	Temperature, °C.	Salinity, °/oo	Depth, meters	Temperature, °C.	Salinity, °/oo	σ_t
0	------	-------	0	15.35	36.02	26.70
21	15.35	36.02	25	15.35	36.02	26.70
40	15.34	36.02	50	15.35	36.02	26.70
61	15.35	36.02	75	15.35	36.02	26.70
81	15.36	36.015	100	15.30	36.00	26.69
122	15.16	35.98	150	15.10	35.97	26.72
162	15.11	35.97	200	14.00	35.84	26.85
243	12.67	35.64	300	10.95	35.33	27.06
265	12.18	35.41	400	8.25	35.13	27.35
422	7.83	35.085	600	5.55	34.92	27.57
595	5.59	34.92	800	3.75	34.79	27.66
761	3.79	34.79	1,000	3.65	34.82	27.70
1,202	3.52	34.845				

Station 6447; 3 May; 41°00′ N., 50°14′ W.; depth 4,024 m.; dynamic height 971.232.

Observed values			Scaled values			
Depth, meters	Temperature, °C.	Salinity, °/oo	Depth, meters	Temperature, °C.	Salinity, °/oo	σ_t
0	13.55	35.705	0	13.55	35.705	26.84
21	13.55	35.71	25	13.55	35.71	26.85
43	13.52	35.70	50	13.50	35.70	26.85
64	13.47	35.69	75	13.45	35.69	26.85
85	13.43	35.69	100	13.45	35.70	26.86
128	13.49	35.695	150	13.40	35.68	26.85
171	13.24	35.65	200	12.20	35.43	26.90
256	10.11	35.07	300	9.20	34.97	27.08
342	8.69	34.935	400	8.00	34.94	27.25
518	6.87	34.96	600	6.10	34.97	27.54
696	5.29	34.98	800	4.90	34.97	27.69
893	4.66	34.965	1,000	4.50	34.96	27.72
1,425	3.84	34.925				

Station 6448; 3 May; 42°04′ N., 49°19′ W.; depth 3,200 m.; dynamic height 971.059.

Observed values			Scaled values			
Depth, meters	Temperature, °C.	Salinity, °/oo	Depth, meters	Temperature, °C.	Salinity, °/oo	σ_t
0	11.29	35.17	0	11.29	35.17	26.88
26	11.33	35.20	25	11.30	35.20	26.90
52	11.34	35.21	50	11.30	35.21	26.91
78	11.47	35.23	75	11.45	35.22	26.89
103	12.06	35.46	100	12.00	35.45	26.96
156	9.58	35.14	150	9.80	35.17	27.14
207	8.62	35.14	200	8.75	35.14	27.29
310	6.07	34.86	300	6.30	34.87	27.44
405	5.53	34.90	400	5.55	34.90	27.55
612	3.87	34.84	600	3.95	34.84	27.68
824	3.73	34.845	800	3.75	34.84	27.70
1,034	3.63	34.86	1,000	3.65	34.86	27.73
1,565	3.53	34.86				

Station 6449; 3 May; 41°34′ N., 48°49′ W.; depth 3,338 m.; dynamic height 971.077.

Observed values			Scaled values			
Depth, meters	Temperature, °C.	Salinity, °/oo	Depth, meters	Temperature, °C.	Salinity, °/oo	σ_t
0	6.50	34.21	0	6.50	34.21	26.89
27	6.30	34.21	25	6.30	34.21	26.91
52	5.89	34.14	50	5.90	34.15	26.91
79	7.39	34.47	75	7.10	34.41	26.96
105	9.54	34.99	100	9.45	34.95	27.02
158	6.66	34.57	150	7.00	34.63	27.14
210	8.36	34.95	200	8.10	34.89	27.19
315	7.58	35.04	300	7.70	35.03	27.36
382	6.66	35.00	400	6.45	35.00	27.51
597	4.95	34.98	600	4.95	34.98	27.68
831	4.52	34.98	800	4.60	34.98	27.72
1,044	4.11	34.95	1,000	4.20	34.96	27.76
1,575	3.69	34.91				

Station 6450; 3 May; 41°00′ N., 48°30′ W.; depth 3,200 m.; dynamic height 971.110.

Observed values			Scaled values			
Depth, meters	Temperature, °C.	Salinity, °/oo	Depth, meters	Temperature, °C.	Salinity, °/oo	σ_t
0	10.77	35.12	0	10.77	35.12	26.94
24	10.79	34.96	25	10.75	35.12	26.94
48	10.38	35.035	50	10.35	35.03	26.93
72	10.21	34.995	75	10.15	34.99	26.93
96	9.94	34.94	100	9.95	34.96	26.95
145	10.23	35.05	150	10.15	35.03	26.96
193	7.43	34.69	200	7.35	34.69	27.14
289	*7.02	34.79	300	6.55	34.74	27.29
346	3.24	34.425	400	3.85	34.58	27.48
529	5.22	34.925	600	4.95	34.94	27.65
720	4.57	34.95	800	4.55	34.95	27.71
910	4.54	34.94	1,000	4.45	34.94	27.71
1,400	3.84	34.91				

Station 6451; 4 May; 40°56.5′ N., 47°41′ W.; depth 3,438 m.; dynamic height 971.101.

Observed values			Scaled values			
Depth, meters	Temperature, °C.	Salinity, °/oo	Depth, meters	Temperature, °C.	Salinity, °/oo	σ_t
0	12.52	35.47	0	12.52	35.47	26.88
27	12.20	35.41	25	12.20	35.41	26.89
52	11.94	35.36	50	11.95	35.36	26.90
79	11.81	35.33	75	11.80	35.33	26.90
104	11.59	35.32	100	11.65	35.32	26.92
157	11.06	35.34	150	11.15	35.34	27.03
210	9.65	35.18	200	9.90	35.21	27.15
314	7.58	35.01	300	7.90	35.04	27.34
356	4.84	34.65	400	4.85	34.71	27.49
547	4.87	34.935	600	4.80	34.94	27.67
748	4.46	34.94	800	4.40	34.94	27.71
945	4.25	-------	1,000	4.20	34.92	27.73
1,452	3.50	34.885				

Station 6452; 4 May; 41°38′ N., 47°16′ W.; depth 4,115 m.; dynamic height 971.200.

Observed values			Scaled values			
Depth, meters	Temperature, °C.	Salinity, °/oo	Depth, meters	Temperature, °C.	Salinity, °/oo	σ_t
0	14.73	35.91	0	14.73	35.91	26.76
25	14.71	35.90	25	14.71	35.90	26.75
51	14.31	35.83	50	14.30	35.83	26.78
77	14.05	35.77	75	14.05	35.77	26.79
102	13.85	35.74	100	13.85	35.74	26.81
153	12.66	35.50	150	12.70	35.51	26.87
204	11.54	35.32	200	11.65	35.34	26.94
306	6.92	34.59	300	7.05	34.61	27.13
358	6.89	34.70	400	6.55	34.76	27.31
535	5.37	34.89	600	5.25	34.94	27.62
713	5.11	34.99	800	4.70	34.96	27.70
897	4.38	34.93	1,000	4.25	34.92	27.72
1,367	3.82	34.91				

TABLE OF OCEANOGRAPHIC DATA—Continued
STATIONS OCCUPIED IN 1957—Continued

Station 6453; 4 May; 42°04.5′ N., 47°45′ W.; depth 3,749 m.; dynamic height 970.984.

Observed values			Scaled values			
Depth, meters	Temperature, °C.	Salinity, °/oo	Depth, meters	Temperature, °C.	Salinity, °/oo	σ_t
0	3.81	33.36	0	3.81	33.36	26.52
25	3.77	33.70	25	3.77	33.70	26.80
50	3.35	34.02	50	3.35	34.02	27.09
75	2.57	34.06	75	2.57	34.06	27.20
100	3.03	34.20	100	3.03	34.20	27.26
150	5.84	34.73	150	5.84	34.73	27.37
200	5.93	34.86	200	5.93	34.86	27.48
300	5.60	34.85	300	5.60	34.85	27.50
413	5.23	34.98	400	5.25	34.97	27.65
620	4.59	34.98	600	4.65	34.98	27.72
828	3.57	34.845	800	3.70	34.85	27.72
1,036	3.51	34.86	1,000	3.50	34.86	27.75
1,558	3.38	34.87				

Station 6454; 4 May; 42°25.5′ N., 48°35′ W.; depth 3,219 m.; dynamic height 971.043.

Observed values			Scaled values			
Depth, meters	Temperature, °C.	Salinity, °/oo	Depth, meters	Temperature, °C.	Salinity, °/oo	σ_t
0	10.10	34.86	0	10.10	34.86	26.85
26	10.18	34.95	25	10.15	34.95	26.90
52	10.20	34.98	50	10.20	34.97	26.92
78	10.26	35.02	75	10.25	35.01	26.94
104	9.58	35.03	100	9.70	35.03	27.04
155	8.61	34.99	150	8.70	35.00	27.18
208	7.09	34.84	200	7.30	34.85	27.28
312	5.86	34.86	300	5.95	34.85	27.46
414	5.47	34.92	400	5.50	34.91	27.57
622	5.01	35.01	600	5.05	35.01	27.70
832	4.26	34.94	800	4.35	34.95	27.73
1,040	3.98	34.92	1,000	4.00	34.92	27.75
1,561	3.52	34.90				

Station 6455; 4 May; 42°49′ N., 49°30′ W.; depth 2,103 m.; dynamic height 970.942.

Observed values			Scaled values			
Depth, meters	Temperature, °C.	Salinity, °/oo	Depth, meters	Temperature, °C.	Salinity, °/oo	σ_t
0	2.20	33.62	0	2.20	33.62	26.87
25	1.26	34.62	25	1.26	33.66	26.97
50	1.01	33.77	50	1.01	33.77	27.08
76	1.22	34.01	75	1.20	34.01	27.26
101	1.60	34.17	100	1.60	34.17	27.36
151	3.56	33.66	150	3.55	34.62	27.55
201	3.42	34.60	200	3.45	34.60	27.54
302	3.47	34.72	300	3.50	34.72	27.64
397	3.41	34.75	400	3.40	34.75	27.67
601	3.58	34.81	600	3.60	34.81	27.70
809	3.55	34.82	800	3.55	34.82	27.71
1,013	3.58	34.835	1,000	3.60	34.83	27.71
1,528	3.50	34.86				

Station 6456; 5 May; 43°21′ N., 48°48′ W.; depth 2,460 m.; dynamic height 970.938.

Observed values			Scaled values			
Depth, meters	Temperature, °C.	Salinity, °/oo	Depth, meters	Temperature, °C.	Salinity, °/oo	σ_t
0	1.86	33.50	0	1.86	33.50	26.81
26	1.97	33.54	25	1.95	33.54	26.83
52	2.08	33.97	50	2.05	33.93	27.13
78	2.88	34.20	75	2.80	34.18	27.27
104	2.96	34.38	100	2.95	34.36	27.40
155	4.42	34.66	150	4.30	34.65	27.50
208	3.62	34.63	200	3.70	34.63	27.54
312	4.69	34.90	300	4.60	34.87	27.64
411	4.33	34.88	400	4.35	34.89	27.68
617	4.09	34.905	600	4.10	34.90	27.72
823	3.56	34.85	800	3.60	34.85	27.73
1,030	3.67	34.89	1,000	3.65	34.89	27.75
1,552	3.41	34.87				

Station 6457; 5 May; 43°06.5′ N., 48°05′ W.; depth 3,347 m.; dynamic height 971.013.

Observed values			Scaled values			
Depth, meters	Temperature, °C.	Salinity, °/oo	Depth, meters	Temperature, °C.	Salinity, °/oo	σ_t
0	6.41	34.09	0	6.41	34.09	26.80
25	6.91	34.29	25	6.91	34.29	26.89
51	7.37	34.44	50	7.35	34.44	26.95
77	7.81	34.60	75	7.75	34.59	27.01
103	6.34	34.48	100	6.55	34.49	27.10
153	4.80	34.43	150	4.80	34.43	27.26
204	5.95	34.72	200	5.90	34.70	27.35
307	5.29	34.84	300	5.35	34.84	27.53
406	4.99	34.90	400	5.00	34.90	27.62
604	3.91	34.86	600	3.90	34.86	27.71
799	4.42	34.94	800	4.45	34.94	27.71
1,006	3.87	34.91	1,000	3.90	34.91	27.75
1,536	3.45	34.88				

Station 6458; 5 May; 42°51.5′ N., 47°26′ W.; depth 3,932 m.; dynamic height 971.042.

Observed values			Scaled values			
Depth, meters	Temperature, °C.	Salinity, °/oo	Depth, meters	Temperature, °C.	Salinity, °/oo	σ_t
0	8.61	34.78	0	8.61	34.78	27.03
25	8.50	34.78	25	8.50	34.78	27.04
50	8.83	34.89	50	8.83	34.89	27.08
75	8.81	34.90	75	8.81	34.90	27.09
100	8.71	34.90	100	8.71	34.90	27.11
150	8.41	34.88	150	8.41	34.88	27.13
199	6.71	34.69	200	6.65	34.69	27.24
299	5.60	34.75	300	5.60	34.75	27.42
393	5.37	34.87	400	5.35	34.87	27.55
593	4.41	34.905	600	4.40	34.90	27.68
796	3.88	34.88	800	3.90	34.88	27.72
996	3.77	34.89	1,000	3.75	34.89	27.74
1,500	3.49	34.875				

Station 6459; 5 May; 42°38′ N. ,46°51′ W.; depth 4,143 m.; dynamic height 971.217.

Observed values			Scaled values			
Depth, meters	Temperature, °C.	Salinity, °/oo	Depth, meters	Temperature, °C.	Salinity, °/oo	σ_t
0	15.64	36.00	0	15.64	36.00	26.61
27	14.84	35.92	25	14.90	35.92	26.72
53	14.28	35.83	50	14.30	35.84	26.79
80	13.93	35.76	75	14.00	35.77	26.80
106	13.65	35.70	100	13.70	35.71	26.82
160	12.23	35.42	150	12.50	35.47	26.88
214	10.48	35.08	200	10.90	35.17	26.95
320	8.00	34.82	300	8.55	34.86	27.10
361	5.38	34.44	400	5.45	34.53	27.27
526	5.59	34.89	600	5.30	34.92	27.60
681	4.91	34.935	800	4.70	34.94	23.68
853	4.63	34.95	1,000	4.40	34.93	27.70
1,286	3.89	34.91				

Station 6460; 5 May; 42°25′ N., 46°08′ W.; depth 4,663 m.; dynamic height 971.590.

Observed values			Scaled values			
Depth, meters	Temperature, °C.	Salinity, °/oo	Depth, meters	Temperature, °C.	Salinity, °/oo	σ_t
0	15.16	36.035	0	15.16	36.035	26.76
25	14.98	36.03	25	14.98	36.03	26.78
50	14.97	36.06	50	14.97	36.06	26.82
75	14.90	36.06	75	14.89	36.06	26.83
100	14.89	36.06	100	14.89	36.06	26.83
149	14.92	36.065	150	14.90	36.06	26.83
199	14.88	36.065	200	14.85	36.06	26.85
299	*14.82	36.07	300	14.80	36.07	26.87
429	*14.82	36.07	400	14.80	36.07	26.87
641	13.06	35.69	600	13.70	35.82	26.90
853	8.41	35.125	800	9.55	35.23	27.22
1,069	5.41	34.925	1,000	6.00	34.95	27.53
1,612	4.25	34.955				

TABLE OF OCEANOGRAPHIC DATA—Continued
STATIONS OCCUPIED IN 1957—Continued

Station 6461; 5 May; 42°47′ N., 45°42′ W.; depth 3,855 m.; dynamic height 971.525.

Observed values			Scaled values			
Depth, meters	Temperature, °C.	Salinity, °/oo	Depth, meters	Temperature, °C.	Salinity, °/oo	σ_t
0	16.07	36.17	0	16.07	36.17	26.66
25	16.08	36.16	25	16.08	36.16	26.65
51	15.91	36.12	50	15.90	36.12	26.65
77	15.92	36.125	75	15.90	36.12	26.65
103	15.26	36.00	100	15.30	36.01	26.70
153	14.96	36.015	150	14.95	36.01	26.79
205	14.87	36.015	200	14.90	36.01	26.80
308	14.88	------	300	14.85	36.04	26.83
419	*14.71	36.02	400	14.75	36.03	26.84
627	10.65	35.33	600	11.15	35.41	27.09
834	6.95	35.02	800	7.45	35.06	27.42
1,040	4.61	34.865	1,000	4.90	34.88	27.61
1,546	4.06	34.92				

Station 6462; 6 May; 43°10.5′ N., 45°22′ W.; depth 4,663 m.; dynamic height 971.460.

Observed values			Scaled values			
Depth, meters	Temperature, °C.	Salinity, °/oo	Depth, meters	Temperature, °C.	Salinity, °/oo	σ_t
0	16.34	36.23	0	16.34	36.23	26.63
25	16.35	36.22	25	16.35	36.22	26.62
50	16.35	36.22	50	16.35	36.22	26.62
75	16.37	36.22	75	16.37	36.22	26.62
100	16.36	36.23	100	16.36	36.23	26.62
150	15.29	35.98	150	15.29	35.98	26.68
200	15.02	35.99	200	15.02	35.99	26.75
300	13.82	35.74	300	13.82	35.74	26.82
397	13.02	35.67	400	13.00	35.67	26.93
586	9.49	35.20	600	9.05	35.16	27.25
769	5.43	34.82	800	5.30	34.82	27.52
957	4.74	34.90	1,000	4.65	34.90	27.66
1,421	4.00	34.94				

Station 6463; 6 May; 43°28.5′ N., 45°56′ W.; depth 3,750 m.; dynamic height 971.005.

Observed values			Scaled values			
Depth, meters	Temperature, °C.	Salinity, °/oo	Depth, meters	Temperature, °C.	Salinity, °/oo	σ_t
0	3.83	33.16	0	3.83	33.16	26.36
26	2.44	33.42	25	2.45	33.39	26.86
52	2.19	33.80	50	2.20	33.75	26.97
78	3.24	34.04	75	3.15	34.03	27.11
104	2.24	34.02	100	2.25	34.02	27.19
155	3.41	34.34	150	3.30	34.31	27.33
208	4.20	34.53	200	4.10	34.50	27.40
312	4.62	34.80	300	4.60	34.78	27.56
406	4.54	34.84	400	4.55	34.84	27.62
617	4.24	34.89	600	4.25	34.89	27.69
832	4.13	34.92	800	4.15	34.92	27.73
1,039	------	------	1,000	3.95	34.92	27.75

Station 6464; 6 May; 43°40.5′ N., 46°44′ W.; depth 4,390 m.; dynamic height 970.964.

Observed values			Scaled values			
Depth, meters	Temperature, °C.	Salinity, °/oo	Depth, meters	Temperature, °C.	Salinity, °/oo	σ_t
0	6.38	34.05	0	6.38	34.05	26.78
24	4.88	34.10	25	4.85	34.10	27.00
49	4.10	34.14	50	4.10	34.14	27.11
73	4.72	34.30	75	4.75	34.32	27.19
98	5.43	34.47	100	5.40	34.47	27.23
147	4.68	34.54	150	4.65	34.55	27.38
195	4.25	34.62	200	4.20	34.63	27.49
293	3.85	34.69	300	3.90	34.70	27.58
388	4.32	34.85	400	4.30	34.86	27.66
584	4.18	34.90	600	4.15	34.90	27.71
781	3.87	34.885	800	3.85	34.89	27.73
979	3.80	34.90	1,000	3.80	34.90	27.75
1,479	3.43	34.87				

Station 6465; 6 May; 43°47.5′ N., 47°22′ W.; depth 4,115 m.; dynamic height 971.086.

Observed values			Scaled values			
Depth, meters	Temperature, °C.	Salinity, °/oo	Depth, meters	Temperature, °C.	Salinity, °/oo	σ_t
0	7.86	34.49	0	7.86	34.49	26.91
26	8.14	34.58	25	8.15	34.57	26.94
52	8.40	34.74	50	8.40	34.73	27.02
78	8.78	34.91	75	8.75	34.90	27.10
104	8.82	34.93	100	8.80	34.93	27.11
155	8.72	34.92	150	8.70	34.92	27.12
207	8.03	34.83	200	8.15	34.84	27.14
311	5.91	34.69	300	6.05	34.70	27.33
407	5.46	34.81	400	5.50	34.71	27.41
617	4.47	34.91	600	4.55	34.90	27.67
832	3.96	34.89	800	4.00	34.89	27.72
1,040	3.69	34.87	1,000	3.70	34.87	27.74
1,561	3.44	34.87				

Station 6466; 6 May; 43°55′ N., 48°03′ W.; depth 3,566 m.; dynamic height 971.066.

Observed values			Scaled values			
Depth, meters	Temperature, °C.	Salinity, °/oo	Depth, meters	Temperature, °C.	Salinity, °/oo	σ_t
0	9.16	34.69	0	9.16	34.69	26.87
25	9.16	34.97	25	9.16	34.97	27.09
50	9.16	34.96	50	9.16	34.96	27.08
76	9.24	34.97	75	9.20	34.97	27.08
101	9.27	34.995	100	9.25	34.99	27.09
150	9.32	35.00	150	9.30	35.00	27.09
200	8.75	35.02	200	8.75	35.02	27.20
301	6.71	34.945	300	6.75	34.95	27.43
373	*6.10	------	400	5.90	34.91	27.52
563	4.78	34.89	600	4.70	34.90	27.65
755	4.44	34.92	800	4.40	34.92	27.70
953	4.11	34.92	1,000	4.10	34.92	27.74
1,467	3.61	34.89				

Station 6467; 6 May; 44°05.5′ N., 48°42′ W.; depth 2,195 m.; dynamic height 970.967.

Observed values			Scaled values			
Depth, meters	Temperature, °C.	Salinity, °/oo	Depth, meters	Temperature, °C.	Salinity, °/oo	σ_t
0	0.49	33.05	0	0.49	33.05	26.52
25	0.25	33.18	25	0.25	33.18	26.65
50	0.91	33.50	50	0.91	33.50	26.87
75	1.20	33.98	75	1.20	33.98	27.23
100	1.29	34.12	100	1.29	34.12	27.34
150	2.25	34.38	150	2.25	34.38	27.48
200	2.78	34.55	200	2.78	34.55	27.56
300	3.24	34.67	300	3.24	34.67	27.62
414	3.32	34.74	400	3.30	34.73	27.66
625	3.57	34.80	600	3.60	34.79	27.68
839	3.56	34.83	800	3.60	34.83	27.71
1,051	3.49	34.84	1,000	3.50	34.84	27.73
1,587	3.44	34.855				

Station 6468; 6 May; 44°07′ N., 48°48′ W.; depth 1,554 m.; dynamic height 970.969.

Observed values			Scaled values			
Depth, meters	Temperature, °C.	Salinity, °/oo	Depth, meters	Temperature, °C.	Salinity, °/oo	σ_t
0	−0.39	32.92	0	−0.39	32.92	26.47
27	−0.13	33.11	25	−0.15	33.10	26.60
53	1.37	33.76	50	1.30	33.69	26.99
81	1.04	34.02	75	1.10	33.98	27.23
107	1.41	34.18	100	1.30	34.14	27.35
161	2.12	34.40	150	2.00	34.36	27.48
215	2.62	34.55	200	2.50	34.52	27.57
322	2.97	34.64	300	2.95	34.62	27.61
394	3.09	34.69	400	3.10	34.69	27.65
595	3.34	34.755	600	3.35	34.75	27.67
800	3.60	34.83	800	3.60	34.83	27.71
999	3.55	34.83	1,000	3.55	34.83	27.71
1,492	3.51	34.845				

TABLE OF OCEANOGRAPHIC DATA—Continued

STATIONS OCCUPIED IN 1957—Continued

Station 6469; 6–7 May; 44°10′ N., 48°59′ W.; depth 622 m.; dynamic height 971.050.

Observed values			Scaled values			
Depth, meters	Temperature, °C.	Salinity, °/oo	Depth, meters	Temperature, °C.	Salinity, °/oo	σt
0	−0.47	32.91	0	−0.47	32.91	26.46
27	−0.59	32.93	25	−0.55	32.93	26.48
53	−1.19	32.99	50	−1.15	32.98	26.54
80	−1.14	33.32	75	−1.15	33.26	26.77
106	−0.58	33.53	100	−0.75	33.48	26.93
160	0.96	34.00	150	0.60	33.92	27.22
213	1.92	34.29	200	1.75	34.23	27.39
319	2.51	34.52	300	2.45	34.50	27.55
396	2.81	34.60	400	2.85	34.60	27.60
601	3.32	34.75	600	3.35	34.75	27.67

Station 6470; 7 May; 44°12.5′ N., 49°08′ W.; depth 169 m.; dynamic height 971.104.

Observed values			Scaled values			
Depth, meters	Temperature, °C.	Salinity, °/oo	Depth, meters	Temperature, °C.	Salinity, °/oo	σt
0	−0.47	32.93	0	−0.47	32.93	26.48
26	−0.52	32.94	25	−0.50	32.93	26.48
51	−0.96	32.98	50	−0.90	32.97	26.53
77	−1.37	33.22	75	−1.35	33.20	26.73
102	−0.59	33.36	100	−0.60	33.35	26.82
154	−0.64	33.48	150	−0.65	33.47	26.93

Station 6471; 7 May; 44°14′ N., 49°13′ W.; depth 71 m.; dynamic height 971.099.

Observed values			Scaled values			
Depth, meters	Temperature, °C.	Salinity, °/oo	Depth, meters	Temperature, °C.	Salinity, °/oo	σt
0	−0.43	32.94	0	−0.43	32.94	26.49
22	−0.08	33.04	25	−0.10	33.06	26.56
44	−0.13	33.21	50	−0.20	33.22	26.70
62	−0.36	33.255				

Station 6472; 7 May; 44°15.5′ N., 49°20′ W.; depth 53 m.; dynamic height 971.098.

Observed values			Scaled values			
Depth, meters	Temperature, °C.	Salinity, °/oo	Depth, meters	Temperature, °C.	Salinity, °/oo	σt
0	0.48	33.13	0	0.48	33.13	26.59
25	0.90	33.16	25	0.90	33.16	26.59
49	−0.16	33.17	50	−0.15	33.17	26.66

Station 6473; 7 May; 45°00′ N., 49°25′ W.; depth 71 m.; dynamic height 971.103.

Observed values			Scaled values			
Depth, meters	Temperature, °C.	Salinity, °/oo	Depth, meters	Temperature, °C.	Salinity, °/oo	σt
0	−0.14	33.00	0	−0.14	33.00	26.53
25	−0.24	33.00	25	−0.24	33.00	26.53
50	−0.78	33.16	50	−0.78	33.16	26.67

Station 6474; 7 May; 44°58′ N., 49°15′ W.; depth 89 m.; dynamic height 971.110.

Observed values			Scaled values			
Depth, meters	Temperature, °C.	Salinity, °/oo	Depth, meters	Temperature, °C.	Salinity, °/oo	σt
0	−0.37	32.89	0	−0.37	32.89	26.43
25	−0.51	32.92	25	−0.51	32.92	26.47
50	−0.62	32.98	50	−0.62	32.98	26.52
75	−0.87	33.07	75	−0.87	33.07	26.60
			(100)	−1.00	33.15	26.68

Station 6475; 7 May; 44°55.5′ N., 49°06′ W.; depth 622 m.; dynamic height 971.096.

Observed values			Scaled values			
Depth, meters	Temperature, °C.	Salinity, °/oo	Depth, meters	Temperature, °C.	Salinity, °/oo	σt
0	−0.21	32.81	0	−0.21	32.81	26.38
23	−0.73	32.94	25	−0.85	32.95	26.50
47	−1.50	33.05	50	−1.50	33.06	26.61
70	−1.30	33.18	75	−1.30	33.20	26.72
93	−1.30	33.24	100	−1.25	33.25	26.76
140	−1.01	33.38	150	−0.85	33.42	26.89
187	−0.20	33.615	200	0.05	33.71	27.09
280	1.87	34.29	300	2.20	34.43	27.52
349	2.81	34.60	400	2.90	34.63	27.62
546	3.05	34.67	(600)	3.10	34.68	27.64

Station 6476; 7 May; 44°51′ N., 48°48′ W.; depth 1,554 m.; dynamic height 971.022.

Observed values			Scaled values			
Depth, meters	Temperature, °C.	Salinity, °/oo	Depth, meters	Temperature, °C.	Salinity, °/oo	σt
0	−0.11	32.90	0	−0.11	32.90	26.43
22	−0.39	32.91	25	−0.40	32.91	26.46
44	−0.51	32.93	50	−0.65	32.99	26.54
67	−1.01	33.30	75	−0.90	33.36	26.84
89	−0.64	33.48	100	−0.45	33.57	27.00
133	0.26	33.78	150	0.90	33.97	27.25
177	2.21	34.29	200	2.40	34.41	27.49
266	2.74	34.59	300	2.85	34.62	27.62
280	2.76	34.39	400	3.05	34.68	27.64
427	3.08	34.69	600	3.25	34.74	27.67
579	3.21	34.735	800	3.45	34.80	27.70
737	3.45	34.795	1,000	3.50	34.83	27.72
1,154	3.53	34.85				

Station 6477; 7 May; 44°47.5′ N., 48°32′ W.; depth 1,737 m.; dynamic height 970.913.

Observed values			Scaled values			
Depth, meters	Temperature, °C.	Salinity, °/oo	Depth, meters	Temperature, °C.	Salinity, °/oo	σt
0	1.04	33.24	0	1.04	33.24	26.66
25	2.08	33.90	25	2.08	33.90	27.10
49	1.34	34.02	50	1.35	34.02	27.26
74	1.49	34.15	75	1.50	34.16	27.36
98	1.97	34.32	100	2.00	34.33	27.45
147	2.54	34.53	150	2.55	34.54	27.58
196	2.94	34.62	200	2.95	34.62	27.61
294	3.36	34.725	300	3.35	34.73	27.65
391	3.66	34.80	400	3.70	34.80	27.68
589	3.60	34.85	600	3.65	34.85	27.72
790	3.51	34.85	800	3.50	34.85	27.74
990	3.47	34.85	1,000	3.50	34.85	27.74
1,497	3.40	34.87				

Station 6478; 7 May; 44°38.5′ N., 47°49′ W.; depth 3,567 m.; dynamic height 970.974.

Observed values			Scaled values			
Depth, meters	Temperature, °C.	Salinity, °/oo	Depth, meters	Temperature, °C.	Salinity, °/oo	σt
0	4.50	33.77	0	4.50	33.77	26.78
25	4.60	33.81	25	4.60	33.81	26.80
50	5.07	34.15	50	5.07	34.15	27.02
75	7.89	34.76	75	7.89	34.76	27.13
99	6.38	34.56	100	6.25	34.55	27.18
149	2.53	34.20	150	2.50	34.20	27.31
199	4.57	34.64	200	4.60	34.65	27.46
298	5.68	34.98	300	5.70	34.98	27.59
413	4.58	34.845	400	4.65	34.90	27.66
621	3.80	34.865	600	3.85	34.87	27.72
830	3.55	34.855	800	3.55	34.86	27.74
1,037	3.48	34.86	1,000	3.50	34.86	27.75
1,555	3.40	34.875				

TABLE OF OCEANOGRAPHIC DATA—Continued

STATIONS OCCUPIED IN 1957—Continued

Station 6479; 8 May; 44°30′ N., 47°11′ W.; depth 3,932 m.; dynamic height 971.023.

Observed values			Scaled values			
Depth, meters	Temperature, °C.	Salinity, °/oo	Depth, meters	Temperature, °C.	Salinity, °/oo	σ_t
0	5.11	33.91	0	5.11	33.91	26.83
25	5.41	33.965	25	5.41	33.965	26.83
49	6.50	34.28	50	6.55	34.29	26.94
74	7.12	34.50	75	7.15	34.51	27.03
98	7.82	34.76	100	7.80	34.76	27.14
147	6.62	34.625	150	6.60	34.63	27.20
197	6.10	34.67	200	6.05	34.67	27.31
295	4.99	34.73	300	4.95	34.73	27.48
396	4.08	34.76	400	4.10	34.76	27.61
595	4.34	34.905	600	4.35	34.91	27.70
794	4.27	34.945	800	4.30	34.94	27.72
993	3.91	34.92	1,000	3.90	34.92	27.76
1,496	3.52	34.89				

Station 6480; 8 May; 44°22′ N., 46°34′ W.; depth 3,932 m.; dynamic height 970.973.

Observed values			Scaled values			
Depth, meters	Temperature, °C.	Salinity, °/oo	Depth, meters	Temperature, °C.	Salinity, °/oo	σ_t
0	6.35	34.25	0	6.35	34.25	26.94
25	6.37	34.25	25	6.37	34.25	26.94
50	7.77	34.67	50	7.77	34.67	27.07
75	7.28	34.71	75	7.28	34.71	27.18
100	6.80	34.66	100	6.80	34.66	27.20
150	6.38	34.78	150	6.38	34.78	27.35
201	5.10	34.67	200	5.10	34.67	27.43
301	5.00	34.86	300	5.05	34.86	27.58
340	5.10	34.90	400	4.90	34.92	27.65
515	4.62	34.935	600	4.30	34.92	27.71
695	3.99	34.89	800	3.90	34.90	27.74
880	3.82	34.90	1,000	3.70	34.89	27.75
1,360	3.42	34.87				

Station 6481; 8 May; 44°19.5′ N., 45°54′ W.; depth 3,932 m.; dynamic height 971.025.

Observed values			Scaled values			
Depth, meters	Temperature, °C.	Salinity, °/oo	Depth, meters	Temperature, °C.	Salinity, °/oo	σ_t
0	10.44	34.92	0	10.44	34.92	26.83
25	10.44	34.92	25	10.44	34.92	26.83
50	9.17	34.85	50	9.17	34.85	27.00
75	8.46	34.79	75	8.46	34.79	27.06
100	8.19	34.82	100	8.19	34.82	27.12
149	7.22	34.74	150	7.20	34.74	27.20
199	6.15	34.72	200	6.15	34.72	27.34
299	5.79	34.86	300	5.80	34.86	27.49
413	4.90	34.845	400	5.00	34.85	27.58
621	4.54	34.94	600	4.55	34.93	27.69
834	4.11	34.93	800	4.20	34.93	27.73
1,044	3.68	34.89	1,000	3.75	34.90	27.75
1,568	3.41	34.88				

Station 6482; 8 May; 44°11.5′ N., 45°16′ W.; depth 4,481 m.; dynamic height 971.058.

Observed values			Scaled values			
Depth, meters	Temperature, °C.	Salinity, °/oo	Depth, meters	Temperature, °C.	Salinity, °/oo	σ_t
0	8.49	34.47	0	8.48	34.47	26.80
25	10.81	35.09	25	10.81	35.09	26.90
51	9.30	34.87	50	9.35	34.88	26.9
76	7.36	34.52	75	7.35	34.52	27.01
152	4.33	34.24	100	6.10	34.38	27.07
203	7.66	34.89	150	4.35	34.24	27.16
305	4.76	34.62	200	7.65	34.88	27.25
391	5.57	34.88	300	4.80	34.63	27.42
590	5.21	35.00	400	5.60	34.90	27.54
791	4.34	34.93	600	5.15	35.00	27.68
1,000	3.85	34.885	800	4.30	34.93	27.71
1,516	3.60	34.89	1,000	3.85	34.89	27.73

Station 6483; 8 May; 44°44.5′ N., 45°10′ W.; depth 4,253 m.; dynamic height 971.058.

Observed values			Scaled values			
Depth, meters	Temperature, °C.	Salinity, °/oo	Depth, meters	Temperature, °C.	Salinity, °/oo	σ_t
0	10.87	35.02	0	10.87	35.02	26.84
21	10.98	35.02	25	10.90	35.02	26.83
43	10.41	34.90	50	10.10	34.88	26.86
64	9.45	34.86	75	8.80	34.76	26.98
86	8.26	34.66	100	8.00	34.67	27.04
128	7.58	34.69	150	7.20	34.69	27.16
170	6.84	34.69	200	6.40	34.70	27.28
256	5.73	34.735	300	5.50	34.78	27.46
246	5.80	34.76	400	5.10	34.84	27.56
386	5.14	34.83	600	4.60	34.93	27.68
538	4.69	34.91	800	4.30	34.94	27.72
696	4.44	34.95	1,000	4.00	34.92	27.75
1,128	3.80	34.905				

Station 6484; 8 May; 45°17.5′ N., 45°15′ W.; depth 4,287 m.; dynamic height 971.087.

Observed values			Scaled values			
Depth, meters	Temperature, °C.	Salinity, °/oo	Depth, meters	Temperature, °C.	Salinity, °/oo	σ_t
0	10.18	34.89	0	10.18	34.89	26.86
27	10.21	34.89	25	10.20	34.89	26.85
53	10.1	34.90	50	10.20	34.90	26.86
79	9.93	34.94	75	10.00	34.93	26.91
105	9.23	34.93	100	9.35	34.93	27.02
159	7.86	34.77	150	8.05	34.80	27.13
211	6.49	34.62	200	6.75	34.65	27.20
316	6.10	34.79	300	6.15	34.76	27.37
392	5.87	34.885	400	5.85	34.88	27.49
595	3.98	34.81	600	4.00	34.81	27.66
805	4.08	34.87	800	4.10	34.87	27.70
1,014	3.94	34.89	1,000	3.95	34.89	27.72
1,548	3.42	34.86				

Station 6485; 9 May; 45°17.5′ N., 45°58′ W.; depth 3,566 m.; dynamic height 970.926.

Observed values			Scaled values			
Depth, meters	Temperature, °C.	Salinity, °/oo	Depth, meters	Temperature, °C.	Salinity, °/oo	σ_t
0	4.08	34.01	0	4.08	34.01	27.01
27	4.06	34.03	25	4.05	34.03	27.03
52	2.48	34.12	50	2.55	34.11	27.24
79	2.71	34.28	75	2.65	34.25	27.34
104	2.98	34.37	100	2.90	34.36	27.41
157	3.30	34.56	150	3.25	34.53	27.50
210	4.38	34.78	200	4.25	34.76	27.59
314	3.92	34.90	300	4.00	34.80	27.65
418	3.43	34.77	400	3.50	34.77	27.68
630	3.67	34.84	600	3.65	34.83	27.70
846	3.57	34.845	800	3.60	34.84	27.72
1,059	3.51	34.86	1,000	3.55	34.85	27.73
1,595	3.37	34.87				

Station 6486; 9 May; 45°18.5′ N., 46°44′ W.; depth 3,219 m.; dynamic height 970.932.

Observed values			Scaled values			
Depth, meters	Temperature, °C.	Salinity, °/oo	Depth, meters	Temperature, °C.	Salinity, °/oo	σ_t
0	3.86	33.88	0	3.86	33.88	26.92
25	3.82	33.88	25	3.82	33.88	26.93
50	3.12	34.05	50	3.12	34.05	27.14
75	4.10	34.25	75	4.10	34.25	27.20
100	4.96	34.52	100	4.96	34.52	27.32
150	3.79	34.51	150	3.79	34.51	27.44
200	3.96	34.67	200	3.96	34.67	27.55
300	4.52	34.87	300	4.52	34.87	27.65
405	4.43	34.92	400	4.45	34.92	27.70
610	3.87	34.88	600	3.90	34.88	27.72
818	3.50	34.86	800	3.50	34.86	27.75
1,026	3.44	34.86	1,000	3.45	34.86	27.75
1,549	3.38	34.88				

TABLE OF OCEANOGRAPHIC DATA—Continued

STATIONS OCCUPIED IN 1957—Continued

Station 6487; 9 May; 45°24′ N., 47°24′ W.; depth 2,561 m.; dynamic height 970.929.

Observed values			Scaled values			
Depth, meters	Temperature, °C.	Salinity, ‰	Depth, meters	Temperature, °C.	Salinity, ‰	σt
0	4.37	33.92	0	4.37	33.92	26.91
24	4.36	33.93	25	4.35	33.93	26.91
49	3.72	34.00	50	3.70	34.03	27.06
73	2.93	34.25	75	2.95	34.28	27.33
98	3.58	34.46	100	3.60	34.47	27.43
147	4.04	34.63	150	4.05	34.63	27.50
196	4.03	34.70	200	4.00	34.70	27.57
294	3.36	34.72	300	3.40	34.72	27.65
357	3.40	34.76	400	3.55	34.79	27.68
541	3.97	34.89	600	3.85	34.88	27.72
729	3.60	34.85	800	3.55	34.85	27.73
918	3.48	34.85	1,000	3.45	34.85	27.74
1,400	3.37	34.87				

Station 6488; 9 May; 45°34.5′ N., 47°38′ W.; depth 1,600 m.; dynamic height 970.935.

Observed values			Scaled values			
Depth, meters	Temperature, °C.	Salinity, ‰	Depth, meters	Temperature, °C.	Salinity, ‰	σt
0	2.96	33.70	0	2.96	33.70	26.87
27	3.26	33.96	25	3.25	33.94	27.03
53	3.48	34.15	50	3.45	34.13	27.16
80	3.21	34.22	75	3.25	34.21	27.25
106	3.14	34.29	100	3.15	34.27	27.31
160	3.52	34.50	150	3.45	34.47	27.44
214	3.79	34.66	200	3.75	34.62	27.53
320	4.20	34.85	300	4.15	34.83	27.65
416	3.97	34.845	400	4.00	34.85	27.69
626	3.68	34.86	600	3.70	34.86	27.73
838	3.51	34.84	800	3.55	34.84	27.72
1,049	3.46	34.85	1,000	3.45	34.85	27.74
1,580	3.36	34.865				

Station 6489; 9 May; 45°44.5′ N., 47°58′ W.; depth 622 m.; dynamic height 971.008.

Observed values			Scaled values			
Depth, meters	Temperature, °C.	Salinity, ‰	Depth, meters	Temperature, °C.	Salinity, ‰	σt
0	0.03	32.97	0	0.03	32.97	26.49
26	−0.71	33.00	25	−0.70	33.00	26.55
52	−0.55	33.36	50	−0.60	33.31	26.78
78	0.64	33.86	75	0.60	33.80	27.12
104	0.83	33.97	100	0.80	33.95	27.23
155	1.15	34.06	150	1.10	34.05	27.30
208	1.44	34.22	200	1.40	34.20	27.40
312	2.51	34.54	300	2.40	34.51	27.57
416	2.97	34.66	400	2.95	34.65	27.63
596	2.97	-------	(600)	3.00	34.68	27.65

Station 6490; 9 May; 45°51′ N., 48°09′ W.; depth 169 m.; dynamic height 971.027.

Observed values			Scaled values			
Depth, meters	Temperature, °C.	Salinity, ‰	Depth, meters	Temperature, °C.	Salinity, ‰	σt
0	0.22	33.00	0	0.22	33.00	26.51
25	−0.54	33.09	25	−0.54	33.09	26.60
51	−1.10	33.31	50	−1.10	33.30	26.79
76	−0.32	33.59	75	−0.35	33.59	27.00
101	−0.18	33.64	100	−0.20	33.64	27.04
152	−0.16	33.64	150	−0.15	33.64	27.04

Station 6491; 9 May; 45°54′ N., 48°15′ W.; depth 115 m.; dynamic height 971.036.

Observed values			Scaled values			
Depth, meters	Temperature, °C.	Salinity, ‰	Depth, meters	Temperature, °C.	Salinity, ‰	σt
0	0.16	32.94	0	0.16	32.94	26.46
25	−0.76	32.98	25	−0.76	32.98	26.53
50	−1.23	33.17	50	−1.23	33.17	26.70
76	−1.09	33.39	75	−1.10	33.38	26.86
101	−0.50	33.54	100	−0.50	33.53	26.96

Station 6492; 9 May; 46°05′ N., 48°33′ W.; depth 91 m.; dynamic height 971.051.

Observed values			Scaled values			
Depth, meters	Temperature, °C.	Salinity, ‰	Depth, meters	Temperature, °C.	Salinity, ‰	σt
0	0.22	32.84	0	0.22	32.84	26.38
25	−0.84	32.90	25	−0.84	32.90	26.46
50	−0.46	33.00	50	−1.06	33.00	26.56
75	−1.12	33.09	75	−1.12	33.09	26.62

Station 6493; 9 May; 46°10.5′ N., 48°47′ W.; depth 82 m.; dynamic height 971.052.

Observed values			Scaled values			
Depth, meters	Temperature, °C.	Salinity, ‰	Depth, meters	Temperature, °C.	Salinity, ‰	σt
0	0.86	32.85	0	0.86	32.85	26.36
25	−0.05	32.87	25	−0.05	32.87	26.41
50	−0.49	32.98	50	−0.49	32.98	26.52
73	−0.83	33.13	75	−0.85	33.14	26.66

Station 6494; 9 May; 46°17.5′ N., 48°59′ W.; depth 71 m.; dynamic height 971.054.

Observed values			Scaled values			
Depth, meters	Temperature, °C.	Salinity, ‰	Depth, meters	Temperature, °C.	Salinity, ‰	σt
0	0.73	32.90	0	0.73	32.90	26.39
25	0.21	32.90	25	0.21	32.90	26.42
49	0.01	32.92	50	0.00	32.92	26.45

Station 6495; 9 May; 46°15′ N., 48°39′ W.; depth 89 m.; dynamic height 971.049.

Observed values			Scaled values			
Depth, meters	Temperature, °C.	Salinity, ‰	Depth, meters	Temperature, °C.	Salinity, ‰	σt
0	0.72	32.82	0	0.72	32.82	26.33
24	0.00	32.84	25	0.00	32.84	26.39
49	−0.65	33.03	50	−0.65	33.04	26.58
73	−0.91	33.145	75	−0.90	33.15	26.68

Station 6496; 10 May; 46°13′ N., 48°10′ W.; depth 115 m.; dynamic height 971.042.

Observed values			Scaled values			
Depth, meters	Temperature, °C.	Salinity, ‰	Depth, meters	Temperature, °C.	Salinity, ‰	σt
0	0.11	32.96	0	0.11	32.96	26.48
25	−0.08	32.95	25	−0.08	32.95	26.48
51	−0.61	32.98	50	−0.60	32.97	26.51
76	−1.07	33.23	75	−1.05	33.21	26.73
102	−0.56	33.50	100	−0.60	33.47	26.92

Station 6497; 10 May; 46°11′ N., 47°50′ W.; depth 169 m.; dynamic height 971.040.

Observed values			Scaled values			
Depth, meters	Temperature, °C.	Salinity, ‰	Depth, meters	Temperature, °C.	Salinity, ‰	σt
0	−0.50	32.96	0	−0.50	32.96	26.50
24	−0.54	32.96	25	−0.55	32.96	26.50
49	−0.99	32.96	50	−1.00	32.96	26.52
73	−1.23	33.20	75	−1.20	33.21	26.73
97	−1.10	33.42	100	−1.05	33.45	26.92
146	0.40	33.83	(150)	0.50	33.86	27.18

Station 6498; 10 May; 46°09.5′ N., 47°27′ W.; depth 649 m.; dynamic height 970.962.

Observed values			Scaled values			
Depth, meters	Temperature, °C.	Salinity, ‰	Depth, meters	Temperature, °C.	Salinity, ‰	σt
0	0.08	33.10	0	0.08	33.10	26.59
25	0.09	33.18	25	0.09	33.18	26.65
51	−0.32	33.46	50	−0.25	33.45	26.89
76	1.01	34.08	75	0.95	34.05	27.30
102	1.58	34.24	100	1.55	34.23	27.40
152	2.26	34.48	150	2.25	34.47	27.55
202	2.56	34.56	200	2.55	34.55	27.59
304	3.03	34.66	300	3.00	34.66	27.64
336	3.08	34.695	400	3.10	34.70	27.66
541	3.15	34.72	(600)	3.15	34.72	27.67

TABLE OF OCEANOGRAPHIC DATA—Continued

STATIONS OCCUPIED IN 1957—Continued

Station 6499; 10 May; 46°08′ N., 47°10′ W.; depth 1,536 m.; dynamic height 970.940.

Observed values			Scaled values			
Depth, meters	Temperature, °C.	Salinity, °/oo	Depth, meters	Temperature, °C.	Salinity, °/oo	σt
0	0.88	33.12	0	0.88	33.12	26.56
23	0.91	33.16	25	0.90	33.16	26.59
46	0.74	33.84	50	0.75	33.90	27.20
69	1.12	34.10	75	1.25	34.14	27.36
93	1.55	34.22	100	1.70	34.25	27.41
138	2.54	34.48	150	2.70	34.52	27.55
184	3.00	34.61	200	3.00	34.62	27.61
277	3.12	34.68	300	3.15	34.69	27.64
373	3.32	34.73	400	3.35	34.74	27.66
587	3.41	34.785	600	3.40	34.79	27.70
801	3.58	34.84	800	3.60	34.84	27.72
1,015	3.49	34.84	1,000	3.50	34.84	27.73
1,418	3.43	34.845				

Station 6500; 10 May; 46°05′ N., 46°35′ W.; depth 521 m.; dynamic height 970.912.

Observed values			Scaled values			
Depth, meters	Temperature, °C.	Salinity, °/oo	Depth, meters	Temperature, °C.	Salinity, °/oo	σt
0	2.36	33.49	0	2.36	33.49	26.75
24	4.05	34.17	25	4.05	34.17	27.15
47	3.69	34.26	50	3.60	34.27	27.27
71	3.13	34.35	75	3.15	34.37	27.39
95	3.39	34.46	100	3.45	34.47	27.44
142	3.72	34.58	150	3.80	34.61	27.52
189	4.28	34.76	200	4.25	34.76	27.59
284	3.48	34.73	300	3.50	34.74	27.65
379	3.66	34.81	400	3.70	34.82	27.70
476	3.68	34.84				

Station 6501; 10 May; 46°03.5′ N., 45°56′ W.; depth 2,012 m.; dynamic height 970.957.

Observed values			Scaled values			
Depth, meters	Temperature, °C.	Salinity, °/oo	Depth, meters	Temperature, °C.	Salinity, °/oo	σt
0	6.31	34.40	0	6.31	34.40	27.05
24	6.29	34.39	25	6.30	34.39	27.05
49	7.63	34.69	50	7.65	34.70	27.11
73	7.90	34.86	75	7.85	34.76	27.13
98	6.55	34.71	100	6.50	34.71	27.28
146	5.99	34.78	150	5.95	34.78	27.40
195	5.48	34.81	200	5.40	34.81	27.50
293	4.62	34.82	300	4.50	34.81	27.60
360	3.55	34.74	400	3.55	34.75	27.65
546	3.62	34.82	600	3.60	34.82	27.71
736	3.52	34.825	800	3.50	34.83	27.72
929	3.46	34.835	1,000	3.45	34.84	27.73
1,432	3.43	34.86				

Station 6502; 10 May; 46°02′ N., 45°17′ W.; depth 3,200 m.; dynamic height 970.892.

Observed values			Scaled values			
Depth, meters	Temperature, °C.	Salinity, °/oo	Depth, meters	Temperature, °C.	Salinity, °/oo	σt
0	5.51	34.43	0	5.51	34.43	27.17
27	5.22	34.42	25	5.25	34.43	27.21
54	4.14	34.54	50	4.30	34.53	27.40
81	3.42	34.56	75	3.50	34.55	27.50
107	3.48	34.615	100	3.45	34.60	27.54
162	3.36	34.65	150	3.40	34.64	27.58
216	3.33	34.71	200	3.35	34.69	27.62
323	3.42	34.75	300	3.40	34.74	27.66
418	3.47	34.79	400	3.45	34.78	27.68
633	3.77	34.87	600	3.75	34.87	27.73
854	3.63	34.86	800	3.70	34.86	27.73
1,072	3.42	34.85	1,000	3.50	34.85	27.74
1,627	3.31	34.87				

Station 6503; 10 May; 46°01.5′ N., 44°36′ W.; depth 2,140 m.; dynamic height 971.119.

Observed values			Scaled values			
Depth, meters	Temperature, °C.	Salinity, °/oo	Depth, meters	Temperature, °C.	Salinity, °/oo	σt
0	12.63	35.46	0	12.63	35.46	26.85
25	12.67	35.45	25	12.67	35.455	26.83
51	12.67	35.445	50	12.70	35.445	26.82
76	12.56	35.435	75	12.55	35.43	26.83
102	10.60	35.07	100	10.70	35.08	26.91
151	11.07	35.32	150	11.05	35.31	27.02
202	10.24	35.23	200	10.30	35.23	27.09
304	6.45	34.74	300	6.55	34.76	27.31
391	6.20	34.88	400	6.15	34.88	27.46
594	4.75	34.905	600	4.70	34.91	27.66
801	4.42	34.94	800	4.40	34.94	27.71
1,006	3.99	34.91	1,000	4.00	34.91	27.74
1,529	3.52	34.88				

Station 6504; 10 May; 46°22.5′ N., 44°33′ W.; depth 1,920 m.; dynamic height 971.016.

Observed values			Scaled values			
Depth, meters	Temperature, °C.	Salinity, °/oo	Depth, meters	Temperature, °C.	Salinity, °/oo	σt
0	11.43	35.23	0	11.43	35.23	26.90
26	11.45	35.24	25	11.45	35.24	26.90
52	11.38	35.22	50	11.40	35.22	26.90
79	9.70	34.97	75	9.80	35.01	27.01
105	9.53	35.05	100	9.55	35.04	27.08
156	6.70	34.65	150	6.85	34.67	27.20
200	6.38	34.75	200	6.45	34.74	27.31
314	5.47	34.86	300	5.60	34.85	27.50
419	4.90	34.90	400	4.95	34.90	27.62
628	3.89	34.87	600	4.00	34.88	27.71
839	3.52	34.84	800	3.55	34.85	27.73
1,049	3.44	34.86	1,000	3.45	34.86	27.75
1,574	3.43	34.88				

Station 6505; 11 May; 46°32.5′ N., 44°37′ W.; depth 640 m.; dynamic height 970.905.

Observed values			Scaled values			
Depth, meters	Temperature, °C.	Salinity, °/oo	Depth, meters	Temperature, °C.	Salinity, °/oo	σt
0	4.64	34.39	0	4.64	34.39	27.25
24	4.65	34.39	25	4.65	34.39	27.25
48	4.25	34.39	50	4.25	34.39	27.29
72	4.27	34.44	75	4.25	34.44	27.33
97	3.62	34.46	100	3.60	34.47	27.43
144	3.50	34.58	150	3.45	34.59	27.53
192	3.28	34.63	200	3.30	34.64	27.59
289	3.51	34.77	300	3.55	34.78	27.67
356	3.56	34.81	400	3.60	34.81	27.70
505	3.53	34.81	(600)	3.50	34.81	27.71

Station 6506; 11 May; 46°37.5′ N., 44°39′ W.; depth 224 m.; dynamic height 970.894.

Observed values			Scaled values			
Depth, meters	Temperature, °C.	Salinity, °/oo	Depth, meters	Temperature, °C.	Salinity, °/oo	σt
0	4.08	34.34	0	4.08	34.34	27.27
25	4.08	34.34	25	4.08	34.34	27.28
49	3.46	34.41	50	3.40	34.42	27.41
74	2.90	34.47	75	2.90	34.46	27.49
98	2.86	34.47	100	2.85	34.47	27.50
147	2.90	34.53	150	2.90	34.54	27.55
196	3.16	34.62	200	3.20	34.63	27.59

Station 6507; 11 May; 46°44′ N., 44°42′ W.; depth 163 m.; dynamic height 970.893.

Observed values			Scaled values			
Depth, meters	Temperature, °C.	Salinity, °/oo	Depth, meters	Temperature, °C.	Salinity, °/oo	σt
0	3.80	34.31	0	3.80	34.31	27.28
24	3.80	34.31	25	3.80	34.31	27.28
49	2.92	34.39	50	2.90	34.40	27.44
73	2.83	34.44	75	2.85	34.45	27.48
97	2.93	34.51	100	2.95	34.52	27.53
146	2.98	34.53	150	3.00	34.53	27.53

TABLE OF OCEANOGRAPHIC DATA—Continued

STATIONS OCCUPIED IN 1957—Continued

Station 6508; 11 May; 46°50′ N., 44°44′ W.; depth 133 m.; dynamic height 970.899.

Observed values			Scaled values			
Depth, meters	Temperature, °C.	Salinity, °/oo	Depth, meters	Temperature, °C.	Salinity, °/oo	σ_t
0	3.83	34.33	0	3.83	34.33	27.29
25	3.83	34.31	25	3.83	34.31	27.28
51	3.78	34.33	50	3.80	34.33	27.29
76	2.90	34.42	75	2.90	34.42	27.46
102	2.84	34.41	100	2.85	34.42	27.46
127	2.89	34.47	150	3.00	34.53	27.53

Station 6509; 11 May; 46°50′ N., 44°57′ W.; depth 169 m.; dynamic height 970.904.

Observed values			Scaled values			
Depth, meters	Temperature, °C.	Salinity, °/oo	Depth, meters	Temperature, °C.	Salinity, °/oo	σ_t
0	4.05	34.33	0	4.05	34.33	27.27
25	4.05	34.34	25	4.05	34.34	27.28
50	4.05	34.33	50	4.05	34.33	27.27
75	3.29	34.35	75	3.29	34.35	27.36
100	2.94	34.38	100	2.94	34.38	27.42
150	2.91	34.47	150	2.91	34.48	27.50

Station 6510; 11 May; 46°49.5′ N., 45°16′ W.; depth 220 m.; dynamic height 970.893.

Observed values			Scaled values			
Depth, meters	Temperature, °C.	Salinity, °/oo	Depth, meters	Temperature, °C.	Salinity, °/oo	σ_t
0	4.23	34.37	0	4.23	34.37	27.28
25	4.21	34.38	25	4.21	34.38	27.29
50	3.20	34.44	50	3.20	34.44	27.44
75	3.01	34.44	75	3.01	34.44	27.46
100	3.18	34.50	100	3.18	34.50	27.48
149	2.93	34.54	150	2.95	34.54	27.54
199	3.15	34.63	200	3.15	34.63	27.59

Station 6511; 11 May; 46°50′ N., 45°43′ W.; depth 274 m.; dynamic height 970.896.

Observed values			Scaled values			
Depth, meters	Temperature, °C.	Salinity, °/oo	Depth, meters	Temperature, °C.	Salinity, °/oo	σ_t
0	3.91	34.21	0	3.91	34.21	27.19
25	3.77	34.24	25	3.77	34.24	27.23
50	2.74	34.26	50	2.74	34.26	27.34
75	2.61	34.31	75	2.61	34.31	27.39
100	2.74	34.38	100	2.74	34.38	27.43
149	3.28	34.61	150	3.30	34.61	27.57
199	3.56	34.75	200	3.55	34.75	27.65
259	3.60	34.78	300	3.60	34.79	27.68

Station 6512; 11 May; 46°50′ N., 46°07′ W.; depth 320 m.; dynamic height 970.907.

Observed values			Scaled values			
Depth, meters	Temperature, °C.	Salinity, °/oo	Depth, meters	Temperature, °C.	Salinity, °/oo	σ_t
0	3.02	33.97	0	3.02	33.97	27.08
25	3.04	34.02	25	3.04	34.02	27.12
50	2.76	34.19	50	2.76	34.19	27.28
75	2.55	34.27	75	2.55	34.27	27.37
100	2.46	34.33	100	2.46	34.33	27.41
150	3.19	34.57	150	3.19	34.57	27.55
201	3.55	34.69	200	3.55	34.69	27.60
301	3.60	34.81	300	3.60	34.81	27.70

Station 6513; 11 May; 46°50′ N., 46°36′ W.; depth 622 m.; dynamic height 970.914.

Observed values			Scaled values			
Depth, meters	Temperature, °C.	Salinity, °/oo	Depth, meters	Temperature, °C.	Salinity, °/oo	σ_t
0	2.30	33.62	0	2.30	33.62	26.87
24	2.15	33.72	25	2.15	33.72	26.96
49	3.00	34.25	50	3.00	34.25	27.31
73	2.93	34.33	75	2.90	34.33	27.38
99	2.90	34.36	100	2.90	34.36	27.41
147	2.42	34.46	150	2.45	34.47	27.53
196	2.92	34.61	200	2.95	34.62	27.61
295	3.21	34.71	300	3.20	34.71	27.66
392	3.55	34.80	400	3.55	34.80	27.69
596	3.55	34.835	600	3.55	34.84	27.72

Station 6514; 11 May; 46°50′ N., 46°52′ W.; depth 1,207 m.; dynamic height 970.889.

Observed values			Scaled values			
Depth, meters	Temperature, °C.	Salinity, °/oo	Depth, meters	Temperature, °C.	Salinity, °/oo	σ_t
0	1.73	33.45	0	1.73	33.45	26.78
26	1.56	33.61	25	1.55	33.60	26.91
51	1.92	34.28	50	1.90	34.26	27.41
77	2.15	34.43	75	2.15	34.42	27.52
103	2.47	34.54	100	2.45	34.53	27.57
153	2.86	34.63	150	2.85	34.63	27.62
204	3.02	34.69	200	3.00	34.69	27.66
307	3.12	34.74	300	3.10	34.74	27.69
406	3.20	34.76	400	3.20	34.76	27.70
610	3.34	34.81	600	3.35	34.81	27.72
815	3.40	34.83	800	3.40	34.83	27.73
1,022	3.42	34.85	1,000	3.45	34.85	27.74
1,190	3.38	34.86				

Station 6515; 11 May; 46°50′ N., 47°12′ W.; depth 622 m.; dynamic height 970.958.

Observed values			Scaled values			
Depth, meters	Temperature, °C.	Salinity, °/oo	Depth, meters	Temperature, °C.	Salinity, °/oo	σ_t
0	−0.22	33.05	0	−0.22	33.05	26.56
25	−0.38	33.19	25	−0.38	33.19	26.68
51	0.92	33.93	50	0.90	33.92	27.21
76	1.32	34.17	75	1.35	34.17	27.38
102	1.40	34.20	100	1.40	34.20	27.40
152	1.81	34.35	150	1.75	34.34	27.48
204	2.39	34.50	200	2.35	34.49	27.55
306	2.98	34.66	300	2.95	34.65	27.63
397	3.15	34.71	400	3.15	34.71	27.66
596	3.18	34.73	600	3.20	34.74	27.68

Station 6516; 11 May; 46°50′ N., 47°20′ W.; depth 311 m.; dynamic height 971.004.

Observed values			Scaled values			
Depth, meters	Temperature, °C.	Salinity, °/oo	Depth, meters	Temperature, °C.	Salinity, °/oo	σ_t
0	−0.62	32.74	0	−0.62	32.74	26.33
24	−0.87	32.96	25	−0.90	32.97	26.53
48	−1.62	33.19	50	−1.60	33.20	26.73
72	−1.37	33.31	75	−1.25	33.36	26.85
97	−0.05	33.72	100	0.05	33.75	27.12
145	1.30	34.13	150	1.40	34.18	27.38
193	2.14	34.45	200	2.20	34.47	27.56
290	2.85	34.63	(300)	2.90	34.64	27.63

Station 6517; 11 May; 46°48′ N., 47°38′ W.; depth 169 m.; dynamic height 971.035.

Observed values			Scaled values			
Depth, meters	Temperature, °C.	Salinity, °/oo	Depth, meters	Temperature, °C.	Salinity, °/oo	σ_t
0	−0.28	32.93	0	−0.28	32.93	26.47
25	−0.36	32.98	25	−0.36	32.98	26.51
51	−1.35	33.06	50	−1.35	33.06	26.61
76	−1.58	33.15	75	−1.60	33.15	26.69
101	−1.45	33.26	100	−1.45	33.26	26.77
152	1.08	34.05	150	0.95	34.03	27.28

TABLE OF OCEANOGRAPHIC DATA—Continued

STATIONS OCCUPIED IN 1957—Continued

Station 6518; 12 May; 46°45′ N., 48°10′ W.; depth 110 m.; dynamic height 971.040.

Observed values			Scaled values			
Depth, meters	Temperature, °C.	Salinity, °/oo	Depth, meters	Temperature, °C.	Salinity, °/oo	σ_t
0	0.11	32.84	0	0.11	32.84	26.38
25	−0.48	32.89	25	−0.48	32.89	26.44
50	−1.08	32.94	50	−1.08	32.94	26.51
76	−0.99	33.27	75	−1.00	33.26	26.76
101	−0.66	33.44	100	−0.70	33.43	26.89

Station 6519; 12 May; 46°42′ N., 48°40′ W.; depth 82 m.; dynamic height 971.050.

Observed values			Scaled values			
Depth, meters	Temperature, °C.	Salinity, °/oo	Depth, meters	Temperature, °C.	Salinity, °/oo	σ_t
0	0.69	32.81	0	0.69	32.81	26.33
25	0.51	32.84	25	0.51	32.84	26.36
49	−0.41	32.95	50	−0.45	32.95	26.50
74	−0.84	33.07	75	−0.85	33.07	26.60

Station 6520; 49°57.5′ N., 48°58′ W.; 22 July; depth 1,920 m.; dynamic height 970.887.

Observed values			Scaled values			
Depth, meters	Temperature, °C.	Salinity, °/oo	Depth, meters	Temperature, °C.	Salinity, °/oo	σ_t
0	9.90	34.59	0	9.90	34.59	26.67
24	7.48	34.58	25	7.40	34.58	27.05
49	4.24	34.50	50	4.15	34.50	27.39
73	3.68	34.54	75	3.70	34.55	27.48
98	3.83	34.66	100	3.85	34.67	27.56
146	3.75	34.72	150	3.75	34.72	27.61
195	3.80	34.76	200	3.80	34.77	27.65
293	3.86	34.84	300	3.85	34.84	27.69
417	3.76	34.84	400	3.80	34.84	27.70
629	3.63	34.86	600	3.65	34.86	27.73
844	3.54	34.87	800	3.55	34.87	27.75
1,055	3.42	34.87	1,000	3.45	34.87	27.76
1,582	3.34	34.88				

Station 6521; 22 July; 49°47.5′ N., 49°30′ W.; depth 1,390 m.; dynamic height 970.912.

Observed values			Scaled values			
Depth, meters	Temperature, °C.	Salinity, °/oo	Depth, meters	Temperature, °C.	Salinity, °/oo	σ_t
0	7.53	33.39	0	7.53	33.39	26.10
25	2.30	34.17	25	2.30	34.17	27.31
50	2.68	34.30	50	2.68	34.30	27.37
75	2.37	34.38	75	2.37	34.38	27.46
100	3.12	34.54	100	3.12	34.54	27.53
150	3.67	34.67	150	3.67	34.67	27.58
201	3.81	34.73	200	3.80	34.73	27.61
301	4.05	34.79	300	4.05	34.79	27.63
408	4.00	34.84	400	4.00	34.84	27.68
611	3.60	34.84	600	3.65	34.84	27.71
812	3.39	34.825	800	3.40	34.83	27.73
1,004	3.33	34.84	1,000	3.35	34.84	27.74
1,331	3.34	34.87				

Station 6522; 22 July; 49°37.5′ N., 50°02′ W.; depth 622 m.; dynamic height 970.961.

Observed values			Scaled values			
Depth, meters	Temperature, °C.	Salinity, °/oo	Depth, meters	Temperature, °C.	Salinity, °/oo	σ_t
0	7.72	33.34	0	7.72	33.34	26.02
25	5.38	33.87	25	5.38	33.87	26.76
50	2.38	34.18	50	2.38	34.18	27.30
75	2.07	34.24	75	2.07	34.24	27.38
101	1.95	34.28	100	1.95	34.28	27.42
150	3.00	34.51	150	3.01	34.51	27.52
200	3.74	34.67	200	3.74	34.67	27.57
301	3.98	34.75	300	4.00	34.75	27.61
389	4.05	34.80	400	4.05	34.80	27.64
589	3.98	34.81	600	4.00	34.81	27.66

Station 6523; 22 July; 49°29′ N., 50°31′ W.; depth 334 m.; dynamic height 970.964.

Observed values			Scaled values			
Depth, meters	Temperature, °C.	Salinity, °/oo	Depth, meters	Temperature, °C.	Salinity, °/oo	σ_t
0	8.84	33.22	0	8.84	33.22	25.77
25	2.16	33.62	25	2.16	33.62	26.88
50	−0.29	33.80	50	−0.29	33.80	27.17
74	0.47	34.01	75	0.50	34.01	27.30
100	0.87	34.14	100	0.85	34.14	27.38
149	1.82	34.35	150	1.85	34.36	27.49
199	2.53	34.50	200	2.55	34.50	27.55
299	3.09	-------	(300)	3.10	34.69	27.65

Station 6524; 22 July; 49°17′ N., 51°01′ W.; depth 338 m.; dynamic height 970.980.

Observed values			Scaled values			
Depth, meters	Temperature, °C.	Salinity, °/oo	Depth, meters	Temperature, °C.	Salinity, °/oo	σ_t
0	9.20	33.16	0	9.20	33.16	25.67
25	2.54	33.55	25	2.54	33.55	26.79
50	0.36	33.76	50	0.36	33.76	27.11
74	0.39	33.94	75	0.40	33.94	27.25
100	0.30	34.04	100	0.30	34.04	27.33
149	1.29	34.24	150	1.30	34.24	27.43
199	1.96	34.40	200	2.00	34.40	27.51
299	2.90	34.605	300	2.90	34.61	27.61

Station 6525; 22 July; 49°11′ N., 51°36′ W.; depth 320 m.; dynamic height 971.043.

Observed values			Scaled values			
Depth, meters	Temperature, °C.	Salinity, °/oo	Depth, meters	Temperature, °C.	Salinity, °/oo	σ_t
0	9.16	31.94	0	9.16	31.94	24.72
25	1.27	33.25	25	1.27	33.25	26.64
50	0.64	33.42	50	0.64	33.42	26.82
75	−0.94	33.49	75	−0.94	33.49	26.95
101	−0.94	33.65	100	−0.95	33.65	27.08
151	−0.35	33.88	150	−0.40	33.87	27.24
202	0.23	34.01	200	0.20	34.00	27.31
303	2.37	34.49	300	2.30	34.47	27.55

Station 6526; 23 July; 49°04.5′ N., 51°54′ W.; depth 302 m.; dynamic height 971.048.

Observed values			Scaled values			
Depth, meters	Temperature, °C.	Salinity, °/oo	Depth, meters	Temperature, °C.	Salinity, °/oo	σ_t
0	8.85	31.92	0	8.85	31.92	24.76
25	1.26	33.18	25	1.26	33.18	26.59
50	0.26	33.31	50	0.26	33.31	26.75
76	0.08	33.44	75	0.10	33.44	26.87
101	−1.01	33.54	100	−1.00	33.54	26.99
151	−0.52	33.82	150	−0.55	33.81	27.19
201	0.48	34.05	200	0.40	34.04	27.33
277	2.33	34.49	(300)	2.75	34.62	27.63

Station 6527; 23 July; 49°00.5′ N., 52°07′ W.; depth 293 m.; dynamic height 971.065.

Observed values			Scaled values			
Depth, meters	Temperature, °C.	Salinity, °/oo	Depth, meters	Temperature, °C.	Salinity, °/oo	σ_t
0	8.78	31.66	0	8.78	31.66	24.57
24	1.21	33.00	25	1.15	33.03	26.48
47	0.34	33.20	50	0.20	33.21	26.68
71	−0.90	33.28	75	−0.90	33.30	26.79
94	−0.77	33.43	100	−0.80	33.46	26.92
142	−0.83	33.68	150	−0.80	33.72	27.13
189	−0.26	33.92	200	0.00	33.98	27.30
260	1.99	34.40	300	2.95	34.63	27.61

TABLE OF OCEANOGRAPHIC DATA—Continued

STATIONS OCCUPIED IN 1957—Continued

Observed values			Scaled values			
Depth, meters	Temperature, °C.	Salinity, °/oo	Depth, meters	Temperature, °C.	Salinity, °/oo	σt
Station 6528; 23 July; 48°54′ N., 52°22′ W.; depth 359 m.; dynamic height 971.065.						
0	6.49	31.69	0	6.49	31.69	24.90
24	2.94	33.10	25	2.80	33.11	26.42
48	0.35	33.24	50	0.35	33.25	26.70
72	0.50	33.38	75	0.50	33.39	26.80
96	−0.59	33.45	100	−0.60	33.47	26.92
143	−0.81	33.70	150	−0.80	33.74	27.14
191	0.23	33.96	200	0.40	34.01	27.31
287	2.08	34.43	(300)	2.25	34.48	27.55
Station 6529; 23 July; 48°47′ N., 52°39′ W.; depth 220 m.; dynamic height 971.188.						
0	7.72	30.58	0	7.72	30.58	23.87
23	−1.19	32.63	25	−1.25	32.66	26.29
46	−1.54	32.78	50	−1.55	32.79	26.40
69	−1.60	32.85	75	−1.60	32.87	26.47
93	−1.60	32.92	100	−1.60	32.93	26.51
139	−1.60	33.00	150	−1.55	33.04	26.60
185	−1.28	33.20	(200)	−1.10	33.26	26.76
Station 6530; 23 July; 48°45.5′ N., 52°48′ W.; depth 132 m.; dynamic height 971.192.						
0	7.91	30.45	0	7.91	30.45	23.75
26	−0.92	32.58	25	−0.75	32.50	26.14
52	−1.59	32.78	50	−1.60	32.77	26.39
79	−1.60	32.88	75	−1.60	32.87	26.47
105	−1.62	32.96	100	−1.60	32.94	26.52
Station 6531; 23 July; 48°43.5′ N., 52°58′ W.; depth 100 m.; dynamic height 971.216.						
0	10.60	30.02	0	10.60	30.02	23.00
26	−0.33	32.17	25	−0.20	32.09	25.79
53	−1.45	32.63	50	−1.40	32.59	26.23
79	−1.59	32.80	75	−1.60	32.78	26.39
			(100)	−1.60	32.89	26.48
Station 6532; 23 July; 48°37.5′ N., 52°44′ W.; depth 279 m.; dynamic height 971.228.						
0	8.44	30.52	0	8.44	30.52	23.72
25	−1.27	32.68	25	−1.27	30.68	24.69
50	−1.26	32.72	50	−1.26	32.72	26.34
75	−1.55	32.85	75	−1.55	32.85	26.45
100	−1.28	32.93	100	−1.28	32.93	26.50
151	−1.53	33.03	150	−1.50	33.02	26.58
201	−1.48	33.26	200	−1.50	33.25	26.77
251	0.20	34.00	300	1.90	34.57	27.66
Station 6533; 23 July; 48°32.5′ N., 52°32′ W.; depth 220 m.; dynamic height 971.143.						
0	8.48	30.43	0	8.48	30.43	23.64
25	−1.09	32.66	25	−1.09	32.66	26.28
49	−1.61	32.83	50	−1.60	32.83	26.43
74	−1.59	32.97	75	−1.60	32.97	26.55
98	−1.53	33.01	100	−1.55	33.02	26.59
147	−1.08	33.26	150	−1.05	33.28	26.78
196	−0.86	33.66	200	−0.85	33.70	27.11

Observed values			Scaled values			
Depth, meters	Temperature, °C.	Salinity, °/oo	Depth, meters	Temperature, °C.	Salinity, °/oo	σt
Station 6534; 23 July; 48°21.5′ N., 52°08′ W.; depth 192 m.; dynamic height 971.139.						
0	10.17	30.75	0	10.17	30.75	23.64
26	−1.05	32.70	25	−0.95	32.63	26.26
52	−1.63	32.90	50	−1.60	32.88	26.47
77	−1.55	33.00	75	−1.55	32.99	26.56
103	−1.40	33.06	100	−1.45	33.05	26.60
155	−1.18	33.24	150	−1.20	33.37	26.86
186	−0.84	33.58	200	−0.50	33.65	27.06
Station 6535; 23 July; 48°15′ N., 51°52′ W.; depth 192 m.; dynamic height 971.133.						
0	9.66	31.26	0	9.66	31.26	24.11
26	−0.08	32.72	25	0.10	32.66	26.24
52	−1.29	32.90	50	−1.20	32.88	26.46
77	−1.66	33.01	75	−1.65	33.00	26.57
103	−1.48	33.10	100	−1.50	33.08	26.63
155	−1.05	33.37	150	−1.10	33.33	26.82
186	0.52	34.045	200	1.35	34.29	27.47
Station 6536; 23 July; 48°07′ N., 51°34′ W.; depth 201 m.; dynamic height 971.131.						
0	11.32	30.99	0	11.32	30.99	23.62
25	−0.45	32.66	25	−0.45	32.66	26.26
51	−1.13	32.94	50	−1.10	32.94	26.50
76	−1.45	33.06	75	−1.45	33.06	26.61
102	−1.33	33.23	100	−1.35	33.21	26.74
152	−0.69	33.44	150	−0.70	33.43	26.89
188	−0.69	33.52	(200)	−0.50	33.60	27.02
Station 6537; 23 July; 47°59.5′ N., 51°15′ W.; depth 169 m.; dynamic height 971.129.						
0	10.90	31.09	0	10.90	31.09	23.78
26	−0.05	32.72	25	0.50	32.66	26.22
51	−1.40	32.90	50	−1.35	32.89	26.47
77	−1.33	33.03	75	−1.35	33.02	26.58
103	−1.41	33.14	100	−1.40	33.13	26.67
154	−0.82	33.43	150	−0.85	33.40	26.87
Station 6538; 23 July; 47°53′ N., 50°58′ W.; depth 123 m.; dynamic height 971.112.						
0	11.05	31.30	0	11.05	31.30	23.92
26	0.44	32.62	25	0.75	32.57	26.13
52	−1.34	33.00	50	−1.30	32.98	26.54
77	−1.32	33.13	75	−1.30	33.12	26.66
103	−1.02	33.34	100	−1.10	33.31	26.80
Station 6539; 23 July; 47°45′ N., 50°40′ W.; depth 129 m.; dynamic height 971.112.						
0	10.34	31.68	0	10.34	31.68	24.34
26	0.81	32.60	25	1.20	32.56	26.10
52	−1.22	32.95	50	−1.20	32.93	26.50
77	−1.26	35.14	75	−1.25	33.13	26.66
103	−0.70	33.26	100	−0.80	33.24	26.74

TABLE OF OCEANOGRAPHIC DATA—Continued

STATIONS OCCUPIED IN 1957—Continued

Station 6540; 23 July; 47°36′ N., 50°18′ W.; depth 159 m.; dynamic height 971.109.

Observed values			Scaled values			
Depth, meters	Temperature, °C.	Salinity, °/oo	Depth, meters	Temperature, °C.	Salinity, °/oo	σt
0	10.16	31.65	0	10.16	31.65	24.34
25	0.80	32.52	25	0.80	32.52	26.09
50	−1.44	32.95	50	−1.44	32.95	26.52
75	−1.08	33.15	75	−1.08	33.15	26.68
100	−0.96	33.31	100	−0.96	33.31	26.80

Station 6541; 24 July; 47°24′ N., 50°01′ W.; depth 95 m.; dynamic height 971.105.

Observed values			Scaled values			
Depth, meters	Temperature, °C.	Salinity, °/oo	Depth, meters	Temperature, °C.	Salinity, °/oo	σt
0	9.86	31.65	0	9.86	31.65	24.39
25	1.46	32.39	25	1.46	32.59	26.11
50	−0.62	32.98	50	−0.62	32.98	26.53
75	−0.93	33.20	75	−0.93	33.20	26.72

Station 6542; 24 July; 47°44′ N., 49°53′ W.; depth 115 m.; dynamic height 971.100.

Observed values			Scaled values			
Depth, meters	Temperature, °C.	Salinity, °/oo	Depth, meters	Temperature, °C.	Salinity, °/oo	σt
0	10.43	31.68	0	10.43	31.68	24.32
26	1.30	32.74	25	2.00	32.70	26.15
52	−1.14	33.12	50	−1.10	33.10	26.63
79	−0.69	33.37	75	−0.75	33.34	26.82
105	−0.56	33.58	100	−0.60	33.54	26.97

Station 6543; 24 July; 47°56.5′ N., 49°49′ W.; depth 169 m.; dynamic height 971.104.

Observed values			Scaled values			
Depth, meters	Temperature, °C.	Salinity, °/oo	Depth, meters	Temperature, °C.	Salinity, °/oo	σt
0	9.64	31.89	0	9.64	31.89	24.61
25	2.50	32.68	25	2.50	32.68	26.10
50	1.41	33.25	50	1.41	33.25	26.64
75	−0.98	33.23	75	−0.98	33.23	26.74
101	−1.04	33.33	100	−1.05	33.32	26.81
151	−0.23	33.72	150	−0.25	33.71	27.10

Station 6544; 24 July; 48°13′ N., 49°44′ W.; depth 220 m.; dynamic height 971.096.

Observed values			Scaled values			
Depth, meters	Temperature, °C.	Salinity, °/oo	Depth, meters	Temperature, °C.	Salinity, °/oo	σt
0	10.32	31.28	0	10.32	31.28	24.02
25	0.03	32.90	25	0.03	32.90	26.43
51	−1.15	33.10	50	−1.15	33.09	26.63
76	−1.33	33.22	75	−1.35	33.21	26.74
102	−1.05	33.41	100	−1.10	33.39	26.87
152	−0.30	33.80	150	−0.35	33.78	27.15
203	1.85	34.38	200	1.70	34.35	27.49

Station 6545; 24 July; 48°36.5′ N., 49°38′ W.; depth 622 m.; dynamic height 971.033.

Observed values			Scaled values			
Depth, meters	Temperature, °C.	Salinity, °/oo	Depth, meters	Temperature, °C.	Salinity, °/oo	σt
0	10.33	32.54	0	10.35	32.54	25.00
25	2.59	33.37	25	2.59	33.37	26.64
51	1.79	33.53	50	1.85	33.53	26.83
76	−0.02	33.76	75	0.00	33.75	27.12
102	1.10	34.02	100	1.10	34.00	27.26
152	1.17	34.20	150	1.15	34.19	27.40
204	2.24	34.41	200	2.15	34.40	27.50
306	3.58	34.66	300	3.55	34.65	27.57
392	3.59	34.69	400	3.60	34.69	27.60
583	3.26	34.68	600	3.25	34.68	27.62

Station 6546; 24 July; 48°43.5′ N., 49°34′ W.; depth 1,088 m.; dynamic height 970.991.

Observed values			Scaled values			
Depth, meters	Temperature, °C.	Salinity, °/oo	Depth, meters	Temperature, °C.	Salinity, °/oo	σt
0	9.23	32.70	0	9.23	32.70	25.31
25	0.80	33.45	25	0.80	33.45	26.83
50	−0.83	33.57	50	−0.83	33.57	27.01
75	1.11	33.93	75	1.11	33.93	27.20
99	1.12	34.00	100	1.15	34.00	27.25
149	2.44	34.36	150	2.45	34.36	27.44
199	3.26	34.58	200	3.25	34.58	27.54
298	3.96	34.75	300	3.95	34.75	27.61
386	3.83	34.74	400	3.85	34.74	27.61
583	3.95	34.80	600	3.95	34.81	27.66
783	3.56	34.84	800	3.55	34.84	27.72
977	3.39	34.85	1,000	3.40	34.85	27.75

Station 6547; 24 July; 49°08.5′ N., 49°20′ W.; depth 1,646 m.; dynamic height 970.891.

Observed values			Scaled values			
Depth, meters	Temperature, °C.	Salinity, °/oo	Depth, meters	Temperature, °C.	Salinity, °/oo	σt
0	8.85	33.73	0	8.85	33.73	26.17
24	5.72	34.59	25	5.55	34.59	27.30
48	4.10	34.57	50	4.10	34.57	27.46
72	4.42	34.69	75	4.35	34.69	27.52
95	3.87	34.68	100	3.85	34.68	27.56
143	3.75	34.72	150	3.75	34.73	27.61
191	3.89	34.76	200	3.90	34.77	27.64
286	3.79	34.81	300	3.80	34.81	27.68
405	3.76	34.83	400	3.75	34.83	27.69
608	3.48	34.83	600	3.50	34.83	27.72
811	3.27	34.825	800	3.30	34.83	27.74
1,014	3.31	34.84	1,000	3.30	34.84	27.75
1,523	3.36	34.87				

Station 6548; 24 July; 49°34′ N., 49°09′ W.; depth 1,737 m.; dynamic height 970.882.

Observed values			Scaled values			
Depth, meters	Temperature, °C.	Salinity, °/oo	Depth, meters	Temperature, °C.	Salinity, °/oo	σt
0	10.02	34.31	0	10.02	34.31	26.44
25	7.04	34.58	25	7.04	34.58	27.10
50	4.52	34.61	50	4.52	34.61	27.44
74	3.76	34.63	75	3.75	34.63	27.53
99	3.61	34.71	100	3.60	34.71	27.62
149	3.61	34.74	150	3.60	34.74	27.64
198	3.65	34.78	200	3.65	34.78	27.66
297	3.62	34.80	300	3.60	34.80	27.69
379	3.50	34.87	400	3.50	34.82	27.72
570	3.34	34.82	600	3.35	34.82	27.73
761	3.34	34.83	800	3.35	34.83	27.73
956	3.30	34.825	1,000	3.30	34.83	27.74
1,450	3.34	34.87				

Station 6549; 25 July; 50°01′ N., 48°58′ W.; depth 1,847 m.; dynamic height 970.893.

Observed values			Scaled values			
Depth, meters	Temperature, °C.	Salinity, °/oo	Depth, meters	Temperature, °C.	Salinity, °/oo	σt
0	10.04	34.42	0	10.04	34.42	26.51
25	7.26	34.60	25	7.26	34.60	27.09
50	4.57	34.58	50	4.57	34.58	27.41
75	3.70	34.54	75	3.70	34.54	27.47
100	3.56	34.61	100	3.56	34.61	27.54
150	3.81	34.74	150	3.81	34.74	27.62
200	3.89	34.78	200	3.89	34.78	27.64
300	3.78	34.81	300	3.78	34.81	27.68
404	3.63	34.83	400	3.65	34.83	27.70
609	3.47	34.84	600	3.50	34.84	27.73
814	3.35	34.83	800	3.35	34.83	27.73
1,018	3.34	34.85	1,000	3.35	34.85	27.75
1,534	3.35	34.87				

TABLE OF OCEANOGRAPHIC DATA—Continued
STATIONS OCCUPIED IN 1957—Continued

Station 6550; 26 July; 53°43.5′ N., 55°48′ W.; depth 114 m.; dynamic height 1937.727.

Observed values			Scaled values			
Depth, meters	Temperature, °C.	Salinity, °/oo	Depth, meters	Temperature, °C.	Salinity, °/oo	σ_t
0	5.91	25.53	0	5.91	25.53	20.13
25	−1.66	32.36	25	−1.66	32.36	26.05
50	−1.70	32.72	50	−1.70	32.72	26.35
76	−1.68	32.82	75	−1.70	32.82	26.43
101	−1.63	32.94	100	−1.65	32.93	26.51

Station 6551; 26 July; 53°51.5′ N., 55°32′ W.; depth 206 m.; dynamic height 1937.673.

Observed values			Scaled values			
Depth, meters	Temperature, °C.	Salinity, °/oo	Depth, meters	Temperature, °C.	Salinity, °/oo	σ_t
0	2.80	28.72	0	2.80	28.72	22.92
26	−1.20	32.34	25	−1.15	32.20	25.91
51	−1.57	32.92	50	−1.55	32.91	26.50
77	−1.29	33.14	75	−1.30	33.13	26.66
102	−1.46	33.26	100	−1.45	33.25	26.76
153	−1.36	33.40	150	−1.40	33.39	26.88
194	−0.56	33.78	(200)	−0.45	33.85	27.22

Station 6552; 26 July; 53°57′ N., 55°22′ W.; depth 169 m.; dynamic height 1937.636.

Observed values			Scaled values			
Depth, meters	Temperature, °C.	Salinity, °/oo	Depth, meters	Temperature, °C.	Salinity, °/oo	σ_t
0	2.96	30.05	0	2.96	30.05	23.97
25	−1.28	32.60	25	−1.28	32.60	26.24
51	−1.60	32.86	50	−1.60	32.86	26.46
76	−1.49	33.17	75	−1.50	33.16	26.69
102	−1.30	33.37	100	−1.35	33.36	26.85
153	−0.71	33.74	150	−0.75	33.72	27.13

Station 6553; 26 July; 54°07.5′ N., 55°02′ W.; depth 167 m.; dynamic height 1937.602.

Observed values			Scaled values			
Depth, meters	Temperature, °C.	Salinity, °/oo	Depth, meters	Temperature, °C.	Salinity, °/oo	σ_t
0	5.54	31.08	0	5.54	31.08	24.54
26	−0.21	33.05	25	−0.10	32.97	26.49
52	−1.18	33.33	50	−1.15	33.31	26.81
78	−1.29	33.50	75	−1.30	33.48	26.95
104	−1.22	33.57	100	−1.25	33.56	27.02
156	−0.59	33.81	150	−0.70	33.78	27.17

Station 6554; 26 July; 54°14.5′ N., 54°50′ W.; depth 183 m.; dynamic height 1937.604.

Observed values			Scaled values			
Depth, meters	Temperature, °C.	Salinity, °/oo	Depth, meters	Temperature, °C.	Salinity, °/oo	σ_t
0	5.25	31.33	0	5.25	31.33	24.77
25	−1.15	32.92	25	−1.15	32.92	26.49
51	−1.42	33.20	50	−1.40	33.18	26.71
76	−1.18	33.39	75	−1.20	33.38	26.87
101	−1.28	33.55	100	−1.30	33.54	27.00
152	−0.77	33.78	150	−0.85	33.77	27.17

Station 6555; 26 July; 54°29′ N., 54°24′ W.; depth 214 m.; dynamic height 1937.628.

Observed values			Scaled values			
Depth, meters	Temperature, °C.	Salinity, °/oo	Depth, meters	Temperature, °C.	Salinity, °/oo	σ_t
0	4.09	30.60	0	4.09	30.60	24.30
25	−0.79	32.45	25	−0.79	32.45	26.10
50	−1.31	33.06	50	−1.31	33.06	26.61
75	−1.28	33.32	75	−1.28	33.32	26.82
100	−1.25	33.48	100	−1.25	33.48	26.95
151	−0.92	33.68	150	−0.95	33.68	27.10
201	−0.18	33.91	200	−0.20	33.90	27.25

Station 6556; 26 July; 54°45′ N., 53°51′ W.; depth 322 m.; dynamic height 1937.614.

Observed values			Scaled values			
Depth, meters	Temperature, °C.	Salinity, °/oo	Depth, meters	Temperature, °C.	Salinity, °/oo	σ_t
0	4.72	30.36	0	4.72	30.36	24.06
25	−1.84	32.19	25	1.84	32.19	25.76
51	−0.36	33.35	50	−0.35	33.31	26.77
76	−0.16	33.64	75	−0.15	33.64	27.04
102	−0.89	33.66	100	−0.90	33.66	27.09
152	0.04	33.90	150	0.00	33.89	27.23
203	1.19	34.14	200	1.15	34.13	27.35
305	3.65	34.63	300	3.50	34.60	27.54

Station 6557; 26 July; 54°52′ N., 53°37′ W.; depth 622 m.; dynamic height 1937.545.

Observed values			Scaled values			
Depth, meters	Temperature, °C.	Salinity, °/oo	Depth, meters	Temperature, °C.	Salinity, °/oo	σ_t
0	6.46	31.24	0	6.46	31.24	24.56
25	−0.11	33.30	25	−0.11	33.30	26.75
51	−0.63	33.66	50	−0.60	33.65	27.06
77	−0.51	33.74	75	−0.55	33.73	27.12
103	−0.03	33.89	100	−0.10	33.87	27.22
153	2.03	34.29	150	1.90	34.27	27.42
204	3.13	34.50	200	3.05	34.49	27.49
307	4.24	34.74	300	4.20	34.73	27.57
402	4.31	34.81	400	4.30	34.81	27.63
602	4.13	34.84	600	4.15	34.84	27.66

Station 6558; 26 July; 54°59′ N., 53°23′ W.; depth 1,554 m.; dynamic height 1937.466.

Observed values			Scaled values			
Depth, meters	Temperature, °C.	Salinity, °/oo	Depth, meters	Temperature, °C.	Salinity, °/oo	σ_t
0	4.25	32.28	0	4.25	32.28	25.62
25	1.19	33.74	25	1.19	33.74	27.04
50	0.75	33.94	50	0.75	33.94	27.23
75	1.78	34.16	75	1.78	34.16	27.34
100	1.77	34.26	100	1.77	34.26	27.42
150	3.51	34.54	150	3.51	34.54	27.49
201	3.65	34.66	200	3.65	34.66	27.57
301	4.64	34.84	300	4.65	34.84	27.61
400	4.15	34.81	400	4.15	34.81	27.64
599	3.83	34.84	600	3.85	34.84	27.69
799	3.70	34.85	800	3.70	34.85	27.72
998	3.46	34.845	1,000	3.45	34.85	27.74
1,495	3.66	34.87	1,500	3.65	34.87	27.74

Station 6559; 26 July; 55°01.5′ N., 53°14′ W.; depth 2,149 m.; dynamic height 1937.397.

Observed values			Scaled values			
Depth, meters	Temperature, °C.	Salinity, °/oo	Depth, meters	Temperature, °C.	Salinity, °/oo	σ_t
0	6.11	32.54	0	6.11	32.54	25.63
25	2.75	34.06	25	2.75	34.06	27.18
50	1.78	34.20	50	1.78	34.20	27.37
75	2.32	34.35	75	2.32	34.35	27.45
100	3.11	34.52	100	3.11	34.52	27.51
150	3.29	34.62	150	3.29	34.62	27.58
201	3.96	34.76	200	3.95	34.76	27.62
301	4.04	34.80	300	4.05	34.80	27.64
378	4.04	34.84	400	4.00	34.84	27.68
570	3.36	34.805	600	3.35	34.81	27.72
764	3.36	34.825	800	3.40	34.84	27.74
960	3.51	34.87	1,000	3.50	34.87	27.76
1,452	3.35	34.875	1,500	3.35	34.88	27.77
1,950	3.24	34.90	(2,000)	3.25	34.90	27.80

TABLE OF OCEANOGRAPHIC DATA—Continued

STATIONS OCCUPIED IN 1957—Continued

Station 6560; 27 July; 55°10.5′ N., 52°52′ W.; depth 3,017 m.; dynamic height 1937.371.

Observed values			Scaled values			
Depth, meters	Temperature, °C.	Salinity, ‰	Depth, meters	Temperature, °C.	Salinity, ‰	σ_t
0	6.87	33.83	0	6.87	33.83	26.54
25	3.14	34.16	25	3.14	34.16	27.22
50	2.35	34.33	50	2.35	34.33	27.42
75	2.58	34.46	75	2.58	34.46	27.51
100	3.42	34.63	100	3.42	34.63	27.57
150	4.16	34.77	150	4.16	34.77	27.61
199	3.89	34.77	200	3.90	34.77	27.64
299	3.94	34.81	300	3.95	34.81	27.66
403	3.95	34.85	400	3.95	34.85	27.69
607	3.69	34.85	600	3.70	34.85	27.72
811	3.63	34.87	800	3.60	34.87	27.75
1,017	3.49	34.87	1,000	3.50	34.87	27.76
1,528	3.35	34.88	1,500	3.35	34.88	27.77
2,039	3.11	34.90	2,000	3.15	34.90	27.81
2,492	2.67	34.895	2,500	2.65	34.89	27.85
2,911	1.81	34.88	(3,000)	1.60	34.88	27.92

Station 6561; 27 July; 55°29′ N., 52°22′ W.; depth 3,292 m.; dynamic height 1937.359.

Observed values			Scaled values			
Depth, meters	Temperature, °C.	Salinity, ‰	Depth, meters	Temperature, °C.	Salinity, ‰	σ_t
	7.14	34.10	0	7.14	34.10	26.71
25	5.69	34.22	25	5.69	34.22	27.00
50	3.47	34.49	50	3.47	34.49	27.45
75	3.23	34.55	75	3.23	34.55	27.52
99	3.60	34.68	100	3.60	34.68	27.59
149	3.45	34.78	150	3.45	34.73	27.64
199	3.40	34.76	200	3.40	34.76	27.68
298	3.31	34.78	300	3.30	34.78	27.70
392	3.36	34.80	400	3.40	34.80	27.71
591	3.55	34.86	600	3.55	34.86	27.74
792	3.41	34.85	800	3.40	34.85	27.75
995	3.38	34.855	1,000	3.40	34.86	27.76
1,499	3.36	34.87	1,500	3.40	34.87	27.77
2,003	3.29	34.90	2,000	3.30	34.90	27.80
2,481	2.93	34.905	2,500	2.90	34.90	27.84
2,976	2.21	34.88	3,000	2.15	34.88	27.88
3,176	1.64	34.87				

Station 6562; 27 July; 55°54′ N., 51°39′ W.; depth 3,517 m.; dynamic height 1937.369.

Observed values			Scaled values			
Depth, meters	Temperature, °C.	Salinity, ‰	Depth, meters	Temperature, °C.	Salinity, ‰	σ_t
0	8.21	34.49	0	8.21	34.49	26.86
25	6.92	34.47	25	6.92	34.47	27.03
50	4.30	34.64	50	4.30	34.64	27.49
75	3.68	34.68	75	3.68	34.68	27.58
100	3.56	34.74	100	3.56	34.74	27.64
150	3.35	34.76	150	3.35	34.76	27.68
201	3.24	34.765	200	3.25	34.76	27.69
301	3.30	34.795	300	3.30	34.79	27.71
402	3.21	34.79	400	3.20	34.79	27.72
607	3.14	34.80	600	3.15	34.80	27.73
814	3.18	34.82	800	3.15	34.82	27.745
1,023	3.25	34.83	1,000	3.25	34.83	27.745
1,535	3.29	34.83	1,500	3.30	34.83	27.745
2,047	3.40	34.88	2,000	3.40	34.88	27.77
2,483	3.41	34.90	2,500	3.40	34.90	27.79
2,997	2.69	34.90	3,000	2.70	34.90	27.85
3,517	1.62	34.86	3,500	1.65	34.86	27.91

Station 6563; 27 July; 56°31.5′ N., 50°38′ W.; depth 3,695 m.; dynamic height 1937.371.

Observed values			Scaled values			
Depth, meters	Temperature, °C.	Salinity, ‰	Depth, meters	Temperature, °C.	Salinity, ‰	σ_t
0	8.23	34.55	0	8.23	34.55	26.90
25	6.67	34.58	25	6.67	34.58	27.15
50	4.20	34.63	50	4.20	34.63	27.49
75	3.77	34.64	75	3.77	34.64	27.54
100	3.33	34.68	100	3.33	34.68	27.62
150	3.43	34.74	150	3.43	34.74	27.66
199	3.35	34.77	200	3.35	34.77	27.69
299	3.22	34.78	300	3.20	34.78	27.71
390	3.17	34.795	400	3.20	34.79	27.72
589	3.14	34.79	600	3.15	34.79	27.72
792	3.16	34.805	800	3.15	34.81	27.74
998	3.22	34.82	1,000	3.25	34.82	27.74
1,498	3.27	34.835	1,500	3.30	34.84	27.75
1,999	3.39	34.88	2,000	3.40	34.88	27.77
2,477	3.40	34.90	2,500	3.40	34.90	27.79
2,976	2.82	34.90	3,000	2.75	34.90	27.85
3,476	1.78	34.865	3,500	1.75	34.865	27.90
3,578	1.72	34.865				

Station 6564; 28 July; 57°03.5′ N., 49°32′ W.; depth 3,695 m.; dynamic height 1937.357.

Observed values			Scaled values			
Depth, meters	Temperature, °C.	Salinity, ‰	Depth, meters	Temperature, °C.	Salinity, ‰	σ_t
0	7.88	34.56	0	7.88	34.56	26.96
25	6.62	34.60	25	6.62	34.60	27.18
50	4.34	34.64	50	4.34	34.64	27.48
75	3.84	34.66	75	3.84	34.66	27.55
100	3.34	34.70	100	3.34	34.70	27.63
150	3.26	34.75	150	3.26	34.75	27.68
201	3.21	34.76	200	3.20	34.76	27.70
301	3.13	34.79	300	3.15	34.79	27.72
402	3.13	34.79	400	3.15	34.79	27.72
604	3.09	34.80	600	3.10	34.80	27.74
805	3.22	34.80	800	3.20	34.80	27.73
1,007	3.28	34.83	1,000	3.30	34.83	27.74
1,509	3.34	34.87	1,500	3.35	34.87	27.77
2,012	3.40	34.885	2,000	3.40	34.88	27.77
2,514	3.15	34.90	2,500	3.20	34.90	27.81
3,009	2.78	34.91	3,000	2.80	34.91	27.85
3,500	1.86	34.87	3,500	1.86	34.87	27.90
3,597	1.70	34.87				

Station 6565; 28 July; 57°36.5′ N., 48°25′ W.; depth 3,493 m.; dynamic height 1937.359.

Observed values			Scaled values			
Depth, meters	Temperature, °C.	Salinity, ‰	Depth, meters	Temperature, °C.	Salinity, ‰	σ_t
0	8.36	34.57	0	8.36	34.57	26.91
25	6.13	34.60	25	6.13	34.60	27.24
50	4.40	34.66	50	4.40	34.66	27.49
75	3.74	34.68	75	3.74	34.68	27.57
100	3.65	34.74	100	3.65	34.74	27.63
150	3.59	34.77	150	3.59	34.77	27.67
199	3.86	34.83	200	3.85	34.83	27.68
299	3.36	34.79	300	3.35	34.79	27.70
500	3.31	34.81	400	3.35	34.80	27.71
698	3.21	34.82	600	3.25	34.82	27.74
898	3.20	34.82	800	3.20	34.82	27.745
1,097	3.27	34.835	1,000	3.25	34.83	27.745
1,596	3.34	34.86	1,500	3.35	34.86	27.76
1,992	3.38	34.89	2,000	3.40	34.89	27.78
2,473	3.05	34.905	2,500	3.05	34.90	27.82
2,946	2.61	34.90	3,000	2.55	34.90	27.87
3,320	1.80	34.87				

TABLE OF OCEANOGRAPHIC DATA—Continued

STATIONS OCCUPIED IN 1957—Continued

Station 6566; 28 July; 58°09.5′ N., 47°13′ W.; depth 3,200 m.; dynamic height 1937.355.

Observed values			Scaled values			
Depth, meters	Temperature, °C.	Salinity, °/oo	Depth, meters	Temperature, °C.	Salinity, °/oo	σt
0	8.91	34.58	0	8.91	34.58	26.83
25	6.16	34.60	25	6.16	34.60	27.24
50	4.47	34.68	50	4.47	34.68	27.50
75	4.22	34.70	75	4.22	34.70	27.54
100	4.04	34.74	100	4.04	34.74	27.59
150	3.97	34.80	150	3.97	34.80	27.65
200	4.20	34.86	200	4.20	34.86	27.68
300	3.91	34.865	300	3.91	34.865	27.71
397	3.61	34.84	400	3.60	34.84	27.72
601	3.42	34.84	600	3.40	34.84	27.74
805	3.16	34.81	800	3.15	34.81	27.74
1,015	3.28	34.835	1,000	3.30	34.83	27.74
1,518	3.31	34.86	1,500	3.30	34.86	27.77
2,019	3.24	34.89	2,000	3.25	34.89	27.79
2,486	2.87	34.91	2,500	2.85	34.91	27.85
2,966	2.02	34.875	3,000	1.90	34.87	27.90
3,087	1.56	34.85				

Station 6567; 28 July; 58°40.5′ N., 46°10′ W.; depth 2,579 m.; dynamic height 1937.350.

Observed values			Scaled values			
Depth, meters	Temperature, °C.	Salinity, °/oo	Depth, meters	Temperature, °C.	Salinity, °/oo	σt
0	7.82	34.61	0	7.82	34.61	27.01
25	5.43	34.62	25	5.43	34.62	27.34
50	4.96	34.70	50	4.96	34.70	27.46
75	4.55	34.77	75	4.55	34.77	27.56
100	4.35	34.74	100	4.35	34.74	27.56
150	4.05	34.81	150	4.05	34.81	27.65
199	4.07	-------	200	4.05	34.83	27.66
299	4.00	34.86	300	4.00	34.86	27.70
402	3.64	34.83	400	3.65	34.83	27.70
602	3.48	34.83	600	3.45	34.83	27.72
802	3.41	34.845	800	3.40	34.84	27.74
1,000	3.40	34.855	1,000	3.40	34.86	27.76
1,502	3.34	34.885	1,500	3.35	34.88	27.77
2,005	3.01	34.90	2,000	3.05	34.90	27.82
2,521	2.10	34.85	2,500	2.15	34.85	27.86

Station 6568; 29 July; 58°58.5′ N., 45°26′ W.; depth 2,469 m.; dynamic height 1937.339.

Observed values			Scaled values			
Depth, meters	Temperature, °C.	Salinity, °/oo	Depth, meters	Temperature, °C.	Salinity, °/oo	σt
0	8.05	34.70	0	8.05	34.70	27.05
25	6.73	34.65	25	6.73	34.65	27.20
50	5.31	34.72	50	5.31	34.72	27.44
75	4.87	34.85	75	4.87	34.85	27.59
100	4.68	34.87	100	4.68	34.87	27.63
150	4.47	34.88	150	4.47	34.88	27.66
199	4.28	34.875	200	4.25	34.87	27.68
299	3.90	34.85	300	3.90	34.85	27.70
402	3.80	34.85	400	3.80	34.85	27.70
604	3.40	34.83	600	3.40	34.83	27.73
806	3.37	34.84	800	3.35	34.84	27.74
1,008	3.45	34.865	1,000	3.45	34.86	27.75
1,508	3.28	34.885	1,500	3.30	34.88	27.78
2,003	2.88	34.895	2,000	2.90	34.89	27.83
2,417	1.91	34.87				

Station 6569; 29 July; 59°11.5′ N., 44°57′ W.; depth 2,103 m.; dynamic height 1937.382.

Observed values			Scaled values			
Depth, meters	Temperature, °C.	Salinity, °/oo	Depth, meters	Temperature, °C.	Salinity, °/oo	σt
0	8.25	34.71	0	8.25	34.71	27.03
25	7.80	34.75	25	7.80	34.75	27.13
50	7.68	34.76	50	7.66	34.76	27.15
75	7.06	34.80	75	7.06	34.80	27.27
100	5.59	34.83	100	5.59	34.83	27.49
150	5.17	34.90	150	5.17	34.90	27.60
200	4.99	34.93	200	4.99	34.93	27.64
300	4.69	34.92	300	4.69	34.92	27.67
401	4.42	-------	400	4.45	34.90	27.68
602	3.83	34.87	600	3.85	34.87	27.72
804	3.70	34.88	800	3.70	34.88	27.74
1,006	3.53	34.88	1,000	3.55	34.88	27.75
1,508	3.32	34.88	1,500	3.35	34.88	27.77
2,009	2.60	34.86	2,000	2.60	34.86	27.83

Station 6570; 29 July; 59°25′ N., 44°29′ W.; depth 1,079 m.; dynamic height 1937.498.

Observed values			Scaled values			
Depth, meters	Temperature, °C.	Salinity, °/oo	Depth, meters	Temperature, °C.	Salinity, °/oo	σt
0	2.63	31.65	0	2.63	31.65	25.27
25	5.44	34.27	25	5.44	34.27	27.07
50	6.96	34.75	50	6.96	34.75	27.24
75	7.11	34.85	75	7.11	34.85	27.31
100	6.92	34.92	100	6.92	34.92	27.39
150	6.29	34.98	150	6.29	34.98	27.52
200	6.05	34.99	200	6.05	34.99	27.56
300	5.98	35.00	300	5.98	35.00	27.57
392	5.26	34.935	400	5.25	34.93	27.61
600	4.87	34.92	600	4.85	34.92	27.65
816	4.66	34.90	800	4.70	34.90	27.65
1,006	4.26	34.885	1,000	4.25	34.89	27.69

Station 6571; 29 July; 59°34.5′ N., 44°14′ W.; depth 172 m.; dynamic height 1937.702.

Observed values			Scaled values			
Depth, meters	Temperature, °C.	Salinity, °/oo	Depth, meters	Temperature, °C.	Salinity, °/oo	σt
0	0.22	29.25	0	0.22	29.25	23.49
25	−0.02	32.35	25	−0.02	32.35	26.00
49	−0.72	32.88	50	−0.75	32.89	26.45
74	−0.84	33.18	75	−0.85	33.19	26.70
98	0.23	33.44	100	0.05	33.49	26.91
147	5.99	34.49	(150)	6.25	34.56	27.19

Station 6572; 29 July; 59°41′ N., 43°58′ W.; depth 148 m.; dynamic height 1937.756.

Observed values			Scaled values			
Depth, meters	Temperature, °C.	Salinity, °/oo	Depth, meters	Temperature, °C.	Salinity, °/oo	σt
0	1.22	29.20	0	1.22	29.20	23.41
24	0.28	31.04	25	0.20	31.09	24.97
47	−0.76	32.30	50	−0.85	32.47	26.12
71	−1.06	32.90	75	−1.05	32.94	26.51
95	−1.06	33.05	100	−1.00	33.08	26.61
128	−0.09	33.38	(150)	0.90	33.71	27.04

GPO 869798

Contribution No. 960

Reprinted from COPEIA, 1958, No. 3, pp. 234–235, August 28
Printed in U. S. A.

A SUMMER SILENCE OF SEA ROBINS, *PRIONOTUS* SPP.—A conclusion that sea robins (*Prionotus evolans* Linnaeus and *P. carolinus* Linnaeus) produce two different calls is based partly on indirect evidence (Moulton, 1956, Biol. Bull., 111: 393–8). The staccato call thought to characterize the breeding season of these fish at Woods Hole, Massachusetts, has not been heard from captive specimens, although it is thought to be spontaneously produced by individuals of a large group of the two species in a live car. The characteristic and more familiar grunts of these species are readily elicited and are often produced spontaneously in captivity. Anatomical considerations, sounds obtained on physiological stimulation of the air bladder muscles, data on the sounds of other kinds of fishes, and extensive sampling of the summer fish population in Great Harbor, Woods Hole, have indicated that male and female sea robins are responsible for staccato calls recorded and studied extensively at Woods Hole during the summers of 1954 and 1955. The most interesting aspect of this latter calling is the possibility of eliciting it by playing into the water imitations and recordings of the call (Moulton, 1955, Bull. Ecol. Soc. Amer., 36: 80; 1956; Moulton and Backus, 1955, Fish. Circ. 17, Me. Dept. Fisheries).

In 1954 and 1955, staccato calls were heard on every day of listening from August 10, 1954, when the first calls of the summer were heard, to August 25, and July 5 to August 30, 1955. The author was away from Woods Hole during the summer of 1956, and returned to the problem of these calls, in connection with other work, in 1957. From June 26 to the last week in August 1957, a single staccato call was heard on the morning of July 22, contrasted with hundreds during equivalent listening of the other summers. The single call followed immediately upon the playing into the water of a signal like those eliciting calling during the other summers. No spontaneous calls were heard during extensive listening periods throughout the summer of 1957.

While sea robins are ordinarily so abundant in Great Harbor during the summer months as to lend doubt to the possibility of their scarcity in 1957, this tentative conclusion seems merited. Although the raft from which listening was performed was anchored in a different position in 1957 than during 1954 and 1955, all three positions were within a radius of 250 yards from a common center, and the depth varied from 54 to 70 feet, with the 1955 position being intermediate. It seems unlikely that change in position alone furnishes an explanation for the absence of staccato calls in 1957.

A more reasonable explanation would seem to lie in the possible absence in 1957 of a breeding population of sea robins in Great Harbor. Fishing from the raft during extensive periods on two weekend occasions failed to raise sea robins by techniques usually successful in obtaining them; conversation with personnel of the supply department of the Marine Biological Laboratory indicated that several kinds of fishes ordinarily common close to shore were difficult to obtain last summer; this evidence and that of local fishermen have indicated that adult sea robins were not commonly caught in Great Harbor nor close to shore generally in the Woods Hole area last summer, despite the fact that during the last half of August young sea robins of between 1½ and 3 inches were common in shallow water off Nobska Beach, facing on Vineyard Sound. While the drought of the early part of the summer of 1957 may be related to a scarcity of sea robins in Great Harbor during July and August, a more likely explanation may lie with unusually high water temperatures at Woods Hole last summer.

Records obtained from Dean Bumpus have shown that from January on in 1957, January being an exception, the mean monthly water temperatures were above 70 year means for the Woods Hole area (Bumpus, 1957, USFW Serv. Spec. Sci. Rep., Fish., No. 214) and that in June, the mean monthly temperature was nearly

4 degrees C. (3.7) above the 70 year mean for that month. Fishing records and acoustical data seem to bear out the relative absence from Great Harbor during the summer of 1957, of a fish population apparently abundant there in 1954 and 1955.

Despite disappointing incidence of sea robin calling, and following the single reception of July 22, a trip was made to the summer's source of sea robin supply, the area between Menemsha Bight and Gayhead, Martha's Vineyard, on July 25 for underwater listening in an area where sea robins were then relatively abundant, to judge from dragger catches. Unfortunately an electronic difficulty and the noise of the several draggers then present over the fishing grounds prevented clear listening and recording, so results were inconclusive. Sea robins of both species contained in a live car hung from the raft in Great Harbor were in ripe condition until mid-August, yet no calling was heard before or subsequent to the single call of July 22, 1957.—JAMES M. MOULTON, *Bowdoin College, Brunswick, Maine, and the Woods Hole Oceanographic Institution, Woods Hole, Massachusetts.* Contribution No. 960 of the Woods Hole Oceanographic Institution.

Contribution No. 963

The Oceanographical Magazine
Vol. 10. No. 1 June 1958

The Response of a Stratified, Bounded Ocean to Variable Wind Stresses.*

By

Takashi ICHIYE**

1. *Introduction*

One of the most interesting and important problems in physical oceanography is to know how oceanic circulation responses to variable wind stresses. The author published a theory of time-dependent wind-driven circulation in a bounded ocean about seven years ago (ICHIYE, 1951), which was shown by Veronis and Morgan (1955) to be incorrect owing to the neglect of the divergence effect, and they gave a more complete theory including this effect. These works treated the problem in a homogeneous ocean. On the other hand, the density stratification is more or less important in the response problem, since in a stratified ocean internal mass adjustment may cause a different mode of motion from a homogeneous ocean. Recently two interesting papers of Charney (1955) and Veronis and Stommel (1956) have been published along this approach, treating a model of two-layered ocean without boundary, which are referred as Ch and VS hereafter. The present paper is only a trivial extension of these two works, just including a frictional force and west and east coast. The historical sketch of the problem and bibliography are given in VS.

Here we treat a two-layered ocean in β-plane with a east and west coast of straight line. As already pointed out in VS, the complete boundary condition, particularly at the west coast, should be non-linear, since inertia terms are predominant near the west coast, owing to a rapid change of vorticity in zonal direction, so that the linearized vorticity equation is no more valid there. However, such condition makes the mathematical treatment of the problem almost prohibitive. Therefore here we treat a simplified boundary condition of linear type and instead we introduce a frictional force. Such procedure might be permissible as the first step towards under-standing more realistic situation, as in the theory of stationary wind-driven oceanic circulation the frictional boundary solution still have a position as a simple picture of the first approximation about oceanic circulation instead of more reasonable inertia boundary theory.

---

* Woods Hole Oceanographic Institution Contribution No. 963

** Woods Hole Oceanographic Institution and also Japan Meteorological Agency

In fact, the introduction of the frictional force seems to be inevitable, so far as we assume that the linearized vorticity equation is valid even near the west coast, because if we neglect the friction in a ocean with east and west coast the boundary conditions at these two coasts give the solution wildly oscillating as indicated in a private manuscript of Dr. Munk (1957). In such situation, only an introduction of the friction makes the physical interpretation of the solution possible by decreasing the amplitude of such solution rapidly from the coast, as will be stated later.

2. *Derivation of the vorticity equations*

The model considered here is essentially the same as that used in Ch and VS, where it consists of two layers of homogeneous water separated by a surface of discontinuity wind stresses act as a body force only in the upper layer. Then the equations of motion and continuity in two layers are given by

$$\frac{\partial u}{\partial t}-fv=-g\frac{\partial(\eta+\eta')}{\partial x}+\frac{\tau_x}{H}+F_x \tag{2.1}$$

$$\frac{\partial v}{\partial t}+fu=-g\frac{\partial(\eta+\eta')}{\partial y}+\frac{\tau_y}{H}+F_y \tag{2.2}$$

$$\frac{\partial \eta}{\partial t}+H\left(\frac{\partial u}{\partial x}+\frac{\partial v}{\partial y}\right)=0 \tag{2.3}$$

$$\frac{\partial u'}{\partial t}-fv'=-g\frac{\partial(\varepsilon\eta+\eta')}{\partial x}+F_x' \tag{2.4}$$

$$\frac{\partial v'}{\partial t}+fu'=-g\frac{\partial(\varepsilon\eta+\eta')}{\partial y}+F_y' \tag{2.5}$$

$$\frac{\partial \eta'}{\partial t}+H'\left(\frac{\partial u'}{\partial x}+\frac{\partial v'}{\partial y}\right)=0 \tag{2.6}$$

where the terms with blime define the quantities in the lower layer and x and y are the horizontal coordinates, directed eastwards and northwards, respectively; H is the equilibrium thickness of the upper layer; η is the deviation of H; τ_x, τ_y are wind stress component; ε is the density ratio ρ/ρ'; and F_x, F_y are component of frictional force: and other quantities are defined by conventional symbols.

Cross differentiating (2.1) and (2.2) and (2.4) and (2.5), we obtain the vorticity equations

$$\frac{\partial\zeta}{\partial t}-\frac{f}{H}\frac{\partial}{\partial t}\eta+\beta v=\frac{1}{H}\operatorname{curl}\boldsymbol{\tau}+\operatorname{curl}\boldsymbol{F} \tag{2.7}$$

$$\frac{\partial\zeta'}{\partial t}-\frac{f}{H'}\frac{\partial}{\partial t}\eta'+\beta v'=\operatorname{curl}\boldsymbol{F}' \tag{2.8}$$

where $\zeta=\partial v/\partial x-\partial u/\partial y$.

In Ch velocity components are assumed to be given by geostrophic relationship. However, in this paper we derive symbolic expression for velocity components from the equations of motion, by putting

$$\boldsymbol{F}=-k\boldsymbol{v},\ \boldsymbol{F}=-k'\boldsymbol{v}'\,;\ \left(\frac{\partial}{\partial t}+k\right)=p,\ \left(\frac{\partial}{\partial t}+k'\right)=p'$$

where k and k' may be taken as a linear operator, which indicates horizontal eddy viscosity term and/or a frictional coefficient simply proportional to the velocity itself such as $-A\nabla^2+k$ and p, p' are linear operator. Then, eliminating v or u from (2.1) and (2.2) or from (2.4) and (2.5), we obtain

$$(p^2+f^2)\,u=pH_x+fH_y \tag{2.9}$$

$$(p^2+f^2)\,v=pH_y-fH_x \tag{2.10}$$

$$(p'^2+f^2)\,u'=p'H_\lambda'+fH_y' \tag{2.11}$$

$$(p'^2+f^2)\,v'=p'H_y'-fH_x' \tag{2.12}$$

where

$$H_x=-g\frac{\partial(\eta+\eta')}{\partial x}+\frac{\tau_x}{H},\quad H_y=-g\frac{\partial(\eta+\eta')}{\partial y}+\frac{\tau_y}{H}$$

$$H_x'=-g\frac{\partial(\varepsilon\eta+\eta')}{\partial x},\quad H_y'=-g\frac{\partial(\varepsilon\eta+\eta')}{\partial y}$$

When we assume that the period of the motion is longer than several days and the coefficient of friction has the similar order of magnitude to such period, then the ratio of p or p' to f is less than 0.1, since $p\sim p'<10^{-5}$. Hereafter we shall make it a rule to neglect the terms of the order less than 10^{-2} of main terms, then we can neglect p^2 and p'^2 in the left hand side of the equations (2.9) to (2.12). Thus we can obtain ζ by use of (2.9) to (2.12) as

$$\zeta=\frac{g}{fH}\left(\nabla^2\overline{\eta+\eta'}-\frac{1}{g}\operatorname{div}\tau+\frac{p}{gf}\operatorname{curl}\tau\right)+\frac{\beta}{f^2}\left(H_y+\frac{2p}{f}H_x\right) \tag{2.13}$$

$$\zeta'=\frac{g}{fH'}(\nabla^2\overline{\varepsilon\eta+\eta'})+\frac{\beta}{f^2}\left(H_y'+\frac{2p'}{f}H_x'\right) \tag{2.14}$$

where the last two terms including β is originated from a result of taking into account of variation of f in differentiation with y, and the ratio of these terms to the ones corresponding to the geostrophic assumption is $\frac{\beta}{f^2H}\frac{\partial(\eta+\eta')}{\partial y} : \frac{g}{fH}\nabla^2\overline{\eta+\eta'} \sim \frac{\beta}{f}\left(\frac{\partial}{\partial y}\right)^{-1}$ which seems to be larger than 0.2 for a circulation with a dimension of larger than 1000 km or 10^8 cm, so that we retain them for some time.

When we put the equations for ζ and v into (2.7) and (2.8) and neglect the terms with a factor p^2/f^2, we obtain

$$\left(p\nabla^2-\frac{2p}{f}\beta\frac{\partial}{\partial y}+\beta\frac{\partial}{\partial x}\right)\overline{\eta+\eta'}-\frac{f^2}{gH}\frac{\partial}{\partial t}\eta=\frac{f}{gH}\left(\mathrm{curl}\,\tau+\frac{p}{f}\mathit{div}\,\tau\right.$$
$$\left.+\frac{\beta}{f}\tau_x-\frac{2\beta p}{f^2}\tau_y\right) \tag{2.15}$$

$$\left(p'\nabla^2-\frac{2p'}{f}\beta\frac{\partial}{\partial y}+\beta\frac{\partial}{\partial x}\right)\overline{\varepsilon\eta+\eta'}-\frac{f^2}{gH'}\frac{\partial}{\partial t}\eta'=0 \tag{2.16}$$

These are different from the original equations of Ch in term $\frac{2p}{f}\beta\frac{\partial}{\partial y}$ in the left hand side and in the last three terms for the disturbing force, which are all originated from derivation of velocity components different from geostrophic assumption.

In order to simplify the mathematical treatment hereafter, we assume that $k=k'$ which is defined as a numerical factor, and we separate the motion into a barotropic and baroclinic mode as in Ch and Vs. Then we obtain

$$\left(\frac{\partial}{\partial t}+k\right)\left(\nabla^2-2\frac{\beta}{\mathrm{f}}\frac{\partial}{\partial y}\right)R_j+\beta\frac{\partial R_j}{\partial x}-\lambda_j^{-2}\frac{\partial}{\partial t}R_j=\frac{f\sigma_j}{gH}F \tag{2.17}$$

where we put $F=\mathrm{curl}\,\tau+\frac{p}{f}\mathrm{div}\,\tau+\frac{\beta}{f}\tau_x-\frac{2\beta p}{f_2}\tau_y$ and $j=r$ or l, and almost similar symbols are used as in Ch, except suffix r and l defines the quantities associated to barotropic and baroclinic mode,. respectively and thus

$$\lambda_r^2=g(H+H')/f^2,\ \lambda_l^2=g'H/f^2,\ \sigma_r\doteqdot r,\ \sigma_l=-1,\ g'=g(\rho'-\rho)/\rho,\ r=H/H'$$

3. *Solution for moving wind stress in a bounded ocean*

As the simplest case of variable wind stress, suppose a wind system moving at a constant speed as a sine wave given by

$$F=F_0\cos(\nu t\pm\theta x)\sin\mu x \tag{3.1}$$

This kind of disturbing force seems to be most interesting, since any type of wind system might be obtained by a linear combination of such harmonic wave train.

When we assume the coasts at $x=a$ and $x=-a$, velocity components u and u' should vanish there. These boundary conditions are expressed in terms of R_j as

$$\text{at } x=\pm a;\ \frac{\partial R_j}{\partial y}+\frac{1}{f}\left(\frac{\partial}{\partial t}+k\right)\frac{\partial R_j}{\partial x}=\frac{\sigma_j}{gH}\left\{\tau_y+\frac{1}{f}\left(\frac{\partial}{\partial t}+k\right)\tau_x\right\} \tag{3.2}$$

As seen at once, these conditions are in homogeneous type, so that we have to divide the solution into two parts, in order to satisfy both the fundamental equation and boundary conditions. Therefore, we put $R=R_{\text{I}}+R_{\text{II}}$, where R_{I} and R_{II} satisfy next relations, respectively $O_f R_{\text{I}}=F_f$, $O_b R_{\text{I}}=O$; $O_f R_{\text{II}}=0$ $O_b R_{\text{II}}=F_b$ in which O_f and O_b are the operational form of the left hand side of the equation (2.17) and the boundary conditions (3.2), and F_f and F_b represents symbolically the right hand side of these relations.

First, we try to obtain the solution R_{I}, and for this purpose we put $F=F_0 k[(e^{i(vt+\theta x)+i\mu y}-e^{i(vt+\theta x)-i\mu y})/2i]$
and express the solution corresponding to the term with factor $e^{i\mu y}$ and $e^{-i\mu y}$as R_1 and R_2, respectively. Further when we put $R_s=K_s P_s(x)e^{ivt\pm i\mu y}$, then we obtain the solution of $P_s(x)$ which satisfy the next relation

$$K_s\left\{(i\nu+k)\left(P_{xx}-\mu^2 P\mp 2\frac{\beta}{f}i\mu P\right)+\beta P_x-i\lambda^{-2}\nu P\right\}=\frac{F_0 f6}{2gHi}e^{i\theta x} \tag{3.3}$$

such as

$$P_s=\frac{1}{2}(e^{i\theta x}+A_{1s}e^{i\delta_1 x}+A_{2s}e^{i\delta_2 x}),\ s=1, 2 \tag{3.4}$$

where

$$K_s=\frac{F_0 f\sigma}{gH\left\{(\nu-ik)\left(\theta^2+\mu^2\pm 2\frac{\beta}{f}\mu i\right)-\beta\theta+\lambda^{-2}\nu\right)} \tag{3.5}$$

and δ_1 and δ_2 are two roots of the characteristic equation

$$\delta^2-\frac{\beta}{\nu-ik}\delta+\frac{\lambda^{-2}\nu}{\nu-ik}+\mu^2\mp 2\frac{\beta}{f}\mu i=0 \tag{3.6}$$

and A_{1s} and A_{2s} are constants determined by the boundary conditions at $x=\pm a$, and the suffix $s=1$ and 2 define the quantities corresponding to upper and lower sign in equations (3.3), (3.5) and (3.6), respectively. Needless to say, σ and λ have the suffix r and l indicating barotropic or baroclinic mode, which are omitted here for avoiding confusion. The boundary conditions are now expressed by

at $$x=\pm a\,;\ e^{i\theta x}(1\pm q\theta i)+A_{1s}e^{i\delta_1 x}(1\pm q\delta_1 i)+A_{2s}e^{i\delta_2 x}(1\pm q\delta_2 i)=0 \qquad (3.7)$$

where $q=(\nu-ik)/f\mu$ and double signs correspond to suffix $s=1$ and 2.

Then the constants A_{1s} and A_{2s} are given by

$$A_{1s}=(1\pm q\theta i)\sin a(\delta_2-\theta)/(1\pm q\delta_1 i)\sin a(\delta_1-\delta_2)$$

$$A_{2s}=-(1\pm q\theta i)\sin a(\delta_1-\theta)/(1\pm q\delta_2 i)\sin a(\delta_1-\delta_2) \qquad (3.8)$$

which are the same explicit form for $s=1$ and 2, since the difference is included implicitely in δ_1 and δ_2. The resultant expression for R_{I} is given by

$$R_{\mathrm{I}}=\frac{1}{2}k\{K_1P_1(x)e^{i(\nu t+\mu y)}-K_2P_2(x)e^{i(\nu t-\mu y)}\} \qquad (3.9)$$

The difference between K_1 and K_2 or P_1 and P_2 exists in the term $2\frac{\beta}{f}\mu i$ in the equations (3.5) or (3.6), or in other words the ratio $2\frac{\beta}{fu}$ determines the importance of this term, which may be neglected for $\mu>10^{-7}$ or for wind stress with a dimension in y-direction smaller than $\pi\times10^2$ km according to the criterion stated above for neglecting p^2 against f^2. In such case the solution (3.9) is expressed simply by

$$R_{\mathrm{I}}=k\{iKe^{i\nu t}(e^{i\theta x}\sin\mu y+e^{i\delta_1 x}\overline{A_{11}e^{i\mu y}-A_{12}e^{-i\mu y}}+e^{i\delta_2 x}\overline{A_{21}e^{i\mu y}-A_{22}e^{-i\mu y}})\} \qquad (3.9a)$$

In any case, as shown in the equation for Ki in (3.5), the amplitude of the response of the ocean gives a resonance for some value of θ with positive value, or for the wave moving westwards, which was also pointed out in VS.

The solution R_{II} corresponding to the homogeneous fundamental equation and inhomogeneous boundary conditions is also expressed by the combination of two proper solutions of the equation (2.17) such as

$$R_{\mathrm{II}s}=(B_{1s}e^{i\delta_1 x}+B_{2s}e^{i\delta_2 x})e^{i(\nu t\pm\mu y)} \qquad (3.10)$$

assuming that

$$\frac{\sigma}{gH}(\tau_y+\frac{p}{f}\tau_x)_{x=\pm a}=i\mu T_s(\pm a)e^{i(\nu t\pm\mu y)} \qquad (3.11)$$

where the suffix $s=1$ or 2 corresponds to $e^{i\mu y}$ or ${}^{-i\mu y}$. The real value of the solution R_{II} may be obtained by taking the real or imaginary part of the combination of $R_{\mathrm{II}1}$ and $R_{\mathrm{II}2}$. For example, when the left hand side of the equation (3.11) is given as $\mu T\sin\nu t\cos\mu y$, then we take the imaginary part of $\frac{1}{2}(R_{\mathrm{II}1}-R_{\mathrm{II}2})$ for the real value of R_{II}. Therefore, here we give the value of the solution $R_{\mathrm{II}s}$ in the complex form. The boundary conditions at $x=\pm a$ becomes for the function given by (3.10)

$$(1+iq\delta_1)B_{1s}e^{i\delta_1 x}+(1+iq\delta_2)B_{2s}e^{i\delta_2 x}=T(\pm a) \tag{3.12}$$

then

$$\begin{aligned} B_{1s}&=\{T_s(a)e^{-i\delta_2 a}-T_s(-a)e^{i\delta_2 a}\}/2(1+iq\delta_1)\sin(\delta_1-\delta_2)a \\ B_{2s}&=\{T_s(-a)e^{i\delta_1 a}-T_s(a)e^{-i\delta_1 a}\}/2(1+iq\delta_2)\sin(\delta_1-\delta_2)a \end{aligned} \tag{3.13}$$

thus

$$\begin{aligned} R_{\text{II}s}=\frac{e^{i(\nu t\pm\mu y)}}{2\sin(\delta_1-\delta_2)a}\Big[&\frac{e^{i\delta_1 x}}{1+iq\delta_1}\{T_s(a)e^{-i\delta_2 a}-T_s(-a)e^{i\delta_2 a}\} \\ &+\frac{e^{i\delta_2 x}}{1+iq\delta_2}\{T_s(-a)e^{i\delta_1 a}-T_s(a)e^{-i\delta_1 a}\}\Big] \end{aligned} \tag{3.10a}$$

$$(s=1 \text{ and } 2)$$

The numerical examples of these solutions are given in the next section, and here only the estimation of the ratio of the order of R_{I} and R_{II} is stated. For complete discussion about the comparison of these two functions we have to know the behaviour of the functions regards to x, but this should be done in next section, and we cansider the ratio of the factor of $e^{i\delta_1 x}$ and $e^{i\delta_2 x}$ in both functions, which is given by

$$\begin{aligned} R_a=|B|:|KA|&\doteqdot\frac{\sigma|\boldsymbol{\tau}|}{|1+iq\delta||\sin(\delta_1-\delta_2)a|\mu gH}:\frac{f\sigma\operatorname{curl}\boldsymbol{\tau}|1+q\theta i||\sin a(\delta-\theta)|}{|1+iq\delta||\sin(\delta_1-\delta_2)a|IgH} \\ &\doteqdot|\boldsymbol{\tau}|I/\mu f\operatorname{curl}\boldsymbol{\tau} \end{aligned} \tag{3.14}$$

where

$$I_j=(\nu-ik)\left(\theta^2+\mu^2\pm2\frac{\beta}{f}\mu i\right)-\beta\theta+\lambda_j^{-2}\nu \tag{3.15}$$

On the other hand, assuming $\boldsymbol{\tau}\sim e^{i(\mu y+\theta x)}$ then $\operatorname{curl}\boldsymbol{\tau}\sim\boldsymbol{\tau}(|\mu|+|\theta)$. Thus we have $R_a\doteqdot I/\mu f(|\mu|+|\theta|)$. When we consider only the negative value of θ, we can avoid the resonance phenomenon and in such case I_j ranges from 10^{-19} to 10^{-21} for the range of ν from 10^{-5} to 10^{-8} and μ, θ from 10^{-7} to 10^{-8}. Thus we get the following table of R_a for μ, $\theta=10^{-8}$ and 5×10^{-8}, the former of which gives the maximum values of the ratio R_a for the range of ν between 10^{-5} and 10^{-8}.

As seen in this table, the effect of the second solution which is originated from the wind stress acting near the coast becomes more important in the baroclinic mode than in barotropic one and also for a rapidly changing wind system of a larger scale than for a slowly changing small scale wind system, although the amplitude of the second solution diminishes from the coast, as will be shown in the next section.

Table 1

ν (sec^{-1})	10^{-5}	10^{-6}	10^{-7}	10^{-8}
$R_a r1$	0.2	0.1	0.1	0.1
$R_a l1$	4.2	4.3	0.5	0.15
$R_a r2$	0.2	0.07	0.04	0.04
$R_a l2$	3.6	0.4	0.07	0.04

(Suffix r=barotropic l=baroclinic
Suffix 1 for $u=\theta=10^{-8}$(cm^{-1}), Suffix 2 for $u=\theta=10^{-7}$(cm^{-1}))

4. *The amplitude of the response of the ocean.*

As seen in the expression of R_I in (3.9), the order of the magnitude of the response is primarily determined by the values of K, so we discuss in this section the results of the numerical values computed by use of the physical constants shown in Table 2.

Table 2

f	β	H	H'	a	$1-\epsilon$	λ_r^{-2}	λ_e^{-2}	r	$f\sigma_r/gH$	$f\sigma_e/gH$
10^{-4}	2.10^{-13}	6×10^4	4×10^5	3×10^8	2.10^{-3}	2.5×10^{-17}	0.83×10^{-13}	0.15	2.55×10^{-13}	1.7×10^{-12}

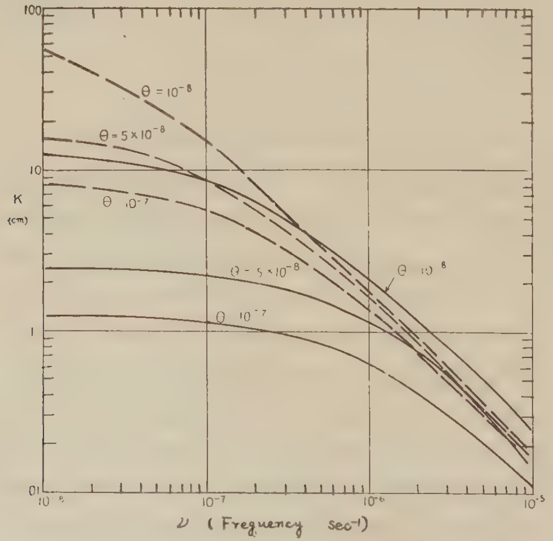

Fig. 1. K for $\mu=10^{-7}$.
(Full lines are barotropic, broken lines are baroclinic. curl $\tau=10^{-7}$)

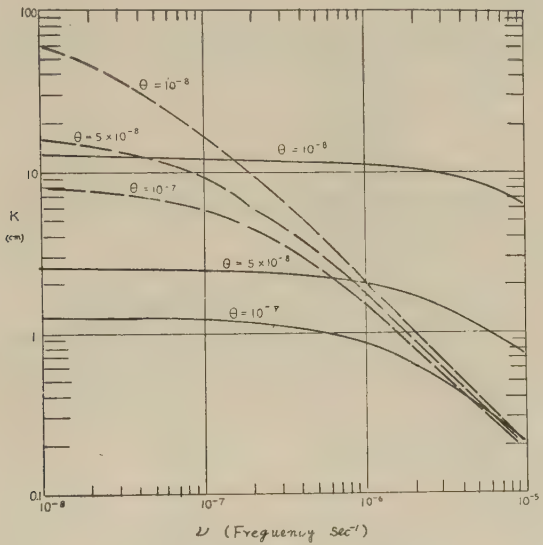

Fig. 2. K for $\mu=10^{-8}$
(Full lines are barotropic, broken lines are baroclinic. curl $\tau=10^{-7}$)

In Fig. 1 and 2 the values of K for $\mu=10^{-7}$ and 10^{-8} and for curl $\boldsymbol{\tau}=10^{-7}$ with the value of $\theta=10^{-7}$, 5×10^{-8}, 10^{-8} are shown as a function of ν. These curves indicate the interesting features of the response that the baroclinic mode increases more rapidly than barotropic as a frequency af the wind system decreases, which gives a quite measurable baroclinic amplitude of the sea surface more than 10 cm for ν less than 10^{-7} or period longer than 70 days with wave numbers less than 5×10^{-8}, although practically the value of curl of wind stress seems to decrease as decreasing frequency, so that such values as 10^{-7} is rather uncommon for longer period fluctuation of the wind system. Therefore the true values of K seems to be less than shown in these curves for smaller values of ν.

The amplitudes of both modes show the increase for constant value of curl $\boldsymbol{\tau}$ and ν as decreasing wave numbers θ and μ, the curves suggesting the changes in θ affects the values of K more than that in μ. However, this is also to be modified somewhat, since in real wind system curl $\boldsymbol{\tau}$ may be changed as according to the scale of the wind system as well as to the frequency. Therefore, as stated in the end of the last section, when we assume $\boldsymbol{\tau}\sim e^{i(\mu y+\theta x)}$, we can take curl $\boldsymbol{\tau}=|\boldsymbol{\tau}|(|\mu|+|\theta|)$. Thus the values of K are computed as a function of θ and the result is shown in Fig. 3, where $|\boldsymbol{\tau}|$ is taken as 1. These curves indicate that the amplitude

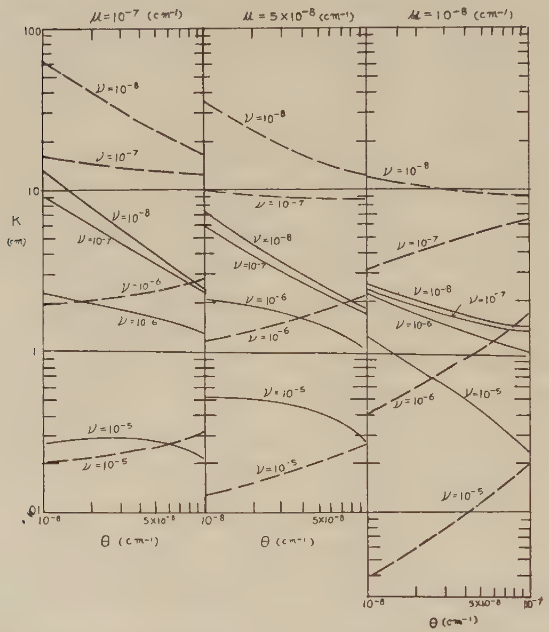

Fig. 3. K as a function of θ (wave number in y direction)
(Full lines are barotropic, broken lines are baroclinic)

of the baroclinic mode with larger frequency ν than 10^{-7} rather decreases with decreasing wave number of θ and μ and these of barotropic mode remain increasing as decreasing wave number θ, though they decrease for decreasing μ. In any way the baroclinic amplitudes have a measurable magnitude for $\nu<10^{-7}$ corresponding to morerealistic value of the curl $\boldsymbol{\tau}$, suggesting that the present problem should have close relationships to the annual change of the mean sea level.

Next the amplitudes K for westwards moving wind system are computed with the same constants, which show the resonance phenomenon for some wave number $\theta=\theta_c$, where the value of K becomes infinitive when we disregard the term $2\frac{\beta}{f}\mu i$ and frictional coefficient k in (3.5) or (3.15). We put θ_c as the value of θ making $I_0=0$, where I is taken as the expression of I_j without the term $2\frac{\beta}{f}\mu i$ and k, then the value of I_j at $\theta=\theta_c$ is given by

$$I_{jc}=-ik(\theta_c^2+\mu^2)\pm 2\frac{\beta}{f}\mu\nu i\mp 2\frac{\beta}{f}\mu k$$

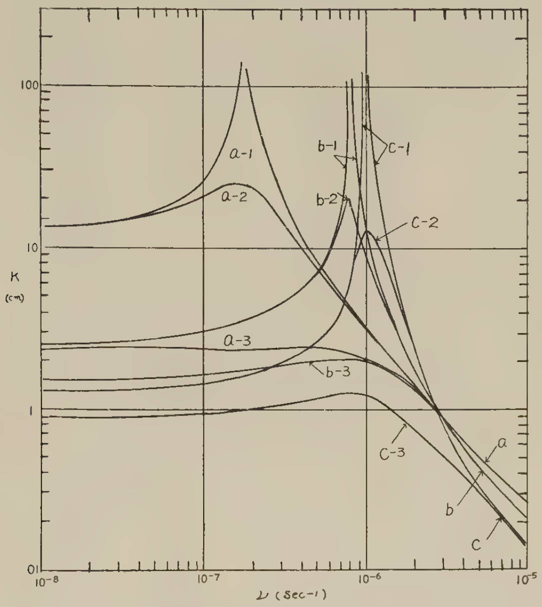

Fig. 4. *K* for westward moving disturbance of barotropic mode, with $\mu=10^{-7}$. ($a: \theta=10^{-8}$, $b: \theta=5\times10^{-8}$, $c: \theta=10^{-7}$, $1: k=10^{-8}$, $2: k=10^{-7}$, $3: k=10^{-6}$)

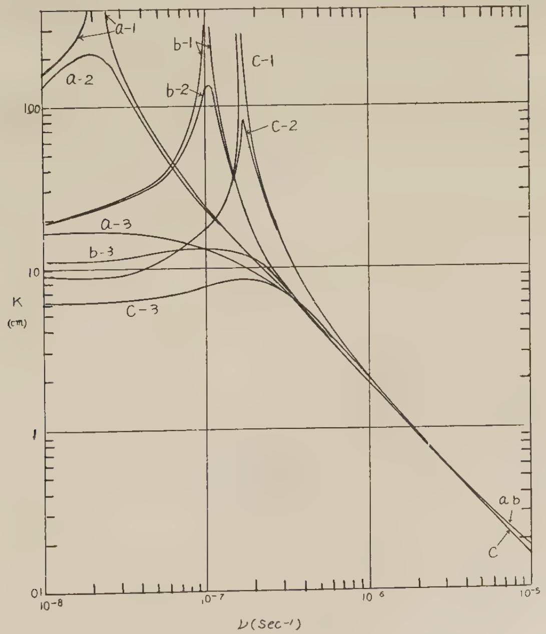

Fig. 5. *K* for westward moving disturbance of baroclinic mode, with $\mu=10^{-7}$ ($a: \theta=10^{-8}$, $b: \theta=5\times10^{-8}$, $c: \theta=10^{-7}$; $1: k=10^{-8}$, $2: k=10^{-7}$, $3: k=10^{-6}$)

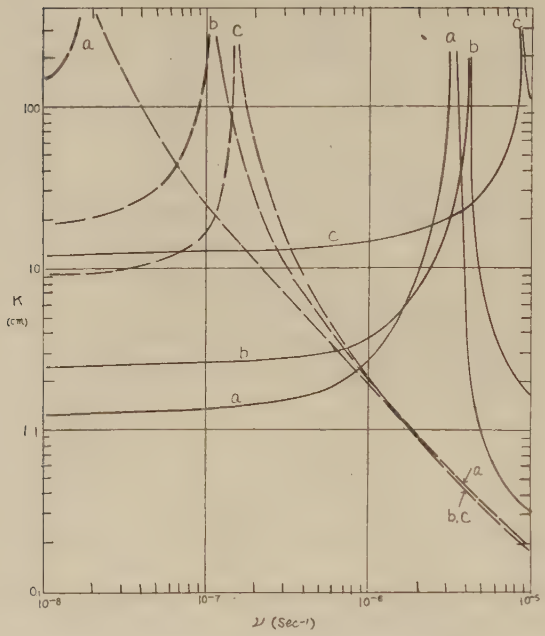

Fig. 6. K for westward moving disturbance with $\mu=10^{-8}$ and $k<10^{-8}$
(Full lines are barotropic, broken lines are baroclinic)
($a:\theta=10^{-8}$, $b:\theta=5\times10^{-8}$, $c:\theta=10^{-7}$)

which prevent the infinitive value of K at $\theta=\theta_c$. The effect of friction and $2\frac{\beta}{f}\mu i$ term may be more or less important near the point θ_c, and in other part of the region they are almost negligible as shown in the figures 4, 5 and 6.

5. *Free waves under the influence of friction.*

The terms having a factor $e^{i\delta_1 x}$ or $e^{i\delta_2 x}$ in P_s of (3.6) or in R_{IIs} of (3.10a) represent free waves in a stratified ocean of planetary type, which is induced by moving disturbance, not directly but rather owing to the effect of the boundaries which reflect the forced waves accompanying with the moving wave system. The wave number δ_1 and δ_2 such waves are given by the equation (3.6) or

$$\delta_s=\frac{\kappa}{1-in}\pm\left\{\left(\frac{\kappa}{1-in}\right)^2-\frac{\lambda_j^{-2}}{1-in}-\mu^2\pm2\frac{\beta\mu}{f}i\right\}^{\frac{1}{2}} \tag{5.1}$$

where $s=1$ corresponds to the plus sign, and we put $\kappa=\beta/2v$, $n=k/v$ The relative magnitude of each term in this equation changes for differcent paysical conditions, but when we consider the range of ν between 10^{-5} and 10^{-8} we have the following list of the order of magnitude of each term within the root sign.

ν	10^{-5}	10^{-6}	10^{-7}	10^{-8}
κ^2	10^{-16}	10^{-14}	10^{-12}	10^{-10}
$n(k=10^{-7})$	$10^{-1}{}_0$	10	1	10

μ^2	10^{-14}	10^{-16}
$2\frac{\beta\mu}{f}$	4×10^{-16}	4×10^{-17}

$\lambda^{-2}{}_r=2.5\times10^{-17}$ $\lambda^{-2}{}_l=8.3\times10^{-14}$

This list gives the rough idea about the relative importance of each term, and we can see that the contribution from $2\beta\mu/f$ is quite small except near $\nu=10^{-5}$ and also the same value of the frictional coefficient has more effect in smaller frequency region.

When we take into account of friction δ_s is generally complex, but even when we neglect the friction and $2\beta\mu/f$ term, still we have complex values of δ_s for a certain range of ν larger than a critical value defined by $\nu_c=\beta(\lambda_j{}^{-2}+\mu^2)^{-\frac{1}{2}}/2$ In such range δ_1 and δ_2 has imaginary part of the same value but opposite sign and therefore we have the term $e^{i\delta_1 x}$ which decreases exponentially as spart from the western coast and the term $e^{i\delta_2 x}$ which decreases in the same manner from the eastern coast. When the imaginary part of $a\delta_s\gg1$, we obtain the following simple expression for R_I

(in the western part)

$$R_\text{I}=\Re\,[K\{-\sin(\nu t-\theta x)\,\sin\mu y-iQ_1e^{i\nu t+i\delta_1(a+x)+ia\theta}\}]$$

(in the eastern part)

$$R_\text{I}=\Re\,[K\{-\sin(\nu t-\theta x)\,\sin\mu y-iQ_2e^{i\nu t+i\delta_2(x-a)+ia\theta}\}] \tag{5.2}$$

where $$Q_s=e^{i\mu y}(1+iq\theta)/(1+q\delta_s)-\mathrm{e}^{-i\mu y}(1-iq\theta)/(1-iq\delta_s)$$

As seen from the equation (5.1), the imaginary part of δ_s increases as increasing frequency for $\nu>\nu_c$, the free waves caused by the disturbance of shorter period attenuates more rapidly as apart from the coast.

In order to give the notion about the change of the values of δ_s as variable physical constants ν, μ and k, we compute the values of δ_s both for barotropic and baroclinic mode for the range of ν between 10^{-5} and 10^{-8} and for $\mu=10^{-7}$, 5×10^{-8}, 10^{-8} and for $k=0$, 10^{-8}, 10^{-7} from the equation (5.1). The results are shown in Table 3. Especially for the range of $\nu\leqslant10^{-6}$ and $\mu\leqslant5\times10^{-8}$ of barotoropic mode and also for $\nu\leqslant10^{-7}$ and $\mu\leqslant10^{-7}$ of both modes we can use the following approximate formula for δ_s

Table 3

	10^{-5}	5×10^{-6}	10^{-6}	5×10^{-7}	10^{-7}	5×10^{-8}	10^{-8}
$\nu=\mu=10^{-7}$	$0.1\pm i$	$0.2\pm0.98i$	$1\pm0.05i$	$3.732,\ 0.268$	$20,\ 0.05$	$40,\ 0.025$	$200,\ 0.005$
	,,	,,	$1.094+0.117i$	$3.732+0.191i$	$19.8+1.98i$	$38.4+7.68i$	$100+100i$
δ_r	,,	,,	$0.906-0.097i$	$0.268-0.111i$	$0.05-0.005i$	$0.025-0.005i$	$0.005-0.005i$
$(\times10^{-7})$	,,	$0.208+0.981i$	$1.31+0.415i$	$3.530+0.824i$	$9.95+10.05i$	$7.98+16.05i$	$1.98+19.9i$
		$0.192\pm0.979i$	$0.67-0.217i$	$0.31-0.056i$	$0.05-0.05i$	$0.025-0.05i$	$0.005-0.05i$
	$0.1\pm3.06i$	$0.2\pm3.03i$	$1\pm2.89i$	$2\pm2.31i$	$20,\ 0.417$	$40,\ 0.208$	$200,\ 0.042$
δ_l	,,	,,	$0.98\pm2.90i$	$2+2.35i$	$19.8+1.97i$	$37.9+4.95i$	$100+100i$
$(\times10^{-7})$			$1.02-2.87i$	$2-2.29i$	$0.45-0.01i$	$0.5-0.005i$	$0.088-0.005i$
	$0.087+3.06i$	$0.17+3.03i$	$0.88+2.95i$	$1.88+2.74i$	$9.54+10.05i$	$7.78+16.05i$	$1.94+19.85i$
	$0.113-3.06i$	$0.23-3.03i$	$1.10-2.75i$	$1.96-1.98i$	$0.46-0.05i$	$0.22-0.05i$	$0.05-0.05i$
$\mu=5\times10^{-8}$	$0.1\pm0.49i$	$0.2\pm0.458i$	$1.87,\ 0.13$	$3.94,\ 0.16$	$19.8,\ 0.0125$	$40,\ 6.25\times10^{-3}$	$200,\ 25\times10^{-4}$
	,,	,,	$1.87+0.023i$	$3.94+0.081i$	$19.8+1.98i$	$38.4+7.64i$	$100+100i$
δ_r			$0.13-0.002i$	$0.16-0.001i$	$(125-25i)\times10^{-4}$	$(63-25i)\times10^{-4}$	$(25-25i)10^{-4}$
$(\times10^{-7})$	,,	$0.202+0.462i$	$1.843+0.225i$	$3.73+0.76i$	$20+20i$	$8+16i$	$1.98+19.8i$
		$0.198-0.454i$	$0.157-0.015i$	$0.11+0.01i$	$(125-125i)\times10^{-4}$	$(63-125i)\times10^{-4}$	$(125-125i)\times10^{-4}$
	$0.1\pm2.93i$	$0.2\pm2.93i$	$1\pm2.75i$	$2\pm2.14i$	$20,\ 0.417$	$40.\ 0.208$	$200.\ 0.042$
δ_l	,,	,,	$0.99+2.76i$	$2+2.18i$	$19.4+1.98i$	$38.2+7.64i$	$100+100i$
$(\times10^{-7})$	,,	,,	$1.01-2.74i$	$2-2.10i$	$0.4-0.0025i$	$0.2-0.0025i$	$0.042-0.0025$
	,,	,,	$0.89+2.85i$	$1.88+2.56i$	$9.57+10i$	$7.8+16i$	$1.95+19.8i$
			$0.11-2.65i$	$1.96-1.80i$	$0.42-0.125i$	$0.21-0.0125i$	$0.04-0.0125i$
$\mu=10^{-8}\nu$	$0.1\pm0.05i$	$0.366,\ 0.034$	$2.005,\ 0.005$	$4,\ 25\times10$	$10,\ 125\times10$	$40,\ 625\times10^{-5}$	$200,\ 5\times10^{-5}$
	,,	$0.366+88i\times10^{-5}$	$1.995+0.02i$	$4+0.08i$	$19.8+1.98i$	$38.4+7.68i$	$100+100i$
δ_r		$0.034-8i\times10^{-5}$	$0.005-5i\times10^{-5}$	$(125-5i)\times10^{-5}$	$(50-5i)\times10^{-5}$	$(25-5i)\times10^{-5}$	$(5-5i)\times10^{-5}$
$(\times10^{-7})$	$0.102+0.05i$	$0.366+88i\times10^{-4}$	$1.985+0.2i$	$3.74+0.77i$	$20+20i$	$8+16i$	$1.98+19.8i$
	$0.098-0.05i$	$0.034-8i\times10^{-4}$	$(50-5i)\times10^{-4}$	$(25-5i)\times10^{-4}$	$(12.5-5i)\times10^{-4}$	$(2.5-5i)\times10^{-4}$	$(0.5-5i)\times10^{-4}$
	$0.1\pm2.89i$	$0.2\pm2.88i$	$1\pm2.70i$	$2\pm2.14i$	$20,\ 0.417$	$40,\ 0.21$	$200,\ 0.04$
δ_l	,,	,,	$0.98+2.72i$	$2+2.12i$	$19.4+1.89i$	$38.2+7.68i$	$100+100i$
$(\times10^{-7})$			$1.02-2.70i$	$2-2.04i$	$0.5-5i\times10^{-5}$	$0.2-5i\times10^{-5}$	$0.04-5i\times10^{-5}$
	,,	,,	$0.87+2.80i$	$1.88+2.52i$	$9.58+10i$	$7.79+16i$	$1.96+19.8i$
			$1.11-2.60i$	$1.96-1.76i$	$0.42-5i\times10^{-4}$	$0.21-5i\times10^{-4}$	$0.04-5i\times10^{-4}$

(1) δ_r means barotropic, δ_l baroclinic.

(2) In the first line, the values of δ for $k=0$ are shown, where δ_1 is given by the plus sign or the larger value.

(3) In the second and third lines, δ for $k=10^{-8}$ and $k=10^{-7}$ are shown, where in each line upper figure indicates δ_1 and lower one δ_2.

$$\delta_{1,2}=\frac{\kappa}{1-n_i}\pm\left\{\frac{\kappa}{1-n_i}-\frac{\mu^2}{2\kappa}(1-n_i)-\frac{\lambda_j^{-2}}{2\kappa}\pm\frac{\beta\mu}{f\kappa}(i+n)\right\} \tag{5.1a}$$

As seen in this table or from (5.1a), the real part of δ_1 of both modes, that is, a wave number for the free waves expressed by $e^{i\delta_1 x}$ exceeds 10^{-6} for $\nu=10^{-7}$, which gives the wave length less than 63*km* and also this wave length becomes shorter as increasing period of the wind system longer than about a half year. When the friction is neglected, these waves have a constant amplitude from east to west all over the ocean. Physical interpretation of such waves is quite difficult and also the evidence of their existense seems to be doubtful. Moreover, when we neglect the friction, we cannot obtain stationary solution which satisfys boundary conditions by decreasing ν towards zero. For, when $\nu\rightarrow 0$ and $k=0$, (2.17) becomes

$$\beta\frac{\partial R}{\partial x}=\frac{f\sigma}{gH}F \tag{5.3}$$

and the solution of this equation can satisfy the boundary condition only at one coast. The generation of the wildly oscillating waves associated with $e^{i\delta_1 x}$ is due to the situation that additional boundary condition at onother coast is impressed to the solution of the above equation which permits only one boundary condition. Therefore, the introduction of the friction is quite reasonable not only from the mathematical point of view but also from physical one because with a finite k the equation (2.17) permits two boundary conditions, even when ν approaches to zero and in fact, it gives the solution treated by Stommel (1948) in this extreme case.

Another justification of the introduction of the friction is given by the physical reasoning, because near the coast the friction should be very important rather than geostrophic effect. In reality, the linearized equation (2.17) seems to be velid only in the interior of the ocean, and as shown by recent theories of Charney (1955b) and Morgan (1956) the non linear effect may play an important role near the coast. However, the simplicity of the mathematical treatment with many results obtained in the stationary circulation problem by the theory of Stommel (1948) and Munk (1950) seems to make it reasonable to use the frictional boundary layer model as the first approximation.

When we lock at the table 3, we can find that the values of δ_1 with a large real part for the values of ν larger than ν_c become to have a large positive imaginary part, too, as a friction is introduced, suggesting that the δ_1 waves (we call the free waves expressed by the term $e^{i\delta_s x}$ as δ_s-waves hereafter) with small wave length attenuate rapidly as apart from the western coast. On the other hand, δ_2 waves with much larger wave length than δ_1 waves decrease from the maximum value at the eastern coast much more gradually than δ_1 waves, because δ_2 has much smaller real and imaginary part, the latter of which is negative. This is a sort of the westward intensification of the induced fluctuations in circulation, which occurs when $\beta_1 a \gg 1$, where we put $\delta_s = \alpha_s + i\beta_s$. We call this range of ν, where such condition is satisfied, as WI range, and also we define the range ν, where the solution is expressed by the equation (5.2), as SC (Subcritical) range hereafter. Then in WI range the approximate form for R_{I} corresponding to (5.2) becomes

$$R_{\mathrm{I}} = -\Re K\{\sin(\nu t+\theta x)\sin\mu y + iQ_1 e^{i\nu t+i\delta_1(a+x)+ia\theta}(1-e^{-2a\overline{\delta_2+\theta}}) + iQ_2 e^{i\nu t+i\delta_2(x-a)-ia\theta}\} \tag{5.4}$$

This expression is valid for all range of x, though in the eastern half the term with $e^{i\delta_2 x}$ is negligible.

In order to show the effect of the friction more clearly, we plot π/β, as a

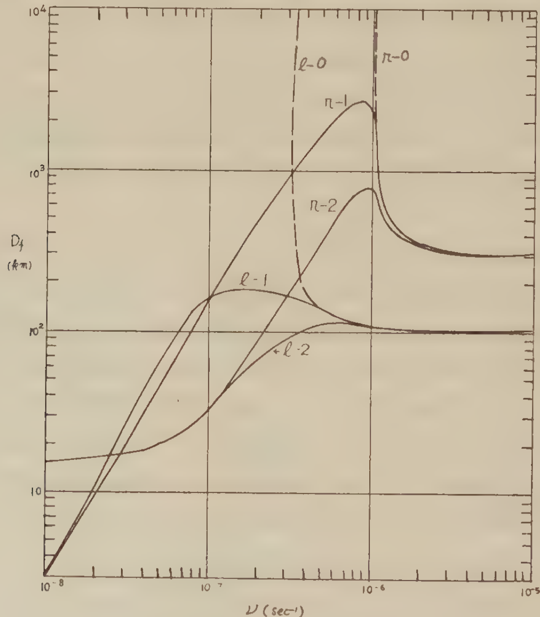

Fig. 7. $Df = \pi/\beta_1$ for $\mu = 10^{-7}$
(r: Barotropic, l: Baroclinic; 0: $k=0$, 1: $k=10^{-8}$, 2: $k=10^{-7}$)

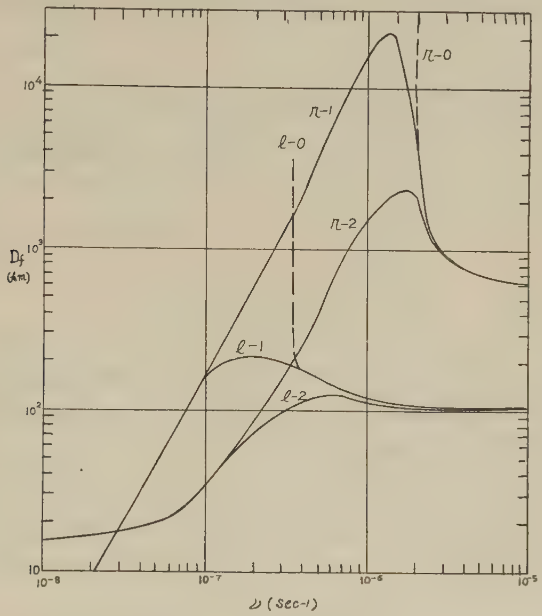

Fig. 8. $D_f=\pi/\beta_1$ for $\mu=10^{-8}$
(r: Barotropic, l: Baroclinic; 0: $k=0$, 1: $k=10^{-8}$, 2: $k=10^{-7}$)

function of frequency ν in fig. 7 and 8, which corresponds to the depth of frictional influence in the wind drift current of Ekman, since it gives the distance from the coast, where the amplitude of δ_1 waves decreases to $e^{-\pi}$ times of the value at the coast, which we shall define as D_f. In the SC range, D_f is finite even when we neglect the friction, and in fact the effect of the friction is very small as seen in Table 3 and the curves. However for $\nu<\nu_c$ this value is finite only when the friction is introduced. In the range of ν intermediate between SC and WI ranges the values of D_f of barotropic mode is much larger than those of baroclinic mode but in the range of WI, say for $\nu<10^{-7}$, they are almost equal, since $\kappa\gg\lambda_l^2$, u^2 and δ_1 is given by $2\kappa/(1-ni)$, approximately. On the other hand, the change of the values in k has much influence in the values of D_f in the WI range, and for the range $\nu<3\times10^{-8}$ the increase in k value rather increases the values of D_f, contrary to the depth of frictional influence.

Anyhow, the values of k adopted here are not so large, since STOMMEL (1948) gave it a value of $k=0.02/H$ or 3.3×10^{-7} in his theory of stationary circulation and NEUMANN (1954) gave it 3.3×10^{-6}. Therefore, the effect of friction for attenuation of δ_1 waves is quite realistic, considering a moderate estimation of the values in k.

6. *Numerical examples for a travelling wind system*

Here we show some examples of numerical computation of the equation (3.9a) or its approximate form (5.2) or (5.4). The disturbance is considered to travel eastwards, since such one seems to be more realistic than westward moving one.

Case I. $\theta=10^{-7}, \quad \mu=10^{-7}, \quad \nu=5\times10^{-6}$

This model corresponds to the smallest wind system considered to give any effect on the circulation of the ocean, and in this model the effect of friction is almost negligible in the values of K and δ_s so far as k is less than 10^{-7}. The numerical values of many quantities in the equation for R_{I} are as follows:

$$q=5\times10^5 \ q\theta=0.05, \quad q\delta_{sl}=0.01\pm0.049_i \quad q\delta_{sr}=0.01\pm0.152_i$$

Both barotropic and baroclinic mode lie in the range of SC and particularly for the barotropic mode the equation (5.2) can be written more simply as

(Western part)

$$R_{\mathrm{I}}=K[-\sin(\nu t-\theta x)\sin\mu y+e^{-\beta(a+x)}\sin(\nu t+\alpha\overline{x+a}+a\theta)\sin\mu y-qe^{-\beta(a+x)}\cos\mu y$$
$$\{\beta\cos(\nu t+\alpha\overline{a+x}+a\theta)+(\theta+\alpha)\sin(\nu t+a\theta)\}] \tag{6.1}$$

because $|q\theta|\ll1, \ |q\delta_{sl}|\ll1$ and also K is real.

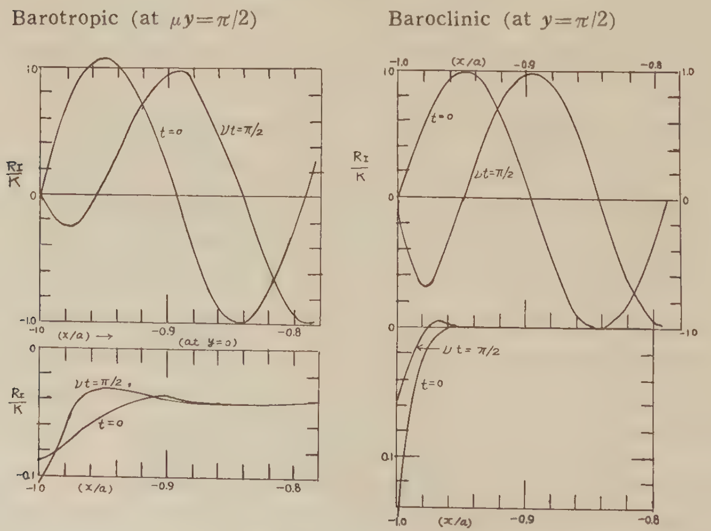
Barotropic (at $\mu y=\pi/2$) Baroclinic (at $y=\pi/2$)

Fig. 9. R_I/K for a model I.

The wave forms of R_1 computed for this model are graphically shown in Fig. 9 for the range of χ near $-a$ or rear the western coast, and those near the eastern coast are symmetric about the point $x=0$, as seen in the equation (5.2). These curves indicate that the effect of the coast is limited within quite a narrow band from the coast, say, of about $0.08a$ for barotropic and $0.04a$ for baroclinic mode.

The condition at the coast $x=\pm a$ is $u=0$, as stated in Section 3, or

$$\frac{\partial R}{\partial y}+\frac{1}{f}\left(\frac{\partial}{\partial t}+k\right)\frac{\partial R}{\partial x}=0$$

and when we neglect the non-geostrophic term in the equation of the boundary value of u, this condition becomes simply $\partial R/\partial y=0$ and we have the solution R which vanishes at the coast. On the other hand, when we take into account of the non-geostrophic term, we have the finite value of R_1 at the coast, although the amplitude is small compared with those in the inner region. This means that the surface elevation and the depth of the upper layer show the fluctuation at the coast due to the moving wind system, and their amplitude seems to be measurable order of magnitude, which may be tested by the observation.

Case II. $\theta=5\times10^{-8}$, $\mu=5\times10^{-8}$, $\nu=5\times10^{-7}$, $k=10^{-8}$ or 10^{-7}

The quantities often used have the following values:

for $k=10^{-8}$ $q=10^5\ (1-0.02i)$, $a\delta_{1\nu}=118.2+2.436i$

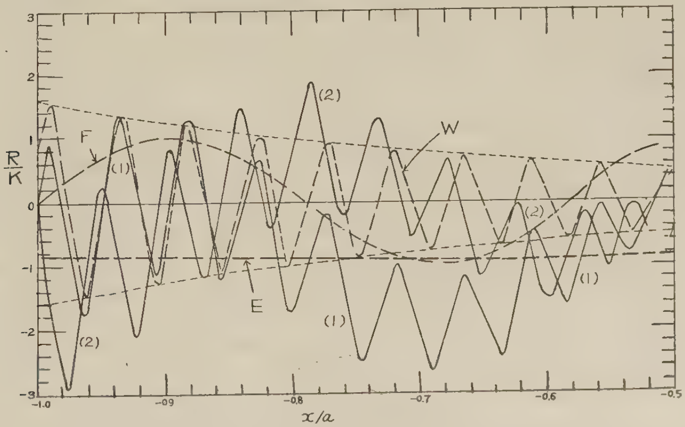

Fig. 10. R/K for model II of barotropic made with $k=10^{-8}$. (Full lines: resultant curve at $t=0$ (1) and $\nu t=\pi/2$ (2). Broken lines: component waves at $t=0$. Forced waves: F, δ_1—waves: W, δ_1—waves: E, Dotted lines: envelope for δ_1—waves.)

$$a\delta_{2r}=1.80-0.036i,\ a\delta_{1l}=60+65.4i,\ a\delta_2 l=60-63_i$$

for $k=10^{-7}$
$$q=10^5\ (1-0.2i),\ a\delta_{1r}=111.9+22.65i$$
$$a\delta_{2r}=3.3+0.39i,\ ad_{1e}==56.3+83.4i,\ a\delta_{2l}=58.7-54.0_i$$

Since $|q\theta|,\ |q\delta_1|\ |q\delta_2|\ll 1$, we can put R_i, for the barotropic mode instead of (5.4), as

$$R=K[-\sin(\nu t-\theta x)\sin\mu y-\Im\{e^{i\delta_1(\theta+x)+ia\theta}(e^{-2i\overline{a\theta+\delta_2}}-1)(\sin\mu y-\overline{q\theta+\delta_1}\cos\mu y)$$
$$-e^{-ia\theta+i\delta_2(x-a)}(\sin\mu y-\overline{q\theta+\delta_2}\cos\mu y)\}] \qquad (6.2)$$

and also for the baroclinic mode we can use the equation (6.1), since ν is larger than ν_c and $|q\delta_s|\ll 1$.

This example gives something interesting feature, since the barotropic mode is in *WI* range and the baroclinic one lies in *SC* range, so that the former is much influenced by the values of k. For $k=10^{-8}$ the value D_f is quite large and the effect of the western coast extends ail over the ocean and δ_1 waves with the wave length of about 159 km are superposed till the eastern coast as shown in

$$-\sin(\nu t-\theta x\overline{+a})-1.945e^{-\beta_1(a+x)}\cos(\alpha_1\overline{a+x}+\nu t+0.004)$$
$$+2.182e^{-\beta_2(a+x)}\sin(\alpha_2\overline{a+x}+\nu t+1.099) \qquad (6.3)$$

Fig. 10 and we know no observed fact corresponding to such waves yet. On the other hand, the waves of the beroclinic mode is much more similar to case I, since they both belong to the range *SC*, so that the graphical representation is not shown

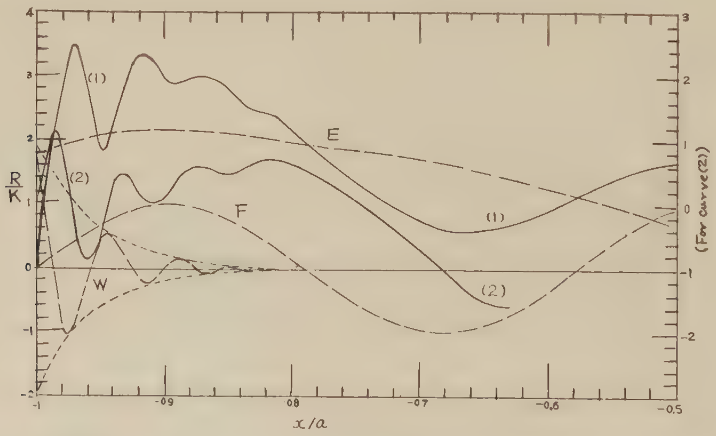

Fig. 11a. R/K for model II of barotropic mode with $k=10^{-7}$ near the western coast. (Full lines: resultant curve at $t=0$ (1) and $\nu t=\pi/2$ (2). Broken lines: component waves at $t=0$. Forced waves: *F*, δ_1—waves: *W*, δ_2—waves: *E*. Dotted lines: envelope for δ_1—waves.)

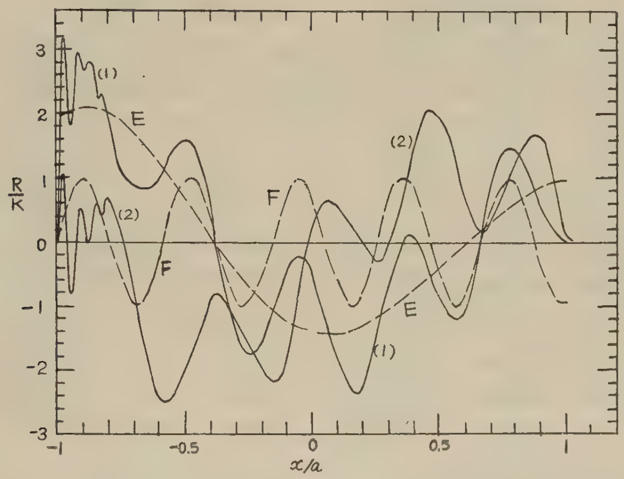

Fig. 11b. The same functions as in Fig. 11a in the whole ocean.

Then we take the frictional coefficient $k=10^{-7}$, then the pattern of barotropic waves seems to be completely changed, since the δ_1 waves become almost negligible for the values of $x>-0.08a$. The more convenient expression of the factor of $\sin\mu y$ for numerical computation is given by

$$-\sin(\nu t-\theta\overline{x+a})-1.945e^{-\beta_1(a+x)}\cos(\alpha_1\overline{a+x}+\nu t+0.004)$$
$$+2.182e^{-\beta_2(a+x)}\sin(\alpha_2\overline{a+x}+\nu t+1.099), \qquad (6.3)$$

From this equation, we can see that the effect of δ_2 waves is rather predominant, except very near to the western boundary, whose weve length is about 6900 km, almost the same as the whole length of the ocean. It is remarkable that the moving wave system with so small wave length as 1250 km can excite a relatively large amplitude of such a long waves as δ_2 waves, which are caused by the boundary condition at the eastern coast, rather than any other effects associated with the condition in the inner part of the ocean.

7. *Numerical examples for a periodically changing wind system.*

In this section we discuss the results obtained for a wind system which is stationary in its location but change periodically with annual period.

Case III. We take the wind stress as follows:

$$\mathrm{curl}\,\boldsymbol{\tau}=F_0\sin\nu t\sin\frac{\pi}{a}x\sin\mu y \qquad (7.1)$$

and the numerical constants as

$$\nu=2\times10^{-2}=2\pi/year, \quad k=2\times10^{-8}$$

$\mu=10^{-8}$ (IIIa), $\mu=5\times10^{-8}$ (IIIb)

This model corresponds to the change of the wind system in the Pacific Ocean, where the eastern and western half have different vorticity of surface wind as stated later. The solution of R_1 itself can be obtained very easily by combination of two solutions for the wind system moving east with a factor $e^{i(\nu t-\theta x)}$ and west with $e^{i(\nu t+\theta x)}$. The δ_1 waves and δ_2 waves in both modes lie in the range of WI, so that δ_1 waves are conspicuous only near the western coast.

Since the value of θ is specified as π/a, the expression for K_1 becomes somewhat more simple than (6 1). Generally K becomes different for $e^{i(\nu t-\theta x)}$ waves and $e^{i(\nu t+\theta x)}$ waves, and we put K_- for the former and K_+ for the latter, then we obtain the relation, such as (In barotropic modes) $K_+=-K_-(1+2\in_r)$, (in baroclinic modes) $K_+=K_-(1+2\in_\iota)$, where $\in_r$ and $\in_\iota$ are both positive number for the range of μ and ν considered here.

Then, for barotropic mode, we have

$$\begin{aligned}R_{\mathrm{I}}=K_-[\{&\sin\nu t\cos\pi/a\,x+\in_r\sin(\nu t+\pi/a\,x)+(1+\in_r)e^{-\beta(a+x)}\sin\overline{\nu t+\alpha_1a+\alpha_1x}\\&-e^{2\beta_2a}\sin\overline{\nu t+\alpha_1a+\alpha_1x-2\alpha_2a})+(1+\in_r)e^{-\beta_2(x-a)}\sin(\nu t+\alpha_2\overline{x-a})\}\sin\mu y\\&+\cos\mu y\Im\{q(\in_r\pi/a+1+\in_r\delta_1)e^{i\delta_1(a+x)}-q(\in_r\pi/a+\overline{1+\in_r}\delta_2)e^{i\delta_2(a-x)}\}]\end{aligned}\tag{7.2}$$

Similarly, for baroclinic mode, we have

$$\begin{aligned}R_{\mathrm{I}}=K_-[\{&-\cos\nu t\sin\pi/a\,x-\in_\iota\sin(\nu t+\pi/a)+\in_\iota e^{-\beta_1(a+x)}\\&\times(e^{2\beta_2a}\sin\overline{\nu t+\alpha_1a+\alpha_1x-2\alpha_2a}-\sin\overline{\nu t+\alpha_1a+\alpha_1x})\\&-\in_\iota e^{-\beta_2(x-a)}\sin(\nu t+\alpha_2\overline{x-a})\}\sin\mu y\\&-\cos\mu y\Im\{q(\overline{1+\in_\iota}\,\pi/a+\in_\iota\delta_1)e^{i\delta_1(a+x)}-q(\overline{1+\in_\iota}\,\pi/a+\in_\iota\delta_2)e^{i\delta_2(a-x)}\}]\end{aligned}\tag{7.3}$$

IIIa $\mu=10^{-8}$ and $2\in_r=0.05$, $2\in_\iota=0.29$

The values of δ_1 and δ_2 are as follows:

(Barotropic)	$a\delta_1=0.467-0.039i$	$a\delta_2=297+29.7i$
(Baroclinic)	$a\delta_1=270+30i$,	$a\delta_2=27-0.33i$

The expression for δ_1 waves with the factor of sin μy which is convenient for numerical computation becomes

(Barotropic)	$0.888\,e^{-\beta_1(a+x)}\cos(\alpha_1\overline{a+x}+\nu t-0.545)$
(Baroclinic)	$-0.211\,e^{-\beta_1(a+x)}\sin(\alpha_1\overline{a+x}+\nu t-0.198)$

The results of the computation are shown graphically in Fig. 12 where the functional form of R_{I} at $\mu y=\pi/2$ is illustrated near the western coast and over the whole ocean separately. Since $\in_r$ is almost negligible compared with 1, the forced motion becomes standing type as the wind system itself, though the

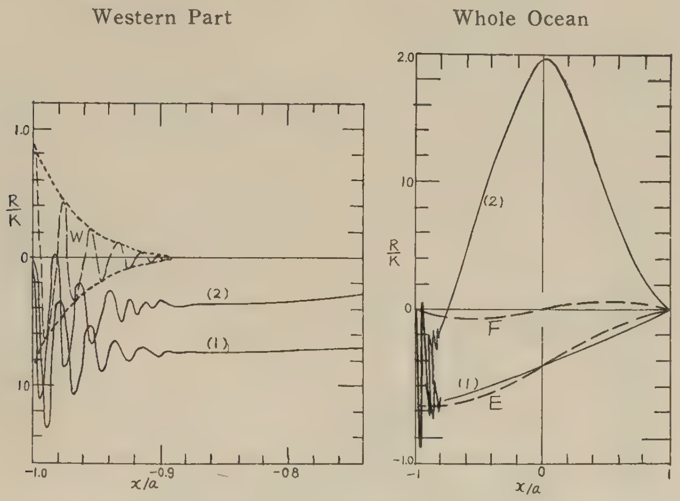

Fig. 12. R/K of barotropic mode for model III with $\mu=10^{-8}$.
(Full lines: resultant curve at $t=0$ (1) and at $t=t$ (2) Broken lines: component waves at $t=0$ Forced waves: F, δ_1—waves: W, δ_2—waves: E Dotted lines: envelope for δ_1—waves)

spatial distribution of the amplitude of the motion is displaced from that of the wind stress curl with a phase of $\pi/2$ and thus the maximum change occurs at the center, with the phase in time being the same as wind stress curl.

The effect of the δ_1 waves is almost negligible beyond $x=-0.1a$ as in Case IIb, though the frictional coefficient here is smaller (2×10^{-8}) than in the previous case (10^{-7}). It is quite interesting that the δ_1 waves with a very short wave length are excited by the large scale wave system and they are limited only in the region of the western current, because these disturbances seem to be associated with the multipie structures of the Gulf Stream which have been often observed and confirmed by Fuglister (1951a) and others.

The effects of δ_2 waves seem to retard the whole pattern with a phase lag of about 1.8 months, because they have a wave length longer than the width of the ocean and their form is expressed with the sine function such as
$\sin\{0.467\,(x/a+1)+\nu t-0.934\}$

On the other hand, the features of baroclinic modes are quite different from the barotropic ones. First, the forced waves have a form such as $-\cos\nu t\sin\theta x$, which means that the response of the ocean to the wind system is retarded by about 1/4 period, though the spatial distribution of the motion is the same as

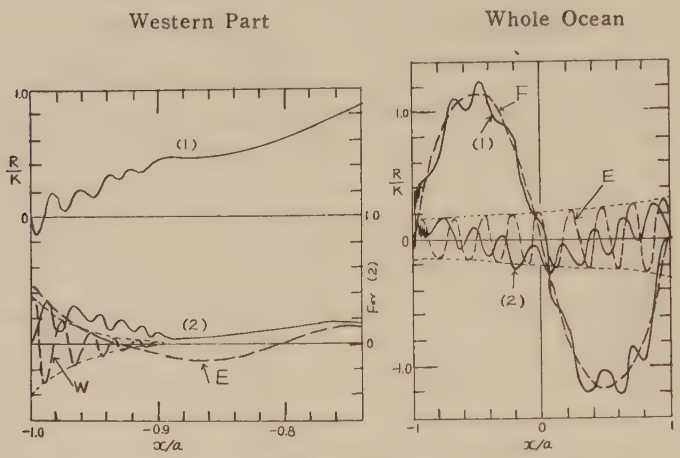

Fig. 13. *R/K* of baroclinic mode for model III with $\mu=10^{-8}$
(See explanation of Fig. 12 for legend)

the wind system. The δ_2 waves have a wave length of about 700 km with the amplitude almost uniform over the whole ocean, so that slight unevenness with a small wave length is recognized in the resultant pattern, although its amplitude is quite small compared with the forced motion.

IIIb′ $\mu=5\times10^{-8}$ and $2\epsilon_r=0.66$, $2\epsilon_i=0.285$

(Barotropic) $a\delta_1=297+29.7_i$ $a\delta_2=0.75-0.075_i$

(Baroclinic) $a\delta_1=269.7+27.0_i$ $a\delta_2=27.5-0.3_i$

The convenient expression for δ_1 waves is given by

$$1.69e^{-\beta_1(a+x)}\sin(\alpha_1\overline{a+x}+\nu t+0.739)\quad\text{(barotropic)}$$

The baroclinic waves are almost similar to the previous case, since the values of ϵ_i, δ_1, δ_2 are almost the same, so that they are not written again.

In this case, the amplitude of westward moving wave $\sin(\nu t+\pi x/a)$ is relatively large, and thus the forced motion has a pattern moving to the west as a whole. Further, both the amplitudes of δ_1 waves and δ_2 waves are larger than in IIIa, so that the difference in amplitude in each stage of phase becomes more conspicuous.

Case. IV. We consider the model discussed by MUNK (1957), where the wind is zonal, with the westerly in the northern half and easterly in the southern half, such as

$$\tau_y=0 \qquad \tau_x=-T_0\cos\nu t\sin\mu y \tag{7.4}$$

in which we take $\mu=1.13\times10^{-8}$, corresponding to the distance of the ocean of about 3000 sm.

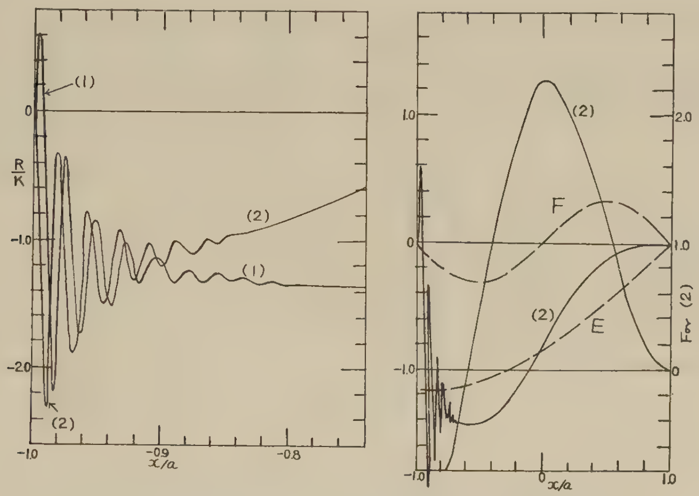

Fig. 14. R/K of barotropic mode for model III with $\mu=5\times10^{-8}$ (See explanation of Fig. 12 for legend)

In this model we retain the term $-2\frac{\beta}{f}\frac{\partial}{\partial y}R_j$ in the equation (2.17). As for the boundary conditions, we can take the exact ones given by (3.2), since the boundary values of τ are given explicitely. However, the contributions from R_{II} can be neglected with a satisfactory exactness, because from the boundary conditions

$$R_{\text{II}y}+\frac{1}{f}\left(\frac{\partial}{\partial t}+k\right)\left(R_{\text{II}x}-\frac{\nu}{f\mu}\frac{\sigma_j}{gH}T_0\cos\nu t\cos\mu y\right)=0$$

we obtain

$$|R_{\text{II}}|\sim\frac{\sigma_j}{gH}T_0\frac{\nu^2}{f^2\mu^2}$$

which gives the ratio

$$|R_{\text{II}}|/|R_{\text{I}}|\sim\nu^2(\mu^2\lambda_j^2)/f^2\mu^2 \qquad (j=r,\ l)$$

$$=4.8\times10^{-6}\ \text{(for barotropic)}=2.7\times10^{-3}\ \text{(for baroclinic)}$$

Therefore the exact solution of R is given by

$$R=-\frac{K}{2}(dS+\bar{d}\bar{S}-ldC+l\bar{d}\bar{C}) \tag{7.5}$$

where

$$\begin{aligned}S=\sin(\varphi+\nu t+\mu y)&-m_1e^{-\beta_1(a+x)}\{\sin(\nu t+\mu y+\alpha_1\overline{x+a}+\varphi+{}_1\psi)\\&-e^{2\beta_2a}\sin(\nu t+\mu y+\alpha_1\overline{x+a}+\varphi+\psi_1-2\alpha_2a)\}\\&-m_2e^{-\beta_2(x-a)}\sin(\nu t+\mu y+\alpha_2\overline{x-a}+\varphi+\psi_2)\end{aligned} \tag{7.6}$$

and in $\overline{S}$, m_1, m_2, 4_1, 4_2, δ_1, δ_2 and φ are replaced with corresponding quantities with a bar and μy is taken by $-\mu y$. . The terms having a factor $l=\beta/\mu f$ are produced by the condition that the wind stress function has a form such as

$$\mathrm{curl}\,\boldsymbol{\tau}+\frac{\beta}{f}\tau x=\mu T_0\cos\nu t\,(\cos\mu y-l\sin\mu y)$$

where the second term produces the l terms in (7.5). The functions C and $\bar{C}$ are expressed by substituting cosine in functions S and $\overline{S}$, respectively. Further the quantities with a bar indicate that they are originated from the term $e^{i(\nu t-\mu y)}$, owing to the condition that $\dfrac{2\beta}{f}\ \dfrac{\partial}{\partial y}R$ term is taken into account of. The equation (7.5) is valid formdally in both modes, where the K, d, φ, m_l, $\overline{m_l}$ and ψ_l, $\overline{\psi_l}$ are defined as

$$K_r=\frac{f_rT_0}{\rho gH\mu\nu}=113T_0,\quad K_l=-\frac{f\mu\beta^2T_0}{\rho gH\,(2\nu)^2}=-1.13T_0 \qquad (7.5\mathrm{a})$$

with r and l indicating barotropic and baroclinic as stated before, and as for d, φ, (in barotropic)

$$de^{i\varphi}=\{(1-2li)\,(1-ni)+\lambda_r^2/\mu^2\}^{-1}\bar{d}e^{i\bar{\varphi}}=\{(1+2l_i)\,(1-ni)\,(-\lambda_r^2/\mu^2\}^{-1} \qquad (7.6\mathrm{a})$$

(in baroclinic)

$$d=\bar{d}=1 \qquad \varphi=\varphi=0$$

Table 4

Iva $k=2\times10^{-8}$	α_1a	β_1a	α_2a	β_2a	$\bar{\alpha}_2a$	$\bar{\beta}_2a$	d	φ	$\bar{d}$
Barotropic	297	29.7	0.460	-0.108	0.473	0.030	0.825	0.23	0.823
Baroclinic	270	30	27	-0.33	α_2a	β_2a	1	0	1
Ivb $k=2\times10^{-7}$									
Barotropic	150	150	0.398	-0.458	0.535	-0.321	0.640	1.032	0.628
Baroclinic	123.5	153	26.5	-3.23	α_2a	β_2a	1	0	1

Iva $k=2\times10^{-8}$	$\bar{\varphi}$	m_1	ψ_1	m_2	ψ_2	$\overline{m_1}$	$\overline{\psi_1}$	$\overline{m_2}$	$\overline{\psi_2}$
Barotropic	-0.063	0.985	-0.174	1	0	m_1	$-\psi_1$	1	0
Baroclinic	0	0.952	-0.317	1	-0.032	m_1	$-\psi_1$	1	-4_2
Ivb $k=2\times10^{-7}$									
Barotropic	0.538	0.985	-0.174	1	0	m_1	$-\psi_1$	1	0
Baroclinic	0	0.985	-0.323	0.965	-0.026	0.922	0.302	1.035	0.028

and also

$$m_l e^{i\psi_l}=(1+p\delta_l)^{-1},\quad \overline{m_l} e^{i\overline{\psi_l}}=(1-p\overline{\delta}_l)^{-1} \tag{7.6b}$$

Practically, $\delta_{1l}=\overline{\delta}_{1l}$, $\delta_{1r}=\overline{\delta}_{1r}$ and $\delta_{2r}=\overline{\delta}_{2r}$ Further, numerical values of these quantities are given by the Table 4.

For the baroclinic mode the expression for R becomes

$$R_l=K_l\{-\sin \nu t\cos \mu y+S_l+l\cos \nu t\cos \mu y+lC_l\} \tag{7.5b}$$

where

$$\begin{aligned}S_l={}&m_1e^{-\beta_1(x+a)}\cos(\mu y+\psi_1)\{\sin(\nu t+\overline{\alpha_1x+a})-e^{2\beta_2a}\sin(\nu t+\alpha_1\overline{x+a}-2\alpha_2a)\\&+\frac{1}{2}e^{-\beta_2(x-a)}\{m_2\sin(\nu t+\mu y+\alpha_2\overline{x-a}+\psi_2)+\overline{m}_2\sin(\nu t-\mu y+\alpha_2\overline{x-a}+\overline{\psi}_2)\}\end{aligned} \tag{7.5c}$$

and for $k=2\times10^{-8}$ the last terms corresponding to δ_2 waves are given by

$$e^{-\beta_2(x-a)}\sin(\nu t+\alpha_2\overline{x-a})\cos(\mu y+\psi_2)$$

and C_l is the substitution of sine in S_l by cosine terms.

Since K_r is about 100 times of K_l in this model, contribution from the baroclinic mode seems to be negligibly small Also the behavior of the function R which is associated with the sea surface and interface has been already discussed in many examples, so that we try to show the velocity distributions here instead of those of R caused by a variable wind stresses.

The western current which is given by the relationship (2.10) and (2.12) becomes very simple, because, for the barotropic mode, only the term which is produced by differentiation of δ_1 waves with x, such as $v_r=\frac{g}{f}\frac{\partial}{\partial x}e^{i\delta_1x}$ term in R_r is predominant. Therefore it is given by

$$v_r=Ve^{-\beta_1\overline{x+a}}\{\sin\Psi_1(\cos\Psi_2+l\sin\Psi_2)-\frac{1}{2}e^{2\beta_2a}(\sin\Phi-l\cos\Phi)-\frac{1}{2}e^{2\overline{\beta}_2\overline{a}}(\sin\Phi+l\cos\overline{\Phi}\} \tag{7.7}$$

where we put

$$\begin{aligned}&V=gK_rdm_1s/f,\quad se^{i\phi}=-\beta_1+\alpha_1i\\&\Psi_1=\nu t+\alpha_1\overline{x+a}+\phi+(\varphi+\overline{\varphi})/2\\&\Psi_2=\mu y+\psi_1+(\varphi-\overline{\varphi})/2\\&\Phi=\nu t+\alpha_1\overline{x+a}+\mu y+\psi_1+\varphi+\phi-2\alpha_2a\\&\Phi=\nu t+\overline{\alpha}_1\overline{x+a}-\mu y-\psi_1+\overline{\varphi}+\phi-2\overline{\alpha}_2a\end{aligned}$$

Similarly, the zonal velocity at the region apart from the western coast is also given by $u_r=\frac{1}{f}\left(-g\frac{\partial R_r}{\partial y}\right)$, because other terms in the original relationship (2.9) and (2.11) are negligibly small. Therefore

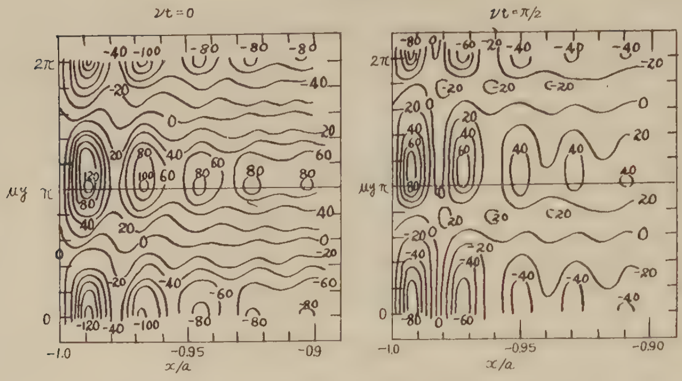

Fig. 17. Isopleths of (R_r/T_0) for $k=2\times10^{-8}$

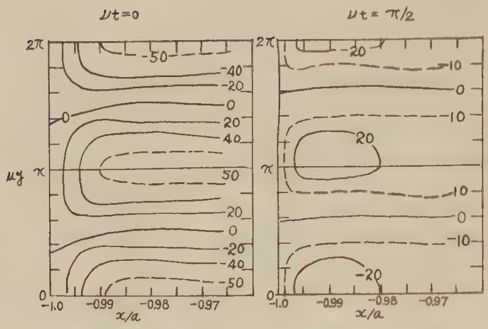

Fig. 18. Isopleths of (R_r/T_0) for $k=2\times10^{-7}$

stage the zonal current in the south or north flows to the opposite direction to the wind stress. Such situation is quite different from the results derived by Fuglister (1951a) from the statistics of the surface currents data, which says that the speed fluctuation of the north equatorial current and the trade wind are approximately the same. Further, even the western current itself shows the time lag, when we take the value at $x=-a$ and $\mu y=\pi$, which also differs from the result of Veronis and MORGAN (1955), because the present model does not correspond exactly to their one.

8. *The response to an asymmetrical wind system*

When the free waves are in SC range, that is, the frequency is larger than critical values, δ_1 waves are only effective near the western coast and δ_2 waves, on the other hand, are important near the eastern coast, and their amplitude is almost symmetric about the center of the ocean, since δ_1 and δ_2 are conjugate complex number. However, in the WI range such symmetry vanishes, because δ_1 waves attenuates conspicuously as apart from the western coast, and yet the imaginary part of δ_2 is much smaller than that of δ_2. Therefore, we can expect much difference between the SC and WI range for an asymmetric wind distribution.

The general solution of the equation (2.17) for a type of the wind stress distribution

$$F=F(x)\cos\nu t\sin\mu y \tag{8.1}$$

is given by

$$R=2\Re\{iP(x)e^{i\nu t}\sin\mu y\} \tag{8.2}$$

where

$$P(x)=J(x)+Ae^{i\delta_1 x}+Be^{i\delta_2 x} \tag{8.3}$$

and also

$$J(x)=\frac{f\sigma j}{2(i\nu+k)(\delta_2-\delta_1)gH}\int_{-a}^{x}F(\xi)\{e^{i\delta_1(x-\xi)}-e^{i\delta_2(x-\xi)}\}d\xi \tag{8.4}$$

in which the numerical constants A and B might be determined by the boundary conditions. Particularly, when we take the most simple boundary conditions, suca as $R_y=0$ at $y=\pm a$, which do not harm the general validity of the discussion here, then we obtain the solution such as

$$P(x)=J(x)+J(a)(e^{i\delta_2 x-i\delta_1 a}-e^{i\delta_1 x-i\delta_2 a})/2\sin(\delta_1-\delta_2)a \tag{8.5}$$

When we take into account of friction having an order of magnitude larger than 10^{-8}, we have a relation such as $|e^{i(\delta_2-\delta_1)a}|\gg|e^{i(\delta_1-\delta_2)a}|$ as seen from Table 3, so that we can put $\sin(\delta_1-\delta_2)a\doteqdot -e^{i(\delta_2-\delta_1)a}/2$ and the above equation becomes

$$P(x)=J(x)+J(a)e^{-i2a\delta_2}\{e^{i\delta_6(a+x)}-e^{i\delta_2(a+x)}\} \tag{8.5a}$$

In this section we assume that the function $F(x)$ is constant over a finite belt and it vanishes outside the belt, weich is called here as "wind belt". For comparison we consider two types of the wind belt, where one locates near the western coast and the other near the eastern coast. In each example the equations $F(x)$ and corresponding $J(x)$ are given as

(Va) $F(x)=F_0$ (in $-a<x<-a+\varDelta$) $=0$ (in $-a+\varDelta<x<a$)

$$J(x)=J_0\left\{\frac{e^{i\delta_1(x+a)}(1-e^{-i\delta_1\varDelta})}{i\delta_1}-\frac{e^{i\delta_2(x+a)}(1-e^{-i\delta_2\varDelta})}{i\delta_2}\right\}$$

(in $a>x>-a+\varDelta$)

$$=J_0\left\{\frac{e^{i\delta_1(x+a)}-1}{i\delta_1}-\frac{e^{i\delta_2(x+a)}-1}{i\delta_2}\right\}$$

(in $-a+\varDelta>x>-a$) (8.6a)

(Vb)

$F(x)-F_0$ (in $a-\varDelta<x<a$) $=0$ (in $-a<x<a-\varDelta$)

$$J(x)=J_0\left\{\frac{e^{i\delta_1(x-a+\Delta)}-1}{i\delta_1}-\frac{e^{i\delta_2(x-a+\Delta)}-1}{i\delta_2}\right\}$$

$$(\text{in } a>x>a-\Delta)$$

$$=0 \quad (\text{in } a-\Delta>x>-a) \tag{8.6b}$$

where $$J_0=f\sigma_iF_0/2(\imath\nu+k)(\delta_2-\delta_1)gH$$

From the same assumption about the frictional coefficient we can deduce the condition $|e^{i\delta_1 a}|\ll 1$, so that the values of $J(a)$ are given by

(Va) $$J(a)=J_0e^{i\delta_2 a}(e^{-i\delta_2\Delta}-1)/(i\delta_2)$$

(Vb) $$J(a)=J_0\left(\frac{e^{i\delta_1\Delta}-1}{i\delta_1}-\frac{e^{i\delta_2\Delta}-1}{i\delta_2}\right)$$

Therefore the equation of $P(x)$ for two examples is expressed as

(Va) inside wind belt or for $-a+\Delta>x>a$

$$P(x)=\frac{J_0}{i}\left\{\left(\frac{1}{\delta_1}-\frac{1}{\delta_2}\right)(e^{i\delta_1\overline{x+a}}-1)+\frac{1}{\delta_2}e^{-i\delta_2\Delta}(e^{i\delta_1\overline{a+x}}-e^{i\delta_2\overline{a+x}})\right\} \tag{8.7a}$$

outside wind belt or for $a>x>-a+\Delta$

$$P(x)=\frac{J_0}{i}e^{i\delta_1(a+x)}\left(\frac{1-e^{-i\delta_1\Delta}}{\delta_1}-\frac{1-e^{-i\delta_2\Delta}}{\delta_2}\right) \tag{8.8a}$$

(Vb) inside wind belt or for $a>x>a-\Delta$

$$P(x)=\frac{J_0}{i}\left\{\left(\frac{1}{\delta_1}-\frac{1}{\delta_2}\right)(e^{i\delta_2(x-a)}-1)+\frac{1}{\delta_1}e^{i\delta_1\Delta}(e^{i\delta_1\overline{x-a}}-e^{i\delta_2\overline{x-a}})\right\} \tag{8.7b}$$

outside wind belt or for $a-\Delta>x>-a$

$$P(x)=\frac{J_0}{i}e^{-i2a\delta_2}(e^{i\delta_1\overline{a+x}}-e^{i\delta_2\overline{x+a}})\left(\frac{e^{i\delta_1\Delta}-1}{\delta_1}-\frac{e^{i\delta_2\Delta}-1}{\delta_2}\right) \tag{8.8b}$$

In SC range, where δ_1 and δ_2 are conjugate complex, we have a relation such that $|e^{-i\delta_2 a}|=|e^{i\delta_1 a}|\ll 1$, thus we can neglect $e^{i\delta_1\overline{a+x}}$ against $e^{i\delta_2\overline{a+x}}$ in the equation (8.8b) and we have instead

$$P(x)=-\frac{J_0}{i}e^{i\delta_2(x-a)}\left(\frac{e^{i\delta_1\Delta}-1}{\delta_1}-\frac{e^{i\delta_2\Delta}-1}{\delta_2}\right) \tag{8.8c}$$

Therefore we obtain a symmetrical distributions of a function $|P(x)|$ about the origin in SC range for the these models of (Va) and (Vb).

For the equation (8.8a) and (8.8c) are conjugate complex for the value of $x=a-x_0$ in (8.8a) and for $x=-a+x_0$ in (8.8c).

The values of (8.7a) and (8.7b) become

$$P(a-x_0)=\frac{J_0}{i}\left\{\left(\frac{1}{\delta_1}-\frac{1}{\delta_2}\right)(e^{i\delta_1 x_0}-1)+\frac{1}{\delta_2}e^{-i\delta_2\Delta}(e^{i\delta_1 x_0}-e^{i\delta_2 x_0})\right\}$$

$$P(x_0-a)=\frac{J_0}{(-i)}\left\{\left(\frac{1}{\delta_2}-\frac{1}{\delta_1}\right)(e^{-i\delta_2x_0}-1)+\frac{1}{\delta_1}e^{i\delta_1\varDelta}(e^{-i\delta_2x_0}-e^{-i\delta_1x_0})\right\}$$

which are also conjugate complex, so that their absolute values are equal to each other. Further, we can see that the value of $|P(x)|$ decreases rapidly as apart from the wind belt, because it is proportional to $exp\{-\beta_1(a+x)\}$ for the case of Va and to $exp\{-\beta_1(a-x)\}$ for (Vb). When $\varDelta$ is not so small and $|e^{i\delta_1\varDelta}|=|e^{-i\delta_2\varDelta}|\ll 1$, the equations (8.7) and (8.8) are expressed more simply as

(Va) inside wind belt

$$P(\lambda)=\frac{J_0}{i}\left\{\left(\frac{I}{\delta_1}-\frac{1}{\partial_2}\right)(e^{i\delta_1\overline{a+x}}-1)-\frac{1}{\delta_2}e^{i\delta_2(x+a-\varDelta)}\right\} \tag{8.9a}$$

outside wind belt

$$P(x)=-\frac{J_0}{i\delta_1}e^{i\delta_1(a+x-\varDelta)} \tag{8.10a}$$

(Vb) inside wind belt

$$P(x)=\frac{J_0}{i}\left\{\left(\frac{1}{\delta_1}-\frac{1}{\delta_2}\right)(e^{i\delta_2\overline{x-a}}-1)+\frac{1}{\delta_1}e^{i\delta_1(x-a+\varDelta)}\right\} \tag{8.9b}$$

outside wind belt

$$P(x)=\frac{J_0}{i\delta_2}e^{i\delta_2(x-a+\varDelta)} \tag{8.10b}$$

On the other hand in the range of WI, $|\delta_2|\ll|\delta_1|$, so that the relation $|e^{-i\delta_2a}|\ll 1$ is no more valid even when $|e^{i\delta_1a}|\gg 1$, thus we have no symmetric distribution of the absolute value of $P(x)$. In fact, from the equation (8.7a) and (8.7b) we have

(Va) outside wind belt (from eq. 8.7a)

$$|P(x)|=P_0\,e^{-\beta_1(a+x)} \tag{8.11a}$$

(Vb) inside wind belt (from eq. 8.7b)

$$|P(x)|=P_0e^{-2a\beta_2}\left|e^{(\alpha_1i-\beta_1)(a+x)}-e^{(\alpha_2i+\beta_2)(a+x)}\right| \tag{8.11b}$$

where

$$P_0=|J_0|\left|\frac{1-e^{-i\delta_1\varDelta}}{\delta_1}-\frac{1-e^{-i\delta_2\varDelta}}{\delta_2}\right|$$

The equation (8.11a) indicates that the absolute value $|P(x)|$ diminishes rapidly as apart from the wind belt the example (Va) since $\beta_1a\gg 1$.

On the contrary, the equation (8.11b) becomes equal to a value of $P_0exp\,\beta_2(x-a)$ as x differs only a little from $-a$, that is, at a short distance from the western coast, because $exp\{-\beta_1(a+x)\}\ll 1$ except near $x=-a$, so that the value of $|P(x)|$ for (Vb) is finite almost all over the outside region of wind belt since $\beta_2a\ll 1$.

Summarizing above results, in the SC range or for shorter period fluctuation of the wind stress curl, the effect of wind decreases rapidly as apart from the wind belt. In the WI range or for a longer period disturbance, the effect of wind diminishes rapidly as apart from the wind belt only when the wind belt coincides with the western part of the ocean and when the wind belt locates in the eastern part, the effect reaches near the western coast and amplitude of surface fluctuation becomes finite very near the western coast.

The function $P(x)$ represents not only the fluctuation of the surface and interface but also zonal velocity, as seen from its definition. Therefore above conclusion is valid in the spatial distribution of zonal velocity. On the other hand the meridional velocity is proportional to $\partial p/\partial x$ and this quantity is more appropriate to show the situation concerning the assymmetry of the amplitude of fluctuation in SC and WI ranges for two types of wind stress distributions. The expressions for $\partial p/\partial x$ for the same wind stress distribution are given by

(Va) inside wind belt $(-a+\varDelta>x>-a)$

$$P_x=J_0\{e^{i\delta_1(x+a)}(1-\frac{\delta_1}{\delta_2}+\frac{\delta_1}{\delta_2}e^{-i\delta_2\varDelta})-e^{i\delta_2(x+a-\varDelta)}\} \qquad (8.12a)$$

outside wind belt $(a>x>-a+\varDelta)$

$$P_x=J_0e^{i\delta_1(x+a)}\{1-e^{-i\delta_1\varDelta}-\frac{\delta_1}{\delta_2}(1-e^{-i\delta_2\varDelta})\} \qquad (8.13a)$$

(Vb) inside wind belt $(a>x>a-\varDelta)$

$$P_x=J_0\{e^{i\delta_1(x-a+\varDelta)}-e^{i\delta_2(x-a)}(1-\frac{\delta_2}{\delta_1}+\frac{\delta_2}{\delta_1}e^{i\delta_1\varDelta})\} \qquad (8.12b)$$

outside wind belt $(a-\varDelta>x>-a)$

$$P_x=J_0e^{-i2\delta_2a}\left\{\delta_1e^{i\delta_1(a+x)}-\delta_2e^{i\delta_2(a+x)}\right\}\left(\frac{1-e^{i\delta_2\varDelta}}{\delta_2}-\frac{1-e^{i\delta_1\varDelta}}{\delta_1}\right) \qquad (8.13b)$$

where we can consider $|e^{i\delta_1a}|\ll 1$.

In *SC* range with moderate value of $\varDelta$, we have

$|e^{-i\delta_2a}|=|e^{i\delta_1a}|\ll 1, \quad |e^{i\delta_1\varDelta}|=|e^{-i\delta_2\varDelta}|\ll 1$

so the equations (8.12) and (8.13) have more simple form such as

(Va) inside wind belt

$$P_x=J_0\{e^{i\delta_1(x+a)}(1-\frac{\delta_1}{\delta_2})-e^{i\delta_2(x+a-\varDelta)}\} \qquad (8.14a)$$

outside wind belt

$$P_x=-J_0e^{i\delta_1(x+a-\varDelta)} \qquad (8.15a)$$

(Vb) inside wind belt

$$P_x=J_0\{e^{i\delta_1(x-a+\Delta)}-e^{i\delta_2(x-a)}(1-\frac{\delta_1}{\delta_2})\} \tag{8.14b}$$

outside wind belt

$$P_x=J_0e^{i\delta_2(x-a+\Delta)} \tag{8.15b}$$

The equation (8.14) and (8.15) indicate similar features as those (8.9) and (8.10) and the amplitude distribution for two types of wind stress is symmetrical about the origin as the absolute valve of $P(x)$ itself.

In the WI range where $|\delta_1|\gg|\delta_2|$ and $|e^{i\delta_1\Delta}|\ll 1$, we obtain

(Va) inside wind belt

$$P_x=-J_0\{e^{i\delta_2(x+a-\Delta)}+\frac{\delta_1}{\delta_2}e^{i\delta_1(x+a)}(1-e^{-i\delta_2\Delta})\} \tag{8.16a}$$

outside wind belt

$$P_x=-J_0e^{i\delta_1(x+a)}\{e^{-i\delta_1\Delta}+\frac{\delta_1}{\delta_2}(1-e^{-i\delta_2\Delta})\} \tag{8.17a}$$

(Vb) inside wind belt

$$P_x=J_0\{e^{i\delta_1(x-a+\Delta)}-(1-\frac{\delta_2}{\delta_1}e^{i\delta_2(x-a)}\} \tag{8.16b}$$

ouside wind belt

$$P_x=J_0e^{-2i\delta_2a}(1-e^{i\delta_2\Delta})\{\frac{\delta_1}{\delta_2}e^{i\delta_1(a+x)}-e^{i\delta_2(x+a)}\} \tag{8.17b}$$

It is remarkable that the value of P_x does not vanish at the coast and as symmetry of the distribution of the value of $|P_x|$ between Va and Vb in WI range is clearly shown by the comparison of the value at the western and eastern coast. In fact, in SC range these values are expressed by

(Va)
$$P_x(a)=J_0e^{i\delta_1(2a-\Delta)}$$
$$P_x(-a)=J_0(1-\frac{\delta_1}{\delta_2})$$

(Vb)
$$P_x(a)=J_0(1-\frac{\delta_1}{\delta_2})$$
$$P_x(-a)=J_0e^{-i\delta_2(2a+\Delta)}$$

Therefore the value of $P_x(-a)$ in (Va) is the same as that of $P_x(a)$ in (Vb) and also $P_x(a)$ in (Va) is the same as $P_2(-a)$ in Vb, where the latter is almost zero. On the other hand, these boundary values in WI range become

(Va)
$$P_x(a)=-J_0e^{2i\delta_1a}\{e^{-i\delta_1\Delta}+\frac{\delta_1}{\delta_2}(1-e^{-i\delta_2\Delta})\}$$

$$P_x(-a)=J_0(1-\frac{\delta_1}{\delta_2})\ (1-e^{-i\delta_2\Delta})$$

(Vb) $$Px(a)=J_0(1-\frac{\delta_2}{\delta_1})$$

$$P_x(-a)=J_0e^{-i2a\delta_2}\left\{\frac{\delta_1}{\delta_2}(1-e^{i\delta_2\Delta})-1\right\}$$

Therefore, in the example (Va) $|P_x(a)| \ll 1$, since $|e^{i\delta_1(2a-\Delta)}| \ll 1$ but in (Vb) the western current $P_x(-a)$ is not so small, because in this case the relation $|e^{-i2a\delta_2}| \ll 1$ is not valid.

Distribution of $F(x)$

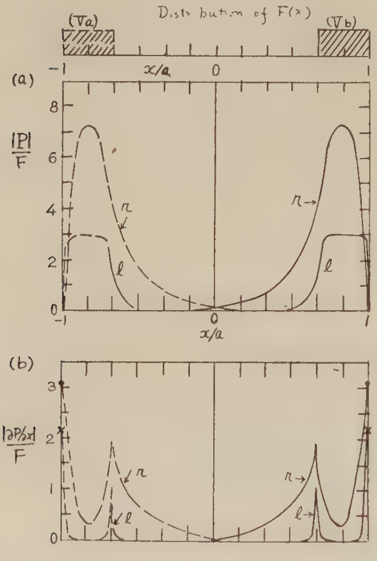

(The scale of ordinates is 10> for r-curves, 10^5 for l-curves.)

(The scale of ordinates is 1 for r-curves, 10^{-2} for l-curves.)

Fig. 19. $|P(x)|$ and $|P_x(x)|$ for SC range.
(Broken lines: V_a model, r: barotropic mode, Solid lines: V_b model, l: baroclinic mode)

In Fig. 19 (a) we show the distribution of $|P(x)|$ about x for two types of wind stress distribution by taking $\mu=5\times10^{-8}$, $\nu=5\times10^{-6}$, $\Delta=10^8$, which corresponds to the SC range. We can sec that the amplitude $|P(x)|$ is finite only within and near the wind belt and also its spatial distibution is symmetrical about the origin for the case (Va) and (Vb), as stated before. Further, the values of $|P(x)|$ for barotropic mode is far larger than that of baroclinic mode, since $|J_{0r}|/|J_{0l}| \doteqdot |(\delta_2-\delta_1)_l/(\delta_2-\delta_1)_r r|$. This is true even in WI range, because $|J_{0r}|/|J_{0l}| \doteqdot \frac{1}{r}$ since $|(\delta_2-\delta_1)_l| \doteqdot |(\delta_2-\delta_1)_r|$ in this range.

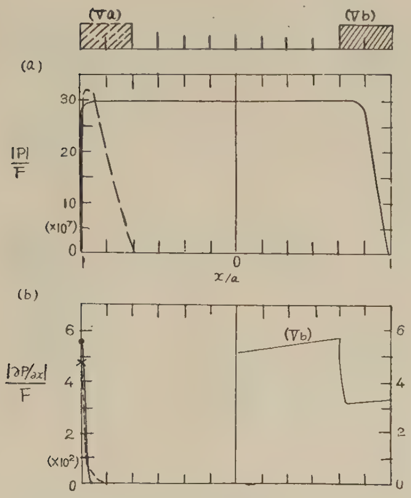

(Scale for V_b curve in east section. Note that the values in east section is 10^{-2} of those at western coast and that these of V_a are so small that the curve almost coincides with the abscissa)

Fig. 20. $|P(x)|$ and $|P_x(x)|$ of barotropic mode for WI range ($\nu=10^{-7}$, $k=10^{-8}$, $\Delta=10^{8}$)
(Broken lines: V_a model, Solid lines: V_b model)

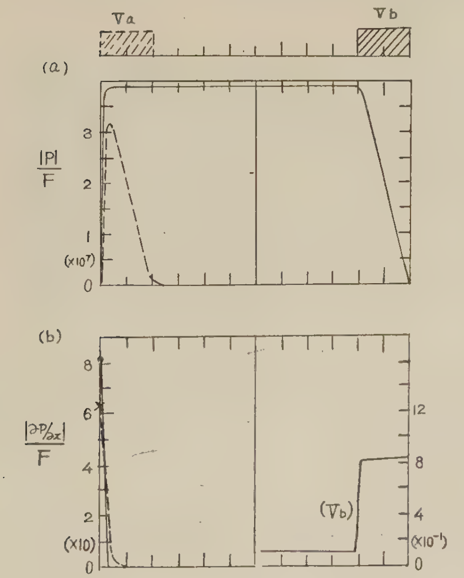

(Scale for V_b curve in east section. The same remark as in Fig. 20b)

Fig. 21. $|P(x)|$ and $|P_x(x)|$ of baroclinic mode for WI range ($\nu=10^{-7}$, $k=10^{-8}$, $\Delta=10^{8}$)

In Fig. 20(a) and 21(a) we indicate the similar distribution of $|P(x)|$ for WI range, by taking the numerical constant such as $\mu=5\times10^{-8}$, $\nu=10^{-7}$, $k=10^{-8}$, Δ

$=10^8$. These figures indicate clearly the difference between WI and SC, since in (Va) the amplitude $|P(x)|$ is finite only in the wind belt which locates in the western part and it dminishes rapidly as apart from it. On the other, hand, the value of $|P(x)|$ has almost constant, equal to $|J_0|\,|1-e^{-i\delta_2\Delta}|/|\delta_2|$ all over the ocean outside wind belt, except at $x=-a$. Especially for barotropic mode this constant has approximate value of $|J_0|\Delta$, since $|i\delta_2\Delta|\ll 1$.

When we compare the values of $|P(x)|$ between SC and WI range, we can see generally that the value in WI is larger than in SC range. When we exress the maximum value of $|P(x)|$ in each range, they are proportional to $|J_0/\delta_2|$ or to $|/\nu|\delta_2(\delta_2-\delta_1)|$ for both range (in SC range we might take this as $|J_0/\delta_1|$ since $|\delta_1|=|\delta_2|$) and in WI range $\nu|\delta_2|$ is quite smaller than that in SC range, and $|\delta_2-\delta_1|$ has a most the same order of magnitude in both ranges.

In Fig. 19(b) we show the similar distribution of $|P_x|$ for (Va) and (Vb) with same numerical constants as In Fig. 19(a), which indicates that the meridional velocity is finite only near the coast and the boundary of the wind belt and its spatial distribution is symmetrical about the origin as in the distribution of P shown in Fig. 19(a).

In Fig. 20(b) and 21(b) the distribution of $|P_x|$ in WI range is shown by taking the same numerical constants as in Fig. 20(a) and 21(a) which indicate that in both types of wind distribution almost the same amount of westeward meridional current is produced notwithstanding the condition that in (Va) the wind acts only near the eastern coast. Especially it is interesting to note that in (Vb) model the meridional current in the wind belt which is near the eastern coast is much weaker than the western coast current. In fact the value of P_x in and near wind belt is expressed as

(inside wind belt or $a>x>a-\Delta$)

$$P_2=J_0\{e^{i\delta_1(x-a+\Delta)}-e^{i\delta_2(x-a)}\} \tag{8.18}$$

(outside wind belt and not near the western coast)

$$P_x=J_0(1-e^{-i\delta_2\Delta})\,e^{i\delta_2(x-a+\Delta)}$$

where the contribution of the first term in (8.18) becomes negligible except very close to $x=a-\Delta$. Therefore, in this type of wind stress distribution the meridional current in the wind belt near the eastern coast has an order of magnitude $|J_0|$ or $J_0|1-e^{-i\delta_2\Delta}|$ which is far smaller than the western current of the order of about $|J_0\delta_1/\delta_2|\,e^{B_2(\Delta-2a)}$.

It is somewhat worthwhile to examine the mode of the western current caused

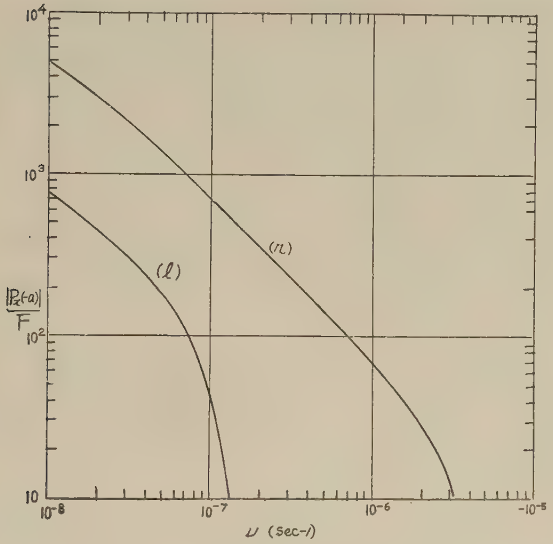

Fig. 22. $P_x(-a)$ as a function of ν (*r*): Barotropic (*l*): Baroclinic

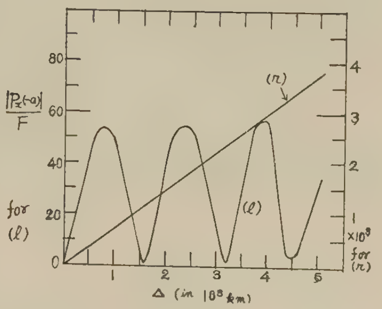

Fig. 23. $P_x(-a)$ as a function of Δ (*r*): Barotropic (*l*): Baroclinic

by the wind stress of type (Vb). Here we show two of such relationships, one is Fig. 22, which gives the value of $|P_x(-a)$ as a function of ν by taking $k=10^{-8}$ $\mu=5\times10^{-8}$ and $\Delta=10^8$. We can see that the value of $|P_x(-a)|$ increases as ν decreases or the period of the fluctuation increases. When ν approaches to the critical value between SC and WI range the value of $|P_x(-a)|$ rapidly decreases, since in SC range it has an order of magnitude of $e^{-2\beta_1 a}$. Further, we can see that the value is always larger for barotoropic mode.

As another example we show the change of $|B_x(-a)|$ as a function of Δ with numerical constants $k=10^{-8}$, $\mu=5\times10^{-8}$, $\nu=10^{-7}$ or in WI range of course. In this example we have a very simple relation for the barotropic mode, since $|i\delta_2\Delta|\ll1$ and $|P_x(-a)|$ increases almost linearly with Δ. On the other hand, for the baroclinic mode

$$|P_x(-a)|\sim|1-e^{i\delta_2\Delta}|$$

and also when we put $\Delta=\frac{a}{3}\Delta_0$, then we have $i\delta_2\Delta=(\Delta i+0.025)\Delta_0$ and thus the value of $|R_x(-a)|$ shows spectral distribution about Δ_0 or there exists some resonance phenomenon.

The difference in the response to the wind stress between two cases of western wind belt and eastern wind belt in WI range is due to the fundamental property of β-plane and this situation can be explained more simply by stationary circulation pattern in a rectangular β-plane of homogeneous ocean with friction proportional to velocity which was treated by Stommel (1948) to prove the westward intensification of oceanic circulation.

In such model the vorticity equation becomes

$$\beta v + k\zeta = \frac{1}{h}\left(\frac{\partial \tau_y}{\partial x} - \frac{\partial \tau_x}{\partial y}\right)$$

where k is friction coefficient, ζ relative vorticity, τ_x, τ_y are stress component, h is depth. Assuming geostrophic relation for velocity, we put

$$u = -\partial P/\partial y \quad v = \partial P/\partial x$$

$$F(x)\sin\mu y = \frac{1}{kh}\left(\frac{\partial \tau_y}{\partial x} - \frac{\partial \tau_x}{\partial y}\right)$$

then we have

$$P_{xy} + \frac{\beta}{k}P_x - \mu^2 P = F(x)$$

Therefore the general solution of $P(x)$ is given by

$$P(x) = J(x) + J(a)e^{-2\lambda_1 a}\{e^{\lambda_2(a+x)} - e^{\lambda_1(a+x)}\}$$

as in (8.5a), where

$$J(x) = \frac{1}{(\lambda_1-\lambda_2)}\int_{-a}^{x} F(\xi)\{e^{\lambda_1(x-\xi)} - e^{\lambda_2(x-\xi)}\}d\xi$$

and

$$\lambda_1 = -(\beta/2k) + \sqrt{(\beta/2k)^2+\mu^2}$$

$$\lambda_2 = -(\beta/2k) - \sqrt{(\beta/2k)^2+\mu^2}$$

and also $|e^{\lambda_2 a}| \ll 1$, unless μ is large and if $k < 10^{-5}$, or in other words, when the north-south pattern of the system is larger than the order of magnitude of 1000 km and friction is not so large.

When we assume the same wind belt as in (Va) and (Vb), we obtain the special solution, corresponding to (8.16) and (8.17), such as

(V′a) inside wind belt $(-a+\Delta > x > -a)$

$$P(x) = \frac{F_0}{(\lambda_1-\lambda_2)}\left\{\left(\frac{1}{\lambda_1} - \frac{1}{\lambda_2}\right)(e^{\lambda_2\overline{a+x}} - 1) + \frac{e^{-\lambda_1\Delta}}{\lambda_1}\left(e^{\lambda_1\overline{(a+x)}} - e^{\lambda_2\overline{a+x}}\right)\right)\right\}$$

outside wind belt $(a > x > -a+\Delta)$

$$P(x) = \frac{F_0 e^{\lambda_2(a+x)}}{(\lambda_1-\lambda_2)}\left(\frac{e^{-\lambda_2\Delta}}{\lambda_2} + \frac{1-e^{-\lambda_1\Delta}}{\lambda_1}\right)$$

(V′b) inside wind belt $(a > x > a-\Delta)$

$$P(x) = \frac{F_0}{(\lambda_1-\lambda_2)}\left\{\left(\frac{1}{\lambda_1} - \frac{1}{\lambda_2}\right)(e^{\lambda_1\overline{x-a}} - 1) + \frac{e^{\lambda_2(x-a+\Delta)}}{\lambda_2}\right\}$$

outside wind belt $(a-\Delta > x > -a)$

$$P(x) = \frac{F_0}{\lambda_1-\lambda_2}\left(\frac{1}{\lambda_2} - \frac{1}{\lambda_1} + \frac{e^{\lambda_1\Delta}}{\lambda_1}\right)e^{-2\lambda_1 a}\{e^{\lambda_2(a+x)} - e^{\lambda_1(a+x)}\}$$

where we assume that Δ is of a moderate magnitude or $e^{\lambda_2\Delta} \ll 1$. In order to give some idea about the magnitude of λ_1 and λ_2 we show the next table which corresponds to Table 3.

$\mu=$	10^{-7}	5×10^{-8}	10^{-8}
$k=10^{-6}$ $\lambda_1(\times10^{-7})$	0.41	0.12	0.005
$\lambda_2(\times10^{-7})$	−2.41	−2.12	2.005

$k=10^{-7}$	$\lambda_1(\times 10^{-9})$	5.0	1.25	0.05
	$\lambda_2(\times 10^{-6})$	2.005	2.000	2.000

Therefore these equations have the same features as the equations (8.16) and (8.17), because in (V′a) model $|P(x)|$ diminishes to zero quite rapidly as apart from the wind belt owing to the exponential factor $\exp \lambda_2(a+x)$. On the other hand, in the model (V′b) in which the wind belt lies near the eastern coast, the function $P(x)$ has a factor $\exp \lambda_1(x-a)$ outside wind belt, which remains finite as we can see from above table.

This similarity between the condition in the stationary circulation and in the range of WI in a text exists also in the spatial distribution of $\partial P/\partial x$. This is quite obvious, because in non-stationary solution we get stationary circulation when we put $\nu=0$ which belongs certainly to WI range as seen in Table 3.

Generally speaking, the absolute values of $P(x)$ and $\partial P/\partial x$ are larger in barotropic mode than in baroclinic mode for both range of *SC* and *WI* and the ratio of these quantities of barotropic to baroclinic mode becomes larger for small values of ν or in *SC* range, so that barotropic mode becomes more predominent as frequency increases as in case of various kinds of wind stress distributions discussed above.

Moreover, it seems to be worthwhile to remark that in certain ranges of ν between very low and high frequencies, for example between $\nu=10^{-6}$ and 5×10^{-7} for $\mu=5\times10^{-8}$ as seen in Table 3, the barotropic mode belongs to *WI* range whereas baroclinic mode belongs to *SC* range. In other words, in such range of ν when wind belt is located near eastern coast the excitation of westward intensification occurs only in barotropic mode.

Summarizing above results, we can conclude that

(1) For a disturbance of a period shorter than a couple of weeks the respons of the ocean is limited only near wind belt, no matter where it is located in the ocean.

(2) For a disturbance of a period longer than half a year, in case wind belt is near the western coast, the response is limitted near wind belt, but in case it is near eastern coast, the response reaches western coast and particularly amplitude of meridional current along the western coast is larger than that along the eastern coast, even though wind belt is near eastern coast. This is true for both modes.

(3) For a disturbance of a period between these two values the response of barotropic mode has the same feature as described in (2), whereas that of baroclinic mode indicates the feature of shorter period as described in (1), so

that when the wind belt is near the eastern coast, strong west coast current is generated only in barotropic mode.

(4) For all periods considered here the amplitude of the response of the ocean is larger for barotropic mode than for baroclinic mode, and such difference in amplitude becomes larger as the period of disturbance decreases.

9. *Application of theoretical models and concluding remarks.*

In this paper we have no space to discuss the application of the models to practical problems in detail, partly because we have not had enough observed facts concerning the response of the ocean to variable wind stresses. However, it seems to be better to show some examples, even though they are very poor as an example of application of the theoretical models, rather than not to mention them.

In Fig. 24 annual variations of the total mass transport of the Kuroshio south off Cape Shionomisaki (Ichiye, 1957) and that of the Gulf Stream in the section between Montauk Pt. and Bermuda (Iselin, 1940) are shown. These two curves are not so adequate to be compared with each other, since the reference level

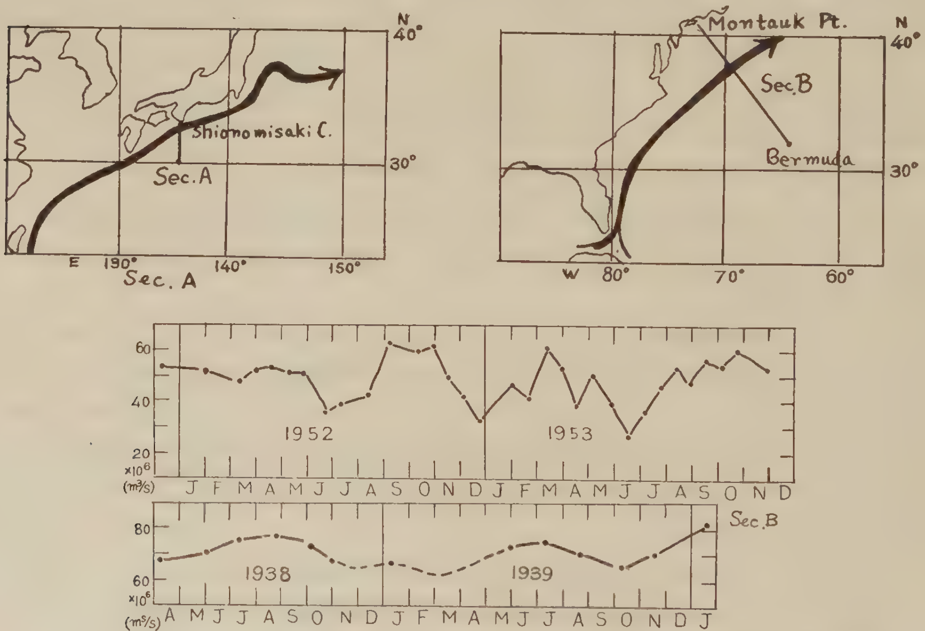

Fig. 24. Annual variations of mass transport in the Kuroshio and the Gulf Stream.

for dynamic computation is different (in the Kuroshio 1000 db, and in the Gulf Stream 2000 db), and also the year of observation, the distances between succesive stations are not the same in two curves. Neverthless, if we examine these curves closely, we can recognize some characteristic features between two current systems. The annual range of fluctuation in the Kuroshio reaches about 20×10^6 m^3/s, whereas that of the Gulf Stream is only about half of it, although the mean transport of the Kuroshio is less than that of the Gulf Stream by about 30×10^6 m^3/s. The difference in the mean values may be partly due to the condition that the reference level in the Kuroshio is more shallow than in the Gulf Stream. Further, the maximum transport seems to occur in spring and autumn in the former, whereas it occurs in summer and winter in the latter, though it is too early to conclude by use of so incomplete data.

The data concerning wind stress distribution over the ocean are also insufficient in the present stage, since such data are given only in the average state, as far as the author knows. However, the voritcity distribution of the

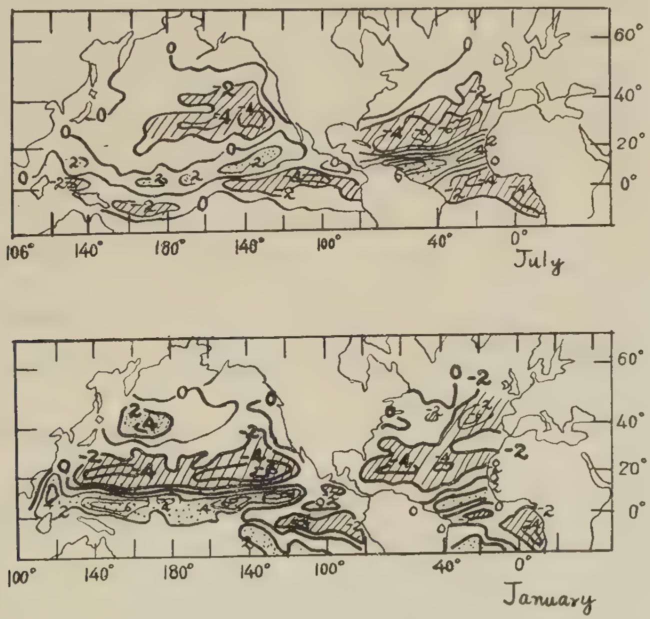

Fig. 25. Vorticity of mean surface wind over the ocean in 10^{-6} S^{-1} after MINTZ and DEAN (1952). (The stippled pattern indicates positive, and the diagonal ruling negative vertical vorticity greater than 2×10^{-6} s^{-1})

surface wind in July and January prepared by Mintz and Dean (1952) which is reproduced in Fig. 25 indicates interesting features of the difference of wind stress condition over the north Atlantic and the north Pacific. When we pay attention to the region between N40° and N20° which corresponds roughly to the rectangular basin considered here, the difference in the vorticity of wind between in winter and summer is more conspicuous over the Pacific than over the Atlantic. Further, the absolute value of negative vorticity in the considered region is higher in summer than in winter over the Atlantic, whereas the condition over the Pacific is reverse. Unfortunately we have no chart of spring and autumn, so that we cannot say about the difference in phase of the annual variation of the transport in two oceans. However, the larger annual fluctuation of the transport of the Kuroshio seems to be associated with the larger annual range (or winter-summer difference) of wind vorticity over the Pacific, particularly over the eastern half of the Pacific, as exlpained in the theoretical model, because the variable wind of annual or semi-annual period can cause a large fluctuation of the western current, even when it is applied to the eastern part of the ocean.

Acknowledgement: The author wishes his thanks to Mr. H. Stommel for his encouragement and advices and also to Dr. G. Veronis, Dr. W. Malkus and Mr. F. Fuglister for their discussions about the present paper.

References

Charney, J.G., 1955 (a) The generation of ocean currents by wind Journ. Mar. Res. 14(4) pp 477-498

Charney, J.G., 1955 (b) The Gulf Stream System as an inertial boundary layer. Proc. N.A.S. (USA) 41(10) pp 731-740

Fuglister, E.C., 1951. (a) Annual variations in current speeds in the Gulf Stream System. Journ. Mar. Res. 10(1) pp 119-127

Fuglister, F.C., 1951 (b) Multiple currents in the Gulf Stream System. Tellus, 4, pp 230-233

Ichiye, T., 1951 On the variation of ocean circulation (1) Oceanog. Mag. 3(2) pp 79-82

Ichiye, T., 1957 On the Hydrography of the Western North Pacific and its seasonal variation. (To be published. The paper was read at the meeting of Ass. d'Ocean. Phys. of IUGG at Toronto in September of 1957)

Iselin, C,O'D., 1940 Preliminary report of long-period variations in the transport of the Gulf Stream. Pap. phys. Oceanog. Met. 3(1) pp 1-40

Mintz, Y. and Dean, G., 1952 The observed mean field of motion of the atmosphere. Geophys. Res. Papers no. 17, (Geophys. Res. Dir. Air Force Cambridge Res. Center)

MORGAN, G.w., 1956 On the wind-driven ocean circulation. Tellus, 8(3) pp 301-320

MUNK, W.H., 1950 On the wind-driven ocean circulation. Journ. Met. 7(2) pp 79-93

MUNK, W.H., 1957 Note on Charney's calculations. (Unpublished manuscript)

NEUMANN, G., 1954 Note on the wind-driven ocean circulation New York University, College of Engineering, Research Division. pp 1-54

STOMMEL, H., 1948 The westward intensification of wind-driven ocean currents. Trans. Amer. Geophys. Un., 29(2) pp 202-207

STOMMEL, H., 1955 Why do our ideas about the ocean circulation have such a peculiarly dream-like quality? (Private printing)

VERONIS, G. and G.W. MORGAN, 1955 A study of the time-dependent wind-driven ocean circulation. Tellus 7(2) pp 232-242

VERONIS, G. and H. STOMMEL, 1956 The action of variable wind stresses on a stratified ocean. Journ. Mar. Res. 15(1) pp 43-75

Contribution No. 965

Reprint OIKOS 9:II 1958

BIOGEOGRAPHICAL STUDIES OF MARINE PHYTOPLANKTON*)

BY

THEODORE J. SMAYDA

(Institute for Marine Biology, Sect. B, University of Oslo)

Introduction

Quantitative biogeographical studies of marine phytoplankton have lagged considerably following the appearance of GRAN's (1902) classical paper more than fifty years ago. In this work he outlined his scheme of "plankton elements" which supplanted CLEVE's (1897, 1900) concept of "plankton types" and has remained of fundamental importance to marine biogeography. Since significant progress has been made in floristic studies following Gran's publication, it seems appropriate at this time to consider these advances and arrive at some general features of phytoplankton biogeography. The fact that culture techniques in phytoplankton research is now a certainty also demands a renewed interest in biogeographical problems. It is clear that a satisfactory knowledge of the underlying biogeographical factors can be obtained only by combining floristic studies—where a species is found or what species are found in a given area—with culture studies—why a species is found in a given area and why it is abundant or unimportant. NORDLI's (1957) study on *Ceratium* reveals how successful this approach can be.

Results of experimental studies have served as standards in discussing or interpreting phytoplankton dynamics. Unfortunately most of the species thus far studied are among the less important in nature or are forms whose metabolic activities probably are not significantly representative. For example, the "guinea pig" *Nitzschia closterium* var. *minutissima* appears not to be a diatom at all but the chrysophycean *Phaeodactylum tricornutum* (HENDEY 1954). Biogeographical studies, however, can provide information as to what organisms are representative of the major thermal zones or specific ecological conditions. Following appropriate selection, experimental treatment then can provide data applicable to these environments or conditions. It is unlikely that one or two species can provide universally applicable data—the metabolism of an arctic representative undoubtedly differs from that of a tropical one. Furthermore, it is becoming especially important to know the distribution of a species since BRAARUD's (1951) observations suggest the existence of clones in nature: species common to the waters of Norway and North America may represent discrete physiological units.

---

*) Contribution No. 965 from the Woods Hole Oceanographic Institution.

Thus the author has attempted to summarize the more important concepts of phytoplankton biogeography as revealed in part by representative arctic, antarctic, tropical and cosmopolitan species. In mapping their distribution the investigation most representative of a given region was selected over minor studies, except when temperature and salinity data were included. These data were compiled irrespective of the accompanying degree of abundance of the species in question. Biogeographically, knowledge of the extremes of tolerable temperature and salinity is equally important to knowing optimal requirements.

The Distribution of Representative Phytoplankton Species and the Accompanying Temperature and Salinity Conditions

Antarctic Representative: *Thalassiosira antarctica* Comber

Thalassiosira antarctica is a characteristic and important component of the antarctic flora. Its distribution (Fig. 1) has been charted from the following sources:

> BODEN 1949; HART 1934; HENDEY 1937; KARSTEN 1905a; MANGIN 1915, 1922; MANGUIN 1954.

T. antarctica appears to be circumpolar, a distribution favored by the prevailing current system (SVERDRUP, JOHNSON and FLEMING 1942, p. 615). Indeed, the majority of antarctic phytoplankton species are probably circumpolar considering the uniform environmental conditions within that area associated with the current systems. Latitudinally, *T. antarctica* is confined almost exclusively to waters within the Antarctic Convergence; occasionally it is encountered north of this boundary. Thus HENDEY (1937) recorded *T. antarctica* near Cape Town and Cape Horn at temperatures of 8.4° and 17.2°C while CLEVE (1901) found it in the "Southern Indian Ocean at 45°S, 26–34°E" at 6.5°C. However, the accompanying temperatures indicate that these occurrences undoubtedly resulted from current transport rather than local, independent stocks.

The conditions of temperature and salinity accompanying *T. antarctica*'s occurrence are plotted (Fig. 2). The salient features of this relationship are probably applicable to antarctic phytoplankton in general. It is seen that in nature *T. antarctic* is stenothermal and stenohaline. The observed temperature

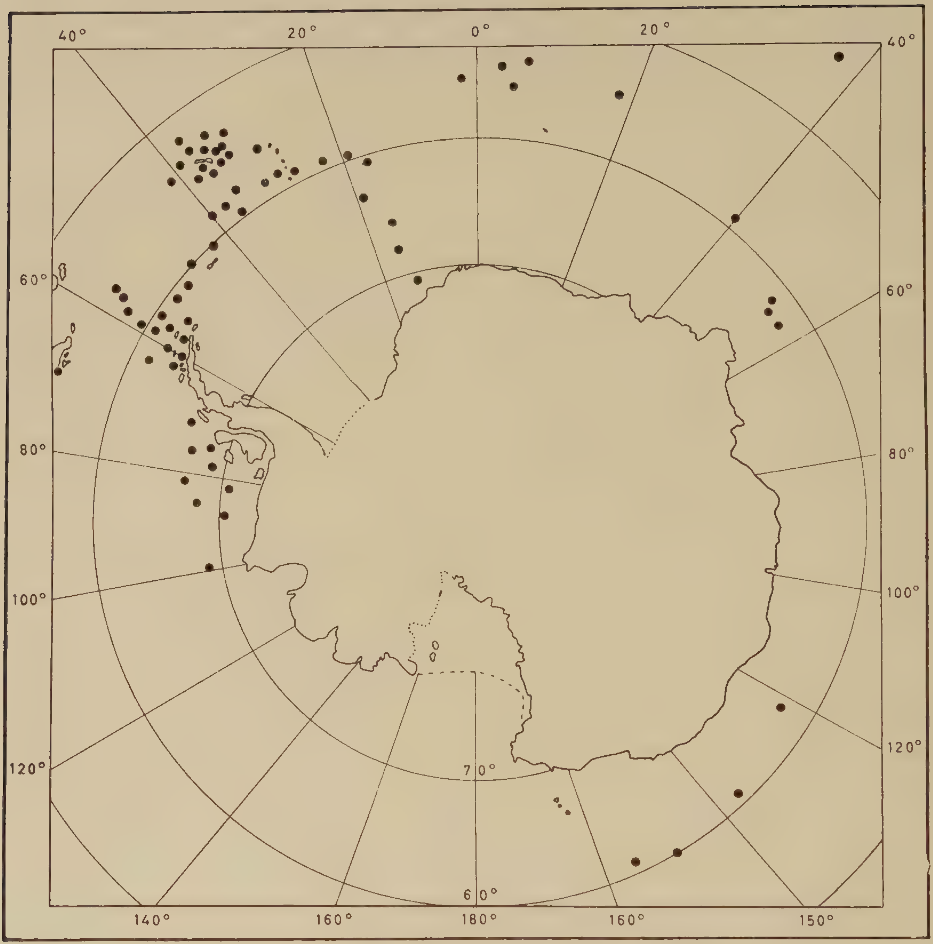

Fig. 1. The geographical distribution of *Thalassiosira antarctica.*

range extends from $-1.77°$ to 3.49°C. It is well represented at temperatures below 0°C, resulting in a mean of $-0.05°$C for 228 observations (including those not plotted)[1]). Its observed salinity range is similarly narrow, 32.61–34.54 $^0/_{00}$. These salinity values reflect the influence of melting ice.

Except for localized conditions, antarctic species in general probably do not have to contend with marked salinity fluctuations or salinities much under 32.00 $^0/_{00}$. The degree of dilution resulting from ice-melting is limited because of the prevailing temperature conditions, and, in addition, the re-formation

---

[1]) Those data not plotted for the species under consideration, as noted, include only those which were not accompanied by the corresponding temperature or salinity, or those which were duplicates.

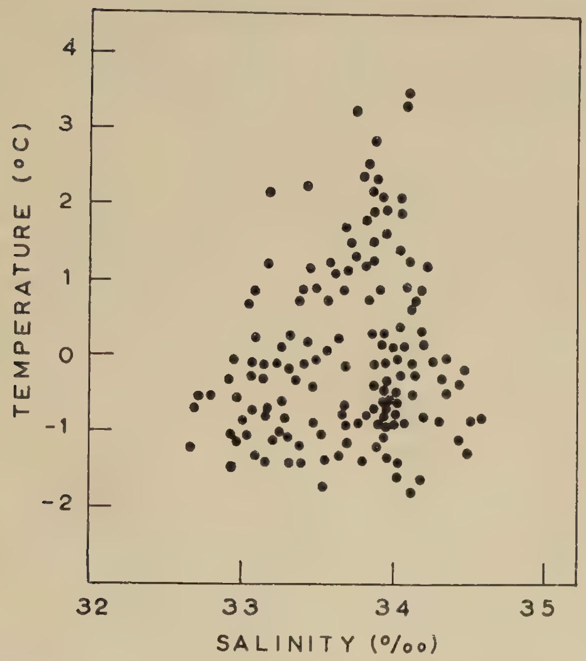

Fig. 2. The temperature-salinity relationships of *Thalassiosira antarctica.*

of ice imposes a limit on the reduction in salinity. These factors, coupled with the effects of turbulence, would maintain the high minimal salinity with which *T. antarctica* and other antarctic species must contend.

The infrequency of *T. antarctica* in adjacent northerly regions, even though transport is accessible, undoubtedly results from its "polar" requirements. Thus a thermal barrier confines *T. antarctica* principally to the region within the Antarctic Convergence. Although specific differences in tolerance can be expected, temperature probably determines the northward extension of all antarctic species. But further observations are needed to establish whether the Antarctic Convergence circumscribes the natural habitat of all true antarctic species.

It may be concluded that for a species to thrive in antarctic waters it must be equipped to tolerate a high and fairly constant salinity and, more critically, extremely low temperatures. Only a few dinoflagellates and perhaps no coccolithoporids can meet these requirements. Diatoms, on the other hand, are well represented. Other antarctic species include:

Chaetoceros criophilus Castr.
Chaetoceros neglectus Karst.
Eucampia balaustium Castr.
Fragilaria curta V. H.
Peridinium applanatum Mangin
Synedra reinboldii V. H.

Arctic Representative: *Thalassiosira hyalina* (Grunow) Gran

Thalassiosira hyalina has been selected to show the distribution of an arctic species (Fig. 3). The taxon as defined by Hustedt (1930) was used. The following sources were used in charting its distribution:

> Aikawa 1936; Bigelow 1926; Braarud 1935; Cleve and Grunow 1880; Damas and Koefoed 1909; Davidson 1931; Fish 1925; Gaarder 1938; Gran 1897a, 1897b, 1897c, 1900, 1902, 1929; Gran and Braarud 1935; Grøntved and Seidenfaden 1938; Hjort and Gran 1899; Jørgensen 1905; Kisselev 1925; Knudsen and Ostenfeld 1899; Marshall 1955; Ostenfeld 1910; Paulsen 1904; Ramsfjell 1957; Skvortzow 1931; Smayda 1958; Wirketiss and Kisselev 1935; Østrup 1895.

The principle features of *T. hyalina*'s distribution suggest an eastern arctic tendency, although additional data might reveal it as circumpolar. The pronounced arctic character of *T. hyalina* is readily discernible. It is resident in all the major polar currents and its distribution closely parallels their courses. It occurs in the East Greenland Current, through which it is in contact with the Labrador Sea stock. It has penetrated into Hudson Bay and through the Labrador Current has extended its range into the Gulf of St. Lawrence (Gran 1919) and south to Nova Scotia. Occasionally stray cells of *T. hyalina* are found in the Gulf of Maine proper and even at Cape Cod.

Within the Norwegian Sea it is confined almost exclusively to the western half where it is a component of the "drift-ice flora". Its absence from the eastern half, through which the warm Gulf Stream flows, is sharply defined. It is also absent along the western coast of Iceland where the warm Irminger Current passes. Neither does it occur off southern Iceland where warm Atlantic water is found; but it is a component of the East Icelandic Current. These features readily confirm its arctic character.

The isolated observations of *T. hyalina* in the Barents Sea, Kara Sea and off Japan probably form part of a continuous distribution. Aikawa (1936) states *T. hyalina* to be common in northern Japanese waters, and Kisselev (1933) has noted the similarity in species composition between the Okhotsk Sea and the Arctic Polar Basin. Thus there is ample reason to believe that *T. hyalina* is more common in this region than its plotted distribution reveals.

The absence of *T. hyalina* along the Alaskan archipelago is unexpected. Cupp (1937) studied the phytoplankton at Scotch Cap, Alaska for seven years and failed to observe it. More modest observations have confirmed this (Aikawa 1936; Motoda and Kawarada 1955). This condition, on the basis of the data available, persists even though Aikawa (1936) claims that an active seeding of phytoplankton from northern Japanese waters takes place into this area—

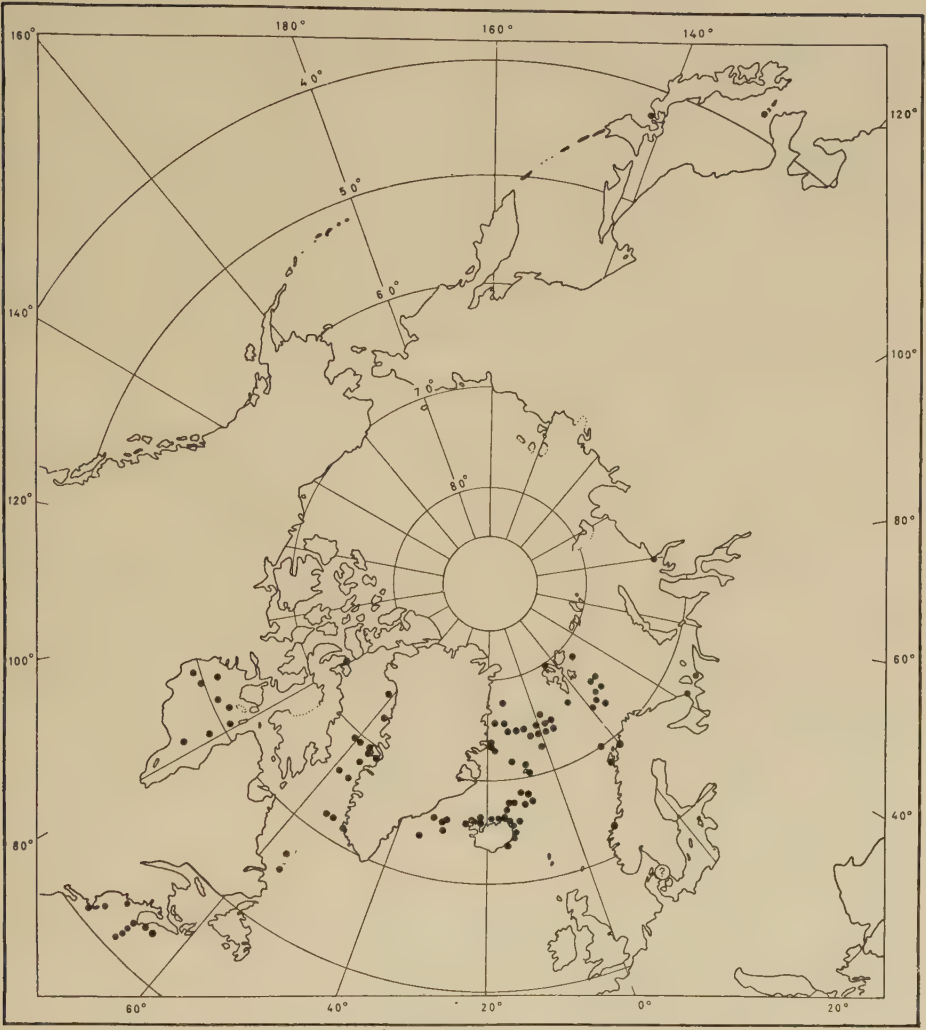
160°
180°
160°
140°
120°
40°
50°
60°
70
80°
140°
100°
120°
80°
100°
60°
80°
40°
60°
40°
20°
0°
20°
?

Fig. 3. The geographical distribution of *Thalassiosira hyalina.*

an avenue readily accessible to *T. hyalina.* Furthermore, the Japanese stock probably was derived originally from the Arctic and is still being supplemented[1]). Should this be a valid assumption, then one would expect that subsequent transport through the Bering Strait would lead to its establishment in the eastern Pacific as well. But it remains for future observations to determine whether *T. hyalina* is found north of the Alaskan archipelago.

---

[1]) The possibility that *T. hyalina* does not occur in Japanese waters must be kept in mind. Aikawa appears to be the only investigator to cite its presence by name. The predilection of Japanese students to lump species according to genus has made it impossible to check Aikawa's claim. Skvortzow's report that *T. hyalina* was found near Tsushima Island is suspect since his drawing also bears a resemblance to *T. rotula,* Meun.

It is of interest to note that relatively higher temperatures prevail on the American side of the Bering Sea than in northern Japanese waters or the Bering Strait. This prompted EKMAN (1953, p. 167) to state that "the American side of the Bering Sea is not distinctly arctic as regards temperature until we reach the Bering Strait". Thus a thermal barrier might prevent *T. hyalina* and other strictly arctic species from inhabiting these waters. MANN (in BIGELOW and LESLIE 1930) reports *T. hyalina* from Monterey Bay, California. However, judging from its distribution pattern and temperature "requirements", this is probably a misidentification.

In spite of suitable temperatures, *T. hyalina* appears to be only an unimportant visitor in isolated fjords along the Norwegian coast. It occurs consistently at the Lofoten Islands, and GRAN (1902) also mentions its presence along the Finnmark coast, although no specific details are given. Stad, south of the Romsdalsfjord, represents its southern-most known extension. The question mark drawn in the Kattegat (Fig. 3) represents CLEVE-EULER's (1937) claim that *T. hyalina* occurs there. She attributed it as a visitor from the Baltic Sea and this led GRØNTVED (1950) to designate *T. hyalina* as having a bicentric distribution: found in the Arctic and Baltic Seas. However, numerous investigations in adjacent waters, including the Baltic, have failed to reveal *T. hyalina*. (CLEVE-EULER (1917) reported this species from the Skagerrak as "united with *T. gravida*"). It seems likely that Cleve-Euler misidentified this species, and she herself professed uncertainty in her identification. Thus it is questionable if this species occurs in the Kattegat and Baltic, or that it has a bicentric distribution.

HENDEY (1937) claimed to have found *T. hyalina* at two stations near Cape Town, Africa at temperatures of 13.97° and 15.33°C, respectively. He acknowledged that previously it was recorded only from northern waters and concluded "its occurrence off the coast of South Africa is somewhat unusual, it had probably been carried northeastwards from the neighborhood of Bouvet Island". However, other investigations in the Antarctic have failed to record it as yet.

The few data available for the conditions of temperature and salinity under which *T. hyalina* has been encountered are presented (Fig. 4). The salient features of this relationship appear to be significantly representative of arctic phytoplankton in general (SMAYDA 1958). Like its ecological homologue *T. antarctica*, *T. hyalina* is both stenothermal and stenohaline. The temperatures accompanying its presence range from −1.35° to 9.03°C, the mean of 125 observations (including those not plotted) being 2.3°C.

The evidence is suggestive that those occurrences of *T. hyalina* at temper-

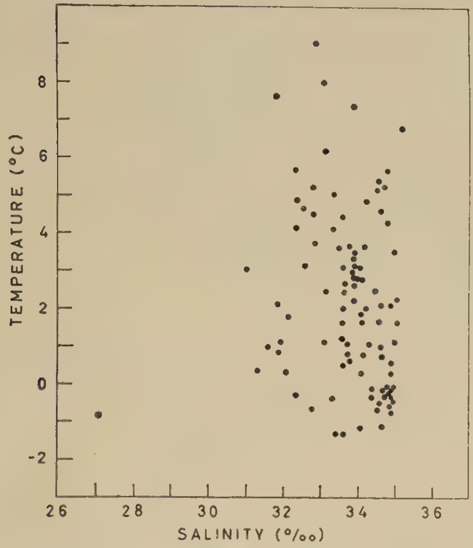

Fig. 4. The temperature-salinity relationships of *Thalassiosira hyalina*.

atures above 5°C represent remnants of earlier populations or merely a transport, rather than instances of active growth. For example, GRAN (1919) found this species during May in the Gulf of St. Lawrence, but not in June when the surface temperatures exceeded 5°C. DAVIDSON (1931) found only traces of *T. hyalina* during August and September in Hudson Bay at temperatures between 4.8° and 8.6°C. Other investigators likewise have found only stray cells of *T. hyalina* above 5°C.

Except for one observation at 27.11 $^0/_{00}$, *T. hyalina* has been observed only in waters above 31 $^0/_{00}$, the mean being 33.88 $^0/_{00}$. The mean value reflects the effect of melting ice and verifies the predominance of *T. hyalina* in polar oceanic water masses rather than neritic ones throughout its range. *T. hyalina*, hitherto, has been called a neritic species.

The conditions of existence as summarized for *T. antarctica* apply in general to *T. hyalina* as well. However arctic species do not have the uniformity of environmental conditions so typical of the Antarctic. The presence of warm Atlantic water within the Norwegian Sea not only renders a significant area uninhabitable but also divides the polar western Norwegian and Barents Seas to near Spitzbergen, ice-free only during the summer. As inhabitants of polar currents which flow away from the Arctic, arctic species are subjected to higher and more variable temperatures throughout their range as a whole than are antarctic species. This has contributed to an essential difference between the communities inhabiting the two polar regions. Whereas the seasonal antarctic flora is comprised principally of true antarctic forms (HART 1942), arctic diatoms are in the minority and relatively unimportant in their habitat. In fact, *Chaetoceros furcellatus* Bail. is outstanding among arctic diatoms in that it appears to be the only one quantitatively significant throughout most of its range. This undoubtedly is related to its ability to withstand relatively higher temperatures than the other arctic forms (Table 1). But it is premature to ascribe temperature as the sole mechanism hindering the success of the arctic flora to attain the dominance enjoyed by its antarctic counterpart. Culture studies on representative forms are needed.

Other arctic species include:

Achnanthes taeniata Grun.
Bacterosira fragilis Gran
Ceratium arcticum (Ehrbg.) Cl.
Chaetoceros furcellatus Bail.
Fragilaria oceanica Cl.
Navicula vanhöffenii Gran

Table 1.
Mean Temperature of Occurrence of Representative Arctic Diatoms (after SMAYDA 1958).

Species	Temperature °C
Achnanthes taeniata	1.0
Bacterosira fragilis	1.4
Chaetoceros furcellatus	3.5
Fragilaria oceanica	2.2
Thalassiosira bioculata	2.8

Tropical Representative: *Planktoniella sol* (Wallich) Schütt

Planktoniella sol has been selected to show the distribution of a tropical form (Fig. 5). The following sources were used to chart its distribution:

> AIKAWA 1930, 1936; ALLEN and CUPP 1935; CORLETT 1953; GAARDER 1951; GILBERT and ALLEN 1943; HART 1934; HENDEY 1937; HENSEN 1911; HENTSCHEL 1932; KARSTEN 1907; KNUDSEN and OSTENFELD 1900; KRASSKE 1941; LEMMERMANN 1899; MANGIN 1922; OSTENFELD 1898, 1902, 1915; OSTENFELD and SCHMIDT 1901; PAVILLARD 1925, 1931, 1935; SCHRÖDER 1906; SILVA 1953, 1956a, 1956b; SKVORTZOW 1931; SUBRAHMANYAN 1946; TAKANO 1955; WANDEL and OSTENFELD, 1898; WOOD 1950.

Planktoniella sol is a circumtropical diatom and found principally in oceanic regions. The gaps in its distribution within the tropics, as charted, reflect areas mainly uninvestigated. It is a component of all the major tropical current systems which ensures a wide distribution. After plotting *Planktoniella sol*'s

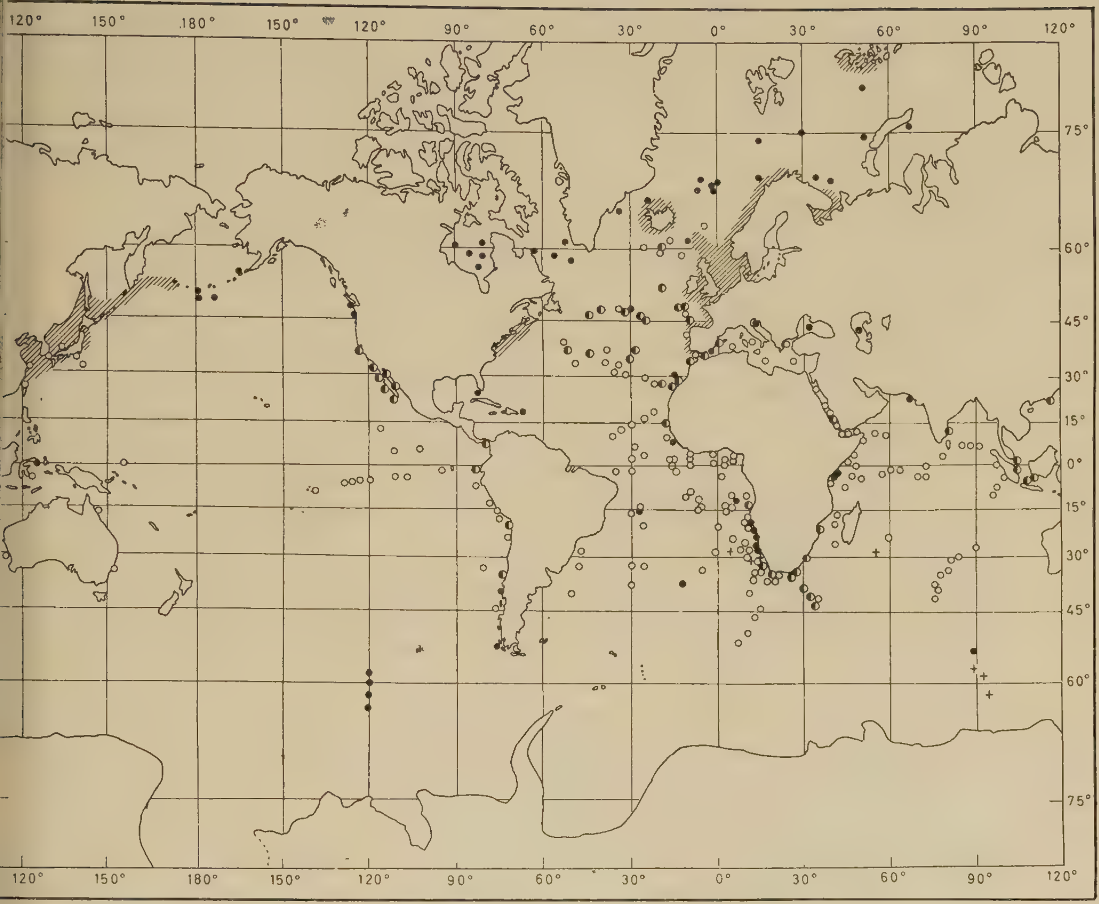

5. The geographical distribution of *Planktoniella sol* (open circles) and *Thalassionema nitzschioides* (hatched , closed circles). The half-filled circles represent occurrences of both species, and pluses indicate finds recorded as varieties of *Thalassionema nitzschioides*.

distribution it became apparent that it is not a tropical species in the strictest sense. Its range extends into subtropical regions and it is even found in the temperate Peruvian Current. It is unknown, however, whether it is a permanent component of this current or whether its occurrence coincides with maximum temperatures. It is also found near 60°N where it can be used as an indicator species of Gulf Stream water near its entrance into the Norwegian Sea.

The conditions of temperature and salinity accompanying *Planktoniella sol*'s occurrence in nature show it to be eurythermal and stenohaline (Fig. 6). Its temperature range extends from 1.9° to 30.5°C. Hendey (1937) recorded *Planktoniella sol* at two stations where the temperature was 1.9° and 5.2°C. Since these occurrences undoubtedly resulted from current transport, they are

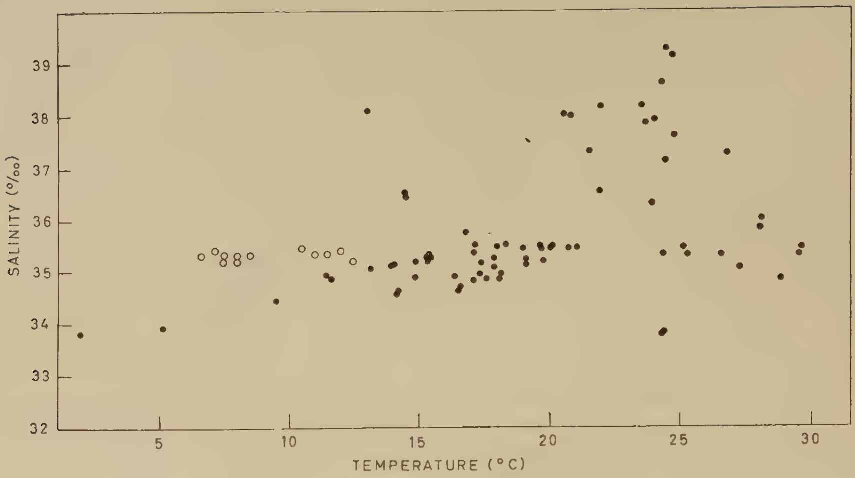

Fig. 6. The temperature-salinity relationships of *Planktoniella sol*, the open circles are explained in the text.

omitted in calculating a mean temperature of 19.2°C (101 observations, including those not plotted). The salinity range found for *Planktoniella sol*, 33.76 $^0/_{00}$ to 39.15 $^0/_{00}$, reveals its tropical character. A mean of 35.71 $^0/_{00}$ is obtained.

The ability of *Planktoniella sol* to withstand a wide temperature range, probably not shared to such a degree by the majority of tropical species, would account for its presence in extra-tropical areas. Since effective cell division is not expected to occur throughout this temperature spectrum, its observed tolerance of temperatures below 10°–15°C may represent sterile distributions. Were effective division possible at these lower temperatures, it would be expected that *Planktoniella sol* would be a more frequent member of the temperate phytoplankton.

Its absence from neritic areas may result from its salinity requirements in combination with some other factor. It is doubtful that salinity alone determines this exclusion.

It may be concluded that in order for a species to inhabit the tropics it must be equipped to tolerate very high temperatures and, secondarily, high salinities. Coccolithophorids and dinoflagellates have been especially successful in meeting these requirements. There are relatively few true tropical pelagic diatoms, but a surprisingly large number of temperate species thrive in tropical waters. Some tropical species are:

Chaetoceros laevis Leud.-Fort.
Coccolithus sibogae (Web. v Bos.) Schill.
Gossleriella tropica Schütt
Hemiaulus membranaceus Cl.
Peridinium elegans Cl.
Rhizosolenia robusta Norm.

Cosmopolitan Representative: *Thalassionema nitzschioides* Grunow

Thalassionema nitzschioides has been selected to show the distribution of a cosmopolitan species (Fig. 5). The taxon as defined by HUSTEDT (1937) was used. The following sources were used to chart its distribution:

> AIKAWA 1930, 1936; ALLEN and CUPP 1935; BIGELOW 1926; BRAARUD 1935, 1945a; BRAARUD and BURSA 1939; BRAARUD, GAARDER and GRØNTVED 1953; CLEVE-EULER 1917, 1949; CORLETT 1953; CUPP 1937; CZAPEK 1909; DAVIDSON 1931; ERCEGOVIC 1936; FISH 1925; GAARDER 1951; GILBERT and ALLEN 1943; GRAN 1915; GRAN and BRAARUD 1935; GRØNTVED 1952; GRØNTVED and SEIDENFADEN 1938; GUDMUNDSSON 1937; HAGELSTEIN 1939; HALLDAL 1953; HASLE 1956; HEIDEN and KOLBE 1928; HENTSCHEL 1932; ISELIN 1930; KING 1950; KISSELEV 1925, 1928; KRASSKE 1941; MANGUIN 1954; MARGALEF and DURAN 1953; MERESCHKOWSKY 1902; MOTODA and KAWARADA 1955; OSTENFELD 1913; PAULSEN 1909, 1911; PAVILLARD 1925, 1931; RAMSFJELL 1957; REINHARD 1910; SABELINA 1930; SCHRÖDER 1906; SILVA 1949, 1952, 1953, 1956a, 1956b; SILVA and PINTO 1948, 1952; SKVORTZOW 1931; SMAYDA 1957, 1958; STEEMANN NIELSEN 1935; SUBRAHMANYAN 1946; TAKANO 1955; USSATCHEW 1935; WIRKETISS and KISSELEV 1935.

Th. nitzschioides is circumglobal and confined primarily to neritic areas. Its distributional pattern supports the contention of some investigators that neritic species can survive in oceanic environments if transported there. Its distribution in the Arctic is somewhat obscure due to the failure of early investigators to distinguish it from *Thalassiothrix frauenfeldii* Grun., a form also found there. *Th. nitzschioides* is ubiquitous and numerically important throughout the northern hemisphere. Additional investigations in the southern hemisphere probably will reveal a similar condition there as well.

An outstanding feature of *Th. nitzschioides*' distribution is the failure to establish itself in the Baltic Sea. Although it occurs sporadically off Bornholm Island and near the Danzig Bay (OSTENFELD 1913), it is not stationary in the Baltic Sea. It is a pronounced euryhaline species (Fig. 7) occurring at salinities down to 4.13 $^0/_{00}$ in Portuguese Guinea (SILVA and PINTO 1952) and 3.60 $^0/_{00}$ in Tscheskaja Bay in the Barents Sea (WIRKETISS and KISSELEV 1935). Except for the Gulfs of Finland and Bothnia where the salinity may decrease to 3.00 $^0/_{00}$ or less, much of the Baltic has a surface salinity of approximately 7.00 $^0/_{00}$ (SVERDRUP, JOHNSON and FLEMING 1942, p. 664). The salinity conditions in the Baltic, then, certainly would seem tolerable to *Th. nitzschioides*. It should be noted that the limnetic *Diatoma elongatum* (Lyngb.) Agardh closely resembles *Th. nitzschioides*. VÄLIKANGAS (1926) classifies *D. elongatum*

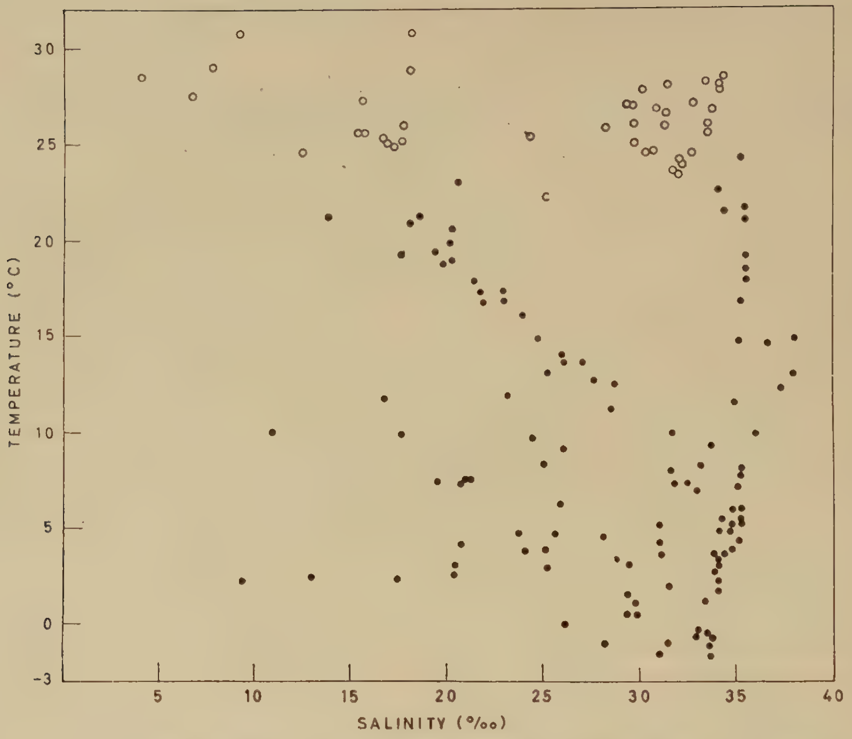

Fig. 7. The temperature – salinity relationships of *Thalassionema nitzschioides*, the open circles represent the stock found in tropical Portuguese Guinea.

as a "Meio- oder β-mesohalin" form showing its greatest development at salinities between 2.00–8.00 °/oo.

The absence of *T. antarctica* from the Antarctic except along 120°W near the Antarctic Convergence (Hasle 1956) and Heard Island (Manguin 1954) is also strange considering that it occurs in the high Arctic at similar temperatures. It is also present in the Caspian Sea where it has persisted as a relict form. It is conceivable that morphological differentiation has accompanied *Th. nitzschioides*' attainment of cosmopolitanism. The pluses drawn in on its distribution map (Fig. 5) represent finds recorded as varieties (Heiden and Kolbe 1928). Gaarder (1951) found this species to be variable and could distinguish between two valve types.

The distribution of *Th. nitzschioides* in relation to temperature and salinity (Fig. 7) reveals it to be pronouncedly eurythermal and euryhaline. Closer inspection shows the similarity in salinity but dissimilarity in temperature encountered by this species in different parts of its range. The stock found in tropical Portuguese Guinea (Silva and Pinto 1952) occurs at temperatures ranging from 22.2° to 30.7°C, the mean being 26.3°C (Fig. 7, open circles).

The salinity ranges from 4.13 to $34.34^{0}/_{00}$ with a mean of $25.04^{0}/_{00}$. On the other hand, the stock found in the Oslofjord and Skagerrak (BRAARUD 1945a; BRAARUD and BURSA 1939; CLEVE-EULER 1917) occurs at a mean temperature and salinity (185 observations) of 8.5°C and $28.86^{0}/_{00}$, respectively. For northern European waters in general, OSTENFELD (1913) gives means of 7.7°C and $31.50^{0}/_{00}$ when *Th. nitzschioides* is "*c* and *cc*" (94 observations). The arctic and temperate stocks would be expected to have different temperature means as well. Thus within the cosmopolitan distribution of *Th. nitzschioides* we can distinguish between different thermal "clones". These are stenothermal in the sense that they are subjected to only slight variations in temperature typical of that part of the range. BRAARUD (1945b) has found that at 10°C the Oslofjord *Th. nitzschioides* is capable of 1.2 divisions per day. It is important to determine whether its temperate and tropical counterparts would react similarly at that temperature.

The term cosmopolitan is used here for those species living in both cold-water and equatorial regions of all oceans. *The most important prerequisite for the attainment of a cosmopolitan distribution by a phytoplankton species is a eurythermal tolerance.* Unlike zooplankton and other animals, there can be no stenothermal, cold-water, cosmopolitan phytoplankton species because avoidance of the warm temperatures of sub-tropical and tropical regions requires a submergence below the euphotic zone. Salinity probably plays a subordinate role in such a distribution, although one can expect cosmopolitan species to have specific requirements.

Diatoms predominate among the known cosmopolitan species. Other cosmopolitan species include:

Chaetoceros compressus Laud.
Coccolithus huxleyi (Lohm.) Kpt.
Exuviaella baltica Lohm.
Leptocylindrus danicus Cl.
Prorocentrum micans Ehrbg.
Skeletonema costatum (Grev.) Cl.

Bipolarity

A bipolar distribution has been ascribed to a number of phytoplankton species. *Thalassiothrix longissima* Cleve et Grunow and *Rhizosolenia hebetata* Bailey f. *semispina* (Hensen) Gran are the classical examples given in the literature. Bipolarity, in its strictest sense, defines the occurrence of an element in both polar regions with its absence in the intervening tropical regions. The concept of bipolarity stresses a discontinuous distribution and actually it is indifferent whether the representative is a polar or subpolar species.

A number of zooplankton species claimed to be bipolar by early investigators have since been found to have a continuous longitudinal distribution. These forms are tropically or equatorially submerged, inhabiting strata thermally similar to those inhabited in the polar regions. Although these discoveries refuted bipolarity for these species, they strengthened the viewpoint that migration is of cardinal importance in effecting a bipolar distribution (CHUN 1897, EKMAN 1953). Neither the "relict theories" of Theel, Pfeffer or Murray (cf. EKMAN 1953, p. 258) nor a polyphyletic origin can be accepted as an adequate explanation of bipolarity. It is unequivocal that the longitudinal migration of planktonic forms is essentially passive and dependent on currents.

Subscribing to the definition of bipolarity given above, we find that *Th. longissima* and *Rh. hebetata* f. *semispina* are not bipolar. Both are widely distributed throughout the tropics. In discussing the latter species, HENDEY (1937, p. 316) states "it was observed in all types of water, but more frequently in the waters of the tropical and subtropical zones". As for *Th. longissima*, it is found in the Mediterranean Sea (PAVILLARD 1925), in the Red Sea, Gulf of Aden, Malay Archipelago, Indian Ocean (OSTENFELD 1902) and South Equatorial Current (PAVILLARD 1935), to name a few of the localities. Admittedly, these species appear to be more important in the polar regions; nonetheless they inhabit and undergo active cell division in the tropics.

KARSTEN (1905a) listed 31 species of marine phytoplankton as being bipolar; but all of these are now known to live within the tropics as well. Indeed true bipolarity at the species level probably is not to be found among marine phytoplankton. The difficulties in establishing such a distribution appear to be insurmountable. Of prime importance in that it is the greatest obstacle is the problem of trans-tropical migration. To pass from one pole to the other entails being transported through the tropics. A stenothermal cold-water form like *T. antarctica* or *T. hyalina* (Figs. 2, 4) must successfully withstand tropical temperatures if it is to reach the opposite pole in a viable state. Unlike zooplankton, phytoplankton cannot take advantage of the suitable thermal conditions in the depths as these invariably lie under the euphotic zone. For a species to traverse these tremendous distances active cell division must take place and for this light is necessary.

It would seem that neritic species are well equipped to become bipolar since many produce resting spores, supposedly capable of withstanding the extremes of an environment. Resting spores having been formed, these might be carried to suitable habitats, germinate, develop resting spores anew and repeat the entire cycle again. Through this process the species could stepwise extend their range in the direction of the opposite pole. But as a general rule, only a small number of the vegetative cells of a given species capable of producing resting spores do so. Of these only a limited number, if any, would gain access to the proper current system. In addition, further dispersal during transport and loss due to sinking and grazing would continue to decimate this number.

Admittedly, a species might succeed in establishing itself in a new area, but eventually it will be confronted with the problem of maintaining itself in a tropical environment as well. If it fails, then from the marginal areas of its range it must have its resting spores transported over a considerable distance to the opposite polar region. Even should these resting spores reach the opposite pole, a bipolarity is still not assured. There remains the problem of achieving a sufficient density enabling the species to withstand extinction due to grazing and assuring the production of resting spores. It is maintained that the attainment of a bipolar distribution through the mechanism of resting spores is ineffective for marine phytoplankton. This is borne out by the absence of a single known bipolar neritic species.

Above we assumed that the species would be unable to establish itself in the tropics. It is suggested, however, that *in order for a species to thrive at both poles it must also become cosmopolitan. Successful trans-tropical transport leading to the establishment of a species at both poles will occur only when the species can maintain itself within the tropics as well.* Karsten's original list of "bipolar" species is offered in evidence.

Indicator Species and Visitors

The species making up the phytoplankton community during a seasonal cycle usually can be grouped into indigenous and visitor forms, or autochthonous and allochthonous species, respectively. Some of the visiting species are especially valuable in that they label the influence or presence of a specific water mass during its incursion into a given area. Such species are called indicator species. A valid indicator species of this type is one whose presence in a given area coincides with the introduction of a specific water mass of known origin. While it need not be an important component in its "native" water mass, it can not normally be found in the recipient one. It is irrelevant whether a phytoplankton indicator species is viable or dead upon its introduction.

Planktoniella sol is an indicator species of the Gulf Stream near its entrance into the Norwegian Sea (Fig. 5). Its specificity for this current is revealed by the salinity values accompanying its occurrence in that region (Fig. 6, open circles). These values concentrate about 35.35 $^0/_{00}$, ranging from 35.21 to 35.44 $^0/_{00}$, in close agreement with the mean of 35.30 $^0/_{00}$ characteristic of inflowing Gulf Stream water (SVERDRUP, JOHNSON and FLEMING 1942, p. 655). The corresponding temperatures range from 6.6° to 12.5°C, representing *Planktoniella*'s occurrence from March through November (WANDEL and OSTENFELD 1898; KNUDSEN and OSTENFELD 1900). *Planktoniella sol* serves also as an indicator species of intrusive offshore water masses in the coastal regions bordering the Benguela Current (HART 1953) and Peru Current (GUNTHER 1936, quoted by HART). The fact that *Planktoniella sol* is easily identifiable, a characteristic of most indicator species, has contributed to its being used as an indicator species so frequently.

SCHÜTT (1893) maintained that each current system possesses its own characteristic flora. Although many species are possessed in common with other currents, the different assemblages often can be used to delimit the currents and areas of their influence within a given thermal zone. But as the currents pass through different regions, thermal changes and admixture take place resulting in considerable changes in composition. The ability of a species to maintain itself in spite of these changes increases its chances of becoming an indicator species. It will suffice to state that relatively few species can be used as indicators of hydrographic phenomena.

Species belonging to a local flora may also be used as indicators of some specific element in their environment. *Eutreptia lanowi* Steuer, for example, serves as an indicator of polluted waters in the inner Oslofjord (BRAARUD 1945a) and the Grand Canal of Venice. The presence of certain diatoms, such as *Thalassiosira baltica* (Grun.) Ostf., indicates a specific salinity range, while others, *Cyclotella caspia* Grun., signal fresh-water dilution. The abundance of the eurythermal *Chaetoceros wighami* Btw. and *Ch. subtilis* Cl. appears to be inversely related to the degree of salinity; these species attaining maximum concentrations in the Baltic and Caspian Seas. That limnetic and brackish diatoms are excellent indicators of the degree of salinity (more specifically Cl ion concentration) enabled KOLBE (1932) to formulate his "Halobion system". The results of culture studies will probably warrant a similar classification for marine forms, if not for total salinity then for specific inorganic ions.

The flora and its seasonal cycle are remarkably constant for a given area. Thus, to an experienced observer, the composition of the phytoplankton community and their relative abundance are a measure of the community's stage of development and previous history, and even relate something about the "natural fertility" of the environment. In many temperate inshore areas, for example, *Skeletonema costatum* (Grev.) Cl. initiates the late-winter or spring flowering, is succeeded by *Thalassiosira* spp., which in turn are replaced by *Chaetoceros* spp., and so on. But the community is likewise sensitive, and any significant environmental changes will become manifested in terms of composition and abundance. Comparison of waters contaminated with domestic and industrial pollutants with non-polluted ones readily reveals this.

As contrasted to hydrographic indicator species, visitor species or guests may indicate the influence of different water masses but give no concrete information as to their origin. The presence of visitor species usually represents a temporary extension of range corresponding to the seasonal changes in temperature. Thus, within a given area, we can distinguish between its local flora and warm or cold-water visitors. The visitors often become important components in the community at times when sub-optimal temperatures suppress active growth of the local representatives.

CLEVE (1897) overemphasized the role of visiting species in contributing to and molding the seasonal phytoplankton cycle. Justly, he concluded that phytoplankton can be grouped into thermal units, called "plankton-types", which have centers of abundance within their respective thermal zones. Accordingly, cold-water forms are concentrated in the polar regions and warm-water ones in the tropics. These plankton-types, he maintained, are constantly "migrating" and in the process serially seeding the areas through which they pass, resulting in the domination of the community by these newly arrived visitors. Thus, he attributed the seasonal changes in composition and dominance of the community to the periodic recruitment of species from these different areas. As an example, he claimed the spring flowering in the Skagerrak to be the result of a seeding by water emanating from the Arctic, while the summer flora was derived from southerly waters. Cleve's viewpoint denied the existence of a stationary population in these waters made possible through the production of resting spores (GRAN 1902) or other means. In propounding his concept, Cleve also failed to recognize the importance of the environment in molding the biological conditions, so aptly described by GRAN (1912): "when the conditions of existence in the flowing water-masses gradually alter, it is the new conditions of existence that decide the character of the flora, since the species best qualified to endure them will very soon get the upper hand over the others." A fact well established today. In reality, the seasonal composition of a developing population is derived primarily from a local stock and secondarily from visitors. Some visitors are certain to appear each year and be of secondary importance. Others are sporadic in occurrence and may suddenly appear in great numbers like *Asterionella japonica* Cl. did along the Norwegian coast in 1927 (GRAN 1929). One visitor, *Biddulphia sinensis* Grev., a "tropical-neritic Indo Pacific form" suddenly appeared in 1903 off Hamburg and quickly spread to much of the North Sea where it has since established itself (OSTENFELD 1909).

Concepts of Neritic, Oceanic, Meroplanktonic and Holoplanktonic

HENSEN'S (1887) coinage of the term plankton replaced the then current Auftrieb. But plankton as defined by Hensen was no improvement over Auftrieb since it included both swimming and planktonic forms. It remained for HAECKEL (1890) to divide up the composite plankton and introduce the classification which persists today: benthos, nekton and plankton. In the same work he introduced the terms neritic, oceanic, meroplanktonic and holoplanktonic.

Neritic and oceanic were established by HAECKEL (1890, p. 22) to characterize the horizontal distribution of plankton: "oceanisches Plankton ist dasjenige des offenen Weltmeeres, mit Ausschluss des schwimmenden Küsten Bios; ... das neritische Plankton umfasst die schwimmende Fauna und Flora der Küsten Regionen, sowohl der Continente, als der Archipele und Inseln." Those organisms independent of the sea bottom he termed holoplanktonic—"Organismen welche gar keine Beziehung zum Benthos haben", and those dependent on it meroplanktonic. It is surprising that Haeckel did not attempt to relate neritic with meroplanktonic, and oceanic with holoplanktonic.

GRAN (1902) noticed that many diatom species forming resting spores were confined primarily to coastal waters, the non-producers to oceanic waters. This observation led him to redefine neritic and oceanic (p. 75–76): "neritisch sind alle Arten, die in irgend einer Weise von der Küste, d. h. vom Meeresboden der seichteren Küstenmeere abhängig sind; sie können z. B. Dauersporen haben; ... oceanisch sind dagegen alle Arten, die vom Meeresboden in ihrem ganzen Lebenscyklus unabhängig sind". Gran then concluded: "nach dieser Definition sind also die Begriffe neritisch und oceanisch mit den ebenfalls von Häckel aufgestellten Begriffen meroplanktonisch und holoplanktonisch vollständig kongruent". Gran's modification of Haeckel's classification has persisted ever since.

Manifest in the concept of neritic and oceanic, in Gran's sense, are two diverse elements. Firstly, a geographical orientation is included which vaguely defines the normal distribution of an organism relative to the coast or open ocean. Secondly, a biological concept is included which characterizes the type of life cycle innate to the organism. Accordingly, neritic, as pertaining to phytoplankton, has come to mean an organism confined to coastal or "inshore" regions and possessing a sedentary stage (resting spore); oceanic designates an organism inhabiting a deep sea environment in a continuously pelagic state. A causal relationship and interdependence of concepts is implied. But, in fact, *a neritic species need not be meroplanktonic* (i. e. *spore producing*) *nor need a meroplanktonic species be neritic. The same applies to the apparent oceanic—holoplanktonic relationship.* Some organisms, including *Asterionella japonica* Cl., *Guinardia flaccida* (Castr.) Perag., *Skeletonema costatum* (Grev.) Cl. and *Thalassionema nitzschioides* Grun., appear to be confined to coastal waters yet fail to form resting spores. Other species do not form resting spores, such as *Nitzschia delicatissima* (Ehrbg.) Sm. and *Thalassiosira decipiens* (Grun.) Jørg., but are equally successful in neritic or oceanic regions. Many species normally inhabiting oceanic regions are periodically introduced into inshore areas where they become active participants in the community. Likewise, many resting spore producers have been found in active growth in oceanic waters. Some, like *Thalassiosira gravida* Cl. and *T. nordenskioeldii* Cl., have a center of abundance in oceanic regions. These two species are found in the ice-floe region of the Norwegian Sea. Even though the ice packs may simulate a neritic environment in providing an effective surface for the deposition of resting spores or congealed vegetative cells, the hydrographic conditions nonetheless reveal an oceanic character. These examples support the contention that using the possession or absence of a resting spore stage as a criterion in delimiting the environment inhabited by a species, and indirectly defining its milieu, is neither completely reliable nor satisfactory. Contrary to Gran's viewpoint, *neritic and meroplanktonic are not synonymous, nor are oceanic and holoplanktonic.* Braarud (BRAARUD, GAARDER and GRØNTVED 1953) also has pointed out the heterogeneity of the concepts of neritic and oceanic and the ensuing difficulties in using them in the sense of Haeckel and Gran.

Thus we have two unrelated sets of terms classifying phytoplankton; one representing a geographical or environmental concept, neritic—oceanic, the other a biological phenomenon, meroplanktonic—holoplanktonic. It is now necessary to consider the fitness of these terms as applied to phytoplankton.

Without doubt, as Haeckel recognized, the distribution of plankton bears some relevance to the coast ("neritisches Plankton") or open ocean ("ozeanisches Plankton"). But, nonetheless, the terms neritic and oceanic, as applied to phytoplankton to describe such a distribution, are of little biogeographical value. They are at best vague generalizations of an environment which does not exist *per se*, and which in reality represents a multitude of environments. The classification of a species as Arctic, for example, conveys a fairly comprehensive picture of its general thermal requirements and distribution. But now the classification of this species as neritic or oceanic is essentially meaningless, for whereas the designation Arctic is a specific and definable biogeographical unit, neritic and oceanic are heterogeneous and not distinguished by any specific element. How, then, does one define neritic and oceanic? Are the parameters used to distinguish between them of importance to the phytoplankton? A species, for example, may be confined to either the neritic or oceanic province, or found in both, because of the absence or presence of a resting spore or sedentary stage, a nutritional reason or a physiological reason other than nutrition. An adequate definition must take into account the nature of the organisms to be classified. Indeed one can arbitrarily select the edge of the continental shelf or a particular depth (see HEDGPETH 1957) as the boundary between the neritic and oceanic provinces. But while this may be appropriate for some aspects of oceanography, it has no value when applied to phytoplankton. Here is also a source of confusion resulting from the usage of neritic and oceanic in all disciplines within oceanography, but with different meanings. *We must recognize, therefore, that the classification of a phytoplankton species as neritic or oceanic places it in an undefined region and tells nothing of its life cycle, or why it is found there.* Neritic and oceanic either should be rejected as biogeographical terms for phytoplankton, or subdivided to accomodate the different ecological groups whose distribution is related to coastal or oceanic waters in some manner. The former alternative would seem preferable.

The terms mero- and holoplanktonic, in general, appear to be quite satisfactory. Many phytoplankton species possess a resting spore stage and must be considered as meroplanktonic. In fact a fundamental and natural biological category exists among phytoplankton based on the production of resting spores. The possibility that holoplanktonic species also possess a pelagic dormant stage in their life cycle can not be dismissed. KARSTEN (1905a) contended that some of the open ocean species actually possess just such a stage, which he called "Schwebesporen". Should this be the case, then the production of a resting stage need not necessarily mean a dependence on the sea bottom.

For most of the diatoms there is little doubt which species produce resting spores and which do not. Gran could use his classification legitimately only for the diatoms, since little was known about the biology of the other components. It is now known that a number of dinoflagellates form resting spores, including representatives of *Ceratium* (JOLLOS 1910) and *Goniaulax* (NORDLI 1951) as well as many *Peridinium* species. Resting spores have also been encountered among the coccolithophorids (KAMPTNER 1937; GAARDER 1954). Thus here is a feature common to certain representatives of the principal groups comprising the phytoplankton.

It appears that certain diatoms must be considered as meroplanktonic even though they do not form resting spores. Their life cycle has been said to include a vegetative sedentary stage, so that one can consider them analogous to tychopelagic species. The essential difference here is that unlike the true tychopelagic forms they are normally planktonic and capable of active cell division at that time. Now the evidence that such species exist is very scanty. OSTENFELD (1913), especially, mentions such species, among which are *Asterionella japonica* Cl., *Eucampia zoodiacus* Ehrbg., *Leptocylindrus danicus* Cl., *Skeletonema costatum* (Grev.) Cl and *Thalassionema nitzschioides* Grun. But at no time does he cite any actual observations to support his claims. This problem is certainly worthy of investigation.

It is commonly observed that many of those species claimed by Ostenfeld to have a sedentary vegetative stage become abundant, decline to trace concentrations and then often become abundant again. Frequently this temporary loss of vigour can not be attributed to nutrient deficiency or any other factor.

Nor is it known whether these cells are in a vegetative or dormant phase, although cytological study should clarify this.

An adequate definition of meroplanktonic and holoplanktonic, as pertaining to phytoplankton, must take into account the considerations discussed above. Hence it is proposed that *meroplanktonic* be retained for those organisms which either produce a resting spore, or possess a sedentary stage or dormant pelagic phase, and hence are *pelagic vegetatively*, except for reproductive stages, *only during part of their life cycle. Holoplanktonic* embraces those organisms not producing a resting spore, or possessing a sedentary or dormant pelagic phase, but being *pelagic vegetatively*, except for reproductive stages, *throughout their life cycle.* These definitions emphasize a biological feature—how they live—and have no geographical connotation.

An adequate biogeographical classification of phytoplankton is dependent on culture studies. Following the systematic study of the requirements for and tolerances of certain parameters by phytoplankton *in vitro*, these parameters should be measured in the natural environment. Then by comparing the normal distribution and dynamics of the organisms in relation to these with what has been found in the laboratory, a satisfactory classification should be possible. Such a classification is not imminent. Thus in the interim it seems advisable to have a provisional classification which recognizes that phytoplankton do have a real, definable horizontal distribution. The inadequacy of the concepts of neritic and oceanic to define this has been pointed out.

Instead, a binary classification (Table 2) is proposed which distinguishes between three distributional types: paractic (Gr. *παράκτιος*, of the coast), anoictic (Gr. *ἀνοικτά*, in the open sea) and adiaphoric (Gr. *ἀδιάφορος*, indifferent). These are then used in combination with the prefix of the term defining the life cycle innate to a given species: meroplanktonic, holoplanktonic. It must be emphasized that paractic, anoictic and adiaphoric do not represent environments. Paractic is conceived of as a concept which recognizes that a given species is bound to, and normally distributed in, certain waters because of

Table 2.
A Classification of Marine Phytoplankton.

	Paractic	Anoictic	Adiaphoric
Mero-	*Chaetoceros laciniosus*	*Rhabdosphaera spinosa*	*Ditylum brightwelli* (?)
–	*Goniaulax polyedra*		*Stephanopyxis turris*
–	*Skeletonema costatum* (?)		*Thalassiosira decipiens*
Holo-	*Cerataulina bergoni*	*Chaetoceros atlanticus*	*Coccolithus huxleyi*
–	*Guinardia flaccida*	*Coccolithus pelagicus*	*Exuviaella baltica*
–	*Rhizosolenia fragilissima*	*Planktoniella sol*	*Nitzschia delicatissima*

requirements attributable to coastal influences. The nature of this attraction is unknown, but may be due to shallowness, nutrients, growth factors or other parameters, singly or in combination. Anoictic defines a distribution limited to those waters free from coastal influences, and adiaphoric is restricted to those species whose requirements and tolerances permit an existence in both types of water.

Thus a mero-paractic species is one which has a dormant or sedentary stage and is distributed in waters modified by coastal influences. Mero-anoictic represents a species with a similar life cycle, but found in waters free from coastal influences, while a mero-adiaphoric species is found in both types of water. Holo- denotes a species pelagic vegetatively throughout its life cycle.

Factors Affecting the Distribution of Phytoplankton

The distribution of marine phytoplankton is governed by essentially the same variables that effect their abundance. Actually there is no marine habitat where a phytoplankton species can not find favorable conditions in some part of its ecological spectrum. But it is the combined effect of these variables which determine distribution, and it is usually difficult to single out the most important one in a given situation.

The spatial relations of phytoplankton distribution can be thought of as three-dimensional, consisting of a latitudinal, longitudinal and vertical component. Using this as a model, the various factors affecting this pattern of distribution can be analyzed.

1. *Light*: The vertical distribution of marine phytoplankton is regulated almost exclusively by light. Under certain conditions thermal stratification or turbulence may cause a gradient in vertical distribution, but these are indirect effects in that they do not elicit a physiological response directly controlling vertical distribution as does light. There is little doubt that phytoplankton have specific light requirements, both qualitatively (Baatz 1940) and quantitatively, but little is known. The vertical distribution of certain dinoflagellates appears to be related in some way to light as these show marked diurnal movements (Hasle 1950, 1954). But light is probably not the sole factor involved as certain ions also influence phototaxis (Halldal 1957). A "shade flora" consisting of diatoms, including *Planktoniella sol*, and dinoflagellates has been claimed to inhabit the greater depths within the tropics (Karsten 1907; Steemann Nielsen 1934, 1939). Steemann Nielsen (1939) distinguished between three groups of *Ceratium* spp. which he termed oligophotic, mesophotic and euphotic.

Light also governs the longitudinal distribution of phytoplankton, principally through its absence. Because of the "midnight sun" phenomenon and presence of ice, aphotic conditions exist periodically or continually throughout much of the polar regions. But whether this precludes the existence of a community is not certain; for RODHE (1955) has found an abundant flagellate population in certain ice-covered arctic lakes. A number of arctic diatoms appear to have low light requirements and are capable of active growth on the under side of ice (see SMAYDA 1958). The periodic colonization in those waters where ice-melting accompanies the "midnight sun" is well marked.

2. *Temperature*: That the distribution of phytoplankton is a function of temperature is manifest in their division into arctic, boreal, temperate or tropical species. Thus temperature regulates the longitudinal distribution of phytoplankton, as shown here more specifically for *T. antarctica* and *T. hyalina.* Unfortunately the classification of phytoplankton as to their thermal requirements is based exclusively on biogeographical data. In many instances insufficient data were had resulting in the classification of an organism inconsistent with its presently known distribution.

The belief that dinoflagellates as a group are warmth-loving organisms is now being borne out by experimental studies. BARKER (1935) found the optimal temperatures of a number of species to lie between 18° and 25°C, of which *Peridinium triquetrum* (Ehrbg.) Leb. (18°C) and *Prorocentrum micans* Ehrbg. (25°C) can be mentioned. NORDLI (1953) obtained a temperature optimum of 15°C for *Ceratium furca* (Ehrbg.) Clap. et Lach. and 20°C for *Ceratium fusus* (Ehrbg.) Duj. Diatoms likewise have been studied *in vitro* (SCHREIBER 1927; BRAARUD 1937, 1945b), but the results are fragmentary. For example, BRAARUD (1937) found *Thalassiosira nordenskioeldii* Cl. to be very prolific at 10°C, although in nature it attains a maximum between 2° to 3°C, and disappears at slightly higher temperatures (GRAN and BRAARUD 1935, SMAYDA 1957). A species' ability to thrive at different temperatures appears to be related to the amount of nutrients available. BRAARUD (1945a) found boreal diatoms in active growth at 20°C in polluted waters of the Oslofjord, whereas growth was negligible in non-polluted areas.

3. *Salinity*: This factor controls distribution primarily in inshore areas, latitudinal distribution, where considerable fluctuations and differences are common. Experimental studies indicate, however, that representative dinoflagellates and coccolithophorids are more or less euryhaline (BRAARUD 1951; BRAARUD and PAPPAS 1951; BRAARUD and ROSSAVIK 1951; NORDLI 1957; MJAALAND 1956). The dinoflagellates tolerated salinities from 5 to 45 $^0/_{00}$, and one clone of *Peridinium trochoideum* (Stein) Lemm. even 55 $^0/_{00}$ (BRAARUD 1951). In all instances, the individual species were characterized by a low optimum, the lowest optimum being 10 $^0/_{00}$ (*Exuviaella baltica* Lohm.) and the highest 25 $^0/_{00}$ (*Ceratium furca* Ehrbg.).

These results, coupled with what can be inferred from biogeographical data, suggest that salinity is more important in governing abundance rather than distribution within the marine environment. It may be that total salinity is not so important a factor of distribution as are specific ions (DROOP 1958; PROVASOLI, McLAUGHLIN and PINTNER 1954). DROOP (1958) draws the tentative conclusion that Na tolerance may be the most important parameter distinguishing between "neritic and supra-littoral or estuarine species".

The best known example of where salinity is a barrier to distribution is the Baltic Sea. The salinity of the Kattegat near the entrance into the Baltic Sea is approximately $15\,^{0}/_{00}$. At nearby Bornholm Island, lying within the Baltic, the salinity is only $7\,^{0}/_{00}$ (DIETRICH and KALLE 1957, p. 417). A number of diatoms that occur in the Kattegat at $15\,^{0}/_{00}$ are absent at Bornholm Island, presumably because of the decreased salinity (OSTENFELD 1913). Some of the species that can be assumed to have a minimal salinity requirement between $7\,^{0}/_{00}$ and $15\,^{0}/_{00}$ are:

Chaetoceros decipiens Cl.
– *laciniosus* Sch.
Guinardia flaccida (Castr.) Perag.
Lauderia borealis Gran
Leptocylindrus danicus Cl.
Rhizosolenia alata Btw.
– *setigera* Btw.
– *styliformis* Btw.
Thalassiosira nordenskioeldii Cl.
– *gravida* Cl.

NORDLI (1953) has shown that the low salinities of the Baltic prevent the occurrence of *Ceratium fusus*, *C. furca* and *C. tripos*, although they show good growth at $15\,^{0}/_{00}$. SEGERSTRÅLE (1951) has found that the salinity of the Baltic is rising, and thus it would be most desirable to follow the ensuing changes in phytoplankton composition.

4. *Pollution*: Pollutants have become important factors of distribution in localized areas. The nature of the pollutant determines whether it will be toxic or beneficial, and may be highly selective in molding the community. In any respect, pollutants are accompanied by changes in composition and abundance. BRAARUD (1945a) concluded that although no organisms could be used as totally specific indicators of domestic pollution in the Oslofjord, in certain cases the species composition and response illustrated different degrees of pollution. RYTHER (1955) showed that the effluent from duck farms had a profound effect on the phytoplankton composition in Moriches Bay. BRAARUD and PAPPAS (1951) found that small amounts of sewage stimulated the growth of *Peridinium triquetrum*, whereas concentrations greater than 75 ml/l retarded growth. ØDEGAARD (1942) found marine diatoms to differ in their resistance to domestic and industrial pollutants.

5. *Fertility*: This represents the gamut of substances having nutritional or other biological significance, and effecting the distribution of phytoplankton. They may be distinguished from certain pollutants in being naturally occurring

substances in a given water mass. Insight into "fertility" as a factor of distribution is dependent upon culture studies of the requirements for and, more important, tolerances of these substances. Basic nutrients, for example, may be present in concentrations inhibitory to certain species, as shown for certain limnetic forms (RODHE 1948). PETERS (1934) claimed that the distribution of certain *Ceratium* spp. was governed by nitrate and phosphate concentrations. Organic factors undoubtedly affect distribution, including indirectly by acting as chelators or forming other complexes allowing the presence of species at nutrient concentrations that normally would be inhibitory (FOGG and WESTLAKE 1955). STEEMANN NIELSEN (1934) postulated that the horizontal distribution of *Ceratium* is governed by organic metabolic substances (Stoffwechselprodukte). The ultimate distinction between paractic, anoictic and adiophoric species may be in their requirements for and tolerances of specific substances.

6. *Currents*: Currents are important, physical factors of distribution. Above all, they provide a species with a range in accordance with the biological factors enumerated above.

Acknowledgements

I wish to extend my deep gratitude to Professor TRYGVE BRAARUD for reading the manuscript and offering valuable criticism, in addition to providing facilities at his Institute. To cand. real. EINAR RAMSFJELL grateful acknowledgement is made for making available unpublished data. Mrs. BJØRG PAULSEN kindly prepared the figures. Finally, the author is deeply indebted to his wife, NORMA LOUISE SMAYDA, without whose understanding and assistance this study would have been impossible. This study was completed during the tenure of a WOODS HOLE OCEANOGRAPHIC ASSOCIATES' FELLOWSHIP.

Summary

1. The distribution of representative arctic, antarctic, tropical and cosmopolitan phytoplankton species was charted. The accompanying temperature—salinity conditions were also presented.

2. Both polar species, *Thalassiosira antarctica* and *Thalassiosira hyalina*, are stenothermal and stenohaline. *T. antarctica* is circumpolar and confined primarily to those waters within the Antarctic Convergence. *T. hyalina* shows an eastern arctic tendency and has an irregular longitudinal distribution. Whereas the seasonal antarctic flora is comprised principally of true antarctic species, arctic diatoms are relatively unimportant in their habitat.

3. The tropical *Planktoniella sol* is eurythermal and stenohaline in its distribution. It is circumtropical and can be used as an indicator species of the Gulf Stream near its entrance into the Norwegian Sea.

4. *Thalassionema nitzschioides* was selected as the cosmopolitan species. It is both eurythermal and euryhaline. Within the range of a cosmopolitan species one can distinguish between different thermal "clones". There can be no stenothermal cold-water cosmopolitan phytoplankton species.

5. The existence of bipolarity claimed for certain phytoplankton species is reconsidered, and the conclusion arrived at that true bipolarity is not to be found among marine phytoplankton at the species level. It is postulated that the presence of a species at both poles is enabled only by the attainment of a cosmopolitan distribution.

6. The different types of phytoplankton indicator species are discussed. The distinction between indicator and visitor species is also considered, and the role of visitor species in the community commented upon.

7. The interrelationships between meroplanktonic and neritic, holoplanktonic and oceanic phytoplankton, as advanced by Gran, are re-evaluated. It is shown that these terms are not synonymous. It was argued that neritic and oceanic have no biogeographical value and should not be used for phytoplankton. The terms meroplanktonic and holoplanktonic were redefined. A meroplanktonic species is one which is pelagic vegetatively only during part of its life cycle; holoplanktonic is pelagic vegetatively throughout its life cycle. It is maintained that a satisfactory biogeographical classification is dependent on culture studies. A provisional, binary classification of marine phytoplankton is then proposed.

8. The roles of light, temperature, salinity, pollution, fertility and currents as factors of distribution are then discussed.

References

AIKAWA, H., 1930: The plankton of the southern seas of Japan considered with reference to their hydrography. Rec. oceanogr. Wks Jap., *3* (1): 17–34.

— 1936: On the diatom communities in the waters surrounding Japan. Rec. oceanogr. Wks Jap., *8* (1): 1–159.

ALLEN, W. E. and E. E. CUPP, 1935: Plankton diatoms of the Java Sea. Ann. Jard. bot. Buitenz., *44* (2): 101–174.

BAATZ, I., 1940: Die Bedeutung der Lichtqualität für Wachstum und Stoffproduktion planktonischer Meeresdiatomeen. Planta, *31*: 726–766.

BARKER, H. A., 1935: The culture and physiology of marine dinoflagellates. Arch. Mikrobiol., *6*: 157–181.

BIGELOW, H., 1926: Plankton of the Gulf of Maine. Bull. U.S. Bur. Fish. (1924), *40* (2): 1–509.

BIGELOW, H. and M. LESLIE, 1930: Reconnaissance of the waters and plankton of Monterey Bay, July 1928. Bull. Mus. comp. Zool. Harv., *70* (5): 430–581.

BODEN, B. P., 1949: The diatoms collected by the U.S.S. CACOPAN in the Antarctic in 1947. J. Mar. Res., *8*: 6–13.

BRAARUD, T., 1935: The Øst Expedition to the Denmark Strait 1929 II. The phytoplankton and its conditions of growth. Norske VidenskAkad. Hvalråd. Skr., No. 10: 1–173.

Braarud, T., 1937: A quantitative method for the experimental study of plankton diatoms. J. Cons. int. Explor. Mer, *12* (3): 321–332.

— 1945a: A phytoplankton survey of the polluted waters of the inner Oslo Fjord. Norske VidenskAkad. Hvalråd. Skr., No. 28: 1–142.

— 1945b: Experimental studies on marine plankton diatoms. Norske VidenskAkad., Oslo. I. Mat.-Naturv. Klasse, 1944 No. 10: 1–16.

— 1951: Salinity as an ecological factor in marine phytoplankton. Physiol. Plant., *4*: 28–34.

Braarud, T. and A. Bursa, 1939: The phytoplankton of the Oslo Fjord 1933–1934. Norske VidenskAkad. Hvalråd. Skr., No. 19: 1–63.

Braarud, T. and I. Pappas, 1951: Experimental studies on the dinoflagellate *Peridinium triquetrum* (Ehrb.) Lebour. Norske VidenskAkad., Oslo. I. Mat.-Naturv. Klasse, 1951, No. 2: 1–23.

Braarud, T. and E. Rossavik, 1951: Observations on the marine dinoflagellate *Prorocentrum micans* Ehrenb. in culture. Norske VidenskAkad., Oslo. I. Mat.-Naturv. Klasse, 1951, No. 1: 1–18.

Braarud, T., K. R. Gaarder and J. Grøntved, 1953: The phytoplankton of the North Sea and adjacent waters in May 1948. Rapp. Cons. Explor. Mer, *133*: 1–87.

Chun, C., 1897: Die Beziehungen zwischen dem arktischen und antarktischen Plankton. Stuttgart, 64 pp.

Cleve, P. T., 1897: A treatise on the phytoplankton of the Atlantic and its tributaries and on the periodic changes of the plankton of the Skagerak. Upsala, 1897.

— 1900: The seasonal distribution of Atlantic plankton organisms. Göteborg, 368 pp.

— 1901: Plankton organisms from the Indian Ocean and the Malay Archipelago. K. svenska VetenskAkad. Handl., *35* (5): 1–58.

Cleve, P. T. and A. Grunow, 1880: Beiträge zur Kenntnis der Arctischen Diatomeen. K. svenska VetenskAkad. Handl., *17* (2): 1–121.

Cleve-Euler, A., 1917: Quantitative plankton researches in the Skager Rak. K. svenska VetenskAkad. Handl., *57* (7): 1–130.

— 1937: Undersökningar över Öresund, XXIV. Sundets Plankton, 1. Sammansättning och Fördelning. K. fysiogr. Sällsk. Lund Handl. N.F., *48* (9): 5–47.

— 1949: Litoral diatoms from Tristan da Cunha. Results Norweg. Exped. T. da Cunha, No. 18: 1–30.

Corlett, J., 1953: Net phytoplankton at ocean weather stations "I" and "J". J. Cons. int. Explor. Mer, *19* (2): 178–190.

Cupp, E. E., 1937: Seasonal distribution and occurrence of marine diatoms and dinoflagellates at Scotch Cap, Alaska. Bull. Scripps Instn Oceanogr. tech., *4* (3): 71–100

Czapek, F., 1909: Zur Kenntnis des Phytoplanktons im Indischen Ozean. S. B. Akad. Wiss. Wien Math.-Naturwiss. Kl., *118* (1): 1–9.

Damas, D. and E. Koefoed, 1909: Le plankton de la Mer du Grönland. Croisière oceanographique accomplie a bord de la Belgica dans la Mer du Grönland, 1905, 109 pp.

Davidson, V. M., 1931: Biological and oceanographic conditions in Hudson Bay. 5. The planktonic diatoms. Contr. Canad. Biol., *6* (26): 497–509.

Dietrich, G. and K. Kalle, 1957: Allgemeine Meereskunde. Gebrüder Borntraeger, Berlin, 492 pp.

Droop, M. R., 1958: Optimum relative and actual ionic concentrations for growth of some euryhaline algae. Verh. int. Ver. Limnol., *13*: 722–730.

Ekman, S., 1953: Zoogeography of the Sea. Sidgwick and Jackson Limited, London, 417 pp.

Ercegovic, A., 1936: Études qualitative et quantitative du phytoplancton dans les eaux cotières de L'Adriatique Oriental Moyen au cours de l'année 1934. Acta adriat., *9*: 1–126.

Fish, C. J., 1925: Seasonal distribution of the plankton of the Woods Hole region. Bull. U.S. Bur. Fish, *41*: 91–179.

Fogg, G. E. and D. F. Westlake, 1955: The importance of extracellular products of algae in fresh water. Verh. int. Ver. Limnol., *12*: 219–232.

Gaarder, K. R., 1938: Phytoplankton studies from the Tromsö district 1930–31. Tromsö Mus. Aarsh., *55* (1): 1–160.

— 1951: Bacillariophyceae from the "Michael Sars" North Atlantic Deep Sea Expedition 1910. Rep. Sars N. Atl. Deep Sea Exped. 1910, *2* (2): 1–53.

— 1954: Coccolithineae, Silicoflagellatae, Pterospermataceae and other forms from the "Michael Sars" North Atlantic Deep Sea Expedition 1910. Rep. Sars N. Atl. Deep Sea Exped. 1910, *2* (4): 1–28.

Gilbert, J. Y. and W. E. Allen, 1943: The phytoplankton of the Gulf of California obtained by the "E. W. Scripps" in 1939 and 1940. J. Mar. Res., *5* (2): 89–110.

Graham, H. W. and N. Bronikovsky, 1944: Scientific results of Cruise VII of the Carnegie during 1928–1929. Biology V. The genus *Ceratium* in the Pacific and North Atlantic Oceans. Car. Inst. Wash. Publ. 565, 209 pp.

Gran, H. H., 1897a: Protophyta, Diatomaceae, Silicoflagellata and Cilioflagellata. The Norwegian North Atlantic Expedition 1876–1878, *24*: 1–36.

— 1897b: Bacillariaceen vom kleinen Karajakfjord. Bibl. bot., Stuttgart, *42*: 1–12.

— 1897c: Bemerkungen über das Plankton des Arktischen Meeres. Ber. dtsch. bot. ges., *15* (2): 132–136.

— 1900: Hydrographic-biological studies of the North Atlantic Ocean and the coast of Nordland. Rep. Norweg. Fish. Invest., *1* (5): 1–92.

— 1902: Das Plankton des Norwegischen Nordmeeres. Rep. Norweg. Fish. Invest., *2* (5): 1–222.

— 1912: Pelagic plant life, pp. 307–386. In Murray and Hjort, Depths of the Ocean. Macmillan, London.

— 1915: The plankton production of the North European waters in the spring of 1912. Cons. Internat. Explor. Mer, Bull. Planktonique p. l'Année 1912, 142 pp.

— 1919: Quantitative investigations as to phytoplankton and pelagic protozoa in the Gulf of St. Lawrence and outside the same. Dep. Naval Service, Canad. Fish. Exped. 1914–1915, pp. 489–495.

— 1929: Investigation of the production of plankton outside the Romsdalsfjord 1926–1927. Rapp. Cons. Explor. Mer, *56*: 1–112.

Gran, H. H. and T. Braarud, 1935: A quantitative study of the phytoplankton in the Bay of Fundy and the Gulf of Maine. J. biol. Bd. Can., *1* (5): 279–467.

Grøntved, J., 1950: Phytoplankton studies I. *Nitzschia frigida* Grun. an arctic—inner Baltic diatom found in Danish waters. K. danske Vidensk. Selsk., Bio. skr., *18* (12): 1–19.

— 1952: Investigations on the phytoplankton in the southern North Sea in May 1947. Medd. Komm. Havundersøg. Kbh., Ser.: Plankton, *5* (5): 1–49.

Grøntved, J. and G. Seidenfaden, 1938: The phytoplankton of the waters west of Greenland, Godthaab Expedition, 1928. Medd. Grönland, *82* (5): 1–380.

Gudmundsson, F., 1937: Das Oberflächennetzplankton der isländischen Küstengewässer nach den Ergebnissen einer Rundfahrt. Ber. dtsch. Komm. Meeresforsch., *8* (4): 220–268.

Gunther, E. R., 1936: A report on oceanographical investigations in the Peru Coastal Current. Discovery Rep., *13*: 107–276 (not seen).

Haeckel, E., 1890: Planktonstudien. Jena, 105 pp.

Hagelstein, R., 1939: Scientific study of Porto Rico and the Virgin Islands. Diatomaceae. N.Y. Acad. Sci., *8* (3): 313–444.

Halldal, P., 1953: Phytoplankton investigation from weather ship M in the Norwegian Sea, 1948–1949. Norske VidenskAkad. Hvalråd. Skr., No. 38: 1–91.

HALLDAL, P., 1957: Importance of calcium and magnesium ions in phototaxis of motile green algae. Nature, *179*: 215.

HART, T. J., 1934: On the phytoplankton of the south-west Atlantic and the Bellinghausen Sea, 1929–1931. Discovery Rep., *8*: 1–268.

— 1942: Phytoplankton periodicity in Antarctic surface waters. Discovery Rep., *21*: 261–356.

— 1953: Plankton of the Benguela Current. Nature, *171*: 631.

HASLE, G. R., 1950: Phototactic vertical migration in marine dinoflagellates. Oikos, *2* (2): 162–175.

— 1954: More on phototactic diurnal migration in marine dinoflagellates. Nytt Mag. Bot., *2*: 139–147.

— 1956: Phytoplankton and hydrography of the Pacific part of the Antarctic Ocean. Nature, *177*: 616.

HEDGPETH, J. W., 1957: Classification of marine environments. Geol. Soc. America, Mem, *67* (2): 93–100.

HEIDEN, H. and R. W. KOLBE, 1928: Die marinen Diatomeen der Deutschen Südpolar Expedition. 1901–1903. Dtsch. SüdpolExped., *8* (5): 447–714.

HENDEY, N. I., 1937: The plankton diatoms of southern seas. Discovery Rep., *16*: 151–364.

— 1954: Note on the Plymouth "*Nitzschia*" culture. J. Mar. biol. Ass. U.K., *33*: 335–339.

HENSEN, V., 1887: Ueber die Bestimmung des Planktons oder des im Meere treibenden Materials an Pflanzen und Thieren. Fünfter Bericht der Kommission zur wissenschaftlichen Untersuchung der deutschen Meere in Kiel für die Jahre 1882–1886, XII bis XVI Jahrgang.

— 1911: Das Leben im Ozean nach Zählungen seiner Bewohner. Ergeb. Plankton Exped. Humboldt Stiftung, *5*: 1–406.

HENTSCHEL, E., 1932: Die Biologischen Methoden und das Biologische Beobachtungsmaterial der Meteor Expedition. Wiss. Ergebn. dtsch. atlant. Exped. "Meteor", *10*: 1–275.

HJORT, J. and H. H. GRAN, 1899: Plankton studies. Currents and pelagic life in the Northern Ocean. Bergens Mus. Skr., *6*.

HUSTEDT, F., 1930–37: Die Kieselalgen Deutschlands, Österreichs und der Schweiz mit Berücksichtigung des übrigen Länder Europas sowie der angrenzenden Meeresgebiete. Dr. L. Rabenhorst's Kryptogamen Flora, *7* (1–2): 920 + 736 pp.

ISELIN, C., 1930: A report on the coastal waters of Labrador, based on explorations of the "Chance" during the summer of 1926. Proc. Amer. Acad. Arts Sci., *66* (1): 1–37.

JOLLOS, V., 1910: Dinoflagellatenstudien. Arch. Protistenk., *19* (2): 178–206.

JØRGENSEN, E., 1905: Protist plankton of northern Norwegian fjords. Bergens Mus. Skr., 1905, pp. 49–151.

KAMPTNER, E., 1937: Über Dauersporen bei marinen Coccolithineen. S. B. Akad. Wiss. Wien Math.-Naturwiss. Kl., *146*: 67–76.

KARSTEN, G., 1905a: Das Phytoplankton des Antarktischen Meeres nach dem Material der deutschen Tiefsee-Expedition, 1898–1899. Dtsch. Tiefsee Exped., *2* (2): 1–136.

— 1905b: Das Phytoplankton des Atlantischen Oceans nach dem Material der deutschen Tiefsee-Expedition, 1898–1899. Dtsch. Tiefsee Exped., *2* (2): 139–219.

— 1907: Das Indische Phytoplankton nach dem Material der Deutschen Tiefsee-Expedition, 1898–1899. Dtsch. Tiefsee Exped., *2* (2): 223–544.

KING, J. E., 1950: A preliminary report of the plankton of the west coast of Florida. Quart. J. Fla. Acad. Sci., *12* (2): 109–137.

KISSELEV, J. A., 1925: Das Phytoplankton des Weissen Meeres. Explor. Mers russes, *2*: 1–43 (Russian, German summary).

— 1928: Contribution to the question of distribution and composition of the phytoplankton in the Barents Sea. Trans. Inst. Expl. North, *37*: 28–42 (Russian, English summary).

KISSELEV, J. A., 1933: The Arctic and Mediterranean elements in the phytoplankton of the Amur Gulf, their origin and distribution. Proc. 5th Pac. Sci. Cong., *3*: 2061.

KNUDSEN, M. and C. H. OSTENFELD, 1899: Iagttagelser over overfladevandets temperatur, saltholdighed og plankton paa islandske og grønlandske skibsrouter i 1898, Kjøbenhavn, 93 pp.

— 1900: Iagttagelser over overfladevandets temperatur, saltholdighed og plankton paa islandske og grønlandske skibsrouter i 1899, Kjøbenhavn, 93 pp.

KOLBE, R. W., 1932: Grundlinien einer allgemeinen Ökologie der Diatomeen. Ergebn. Biol., *8*: 221–348.

KRASSKE, G., 1941: Die Kieselalgen des Chilenischen Küstenplanktons. Arch. Hydrobiol., *38*: 260–287.

LEMMERMANN, E., 1899: Ergebnisse einer Reise nach dem Pacific. Abh. naturw. Ver. Bremen, *16* (2): 313–398.

MANGIN, L., 1915: Phytoplancton de l'Antarctique. Deuxiéme Expédition Française (1908–1910). Paris, 95 pp.

— 1922: Phytoplancton Antarctique. Expédition Antarctique de la "Scotia", 1902–1904. Mem. Acad. Sci. Paris, *67*: 1–134.

MANGUIN, E., 1954: Diatomées marines provenant de l'Ile Heard. Rev. algol., *1* (1): 14–24.

MARGALEF, R. and M. DURAN, 1953: Microplancton de Vigo, de octubre de 1951 a septiembre de 1952. Publ. Inst. Biol. apl. Barcelona, *13*: 5–78.

MARSHALL, P. T., 1955: Phytoplankton production in the western Barents Sea 1949–1954. Int. Cons. Explor. Mer Meeting, Plankton Committee No. 49.

MERESCHKOWSKY, C., 1902: Liste des Diatomées de la mer Noire. Scripta bot. petropol., *19*: 1–42 (Russian, French summary).

MJAALAND, G., 1956: Some laboratory experiments on the coccolithophorid *Coccolithus huxleyi*. Oikos, *7* (2): 251–255.

MOTODA, S. and Y. KAWARADA, 1955: Diatom communities in western Aleutian waters on the basis of net samples collected in May–June 1953. Bull. Fac. Fish. Jap., *6* (3): 191–200.

NORDLI, E., 1951: Resting spores in *Goniaulax polyedra* Stein. Nytt Mag. Naturv., B *88*: 207-212.

— 1953: Salinity and temperature as controlling factors for distribution and mass occurrence of Ceratia. Blyttia, *11*: 16–18.

— 1957: Experimental studies on the ecology of *Ceratia*. Oikos, *8* (2): 200–265.

OSTENFELD, C. H., 1898: Lidt tropiskt og subtropiskt phytoplankton fra Atlanterhavet. Vidensk. Meddel. dansk naturh. Foren. Kbh., pp. 427–430.

— 1902: Flora of Koh Chang. VII. Marine plankton diatoms. Bot. Tidsskr., *25*: 219–245.

— 1909: Immigration of a plankton diatom into a quite new area within recent years; *Biddulphia sinensis* in the North Sea waters. Int. Rev. Hydrobiol., *2*: 362–374.

— 1910: Marine plankton from the East Greenland Sea. I. List of diatoms and flagellates. Danmark-Ekspeditionen til Grønlands Nordøstkyst 1906–1908. Medd. Grønland, *43*: 260–285.

— 1913: On the distribution of Bacillariales (diatoms). Résumé des observations sur le plankton des mers explorées par le Conseil pendant les années 1902–1908. Bull. Planktonique 1902–1908.

— 1915: A list of phytoplankton from the Boeton Strait, Celebes. Dansk bot. Ark., *2* (4): 1–18.

OSTENFELD, C. H. and J. SCHMIDT, 1901: Plankton fra det Røde Hav og Adenbugten. Vidensk. Meddel. naturh. Foren. Kbhvn., pp. 141–182.

PAULSEN, O., 1904: Plankton investigations in the waters around Iceland in 1903. Medd. Komm. Havundersøg. Ser. Plankton, *1* (1): 1–40.

— 1909: Plankton investigations in the waters around Iceland and in the North Atlantic in 1904. Medd. Komm. Havundersøg. Ser. Plankton, *1* (8): 1–57.

PAULSEN, O., 1911: The plankton on a submarine bank. Biologiske Arbejder tilegnede Eug. Warming, pp. 231–239.

PAVILLARD, J., 1925: Bacillariales – Rpt. on the Danish Oceanographical Expeditions 1908–10 to the Mediterranean and Adjacent Seas, *2* (4): 1–72.

— 1931: Phytoplankton (Diatomées, Peridiniens) provenant des campagnes scientifiques du Prince Albert Ier de Monaco. Resul. Camp. sci. Monaco, *82*: 1–203.

— 1935: Peridiniens et diatomées pelagiques recueillis par Alain Gerbault entre les îles Marquises et les îles Galapagos. Bull. Inst. océanogr. Monaco, *669*: 1–7.

PETERS, N., 1934: Die Bevölkerung des Südatlantischen Ozeans mit Ceratien. Wiss. Ergebn. dtsch. atlant. Exped. "Meteor.", *11*: 1–69.

PROVASOLI, L., J. J. A. MCLAUGHLIN and I. J. PINTNER, 1954: Relative and limiting concentrations of major mineral constituents for the growth of algal flagellates. Trans. N.Y. Acad. Sci. Ser. II, *16* (8): 412–417.

RAMSFJELL, E., 1957: Hovedtrekkene i nannoplanktonets fordeling i Norskehavet og deres hydrografiske bakgrunn. (MS).

REINHARD, L., 1910: Vorläufige Mitteilung über das Phytoplankton des Schwarzen Meeres, der Meeresstrasse von Kertsch, des Bosphorus und des Marmara Meeres. Trud. Obshch. Ispuit. Prir. Kharkov, *43*: 1–31. (Russian).

RODHE, W., 1948: Environmental requirements of freshwater plankton algae. Symb. bot. upsaliens, *10* (1): 1–149.

— 1955: Can plankton production proceed during winter darkness in subarctic lakes? Verh. int. Ver. Limnol., *12*: 117–122.

RYTHER, J. H., 1955: The ecology of phytoplankton blooms in Moriches Bay and Great South Bay, L. I., N.Y. Biol. Bull., Woods Hole, *106* (2): 198–209.

SABELINA, M. M., 1930: Einige neue Daten über das Phytoplankton des Karischen Meeres. Expl. Mers russe, *13*: 105–143. (Russian, German summary).

SCHREIBER, E., 1927: Die Reinkultur von marinem Phytoplankton und deren Bedeutung für die Erforschung der Produktionsfähigkeit des Meerwassers. Wiss. Meeresuntersuch. N.F. Abf., *16* (10): 1–35.

SCHRÖDER, B., 1906: Beiträge zur Kenntnis des Phytoplanktons warmer Meere. Vjschr. naturw. Ges. Zürich, *51*: 319–377.

SCHÜTT, F., 1893: Das Pflanzenleben der Hochsee. Kiel und Leipzig, 76 pp.

SEGERSTRÅLE, S. G., 1951: The recent increase in salinity off the coasts of Finland and its influence upon the fauna. J. Cons. int. Explor. Mer, *17* (2): 103–110.

SILVA, E. S., 1949: Diatomáceas e dinoflagelados de Baía de Cascais. Portug. acta biol. (B) vol. "Julio Henriques", pp. 300–383.

— 1952: Estudos de plancton na Lago de Óbidos 1. Diatomáceas e dinoflagelados. Rev. Fac. Sci. Lisboa, 2a Sér. (C), *2* (1): 5–44.

— 1953: Diatomáceas do plâncton marinho de Angola. An. Jta. Inv. Ultramar, *8* (2): 3–56.

— 1956a: Contribution à l'étude du microplankton de Dakar et des régions maritimes voisines. Bull. Inst. franc. Afr. noire, Ser. A, *8* (2): 335–371.

— 1956b: Contribuição para o estudo do microplâncton marinho de Moçambique. Junta Inv. Ultramar., Estudos, Ensaios e Documentos, *28*: 9–97.

SILVA, E. S. and J. S. PINTO, 1948: O plâncton da Baía de S. Martinho do Porto I. Diatomáceas e dinoflagelados. Bull. Soc. Portug. Sci. nat., *16* (2): 134–187.

— 1952: Estudo do ciclo sazonal do plâncton marinho da Guiné Portuguesa. Bol. cult. Guine portug., No. 25: 131–155.

SKVORTZOW, B. W., 1931: Pelagic diatoms of Korean Strait of the Sea of Japan. Philipp. J. Sci., *36* (1): 95–122.

Smayda, T. J., 1957: Phytoplankton studies in lower Narragansett Bay. Limno. Oceanogr., *2* (4): 342–359.

— 1958: Phytoplankton studies around Jan Mayen, March–April 1955. Nytt Mag. Bot., *6*: 75–96.

Steemann Nielsen, E., 1934: Untersuchungen über die Verbreitung, Biologie und Variation der Ceratien im südlichen Stillen Ozean. Dana Rep. No. 4.

— 1935: The production of phytoplankton at the Faroe Isles, Iceland, East Greenland and in the waters around. Medd. Komm. Havundersøg. Kbh. Ser. Plankton, *3* (1): 1–93.

— 1939: Über die vertikale Verbreitung der Phytoplankton im Meere. Int. Rev. Hydrobiol., *38*: 421–440.

Subrahmanyan, R., 1946: A systematic account of the marine plankton diatoms of the Madras Coast. Proc. Indian Acad. Sci., *24*: 85–197.

Sverdrup, H. U., M. W. Johnson and R. H. Fleming, 1942: The Oceans. Prentice-Hall, Inc. New York, pp. 1087.

Takano, H., 1955: Plankton diatoms collected off Bôsô District in August, 1951. Bull. Jap. Soc. sci. Fish., *21* (2): 55–61.

Ussatschew, P. I., 1935: Die Zusammensetzung und Verteilung des Phytoplanktons des Barents-Meeres im Sommer 1931. Trans. arct. Inst., Leningr., *21*: 5–94. (Russian, German summary).

Välikangas, I., 1926: Planktologische Untersuchungen im Hafengebeit von Helsingfors I. Über das Plankton insbesondere das Netz-zooplankton des Sommerhalbjahres. Acta zool. fenn., *1*: 1–298.

Wandel, C. F. and C. Ostenfeld, 1898: Iagttagelser over overfladevandets temperatur, saltholdighed og plankton paa islandske og grönlandske skibsrouter i 1897. Kjøbenhavn, 1898, 1–49.

Wirketiss, M. A. and J. A. Kisselev, 1935: Zur Kenntnis des Planktons der Tscheskaja Bucht. Explor. Mers russes, *18*: 115–144. (Russian, German summary).

Wood, E. J. F., 1950: Phytoplankton studies in eastern Australia. Proc. Indo-Pac. Fish Counc., S 2/2: 60–63.

Ødegaard, K., 1942: De økologiske virkninger av kloakkforurening med særlig henblikk på giftvirkningen. Sammenliknende forsøk over marine fytoplanktonalgers giftresistens. Thesis at the University of Oslo.

Østrup, E., 1895: Marine diatomeer fra Østgrønland. Medd. Grønland, *18*: 397–476.

Addenda

The occurrence of *Thalassiosira hyalina* north of the Alaskan archipelago (Kawarada and Ohwada 1957) and Okhotsk Sea (Jousé 1957) has been reported. These observations confirm the presence of *T. hyalina* in Pacific waters and indicate a circumpolar distribution.

Only Hendey's (1937) report of *T. hyalina* in the southern hemisphere was briefly discussed earlier, as all other known reports (Boden 1950; Krasske 1941; Zacharias 1906) were deemed not to warrant discussion. But as they might be offered in evidence against *T. hyalina*'s arctic nature or in support of the existence of bipolarity of marine phytoplankton at the species level, a brief discussion of these reports is in order. Boden appears not to have found *T. hyalina* along the west coast of South Africa; the inclusion of this species in his handbook stems from HENDEY's claim that it is present in those waters. KRASSKE's viewpoint that *T. hyalina* and *T. decipiens* are identical can not be accepted. Hence, *T. hyalina* probably does not occur along the Chilean coast. ZACHARIAS' claim that he found *T. clevei* (a synonym of *T. hyalina*) in the Gulf of Valparaiso, and also in the Adriatic Sea, seems improbable.

LEWIN (1958) has reinvestigated the taxonomic position of *Phaeodactylum tricornutum* and concluded that it is a diatom rather than a chrysophycean. She has also compiled a bibliography of those investigations employing *P. tricornutum*, but erroneously identified as *Nitzschia closterium* or its *minutissima* form.

GRAN and ANGST (1931) report *Planktoniella sol* from Puget Sound, Washington, its most northerly known extension in the eastern Pacific. The criticism has been received that the literature has not been thoroughly searched in mapping the distributions of the species considered herein. It must be stressed that it was not the purpose to record every known observation of these species, but rather to provide an insight into the general features of distribution and the accompanying temperature and salinity conditions. Accordingly, a single, reliable report of occurrence from a given area was frequently selected over other confirmatory observations. However, all known reports containing applicable temperature and salinity data were used in calculating the respective means of occurrence.

BODEN, B. P., 1950: Some marine plankton diatoms from the west coast of South Africa. Trans. Roy. Soc. South Africa, *22* (4): 321–434.

GRAN, H. H. and E. C. ANGST, 1931: Plankton diatoms of Puget Sound. Pub. Puget Sound Biol. Sta., *7*: 417–519.

JOUSÉ, A. P., 1957: Diatoms from the Okhotsk Sea. Trudy Inst. Okeanol. SSSR, *22*: 164–220 (Russian).

KAWARADA, Y. and M. OHWADA, 1957: A contribution of microplankton observations to the hydrography of the northern North Pacific and adjacent seas (1. Observations in the western North Pacific and Aleutian waters during the period from April to July 1954). Oceanogr. Mag., *9* (1): 149–157.

LEWIN, J. C., 1958: The taxonomic position of *Phaeodactylum tricornutum*. J. gen. Microbiol., *18* (2): 427–432.

ZACHARIAS, O., 1906: Über Periodizität, Variation und Verbreitung verschiedener Planktonwesen in südlichen Meeren. Arch. Hydrob. u. Planktonk., *1*: 498–575.

Contribution No. 968

Second United Nations
International Conference
on the Peaceful Uses of
Atomic Energy

PAPER: UN402-01C724
SEPTEMBER 1-15, 1958

BIOLOGICAL FACTORS DETERMINING THE DISTRIBUTION OF RADIOISOTOPES IN THE SEA.

By

B. H. Ketchum and V. T. Bowen[1]

INTRODUCTION

With the anticipated considerable increase in the peaceful uses of atomic energy the addition of radioisotopes to the sea is inevitable, whether intentionally as a waste disposal measure, or accidentally. The seas are vast and enormous possibilities for dispersion of radioisotopes are available, but it is imperative that the problems associated with radioactive contamination of the oceans be carefully evaluated in advance. The deep sea offers considerable promise for containing large amounts of radioisotopes since it is known that the waters at considerable depths are isolated from the surface layers of the ocean for periods which are measured in terms of centuries. Craig (1957), using 300 years for the mean residence time in the deep sea, has evaluated the ultimate steady state distribution of radioisotopes between the upper layers and the deep water and the rate at which the steady state distribution would be approached if large amounts of fission products were introduced into the ocean below the density gradient (the thermocline).

If considerable amounts of fission products were to be added to the oceans, the ultimate distribution would depend not only upon the current systems and mixing processes which determine the exchanges of water between the deep and the surface layers, but also upon geochemical and biological factors. Many of the elements present in a fission product mixture are insoluble in sea water; these would tend to settle out of the system and not approach equilibrium in the same way that would be expected for soluble materials. Organisms in the water may be expected to accumulate various elements of the fission product mixture to a degree which will depend on the character of the element and the species of organism involved. Part of the accumulation within the organism would depend upon direct assimilation or absorption from the water; part would depend upon the ability of some filter feeding organisms to remove particles from the water. Whether these particles be precipitated fission products or other organisms containing fission products, these elements could also be incorporated into the living tissue. Evidence that marine plankton do concentrate fission products is afforded by observations in the Pacific. Hàrley (1956) reports determinations of the gross radioactivity of both sea water and plankton organisms to the west of the Bikini test area. The analyses indicate that the gross radioactivity was on the average 470 times more concentrated in the plankton than in the water itself when both are expressed on an equivalent basis.

---

[1] Contribution No. 968 from the Woods Hole Oceanographic Institution.

Once organisms have accumulated a radioisotope they may modify its distribution in a variety of ways. Following their death the organisms may be expected to sink towards the bottom and to carry with them those elements which are tightly bound within the organic or skeletal structures. While living, the organisms may make extensive vertical migrations within the water column, migrations which could transport radioisotopes from a contaminated layer to an uncontaminated zone. The materials which would be transported most effectively by living organisms during migration are those which are readily labile, i.e., those which reach equilibrium rapidly with the dissolved phase. In such a case an organism could accumulate a considerable amount of an isotope while in contaminated water and release most of this accumulation by approaching equilibrium again in uncontaminated water.

In this paper we make a preliminary evaluation of the relative effectiveness of the biological and physical systems in the vertical transport of isotopes in the ocean. From analyses of the elemental composition of various planktonic organisms the effectiveness of biological transport of specified isotopes is also evaluated. Much more needs to be known before a complete evaluation of this problem is possible. The treatment presented in this paper is less in the character of an answer to the problem and more a definition of the types of biological and oceanographic investigations which are necessary before the evaluation can be completed.

ELEMENTAL COMPOSITION OF PLANKTON

The elemental composition of organisms in the sea must be known in order to evaluate the importance of biological transport. The results of spectrographic analysis of eleven samples of marine plankton, mostly single species samples, have been reported by Nicholls, Curl, and Bowen (1958). The results reveal wide differences in the trace element content of different species, and considerable concentration of each element by at least one of the species. It is clear that biological concentration of radioisotopes will depend upon the species of organism and upon the element considered.

For the purposes of this paper we have estimated the concentration factors for a variety of radio elements important in nuclear technology for several types of planktonic organisms. The analytical data on organisms are from Nicholls, Curl and Bowen (1958) or are based on analyses published in Vinogradov (1953). The sea water figures are from Vinogradov or from recent separate publications. The genera selected are known to occur in considerable abundance in the sea. The data for the pelagic squid, Ommostrephes, is included since it is known to carry out vertical migrations of several hundred meters in extent. The blank spaces in Table II, plus the fact that many of the values had to be derived from closely related genera or from assumed constant ratios between closely related elements, emphasize the paucity of basic information. The sea water values used give the concentration of the element, so that the actual concentration in the organisms can be calculated.

In general, the concentration factors for radio elements occupy a range of about 10^6, similar to that described by Nicholls et al (1958) for various other elements. The greatest range for a single element among different species is shown by cobalt which varies from a concentration factor of 60 in a salp to 10^4 in Sagitta and Limacina. The concentration factors quoted for iron have been calculated relative to "soluble iron" data of Lewis and Goldberg (1954). They would be lower if total iron were used, but this is variable and should properly be determined on the water from which the organisms were collected. The factors for cesium, on the other hand, are probably low since they are based on the assumption of an unchanged ratio of potassium to cesium in tissues. Chipman et al. (1954) have described much higher levels of radio cesium in oyster tissues, and it seems probable that similar values will be found for some planktonic species.

An estimate for the concentration of cerium by a factor of 10^3 can be derived from Harley's (1956) measurement of cerium^{144} in Pacific macroplankton in comparison with the measurement of the same isotope in Pacific waters by Miyake and Sugiura (1955).

In addition to the concentration factor, which represents the steady state condition, it would be desirable to know the rate at which equilibrium is reached. Unfortunately there seems to be no experimental data to indicate the equilibrium times for the various isotopes in macroplankton. For the above radio elements we estimate that iodine is of very low lability; that cesium and strontium, and, through isotopic exchange, cerium are of very high lability; that for the others rates of exchange ranging from 1 to 15 per cent per hour may be reasonable. The elements transported most readily by vertical migrations will be those most rapidly exchanged with the medium. In contrast, the elements most effectively transported by sedimentation will be those which are tightly bound in the tissues or in skeletal material.

Table I. Concentration factors in some marine organisms (wet weight:volume basis). Values in parentheses are for analyses made on closely related genera.

Elements	Cesium	Strontium	Iron	Cobalt	Zinc	Cadmium	Iodine
Sea water g/cc	5.10^{-10}	9.10^{-6}	4.10^{-9}	$2.5.10^{-10}$	$1.4.10^{-9}$	5.10^{-11}	5.10^{-8}
Organism							
Limacina	$(0.2)^{\pm}$	--	(5.10^{4})	10^{4}	(3.10^{4})	(7.10^{5})	(5.10^{4})
Centropages	0.1-1	--	--	600	--	--	(6.10^{3})
Calanus	0.1-1	0.28^{x}	$2.5.10^{4}$	200	--	--	100
Ommastrephes	$(0.1)^{\pm}$	$(0.3)^{x}$	10^{4}	200	(2.10^{4})	2.10^{5}	(10^{4})
Sagitta	--	70	5.10^{4}	10^{4}	--	--	--
Euphausia	--	$(0.3)^{x}$	--	800	--	--	--
Salpa	--	--	--	60	--	--	--

x Derived from Ca analysis and Sr/Ca ratio given by Chow and Thompson (1956).

± Based upon analyses for potassium, assuming the Cs/K ratio in the organisms to be the same as that in sea water.

TRANSPORT BY VERTICAL MIGRATION

Planktonic organisms which migrate vertically on a diurnal cycle in the ocean could transport readily labile elements absorbed from the water from layers of high to layers of low concentration. If radioisotopes should be introduced below the thermocline of the ocean in the hope of prolonged retention, the possible transport by this means requires evaluation.

Relative effectiveness of the vertical transport of elements in the sea by biological and physical processes can be evaluated using a simplified model of the distribution which might be expected. This model involves a low or negligible concentration in the upper layer; a higher concentration in the deep layer; and a uniform gradient of concentration through the thermocline or density discontinuity layer. The treatment developed is equally applicable to any other situation in which a layer of high concentration is separated vertically from a layer of low concentration by a uniform gradient. If the organisms migrate from the bottom of the discontinuity layer to the top on a diurnal cycle, the biological transport (T_B) of any given element may be represented by the following:

$$T_B = \frac{\mathcal{E}_o}{\mathcal{E}_\omega} V_o \left(C_b \alpha_b - C_t \alpha_t\right) \frac{d_m}{P_m} \tag{1}$$

in which $\mathcal{E}_o/\mathcal{E}_\omega$ is the concentration factor (f_o) i.e. the ratio of the concentration of the element in the organisms to the total concentration in the water, V_o is the volume of the organism per unit volume of water, C_b and C_t are the concentrations of the element respectively at the bottom and top of the gradient layer, α_b and α_t are the specific activities of the radioisotope at these two levels, d_m is the distance over which the organism migrates and P_m is the period of migration.

The physical transport (T_p), expressed in finite terms, is given by:

$$T_p = A_z \frac{C_b \alpha_b - C_t \alpha_t}{d} \tag{2}$$

where A_z is the vertical coefficient of eddy diffusion and d is the depth of the gradient zone considered. The ratio of the biological transport to the physical transport is therefore given by the following:

$$\frac{T_B}{T_p} = V_o \frac{f_o}{A_z} \cdot \frac{d \cdot d_m}{P_m} \tag{3}$$

Assuming reasonable values for the various parameters the relative importance of biological to physical transport has been calculated with the results shown in Table II. For this computation it has been assumed that $d = d_m = 100$ meters, that the period of migration is 10^5 sec and that the volume of organisms in the water is 1 cc per cubic meter ($V_o = 10^{-6}$). As expected, the relative importance of the biological process increases as the concentration factor within the organism increases, and also increases as the eddy diffusion decreases.

Table II. The ratio of biological to physical transport of elements in the sea for various mixing coefficients and concentration factors, assuming the organism reaches equilibrium for the isotope in the time spent in each layer. Other parameters are defined as follows: $d = d_m = 100$ meters, $P_m = 10^5$ seconds, $V_o = 10^{-6}$ (1 cc/m3).

A_z	$f_o = 1$	10	10^2	10^3	10^4	10^5
.01	10^{-1}	1	10	10^2	10^3	10^4
.1	10^{-2}	0.1	1	10	10^2	10^3
1.0	10^{-3}	10^{-2}	0.1	1	10	10^2
10	10^{-4}	10^{-3}	10^{-2}	0.1	1	10
100	10^{-5}	10^{-4}	10^{-3}	10^{-2}	0.1	1

As shown in Table I, the biological concentration factors range up to values of 10^5. With this concentration factor, and the assumed volume of organisms in the water, the biological transport of readily labile elements will equal the physical diffusion of the element even in moderately turbulent conditions ($A_z = 100$). For very stable conditions in the water ($A_z = 0.1$ or less) the biological transport will equal or exceed the physical transport with concentration factors of 100.

Craig (1957) has calculated the ultimate steady state distribution of radioisotopes which might be added to the deep sea as fission product activities. He used a mean retention time of 300 years in the deep water, from the bottom of the thermocline at 100 meters to the average depth of 3800 meters. The mean transport per day from this layer to the surface is thus:

$$\frac{C_b \times 3.7 \times 10^5}{300 \times 365} = 3.4\, C_b$$

in which C_b is the concentration in the deep water of the isotope considered per cm^3 of water.

The concentration factor necessary to give equivalent biological transport can be computed from our equation (1), assuming a surface concentration of zero initially, and, as above, the depth of migration of 100 meters, a period of one day, and a population of 1 cc/m^3. The resultant concentration factor is 340. Since concentration factors of this magnitude and greater are not uncommon, it seems inevitable that the ultimate distribution of radioisotopes added to the deep sea would be profoundly influenced by the biological processes.

TRANSPORT BY SEDIMENTATION

It has long been known that the distribution of essential nutrient elements in the sea is markedly affected by their assimilation in living tissues, and the subsequent sedimentation of dead organisms, whether intact or as fecal matter of predators. This produces the typically low concentrations in surface layers, where the light is sufficient for photosynthesis, and an increasing concentration with depth below the euphotic zone. Because of the gradient thus developed the physical processes and the transport by vertical migration of plankton must constantly deliver new supplies to the surface. The rate of sedimentation must be sufficient to balance this in areas where a steady state distribution persists.

The downward gravitational transport (T_g) of elements may be expressed, for particles of uniform properties, by the following:

$$T_g = \frac{\varepsilon_o}{\varepsilon_w} V_o C_t v \qquad (4)$$

in which v is the settling velocity, which is negative downwards. This process will be most effective for elements which are tightly bound in the organic or skeletal structure of organisms and which, therefore, do not exchange rapidly but await the slower remineralization by bacteria, autolysis or resolution.

This equation can be added to equation (1), the biological transport resulting from vertical migration, to give the combined transport. For particles of uniform properties the rate could be evaluated. However, the particles in the sea are far from uniform, and vary greatly in size, density and shape, all of which will modify the settling velocity. No simple generalization which would provide an evaluation of this process seems possible considering the wide variety of materials which are settling in the sea. Redfield (1955) has shown the results of this process in developing high concentrations of elements in deep waters where surface and deep currents are opposed. In addition to the nutrient maxima, similar, though generally less extensive, maxima have been reported for other elements, as nickel (Laevastu and Thompson 1956), cooper and zinc (Morita 1952).

RETENTION BY RESISTANCE TO SINKING

Some planktonic organisms aggregate at the surface and thus produce considerable concentrations of trace elements. In "red tide" blooms of the dinoflagellate, *Gymnodinium brevis*, concentrations of total phosphorus ten times greater than the maximum in adjacent waters were described by Ketchum and Keen (1948). Collier (1953) also observed unusually high concentrations of zirconium and titanium in a similar bloom. These blooms tend to occur in surface lenses of low salinity (see Slobodkin 1953) so that physical transport is minimal, and the toxicity of the bloom would minimize grazing and transport of the elements away from the center of concentration.

The observed accumulation of elements in such plankton blooms are clearly the result of the unique properties of the organisms involved. These tend to aggregate at the surface, either by migration or flotation. Greater concentrations may subsequently be achieved, as discussed by Ryther (1955), along convergences at the surface.

Those articifical radioisotopes which are now found in the sea have been added at the surface as fallout from weapons tests. Analyses of surface sea water have shown a striking enrichment of cerium or promethium relative to strontium. This has been demonstrated near Bikini by Miyake and Sugiura (1955) and in both the north and south Atlantic by Bowen and Sugihara (1958). Harley's (1956) radiochemical analyses showed that the ratio of Ce^{144}:Sr^{89,90} was higher in the macroplankton than in the water.

The microplankton will preferentially concentrate the rare earth "radio colloids" even more than the macroplankton. Bowen and Rubinson (1951 and unpublished) have shown that yeast cells act as very efficient collecting surfaces for these materials, and Rice (1956 and unpublished) has demonstrated considerable accumulations of yttrium and cerium by cultures of planktonic algae. A large fraction of the microplankton population can maintain its position in the upper layers, thus resisting both sinking and physical eddy diffusion, which in this case would transport elements downward from the higher concentrations at the surface. Since the rare earth elements are concentrated more actively than strontium by three or four orders of magnitude their accumulation by phytoplankton would produce the observed retention in the surface water.

DISCUSSION

The treatment presented above appears to us sufficient to show that the movements of organisms and their activities as concentrators of elements will be of real quantitative significance in modifying any concentration gradients created by the addition of radioisotopes to the sea. Adequate data are presented to indicate that estimates of vertical transport based upon physical considerations alone may be in error by a factor of two or more. Since the affinity of organisms for individual isotopes differs widely, preferential transport by the biological agents may be expected.

Ultimate evaluation of the problem requires basic information which is unavailable as yet. The paucity of information is apparent in both the rate of physical processes of mixing and exchange between different layers in the ocean, and in the biological field concerning the distribution of organisms and their affinity for various radio elements.

The physical oceanographers are unable as yet to define the coefficient of eddy diffusion precisely enough to allow intercomparison of a variety of places. The biological transport of elements may augment the physical transport or oppose it, and it is,therefore, essential in each case to evaluate both processes. For this reason we have, where possible, expressed the biological transport in terms of what may be expected from physical mixing. The values for the mixing coefficient used in calculating relative transports in Table II range from very stable to moderately turbulent conditions. Values less than unity are typical of conditions in the gradient layer of the open sea, and values of 100 or more may be observed in turbulent coastal waters. For a complete evaluation of the vertical transport of elements much more precise data on vertical eddy diffusion in the sea are required.

It is equally true that the biological oceanographers do not have adequate data to evaluate the concentration of organisms to be expected in various areas at various times of the year. We do know that the biological sampling techniques with nets do not collect all of the populations but that the value of 1 cc per cubic meter used in the above examples is common in coastal areas and is not infrequently found in the open sea. In the Sargasso Sea, and in other comparable marine "deserts", however, the populations rarely exceed one tenth of this value. In such areas the physical mixing processes are also very small.

The basic biological information needed includes all stages of the ecological cycle in the sea, i.e.,the biomass of various populations, the rate of reproduction and the exchanges of energy and of elements from one component of the community to another. For problems of sorption, not only the biomass but also the surface area must be known. This is particularly true of the microplankton which afford by far the greatest surface area in the open sea where other suspended materials are rare. The size, density and shape of the organisms determine settling rates which control the downward transport of elements by sedimentation.

The importance of determining the accumulation of various elements by different species of plankton cannot be overemphasized. The data already available suggests considerable concentration by at least one species of each element which has been studied. The effectiveness of transport depends, in each case, on both the concentration factor and on the rate at which the organism reaches equilibrium with materials in the water. Extensive studies of the rates of uptake and exchange are needed, since this information is available in very few instances.

REFERENCES

Bowen, V. T. and Rubinson, J., Uptake of lanthanum by a yeast, Nature 167:1032, (1951).

Bowen, V. T. and T. G. Sugihara, Marine geochemical studies with fallout radioisotopes, (in prep.).

Chipman, W. A., T. R. Rice and T. J. Price, Accumulation of fission product by marine plankton, fish and shellfish, U. S. Fish and Wildlife Radioisotope Lab. Progress Report, July-December, (1954).

Chow, T. J. and T. G. Thompson, Flame photometric determination of strontium in sea water, Anal. Chem. 27:18-21, (1955).

Collier, A., Titanium and zirconium in the bloom of Gymnodinium brevis Davis, Science 118:328, (1953).

Craig, H., Disposal of radioactive wastes in the ocean: The fission product spectrum in the sea as a function of time and mixing characteristics, Chapt. 3. In: The effects of atomic radiation on oceanography and fisheries. Pub. No. 551, Nat. Acad. of Sci. -Nat. Res. Counc. 34-42, (1957).

Harley, J. F. (Editor), Operation Troll, U. S. Atomic Energy Comm., New York Operation Office, v + 37 pp., (1956).

Ketchum, B. H. and D. J. Keen, Unusual phosphorus concentrations in the Florida "red tide" sea water, Jour. Mar. Res. 7:17-21, (1948).

Lewis, G. J., Jr. and E. D. Goldberg, Iron in marine waters, Jour. Mar. Res. 193(2):183-197, (1954).

Laevastu, T. and T. G. Thompson, The determination and occurrence of nickel in sea water, marine organisms and sediments, J. du Conseil 21:125-143, (1956).

Miyake, Y. and Y. Sugiura, Radiochemical analysis of radionuclides in sea water collected near Bikini Atoll. Pap. Met. Geophy., 7(1):33-37, (1955).

Morita, Y., Copper and zinc in Pacific waters, Rec. Oceanographic Works in Japan 1:49-51, (1953).

Nicholls, G.K., H. Curl, Jr., and Bowen, V. T., Spectrographic analyses of plankton, Limnol. and Oceanogr.,(in press).

Redfield, A. C., The hydrography of the Gulf of Venezuela. Pap. Mar. Biol. & Oceanogr., Deep-Sea Res. Suppl. 3:115-133, (1955).

Rice, T. R., The accumulation and exchange of strontium by marine planktonic algae, Limnol. and Oceanogr. 1(2):123-138, (1956).

Ryther, J. H., Ecology of autotrophic marine dinoflagellates with reference to red water conditions, In: Luminescence of Biological Systems, 387-414, (1955).

Slobodkin, L. B., A possible initial condition for red tides on the coast of Florida, Jour. Mar. Res. 12(1):148-155, (1953).

Vinogradov, A. P., The elementary chemical composition of marine organisms, Memoir Number Two, Sears Found. Mar. Res., New Haven, Conn., pp. 647, (1953).

Contribution No. 970

Second United Nations
International Conference
on the Peaceful Uses of
Atomic Energy

PAPER: UN403-01C902
SEPTEMBER 1-15, 1958

MARINE GEOCHEMICAL STUDIES WITH FALLOUT RADIOISOTOPES[1]

V. T. BOWEN[2] AND T. T. SUGIHARA[3]

Fallout from the various military tests of nuclear explosive devices has delivered to the surface waters of the Atlantic Ocean very considerable amounts of radioactive material. Reasonable calculations of the actual delivery per unit area show that the contribution from all other sources such as waste material dumping (Joseph 1957) or waste release from shore line reactor operations (Anon. 1956) so far represents a negligible fraction of the total. It is emphasized (Nat. Acad. Sci. 1957) that the amount of radioactivity discussed here, are truly negligible with respect to biological effects, but because of the essentially one-path avenue of delivery to the Atlantic Ocean, they afford us a gigantic and unique geochemical tracer experiment. Our first study of strontium 90 (Bowen and Sugihara 1957) distribution revealed the usefulness of this data, and Craig (1958) has since also discussed the problem.

Because of the extreme dilution of radioactivity in Atlantic waters even at the surface, special separation methods for the radioelements selected have had to be devised. The procedure for strontium 90 has already been summarized (Bowen and Sugihara 1957) and a detailed description of our methods for strontium 90, cesium 137, cerium 144, and promethium 147 is to be presented to the American Chemical Society Symposium on Radiochemical Methods in Analytical Chemistry (1958, Sugihara et al.). We have also developed a method for antimony 125 (Bowen and Campbell, unpublished). Selection of these five radioelements (Sr 90, Sb 125, Cs 137, Ce 144, Pm 147) was based on the fact that their relatively long half-lives and relatively high yields in fission gave promise that detectable amounts would be found, and that their chemical behavior was well enough known to permit a meaningful analysis of the data when obtained. This latter condition does not seem to be well enough fulfilled for ruthenium 106, and the fission yield of cadmium 113m (Bowen 1956) appears to be too low.

---

[1] Contribution number 970 from the Woods Hole Oceanographic Institution. This work has been supported in part by the U. S. Office of Naval Research under contract NONR-1238(00), by the National Science Foundation, and by the U. S. Program for the International Geophysical Year under grant NS8 Y/9.12/143.

[2] Woods Hole Oceanographic Institution

[3] Dept. of Chemistry, Clark University

Also because of the extreme dilution, a large volume sampler has been devised, capable of being handled on the conventional hydrographic winch and wire, and of collecting 220-liter samples at any depths. Initially this whole volume was processed for the radioelements, but because of limitations of space on shipboard, we have had to limit ourselves to bringing back two 60-liter aliquots of each sample. Of these one is processed for the five isotopes listed above, and the other is reserved for check or supplementary analyses. The counting procedures and methods of radio-chemical identification are described elsewhere (Bowen and Sugihara 1957; Sugihara et al. 1958).

The program of sample collection has been extensive, through the support of a number of agencies. In connection with a continuing series of studies of related hydrological, chemical, and biological processes on the continental shelf in the area 41°N 71°W, to 39°N 71°W to 39°30'N 74°W, suites of surface samples have been collected in midwinter 1956, 1957, and 1958. Analyses on the 1956 and 1957 samples are reported below (Table I). For comparison, in 1956, 1957, and 1958, surface samples were collected in the Sargasso Sea south of Bermuda, in the Caribbean Sea, and in the Gulf Stream. Analyses on these 1956 samples are reported in Table II. In connection with the U. S. International Geophysical Year program, samples have been collected at 16°S, 8°S, 8°N, and 16°N in each basin of the Atlantic, usually at surface, 1000m, 2500m, 4000 to 4500m, although on the last named parallel, shallower samples were added between 100 and 1000m. The surface samples which have been analysed from this series are reported in Table II and the completed stations in Table III.

In all cases the errors quoted are estimated from counting statistics only.

DISCUSSION

STRONTIUM 90 IN SURFACE WATERS

In our first discussion of the surface water strontium 90 analyses over the shelf area we were led by the large amounts of Sr 90 in some samples relative to the total amount estimated (Libby 1956) to have been delivered to this area, and by the variation between samples (a factor of five between the extremes) to postulate that the mechanics of convective overturn in northern waters operate to inhibit the ability of wind-stirring to produce homogeneous distribution of materials which were added in a highly non-homogeneous pattern. Abundant evidence exists (Clark 1954; Miyake 1954, 1955;) that local high-fallout areas are frequently found on land. We believe it is highly improbable that similar variations are not the rule over the sea surface.

In developing this idea, because we have not yet completed analyses on any closely space vertical series of samples, we have been greatly aided by the tritium data reported by Begemann and Libby (1957). For convenience of reference we have summarized (Table IV) what appear to us to be the most pertinent analyses. The random distribution, vertically, of high and low tritium values in the northern samples contrasts strikingly with the regular reduction with depth at the Saragasso Sea station. Since their samples were collected as have been our "shelf" samples, slowly over distances of 0.5 to 2 km. it is necessary to assume that the concentration variations which both series of samples reveal are representative of masses extending horizontally for distances of 1 to as much as 5 km. And the Begemann and Libby data show these masses to have thicknesses of 30 to 50 meters. Convective sinking of masses of this size and shape is by no means unreasonable. When such a mass is below the surface, only relatively slowly acting physical or biological (Ketchum and Bowen 1958) processes will act to change the isotope concentration. And even when on the surface, it is only at the periphery of each mass that wind-stirring will act effectively to mix adjacent waters of different isotope concentration.

Our confidence in the general validity of the picture has been strengthened by the Sr 90 analyses of 1957 samples in Table I. The variation in concentration is still striking, though reduced somewhat from 1956. It cannot be told whether the change in variation is real or the result of the small number of samples taken, compared to the total number of "convective masses" represented. There is in any case, no evidence of a general increase produced by the increment from the 1956 testing program.

By contrast the warm water samples, summarized in Table II, show amazing homogeneity over very large areas. The consistency of Sr 90 content in the group of samples collected in 1956, along the line south from Bermuda to the Antilles, from the Yucatan Strait, and from the Gulf Stream fits very well the classical picture of surface circulation in the North Atlantic (Sverdrup et al. 1946, P. 684). In fitting this picture so well, it confirms our feeling that long-term retention of isotopic inhomogeneity in surface ocean waters depends upon the peculiarities of convective over-turn.

The samples collected in 1957 show a similar Sr 90 consistency within the set, and indicate as expected, that these are from a different surface water mass. Unfortunately, accepting the classical picture again (Sverdrup et al. 1946, P. 684), the samples from 21° and 8°N should represent the easternmost stream of N. Atlantic surface water, somewhat admixed with deeper water upwelled off the North African coast and in the case of the 8°N 49°W sample, somewhat admixed with S. Atlantic surface water as well. That these samples should show no difference from the 8°S samples was not expected. Fallout delivery to the southern hemisphere is estimated to have been only a small fraction of that to the northern hemisphere (Libby 1957). It is our hope that this situation will be clarified by the analyses on the 16°S samples, and still further by samples at 24°S and at the equator, which we are assured of obtaining later in 1958.

STRONTIUM 90 AT DEPTHS

The data in Table III show that, within the precision of analysis, none of the samples below 800m contained as much as 10 per cent of the surface value of Sr 90. At the 8°S 7°E station, however, approximately 50 per cent of the surface value was found at 300m. At this station the main thermocline was from 300 to 600m, so that the 800m sample, showing less than 0.3 d/min/100L Sr 90, may be viewed as well isolated from the surface. As we have stated above more recent stations have included samples closely spaced in the upper layers, from which we expect to be able to infer actual rates of vertical transport of the various isotopes. It is gratifying that the reduction to 50 per cent Sr 90 concentration in passing from surface to

300m at 8°S should so closely approximate the reduction in passing from 100m to 200m for tritium in the Sargasso Sea (Begemann and Libby, 1957; and Table IV). The thermal structure of the Sargasso station closely resembles that of our 8°S 7°E station. In both cases we believe that horizontal transport is most unlikely to have been responsible for any large fraction of the radioisotope content of the deeper samples.

CERIUM 144 AND PROMETHIUM 147

The analyses for cerium 144 and for promethium 147 reported in Tables I, II, and III present two problems: first that of the cerium 144: promethium 147 ratios, and second that of the cerium 144: strontium 90 ratios. So far as we are aware no other determinations of promethium 147 in fallout have been published, and it is quite likely that this isotope has often been reported as cerium 144 in samples separated by such relatively primitive ion-exchange procedures as have been used in most published sea-water studies (Miyake and Sugiura 1955). This should not be thought of as providing a large source of error in the published cerium 144 data, because of the low beta energy of the promethium 147 spectrum and its consequent low counting efficiency in most systems.

The half-lives of the two rare earth isotopes differ from each other and both differ from that of Sr 90 or Cs 137. In Table V, based on reports of Libby (1958) and of Struxness (1955), we have set out in arbitrary numbers, the pattern of change with time which will occur in the fission product mixture.

As stated above, the cerium and promethium figures in Table I, II, and III have not been corrected for radioactive decay, since no standard T_o was available. If we make the simplifying assumption that geochemical processes in the sea are unlikely to have greatly altered the Ce:Pm ratio, then the data of Table V permits estimation of an "effective decay time", from the ratio Ce 144: Pm 147. The highest ratios found, 4.1 and 3.4 on the two highest Ce 144 concentrations, indicate a decay time of about 1 year, approximately the time elapsed between sample collection (XII-10-56) and combining (III-1-58). Libby (1957 and 1958) has presented graphical summaries of Sr 90 recovery in Pittsburgh, Pennsylvania, U. S. A., compared to the times of known bomb test detonations. This reveals as quite possible that the two high Ce 144: Pm 147 ratios (Table II) represent quite recent fission product mixtures. The calculations of Table V indicate that addition of these amounts of fresh Ce 144 as fission mixture would supply only one tenth as much Sr 90.

Thus in cases where the Ce 144: Pm 147 ratio indicates a significant amount of quite recently produced fallout, we can reasonably subtract from the Sr 90 analyses that corresponding amount of Sr 90, which is indicated as having been added too recently for mixing to have been possible.

Both Miyake (Miyake and Sugiura 1955) and Harley (1956) reported finding in Pacific surface waters unexpectedly high ratios of cerium to strontium radioactivity. It was our initial belief that the cerium 144 data presented for the 1956 samples (Table II) represented a comparable retention of cerium 144 in Atlantic surface water (Ketchum and Bowen 1958). But as more analyses have been completed, this view has had to be abandoned.

Wherever high Ce 144: Sr 90 ratios have been found, the Ce 144: Pm 147 ratio has indicated the mixture to be quite young, and even in the 300m sample from 8°S, the age since fission is indicated as less than three years. On the basis of the data so far accumulated, we are forced to conclude that the rare earth radioactivities delivered to Atlantic waters are removed from the surface layers at rates which are very much higher than apply to the removal of Sr 90. It is generally accepted that the Atlantic receives a higher terrigenous contribution to its sediments than does the Pacific (Kuenen 1950). This makes at least plausible the idea that in a competition between silt-particles sweeping down rare earths, and microplankton retention of them in the surface, the balance in the Pacific is in favor of retention, while that in the Atlantic is in favor of sedimentation.

It is apparent even at this relatively early stage in the study, that the time estimates permitted by the cerium 144: promethium 147 data greatly extend the usefulness of the isotope analysis of marine processes of mineral transport.

ANTIMONY 125

So far we have analysed three surface water samples for antimony 125. The method has given acceptable yields of tracer Sb 124 added to 10 and 50 liter samples, whether the tracer was in three-valent or five-valent form. One of the three samples was that giving our second highest figure for Ce 144 and Pm 147. Unfortunately, however, no unequivocally identifiable Sb 125 was found in any sample, the counting rates varying from statistically zero, to a high of 0.09 cpm. We are now in process of examining some zooplankton and algal samples to determine whether biological withdrawal of Sb may be involved. Our method would not have recovered organic antimony compounds like those which have been described for dissolved arsenic (Gorgy et al. 1948), nor would it have recovered protein-bound antimony of organisms, should this be a major reservoir of this element in the sea.

BIBLIOGRAPHY

Anon., Report of a meeting of United Kingdom and United States scientists on biological effects of radiation in oceanography and fisheries, U. S. Nat. Acad. Sci.-Nat. Res. Council, Oct. 31, 1956, 8pp. (mimeographed), (1956).

Begemann, F. and W. F. Libby, Continental water balance, ground water inventory and storage times, surface ocean mixing rates and world-wide water circulation patterns from cosmic ray and bomb tritium, Geochim. Cosmochim. Acta, 12:277-296, (1957).

Bowen, H. J. M., *The Biogeochemistry of Strontium*, Advancement of Science, 12:585-594, (1956).

Bowen, V. T. and T. T. Sugihara, *Strontium 90 in North Atlantic surface waters* Proc. Natl. Acad. Sci., 43:576-580, (1957).

Clark, H. M., *The Occurrence of an unusually high level Radioactive Rainout in the area of Troy, N. Y.*, Science, 119:619-622, (1954).

Craig, H., Disposal of Radioactive Wastes in the Ocean., U. S. Natl. Acad. Sci.-Natl. Res. Council publication, 551:34-42, (1957).

Gorgy, S., N. W. Rakestraw, and D. L. Fox, *Arsenic in the Sea*, J. Mar. Res., 7:22-32, (1948).

Harley, J. E. (Editor), *Operation Troll.*, U. S. A. E. C., N. Y. Operations Office, 37pp., (1956).

Joseph, A. B., *Waste Disposal at Sea*, Press Release, (1957).

Ketchum, B. H. and V. T. Bowen, Biological factors determining the distribution of radioisotopes in the sea. This conference.

Keunen, P. H., *Marine Geology*, John Wiley and Sons, New York, (1950).

Libby, W. F., *Radioactive Fallout*, Proc. Natl. Acad. Sci., 43:758-775, (1957).

Libby, W. F., Radioactive Fallout, Remarks prepared for delivery before the Swiss Academy of Medical Sciences, March 27, 1958, Typewritten press release 26 pp. and figures, (1958).

Miyake, Y., *The Artificial Radioactivity in Rain Water observed in Japan from May to August 1954*, Pap. Meteorol. Geophys., Tokyo, 5:173-177, (1954).

Miyake, Y., *The Artificial Radioactivity in Rain Water observed in Japan from Autumn 1954 to Spring 1955*, Pap. Meteorol. Geophys., Tokyo, 6:26-32, (1955).

Miyake, Y. and Y. Sugiura, Radiochemical analysis of radionuclides in sea water collected near Bikini Atoll, Records of Oceanographic Works in Japan, 2:1-5, (1955).

Natl. Acad. Sci.-Natl. Res. Council, Effect of Atomic Radiation on Oceanography and Fisheries, U. S. Natl. Acad. Sci.-Natl. Res. Council, Washington, D. C. , publication 551, (1957).

Struxness, E. G., Radioactive wastes in a power program in USAEC New York Operations Office Report Ocean Disposal of Reactor Wastes, May 15, 1955: 35-39, (1955).

Sugihara, T. T., E.J. Troianello, and V. T. Bowen, Radiochemical studies of fission products in Atlantic waters. To be published.

Sverdrup, H. U., M. W. Johnson, and R. H. Fleming, The Oceans, Prentice-Hall, New York, pp X-1087, (1942).

Table I

Radioisotopes in Surface Water - I. Shelf Area

	Position					Radioactivity in Disintegrations/min./100 L.			
Year	Lat.	Long.	Date	Total Depth m.	Isothermal Depth m.	Sr^{90}	Cs^{137}	Ce^{144}	Pm^{147}
1956	41°31'N.	70°40'W.	VI-4-56	5		12.7±3.4			
	40°18'N.	71° W.	II-9-56	110	75	15.0±3.0			
	40° N.	71° W.	II-10-56	275	35	30.0±1.6			
	39°42'N.	71° W.	II-10-56	2000	120	10.3±1.6			
	39°10'N	71° W.	II-11-56	2750	150	6.3±1.6			
1957	40°19'N.	71°29'W.	II-14-57	78	60	12.8±2.0		3.3±0.10	2.2±0.2
	39°18'N.	71°40'W.	II-15-57	1630	200	8.6±2.0		4.1±0.1	2.1±0.2
	39°19'N.	72°02'W.	II-15-57	1550	200	6.7±1.7		1.5±0.22	0.7*±0.3
	39°26'N.	72°10'W.	II-16-57	784	175	10.2±2.0			
	39°39'N.	73°07'W.	II-16-57	39	30	8.6±2.0			
	39°46'N.	73°57'W.	II-16-57	24	15	18.8±3.0		3.2±0.2	0.7*±0.3

Footnote: *Unusually low chemical yield caused these values to be of low precision.

Table II

Radioisotopes in Surface Water - II. Southerly Samples.

Position						Radioactivity in Disintegrations/min/100 L.			
Year	Lat.	Long.	Date	Total Depth m.	Isothermal Depth m.	Sr^{90}	Cs^{137}	Ce^{144}	Pm^{147}
1956	21°34'N.	86°12'W.	V-18-56	550	75	10.0±1.5			
	38°17'N.	69°02'W.	VI-4-56		125	9.1±1.8			
1956	17°49'N.	60°07'W.	XII-9-56	6600	50	10.3±1.7		7.78±0.23	2.3±0.3
	20°15'N.	60°05'W.	XII-10-56	5340	60	10.0±2.5			
	22°00'N.	60°09'W.	XII-11-56	6300	40	8.1±1.5			
	24°50'N.	61°55'W.	XII-12-56	5700	100	12.0±2.0		22.8±0.5	5.6±0.3
	27°47'N.	63°41'W.	XII-13-56	5120	260	12.2±1.5			
1957	21°08'N.	33°20'W.	II-13-57	5100	150	4.7±1.0			
	8°18'S.	7°42.5'W.	III-7-57	4582	20	5.0±1.0		3.0±0.1	1.5±0.2
	8°18'S.	31°17'W.	III-20-57	5300	125	3.4±0.5		2.8±0.2	1.6±0.4
	8°16'N.	17°19'W.	V-8-57	4600	30	4.5±1.0			
	8°17'N.	49°15'W.	V-18-57	4400	80	5.4±1.0			
	15°49'S.	35°50'W.	IV-1-57	4230		4.1±0.5			
	15°40'S.	7°0'E	IV-22-57	5070		3.1±0.4			
	15°26'N.	68°29.5'W.	XI-15-57			5.8±0.6			
	15°23'N.	70°48'W.	XI-18-57			6.0±0.6			
	16°31'N.	73°16'W.	XI-19-57			6.8±0.6			
	17°38'N.	76°02'W.	XI-20-57			10.5±0.6			
	13°46'N.	73°54'W.	II-27-58			7.3±0.6			
	15°39'N.	73°54'W.	II-28-58			6.4±0.6			
	17°46'N.	84°29'W.	III-13-58			7.0±0.6			
	18°30'N.	79°13'W.	III-16-58			6.2±0.6			

Table III

Radioisotopes in Atlantic Water Columns

Position						Radioactivity in Disintegrations*/min./100 L.			
Lat.	Long.	Date	Total Depth m.	Isothermal Depth m.	Sample Depth m.	Sr^{90}	Cs^{137}	Ce^{144}	Pm^{147}
8°26'S	7°45'E.	III-1-57	4620	20	0	4.9±1.0*			
					295	2.4±1.0		1.5±0.1	1.3±0.4
					795	< 0.3		0.8±0.3	1.8±0.3
					2425	< 0.3			
					3915	< 0.3			
8°18'S.	7°42.5'W.	III-7-57	4460		10	5.0±1.0		3.0±0.1	1.5±0.2
8°18'S.	31°17'W.	III-20-57	5300	125	10	3.4±0.5		2.8±0.2	1.6±0.4
					985	< 0.6		1.3±0.2	0.7±0.3
					2420	< 0.6			
					4440	< 0.6			
8°16'N.	17°19'W.	V-8-57	4600	30	20	4.5±1.0			
					995	< 0.3			
					2480	0.6±0.6			
					4535	< 0.5			
8°17'N.	49°15'W.	V-18-57	4400	80	50	5.4±1.2			
					990	< 0.3			
					2480	< 0.5			
					4390	< 0.4			
36°23'N.	70°33'W.	VII-13-57	4200	30	40	10.2±0.6		18.0±0.5	6.8±0.7
					500	4.1±0.6			

Footnote: *No sample - value calculated from other southerly surface samples.

Table IV

Tritium in North Atlantic Water (from Begemann and Libby 1957)

$T/H \cdot 10^{18}$ April to July 1955

Highest T/H	Depth	Lowest T/H	Depth
3.25	62m.	0.40	56m.
3.10	0	0.60	170
3.0	180	0.80	0
2.4	85	1.10	120

Profile 7-15-55
55°N. 53°W.

$T/H \cdot 10^{18}$	Depth
2.2	0m.
0.40	56
2.2	111
0.60	170

Profile 9-24-54
36°N. 65°W. Sargasso Sea

$T/H \cdot 10^{18}$	Depth
2.8	100m.
1.33	200
0.48	600

Table V

Changes in Disintegration Rates with Time after Fission

in arbitrary units relative to initial Sr 90 as 100

Time after fission	Sr 90 $T_{1/2}$ 28 y.	Cs 137 $T_{1/2}$ 28 y.[1]	Ce 144 $T_{1/2}$ 285 d.[2]	Pm 147 $T_{1/2}$ 2.8 y.[2]
T_1= 30 d.	100.	150.	2280.	488.
T_1+ 1 y.	97.5	146.	1021.	381.
T_1+ 2 y.	95.3	143.	459.	297.
T_1+ 3 y.	93.0	139.	205.5	232.
T_1+ 4 y.	90.6	136.	92.0	181.
T_1+ 5 y.	88.4	132.	41.2	141.
T_1+ 6 y.	86.2	129.	18.4	110.
T_1+ 7 y.	84.0	126.	8.2	85.8

Footnote: 1. from Libby (1958) estimate for bomb production.

2. from Struxness (1955), estimate for slow-neutron fission.

ACKNOWLEDGEMENTS

It is a real pleasure to express our best thanks to the many co-workers on whose efforts this study depends: in connection with the deep sample collections, Mr. John Schilling, and Captain David Casiles and his crew of the R. V. Crawford, and Messrs. Fritz Fuglister, L. V. Worthington, D. F. Bumpus and W. G. Metcalf; in the chemical processing and final counting of samples Miss Sybil Campbell, Mrs. Eileen McCormack, and Mr. H. Caron.

Contribution No. 972

Reprinted from LIMNOLOGY AND OCEANOGRAPHY
Vol. 3, No. 4, October, 1958
Printed in U.S.A.

Phytoplankton Nitrogen in the Oceans[1]

CHARLES S. YENTSCH AND RALPH F. VACCARO
Woods Hole Oceanographic Institution, Woods Hole, Mass.

ABSTRACT

The ratio of cellular nitrogen and chlorophyll has been studied in cultures of marine phytoplankton during and after recovery from nitrogen deficiency. The time factors were observed to vary together; however, the ratio was only constant when the cells were sufficient in nitrogen. Since nitrogen deficiency produced chlorotic cells in all species studied, the degree of deficiency could be ascertained by measuring the ratio of carotenoid to chlorophyll *a*. Thus an expression utilizing the ratio of plant pigments has been formulated to compute cellular nitrogen from chlorophyll *a*. This pigment:nitrogen relationship has been applied to estimate the quantity of nitrogen in natural populations of phytoplankton.

The amounts of nitrogen in phytoplankton estimated from plant pigment measurements has been observed to vary between 18–70% of the total particulate matter.

INTRODUCTION

In the surface waters of the oceans particulate nitrogen occurs in planktonic plants, animals, bacteria, and detritus. The contribution of any one of these categories to the total particulate nitrogen is difficult to evaluate because of non-uniformity as to shape, numbers, and particle-size distribution. One promising approach, however, toward indirect estimates of the amount of organic nitrogen in phytoplankton is the use of a nitrogen:chlorophyll equivalent. That nitrogen and chlorophyll are closely related in plant material has been observed by numerous workers. Noack (1925, 1926), Pirson (1937), Fleischer (1935), and Harvey (1953) reduced the chlorophyll content of plants by rendering them deficient in nitrogen. Michael (1935) found leaves high in chlorophyll also high in protein; Boersch (1932) and Kingsbury (1956) have observed changes in the proportions of chlorophyll and carotenoid in nitrogen-deficient cultures in blue-green algae.

Since the ratio of cellular nitrogen:chlorophyll in the phytoplankton cannot be evaluated in nature, we have used laboratory cultures of marine phytoplankton for this purpose. The changes in chlorophyll *a* and cellular nitrogen were determined in a culture of *Phaeodactylum tricornutum* (Hendy) during and after recovery from nitrogen deficiency. Under these conditions the nitrogen:chlorophyll ratio is not a constant, but varies in a way closely correlated with the degree of chlorosis of the cell which can be represented by a carotenoid:chlorophyll ratio.

The application of the N:Chl^a ratios, derived from nitrogen-deficient culture experiments, to natural plant communities makes the assumption that similar ratios would obtain for a variety of species under similar physiological conditions. Pigments and cellular nitrogen, measured simultaneously in other species of diatoms and flagellates, tend to confirm this assumption.

METHODS

Nitrate-nitrogen was determined colorimetrically in a Beckman DU spectrophotometer according to the hydrazine sulfate method proposed by Mullen and Riley (1955). Cell material was removed from suspension by flocculation and centrifuging by the von Brand (1935) method. The washed cells were then subjected to a Kjeldahl digestion and the associated nitrogen measured colorimetrically as ammonia according to Riley (1953).

Chlorophyll *a* and carotenoid were measured spectrophotometrically in acetone extractions by the Richards with Thompson (1952) method, as modified for use with the millipore filter by Creitz and Richards (1955). The computations for chlorophyll *a* and carotenoid pigments were made from nomographs prepared by Duxbury and Yentsch (1956). Cell numbers were estimated in a Levy Hemocytometer under a 10 x objective.

---

[1] Contribution No. 972 from the Woods Hole Oceanographic Institution. This work was supported by the National Science Foundation and the Atomic Energy Commission. The authors wish to express their sincere thanks to Dr. Bostwick H. Ketchum for many helpful suggestions.

NITROGEN DEFICIENCY AND CHLOROSIS

A unialgal culture in the logarithmic stage of growth was harvested by centrifuging. The cells were thoroughly washed in nitrate-free millipore-filtered seawater to assure complete removal of any associated available nitrogen. The washed cells were then resuspended in a nitrogen-free medium of the following composition:

Na_2HPO_4	.0002	g
Na_2SiO_3	.005	g
$Na_2S_2O_3$	.0012	g
Ferric citrate	.0003	g
Citric acid	.0003	g
Vitamin B_{12}	.072	μg
Nitrate-free, millipore-filtered seawater	100	ml
pH after autoclaving	7.8–8.0	

The nitrogen-deficient culture was exposed to 1800 foot-candles of fluorescent illumination in a two-liter cotton-stoppered glass flask at 18 ± 2°C. After four days the cells had become visibly chlorotic. They were then placed in the dark for 15 hours, after which estimations were made of the cell count, cellular nitrogen, and chlorophyll. Enough KNO_3 solution was then added to give an initial concentration of 2.68 mg NO_3-N per liter, and the culture was placed in the light. Aliquot samples were removed at intervals for the estimation of nitrate, cellular nitrogen, and chlorophyll, carotenoid, and cell numbers.

The nitrogen-starved culture removed the added nitrate rapidly during the first six hours of illumination, and continued to assimilate nitrate at a slower rate during the remainder of the experiment (Table 1). The nitrate removed was never completely recovered as cellular nitrogen, suggesting either the formation of nitrogen compounds not recovered by the Kjeldahl digestions, or an excretion of extracellular nitrogen compounds into the medium. After 47 hours 93% of the added nitrate was removed, and 79% of this amount was recovered as cellular nitrogen. The nitrogen per cell increased rapidly at first (Fig. 1A), then became constant and declined thereafter. The values for nitrogen per cell after 26 hours agree with those found by Ketchum and Redfield (1949) for normal *Nitzschia closterium*[2] cells.

TABLE 1. *Changes in cell number, nitrogen, and pigments in an enriched culture of* Phaeodactylum tricornutum

Time hrs	Cells × 10^7/L	Residual NO_3-N mg/L	Cellular nitrogen mg/L	Chlorophyll *a* mg/L	Carotenoid SPU/L	$\frac{\text{Cellular nitrogen}}{\text{Chlorophyll } a}$	$\frac{\text{Carotenoid}}{\text{Chlorophyll } a}$
0	70	2.68	.21	.080	.050	2.64	.62
5	72	2.04	—	.090	.042	—	.47
6.5	73	1.69	.83	.091	.020	9.10	.22
23.5	100	1.02	1.34	.174	.060	7.72	.34
26.5	118	0.77	1.43	.201	.080	7.12	.47
29.5	135	0.48	1.48	.210	.100	7.05	.47
47.5	340	0.18	1.98	.302	.138	6.57	.46

Chlorophyll *a* per cell reached a maximum between 20 and 24 hours after enrichment and then declined (Fig. 2B). Carotenoid initially was high in the cells, then declined rapidly as chlorophyll *a* increased; however, carotenoid synthesis resumed after eight hours, reached a maximum at 28 hours, then declined. Hence the carotenoid:chlorophyll ratio was high at the start of the experiment, reached a low eight hours after enrichment, then increased (Fig. 2C).

The largest increase in chlorophyll *a*, carotenoid, and cell numbers occurred between six and 23 hours, which corresponded to the maximum increase in cellular nitrogen. The increase in the nitrogen per cell also corresponded with decreases in the carotenoid:chlorophyll *a* ratio. Highest values for chlorophyll *a* occurred when the nitrogen per cell was highest, while the pigment ratio (carot.:chl^a) reached a minimum somewhat earlier than the other maxima. The ratio between cellular nitrogen and

---

[2] Probably *Phaeodactylum tricornutum*.

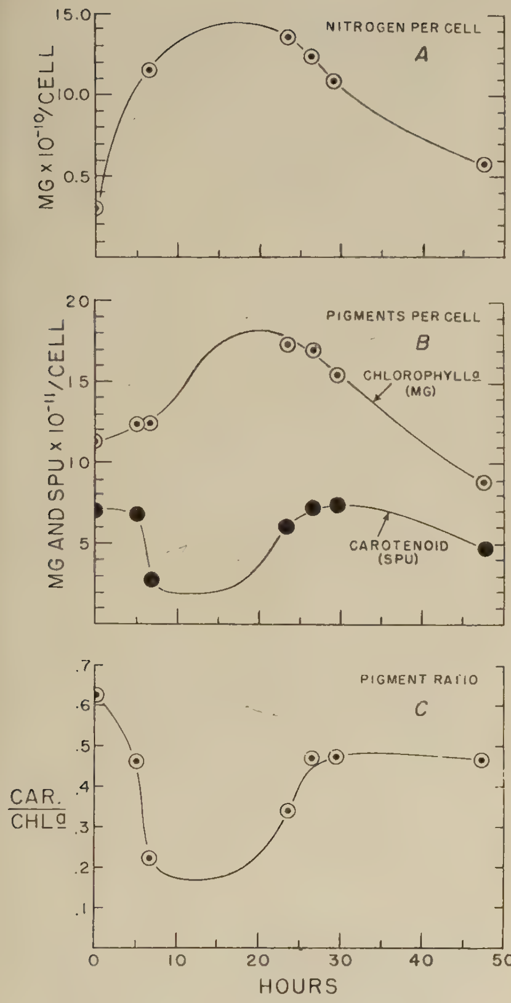

FIG. 1. Changes in chlorophyll *a*, carotenoid, and cell nitrogen in a culture of *Phaeodactylum tricornutum*.

chlorophyll *a* (Table 1) increased from 2.6 to 9.1 at 6.5 hours, and then decreased to values ranging from 7.72 to 6.57 for the remainder of the experiment.

Analyses of cellular nitrogen, chlorophyll *a*, and carotenoid have also been made on cultures of other species, and these are compared in Table 2 with some analyses made on natural populations. All N:Chl^a ratios for algal cultures fall in the range of 1.7–9.1. Young and senescent cultures of the green flagellate *Dunaliella* had ratios of 7.0 and 1.7, respectively. Nitrogen-to-chlorophyll values for the three diatom cultures, *Ditylum*, *Cyclotella*, and *Melosira* average 6.7. Harris and Riley (1956) determined particulate nitrogen and chlorophyll content of net hauls of *Coscinodiscus* and *Goniaulax* which give unusually high values for the N:Chl^a ratio. This is probably due to the unavoidable inclusion of detrital and zooplankton contaminates. Their average N:Chl^a ratio for all net hauls in Long Island Sound was 9.4 on a dry weight basis. Nitrogen-to-chlorophyll ratios given by different workers for "marine phytoplankton" vary considerably. Computed from protein, Krey's (1953) average value is 6.3, while Fleming's (1940) ratio is 3.0.

TABLE 2. *Pigment nitrogen relationship in natural populations and cultures of marine phytoplankton*

Organisms	N:Chl^a	Carot.: Chl^a
Phaeodactylum tricoruntum		
Nitrogen deficient	2.64	.66
Nitrogen enriched	9.10	.22
Dunaliella euchlora		
Nitrogen deficient	1.70	.59
Nitrogen enriched	7.00	.40
Ditylum Brightwellii		
Stock culture	8.3	.29
Melosira sp.		
Stock culture	4.6	.67
Cyclotella sp.		
Stock culture	6.0	.59
Cosinodiscus sp.[1]		
Net haul	13.2	—
Goniaulax sp.[1]		
Net haul	14.7	—
Av. for natural population in Long Island Sound. Based on dry weight in net hauls.[1]	9.4	—
Natural populations of marine phytoplankton.[2]	6.3	—
Natural populations of marine phytoplankton.[3]	3.0	—

[1] Harris and Riley (1956)
[2] Krey (1953)
[3] Fleming (1940)

In culture experiments the cells become visibly chlorotic as the deficiency of nitrogen develops. This is reflected by an increase in the ratio of carotenoid:chlorophyll *a*, and by a closely correlated decrease in the N:Chl^a ratio. These ratios are compared in Figure 2, which includes not only the experimental results with *Phaeodacylum tricornutum* but also data from cultures of other species. Except for two aberrant values these results are related by the equation[3]:

$$N/Chl^a = 11.4 - Carot./Chl^a \qquad (1)$$

The two aberrant points in Figure 2 were for grossly nitrogen-deficient cultures. It seems probable that the extreme nitrogen deficiency induced in these cultures is never duplicated in nature. Numerous Carot.: Chl^a ratios observed by the senior author for natural populations of marine phytoplankton in Atlantic coastal waters have ranged from 0.15–0.55. The most deficient cultures had pigment ratios of 0.59–0.67, suggesting that nitrogen-starved cultures become more chlorotic than natural populations in the sea.

NITROGEN CONTENT OF NATURAL POPULATIONS

We have made measurements of particulate nitrogen, chlorophyll, and carotenoid in Vineyard Sound and the Atlantic coastal slope waters. The observed total particulate N:Chl^a ratios in Vineyard Sound are approximately five times larger than any of the values obtained in our culture experiments (Table 3), suggesting a large amount of non-phytoplankton nitrogen. The ratios in the coastal and slope waters are closer to our culture values.

The ratio of N:Chl^a in the phytoplankton was calculated from the observed pigment ratio by Equation (1). The former ratio was then multiplied by the chlorophyll content in order to estimate the portion of the total particulate nitrogen which was contained in the phytoplankton. In the Vineyard Sound populations the carotenoid: chlorophyll ratios ranged between 0.23 and 0.18, giving calculated N:Chl^a ratios of 8.6 to 9.1 for the phytoplankton fraction of the particulate nitrogen. The carotenoid: chlorophyll values for the coastal and slope waters were 0.37–0.27, giving calculated N:Chl^a ratios of 7.3 to 8.3. The calculated phytoplankton nitrogen comprised 13 to 25% of the total in Vineyard Sound, 43 to 58% at the inshore stations on the conti-

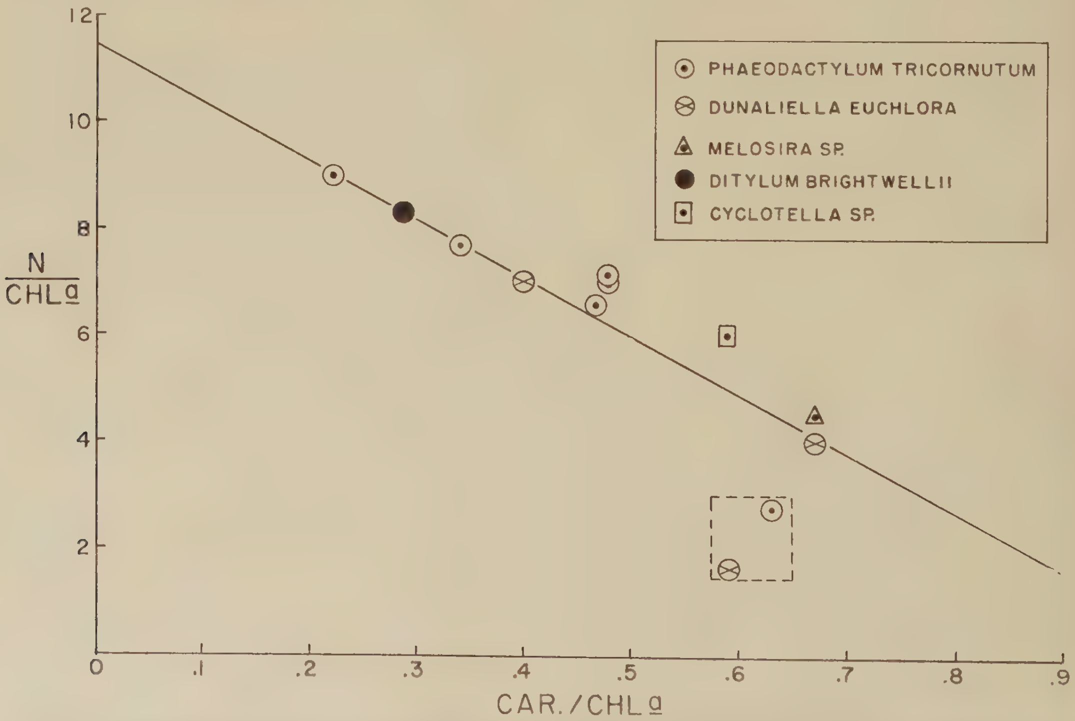

Fig. 2. Relationship between Nitrogen:Chl^a and Carotenoid: Chl^a in 5 cultures of marine phytoplankton.

---

[3] Nitrogen and chlorophyll *a* in milligrams, carotenoid in SPU units.

TABLE 3. *Percentage of organic nitrogen in phytoplankton in surface waters*

Location	Date	Particulate nitrogen µg/L	Chl^a mg/m^3	$\frac{\text{Carot.}}{\text{Chl}^a}$	Observed N:Chl^a	Calculated* N:Chl^a	Phytoplankton nitrogen µg/L	Phytoplankton nitrogen % total
Vineyard Sd.	7/2/57	140.0	2.73	0.18	51.3	9.1	25.0	18.0
Vineyard Sd.	7/10/57	74.0	1.54	0.23	48.2	8.6	13.4	18.1
Vineyard Sd.	7/23/57	94.0	2.00	0.20	47.0	9.0	18.0	19.2
Vineyard Sd.	7/31/57	57.0	1.50	0.22	38.0	8.7	13.1	23.1
Continental Shelf								
Sta. U, 25 fath.	11/14/57	53.1	3.75	0.27	14.2	8.3	31.1	58.5
Sta. N, 100 fath.	11/14/57	36.0	1.86	0.27	19.3	8.3	15.5	43.0
Sta. G., 1000 fath.	11/14/57	4.1	0.39	0.37	10.4	7.3	2.8	70.0

* From relation given by Equation (1).

nental shelf, and 70% for offshore stations. This general increase with increasing distances from land reflects a diminution of non-phytoplankton bacterial and detrital nitrogen.

DISCUSSION

Our experiments show that nitrogen deficiency produces a simultaneous decrease in both cellular nitrogen and chlorophyll. Thus the hydrolysis of cytoplasmic and chloroplastic proteins appear to take place concurrently, or nearly so, and the loss in chlorophyll may be attributed to the decomposition of the pigment protein complex. Therefore, the synthesis or decomposition of chlorophyll is closely associated with nitrogen metabolism, and any environmental factor which modifies nitrogen metabolism may be expected to have an associated influence on the chlorophyll content.

The onset of nitrogen deficiency is accompanied by a gradual loss of carotenoid as well as chlorophyll. Since the loss of the chlorophyll is much faster the ratio of the pigments changes. Our field observations show that in general inshore natural populations have lower pigment ratios than do offshore populations. Furthermore, in the surface waters, diurnal changes in the pigment ratios have been observed which could be interpreted to mean, from the results reported in the paper, that cellular nitrogen also varies with changing light intensity. Harvey (1953) has observed that the nitrogen per cell in cultures decreased as the light intensity was increased. He suggested that phytoplankton might be nitrogen deficient during the day and make up the deficiency at night.

The percentages of the total particulate nitrogen attributed to the phytoplankton in this paper are considerably higher than values given by Fox *et al.* (1952). This discrepancy is undoubtedly due to differences in techniques used to concentrate particulate matter. It is our opinion that Fox *et al.* (1953) have not definitely shown that their method of filtration is not adsorbing dissolved materials. We have also measured total amine-amide nitrogen which includes the dissolved organic matter. If our values for phytoplankton nitrogen were compared with the total amine-amide nitrogen rather than with particulate nitrogen the percentage of nitrogen in the plants would be lower and in agreement with the data of Fox *et al.* (1952). If particulate nitrogen is defined as the material retained by von Brand's (1935) flocculation method then the phytoplankton fraction is always sizable.

REFERENCES

BORESCH, K. 1932. Algenfarbstoffe. In: Handbuch der Pflanzenanalyse, G. Klein, ed. III/2, Spezielle Analyse II: 1382–1410.

VON BRAND, T. 1935. Methods for the determination of nitrogen and carbon in small amounts of plankton. Biol. Bull., **69**(2): 221–232.

CREITZ, G. I., AND F. A. RICHARDS. 1955. The estimation and characterization of plankton populations by pigment analysis. III. A note on the use of "millipore" membrane filters in the estimation of plankton pigments. J. Mar. Res., **14**(3): 211–216.

DUXBURY, A. C., AND C. S. YENTSCH. 1956. Plankton pigment nomographs. J. Mar. Res., **15**: 92–101.

FLEISCHER, W. E. 1935. The relation between chlorophyll content and the rate of photosynthesis. J. Gen. Physiol., **18**: 573–597.

FLEMING, R. H. 1940. Composition of plankton. Proc. 6th Pac. Sci. Cong., **3**: 535.

FOX, D. L., J. D. ISAACS, AND E. F. CORCORAN. 1952. Marine leptopel, its recovery, measurement and distribution. J. Mar. Res., **11**(1): 29–46.

FOX, D. L., C. H. OPPENHEIMER, AND J. S. KITTREDGE. 1953. Microfiltration in oceanographic research. II. Retention of colloidal micelles by adsorption filters and by filter-feeding invertebrates; proportions of dispersed organic to dispersed inorganic matter and to organic solutes. J. Mar. Res., **12**(1): 233–243.

HARRIS, E., AND G. A. RILEY. 1956. Oceanography of Long Island Sound 1952–1954. VIII. Chemical composition of the plankton. Bull. Bingham Oceanogr. Coll., **15**: 315–323.

HARVEY, H. W. 1953. Synthesis of organic nitrogen and chlorophyll by *Nitzschia closterium.* J. Mar. Biol. Ass. U. K., **31**: 477–478.

KETCHUM, B. H., AND A. C. REDFIELD. 1949. Some physical and chemical characteristics of algae grown in mass culture. J. Cell. Comp. Physiol., **33**: 281–300.

KINGSBURY, J. M. 1956. On pigment changes and growth in the blue-green alga, *Plectonema nostocorum* Bornet ex Gomont. Biol. Bull., **110**(3): 310–319.

KREY, J. 1953. Plankton- und Sestonuntersuchungen in der südwestlichen Nordsee auf der Fahrt der "Gauss" Februar–Marz 1951. Ber. & tsch. Komm. Meeres Forsch., **8**(2): 136–153.

MICHAEL, G. 1935. Über die Beziehungen zwischen Chlorophyll Eiweissabbau im vergilbenden Laubblat von *Tropaeolum.* Zeit. Bot., **29**(8): 385.

MULLEN, J. B., AND J. P. RILEY. 1955. The spectrophotometric determination of nitrate in natural waters, with particular reference to sea water. Analyt. Chim. Acta., **12**(5): 464–480.

NOACK, K. 1925. Photochemische Wirkungen des Chlorophylls und ihre Bedeutung für die Kohlensäureassimilation. Zeit. Bot., **17**: 481–548.

———. 1926. Photochemische Wirkungen des Chlorophylls. Naturwissensch., **14**(18): 383–389.

PIRSON, A. 1937. Ernährungs- und stoffwechselphysiologische Untersuchungen an *Fontinalis* und *Chlorella.* Zeit. Bot., **31**: 193–267.

RICHARDS, F. A., WITH T. G. THOMPSON. 1952. The estimation and characterization of plankton populations by pigment analyses. II. A spectrophotometric method for the estimation of plankton pigments. J. Mar. Res., **11**: 156–172.

RILEY, J. P. 1953. The spectrophotometric determination of ammonia in natural waters with particular reference to sea water. Analyt. Chim. Acta., **9**(6): 575–589.

Contribution No. 976

Reprinted from AMERICAN SCIENTIST, Vol. 46, No. 3, September 1958

THE BIOLOGICAL CONTROL OF CHEMICAL FACTORS IN THE ENVIRONMENT[1]

By ALFRED C. REDFIELD

IT IS a recognized principle of ecology that the interactions of organisms and environment are reciprocal. The environment not only determines the conditions under which life exists, but the organisms influence the conditions prevailing in their environment. The examples on which this principle rests are usually difficult to describe in quantitative terms and are frequently local in their application. In the ocean the principal interactions between organisms and environment are chemical. Because of its unity, its fluid nature, and the intensity of the mixing to which the water is subject their relations can be examined statistically and expressed in quantitative terms.

The purpose of this essay is to discuss the relations between the statistical proportions in which certain elements enter into the biochemical cycle in the sea, and their relative availability in the water. These relations suggest not only that the nitrate present in sea water and the oxygen of the atmosphere have been produced in large part by organic activity, but also that their quantities are determined by the requirements of the biochemical cycle. The argument is not simple and in order that it may be understood the nature of the biochemical cycle and the circulation of the elements involved are reviewed.

The Biochemical Cycle

The production of organic matter in the sea is due to the photosynthetic activity of microscopic floating plants, the phytoplankton, and is limited to the surface layers where sufficient light is available. The formation of organic matter in the autotrophic zone requires all the elements in protoplasm, of which carbon, nitrogen, and phosphorus are

---

[1] A Sigma Xi National Lecture for 1957–58. Contribution No. 976 Woods Hole Oceanographic Institution.

Copyrighted 1958, by The Society of the Sigma Xi
and reprinted by permission of the copyright owner

of particular concern. These are drawn from the carbonate, nitrate, and phosphate of the water. Following the death of the plants the organic matter is destroyed, either by the metabolism of animals or the action of microorganisms. Normally, decomposition is completed by oxidation so that carbon, nitrogen, and phosphorus are returned to the sea water as carbonate, nitrate, and phosphate, while requisite quantities of free oxygen are withdrawn from the water.

The autotrophic zone has a depth of 200 meters at most and includes less than five per cent of the volume of the ocean. Below this zone, life depends on organic matter carried down by organisms sinking from above or by the vertical migrations of animals back and forth between the depths. Although the greater part of the nutrient chemicals absorbed in the autotrophic zone complete the cycle in this layer, the portion which sinks as organic matter tends to deplete the surface layers of these chemicals and, with the decomposition of the organic matter in the depths, to enrich this heterotrophic zone with the products of decomposition.

The existence of the vast reservoir of deep water in which organic matter may accumulate and decay out of reach of autotrophic resynthesis is a distinctive feature of the oceanic environment which enables one to separate, in observation and thinking, the constructive and destructive phases of the biochemical cycle.

The synthesis of organic matter is a highly selective process which results in products having specific composition. Differences in the composition of various species or individuals exist, of course, but the similarities on the whole are greater than the differences. When the population of a large region of the sea is considered it seems reasonable that its composition will be uniform in a statistical sense, and will be reflected in the changes in the chemistry of the water from which its materials are drawn or to which they are returned. In the decomposition of a given amount of organic matter the quantity of oxygen consumed must be determined exactly by the quantities of carbon, nitrogen, etc., to be oxidized, and the relative changes in the quantity of oxygen, phosphate, nitrate, and carbonate in the water must depend exactly on the elementary composition of the plankton [1].

The validity of this concept is shown by a comparison of the proportions in which the elements exist in the plankton and the proportions in which they vary in samples of water from the open sea. The analysis of many samples of plankton, taken in a variety of places with nets designed to take organisms of different size indicates that atoms of phosphorus, nitrogen, and carbon are present on the average in the ratios: 1:16:106 [2]. The oxidation of this material is estimated to require 276 atoms of oxygen. In comparison, data on the phosphate, nitrate, and carbonate content of sea water collected from various depths in the several oceans show that the available phosphorus, nitrogen, and carbon vary from sample to sample in the atomic ratios: 1:15:105 and that about 235 atoms of oxygen disappear for each addition of one phosphorus atom, assuming the water to have been in equilibrium with the oxygen of the atmosphere when it was last at the sea surface [3–5]. It is as though various quantities of material containing phosphorus, nitrogen, and carbon in these ratios had decomposed in the water samples. The correspondence of these ratios with those obtained from the analysis of plankton, as shown in Table 1, leaves little doubt that these elements vary in sea water almost entirely as the result of the synthesis or decomposition of organic matter [1].

This conclusion permits one to approach the biochemical cycle in the sea in much the same way as the physiologist examines the general metabolism of an individual organism. It defines the quantitative relations of the cycles of the separate elements which are involved in the biochemical cycle as a whole. It provides a quantitative criterion, similar to the principle of combining proportions in chemistry, for examining many problems in marine ecology. Consider, for example, the question of the relative availability in the sea of the various substances required for the growth of organisms. In accordance with Liebig's law of the minimum, that constituent of the sea water present in smallest quantity relative to the requirement for growth of organisms will become the limiting factor. The ratios shown in Table 1 define precisely what these relative requirements are. When the composition of sea water is examined it is found that phosphorus and nitrogen are usually available in about the proportions, 1:15, required for the formation of the plankton. Carbon, as carbonate, in contrast, is present in great excess, the phosphorus-carbon ratio being about 1:1000 whereas the required ratio is 1:105. Consequently, carbonate never becomes a limiting factor. In a similar way sulfur, an important plant nutrient, is available in great quantities relative to phosphorus and nitrogen, and the same is true of calcium, magnesium, and potassium.

TABLE 1

ATOMIC RATIOS OF ELEMENTS IN THE BIOCHEMICAL CYCLE

	P	*N*	*C*	*O*
Analyses of plankton	1	16	106	−276
Changes in sea water	1	15	105	−235
Available in sea water	1	15	1000	200–300

Phosphorus and nitrogen thus appear to be the constituents of sea water present in limiting quantities. It was pointed out by Harvey in 1926 that it is a remarkable fact that in the English Channel plant growth should strip sea water of both nitrates and phosphates at about the same time [6]. To this coincidence I will return. Data for the oceans indicate that this is a world-wide occurrence in the surface waters of tropical and temperate seas. This would not be the case were other substances, such as the various trace elements, generally limiting factors for growth in the sea.

It should be recognized that in coastal waters and in the surface of the open ocean the ratios of the elements under discussion frequently depart widely from those which are here attributed to the oceans as a whole. This is due, in part at least, to the fact that where the elements are substantially depleted by the growth of plants small unused residues of one or another element may greatly alter the ratios, and also because in the process of decomposition phosphorus tends to be regenerated more rapidly than nitrogen. It is believed, however, that in the great bulk of the open sea the ratios presented represent the statistical composition of the water and of the organisms living in it sufficiently well to serve for the argument to be developed. This argument depends upon the consideration that the physiology of marine plants places definite restrictions on the proportions in which certain elements participate in the biochemical cycle, rather than on the exactness with which these proportions can be stated at present.

The Biochemical Circulation

The withdrawal of nutrients from the autotrophic zone would soon exhaust its fertility and bring the cycle to a close if means did not exist to restore them to the surface. This is done by purely physical processes, the vertical mixing of water by turbulence and by direct upwelling of deeper water to the surface—frequently after transport for great distances by currents in the depths of the sea [7].

The production of organic matter in the autotrophic zone at the surface of the sea depends upon how fast the biochemical cycle runs its course. Many factors, such as the temperature and light intensity, may intervene, but it is clear that the cycle is limited by the return of nutrient materials to the surface by the motion of the water. This, in turn, depends in part upon the quantities of nutrients available in the subsurface waters. We may consequently inquire with interest into the concentrations of nutrients in the deeper layers of the sea as they are distributed throughout the world.

The sea water of the oceans may be considered to be thoroughly mixed. The major ions of sea water occur so nearly in the same proportions that by this criterion one cannot distinguish water from one part of the ocean from another. The principal variables used by oceanographers to distinguish different waters are the temperature and salinity. Changes in these properties are produced at the sea surface, and while the effects may be relatively large they influence only a small part of the total mass of water. Ninety per cent of the water in the oceans differs by less than 3 per cent from the average in its salinity or its heat content.

In contrast, the principal elements involved in the biochemical cycle differ greatly in their abundance in different parts of the sea. It was first shown by the cruises of the Danish research vessel "Dana" and the "Carnegie" that phosphate and nitrate were much more abundant in the Pacific and Indian Oceans than in the Atlantic [8, 9]. A chart showing the quantities of phosphorus present in the world oceans at a depth of 2000 meters, which represents adequately the concentrations present in the great reservoir of deep water, is shown in Figure 1. The variation in phosphorus content is widespread and systematic, the values increasing from less than 1.25 mg atoms per cubic meter in the North Atlantic to more than 3.0 of these units in the North Pacific and Indian Oceans. In the Mediterranean Sea comparable values are less than 0.5 unit, so that there is a variation of more than sixfold in the potential fertility of the deep reservoirs of the major seas.

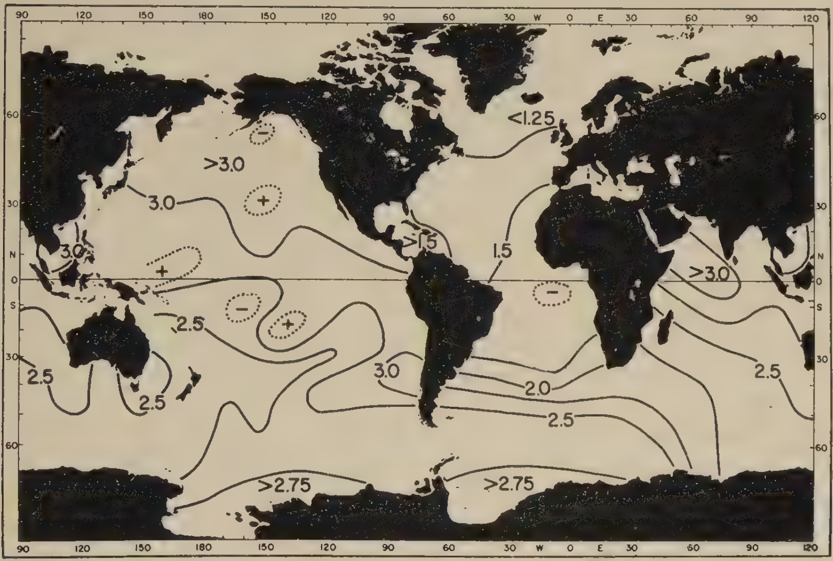

FIG. 1. Distribution of phosphorus at depth of 2000 meters in Oceans of World. Contour interval 0.25 mg atoms/m³. This diagram is based on some 1600 measurements between depths of 1900 and 2100 meters. Data are available from about 75 per cent of the 10° squares. About half the observations fall within the designated contour interval, the remainder within the adjacent intervals.

It is evident that there is some world-wide mechanism at work producing this distribution. Since the elements involved are those which enter the biochemical cycle this mechanism must be biological.

Since the distribution differs from that of the biologically inactive components of the water there must be a biochemical circulation which is different from, though dependent upon, the physical circulation of the water [10]. How can this difference in behavior be explained?

The presumptive agency of fractionation which separates the biochemical from the inactive elements in sea water is the selective absorption of the former in the synthesis of protoplasm near the surface, followed by the sinking of the organized matter to greater depths prior to its decomposition. In addition the differential motions of the water at different depths must be taken into account if substantial differences in concentration and their redistribution are to be explained.

The foregoing discussion is intended to bring out two points of importance, namely, that the principal elementary constituents of protoplasm enter the biochemical cycle statistically in definite proportions, and that the cycle of movement of these elements between the surface layers and the deep waters runs with sufficient intensity to influence markedly their distribution on an ocean-wide scale. We may now turn to two remarkable coincidences which have led to the inquiry which is our major concern.

Correspondence Between Requirement and Availability of Phosphorus, Nitrogen, and Oxygen

The stoichiometric relations summarized in Table 1 indicate that phosphorus, nitrogen, and oxygen are available in ocean water in very nearly the same proportions as those in which they enter the biochemical cycle. In discussing the remarkable coincidence in the supply and demand for nitrogen and phosphorus it has been pointed out that it might arise from: (1) a coincidence dependent on the accidents of geochemical history; (2) adaptation on the part of the organisms; or (3) organic processes which tend in some way to control the proportions of these elements in the water [1].

Of the first alternative not much can be said except that the probability that the ratio in the sea be what it is rather than any other is obviously small. That the coincidence applies to the oxygen as well as to the nutrient elements compounds the improbability.

For the second alternative, it may be said that the phytoplankton do have some ability to vary their elementary composition when one element or another is deficient in the medium in which they grow. Such physiology might account for the coincidence in the nitrogen-phosphorus ratios. However, it is not evident how adaptation could determine the oxygen relation since this depends more on the quantity than the quality of the organic matter formed, and the oxygen requirement is felt only after the death of the living plant.

For these reasons the third alternative deserves serious consideration. Mechanisms should be examined by which organic processes may have tended to control the proportions of phosphorus, nitrogen, and oxygen available for life in the sea.

The Phosphorus-Nitrogen Ratio

When the coincidence between the elementary composition of marine plankton and the proportions of available nitrogen and phosphorus in sea water was first noted, it was suggested that it might have been brought about by the activity of those microorganisms which form nitrogenous compounds from atmospheric nitrogen, or liberate nitrogen gas in the course of their metabolism. The composition of such organisms must be more or less fixed in regard to their relative phosphorus and nitrogen content. When living in an environment containing a deficiency of nitrate relative to phosphate, the growth and assimilation of the nitrogen-fixing organisms might tend continually to bring the proportions of nitrogen and phosphorus nearer to that characteristic of their own substance. Thus, in the case of Azotobacter, it has been found that for every atom of phosphorus available in the medium about 10 atoms of nitrogen are fixed or assimilated into microbial protein [11]. In an environment populated by organisms of this type, the relative proportion of phosphate and nitrate must tend to approach that characteristic of their protoplasm. Given time enough, and the absence of other disturbances, a relation between phosphate and nitrate such as observed in the sea may well have arisen through the action of such organisms.

Nitrogen fixation is employed practically in agriculture whenever leguminous plants are used to enrich the soil. It is not unreasonable to assume that the same process has been effective on a larger scale in nature. Hutchinson has estimated that nitrogen is being fixed on the earth's surface at the annual rate of 0.0034 to 0.017 mg/cm^2 [12]. At the lesser value it would require only 40,000 years to fix the 7×10^{14} kilograms of nitrogen estimated to be available as nitrate in the ocean.

Nitrogen fixation is so active that there is no difficulty in assuming that it might serve in adjusting the phosphorus nitrogen ratio in the sea. The difficulty is rather in explaining why there is not a great excess of nitrate nitrogen in the water. The ratio of nitrogen to phosphorus in fresh waters is higher than that in ocean water, while the ratio in sedimentary rocks is very much lower. Consequently the ratio in the sea must tend to increase, unless some process is returning nitrogen to the atmosphere. Denitrifying bacteria might operate in this sense, in which case the phosphorus-nitrogen ratio is fixed by a complex balance.

Biological mechanisms adequate to influence the phosphorus-nitrogen ratio in sea water are known. Whether they do in fact operate in a regulatory sense is a subject for future investigation.

The Phosphorus-Oxygen Ratio

The relation between the quantity of phosphorus present in sea water and the amount of oxygen available for the decomposition of organic matter is less obvious than the relation of phosphorus and nitrogen. The quantity of oxygen dissolved in sea water when it is at the sea surface appears to be fixed by equilibrium with the atmosphere, which contains about 21 per cent oxygen. Consider what would happen if a unit volume of water, containing its characteristic quantities of plant nutrients, was brought from the depths of the ocean to the surface. There, under the influence of light, photosynthesis would convert the available nutrients to organic matter until all the phosphate is exhausted. At the same time the water is saturated with oxygen by equilibration with the atmosphere. If the unit volume of water is now returned to the depths where the organic matter is decomposed and oxidized, will the dissolved oxygen present be sufficient for the purpose, will there be a large excess of oxygen, or will the oxygen be deficient?

TABLE 2

UTILIZATION OF OXYGEN IN OCEAN WATER

	Average S. W.	*North Atlantic*	*North Pacific*
Phosphorus content mg atoms/m^3	2.3	1.25	3.0
Equivalent oxygen Utilization* ml/liter	6.9	3.75	9.0
Oxygen content of saturated S. W.	7.1	6.7	7.5
Excess oxygen	0.2	2.95	−1.5
Oxygen in "minimum oxygen layer"		3.0	0.01

* Calculated allowing 276 atoms of oxygen to be used in oxidizing a quantity of organic matter containing one atom of phosphorus in which case 1 mg atom P/m^3 is equivalent to 3 milliliters O_2/liter.

The answer can be given only within approximate limits, for two reasons. First, the quantities of nutrients are different in the deep waters of the several oceans, as we have seen. We can consider the extreme cases of the North Atlantic containing phosphorus in the concentration of 1.25 mg atoms per m^3, the North Pacific containing 3.0 mg atoms per m^3, and an "average" sea water containing, say, 2.3 mg atoms per m^3. Second, the quantity of oxygen dissolved in the water when it is at the surface will vary depending upon the temperature, and to a lesser degree upon the salinity.

The lowest oxygen concentrations are not found at the bottom of the oceans, but at some intermediate depth, where also maximum concentrations of phosphate and nitrate occur. The temperature at this depth in the North Atlantic is about 8°C. and when at the surface at this temperature the water would have taken up 6.7 milliliters of oxygen per liter. The corresponding temperature of the minimum oxygen layer in the North Pacific is about 3°C. and the oxygen solubility 7.5 milliliters per liter.

From these numbers Table 2 has been prepared to show the excess oxygen which might be expected to remain in the minimum oxygen layer if all the phosphorus present has been derived from the oxidation of organic matter. In the case of the "average" sea water it appears that the quantity of organic matter which can be formed from the nutrients in a unit of volume of "average" sea water is almost exactly that which can be completely oxidized by the oxygen dissolved at the surface. In the North Atlantic, where the phosphorus content is reduced, only about one half of the dissolved oxygen would be consumed and the excess oxygen corresponds well with the quantities observed to remain in the zone of minimum oxygen content. In the North Pacific, the phosphate content of the deep water is so great that the dissolved oxygen would be more than exhausted if the process went to completion as postulated.

Actually the Pacific Ocean does not appear to be anaerobic at any depth. However, large volumes of water at intermediate depths contain only small traces of oxygen [4]. In high latitudes where the deep water of the oceans originates the photosynthetic processes do not convert all of the available nutrients into organic matter before the water sinks. Consequently, the deep water contains phosphates which have not been liberated by oxidation during the preceding turn of the cycle. Presumably this effect accounts for traces of oxygen which remain in the minimum oxygen layer of the North Pacific.

Although the oxygenation of the oceans appears to be adequate to oxidize the products of the biochemical cycle at present the margin is not large. Actually anaerobic conditions exist in a number of isolated areas, such as the Black Sea and the Sea of Azov, Kaoe Bay in the East Indies, the Cariaco Trench, and numerous fjords in Norway and elsewhere [4]. A decrease in the oxygen content of the atmosphere, an increase in surface ocean temperatures or reduction in the vertical circulation of the water might lead to the extension of anaerobic conditions over much wider areas.

It is widely held among geochemists that the primitive atmosphere was devoid of oxygen, or at least contained very much less oxygen than at present. During the course of geological history atmospheric oxygen is thought to have been produced by the photochemical dissociation of water in the upper atmosphere and by the photosynthetic reduction of carbon dioxide, previously present in much greater quantities [13].

Estimates of the quantity of reduced carbon present in the earth's crust as coal and petroleum indicate that photosynthetic processes have been much more than adequate to produce the present oxygen content of the atmosphere. It has not been suggested, to my knowledge, why this process has proceeded just so far as it has; that is, why there is 21 per cent of oxygen in the atmosphere at present, no more or no less. It is, however, on this fact that the quantity of oxygen dissolved in the sea depends.

My supposition is that the actual quantities of oxygen present in the sea may have been regulated by the activities of sulfate-reducing bacteria. This group of bacteria are known to have the ability to use sulfates as a source of oxygen when free oxygen is absent and organic compounds are present to supply a source of energy [14]. The over-all reaction is

$$SO_4^{=} \longrightarrow S^{=} + 2O_2$$

The process should be broken down into two steps, each of which takes place in the sea under different environmental conditions, (1) Sulfate Reduction, $SO_4^{=} + 2C \rightarrow 2CO_2 + S^{=}$ which occurs at depth under anaerobic conditions, and (2) Photosynthesis $2CO_2 \rightarrow 2C + O_2$ which occurs near the surface in the presence of light.

In these equations C represents the reduced carbon present in organic matter. The decomposition of this material by sulfate-reducing bacteria according to the first step also liberates a corresponding quantity of nitrogen and phosphorus, which permit the CO_2 formed to re-enter the biological cycle when the second step comes into play. The CO_2 produced in this way can thus contribute to the production of oxygen in a way in which the excess carbonate normally present in sea water cannot.

The first step, which depends upon the presence of organic matter in excess of the free oxygen required to complete its decomposition, will initiate a mechanism which will tend to increase the oxygen when, and only when, the quantity of available free oxygen is deficient. If the total mechanism has operated on a large enough scale in the course of geochemical history, it may have kept the supply of oxygen available in the sea adjusted to the requirements of the biochemical cycle.

There is very good evidence that sulfate reduction does operate on a large scale in the sea wherever anaerobic conditions exist. Figure 2 shows the relations between the phosphorus content and the combined utilization of oxygen and sulfate in the waters of the Black Sea and Cariaco Trench, both anaerobic basins. The phosphorus content may be taken as an indication of the quantity of organic matter which has decomposed in the water. The combined utilization is the quantity of free oxygen which has disappeared from the water since it left the surface, plus *four times* the quantity of sulfide present. That is to say, it is assumed that for each ion of sulfide liberated in the water four atoms of oxygen have been produced by sulfate reduction and utilized in oxidizing organic matter. The figure shows that as increasing quantities of organic matter decompose in the water the utilization of oxygen increases approximately in the ratio of 235 atoms for each atom of phosphorus set free [3]. After the phosphorus content reaches a little more than 2 mg atoms per m^3 the free oxygen is exhausted and hydrogen sulfide appears in the water. The increase in hydrogen sulfide continues as though it were produced by the reduction of the quantity of sulfate required to oxidize the accumulated organic matter. In the depths of the Black Sea more than two thirds of the phosphorus present may be attributed to the decomposition of organic matter through sulfate reduction. If the products of such decomposition find their way back to the surface, then the oxygen derived from sulfate will be liberated by the photosynthetic process and will be added to the supply of free oxygen in the environment.

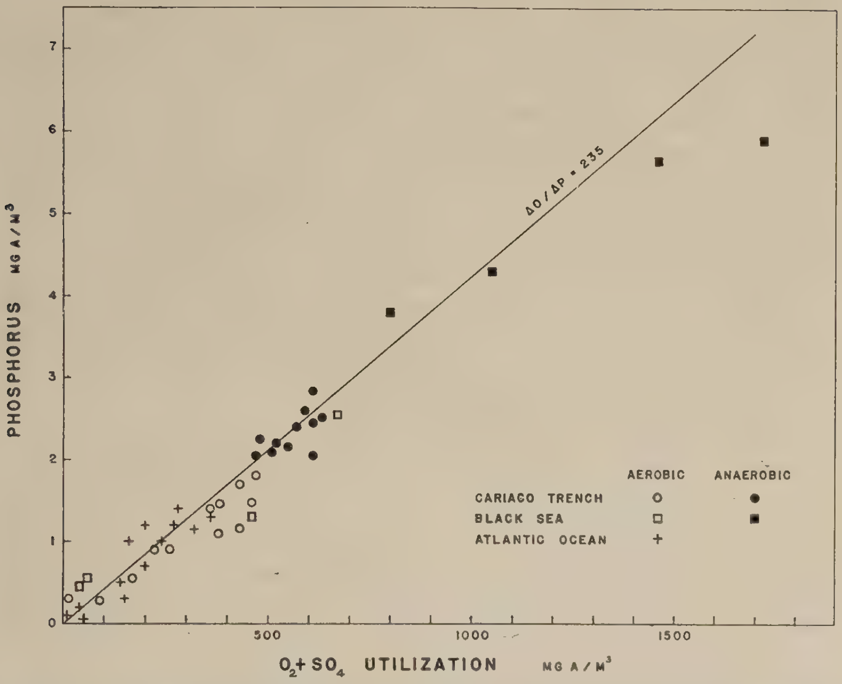

FIG. 2. Relation between the inorganic phosphorus and the combined utilization of oxygen and sulfate in waters of Cariaco Trench, Black Sea, and western Atlantic Ocean. After Richards and Vaccaro [3].

At the present time, anaerobic basins such as the Black Sea and the Cariaco Trench are rarities and the greater part of the ocean is well oxygenated. Extensive areas of marsh and estuary present anaerobic conditions, as do quite generally marine muds. At present the production of oxygen through sulfate reduction in such situations may not be more than sufficient to balance the losses due to the oxidation of eroding terrestrial surfaces. If, however, in the past the oxygen of the atmosphere were lower than at present, anaerobic conditions may have been much more prevalent. The reduction of sulfates may then have served to bring the oxygen content of the atmosphere and sea into correspondence with the requirements set by the quantities of phosphorus available.

In considering the influence of the biochemical cycle on the environment it should be remembered that the cycle can, and apparently for the most part does, run its course without adding more to the environment at one phase than it withdraws at another. Photosynthesis cannot increase the oxygen content of the environment unless the products of photosynthesis are in some way withdrawn from reoxidation. The reduction of sulfates will not make more oxygen available in the sea if the sulfides produced are reoxidized in the sea water. Fractionating mechanisms are required which separate the products of the cycle, so that they cannot re-enter it. Such mechanisms exist at the sea bottom, where materials may be buried in the sediments, and at the surface where volatiles may pass into the atmosphere.

Consider the fate of the sulfide and oxygen which are produced in anaerobic basins by the activity of sulfate-reducing organisms. When the water containing these products is brought to the surface layers of the sea by mixing processes the sulfide will be reoxidized to sulfate, consuming a quantity of free oxygen equivalent to that produced by the original reduction. No change in the total oxygen in the water column would result if this were the complete picture. However, if a portion of the sulfide forms insoluble compounds, such as iron sulfide, which settle into the bottom sediments, or if a portion of the oxygen liberated near the sea surface passes into the atmosphere, these portions cannot re-enter the cycle immediately and a net increase in the oxygen of the environment will be produced.

Conditions on the land, in contrast with the sea, appear to be much less favorable for producing changes in the free oxygen of the atmosphere, either by photosynthesis or in response to anaerobic conditions through sulfate reduction. The predominance of erosion does not permit the permanent entrapment of large quantities of organic matter on land. Soils are usually well aerated so that organic carbon does not remain long out of circulation. Anaerobic conditions do exist in swamps, and many coal deposits must represent reduced carbon formed in such places which have contributed oxygen to the atmosphere, but such withdrawals must be small compared to the quantities of organic matter accumulated in marine sediments.

The exchange of oxygen across the sea surface must be important in this connection. The solubility of oxygen in water is such that under equilibrium conditions more than twenty times as much oxygen occurs in a unit volume of air than in a comparable volume of water at the sea surface. Of any increase in the quantity of oxygen in the water, whether produced by the reduction of sulfates or the photosynthetic reduction of carbonates, only a small portion would remain in the water since a larger fraction would pass into the atmosphere.* In this way the biochemical cycle of the sea can continue to add to the oxygen content of the environment until a new equilibrium is established between the atmosphere, the sea, and the available nutrient materials.

It appears, then, that the biochemical cycle in the sea may have produced the major amount of oxygen in the atmosphere and that conditions in the sea have adjusted its level to that which occurs at present. We think of the atmosphere as determining the oxygen content of the sea. This is because the atmosphere is the great reservoir of oxygen on the earth's surface and because the motion of the air gives it a conveniently constant composition. Perhaps it is more correct, however, to think of the sea, and particularly of its nutrient content, as determining the composition of the atmosphere.

Geochemical Considerations

As a final check on these speculations, we can look at the relative availability of the principal materials of the biochemical cycle on the earth's surface, to see if they conform to the postulates. In Table 3 estimates are given of the total quantities of the pertinent elements in the atmosphere, the ocean, and the sedimentary rocks. The content of the atmosphere is quite accurately known; that of the ocean can be approximated since the greater part of its water is of relatively uniform composition. The values for the sedimentary rocks are quite uncertain, partly because of the variability in their composition and the incompleteness in sampling, and partly because the volumes in question are arbitrarily chosen. However, we are concerned with orders of magnitude so the numbers are useful.

The first column of numbers in Table 3 are the estimated weights of each element on the earth's surface. Divided by the phosphorus content of the ocean and adjusted for atomic weights, the second column gives the numbers of atoms relative to the atoms of phosphorus in the ocean.

---

* The intensity of the exchange of oxygen across the sea surface is indicated by the observations that in the Gulf of Maine a quantity of oxygen sufficient to form a layer 0.9 meters in depth enters the atmosphere each spring as the result of photosynthetic activity by phytoplankton. This is about 15 per cent of the oxygen locally present to a depth of 200 m. This quantity of oxygen returns to the water during the following fall and winter to replace that used in the oxidation of the summer crop of organic matter [15].

So reduced, the relative quantities are indicated in Figure 3 which presents in diagrammatic form the biochemical cycle as described.

TABLE 3

QUANTITIES AND PROPORTIONS OF ELEMENTS AT THE EARTH'S SURFACE*

Ocean	P	1×10^{14}	1
	N as NO_3	7×10^{14}	15
	as N_2	2.3×10^{16}	510
	C	4×10^{16}	1,000
	S	1×10^{18}	10,000
	O	1.4×10^{16}	270
Atmosphere	N as N_2	3.8×10^{18}	62,000
	C	6.4×10^{14}	16
	O	1.2×10^{18}	23,000
Earth's crust			
Sedimentary rocks	P	4×10^{18}	40,000
	N	4.4×10^{17}	10,000
	S	1×10^{18}	10,000
	C	1.5×10^{19}	400,000
Coal and petroleum	C	6×10^{18}	160,000

* Estimates are based on following sources: Atmosphere [19]; Ocean, volume 1.37 $\times$ 10^9 Km^3 [20], P 71 $\times$ 10^{-6} gr/Kg(original), N as NO_3 15 $\times$ P, N as N_2 17.3 $\times$ 10^{-3} gr/Kg assuming saturation at 2°C. and 34.33 % S [21], O as O_2, including consumption in biochemical cycle, 10.7 $\times$ 10^{-3} gr/Kg assuming saturation at 2°C. and 34.5 % S [22], C as HCO_3 0.028 gr/Kg [20] S as SO_4 0.884 gr/Kg [20]; Earth's crust, area 5.1 $\times$ $10^{18}/cm^2$, Sedimentary rocks 170 Kg/cm^2, P 0.46 per cent (arbitrary weighting of analyses by Stokes and Steiger) N 0.051 per cent, S = 0.12 per cent (arbitrary weighting of analyses by Stokes), C 3 Kg/cm^2, and coal and petroleum 1.26 Kg/cm^2 after Kalle [19].

The diagram shows phosphate, nitrate, and carbonate entering the organic phase of the biochemical cycle near the sea surface, through the process of photosynthesis. Phosphorus, nitrogen, and carbon are selected by the synthetic process in the proportions of 1:15:105. This is the step which coordinates the cycles of the several elements in a unique way and gives meaning to the comparisons. The elements are carried in these proportions to the point of decomposition where they are oxidized to their original state as phosphate, nitrate, and carbonate. The oxygen required is just that set free by photosynthesis. Such a cycle could run indefinitely in an otherwise closed system so long as light is supplied.

To account for the correspondence in the ratios of phosphorus and nitrogen in the organic phase of the cycle and in the inorganic environment, bacterial processes of nitrogen fixation and denitrification are indicated at the upper right and, similarly, the sulfate reduction process is shown at the lower left. This latter is assumed to operate effectively only when the environment becomes anaerobic. Finally, the exchanges with the atmosphere and the sediments of the sea bottom are shown. If these processes are operative it is necessary that supplies are adequate and that their products exist in suitable quantities.

Considering first nitrogen, there exist in sea water for each atom of phosphorus 15 atoms of nitrogen available as NO_3 and a reserve of 510 atoms of nitrogen as dissolved N_2 which may be drawn on by nitrogen-fixing bacteria. In addition, there is a reserve of nitrogen in the atmosphere equivalent to 86,000 atoms of phosphorus, which is available to replace that dissolved in the sea were it to be drawn on. The nitrogen of the sedimentary rocks is about one-sixth that in the atmosphere and twenty times that in the ocean. More than four-fifths of this is fossil nitrogen which may be assumed to be derived from organic matter [12]. Consequently, large quantities of nitrogen have passed through the biochemical cycle in its passage from the atmospheric reserves to be deposited in sediments at the sea bottom. The quantity withdrawn in this way is small, however, in comparison to the reserve in the atmosphere. Clearly, the nitrogen supply is adequate.

Sulfate is one of the most abundant ions in sea water. In this form there is present sulfur equivalent to 10,000 atoms of phosphorus. It would be capable of supplying oxygen equivalent to 40,000 atoms of phosphorus on reduction. Clearly, the sulfate reduction mechanism could continue to operate for a long time. If it has operated as postulated in the past much sulfide may have been removed from the sea. Sedimentary rocks are estimated to contain sulfur equivalent to 10,000 atoms of oceanic phosphorus. If this were all the product of sulfate reduction, this would have produced oxygen equivalent to 40,000 atoms of oceanic phosphorus, which is almost twice that present in the atmosphere. It is not clear how much of the sulfur in sedimentary rocks is present as sulfides, but much of it is. Clearly, much oxygen can have been produced in the past by sulfate reduction and possibly this process has contributed to an important degree in producing the oxygen of the atmosphere.

Carbon is present in the sea, chiefly as carbonate ions, in about ten times the quantity required for the biochemical cycle. Much of the large deposits of carbon in the sedimentary rocks is present as carbonates and cannot have contributed to the production of free oxygen. The estimated carbon present as coal and petroleum, equivalent to 160,000 atoms of oceanic phosphorus, is sufficient to yield oxygen on reduction equivalent to 320,000 atoms of oceanic phosphorus, which is more than ten times the present content of the atmosphere.

The known facts of geochemistry do not appear to contradict the suppositions presented on the mechanism which may have controlled the relative availability of phosphate, nitrate, and oxygen in the sea. Sources of nitrogen and sulfate are available in great excess and the by-products of the reactions can be adequately accounted for. According to these suppositions, phosphorus is the master element which controls the availability of the others. How about phosphorus itself?

In the sedimentary rocks, formed for the most part by marine deposition, there are present some 40,000 atoms of phosphorus for every atom in the sea water. Evidently large quantities of phosphorus, carried into the sea from the rivers in past times, have passed through the sea to contribute to these deposits. The concentration of phosphorus in average sea water is very small, amounting to less than one part in 10 million. Probably this represents a condition determined by the low solubility of phosphates under the conditions existing in sea water at the sea bottom. Dietz, Emery, and Shepard [16] have suggested that sea water deeper than a few hundred meters is essentially saturated with $Ca_3(PO_4)_2$. It is not possible to be exact in this regard because the solubility will vary with the conditions, and the physical constants are not well known. However, they have described the presence of phosphorite deposits on the floor of the North Pacific ocean which they explain in this way. The high ratio of phosphorus to nitrogen in sedimentary rocks, 4:1, when compared to the ratio characteristic of the plankton, 1:15, also suggests that phosphorus has been introduced into the sediments by some mechanism other than the entrapment of organic matter.

If the argument presented is sound it may be concluded that the quantity of nitrate in the sea, and the partial pressure of oxygen in the atmosphere are determined through the requirements of the biochemical cycle, by the solubility of phosphate in the ocean. This is a physical property of a unique chemical compound and as such is not subject to change except in so far as alterations in conditions may influence the activity coefficients of the ions involved. It follows then that the nutrient supplies in sea water, and the oxygen content of the atmosphere have been about as at present for a long time in the past and will remain at much the same level into the future. This argument may then be added to those reviewed by Rubey [17] that the composition of sea water and atmosphere has varied surprisingly little at least since early geologic time.

Speculations about geochemical history are obviously not subject to proof in the ordinary sense. The best one can do is to develop circumstantial evidence which shows that known processes occur which are adequate to produce the effects postulated, and to demonstrate that the quantities of matter and its distribution as presently observed are concordant with the hypotheses. The present hypothesis appears to be supported by evidence of this sort. What is lacking is direct evidence that the postulated processes do, in fact, act in a regulatory way so as to bring the atomic ratios of phosphate nitrate and oxygen in the environment into conformity with the requirements of the biochemical cycle. It is desirable, and would seem quite possible, to set up controlled microcosms in the laboratory, such as von Brand, Rakestraw, and Renn [18] employed to demonstrate the steps in the nitrogen cycle, which would test whether the physiology of the nitrogen and sulfur manipulating bacteria is such as to provide the homeostatic regulation which has been assumed.

REFERENCES

1. A. C. Redfield, "On the proportions of organic derivatives in sea water and their relation to the composition of plankton," James Johnstone Memorial Volume, pp. 176–192, Liverpool (1934).
2. R. H. Fleming, "The composition of plankton and units for reporting populations and production," *Proc. Sixth Pacific Sci. Congress, 3*, pp. 535–540 (1940).
3. F. A. Richards and R. F. Vaccaro, "The Cariaco Trench, an anaerobic basin in the Caribbean Sea," *Deep-Sea Research*, 3, pp. 214–228 (1956).
4. F. A. Richards, "Oxygen in the Ocean," Treatise on Marine Ecology and Paleoecology, J. W. Hedgpeth, Ed., Vol. 1, Chapter 9, pp. 185–238 (1957).
5. L. H. N. Cooper, "On the ratio of nitrogen to phosphorus in the sea," *Jour. Marine Biol. Assn., 22*, pp. 177-182 (1937).
6. H. W. Harvey, "Nitrate in the Sea," *Jour. Marine Biol. Assn., n.s. 14*, pp. 71–88 (1926).
7. A. C. Redfield, "The processes determining the concentration of oxygen, phosphate and other organic derivatives within the depths of the Atlantic Ocean," *Papers in Physical Oceanography and Meteorology, 9(2)* 22 pp. (1942).
8. H. Thomsen, "Nitrate and phosphate contents of Mediterranean Water," Report on the Danish Oceanographical Expeditions 1908–1910 to the Mediterranean and Adjacent Seas. No. 10 (3) pp. 1–11 (1931).
9. H. W. Graham and E. G. Moberg, "Chemical results of the last cruise of the Carnegie," Sci. Results of Cruise VII of the Carnegie during 1928–29 under Command of Captain J. P. Ault, Chemistry I, v plus 58 pp., Washington (1944).
10. A. C. Redfield, "The hydrography of the Gulf of Venezuela," Papers in Marine Biology and Oceanography, Supplement to *Deep-Sea Research*, 3, pp. 115–133 (1955).
11. J. Stoklasa, "Biochemischer Kreislauf des Phosphat-Ions im Boden," *Centrbl. Bakt.* II, 29; 385–419 (1911).
12. G. E. Hutchinson, "Nitrogen in the biogeochemistry of the atmosphere," *Am. Scientist, 32*, pp. 178–195 (1944).
13. J. H. J. Poole, "The evolution of the atmosphere," *Royal Dublin Soc., Sci. Proc., 22* (n.s.), pp. 345–365 (1941).
14. S. A. Waksman, "Principles of soil microbiology," Ed. 2, 894 pp., Baltimore (1932).
15. A. C. Redfield, "The exchange of oxygen across the sea surface," *Jour. Marine Research, 7*, pp. 347–361 (1948).
16. R. S. Dietz, K. O. Emery, and F. P. Shepard, "Phosphorite deposits on the sea floor off southern California," *Bull. Geol. Soc. America, 53*, pp. 815–847 (1942).
17. W. W. Rubey, "Geologic history of sea water," *Bull. Geol. Soc. America, 62*, pp. 1111–1147 (1951).
18. T. von Brand, N. W. Rakestraw, and C. E. Renn, "Further experiments on the decomposition and regeneration of nitrogenous organic matter in sea water," *Biol. Bull., 77*, 285–296 (1939).
19. K. Rankama and T. G. Sahama, "Geochemistry," 912 pp., Chicago (1950).
20. H. U. Sverdrup, M. W. Johnson, and R. H. Fleming, "The Oceans," 1087 pp., New York (1942).
21. N. W. Rakestraw and V. M. Emmel, "The solubility of nitrogen and argon in sea water," *Jour. Phys. Chem., 42*, pp. 1211–1215 (1938).
22. F. A. Richards and N. Corwin, "Some oceanographic applications of recent determinations of the solubility of oxygen in sea water," *Limnology and Oceanography*, 1, pp. 263–267 (1956).

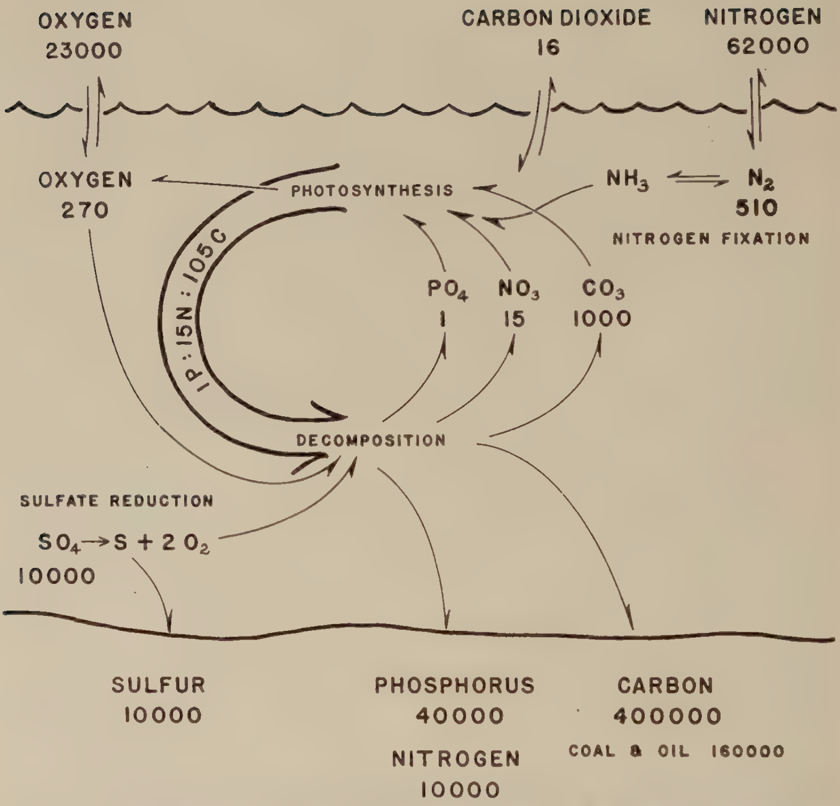
OXYGEN
23000
CARBON DIOXIDE
16
NITROGEN
62000
OXYGEN
270
PHOTOSYNTHESIS
NH$_3$ ⇌ N$_2$
510
NITROGEN FIXATION
1P : 15N : 105C
PO$_4$
1
NO$_3$
15
CO$_3$
1000
DECOMPOSITION
SULFATE REDUCTION
SO$_4$ → S + 2 O$_2$
10000
SULFUR
10000
PHOSPHORUS
40000
NITROGEN
10000
CARBON
400000
COAL & OIL 160000

Fig. 3. The Biochemical Cycle. Numbers represent quantities of respective elements present in the atmosphere, the ocean, and the sedimentary rocks, relative to the number of atoms of phosphorus in the ocean.

Contribution No. 977

UNITED STATES DEPARTMENT OF THE INTERIOR, Fred A. Seaton, *Secretary*
FISH AND WILDLIFE SERVICE, Arnie J. Suomela, *Commissioner*

SURFACE CIRCULATION IN THE GULF OF MAINE AS DEDUCED FROM DRIFT BOTTLES

By C. Godfrey Day

March 3, 1849

FISHERY BULLETIN 141
From Fishery Bulletin of the Fish and Wildlife Service
VOLUME 58
(Contribution No. 977, Woods Hole Oceanographic Institution)

CONTENTS

Page

Introduction 443
Bottle types and distribution 443
Interpretation of drift-bottle returns 443
Surface circulation patterns in the Gulf of Maine 446
  Group *A* cruises: late February and early March 446
    Albatross III cruise 57, 1955 446
    Albatross III cruise 71, 1956 446
  Group *B* cruises: late March and early April 450
    Albatross III cruise 46, 1953 450
    Albatross III cruise 58, 1955 452
    Albatross III cruise 72, 1956 452
  Intermediate cruise: *Albatross II* cruise, 1932 452
  Group *C* cruises: late April and early May 456
    Albatross II cruise, 1931 456
    Atlantis cruise 28, 1934 456
    Albatross III cruise 48, 1953 456
    Albatross III cruise 60, 1955 460
    Albatross III cruise 73, 1956 460
  Group *D* cruises: late May and early June 463
    Albatross II cruise, 1931 463
    Albatross III cruise 50, 1953 463
    Albatross III cruise 61, 1955 463
    Albatross III cruise 75, 1956 463
  Group *E* cruises: late June 468
    Atlantis cruise 16, 1933 468
    Albatross III cruise 76, 1956 468
Indications of bottom drift 471
Conclusions 471
References 472

ABSTRACT

Drift-bottle returns from 17 cruises over the Gulf of Maine and Georges Bank are compared. Seasonal and year-to-year differences in surface water circulations are noted. Wind values for 60 days following each cruise are presented in an effort to determine wind influence on surface circulation within the area.

SURFACE CIRCULATION IN THE GULF OF MAINE AS DEDUCED FROM DRIFT BOTTLES

By C. Godfrey Day, *Research Assistant*
Woods Hole Oceanographic Institution

Between 1931 and 1956, the United States Fish and Wildlife Service made a number of cruises to the Gulf of Maine and Georges Bank as part of a study of the distribution and movement of the eggs and larvae of commercially important food fishes. On 17 of these cruises, during the years 1931, 1932, 1933, 1934, 1953, 1955, and 1956, drift bottles were launched throughout the area.[1] The seasonal coverage of these bottle seedings extends from late February through June.

Plots of drift-bottle returns showed such marked differences that a careful analysis of these data was necessary. This paper reports the results of a study of the surface circulations as deduced from bottle returns. Seasonal and year-to-year differences are noted. Daily values for surface-wind direction and force for the period of each cruise and for 60 days following have been taken from the daily weather maps in an effort to determine the effect wind may have had on the surface-water movement.

The original data, the result of studies by the United States Bureau of Fisheries and the United States Fish and Wildlife Service, are on file at the Woods Hole Oceanographic Institution, where a punchcard system is maintained and supplemented as new drift-bottle returns are received and further studies initiated.

The basic data used in the present paper are available in tabular form in Special Scientific Report: Fisheries No. 242.

BOTTLE TYPES AND DISTRIBUTION

The bottles employed were those commonly used for carbonated drinks. They were of clear glass and measured approximately 22 cm. in height and 6 cm. in diameter, with a capacity of 8 fluid ounces.

Some of the bottles released on the 1931–34 cruises were equipped with drogues and some were not. The pattern of distribution during this period was confined to Georges and Browns Banks, but otherwise it followed no clear-cut system. Usually from 5 to 15 bottles were launched at a station, but occasionally they were distributed over a short track at the rate of 2 bottles every 2 miles. (These tracks of release are not indicated in the figures as they would needlessly confuse the drawing; all returns, however, are accounted for.)

During the 1953–56 cruises, half of the bottles were ballasted with dry sand so that they would float vertically at or near the surface; the other half contained no ballast. The bottles were distributed over a grid of stations fairly evenly covering the Gulf of Maine and Georges Bank. Twelve bottles were released at each station, 6 with ballast and 6 without.

INTERPRETATION OF DRIFT-BOTTLE RETURNS

The trajectories shown in the figures which follow represent general directional trends and in no case should they be considered to indicate the actual routes followed. For each bottle there are but two knowns with which to work: the place and date of launching and the place and date of recovery.

The method by which tracks were constructed from these meager data is best illustrated by an example. To this end, figure 1—*a*, *b*, *c*, and *d*—was prepared, showing the initial treatment of data from cruise 48 of the *Albatross III*.

The first step was to select the bottles with the shortest period of drift and plot their net movement by straight lines (fig. 1, *a*). Usually, as in

---

[1] Walford (1938) has discussed the results of the 1931 and 1932 drift-bottle returns; the others have not previously been reported.

Note.—Approved for publication, September 30, 1957. Fishery Bulletin 141.

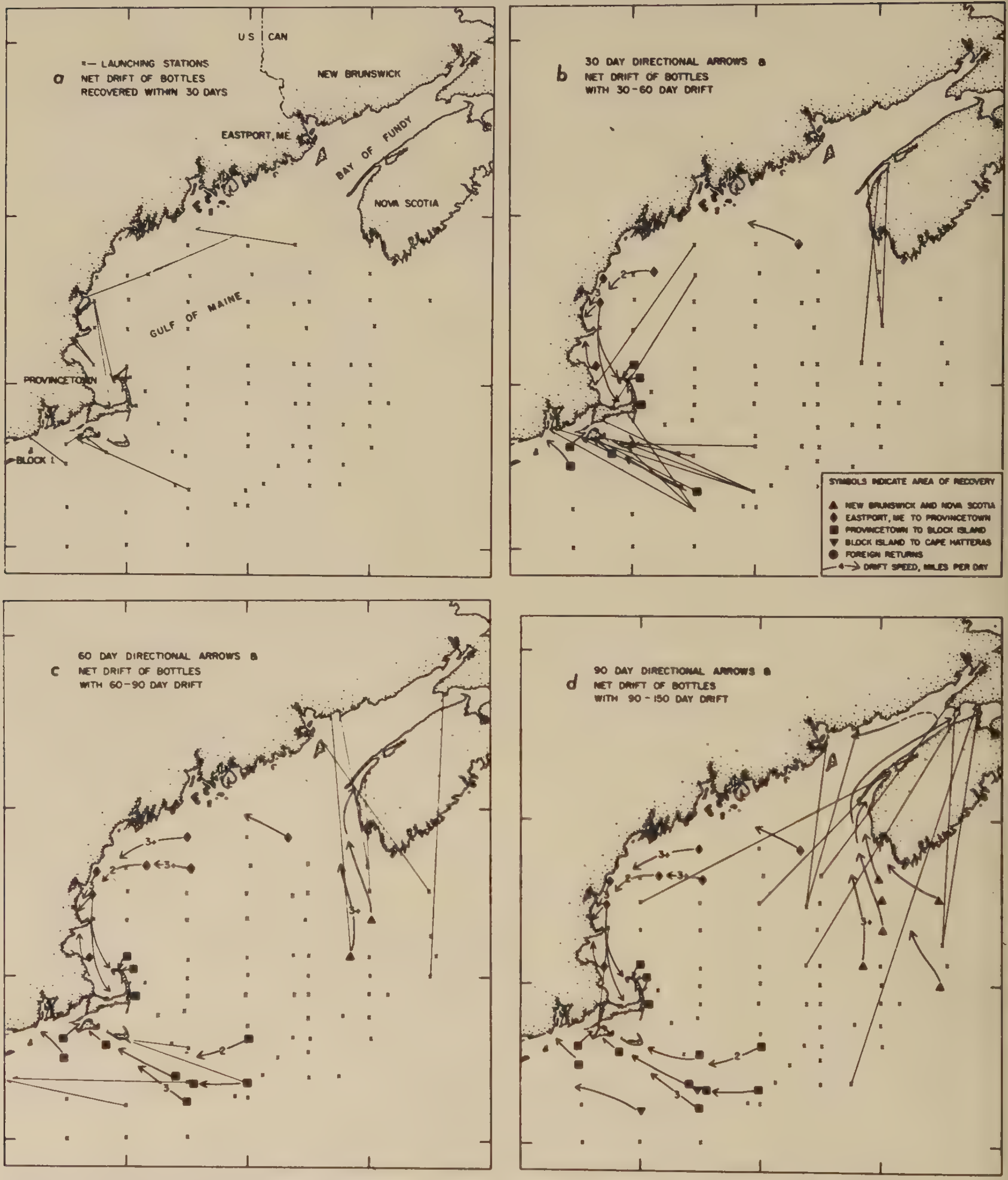
US
CAN
a
x— LAUNCHING STATIONS
NET DRIFT OF BOTTLES
RECOVERED WITHIN 30 DAYS
NEW BRUNSWICK
EASTPORT, ME
BAY OF FUNDY
NOVA SCOTIA
GULF OF MAINE
PROVINCETOWN
BLOCK I.
b
30 DAY DIRECTIONAL ARROWS &
NET DRIFT OF BOTTLES
WITH 30-60 DAY DRIFT
SYMBOLS INDICATE AREA OF RECOVERY
▲ NEW BRUNSWICK AND NOVA SCOTIA
◆ EASTPORT, ME TO PROVINCETOWN
■ PROVINCETOWN TO BLOCK ISLAND
▼ BLOCK ISLAND TO CAPE HATTERAS
● FOREIGN RETURNS
—4→ DRIFT SPEED, MILES PER DAY
c
60 DAY DIRECTIONAL ARROWS &
NET DRIFT OF BOTTLES
WITH 60-90 DAY DRIFT
d
90 DAY DIRECTIONAL ARROWS &
NET DRIFT OF BOTTLES
WITH 90-150 DAY DRIFT

FIGURE 1.—Example of method of interpretation of bottle returns. *a*. Bottles recovered within 30 days of launching; *b*. bottles recovered within 30 to 60 days; *c*. bottles recovered within 60 to 90 days; *d*. bottles recovered within 90 to 150 days. (x indicates station of launching; arrow, direction of drift; figure on arrow, speed of drift.)

this example, enough bottles were found within 30 days of their launching to allow construction of this initial picture. It was felt that these early returns, because of time limitations, came closest to showing the actual path of drift. They came, of course, from the inshore launching stations. These straight lines were then reduced to the first few directional arrows (fig. 1, *b*), and symbols indicating areas of recovery were placed at launching points.

Similarly, the next group of bottles having drifts of from 30 to 60 days was plotted (fig. 1, *b*), showing straight line or net movement. Again, these straight lines were reduced to directional arrows, drawn to conform as nearly as possible to the first set. This process was repeated for the 60- to 90-day drifts which were superimposed as straight lines (fig. 1, *c*). The whole process was repeated (fig. 1, *d*) as often as the data required, until all returns had been accounted for.

It will be noticed that in the final chart for cruise 48 (fig. 11), a cyclonic eddy was shown in the northern Gulf of Maine. This was deduced from the pattern already established (fig. 1, *d*) and from the fact that some bottles recovered from these stations had been adrift for more than 100 days, indicating little likelihood of direct movement toward their recovery point. In addition, the period of drift for the bottle launched in the north-central part of the eddy exceeded considerably the period of drift of those bottles launched in the southern part, though all were found in the same recovery area.

In following the method of charting water movements from bottle recoveries outlined here, certain general principles have been adhered to. The first-drawn directional arrows, which were based on relatively few returns, were subject to minor modifications by subsequent, more numerous recoveries. Such changes, never radical in nature, seldom had to be made, however. Very late returns, which came in after many months or even years, were arbitrarily made to fit the previously established pattern.

Where a concentration of release stations appeared from which there were no returns, directional arrows were made to avoid this area, which was assumed to be characterized by an offshore movement. (Note the northward confinement of the Gulf eddy in figure 11.) Where alternate routes appeared possible, the one more consistent in terms of drift velocity was chosen. Where velocities have been entered, they indicate the fastest drift as being most representative, since other slower bottles may have lain undiscovered on the beach for some time. Where routes were most open to question, a dashed line was used in plotting.

Finally, it should be stated that the plots were completed before the surface wind vectors were read from daily weather maps and graphed. Thus, knowledge of wind patterns in no way influenced the assumed course of bottles.

The end result of this treatment is seen in the charts for each cruise. In referring to them it should be remembered that—

1. Arrows show directional trends, not actual routes followed.

2. A single arrow may show the trend of a number of bottles.

3. Symbols—used in figures 3 to 19—at the point of release (near the base of an arrow) indicate the general region of ultimate recovery.

4. Positions of all stations at which bottles were dropped are shown with the exception of a few instances during the 1931–34 cruises where bottles were set out in short lines of 2 bottles every 2 miles. In some instances where bottles from the same launching position stranded in different recovery areas, two or more symbols are grouped together.

For purposes of comparison, the 17 cruises considered here have been divided on a seasonal basis into five groups (table 1): Group *A*, late February and early March; group *B*, late March and early April; group *C*, late April and early May; group *D*, late May and early June; and group *E*, late June.

Each cruise is considered from the following aspects:

1. How does it agree or disagree with other cruises in the same seasonal category?

2. Are there any seasonal circulatory characteristics?

Table 1.—*Summary of drift-bottle releases in the Gulf of Maine, by cruise and year*

Cruise	Date	Number released	Number returned [1]	Percentage recovered
Group *A*:				
Albatross III:				
Cruise 57	Feb. 21–Mar. 2, 1955	648	34	5.2
Cruise 71	Feb. 20–Mar. 2, 1956	719	54	7.5
Group *B*:				
Albatross III:				
Cruise 46	Mar. 19–Apr. 2, 1953	801	58	7.2
Cruise 58	Mar. 19–Apr. 1, 1955	826	76	9.2
Cruise 72	Mar. 21–31, 1956	633	47	7.4
Albatross II	Apr. 4–18, 1932	737	77	10.4
Group *C*:				
Albatross II	Apr. 17–29, 1931	450	49	10.9
Atlantis: Cruise 28	Apr. 27–May 13, 1934	629	101	16.1
Albatross III:				
Cruise 48	Apr. 24–May 8, 1953	970	108	11.1
Cruise 60	Apr. 19–May 3, 1955	1,235	139	11.3
Cruise 73	Apr. 17–28, 1956	780	72	9.2
Group *D*:				
Albatross II	May 26–June 7, 1931	352	58	16.5
Albatross III:				
Cruise 50	May 25–June 2, 1953	552	39	7.1
Cruise 61	May 16–28, 1955	672	77	11.5
Cruise 75	May 16–29, 1956	1,078	119	11.0
Group *E*:				
Atlantis: Cruise 16	June 19–28, 1933	532	93	17.5
Albatross III: Cruise 76	June 11–24, 1956	1,137	90	7.9
Total		12,751	1,290	

[1] As of December 1956.

3. To what extent can differences or similarities be accounted for by the wind patterns during and immediately following each cruise?

4. How does it agree with or depart from Bigelow's (1927, fig. 207) schematic diagram of the circulation in this area?

Although figure 2, based on Bigelow's diagram of nontidal circulation is for July and August, it is used throughout this discussion as a convenient norm for comparison with each of the cruises.

Bigelow summarized the circulation in the Gulf of Maine as a general anticlockwise eddy around the basin of the Gulf. He called this the "Maine" or "Gulf of Maine" eddy. We have called it the "Gulf" eddy. He pointed out (p. 972) that—

> The eddying drift is operative throughout the year, but differs in velocity and generally in detail, from season to season. It is also complicated by subsidiary eddying movements in the Bay of Fundy, Massachusetts Bay, Vineyard Sound, around Nantucket and Nantucket Shoals, and around and over Georges Bank, which are clockwise around these shoals but counterclockwise in the bays and basins * * *

We shall call the clockwise eddy around Georges Shoals the "Georges" eddy.

For convenience, reference is made in the discussion of cruises, which follows, to four arbitrarily defined areas within the region of study. These are superimposed on Bigelow's schematic diagram as well as on the subsequent plots.

SURFACE CIRCULATION PATTERNS IN THE GULF OF MAINE

GROUP *A* CRUISES: LATE FEBRUARY AND EARLY MARCH

Albatross III cruise 57, February 21–March 2, 1955 (Figure 3)

In area I, there is a pronounced southerly movement along the western shore of the Gulf and there are indications of a strong seaward movement east of Cape Cod through South Channel, breaking the southwestern sector of the Gulf eddy. Maximum velocities are in the order of 2 miles a day. Water movement in area II differs from Bigelow's diagram in that the northward flow from Browns Bank into the Bay of Fundy is not clearly established, two stations showing movement to southeastern Nova Scotia and one station showing a 540-day drift to Maine. Area III shows the return of 1 bottle out of 84 bottles put out at 7 stations (12 per station). At other times, returns would have been had from Long Island and the southwest as far as Cape Hatteras.

The best agreement with Bigelow, though the data are scarce, is found in area IV. On the northern edge of the Bank, the Gulf eddy is indicated by 3 returns from 1 station; 1 bottle entered the Bay of Fundy and 2 reached the western shore of the Gulf. Anticyclonic movement around Georges Bank is suggested by westward drift from two stations and pronounced seaward movement from the eastern and southern edges by the concentration of no-return stations and the scattered foreign returns.

The apparent resultant of wind vectors for 40 days following the cruise shows a dominant wind from about west-northwest. Whether one assumes a movement of surface water to the right of the wind in accordance with Ekman (1902) or a direct downwind transport, winds could well account for the departures from the norm, as taken from Bigelow.

Albatross III cruise 71, February 20–March 2, 1956 (Figure 4)

Area I, for this period, is in close agreement with area I, cruise 57, of 1955, in the pronounced southward movement of bottles toward Cape Cod and the lack of bottles returning via the Gulf eddy to northern and eastern waters. Velocities are

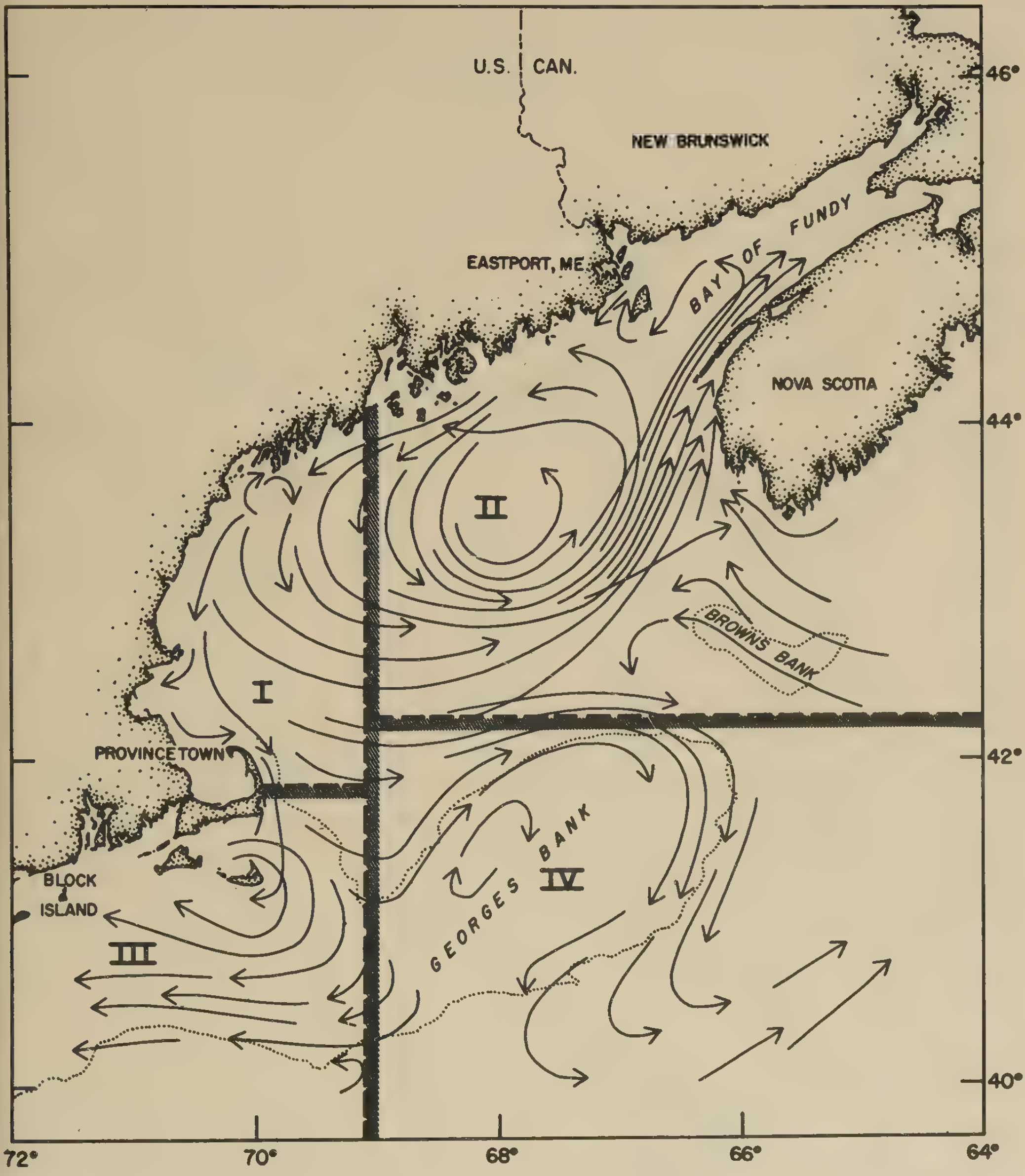
U.S.
CAN.
46°
NEW BRUNSWICK
EASTPORT, ME.
BAY OF FUNDY
NOVA SCOTIA
44°
II
I
BROWNS BANK
PROVINCETOWN
42°
BLOCK ISLAND
III
GEORGES BANK
IV
40°
72°
70°
68°
66°
64°

Figure 2.—Orientation chart based on Bigelow's diagram of water circulation during July and August in the Gulf of Maine.

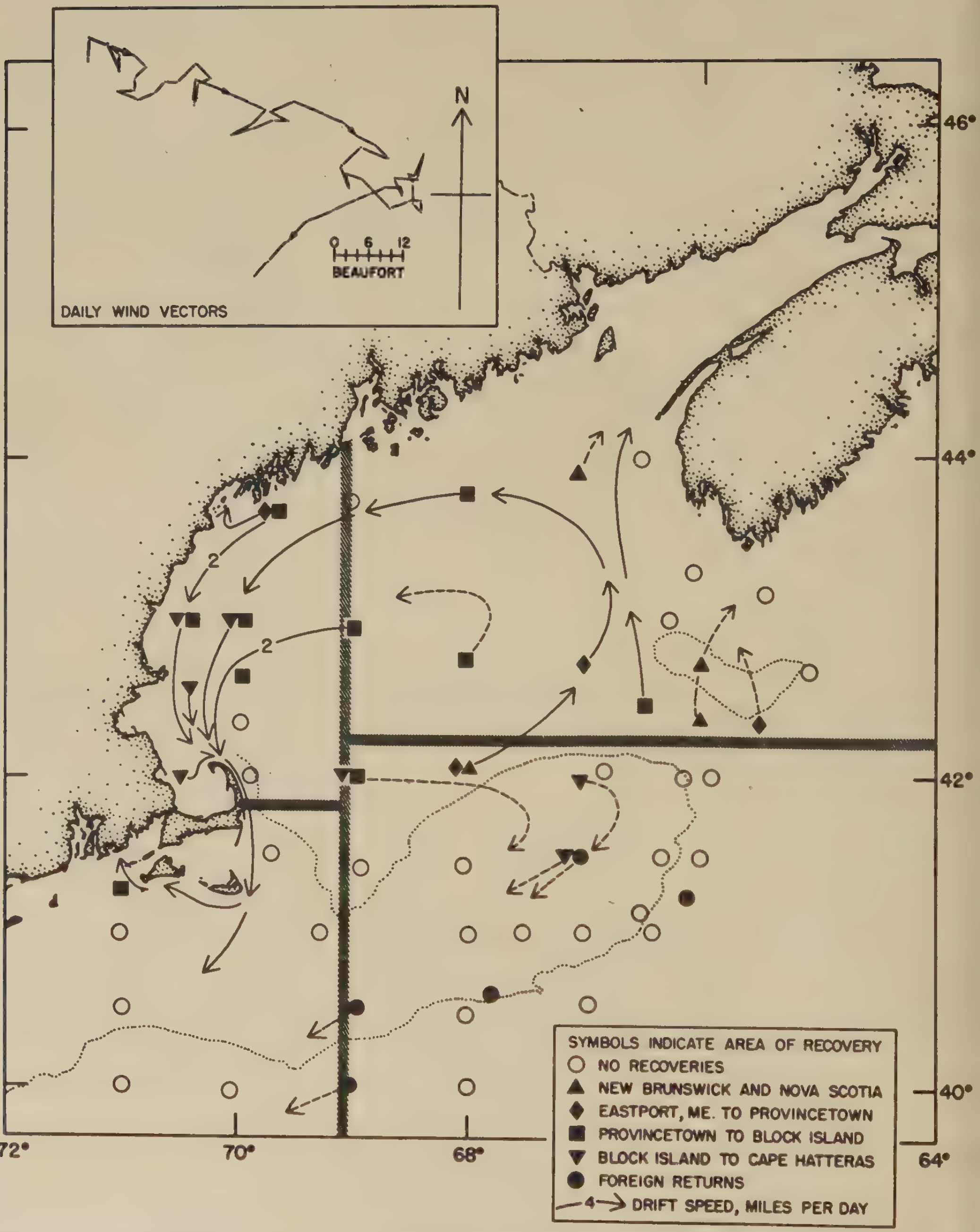
DAILY WIND VECTORS
N
0 6 12
BEAUFORT
46°
44°
42°
40°
72°
70°
68°
64°
2
2
SYMBOLS INDICATE AREA OF RECOVERY
○ NO RECOVERIES
▲ NEW BRUNSWICK AND NOVA SCOTIA
◆ EASTPORT, ME. TO PROVINCETOWN
■ PROVINCETOWN TO BLOCK ISLAND
▼ BLOCK ISLAND TO CAPE HATTERAS
● FOREIGN RETURNS
—4→ DRIFT SPEED, MILES PER DAY

FIGURE 3.—Surface circulation in the Gulf of Maine as deduced from recoveries of drift bottles launched by *Albatross III*, on cruise 57, February 21–March 2, 1955.

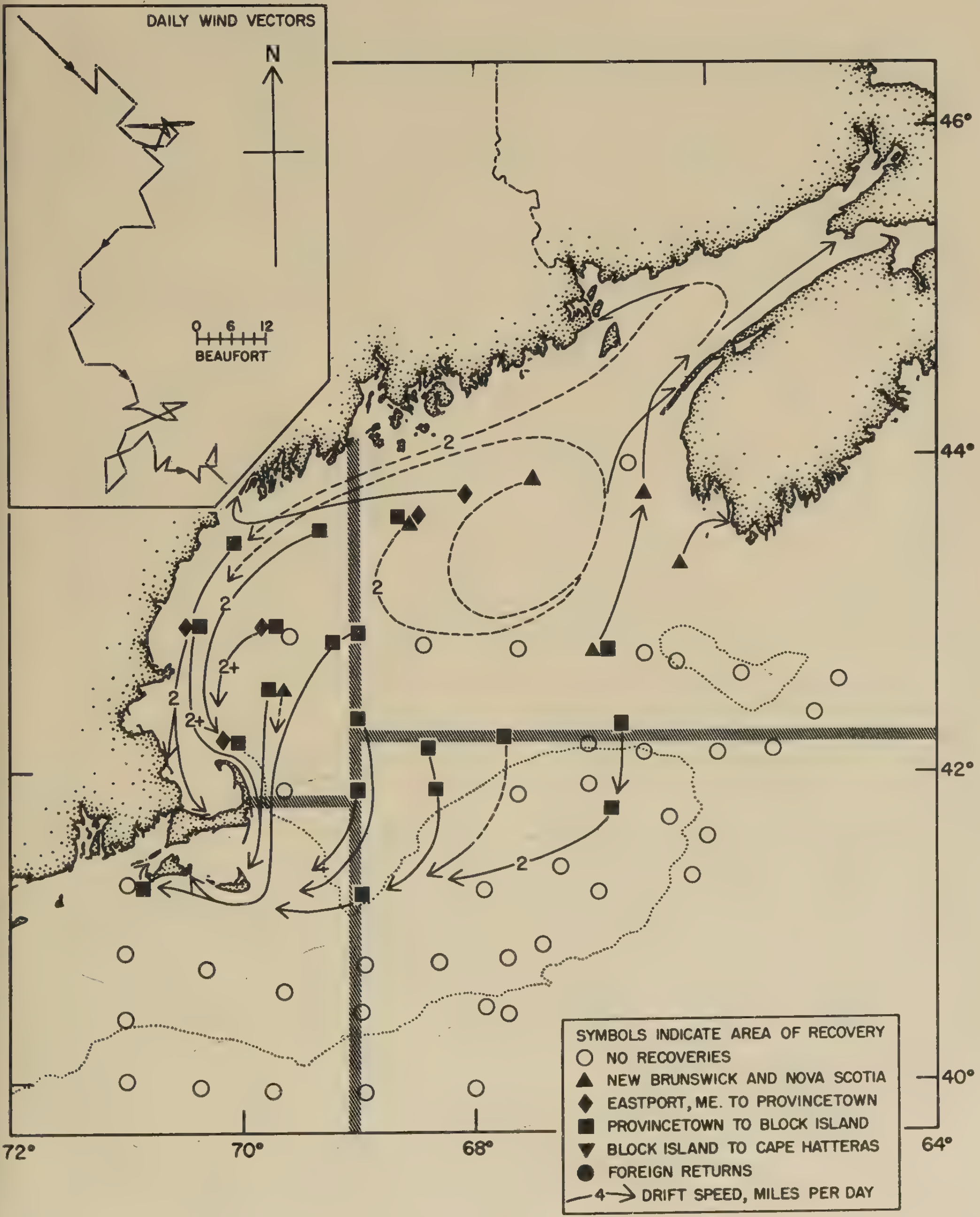
DAILY WIND VECTORS
N
0 6 12
BEAUFORT
46°
44°
42°
40°
72°
70°
68°
64°
2
2
2
2+
2
2+
2
SYMBOLS INDICATE AREA OF RECOVERY
○ NO RECOVERIES
▲ NEW BRUNSWICK AND NOVA SCOTIA
◆ EASTPORT, ME. TO PROVINCETOWN
■ PROVINCETOWN TO BLOCK ISLAND
▼ BLOCK ISLAND TO CAPE HATTERAS
● FOREIGN RETURNS
—4→ DRIFT SPEED, MILES PER DAY

FIGURE 4.—Surface circulation deduced from recoveries of drift bottles launched by *Albatross III*, on cruise 71, February 20–March 2, 1956.

comparable though slightly in excess of those for 1955.

In area II, three salient features appear: The Gulf eddy has been confined to the northeast; there are no returns from the Browns Bank region and the northward flow toward the bay of Fundy is singularly weak and displaced westward; and there appears no flow from northern Georges Bank toward the Bay of Fundy. The movement here is sharply toward Cape Cod and the islands.

Conditions in area III are very like those of a year earlier. Only one out of nine stations has been heard from to date, this one being close to Gay Head. No bottles have been picked up to the westward, contrary to the pattern of later seasons.

Area IV shows conditions during cruise 71 that are unique among our 17 cruises. All signs point to strong southerly movement normal to the usual easterly flow at the confluence of the Gulf and Georges eddies, along the north edge of the Bank. As was the case in cruise 57, no local United States returns have been had from stations south of 41°N. latitude.

The wind vectors following this cruise show 10 days of winds from different quarters, essentially canceling each other, and then a period of northerlies of more than usual force for 20 days. This latter period, it appears, could well account for all the features described in the four areas. That the surface waters were wind influenced is apparent from a comparison of the first and last stations for the cruise, which were made to the southwest of Gay Head. There were no returns from station 1, which was followed by 11 days of northwesterlies; there were four returns from Vineyard Sound from station 60, which was followed by 10 days of mutually negating winds.

If one may make generalizations on the basis of two cruises, it may be said that when winds from the northwest quarter prevail during late February and early March, the idealized circulation in the region will be modified thus:

1. Surface waters from the western Gulf will tend to flow southward past Cape Cod and out South Channel, thus interrupting the Gulf eddy in this area and tending to confine it to the north and east.
2. The northward movement from Browns Bank into the Bay of Fundy will be greatly diminished, some water being deflected along the southeastern coast of Nova Scotia.
3. The usual westward movement of waters south of Nantucket and Martha's Vineyard will be deflected offshore or temporarily interrupted.
4. The Georges eddy will be ill-defined and tend to disappear as winds become more northerly.

Under these conditions, the survival chances for eggs or larvae are small, unless confined to the northeastern sector of the Gulf.

GROUP *B* CRUISES: LATE MARCH AND EARLY APRIL

Albatross III cruise 46, March 19–April 2, 1953 (Figure 5)

A southerly movement of 4 miles per day generally parallel to the coast characterizes the waters in area I for this period. There is no indication from drifts for this cruise that the Gulf eddy is yet established, as there appears to be no return flow from this region to the northeast.

The northward flow from Browns Bank and the tip of Georges Bank in area II is firmly established, as is the veering to the northwest toward the coast of Maine, thus completing the eastern and northern segments of the eddy. Velocities up to 4 miles a day agree with those in area I. The picture agrees well with that of Bigelow, except in the southwestern part of the area.

The westerly drift south of Cape Cod and the islands is established in area III. Three unballasted bottles launched just east of the Cape moved northwest at 5 miles a day, driven by 5 days of wind from the southeast and east. The expected movement here is southerly.

Only three drift-bottle returns were had from Georges Bank in area IV. Two of these bottles moved westward to Long Island and Oregon Inlet at better than 2 miles a day. The third probably followed the path suggested by Bigelow, veered off the southern edge of the Banks and traveled at nearly 4 miles a day to the neighborhood of Sable Island.

The pattern of no-return stations for this cruise suggests an outflow from the Gulf across eastern Georges Bank, breaking the southern segment of the Gulf eddy. It is unusual to have a concentration of no-return stations occur so far to the north in the Gulf as it did on this cruise.

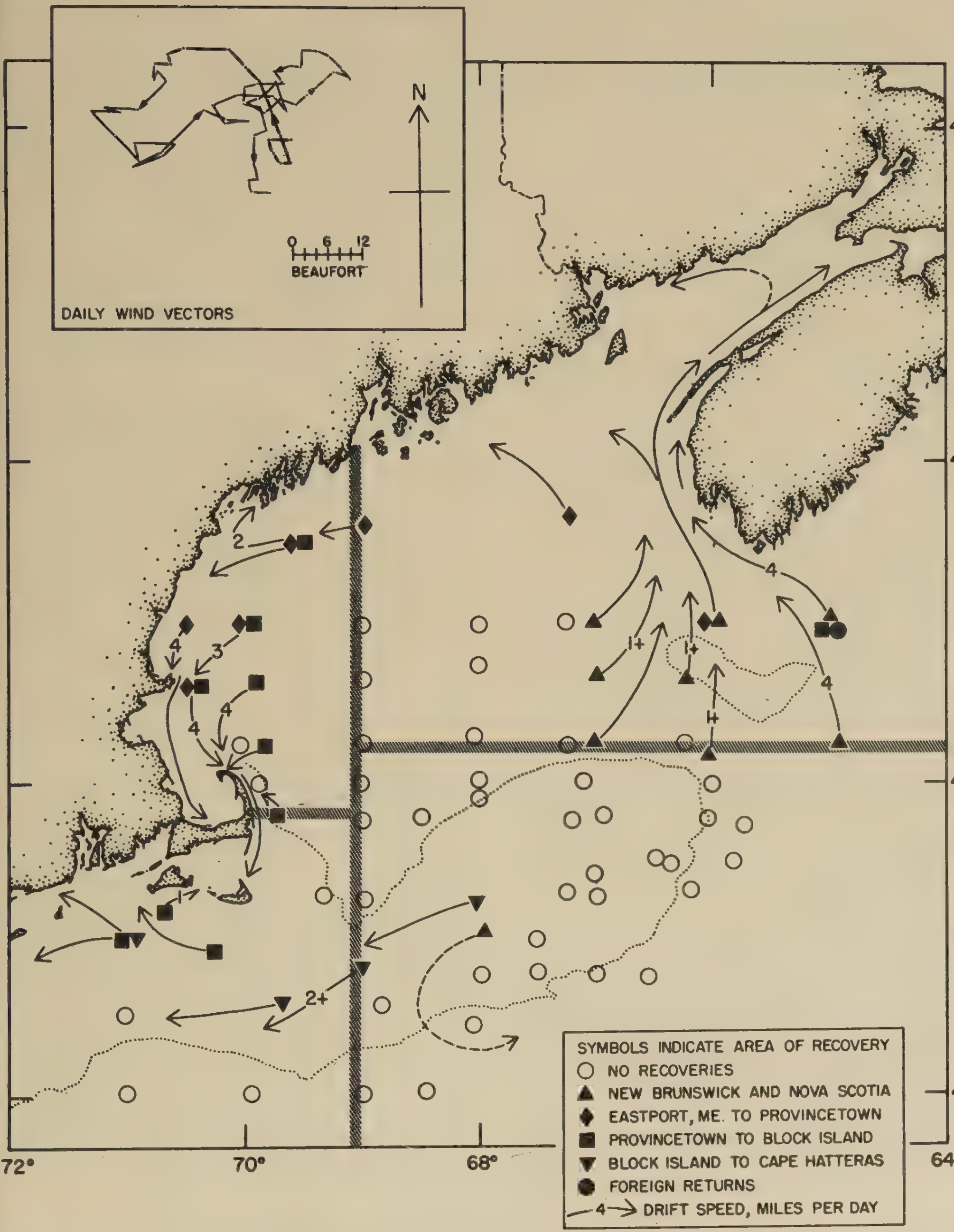
DAILY WIND VECTORS
N
0 6 12
BEAUFORT
46°
44°
42°
40°
72°
70°
68°
64°
2
4
3
4
4
1
1+
1+
1+
4
4
2+
SYMBOLS INDICATE AREA OF RECOVERY
○ NO RECOVERIES
▲ NEW BRUNSWICK AND NOVA SCOTIA
◆ EASTPORT, ME. TO PROVINCETOWN
■ PROVINCETOWN TO BLOCK ISLAND
▼ BLOCK ISLAND TO CAPE HATTERAS
● FOREIGN RETURNS
—4→ DRIFT SPEED, MILES PER DAY

FIGURE 5.—Surface circulation deduced from recoveries of drift bottles launched by *Albatross III*, on cruise 46, March 19–April 2, 1953.

It is not possible to see any wind influence during this cruise except on the very short drifts we have mentioned. Wind vectors for the 60 days following the last bottle drop tend to counteract one another.

Albatross III cruise 58, March 19–April 1, 1955 (Figure 6)

The net drift in area I during this period is southerly, but there appears to be a strong westward, onshore component with no sign of an eastward return of the Gulf eddy.

Circulation in area II is in general agreement with that described by Bigelow for this area, except that the southern segment of the Gulf eddy is broken.

Of 120 bottles launched in area III, only two returns were had, they being from Maryland and Virginia. This agrees with the large number of bottles from north of Cape Cod and from Georges Bank which ultimately stranded to the west.

A good number of drift-bottle returns were had from Georges Bank, all showing a southwest movement but giving little indication of an anticyclonic eddy around the Bank.

The wind vectors show the first directional dominance to be northeasterly beginning 20 days after the end of the cruise, when there were 5 consecutive days of force-5 winds from this quarter. There is little doubt that winds of this force and duration influenced surface movement, but whether they alone produced the southwesterly movement which characterizes this group of bottles cannot be stated.

Albatross III cruise 72, March 21–31, 1956 (Figure 7)

Unfortunately, this cruise did not cover the northern part of the Gulf of Maine; as a result, little can be deduced about the state of the Gulf eddy at this time.

Only three bottle-drop stations were made in area I. Of the total of 36 bottles put out, 2 were recovered in area III some months later.

Area II shows surface water movement of better than 2 miles a day from western Browns Bank north into the Bay of Fundy. Stations east of Browns Bank were not heard from.

There were good returns from offshore stations in area III, which show a pronounced northerly component to the usual westward flow expected here.

Returns from Georges Bank (area IV) indicate a southwest movement, probably becoming more westerly somewhere in the vicinity of South Channel. There are no returns to indicate the existence of the Georges eddy. The tendency for bottles to move westward beyond Block Island, as in the previous cruise, is not seen here.

Vectors show winds to be more directional for this cruise than for the two other cruises in group *B*. There was a slight northwesterly set during the first 38 days following the last bottle-drop station. This gave way to southwesterlies which predominated for the next 30 days and so markedly influenced the results of the succeeding cruise (cruise 73, fig. 13). Comparison of cruises 72 and 73 indicate that the critical winds occur during the first month following a cruise. Thus, to estimate loss or survival of fish eggs and larvae, accurate knowledge as to dates and location of the heaviest spawning is essential.

The three cruises of group *B*, which cover the last 10 days of March for 3 different years, have these points in common.

1. The Gulf eddy is complete on the eastern, northern, and western segments in 1953 and 1955 (cruises 46 and 58), but appears broken on the southern segment, the movement here being either offshore or southwesterly across Georges Bank and out of the Gulf.
2. The northern sector of the Georges eddy, where it sometimes becomes confluent with the Gulf eddy, is not apparent. The surface-water movement is southwesterly across the Bank.
3. The generally westward movement south of Cape Cod and the islands appears established.
4. It would appear that surface plankton in the central and western Gulf of Maine or over Georges Bank would have been carried out of the region in a southwesterly direction in 1955 and 1956 and possibly offshore in 1953.

INTERMEDIATE CRUISE

Albatross II cruise, April 4–18, 1932 (Figure 8)

This cruise is intermediate, seasonally speaking, between groups *B* and *C*, and is treated separately. Bottles were seeded only over the south-

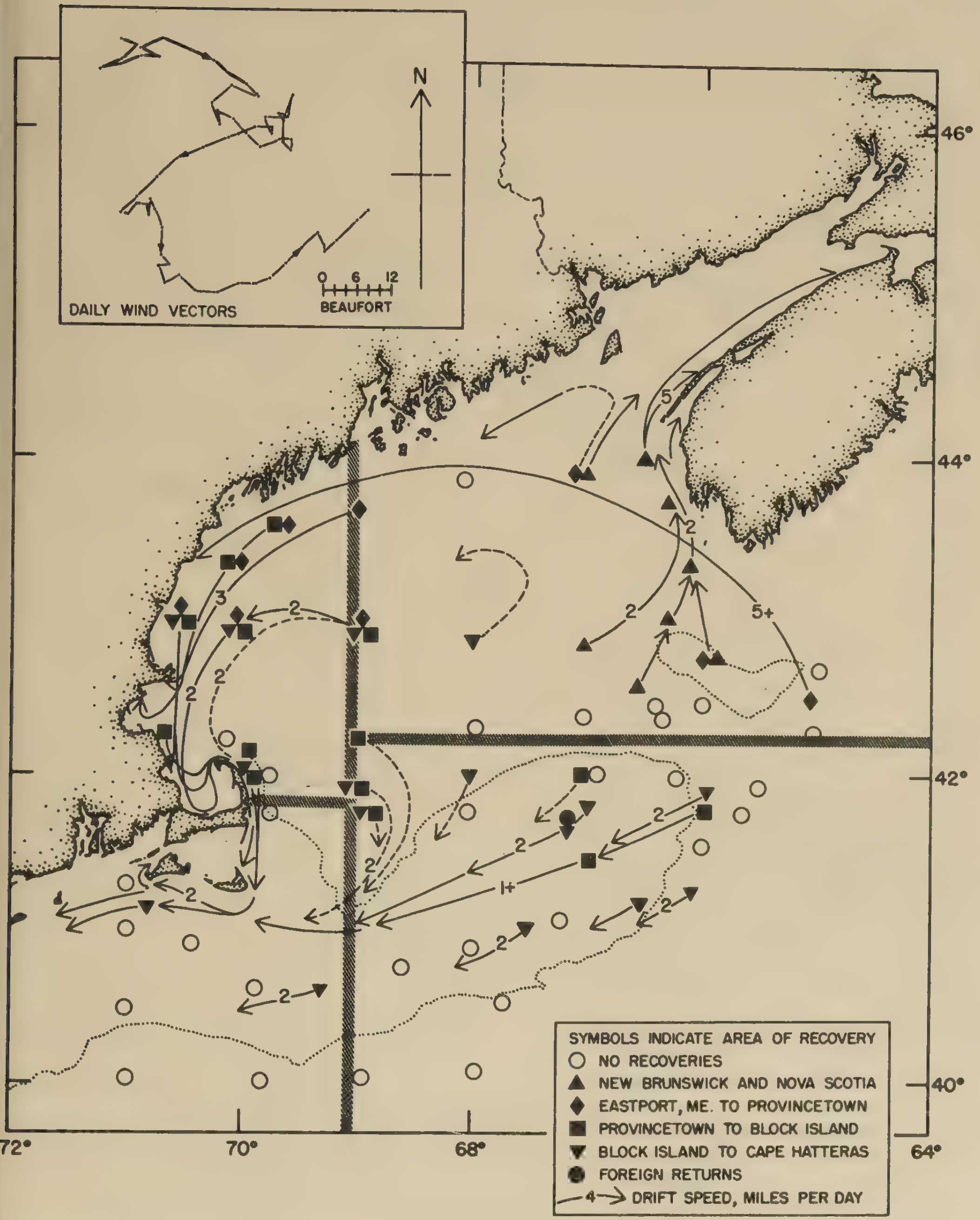
DAILY WIND VECTORS
N
0 6 12
BEAUFORT
46°
44°
42°
40°
72°
70°
68°
64°
5
2
3
2
2
2
5+
2
2
2
2
1+
2
2
2
2
2
2
SYMBOLS INDICATE AREA OF RECOVERY
○ NO RECOVERIES
▲ NEW BRUNSWICK AND NOVA SCOTIA
◆ EASTPORT, ME. TO PROVINCETOWN
■ PROVINCETOWN TO BLOCK ISLAND
▼ BLOCK ISLAND TO CAPE HATTERAS
● FOREIGN RETURNS
—4→ DRIFT SPEED, MILES PER DAY

IGURE 6.—Surface circulation deduced from recoveries of drift bottles launched by *Albatross III*, on cruise 58, March 19–April 1, 1955.

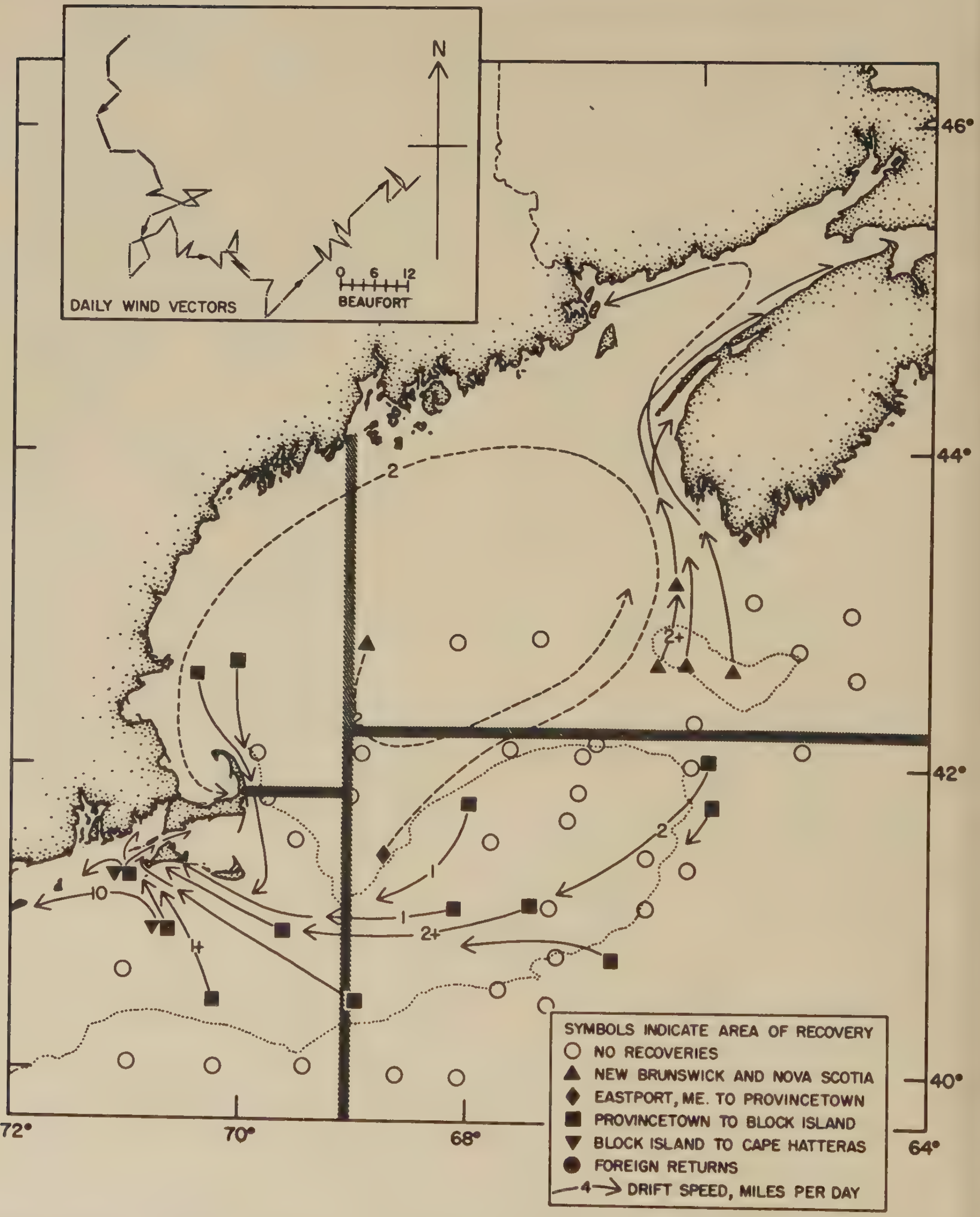
DAILY WIND VECTORS
N
0 6 12
BEAUFORT
46°
44°
42°
40°
72°
70°
68°
64°
2
2+
2
1
1
2+
2
10
4
SYMBOLS INDICATE AREA OF RECOVERY
○ NO RECOVERIES
▲ NEW BRUNSWICK AND NOVA SCOTIA
◆ EASTPORT, ME. TO PROVINCETOWN
■ PROVINCETOWN TO BLOCK ISLAND
▼ BLOCK ISLAND TO CAPE HATTERAS
● FOREIGN RETURNS
—4→ DRIFT SPEED, MILES PER DAY

FIGURE 7.—Surface circulation deduced from recoveries of drift bottles launched by *Albatross III*, on cruise 72, March 21–31, 1956.

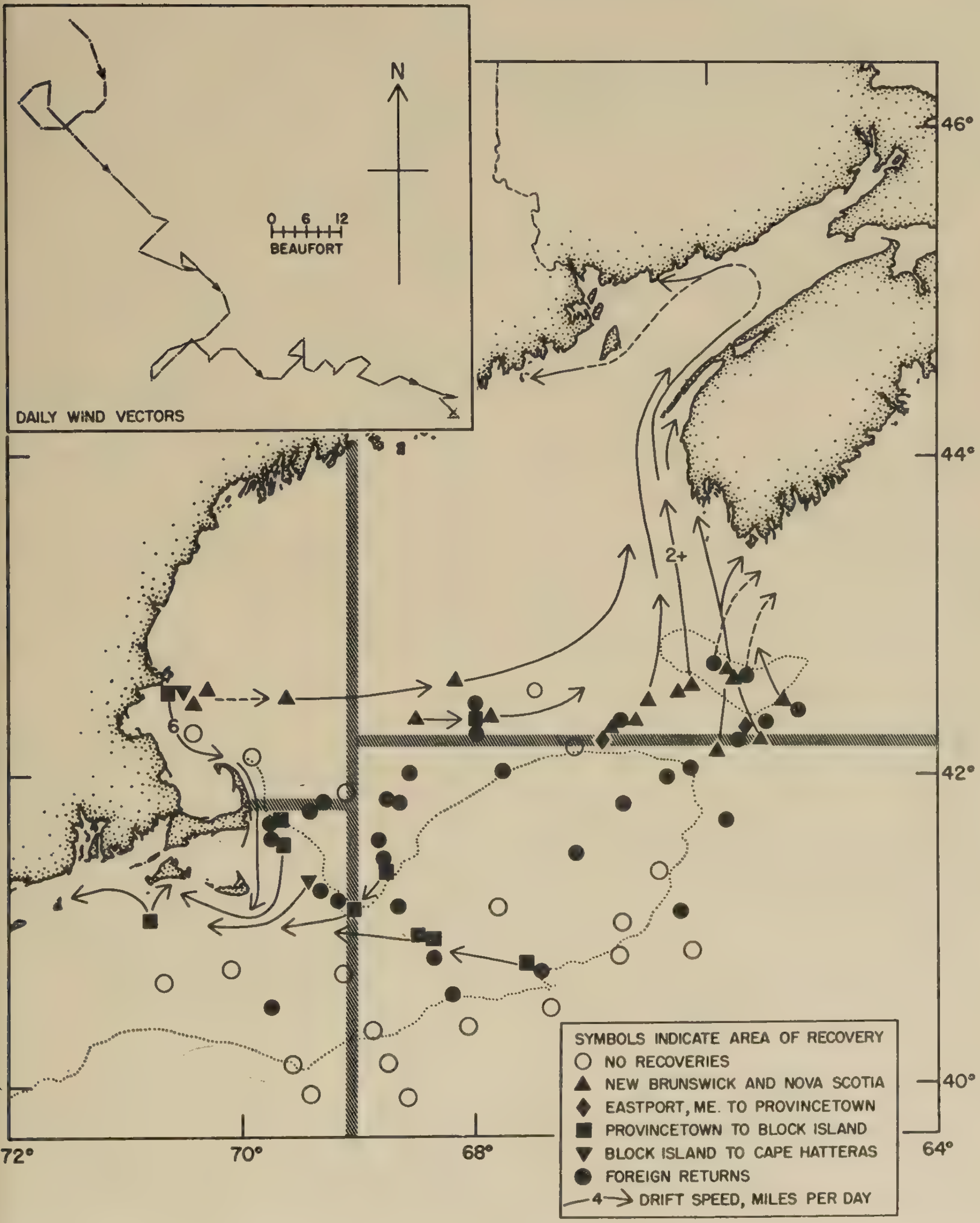
N
0 6 12
BEAUFORT
DAILY WIND VECTORS
46°
44°
42°
40°
72°
70°
68°
64°
2+
6
SYMBOLS INDICATE AREA OF RECOVERY
○ NO RECOVERIES
▲ NEW BRUNSWICK AND NOVA SCOTIA
◆ EASTPORT, ME. TO PROVINCETOWN
■ PROVINCETOWN TO BLOCK ISLAND
▼ BLOCK ISLAND TO CAPE HATTERAS
● FOREIGN RETURNS
4→ DRIFT SPEED, MILES PER DAY

FIGURE 8.—Surface circulation deduced from recoveries of drift bottles launched by *Albatross II*, April 4–18, 1932.

ern part of our region of study, but certain characteristics are well defined.

For the first time, seasonally speaking, the southern segment of the Gulf eddy appears clearly, with bottles seeded north of Cape Cod returning to Canadian waters. The northward movement from Browns Bank toward the Bay of Fundy is apparent.

From Georges Bank and South Channel, there is a preponderance of returns from abroad with little indication of the initial route followed by the bottles. Whether the bottles first started toward the west or traveled downwind in a southeasterly direction, it is apparent that the surface-water movement was away from the region of study. As there were more returns than normal from Newfoundland, Sable Island, and eastern Nova Scotia, and fewer than usual from Long Island, it would seem reasonable to assume that the bottles followed a downwind course in moving out of the region.

In discussing the circulation deduced from the *Albatross II* cruises (figs. 8 and 9), Walford (1938, p. 49) states: "It is evident * * * that there was a very important difference between the circulatory picture in the season of 1932 and that of the corresponding period of 1931."

Inspection of the wind vectors for these cruises appears to indicate wherein the difference lies. In 1931 they show little directional dominance, while in 1932 the offshore tendency is clearcut. That winds are often responsible for anomalies in circulation in this region cannot be denied. Better understanding is needed of how winds from different quarters may establish or modify the circulation of water depending on their force and duration.

GROUP *C* CRUISES: LATE APRIL AND EARLY MAY

Albatross II cruise, April 17–29, 1931 (Figure 9)

This cruise, confined to Georges Bank, covers areas III and IV only. The drift-bottle returns, however, indicate that the southern segment of the Gulf eddy has appeared, joining the northward-moving water over Browns Bank.

Area III shows a strong northerly set which is eventually deflected westward closer to land. This movement agrees with the clockwise eddy which is now firmly established around Georges Bank at a minimum rate of 2 miles a day. The six foreign returns were from stations along the southern edge of the Bank; they could have veered southward from the eddy in the manner suggested by Bigelow or have moved southwest toward Cape Hatteras and there entered the Gulf Stream.

Winds for 30 days following the cruise show that they probably had little effect on the surface-water movement.

Atlantis cruise 28, April 27–May 13, 1934 (Figure 10)

This cruise, also limited to the south and east, nevertheless shows the Gulf eddy as established in these areas, and it seems reasonable to assume that it was complete on the northern and western sectors as well. From Browns Bank, some bottles tended eastward and some into the Bay of Fundy, a situation which may reflect the conflicting winds which characterize the 50-day period following the cruise.

The surface movement in area III is southward out South Channel and thence westward, with none of the northerly motion noticeable in the preceding cruise. Only 1 of the 101 returns came from the Nantucket-Martha's Vineyard area, while many came ashore on Long Island and points west.

The Georges eddy in area IV is quite apparent at this time, as is the southern segment of the Gulf eddy where the two seem to meet north of the Bank. A surprising aspect is the fact that 36 of the 101 bottle returns came from overseas; stranding points were widely distributed between Norway and the Bahamas. There is nothing in the wind pattern to explain this offshore tendency. In view of the large number of recoveries between Long Island and Cape Hatteras, it may well be that the "foreign" bottles initially moved in this direction before entering the Gulf Stream near Cape Hatteras.

Albatross III cruise 48, April 24–May 8, 1953 (Figure 11)

The drift pattern in area I agrees well with Bigelow, except that the return flow of the Gulf eddy does not extend as far south as he shows it. Southward velocities along the coast are 3 miles a day.

Water movement in area II agrees almost exactly with Bigelow, as does that in area III.

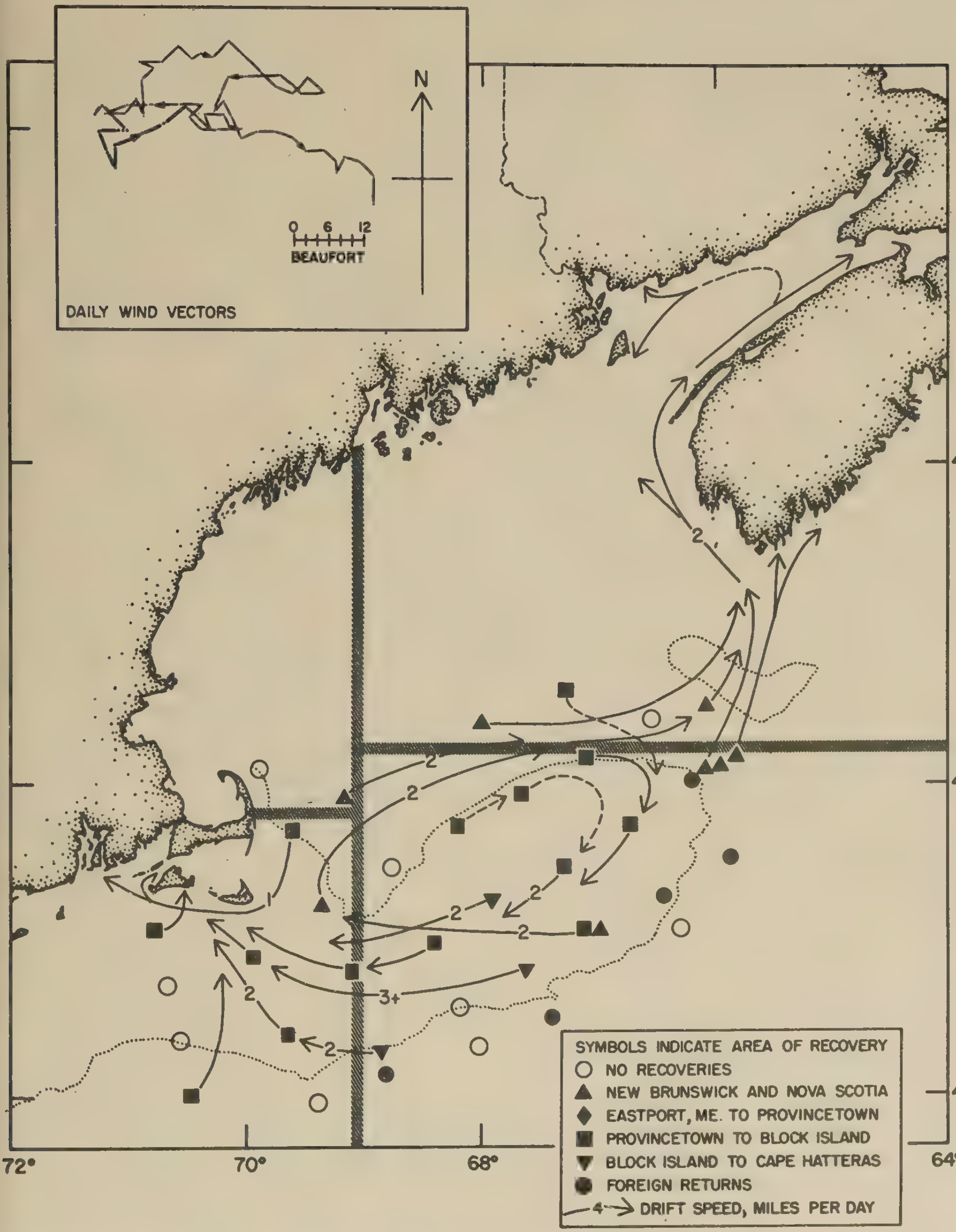
DAILY WIND VECTORS
N
0 6 12
BEAUFORT
44°
42°
40°
72°
70°
68°
64°
2
2
2
1
2
2
2
2
3+
2
SYMBOLS INDICATE AREA OF RECOVERY
○ NO RECOVERIES
▲ NEW BRUNSWICK AND NOVA SCOTIA
◆ EASTPORT, ME. TO PROVINCETOWN
■ PROVINCETOWN TO BLOCK ISLAND
▼ BLOCK ISLAND TO CAPE HATTERAS
● FOREIGN RETURNS
—4→ DRIFT SPEED, MILES PER DAY

FIGURE 9.—Surface circulation deduced from recoveries of drift bottles launched by *Albatross II*, April 17–29, 1931.

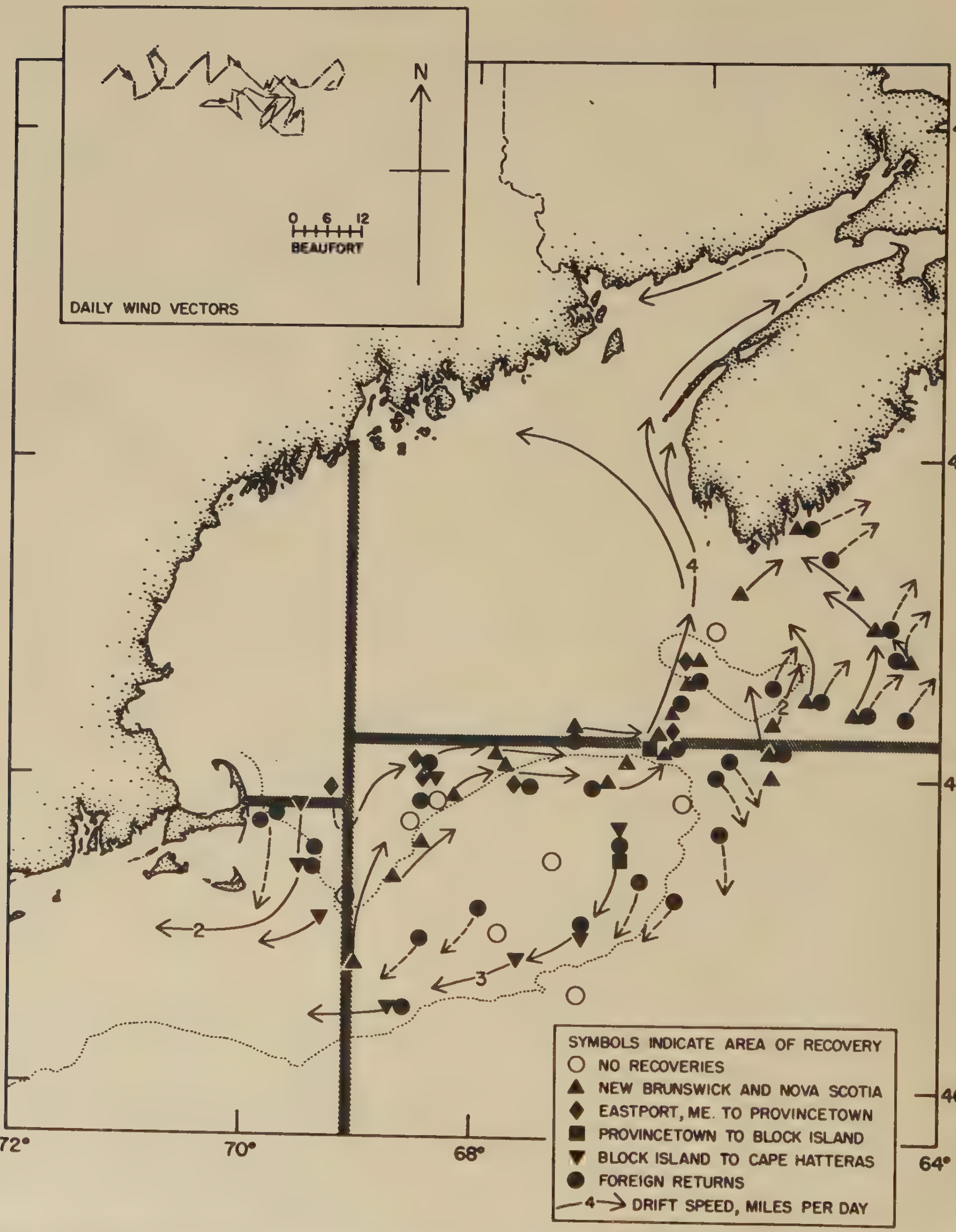
DAILY WIND VECTORS
0 6 12
BEAUFORT
N
46°
44°
42°
40°
72°
70°
68°
64°
4
2
2
3
SYMBOLS INDICATE AREA OF RECOVERY
○ NO RECOVERIES
▲ NEW BRUNSWICK AND NOVA SCOTIA
◆ EASTPORT, ME. TO PROVINCETOWN
■ PROVINCETOWN TO BLOCK ISLAND
▼ BLOCK ISLAND TO CAPE HATTERAS
● FOREIGN RETURNS
—4→ DRIFT SPEED, MILES PER DAY

FIGURE 10.—Surface circulation deduced from recoveries of drift bottles launched by *Atlantis*, on cruise 28, April 27–May 13, 1934.

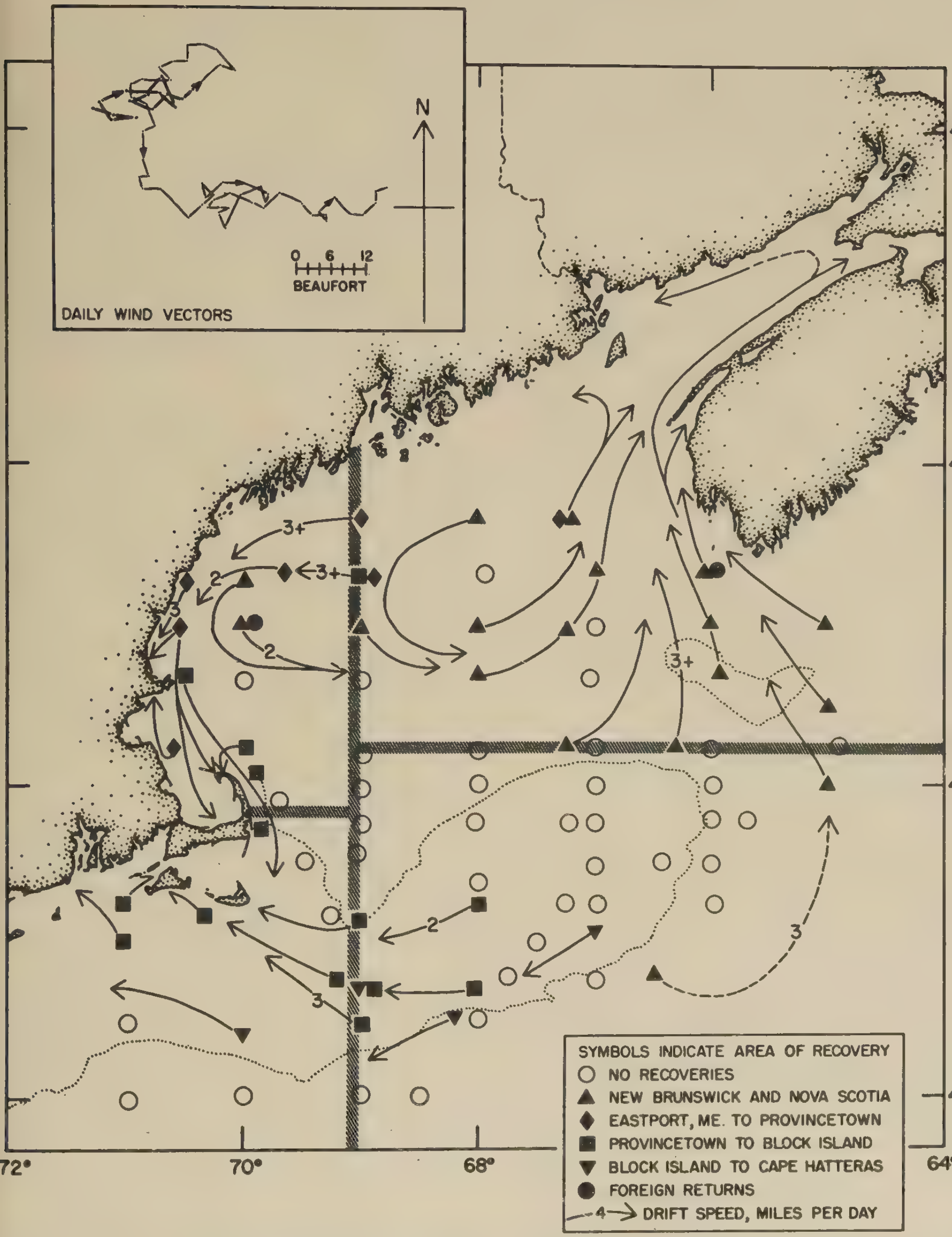
DAILY WIND VECTORS
N
0 6 12
BEAUFORT
46°
44°
42°
40°
72°
70°
68°
64°
3+
2
3
2
3+
2
3
3
3+
SYMBOLS INDICATE AREA OF RECOVERY
○ NO RECOVERIES
▲ NEW BRUNSWICK AND NOVA SCOTIA
◆ EASTPORT, ME. TO PROVINCETOWN
■ PROVINCETOWN TO BLOCK ISLAND
▼ BLOCK ISLAND TO CAPE HATTERAS
● FOREIGN RETURNS
—4→ DRIFT SPEED, MILES PER DAY

FIGURE 11.—Surface circulation deduced from recoveries of drift bottles launched by *Albatross III*, on cruise 48. April 24–May 8, 1953.

Though bottle returns from area IV indicate no Georges eddy, the number of no-return stations in the southern Gulf and northern edge of the Bank can reasonably be assumed to show a general eastward movement through the region with a pronounced outflow off eastern Georges Bank. If this were the case, then the circulation could be said to agree very well with Bigelow's diagram.

All told, this cruise in late April and early May of 1953 is the first to agree with Bigelow in all four areas.

Albatross III cruise 60, April 19–May 3, 1955 (Figure 12)

There were 21 drift-bottle returns from the five stations north of Cape Ann in area I, which show the occurrence of unusual velocities of from 8 to 12 miles a day. Thirteen of these bottles (three with and ten without ballast) came ashore before the end of the cruise on May 4 and very obviously owe their high speeds to a fair wind augmenting the usual southwesterly movement (see vectors, fig. 12). In the southern part of the area, the same winds undoubtedly account for the pronounced water movement out South Channel with no indication of easterly flow in the Gulf eddy.

The cyclonic movement around Browns Bank in area II was drawn because it best fits the wind pattern and logically explains the no-return stations immediately to the northwest. The Gulf eddy is firm on the east and north.

Surface water in area III shows marked movement out South Channel. It is to be noted that there were no local returns from stations made at the start of the cruise in the region south of the islands when winds were northeasterly for some days: but four stations in this area were heard from locally at the end of the voyage, during a time that was characterized by calms and light westerlies. Thus, wind influence on the bottles released in this area may be called "marked."

The Georges eddy on the north is confirmed by one return from the Bay of Fundy with a second possibly making the circuit before going to the west. There were many returns from southern Georges Bank, which fit well with the northwesterly movement seen in area III during this period.

As has been noted previously, the wind pattern, which is relatively clear-cut during and after the cruise, could be said to have had a marked influence on the drift of bottles released at this time.

Albatross III cruise 73, April 17–28, 1956 (Figure 13)

To date, there are only 7 returns from the 84 bottles put out at 7 stations in area I during this cruise. The difference here between this cruise and the other cruises in group *C* is marked and can only be attributed to the winds prevailing at this time. With the exception of two bottles coming into the area from the east, little or no southerly movement of surface water is indicated. That there were no returns from the station immediately south of Cape Ann can only be explained by the winds.

The northward movement of water into the Bay of Fundy appears displaced slightly to the west, with velocities of 4 miles a day. The one return from south of Browns Bank shows a net movement of 75 miles in 95 days, which tells little. The northeasterly motion along the Nova Scotian side of the Bay of Fundy is accelerated to 6 miles a day.

Area III shows no southerly movement of bottles through South Channel, while south of the islands the usual westward flow is strongly deflected shoreward. The appearance and progression of this northerly deflection are apparent in the sequence of the five cruises in 1956, the deflection becoming more pronounced as the season advanced.

Two returns only were had from the entire Georges Bank region: one at Gay Head and the other in Buzzards Bay. It is hard to believe that these returns represent the dominant movement from the Bank, in view of the many no-return stations which surround the two points of release.

The first three cruises discussed under group *C* have wind patterns showing no very clear directional dominance. Thus it would appear possible to consider the deduced surface movement in these years to be fairly typical for the season. The cruises themselves agree reasonably well, and show, in general, that the idealized surface circulation as seen by Bigelow is taking shape for the first time, seasonably speaking. All three cruises show the Gulf eddy to be completed in its southern sector, a condition not noticeable in earlier cruises. The Georges eddy was clearly present in

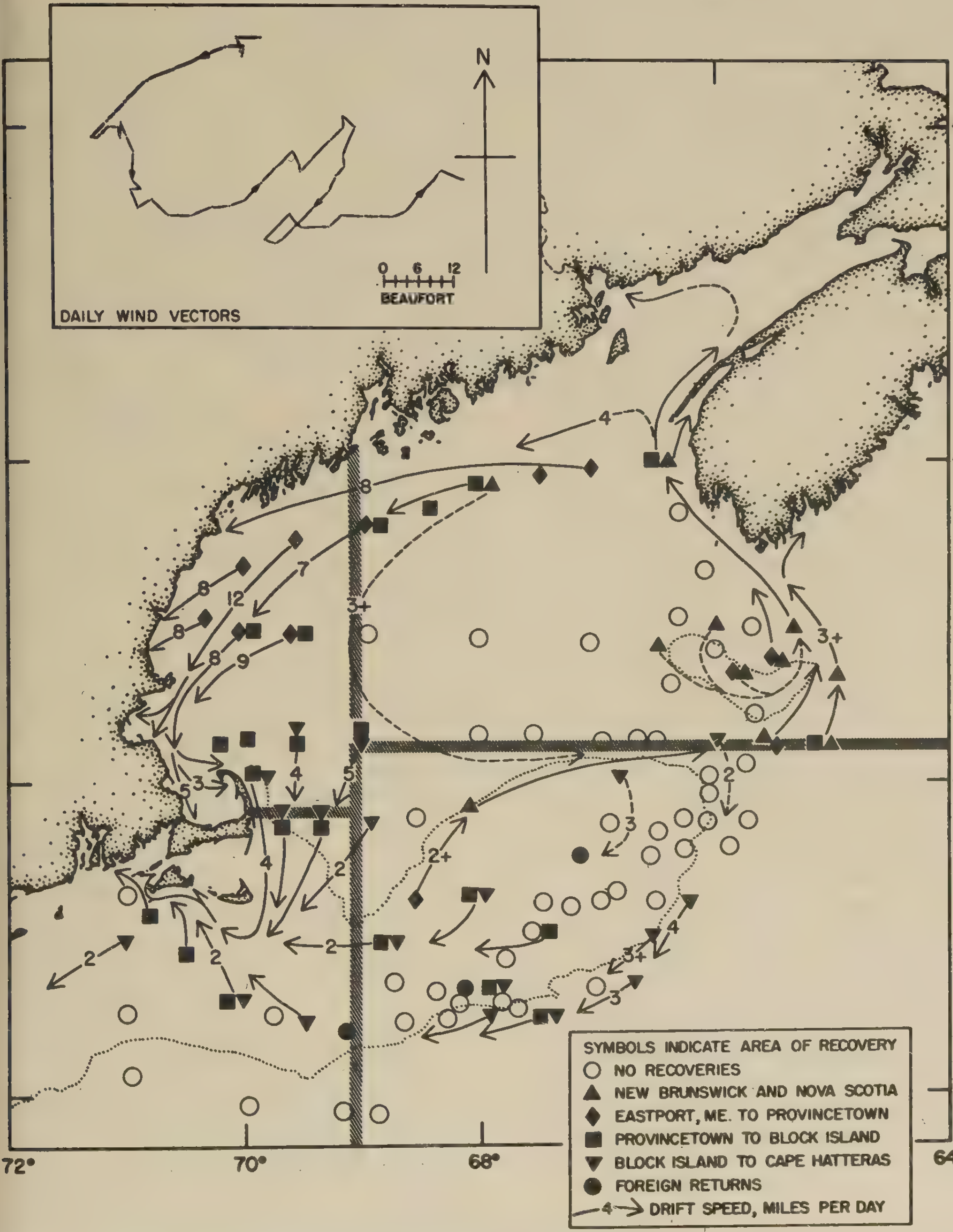
DAILY WIND VECTORS
N
0 6 12
BEAUFORT
46°
44°
42°
40°
72°
70°
68°
64°
SYMBOLS INDICATE AREA OF RECOVERY
○ NO RECOVERIES
▲ NEW BRUNSWICK AND NOVA SCOTIA
◆ EASTPORT, ME. TO PROVINCETOWN
■ PROVINCETOWN TO BLOCK ISLAND
▼ BLOCK ISLAND TO CAPE HATTERAS
● FOREIGN RETURNS
—4→ DRIFT SPEED, MILES PER DAY

Figure 12.—Surface circulation deduced from recoveries of drift bottles launched by *Albatross III*, on cruise 60, April 19–May 3, 1955.

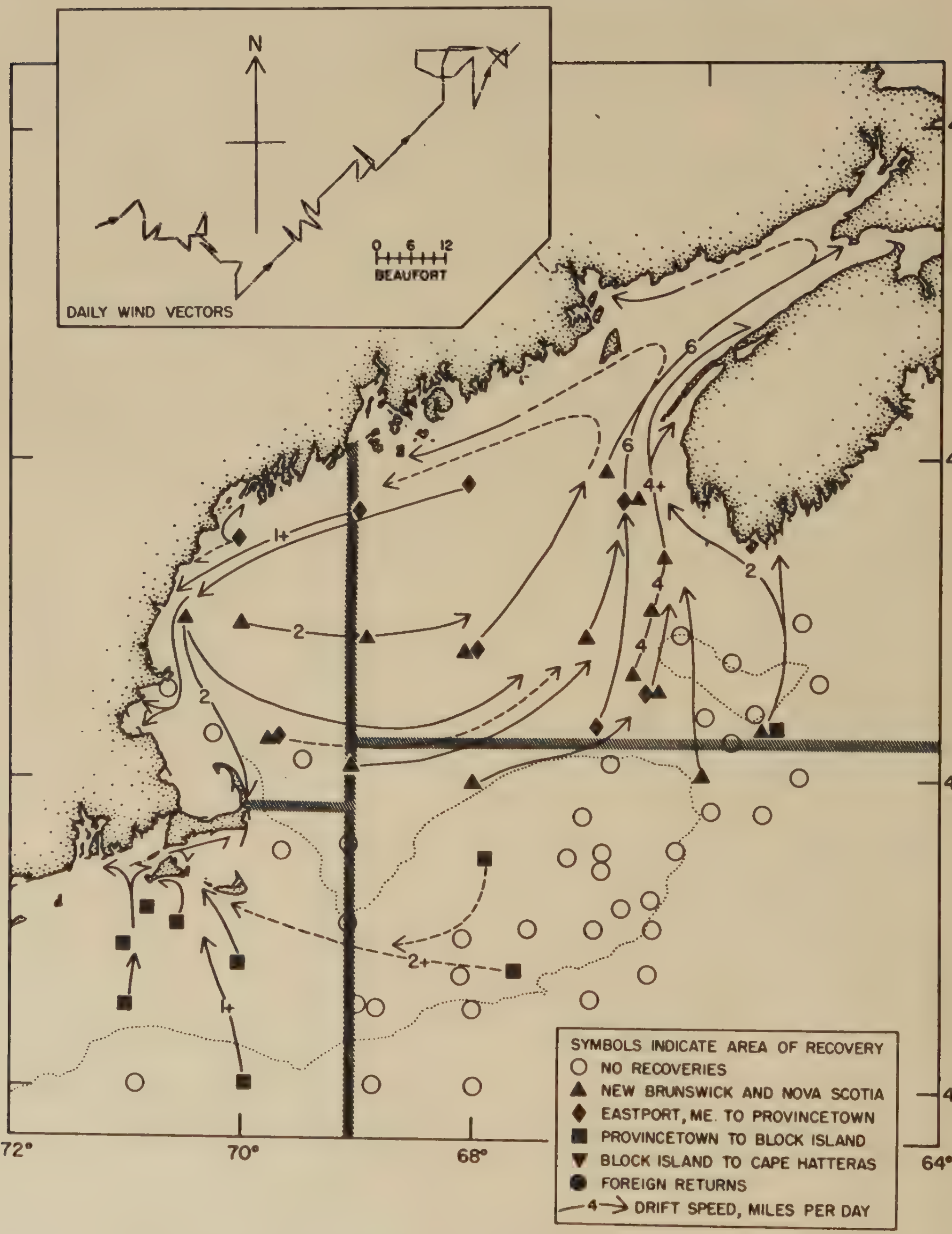
N
0 6 12
BEAUFORT
DAILY WIND VECTORS
46°
44°
42°
40°
72°
70°
68°
64°
1+
2
6
4+
4
2+
SYMBOLS INDICATE AREA OF RECOVERY
○ NO RECOVERIES
▲ NEW BRUNSWICK AND NOVA SCOTIA
◆ EASTPORT, ME. TO PROVINCETOWN
■ PROVINCETOWN TO BLOCK ISLAND
▼ BLOCK ISLAND TO CAPE HATTERAS
● FOREIGN RETURNS
—4→ DRIFT SPEED, MILES PER DAY

FIGURE 13.—Surface circulation deduced from recoveries of drift bottles launched by *Albatross III*, on cruise 73, April 17–28, 1956.

1931 and 1934, while in 1953 it can be considered present except on the eastern end where movement was probably offshore.

Cruise 60, in 1955, while indicating the presence of both the Georges Bank and Gulf eddies, clearly shows the effect of winds. The continuous northeast winds during the cruise and northerly winds for the 12 days following apparently accelerated water movement along the northern and western edges of the Gulf and greatly augmented the seaward flow through South Channel. The western segment of the Gulf eddy was probably displaced eastward. The winds were not strong enough or of sufficient duration to destroy the northeastward flow of the Georges eddy, however.

Cruise 73, in 1956, shows even more wind dominance. The northwest winds during and for 10 days following the cruise appear to have lasted long enough to move bottles offshore along the western edge of the Gulf and confine the southern edge of the Gulf eddy to the north. Bottles from the eastern half of Georges Bank were moved out of the area, probably to the east, and the presence of a Georges eddy is in question. Movement south of Cape Cod and the islands has a pronounced northerly direction, probably being deflected by the southwest winds starting 11 days after the cruise (see cruises 75 and 76, p. 468).

GROUP *D* CRUISES: LATE MAY AND EARLY JUNE

Albatross II cruise, May 26–28 and June 3–7, 1931 (Figure 14)

The Georges eddy is clearly delineated here, the southwestward movement over the southern part being the most pronounced. The southerly flow out of South Channel is evident, as is the westward flow south of the islands. Winds immediately following the end of the cruise are contradictory.

Albatross III cruise 50, May 25–June 2, 1953 (Figure 15)

From the northern part of area I, the Gulf eddy carried bottles to the tip of Cape Cod at speeds of 5 miles a day and thence northeast into Canadian waters at better than 2 miles a day. From the southern stations, bottles were probably swept offshore into the Georges Bank region by the dominant northerly and westerly winds.

In area II, the southern segment of the Gulf eddy moved slightly northward, there being no returns from South Channel or northern Georges Bank. The northward flow into the Bay of Fundy is represented by returns from four stations, giving a velocity of 4 miles a day.

Area III showed a few scattered returns from stations near shore.

In area IV, cruise 50 is unique among the 17 cruises in that there were no returns from the numerous stations over Georges Bank. While it was in this year (cruises 46, 48, and 50) that some of the ballasted bottles sank (see p. 471), it is still remarkable that none of those without ballast (114 bottles seeded in area IV) have turned up locally or from abroad. The scatter of no-return stations for this cruise indicates a pronounced offshore movement of surface water from the southern Gulf and from Georges Bank to an extent that would have removed any surface eggs and larvae in those regions.

Albatross III cruise 61, May 16–28, 1955 (Figure 16)

The overall picture for this cruise agrees well with Bigelow. The southerly movement through area I and the return flow of the Gulf eddy are both present, as is the flow out South Channel.

Area II shows the eddy complete with speeds of 3 miles a day on the south and east and of 5 miles a day along the coast of Maine.

Surface water drift in area III agrees with Bigelow's diagram, except that the onshore movement south of the islands is again present.

It is probably safe to assume a northeasterly flow along the inner edge of Georges Bank and a seaward movement over the eastern end of the Bank. The southern part has a movement to the westward of 3 miles a day. Returns were had from well offshore which confirms the northwesterly movement apparent in area III.

The northerly component found in area III, and sometimes in area IV, seems to develop when winds are from the west and southwest, as they were during and after this cruise.

Albatross III cruise 75, May 16–29, 1956 (Figure 17)

Area I shows the influence of the dominant offshore wind system during this period. The return flow of the Gulf eddy is clearly marked but is dis-

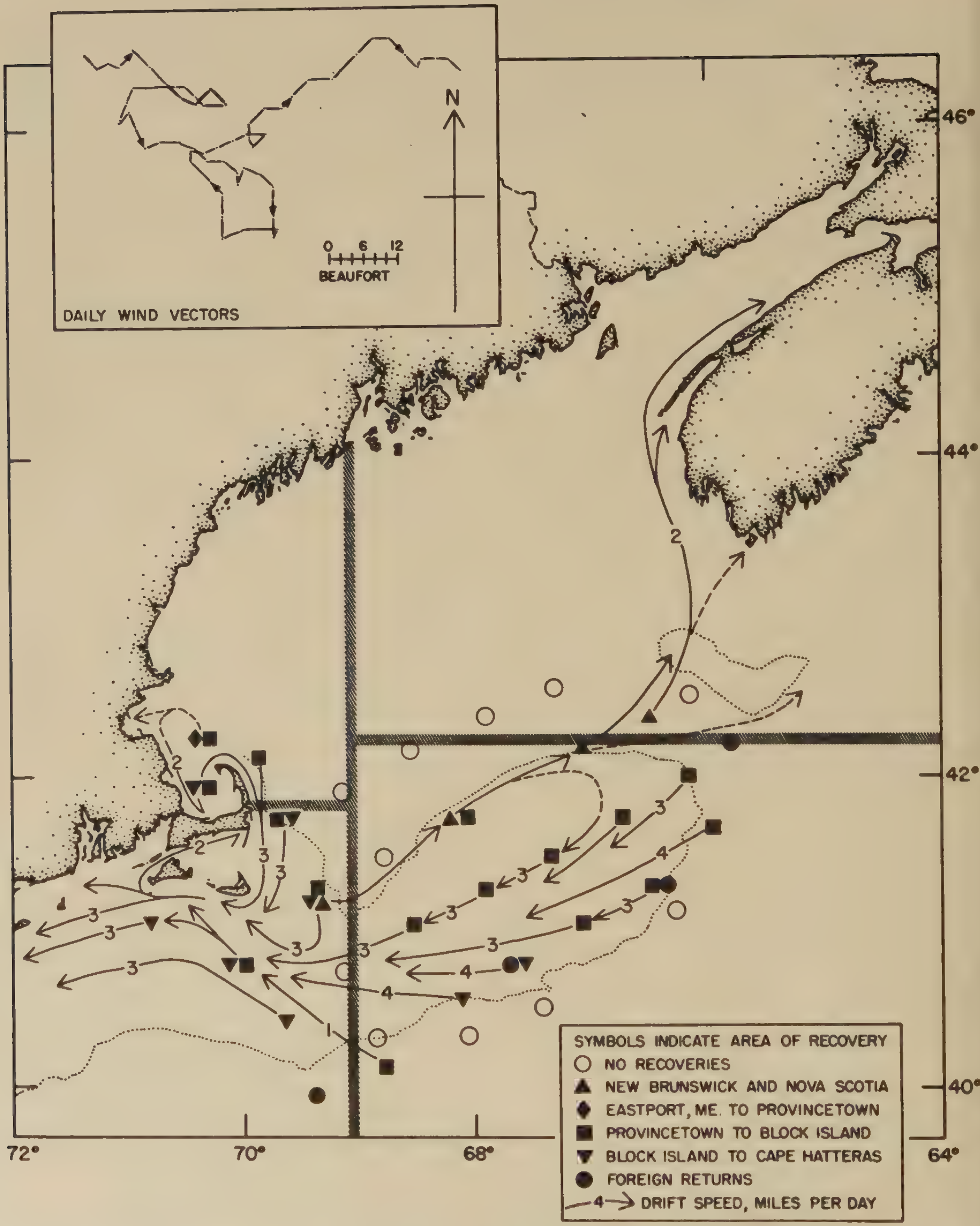
DAILY WIND VECTORS
N
0 6 12
BEAUFORT
46°
44°
42°
40°
72°
70°
68°
64°
2
2
2
3
3
3
3
3
3
3
3
3
3
3
4
4
4
1
SYMBOLS INDICATE AREA OF RECOVERY
○ NO RECOVERIES
▲ NEW BRUNSWICK AND NOVA SCOTIA
◆ EASTPORT, ME. TO PROVINCETOWN
■ PROVINCETOWN TO BLOCK ISLAND
▼ BLOCK ISLAND TO CAPE HATTERAS
● FOREIGN RETURNS
—4→ DRIFT SPEED, MILES PER DAY

FIGURE 14.—Surface circulation deduced from recoveries of drift bottles launched by *Albatross II*, May 26–28 and June 3–7, 1931.

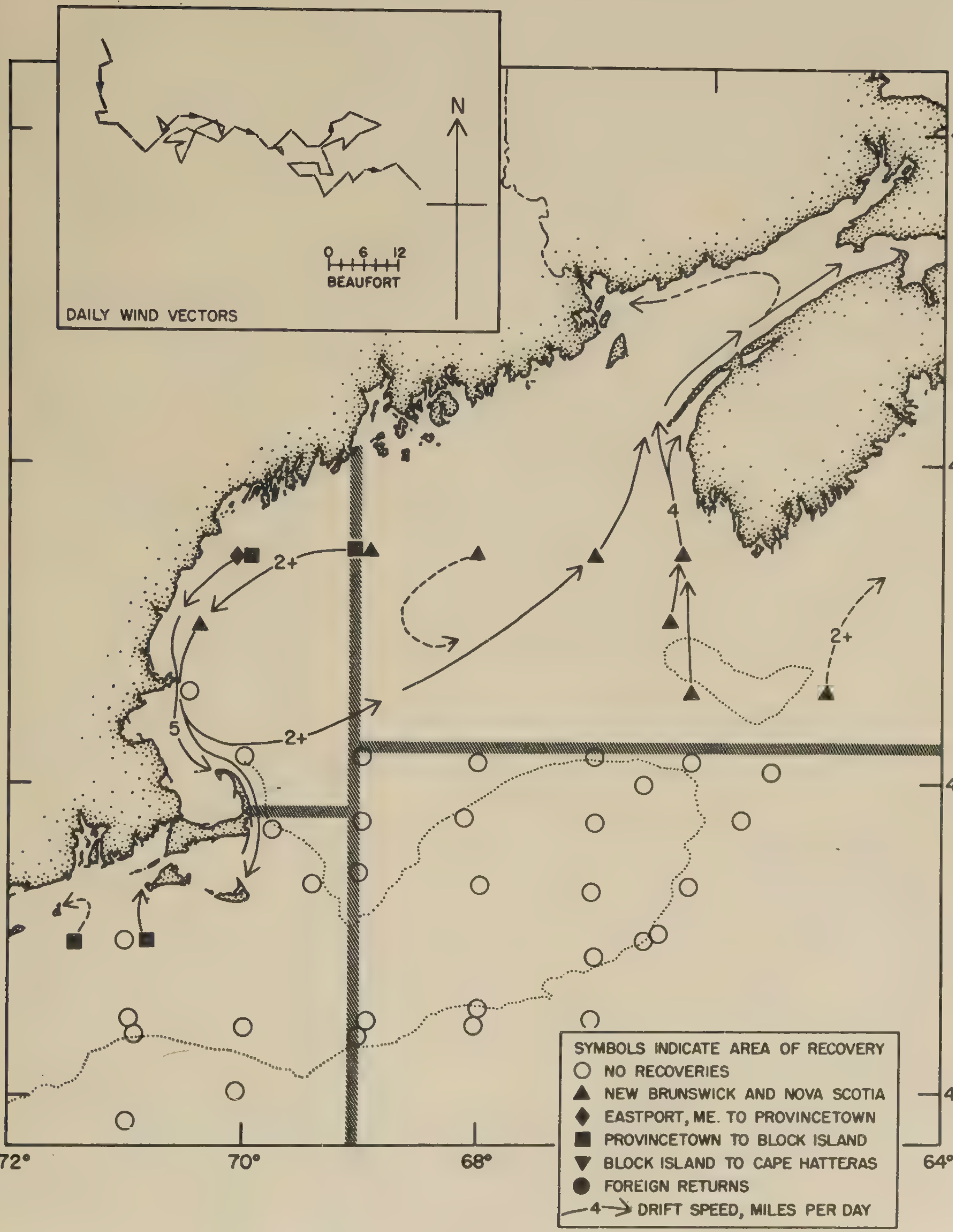
DAILY WIND VECTORS
N
0 6 12
BEAUFORT
46°
44°
42°
40°
72°
70°
68°
64°
2+
2+
2+
5
4
2+
SYMBOLS INDICATE AREA OF RECOVERY
○ NO RECOVERIES
▲ NEW BRUNSWICK AND NOVA SCOTIA
◆ EASTPORT, ME. TO PROVINCETOWN
■ PROVINCETOWN TO BLOCK ISLAND
▼ BLOCK ISLAND TO CAPE HATTERAS
● FOREIGN RETURNS
—4→ DRIFT SPEED, MILES PER DAY

FIGURE 15.—Surface circulation deduced from recoveries of drift bottles launched by *Albatross III*, on cruise 50. May 25–June 2, 1953.

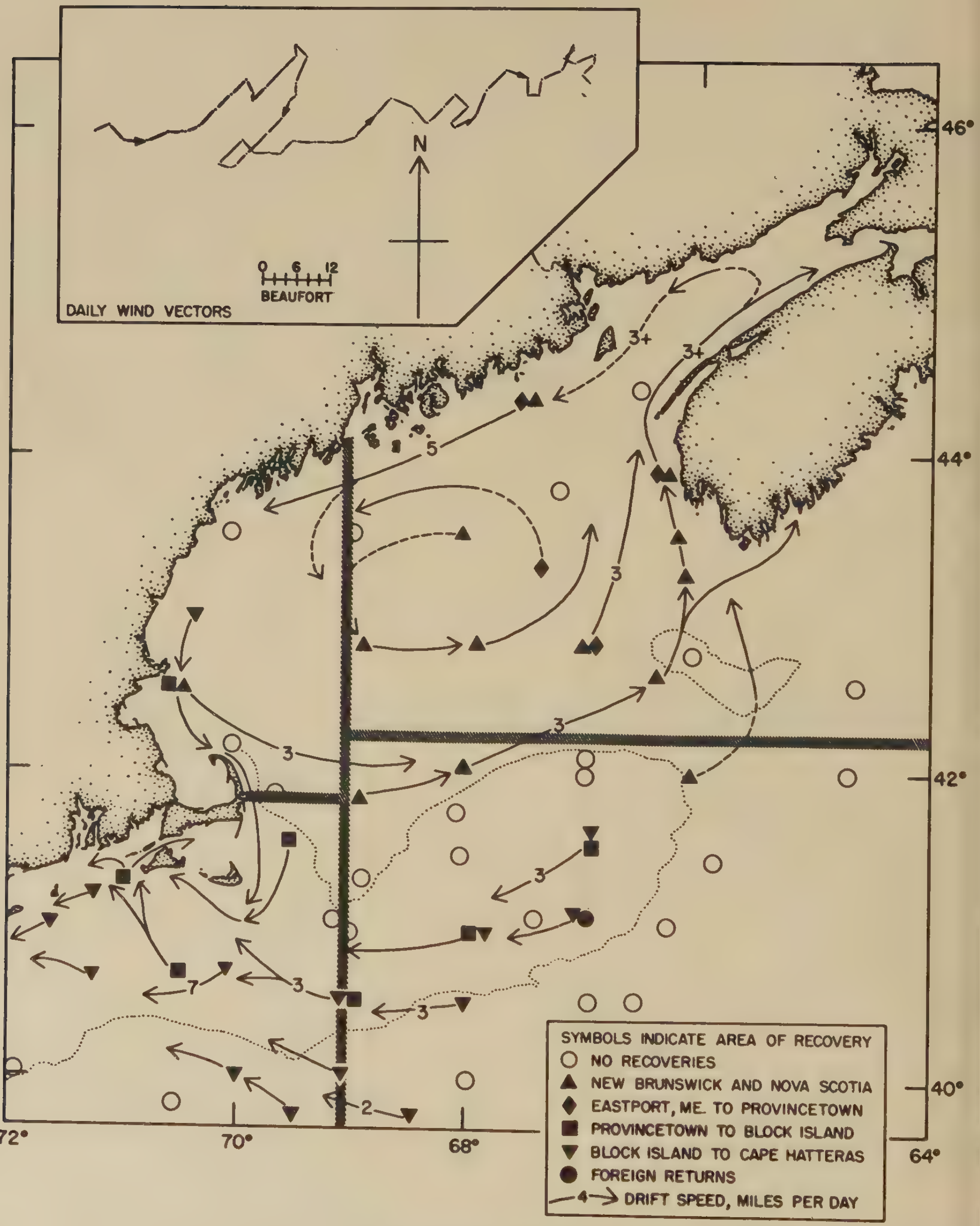
DAILY WIND VECTORS
0 6 12
BEAUFORT
N
46°
44°
42°
40°
72°
70°
68°
64°
3+
3+
5
3
3
3
3
7
3
3
2
SYMBOLS INDICATE AREA OF RECOVERY
○ NO RECOVERIES
▲ NEW BRUNSWICK AND NOVA SCOTIA
◆ EASTPORT, ME. TO PROVINCETOWN
■ PROVINCETOWN TO BLOCK ISLAND
▼ BLOCK ISLAND TO CAPE HATTERAS
● FOREIGN RETURNS
—4→ DRIFT SPEED, MILES PER DAY

FIGURE 16.—Surface circulation deduced from recoveries of drift bottles launched by *Albatross III*, on cruise 61, May 16–28, 1955.

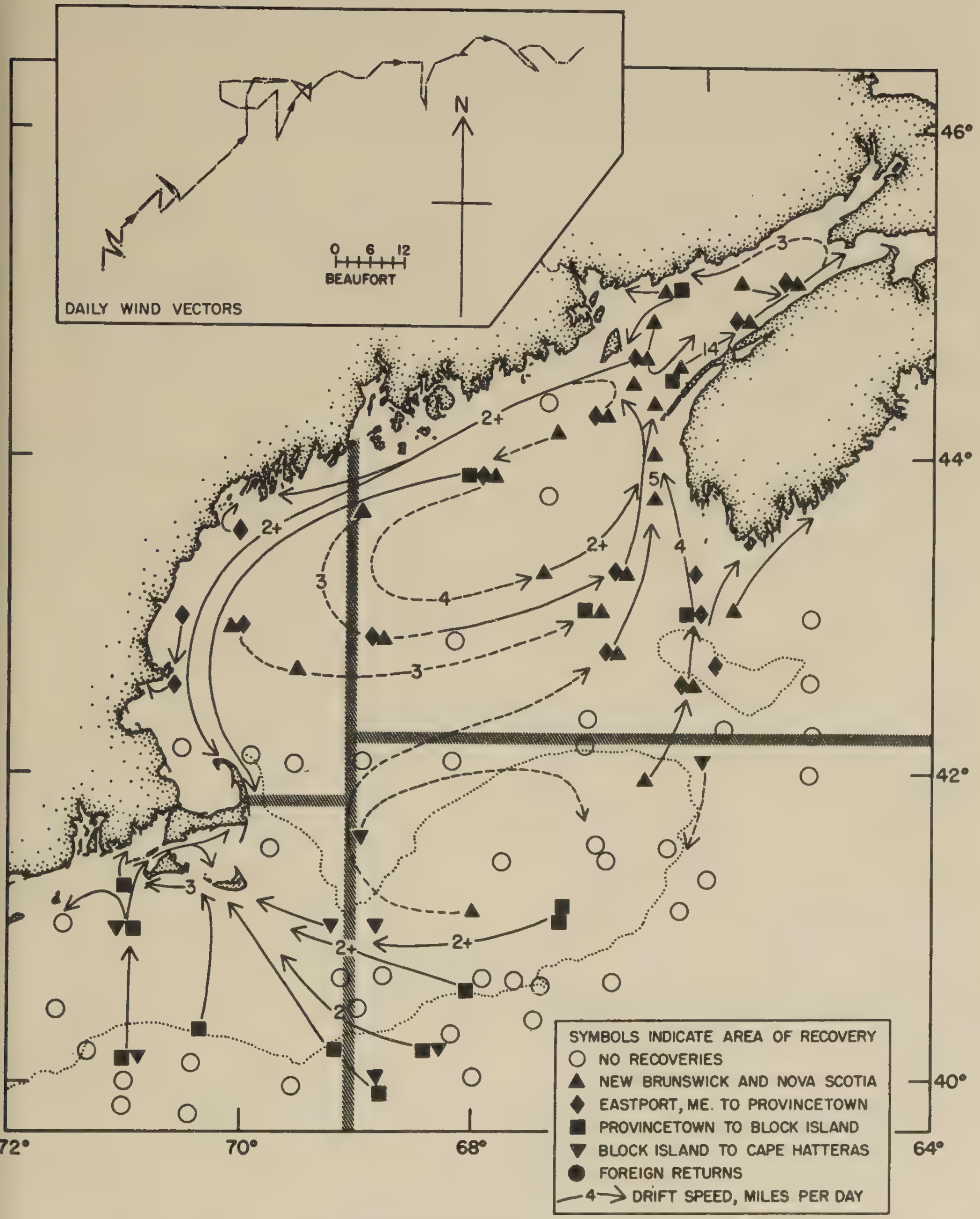
DAILY WIND VECTORS
N
0 6 12
BEAUFORT
46°
44°
42°
40°
72°
70°
68°
64°
2+
3
4
5
14
SYMBOLS INDICATE AREA OF RECOVERY
○ NO RECOVERIES
▲ NEW BRUNSWICK AND NOVA SCOTIA
◆ EASTPORT, ME. TO PROVINCETOWN
■ PROVINCETOWN TO BLOCK ISLAND
▼ BLOCK ISLAND TO CAPE HATTERAS
● FOREIGN RETURNS
—4→ DRIFT SPEED, MILES PER DAY

IGURE 17.—Surface circulation deduced from recoveries of drift bottles launched by *Albatross III*, on cruise 75, May 16–29, 1956.

placed to the north, while the movement out South Channel is not apparent.

In area II, there is a pronounced northward flow from the region of Browns Bank, with a velocity of 5 miles a day. This increased to a velocity of 14 miles a day along the southeastern shore of the Bay of Fundy. The return flow along the coast of Maine dropped to 2 miles a day.

Area III shows the westward flow pushed sharply onshore and thence, in many cases, to the northeast into Buzzards Bay and the sounds. Southerly flow out South Channel is not apparent.

In area IV, the Georges eddy does not appear. However, it seems reasonable to assume a southeasterly movement from the western and southern Gulf outward across the tip of Georges Bank. Returns from the southern half of the Bank seem to have moved westward and northward exhibiting the same onshore tendency seen in area III.

There is no doubt that the surface movement in the area of study was strongly influenced by the dominant southwest and west wind system here.

Of the four cruises in group *D*, only the first (*Albatross II*) can be considered free from wind influence. Unfortunately, bottles were put out only in the southern portion of the area of study, but from the drift characteristics of these it is fair to assume that the circulation agreed well with the Bigelow diagram. Assuming this is true and that such movement—which we saw developing in the cruises of group *C*—can be considered normal circulation at this season, the following departures from normal in the last three cruises appear:

1. The offshore winds which characterized cruise 50 confined the Gulf eddy well to the north while the Georges Bank–South Channel region was virtually swept clean.
2. Wind vectors for cruise 61 averaged slightly to the south of west and the drift pattern agreed with Bigelow's, with one exception: the westerly flow south of the islands was strongly deflected northward.
3. In 1956 winds during cruise 75 were uniformly from the southwest. They probably served to confine the Gulf eddy to the northeastern part of the Gulf of Maine, piling up water in this region. As we have seen before, winds from this direction again served to give a strong northerly component to the westerly drift from Georges Bank and south of the islands. Surface outflow from the region came from the western Gulf out across the east end of the Banks.

GROUP *E* CRUISES: LATE JUNE

Atlantis cruise 16, June 19–28, 1933 (Figure 18)

The eastern and southern regions of the Gulf of Maine covered by this cruise are in good agreement with the Bigelow norm. The Georges eddy is apparent, as is the northward movement of surface water across Browns Bank. South of the islands in area III the westerly motion lacks the northward set which appears to occur with southwest winds (cf. 1956 cruises).

Albatross III cruise 76, June 11–24, 1956 (Figure 19)

Bottles launched in area I moved eastward into Canadian waters, penetrating well into the Bay of Fundy at a rate of 4 miles a day. Among all the cruises, this cruise represents the best agreement with the Bigelow diagram in this area. The northerly flow from Browns Bank is clearly marked. Thus, the west winds appear to have closed off the Gulf circulation.

In area III, the onshore set seen earlier (cruises 72, 73, and 75) has been intensified and many bottles moved eastward into Vineyard and Nantucket Sounds. Area IV produced few returns, these being from Virginia and North Carolina and indicating, along with the no-return stations, a pronounced movement away from the region.

Of these two June cruises, the first cruise, though of limited coverage, can be said to represent normal circulation for the season and to agree well with the Bigelow diagram, being relatively uninfluenced by winds.

The second cruise, in 1956, which is characterized by fairly consistent westerlies, shows that such winds can be expected to modify the Bigelow norm in the southern portion of the area of study in that movement from Georges Bank will be generally offshore away from the area, and the usual westward flow south of Cape Cod and the islands will be deflected northward and onshore. The surface plankton from the Bank would be lost to the area, while that which may have drifted westward would be moved shoreward.

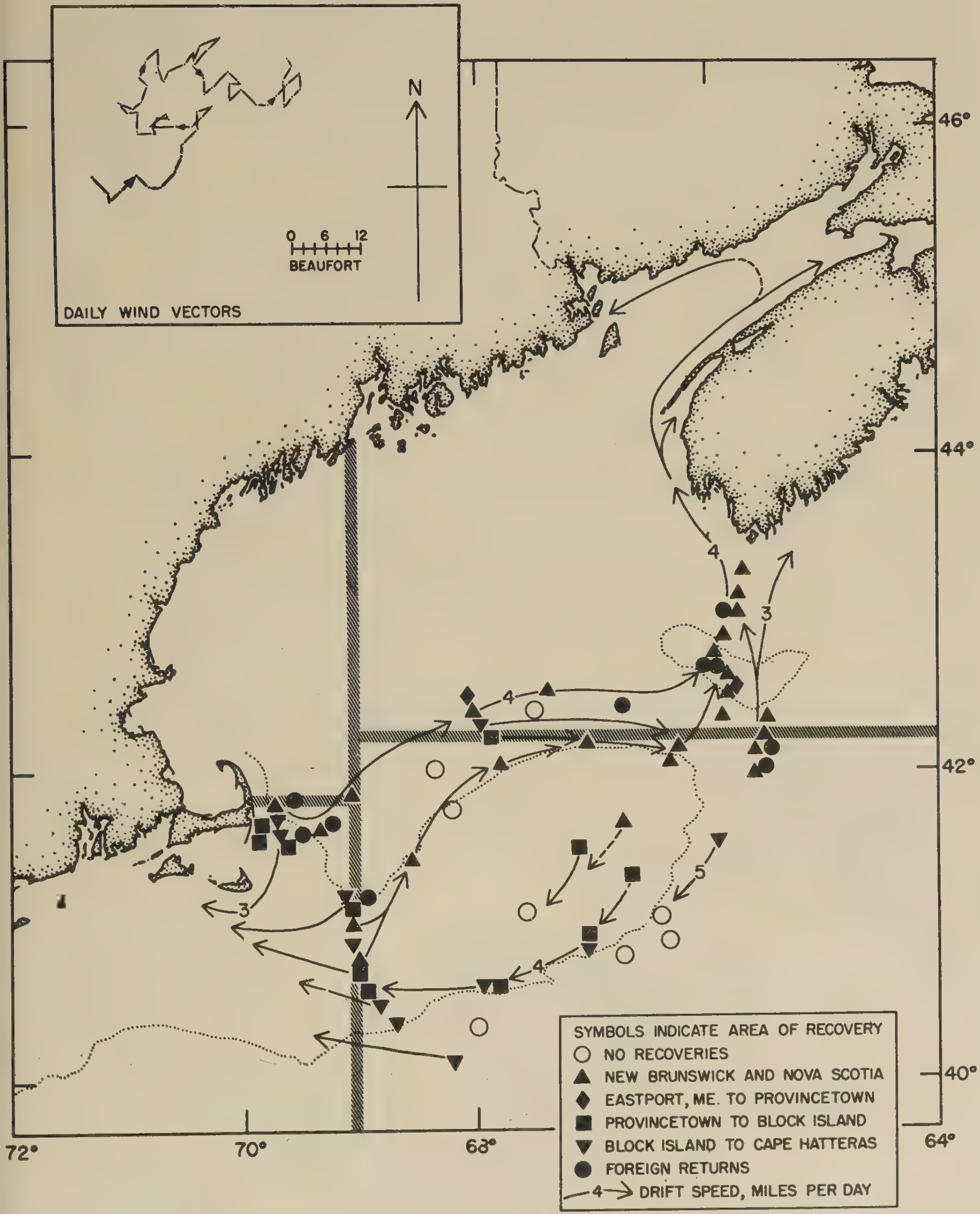
DAILY WIND VECTORS
0 6 12
BEAUFORT
N
46°
44°
42°
40°
72°
70°
68°
64°
4
3
4
3
5
4
SYMBOLS INDICATE AREA OF RECOVERY
○ NO RECOVERIES
▲ NEW BRUNSWICK AND NOVA SCOTIA
◆ EASTPORT, ME. TO PROVINCETOWN
■ PROVINCETOWN TO BLOCK ISLAND
▼ BLOCK ISLAND TO CAPE HATTERAS
● FOREIGN RETURNS
—4→ DRIFT SPEED, MILES PER DAY

FIGURE 18.—Surface circulation deduced from recoveries of drift bottles launched by *Atlantis*, on cruise 16, June 19–28, 1933.

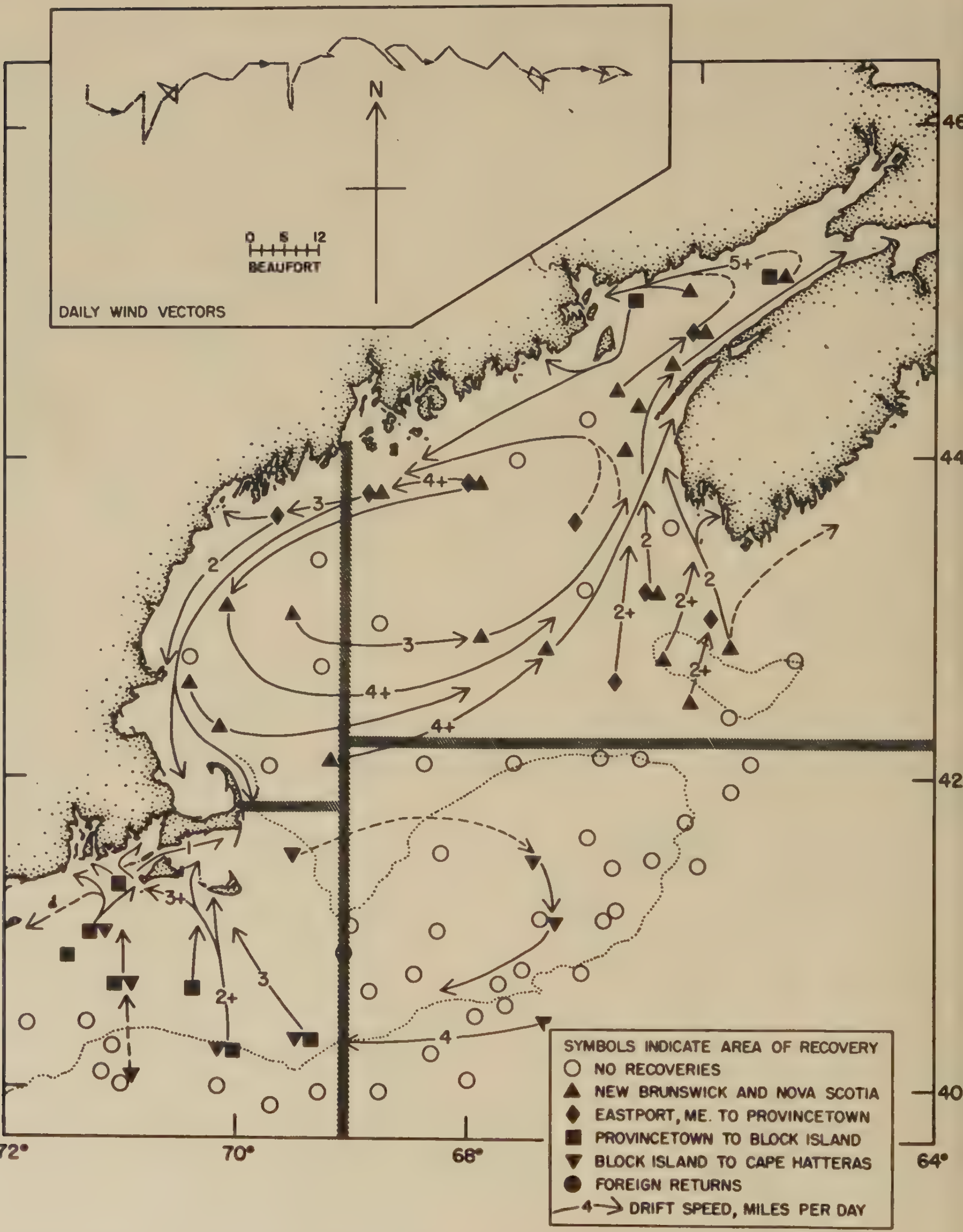
DAILY WIND VECTORS
N
0 6 12
BEAUFORT
46°
44°
42°
40°
72°
70°
68°
64°
5+
4+
3
2
4+
3
4+
4+
2
2
2+
2+
2
2+
1
3+
2+
3
4
SYMBOLS INDICATE AREA OF RECOVERY
○ NO RECOVERIES
▲ NEW BRUNSWICK AND NOVA SCOTIA
◆ EASTPORT, ME. TO PROVINCETOWN
■ PROVINCETOWN TO BLOCK ISLAND
▼ BLOCK ISLAND TO CAPE HATTERAS
● FOREIGN RETURNS
—4→ DRIFT SPEED, MILES PER DAY

FIGURE 19.—Surface circulation deduced from recoveries of drift bottles launched by *Albatross III*, on cruise 7 June 11–24, 1956.

INDICATIONS OF BOTTOM DRIFT

An interesting and unexpected result of the drift-bottle seedings in the Gulf of Maine is found in the returns for 1953. By a fortunate accident, some of the ballasted bottles apparently sank, either because too much sand had been added or because the bottles themselves were heavier than normal.

The inference that these bottles sank seems justified. In four cases, fishermen stated that the bottles were brought up from the bottom in nets. Thus, it is thought reasonable to assume that the other ballasted bottles found at sea by fishermen also sank, as it is improbable that they could have remained afloat in the same area of swift tidal currents for periods ranging from 4 to 37 months.

The net direction and distance of drift of 12 of these bottles are shown in figure 20. In only two instances is there any indication of rate of drift: bottle No. 13339 shows a net movement of 1 mile a day and No. 13827 of 0.7 mile a day. Of interest is the uniform picture of southwesterly movement of water at the bottom along the southern edge of Georges Bank and the general southerly movement out South Channel. This, in general, fits well with the surface water movement in these areas.

CONCLUSIONS

A consideration of the 17 cruises in the Gulf of Maine from the point of view of the conditions tending to conserve or disperse planktonic forms within the region of study leads to three conclusions.

1. Bigelow's (1927, pp. 972–3) July–August pattern, a relatively closed circulation and hence highly conservative, seems to evolve with the seasons, possibly as a result of vernal warming and the consequent formation of density structure. In February and March, the Gulf eddy is ill-defined on the south as water from area I moves seaward out South Channel. The Georges eddy is not apparent, the net movement of surface water being southwest. By late April, the two counterrotating

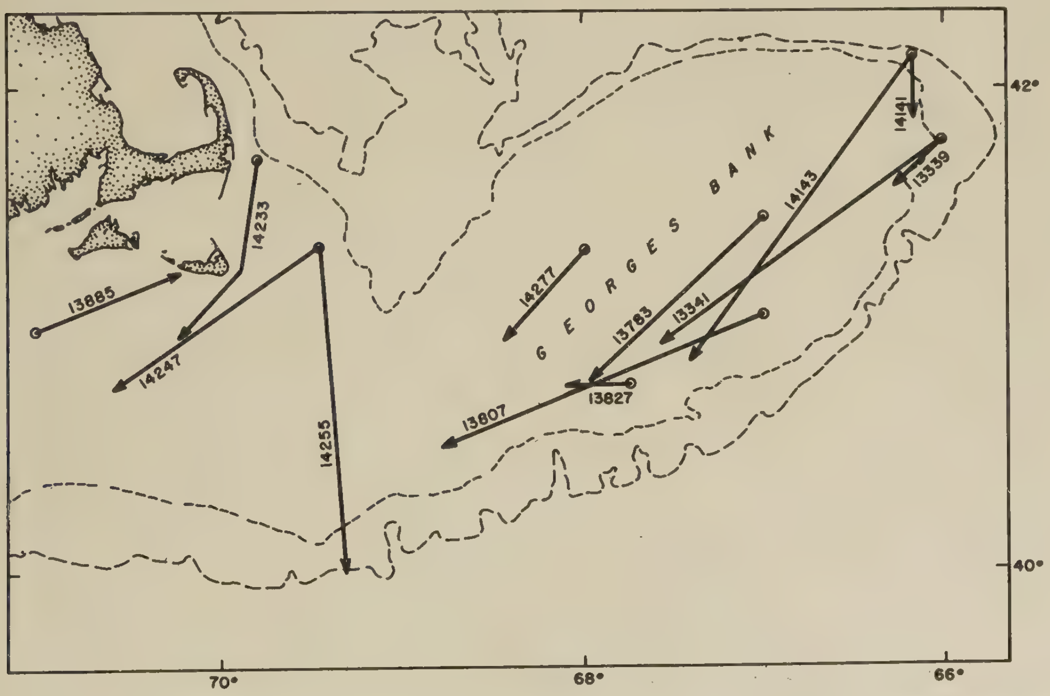

Figure 20.—Net movement of drift bottles which apparently sank and were recovered from the bottom by fishermen.

eddies are taking form with the appearance of a northeasterly movement along the northern edge of Georges Bank where the two eddies become confluent. After this development, plankton within the Gulf would probably be retained.

2. At any time during the seasons considered, the prevailing circulation may be strongly modified by winds. Offshore winds from the northwest quadrant have a pronounced effect on the Georges Bank region, tending to destroy the eddy (figs. 3, 4, 8, and 15). Northeasterly winds, even of short duration as during cruise 60 of the *Albatross III* (fig. 12), speed up the northern segment of the Gulf eddy and increase the flow out South Channel. Winds from the west and southwest (figs. 13, 16, 17, and 19) seem to give a strong onshore component to the waters south of Cape Cod and to accentuate the northward flow from Browns Bank into the Bay of Fundy.

3. In the region of Georges Bank, a marked difference between conditions in the 1930's and 1950's is apparent. With the exception of the April cruise of 1932 (fig. 8), when winds were uniformly offshore, the Georges eddy during the 1930's was far more pronounced than during the last few years. Though there are indications of an eddy in 1955 (fig. 12), it is markedly absent in 1953 and 1956 (figs. 4, 5, 7, 11, 13, 15, 17, and 19). Plankton on the Bank had more chance of surviving locally in the early 1930's than in 1953 and 1956.

Efforts to assess the potential of any given spawning season within the area should certainly involve accurate knowledge of the time and place of spawning and a careful consideration of wind patterns during the period of the planktonic stage of the fish in question.

REFERENCES

BIGELOW, HENRY B.,

1927. Physical oceanography of the Gulf of Maine. Bull. United States Bureau of Fisheries, vol. 40 (1924), Pt. II, Doc. No. 969, pp. 511–1027.

BUMPUS, DEAN F., and C. GODFREY DAY.

1957. Drift bottle records for Gulf of Maine and Georges Bank, 1931–56. United States Fish and Wildlife Service, Special Sci. Rept.: Fisheries No. 242, 61 pp.

EKMAN, V. WALFRID.

1902. Om jordrotationens inverkan på vindströmmar i hafvet. Nyt Magazin for Naturvidenskaberne, bd. 40, S. 37–63. Christiania.

WALFORD, LIONEL A.

1938. Effect of currents on distribution and survival of the eggs and larvae of the haddock (*Melanogrammus aeglefinus*) on Georges Bank. Bull. United States Bureau of Fisheries, vol. 49, No. 29, pp. 1–73.

The Library of Congress has cataloged Fishery Bulletin 141 as follows:

Day, Charles Godfrey.
Surface circulation in the Gulf of Maine as deduced from drift bottles. Washington, U. S. Govt. Print. Off., 1958.

443–472 p. illus. 26 cm. (Fishery bulletin 141)

Woods Hole Oceanographic Institution. Contribution no. 977.
"From Fishery bulletin of the Fish and Wildlife Service, volume 58."
Includes bibliography.

1. Ocean currents—Maine, Gulf of. I. Title.

SH11.A25 vol. 58, no. 141 58–62420 ‡
*551.46 551.471

The series, Fishery Bulletin of the Fish and Wildlife Service, is cataloged as follows:

U. S. *Fish and Wildlife Service.*
Fishery bulletin. v. 1–
Washington, U. S. Govt. Print. Off., 1881–19

v. in illus., maps (part fold.) 23–28 cm.

Some vols. issued in the congressional series as Senate or House documents.
Bulletins composing v. 47– also numbered 1–
Title varies: v. 1–49, Bulletin.
Vols. 1–49 issued by Bureau of Fisheries (called Fish Commission, v. 1–23)

1. Fisheries—U. S. 2. Fish-culture—U. S. I. Title.

SH11.A25 639.206173 9–35239 rev 2*

Library of Congress [r55e⅟₂]

Contribution No. 978

Reprinted from BIOLOGICAL BULLETIN, Vol. 115, No. 2, pp. 257–268, October, 1958
Printed in U. S. A.

THE DYNAMICS OF A DIATOM BLOOM[1]

J. H. RYTHER, C. S. YENTSCH, E. M. HULBURT AND R. F. VACCARO

Woods Hole Oceanographic Institution, Woods Hole, Mass.

Phytoplankton cells respond so rapidly to their environment that conventional methods of studying their populations fail to reveal many of the more subtle and more interesting aspects of their dynamic ecology. This is particularly true of surveys in which observations are made at intervals of weeks or months, where the very use of the term "the phytoplankton population," when carried over from one set of observations to the next, implies more knowledge than is available. It is also true of productivity measurements made over 24 hours or the daylight portion of a day, since Rodhe (personal communication), Doty and Oguri (1957), Yentsch and Ryther (1957) and others have shown that the plants vary in their composition and react differently to their environment at different times of the day. To study such phenomena it is obviously necessary to make intensive observations at very frequent intervals throughout one or more days on single, isolated populations.

This type of study presents obvious difficulties. The average natural population is sparse enough so that its properties can be measured only with rough accuracy, and the errors of such measurements may be larger than the changes in the organisms and their environment which are under investigation. Some insight into these problems may be had by studying cultures, but the difficulties of growing organisms under completely natural conditions need no elaboration here. A compromise may be reached, however, by working with a dense phytoplankton bloom. Here natural populations may be studied under their natural growing conditions and very rapid responses of the organisms to changes in their physical or chemical environment may be detected and measured.

The authors encountered such a diatom bloom in a small tidal creek on the south shore of Long Island, N. Y., in June, 1957. The following report will describe the studies of this bloom which were made over a 40-hour period including two days and one night.

DESCRIPTION OF THE AREA

Senix Creek is approximately one mile long, tapering from a width of about 300 meters at its mouth to less than 10 meters at its upper end in the town of Center Moriches. Our observations were made about halfway up its length where the water depth is approximately one meter. Underlying this shallow body of water is a thick deposit of black, organic muck which discharges H_2S gas when disturbed.

There is no river or other obvious source of fresh water to Senix Creek except for local runoff. The latter was negligible in the early summer of 1957 due to

---

[1] Contribution No. 978 from the Woods Hole Oceanographic Institution. This study was made with the assistance of research grants from the National Science Foundation.

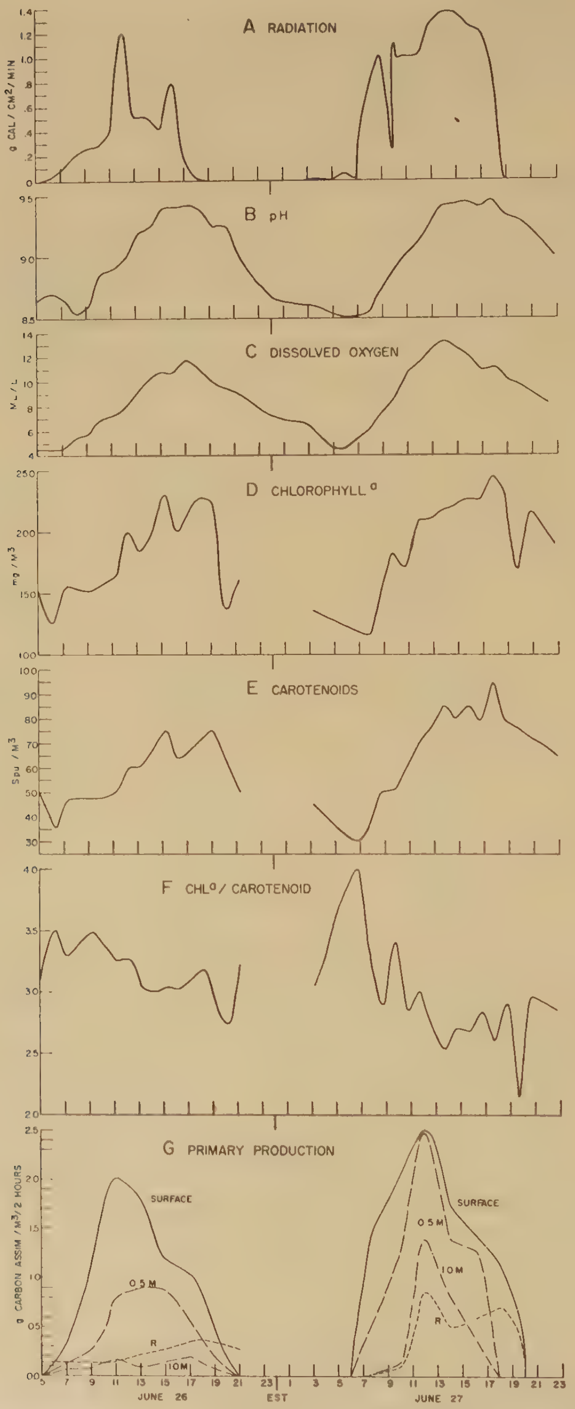

FIGURE 1. Variables measured in Senix Creek between 05:00, June 26 and 20:00, June 27.

as the diatoms, were probably insignificant in terms of total biomass since their cell volume is several hundreds of times smaller than that of the average diatom.

b. The physical environment

Figure 1A shows the incident radiation for the two days. The total daily radiation, obtained by integration of these curves, was 300 gram-calories/cm². on June 26 and 740 gram-calories/cm². on June 27.

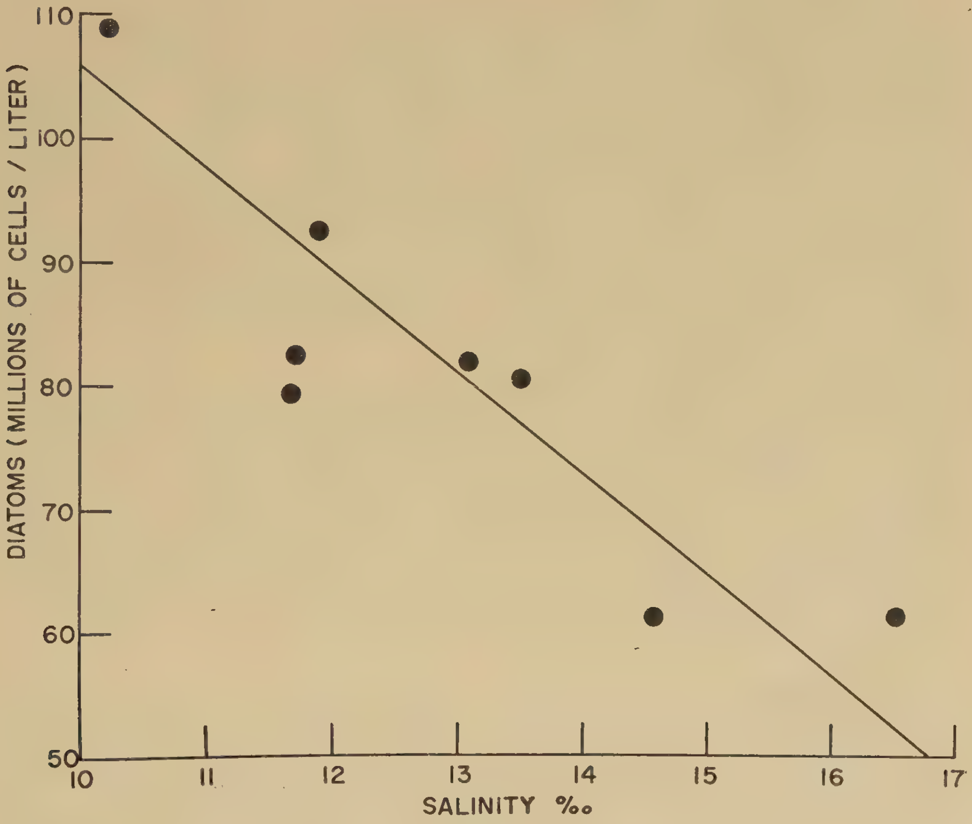

FIGURE 2. The relation between salinity and total diatom concentration, showing least squares line (R = –.875). Data from Table I.

The tidal influence in Senix Creek is extremely small. The range between high and low water on both days was approximately seven inches. Salinities ranged from 10–15 ‰ and showed no obvious correlation with the stage of the tide. However, salinities at the bottom were slightly higher than those at the surface, and salinities were higher the second day of observations than on the first (Table I).

Diatom counts were slightly lower at the bottom than at the surface and lower at both depths on the second day. Again there was no obvious relation to the tide, but there was a good inverse correlation ($r = -0.875$) between the diatom concentration and the salinity (Fig. 2). This correlation suggests that the diatom population did not change over the two-day period as a result of growth or death, but that the population was being diluted slowly with water from Moriches Bay, where the salinity ranged from 20 to 25 ‰ and diatom concentrations were generally less than one million cells per liter.

c. Dissolved oxygen and pH

Both pH and dissolved oxygen behaved in essentially the same manner, as may be seen by comparing Figures 1B and C. However, the high pH attained in the late afternoon of both days was maintained for several hours whereas the oxygen concentration reached its peak at the same time but then began to decline immediately. Water temperatures (which are not shown) ranged from 25° C. to 28° C. during the two-day period. Assuming a mean salinity of 12‰, the water was approximately 90% saturated with oxygen at daybreak, about 270% saturated at 14:00 on June 27. Despite this supersaturation, there did not appear to be a significant loss of oxygen to the air by diffusion since the decrease in oxygen concentration at night by respiration appears to have occurred at a constant rate. If appreciable loss by diffusion had occurred, this would have been dependent upon the oxygen concentration, and the decrease due to both causes (respiration and diffusion) would have been non-linear.

The pH reached a minimum of about 8.5 early in the morning and a maximum of almost 9.5 in the afternoon. Presumably at its maximum, no free CO_2 was available and any further photosynthesis was dependent upon bicarbonate or carbonate ions. Unfortunately no measurements were made of CO_2 in any of its fractions, nor may these values be calculated from pH, salinity, and temperature for these estuarine conditions as they may for either fresh or sea water. Again the regular behavior of the pH curve with time, shown in Figure 1C, indicates that CO_2 diffusion from air to water was negligible in comparison to the changes caused by photosynthesis and respiration.

d. Plant pigments

Figure 1D shows the concentration of chlorophyll *a* in the composite samples taken during the two-day period. Since the cell counts were not made on the same samples, it is not possible to represent chlorophyll on a cellular basis. The chlorophyll concentration in the water ranged from 116 to 245 mg./m^3., about a two-fold variability. Although the highest concentrations coincided on both days with low water, the connection between these factors is probably fortuitous. Certainly the variations in the pigment concentration are far greater than the observed differences in the diatom counts, caused by tidal fluctuations or otherwise. Despite the somewhat erratic distribution of the pigment concentration, it is still obvious that the chlorophyll increased gradually throughout the day, reaching its peak at about sunset, after which it decreased rapidly throughout the night until daybreak.

Similarly the plant carotenoid pigments increased during the day and decreased at night (Fig. 1E). Both chlorophyll and carotenoids increased to higher values on the second day, which differed from the first primarily in the amount of incident

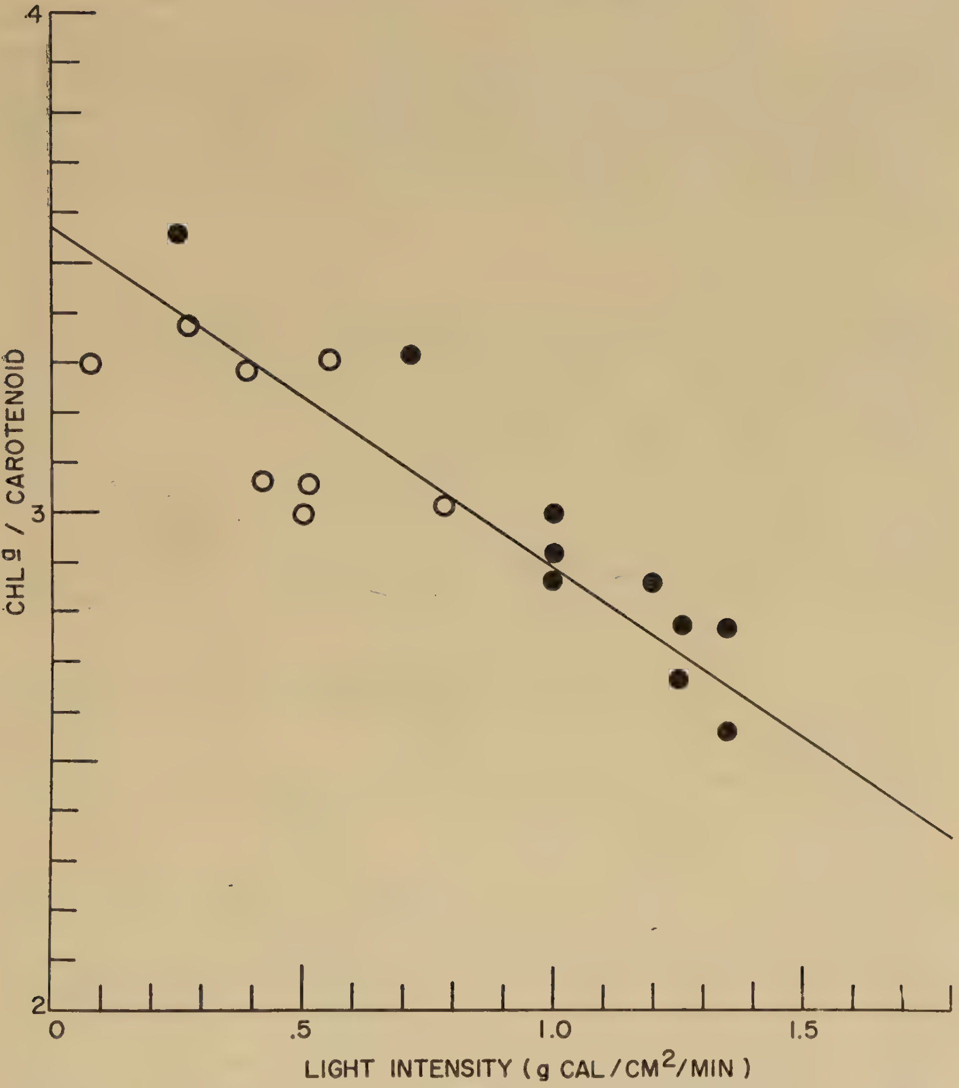

FIGURE 3. The relation between incident radiation and the ratio chlorophyll *a*:carotenoid pigments in the diatom population. Open circles, June 26. Closed circles, June 27.

radiation. The carotenoid pigments ranged on June 27 from a minimum of 30 SPU[3] at 05:45 to 95 SPU at 17:45, more than a three-fold variation.

The ratio chlorophyll *a*:carotenoid pigments (Fig. 1F) decreased throughout the daylight periods of both days from maximum values observed at sunrise, the more rapid decrease on June 27 again correlated with the greater incident radiation on that day. Figure 3 shows the inverse relationship which was found between the intensity of solar radiation and the chlorophyll: carotenoid ratio. The variations in this ratio are the result of a differential effect of light on pigment synthesis and decomposition where the chlorophyll changes are of much greater magnitude than are the carotenoid changes (Yentsch and Scagel, unpublished). The significance and interpretation of the magnitude and changes in this ratio will be discussed in the final section of this paper.

---

[3] The spectrophotometric analysis of carotenoid pigments has not been standardized in absolute units and they are reported in specific pigment units after Richards with Thompson (1952). One SPU, however, is closely equivalent to one milligram of pigment.

e. Primary production

Primary production was calculated by the following three methods: (1) the *in situ* changes of oxygen in the water, (2) the "light-and-dark-bottle" oxygen measurements, (3) the "chlorophyll-radiation" method of Ryther and Yentsch (1957). The inability to measure or calculate total CO_2 prevented the use of pH changes or the C^{14} method for this purpose.

On June 26, the dissolved oxygen in the integrated sample collected over the one-meter water column increased from a minimum of 4.5 ml./liter at 07:00 hours to a maximum of 11.8 ml./liter at 17:00 hours, a difference of 7.3 ml./liter. If an assimilatory quotient of 1.25 is used, this change in oxygen is equivalent to a carbon fixation of 3.15 grams/m^2./day. As mentioned earlier, the decrease in oxygen at night appears to have been due almost entirely to respiration. This loss was equivalent to 0.5 ml. oxygen/liter/hour. During the 10 hours of daylight, if respiration occurred at the same rate, this would account for a total of 5.0 ml. O_2/liter or 2.15 grams carbon/m^2./day. Adding this respiratory loss to the observed net production of 3.15 grams carbon/m^2./day gives a total or gross production of 5.20 grams carbon/m^2./day.

In the same way production was calculated for June 27, the net change in oxygen being equivalent to assimilation of 3.8, the respiration loss 1.7 and the gross production 5.5 grams carbon/m^2./day.

The two-hour "light-and-dark-bottle" experiments which were described above were also used to calculate gross and net production. The differences between the oxygen concentration of the light bottles at 0, 0.5, and 1.0 meter and that of the accompanying dark bottle over the two-hour experimental periods, converted to carbon assimilation as above, are shown in Figure 1G. The carbon equivalent of respiration for the same two-hour periods was obtained from the difference between the oxygen content of the water at the beginning of the two-hour period and that of the dark bottle. These curves were integrated to obtain daily photosynthesis at each depth and daily respiration. These values in turn were plotted against depth and integrated to give daily photosynthesis and respiration beneath a square meter of surface. Gross photosynthesis for June 26 calculated by this method was 3.5, respiration was 1.7 and net photosynthesis 1.8 grams carbon/m^2./day. On June 27 the values were 6.2, 2.8 and 3.4 grams carbon/m^2./day for gross production, respiration and net production, respectively.

The *in situ* oxygen changes at night appeared to indicate a constant respiration rate of 0.5 ml. O_2/liter/hour, and this, as described above, was used to correct the net *in situ* change observed in daylight to give gross production. An examination of the two-hour bottle experiments during the day shows that, when measured in this way, respiration was by no means constant but varied roughly in proportion to the rate of photosynthesis. On June 27, for instance, the respiratory rate ranged from 0.06 ml./liter/hour in the early morning to about 1.00 ml./liter/hour at midday. These measurements, though somewhat crude, emphasize the need for a reconsideration of the tacit assumption made by most ecologists that respiration measured at night, or for long periods in dark bottles, is the same as that which occurs in the light in conjunction with photosynthesis.

The third method for estimating production is that developed by Ryther and Yentsch (1957). This method requires measurement of the concentration of chlorophyll *a*, the total daily incident radiation, and the extinction coefficient of visible light in the water. The latter was determined by the measurement of light penetration to one meter with a submarine photometer at 13:30 hours on June 26. The extinction coefficient (k) so determined was 4.0. Use of this method required an obvious over-simplification, since the chlorophyll *a* concentration, as has been pointed out, varied throughout the day. A mean value of 200 mg. chl*a*/m^3. was used for the calculation for both days, and this was assumed to be uniformly distributed over the one-meter water column. The resulting values for gross production were 3.2 and 5.1 grams carbon/m^2./day for June 26 and 27, respectively.

The results obtained by these three methods are summarized in Table II. They show rather good agreement except for the values obtained by *in situ* oxygen changes on June 25 which are almost twice as high as those obtained by the other two methods. It should be pointed out that the net production values which have been discussed refer to this process during the daylight hours only. The only estimates over a 24-hour period which can be made are based upon the *in situ* oxygen changes (and pH changes) which clearly reflect a net production for this period of zero. Finally, the net changes observed *in situ* and *in vitro* are acknowledged as representing changes brought about by the whole community including animals and bacteria, and do not characterize the plant population alone.

TABLE II

Primary production in Senix Creek on June 26 and June 27, as measured by three methods (grams carbon assimilated/m.^{2}/day)

Method	Gross	Net (day)	Net (24 hrs.)	Gross	Net (day)	Net (24 hrs.)
In situ O_2	5.3	3.15	0	5.5	3.8	0
L-D bottle O_2	3.5	1.76	—	6.2	3.4	—
Chlorophyll	3.2	—	—	5.1	—	—

The efficiency of production on the two days may be roughly estimated by taking the median of the values obtained by the three methods for daily gross production, 3.5 and 5.5 grams carbon/m^2. on June 26 and 27, respectively. If the assumption is made that 50% of the photosynthetic production is carbon and has a heat of combustion of 5.5 *k* cal./gr. (see Krogh and Berg, 1931), and further that half the incident radiation may be used for photosynthesis, the efficiency may be calculated as:

$$\text{a) June 26} \quad \frac{3.5 \times 2 \times 5{,}500}{1{,}500{,}000} = 2.6\%$$

$$\text{b) June 27} \quad \frac{5.5 \times 2 \times 5{,}500}{3{,}700{,}000} = 1.6\%$$

f. The physiology of the bloom

There are several indications that the diatom population in Senix Creek was a non-growing one which had exhausted its supply of available nutrients and was able to subsist at a basal level, photosynthesizing just enough during the day to compensate for its metabolic requirement over a 24-hour period. This is best illustrated by the *in situ* oxygen and pH values, in which the net oxygen produced and CO_2 assimilated during the day are exactly compensated by the reverse processes at night. Further evidence of this is the fact that the concentration of diatoms remained unchanged over the 48 hours of observation except where such changes are attributable to tidal flushing.

The evidence that the bloom was nutrient-limited is somewhat sparse and indirect, but rather convincing. At 10:30 hours on June 27 an integrated water sample was collected and frozen. This was later analyzed for nitrogen and phosphorus fractions at the Woods Hole Oceanographic Institution. The results of these analyses are given below.

	μg Atoms/liter
$NO_2- + NO_3-$	3.40
NH_3+	1.49
PO_4	3.80
Total P	16.0

A photosynthetic rate of 5.5 grams carbon/m^2./day in a one-meter water column represents a requirement of 460 μgA carbon/liter/day. As Redfield (1934) and others have pointed out, marine phytoplankton assimilate carbon, nitrogen and phosphorus at an atomic ratio closely approaching 100 : 15 : 1. This rate of carbon assimilation is therefore equivalent to a daily requirement of 71 μgA/liter of nitrogen and 4.6 μgA/liter of phosphorus. Thus, the concentrations of these elements in the mid-morning of June 27 represented no more than a fraction of a day's supply of either nitrogen or phosphorus. These calculations were based upon the requirement of normal cells. Photosynthesis may of course continue after nitrogen and phosphorus are exhausted with the storage of carbohydrates and lipids. This is presumedly what was happening in this population, the cells using these stored materials to satisfy their metabolic requirements at night. Further studies of this type of population, with emphasis placed upon the diurnal cycle of nutrients, would be particularly interesting.

The behavior of the plant pigments is a further indication of the physiological condition of the population. The fact that both chlorophyll *a* and the carotenoids were synthesized during the day and decomposed at night signifies that the plants were drawing upon their cellular reserves to maintain themselves in the dark. When nutrients are available, this does not occur; in fact, chlorophyll may be synthesized in the dark under favorable growing conditions if the cells have sufficient respiratory reserves (Harvey, 1953).

Experiments in this laboratory (Ketchum *et al.*, 1958) and elsewhere have shown that both chlorophyll *a* and the carotenoid pigments decrease in diatoms in response to nitrogen, phosphorus or iron deficiency or excessive illumination. This nutritional chlorosis results in a more rapid decomposition of chlorophyll than carotenoid pigments. As the day progressed the pigment ratio decreased, presumably in part because of nutrient exhaustion which was hastened by greater demands of photosynthesis at high light intensities (Fig. 3).

The picture which emerges from these various bits of evidence, then, is that of a static diatom bloom of great magnitude, its nutrient supply exhausted or at least reduced to the level where growth could not occur. Yet it was not a dying population, except insofar as physical forces tended to disperse it. It was capable of carrying out organic synthesis at a rate some 10–100 times that of normal plankton communities, drawing upon these materials for its metabolic requirements much the same as a mature animal maintains a balance between its assimilation and metabolism.

It would appear, then, that populations of phytoplankton such as we have described here, though not actively growing, are not necessarily dying either. They are merely living in a different growth phase, a condition in which they may persist for long periods of time if they are not destroyed or dispersed by external factors. Perhaps in diatom populations, as elsewhere, the bloom of maturity may outlast the bloom of youth.

SUMMARY

1. A dense population of planktonic diatoms was studied over a 40-hour period in a small tidal creek on the south shore of Long Island, New York.

2. Measurements were made at frequent intervals of incident radiation, light penetration, salinity, temperature, dissolved oxygen, pH, concentration of diatom cells and their pigments, and dissolved inorganic nutrients. Photosynthesis and respiration were measured by oxygen changes in bottle experiments and estimated from *in situ* oxygen changes and from chlorophyll *a* and radiation.

3. The plankton community appeared to be nutrient-limited and consisted of a static, non-growing diatom population which was being slowly diluted by tidal action. This was indicated by the diatom counts, the behavior of their pigments (which increased throughout the day and decreased during the night) and the concentration of available plant nutrients.

4. Rates of primary production measured by three methods showed good agreement, the values ranging from 3.2 to 5.3 grams carbon assimilated/m^2./day on June 26, from 5.1–6.2 on June 27. Total incident radiation for the two days was 300 and 740 gram calories/cm^2./day, respectively, and the efficiency of the photosynthetic utilization of visible radiation for the two days was estimated at 2.6% and 1.6%, respectively.

LITERATURE CITED

AMERICAN PUBLIC HEALTH ASSOCIATION, 1955. Standard methods for the analysis of water, sewage, and industrial wastes. Tenth Edition. American Public Health Assoc., Inc., New York. 259 pp.

CREITZ, G. I., AND F. A. RICHARDS, 1955. The estimation and characterization of plankton populations by pigment analyses. III. A note on the use of "millipore" membrane filters in the estimation of plankton pigments. *J. Mar. Res.*, **14**: 211–216.

DOTY, M. S., AND M. OGURI, 1957. Evidence for a photosynthetic daily periodicity. *Limnol. and Oceanogr.*, **2**: 37–40.

DUXBURY, A. C., AND C. S. YENTSCH, 1956. Plankton pigment nomographs. *J. Mar. Res.*, **15**: 92–101.

HARVEY, H. W., 1948. The estimation of phosphate and total phosphorus in sea waters. *J. Mar. Biol. Assoc.*, **27**: 337–359.

HARVEY, H. W., 1953. Synthesis of organic nitrogen and chlorophyll by *Nitzschia closterium. J. Mar. Biol. Assoc.*, **31**: 477–478.

KETCHUM, B. H., J. R. RYTHER, C. S. YENTSCH AND N. CORWIN, 1958. Productivity in relation to nutrients. *Rapp. et Proc. Verb. Cons. Internat. Explor. Mer.*, **144**: 132–140.

KROGH, A., AND K. BERG, 1931. Über die chemische Zusammensetzung des Phytoplanktons aus dem Fredriksborg-Schlossee und ihre Bedeutung für die Maxima der Cladoceren. *Int. Rev. Gesamt. Hydrobiol. u Hydrog.*, **25**: 205–218.

MULLIN, J. B., AND J. P. RILEY, 1955. The spectrophotometric determination of nitrate in natural waters, with particular reference to sea water. *Analyt. Chim. Acta*, **12**: 464–480.

REDFIELD, A. C., 1934. On the proportions of organic derivatives in sea water and their relation to the composition of plankton. James Johnstone Memorial Vol., The University Press, Liverpool. Pp. 176–192.

RICHARDS, F. A., WITH T. G. THOMPSON, 1952. The estimation and characterization of plankton populations by pigment analysis. II. A spectrophotometric method for the estimation of plankton pigments. *J. Mar. Res.*, **11**: 156–172.

RIDER, B. F., AND M. G. MELLON, 1946. Colorimetric determination of nitrites. *Ind. Engin. Chem. Anal. Edit.*, **18**: 96–99.

RILEY, J. P., 1953. The spectrophotometric determination of ammonia in natural waters with particular reference to sea water. *Analyt. Chim. Acta*, **9**: 575–589.

ROBINSON, R. J., AND T. G. THOMPSON, 1948. The determination of phosphates in sea water. *J. Mar. Res.*, **7**: 33–41.

RYTHER, J. H., 1954. The ecology of phytoplankton blooms in Moriches Bay and Great South Bay, Long Island, New York. *Biol. Bull.*, **106**: 198–209.

RYTHER, J. H., AND C. S. YENTSCH, 1957. The estimation of phytoplankton production in the ocean from chlorophyll and light data. *Limnol. and Oceanogr.*, **2**: 281–286.

YENTSCH, C. S., AND J. H. RYTHER, 1957. Short-term variations in phytoplankton chlorophyll and their significance. *Limnol. and Oceanogr.*, **2**: 140–142.

Contribution No. 979

Vol. 39, No. 5 TRANSACTIONS, AMERICAN GEOPHYSICAL UNION October 1958

A Portable Raindrop Recorder for Semi-Continuous Determination of Size Distributions*

A. T. SPENCER AND D. C. BLANCHARD

Abstract—The recorder was designed to obtain adequate drop samples, in the size range of 50 to 2000 microns diameter, at about two-minute intervals for a period in excess of 24 hrs. Successful field use of several instruments in a cloud physics study is indicated and they are described in some detail.

Introduction—During the planning stages of Project Shower [*Blanchard* and *Spencer*, 1957; *Squires*, 1955] the need arose to obtain continuous records of the fluctuation of the raindrop size in the orographic clouds on the Island of Hawaii. This need grew out of earlier ideas [*Blanchard*, 1953; *Woodcock*, 1952] of the importance of detailed knowledge of raindrop size distributions as an aid to understanding 'warm' rain formation. The purpose of this paper is to describe the instrument which was designed to answer our questions about drop size and number differences as a function of time and substance within orographic clouds.

A variety of automatic sampling devices have been developed and used [*Bowen* and *Davidson*, 1951; *Cooper*, 1951; *Fugiwara*, 1954; *Katz*, 1952; *Maulard*, 1951], but none of them, with the possible exception of the raindrop spectrograph of Bowen and Davidson [1951], appeared to have sufficient accuracy, compactness, and portability for the present work. Thus it seemed advisable to design and build a small device that would incorporate the above features.

Earlier work in Hawaii had shown that the rain from orographic clouds was not uniform but that great fluctuation in intensity and rain drop size occurred. Individual showers, imbedded within the orographic cloud system, appeared to move up the mountain slopes while the median raindrop size progressively decreased with increasing elevation [*Blanchard*, 1953].

Since we needed to determine the rate of change of the drop distribution as a function of time and distance along the mountain slope, it was necessary to construct a number of portable instruments that could be used to obtain measurements simultaneously at several elevations. As no source of power was available on the mountain, the instruments had to be self-contained and portable. It was decided to build instruments that would expose a section of dye treated paper tape at intervals of about two minutes. The splash pattern on the tape could then be related to raindrop size by appropriate calibration methods.

Although the instrument to be described in this paper was designed specifically for use in Hawaiian orographic rains where the raindrops seldom exceed two millimeters diameter, there is no reason why minor changes in the design could not make it adaptable for use in heavier rains. The present design should also be adequate for the light steady rains that are commonly associated with the passage of a warm front.

Instrument description—The dimensions of the drop recorder shown in Figures 1–3, are 6 × 8 × 11 inches. It weighs twelve pounds, excluding the weight of the power source. The operation of the recorder is as follows: at two minute intervals a sliding shutter opens and exposes a section of paper tape to the rain. The shutter remains open for approximately 2.7 sec. During the nearly two-minute period that the shutter is closed, the paper tape is dried by a heating coil and the 'take up' spool advances an unexposed section of paper tape into position for the next exposure.

The tape is standard, 3½ inches wide, adding machine paper which was impregnated with dry methylene blue chloride powder. Sufficient dye was polished into the paper, as illustrated on Figure 4, to produce a uniform pale blue color.

The opening in the cover, through which the rain falls (see Fig. 2) has an area of only 33 cm². However, past studies of typical trade-wind shower rains [*Blanchard*, 1953] show that a two or three-second exposure allows from 60 to 200 drops to be collected on a 33 cm² surface. In most cases this is a sufficient number to establish the drop size distribution with useful accuracy.

The two small, 12-v dc motors and the 16-watt

---

* Contribution number 979 from the Woods Hole Oceanographic Institution.

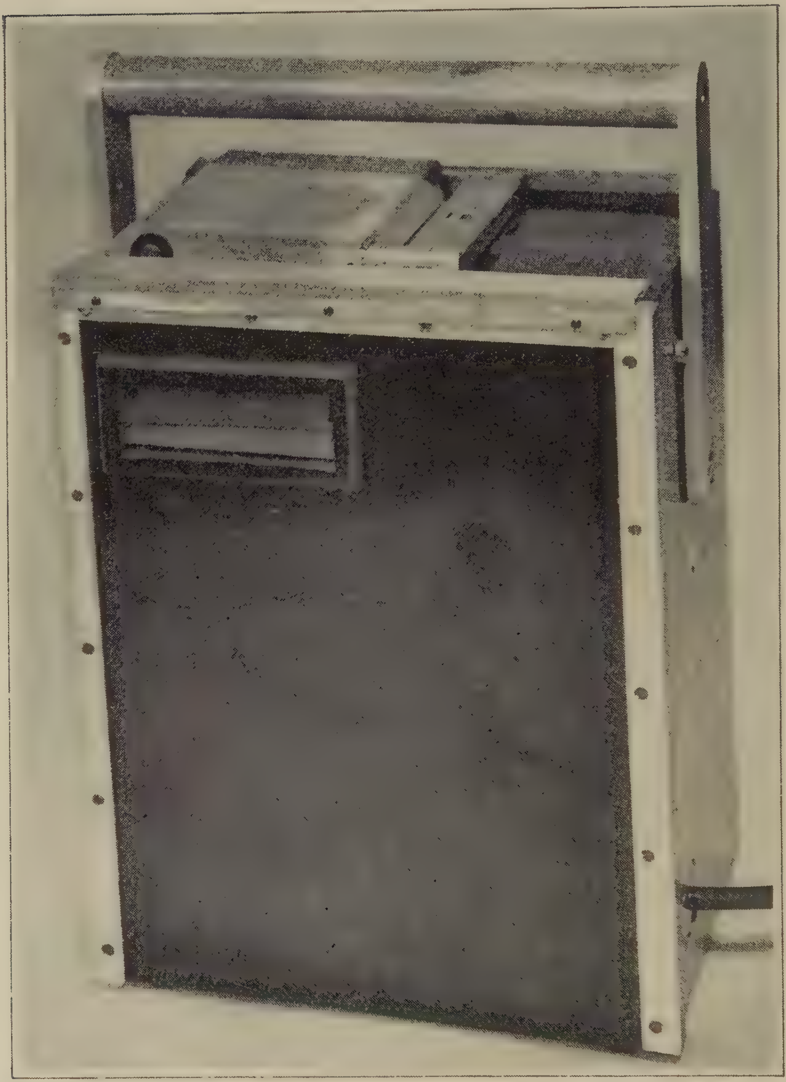

FIG. 1 – Front view of recorder showing ventilation louvers in access door and sliding door in closed position

heater coil of the recorder, are powered by a 12-v dc automobile battery. This battery will operate the recorder for 24 hrs without recharging. One of the two motors runs continuously as a timing motor. The second motor transports the paper and opens the sliding hatch to expose the tape. The heating coil is turned off, shortly before the tape is exposed, to prolong the life of the battery between charging periods.

The top surface of the case, as well as the sliding shutter, are made of Formica, a laminated plastic material of low heat conductivity. This allows the inside surface of the cover and hatch to attain a sufficiently high temperature so that condensation of the water vapor, which is evaporated from the tape does not take place. There is sufficient space between the sliding hatch or shutter, and the top surface for the vapor from the drying tape to escape to the outside air. Circulation is facilitated by the ventilation louvres revealed on Figure 1.

The fine wire mesh, which stands approximately $\frac{1}{4}$ inch above the top surface, prevents raindrops from striking the outside rigid surfaces and splashing onto the tape when the shutter is open. The splash of raindrops striking the wire mesh or the paper tape was negligible for drops of less than two

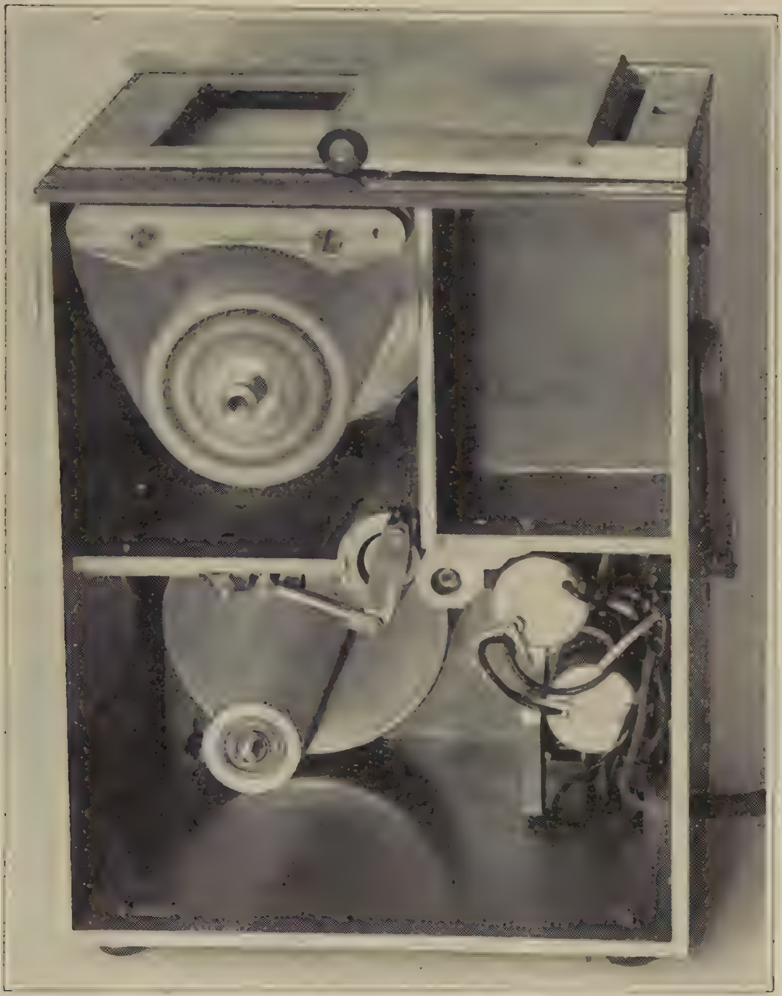

FIG. 2 – Front view of raindrop recorder with access door removed, and showing sliding door in open position

millimeters diameter. For drops larger than two millimeters the splashed drops were generally smaller than 0.2 mm.

The relatively constant rate of rotation of the small dc motors, produces a usefully constant relationship between the length of paper tape exposed and time. Thus the time of exposure of any given rain record can be extrapolated or interpolated from a few time marks manually placed on the tape during a 24-hr period.

Discussion—The drop recorders obtained excellent records in the Hawaiian orographic rains when the rain did not exceed intensities of about 25 mm hr^{-1} (see Fig. 5). The exposure time of 2.7 sec was satisfactory even when sampling the very light rains in the range of 0.1 to 1 mm hr^{-1}. Although the drops in these light rains are generally less than 500 microns diameter and thus have a low settling speed, they are present in great numbers. Consequently, the number of drops striking the recorder tape per unit time will often equal, if not exceed, that when the rain intensity is higher. This will hold true only when the sampling is done in a region where the small drops are not subject to evaporation in their fall from source to ground. At intensities greater than about 25 mm hr^{-1} the increased size of the imprint pattern of the drops resulted in overlapping and in the production of small drops by splashing.

The calibration of the recorder tape was done by letting various sized drops strike the tape at terminal velocity. Drops as small as 50 microns

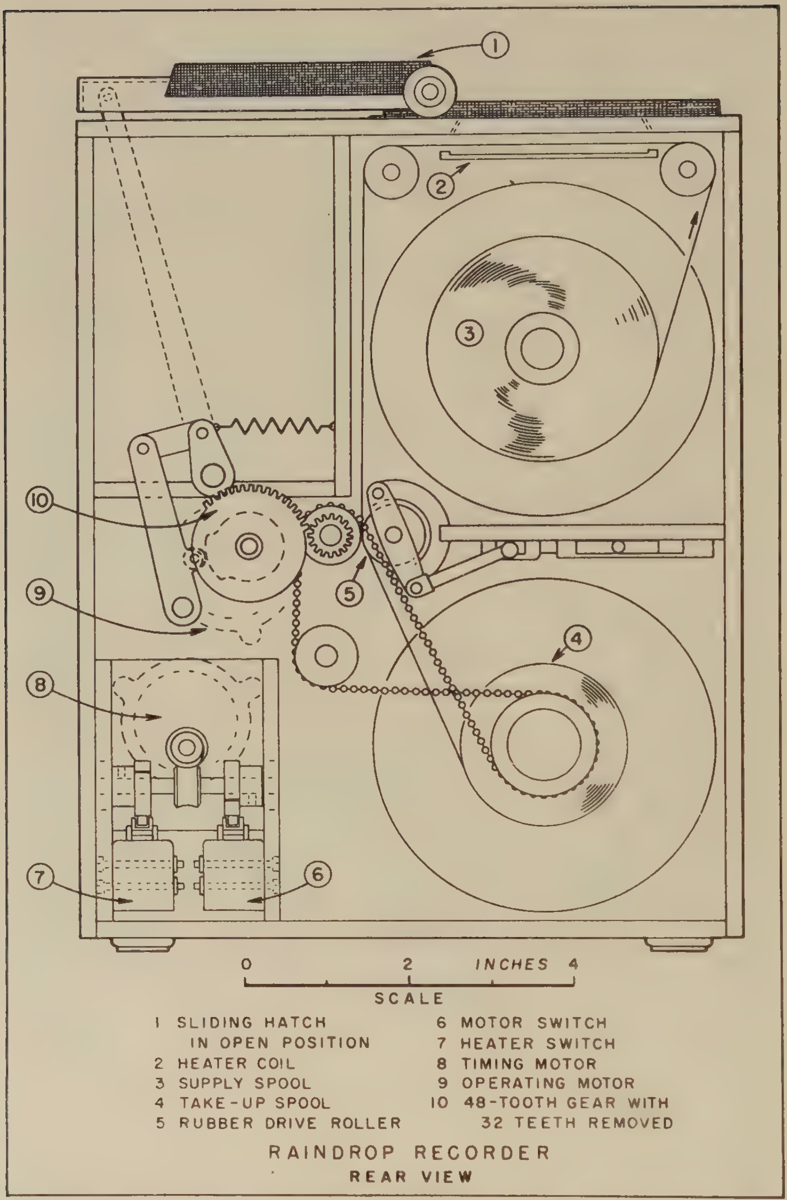
①
②
③
④
⑤
⑥
⑦
⑧
⑨
⑩
0
2
INCHES
4
SCALE
1 SLIDING HATCH IN OPEN POSITION
2 HEATER COIL
3 SUPPLY SPOOL
4 TAKE-UP SPOOL
5 RUBBER DRIVE ROLLER
6 MOTOR SWITCH
7 HEATER SWITCH
8 TIMING MOTOR
9 OPERATING MOTOR
10 48-TOOTH GEAR WITH 32 TEETH REMOVED
RAINDROP RECORDER
REAR VIEW

Fig. 3 – Sectional view of recorder with back removed; this view shows the mechanisms for transporting the paper tape and opening the sliding hatch; a cam and switch which stops the operating motor (see Fig. 3, no. 9) after 360° of rotation, is not shown here

diameter leave imprints on the dyed tape that are sharp and clear. With such small drops a low-power microscope is necessary to measure the imprint. The imprint diameter is a function of raindrop size and is from 1.5 times the drop diameter at 50 microns to about ten times the drop diameter at two millimeters. In the range commonly associated with raindrops (> 200 micron diameter) the original drop size may be determined from the imprint diameter by using a properly calibrated scale. With the aid of graphs, the drop distribution thus obtained may be converted into rain intensity or the volume distribution of raindrops.

An instrument of the type here described is useful in many cloud physics and radar weather studies. Further discussion of the use of the re-

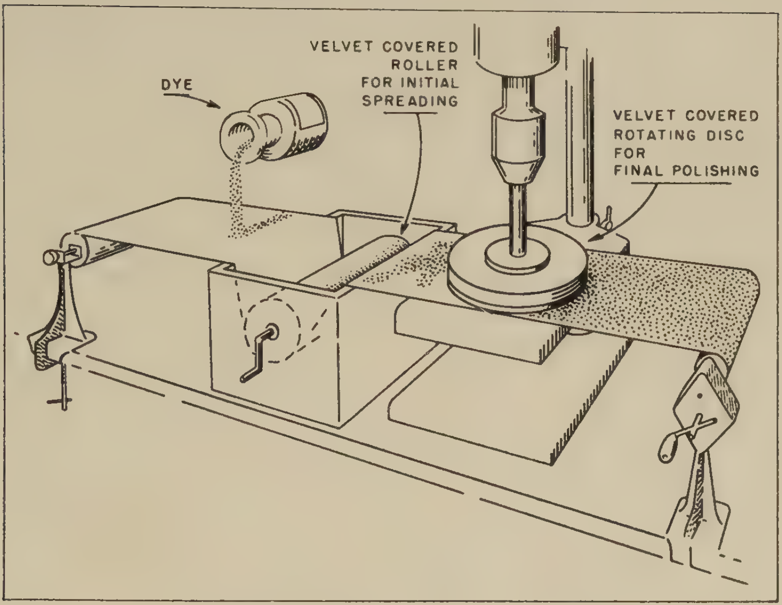
DYE
VELVET COVERED ROLLER FOR INITIAL SPREADING
VELVET COVERED ROTATING DISC FOR FINAL POLISHING

FIG. 4 – Method of impregnating paper

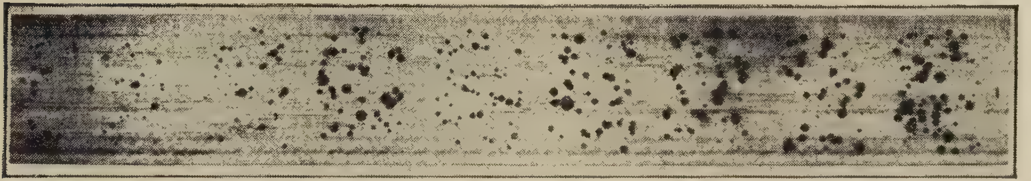

FIG. 5 – Portion of an exposed three-inch paper tape from the recorder, showing consecutive samples

corders in Hawaii are available [*Blanchard*, 1957; *Blanchard* and *Spencer*, 1957].

Acknowledgements—This paper represents the results of research carried out by the W.H.O.I. under contract with the Office of Naval Research.

REFERENCES

BOWEN, E. G., AND K. A. DAVIDSON, A raindrop spectrograph, *Q. J. R. Met. Soc.*, **77**, 445–449, 1951.

BLANCHARD, D. C., Raindrop size distribution in Hawaiian rains, *J. Met.*, **10**, 457–473, 1953.

BLANCHARD, D. C., Discussion of raindrop distribution made during Project Shower, Hawaii, 1954, *Artificial stimulation of rain*, Pergamon Press, 213–223, 1957.

BLANCHARD, D. C., AND A. T. SPENCER, Raindrop measurements during Project Shower, *Tellus*, **9**, 541–552, 1957.

COOPER, B. F., A balloon-borne instrument for telemetering raindrop size distribution and rain water content of a cloud, *Austral. J. Appl. Sci.*, **2**, 43–45 1951.

FUGIWARA, M., A new radio telemetering apparatus for measuring raindrop size, *Met. and Geophys.*, **5**, 41–46, 1954.

KATZ, I., A momentum disdrometer for measuring raindrop size from aircraft, *Bul. Amer. Met. Soc.*, **33**, 365–368, 1952.

MAULARD, J., Measure du nombre de gouttes de pluie, *J. Sci. Met.*, **10**, 69–71, 1951.

SQUIRES, P., Project Shower, an investigation of warm rain in the Hawaiian Islands, *Nature*, **175**, 748–750, 1955.

WOODCOCK, A. H., Atmospheric salt particles and raindrops, *J. Met.*, **9**, 200–212, 1952.

Woods Hole Oceanographic Institution, Woods Hole, Massachusetts

(Communicated manuscript received May 19, 1958; open for formal discussion until March 1, 1959).

Contribution No. 981

The Oceanographical Magazine
Vol. 10. No. 1 June 1958

On Convective Circulation and Density Distribution in a Zonally Uniform Ocean*

By

Takashi ICHIYE**

1. *Introduction*

Many oceanographers have worked on oceanic circulation from point of view of wind driven theory since a pioneer work of Henry STOMMEL in 1948 and it is generally accepted that the primary cause of upper circulation of the ocean may be wind stresses. However, the importance of thermal or convective circulation, particularly as a main driving force of deep sea circulation, has become confirmed recently (STOMMEL 1957, VERONIS 1957) and also some theoretical works on the subject were published (FOFONOFF 1954, LINEYKIN 1955), though the complete understanding of the problem seems to be still difficult, chiefly owing to non-linearity accompanying with the analysis of the motion.

The present study aims at obtaining the relationships between circulation and density distribution, considering a simple model of circulation in a meridional section.

2. *Fundamental equations*

In this paper the condition in the midst of the ocean far from the coast is discussed, since the existence of coastal barriers just adds an analytical difficulty which is not an essential part of convective circulation. By such assumption we can neglect east-west difference of all quantities and thus the motion can be fully described only on a meridional section. When we take y-axis as northwards and z-axis as upwards, equations of motion, continuity and mass flux are written as follows:

---

* Woods Hole Oceanographic Institution Contribution No. 981.

** Woods Hole Oceanographic Institution.

$$-fv = A\frac{\partial^2 u}{\partial z^2} \qquad (1) \qquad fu = -\frac{1}{\rho}\frac{\partial p}{\partial y} + A\frac{\partial^2 v}{\partial z^2} \qquad (2)$$

$$g\rho = -\partial p/\partial z \qquad (3) \qquad \partial v/\partial y + \partial w/\partial z = 0 \qquad (4)$$

$$v\frac{\partial \rho}{\partial y} + w\frac{\partial \rho}{\partial z} = K\frac{\partial^2 \rho}{\partial z^2} \qquad (5)$$

where u, v and w are zonal, meridional and vertical component of velocity and A and K are eddy viscosity and diffusivity. From (4) we can introduce current function φ which gives

$$v = \partial\varphi/\partial z, \qquad w = -\partial\varphi/\partial y$$

By differentiating (2) with z and substituting $\partial p/\partial z$ from (3) we have

$$f\frac{\partial u}{\partial z} = \frac{g}{\rho}\frac{\partial \rho}{\partial y} + A\frac{\partial^4 \varphi}{\partial z^4} \qquad (6)$$

We put $v = \partial\varphi/\partial z$ into (1) and integrate it with z under the boundary conditions at the surface

$$\varphi = 0, \qquad A\partial u/\partial z = T(y)$$

where $T(y)$ is zonal wind stress, we have

$$f\varphi = -A\partial u/\partial z + T \qquad (7)$$

We eliminate $\partial u/\partial z$ from (6) and (7), then we have

$$A^2\frac{\partial^4 \varphi}{\partial z^4} + A\frac{g}{\rho}\frac{\partial \rho}{\partial y} + f^2\varphi - fT = 0 \qquad (8)$$

and also from (5)

$$\frac{\partial \varphi}{\partial z}\frac{\partial \rho}{\partial y} - \frac{\partial \varphi}{\partial y}\frac{\partial \rho}{\partial z} = K\frac{\partial^2 \rho}{\partial z^2} \qquad (9)$$

These two equations (8) and (9) are basic equations for unknown functions ρ and φ.

For convenience of further computation we introduce non-dimensional variables such as

$$\varphi = \varphi_0\Psi, \quad \rho = \rho_0\sigma, \quad y = aY, \quad z = hZ, \quad T = T_0\tau$$

where a and h are meridional distance and depth of the ocean and we assume that Coriolis' parameter is linear function of y such as

$$f = f_0 + \beta y = f_0(1+\gamma Y) \quad \text{with} \quad \gamma = \beta a/f_0$$

Then we have next equations from (8) and (9)

$$\epsilon^2\frac{\partial^4 \Psi}{\partial Z^4} + (1+\gamma Y)^2\Psi = -\alpha\frac{\partial \sigma}{\partial Y} + (1+\gamma Y)\delta\tau \qquad (10)$$

$$\frac{\partial^2 \sigma}{\partial Z^2} = \kappa\left(\frac{\partial \Psi}{\partial Z}\frac{\partial \sigma}{\partial Y} - \frac{\partial \Psi}{\partial Y}\frac{\partial \sigma}{\partial Z}\right) \qquad (11)$$

where
$$\kappa = h\varphi_0/aK, \qquad \epsilon = A/h^2 f_0$$
$$\alpha = gA/f_0^2\varphi_0 a, \quad \delta = T_0/f_0\varphi_0$$

3. *Boundary layers and interior region*

Now the whole prolem is to solve the two equations (10) and (11) for unknown quantities Ψ and σ under suitable boundary conditions. The wind stress τ is given as a function of Y, but for a while we disregard this term for simplicity and we consider only convective circulation caused by the density field.

As suitable and yet simple boundary conditions, we assume that the density at the top and bottom of the ocean is given and further the density at the bottom is constant. This condition corresponds to the situation in the ocean that some meteorological condition maintains the surface density variable only in latitudes and also at the bottom (or more properly the lower boundary where the present dynamic model is valid) the density is kept constant by some dynamic process of the deep sea. As for the conditions for velocity field, we can assume that at the surface $Z=1$, $W=0$ or $\Psi=0$ and at the bottom $Z=0$, $V=W=0$ or $\Psi=0$, $\partial\Psi/\partial Z=0$, which seems to be more reasonable than the boundary conditions for density.

Then, as easily seen, the equation (10) is of boundary layer type, so that we can obtain seperate solutions for upper and lower boundary layers and interior region (FORONOFF, 1954). Especially for the boundary condition that the bottom density is constant, the lower boundary layer vanishes, since the value of $\partial\sigma/\partial Y$ is equal to zero and also $\partial^2\sigma/\partial Y\partial Z$ is small near the bottom as shown in later analysis.

The solution of the equation (10) in the upper boundary layer is obtained by neglecting the change of $\partial\sigma/\partial Y$ with the depth in this layer and it is similar to the solution of EKMAN (1905), given by

$$\Psi = -\alpha\frac{\partial\sigma}{\partial Y}[1-\exp\{-k(1-Z)\}\cos k(1-Z)]/(1+\gamma Y)^2 \qquad (13)$$

where $k=[(1+\gamma Y)/2\epsilon]^{\frac{1}{2}}$. The thickness of the boundary layer is given by $Z_0=3\pi/4k$, which is the same as the depth of friction of EKMAN. This quantity is very small compared with 1 in the present non-dimentional form, since $k \gg 1$.

In the interior region below this boundary layer, we can neglect the term with the coefficient ϵ^2 and we get

$$(1+\gamma Y)^2\Psi = -\alpha\partial\sigma/\partial Y \qquad (14)$$

When we substitute this into (11) we have

$$\frac{\partial^2\sigma}{\partial Z^2}=\frac{\alpha\kappa}{(1+\gamma Y)^2}\left(\frac{\partial^2\sigma}{\partial Y^2}\frac{\partial\sigma}{\partial Z}-\frac{\partial^2\sigma}{\partial Y\partial Z}\frac{\partial\sigma}{\partial Y}\right)-\frac{2\alpha\kappa\gamma}{(1+\gamma Y)^3}\frac{\partial\sigma}{\partial Y}\frac{\partial\sigma}{\partial Z} \tag{15}$$

which contains only one unknown variable σ and when we give boundary values at the top (or at the upper boundary layer) and the bottom of the ocean we can get the distribution of σ which in turn gives the velocity field by the equation (14).

4. *Uniformly rotating system*

As the first step we consider a simple model of uniformly rotating system, where CORIOLIS' coefficient is constant or $\gamma=0$ in the equation (15). In this model, a solution which is mathematically simple and yet represents the actual condition of the ocean in some way is expressed by a power series of Y. The solution can be obtained by equaling the coefficients of the same power of Y in the equation (15), so that only the solution of less than the second power of Y is possible.

When we put

$$\sigma=F_0(Z)+F_1(Z)Y+F_2(Z)Y^2 \tag{16}$$

then the ordinary differential equations for $F_i(Z)$ become

$$F_0''=p(2F_2F_0'-F_1'F_1) \tag{17}$$

$$F_1''=-2pF_1F_2' \tag{18}$$

$$F_2''=-2pF_2F_2' \tag{19}$$

where $p=\alpha\kappa$,

whereas the boundary conditions that the density at the surface is a function of Y and that at the bottom is constant are expressed as

$$\text{at } Z=1,\ F_0=\sigma_0,\ F_1=\sigma_1,\ F_2=\sigma_2;\quad \text{at } Z=0,\ F_0=\sigma_b,\ F_1=F_2=0 \tag{20}$$

In this solution, we cannot demand another condition at the bottom corresponding to the condition that $V=0$ or $\partial\psi/\partial Z=0$, since this leads to additional requirement such as $\partial^2\sigma/\partial Y\partial Z=0$ or $F_1'=F_2'=0$ at $Z=0$ so far as we use the relation (14) near the bottom instead of (10). This additional boundary condition can be satisfied only when we introduce the lower boundary layer, in which the stream function ψ is expressed by a similar equation to (13), with the term including the coefficient k replaced by $\exp(-kZ)(\cos kZ+\sin kZ)$ (FOFONOFF, 1954). However, since $\partial\sigma/\partial Y=F_1+2F_2Y$ is small near the bottom so long as we adopt the boundary condition $F_1(0)=F_2(0)=0$, the introduction of the lower boundary layer does not much affect the values of σ and Ψ near the bottom.

On the other hand, we cannot take the boundary condition for $F_2(Z)$ such that $F_2'=0$ at $Z=0$, regardless of any other boundary conditions. For, when we expand F_2 in power series of Z near $Z=0$, such as

$$F_2=C_0+C_1Z^s+C_2Z^{s+1}+\cdots\cdots$$

then $s>1$, if we demand the condition that $F_2'(0)=0$. Substituting this series in the equation (19), we have

$$F_2''=s(s-1)C_1Z^{s-2}+s(s+1)C_2Z^{s-1}+\cdots\cdots$$
$$F_2F_2'=C_0C_1Z^{s-1}+C_0C_2(s+1)Z^s+C_1^2Z^{2s-1}+\cdots\cdots$$

Therefore, by equaling the coefficient of the same power of Z, we have $C_1=0$, since the lowest power of Z in F_2F_2' is $Z^{s-1}(s>1)$. Then we get succesively $C_2=C_3=$ $=\cdots\cdots 0$.

The solutions of the equation system (17)—(19) is obtained by integrating first the equation (19), which gives

$$F_2'=-p(F_2^2\pm C^2) \tag{21}$$

where C is a positive integration constant, and plus sign corresponds to a negative value of σ_2 and minus to a positive σ_2. For by integrating (21) again we get

$$\left.\begin{aligned} F_2&=c\tanh cpZ \quad (\text{for } \sigma_2>0) \quad (\text{A}) \\ F_2&=-c\tan cpZ \quad (\text{for } \sigma_2<0) \quad (\text{B}) \end{aligned}\right\} \tag{22}$$

where the constant C is determined by the boundary condition at $Z=1$, which gives

$$c\tanh cp=\sigma_2 \quad (\text{A}), \qquad c\tan cp=-\sigma_2 \quad (\text{B}) \tag{23}$$

The equation (18) becomes

$$\left.\begin{aligned} F_1''&=-(2p^2c^2\operatorname{sech}^2 cpZ)F_1 \quad (\text{A}) \\ F_1''&=(2p^2c^2\sec^2 cpZ)F_1 \quad (\text{B}) \end{aligned}\right\} \tag{24}$$

These equations cannot be integrated by use of elementary functions, so that we have to resort to numerical integration or approximate integration.* However, as shown later, numerical value of cp is generally small compared with 1 for reason-

---

* More exact approximate solution of the equation (24) is expressed by use of Bessel functions. First, we change a variable Z to $\xi=mZ+n$ by a linear transformation. Then we can express the coefficient of F_1 in the equation (24) by some power or ξ such as

$$d^2F_1/d\xi^2+\beta\xi^sF_1=0$$

for the interval of $Z=0$ to 1 by taking suitable numerical constants m, n, β and s, so that $\beta\xi^s$ may give the value as close to the original coefficient of F_1 as possible. Then this equation has a solution of a type

$$F_1(\xi)=C_1\sqrt{\xi}\,J_{\frac{1}{s+2}}\Big(\frac{2\sqrt{\beta}}{s+2}\xi^{\frac{s+2}{2}}+C_2\sqrt{\xi}\,Y_{\frac{1}{s+2}}\Big(\frac{2\sqrt{\beta}}{s+2}\xi^{\frac{s+2}{2}}\Big)$$

where C_1 and C_2 are integration constant to be determined from the boundary conditions.

able physical constants in the ocean, we can consider $\operatorname{sech}^2 cpZ$ or $\sec cpZ$ almost constant between $Z=0$ and 1 and replace them by their mean value in this interval, then we have

$$F_1'' \doteqdot -2p\sigma_2 F_1 \quad \text{(A) and (B)} \tag{25}$$

as easily verified by use of the condition (23). Thus the solution satisfying the boundary condition (20) is given by

$$F_1 = \frac{\sigma_1 \sin\sqrt{2p\sigma_2}\,Z}{\sin\sqrt{2p\sigma_2}} \quad \text{(A)}, \qquad F_2 = \frac{\sigma_1 \sinh\sqrt{-2p\sigma_2}\,Z}{\sinh\sqrt{-2p\sigma_2}} \quad \text{(B)} \tag{26}$$

The solution F_0 of the equation (17) is also given by a simple integration which is

$$F_0' = A\exp\left(2p\int_0^z F_2 dz\right) - p\exp\left(2p\int_0^z F_2 dz\right)\int_0^z F_1 F_1' \exp\left(-2p\int_0^{z_1} F_2 dz\right) dz_1 \tag{27}$$

or

$$\left.\begin{aligned} F_0' &= A\cosh^2 cpZ - B\cosh^2 cpZ \int_0^z \sin 2\sqrt{2p\sigma_2}\,Z \cosh^{-2} cpZ dz \quad \text{(A)} \\ F_0' &= A\cos^2 cpZ - B\cos^2 cpZ \int_0^z \sinh 2\sqrt{-2p\sigma_2}\,Z \cos^{-2} cpZ dz \quad \text{(B)} \end{aligned}\right\} \tag{28}$$

where A is an integration constant determined by the boundary condition and B represents

$$B = \frac{\sigma_1{}^2\sqrt{2\sigma_2 p}}{\sin^2\sqrt{2\sigma_2 p}} \quad \text{(A)}, \qquad B = \frac{\sigma_1{}^2\sqrt{-2\sigma_2 p}}{\sinh^2\sqrt{-2\sigma_2 p}} \quad \text{(B)}$$

Since the function $F_0(z)$ represents the vertical profile of the density at $Y=0$ or, so to speak, at the reference station, we had better state physical explanation of each term of (27) or (28). When we consider the equation (14), the function F_2 represents the vertical current, as easily seen from the relationship

$$W = -\frac{\partial\Psi}{\partial Y} = \alpha\frac{\partial^2\sigma}{\partial Y^2} = 2\alpha F_2$$

Therefore we can consider that the first term represents the effect of vertical current upon the density profile. On the other hand, even when F_2 vanishes, or there is no vertical motion, the second term gives the distribution of density different from constant, if F_1' is not zero, so that this term may be interpreted as giving the effect of horizontal current. Thus we call these two terms convective and advective term, respectively. The advective term vanishes at the bottom, and when we demand the flux of mass to vanish at the bottom at $Y=0$, $A=0$ or only the advective term remains.

The complete solution of (17) satisfying the boundary condition (20) is thus written as

$$\left.\begin{array}{ll} F_0=(J(1)-\sigma_b+\sigma_0)\tanh cpZ/\tanh cp+\sigma_b-J(Z) & \text{(A)} \\ F_0=(J(1)-\sigma_b+\sigma_0)\tan cpZ/\tan cp+\sigma_b-J(Z) & \text{(B)} \end{array}\right\} \qquad (29)$$

where
$$J(z)=B\int_0^z \cosh^2 cpZ_1\int_0^{z_1}\sin 2\sqrt{2p\sigma_2}Z_2\cosh^{-2} cpZ_2 dz_1 dz_2 \quad \text{(A)}$$

$$J(z)=B\int_0^z \cos^2 cpZ_1\int_0^{z_1}\sinh 2\sqrt{-2p\sigma_2}Z_2\cos^{-2} cpZ_2 dz_1 dz_2 \quad \text{(B)}$$

Numerical Computation: The parameter p is given by $p=\alpha\kappa=gAh/Kaf_0^2$, and we give next geometrical and physical constants corresponding to the ocean (here we have to remind that we assume that Coriolis' coefficient is constant, so that we cannot discuss the condition of the whole scale ocean)

$$f_0=10^{-4}, \quad a=10^8, \quad h=10^5, \quad g=10^3$$

then we have $p=A/K$. As stated before, cp must be small compared with 1, so that the approximation (20) may be valid, and this condition is satisfied so long as $p<10^3$, when we determine c from the condition (23) for a reasonable value of $\sigma_2=10^{-3}$. Actually we have no conclusive knowledge about the magnitude of eddy viscosity and eddy diffusivity in the ocean, but there are many evidences (for example, Sverdrup *et al*, Ocean) that the ratio A/K is larger than 1 and smaller than 10^3. Therefore we compute the density distribution expressed by (22), (26) and (29) with $p=10^3$ and $p=10$. Further, we take

$$\sigma_0-\sigma_b=3\times10^{-3}, \quad \sigma_1=2\times10^{-3}, \quad \sigma_2=\pm10^{-3}$$

where these values of σ_t can be given in σ_t values instead density itself.

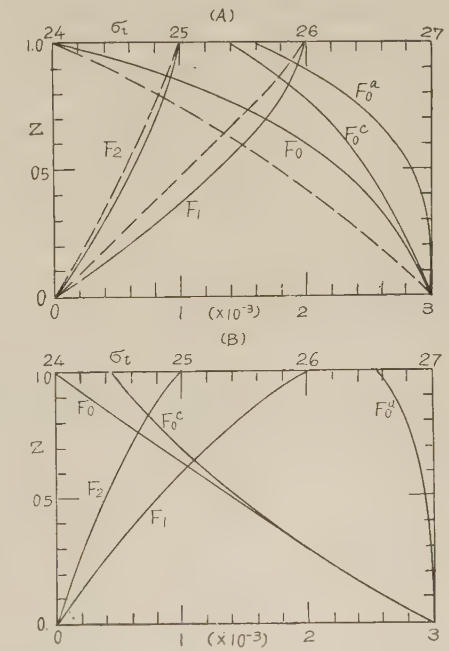

Fig. 1. Profiles of F_i, in two models for $A/K=10^3$ (In (A), broken lines are curves for $A/K=10^2$).

In Fig. 1 we indicate vertical profiles of F_0, F_1 and F_2 for model (A) ($\sigma_2=10^{-3}$) and (B) ($\sigma_2=-10^{-3}$) by use of these numerical values. As stated in the beginning of this section, these curves represent the values of functions F_0, F_1 and F_2 only in the interior region of the ocean where $\epsilon^2\Psi^{(IV)}$ can be neglected, so that we might avoid additional complication. Therefore, in order to obtain complete pictures of the distribution of the density in the whole depth of the ocean we have to add upper and lower boundary layer outside the considered region, where F_i is constant with the depth.

When we look at the curves, we can see that all F_i are linear function of Z for $p=10$, which means that in the present model the water mass is almost thoroughly mixed in a vertical direction already for a eddy diffusivity of about one tenth of an eddy viscosity. When the ratio A/K increases, the effect of convection also increases, since the whole system of current on meridional section in this model is produced by frictional force even in the interior region (as seen in the equation (1) menidional velocity V is caused by frictional force) and thus the increase of A produces stronger current on this section. The difference between (A) and (B) is clearly seen in the profile of $F_0(z)$ for $p=10^3$, where in (A) vertical current is upwards and thus it brings the heavy water towards surface, resulting in producing more shallow thermocline than in the model (B). Further, in this figure we show the advective (F_0^a) and convective term (F_0^c, the first

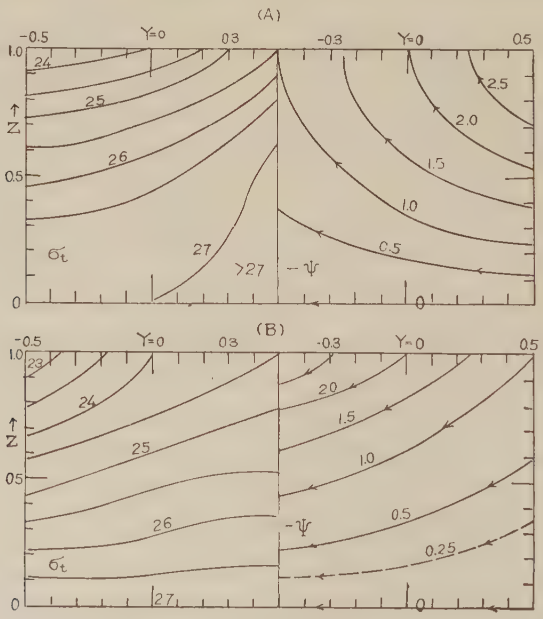

Fig. 2. Density field (in σ_t) and stream function (in A/φ_0).

term including tanh cpZ or tan cpZ) in the equation (29). We can see that the relative magnitude of these two terms are different in two models and in the model (A) they are almost of the same order, whereas in the model (B) the advective term F_0^a is quite small compared with F_0^c. The reason of this difference is more clearly illustrated by vertical sections of density and stream pattern which are shown in Fig. 2. (Stream function Ψ is shown with a unit of $\frac{A}{\varphi_0}$.) We can see at once that in the model (A) stream lines cross isopicnals, whereas in (B) they are almost parallel. Moreover, in the model (A) thermocline becomes more shallow towards north, but in (B) in it is almost the same, slightly deeper towards north. (In this numerical example the density decreases downwards in the layer of about $0.4>Z>0$ at $Y=0.5$, so that in this layer instability occurs. However, the present model is only a schematical one and we are not concerned with stability problem).

As one more simple model, we show the density distribution for $\sigma_2=0$, where there is no vertical motion since $F_2=0$ and thus

$$F_1=\sigma_1 Z, \quad F_0=(\sigma_0-\sigma_b)Z+\sigma_b+p\sigma_1^2(Z-Z^3)/\sigma \tag{30}$$

The density field is rather similar to that of the model (B), because, as seen from the distribution of $F_0(z)$ in Fig. 1. $F_0(z)$ is almost the same in these two models.

5. *Circulation produced by a density field increasing uniformly polarwards in β plane.*

In a uniformly rotating system we have an exact solution for a given distribution of density at the surface expressed by up to the square equation of Y. On the other hand, in a $\beta-$ plane, the solution of (15) is expressed exactly with finite series of Y only when the surface density is given as a linear function of Y. In fact, we may assume that

$$p=\alpha\kappa(1+\gamma Y)^{-2}=\text{const.}, \quad q=2\alpha\kappa\gamma(1+\gamma Y)^{-3}=\text{const.} \tag{31}$$

in β=plane, since p is proportional to f^{-2} and q is to βf^{-2}. Then when we put (16) into

$$\frac{\partial^2\sigma}{\partial Z^2}=p\left(\frac{\partial^2\sigma}{\sigma Y^2}\frac{\partial\sigma}{\partial Z}-\frac{\partial^2\sigma}{\partial Y\partial Z}\frac{\partial\sigma}{\partial Y}\right)-q\frac{\partial\sigma}{\partial Y}\frac{\partial\sigma}{\partial Z} \tag{15'}$$

equations which are obtained by equaling the same degree of Y in both side of (15′) are as follows:

$$F_0''=p(2F_0'F_2-F_1'F_1)-qF_1F_0' \tag{32}$$

$$F_1''=-2pF_1F_2'-q(F_1'F_1+2F_0'F_2) \tag{33}$$

$$F_2''=-2pF_2F_2'-q(2F_2F_1'+F_1F_2'') \tag{34}$$

and also there exists a term $-qF_2F_2'Y^3$ in the right hand side of the equation (15′), which should vanish. However, this is impossible, so that we have to express σ in infinite series of Y or if we want to have finite form of the solution, we should put $F_2=0$. In this section we follow the second approach and we shall compare the results with those of the previous model.

By taking the type of solution $\sigma=F_0+YF_1$, we have the ordinary differential equations for F_0 and F from (32) and (33) such as

$$F_0' = -pF_1'F_1 - qF_1F_0' \tag{35}$$

$$F_1'' = -qF_1'F_1 \tag{36}$$

where the second equation is integrated at once by the same process described in the previous section and the solution is

$$F_1 = c\tanh(qcZ/z) \tag{37}$$

in which the integration constant c is determined from the relation such as $\sigma_1=c\tanh(qc/2)$ for the boundary condition that $F_1(0)=0$, $F_1(1)=\sigma_1$.

The solution of the first equation F_0' is also given by

$$F_0' = \mathrm{sech}^2(qcZ/2)\,(A - pc^2\log\cosh(qcZ/2)) \tag{38}$$

where A is an integration constant. Further, when we take the same boundary condition as given in (20), we have

$$F_0 = (\sigma_0 - \sigma_b + I(1))\tanh\frac{qcZ}{2}\Big/\left(\tanh\frac{qc}{2}\right) - I(Z) + \sigma_b \tag{39}$$

where $$I(Z) = pc^2\int_0^z \mathrm{sech}^2(qcZ/2)\log\cosh(qcZ/z)\,dz$$

Numerical computation. For numerical computation of these equations, we use the following constants

$$\beta=2\times10^{-13},\quad \gamma=0.4$$

in addition to the physical and geometrical constants already introduced in the previous section. Since the analysis of this section include the effect of β, we can assume that the present model is valid for larger range of Y than the previous model, so that we shall compute the distribution of σ and Y from $Y=-1$ to 1. Then the average values of p and q in this range of Y are

$$p=1.774\,A/K,\qquad q=1.872\,A/K$$

Here we should remind that the solution (37) and (39) are valid only in the interior region, therefore we have to take the upper boundary of the solutions as $1-Z_0$ instead of 1. However, this only contributes to make the mathematical form more complicated, so that we keep the mathematical formula simple and yet in numerical computation of the distribution of σ and ψ

we introduce the upper boundary layer. This layer is located from $Z=1-Z_0$ to $Z=1$ as stated in section 3, and the distribution of ψ is computed from the equation (13).

The results are shown in Fig. 3 and 4, where meridional section of σ and ψ are indicated for the ratio $A/K=10$ and 10^3. As stated in the previous section, the vertical profile of $F_0(z)$ and $F_1(z)$ approaches to linear function of depth Z as the ratio A/K decreases, so that they are almost expressed by linear function of Z for $A/K=10$. On the other hand, in the interior region

$$\psi=-\alpha F_1(Z)/(1+\partial Y)^2$$

and $F_1(z)>0$ in this model, we have a downwards vertical motion throughout the interior region from the relation $W=-\partial\Psi/\partial Y$, even though in case of $F_2\equiv0$, which gives no vertical current in an uniformly rotating system. Therefore, in the previous model the density profiles show deeper thermocline generally than in the previous model, owing to the sinking motion.

However, the response of the density distribution for such vertical movement is different for different values of A/K, and indeed for $A/K=10^3$, the isopicnals are more horizontal than for $A/K=10$, indicating that the depth of maximum

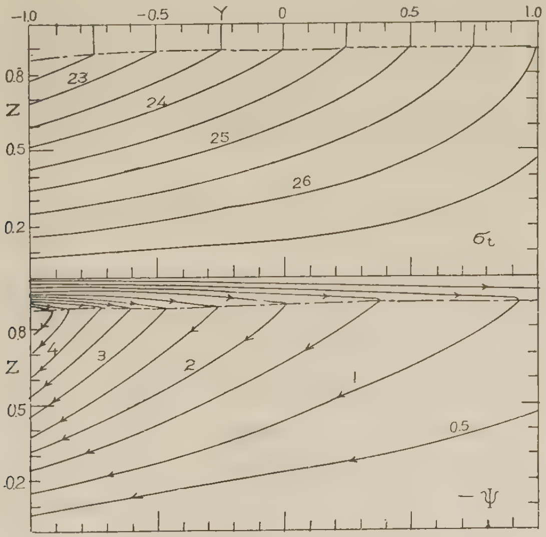

Fig. 3. Density field (in σ_t) and stream function (in A/φ_0) for $A/K=10$. (Chain lines indicate a limit of upper boundary layer).

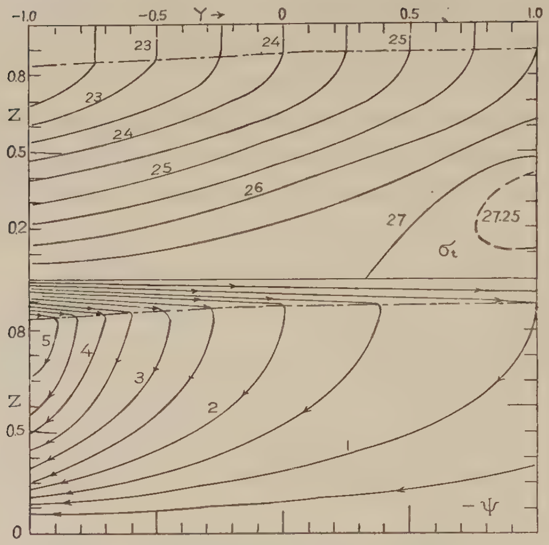

Fig. 4. Density field and stream function for $A/K=10^3$.

gradient becomes deeper towards low latitude. On the other hand, current pattern indicated by the distribution of ψ shows that in low latitudes sinking motion is stronger for $A/K \doteq 10^3$ than for $A/K=10$. Therefore, in the former case the streamlines and isopicnals cross each other, whereas in the latter they are almost parallel, which is explained by considering the relative magnitude of the advective effect and diffusion effect.

6. *Circulation produced by the uniformly increased surface density in a variable p, q.*

In the previous section we assume that p and q are constant throughout the domain $-1 \leqslant Y \leqslant 1$, which is rather bold assumption, because they are variable in this range of Y such as $2.78 \geqslant p(K/A) \geqslant 0.51$, $3.70 \geqslant q(K/A) \geqslant 0.29$. In order to improve this approximation, we divide this range of Y into small intervals, where p and q are safely assumed to be constant. Then in each of such intervals we apply the procedure descrided in the previous section to obtain the solution. The values of the solutions at a boundary of successive intervals which are computed by use of the formula (37) and (39) in each interval are not equal to each other mathematically. However, so long as we consider the boundary condition that the surface density is linear function of Y, these two values are almost the same practically by taking the distance of such interval to be small enough. Therefore, we can consider such procedure gives an accurate solution numerically. Here we divide the whole range of $-1 \leqslant Y \leqslant 1$ into 10 intervals of equal distance of 0.2, and compute the values of σ and Ψ for the ratio $A/K=10^3$ and same physical constants as in the previous section.

The result which is shown in Fig. 5 indicate us that the isopicnals and streamlines become more vertical in the lower latitudes than in the previous model shown in Fig. 3 and 4, suggesting that vertical current in the lower latitudes is stronger than in the model of constant p and q, as easily verified by the relation of Ψ and p. When the ratio A/K decreases and is equal to about 10, the distributions of σ and ψ are almost the same as in the previous model, so that they are not shown here.

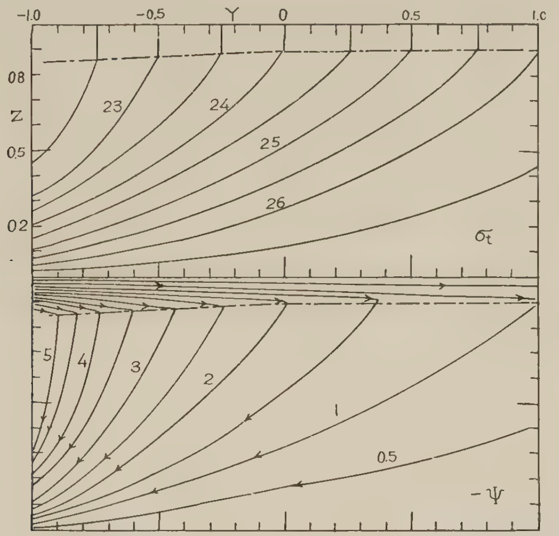

Fig. 5. Density field (in σ_t) and stream function (in A/φ_0) with varying p and q for $A/K=10^3$.

On the other hand, in an interval where Y is variable within a small fraction of 1, we can assume $p=\alpha\kappa/(1+\gamma Y)^2=-q_1Y+p_1$. Then equations for F_0 and F_1 become

$$F_0''=-p_1F_1'F_1-qF_0'F_1 \tag{40}$$

$$F_1''=(q_1-q)F_1'F_1 \tag{41}$$

instead of (35) and (36). Generally $q_1 \fallingdotseq q$ in an interval of small distance, so that we have simply $F_1=\sigma_1 Z$. Also the solution of (40) is given by

$$F_0'=A\exp\left(-\frac{q\sigma_1}{2}Z^2\right)-\frac{p_1\sigma_1}{q}\left\{1-\exp\left(-\frac{q\sigma_1}{2}Z^2\right)\right\} \tag{42}$$

or

$$F_0=(\sigma_0-\sigma_b+H(1))\,Erf(\beta Z)/Erf(\beta)-H(Z)+\sigma_b \tag{43}$$

where A is an integration constant and $Erf(Z)$ is an error function. Also $H(Z)$ is given by

$$H(Z)=\frac{p_1\sigma_1}{q}\left\{Z-\frac{\sqrt{\pi}}{2\beta}Erf(\beta Z)\right\},\quad \beta=\sqrt{q\sigma_1/2}$$

The result of numerical computation of this model by dividing the range into the same small intrervals as in the previous case is shown in Fig. 6. by use of the same constants, which gives the intermediate pattern of the density between the model of the previous section and that described just above, although current pattern is the same as that of the case $A/K=10$ shown in Fig. 4.

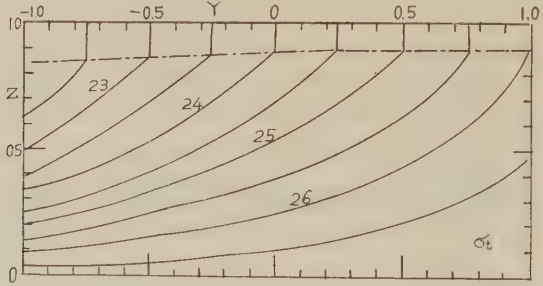

Fig. 6. Density field with linearly varying p for $A/K=10^3$.

7. *Ciruculation produced by arbitrary distribution of the surface density*

The solution which is expanded in power series of Y can be obtained only in a limited case of the boundary condition that the surface density is expressed by linear function of Y. In any other form of the boundary value, the series become infinite and ordinary differential equations for each coefficient F_i of Y^i are non-linear and prohibitively complicated.

On the other hand, when we give up the boundary condition which demands a predescribed surface value of density, we can obtain finite form of the solution of type $F(Y)\ G(Z)$ which is mathematically exact. This type of solution gives the density distribution which has a similar vertical profile all over the ocean, which is not true in actual case, since generally thermocline in the lower latitudes are more shallow than that of higher latitudes. Moreover, in this type of a solution we cannot specify the surface value of density except at two points of the surface, because for definite function $G(Z)$, $F(Y)$ is defined as a solution of the second order ordinary differential equation.

Neverthless, we can obtain various kinds of distribution of density by changing parameters, which correspond to many actual conditions of the ocean, and comparison of such density field with corresponding current pattern gives some interesting explanation concerning the relationships between circulation and density distribution.

The solution within the boundary layer is the same as in the previous section and we have only to consider the solution of (15). When we introduce a new variable defined by

$$(1+\gamma Y)^2 dY = dX \qquad \text{or} \qquad X = (1+\gamma Y)^3/3\gamma \tag{44}$$

the equation (15) is transformed into

$$\frac{\partial^2\sigma}{\partial Z^2} = \alpha\kappa\,(3\gamma X)^{\frac{2}{3}}\left(\frac{\partial^2\sigma}{\partial X^2}\,\frac{\partial\sigma}{\partial Z} - \frac{\partial\sigma}{\partial Z}\,\frac{\partial^2\sigma}{\partial X\partial Z}\right) \tag{45}$$

This equation has a type of solution $F(X)G(Z)$ and also the general form of the solution is expressed by

$$\sigma = F(X)\,G(Z) + f(X) + \sigma_b \tag{46}$$

where σ_b is an arbitrary constant and $f(X)$ is a function having a next form

$$f(X) = b + a\int^{x} F dX \tag{47}$$

in which a and b are integral constants.

The main problem of solving (28) is therefore to get $F(X)$ and $G(Z)$ and when we substitute (29) into (28), we have

$$\frac{G''(Z)}{\alpha\kappa G(Z)\,G'(Z)} = \frac{F''(X)\,F(X) - \{F'(X)\}^2}{(3\gamma X)^{-\frac{2}{3}}F(X)} = \text{const.} \tag{48}$$

This constant may be taken arbitrary, so that we put it 1 or -1 without losing generality.

The equation concerning $G(Z)$ is integrated immediately, by use of the same method as in previous sections. As the first step, we assume that $f(X)=0$, in order to simplify the solution. Thus the boundary condition at the bottom for $G(Z)$ is such that $G(0)=0$, corresponding to the condition that vertical current vanishes there or $\partial\sigma/\partial Y=0$. Further, we can consider $F(X)>0$ without loss of generality, since when $F(X)<0$, we only have to change of the sign of constant of the equation (48). Then we should put $G'(Z)<0$ corresponding to stable stratification in the ocean. Then we obtain two types of solution for $G(Z)$ to different values of integration constant of (48), such as

$$\left.\begin{array}{lll} G=-c\tanh rcZ & \text{(for 1)} & \text{(C)} \\ G=-c\tan rcZ & \text{(for }-1\text{)} & \text{(D)} \end{array}\right\} \qquad (49)$$

where c is an integration constant to be determined from the boundary conditions such that

$$c\tanh rc=m \quad \text{(C)} \qquad c\tan rc=m \quad \text{(D)} \qquad \left(r=\frac{\alpha\kappa}{2}\right)$$

These two types of solution give quite different profiles in vertical section of density, so that it is important to include both signs in the constant of (48), whereas its numerical values are adjusted by changing the boundary values of $G(1)=-m$, so that it does not harm generality to put it ±1.

The differential equation for $F(X)$ becomes

$$F''F-(F')^2=\pm(3\gamma X)^{-\frac{2}{3}}F \qquad \text{(for C and D)} \qquad (50)$$

is also non-linear type and it can be integrated by some approximate process. First of all we express the function $(3\gamma X)^{-\frac{2}{3}}$ approximately by an exponential function of a type

$$j(X)=\exp\left(a_0+a_1X+a_2X^2\right) \qquad (51)$$

by taking suitable constants a_c, a_1 and a_2, which is possible as shown in the next section. Then we put

$$F(X)=j(X)\exp\{\phi(X)\} \qquad (52)$$

and we have

$$F''F-(F')^2=(\phi''+2a_2)F^2.$$

Therefore the equation (50) is transformed into

$$F''+2a_2=\pm\exp(-\phi) \qquad \text{(for C and D)} \qquad (53)$$

By multiplying ϕ' to both sides of this equation, we can integrate, because $\phi'\exp(-\phi)=\dfrac{-d\exp(-\phi)}{dX}$, and we have

$$(\phi')^2=\mp 2\exp(-\phi)-4a_2\phi+l \qquad (54)$$

where l is an integral constant and minus sign corresponds to the case (C) and plus corresponds to (D). From (54) we get easily

$$\phi'=\pm\{\mp 2\exp(-\phi)-4a_2\phi+l\}^{\frac{1}{2}} \qquad (55)$$

or

$$\pm\int_{\phi_0}^{\phi}\{\mp 2\exp(-\phi)-4a_2\phi+l\}^{-\frac{1}{2}}\,d\phi=X-X_0 \tag{56}$$

where ϕ_0 corresponds to the value of ϕ at X_0, the lower limit of X in the considered domain and the double sign before the integral sign should be taken so as to give the positive value of the left hand side of the equation, whereas the minus sign within the parentheses corresponds to (C) and the plus corresponds to (D).

8. *Preliminary discussion for numerical computation of Section 7.*

The behavior of the function $F(X)$ is rather complicated, because has very intricate form and also it has two integration constants to be determined from the boundary conditions, whereas $G(Z)$ is simple in its integrated form and only one parameter However, the difference of vertical profile of $G(Z)$ in two cases (C) and (D) gives a remarkable contrast in a vertical distribution of density pattern, which, in turn, is closely associated with current system, since $F(X)$ is also different in two cases.

In order to illustrate the contrast between (C) and (D), we show vertical distributions of $G(Z)$ for $2r=\alpha\kappa=1$ to 10^2 by taking $m=1$ in Fig. 7, which indicates that the profile of (C) gives thermocline deeper than that of (D). As shown later, different function $F(X)$ corresponds to different value of m, so that we cannot compare this vertical profile with the previous models. However, it is interesting to note that the vertical profiles of this model are almost similar to the models treated by the author (Ichiye, 1958). which is derived on the basis of balance between planetary vorticity and divergence. Thus, the present case of (C) give profiles similar to vertical density distribution obtained for a westward increasing density field in the previous model, with homogeneous layer in the upper layer. On the other hand, the profiles corresponding to (D) have homogeneous layer near the bottom, similar to those of a eastwards increasing density field. Moreover, in the present model too, a decreasing value of $2r=A/K$ produces the profiles approaching to linear

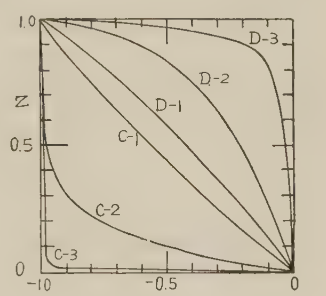

Fig. 7.

Curves of G(Z)
C—Model (C)
D—Model (D)
1—$\alpha\kappa=1$
2—$\alpha\kappa=10$
3—$\alpha\kappa=10^2$

function with the depth, which is considered as a well-mixed state.

For computing $F(X)$, first we have to determine the numerical constants a_0, a_1 and a_2, so that $j(X)$ may give a close approximation to $(3\gamma X)^{-\frac{2}{3}}$, This estimation is done by use of least squares and the result is

$$a_0=1.770, \qquad a_1=-1.937, \qquad a_2=0.572$$

The exact curve of $(3\gamma X)^{-\frac{2}{3}}$ and the approximate curve are shown in Fig. 8, which indicate that the correspond between two curves is good only in a range of X from 0.2 to 1.6 or in a range of Y from -0.9 to 0.6. However, this does not hurt the applicability of the present model, since is we take a larger value of γ, we can cover wider range of X by such approximation. We can integrate the equation (56) by numerical method. or ther approximation process which is to be described in the following sections.

The analytic property of the integral (56) is much changed for different values of parameters ϕ_0 and l. The value of ϕ_0 can be determined from the surface value of density $\sigma(X, 0)$ at the lowest latitude $X=X_0$ and also the parameter m for the function $G(Z)$. When we put $\sigma(X_0, 0)=-\sigma_0+\sigma_b$, then $F(X_0)=\sigma_0/m$ and

$$\phi_0=\log(\sigma_0/m)-\log j(X_0)$$

The integration constant l is determined by another boundary condition. When we put $\eta=\phi-\phi_0$, the equation (56) becomes

$$\pm\int_0^\eta e^{\phi_0/2}(\mp 2e^{-\eta}-4a_2\eta e^{\phi_0}+k)^{-\frac{1}{2}}\,d\eta=X-X_0 \tag{57}$$

Further, when we put the value or $\eta=\eta_1$ at $X=X_1$, this is determined only by the ratio of the surface density at $X=X_0$ and $X=X_1$ since

$$\eta_1=\phi_1-\phi_0=\log\sigma_1/\sigma_0-\log j(X_0)/j(X_1)$$

where $\qquad \sigma(X_1, 0)=-\sigma_1+\sigma_b$ and $\phi(X_1)=\phi_1$.

When η is monotonous function of X in the range $X_0\leqslant X\leqslant X_1$ we have take positive or negative sign before the integral of (57) according to positive or negative value of η_1. On the other hand, when η has maximum or minimum in this range, for example, maximum η_m at $X=X_m$, we can express the relation (57) for (C) as

$$\left.\begin{aligned}
&(\text{for } X_0<X<X_m) \quad X-X_0=e^{\frac{\phi_0}{2}}\int_0^\eta\{2(e^{-\eta_m}e^{-\eta})+4a_2e^{\phi_0}(\eta_m-\eta)\}^{-\frac{1}{2}}\,d\eta\\
&(\text{for } X_m<X<X_1) \quad X-X_m=e^{\frac{\phi_0}{2}}\int_\eta^{\eta_m}\{2(e^{-\eta_m}-e^{-\eta})+4a_2e^{\phi_0}(\eta_m-\eta)\}^{-\frac{1}{2}}\,d\eta
\end{aligned}\right\} \tag{58}$$

and for (D) we only have to change the sign before e^{η}.

9. *Various examples of density distribution and circulation pattern*

Now we can compute any density destribution and stream function induced by such density pattern by use of (49) (52), (56) and (58). Here we summarize the process to compute these equations so as to give a density distribution which is plausible in the actual ocean. As stated in section 8, we shall determine a value of σ which satisfys the boundary condition that $\sigma=\sigma_b$ at the bottom $Z=0$ and $\sigma=\sigma_b-\sigma_0$ at $X=X_0$ and $\sigma=\sigma_b-\sigma_1$ at $X=X_1$ at the surface (or more precisely at the upper boundary layer).

First we take arbitrarily ϕ_0 (actually the range is limitted in order to obtain a reasonable result) and we determine integration constant k in the equation (57) or η_m in (58) from the boundary condition at $X=X_1$ that $\eta(X_1)=\eta_1=\phi_1-\phi_0$ This process is generally carried out by trial and error method, but actually the range of η_1, η_m is not so large compared with 1 we can express the integral (57) or (57) by elementary functions as described below, so that we can compute these constants rather analytically in most cases. From the relation between η and X thus determined we can compute a function $F(X)$.

For each function $F(X)$ or for each initial constant ϕ_0 one value of m is determined from the relation $m=\sigma_0/F(X_0)$. Then we can compute the function $G(Z)$ from the equation (49) where c is determined from the boundary condition for different values of $r=\alpha\kappa/2$. Therefore for each surface density distribution we can assort various kinds of vertical profiles represented by the function $G(Z)$ according to different values of the ration A/K, say, from the profile with very shallow thermocline for a large value of the ratio, when the function $G(Z)$ belongs to the type (D), to the linear function of Z for a small value of it.

As easily seen, the solution $F(X)$ cannot be uniquely determined only by specifying the surface density at two points, because we can take ϕ_0 arbitrarily and adjust m. Also it is important that we cannot specify the surface density distribution all over the region in the present approach as in the process of section 5 and 6, so that we have to seek various kinds of solution by changing parameters so as to give plausible surface density distribution instead of impose it as a boundary condition.

Singular solution. When $\phi_0 \gg 1$, the integral (57) can be integrated by use of elementary function, since the exponential term in the integrand is negligibly small, so that for example the equation (56) is written as

$$X-X_0=\frac{1}{2a_2}(l^{\frac{1}{2}}-\overline{l-4a_2\eta}^{\frac{1}{2}})$$

On the other hand, this type of solution corresponds to a singular solution of the original equation (45), since in such condition the equation (53) becomes $\phi''+2a_2=0$. Therefore we have

$$F(X)=F_0e^{\gamma X}$$

where F_0 and γ are constants to be determined from boundary conditions. As we can see at once by substituting this $F(X)$ into (45), $G''(Z)=0$. Therefore the solution for density σ which satisfys the boundary condition described in the last section

(At the surface $Z=1$) $\quad\sigma=\sigma_b-\sigma_0$ at $X=X_0$, $\sigma=\sigma_0-\sigma_1$ at $X=X_1$
(at the bottom $Z=0$) $\quad\sigma=\sigma_b \qquad (59)$

is represented by

$$\sigma=-\sigma_0 Z\exp\gamma(X-X_0)+\sigma_b \qquad (60)$$

where $\quad\gamma=[\log(\sigma_1/\sigma_0)]/(X_1-X_0)$

$$X=(1+\gamma Y)^3/\gamma$$

Since this solution does not include the ratio $\alpha_K=A/K$, it is considered to represent the condition that the density field and current system adjust themselves so as to annul the effect of vertical mixing.

We take $\sigma_0=5\times10^{-3}$, $\sigma_1=2\times10^{-3}$, $X_0=0.2$, $X_1=1.6$ which corresponds roughtly to the condition treated in section 5 and 6, and numerical results are shown in Fig. 8, where curves of surface density and Ψ, and vertical profiles of density and ψ are drawn against Y. The vertical sections of σ and Ψ are very similar to the model of section 5 and 6 of well mixed state with a small value of A/K, since the surface density is almost uniformly increased with Y and also it is linear function of Z in the present model.

Approximate form to the integral (57) and (58).

When $\eta<1$ and we can put $e^{-\eta}=1-\eta+\frac{\eta^2}{2}$, the integral (57) is written as

$$\text{(C)}\quad \sin^{-1}\left(\frac{\eta_c}{\sqrt{k_c^2+\eta_c^2}}\right)-\sin^{-1}\left(\frac{\eta_c-\eta}{\sqrt{k_c^2+\eta_c^2}}\right)=(X-X_0)^{-\phi_0/2} \qquad (61)$$

where $\quad k_c^2=k-2, \qquad \eta_c=1-2a_2e^{\phi_0}$

$$\text{(D)}\quad \sinh^{-1}\left(\frac{\eta_d}{\sqrt{k_d^2-\eta_d^2}}\right)-\sinh^{-1}\left(\frac{\eta_d-\eta}{\sqrt{k_d^2-\eta_d^2}}\right)=(X-X_0)e^{-\phi_0/2} \qquad (62)$$

where $\quad k_d^2=k+2, \qquad \eta_d=1+2a_2e^{\phi_0}$

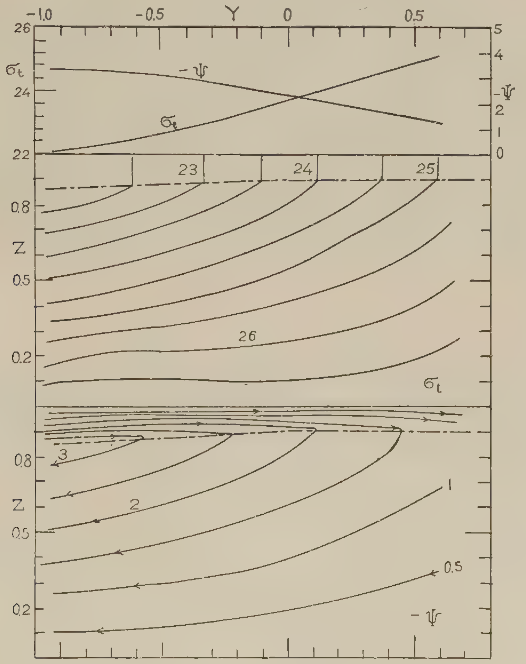

Fig. 8. Surface values (the upper most curves) and vertical sections of density (σ_t) and stream function (in A/φ_0).

Further, when $\eta_1<1$, $\eta_m-\eta_1<1$, we can put

(C) (for $0<\eta<\eta_1$) The same equation as (61) with

$$k_c^2=2(e^{-\eta_m}-1+2a_2e^{\phi_0}\eta_m)$$

(for $\eta_1<\eta<\eta_m$)

where $\sin^{-1}(\xi_c-\eta_m+\eta)/\xi_c \quad \sin^{-1}(\xi_c-\eta_m+\eta_1)/\xi_c=(X-X_m)e^{-\frac{1}{2}(\phi_0+\eta_m)}$ (63)

$\xi_c=2a_2e^{\phi_0+\eta_m}-1$

(D) (for $0<\eta<\eta_1$) The same equation as (62) with

$$k_d^2=2(1-e^{-\eta_m}+2a_2e^{\phi_0}\eta_m)$$

(for $\eta_1>\eta>\eta_m$)

$$\cosh^{-1}(\xi_d+\eta_m-\eta)/\xi_d=(X-X_m)e^{-\frac{1}{2}(\phi_0+\eta_m)} \tag{64}$$

where $\xi_d=1+2a_2e^{\phi_0+\eta_m}$

Examples for different ϕ_0 with the same function $G(Z)$.

Here we discuss the solutions obtained under the same boundary condition (59) with numerical constants equal to those of Fig. 8, whereas we change the constant ϕ_0 from 4 to -1.5. We can determine $F(X)$ for each ϕ_0 and we can combine various kinds of $G(Z)$, but here we assort only one $G(Z)$, in order to show more instructively how is the relationship between mass distribution and circulation which is deduced from the basic relations given in section 2. Here we chose a function $G(Z)$ corresponding to $r'=5$ which is drawn in Fig. 7, where we use r' instead r in order to indicate the parameter in Fig. 7 being for $m=1$. Therefore, the ratio A/K for each value of m with different value of ϕ_0 is computed from

$$A/K \fallingdotseq \alpha_K = 2r = 2r'/m$$

whereas m is given by $m=\sigma_0/F(X_0)=\sigma_0/j(X_0)\exp(\phi_0)$. The reason why we chose the value $r'=5$ is that the function $G(Z)$ obtained is intermediate between the extremely shallow or deep thermocline for larger r' and uniformly changing vertical profile for smaller r', which gives more realistic picture of density distribution.

The results are represented in similar way to Fig. 8 and the values of ϕ_0 for each figure and corresponding ratio A/K are shown below. The function $F(X)$ for each ϕ_0 is mostly computed for the case (D), since this type of vertical profile is more realistic in the ocean.

Table

No. of Model	I	II	III	IV	V	VI	VII
No. of Fig.	9	10	11	12	13	14	15
ϕ_0	4	1	0	$-.5$	$-.75$	$-.954$	-1.5
A/K	2.84×10^5	1.44×10^4	5.2×10^3	3.2×10^3	2.5×10^3	2.0×10^3	1.1×10^3

The model I is similar to the previous solution of (60) except its vertical profiles, and it has abnormally high value of A/K in order to maintain vertical profile similar to other cases described in this paragraph, so that it is rather a theoretical purpose to show it here than a purpose for applying the obtained distribution to the actual ocean. On the other hand, the model II, III and so on gives interesting picture, which deviates from the linear surface distribution in section 5 and 6. Generally the surface density or $F(X)$ increases very slowly with Y in lower latitudes or for smaller values of Y and indeed in model VI and VII it decreases in some range thus it has minimum surface density.

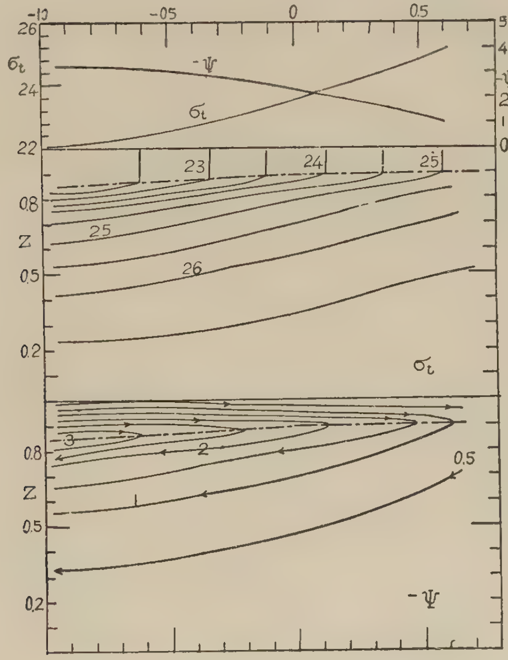

Fig. 9.
Surface values (the upper most curves) and vertical sections of density (in σ_t) and stream function (in A/φ_0) of Model (I).

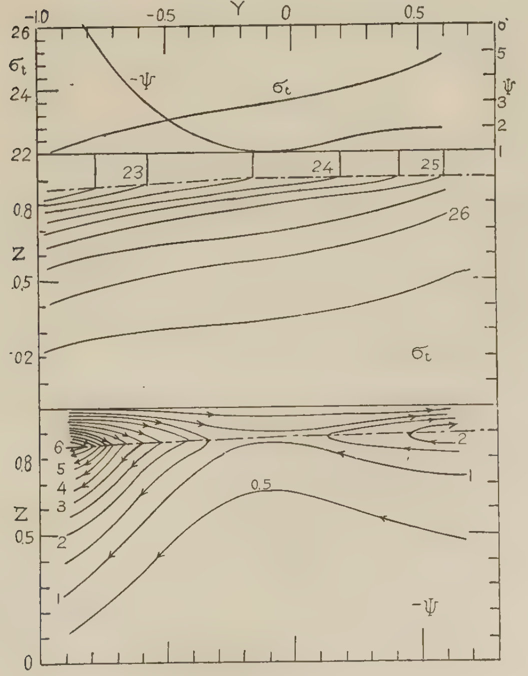

Fig. 10.
Model (II).

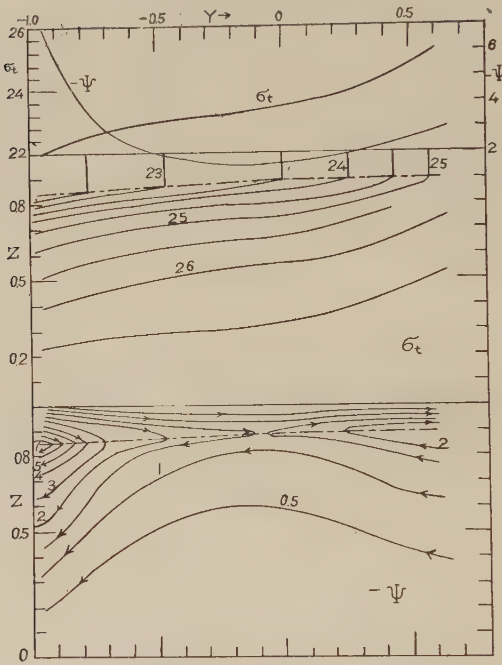

Fig. 11.
Model (III).

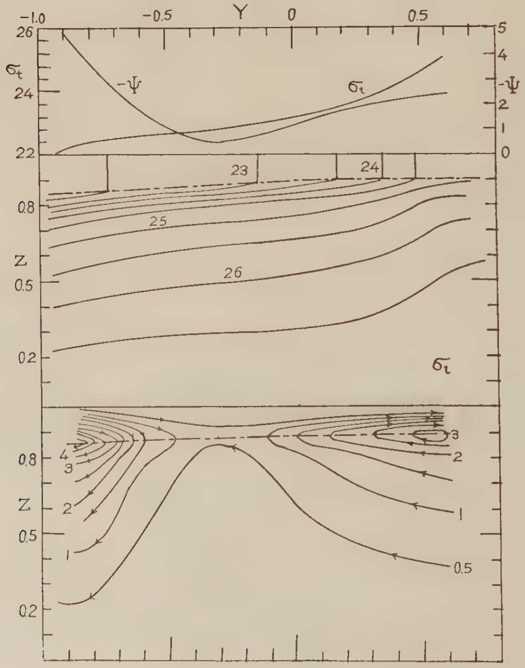

Fig. 12.
Model (IV).

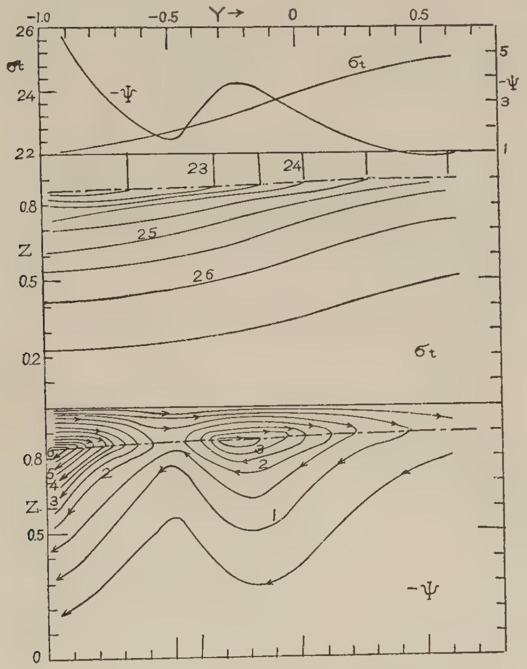

Fig. 13.
Model (V).

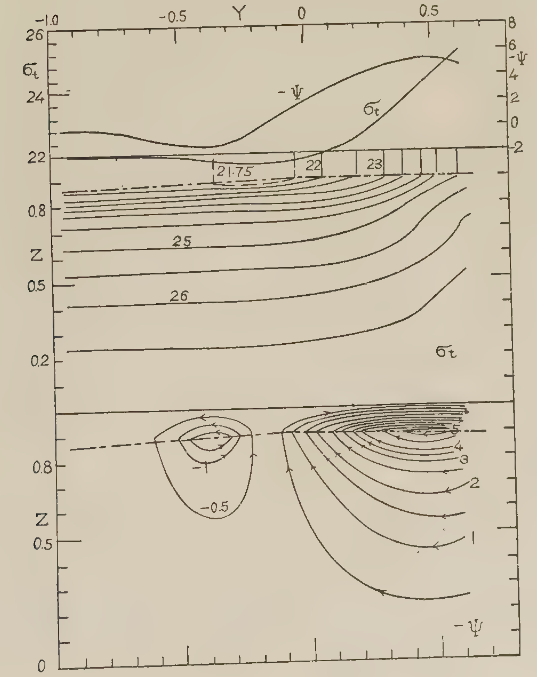

Fig. 14.
Model (VI).

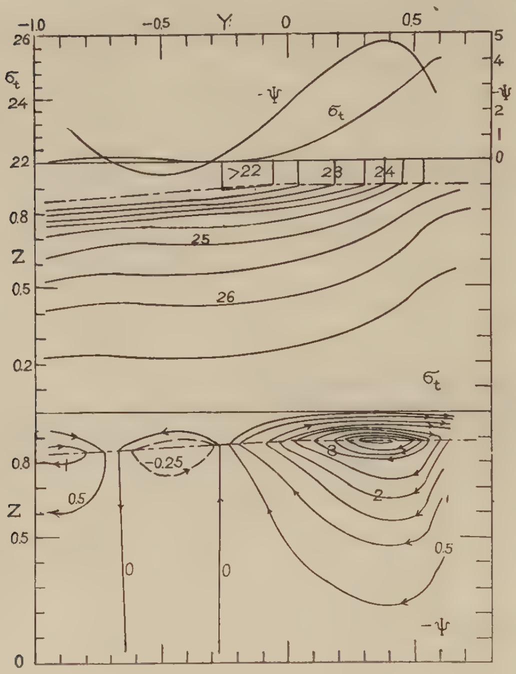

Fig. 15. Model (VII).

On the other hand, in higher latitudes it increases rapidly with Y. (This is described about model (D) of $G(Z)$, and for (C) this statement is not valid as seen later.) Such surface density is reflected in current pattern and there appear two gyres in models II to V, where that in lower latitudes produces sinking motion in the interior region and the in higher latitude causes upwelling, the relative intensity of which charges as changing φ_0. In the model VII, there appears three gyre, corresponding to the minimum of surface density, and also the strength of higher latitude gyre is maximum among three, thus producing strong upwelling in the middle latitude. The model VI shows intermediate nature between these two types.

As one model corresponding to the vertical profile of type (C), we get Fig. 16, which is computed for $\phi_0=-.954$ and $A/K=2\times10^2$, with the same constants as the models stated above. The surface density shows a rapid increase for smaller value of Y, contrary to the above models. Therefore, the general vertical current in the interior region is downwards, which contributes to make the thermo-

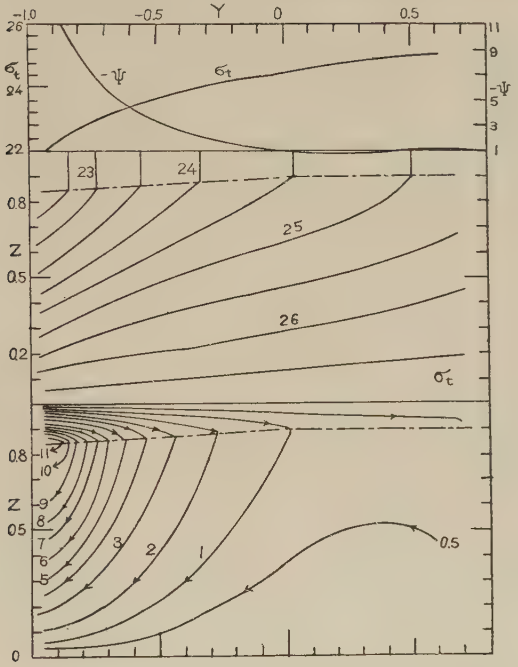

Fig. 16.
Example of a vertical profile of type (C).

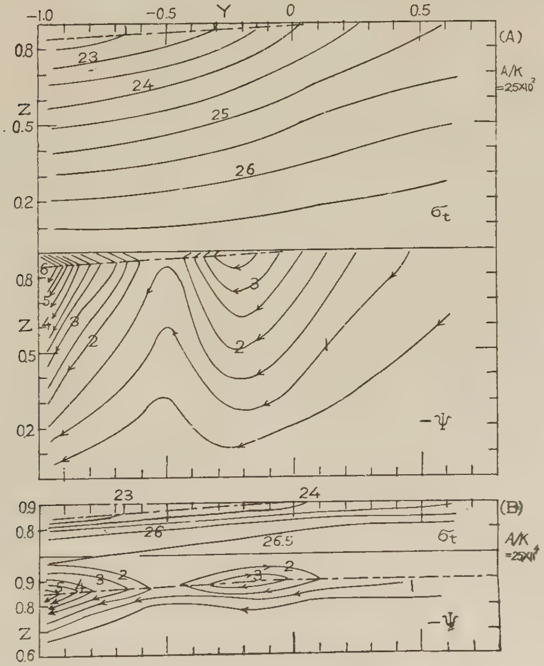

Fig. 17.
Models equivalent to (V) with different ratio *A*/*K*.

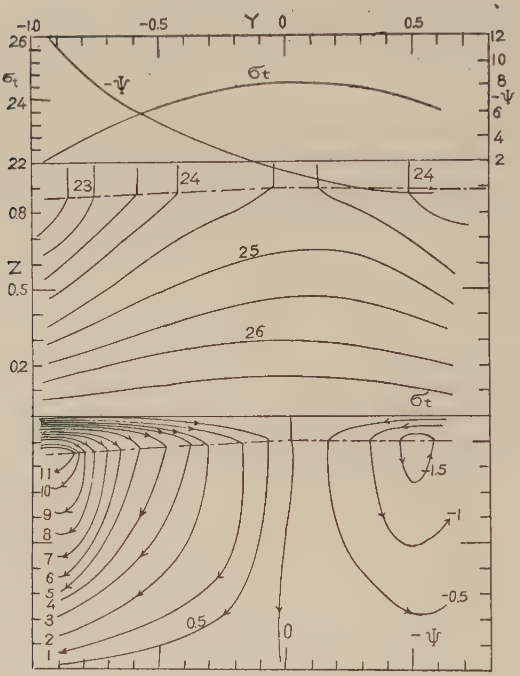

Fig. 18.
Examples of a profile of type (C) with $A/K = 2.5\times10^2$.

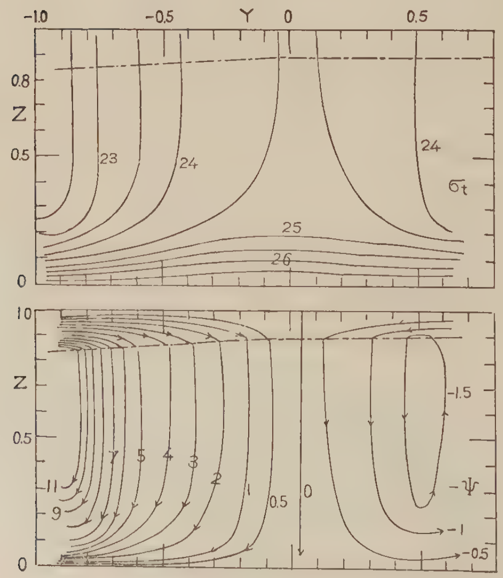

Fig. 19.
Example of a profile of type (C) with $A/K = 2.5\times10^3$. (Surface values of σ_t and ψ are equal to those of Fig. 18).

cline deeper than the last cases.

Change of pattern as variable ratio A/K. For the same surface distribution of density or function $F(X)$, vertical profile changes as the ratio A/K has a different value. Examples of such change are illustrated in Fig. 17, where the model V of the last paragraph is taken and patterns of density and current for $A/K=2.5\times10^2$ and 25×10^4 are shown. We can see that increase of A/K to ten times from the original value in the last paragraphy changes the pattern quite remarkably, whereas the decrease to one tenth gives no such conspicuous change.

As another example, we show the model for vertical profile of type (C) in Fig. 18 and 19, with $\phi_0=-.75$ and the ratio A/K is 2.5×10^2 and 2.5×10^3, respectively. This model does not satisfy the condition that $\sigma_1=2\times10^{-3}$, but it gives an example that there exist two gyres, owing to the condition that there is a maximum in the surface density distribution, although these two gyres give both sinking motion below the upper boundary layer. Further, in this (C) type, change of the ratio A/K is reflected in the pattern more sensitively than in the type (D), and thus the increase of A/K to ten times of 2.5×10^2, which gives almost uniformly changing vertical profile, change the whole pattern conspicuously, so that in the case of $A/K=2.5\times10^3$, the thermocline is almost near the bottom.

Miscellaneous patterns for $\phi_0=-1.5$. Since the model VII gives some interesting features, we shall compute further some examples for $\phi_0=1.5$, but for different values of σ_1. Two of these are shown in Fig. 20, both for the ratio $A/K=1.1\times10^3$ as in the model VII. We can see that the decrease of the end value of surface denisty at $X=X_1$ produces more and more intense middle gyre, since the value of σ_1 corresponding to the model VII (Fig. 15) is 1.8×10^{-3} (we specify σ_1 in the model VII as 2×10^{-3}, but we have to determine integral constants by trial and error method, so that some difference exists at the end value.), whereas the pattern of Fig. 20 corresponds to $\sigma_1=0.9\times10^{-3}$ and 2.6×10^{-3}, respectively. This state of condition suggests that the absolute difference in density of the surface water between in polar region and tropical region affects the whole pattern of vertical circulation.

A solution containing an additional term (47). This is rather hypothetical model, but it is obtained from mathematically possible solution, by adding a term (47) to a solution heretofore determined. In present model we take a function $F(X)$ similar to the model VI of the previous paragraph, then we add a term $0.3\int_{X_0}^{X}F(x)\,dx$, as stated in the equation (46). The resultant pattern of σ and Ψ are shown in Fig. 21, where we should in-

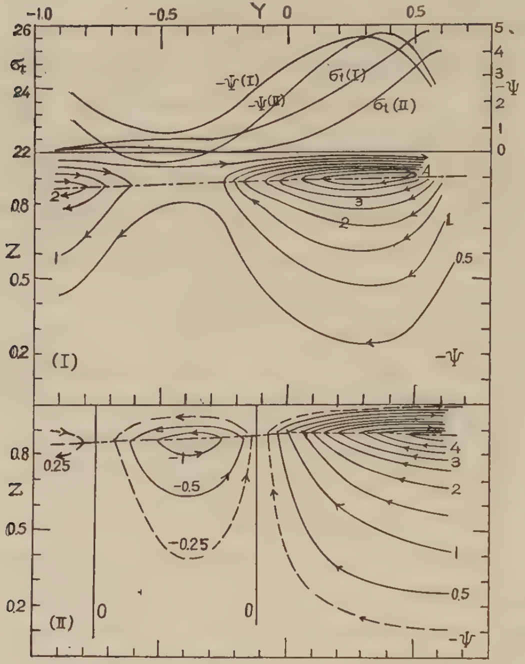

Fig. 20. Two examples equivalent to Model VII with different density at the polarward limit.

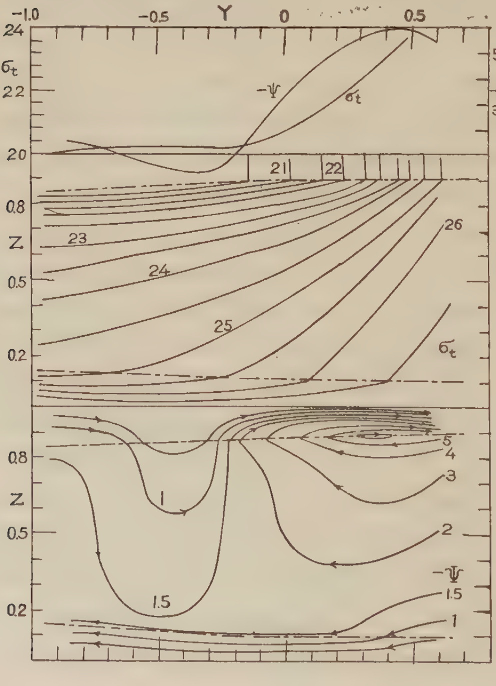

Fig. 21. Example with a lower boundary layer

triduce lower boundary layer, so as to make vertical current at the bottom vanish. Comparison of this pattern with that of Fig. 14 suggests us that change in the general current pattern in the interfor region is rather small, although near the lower boundary layer the pattern of the present model is quite different from the previous one. An approximate solution for arbitrarily given surface density.

When we assume that the density distribution is represented by a form as (46) without $f(X)$ term, or by a equation such as

$$\sigma=E(Y)G(Z)+\sigma_b \tag{64}$$

then we have from the equation (15)

$$G''=2R(Y)GG' \tag{65}$$

where

$$2R(Y)=\frac{\alpha\kappa}{(1+\gamma Y)^2E}\left\{(E''E-E'^2)-\frac{2\gamma}{(1+\gamma Y)}EE'\right\} \tag{66}$$

Therefore, when we divide the interval of Y into small divisions, in which the change of $R(Y)$ is so small that it can be considered constant, we can integrate $G(Z)$ as stated in the section 7 and this function is expressed by formula (49), by replacing r with $R(Y)$. When R is positive, the formula for (C) is applied, and when R is negative, that of (D) is valid. Since $E(Y)$ or $F(X)$ of the previous paragraphs is known when the surface desity distribution is given, so that the resultant vertical profiles are determined for any surface density. In this solution, it depends on a local value of $E(Y)$, $E'(Y)$ and $E''(Y)$ which type of (C) or (D) a vertical profile belongs to.

As an example, we take a linear function for $E(Y)$ such as

$$E(Y)=\sigma_1 Y-\sigma_0$$

and divide the interval $(-1, 1)$ of Y into ten divisions, using the same constant $\sigma_0=3\times10^{-3}$, $\sigma_1=2\times10^{-3}$ and $\alpha\kappa=10^3$ as in the sections 5 and 6. The result of computation is shown in Fig. 22, which is quite similar to the previous example of Fig. 7, which is computed with more tedious process. In this example, we can see that at about $Y=0.2$ the vertical profile changes from type (C) in lower latitudes to type (D) in higher latitudes.

When we assume that $R(Y)$ is constant in the whole region of Y, we can obtain the solutions which has been discussed in the previous paragraphs (written as $F(X)$). Generally, we can conclude, from the results obtained by numerical calculation, that for a vertical profile of (C) the surface density when plotted against Y, has a curve convex downwards, and for type (D) it is

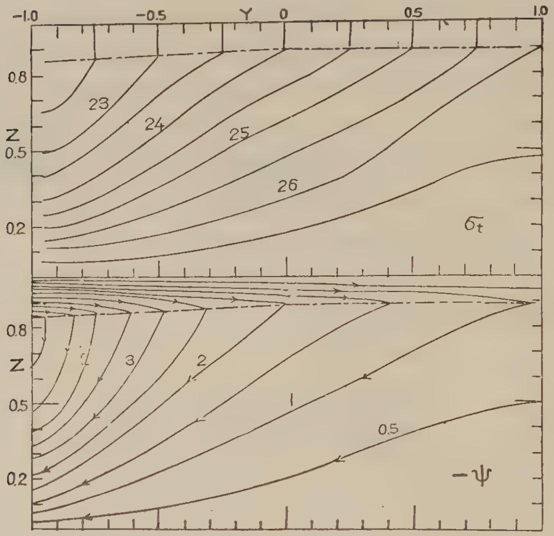

Fig. 22. Model of linearly increasing surface density computed by approximation (65) for $A/K=10^3$.

represented by a curve concave downwards. Such density distribution produces various kinds of current pattern, which are not so simple that we cannot say that (C) is accompanied with sinking and (D) is caused by upwelling, as described in the previous paragraphs.

10. *Comparison with observed data.*

The models described above are expressed with non-dimensional parameters, which is very convenient particularly to show density distribution. However, for the purpose of estimation of velocity from a chart of stream function ψ, we should give some remarks The values of Ψ in these charts are expressed by an unite of $A/2\varphi_0$, when we take numerical constants such as $f_0=10^{-4}$, $a=2\times10^8$, $g=10^3$. Therefore, when we take $A=4(\text{cm}^2/\text{sec})$, a vertical velocity w and horizontal velocity v expressed by $w=-\frac{A}{2a}\frac{\partial}{\partial Y}\Psi$, $v=\frac{A}{2h}\frac{\partial}{\partial Z}\Psi$, respectively, has a numerical value of $w=-10^{-8}\,\partial\psi/\partial Y$ and $v=10^{-5}\,\partial\psi/\partial Z$, for $h=2\times10^5$. Therefore, one unit difference of Ψ at a distance of $Y=0.1$ corresponds to $w=10^{-7}$(cm/sec), and that of Ψ at a distance of $Z=0.1$ gives $v=10^{-4}$(cm/sec).

In this theoretical model we neglect the zonal pressure difference and we have assumed that meridional components of flow is not geostrophic but is driven through frictional force produced by geostrophic zonal flow which, in turn, is caused by meridional pressure difference due to density gradient in this direction. Therefore eddy viscosity is rather essential to the meridional circulation in this model, so that this model seems to be valid only in the upper layer of the ocean, say, of about 1000 m thickness, because eddy viscosity is presumably ineffectice below this level in the actual ocean. In a deeper layer, current is actually geostrophic in most cases even in meridional component, toerefore, the model of STOMMEL (1957b), STOMMEL and VERONIS (1957) or that described in another paper by the author (1958).

Indeed, we show the vertical section of σ_t along the middle section of the Atlantic from the Meteor Report (DEFANT, 1936, WÜST, 1936) where the upper

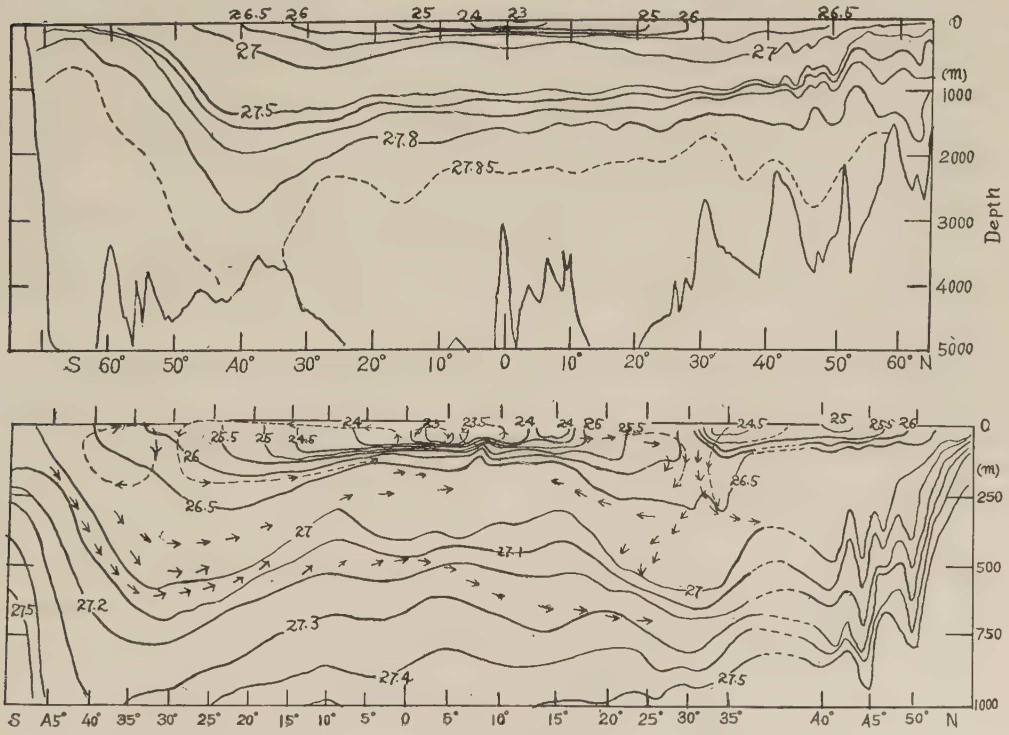

Fig. 23. Vertical section of σ_t along the central part of the Atlantic (after Wüst (1936) for upper chart and Defant (1936) for lower chart)

chart gives the distribution of σ_t to the bottom, and the lower one to 1000 m depth. A glance of the upper chart suggest us that vertical gradient of density below about 1000 m is quite small, so that we need a large value of the ratio A/K for explaining the observed profile from the present theory (of course the profile is type (D) defined in section 9) if we include the ocean to the bottom. A brief estimation gives the ratio A/K of about 10^4 to 10^5 corresponding to the actual profiles of, which gives the value of A 13 to 130 (cm²/sec) even for a molecular diffusivity of K, since molecular K is about 1.3×10^{-3} when we assume that change of density is mainly due to that of water temperature. Such discrepancy with observed facts seems to be due to the assumption that meridional circulation is caused by frictional force even to the great depth.

Anyhow, hereafter we restrict our discussions within upper 1000 m layer. The first glimpes of the lower chart suggests us that in the polar region, especially in the southern hemisphere, the observed density distribution and meridional circulation seems to correspond to the theoretical model of uniformly increasing surface density described in section 5 and 6, but in middle and lower latitude correspondence between the observed and theoretical distribution fils rather poor. This is due to the fact that the density distribution in the upper layer is not only governed by convective circulation but also of wind current which produces rather intense vertical current below the upper boundary layer or Ekman layer, as stated below. However, some resemblance is recognized between model VI or VII and middle latitude of the northern Atlantic in circulation pattern.

Representation of density in power series. First we expressobserved σ_t in power series of Y, where we take the whole distance of theregion $2a=40$ deg. latitude (from 10 degrees to 50 degrees), from 200 m to 1000 m depth. As a series we take up to cubic powers of such as

$$\sigma_t=F_0(Z)+F_1(Z)Y+F_2(Z)Y^2+F_3(Z)Y^3$$

and practically $F_i(Z)$ is computed by the estimation of momentum $\int_{-1}^{1}\sigma_t Y^i dY$ from observed values of σ_t. The results are plotted in Fig. 24, which indicate that the term $F_3(Z)$ is very small compared with other terms. Further the positive value of $F_2(Z)$ suggests that circulation induced by density distribution is generally upwelling all over the region as stated in section 4. Comparison of vertical profiles of $F_0(Z)$, $F_1(Z)$ $F_2(Z)$ obtained empirically with theoretical ones of Fig. 1 suggests us that the ratio A/K is about 10^3 if we assumed that the meridional circulation is produced only by convection. Stream function computed

(A) Northern Hemisphere

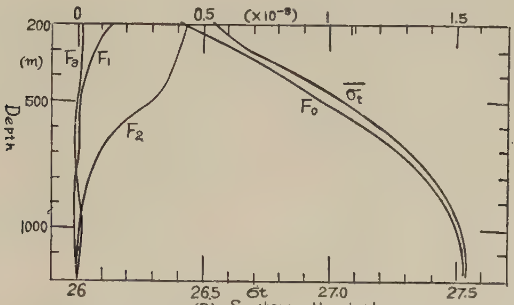

(B) Southern Hemisphere

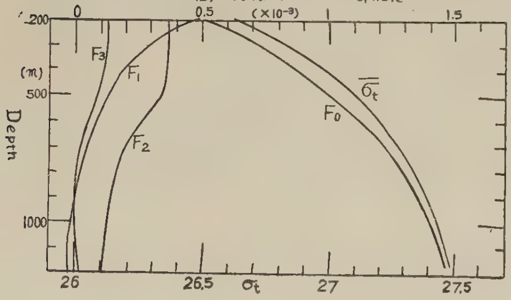

Fig. 24. Vertical profiles of $\overline{\sigma_t}$ (mean value of σ_t at each depth) and F_i. (Upper scale should be used for F_1, F_2 and F_3, lower scale be used for F_0 and $\overline{\sigma_t}$).

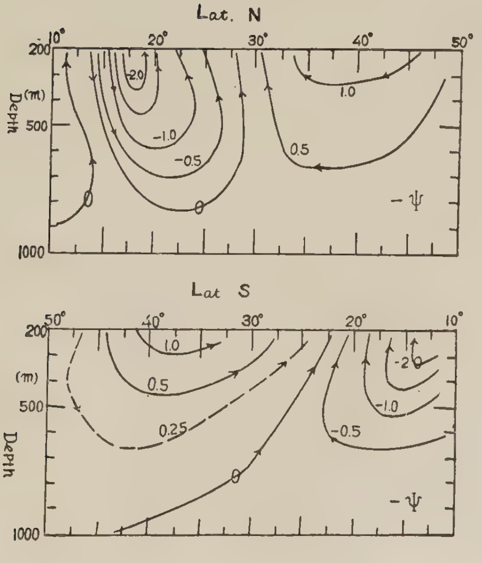

Fig. 25. Stream function (A/φ_0) computed from observed density field in the Atlantic.

from observed density distribution.

We can compute directly stream function in the considered region from observed density distribution by use of the formula (14). The results are shown in Fig. 25, where some smoothing of original data is applied. These pictures do not represent a real circulation pattern, since the wind stress term in the equation for Ψ is more predominent actually, as stated below. However, it gives some ideas about convective circulation, if it is assumed to be a main factor in the ocean, which produces generally sinking motion in polar region and upwelling in subtropical region.

The effect of wind-driven current on density distribution.

So far as we are concerned with theoretical model, we have neglected wind-stres term in the equation (10). However, rough estimation of this term in the ocean indicates that this term is far more important than density gradient term so long as the value of eddy viscosity is not abnormally large. Since the wind stress term increases with Y, the resultant vertical motion is downwards all over

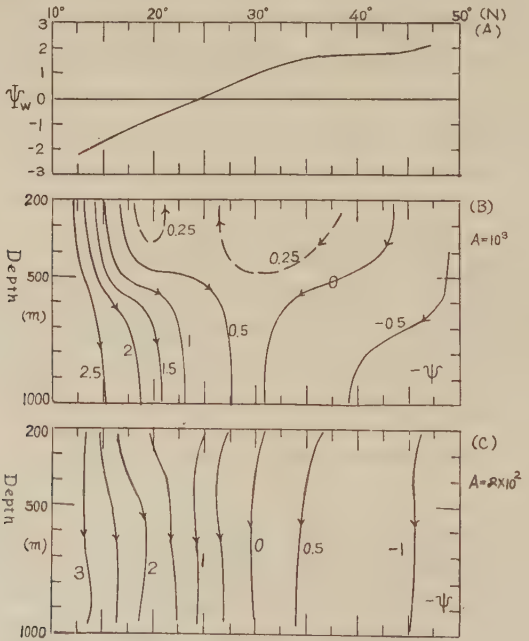

Fig. 26. Stream function induced by wind stress (A) and by combined effect of density field (B and C) in the North Atlantic.

the region and also this motion is constant with the depth below the Ekman layer, although there is no horizontal motion induced by wind stress there. In Fig. 26 we plot the computed value of stream function due to the wind stress $\Psi_w=\delta\tau/(1+\gamma Y)$ by use of the data of Munk (1950) over the north Atlantic, and also the resultant value of Ψ due to both convection and wind-driven circulation. We can see at once that the latter effect is predominent already for a value of A less than 2×10^2, and only for an abnormally large value of A more than 10^3 the former effect is recognizable.

On the other hand, when we assumed that wind-driven circulation is predominant, we can compute density distribution very simply from the equation

$$\frac{\partial^2\sigma}{\partial Z^2}=W(Y)\frac{\partial\sigma}{\partial Z} \tag{67}$$

where $W(Y)$ is a known function of Y such as

$$W(Y)=-\delta æ\frac{\partial}{\partial Y}\left(\frac{\tau}{1+\gamma Y}\right) \tag{68}$$

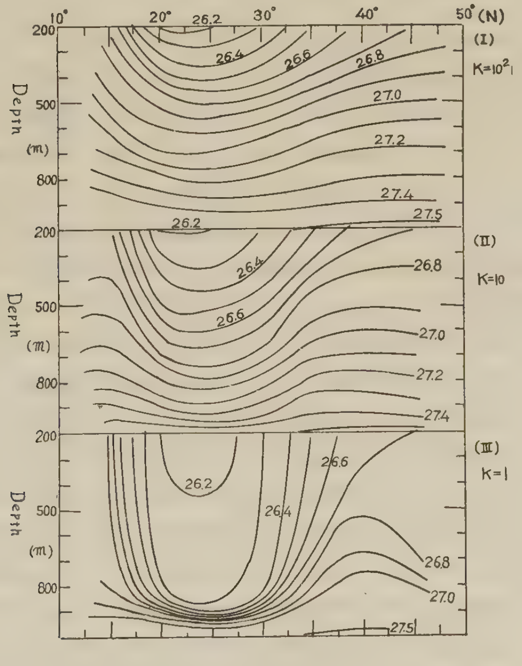

Fig. 27. Density field produced by wind-driven vertical current in the North Atlantic.

and thus the density is given by

$$\sigma=\sigma_b-(\sigma_b-\sigma_s)(1-e^{wz})/(1-e^{w}) \tag{69}$$

where σ_b, σ_s are bottom and surface value of b.

We compute the density distribution from this equation by use of observed values of Ψ shown in Fig. 27 and σ_s, σ_b for $K=1,10$ and 100. The result suggests us that we should take an extraordinary large value of K in order to get a picture similar to the observed density distribution. This means that a much larger contribution of vertical diffusion is necessary to counteract the strong downwards current induced by wind stress if we neglect the convective motion. However, it is not the main purpose of present research to discuss in details about the interaction of wind-driven current and convection current, and also it seems that we should build more complicated theory in order to get complete picture of circulation in such intermediate layer, which is another problem different from the present one.

11. Summary and concluding remarks

Assuming zonal ocean, or neglecting zonal difference of all physical quantities, we derived two equations which give the relationships between density structure and current system, where zonal current is produced by geostrophic relation due to meridional gradient of density and meridional circulation is induced by frictional force. When we give the surface density, which is linearly increased polarwards changed, we can get approximate solution of this equation system approximately by several processes, which gives a circulation pattern that in the upper boundary layer or EKMAN layer there is a flow almost horizontal and polarwards and below this layer there is an equatorwards flow accompanying sinking motion. The depth of thermocline decreases as increasing ratio of A/K especially in the polar region, but in lower latitudes it is rather more shallow than in the polar region, contrary to the observed density distribution.

We can get only an approximate solution under the boundary condition that surface density is a linear function of latitude, but we can get exact solution under various kinds of surface density distribution Therefore we can build many circulation pattern induced by each of such surface condition, which have two or three gyres in some cases quite similar to the actual circulation in the meridional section of the ocean. Further, such circulation pattern belongs to two different types according to vertical profiles, one of which has deeper thermocline than the other type. Also the surface density which belongs to a type of deeper thermocline increases rapidly in higher latitudes, whereas that of the other type increases rapidly in lower latitudes. Both types of vertical profiles approaches to the linear distribution with depth when the ratio A/K decreases, which is considered as a well-mixed state of surface and bottom water.

These theoretical models of convective circulation do not agree with observed density distribution and circulation so well, because in the actual ocean vertical current induced by wind driven circulation below EKMAN layer is more predominant. However, this type of circulation induced by convection seems to counteract the effect of wind-driven sinking motion, particularly in middle and lower latitudes, thus we need not so large effect of vertical mixing in order to main tain the observed density structure against such sinking motion.

This work is rather incomplete in regards to applicability to the real condition. However, it gives many examples of convective current from exact solutions of non-linear equation, so that they might be used for interpretation of actual data in many cases.

Acknowledgement

The author wishes his hearty thanks to Mr. Henry STOMMEL for his encouragement and many advices.

References

DEFANT, A., 1936: Schitung und Zirkulation des Atlantischen Ozeans. Die Troposphäre. Wiss. Erg. Deutsch. Atlant. Exp. "Meteor" 1925–27, 6–1.

EKMAN, V. W., 1905: On the influence of the earth's rotation on ocean current. Arkiv för Mat. Astron. och Fysik, 2 (11).

FOFONOFF, N. P., 1954: A theoretical study of zonally uniform ocean flow. Tech. Report 4 for Office of Naval Res. Brown Univ.

ICHIYE, T., 1958: A theory of vertical structure of density. (To be published in Journ. Oceano. Soc. Japan and WHOI Contr. No. 953).

LINEYKIN, P. C., 1955: On the determination of the thickness of the baroclinic layer in the sea. Docklady SSSR Akad. Nauk, 101.

MUNK, W. H., 1950: On the wind-driven circulation. Journ. of Meteor. 7 (2).

STOMMEL, H., 1957a: A survey of ocean current theory. Deep Sea Res. 4 (3).

STOMMEL, H., 1957b: Reflections on the mechanism of the main thermocline. (Unpublished manuscript).

STOMMEL, H. and G. VERONIS, 1957: Steady convective motion in a horizontal layer of fluid heated uniformly from above and cooled non-uniformly from below. Tellus 9 (3).

VERONIS, G., 1957: Thermal circulation. Oceanus 5 (3).

WÜST, G., 1936: Schichtung und Zirkulation des Atlantischen Ozeans. Das Bodenwasser und die Stratosphäre. Wiss. Erg. Deutsch. Atlanti. Exp. "Meteor" 1925–27 6 (1).

Contribution No. 983

DET NORSKE VIDENSKAPS-AKADEMI I OSLO

HVALRÅDETS SKRIFTER

SCIENTIFIC RESULTS OF MARINE BIOLOGICAL RESEARCH

EDITED BY
UNIVERSITETETS INSTITUTT FOR MARIN BIOLOGI AND
STATENS INSTITUTT FOR HVALFORSKNING

Nr. 44

P. F. SCHOLANDER
INSTITUTE OF ZOOPHYSIOLOGY, UNIVERSITY OF OSLO
and
WOODS HOLE OCEANOGRAPHIC INSTITUTION

COUNTER CURRENT EXCHANGE

A PRINCIPLE IN BIOLOGY

WITH 11 FIGURES IN THE TEXT

Contribution No. 983 from the Woods Hole
Oceanographic Institution

OSLO
I KOMMISJON HOS H. ASCHEHOUG & CO. (W. NYGAARD)
1958

A. W. BRØGGERS BOKTRYKKERI A/S, OSLO

Contents.

Page
Introduction 5
Counter current exchange in the swimbladder 6
Counter current exchange in the gills of fishes 11
Counter current exchange in the placenta 12
Counter current heat exchangers in mammals and birds .. 13
Counter current exchange and renal function 18
Literature cited 22

Introduction.

All living cells depend upon an exchange of material and energy with the environment. Much of this exchange takes place as a result of simple diffusion, i. e., differences in concentration are evened out from one place to another by the random movements of the molecules involved. Thus, the carbon dioxide and heat generated in a respiring cell diffuse to the surroundings where the concentration of carbon dioxide and the temperature are lower. Diffusion, however, is a very slow process, so slow indeed that it cannot satisfy the exchange needs of an active animal larger than one millimeter in diameter unless the animal is endowed with some internal transport system. In bulky animals, therefore, the diffusion exchange generally takes place through large, thin surfaces well backed with capillary circulation, such as we find in our lungs or digestive tract. In certain cases, however, when diffusion exchange occurs between two flowing systems we may find realized a piece of truly remarkable bioengineering, which not only vastly increases the efficiency of the exchange, but which may also sometimes lend to the system new and unexpected features. This is diffusion exchange by counter current flow, and although this fundamental principle has not been widely recognized in biology we shall see that it exists in several different manifestations along the vertebrate system, all the way from fishes to man.

In engineering, of course, counter current flow exchange is a basic concept, and it has many applications in industry. We might mention heat exchangers, for example, which save expensive calories by using the hot exhaust gases from a furnace to preheat the air for the combustion. This can be most efficiently accomplished by a counter current system.

---

[1] Based on a lecture of the same title given for the Nordisk Insulin Fond in Oslo, November 23, 1954, in memory of Professor Hans Christian Jacobaeus. Part of the material was originally presented at the Federation of American Societies for Experimental Biology Symposium on Environmental Physiology at Atlantic City, April 15, 1954, and later adapted for publication in the *Scientific American* (Scholander, 1957).

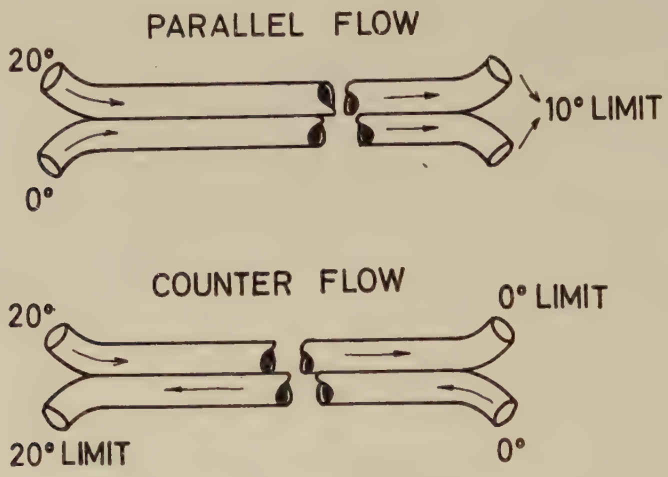

Fig. 1. Exchange through parallel and counter flow.

Suppose that we have two pipes running parallel and in contact with each other. With parallel flow, both streams pass out of the system with, at best, nearly the same intermediate temperature. In an efficient counter current flow each stream will leave at the approximate temperature with which the other enters, and most of the heat will accordingly pass over to the meeting stream, leaving very little to escape from the system in a lengthwise direction (Fig. 1).

These two properties, i. e., efficient diffusion exchange and maintenance of a diffusion barrier in spite of flow, are of fundamental importance in biology. A third important property of the counter current system is its capacity to maintain, or sometimes build up, large gradients along the flow direction. These three properties are, of course, all interdependent.

Where now do we find counter current flow systems realized and useful in biology? In several locations they can be seen quite clearly, namely, in the swimbladder of fishes, in the gills of fishes, in the placenta of mammals, in the extremities of mammals and birds, and possibly in the kidney.

Counter current exchange in the swimbladder.

Nowhere in nature is the counter current system so strikingly developed nor the fundamental principle so clearly indicated as in the capillary bundles in the swimbladder wall of deep sea fishes. Even at great depths, 2000 to 3000 meters and more, fishes can keep their swimbladders filled with gas. The gas is more than 90 % oxygen, and at such depths the pressure at which this oxygen must be maintained amounts to as much as 200—300 atmospheres. This corresponds to nearly double the pressure in a conventional steel oxygen cylinder fully charged (cp. Scholander and van Dam, 1953).

The atmospheric oxygen which is dissolved in the sea water has a gas pressure of no more than one fifth of an atmosphere at any depth, and the arterial oxygen pressure in the fish is slightly below this. So across the thin swimbladder wall of a fish living at a depth of 2000 meters there is a drop in oxygen pressure of nearly 200 atmospheres. The swimbladder is a living organ and is circulated with blood. At a pressure of 200 atmospheres this blood becomes charged with ten times its own volume of oxygen by simple physical solution, and if such amounts were to leave the bladder there would soon be no oxygen left. Obviously there must be some mechanism that is capable of lowering the oxygen pressure in the blood before it leaves the swimbladder. In more general terms one may state the problem thus: How can a steep concentration gradient be maintained across a barrier in spite of the fact that liquid is continuously streaming through it? The answer lies in the arrangement of the vascular channels. In the wall of the swimbladder this is represented by bundles of fine capillaries, known as *rete mirabile*. The arteries entering the wall break up into thousands (often millions) of parallel capillaries. These loop around inside the swimbladder and return as thousands of venous capillaries intermingled with the arterial ones to form a counter current exchange system (cp. Woodland, 1911; Haldane, 1922; Hall, 1924, and others). As the blood, highly charged with oxygen, starts to run out through the venous *rete* capillaries the oxygen passes over to the inflowing blood and the pressure drops steadily until the blood leaves the *rete* (Fig. 2). The magnitude of this drop depends upon the dimensions and arrangement of the intermingled capillaries.

In such a network or *rete* let us consider what geometrical configuration would provide the maximum surface for diffusion exchange between inflowing and outflowing capillaries. This might be expressed as a problem in topology: How can we arrange black and white polygons in a pattern so that black always borders white, allowing no more than four polygons to meet at each corner? Only two different solutions present themselves, namely, a checkerboard arrangement and a combination of hexagons with triangles in a star pattern (Fig. 3). We must acknowledge that evolution has indeed reached the ultimate in efficient design by producing both these patterns in the *retes* of deep sea fishes (Fig. 4, below).

Because of the simple geometry of the *rete* we may venture to estimate quantitatively some of its diffusion properties. From the number, length, wall thickness and circumference of the *rete* capillaries we may calculate how much oxygen would diffuse across the rete per minute at a pressure difference of one atmosphere (cp. Scholander, 1954).

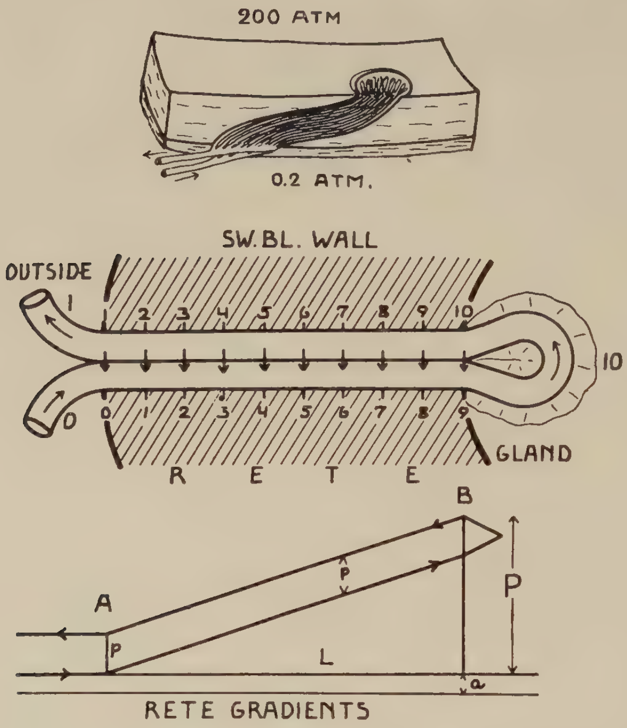

Fig. 2. Above: Section of swimbladder wall penetrated by *rete*. Middle: Counter current exchange, numbers denoting concentration. Below: *Rete* gradients (Scholander, 1954).

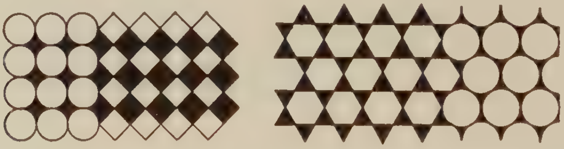

Fig. 3. Left: Checkerboard pattern, derivable from non-staggered primary vessels with secondary vessels in the interstices. Right: Hexagonal star pattern, derivable from staggered primary vessels with secondary vessels in interstices (Scholander, 1954).

The diffusion events through such a structure (cp. Fig. 2) may be described approximately by two equations, using the following symbols: blood flow, V ml/min; oxygen diffusion across rete, Q ml/min/atm.; pressure difference from one end of the *rete* to the other, P; pressure drop across the *rete* at any level, p; O_2 secreted from blood, D ml/ml; O_2 lost by diffusion and respiration, R ml/min; solubility coefficient of oxygen, α ml/atm./ml.

$$V\alpha P = pQ + V\alpha p \tag{1}$$

$$VD = V\alpha P + R \tag{2}$$

Equation (1) states that the amount of oxygen entering at B (Fig. 2) equals one part diffusing across the *rete* to the inflowing blood, and one part flowing out at A. The other equation (2) states that the amount of oxygen released from the blood equals the amount lost at A plus the amount covering diffusion losses and respiratory needs of the swimbladder (cp. Scholander, 1954).

Using these equations and reasonable values for the various constants it can be calculated that the exchange through the *rete* in a deep sea eel is so great that if the blood in the swimbladder has an oxygen tension of two hundred atmospheres it will leave the bladder with an oxygen tension only a few millimeters higher than in the arterial blood. This cuts the oxygen loss from the swimbladder down to only a few per cent of the total oxygen consumption of the fish, which is what we would expect.[1] Hence we have realized in the *rete* of the swimbladder two important features of the counter current system, namely, an incredibly efficient pressure exchange across the *rete,* and consequently an almost complete diffusion barrier along the *rete.*

There is a third important aspect of a counter current system which may possibly be applicable to the fish *rete.* If in such a system a small increment in pressure or concentration (p in Fig. 2) is actively produced along one leg of the *rete* this small primary effect will be multiplied by cross diffusion and counter current flow so that very big gradients (P/p) can be built up from one end of the *rete* to the other. The pressure or concentration (P) that can be produced in such a system by the primary effect (p) can be calculated from the equation. It is ultimately limited, however, by the amount of pressure which will stop by mass action the reaction responsible for p.

It will be realized that what has just been described approaches in principle one of the modern methods for isotope separation, namely, the thermo diffusion tube developed by Clusius and Dickel in 1938, and used, for example, to separate the hexafluoride of uranium 235 from that of U 238 during one phase in the development of the atom bomb. In this system a heated wire is suspended in a vertical tube several meter long, which contains the mixture. Thermal diffusion produces a very slight concentration of the lighter component along the whole length of the hot wire and conversely a slight increase of the heavier component along the cold wall. At the same time as the hot wire maintains this primary concentration effect (p), the warm gases rise along the wire and the cold sink along the wall, recirculating in a counter current fashion. Hence

---

[1] It will perhaps be even more graphic to describe the situation in terms of heat exchange. If ice water were to enter such a *rete* from one end and boiling water from the other exchange of heat would be complete within 0.0001°.

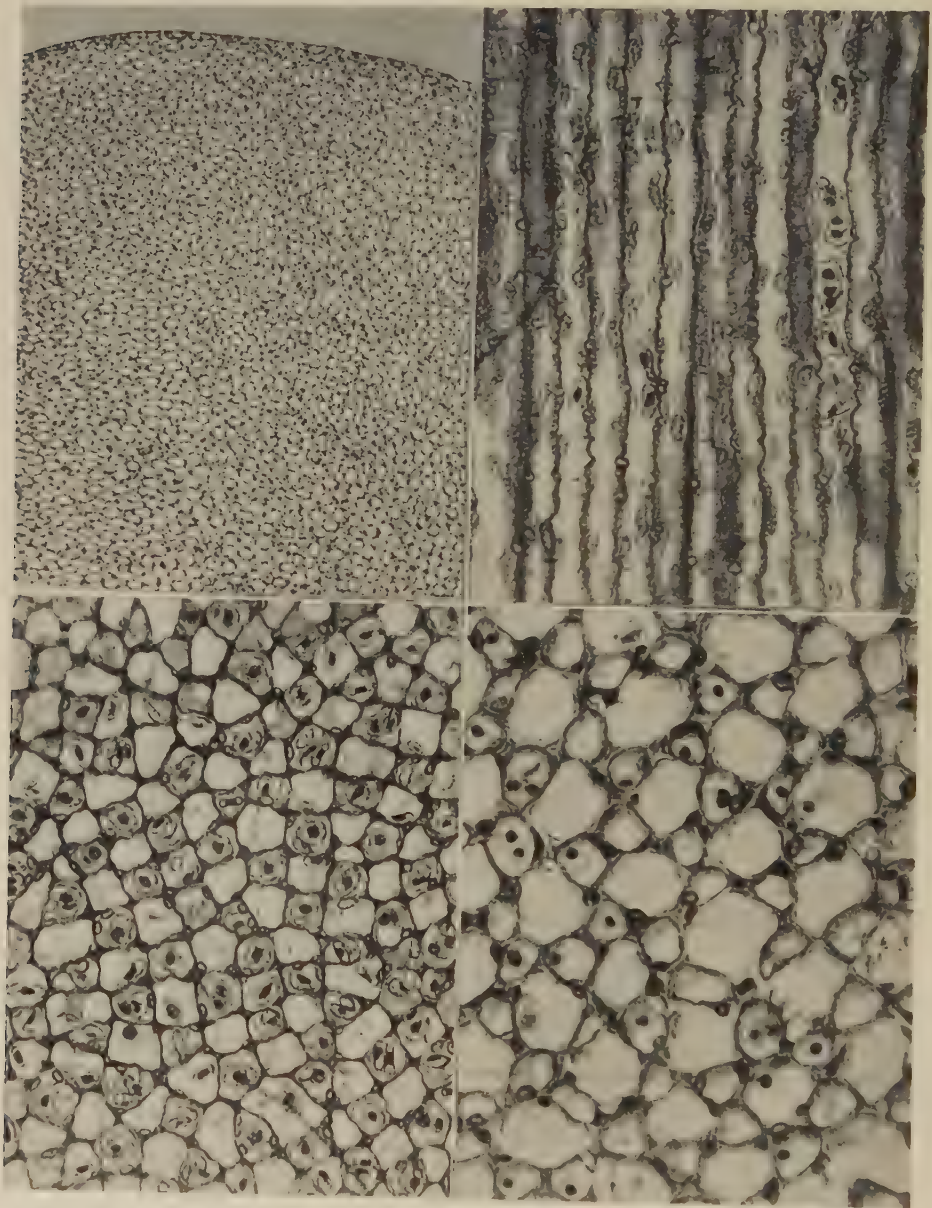

Fig. 4. Left above: Cross section of checkerboard *rete* in deep sea eel (*Synaphobranchus*) which can maintain a gradient of at least 250 atmospheres' oxygen through the *rete*. Each squae is a capillary about 13 × 13 microns and a centimeter or more long, approximately every other one arterial, every other one venous, with one or two red cells in the alternate capillaries. The wall thickness is 1—$1^{1}/_{2}$ microns, i. e. the same as for lung epithelium. Left below: The same, magnification 300. Right above: The same in longitudinal section, magnification 300. Right below: Cross section of *rete* in rosefish (*Sebastes*) showing the hexagonal star pattern. Magnification 400. In many fishes the *rete* capillaries may be counted in millions. (Sections, courtesy of Department of Anatomy, Harvard Medical School, photographs by C. Lloyd Claff).

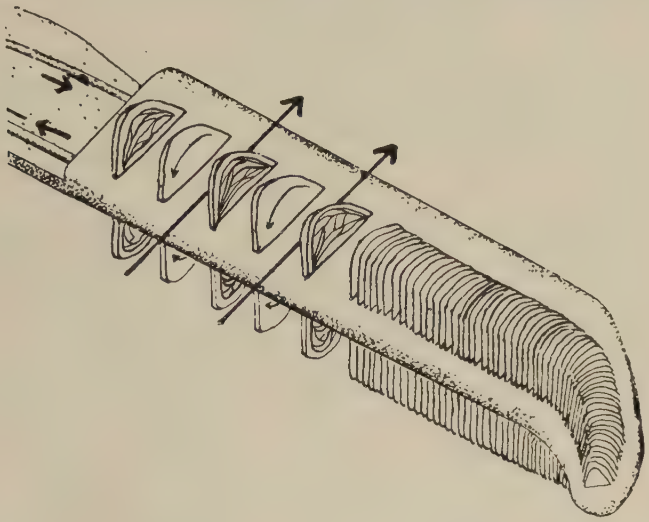

Fig. 5. Counter current flow between sea water and blood in gill lamellae of fish (Van Dam, 1938).

we get an accumulation of the lighter component at the top of the tube and the heavier at the bottom, with a gradient, or separation, which may exceed the primary thermal separation by as much as a hundred- to a thousand-fold (Jost, 1952). In the swimbladder there is no recirculation, but nevertheless, in one single pass through a *rete* only one centimeter long, the multiplication factor P/p reaches well over 3000, which leaves industrial engineering far behind. We shall return to this third aspect of the counter current system in the discussion of the kidney function.

Counter current exchange in the gills of fishes.

In the normal process of breathing, fishes can extract as much as 80 % of the oxygen from the water passing over their gills. When van Dam (1938) found that the capillary blood in the gill lamellae runs in a counter current direction to the flow of water (Fig. 5), he considered this to be an important factor in the high efficiency of the gills, and its significance was demonstrated later by Hazelhoff and Evenhuis (1952). They experimentally reversed the water current over the gills and found that the fish then extracted only one fifth as much oxygen from the water as it could obtain when the water flowed normally in counter current to the blood.

One may wonder why no such system has been realized in air breathing animals. There may be various reasons. Air represents an ocean of oxygen when compared to sea water. Whereas one liter of air contains

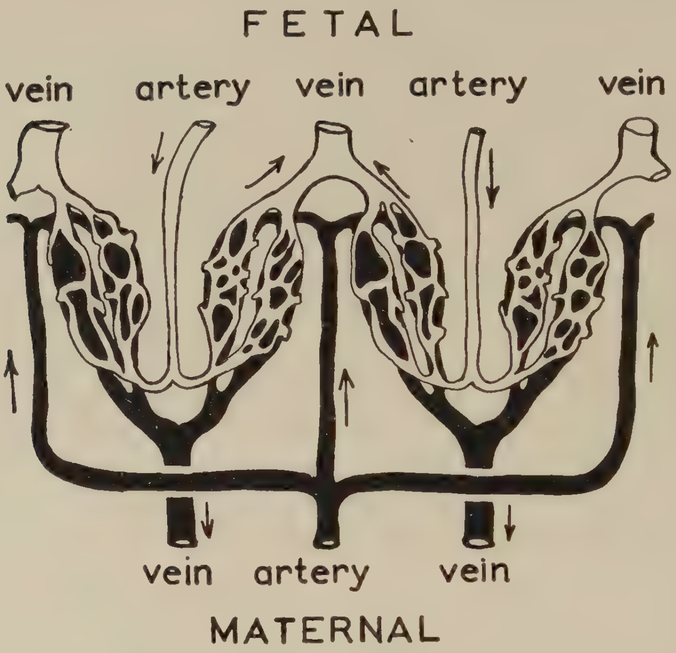

Fig. 6. Counter current flow in villi of placenta of rodent (*Citellus tridecemlineatus*) (after Mossman, 1937).

200 cubic centimeters of oxygen, one liter of sea water contains only 5 cubic centimeters, i. e., forty times less. Oxygen diffuses through water many thousand times more slowly than through air, and as a medium to pump over the exchange area water is also a thousand times heavier than air. It is no wonder then that the utmost in bio-engineering is necessary to provide the fishes with an adequate gas exchange.

Counter current exchange in the placenta.

In mammals the life of the embryo depends largely upon a diffusion interchange between its blood and the maternal blood, with respect to respiratory gases, nutrients, waste products, and heat. Mossman (1926) discovered that a counter current arrangement obtains between the fetal and maternal capillaries in the villi of the placenta of the rabbit. Similar arrangements have since been found in a great many other mammals, such as the ground squirrel (Fig. 6), sheep, cows, cats and dogs (Mossman, 1937; Barcroft and Barron, 1946; Amoroso, 1952). The diffusion distance between the placental counter current capillaries may be considerable, some 20—120 microns in the sheep, but the capillaries may run together for as much as one centimeter. The high oxygenation which the fetal blood acquires on its way through the placenta may be attributed partly to the counter current exchange and partly to the fact that fetal blood has a higher affinity for oxygen than has adult blood. In the human placenta a clear counter current scheme does not seem to be realized inasmuch as the capillary loops of the fetus are bathed directly in pools of the maternal blood.

Counter current heat exchangers in mammals and birds.

We shall now turn to an entirely different application of the counter current principle, namely, to heat exchange in warm-blooded animals.

The mechanism of cold adaptation in warm-blooded animals, as well as man, has attracted much interest during the last decade. A major problem of survival in the arctic winter is, of course, the preservation of heat. Theoretically this can be accomplished in three different ways: (1) by decreasing the temperature gradient, (2) by increasing the heat production, and (3) by increasing the insulation. It has long been known that the body temperature of mammals and birds is the same in tropical forms as it is in arctic forms (Morrison and Ryser, 1952; Irving and Krog, 1954), and the metabolic resting rate for similar size in the thermoneutral zone is the same in all latitudes. That leaves reduced heat dissipation as the main factor in phylogenetic cold adaptation. Animals are protected from heat loss largely by their fur insulation, which in larger forms increases more or less in proportion to the coldness of the climate (Scholander *et al.,* 1950, a, b, c).[1]

Yet it is a striking thing that arctic mammals and birds are so poorly insulated on their legs and other appendages. A reindeer has only one quarter to one fifth as much insulation on its legs as on the trunk (Scholander *et al.,* 1950 c) and seals, whales, otters, beavers, and ducks swim about in ice water with naked and expanded flippers or feet. If these were kept warm the heat loss would be tremendous (cp. Fig. 8). It has been shown, especially through the work of Irving and Krog (1954) in Alaska, that many arctic animals have a leg temperature far below their body temperature, i. e., 10° or even less. Still these extremities remain fully functional (Chatfield, Lyman and Irving, 1953). Cold extremities are therefore a major factor in heat conservation. How is this engineered? Either the blood flow might be grossly reduced, or there might be a vascular arrangement which shunts the arterial heat back into the body by counter current exchange with the veins, before it reaches the extremity. Anatomical and physiological studies strongly suggest that such heat shunts are of great importance.

---

[1] In smaller forms, like little birds, insulation by itself is insufficient and to survive the winter cold they must seek shelter and/or raise their resting heat production by shivering even during sleep (cp. Steen and Enger, 1957).

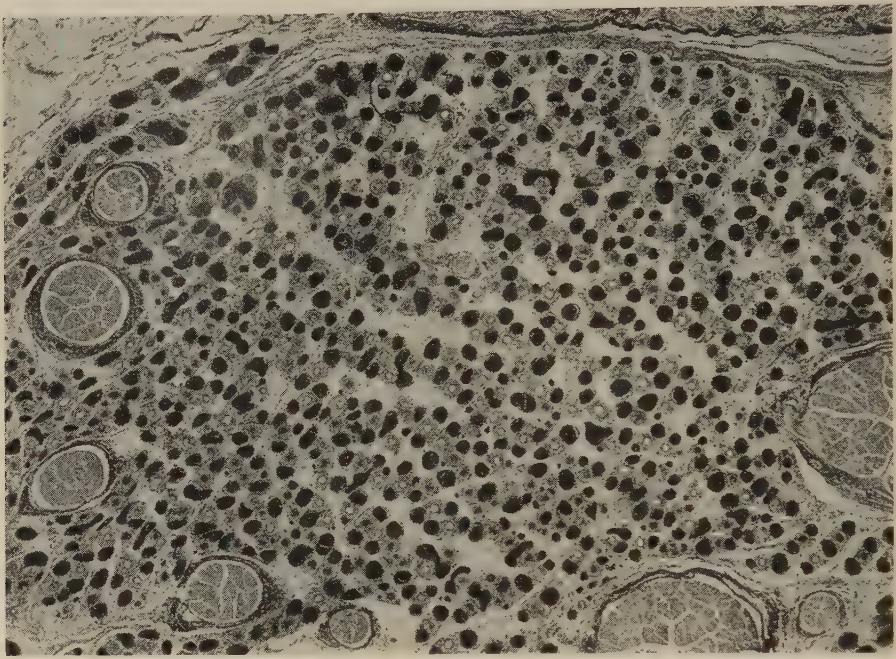

Fig. 7. Section of brachial vascular bundle in Florida manatee (*Trichechus latirostris*). Arteries (white) accompanied usually by two venules (black). Large peripheral structures are brachial nerve plexus (Fawceft, 1942).

Many years ago Claude Bernard (1876) pointed out that wherever veins are found running next to arteries there must be a transfer of heat between them. By such an arrangement some of the arterial heat could be saved and returned to the body before it is dissipated in the extremities. In recent years Bazett and his collaborators (1948) made fundamental studies of this heat exchange mechanism in man, and found that the temperature in the brachial artery might drop as much as 3 degrees per decimeter by transmitting heat to the adjacent veins.

This simple heat exchange system in man is a mere rudiment compared to the multichannel arterio-venous *rete* systems which anatomists have found in many mammals and birds. Some of these will be mentioned below.

The flippers and fluke of the Florida manatee are supplied through a bundle of several hundred small arteries and veins intermingled in a *rete* (Murie, 1872; Fawcett, 1942, cp. Fig. 7). Arterio-venous *retes* in peripheral structures are also prevalent in seals (Erikson, unpublished). The fluke and fins of whales are supplied through similar *retes* (cp. Slijper, 1936; Fawcett, 1942). Indeed, all major arteries entering the fins and flukes of whales are suspended within trabeculate venous channels (cp. Tomilin, 1951). The venous return, however, may take place along two alternative routes, either through the counter current system just mentioned, or through separate superficial veins (cp. Figs. 8 and 9), which makes a differential control of the heat loss possible (Scholander and Schevill, 1955).[1] Tall wading birds, like cranes and herons, have tarsal arterio-venous *retes* (Hyrtl, 1863).

In many terrestrial tropical mammals we find conspicuous *retes,* where instead of the typical brachial or femoral artery there are numerous smaller arteries and veins all mixed together in a bundle. *Retes* of this type are found in monotremes, loris (Fig. 10), sloths, anteaters, and armadillos (cp. Hyrtl, 1853; Rao and Rau, 1930; Wislocki and Straus, 1932; Scholander, 1955).

What is the meaning of these *retes*? No matter what other function they may have, they are by physical necessity heat exchangers and economizers of body heat. They are generally situated at the base of limbs, tail or fins. Consider an arctic whale, or seal, swimming in icy waters, with its greatly expanded and well vascularized fins and fluke (Fig. 8). How could this animal maintain its body heat unless it had some such heat exchange mechanism as the *retes* to keep the heat confined to the trunk (cp. Fig. 10)? The same holds true for waders, standing with their tall legs in cold water. The fact that we also find these structures in some tropical aquatic forms, such as manatees, whales, and the capybara, need not surprise us. Sea or lake water is chilling, as everyone knows from personal experience. Its cooling capacity is easily some 20—50 times greater than that of air of the same temperature.

In many other cold water forms, however, such as ducks, geese, sea gulls, and swans, *retes* have not ben observed (Hyrtl, 1863), and the fact that they have been found, on the other hand, in several land animals of the Tropics is also puzzling. At first sight this is a contradiction of the thesis that the *retes* are structures concerned with heat economy. We must remerber, however, that in temperature regulation, heat dissipation may be just as critical a factor as heat conservation. Consider, for instance, an arctic mammal, such as a husky or a fox, which is so well insulated that it can sleep on top of the snow at —40° with no more than a basal rate of heat production. When this animal gets up and runs, let us say in the warm sun after a night at —40°, it is immediately faced with the problem of getting rid of a ten to twenty times greater heat production. Man can do this easily by stepping out of his sleeping bag and adjusting his clothing, but the husky cannot throw off its coat, and it is impossible to change the heat transmission effectively through dense fur 5—6 centimeters thick. It can lose heat only through poorly insulated surfaces, such as the legs, face and tongue. Since the maintenance of

---

[1] Whales have conspicuous retes situated in various locations deep in the interior of the body. These are formed by strongly contorted arteries and veins, but bear no obvious relation to heat conservation (cp. Scholander, 1940).

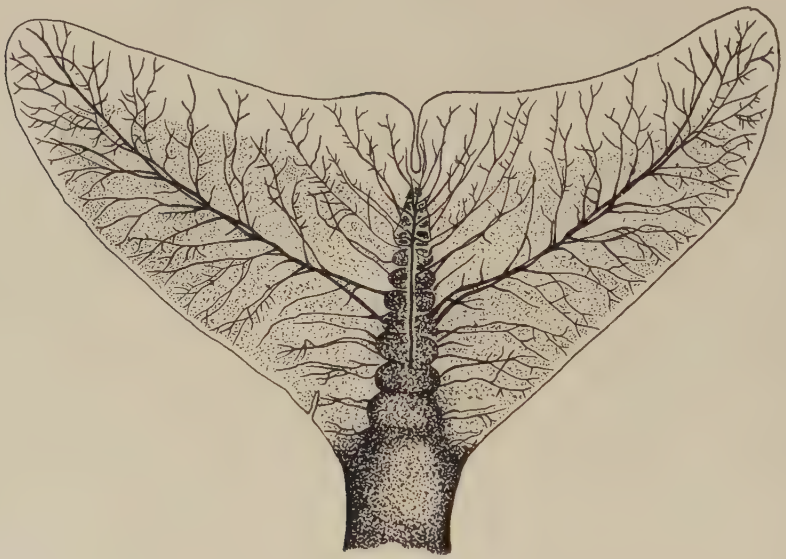

Fig. 8. Arterial blood supply to the flukes in common porpoise (*Phocaena phocaena*), drawn from an X ray picture by Braun (1905).

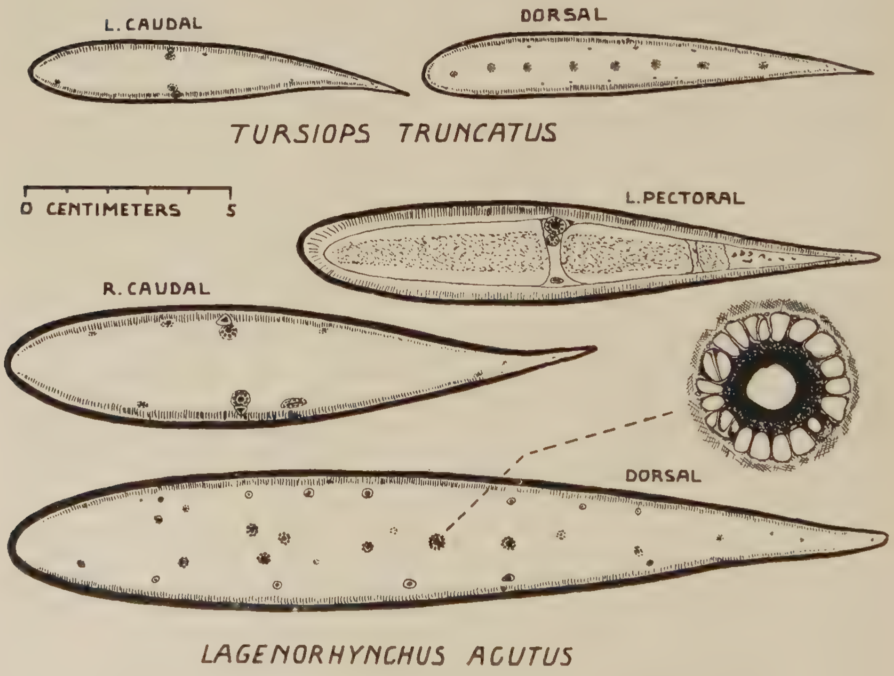
L. CAUDAL
DORSAL
TURSIOPS TRUNCATUS
0 CENTIMETERS 5
L. PECTORAL
R. CAUDAL
DORSAL
LAGENORHYNCHUS ACUTUS

Fig. 9. Sections near base of fins and flukes of two species of porpoise. Each artery is surrounded by a multiple venous channel. Simple veins are found near the surface, only the larger ones indicated here. (After Scholander and Schevill, 1955.)

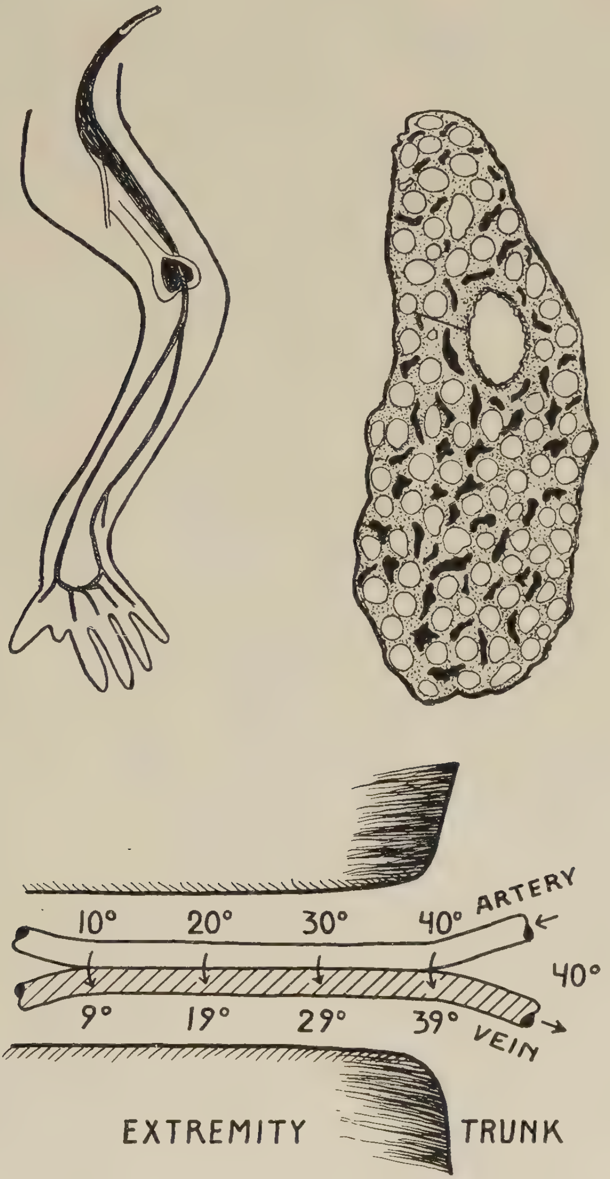

Fig. 10. Left: Front limb of loris (*Loris lyddekerianus*), showing brachial vascular rete. Right: cross section of femoral *rete* of same animal, arteries white, veins black. (After Rau and Rao, 1930). Below: Diagram of counter current transfer of heat in *rete* located at base of extremity (Scholander, 1955).

body temperature depends upon the balance between two opposite factors, heat dissipation and heat conservation, it is not always easy to predict where counter current heat exchangers would be needed.

Ducks and penguins, for example, are extremely well insulated birds, which probably depend upon their webbed feet for heat dissipation. Arterio-venous heat exchangers would directly counteract body cooling through the feet, and in this case it would be more reasonable to expect that the arteries and veins would run separately in the legs and feet and meet in networks near the surface. The sloth, on the other hand, living in the warm Tropics, is nevertheless so sensitive to temperature changes that it commences to shiver and to raise its metabolic rate as soon as the air temperature drops below + 27°. And yet the sloth must face this situation almost every night. It may well have to depend upon letting its long arms and legs cool at night to a reptilian temperature in order to preserve its body heat. It has been demonstrated that the sloth achieves just such a thermal separation by means of its brachial and femoral retes (Scholander and Krog, 1957).

The conspicuous development of arterio-venous retes at the base of the extremities in many warm-blooded animals seems to indicate that counter current exchange is a fundamental feature in the engineering of heat conservation, but more measurements must be made before we can fully evaluate the significance of these striking anatomical structures.

As an interesting variation on this theme it may be mentioned that the testes in most mammals are provided with a counter current vascular system. Here it seems that the maintenance of testicular coolness, essential to spermo genesis, is more important than the saving of general body heat. By means of a counter current vascular supply, the testes remain cool, although fully circulated.

Counter current exchange and renal function.

The possibility has recently been suggested that counter current exchange is involved in the renal mechanism for concentrating the urine.

We shall briefly call to mind the relevant part of the kidney structure. Urine starts its course of formation in the glomerulus capsule, it runs through the proximal convoluted tubule down into the loop of Henle, back through the distal convoluted tubule, and finally out through the collecting duct (cp. Fig. 11). There may be several millions of these units (nephrons) in a kidney. The loops of Henle and the lower parts of the collecting ducts project into the kidney papilla. The glomerulus capsules and the tubules are in the kidney cortex.

A number of years ago, Richards and his collaborators proved by the most subtile technique that the fluid produced by the glomerular capsule is simply a protein-free filtrate of the blood plasma, and is therefore essentially of the same concentration as the blood, i. e., it is isosmotic with the blood (Walker, Hudson, Findley and Richards, 1937). It re-

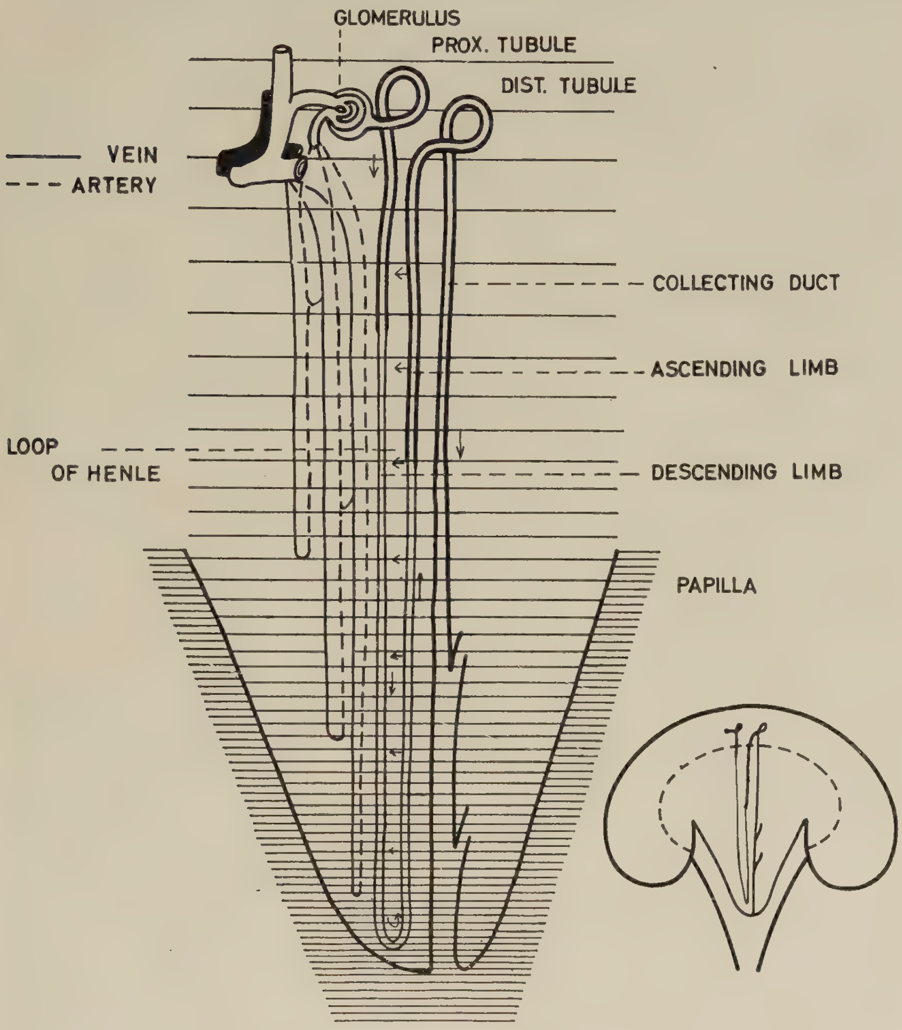
GLOMERULUS
PROX. TUBULE
DIST. TUBULE
VEIN
ARTERY
COLLECTING DUCT
ASCENDING LIMB
LOOP OF HENLE
DESCENDING LIMB
PAPILLA

Fig. 11. Diagram of nephron in rodent. Cross hatching indicates increasing osmoconcentration of all elements towards tip of papilla, which is isosmotic with the urine. Horizontal arrows indicate active transport of salts, vertical arrows direction of flow. Insert shows location of nephron in rodent kidney.

mained isosmotic in the proximal tubule, although much of it was reabsorbed (Walker, Bott, Oliver and MacDowell, 1941). There are no observational data on the concentration of the fluid in the loop of Henle, but it was generally believed that also there it remains essentially isosmotic with the systemic blood, so that the final concentration of the fluid into urine takes place in the distal tubules and the collecting ducts. The urine is often three to four times as concentrated as the blood.

A radically new idea was introduced by Hargitay and Kuhn in 1951.

They suggested that Henle's loop might reflect a counter current system involved in the process of concentrating the urine, and they pointed out a fact, which Sperber (1944) had already noted, namely, that only those animals that have Henle's loop, i. e., mammals and birds, are able to produce concentrated urine. Desert rodents, in particular, have well developed loops and can produce an extremely concentrated urine (cp. Schmidt-Nielsen et al., 1952). Hargitay and Kuhn (1951) postulated that some unknown process maintains a migration of salts from the ascending limb of the loop across the intervening tissue into the descending limb, or possibly a migration of water in the opposite direction. In either case, if such a cross migration were superimposed upon the counter current flow, it would build up a concentration gradient along the loop. It was further proposed that the concentration gradients originating in the loops would be transmitted to the surrounding tissues, involving both collecting ducts and blood capillaries. One would hence have a tissue gradient running from blood concentration in the cortex region to full urinary concentration towards the tip of the papilla, and the blood entering the papilla would transiently undergo a three- to fourfold concentration (cp. Fig. 11).

Wirz, Hargitay, and Kuhn (1951) put these ideas to a test by freezing rat kidneys which were secreting a concentrated urine. The frozen kidneys were sectioned and the melting point of the sections was observed under a microscope. They found that the melting point of the tissue in the papilla region indeed equalled that of the urine, and the melting point in the cortex tissue equalled that of the blood. Since, however, permeability damage from freezing might have allowed the urine to seep out on thawing from the collecting ducts into the papilla tissue, Wirz (1953, 1954) developed a micro puncture technique and managed to obtain blood samples from the papilla capillaries in a hamster. This blood had the same melting point as the urine, i. e., it was up to three times as concentrated as the systemic blood.

These findings, although indicating the existence of an osmotic gradient down the papilla, unfortunately leave the main issue unsettled. Such a gradient could indeed developed from the postulated active cross migration in Henle's loop, but it could also develop passively from a concentrated urine formed by other means. (Compare the relation between P and p expressed in equation (1).). The idea that counter current exchange may play an important role in the mechanism for concentrating the urine remains, however, an interesting possibility, especially when we realize that there are so many other simpler cases of counter current systems which are functional in biology.[1]

---

[1] For a full account of recent developments in this subject the reader is referred to surveys by Berliner *et al.* (1958) and Schmidt-Nielsen (1958).

It may be concluded from the examples which have beeen described that counter current exchange is a principle of wide and varied application in biology. We find it as a means of greatly increasing the efficiency of diffusion exchange in the gills of fish and in the placenta of mammals. It acts as a potent diffusion barrier against circulatory gas loss from the swimbladder in fishes, and it also establishes barriers against excessive peripheral heat loss in the extremities of mammals and birds. Finally it represents a means for producing high concentrations by a gentle, stepwise summation of a small primary concentration effect, which may be the mechanism involved in producing the tremendous gas pressures in the swimbladder of fishes or the concentration of urine in the mammalian kidney.

Literature cited.

Amoroso, E. C., 1952. Placentation. *In* Parkes, A. S., ed., Marshall's Physiology of Reproduction, vol 2, Chapt. 15, pp. 127—311, London.

Barcroft, J., and D. H. Barron, 1946. Observations upon the form and relations of the maternal and fetal vessels in the placenta of the sheep. Anat. Rec., *94*: 569—595.

Bazett, H. C., L. Love, M. Newton, L. Eisenberg, R. Day, and R. Forster II, 1948. Temperature changes in blood flowing in arteries and veins in man. Journ. Appl. Physiol., *1*: 3—19.

Berliner, R. W., N. G. Levinsky, D. G. Davidson and M. Eden, 1958. Dilution and concentration of the urine and action of antidiuretic hormone. Am. Journ. Med. *24*: 730—744.

Bernard, C., 1876. Leçons sur la chaleur animale, Paris.

Braun, M., 1905. Einiges über *Phocaena communis* Less. Zool. Anz. *29*: 145—149.

Chatfield, P. O., C. P. Lyman, and L. Irving, 1953. Physiological adaptation to cold of peripheral nerve in the leg of the herring gull (*Larus argentatus*). Amer. Journ. Physiol., *172*: 639—644.

Clusius, K., and G. Dickel, 1938. Neues Verfahren zur Gasentmischung und Isotopentrennung. Naturwissensch., *26*: 546.

Dam, L. van, 1938. On the utilization of oxygen and regulation of breathing in some aquatic animals. Groningen.

Erikson, H. Unpublished material.

Fawcett, D. W., 1942. A Comparative study of blood-vascular bundles in the Florida manatee (*Trichechus latirostris*) and in certain cetaceans and edentates. Journ. Morph., *71*: 105—133.

Haldane, J. S., 1922. Respiration. New Haven.

Hall, F. G., 1924. The functions of the swimbladder of fishes. Biol. Bull., *47*: 79—126.

Hargitay, B., and W. Kuhn, 1951. Das Multiplikationsprinzip als Grundlage der Harnkonzentrierung in der Niere. Zeitschr. Elektrochem. angewandte Physik. Chem., *55*: 539—558.

Hazelhoff, E. H., and H. H. Evenhuis, 1952. Importance of the "counter current Principle" for the oxygen uptake in fishes. Nature *169*: 77.

Hyrtl, J., 1853. Beiträge zur vergleichenden Angiologie. IV. Das arterielle Gefäss-System der Monotremen. Denkschr. K. Akad. Wissensch., Math.-Naturwiss. Classe, Wien, vol. 5, Abth. 1, 1—20.

— 1863. Neue Wundernetze und Geflechte bei Vögeln und Säugethieren. Denkschr. Math.-Naturwiss. Classe K. Akad. Wissensch., Wien, *22*: 113—152.

Irving, L., and J. Krog, 1954. Body temperature of arctic and subarctic birds and mammals. Journ. Appl. Physiol., *6*: 667—680.

Jost, W., 1952. Diffusion in solids, liquids, gases. New York.

Morrison, P. R., and F. A. Ryser, 1952. Weight and body temperature in mammals. Science, *116*: 231—232.

Mossman, H. W., 1926. The rabbit placenta and the problem of placental transmission. Amer. Jour. Anat., *37*: 433—497.

— 1937. Comparative morphogenesis of the fetal membranes and accessory uterine structures. Contr. Embryology, *26*: 129—246, Carnegie Inst. Washington Publ. no. 479.

Murie, J., 1872. On the form and structure of the manatee (*Manatus americanus*). Trans. Zool. Soc. London, *8*: 127—202.

Rau, A. Subba, and P. Krishna Rao, 1930. Contributions to our knowledge of the anatomy of the Lemuroidea. I. Arterial system of *Loris lyddekerianus*. Half-yearly Journ. Mysore Univ., *4*: 90—121.

Schmidt-Nielsen, K., and B. Schmidt-Nielsen, 1952. Water metabolism of desert mammals. Physiological Rev. *32*: 135—166.

Schmidt-Nielsen, B., 1958. Urea excretion in mammals. Physiol. Rev. *38*: 139—168.

Scholander, P. F., 1940. Experimental investigations on the respiratory function in diving mammals and birds. Hvalrådets skrifter nr. 22.

— 1954. Secretion of gases against high pressures in the swimbladder of deep sea fishes. II. The *rete mirabile*. Biol. Bull., *107* :260—277.

— 1955. Evolution of climatic adaptation in homeotherms. Evolution, *9*: 15—26.

— 1957. "The wonderful net". Scientific American, *196*: 4: 96—107.

— and L. van Dam, 1953. Composition of the swimbladder gas in deep sea fishes. Biol. Bull., *104*: 75—86.

— R. Hock, V. Walters, and L. Irving, 1950 a. Adaptation to cold in arctic and tropical mammals and birds in relation to body temperature, insulation, and basal metabolic rate. Biol. Bull., *99*: 259—271.

— R. Hock, V. Walters, F. Johnson, and L. Irving, 1950 b. Heat regulation in some arctic and tropical mammals and birds. Biol. Bull., *99*: 237—258.

— and J. Krog, 1957. Countercurrent heat exchange and vascular bundles in sloths. J. Appl. Physiol. *10*: 405—411.

— and W. E. Schevill, 1955. Counter-current vascular heat exchange in the fins of whales. J. Appl. Physiol., *8*: 279—282.

— V. Walters, R. Hock, and L. Irving, 1950 c. Body insulation of some arctic an tropical mammals and birds. Biol. Bull., *99*: 225—236.

Slijper, E. J., 1936. Die Cetaceen vergleichend-anatomisch und systematisch. Capita zoologica, vol. 7.

Sperber, I., 1944. Studies on the mammalian kidney. Zool. bidrag, Uppsala, *22*: 249—431.

Steen, J., and P. S. Enger, 1957. Muscular heat production in pigeons during exposure to cold. Am. J. Physiol. *191*: 157—158.

Tomilin, A. G., 1951. On the thermoregulation in cetacea. "Priroda", n. 6, pp. 55—58.

Walker, A. M., P. A. Bott, J. Oliver, and M. C. MacDowell, 1941. The collection and analysis of fluid from single nephrons of the mammalian kidney. Amer. Journ. Physiol., *134*: 580—595.

— C. L. Hudson, T. Findley, Jr., and A. N. Richards, 1937. The total molecular concentration and the chloride concentration of fluid from different segments of the renal tubule of amphibia. Amer. Journ. Physiol., *118*: 121—129.

Wirz, H., 1953. Der osmotische Druck des Blutes in der Nierenpapille. Helvetica Physiol. Pharmacol. Acta, *11*: 20—29.

— 1954. The production of hypertonic urine by the mammalian kidney. *In* Lewis, A. A. G., and G. E. W. Wolstenholme, eds., Ciba Foundation Symposium on the Kidney, pp. 38—49. Boston.

— B. Hargitay, and W. Kuhn, 1951. Lokalisation des Konzentrierungsprozesses in der Niere durch direkte Kryoskopie. Helvetica Physiol. Pharmacol. Acta, *9*: 196—207.

Wislocki, G. B., and W. L. Straus, Jr., 1932. On the blood vascular bundles in the limbs of certain edentates and lemurs. Bull. Mus. Comp. Zool., *74*: 1—15.

Woodland, W. N. F., 1911. On the structure and function of the gas glands and *retia mirabilia* associated with the gas bladder of some teleostean fishes, with notes on the teleost pancreas. Proc. Zool. Soc. London, pp. 183—248.

Contribution No. 994

Reprinted from
BULLETIN OF MARINE SCIENCE
OF THE GULF AND CARIBBEAN
Vol. 8, No. 4, pp. 369-389
DECEMBER, 1958

THE CEPHALOPODS COLLECTED BY THE R/V ATLANTIS DURING THE WEST INDIAN CRUISE OF 1954.[1,2]

GILBERT L. VOSS
The Marine Laboratory, University of Miami

ABSTRACT

The present report is based upon a collection of cephalopods made by the Woods Hole Oceanographic Institution's research vessel ATLANTIS in the West Indies in 1954. The collection consists of 83 specimens representing 17 genera and 18 species of which one genus, *Selenoteuthis,* and two species, *Selenoteuthis scintillans* and *Abralia grimpei,* are new to science.

INTRODUCTION

This study is based upon a small collection of cephalopods collected by the Woods Hole Oceanographic Institution's research vessel ATLANTIS during a cruise to the West Indies in 1954. The material, consisting of 83 specimens, is very rich and contains 17 genera and 18 species of which one genus and two species are new to science. Of particular interest in the collection is the new species of lycoteuthid squid which, by the arrangement and size of its light organs, must rank among the most brilliant of all of our luminous bathypelagic species. Also worthy of note is the new species of *Abralia.* For many years this genus was thought to be primarily Indo-Pacific in distribution and was represented in the Atlantic by a single species. Within only a few years the number of species of this genus has been raised to three and the whole Atlantic cephalopod fauna is being shown to be equal in importance to that of the other large oceanic areas.

The author is indebted to Dr. Richard H. Backus of the Woods Hole Oceanographic Institution for the opportunity to study this collection made by him during the 1954 cruise, for reading the manuscript, and for observations concerning the gear used. In particular he wishes to thank the Woods Hole Oceanographic Institution and Dr. Alfred C. Redfield, formerly Associate Director, for the financial support in the form of a Fellowship which enabled him to carry out the study both at Miami and the Museum of Comparative Zoology at Harvard College. The illustrations of *Abralia* are by the author's wife, Nancy A. Voss; the others were drawn by the author. All abbreviations and measurements are as defined by Voss (1956).

---

[1] Contribution No. 994 from the Woods Hole Oceanographic Institution.
[2] Contribution No. 213 from The Marine Laboratory, University of Miami.

The specimens were captured by means of an Isaacs-Kidd Midwater Trawl (IKMT). Since this is not a closing net, the specimens might have been taken anywhere between the surface and the depths indicated. As the net fishes at the depth indicated for a period considerably longer than the time needed for lowering or hauling in, statistically the chances are greater that they came from the depth recorded. The depth in meters was obtained by a telemetering device and represents the actual depth fished instead of meters of wire out.

Order SEPIOIDEA

Family SPIRULIDAE Orbigny

Spirula spirula (Linnaeus, 1758)

Nautilus spirula Linnaeus, 1758, p. 710.

Material. 2 ♀♀, ML 32.0 and 42.0 mm, Stn. RHB 582, in 504 meters, March 2, 1954. UMML 31.175.

Both specimens were taken alive and are in an excellent state of preservation. The larger one is intact, with the skin covering the shell both dorsally and ventrally; the smaller one has the skin ruptured and several chambers of the shell are crushed.

Bruun (1943) has summarized the present information on the biology and distribution of this interesting species. In 1955 he also published a more detailed account of the vertical distribution and has suggested the term "mesopelagic" for the level at which they are found. According to his table (1955, p. 67) the present specimens came from a greater depth than any yet recorded from the West Indies.

Order TEUTHOIDEA

SUBORDER *OEGOPSIDA*

Family LYCOTEUTHIDAE Pfeffer

Selenoteuthis, new genus

Lycoteuthids with short, wide fins; a large round light organ at the end of the mantle and a small round light organ at the tip of the 2nd and 3rd arms; 10 light organs within the mantle cavity and two on each of the tentacular stalks; buccal membrane 8 lobed with 8 supports.

Type species: Selenoteuthis scintillans, n. sp.

Selenoteuthis scintillans, n. sp.

Figure 1 a-e

Holotype. A male, in alcohol, ML 32.5 mm, from Stn. RHB 587, 26°22′N, 76°10′W, IKMT net, from 46 meters; 2003 - 2111 hours, March 21, 1954. To be deposited in the Museum of Comparative Zoology.

Description. I have referred this specimen to the lycoteuthids with some reservation. It is a remarkable species and a living individual must be spectacular.

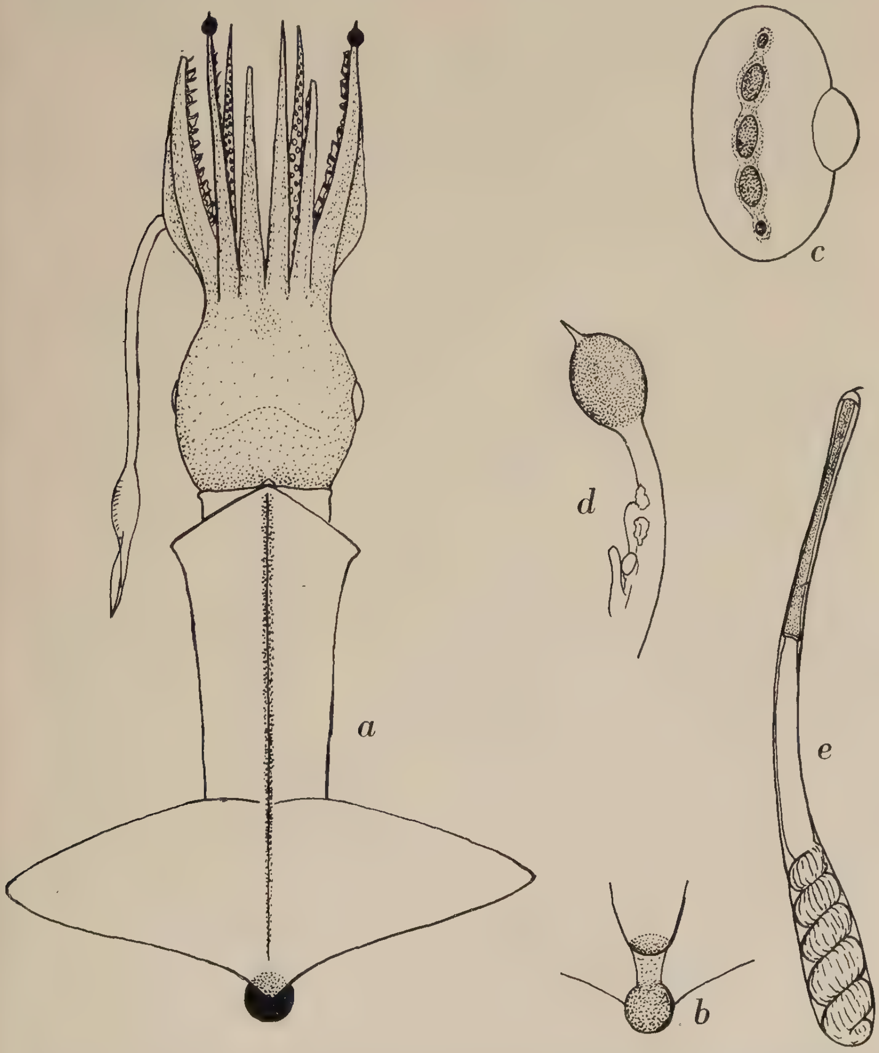

FIGURE 1. *Selenoteuthis scintillans* n. sp. a. Dorsal view, b. Terminal light organ of mantle, c. Left eyeball, ventral view to show light organs, d. Apical light organ of left dorso-lateral arm, e. Spermatophore.

The *mantle* is rather long and slender (Fig. 1 a), the anterodorsal margin sharply produced. There is no excavation in the ventral mantle margin beneath the funnel. The posterior end is bluntly pointed, but the mantle is somewhat curved downward due to fixation and a break in the dorsal surface of the mantle, so that the true contour is difficult to see. At the end of the mantle and entirely projecting beyond the fins is a large round light organ (Fig. 1 b). This does not occur in any other lycoteuthid.

The *fins* are short and very broad, terminal except for the black photophore projecting beyond them. The anterior margins are convex, the posterior margins concave. The lateral corners are sharply pointed.

The *funnel* is large and stout, free for only the distal ¼ of its length and provided with a small but strong dorsal support. The funnel organ is uncomplicated and consists of an inverted V shaped dorsal member with short, shouldered limbs, and fat, thick ventral pads. The funnel valve is large, sub-terminal and slightly bilobed. The mantle locking apparatus consists of a simple, slightly curved funnel groove on each side and a corresponding ridge on either side of the mantle. The nuchal cartilage is elongate, swollen and rounded posteriorly and widely pointed anteriorly.

The *gladius* may be seen through the dorsal mantle wall but was not dissected out.

The *head* is short and broad, nearly as wide as the mantle, with large eyes. The eyes are equipped with five light organs around their periphery ventrally. At each end there is a very small round organ, separated by three large round organs (Fig. 1 c). All appeared to have been bright red in the living animal and in the preserved specimen they had a distinct reddish hue. The light organs on both eyes were somewhat damaged. The beaks were not dissected out but appeared normal. The buccal membrane is 8 lobed with 8 prominent supports. The entire membrane is reddish purple and is strongly papillose on the outer surface.

The *arms* are in the order 2 = 3.1 = 4. No keels could be seen, but all of the arm tips are very attenuate. In addition, there is a small brownish black light organ just below the tip on the 3rd arm of the right side and the 2nd arm of the left side (Fig. 1 d). The tips of the corresponding arms of these pairs were missing. The suckers of the arms are biserially arranged, bordered dorsally by a low indistinct protective membrane and ventrally by a very broad membrane with stout supports. The supports, however, are torn free from the membrane and present a fringed appearance. The suckers are equipped with about 7-9 long teeth on the distal margin of the horny ring. The proximal edge of the ring is entire. There is no apparent hectocotylization of any of the arms.

Only the left *tentacle* is present. It is long and stout and bears a short club which is broad basally but attenuate for the distal 2/3. The suckers are in four rows upon the hand part with the entire margin finely toothed. The carpal cluster is compact and consists of five suckers and about three discernible buttons. A protective membrane with prominent supports is located ventrally and a swimming membrane occupies about 1/3 of the distal border on the dorsal side. Two large light organs of a silvery appearance are embedded on the aboral surface of the tentacular stalks, one basally, the other near the carpal section.

Internally there are 10 *light organs*. Two elongate, oval light organs lie within the funnel chamber, one on each side of the rectum. In the midsection of the mantle cavity are five light organs: a small longitudinally oval central organ, a large transversely oval light organ on each side, and a small round light organ attached to the base of each gill. In the posterior part of the mantle cavity there appear to be three photophores arranged in a transverse row, but these organs are badly damaged and their exact shape and number cannot be ascertained.

The spermatophores are short and stout and there are only a few turns of the sperm reservoir. The structure of the spermatophores is different from any yet described and is illustrated in Figure 1 e.

TABLE 1

MEASUREMENTS (IN MM) OF THE HOLOTYPE OF *Selenoteuthis scintillans* n. sp.

Sex	♂	Arms, I	12.0
ML	32.5	II	12.9
MW	12.0	III	12.9
HW	—	IV	12.0
HL	11.5	TL	27.5
FL	11.0	CL	6.8
FW	30.0	Diam. terminal light organ	3.0

The generic name *Selenoteuthis* or moon squid is derived from the Greek SELENE—moon and TEUTHIS—a squid, in reference to the large terminal light organ, and is in the feminine gender. The specific name *scintillans* is the present participle of the Latin *scintillo,* to glitter, sparkle or shine, here used as an adjective, sparkling.

Discussion. Selenoteuthis scintillans is the sixth species to be included in the family Lycoteuthidae, and all six belong to monotypic genera. In general, in modern systematics, such generic splitting is frowned upon, but in the present situation no other recourse is at hand. With the exception of *Lycoteuthis diadema* (Chun, 1900) all of the other genera and species are known from unique specimens only. Lycoteuthids are rarely obtained, living apparently in the bathypelagic habitat, and little is known of their life history. Also, as most of the species are known only from females, the morphology of the males and differences in the genitalia are unknown.

Lycoteuthis diadema (Chun, 1900)

Enoploteuthis diadema Chun, 1900, p. 532.
Lycoteuthis diadema, Pfeffer, 1908, p. 294; 1912, p. 114; Voss, 1956, p. 118.
Asthenoteuthion planctonicum Pfeffer, 1912, p. 172, Pl. 15, figs. 8-14.

Material. 2 juveniles, ML 8.3 and 7.2 mm, from Stn. RHB 553, in 57 meters, Feb. 7, 1954. UMML 31.194.

1 juvenile, ML 8.7 mm, from Stn. RHB 574, in 46 meters, Feb. 25, 1954. UMML 31.194.

These three specimens seem definitely referrable to this species on the basis of the shape of the fins, the light organs on the ventral surface of the eyeball, and the arrangement and number of the light organs within the mantle cavity.

In 1912 Pfeffer described a new genus and species, *Asthenoteuthion planctonicum,* based upon three larval specimens obtained by the German Plankton-Expedition. The mantle lengths were 4.5, 3.5 and 2.0 mm respectively. Due to the shape of the gladius in the largest of these, he considered them to belong to the family Enoploteuthidae and suggested relationship to the larvae of *Abraliopsis, Abralia,* etc. because of the shape and position of the fins. Finally he remarks, "Man könnte auf Grunde der Fünfzahl der Leuchtorgane des Bulbus vielleicht an eine Verwandtschaft mit *Lycoteuthis* denken; aber der Gladius von *Asthenoteuthion* ist ein echter Enoploteuthiden-Gladius."

In the present specimens the gladius of the 8.3 mm specimen was dissected out and found to lie midway between the enoploteuthid like gladius described by Pfeffer and the true lycoteuthid gladius. Evidently Pfeffer's younger specimen was not far enough advanced in development to show its true affinities.

The most notable character of these larvae or juveniles, as well as in *Asthenoteuthion,* is the presence of five light organs on the ventral surface of the bulbus. The five organs are large, crowded and round, but as in *Lycoteuthis* the middle or 3rd organ is distinctly different in color from the others. It is reddish in contrast to the clear opaque appearance of the other four and in the largest specimen available, 8.7 mm, a purplish sheen is distinctly visible. This coincides exactly with the organs in *Lycoteuthis*.

The mantle cavity of each specimen was opened and the visceral mass searched for the presence of the light organs peculiar to the lycoteuthids. In the 7.2 mm specimen, there were two light organs in the funnel, one on each side of the rectum, a small light organ at the base of the gills, and two light organs lying between the gills in a line across the visceral mass. In the 8.7 mm specimen there was a minute light organ lying between the median pair between the gills. These light organs correspond to those found in *Lycoteuthis* with the exception of the posterior three photophores which were completely missing in the present specimens, nor was there any evidence of the photophores in the tentacular stalks. Evidently these missing organs develop at a later stage.

The fins are small but have already attained their typical wide, pointed, lycoteuthid appearance.

Family ENOPLOTEUTHIDAE Pfeffer

Abralia grimpei, n. sp.

Holotype. ♀, preserved in alcohol, ML 27.0 mm, from Stn. RHB 551, 26°25′N, 79°45′W, IKMT net, from 57 meters, Feb. 6, 1954. To be deposited in the Museum of Comparative Zoology.

Diagnosis. Two rows of suckers on tips of arms; fins half the length of the mantle or less; two hooks on tentacular clubs; six to seven light organs on ventral periphery of eyeball; about nine rows of photophores on ventral surface of head.

Description. A single female of an *Abralia* was found in the collections. A number of characters distinguish it from the other members of the genus found in the Atlantic and Indo-Pacific areas and warrant its description here as a new species.

The *mantle* is long and cylindrical (Figs. 2 a, b), slightly produced in the midline dorsally and emarginated beneath the funnel. The posterior end is bluntly pointed.

The *fins* are of moderate length, united posteriorly, and with free anterior lobes. The anterior margin is strongly convex, the posterior margin concave. The mantle locking apparatus is slightly curved and strong.

The *funnel* is strongly developed (Fig. 2 c). The funnel organ (Fig. 2 d) is composed of a dorsal member shaped like an inverted

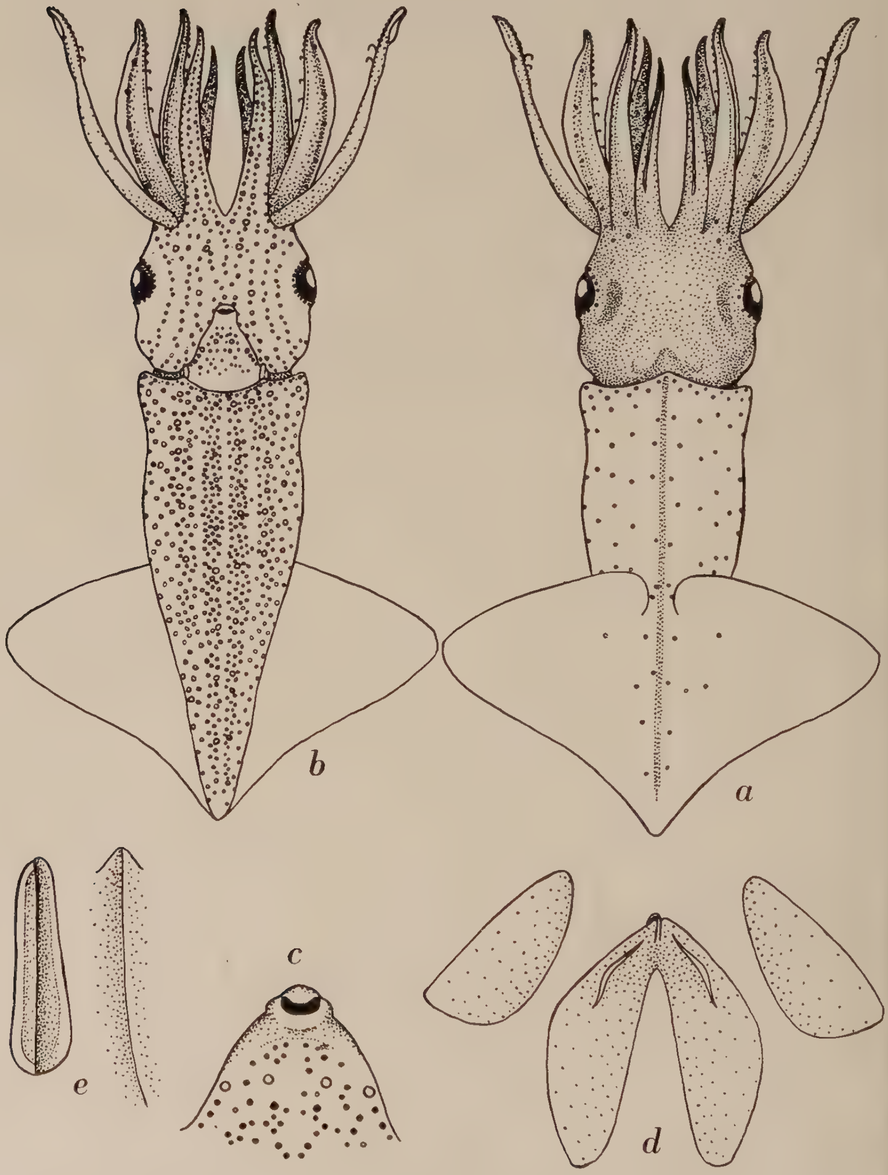

FIGURE 2. *Abralia grimpei* n. sp. a. Dorsal view, b. ventral view, c. Funnel, d. Funnel organ, e. Locking apparatus.

V with angled shoulders and two ventral pads which are large and slightly angled. The locking apparatus is shown in Figure 2 e.

The *arms* are in the order 4.1.2 = 3. All of the arms, with the exception of those of the fourth pair, are keeled at least distally. The third pair is equipped with a strong swimming membrane. All of the arms (Fig. 3 a) bear about 13 hooks on the proximal 2/3 of the arms (12 in IV) after which there are about 10-12 small suckers followed distally by a few minute suckers in two rows. The hooks (Fig. 3 b) and suckers are bordered by low protective membranes, the ventral one of III being somewhat larger than the others. The sucker rings are toothed on their outer margins but are entire on the inner margin (Fig. 3 c).

The *tentacles* are short and stout, the stalks oval in cross section and grooved orally. The clubs (Fig. 3 d) are moderately expanded and on the hand part are equipped with two rows of suckers with finely toothed margins (Fig. 3 e) and two large hooks (Fig. 3 f) on the ventral row. Distally the club bears four rows of small suckers. The carpal cluster consists of a block of five small, smooth ringed suckers and

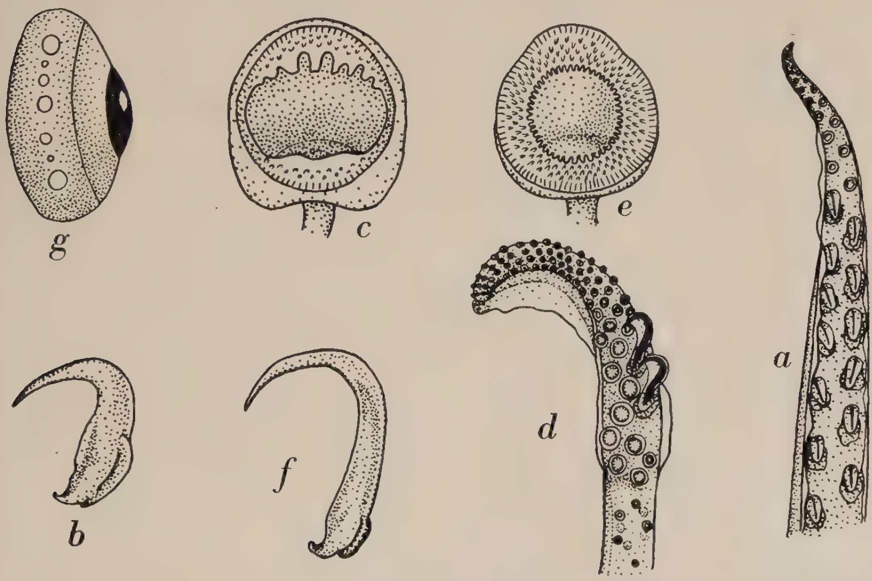

FIGURE 3. *Abralia grimpei* n. sp. a. Right dorso-lateral arm, b. Hook from fifth pair of dorso-lateral arm, c. Sucker from second pair of right dorso-lateral arm, d. Left tentacular club, e. Sucker from left tentacular club, inner row, third pair, f. Distal hook from left tentacular club, g. Left eyeball, ventral view.

about four low pads. Ventrally there is a semicircular protective membrane originating near the carpus and ending at the base of the distal hook. Beyond this is a low protective membrane which extends to the tip of the club. Aborally there is a strong keel on the distal half. Dorsally there is a low protective membrane originating at the carpus and extending over about half of the club.

As in all *Abralia* the specimen is liberally supplied with light organs. These are of the typical three types on the ventral surface of the head, funnel and mantle. There are large clear-centered organs, medium size dark ones and small dark organs with minute clear centers. They are arranged as follows.

On the ventral surface of the mantle and extending over the lower part of the sides are numerous light organs separated in the ventral midline and laterally by distinct bands of clear skin. This apparent orderly distribution may well be due to the action of the preservative. There are also scattered photophores on the dorsal side of the mantle. The ventral surface of the funnel (Fig. 2 c) bears about 56 light organs, 28 on each side, besides a patch of about 16 on each side of the funnel on the dorsal surface, squeezed in against the posterior surface of the head.

The ventral surface of the head bears about nine indistinct rows of photophores which unite anteriorly to form three distinct rows of light organs on the ventral arms occupying about 4/5 of the length of the arms. The dorsal row terminates here but the other two rows continue to just short of the tip. Only the median row continues to the extremity of the arm. There are about five small light organs on the ventro-lateral arms, distributed along the base of the swimming membrane. In addition, there are two light organs on the head at the base of the dorsolateral arms and a single photophore a few millimeters from the base of these arms. Each eye has a distinct and orderly row of small light organs bordering the eyelids.

TABLE 2

MEASUREMENTS (IN MM) OF THE HOLOTYPE OF *Abralia grimpei* n. sp.

Sex	♀	Arms	I	12.0
ML	34.0		II	11.5
MW	11.4		III	11.5
HW	12.4		IV	12.5
HL	11.0	Hooks	I	13
FL	18.6		II	13
FW	28.0		III	13
TL	16.0		IV	12
CL	6.0			

The eyeballs bear light organs on the lower half of their periphery, arranged in a single row. The photophores are six in number on the right eyeball, consisting of a posterior and anterior roundish organ with three slightly smaller and less well-defined light organs between them and a minute light organ between the anteriormost one and its fellow. In addition to these, on the left eyeball (Fig. 3 g) a minute organ lies between the posteriormost light organ and its adjacent fellow, making seven photophores in all.

The beaks and radula were not examined.

Discussion. With the description of this species, the number of species of *Abralia* in the Atlantic is raised to three, each of which is easily distinguished from the others. These are compared below and a key is given to the Atlantic species. The species of the genus *Abralia* of the Pacific and Indian Oceans are presently being revised and will be published upon shortly.

The first Atlantic species, *Abralia veranyi,* was described from the Mediterranean in 1844 by Rüppell. It is characterized by the presence of five light organs on the eyeball of which the first and the last members are large and oval, the posterior one with a slight sinus, and there are four hooks on the tentacular club of which the proximal is minute, the second largest, and the others decreasing in size. There are four rows of minute suckers on the ends of the arms. The second species, *Abralia redfieldi,* was described by the author in 1955 and separated from the preceding species by the presence of five light organs on the eyeball all of which are round, three hooks on the tentacular club and two rows of suckers on the sessile arm tips.

A. veranyi is recorded from the Mediterranean, the eastern Atlantic from Madeira to West Africa, and the Western Atlantic from the Bahamas, Cuba and the Gulf of Mexico. *A. redfieldi* is known at present from the Florida Current off Miami and the coast of Cuba. The present species. It has been well figured and described by Pfeffer (1912). ing only two rows of minute suckers on the ends of the arms. It differs from both in having only two large hooks on the tentacular club and differs also from both in the arrangement and size of the light organs on the eyeball. It does not correspond to any of the known Indo-Pacific forms.

The specific name *grimpei* is given in honor of Dr. Georg Grimpe, the noted German teuthologist who contributed greatly to our knowledge of this genus.

KEY TO THE ATLANTIC SPECIES OF *Abralia*

1. 4 rows of suckers on the tips of the sessile arms; 4 hooks on the tentacular club; light organs on eyeball with large oval anterior and posterior members with a sinus in the dorsal margin of the posterior one; fins large, well over half the mantle length in the adult.
Abralia veranyi Rüppell, 1844
2 rows of suckers on the tips of the sessile arms; less than 4 hooks on the tentacular club; light organs on the eyeball all round; fins small. 2
2. 3 hooks on the tentacular club; light organs on eyeball round, 1st, 3rd and 5th large, 2nd and 4th small; body large and stout.
Abralia redfieldi Voss, 1955
2 hooks on the tentacular club; light organs on eyeball less clearly defined, 6-7 in number with anterior and posterior ones largest, 2nd and often next to last minute; mantle long and slender.
Abralia grimpei, n. sp.

Abralia juv.

Material. 1 juv., ML 6.8 mm, from Stn. RHB 551 from 57 meters, Feb. 6, 1954.

3 juv., ML 10.5, 9.5 and 11.6 mm, from Stn. RHB 560 from 46 meters, Feb. 22, 1954.

It does not seem possible to make a definite identification of the four specimens listed above. The tentacles are missing in all but the largest specimen from Stn. 560, in which it appears that the distalmost hook on the club is the largest. In this specimen the 1st and 5th light organs on the eyeball are nearly the same size as the 3rd and in this respect it most closely resembles *A. redfieldi*, but there seem to be four rows of suckers on the tips of the sessile arms which would place it in *A. veranyi*. The remaining two specimens from Stn. 560 have very large, rather round 1st and 5th photophores which would place it in the same species.

The smallest specimen in the series, from Stn. 551, seems to have smaller fins and a narrower body and the light organs of 1, 3 and 5 on the eyeball are of equal size. From these characters it would seem best to call it *A. redfieldi* but I hesitate to do so until the larval and juvenile stages and the accompanying morphological changes are known. In all of the specimens, the dorsal row of light organs on the ventral arms alone is present, and the photophores on the ventral surface of the head and mantle are much less numerous than in the adults.

? *Abraliopsis morissi* (Verany, 1837)

Onychoteuthis Morissii Verany, 1837, p. 100.
Enoploteuthis Morissii, Orbigny, 1848, p. 338.
Abralia Morissii, Gray, 1849, p. 50.
Abraliopsis Morissii, Pfeffer, 1900, p. 168.

Material. 1 ♂, damaged, ML 18.6 mm, from Stn. RHB 572 in 505 meters, Feb. 25, 1954.

1 ♀, damaged, ML 16.5 mm, from Stn. RHB 589, in 370 meters, March 22, 1954.

The present specimens are in such a poor state of preservation that definite identification is impossible. The distal ends of the ventral arms are missing in both specimens so that it cannot be determined if they possessed the three photophores at their tips. However, the much larger fins, the light organs arranged in more or less regular rows on the mantle, and the dark purplish violet buccal membrane all indicate that the specimens are referrable to this species.

Pyroteuthis margaritifera (Rüppell, 1844)

Enoploteuthis margaritifera Rüppell, 1844.
Pterygioteuthis margaritifera, Pfeffer, 1900, p. 166.
Pyroteuthis margaritifera, Hoyle, 1902, p. 1.

Material. 2 ♀ ♀, ML 14.5 and 13.5 mm, from Stn. RHB 552, in 485 meters, Feb. 7, 1954.

These two specimens were the sole representatives of this common species. It has been well figured and described by Pfeffer (1912). They are easily differentiated from *Pterygioteuthis giardi* Fischer by the wide insertion of the fins, the presence of suckers on the ventral arms and the numerous large chromatophores on the dorsal surface of the head and mantle. This is a widely distributed species occurring in the Mediterranean Sea, Azores (Joubin), Madeira (Rees), Cuba (Voss). Joubin's specimen from the Azores was described as a new subspecies, *P. m. aurantiaca.*

Pterygioteuthis giardi H. Fischer, 1896

Pterygioteuthis giardi H. Fischer, 1896, p. 205.

Material. 4 ♂ ♂, ML 10.5 - 16.5 mm, 3 ♀ ♀, ML 8.4 - 19.0 mm, from Stn. RHB 553, in 57 meters, Feb. 7, 1954.

2 ♀ ♀, ML 18.0 and 14.0 mm, 2 ♀ ♀ damaged from Stn. RHB 555 in 560 meters, Feb. 10, 1954.

2 ♂ ♂, ML 12.8 and 8.3 mm, 3 ♀ ♀, ML 8.0 - 18.0 mm, and 1 damaged specimen, from Stn. 560, in 46 meters, Feb. 22, 1954.

1 ♂, ML 14.3 mm, 1 ♀, ML 15.6 mm and 3 badly damaged specimens from Stn. RHB 572, in 505 meters, Feb. 25, 1954.

1 ♂, ML 11.8 mm, 7 ♀ ♀, ML 5.3 - 18.0 mm, from Stn. RHB 574, in 46 meters, Feb. 25, 1954.

2 ♂ ♂, ML 11.0 and 13.4 mm, from Stn. RHB 575, in 505 meters, Feb. 26, 1954.

2 ♀♀, ML 16.0 and 20.0 mm, from Stn. RHB 587, in 46 meters, March 21, 1954.

The 34 specimens listed above were the most numerous of any species taken by the ATLANTIS on this cruise and the females were nearly twice as numerous as the males (10 males, 18 females). Their vertical distribution extended from 46 meters to 560 meters but no particular change in level seemed to occur with increase in size.

Pfeffer (1912) has discussed the relationship of this genus with *Pyroteuthis* and considered it to be a subgenus of the latter. However, the hectocotylization of the left arm in *Pterygioteuthis* in contrast with the right arm in *Pyroteuthis* seems alone to be of sufficient weight to keep it at the generic level.

Whether, as Pfeffer suggests, there are two races or subspecies of this species, one in the Atlantic and the other in the Pacific *(P. giardi hoylei)* must await the analysis of a larger number of specimens than is now available. Apparently a closely related species, *P. gemmata* Chun, occurs in the South Atlantic, but the author has seen specimens from the tropical Atlantic referred to *P. giardi* which had the peculiar faceted light organs of the former species.

Family OCTOPODOTEUTHIDAE Berry

Octopodoteuthopsis megaptera (Verrill, 1885)

Ancistrocheirus megaptera Verrill, 1885, p. 399.
Octopodoteuthopsis megaptera, Pfeffer, 1912, p. 223; Voss, 1955, p. 125.

Material. 1 juv., ML 11.7 mm, from Stn. RHB 550, in 329 meters, Feb. 6, 1954.

This small specimen has had the posterior end of the mantle cut off even with the fins, and if intact would probably have measured about 14.0 mm. The fins are very broad and somewhat narrow, 19.0 mm by 11.0 mm. The funnel organ has the peculiar hollowed out ventral pads described by Voss (1955, p. 125). The arms are apparently in the order 3.4.2.1, the third pair much longer than the others. None of the light organs described for this species were observable.

The ventral surface of the head and mantle is liberally spotted with small reddish brown chromatophores, and there is a transverse row of larger, dark brown chromatophores across the ventral surface of the head at the midpoint of the eyes.

Family ONYCHOTEUTHIDAE Gray

Onychoteuthis banksi (Leach, 1817)

Loligo banksi Leach, 1817, p. 141.
Onychoteuthis banksi, Orbigny, 1826, p. 61; Voss, 1955, p. 129.

Material. 1 juv., ML 16.5 mm, from Stn. RHB 551, in 57 meters, Feb. 26, 1954.

1 juv., ML 10.5 mm, from Stn. RHB 553, in 57 meters, Feb. 7, 1954.

5 juv., ML 6.6-9.5 mm, from Stn. RHB 574, in 46 meters, Feb. 25, 1954.

3 juv., ML 5.3-17.0 mm, from Stn. 581, in 95 meters, Feb. 26, 1954.

The 10 juveniles listed above were easily distinguished as belonging to this species. The rows of chromatophores in the midline on the dorsal surface, small fins, and sharply curved and projecting end conus of the gladius serve to distinguish this from all other known teuthoid larvae and juveniles. As might be expected of a surface pelagic species, the larvae all came from the shallower stations.

Family HISTIOTEUTHIDAE Verrill

Calliteuthis reversa Verrill, 1880

Calliteuthis reversa Verrill, 1880, p. 393.

Material. 1 ♂, ML 33.5 mm, Stn. RHB 450, in 137 meters, July 16, 1953. UMML 31.190.

1 ♀, ML 42.0 mm, Stn. RHB 584, in ??? meters, March 4, 1954. UMML 31.192.

1 ♀, ML 34.5 mm, Stn. RHB 591, in 524 meters, March 22, 1954. UMML 31.191.

2 ♀ ♀, ML 22.5 - 25. 0 mm, Stn. RHB 555, in 560 meters, Feb. 10, 1954. UMML 31.193.

Five specimens, tentatively identified as *C. reversa,* were taken by the BLUE DOLPHIN and the ATLANTIS. Four of these, all females, seem similar to those described by me (Voss, 1956) from the Gulf of Mexico. Their measurements and indices are given in Table 3.

The mantle is short, cone-shaped, widest at the anterior margin and bluntly pointed. The fins are small, round, indented posteriorly, and projecting slightly beyond the end of the mantle. In all the arm suckers are smooth on the proximal half and bear about twelve small, semicircular teeth on the distal half, the teeth minute and difficult to see basally, distinct distally. The tentacular suckers are minutely but distinctly armed with sharp teeth numbering about 60 on the largest sucker of the largest specimen. This may be compared with about 33 teeth from the Gulf of Mexico specimens. The photophores are few and scattered with three rows on the ventral arms. The dorsal member of the funnel organ bears a large flap on each lateral arm.

The fifth specimen, a male, differs considerably from the others. The mantle is more elongate and slender, with nearly parallel sides on the anterior half. The arm suckers are nearly smooth proximally armed with very minute teeth which are hardly discernible, but are more evident distally. The tentacular suckers are also toothed, but very minutely. In addition, the tentacles are quite short. There are no flaps on the dorsal member of the funnel organs, these being replaced by low mounds.

TABLE 3
Measurements and Indices of 5 Specimens of
Calliteuthis reversa Verrill, 1880.

Stn. No.	584	591	555	555	450
Sex	♀	♀	♀	♀	♂
ML	42.0	34.5	22.5	25.0	33.5
MWI	56.0	58.0	55.5	54.0	37.4
HWI	64.2	66.8	66.7	56.0	43.3
HLI	69.0	66.8	66.7	68.0	40.3
FLI	37.0	36.3	37.3	38.0	32.9
FWI	71.5	65.2	62.3	66.0	53.8
Arms I	85.0	63.0	33.0	41.0	33.5
II	101.0	61.0	37.0	44.0	38.0
III	101.0	70.0	38.0	44.0	37.5
IV	87.5	57.0	33.0	39.0	32.0
TLI	303.0	336.0	235.0	280.0	110.0
CLI	47.7	49.3	35.6	40.0	26.9
MAI	241.0	200.0	169.0	176.0	113.0

This last specimen compares very favorably with the original description and measurements of the holotype given by Verrill (1880). However, at this time we know too little about sexual differences in this group to even surmise whether all five specimens belong to *C. reversa* or whether they represent two distinct species. A revision of this genus is now underway by the author and it is hoped that some of the perplexing problems in this group may be cleared up.

Family OMMASTREPHIDAE Gill

Ommastrephid larvae *(Rhynchoteuthis)*

Material. 1 juv., ML 3.3 mm, Stn. RHB 560 in 46 meters, Feb. 22, 1954.

2 juv., ML 5.1 mm, one damaged, Stn. RHB 574 in 46 meters, Feb. 25, 1954.

These three small larvae cannot be identified to species at this time. The entire problem of the *Rhynchoteuthis* larvae has yet to be solved, although it has been assumed that at least some of the known larvae belong to *Ommastrephes pteropus* and *O. bartrami*. Various stages in the development of these larvae have been illustrated by Pfeffer (1912), who considered that there might be two species represented in his material. Additional comments on this problem have been given by Robson (1948). This form is commonly found in the plankton and it is somewhat surprising that the ATLANTIS took so few during this cruise.

Family CHIROTEUTHIDAE Gray

Mastigoteuthis sp.

Material. 1 specimen, ML 36.0 mm, Stn. RHB 572 in 505 meters, Feb. 25, 1954.

A single specimen, very badly damaged, with all of the arms mutilated and tentacles missing, was obtained at the above station. Because of its condition the specimen is unidentifiable. The skin is lacking over almost the entire surface, the greater part of all of the arms is missing and the head is detached from the body. However, just anterior to and somewhat ventral to the eyes is a large photophore on either side. These may be double or both may have been torn in two. According to Degner (1925), only two species of this genus have photophores on or near the eyes, *M. glaucopis* and *M. hjorti*. The shape of the fins and the posterior extremity of the body do not agree with the figures of *glaucopis* nor does the animal fit the description of *hjorti* in all respects.

Liocranchia reinhardti (Steenstrup, 1856)

Leachia Reinhardti Steenstrup, 1856, p. 200.
Cranchia Reinhardti, Steenstrup, 1861, p. 76.
Loligopsis Reinhardti, Tryon, 1879, p. 165.
Perothis Reinhardti, Rochebrune, 1884, p. 25.
Liocranchia Reinhardti, Pfeffer, 1900, p. 194.

Material. 1 specimen, ML 38.5 mm, Stn. RHB 560 in 46 meters, Feb. 22, 1954.

The present specimen shows some small differences from the typical specimens of this species, but they do not warrant any change in the identification. The fins are large and slightly broader than long, with no indentation on the posterior median border. The V shaped rows of tubercles on either side of the mantle at the fusion with the funnel are large with conspicuous tubercles, roughly alternating between large tri- or quadrifid tubercles and simple ones. At the apex of the V is a large multicuspid tubercle much larger than any described or figured in the literature. Dorsally there is a row of widely spaced simple tubercles in the midline on the gladius or lanceola, but in the posterior widened section the tubercles are few and small.

In my paper on the Cuban cephalopods (Voss, 1955), I erroneously gave the specimen recorded in that paper as the first record from the Western Atlantic, but a perusal of Pfeffer's 1912 monograph yielded a record by Issel from the Caribbean.

Pyrgopsis lemur Berry, 1920

Pyrgopsis lemur Berry, 1920, p. 298.

Material. 1 specimen, ML 21.0 mm, Stn. RHB 560, in 46 meters, Feb. 22, 1954.

This specimen seems to be conspecific with Berry's species according to the published preliminary description. The mantle is long and slender, completely colorless and tapers to a long narrow point posteriorly. The ventral surface of the mantle bears two longitudinal rows of cartilaginous tubercles consisting of large, spinous tubercles with small simple ones between them. The tubercle rows appear to be less than ¼ the mantle length. The fins are slightly broader than long, transversely elliptical with smooth outlines. The gladius is visible through the mantle but was not distinct enough for descriptive purposes.

Degner (1925) has compared his material of *P. atlantica* with the present species, and has remarked upon its similarity to *P. pacifica* and *P. schnehageni*.

The present specimen is apparently only the second record of this small cranchiid.

Order OCTOPODA

Family OCTOPODIDAE Orbigny

Scaeurgus unicirrhus (Orbigny, 1840)

Octopus unicirrhus Orbigny, 1840, p. 70.
Scaeurgus unicirrhus, Tiberi, 1880, p. 12.

Material. 3 juv., ML 5.1, 6.0 and 7.5 mm, Stn. RHB 560, in 46 meters, Feb. 22, 1954.

4 juv., badly damaged, Stn. RHB 572, in 505 meters, Feb. 25, 1954.

2 juv., ML 7.5 and 7.5 mm, Stn. RHB 574, in 46 meters, Feb. 25, 1954.

Macrotritopus stage

The present specimens are all larval or juvenile forms with the typical extreme elongation of the third arms which has given this stage the generic name *Macrotritopus*. The identity of this species has long been in doubt and until recently about six separate species have been described. In 1954 Rees showed that all of the known specimens of this genus are young specimens of *Scaeurgus unicirrhus.* The present specimens present no unusual features and agree well with all of the particulars enumerated by Rees. The various species assigned to the genus *Macrotritopus* are not listed here but a full larval synonymy is given in the paper cited above.

Eledonella pygmaea Verrill, 1884

Eledonella pygmaea Verrill, 1884, p. 145.

Material. 1 ♂, ML ?, from Stn. RHB 572, in 505 meters, Feb. 25, 1954.

This small specimen is in very poor shape and is listed here only to complete the record of the specimens in the collection.

TABLE 4

DATA FOR ALL STATIONS AT WHICH CEPHALOPODS WERE TAKEN.

Station	Date	Location	Gear	Time	Depth in meters
450	VII/16/54	39°45′N, 71°08′W	IKMT	2018-2125	137
550	II/6/54	25°53′N, 79°46′W	IKMT	1513-1718	330
551	II/6/54	26°25′N, 79°45′W	IKMT	1957-2159	57
552	II/7/54	26°34′N, 79°04′W	IKMT	1545-1722	485
553	II/7/54	26°35′N, 79°28′W	IKMT	2339-0144	57
555	II/10/54	25°26′N, 76°03′W	IKMT	0110-0419	560
560	II/22/54	18°43′N, 65°10′W	IKMT	2000-0040	46
572	II/25/54	20°17′N, 65°02′W	IKMT	0242-0606	505
574	II/25/54	20°12′N, 65°19′W	IKMT	2000-2400	46
575	II/26/54	19°22′N, 65°57′W	IKMT	1047-1453	505
581	III/2/54	19°21′N, 66°20′W	IKMT	0328-0603	95
582	III/2/54	18°37′N, 66°05′W	IKMT	1939-2311	505
584	III/4/54	18°55′N, 66°10′W	IKMT	2000-0015	Surface to 415
587	III/21/54	26°22′N, 76°10′W	IKMT	2003-2111	46
589	III/22/54	26°08′N, 76°23′W	IKMT	0310-0542	370
591	III/22/54	25°32′N, 77°15′W	IKMT	2135-0103	524

LITERATURE CITED

BERRY, S. STILLMAN
1920. Preliminary diagnoses of new cephalopods from the Western Atlantic. Proc. U. S. Nat. Mus., *58*: 293-300, 1 pl.

BRUUN, ANTON FR.
1943. The biology of *Spirula spirula* (L). Dana Rep., 24: 1-42.
1955. New light on the biology of *Spirula*, a mesopelagic cephalopod. Essays in the natural sciences in honor of Captain Allan Hancock, pp. 61-72.

CHUN, CARL
1900. Aus den Tiefen des Weltmeeres. Jena.

DEGNER, EDUARD
1925. Cephalopoda. Rep. Danish oceanogr. Exped. 1908-10. *2*(C.1): 1-94.

FISCHER, H.
1896. Note préliminaire sur le *Pterygioteuthis Giardi*, céphalopode nouveau recueilli dans le cours de l' Expedition scientifique du Talisman (1883). J. Conchyl., *43*.

GRAY, J. E.
1849. Catalogue of the mollusca in the collection of the British Museum. I. Cephalopoda antepedia. London.

HOYLE, W. E.
1902. The luminous organs of *Pterygioteuthis margaritifera*, a Mediterranean cephalopod. Mem. Manchester Soc., *46*(16): 14 pp.

LEACH, W. E.
1817. Synopsis of the orders, families and genera of the class cephalopoda. Zool. Miscell., *3*: 137-141.

LINNAEUS, CAROLUS
1758. Systema naturae, Edit. 10.

ORBIGNY, A. D'
1826. Tableau methodique de la Classe des Céphalopodes. Ann. sci. nat. Paris, *7*: 96-169.
1848. *In* Ferussac and Orbigny, 1834-1848, Histoire naturelle générale et particulière des Céphalopodes acétabulifères, etc. Paris, ix, 1-361, 143 pls.

PFEFFER, GEORG
1900. Synopsis der oegopsiden Cephalopoden. Mitteil. naturhist. Mus., *17*: 145-198.
1908. Teuthologische Bemerkungen. Mitteil. naturhist. Mus., *25*: 287-295.
1912. Die Cephalopoden der Plankton Expedition. Ergebn. Plankton Exped., *2*: 1-815, Atlas.

REES, W. J.
1954. The *Macrotritopus* problem. Bull. Brit. Mus. Zool., *2*(4): 69-99, 1 pl.

ROBSON, G. C.
1948. The cephalopoda decapoda of the Arcturus oceanographic expedition, 1925. Zoologica, *33*(3): 115-132.

ROCHEBRUNE, A. T. DE
1884. Étude monographique sur la famille des Loligopsidae. Bull. soc. phil. Paris, *8*: 7-28, 2 pls.

RÜPPELL, E.
1844. Intorno ad alcuni Cefalopodi del mare di Messina. Messina.

STEENSTRUP, JOH. JAPETUS SM.
1856. Hectocotyldannelsen hos Octopodslaegterne *Argonauta* og *Tremoctopus*, oplyst ved Iagttagelse af lignende Dannelser hos Blaeksprutterne i Almindelighed. Vedensk. Selsk. Skr. 5 Raekke, *4*: 187-216.
1861. Overblick over de i Kyöbenhavns Museer opbevarede Blaeksprutter fra det aabne Hav. Overs. Dansk. Ved. Selsk. Forh., 1861: 69-86.

TIBERI, N.
1880. Cefalopodi . . . viventi nel Mediterraneo. Boll. Soc. Mal. Ital., *6*.

TRYON, G. W.
1879. Manual of Conchology. I. Cephalopoda.

VERANY, J. B.
1837. Mémoires sur deux nouvelles espèces de Céphalopodes, trouves dans l'ocean. Mem. Accad. Torino, *1*: 99-101.

VERRILL, A. E.
1880. Notice of the remarkable marine fauna occupying the outer banks off the southern coast of New England. Amer. J. Sci., *20*(119): 390-403.
1884. Second catalogue of the mollusca, etc. Trans. Conn. Acad. Arts Sci., *6*(1): 139-294.
1885. Third catalogue of the mollusca, etc. Trans. Conn. Acad. Arts Sci., *6*(2): 395-452.

VOSS, GILBERT L.
1955. The cephalopoda obtained by the Harvard-Havana Expedition off the coast of Cuba in 1938-39. Bull. Mar. Sci. Gulf & Carib., *5*(2): 81-115.
1956. A review of the cephalopods of the Gulf of Mexico. Bull. Mar. Sci. Gulf & Carib., *6*(2): 85-178.

Contribution No. 998

Reprint OIKOS 9:II 1958

REGARDING THE SOUTHERN LIMITS OF *BALANUS BALANOIDES* (L.)

BY

*H. BARNES**)

(The Marine Station, Millport, Scotland)

Balanus balanoides (L.) is perhaps the most abundant intertidal cirripede of boreo-arctic regions, being present not only on both sides of the Atlantic but also on northern Pacific shores; indeed, in the more northerly parts of its range it is the only barnacle of the open coast, where it is a constant component of the shore fauna. In its life history it appears to be a typical arctic species that extends into boreal regions where, however, in various features of its life cycle, characters adapted to existence in the Arctic are still maintained. This is particularly evident in the synchrony of the annual larval outburst and the spring diatom increase; this synchrony persists in warmer waters even though it may then result in certain later phases of the life history being ill-adjusted to the enviromnent (BARNES, 1957a, 1958; BARNES and BARNES, 1958a, 1958b). The northern limits have already been considered (BARNES, 1957b). The northern character of this species lead HUTCHINS (1947) to consider that it was typical of those animals whose southern limit was determined by a low temperature requirement for breeding – and he suggested that this limit in the case of *B. balanoides* is set where the winter sea surface temperature does not exceed 8°C. The position of this winter isotherm does indeed approximate to the southern limits of the species in eastern America and Europe, but it will be shown that it is not winter sea surface temperature *per se* that is the significant limiting factor.

The Southern Limits of the Distribution

B. balanoides is present along European coasts as far south as the Atlantic coast of France, varying in quantity to the south but reaching the Gironde Estuary and, after a break, east Galicia (BISHOP, CRISP, FISCHER-PIETTE and

---

*) Contribution No. 998 from the Woods Hole Oceanographic Institution. A Research Fellowship of the Woods Hole Oceanographic Institution and support from the Office of Naval Research (Contract No. NR. 165/142, Dr. D. L. Ray, University of Washington) allowed the observations on the United States Coast to be made. Thanks are due to both these authorities and to the Council of the Scottish Marine Biological Association for leave of absence.

Prenant, 1957). It is absent from the Scilly Isles and Weltner's (1900) records for the Azores and Portugal have not been confirmed (Southward and Crisp, 1956; Bishop, *et al.*, *loc. cit.*) The southern limit in Europe may be set at about latitude 44–46^{0}N.

On western Atlantic shores it is abundant southwards from the Canadian Arctic (Ellis, 1955; Bousfield, 1954, 1955) to the coast of New Jersey. Beyond Cape Cod, however, when it becomes associated with *Chthamalus fragilis* Darwin, suitable rocky shores become less frequent as one moves further south. Nevertheless, it is common in both Rhode Island and Connecticut when there are rocky outcrops, protected stony beaches or artificial structures capable of supporting settlement and growth. Although reported by Darwin (1854) from Delaware Bay, Pilsbry (1916) failed to find it south of Ocean City, N.J. Ferguson and Jones (1949) have recorded it as abundant in the intertidal region at Hampton Roads, Norfolk, Virginia. However, the fact that they did not record one of the commonest barnacles in this region, namely *Balanus improvisus* suggests that this species was confused with *B. balanoides.* Dr. J. D. Andrews (Virginia Fisheries Laboratory) has kindly confirmed that *B. balanoides* is absent from Chesapeake Bay and Gloucester Point, Virginia and Dr. F. W. Sieling that it is not present in the area of Chinconteague Bay, Maryland. It was sought in vain by McDougall (1943) at Beaufort, North Carolina. I have not found it further to the south. The limit on the western Atlantic seaboard may then be as far south as 38°N. latitude.

In the Pacific the species appears to be frequent on the Alaskan coast of the Bering Strait and is present in the Aleutians and as far south as Sitka (Pilsbry, 1916; Barnes, 1957b). Little collecting has been done on this coast to the south of Alaska but it is certainly absent from the coasts of southern British Columbia, Washington and Oregon (personal investigation). It has been recorded as present in Japan by Hiro (Hiro, 1935; see also Henry, 1942) and Tarasov (1937) found it in Amur Bay and in the Ochotsk Sea. Perhaps 57°N. latitude may be taken as the southern limit.

We have then the following major limits: eastern Atlantic 46°N, western Atlantic 38°N, eastern Pacific 57°N and these as well as minor variations of a regional and local character must be considered in any attempt completely to explain the distribution. We are here concerned only with broad geographical limits.

Temperature and the Behaviour of *B. balanoides*

It is generally agreed that over wide geographical ranges the distribution of species is very much under temperature control. A preliminary account of the effect of temperature at various stages of the life cycle of *B. balanoides* has already been given (Barnes, 1958).

It is perhaps first worth commenting upon those parts of the life cycle where, within wide limits, temperature alone is unlikely to *limit* the animal's distribution. It is hardly necessary to point out that its existence in the Arctic indicates that low temperatures, although they may reduce the intensity of various rate processes, are no bar either to growth or reproduction. According to SOUTHWARD (1955) the optimal range of temperature for the frequency of cirral beat lies between 0–18°C. General metabolic activities and growth under natural conditions do not appear to be grossly impaired by moderately high temperatures. They take place at temperatures up to 20°C (sea water) at Woods Hole and elsewhere on this western Atlantic coast. Here too, gonads are laid down and develop during the warm summer months. Development of the embryos, which are incubated in the mantle cavity of the adult, normally occurs at relatively low temperatures since this phase of the life history follows one in which it is believed that a low temperature is essential (see below). However, egg masses have now been developed *in vitro* outside the adult from the earliest stages to vigorously swimming (and to all appearances fully viable) Stage I nauplii at temperatures up to 15°C. Further, metabolic studies on developing embryos indicate no adverse effect of temperature up to 15–20°C on their oxygen uptake (BARNES and BARNES, 1958b). Little is known of the effect of temperature on the free swimming planktonic larval phase; here only water temperatures need be considered. It has been shown that the Stage I to Stage II transition can take place up to 18°C, the value of Q_{10} for the transition rate being about 2.0 (BARNES and BARNES, 1958c). Under natural conditions it is, however, true that larval development takes place at relatively low temperatures and this, as is the case for embryonic development, is because it succeeds a period in the life history when low temperature is essential. In nature the temperature during the planktonic phase is of the order of 0–6°C according to the region so that continued higher temperatures may possibly be deleterious to full larval development. Nevertheless temperature alone is relatively non-critical for many phases of the life history.

Even so, *B. balanoides* is no exception to the general rule that temperature sensitivity may refer particularly to some stage of the breeding cycle. It has been shown that at Woods Hole, Mass., although the gonads are developed during the warm summer months the final maturation and fertilisation does not take place until the autumn (BARNES, 1958). At this time sea temperatures were relatively high (15°C) and the important factor appeared to be the autumnal drop in air temperature; the question was then left open as to whether the form of this temperature dependence was an upper critical limit, a critical departure from a mean level or even a critical oscillation about some specific but unknown level. The available field evidence suggested that the requirement was a fall below a critical level followed by a degree of maintenance below this critical temperature and this was in agreement with earlier (unpublished) experimental results and has also been confirmed by CRISP (1957). Attention was also drawn to the possibility that any temperature effects may be mediated through neurosecretory or other hormonal activities (LUBET, 1955, 1956; BARNES and GONOR, 1958).

The Western Atlantic Seaboard

It will be convenient to deal first with this region, for here there is a long unbroken coast and the inter-play of various factors is perhaps more easily resolved. The old evidence and newer data will be considered in detail. Fig. 1 shows the mean sea surface temperatures (U.S. Department of Commerce, Special Publication No. 278) for a number of places along the east coast of America. Accepting the southern limits on this coast at about 38°N. latitude it is clear that, as pointed out by HUTCHINS (1947), the southern limit does lie close to the winter isotherm for 8°C (45°F), (see Fig. 1). Towards the southern limit the general development of the gonads in *B. balanoides* takes place, as already stressed, at relatively high temperatures – both sea and air. For example, at Woods Hole, they develop during the summer months when both sea and air temperatures are around 20°C (Figs. 1 and 2). At the end of August these ripening gonads are very prominent. The ovaries are of a thick consistency and creamy yellow in colour; at the same time the large and swollen *vesicula seminales* are very conspicuous on opening an animal. This was equally true of animals further south at Sandy Hook, N.J., where both sea and air temperatures were somewhat higher, but it must be emphasised that here the animals were only common locally in relatively sheltered places (BARNES and BARNES 1958a; see also p. 146). It was possible during the late summer and autumn of 1956 to make frequent examinations of the Woods Hole population to ascertain the date of fertilisation both here and elsewhere on the coast. These 'ripe' ovaries remained unfertilised until early October, when fertilisation began at about the same time at Sandy Hook, N.J., Woods Hole and Portland, Maine. It is suggested that the delay was due to high temperatures prevailing during the late summer and that maturation of the ovaries will not take place above a critical temperature. Fig. 3 shows the daily sea surface temperatures and the daily maximum and minimum air temperatures for this period (late summer and autumn 1956) for Sandy Hook, N. J. and Woods Hole, Mass., as well as for Charleston, S.C. to the south and Portland, Me. to the north. (New York and Sandy Hook can be considered equivalent; each station was used according to the data available.)

It may first be pointed out that when the animals began to be fertilised, on or about October 11th., the sea surface temperatures at both Sandy Hook and

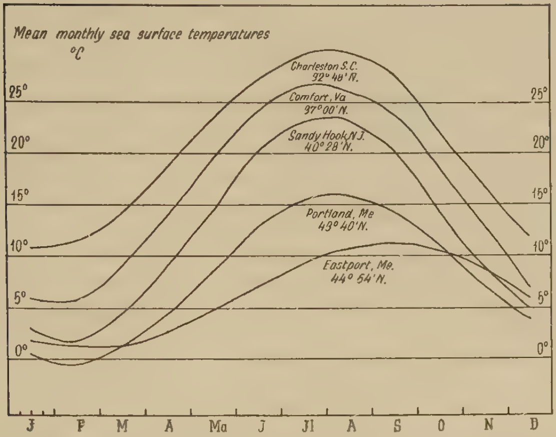

Fig. 1. Some mean monthly sea temperatures, U S. Atlantic coast. Data from U.S. Department of Commerce. Special Publication, N. 278. (New York and Sandy Hook can be taken as equivalent places; more detailed air temperature data are available for New York but sea water temperatures are more typical of the open coast).

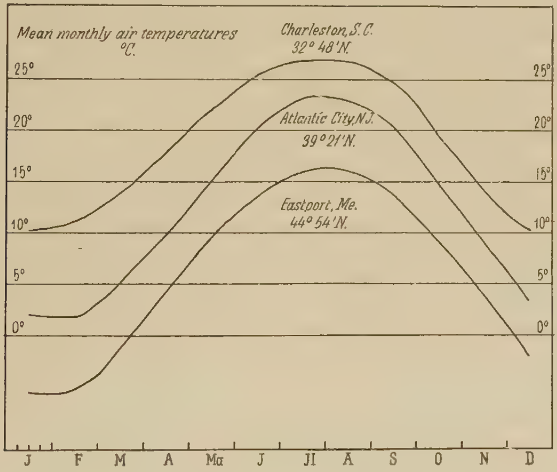

Fig. 2. Some mean monthly air temperatures, U.S. Atlantic coast. Data for 1956 obtained from Local Climatological Data, U.S. Department of Commerce, Weather Bureau have been used; this was the year when the detailed observations were made and the data were being worked up from these records for other purposes. The selection of places, therefore, again depends in part on the availability of these detailed records of hourly temperatures.

Woods Hole were about 15°C; if the above hypothesis is correct, that the limiting factor is acting on this phase of the life cycle, then clearly a sea surface temperature of 8°C is not essential since maturation and fertilisation take place at both these places long before the sea temperature has reached 8°C; this is

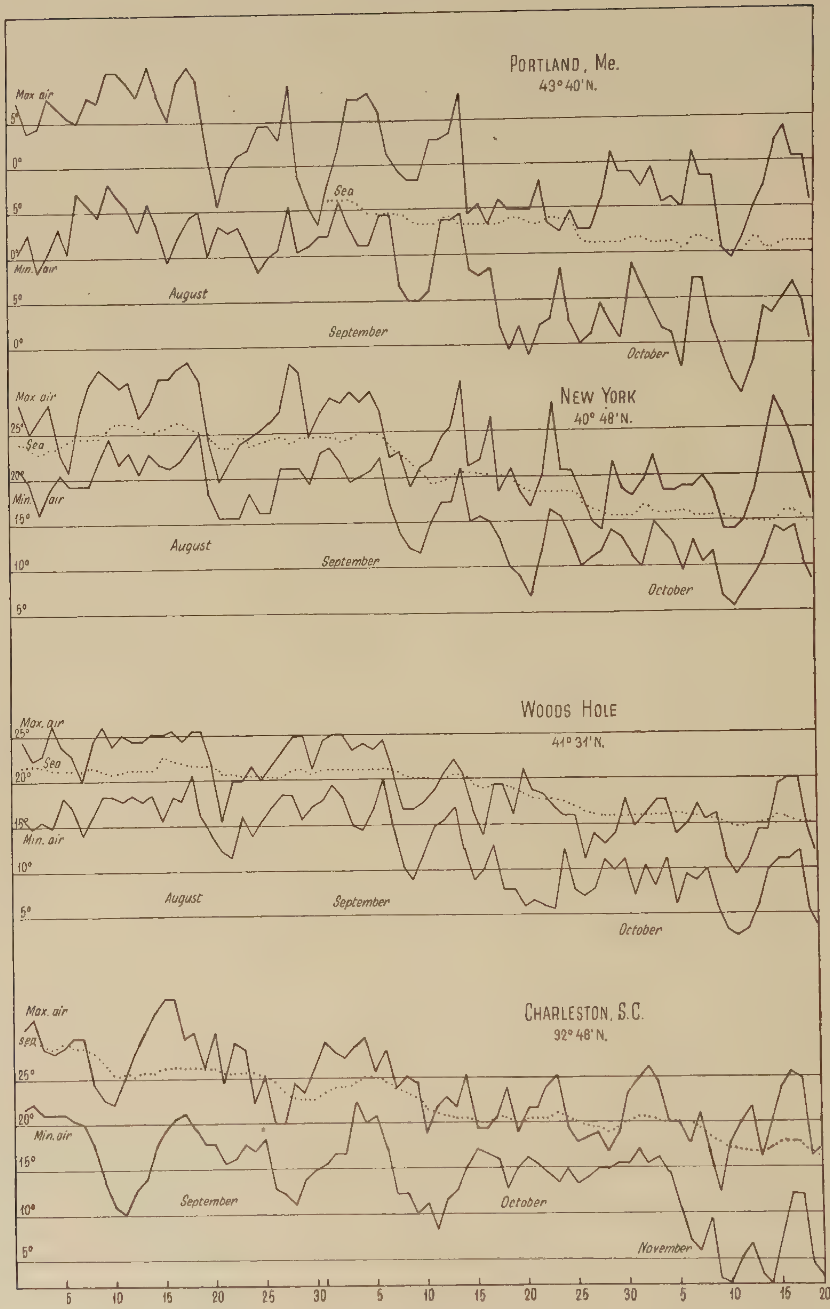

Fig. 3. Daily maximum, minimum and sea surface temperatures U.S. Atlantic Coast. Data 1956 for New York, Charleston, S.C. and Portland, Me. from Local Climatological Data and daily sea temperatures from surface water temperatures at tide stations supplied on request by U.S. Department of Commerce, Woods Hole data kindly supplied by Mr. Dean F. Bumpus.

not until November. The air temperatures are, however, much lower and it is suggested that in this intertidal species low air temperatures will allow the final ripening of the gametes. The critical character of the sea surface isotherm is, therefore, only an empirical expression of the animals limit and indicates that the required air temperature is reached at an earlier date.

As already pointed out (p. 141) the nature and mode of action of this barrier is not yet certain; again, whether this temperature block acts only on the maturation process or whether low temperature is also essential for the initiation of the behaviour pattern associated with copulation is not known. Although the normal habitat is intertidal, copulation takes place *under* water and the fact that water temperatures are still high when the suggested block to maturation is removed by low air temperatures suggests that only the maturation of the gonads is primarily involved; initiation of copulation may, in turn depend upon maturation having taken place. The minimum air temperatures at Sandy Hook indicate that the barrier is in the neighbourhood of 10°C and that repeated falls with some maintenance at this temperature is adequate; experiments already referred to (p. 141) whereby maturation was induced were conducted at lower temperatures (4–6°C) but a value of the order of 10°C is in agreement with CRISP's results (1957). The Woods Hole data for 1956 suggest a period of perhaps 20 days or so is required for the process. In 1956 it was possible to determine the approximate date at which the animals were initially fertilised over several hundred miles of this coast by repeated visits and estimations based on the first few egg divisions; the effect of temperature on the latter has to be assumed but the evidence suggests that the beginning of fertilisation was roughly synchronous over a wide latitudinal range – from New Jersey to Maine – and that it followed a sudden excessive drop in air temperature about October 11th. Other work on the maturation and emission of gametes (LOOSANOFF and DAVIES, 1950, 1952) indicates that a sudden temperature change (in their case raising the temperature above the so called 'conditioning level' may act as a shock reaction stimulating emission of gametes following maturation over a longer period at the appropriate temperature level.

In view of the fact that the 8°C winter isotherm is only empirically indicative of the limit of the species rather than directly causal, it is necessary to examine the details of the air and sea temperatures farther south. Charleston, S.C., for which there is adequate data may be considered for it is several hundred miles south of where the species is found. The mean sea surface temperature does not fall to 8°C during the winter (Fig. 1) and on HUTCHINS' (1947) empirical basis *B. balanoides* would not be expected to occur. However, an inspection of the air temperatures reveals a situation in November – one month later than at Sandy Hook, N.J. – in which, on the hypothesis advanced above, breeding should be possible. The daily curves (Fig. 3) indicate adequately low temperature conditions in this month for maturation of the gametes (compare New York). On this basis then and in the absence of other restricting factors, *B. balanoides* would not be barred from this region. The fact that it does not reach this region requires, therefore, an explanation in which low temperature may not play a part.

It is suggested that two further factors must be considered, namely, high summer temperatures and competition. On this coast (Barnes and Barnes, 1958a), as elsewhere (Southward and Crisp, 1954), when the southern limit is approached the animal tends to be restricted to the more sheltered places – under various artificial structures as well as under rocks; this was particularly noticeable even at Sandy Hook, N.J. This in itself would suggest that conditions for growth and survival either of spat or adults, as distinct from reproduction, are involved and that a 'retreat' to, or more strictly, since the animal is sedentary, a survival in, micro-habitats where conditions more closely approach the normal for the species, is taking place. That this phenomenon occurs even in places where spring temperatures are moderate suggests that high summer temperatures and their effect upon adult survival rather than spat is involved.

There are more indications of the adverse effects of high summer temperature from detailed observations in the Woods Hole district. Here, although both air and sea temperatures are low during the winter months, the extremes are much greater than further north; during the summer, air temperatures with a mean of the order of 20°C frequently reach the 25°C level (see, for example, Fig. 2) in June, July and even August.

It was noted in the late summer of 1956 that on the larger boulders of the upper shore there were vast numbers of empty shells of *B. balanoides*. On the lower shore predation by *Thais lapillus* was evident but not excessive. However, the mortality that was so striking, increased higher up the shore. Further, all the shells were very uniform in size, some 5 mm basal diameter. Now this is the size reached at such places on the shore by June–July following spring settlement and this is the time when air temperatures rose from 17.2° in May to 20° in June and 25°C in July, the maxima in the second two of these months being 26° and 27°C. Measurement had shown that the temperature at the rock surface may be 5–10° higher than the air temperature and there is little doubt that this excessive air temperature was fatal to those relatively young individuals of the current year's spat. Further, the mortality was far greater on the top and south facing parts of the boulders than on the north facing or more protected parts (Table 1).

As temperatures, both sea and air rise, severe competition from *Balanus eburneus* takes place. Although this barnacle, a warm-temperate species, reaches to the north of Cape Cod (Dexter, 1947) and in some places is common at Woods Hole (Sumner, Osburn and Cole, 1911) it is essentially a warm

Table 1.
Average mortality of young *B. balanoides* on boulders, Woods Hole.

Position	% age dead
Top of boulders	95
South side of boulders	93
Seaward side of boulders	53
North side of boulders	50

water species, being abundant from North Carolina to the Caribbean. Even at Woods Hole where it is largely in the lower intertidal or sub-littoral, it may be completely decimated in the intertidal during moderately severe winters (personal information, Mr. S. GRAY). At Beaufort, N.C., well north of Charleston, it is the most abundant barnacle in the intertidal (MCDOUGALL, 1943); it breeds continously from March to December with a peak period in July and reaches sexual maturity in 60 days; the productivity, therefore, compared with *B. balanoides* with its single annual brood, is very high. Further, unlike *Chthamalus fragilis*, *Balanus eburneus* is a large barnacle with a high growth rate occupying, further south, much of the nîche that characterises *B. balanoides* (although it is much more abundant than the latter sub-littorally). In addition, as one proceeds further south, *B. amphitrite*, another warm water species becomes common in the higher parts of the intertidal zone; this too has numerous broods in warmer waters, is large and has a high growth rate. To the south conditions become increasingly adverse for *B. balanoides* and increasingly favourable for both *B. eburneus* and *B. amphitrite*; this competition from these species together with the high summer air temperatures is considered to effectively bar penetration of *B. balanoides* further south into regions where, on the basis of the winter temperatures alone, breeding should be possible.

A further point must receive comment; as one proceeds further south into warm temperate regions, the annual temperature minimum is reached later in the year (and eventually in the early months) and a sufficiently low temperature to remove the barrier to maturation of the gonads may be found very much later than in the temperate zones. The eventual attainment later in the season of a sufficiently low temperature for maturation of the gonads need not necessarily give adequate conditions for breeding. First, ripe gonads developed early in the warmer summer may not be able to remain viable indefinitely while 'awaiting' low temperatures for maturation. Secondly, if the wait were prolonged and the subsequent seasonal rise in temperature following the minimum should take place fairly sharply, it is conceivable that water temperatures would become too high for survival of the larvae (see p. 145) after the incubation period in the adult mantle cavity.

The Pacific Coast of America

We may now consider conditions on the Pacific coast. There has been relatively little intensive shore investigation along the Alaskan coast, but as already pointed out (p. 140) the southern limit of *B. balanoides* appears to lie roughly at the latitude of Sitka. Sea and air temperatures for this region are shown in Figs. 4 and 5.

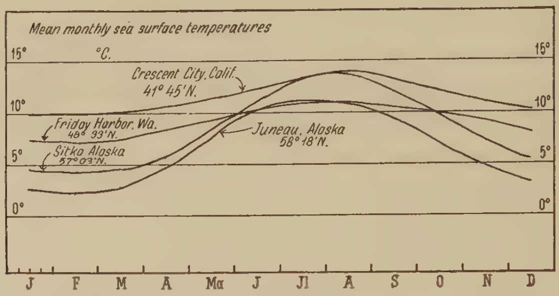

Fig. 4. Some mean monthly sea surface temperatures, U.S. Pacific Coast. Data from U.S. Department of Commerce, Special Publication 280.

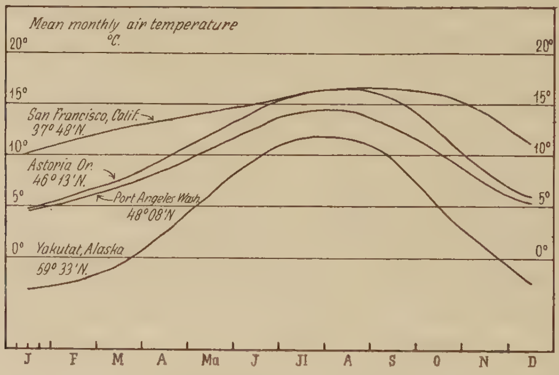

Fig. 5. Some mean monthly air temperatures, U.S. Pacific Coast. Data for 1956 obtained from Local Climatological Data, U.S. Department of Commerce, Weather Bureau.

On comparing these Figures with those given previously it is quite evident that on the basis of the foregoing discussion concerning the effect of temperature on the limit of *B. balanoides* on the east American coast, temperature conditions on this west coast, both as regards breeding and growth, are suitable and indeed well adapted for the species much further to the south (possibly 1000 miles) than where it is found. (Compare also, for example the temperature regime at Millport, Scotland, and Friday Harbor, Washington). However, south of Sitka two common intertidal barnacles are found in the normal nîche of *B. balanoides*, namely *B. glandula* and *B. cariosus*. Now both these species closely resemble *B. balanoides* in their life histories and in particular in their breeding behaviour; the major spat fall takes place in the spring although this becomes earlier further south (Barnes and Barnes, 1956) and although over part of its range *B. glandula* (as *B. crenatus* at Millport, Scotland) may produce a second smaller brood. Both *B. glandula* and *B. cariosus* are the typical intertidal barnacles of the north Pacific coast, the former extending as far south as Ensenada in Baja California and the latter to about the latitude of southern Oregon (it is common, for example at Coos Bay); further south *B. cariosus* gives way to *Tetraclita squamosa* in the lower intertidal. It is suggested that *Balanus glandula* in particular, and on the lower shore *B. cariosus*, have prevented further southward spread of *B. balanoides* whose entrance to the Pacific was made through the Bering Strait when these typical Pacific species were already well established.

It is not intended to discuss the evidence for a circumpolar distribution with extensions into the north Pacific but the following facts appear to be relevant. According to Dall (1920) there is much evidence of a temperate molluscan fauna in the Pleiocene of Nome and the arctic coast of North America. In addition to two present day sub-littoral cirripedes (*B. rostratus* and *B. evermanni*) he records *B. balanoides* from Nome on the Seward Peninsula at the eastern side of the Bering Strait and at Camden Bay on the north coast of Alaska east of Point Barrow. This would indicate a continuous distribution in the Pleiocene (possibly only the upper Pleiocene) when the climate was relatively mild. On the other hand Broch (1924) relates the current distribution to the Post-glacial warm period.

Again, Feyling-Hanssen (1953) has pointed out that records of *B. balanoides* from the Arctic Pleistocene are comparatively rare. He stresses, however, that this lack of records may not indicate its real status in the period since, lacking a calcareous base, it remains only in form of separate compartments and fragments that are usually recorded as *Balanus* sp. He comes to the conclusion that "*B. balanoides* presumably occurs in the Arctic Pleistocene deposits of a great many more localities than those stated. Probably the species may be found in any deposit from the Post-glacial warm period within the region [Arctic] containing littoral forms. The finds of the species in Greenland and Spitzbergen were made in deposits dating from that Period".

Clearly in the colder periods of the Pleistocene, with abundant glaciation of the coastal regions of the north Pacific there must have been retreat southwards of the indigenous fauna. Amelioration of conditions, at whatever period is considered to be most significant would still leave the indigenous species in possession and later bar the soutward spread of *B. balanoides*. Nothing is known of the factors limiting the northward extension of the endemic Pacific species.

European Shores

We may now consider European shores. Millport, Scotland is a typical situation for northern Britain and there is much available data. Here *B. balanoides* is the dominant barnacle on the shore and *Chthamalus stellatus*, although quite common is, in general, restricted by competition to the upper levels, where it is able to exist by virtue of its greater ability to withstand dessication.

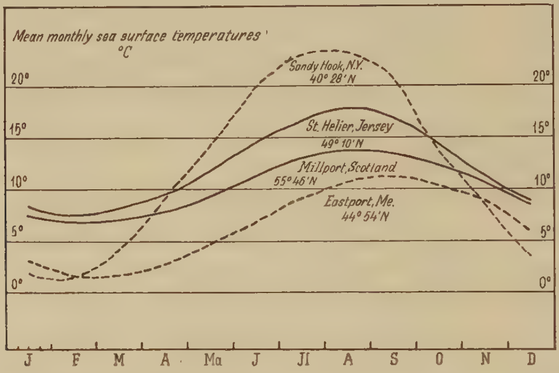

Fig. 6. Some mean monthly sea surface temperatures, Europe: various sources.

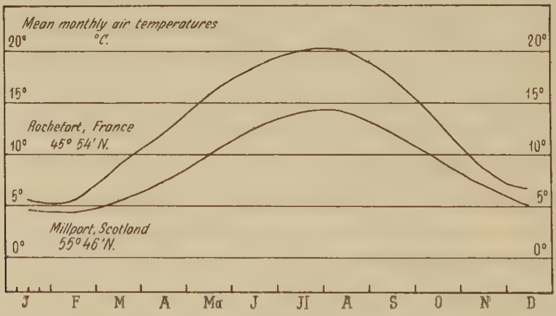

Fig. 7. Some mean monthly air temperatures, Europe: various sources.

The sea and air temperatures are shown in Figs. 6 and 7 (see Barnes, 1955, for further data). It is first to be noted that, compared with say Woods Hole, fertilisation is delayed by about one month; it takes place regularly in early November.

The interpretation to be placed on this later date is not, however, that the increased delay is due to the necessity for the temperature to fall to the appropriate low level (Fig. 8 for 1956 data). Minimum air temperatures are falling throughout the autumn and even in early October their minima are oscillating near 10°C. A period, however, between 5–10°C usually precedes fertilisation.

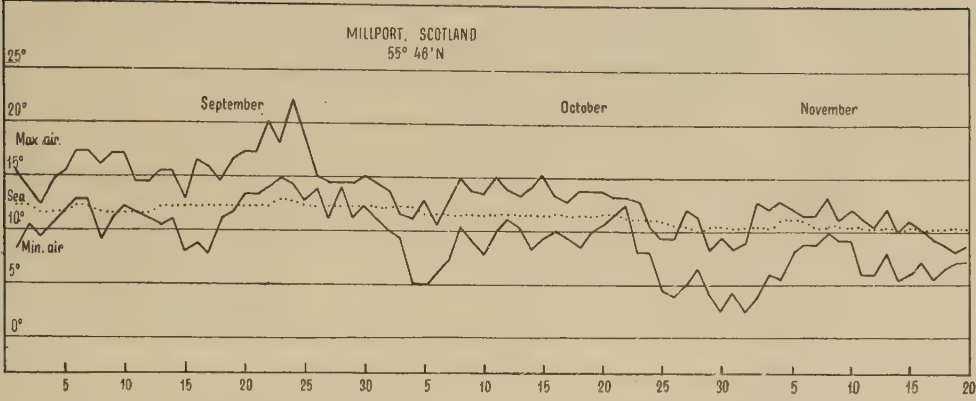

Fig. 8. Daily maximum and minimum air, and sea temperatures Millport, Scotland, 1956.

It is suggested that here – as indeed in regions further north where the temperature may even never exceed that required for maturation – any delay is a consequence of the slower ripening of the ovary; gonad development has been taking place at much lower summer temperatures. It may be noted, that gonad development is also closely related to food supply so that even at the lower temperatures of the Arctic the abundant food supply over a restricted period may result in a faster rate of development than at certain seasons in the warmer boreal regions. During certain parts of the year the suppply of food rather than temperature has been shown to control the length of the brood period in *Elminius modestus* (CRISP and DAVIES, 1955).

The general conditions in Europe may now be examined, particularly in ralation to the hypotheses already put forward. First, it is instructive to consider the general distribution of air and sea temperatures over the European coasts since the evidence already advanced suggests that temperature is of primary importance. It is first to be noted that whereas the winter isotherms on the western Atlantic seaboard run almost east and west so that temperatures decrease progressively on passing from south to north, this is not the case in Europe (Fig. 9). With the advent of autumn, the isotherms (roughly east and west during the summer) swing southwards as they approach the European coasts so that the mid-winter isotherms run almost due north and south over the west coast of Britain and the Atlantic coast of France. This is made abundantly clear on examination of the temperature data for say Millport, Scotland and Rochefort, France (the last at about the southern limit of *Balanus balanoides*, see p. 140). The air temperatures for these two places for the autumn and winter months are set out in more detail in Table 2.

Clearly over these coast lines, a distance of almost 1000 miles, the mean

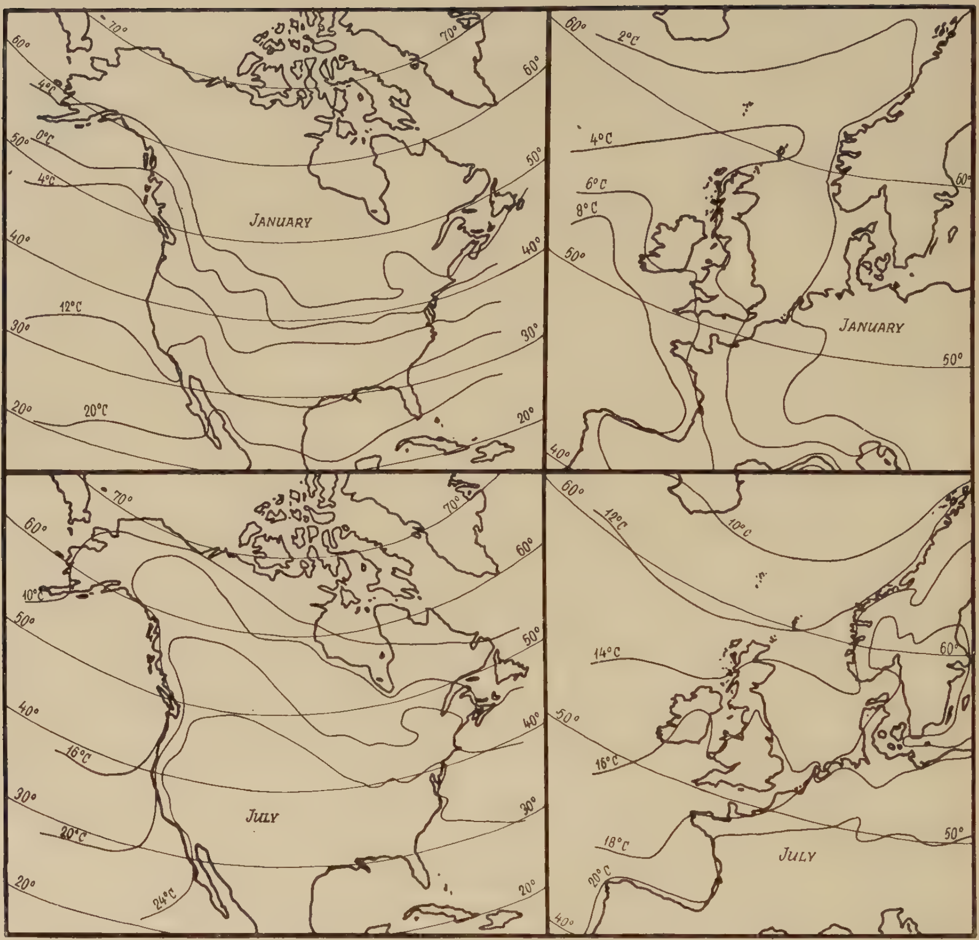
70°
70°
60°
60°
4°C
50°
0°C
4°C
50°
JANUARY
40°
40°
12°C
30°
30°
20°
20°C
20°
60°
2°C
4°C
6°C
8°C
50°
60°
JANUARY
50°
40°
70°
70°
60°
60°
10°C
50°
50°
40°
40°
16°C
30°
30°
20°C
JULY
20°
24°C
20°
60°
12°C
10°C
14°C
60°
50°
16°C
18°C
50°
JULY
20°C
40°

Fig. 9. January and July isotherms, Europe and America.

temperatures in November and December differ by only 1–3°C. Further, by reference to the data for, say New York, (see Figs. 2 and 3) it is clear that the temperature conditions as far south as Rochefort are such as to allow maturation of the gonads of *B. balanoides* in November; indeed the Gironde Estuary is near the southern latitudinal limit of the species and this agrees, therefore, with the suggestion that such a bar is acting as the ultimate geographical limit to the species.

Although the winter air isotherms run almost north and south the midsummer isotherms in Europe resemble those over the American coast. The values for Rochefort may be compared with those for Atlantic City, N.J., (Table 3).

Table 2.
Maximum, minimum and mean air temperatures (°C).
(Data from various sources).

Place	Month							
	October		November		December		January	
	Max.	Min.	Max.	Min.	Max.	Min.	Max.	Min.
Millport (Scotland) ...	11.7	6.7	8.8	2.6	7.2	2.9	6.6	2.1
Mean...	9.2		5.7		5.1		4.4	
Rochefort (France) ...	17.2	9.4	11.7	5.0	9.4	4.4	8.3	2.8
Mean...	13.3		8.4		6.9		5.6	

Table 3.
Maximum, minimum and mean air temperatures (°C).
(Data from various sources).

Place	Month					
	June		July		August	
	Max.	Min.	Max.	Min.	Max.	Min.
Atlantic City (U.S.A.)...........	23.9	16.9	26.2	20.0	26.0	19.7
Mean...	20.4		23.1		22.9	
Rochefort (France)	25.0	15.0	25.0	15.0	22.2	12.8
Mean...	20.0		20.0		17.5	

We may therefore consider that winter air temperatures together with the increased summer temperatures limit *B. balanoides* on the European coasts. In contrast with the east American coast these two factors appear to be almost self sufficient in that competition from a warm water species need not be invoked to explain the southern limit; locally this and topographical effects – such as long stretches of sandy beach – could be of some importance.

One further feature of the distribution may be stressed. The species is accompanied by *Chthamalus stellatus* over the southern parts of its range in Europa and by *C. fragilis* on American shores to the south of Cape Cod. The relation between *Balanus balanoides* and *Chthamalus stellatus* had recently received considerable attention in those regions where both are reaching their limits (SOUTHWARD and CRISP, 1954, 1956; BARNES, 1956). It is not proposed to discuss this competition but only to stress that the wide zone of co-existence on European shores of these two species, with their contrasting temperature requirements for breeding, is related to the form of the summer and winter isotherms. The north and south course of these isotherms along the European coasts in winter would seem to allow considerable fluidity in the eco-system, particularly as it affects competition between the two species. The north and south demarcation becomes less clearly defined and annual variations or local changes in temperature and other significant variables become important in the regional and local status of the two populations which may react more immediately to any such changes; the dynamic character of the eco-system is accentuated.

Nothing has so far been said regarding sub-speciation of *Balanus balanoides.* DARWIN (1854) stressed that there was considerable variation and a number of sub-species have been described by PILSBRY (1916). There is little doubt that many of the variations in external form are the result of the environment on an animal capable of adjusting its growth form to micro-variations in the habitat – in particularly to crowding, (TRUSHEIM, 1931; MOORE, 1934; BARNES and POWELL, 1950). The Variety (a), of Darwin, in which the parietes are permeated by tubes was rejected as a sub-species by that author because its most distinctive character, namely, the number of spines on the posterior cirri, was variable and all the characters by which the variety was separated were variable in typical *B. balanoides.* Further Darwin found specimens from Europe resembling in part this variety which was taken from the east American coast. Further evidence suggesting that there has been no significant sub-speciation on the Atlantic Coast of America has been summarised by BARNES and BARNES (1958a). The likelihood of sub-speciation is greatest on the Pacific coast following isolation from what has been presumed to be an Atlantic stock. There is, in any case, no indication that such morphological variation as exists is accompanied by any physiological differences. Again although details of the mechanism by which temperature effects the distribution must await further experimentation, the fact that a reasonable hypothesis can be erected to explain the whole geographical distribution does in itself indicate that any sub-speciation is of relatively little importance over wide ranges.

Summary

1. The available evidence concerning the southern limits of *Balanus balanoides* as indicated by the literature and recent investigations is presented. These limits approximate to 46°N in the eastern Atlantic, 38°N in the western Atlantic and 57°N on eastern Pacific shores.

2. A sea temperature of 8°C does not *per se* limit the animal but the winter isotherm of 8°C indicates conditions that approximate to the limits of the species.

3. The effect of temperature on various phases of the life cycle are discussed in some detail; many processes proceed normally (although their rate may be affected) over wide ranges of temperature.

4. In the more southerly parts of its range warm summer temperatures lead

to well developed gonads in late summer, but fertilisation is delayed until autumn. The interpretation is an upper limit for the maturation process. Detailed results for U.S. coast are presented.

5. A temperature bar may take a number of forms; the evidence so far available indicates that the temparature must fall below an upper critical limit (near 10°C and remain below this level for some time.
6. The limitation southwards on the eastern American coast, is not entirely due to this temperature bar to breeding. Deleterious effects of high summer temperatures on the adults and severe competition from the warm temperate species, *B. eburneus* and *B. amphitrite*, also play an important part.
7. A sudden temperature shock may synchronize breeding.
8. Temperature conditions do not determine the southern boundary on the Pacific coast of this species; it is suggested that the endemic species, *B. glandula* and *B. cariosus* have limited the southward spread as the penetration via the Bering Strait progressed.
9. Winter air temperatures appear to set a limit in Europe although high summer temperatures will also play a part. There is no need to invoke competition from warm water species to explain the general distribution although doubtless locally they may be of some importance.
10. Attention is drawn to the contrast between the form of the winter isotherms over the European and American coasts. The fact that they run roughly north and south on European coasts is considered to lead to considerable fluidity, where annual changes and local conditions become important.

References

Barnes, H., 1955: Climatological and salinity data for Millport, Scotland. Glasgow Naturalist, *17*, 193–204.

— 1956: The growth rate of *Chthamalus stellatus* (Poli). J. Mar. biol. Ass. U.K., *35*, 355–361.

— 1957a: Processes of restoration and synchronization in marine ecology; the spring diatom increase and the "spawning" of the common barnacle, *Balanus balanoides* (L.). Ann. Biol. *33*, 67–85.

— 1957b: The northern limits of *Balanus balanoides* (L.). Oikos, *8*, 1–14.

— 1958: Temperature and the life-cycle of *Balanus balanoides* (L.). Friday Harbour Symposium on Limnoria and Barnacles. Univ. of Washington (in press).

Barnes, H. and M. Barnes, 1956: The general biology of *Balanus glandula*, Darwin. Pacific Science, *10*, 415–422.

— 1958a: A comparison of the annual growth patterns of *Balanus balanoides* (L.) with particular reference to the effect of food and temperature. Oikos (in press).

— 1958b: The respiration and development of cirripede egg lamellae. In preparation.

— 1958c: The rate of development of *Balanus balanoides* (L.) larvae. Oceanogr. and Limnology *3*, 19–32.

Barnes, H. and J. J. Gonor, 1958: Neurosecretory cells in some cirripedes. Nature, Lond., *181*, 194.

BARNES, H. and H. T. POWELL, 1950: The development, general morphology and subsequent elimination of barnacle populations, *Balanus crenatus* and *B. balanoides*, after a heavy settlement. J. Anim. Ecol. *19*, 175–179.

BISHOP, M. W. H., D. J. CRISP, E. FISCHER-PIETTE and M. PRENANT, 1957: Sur l'écologie des Cirripèdes de la côte atlantique française. Bull., L'Inst. Océanogr. Monaco, No. 1099

BOUSFIELD, E. L., 1954: The distribution and spawning seasons of barnacles on the Atlantic coast of Canada. Ann. Rep. National Museum of Canada. Bull. 132, (1952–53), 112–154.

— 1955: The cirripede crustacea of the Hudson Strait region, Canadian Eastern Arctic. J. Fish. Res. Bd. Canada, *12*, 762–767.

BROCH, H. J., 1924: Cirripedia Thoracica von Norwegen und dem norwegischen Nordmeere. Vidensk. selsk. Skrifter 1. Mat.-Naturv. Klasse No 17.

CRISP, D. J., 1957: Effect of low temperature on the breeding of marine animals. Nature, Lond., *179*, 1138–1139.

CRISP, D. J. and P. A. DAVIES, 1955: Observations *in vivo* on the breeding of *Elminius modestus* grown on glass slides. J. Mar. biol. Ass. U.K., *34*, 357–380.

DALL, W. H., 1920: Pleiocene and Pleistocene fossils from the Arctic coast of Alaska and the auriferous beaches of Nome, Norton Sound, Alaska. U.S. Geol. Survey, Professional Paper, 125-C, 23–37.

DARWIN, C. R., 1854: A monograph of the sub-class Cirripedia. Vol. II. The Balanidae. Ray. Soc. Lond., 684 pp.

DEXTER, R. W., 1947: The marine communities of a tidal inlet at Cape Ann, Mass. A study in bio-ecology. Ecol. Monogr., *17*, 261–294.

ELLIS, D. V., 1955: Some observations on the shore fauna of Baffin Island. Arctic, *8*, 224–236.

FERGUSON, F. F. and E. R. JONES (Jr.), 1949: A survey of the shore line fauna of the Norfolk Peninsula. Amer. Midl. Nat., *41*, 436–446.

FEYLING-HANSSEN, R. W., 1953: The barnacle *Balanus balanoides* (L.) in Spitzbergen. Norsk Polarinst. Skrifter. No. 98, 64 pp.

HENRY, D. P., 1942: Studies on the Cirripedia of the Pacific coast of North America. Univ. Wash. Publ. Oceanogr., *4*, 95–134.

HIRO, F., 1935: The fauna of Akkeshi Bay. II. Cirripedia. J. Fac. Sci. Hokkaido Univ. Ser. VI, Zoology, *4*, 213–229.

HUTCHINS, L. W., 1947: The bases for temperature zonation in geographical distribution. Ecol. Monogr., *17*, 325–335.

LOOSANOFF, V. L. and H. C. DAVIES, 1950: Conditioning *V. mercenaria* for spawning in winter and breeding its larvae in the laboratory. Biol. Bull. *98*, 60–65.

— 1952: Temperature requirements for maturation of gonads of northern oyster. Biol. Bull., *103*, 80–96.

LUBET, P., 1955: Cycle neurosécrétoire chez *Chlamys varia* L. et *Mytilus edulis* L. (Mollusques lamellibranches). Compt. Rend., *241*, 119–121.

— 1956: Effects de l'ablation des centre nerveux sur l'émission des gamètes chez *Mytilus edulis* L. et *Chlamys varia* L. (Mollusques lamellibranches). Ann. Sc. Nat. Zool. IIe Series, 175–183.

McDOUGALL, K. D., 1943: Sessile marine invertebrates at Beaufort, N.C. Ecol. Monogr., *13*, 321–374.

MOORE, H. B., 1934: The biology of *Balanus balanoides*. I. Growth rate and its relation to size, season and tidal level. J. Mar. biol. Ass. U.K. *19*, 851–866.

PILSBRY, H. A., 1916: The sessile barnacles (Cirripedia) contained in the collections of the U.S. National Museum including a monograph of the American species. U.S. Natl. Mus. Bull. *93*, 366 pp.

SOUTHWARD, A. J., 1955: On the behaviour of barnacles. I. The relation of cirral beat and other activities of temperature. J. Mar. biol. Ass. U.K., *34*, 403–422.

SOUTHWARD, A. J. and D. J. CRISP, 1954: Recent changes in the distribution of the intertidal barnacles *Chthamalus stellatus* and *Balanus balanoides* in the British Isles. J. Anim. Ecol. *23*, 163–177.

SOUTHWARD, A. J. and D. J. CRISP, 1956: Fluctuations in distribution and abundance of intertidal barnacles. J. Mar. biol. Ass. U.K., *35*, 211–229.

SUMNER, F. B., R. C. OSBURN and L. I. COLE, 1911: A biological survey of the waters of Woods Hole and vicinity. Part 1. Section I. Physical and zoological. Bull. U.S. Bur. Fish., *31*, 1–411.

TARASOV, N., 1937: Contribution to the fauna of Cirripedia Thoracica of the Arctic Ocean. III. Trans. Arctic. Inst. Leningrad, *2*, 59–62.

TRUSHEIM, F., 1931: Spülsäme am Meeresstrand. Nat. and Mus. *61*, 235–241.

U.S. DEPARTMENT OF COMMERCE, 1955: Surface water temperatures at tide stations. Pacific coast North and South America and Pacific Ocean Islands. Special Publication No. 280.

— 1955: Surface water temperatures at tide stations. Atlantic Coast North and South America. Special Publication No. 278.

— 1956: Local climatological Data Sheets. 1956.

WELTNER, W., 1900: Die Cirripeden der Arktis. Fauna Arctica, *1*, 289–312.

Contribution No. 1001

The Luminescence Camera

L. R. BRESLAU and H. E. EDGERTON

Woods Hole Oceanographic Institution, Woods Hole, Massachusetts and
Massachusetts Institute of Technology, Cambridge, Massachusetts

Reprinted from
JOURNAL OF THE BIOLOGICAL PHOTOGRAPHIC ASSOCIATION
May, 1958 — Copyright, 1958

Journal of the Biological Photographic Association Vol. 26, No. 2 May, 1958

The Luminescence Camera

L. R. BRESLAU and H. E. EDGERTON
Woods Hole Oceanographic Institution, Woods Hole Massachusetts and
Massachusetts Institute of Technology, Cambridge, Massachusetts

Abstract

AN instrument was designed and constructed for the purpose of causing the flashes of luminescence in the sea to trigger an underwater camera device and thus take photographs of the animals producing the flashes. A photomultiplier detector is utilized which, upon stimulation by the flash of a luminescent animal, triggers an electronic flash and camera combination. Simultaneously, a sonar pulse is emitted from an attached transducer, which announces that a picture has been taken and relays information to the surface concerning the depth of the instrument. After this the camera automatically advances its film to complete the cycle. The instrument described is entirely self-contained and requires only mechanical support from the cable to the surface. It has been designed to operate at any depth down to 6000 meters. The length of film used during each lowering is sufficient for 800 frames. The instrument was operated successfully during the summer of 1957 aboard the Research Vessel Crawford and the Coast Guard Cutter Yamacraw.

General Design

This instrument was especially designed to investigate the light flashes previously observed by Clarke and Wertheim (1956), Clarke and Backus (1956), and Clarke and Hubbard (1958), while using the Bathyphotometer. Information from their work showed that the luminescence detector should be triggered by flashes with an irradiance of 10^{-5} u watts /cm^2 or greater in order to obtain a satisfactory number of photographs (Figure 1). Due to the high sensitivity demanded, a photomultiplier trigger was required. This was designed so as not to be injured by direct sunlight or by the light flash emitted from the electronic lamp. The circuits are so designed that only pulses of light are accepted. Provision is made for manual pre-selection of the threshold level of the photomultiplier trigger.

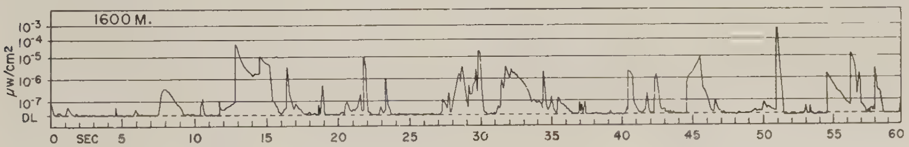

FIG. 1

The instrument is entirely self-con-

---

*Work supported by funds from the National Science Foundation Grant No. 3838 and Office of Naval Research, Nonr—1720(00) (NR-083-116) and the National Geographic Society contribution No. 1001 of the Woods Hole Oceanographic Institution.

tained, thereby eliminating any dependence upon electrical conductors in the cable. The circuitry is such that the device can operate continuously for at least ten hours before the batteries need recharging. Mercury switches are employed so that the instrument can be loaded and stored in a prepared state.

The camera and film advancing circuitry are contained in one cylindrical housing, and the electronic flash and photomultiplier trigger are in another (Figure 2). These fit into a rigid cradle which fixes the overall geometry of the instrument. The cradle is so designed that each cylindrical house can be easily detached for facility in servicing and transportation.

Although the overall instrument is electrically self-contained, signals must be exchanged among its various units. Electrical pulses leave the flash unit, pass through the sonar, and then enter the camera unit. By utilizing the instrument ground, only one electrical lead-in is needed on each cylindrical housing.

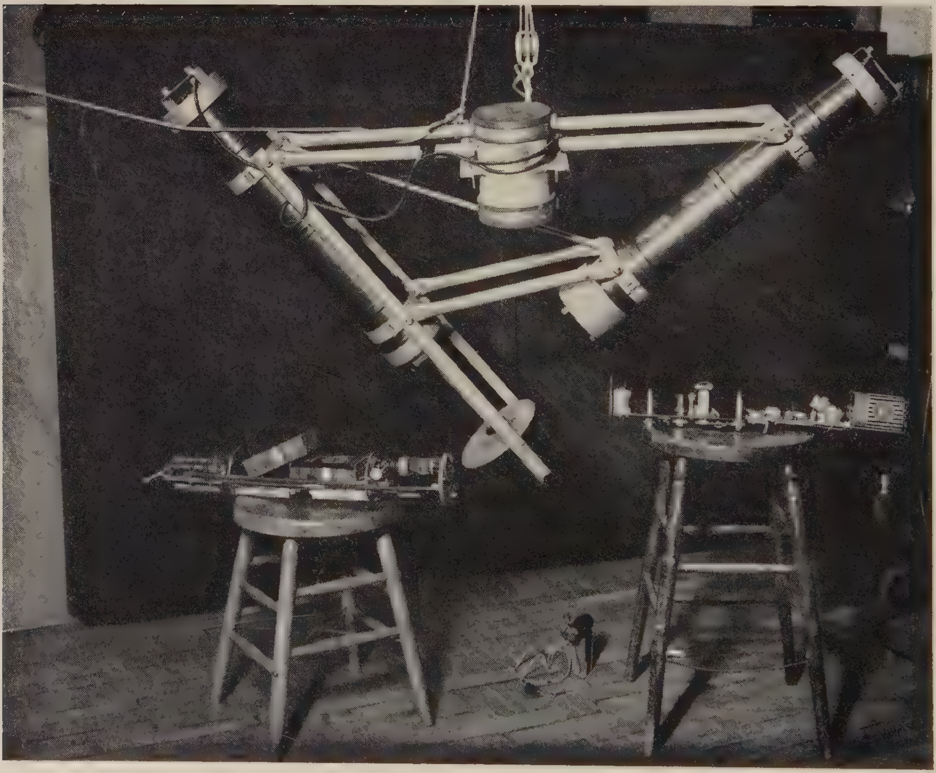

Figure 2

The entire volume of water observed by the photomultiplier lies in the field of view of the camera and is illuminated by the electronic flash. Since many luminescent animals have translucent bodies, side lighting was deemed to be most desirable. Naturally a compromise must be made concerning the field included and the magnification of the object photographed. Since most of the luminescent animals the photographic record of which was desired were expected to be less than 3 inches in length, an observed volume of about 1/10 of a cubic foot was decided upon. A second position of the tubes in the cradle allowed the camera to photograph only half of the volume observed by the photomultiplier, but produced twice the magnification. Each time a photograph was taken both an upward and downward ray are transmitted by the sonar. By recording the difference in arrival times of these rays at the surface, the depth of the instrument can be calculated. Since it is impractical to keep exact tally of the depth corresponding to each frame for the entire length of film, a small watch in a water-tight case was attached to the device in such a manner as to appear in each photograph. By the coordination of records on a time basis, the depth, location, and other circumstances for each picture are determined.

Mechanical Design

The cylindrical housings for the camera and flash units as well as the end plates are made of centrifugally cast 17-4 PH stainless steel. Heat treatment after machining brought the steel to a chardness of Rockwell 41. The cylinder has an inside diameter of 4.050 inches with a ⅜ inch wall thickness and a theoretical strength of 24,000 psi. The thinnest end plate is 1 inch thick with a theoretical strength of 40,000 psi. Each of the rear end plates on both units has a single electrical lead brought through it. A gland type fitting (Conax Mfg. Co., 4514 Main Street, Buffalo, New York) is utilized in conjunction with a plastic insulated solid wire. The use of a stranded wire in the gland may result in a leak through the space between the strands if the rubber wire does not completely seal. Single prong water-tight molded plugs (Joy Co., Henry W. Oliver Building, Pittsburgh 22, Pa.) are attached to the solid wire on the outside of the end plate.

The face plate of the camera unit is 1.5 inches thick to form a rigid seat for the glass, and is provided with a 1 inch hole in the center through which the camera received light. Two concentric "O" rings form a water seal with the glass plate window. The plate glass window is 1 inch thick, and has the same outside diameter as the end plate. The surface of the glass is polished to increase its strength. The end plate of the flash unit is 1 inch thick and is provided with ½ inch holes spaced 2¼ inches apart. One of these is the receiving window of the photomultiplier and utilizes an "O" ring waterseal against a 1 inch thick plexiglass plate. The second hole is used for the connection of the electronic lamp housing.

The electronic flash lamp and associated spark coil are contained in a pyrex housing which is 12 inches long, 1 inch inside diameter, ¼ inch wall thickness (Macalaster Bicknell Co., 243 Broadway, Cambridge, Mass.). This tube is closed with a rounded seal at one end and open with a flared edge ground flat at the other end. A metal clamp with a fiber insert fits over the flared end and secures the pyrex housing to the face end plate. A neoprene gasket provides a water seal between the flat end of the housing and the face end plate. The rubber gasket compresses under pressure and seldom has time to regain its original thickness when the instrument is retrieved. Therefore it is important to use a thin gasket and to provide some type of take-up mechanism on the metal clamp holding the tube. In this instrument the gasket is 1/32 inch thick and there are lock washers under the clamp holding bolts to insure a tension on it at all times.

The cradle for holding the two main tubes is constructed of 1 inch stainless steel tubing. Each tube is held in place by two clamps which may be opened and closed quickly by means of a thumb screw. The sonar transducer is of the crystal-in-oil type (EDO # X-18517) employing a rubber diaphragm on each end from which sonar beams are emitted. The transducer is positioned on the cradle so that the sonar beams are directed approximately vertically up and down.

The field of view of the photomultiplier is a right circular cone of about 25° with its apex located at the face plate of the flash unit. A baffle attached to the cradle truncates this cone at a distance of 10 inches from the face plate. A sensitivity zone is thus delineated into which a luminescent animal must enter in order that its flash will trigger the instrument.

Camera Design

Many underwater cameras have been designed by putting a watertight case around a standard camera. Experience has shown however, that for great depths it is more advisable to design the camera to fit in the housing. The present instrument incorporates an "in-line" camera which has been specially designed by Edgerton for a cylindrical housing. The camera uses a standard 100 ft 35 mm motion picture reel. The film transportation is accomplished by using two "O" rings as belts from a motor to the sprocket shaft and to the take-up reel shaft. One main sprocket is used to meter the film. A microswitch operated by a cam on the sprocket shaft, is used to stop the film motion after each frame has been advanced. The take-up reel shaft is driven by a loose "O" ring belt that slips as the film builds up on the reel. The 6-volt motor (Hansen Manufacturing Co., Princeton, Indiana) turns at 18 rpm and is attached as a unit with the reducing gears to the camera plate.

Since the camera is shutterless, the electronic light flash takes the picture. The lens used is a Leitz Elmar f 3.5 with a 50 mm focal length. Since this lens with its adjustment cannot focus on points closer than 43 inches, lens extenders are used for each operating condition. Under "general" operating conditions the camera photographs a field 5 inches wide and 7 inches long, in the direction of the axis of the photosensitive cone. With "close up" operation the field is reduced to about half of this. Laboratory tests indicated that the most suitable aperture was f 16. The depth of field obtained at this aperture is sufficient to take in the entire photosensitive cone.

Electronics

The circuit diagram of the photomultiplier trigger and electronic light is shown in figure 3. Photomultiplier tube R.C.A. 6199 was chosen because of its high sensitivity, convenient size, and a spectral response peaked in the region of maximum transmission of sea water, which is also probably the region of most bioluminescent emission. The photosensitive surface of the S11 type is the same as that employed in the bathyphotometer. Were this not so, it would be impossible to form any correlation between the results of the two instruments. The device will be triggered by a pulse of light as small as 5×10^{-6} uw/cm^2 as measured with the bathyphotometer.

The high voltage is supplied by two 510 volt photoflash batteries (Eveready 497 or Burgess 320) placed in series.

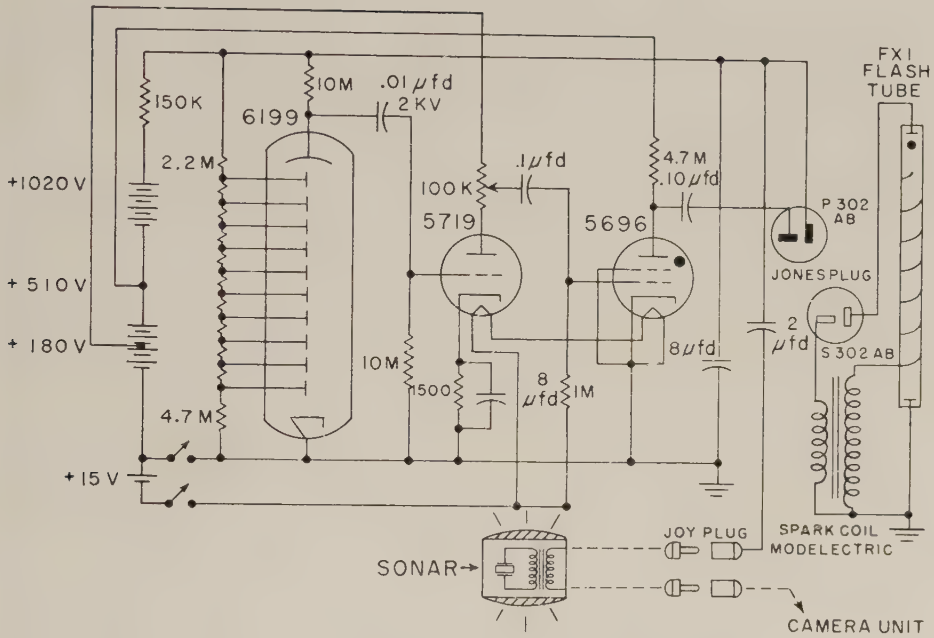
FX I
FLASH
TUBE
150 K
10 M
.01 μfd
2 KV
6199
2.2 M
+1020 V
+ 510 V
+ 180 V
4.7 M
+ 15 V
.1 μfd
100 K
5719
10 M
500
8
μfd
IM
4.7 M
.10 μfd
5696
8 μfd
P 302
AB
JONES PLUG
2
μfd
S 302 AB
JOY PLUG
SPARK COIL
MODELECTRIC
SONAR
CAMERA UNIT

LUMINESCENCE CAMERA—FLASH UNIT
FIG. 3

These were chosen because of their convenient size and 180 volt tap. The full 1020 volts, charging through the 150 k ohm resistor, are placed across the 8 ufd flash condenser and 2 ufd sonar condenser. These in turn hold up the voltage across the FX-1 electronic flash lamp (Edgerton, Germeshausen, and Grier, Incorporated, 160 Brookline Ave., Boston, Mass.) and the photomultiplier resistor bank. When the electronic flash lamp fires, these condensers discharge, and in so doing, drop the voltage across the photomultiplier bank to zero. This has the effect of temporarily desensitizing the photomultiplier and thus preventing it from injury by the high intensity electronic flash.

The photomultiplier resistor bank is composed of 2.2 M ohm resistors with the exception of a 4.7 M ohm resistor between the cathode and first dynode. The load imposed by this high resistance is negligible. Consequently the voltage across the photomultiplier is essentially the same as the battery open circuit voltage which makes for maximum sensitivity obtainable. Incremental voltage drops across the last few dynode resistors are of no consequence here since this is a trigger circuit rather than a linear amplifier.

The signal is developed across the 10 M ohm resistor in series with the photomultiplier anode. This very large value of resistance gives the stage a high sensitivity and serves to protect the photomultiplier from overload when subjected to a large value of ambient light. The photomultiplier generates a negative pulse across its anode resistor, whereas the thyratron can only be triggered by a positive pulse. Therefore a stage of voltage amplification is inserted between them and this serves to invert the phase.

The voltage amplifier utilizes a 5719 subminiature triode. This tube is used for missile circuitry and is supposed to be mechanically rugged and electrically stable. These factors, in addition to its small physical size, low quiescent power dissipation, and convenient filament rating influenced the choice of this tube.

The grid resistor used is 10 M ohm which provides a high degree of coupling to the photomultiplier. This has the advantage of producing a high sensitivity, but at the same time requires that the 5719 tube draws very little grid current. All the 5719 tubes used worked satisfactorily, but since the tube is being pushed beyond the manufacturers specifications, a "good" tube might have to be selected. The plate is fed from a 180 volt tap and passes through a 100 K ohm potentiometer. The output signal, developed across the potentiometer provides the manual sensitivity control.

Thyratron tube 5696 was chosen because of its small size and low filament dissipation. The thyratron is biased to cut-off by tapping off the negative side of the filament battery. A one M ohm resistor is injected here so as to provide the high impedance necessary in a thyratron grid circuit. The plate is fed from a 510 volt tap through a 1 M ohm resistor. A .25 ufd condenser in series with the spark coil primary is placed directly across the thyratron. When no signal current is applied, the thyratron is cut off. The full 510 volts is supplied to the plate and develops across the .25 ufd condenser. When a signal is applied, the thyratron fires. The condenser then discharges through the thyratron and energizes the spark coil. During the condenser recharge transient, most of the supply voltage falls across the 1M ohm resistor. This lowers the plate voltage of the thyratron and prevents it from holding over.

One side of the spark coil secondary goes to a spiral of wire wound around the FX1 xenon flash lamp. When energized, this ionizes the xenon and serves to set off the flash lamp. Once triggered the 8 ufd flash condenser discharges through the flash lamp. This produces a light flash with a peak intensity of .4 million horizontal candlepower and a time duration of 30 microseconds. After the electronic flash has occurred, the discharge condenser requires three seconds to recharge before another flash can be made.

The resistance of the xenon flash lamp drops to a very low value when it is energized. This property allows it to be exploited as a switch. Each time the lamp flashes, a path is completed between the sonar condenser, sonar transducer, and camera recycle unit. Consequently at 12.5 Kc impulse is emitted from the sonar transducer, and a syncronizing signal is sent to the camera unit for film recycle purposes. Filament power for both tubes is provided by eight Yardney LR 1 silver cells connected in series to produce 14 volts under load. Silver cells were used because of their high stored energy versus physical volume ratio.

The circuit diagram of the film recycle unit is shown in figure 4. The synchronizing signal is developed across the 1 ohm resistor. Duration of the signal is much too short to energize a relay and must be lengthened. This is accomplished by the 50 ufd condenser and diode combination. The relay employed is of the double coil polarized latching type. When either coil is energized in the direction of the indicated polarity, it will close and remain closed until either coil is energized in the reverse direction.

The film advance motor is mechanically coupled to a cam which activates a microswitch. The purpose of this cam is to inform the microswitch that the film has been advanced sufficiently. One six volt lantern battery (Burgess F4BP) is used to provide power for the film advance motor. This contains ample energy for the 800 recycle operations necessary to move the entire film through the camera.

At the beginning of the cycle the relay is open and the microswitch is in the down position. When the synchronizing signal is received, the relay closes and thus energizes the motor. While the motor is running, the cam causes the microswitch to assume the "up" position, and thus the 100 ufd condenser is charged. After the film has advanced sufficiently, the cam causes the microswitch to assume the "down" position, thus allowing the 100 ufd condenser to discharge into the relay. This causes the relay to open and consequently halts the film advance motor. The film is now in position, the relay has been reset, and the cycle is complete. The complete recycle process requires four seconds.

Observations at Sea

The luminescence camera was operated from the Research Vessel Crawford and Coast Guard Cutter Yamacraw in the waters south of Woods Hole during the summer of 1957. The instrument was used independently on certain occasions but improved results were obtained when it was employed in conjunction with the bathyphotometer and with the Precision Graphic Recorder (Knott and Hersey, 1956) for echo sounding.

The bathyphotometer used is a wide-range, logarithmic device sensitive enough to observe bioluminescence but not injured by a high intensity electronic flash. Since the light values received by the bathyphotometer at various depths are displayed on the Sanborn Recorder,

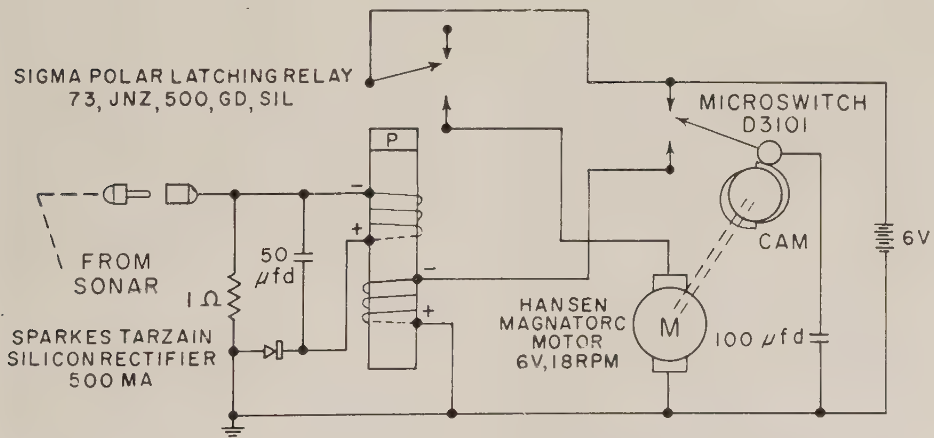

NOTE: THE MICROSWITCH RIDES ON A CAM GANGED TO THE FILM ADVANCE MOTOR

LUMINESCENCE CAMERA—CAMERA UNIT

FIG. 4

it is possible to lower the camera to regions of maximum bioluminescent activity. In addition the simultaneous use of the photometer serves to verify that the luminescence camera is operating since the occurrence of each electronic flash is visible on the record of the Sanborn Recorder.

The precision graphic recorder used is of the high-resolution, sonar type. By recording the sonar impulse emitted from the luminescence camera this device is able to discern the distance from the ship to the instrument and hence its vertical depth when the wire angle is low.

The camera may be loaded and unloaded without the use of a dark room, but opening the camera on deck causes about 3 ft. of film to be fogged. In this case about 25 frames should be run through before and after the lowering.

Open cameras at sea can become filled with warm, humid air. As a result, when the cameras are lowered into the cold sea, moisture condenses on the inside of the glass window, destroying its photographic quality. Every effort must be made to keep the inside of the camera case dry. When a camera emerges from the cold sea water, it should not be opened until it has warmed to air temperature since otherwise moisture would immediately condense over the entire interior. Thermal equalization can be hastened by bathing the camera housing in warm water.

The film used was Kodak plus X in 100 ft. spools. This was processed at sea using a Morse tank in order that the results could be evaluated immediately.

The operation of the entire instrument may be conveniently tested on deck by exposing it to a flashlight, match, cigarette, or other small light source. The electronic flash should be seen and the recycle of the film and the click of the sonar transducer should be heard.

A convenient test for the recycle circuit is to apply a six volt negative pulse between the Joy plug input and the housing ground. This technique may also be used to advance the film when desired. The electronic light section of the photomultiplier and electronic light unit may be checked by short circuiting the grid of the thyratron to ground. This should produce an electronic flash.

A portable test light was designed and constructed for facility in determining sensitivity of the instrument. This device consisted of a 700 ufd condenser charging up to 22.5 volts and then discharging through a 30 ohm rheostat into a 3 volt tungsten flashlight bulb. The light pulse generated was found to have essentially the same shape as that of many luminescent animals. A wooden calibration box was constructed. This fits over the head of the photomultiplier unit and provides a light tight chamber into which the portable test light may be introduced. The rheostat on the portable test light is then varied until the threshold of the photomultiplier trigger is found. The portable test light is then placed in the calibrating box of the bathyphotometer and its value determined by that instrument.

Sample photographs of animals which took their own pictures by means of the luminescence camera are reproduced in Figures 5 and 6. The siphonophore (about 6 cm in diameter), shown in Figure 5a, was taken in August 1957 about 170 miles east of Cape Hatteras at a depth not accurately determined but probably about 100 m. Figure 5b shows a ctenophore (about 2.8 cm in diameter) at a depth of 10 m; Figure 6a shows a medusa (about 1 cm in diameter at 100 m; and Figure 6b shows

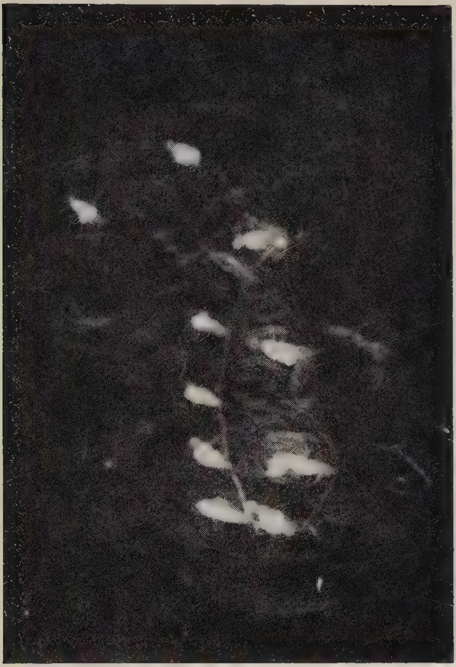

Figure 5a.

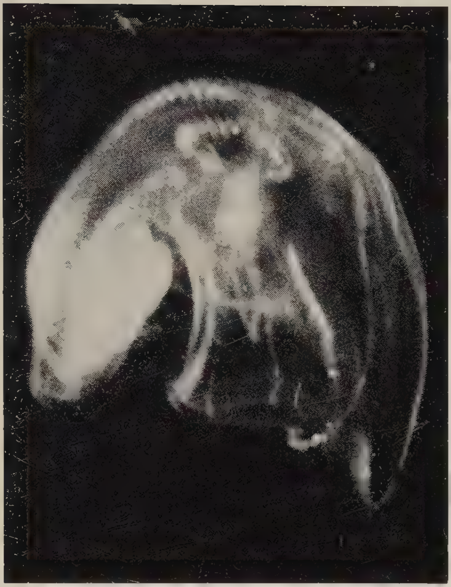

Figure 5b.

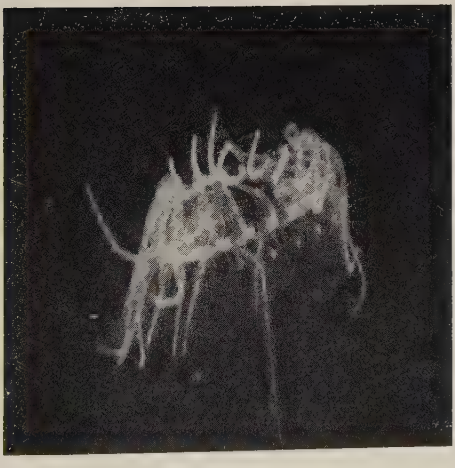

Figure 6a.

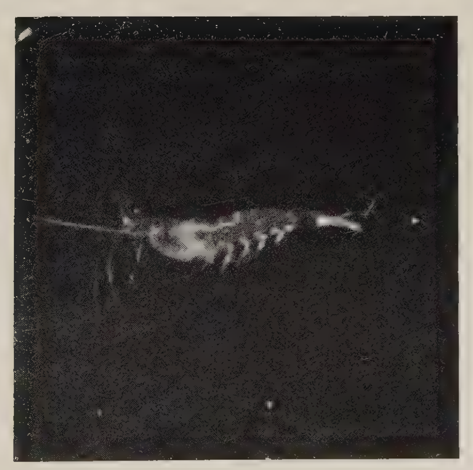

Figure 6b.

a euphausid (about 1½ cm long) at 50 m, all taken at stations north of Cuba in February 1958, after slight modifications of the camera device which will be described subsequently. A fuller account of the results obtained with the luminescence camera and their application to problems in the ecology of the deep sea will be presented in a separate report by Dr. G. L. Clarke.

ACKNOWLEGEMENTS

The authors are indebted to G. L. Clarke of Woods Hole Oceanographic Institution for his numerous suggestions as a biologist concerning the desirable features to be incorporated into the design of this instrument and for his criticism of this manuscript. We also wish to acknowledge the able assistance of V. MacRoberts of Massachusetts Institute of Technology in the construction of the instrument. L. Hoadley assisted in pressure testing of this device. The machine work was done in the machine shop of the Research Laboratory of Electronics at MIT under the supervision of foreman J. Keefe.

We wish to thank the many people who helped us during the testing of the device at sea on the R/V Crawford and CGC Yamacraw, in particular J. B. Hersey, C. J. Hubbard, W. A. Richardson, E. E. Hays, R. C. Stross, D. B. Clarke, and T. Stetson.

REFERENCES

Clarke, G. L. and Backus, R. H. (1956)
Measurements of light penetration in relation to vertical migration and records of luminescence of deep sea animals. *Deep Sea Research,* 4, 1-14.

Clarke, G. L. and Hubbard, C. (1958)
(In preparation).

Clarke, G. L. and Wertheim, G. K. (1956)
Measurements of illumination at great depths and at night in the Atlantic Ocean by means of a new bathyphotometer. *Deep Sea Research,* 3, 189-205.

Edgerton, H. E. and Hoadley, L. D. (1955)
Camera and lights for underwater use. *Society of Motion Picture and Television Engineers,* 64, 345-350.

Hubbard, C. J. (1956)
A wide range, high-speed bathyphotometer. Woods Hole Oceanographic Institution, unpublished manuscript. Ref. No. 56-68.

Knott, S. T. and Hersey, J. B. (1956)
Interpretation of high-resolution echo sounding techniques and their use in Bathymetry, Marine Geophysics and Biology, *Deep Sea Research,* 4, 36-44.

Report for the year 1958

THE
WOODS HOLE OCEANOGRAPHIC INSTITUTION

REPORT FOR THE YEAR
1958

1959

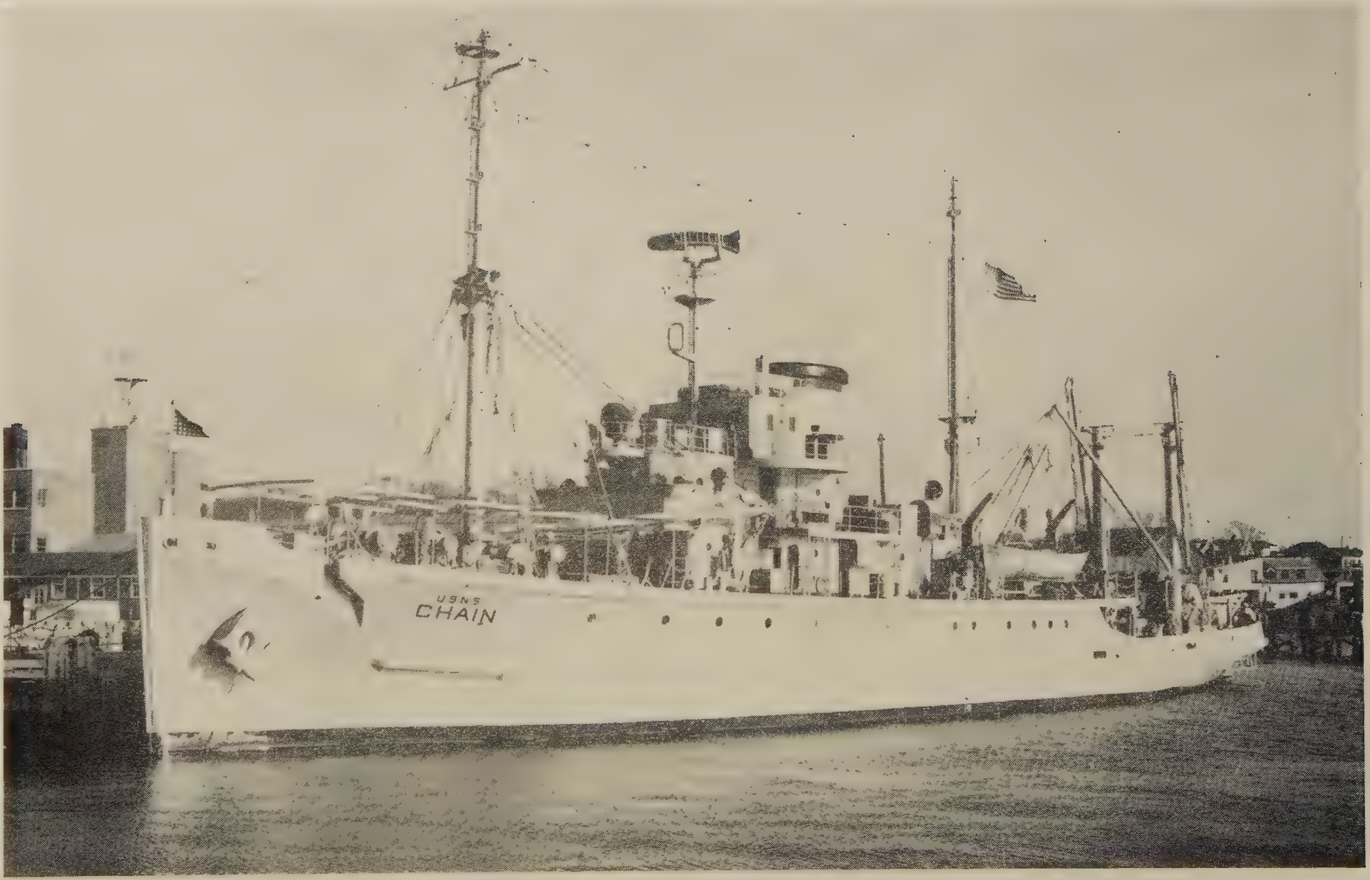

The New Research Vessel "Chain"

TABLE OF CONTENTS

		PAGE
I.	Trustees, as of December 31, 1958	5
II.	Members of the Corporation, as of December 31, 1958	6
III.	Research Staff	8
IV.	Director's Report	12
V.	Treasurer's Report for the Year 1958	55

I. TRUSTEES

(as of December 31, 1958)

Honorary Trustees

Henry B. Bigelow, Museum of Comparative Zoology, Cambridge 38, Mass.
L. O. Colbert, 4408 29th Street, N.W., Washington, D. C.
Marion Eppley, 510 Park Avenue, New York, N. Y.
Alexander Forbes, 610 Harland Street, Milton, Mass.
Horace S. Ford, 77 Massachusetts Avenue, Cambridge 39, Mass.
Arnaud C. Marts, 521 Fifth Avenue, New York, N. Y.
Lawrason Riggs, Riggs, Ferris and Geer, Room 1201, 74 Trinity Place, New York 6, N. Y.
Henry L. Shattuck, 10 Milk Street, Boston, Mass.
Selman A. Waksman, Institute of Microbiology, Rutgers University, New Brunswick, N. J.

To serve until 1962

Charles Francis Adams, Raytheon Manufacturing Company, 138 River Street, Waltham 54, Mass.
Columbus O'D. Iselin, Woods Hole Oceanographic Institution, Woods Hole, Mass.
Augustus P. Loring, Loring, Walcott Office, Inc., 35 Congress Street, Boston, Mass.
Albert E. Parr, American Museum of Natural History, Central Park West at 79th Street, New York, N. Y.
Athelstan F. Spilhaus, Institute of Technology, University of Minnesota, Minneapolis 14, Minn.
Alfred M. Wilson, Minneapolis-Honeywell Regulator Co., 2747 4th Avenue, South, Minneapolis 8, Minn.

To serve until 1961

Harvey Brooks, Division of Applied Science, Harvard University, Cambridge 38, Mass.
Frank A. Howard, 30 Rockefeller Plaza, New York, N. Y.
Robert R. Shrock, Department of Geology and Geophysics, Massachusetts Institute of Technology, Cambridge 39, Mass.
Edward H. Smith, Woods Hole, Mass.
Raymond Stevens, c/o Arthur D. Little, Inc., 30 Memorial Drive, Cambridge 42, Mass.
E. Bright Wilson, Jr., Department of Chemistry, Harvard University, Cambridge 38, Mass.

To serve until 1960

Detlev W. Bronk, The Rockefeller Institute of Medical Research, 66th Street and York Avenue, New York 21, N. Y.
Noel B. McLean, Edo Corporation, College Point 56, N. Y.
Daniel Merriman, Bingham Oceanographic Laboratory, Yale University, New Haven, Conn.
Emanuel R. Piore, International Business Machines Corp., 590 Madison Avenue, New York 22, N. Y.
Alfred C. Redfield, Woods Hole Oceanographic Institution, Woods Hole, Mass.
Gerard Swope, Jr., c/o International General Electric Co., 570 Lexington Avenue, New York, N. Y.

To serve until 1959

J. S. Coles, Bowdoin College, Brunswick, Maine
Carl H. Eckart, Scripps Institution of Oceanography, La Jolla, Calif.
Ross G. Harrison, Osborn Zoological Laboratory, Yale University, New Haven, Conn.
Milford R. Lawrence, Siders Pond Road, Falmouth, Mass.
Harlow Shapley, Sharon Cross Road, Peterborough, N. H.
Francis C. Welch, 73 Tremont Street, Boston, Mass.

Ex Officio

Edwin D. Brooks, Jr., P.O. Box 1135, Boston 3, Mass.
Mary Sears, Woods Hole Oceanographic Institution, Woods Hole, Mass.
Paul M. Fye, Woods Hole Oceanographic Institution, Woods Hole, Mass.

Officers

Raymond Stevens, President of the Corporation, c/o Arthur D. Little, Inc., 30 Memorial Drive, Cambridge 42, Mass.
Henry B. Bigelow, Chairman of the Board of Trustees, Museum of Comparative Zoology, Cambridge 38, Mass.
Edwin D. Brooks, Jr., Treasurer, P.O. Box 1135, Boston 3, Mass.
Mary Sears, Clerk of the Corporation, Woods Hole Oceanographic Institution, Woods Hole, Mass.

II. MEMBERS OF THE CORPORATION

Charles Francis Adams, Raytheon Manufacturing Company, 138 River Street, Waltham 54, Mass.

Oliver Ames, III, "Edgewater", Beverly Farms, Mass.

Philip Armstrong, Medical Center of Syracuse, State University of New York, Syracuse, N. Y.

Eric G. Ball, Harvard Medical School, Shattuck Street, Boston, Mass.

Henry B. Bigelow, Museum of Comparative Zoology, Cambridge 38, Mass.

Lindsay Bradford, 215 East 72nd Street, New York, N. Y.

Detlev W. Bronk, The Rockefeller Institute of Medical Research, 66th Street and York Avenue, New York 21, N. Y.

Edwin D. Brooks, Jr., P.O. Box 1135, Boston 3, Mass.

Harvey Brooks, Division of Applied Science, Harvard University, Cambridge 38, Mass.

C. Lloyd Claff, Single Cell Research Foundation, Inc., 5 Van Beal Road, Randolph, Mass.

E. L. Cochrane, Office of Vice President for Industrial and Governmental Relations, Massachusetts Institute of Technology, Cambridge 39, Mass.

L. O. Colbert, 4408 29th Street, N.W., Washington, D. C.

Kenneth S. Cole, National Institutes of Health, Bethesda 14, Md.

J. S. Coles, Bowdoin College, Brunswick, Maine

Henry B. Dupont, Wilmington, Del.

Ferdinand Eberstadt, 39 Broadway, New York 6, N. Y.

Carl H. Eckart, Scripps Institution of Oceanography, La Jolla, Calif.

Harrison P. Eddy, c/o Metcalf & Eddy, 1300 Statler Building, Boston, Mass.

Marion Eppley, 510 Park Avenue, New York, N. Y.

Alexander Forbes, 610 Harland Street, Milton, Mass.

Horace S. Ford, 77 Massachusetts Avenue, Cambridge, Mass.

Paul M. Fye, Woods Hole Oceanographic Institution, Woods Hole, Mass.

John A. Gifford, 14 Wall Street, New York 5, N. Y.

Paul Hammond, 230 Park Avenue, New York 17, N. Y.

Ross G. Harrison, Osborn Zoological Laboratory, Yale University, New Haven, Conn.

Hudson Hoagland, Worcester Foundation for Experimental Biology, 222 Maple Avenue, Shrewsbury, Mass.

Frank A. Howard, 30 Rockefeller Plaza, New York, N. Y.

Columbus O'D. Iselin, Woods Hole Oceanographic Institution, Woods Hole, Mass.

Augustus B. Kinzel, Union Carbide Corporation, 30 East 42nd Street, New York 17, N. Y.

Milford R. Lawrence, Siders Pond Road, Falmouth, Mass.

Alfred L. Loomis, Room 2420, 14 Wall Street, New York, N. Y.

Augustus P. Loring, Loring, Walcott Office, Inc., 35 Congress Street, Boston, Mass.

Arnaud C. Marts, 521 Fifth Avenue, New York, N. Y.

Robert E. McConnell, First National Bank, Hobe Sound, Fla.

Noel B. McLean, Edo Corporation, College Point 56, N. Y.

Daniel Merriman, Bingham Oceanographic Laboratory, Yale University, New Haven, Conn.

Henry S. Morgan, 2 Wall Street, New York, N. Y.

Frank A. Pace, General Dynamics Corporation, 445 Park Avenue, New York 22, N. Y.

Albert E. Parr, American Museum of Natural History, Central Park West at 79th Street, New York, N. Y.

Sumner T. Pike, Lubec, Maine

Emanuel R. Piore, International Business Machines Corp., 590 Madison Avenue, New York 22, N. Y.

Alfred C. Redfield, Woods Hole, Mass.

George H. Richards, 68 William Street, New York, N. Y.

Lawrason Riggs, Riggs, Ferris and Geer, Room 1201, 74 Trinity Place, New York 6, N. Y.

Francis C. Ryder, 37 Larchwood Drive, Cambridge 39, Mass.

Mary Sears, Woods Hole Oceanographic Institution, Woods Hole, Mass.

Harlow Shapley, Sharon Cross Road, Peterborough, N. H.

Henry L. Shattuck, 10 Milk Street, Boston, Mass.

Robert R. Shrock, Department of Geology and Geophysics, Massachusetts Institute of Technology, Cambridge 39, Mass.

Edward H. Smith, Woods Hole, Mass.

Athelstan F. Spilhaus, Institute of Technology, University of Minnesota, Minneapolis 14, Minn.

Lyman Spitzer, Jr., Princeton University Observatory, 14 Prospect Ave., Princeton, N. J.

Raymond Stevens, c/o Arthur D. Little, Inc., 30 Memorial Drive, Cambridge 42, Mass.

Julius A. Stratton, Office of the Vice President and Provost, Massachusetts Institute of Technology, Cambridge 39, Mass.

Gerald Swope, Jr., c/o International General Electric Co., 570 Lexington Avenue, New York, N. Y.

J. H. Van Vleck, Lyman 332, Harvard University, Cambridge 38, Mass.

Selman A. Waksman, Institute of Microbiology, New Brunswick, N. J.

Thomas J. Watson, Jr., International Business Machines Corporation, 590 Madison Avenue, New York 22, N. Y.

Francis C. Welch, 73 Tremont Street, Boston, Mass.

Alfred M. Wilson, Minneapolis-Honeywell Regulator, 2747 4th Avenue, South, Minneapolis 8, Minn.

E. Bright Wilson, Jr., Department of Chemistry, Harvard University, Cambridge 38, Mass.

III. RESEARCH STAFF

(As of December 31, 1958)

ARNOLD B. ARONS, Associate in Physical Oceanography.
Professor of Physics, Amherst College.

WILLIAM D. ATHEARN, Research Associate in Geology.

JOHN C. AYERS, Associate in Marine Biology.
Associate Professor, Great Lakes Research Institute, and Associate Professor of Zoology, Department of Zoology, University of Michigan.

RICHARD H. BACKUS, Research Associate in Marine Biology.

JOHN P. BARLOW, Associate in Marine Biology.
Assistant Professor of Oceanography, Cornell University.

LINCOLN BAXTER II, Research Associate in Physics.

DAVID L. BELDING, Associate in Marine Biology.
Professor of Bacteriology and Experimental Pathology (Emeritus), Boston University; Consultant, U. S. Fish & Wildlife Service.

BRUCE BENSON, Associate in Physics.
Associate Professor of Physics, Amherst College.

HENRY B. BIGELOW, Associate in Oceanography.
Professor of Zoology (Emeritus), Harvard University; Research Oceanographer, Museum of Comparative Zoology.

DUNCAN C. BLANCHARD, Research Associate in Meteorology.

BERT BOLIN, Associate in Meteorology.
Director, Institute of Meteorology, University of Stockholm.

VAUGHAN T. BOWEN, Geochemist.
Lecturer in Zoology, Yale University.

ROBERT R. BROCKHURST, Research Associate in Physics.

JOHN G. BRUCE, JR., Research Associate in Oceanography.

DEAN F. BUMPUS, Oceanographer.

ELIZABETH T. BUNCE, Research Associate in Physics.

ANDREW F. BUNKER, Meteorologist.

CORNELIA L. CAREY, Associate in Marine Bacteriology.
Associate Professor of Botany (retired), Barnard College.

CHARLES E. CARVER, JR., Associate in Hydraulics.
Associate Professor of Civil Engineering, University of Massachusetts.

JOSEPH CHASE, Research Associate in Physical Oceanography.

GEORGE L. CLARKE, Marine Biologist.
Associate Professor of Zoology, Harvard University.

NATHANIEL CORWIN, Research Associate in Chemistry.

HERBERT CURL, JR., Research Associate in Marine Biology.

WILLARD DOW, Electronics Engineer.

RICHARD S. EDWARDS, Research Associate in Geophysics.

MAURICE EWING, Associate in Geophysics.
Professor of Geology, Columbia University; Director, Lamont Geological Observatory.

ALAN J. FALLER, Research Associate in Meteorology.

HARLOW G. FARMER, JR., Research Associate in Hydraulics.

CHARLES J. FISH, Associate in Marine Biology.
Professor of Marine Biology, University of Rhode Island; Director, Narragansett Marine Laboratory.

DAVID H. FRANTZ, JR., Research Associate in Engineering.

FREDERICK C. FUGLISTER, Physical Oceanographer.

PAUL M. FYE, Chemist.

MICHAEL GARSTANG, Research Associate in Meteorology.

ROBERT H. GIBBS, JR., Associate in Marine Biology.
Assistant Professor of Biology, Boston University.

JOHN W. GRAHAM, Research Associate in Geology.

DONALD R. GRIFFIN, Associate in Physiology.
Professor of Zoology, Harvard University.

ROBERT R. L. GUILLARD, Research Associate in Marine Biology.

Bernard J. Haurwitz, Associate in Meteorology.
Professor of Meteorology and Chairman of the Department of Meteorology and Oceanography, New York University.

Earl E. Hays, Physicist.

John B. Hersey, Geophysicist.
Associate Professor of Oceanography, Massachusetts Institute of Technology.

Edward M. Hulburt, Research Associate in Marine Biology.

Columbus O'D. Iselin, Henry Bryant Bigelow Oceanographer.
Associate Professor of Physical Oceanography, Harvard University; Research Oceanographer, Museum of Comparative Zoology.

Henry R. Johnson, Research Associate in Underwater Acoustics.

John W. Kanwisher, Research Associate in Biophysics.

Bostwick H. Ketchum, Senior Oceanographer.

David D. Ketchum, Research Associate in Electronics.

Sydney T. Knott, Jr., Research Associate in Engineering.

Bernhard Kummel, Associate in Submarine Geology.
Associate Professor of Geology, Harvard University.

Richard G. Leahy, Research Associate in Geology.

Benjamin B. Leavitt, Associate in Marine Biology.
Associate Professor of Biological Sciences, University of Florida.

Joyce C. Lewin, Research Associate in Marine Biology.

Robert A. Lufburrow, Associate in Physics.
Assistant Professor of Physics, St. Lawrence University.

Joanne S. Malkus, Meteorologist.

Willem V. R. Malkus, Physical Oceanographer.

Frank J. Mather III, Research Associate in Oceanography.

James W. Mavor, Jr., Associate in Applied Physics.
Associate Professor of Mechanical Engineering, Northeastern University.

William G. Metcalf, Physical Oceanographer.

Arthur R. Miller, Physical Oceanographer.

Robert L. Miller, Associate in Submarine Geology.
Associate Professor in Qualitative Sedimentology, The University of Chicago.

Raymond B. Montgomery, Associate in Physical Oceanography.
Associate Professor of Oceanography, Chesapeake Bay Institute, The Johns Hopkins University.

Hilary B. Moore, Associate in Marine Biology.
Professor in Marine Biology and Assistant Director, Marine Laboratory, University of Miami.

James M. Moulton, Associate in Marine Biology.
Assistant Professor of Biology, Bowdoin College.

Jerome Namias, Associate in Meteorology.
Chief, Extended Forecast Section, U. S. Weather Bureau.

A. Conrad Neumann, Research Associate in Sedimentary Geology.

Geoffrey D. Nicholls, Associate in Geochemistry.
Lecturer, Department of Geology, University of Manchester, Manchester, England.

Daniel R. Norton, Associate in Chemical Oceanography.
Research Chemist, Sprague Electric Co., North Adams, Massachusetts.

Charles B. Officer, Jr., Geophysicist.
Associate Professor of Geology, Rice Institute.

David M. Owen, Research Associate in Underwater Photography.

Mary Alys Plunkett, Associate in Chemistry.
Associate Professor of Chemistry, Vassar College.

Alfred C. Redfield, Senior Oceanographer (Emeritus).
Professor of Physiology (Emeritus), Harvard University.

Charles E. Renn, Associate in Engineering.
Professor of Sanitary Engineering, School of Engineering, The Johns Hopkins University.

Francis A. Richards, Chemical Oceanographer.

William S. Richardson, Physical Chemist.

GORDON A. RILEY, Associate in Marine Physiology.
Associate Director, Bingham Oceanographic Laboratory, Yale University.

NATHAN W. RISER, Associate in Marine Biology.
Professor of Zoology, Northeastern University.

HELEN M. ROBERTS, Associate in Mathematics.
Assistant Professor of Mathematics, University of Connecticut.

F. CLAUDE RONNE, Research Associate in Photography.

JOHN H. RYTHER, Marine Biologist.

HOWARD L. SANDERS, Research Associate in Marine Biology.

HAROLD E. SAWYER, Research Engineer.

IRVING I. SCHELL, Associate in Meteorology.
Research Associate, Department of Geology, Tufts University.

WILLIAM E. SCHEVILL, Associate in Oceanography.
Research Associate in Zoology, Museum of Comparative Zoology, Harvard University.

KARL E. SCHLEICHER, Research Associate in Physics.

WILLIAM C. SCHROEDER, Ichthyologist.
Associate Curator of Fishes, Museum of Comparative Zoology, Harvard University.

MARY SEARS, Planktonologist.

RAYMOND SIEVER, Associate in Geology.
Assistant Professor of Geology, Harvard University.

EDWARD H. SMITH, Associate in Oceanography.
Development Office, The Cooper Union for the Advancement of Science and Art.

PAUL FERRIS SMITH, Associate in Physical Oceanography.
Electronics Engineer, Rockefeller Institute for Medical Research.

FLOYD M. SOULE, Associate in Physical Oceanography.
Oceanographer, U. S. Coast Guard.

ALLARD T. SPENCER, Research Associate in Engineering.

ATHELSTAN F. SPILHAUS, Associate in Physical Oceanography.
Dean, Institute of Technology, University of Minnesota.

MELVIN E. STERN, Research Associate in Physics.

HENRY M. STOMMEL, Physical Oceanographer.

EDWARD D. STROUP, Research Associate in Physical Oceanography.

THOMAS T. SUGIHARA, Associate in Geochemistry.
Associate Professor of Chemistry, Clark University.

WILLIAM H. SUTCLIFFE, JR., Associate in Marine Biology.
Director, Bermuda Biological Station for Research, Inc.

PARKER D. TRASK, Associate in Submarine Geology.
Professor of Geological Engineering, University of California.

HARRY J. TURNER, JR., Marine Biologist.
Lecturer in Zoology, University of New Hampshire.

RALPH F. VACCARO, Research Associate in Microbiology.

GEORGE VERONIS, Research Associate in Mathematics.

ALLYN C. VINE, Physical Oceanographer.

GORDON H. VOLKMANN, Research Associate in Physical Oceanography.

WILLIAM S. VON ARX, Physical Oceanographer.
Associate Professor of Oceanography, Massachusetts Institute of Technology.

ARTHUR D. VOORHIS, Research Associate in Physics.

ROBERT G. WALDEN, Research Associate in Electronics.

EDMOND E. WATSON, Associate in Physical Oceanography.
Professor of Physics, Queen's University, Kingston, Ontario.

STANLEY W. WATSON, Research Associate in Bacteriology.

RAYMOND WEXLER, Associate in Meteorology.
Allied Research Associates, Inc., Boston, Massachusetts.

GEOFFREY G. WHITNEY, JR., Research Associate in Physical Oceanography.

ALFRED H. WOODCOCK, Oceanographer.

GEORGE P. WOOLLARD, Associate in Geophysics.
Professor of Engineering Geology and Geophysics, University of Wisconsin.

L. VALENTINE WORTHINGTON, Physical Oceanographer.

CHARLES S. YENTSCH, Research Associate in Marine Biology.

JOHN M. ZEIGLER, Research Associate in Marine Geology.

ADMINISTRATIVE STAFF

PAUL M. FYE	Director
RICHARD G. LEAHY	Assistant to the Director
RONALD A. VEEDER	Assistant to the Director
JOHN MCGILVRAY	Business Manager
JAN HAHN	Public Information
NORMAN T. ALLEN	Administrator
HARVEY MACKILLOP	Controller
JOHN F. PIKE	Port Captain

IV. DIRECTOR'S REPORT

Introduction

This has been an interesting and exciting year in science. The period following the first satellites has been alive with a resurging interest in science and cultural pursuits. The International Geophysical Year has proven to be a huge success and oceanography has shared in this resurgence and these successes.

The Institution's contribution to the I.G.Y. has been outstanding. In all, approximately 1,000 hydrographic stations have been taken during the total period and over 24,000 samples of water obtained for analysis. Staff members have participated in twelve complete sections of the North and South Atlantic Oceans and in four partial crossings east of the Mid-Atlantic Ridge. The I.G.Y. funds helped oceanography weather a difficult financial period and the returns have been rewarding. One of the most important results has been a new high in international cooperation among scientists the world over. Dr. Arnold B. Arons represented the Institution at the I.G.Y. meetings in Moscow in August and Dr. Columbus O'D. Iselin attended the second meeting of the Special Committee for Oceanic Research (SCOR) of the International Council for Scientific Unions in Paris in September. It is sincerely hoped that these evidences of scientific goodwill throughout the world will increase and that this Institution will play an important role in continued international cooperation.

The National Academy of Sciences' Committee on Oceanography headed by Professor Harrison Brown has been holding frequent and energetic meetings throughout the year. Dr. Iselin has represented Woods Hole on this important committee and now reports as the year ends that we can shortly expect to see the first fruits of these endeavors. There has been much talk of expansion in oceanography and of large sums of money to be made available for research in the earth sciences. Actually this year has seen very little real money resulting from these post-Sputnik discussions. The main evidence of improved solvency in oceanography is that, whereas it was impossible in the beginning of the year to prepare a budget, by the year's end a budget for 1959 had been prepared which in almost all respects was based on firm commitments of money. This budget was, however, only ten percent higher than the three million dollars expended during 1958.

In accordance with the Trustees' directive of the last Annual Meeting that the Institution plan for further orderly expansion while maintaining the high excellence of its scientific program, the Director has established committees for the design of new research vessels, for land acquisition, for a building program and an educational policy committee. The need for training of capable young people in marine science is very apparent and the educational policy committee, although established late in the year, has been most active in reviewing our association with universities, in improving our fellowship program, in providing adequate teaching opportunities for our senior staff and in setting up training courses for the younger members.

The establishment of the Carl-Gustaf Rossby Memorial Fellowship by the Executive Committee in October is considered a fitting fulfillment of the Trustees' request for an appropriate memorial to our beloved Senior Meteorologist. Preference will be given to applicants interested in those areas of study, sufficiently numerous, which engaged Professor Rossby's own attention. As our contribution to the American Meteorological Society's Rossby Memorial, the Society was invited to name the first Rossby Fellow. Dr. P. M. Saunders of the Imperial College of Science and Technology in England, who will spend a year in Woods Hole working with Dr. Joanne S. Malkus, was selected.

In this, my first Annual Report, perhaps I may be permitted a few personal observations and initial impressions. Seldom, if ever, has a new Director of a research institution been so fortunate as to have available for advice and help all the previous directors. The helpful discussions with Dr. Bigelow, Admiral Smith and Dr. Redfield have been greatly appreciated by me. To have Dr. Iselin as my constant mentor has been a source of strength and a very great personal pleasure. He is filling the Henry Bryant Bigelow Chair of Oceanography with great distinction and continues to be an inspiring leader for all of us.

Although I had spent a little time each year during the past decade in visits to Woods Hole there appear to be a number of noteworthy changes and advances of which I was not wholly aware. The most obvious of these changes, and perhaps the most predictable, has been the introduction of new techniques and new instrumentation. The use of drift buoys and neutrally buoyant floats permitting a recording of data in the absence of an observer, the use of the tow chain permitting the virtually continuous recording of the thermal structure from a vessel underway at speeds up to 12 knots and the use of an airplane as a research vessel from which oceanographic observations are made are examples of such new techniques in physical oceanography.

A second and perhaps more significant change relates to the type of thinking which is being done today. The use of models, particularly in large-scale circulation studies and in wave investigations, and a much greater acceptance of theoretical studies are examples of such changes. The recent successful prediction by theory of the deep-water circulation pattern is perhaps one of the few examples of modern oceanography where theory has preceded experiment. This represents a degree of sophistication not previously available in oceanography and may indicate that we are about to evolve out of the descriptive phase of the science into one in which the scientific methods will have more application. Finally, the inclusion on the staff of the excellent group engaged in beach studies, marine meteorology, hydrodynamics and theoretical work is undoubtedly the most significant change which has occurred during the past decade.

Today oceanography is occupying an increasingly important place as a major science. A number of the larger industrial companies are seeking assistance in studies involving either operational analysis or the feasibility of developing much improved high-performance weapon systems. Thus there is a sudden demand for the services of experienced physical oceanographers in industry. A course for industry in the "Environmental Factors Influencing the Performance of Naval Weapon Systems" was received with great enthusiasm.

The studies concerning the future of oceanography within the National Academy of Sciences and the Federal Government will undoubtedly bear much fruit. It is commonly assumed by these study groups that oceanography will expand very much in the near future. The only question appears to be how much and by what means. One of the most important decisions the Institution has ever had to make is what role it should play in this expansion. Everyone concedes that we should retain our well-established leadership in the field but it is not yet clear to what extent we should increase the size of our plant and staff. Undoubtedly it does mean increased stature for our staff members regardless of our total size. It is our strong opinion that our destiny should be determined by serious thought and planning in Woods Hole rather than in Washington.

The chief uncertainty at present is just how far-reaching a change will be made in the present method of selecting and supporting the kinds of basic research of interest to the Department of Defense and to the Federal Government in general. No doubt the changes will not go as far as some now hope. It is hoped that the thinking and planning for earth sciences in Washington will be able to keep up with events and to influence research budgets in sufficient time. Moreover, our reputation is such that, to a considerable degree, we should be able to influence the planning.

The health of the Institution appears to be excellent. With oceanographic data being compiled during the I.G.Y. at a rate greater than ever before in the history of the science and with the present excellence and enthusiasm of the staff, we can look to the future with great confidence. I am most happy for the opportunity to have a part in that future.

Physical Oceanography

The Institution's participation in the 1957–58 International Geophysical Year oceanographic program continued and expanded during 1958. This project has been directed by Dr. Columbus O'D. Iselin and is proving to have been one of the major contributions to the United States I.G.Y. oceanography program. We again joined with England's National Institute of Oceanography and together we have virtually completed a new systematic survey of the main body of the Atlantic Ocean. The sea-going part of the program would have been finished but for the engine break-down which prevented the ATLANTIS from going to the South Atlantic early in the year. Nevertheless over eight months of ship time were used on this program and an unprecedented number of successful, deep oceanographic stations were occupied during the year. This work, plus the painstaking task of evaluating and checking the data and preparing them for publication, occupied many man-hours of a group of scientists, technicians, secretaries, service personnel and the officers and crews of the CRAWFORD and DISCOVERY II.

In January Mr. Frederick C. Fuglister, after taking part in the second I.G.Y. cruise of the DISCOVERY II, visited the West German Hydrographic Office in Hamburg, the Service Hydrographique de la Marine in Paris and the National Institute of Oceanography in Surrey. In Germany he arranged for Mr. Karl E. Schleicher to take part in the German I.G.Y. survey, aboard the ANTON DOHRN, in Greenland waters during August and September. His visit to Surrey and Paris bore fruit in November when he and Mr. Arthur R. Miller joined the DISCOVERY II on its fourth I.G.Y. cruise. This cruise consisted of an intensive study, in the Bay of Cadiz, of the core of high salinity water flowing out from the Mediterranean Sea. Although the thermohaline data showed steady state conditions over a period of several weeks, observations made by Dr. John C. Swallow with his neutrally buoyant floats revealed the existence of currents that would have been plotted quite differently from a classical interpretation of the data.

Following this cruise, Mr. Fuglister went to the University of Kiel where he had been invited to give a talk on the Atlantic survey. An unusual feature of his talk was the fact that, although he had just left the DISCOVERY II, he was able to show completed temperature, salinity, oxygen and phosphate "profiles" and plots of direct current measurements for the Bay of Cadiz study. This was made possible by use of the newly developed conductivity bridge salinometer.

In June Mr. L. Valentine Worthington completed and distributed a report on the oceanographic data from the first and second I.G.Y. cruises aboard the R.R.S. DISCOVERY II. In August he again went aboard the

British ship to make four sections across the eastern basin of the North Atlantic. After this third I.G.Y. cruise of the DISCOVERY II he spent a month at the National Institute of Oceanography where he completed his joint paper with Dr. Swallow on the undercurrent of the Gulf Stream.

Mr. Worthington also completed a study of the "Eighteen Degree Water in the Sargasso Sea." In this paper he discusses some of the implications of the layer of water which lies at a depth of 300 meters and extends throughout the Sargasso Sea. He points out a parallel between the formation of this water and North Atlantic Deep Water. In both cases the water masses are considered to have been formed on the surface during the winter and to have sunk to their present depth due to increased densities as a result of the period of winter cooling.

Mr. William G. Metcalf spent a considerable portion of 1958 at sea on the I.G.Y. program. During February and March he took the CRAWFORD to the Caribbean Sea where he completed four meridional profiles. On the way to the Caribbean he made a section of oceanographic stations running from Bermuda to Hispaniola. In June Mr. Metcalf completed a report on the oceanographic data from CRAWFORD Cruise 16, obtained for the I.G.Y. during October and November 1957. He ended this busy year by successfully completing transatlantic sections in 24° South latitude and the Equator.

Oceanographic data were obtained from two bases on the ice in the Arctic Ocean for the I.G.Y. by Mr. John S. Farlow III. These observations, which were taken by Mr. Farlow during the fall of 1957 and the spring of 1958, further substantiated the clockwise circulation in the Beaufort eddy which had been postulated earlier by Mr. Worthington.

In addition to the oceanographic data obtained in the Atlantic, a total of 51 stations were occupied in the Mediterranean Sea, Red Sea and Indian Ocean during the summer. These stations were mostly concentrated in the Red Sea and the Straits of Bab-El-Manded connecting the Red Sea to the Gulf of Aden in the Indian Ocean.

A series of five short cruises, one each month from May to September, was made over the continental shelf and slope south of Martha's Vineyard and Nantucket. The purpose of these cruises was the study of the monthly and shorter period variations in the temperature and salinity of the cold wedge of water on the shelf and the transitional region between the coastal and slope water.

Mr. Arthur R. Miller made a study of the oxygen distribution in the Atlantic section of the Southern Ocean where he compared data taken by the METEOR and the DISCOVERY II. He found seasonal and geographical variations that led him to some new ideas on the formation of Antarctic Bottom Water by mixing of the brine from growing sea ice and subsurface water.

Mr. Joseph Chase used data obtained from east coast lightships and weather maps to show some relationships between wind patterns and the movement of water along the coast in the Chesapeake-Hatteras area. In the study of seasonal secular and long-term fluctuations, Mr. Dean F. Bumpus, assisted by Mr. C. Godfrey Day, has continued to compile synoptic temperature and salinity data from lightships, Texas Towers and shore locations along the coast from Maine to Georgia. Summertime intrusions of offshore water along the bottom as the result of offshore wind-driven surface movements along the Virginia and New Jersey coasts, which heretofore were not known to exist, are now commonly observed.

They have continued to study the circulation in the Gulf of Maine throughout the whole year using drift bottles. The effect of the coastal runoff has been observed to have a marked effect on the currents on the northern and western side of the Gulf of Maine. Fortunately, from the standpoint of experimentation, the runoff in 1957 which was much below normal gave way to a runoff much greater than average in 1958. Experiments with radio drift buoys on Georges Bank during the autumn suggest that the southwesterly set commonly observed there, March through July, gives way in the autumn to an easterly drift.

In addition to her duties of maintaining and adding to the WHOI Atlantic thermohaline data collection and keeping up the data tabulations of monthly mean temperatures and salinities, Miss Elizabeth H. Schroeder collaborated with Mr. Henry Stommel, Dr. David Menzel and Dr. W. H. Sutcliffe, Jr., on a paper dealing with the climatic stability of the 18° water at Bermuda. This paper deals with the same water mass as that studied by Mr. Worthington but concentrates its attention on observations made in the vicinity of Bermuda.

During May and June Dr. William S. von Arx, Mr. Bumpus and Mr. Day used the CRAWFORD to make 119 consecutive sections of the Gulf Stream off the coast of North Carolina as part of a second attempt to measure the short-period variations of the position and structure of the current. While the series of transverse sections was being made with the ship, the longitudinal changes were being plotted from the R4D aircraft by Dr. William S. Richardson and Mr. Charles H. Wilkins both visually and with the aid of the airborne radiation thermometer. These new data cover a period of one lunar month and give evidence that the Gulf Stream is moved bodily on and off the coast with the rise and fall of the local tide as well as possibly being pulsed by the tides in the Gulf of Mexico. The current was observed to change its regime of motion every seven and every fourteen days.

In the period from late August through the end of the year Dr. von Arx served as a member of the staff of the University Committee for Atmospheric

Research concerned with the preparation of plans for a National Institute for Atmospheric Research. This study was made at the suggestion of the Committee on Atmospheric Research of the National Academy of Sciences and sponsored by the National Science Foundation as part of an effort to facilitate research in the atmospheric and oceanographic phases of earth science.

During this year the last two of the four planned salinometers were completed by Mr. Karl E. Schleicher and Mr. Alvin L. Bradshaw. All four salinometers are available for active duty and the first instrument is now used to do all routine shore-based analyses at the Institution formerly done by Knudsen titration.

An attempt was also made to resolve the question of the accuracy of Copenhagen normal water as a sea-water conductivity standard by sending samples of this water to the Bureau of Standards for specific conductance determination and comparing these results with those of previous determinations on sea water. There was agreement within the experimental uncertainty of the comparison.

Mr. Schleicher was a guest aboard the German vessel ANTON DOHRN for a two months' cruise in the waters southwest of Iceland. One of the salinometers was used on this cruise to analyze the 3,000 salinity samples obtained. As a result of this trip the Germans have shown great interest in the instrument and are planning to build one of their own. As the September meeting of the Bureau du Conseil International pour L'Exploration de la Mer in Copenhagen a paper on the salinometer was read and a very encouraging amount of interest was demonstrated by the members of the Hydrographical Subcommittee. Personnel from the Lamont Geological Observatory were trained in the use of the salinometer and one of the instruments was loaned for the long cruise by the VEMA around the coast of South America.

Theoretical Oceanography

Dr. Allan R. Robinson and Mr. Henry M. Stommel have worked out a theoretical model of the oceanic thermocline and the associated thermohaline circulation. Previously, the only theories of oceanic circulation which had been reduced to a mathematical form were ones which attributed the cause of circulation to the prevailing wind systems. Now it is possible to compute various features of the circulation determined by the unequal heating of the ocean at the equator and poles; and for the first time we have a theoretical basis for explaining the vertical distribution of properties in the ocean.

Earlier in the year Mr. Stommel and Dr. Arnold B. Arons worked on the development of a theoretical model for the abyssal circulation which would take into account the effects of lateral mixing and permit the extension of the original simpler theory to cover the observed distributions of temperature, salinity and oxygen in the deep water.

Dr. Arons spent a sabbatical year at the Institute of Meteorology of the University of Stockholm. During this period he continued his collaboration with Mr. Stommel on the development of a theoretical model of the abyssal circulation of the world ocean. He was also able to complete some interesting work on flows induced by source and sink distributions in a rotating tank. These studies, which were initiated by the theoretical group in Woods Hole in 1957, have provided experimental insight and verification of theoretical considerations which underlie the present concept of abyssal circulation.

Dr. George Veronis worked on an analysis of the finite amplitude behavior of a rotating fluid which is heated from below and cooled from above. An interesting result of this investigation is that the non-linear interactions of the fluid tend to offset the effects of the constraint of the imposed rotation. This result is of considerable interest in planetary flow problems where the rotational constraint is the principal mechanistic constraint which governs the flow. A generalization of this result is that the dual role of viscosity, viz., as an energy releasing mechanism, as well as the more familiar dissipative mechanism, is a necessary condition for the fluid to become unstable to finite amplitude disturbances before it becomes unstable to infinitesimal perturbations.

Dr. Alan J. Faller returned in June after a stimulating nine months at the Hydrodynamics Laboratory of the University of Chicago and resumed his experimental studies of simple analogues of the ocean circulation. While the circulations produced in these experiments resemble the features of the large-scale ocean currents to a remarkable degree they are of more general hydrodynamic interest and have been compared with secondary flows in curved pipes. Some new thermal-circulation experiments have been initiated in collaboration with Dr. Robinson, a WHOI Fellow at Harvard University, to test his theoretical predictions of thermal circulations in rotating systems.

Dr. Melvin Stern made use of the rotating apparatus to test his non-linear mathematical theory for the decay of the relative circulation when there is an abrupt change in the rate of rotation of a tank of water. During these experiments some interesting instabilities of the flow were evident and plans are being made to investigate these instabilities under more controlled conditions on the very large floating turntable built by Dr. von Arx.

A new member of our staff is Dr. Kirk Bryan, Jr., who joined us in August after spending a year in Sweden on a Swedish-American Fellowship. In order to study the instabilities of large-scale atmospheric circulations Dr.

Bryan has built a small temporary rotating table and uses two fluids of different density to simulate the thermal structure of the atmosphere.

Dr. Willem V. R. Malkus has been involved in a variety of projects which include a theoretical study on magneto-convection of a conducting fluid heated steadily from below and studies on thermal turbulence and investigations with Dr. Veronis on electro-convective processes in dielectric fluids. Experimental or observational confirmation of some of this work has already been achieved.

In theoretical and experimental work on electro-convection it is possible to deal with convective cells and transitions from one regime of flow to another under easily controlled and precisely measurable conditions. Aside from the fact that these flows are interesting in themselves, there also exists a direct analogy between such systems and the thermally convective ones which are of basic interest in meteorology and oceanography. For example, the electric potential is the analogue of temperature, electric current of heat flow, and the superposition of a magnetic field imposes forces which are analogous to Coriolis forces.

The work of the theoretical group at Woods Hole is becoming recognized as outstanding throughout several related areas of science. For example, the theory of turbulence set forth by Dr. Malkus over recent years is a significant fundamental contribution to the understanding of all flow processes and will undoubtedly prove of great value in oceanography, meterology and astronomy. The explanation of vertical temperature distribution in the ocean and the model for abyssal circulation by Mr. Stommel and others are conceptual developments that have proven to be immensely stimulating to physical oceanographers. The contributions to an understanding of non-linear phenomena are of far-reaching importance and can be expected to contribute immeasurably to the theoretical understanding of natural phenomenon. Over the past three years an inspiring series of colloquia have been held jointly with the Meterology Department of the Massachusetts Institute of Technology and have proven to be a source of stimulation for all concerned.

Marine Meteorology

The instrumentation of the Institution's R4D airplane was continued throughout the year and two flights were made to the Caribbean area in February and November to study turbulence, heat and water vapor flux and the effects of clouds upon the flux in the environment. Net radiation measurements were made at various altitudes in the trades by an airborne radiometer designed by Mr. David B. Clarke.

The turbulence and heat flux data reduction problem has been eased with the development of a vertical velocity computer by Mr. Andrew F.

Bunker for use in the aircraft and by programming these data for the Arthur D. Little, Inc., "Datatron" computer. These steps have reduced reduction time by a factor of eighty.

The relation of the vertical flux of heat in the air-to-air stability, the relative importance of the water vapor flux and the interpretation of these measurements as obtained from the field data are discussed by Mr. Bunker in a paper that has been submitted for publication.

The results of a 1957 CRAWFORD cruise were reported by Mr. Michael Garstang. This expedition brought back the first documentation of an early-stage tropical vortex in the low latitudes (5° N), unhampered by land effects. Many of the computations described in the report were not previously possible.

The analysis of the cloud films obtained by Dr. Joanne S. Malkus and Mr. F. Claude Ronne in flights over the Pacific Ocean in MATS Globemaster aircraft during the summer of 1957 progresses well. This work is being done in conjunction with Professor Herbert Riehl and associates of the University of Chicago who are carrying out an intensive synoptic study of the period investigated. Several exciting results have emerged, among them being (1) the controlling role on cumulus structure played by the large-scale flow patterns and (2) the degree of organization of oceanic cumulus clouds into lines, particularly in convergent regions.

Dr. Malkus has also been working with Dr. Riehl on a problem concerning the dynamics and energetics of the hurricane rain area and the question of how latent heat is released to establish the pressure gradients which maintain the flow against friction and maintain winds of hurricane strength.

Mr. Joseph Levine has evolved recently a theoretical model described in a paper entitled "Spherical Vortex Theory of Bubble-like Motion in Cumulus Clouds" which mathematically predicts bubble behavior (cumulus convection) under given conditions. Dr. Malkus has extended this model to hurricane clouds and with data furnished by the National Hurricane Research Project (West Palm Beach, Florida) has developed theoretical models of hurricane cumulonimbus convection. These cloud towers play a major role in the mass and heat budget of the storm and are vital in maintaining its pressure gradients. The accumulated work of this group under Dr. Malkus has resulted in a greatly improved understanding of hurricane formation and maintenance.

Work on the salt nuclei project has proceeded during 1958 with Mr. Alfred H. Woodcock, Mr. Duncan C. Blanchard and Mr. Allard T. Spencer being engaged in various phases of the study. Mr. Blanchard, who recently returned from M.I.T. where he has completed his course work for a doctorate in meteorology, spent the summer months in the laboratory attempting to determine if the composition of droplets as they are initially ejected by bubbles bursting at a sea-water surface is identical to the composition of sea water. During the fall he began his present study of the origin of the charge which he had previously found on droplets ejected by bursting bubbles.

Mr. Woodcock and Mr. Spencer made two field trips with Mr. Bunker during the spring and fall on the R4D aircraft to the West Indian area. Their purpose was to add to our information on the distribution of salt particles as a function of altitude and wind force. The airborne flame photometer was used in testing some ideas about the effects of trade-wind cumulus clouds upon aerosol concentrations. The need for detailed exploration of the sea-salt load of the air in and around clouds originated from the idea that high concentrations of salt will significantly alter the humidity at which latent heat is released within masses of salt-laden air.

Mr. Spencer used most of his time in an attack upon the instrumental problems associated with the use of the flame spectophotometer within clouds. An effort to achieve a full recorder response to the great short-duration differences in signal strength from the photo-multiplier led to a modified approach to the problem of measuring the weight of sodium in cloud droplets and the number of these sodium-bearing droplets.

Mr. Woodcock expanded further his extensive data on the distribution of sea-salt particles in the atmosphere in order to learn more about the contribution of these particles to the well-known salt cycle (ocean-atmosphere-continent-ocean), and to explore further the precipitation mechanism in marine cumulus clouds by tracing the salts in the airborne particles to the salts in solution in the rains.

Geophysics, Underwater Acoustics and Geology

The year 1958 was a sea-going year for the underwater acoustics and geophysics group at the Institution. The Coast Guard Cutter YAMACRAW worked in the Gulf of Mexico during January and February, south of Cuba during April and in the Mediterranean from June to September. The YAMACRAW then made her last cruise for Woods Hole in October to the Tongue of the Ocean, returning to Savannah, Georgia, where all laboratory equipment was transferred to USNS CHAIN. The CHAIN's first cruise was from Savannah to Woods Hole in November making observations on the Blake Plateau en route. A December cruise of the CHAIN to Bermuda and return was shared with Dr. Ketchum's group to complete the year's cruises for the YAMACRAW and the CHAIN.

The ATLANTIS made an extended cruise to the Indian Ocean, the Red

Sea, and worked in the Mediterranean with the YAMACRAW and the VEMA of the Lamont Geological Observatory.

The BEAR was used by the group for a two-week cruise on the shelf of Long Island in August and made numerous short cruises near Woods Hole.

R/V ASTERIAS was used on many local cruises and also made several cruises to the Gulf of Maine for ambient noise studies.

The underwater acoustics work, headed by Dr. J. B. Hersey and Dr. Earl E. Hays, is providing a better understanding of sound propagation in the oceans by studying the effects of the water temperature structure, bottom topography and other associated features on sound transmission. Such studies were pursued on all these major cruises which are described in more detail below.

Dr. Hays led the two cruises to the Gulf of Mexico and Caribbean Sea which had the principal objectives of studying the relationship between sound transmission and the horizontal and vertical sound velocity variations in the ocean and in testing and making shallow temperature measurements with the new thermistor chain. The chain towed very successfully, but somewhat more time and effort were required to fit it to the winch than had been anticipated.

The four month cruise of the YAMACRAW in the North Atlantic and western Mediterranean Sea had a program of bathymetric, thermometric, acoustic and seismic measurements. Chief scientists for different portions of the trip were Drs. Hersey, Backus, Hays and Mr. Allyn C. Vine. Members of the scientific party included nine summer student employees. Introductory classes in oceanography were conducted daily for these students during the first Atlantic crossing. Later the party on the YAMACRAW worked with the ATLANTIS and the VEMA while they were returning from a cooperative cruise in the Indian Ocean and Red Sea.

On the westward passage of the Strait of Gibraltar, Mr. Roberto Frassetto of Hudson Laboratories, Columbia University, joined the ship to make observations of water exchange over the sill at Gibraltar. Mr. Vine made subsurface current measurements with the parachute drogue technique, but most of the available time was spent in making 78 north-south temperature sections across the straits with the thermistor chain. This operation placed heavy demands on the ship handler because of the confined waters, the heavy east-west traffic and a ship with an effective 600-foot draft. An excellent series of temperature sections spanning several tidal cycles resulted from this work, and we are most appreciative of the efforts of the captain and crew of the YAMACRAW for their considerable contribution to this difficult project. A clearer picture of the water flow between the Mediterranean Sea and the Atlantic Ocean has resulted from this work. A combination of information from the Precision Graphic Recorder and the thermistor chain indicated that the lower boundary of the scattering layer stayed close to one of the isotherms.

Various staff members had a key role in the ATLANTIS cruise into the Gulf of Aden in the Indian Ocean by way of the Mediterranean and Red Seas. Mr. Thomas R. Stetson took charge of bathymetric measurements from Woods Hole to Suez. Dr. John W. Graham acted as chief scientist on a program of seismic refraction measurements with the VEMA, hydrographic and bathymetric measurements, and bottom photography from Suez to the Gulf of Aden and return. Mr. Richard S. Edwards supervised a program of seismic refraction measurements with the VEMA, sound transmission measurements with the YAMACRAW and continuous bathymetric observations from Suez to Cadiz, Spain. Mr. Jan Hahn supervised a program of bathymetric and bathythermograph measurements between Cadiz and Woods Hole.

During the fall, Dr. Hays supervised the general environmental study of the Tongue of the Ocean, Bahamas. This included bathymetric, temperature and sound-velocity measurements of the water and studies of reflection of sound from the bottom. Interesting observations of large internal waves were made with the continuous temperature recorder. These may have resulted from a hurricane which passed through the area shortly before the measurements were made.

The work with seismic reflection techniques has continued to expand and there has been considerable commercial interest in it as well. In particular Dr. Charles B. Officer, Jr., an Institution Associate and former staff member, applied for permission to use the WHOI "Seismic Profiler" for commercial exploration. Dr. Officer has pursued a vigorous program including surveys along the Gulf Coast, the West Coast, in the Great Lakes, in Nova Scotia, in the Persian Gulf, and off the Nigerian Delta and more recently in Alaska. As part of our agreement with Dr. Officer we will exchange technical improvement and he will report to us the scientific content of his findings.

Our own work with the Seismic Profiler has included completion of the Narragansett Bay survey for the Corps of Engineers, plans for which were reported last year. The field work was carried out by Mr. Don R. Fink and Miss Elizabeth T. Bunce. Mr. Sidney T. Knott, Jr., also made a most interesting series of profiles over the outer part of the continental shelf south of New England last summer, and several of our staff have assisted students in using the Seismic Profiler to help to understand problems of local submarine geology. Both Mr. Fink's and Mr. Knott's work clearly demonstrate the potential value as well as the several pitfalls of this technique as a tool for study of shallow water sediments. In Narragansett Bay the depth of bed-rock could be measured over much of the west passage around Conanicut Island and along the sides of the east passage. The overlying sediment, probably largely deposited by glaciers but with a thinner deposit of recent sediments, was charted in some detail. Mr. Knott's study over the continental shelf indicates that the structure near the edge is dominated by bedding that dips seaward capped by nearly flat-lying beds. Profiles across the Hudson Canyon show that it is cut through flat-lying beds on the shelf.

Repeated attempts have been made to use the Seismic Profiler to record soundings below the bottom in deep water. While limited success has been achieved, it is evident that our present sound source is too weak to overcome the problems of depth and the sea noise which must be put up with if the ship is to move about while recording. Improvements are steadily being made in the sound source and in reducing noise, hence it is expected that echo sounders of the near future will allow charting of the bottom sediment structures as well as water depth in vast ocean areas.

Relative to this same question of shallow sediment structures in deep water, our efforts to improve the resolving power of deep-water echo sounders have paid interesting dividends. Using our fish-shaped transducer on the YAMACRAW during the Mediterranean cruise it was found possible to sound at 10 knots cruising speed while employing an exceedingly short sound pulse or ping (0.5 milliseconds). Echoes the equivalent of two feet apart in travel path could thus be resolved. In places where the bottom is smooth-looking to the echo sounder we have frequently found that two or more echoes are consistently recorded in such a pattern as to suggest that the later ones are reflections from layers below the bottom. This interpretation of echo sounder records is best confirmed by sampling the bottom with long cores. Fortunately one series of such recordings was made in the Tyhrennian Sea off Naples by Dr. Hersey on the YAMACRAW last summer which are within 50 miles of a coring station of the Swedish Albatross Expedition. The reflections recorded by the echo sounder match very closely with volcanic ash beds in the log of this core. Elsewhere in the western Mediterranean, Dr. Richard H. Backus recorded many more of these multiple echo sequences, suggesting not only flat-lying sediment structures but also local slumping where the beds are sloping. While crossing the flat abyssal plains of the North Atlantic, YAMACRAW echo soundings frequently showed multiple echo sequences, suggesting thin bedding (two to ten feet) below the bottom; occasionally over the eastern part of the Atlantic passage multiple echo sequences were observed similar to those described for the Mediterranean.

The geological group headed by Dr. John M. Zeigler has also worked on several sedimentation problems. The interrelationship of water and sediment movement in the surf zone and nearshore areas has been studied in collaboration with Professor Robert C. Miller of the University of Chicago. A point has been reached where it is possible to predict the sediment pattern from sea state and such predictions are being tested by comparing the predicted pattern with the actual depositional situation. Problems relating to the fall velocity of sand in water were examined by a specially designed settling tube which makes a rapid mechanical analyses of the sorting sands. Many of the problems related to the general operation of settling tubes have been examined and the mathematics have been condensed into graphs and tables. The geological aspects of the continental shelf off South America were investigated during a winter cruise on the ATLANTIS. This work has encouraged the Venezuelans to study oceanography and it appears they are going to establish an Oceanographic Department in the Government. Mr. William D. Athearn has examined most of the material from the Cariaco Trench and Dr. Zeigler is working on sediments from the Gulf of Venezuela. Interest of the various oil companies is quite high because of the possibility that this Gulf will one day be an important oil province.

Professor Raymond Siever of the Harvard University Geology Department is associated with the Institution's geology program. His investigations during the past year have been particularly concerned with the geochemistry of silica in the interstitial material in sediments. He has also continued to work up cores obtained by Mr. Henry C. Stetson on his last cruise on the ATLANTIS.

Dr. Graham has continued his interest in manganese nodules. His analysis of collections made on the Blake Plateau led him to re-examine the possibility of biological concentrating agents, an old approach which has not been entertained seriously in recent years. He has thus constructed an hypothesis which supposes the existence of nuclei of heavy ions chelated by organic molecules, such as the amino acids. These he supposes are absorbed as food by micro-organisms which dispose of the heavy ion, whether manganese, cobalt, iron or other elements in nodular form or as encrustations. Mr. Worthington has been collecting bottom samples in the course of his more recent hydrographic observations. These appear to support Dr. Graham's hypothesis.

Dr. Backus and Dr. Hersey have continued their study of the deep scattering layers, having received a grant from the National Science Foundation to this end. A new instrument which permits direct acoustical and photographic examination of individual sound scatterers was designed and built by Mr. Thomas H. Gifft. This makes use of a clever combination of directional effects in the receiving part of the acoustical apparatus to insure that a scatterer is near the center of view of an underwater camera when it is automatically triggered. Observations of sound scattering with explosive sources have been extended by recording several dawn and sunset migration sequences of the layer both in the Atlantic and the Mediterranean. It is evident from these observations that dawn and sunset migrations are indeed different with respect to their depth/frequency relationships. Dr. Per F. Scholander has predicted that they would be different if the scattering is from the swim bladders of fishes as suggested, since the mode of accommodation to increasing and decreasing pressure would be expected to be different.

The investigation of sound scattering by fishes of the deep scattering layer, and the study of the sounds made by fishes and cetaceans which continue to interest Dr. Backus and Mr. William E. Schevill, have been greatly aided by the visible speech wave analyzers developed some years ago at the Bell Telephone Laboratories. The discoveries in oceanographic acoustics which these instruments facilitated have put such an analysis load on our staff that the original instruments have been made nearly obsolete. During the past year, several of the staff have examined ways of improving and speeding spectrum analysis of the transient sounds of interest here, and they are hopeful of putting together new equipment that is both better and within our means.

Geochemistry

Studies of the horizontal and vertical distribution of the fallout radioisotopes, strontium 90, antimony 125, cesium 137, cerium 144, and promethium 147, have been continued. This program, under the direction of Dr. Vaughan T. Bowen and Dr. Thomas T. Sugihara, is currently supported by contracts with the Atomic Energy Commission and the Office of Naval Research and by portions of the I.G.Y. funds from the National Science Foundation. A summary of the analytical data up to August 1, 1958 has been published as has a description of the analytical methods employed.

Sample collection for this program has continued at a rapid rate and has been stimulated by the construction of new samplers of an improved design. With these samplers four stations were made from the CRAWFORD in July between Woods Hole and Bermuda, one from the BEAR in September on the continental shelf south of Montauk, one from the PANULIRUS in October off Bermuda, two from the CRAWFORD in November on the equator, one from the CRAWFORD in March north of Bermuda and one from the PANULIRUS in April off Bermuda. Mr. Henri Caron and Dr. Sugihara supervised the last two stations and Dr. Bowen all the others.

The complicated and prolonged operations involved in chemical processing and low-level beta counting of these samples continues to produce a disheartening lag between collection and completed analysis. This has been significantly eased by having, since June, Mr. Caron to assist Dr. Sugihara on a full-time basis. The group now has, among other interesting sets of data, three stations analyzed from the Sargasso Sea, July 1957, December 1957 and July 1958. The consistent shape of the curves for Sr^{90} from surface to 1,000 meters where it is now readily detectable indicate, as we hoped, that these data will provide a unique approach to the measurement of vertical mixing. Comparison of the surface values for December and for July indicates that these may provide a measure of the seasonal value for rainfall in remote ocean areas.

The ratios of Sr^{90}, Ce^{144}, Pm^{147} in surface samples even from low-productivity areas of open ocean indicate that some process — sedimentation on particle surfaces is postulated — rapidly removes the latter two isotopes from the upper layers of the sea. At 8° S, 7° E the cerium-promethium ratio at 300 meters indicated a decay time since production of about 2.7 years, and that at 800 meters a decay time of about 4.4 years, whereas surface values very rarely indicate more than one year of decay. Accumulation of more of this type of data, combined with analyses, already begun, of the isotope ratios in plankton and detritus in both shelf and offshore areas, should give us new insight into the relative importance and effective rates of biological and inorganic processes in sedimentation.

As a by-product of Dr. Herbert Curl's analyses of the composition of various plankton species, a large number of ash samples have been prepared for spectrographic analyses. One group of eleven samples was analyzed by Dr. Geoffrey D. Nicholls of the Department of Geology, University of Manchester, England, during his tenure of a fellowship at the Massachusetts Institute of Technology. The appointment of Dr. Nicholls as Associate in Geochemistry on the research staff of the Institution projects a continued collaboration in Manchester on this interesting work. This program is giving us new insight into the diversity of chemical behavior taking place within the various forms of planktonic life. Combined with the data on population composition and size being obtained as part of the broad plankton program under Dr. Ketchum, these analyses permit quantitative evaluation of the biota as factors in the marine geochemistry of the rarer elements.

A reliable and sensitive method for vanadium analysis has been worked out and Miss Sybil A. Campbell has been accumulating data, mostly relevant to radioactive tracer experiments made in 1957 by Dr. Bowen and Professor L. S. Ciereszko of the University of Oklahoma. Culture conditions are being established for several local tunicates, both accumulators of vandium and non-accumulators; also conditions for inducing production of larvae by some of these tunicates is being studied. In the next few months an intensive attack on the questions of uptake mechanisms for vandium, of vanadium-phosphate competition and metabolic cycles of vanadium and niobium in ascidia will be started.

The biological deposition of silica by diatoms and factors affecting its resolution after the cells die have been under investigation by Dr. Joyce C. Lewin. In order to gain information concerning the nature of the organic membrane upon which the silica is deposited by the living diatom cell, ultrathin sections of various species have been examined with the electron microscope. The physiology of *Phaeodactylum tricornutum*, an unusual marine diatom with unsilicified (or only partially silicified) cell membranes, has been studied in detail with a view to understanding and controlling the complete life cycle. For sustained growth of *Navicula pelliculosa* high concentrations of calcium are required, correlated with the observed fact that this cation is essential for silica deposition.

Studies have been carried out on the dissolution of silica at 20° C from marine plankton diatoms, from fresh-water diatoms grown in culture in the laboratory and from fossil diatom walls. The ability of certain cations to combine with the silica walls and inhibit their subsequent dissolution has been studied.

Vitamin requirements and heterotrophic growth studies on forty-four pure cultures of marine littoral diatoms have been completed.

Dr. Richard G. Leahy has continued the studies of atmospheric CO_2 variations which were begun early in the I.G.Y. Data collected along the eastern coast of North America have continued to indicate a high degree of variability in CO_2 levels, and the records obtained are very similar to those reported by the Scandinavian network. These measurements have been made at both local ground stations and from the Institution R4D aircraft. The vertical profiles made in the aircraft indicate a greater range in CO_2 level than was expected before the sampling program was undertaken.

Biology and Chemistry

The studies of the biology and chemistry of marine plankton populations have been continued. In May 1958 two years of observations were completed at a series of stations which provided two cross sections of the continental shelf and some stations in the slope water just beyond the edge of the shelf. In these field observations the conditions ranged from coastal waters with depths of 30 meters to observations where the depth was greater than 2,000 meters. Thus a wide range of conditions was obtained. In 1958 the cruises were extended seaward on a section from Montauk Point, Long Island, to Bermuda. The inshore seven stations of this section repeat some of those previously occupied on the continental shelf, but the extension provides the opportunity to make studies of the deeper water, to observe the unique populations in the Gulf Stream and to include the truly oceanic conditions of the Sargasso Sea in our investigations.

This program continues to be supported jointly under a contract with the Atomic Energy Commission, by several grants with the National Science Foundation and by Institution funds. The work under the AEC contract is supervised by Dr. Bostwick H. Ketchum and Dr. Vaughan T. Bowen. Dr. Ketchum and Dr. John H. Ryther are principal investigators on the associated NSF grants.

At the Conference on the Peaceful Uses of Atomic Energy held in Geneva in September, Dr. Ketchum presented a paper prepared in collaboration with Dr. Bowen entitled "Biological Factors Determining the Distribution of Radioisotopes in the Sea." This was the only U. S. paper selected for presentation at the session dealing with the marine sciences. A paper by Dr. Bowen and Dr. Thomas T. Sugihara "Marine Geochemical Studies with Fall-out Radioisotopes" will be published in the proceedings of the Conference but was not presented orally at Geneva.

Studies of the distribution of the essential plant nutrients, particularly phosphorus and nitrogen, have been an integral part of our plankton investigations. A general description of the annual cycle in the coastal waters has been submitted for publication by Dr. Ketchum with Mr. Ralph F. Vaccaro and Mr. Nathaniel Corwin. Mr. Charles S. Yentsch and Mr. Vaccaro have completed and published the results of laboratory and field studies of the relationship between the available nitrogen and the chlorophyll content of the plant cells.

Dr. Mary Sears and Miss Constance W. Chadwick have continued the analysis of the zooplankton and Dr. Edward M. Hulburt is identifying species of phytoplankton collected during our coastal and Bermuda cruises. Dr. Sears has also done a splendid job of organizing the first International Oceanographic Congress which is sponsored by the American Association for the Advancement of Science in cooperation with UNESCO and the Special Committee for Oceanic Research (SCOR) of the International Council of Scientific Unions. This Congress will be held in September of 1959 at the United Nations headquarters in New York City. At least 600 oceanographers from all over the world are expected to participate in this Congress.

In the fall, Mr. John H. Steele of the Fisheries Laboratory at Aberdeen, Scotland, visited Woods Hole on one of our fellowships. He and Mr. Yentsch studied the effects of deficiencies of nutrients in algal cultures upon the sinking rate of the cells. They found the deficient cells sank more rapidly than those that were grown in adequate media. This observation may help to explain the accumulations of chlorophyll below the zone of optimum photosynthesis, frequently observed when the nutrient conditions in the water are poor. Also, in cooperation with Mr. Vaccaro, it was found that deficient cells excrete nitrite while assimilating nitrate from water. This observation may help to explain the maximum concentrations of nitrite which are found below the illuminated zone in the summertime. It has previously been thought that these must be due to nitrifying bacteria, but our extensive studies of this process have failed to isolate the appropriate bacteria from the water. If the nitrite is formed by the phytoplankton rather than by bacterial action it may help to explain many of the poorly understood distributions of nitrogen compounds in the ocean.

Dr. Stanley W. Watson has continued his bacteriological studies and has determined, at several stations, the rate of oxygen consumption in samples of water collected from various depths. Direct observations of bacteria on fine filters have demonstrated many forms which are not found by previous methods of counting. Attempts will be made to isolate, culture and identify these unknown microscopic specimens.

Dr. Herbert Curl, Jr., has completed an extensive study of the environmental factors which influence the growth of an important coastal diatom, *Skeletonema costatum*. The results of this investigation on the interaction of nutrients, light and temperature appear to correlate closely with seasonal distribution of this common diatom. Dr. Curl has also continued the collection of plankton samples for spectrographic elemental analysis. The differences in the elemental composition of the various species will influence greatly the fate of radionucleides which may be added to the sea either through fall-out or as waste materials resulting from the development of atomic energy.

Dr. Ryther has continued his studies of the primary production of organic matter in the sea. Routine measurements of productivity have been made on all of the Woods Hole-Bermuda sections as part of the plankton program described above. In addition, Dr. Ryther has been directing a similar, though more limited, plankton investigation in the Sargasso Sea off Bermuda. This study has been carried out by Dr. David Menzel from the Bermuda Biological Station and has made use of their facilities including the Research Vessel PANULIRUS. It has involved routine hydrographic, chemical, and biological measurement at two-week intervals throughout the year at a station 15 miles southeast of Bermuda in 1500 fathoms of water. A unique record of the annual cycle of primary production and the related chemistry and hydrography of these semitropical waters has been obtained.

In addition to the measurement of primary production in these two areas, studies of the environmental physiology of the phytoplankton under natural conditions have been undertaken whenever possible. Examples of such work include two manuscripts currently in press, one dealing with light adaptation of the plankton algae living under conditions of low illumination at the lower limit of the euphotic zone, the other demonstrating that iron and/or other trace metals and silicon, rather than nitrogen and phosphorus, may be the principal limiting factors to organic production in the nutrient-poor Sargasso Sea.

In the laboratory, Dr. Robert L. Guillard has developed a collection of some 75 species of plankton algae including representatives of all the major algal groups, mostly in bacteria-free or "pure" culture. This collection, probably unique in the world, has proved extremely useful both to biologists at Woods Hole and elsewhere and is becoming widely recognized. Dr. Guillard and Dr. Ryther are currently undertaking a study of the taxonomy and physiology of several closely related species of small diatoms collected from widely differing types of marine environments.

In addition to these specific research problems, Dr. Ryther has prepared two review papers on the productivity of the seas. The first was included as part of a symposium on "The Physiology of the Algae" sponsored by the AAAS at its annual meeting in Washington in December 1958. The second is part of an NSF-sponsored symposium on "The Ecology of the Algae" to be given at Pymatuning, Pa., in June 1959.

The extension of our cruises to include crossings of the Gulf Stream has permitted a study of the distribution of phosphorus compounds in the deeper waters of the North Atlantic Ocean. In general, organic compounds of phosphorus are not found in water much deeper than 1000 meters in the Atlantic Ocean. However, in water of depths greater than 2,000 meters directly below and to the south of the Gulf Stream, high concentrations of organic phosphorus have been found on all of our crossings. A similar observation was made for the first time in crossings of the Gulf Stream by Mr. David A. McGill during one of the I.G.Y. cruises in 1957. It is interesting that these concentrations of organic phosphorus occur in just the region where one would expect to find the recently described deep countercurrent below the Gulf Stream. The presence of the organic phosphorus at these depths suggests that the water is comparatively "new" and had recently been near enough to the surface to accumulate these organic compounds before sinking.

The cruises of the I.G.Y. have again given us an opportunity to extend our observations of the distribution of phosphorus throughout the North and South Atlantic Oceans. On these same cruises, samples of chlorophyll have been obtained in the surface layers so that estimates of the productivity of the different waters can be made. Mr. McGill accompanied the CRAWFORD on Cruise #22 when two sections were completed in the South Atlantic Ocean, one at approximately 24° S and the other on the Equator. Mr. John L. Shilling accompanied CRAWFORD Cruise #17 during which the eastern North Atlantic and the Caribbean were traversed by five sections.

Dr. Francis A. Richards and Dr. Curl accompanied a cruise to investigate the hydrography and biological and chemical oceanography of the north coast of South America from Trinidad to the Gulf of Darren, and to repeat observations on the anaerobic basin, the Cariaco Trench. Dr. Richards has analyzed the data with particular attention to the nitrogen cycle. Ammonia, the only nitrogen compound found in the anaerobic water, was measured by a new method, and the nitrogen/argon ratio and the nitrogen isotope ratios have been determined by Dr. Bruce B. Benson of Amherst College. These data demonstrate the release, under anaerobic conditions in the Cariaco Trench, of free nitrogen from nitrogen of organic origin, permitting the striking of a nitrogen balance on the water column. Samples from the Dramsfjord in Norway have also been analyzed with similar results.

Dr. Richards has also completed an analysis of the distribution of silicate in the western Atlantic and Caribbean. In much of the water column, silicate concentrations are closely correlated with phosphate and nitrate concentrations, thus relating silicate to the biological cycles of phosphorus, nitrogen and oxygen.

As co-chairman of a special committee appointed by the editor of the Journal of Marine Research, Dr. Richards shared in the arrangements for the publication of a special volume of that journal honoring the 70th birthday of Professor Thomas G. Thompson of the University of Washington, and most of the editing of the volume was completed.

Dr. George L. Clarke and Mr. Lloyd R. Breslau obtained quantitative records of luminescent flashing of animals at great depths in the Mediterranean Sea during a visit to the Oceanographic Institute of Monaco. The amount of bioluminescence was found to be decidedly less than in the waters of the North Atlantic, but the vertical distribution of flashing organisms was similar in both locations. Additional observations with the light-triggered camera suggest that most of the flashing organisms in the depths are too small to be photographed. Some excellent photographic records of deep-water coelenterates and crustaceans have been obtained, however. A series of measurements of light conditions with records of bioluminescence was made from the CRAWFORD during August at stations to the south, east and north of Cape Cod. Luminescent flashing was encountered at every station from the shallowest on Georges Bank to the deepest in the Gulf Stream. The results indicate that bioluminescence occurs far more generally and is of greater ecological significance in the deep sea than previously supposed. A portable photometer suitable for use with a small boat but with the same degree of sensitivity as the larger bathyphotometer has been developed.

Drs. S. M. Marshall and A. P. Orr of the Marine Biological Station, Millport, Scotland, visited the laboratory in the spring on Institution fellowships. With Dr. Robert J. Conover, who joined the project in March, they completed a series of feeding, respiration and excretion studies on the copepod, *Calanus*. They found a surprisingly rapid excretion of phosphorus in these studies, suggesting that the importance of zooplankton in returning nutrients to the ecological cycle may have been underestimated. Dr. Conover is continuing these studies on neritic and oceanic zooplankton.

Dr. Raymond G. Stross held a fellowship from the National Institute of Health and worked in the Institution during 1958. His studies were concerned with the interrelationships between phytoplankton and zooplankton. Dr. Jack McLachlan, also an NIH Fellow, worked at the Institution on studies of the physiology of algal cultures.

Dr. Edward R. Baylor continued his investigations on dark adaptions in horseshoe crabs, copepods and honey bees and examined the dioptrics of marine invertebrate visual systems. He also has pursued the question of polarized light detection to satisfactory conclusions for the horseshoe crab (*Limulus*), the bee and a snail (*Nassa*).

Mr. Harry J. Turner has continued his studies of the commercial shellfish in local waters. The productivity of a large population of quahogs in the waters of Nantucket Sound was evaluated by bringing specimens into the laboratory, holding them under warmer conditions and attempting to stimulate spawning by adding suspensions of sperm. This system invariably produces spawning in breeding stocks of quahogs. However, the quahogs from the deepest parts of Nantucket Sound would not spawn under these conditions. It appears, therefore, that this population is not the source of new seed for commercial stocks of quahogs, although it was the opinion of the local clamdiggers that this was an important source. Studies were also made of the transplanting and growth of European oysters in local waters.

Mr. James E. Hanks has completed his course work for the Ph.D. degree at the University of New Hampshire and has been conducting his thesis research at the Institution under the direction of Mr. Turner. His problem is concerned with the breeding and early life history of three species of the clam drill, *Polynices*. It appears that in the natural environment the time of settlement of the drills is nicely synchronized with that of the shellfish. Because of the voracious appetite of the drills they consume enormous quantities of freshly settled shellfish, and this may be the explanation of the failure of many sets of clams to mature to the adult and edible size.

Dr. Howard L. Sanders has continued his investigations of the benthic animal communities in Buzzards Bay. He has recently completed a paper concerned with the structure of the animal assemblages present in the softer sediments. Dr. Sanders is also studying the morphology, development and ecology of the remarkable crustacean, *Hutchinsoniella macracantha* and its significance to the understanding of evolution of crustaceans. He presented some of these findings last summer at the International Zoological Congress in London.

Dr. John W. Kanwisher has studied the carbon dioxide balance in sea water using an equilibration system and infrared analyzer. The CO_2 tension increases rapidly with increases in total carbonate and with temperature. At constant temperature, measurement of CO_2 tension gives a sensitive index of biological activity. These studies of the equilibrium between CO_2 and sea water indicate that the CO_2 released by the burnings of fossil fuels has been effective in increasing the atmospheric CO_2 content.

Dr. Wolfgang Wieser of the University of Vienna is making a study of quantitative distribution of nematodes using respiration measurements to assess their metabolic importance. A Cartesian diver system has been built capable of measuring the respiration of individual small animals. The distribution of a varied bottom fauna that can survive for weeks in the laboratory without oxygen is being correlated with the chemistry of the bottom habitat as defined by oxygen tension and oxidation reduction potential. We are haunted by the uncertain implications of taking animals from such an environment and measuring their oxygen uptake.

A paper by Dr. Henry B. Bigelow and Mr. William C. Schroeder describing four new species of skates from the Gulf of Mexico was published in July 1958 and they have completed an account of the family Osmeridae, the capelin and smelts, to be included in Part 3 of "Fishes of the Western North Atlantic." At present they are working on a very interesting collection of batoids (skates and rays) received from Mr. Harvey R. Bullis, Jr., collected by the U. S. Fish and Wildlife Service Research Vessel OREGON, chiefly between Trinidad and the Equator, in depths down to about 400 fathoms in a region that had not previously been fished with otter trawls. Mr. Schroeder completed a report on the offshore lobster fishery and the deep-water red crab, the latter as yet unexploited but which at some future time might prove of importance commercially.

The research program dealing with the biology of the larger pelagic fishes, supported by a grant from the National Science Foundation, has progressed under the direct supervision of Mr. Frank J. Mather III. The collection of biometric and other biological data has yielded desirable information especially for the tunas and the amberjacks. Sport fishermen have continued to cooperate in the tagging of pelagic gamefish. Mr. Mather conducted a research cruise to the southeastern Bahamas, sponsored by Mr. Louis E. Marron, an Associate of the Woods Hole Oceanographic Institution, carried out on his cruiser, EUGENIE VIII. In November Mr. Mather delivered a paper concerning the amberjacks (*Seriola*) of the western Atlantic at the International Gamefish Conference at Miami Beach, Florida.

Oceanographic Instrumentation

During the summer Mr. Allyn C. Vine undertook to design a deep-water mooring for an automatic weather station for the middle of the Gulf of Mexico. This boat-shaped buoy, 20 ft. by 12 ft., contained electronic weather sensing and telemetering equipment. The buoy was built by the David Taylor Model Basin and instrumented by the National Bureau of Standards. With the cooperation of the Coast Guard the mooring was set out in early September and promptly rode out near-hurricane force winds when Hurricane Ella passed within 50 miles of its position. This mooring utilizes the positive buoyancy of the new polypropylene line to minimize fouling and chafing on the bottom while using heavier-than-water dacron line to minimize it at the surface. Attacks by sharks are considered to be the only serious threat to this type of mooring.

The electronics group, under the direction of Mr. Robert G. Walden, spent about forty percent of its time on the installation and maintenance of navigation and communication equipment aboard the various vessels of our fleet. The remaining time was devoted to assistance in instrumentation for various projects and to the program in buoy development. A transponding telemetering buoy which is an exact copy of the one designed by Messrs. Walden, David D. Ketchum and David H. Frantz is now available commercially. This has relieved the electronics group of construction of these useful devices and more time has been spent on assisting various projects in using them and in working on new techniques of data transmission. The buoys now have a reliable telemetering range of over 100 miles.

Mr. Frantz has constructed a data processing system for these buoys which permits the storage and later transmission of eight temperature measurements. The temperature data are telemetered digitally and may be obtained at preselected times or at any desired time by radio interrogation. He has also continued his work on the "pop-up" buoy as an instrument vehicle and has been working on the problem of anchoring surface buoys in the deep sea.

Mr. Harlow G. Farmer, Jr., with the assistance of Mr. Ketchum, has continued his work on surface waves. During the summer a tower was set up in Buzzards Bay on which wave recording instrumentation was installed. This consisted of a series of fine wires whose resistance is changed by the passage of the waves. The information from the wires is telemetered to the laboratory by means of a VHF radio link and is processed to give a measure of wave height and slope. The data are automatically reduced to digital form and stored on punched tape for later conversion to IBM cards for machine computation of energy spectra.

Dr. Charles J. Hubbard and Dr. William S. Richardson have completed an underwater spectrometer which records on deck the spectral distribution of underwater light. They also changed the recording system of the towed thermistor chain so that it automatically contours the depth of isotherms as the ship proceeds on course. This equipment was towed by the USCGC YAMACRAW to the Mediterranean during the summer and fall and on several coastwise cruises. During the late fall it was transferred to the USNS CHAIN and modifications to improve the electronics were started.

Mr. Gordon H. Volkmann has been engaged in the development of a neutrally buoyant "pinger" of the Swallow-type for use in the direct measurement of deep currents. During the sea tests two pingers were followed long enough to provide a measure of the current, one off Woods Hole and one off Eleuthera in the Bahamas. While of no significance in themselves, it is hoped that they will form part of a series of measurements of the deep currents along the western boundaries of the ocean. With the series in the central ocean areas planned by Mr. Henry M. Stommel and Dr. John C. Swallow, we hope for a better understanding of deep circulations.

For many years ocean seismographers have been thwarted in their attempts to observe near the bottom elastic waves that have traveled through the bottom. Mr. Willard Dow has successfully completed development of telemetering circuitry for a hydrophone that may be suspended to any ocean depth on a single conductor well-logging cable. This hydrophone has been tested and used routinely in receiving sounds at depths greater than 2000 fathoms. Thus this design is a promising candidate for a deep detector, and should prove extremely valuable in resolving some of the questions of sediment structures at shallow depth below the bottom in deep water.

The relative inaccessibility of the ocean floor for direct observation has long made underwater photography a valuable tool to the geologist, but he has been somewhat hampered and discouraged in its use by camera design, which limited the control he could exercise over his observations. The development by Dr. Harold E. Edgerton of the Massachusetts Institute of Technology of a repeating camera that can be positioned above the bottom by means of an acoustic link has greatly increased the attractiveness of this instrument. This year he has put together a stereoscopic camera designed with an improved acoustic link which Dr. John W. Graham employed in seven locations in the Indian Ocean and Red Sea from the ATLANTIS. Since several hundred pictures are commonly taken at each location, the results of this work are still being processed. It is evident from the detail and clarity of the resulting photographs that much can be learned with these instruments and that considerable effort to improve the ease and versatility of handling will be well repaid in scientific results.

The towed thermistor array, which was described last year by Dr. Iselin, was used on the cruises of the YAMACRAW. On the Mediterranean cruise Dr. Richardson and Dr. Hubbard installed and tested a completely new recorder for the instrument. This recorder incorporates a computer which automatically feeds a series of pulses corresponding to integral and tenths of degrees centigrade to a facsimile recorder as the computer scans the series of 23 thermistors distributed equally in depth along the chain. By repeated and rapid scanning (1 scan per 8 to 10 seconds) the recorder presents a quasi-continuous plot of isotherms along the track of the ship if it is underway, or the variation of temperature with time at a place if it is standing still. This instrument demonstrates dramatically the large and small-scale variability of temperature in near-surface waters. Recordings from the Mediterranean cruise indicated that temperature variation with position is so rapid that even higher scan rates were required. Accordingly, Dr. Hubbard has designed a new recorder incorporating a choice of much higher scan rates.

For many years underwater acousticians have wanted a precise, reliable instrument for direct measurement of the velocity of sound in sea water. Many attempts have been made at developing such an instrument and from time to time our staff have assisted others in testing various models. A few years ago the National Bureau of Standards staff, under Dr. Martin Greenspan, completed a promising instrument which gave good results in shallow water. More recently Dr. Greenspan and Mr. Tschiegg of NBS have developed a similar instrument for use in any ocean depth. Dr. Earl Hays supervised the testing of this instrument on the Mediterranean cruise of the YAMACRAW and on subsequent cruises. The instrument is clearly capable of high precision and gives results that compare well with sound velocities computed from temperature and salinity data taken in the same region but at other times. Thus far it has not been possible to combine its use with hydrographic observations but it is hoped to do so in the near future.

Research Fleet

As may be noted from the accompanying tabulation of ship activities, the ATLANTIS spent 226 days at sea, the CRAWFORD 216, the BEAR 138, and the YAMACRAW and CHAIN combined 161 days. Thus, it has been an active, sea-going year for much of our staff.

During January and February what seemed to be an endless struggle with the ATLANTIS' main engine occurred. This started off by iron grit being found in the crankcase and ended up with the installation of a new crankshaft. In the end the grit turned out to be a red herring; the real trouble was caused by an "improvement" in the design of some new bearings which had been installed during the last two weeks in 1957.

The cost of all this was very heavy indeed but fortunately, in good part, was covered by insurance. Not only did we have to buy and install a new crankshaft and several sets of new bearings but also our carefully laid plans to complete the re-survey of the South Atlantic during the winter months were disrupted. The ATLANTIS did not meet the VEMA in Cape Town as had been planned. The CRAWFORD was also delayed and could not undertake two tropical crossings of the Atlantic. Instead she was sent to the Caribbean while the ATLANTIS raced via the Mediterranean Sea to join the VEMA in the Indian Ocean. Fortunately, both of these operations appear to have been a complete scientific success.

Since the ATLANTIS is due for her quadrennial inspection in 1959 and since a decision was necessary concerning the proposed long cruise into the South Atlantic, a preliminary survey of her hull was made at the end of August. This inspection showed no excessive thinning of the hull plates and indicated that, for relatively nominal costs, we should be able to continue the ATLANTIS in service until June of 1960. At that time it is predicted that extensive repairs would be required. A preliminary estimate of the costs of these repairs indicates that an amount approximating the original construction cost ($218,000) may be required. On this basis it is now planned to keep the ATLANTIS in operation only until that time.

Knowing that the research days of the ATLANTIS are numbered, a research vessel design committee was set up under the direction of Mr. Francis Minot, who was one of the original designers of the ATLANTIS. Staff members representing all aspects of oceanography have shared the work of this very active committee. In all, preliminary designs of some ten types of research vessels have been drawn up and a design for the ATLANTIS' replacement has been selected. Work on this is still progressing but it appears that this vessel should be approximately 175 feet long and have a total displacement of about 1,000 tons. Special features include a center well, active stabilization devices, bow propulsion and special equipment for handling scientific gear at sea. The general hull form is a blend of the characteristics of the deep-sea trawler and the offshore Coast Guard cutter. The cost of this ship, together with final design, model testing and equipment, is estimated at three and one-half to four million dollars.

During June the efforts of the Office of Naval Research to secure some larger vessels for oceanographic research were successful. Emergency funds were secured in time to enable contracts to be signed before July first for the conversion of three ships from the mothball fleet. By November the USNS CHAIN was placed in service by the Military Sea Transportation Service to be operated in support of the Institution's scientific program.

The assignment of the CHAIN to oceanographic service is the result of accumulated pressures created by the Institution's deep-sea research programs. It was found to be increasingly difficult to operate with reasonable efficiency on our small ships, particularly in studying the relationship between shallow temperature structures and sound transmission and in submarine geophysics. Nor has it been possible to attack many problems at all in high latitudes where moderate to rough seas are to be anticipated much of the time. Another limitation has been the small working space available on our ships for the increasingly complex apparatus of modern oceanography. The thermistor chain is an obvious example, but it is only one of several developments which have to be carried on from larger ships.

Realizing that new ships especially designed for oceanography would inevitably not be available for several years, Mr. Vine collaborated with the Office of Naval Research in making a careful feasibility study of ships up to about 2,000 gross tons in size available for conversion. Many classes of naval and civilian service craft such as ocean-going tugs and re-supply ships were considered, but each had rather apparent shortcomings. Large trawlers and small freighters have many desirable characteristics which can be incorporated in a new design but the available types were not suitable for conversion. In the end the Navy salvage and rescue ARS-type ship was selected because it provided most of the features desired by the staff.

On the ARS space had been provided for quarters for the salvage crew as well as the operating crew. This in part provided for the scientific party. The large (28 by 40 foot) salvage workshop and several salvage storage spaces provided excellent laboratory and storage space. The large main deck aft provided excellent open deck working space and the versatile power plant included most of the power sources needed, both for our deck gear and electronics. Perhaps most important of all was the excellent sea-keeping ability reported by former officers.

In the spring of 1958 two ARS-type ships were assigned by the Navy Department through the Office of Naval Research, one for use by this Institution and the other for the Scripps Institution of Oceanography. The CHAIN (T-ARS-20) was assigned to Woods Hole to be put in service and operated for the first year by the Military Sea Transportation Service (MSTS).

The CHAIN is a 1,800 ton ship, 215 feet long, 40 foot beam, 14 foot draft with a twin-screw diesel electric power plant. Plans for her conversion were worked out jointly by members of the Institution staff with representatives of MSTS and ONR. Mr. Edwards represented the Institution at the Savannah Machine and Foundry Company during her conversion and his efforts were an important factor in making the conversion a successful one for science. The CHAIN has been fitted with four large laboratories and an explosives magazine. She also has two somewhat smaller compartments reserved entirely for writing, reading or conferences. Her large afterdeck is fitted with an excellent constant-tension winch for handling heavy steel cable for coring and trawling, a high-capacity hydraulically operated "A"-frame and various booms, winches and a heavy-duty capstan. Living accommodations provide for a scientific party of 26 and a crew of 39. These features all represent in one way or another completely new sea-going research facilities. We look forward with much anticipation to making use of this fine ship.

The CARYN was finally sold in December 1958 to Mr. Stephen H. Swift, Jr., of Milton, Massachusetts.

ATLANTIS ACTIVITIES FOR YEAR 1958

Cruise No.	Depart	Arrive	From	To	Days	Ch. Scientist
241	23 Jan.	27 Jan.	Woods Hole	St. Georges	5	Miller
	27 Jan.	14 Feb.	(Delayed in St. Georges for engine repairs)		18	
	14 Feb.	25 Feb.	St. Georges	Brooklyn, N.Y.	12	
	25 Feb.	29 Mar.	(In shipyard, Brooklyn for engine repairs)		33	
	29 Mar.	30 Mar.	Brooklyn	Woods Hole	2	
242	3 Apr.	4 Apr.	Woods Hole	Earle, N. J.	2	Stetson (Medit. and Red Seas)
	5 Apr.	9 Apr.	Earle	St. Georges	5	
	11 Apr.	25 Apr.	St. Georges	Gibraltar	15	
	28 Apr.	28 Apr.	Gibraltar	Ceuta (Rota)	1	
	28 Apr.	8 May	Ceuta	Alexandria	11	
	12 May	13 May	Alexandria	Port Said	2	Graham
	13 May	21 May	Port Said	Aden, Arabia	9	
	23 May	7 June	Aden	Aden	16	
	10 June	20 June	Aden	Port Sudan	11	
	21 June	29 June	Port Sudan	Suez	9	
	29 June	30 June	Suez	Port Said	2	
	1 July	4 July	Port Said	Alexandria	4	
	7 July	18 July	Alexandria	Naples	12	Edwards
	23 July	2 Aug.	Naples	Ceuta (Rota)	11	
	2 Aug.	3 Aug.	Ceuta	Cadiz	2	
	7 Aug.	12 Aug.	Cadiz	Ponta Delgada	6	Hahn
	14 Aug.	25 Aug.	Ponta Delgada	St. Georges	12	
	28 Aug.	31 Aug.	St. Georges	Woods Hole	4	
243	4 Sept.	4 Sept.	Woods Hole	Chelsea	16	Shipyard overhaul/repairs
	18 Sept.	19 Sept.	Chelsea	Woods Hole		
244	20 Sept.	20 Sept.	Woods Hole	Woods Hole	1	WHOI Associates Cruise
245	13 Oct.	13 Oct.	Woods Hole	Woods Hole	1	Student Cruise
246	15 Oct.	24 Oct.	Woods Hole	Port-of-Spain	10	Zeigler
	27 Oct.	6 Nov.	Port-of-Spain	Willemstad, Curaçao	11	
	9 Nov.	16 Nov.	Willemstad	Amuay	8	
	16 Nov.	17 Nov.	Amuay	Maracaibo	2	
	19 Nov.	19 Nov.	Maracaibo	Maracaibo	1	
	20 Nov.	24 Nov.	Maracaibo	Barranquilla	5	
	27 Nov.	1 Dec.	Barranquilla	Cristobal, C.Z.	5	
	3 Dec.	15 Dec.	Cristobal	Woods Hole	13	

CRAWFORD ACTIVITIES FOR YEAR 1958

Cruise No.	Depart	Arrive	From	To	Days	Ch. Scientist
17	6 Feb.	9 Feb.	Woods Hole	Bermuda	4	Metcalf
	11 Feb.	17 Feb.	Bermuda	St. Thomas	7	
	21 Feb.	6 Mar.	St. Thomas	Kingston	14	
	11 Mar.	20 Mar.	Kingston	Cristobal	10	
	25 Mar.	28 Mar.	Cristobal	Guantanamo	4	
17D	1 Apr.	9 Apr.	Guantanamo	Guantanamo	9	Gendreau of
	11 Apr.	23 Apr.	Guantanamo	Guantanamo	13	Daystrom Corp.
	25 Apr.	30 Apr.	Guantanamo	Woods Hole	6	
18	15 May	19 May	Woods Hole	Morehead City	5	von Arx
	19 May	2 June	Morehead City	Morehead City	15	
	3 June	18 June	Morehead City	Morehead City	16	
	19 June	21 June	Morehead City	Woods Hole	3	
19	7 July	12 July	Woods Hole	St. Georges	6	B. Ketchum
	14 July	19 July	St. Georges	Woods Hole	6	
	20 July	20 July	Woods Hole	Chelsea	1	Shipyard, repairs
	11 Aug.	11 Aug.	Chelsea	Woods Hole	1	
20	14 Aug.	20 Aug.	Woods Hole	Woods Hole	7	Clarke
21	28 Aug.	28 Aug.	Woods Hole	Chelsea	1	Shelter from
	30 Aug.	30 Aug.	Chelsea	Woods Hole	1	Hurricane Daisy
22	3 Sept.	10 Sept.	Woods Hole	Port-of-Spain	8	Metcalf
	13 Sept.	26 Sept.	Port-of-Spain	Rio de Janeiro	14	
	1 Oct.	5 Oct.	Rio de Janeiro	Rio de Janeiro	5	
	8 Oct.	26 Oct.	Rio de Janeiro	Walvis Bay	19	
	29 Oct.	1 Nov.	Walvis Bay	Luanda	4	
	5 Nov.	14 Nov.	Luanda	Monrovia	10	
	17 Nov.	1 Dec.	Monrovia	Belem	15	
	10 Dec.	15 Dec.	Belem	St. Thomas	6	
	16 Dec.	21 Dec.	St. Thomas	Woods Hole	6	

BEAR ACTIVITIES FOR YEAR 1958

Cruise No.	Depart	Arrive	From	To	Days	Ch. Scientist
182	21 Jan.	24 Jan.	Woods Hole	St. Georges	4	B. Ketchum
	26 Jan.	28 Jan.	St. Georges	Woods Hole	3	
183	6 Mar.	10 Mar.	Woods Hole	Woods Hole	7	Ryther
184	19 Mar.	25 Mar.	Woods Hole	Ft. Lauderdale	7	Daystrom
	26 Mar.	29 Mar.	Ft. Lauderdale	Guantanamo	4	
	1 Apr.	9 Apr.	Guantanamo	Kingston	9	
	11 Apr.	20 Apr.	Kingston	Guantanamo	10	
	21 Apr.	25 Apr.	Guantanamo	Charleston	5	
	28 Apr.	1 May	Charleston	Woods Hole	4	
185	12 May	16 May	Woods Hole	Woods Hole	5	B. Ketchum
186	21 May	26 May	Woods Hole	Woods Hole	6	Creswell
187	3 June	3 June	Woods Hole	Woods Hole	1	Compass adjustment
188	10 June	11 June	Woods Hole	Woods Hole	2	Frantz Fraser
189	18 June	25 June	Woods Hole	Woods Hole	8	Creswell
190	15 July	17 July	Woods Hole	Woods Hole	3	Frantz Walden
191	18 July	24 July	Woods Hole	Woods Hole	7	Creswell
192	4 Aug.	15 Aug.	Woods Hole	Woods Hole	12	Schevill Knott
193	19 Aug.	28 Aug.	Woods Hole	Woods Hole	10	Creswell
194	28 Aug.	28 Aug.	Woods Hole	Chelsea	1	Shelter from
	30 Aug.	30 Aug.	Chelsea	Woods Hole	1	Hurricane Daisy
195	5 Sept.	8 Sept.	Woods Hole	Woods Hole	4	Bowen
196	15 Sept.	19 Sept.	Woods Hole	Woods Hole	5	Yentsch
197	20 Sept.	21 Sept.	Woods Hole	Woods Hole	2	Voorhis
198	23 Sept.	28 Sept.	Woods Hole	Woods Hole	6	Creswell
199	6 Oct.	8 Oct.	Woods Hole	Woods Hole	3	Voorhis
200	20 Oct.	21 Oct.	Woods Hole	Woods Hole	2	Voorhis
201	4 Nov.	8 Nov.	Woods Hole	Woods Hole	5	Volkmann
202	12 Nov.	12 Nov.	Woods Hole	Chelsea	1	Shipyard, repairs
	30 Dec.	30 Dec.	Chelsea	Woods Hole	1	

USCGC YAMACRAW ACTIVITIES FOR YEAR 1958

Cruise No.	Depart	Arrive	From	To	Days	Ch. Scientist
8	27 Jan.	3 Feb.	Woods Hole	Key West	8	E. Hays
	3 Feb.	9 Feb.	Key West	Havana	7	
	12 Feb.	13 Feb.	Havana	Key West	2	
	13 Feb.	18 Feb.	Key West	Boston	5	
9	25 Mar.	31 Mar.	Woods Hole	Galveston	7	Hersey
	3 Apr.	9 Apr.	Galveston	Guantanamo Bay	7	
	11 Apr.	18 Apr.	Guantanamo Bay	Kingston	8	
	18 Apr.	23 Apr.	Kingston	Kingston	6	
	25 Apr.	26 Apr.	Kingston	Guantanamo Bay	2	
	27 Apr.	3 May	Guantanamo Bay	Newport, R. I.	7	
	5 May	5 May	Newport	Woods Hole	1	
10	21 June	1 July	Woods Hole	Ponta Delgada	11	Hersey
	3 July	7 July	Ponta Delgada	Gibraltar	5	
	7 July	11 July	Gibraltar	Palma	5	
	14 July	19 July	Palma	Naples, Italy	6	
	23 July	4 Aug.	Naples	Cadiz, Spain	13	
	8 Aug.	11 Aug.	Cadiz	Rota, Spain	4	
	12 Aug.	14 Aug.	Rota	Lisbon	3	
	17 Aug.	24 Aug.	Lisbon	Belfast, Ireland	8	
	29 Aug.	6 Sept.	Belfast	Argentia	9	
	6 Sept.	9 Sept.	Argentia	Boston	4	
11	28 Sept.	5 Oct.	Woods Hole	Jacksonville	8	Hersey
	7 Oct.	16 Oct.	Jacksonville	Savannah	10	

USNS CHAIN ACTIVITIES FOR YEAR 1958

Cruise No.	Depart	Arrive	From	To	Days	Ch. Scientist
(17 November 1958—Placing in service ceremonies. WHOI staff members attended.)						
1	18 Nov.	24 Nov.	Savannah	Woods Hole	7	
2	8 Dec.	13 Dec.	Woods Hole	Bermuda	6	Hersey
	17 Dec.	20 Dec.	Bermuda	Woods Hole	4	
3	23 Dec.	23 Dec.	Woods Hole	East Boston	1	Shipyard, repairs

R4D-6R, BUNO 39106 ACTIVITIES FOR YEAR 1958

Flight No.	Departure and Return	Days Duration	Bases	Scientist in Charge
	2 Jan.–18 Jan.	3	Local flights	
87	19 Jan.		Otis to Charleston AFB	Zeigler
	20 Jan.		Charleston AFB to Key West	
	22 Jan.		Key West to New Orleans	
	23 Jan.		New Orleans local	
	24 Jan.		New Orleans to Brownsville	
	25 Jan.		Brownsville local	
	26 Jan.		Brownsville to Memphis NAS	
	27 Jan.		Memphis to Chicago (Glenview)	
	29 Jan.	11	Glenview NAS to Otis	
88	31 Jan.		Otis to Kindley	Pike
	3 Feb.	4	Kindley to Otis	
	4 Feb.–7 Feb.	2	Local flights	
91	8 Feb.		Otis to Kindley	Pike
	9 Feb.	2	Kindley to Hyannis	
	12 Feb.–14 Feb.	2	Local flights	
94	17 Feb.		Otis to Charleston AFB	Bunker
	18 Feb.		Charleston to Guantanamo	
	19 Feb.		Guantanamo NAS to San Juan	
	20 and 22 Feb.		San Juan local	
	23 Feb.		San Juan to Piarco	
	24 to 28 Feb.		Daily — Piarco local	
	1 Mar.		Piarco to San Juan	
	2 Mar.		San Juan to Miami	
	3 Mar.	15	Miami to Otis	
	5 Mar.–21 Mar.	2	Local flights	
97	24 Mar.		Otis to Savannah	Redfield and group to attend conference
	25 Mar.		Savannah to Glynco NAS	
	26 Mar.		Glynco local	
	27 Mar.		Glynco to Savannah	
	28 Mar.		Savannah local	
	29 Mar.	6	Savannah to Otis	
	31 Mar.–2 May	11	Local flights	
108	5 May		Otis to Moncton N. B.	Bunker/Leahy
	6 May		Moncton to Argentia	
	7 May		Argentia local	
	9 May	5	Argentia to Otis	
	13 May–15 May	3	Local flights	
115	18 May		Otis to Cherry Point	Richardson
	19 to 24 May		Daily — Cherry Point local	
	25 May	8	Cherry Point to Otis	
123	27 May		Otis to Cherry Point	D. Ketchum
	28 May to 1 June		Daily — Cherry Point local	
	2 June	7	Cherry Point to Quonset	
	6 June	1	Local flight	

R4D-6R, BUNO 39106 ACTIVITIES FOR YEAR 1958 (CONTINUED)

Flight No.	Departure and Return	Days Duration	Bases	Scientist in Charge
131	7 June		Otis to Cherry Point	Walden/ Wilkins
	8 to 14 June		Daily — Cherry Point local	
	15 June	9	Cherry Point to Otis	
	17 June–22 Aug.	24	Local flights	
164	25 Aug.		Otis to Kindley	Leahy
	26 Aug.	2	Kindley to Otis	
	3 Sept.-3 Oct.	16	Local flights	
182	4 Oct.		Otis to Miami	Walden/Frantz
	7 and 10 Oct.		Miami local	
	11 Oct.	8	Miami to Otis	
	14 Oct.–7 Nov.	6	Local flights	
192	11 Nov.		Otis to Miami	Bunker/ Woodcock
	12 Nov.		Miami to San Juan	
	13 and 14 Nov.		San Juan local	
	15 Nov.		San Juan to Trinidad	
	16 to 21 Nov.		Trinidad local	
	22 Nov.		Trinidad to San Juan	
	23 Nov.		San Juan to Miami	
	24 Nov.	14	Miami to Otis	
	2 Dec.–8 Dec.	4	Local flights	
197	11 Dec.		Otis to Kindley	Woodcock
	13 Dec.	2	Kindley to Otis	
	17 Dec.–23 Dec.	3	Local flights	

STINSON N-408 ACTIVITIES FOR 1958

January	13 Local flights		
February	3 Local flights		
March	27 Local flights		
April	27 Local flights		
May	34 Local flights		
Passenger flight	19 May	Falmouth to New London	Walden/Vine
		New London to Atlantic City	Walden
		Atlantic City to Kellam, Md.	
		Kellam to Morehead City	
	20 May	Morehead City to Kellam	
		Kellam to Monmouth, N. J.	
		Monmouth to Coonamessett	
June	11 Local flights		
Ferry flight	1 June	Falmouth to Monmouth	
		Monmouth to Kellam, Md.	
		Kellam to Morehead City	
	2 June	Morehead City to Elizabeth City	
		Elizabeth City to Whitehouse, Del.	
		Whitehouse to Cape May	

STINSON N-408 ACTIVITIES FOR 1958 (CONTINUED)

	3 June	Cape May to Westerly	
		Westerly to New Bedford	
		New Bedford to Coonamessett	
July	23 Local flights		
August	15 Local flights		
September	9 Local flights		
Passenger flight	9 Sept.	Falmouth to Bedford	Watkins/Schevill
Passenger flight		Bedford to Portland	
Whale searching		Portland local	Schevill
Whale searching	10 Sept.	Portland local	Backus
Radio check		Portland local	Watkins
Whale searching	11 Sept.	Portland local	Schevill
Whale searching	Sept.	Portland local	Schevill
Whale searching	12 Sept.	Portland local	Schevill/Watkins/Backus
Passenger flight		Portland to Bedford	Schevill/Watkins/Backus
Passenger flight		Bedford to Falmouth	Watkins/Backus
October	9 Local flights		
Ferry flight	6 Oct.	Falmouth to Bedford	
Passenger flight		Bedford to Old Town	Schevill
Passenger flight		Old Town to Caribou	Schevill
Passenger flight		Caribou to Mont Joli	Schevill
Passenger flight		Mont Joli to Forestville	Schevill
Whale hunting	7 Oct.	Forestville local	Schevill
Whale hunting		Forestville local	Schevill
Passenger flight	10 Oct.	Forestville to Mont Joli	Schevill
Passenger flight		Mont Joli to Caribou	Schevill
Passenger flight		Caribou to Portland	Schevill
Passenger flight		Portland to Bedford	Schevill
Ferry flight		Bedford to Hyannis	
Ferry flight	22 Oct.	Falmouth to Portland	Backus/Johnson/Watkins
Ferry flight		Portland to Biddeford	
Passenger flight		Biddeford to Coonamessett	Watkins
Ferry flight		Coonamessett to Portland	
Ferry flight	30 Oct.	Portland to Biddeford	
Whale spotting		Biddeford to Portland	Schevill
Ferry flight		Portland to Biddeford	
Whale spotting	31 Oct.	Biddeford to Portland	Schevill
Whale spotting		Portland local	Schevill
Whale spotting	1 Nov.	Portland local	Schevill
Whale spotting		Portland to Biddeford	Schevill
Whale spotting	2 Nov.	Biddeford to Portland	
Whale spotting		Portland local	
Whale spotting	4 Nov.	Portland local (twice)	
Whale spotting	5 Nov.	Portland local (twice)	
Ferry flight	5 Nov.	Portland to Hyannis	
November	4 Local flights		
December	16 Local flights		

Publications

During 1958, forty-nine papers bearing contribution numbers were published. See Author, Subject-Locality, Taxonomic Index published in 1957 for a complete list up to 1956.

No. 784 Alfred C. Redfield. Preludes to the Entrapment of Organic Matter in the Sediments of Lake Maracaibo. In: Habitat of Oil. Amer. Assoc. Petrol. Geologists, June, 1958.

No. 849 Duncan C. Blanchard. Electrically Charged Drops from Bubbles in Sea Water and their Meteorological Significance. *Jour. Meteorol.*, Vol. 15, No. 4, pp. 383–396. 1958.

No. 874 J. B. Hersey. Electronics in Oceanography. (Dated 1957.) In: Advances in Electronics and Electron Physics. Vol. 9, pp. 239–295. Academic Press, Inc., New York. 1957.

No. 877 Floyd M. Soule and J. E. Murray. Physical Oceanography of the Grand Banks Region and the Labrador Sea in 1956. (Dated 1957.) *U. S. Coast Guard Bull.*, No. 42, pp. 35–100. 1957.

No. 900 Arthur R. Miller. The Effects of Winds on Water Levels on the New England Coast. *Limnol. and Oceanogr.*, Vol. 3, No. 1, pp. 1–14. 1958.

No. 906 John H. Ryther and Charles S. Yentsch. Primary Production of Continental Shelf Waters off New York. *Limnol. and Oceanogr.*, Vol. 3, No. 3, pp. 327–335. 1958.

No. 915 Joanne S. Malkus. On the Structure and Maintenance of the Mature Hurricane Eye. *Jour. Meteorol.*, Vol. 15, No. 4, pp. 337–349. 1958.

No. 920 A. H. Woodcock. The Release of Latent Heat in Tropical Storms due to the Fall-Out of Sea-Salt Particles. *Tellus*, Vol. 10, No. 3, pp. 355–371. 1958.

No. 923 Alfred C. Redfield. The Inadequacy of Experiment in Marine Biology. In: Perspectives in Marine Biology. Symposium held at Scripps Inst. of Oceanogr., Univ. Cal., March 24–April 2, 1956. 1958.

No. 928 H. Barnes and Margaret Barnes. The Rate of Development of *Balanus balanoides* (L.) Larvae. *Limnol. and Oceanogr.*, Vol. 3, No. 1, pp. 29–32. 1958.

No. 930 William S. von Arx. "Dister": A Displacement Sequence Stereoscope. *Jour. Meteorol.*, Vol. 15, No. 2, pp. 230–231. 1958.

No. 931 William S. von Arx. Synoptic Photography. *Weather, Royal Meteorol. Soc.*, London, pp. 179–197. 1958.

No. 932 Henry B. Bigelow and William C. Schroeder. Four New Rajids from the Gulf of Mexico. *Bull. Mus. Comp. Zool.*, Vol. 119, No. 2, pp. 201–233. 1958.

No. 933 G. Veronis. On the Transient Response of a β–plane Ocean. *Jour. Oceanogr. Soc. Japan*, Vol. 14, No. 1, pp. 1–5. 1958.

No. 934 William S. Richardson and Charles H. Wilkins. An Airborne Radiation Thermometer. *Deep-Sea Research*, Vol. 5, pp. 62–71. 1958.

No. 935 Joyce C. Lewin, R. A. Lewin and D. E. Philpott. Observations on *Phaeodactylum tricornutum. Jour. Gen. Microbiology,* Vol. 18, No. 2, pp. 420–426. 1958.

No. 936 Joyce C. Lewin. The Taxonomic Position of *Phaeodactylum tricornutum. Jour. Gen. Microbiology,* Vol. 18, No. 2, pp. 427–432. 1958.

No. 938 Harry J. Turner. The Effect of Nutrition on the Color of the Callus of *Polinices duplicatus. The Nautilus,* Vol. 72, No. 1, pp. 1–3. 1958.

No. 939 Henry Stommel, A. B. Arons and A. J. Faller. Some Examples of Stationery Planetary Flow Patterns in Bounded Basins. *Tellus,* Vol. 10, No. 2, pp. 179–187. 1958.

No. 940 Howard L. Sanders. Benthic Studies in Buzzards Bay. I. Animal-Sediment Relationships. *Limnol. and Oceanogr.,* Vol. 3, No. 3, pp. 245–258. 1958.

No. 942 Frank J. Mather, III and Robert H. Gibbs, Jr. Distribution of the Atlantic Bigeye Tuna, *Thunnus obesus,* in the Western North Atlantic and the Caribbean Sea. *Copeia,* 1958, No. 3, pp. 237–239. 1958.

No. 943 W. V. R. Malkus and G. Veronis. Finite Amplitude Cellular Convection. *Jour. Fluid Mech.,* Vol. 4, Pt. 3, pp. 225–260. 1958.

No. 944 J. B. Hersey and M. S. Rutstein. Reconnaissance Survey of Oriente Deep (Caribbean Sea) with a Precision Echo Sounder. *Bull. Geol. Soc. Amer.,* Vol. 69, pp. 1297–1304. 1958.

No. 945 Alan J. Faller. An Optical Method for the Measurement of Surface Waves in the Laboratory. *Trans. Amer. Geophys. Union,* Vol. 39, No. 4, pp. 716–720. 1958.

No. 946 Bostwick H. Ketchum, John H. Ryther, Charles S. Yentsch and Nathaniel Corwin. Productivity in Relation to Nutrients. *Rapp. et Proc.-Verb., Cons. Internat. Explor. de la Mer,* Vol. 144, pp. 132–140. 1958.

No. 949 H. Barnes and Margaret Barnes. Further Observations on Self-Fertilization in *Chthamalus* sp. *Ecology.* Vol. 39, No. 3, p. 550. 1958.

No. 951 Takashi Ichiye. A Theory of Vertical Structure of Density in the Ocean. *Jour. Oceanogr. Soc. Japan,* Vol. 14, No. 2, pp. 35–40. 1958.

No. 952 Takashi Ichiye. Tsunami Waves — What are known about them — How we have studied them. *The Port Engineer,* Vol. 7, No. 1, pp. 5–19 [1–14]. Calcutta, India. 1958.

No. 953 Henry Stommel. Letter to the Editors: The Abyssal Circulation. *Deep Sea-Research,* Vol. 5, pp. 80–82. 1958.

No. 955 G. C. McLeod. Delayed Light Action Spectra of Several Algae in Visible and Ultraviolet Light. *Jour. Gen. Physiol.,* Vol. 42, No. 2, pp. 243–250. 1958.

No. 957 James M. Moulton. The Acoustical Behavior of some Fishes in the Bimini Area. *Biol. Bull.,* Vol. 114, No. 3, pp. 357–374. 1958.

No. 958 Robert L. Miller and John M. Zeigler. A Model Relating Dynamics and Sediment Pattern in Equilibrium in the Region of Shoaling Waves, Breaker Zone, and Foreshore. *Jour. Geology,* Vol. 66, No. 4, pp. 417–441. 1958.

No. 959 Floyd M. Soule and R. M. Morse. Physical Oceanography of the Grand Banks Region and the Labrador Sea in 1957. *U. S. Coast Guard Bull.*, No. 43, pp. 81–131. 1958.

No. 960 James M. Moulton. A Summer Silence of Sea Robins, *Prionotus* spp. *Copeia* 1958, No. 3, pp. 234–235. 1958.

No. 963 Takashi Ichiye. The response of a Stratified Bounded Ocean to Variable Wind Stresses. *Oceanogr. Mag.*, Vol. 10, No. 1, pp. 19–63. Tokyo, Japan. 1958.

No. 965 Theodore J. Smayda. Biogeographical Studies of Marine Phytoplankton. *Oikos*, Vol. 9, No. 2, pp. 158–191. 1958.

No. 968 Bostwick H. Ketchum and Vaughan T. Bowen. Biological Factors Determining the Distribution of Radio-isotopes in the Sea. Proc. 2nd Internat. Conference on the Peaceful Uses of Atomic Energy, Geneva, Sept. 1–15, 1958. Paper UN402-01C724, 11 pp. 1958.

No. 969 Joanne Starr Malkus. On the Structure of the Trade Wind Moist Layer. *Papers in Physical Oceanography and Meteorology*, Vol. 13, No. 2, pp. 1–47. 1958.

No. 970 Vaughan T. Bowen and T. T. Sugihara. Marine Geochemical Studies with Fallout Radioisotopes. Proc. 2nd Internat. Conference on the Peaceful Uses of Atomic Energy, Geneva, Sept. 1–15, 1958. Paper UN403-01C902, 12 pp. 1958.

No. 972 Charles S. Yentsch and Ralph F. Vaccaro. Phytoplankton Nitrogen in the Oceans. *Limnol. and Oceanogr.*, Vol. 3, No. 4, pp. 443–448. 1958.

No. 976 Alfred C. Redfield. The Biological Control of Chemical Factors in the Environment. *Amer. Scientist*, Vol. 46, No. 3, pp. 205–222. 1958.

No. 977 C. Godfrey Day. Surface Circulation in the Gulf of Maine Deduced from Drift Bottles. U. S. Fish and Wildlife Service, Vol. 58, *Fish. Bull.* 141, pp. 443–472. 1958.

No. 978 John H. Ryther, Charles S. Yentsch and Ralph F. Vaccaro. The Dynamics of a Diatom Bloom. *Biol. Bull.*, Vol. 115, No. 2, pp. 257–268. 1958.

No. 979 A. T. Spencer and D. C. Blanchard. A Portable Raindrop Recorder for Semi-Continuous Determination of Size Distributions. *Trans. Amer. Geophys. Union*, Vol. 39, No. 5, pp. 853–857. 1958.

No. 981 Takashi Ichiye. On Convective Circulation and Density Distribution in a Zonally Uniform Ocean. *Oceanogr. Mag.*, Vol. 10, No. 1, pp. 97–135. Tokyo, Japan. 1958.

No. 983 P. F. Scholander. Counter Current Exchange: A Principle in Biology. *Hvalrådets Skrifter*, No. 44, 24 pp. Oslo. 1958.

No. 994 Gilbert L. Voss. The Cephalopods Collected by the R/V Atlantis during the West Indian Cruise of 1954. *Bull. Mar. Sci., Gulf and Caribbean*, Vol. 8, No. 4, pp. 369–389. 1958.

No. 998 H. Barnes. Regarding the Southern Limits of *Balanus balanoides* (L.) *Oikos*, Vol. 9, No. 2, pp. 139–157. 1958.

No. 1001 L. R. Breslau and H. E. Edgerton. The Luminescence Camera. *Jour. Biol. Photogr. Assoc.*, Vol. 26, No. 2, pp. 49–58, 1958.

Personnel

The following persons were awarded grants, honoraria or fellowships during 1958:

John P. Barlow	Cornell University
Duncan C. Blanchard	Massachusetts Institute of Technology
Henri Caron	Clark University
William A. Dawson	Harvard University
John L. Edgar	Antioch College
Michael Garstang	Florida State University
Ilmo Hela	Institute of Marine Research, Helsinki, Finland
Bruce Hopper	Alabama Polytechnic Institute
Takashi Ichiye	Central Meteorological Observatory, Tokyo, Japan
Alexandre Ivanoff	École Supérieure de Physique et de Chimie, Paris, France
James B. Lachey	University of Florida
Benjamin B. Leavitt	University of Florida
Joseph Levine	Massachusetts Institute of Technology
Frederick C. Marland	Agricultural and Mechanical College of Texas
Sheina Marshall	Marine Station, Millport, Isle of Cumbrae, Scotland
George C. Mattheissen	Harvard University
Guy C. McLeod	Harvard University
Sigeru Motoda	Hokkaido University, Hokkaido, Japan
Daniel R. Norton	Sprague Electric Company
Andrew P. Orr	Marine Station, Millport, Isle of Cumbrae, Scotland
Peter D. Parker	Amherst College
Owen Phillips	The Johns Hopkins University
Carol Ann Reichert	Antioch College
Allan R. Robinson	Harvard University
Ellen Ruby	Antioch College
Rudolf S. Scheltema	University of North Carolina
David H. Shonting	Massachusetts Institute of Technology
Theodore J. Smayda	University of Oslo
Joseph Stampfli	University of Michigan
John H. Steele	Marine Laboratory, Aberdeen, Scotland
Edward D. Stroup	The Johns Hopkins University
T. Ferris Webster	Massachusetts Institute of Technology
Peter Wanggersky	Yale University
Judith Witkin	Hunter College

We were honored during the year by receiving visits from distinguished colleagues from other countries. Among these the following spent a considerable period of time:

Dr. Bruce B. Benson	Amherst College
Mr. Thanon Charenlarb	Royal Thai Navy, Thailand
Mr. Charles P. Cook	Commercial Products, Inc.
Dr. Edgar L. Deacon	Commonwealth Scientific and Industrial Research Organization, Australia
Dr. G. E. R. Deacon	National Institute of Oceanography, England
Mr. Robert L. Erath	Grumman Aircraft Corporation
Mr. Richard Fay	United States Weather Bureau
Dr. Sadahyo M. Hori	Japanese Hydrographic Office
Dr. Kiyashi Horikawa	University of Tokyo, Japan
Dr. S. Ishiguro	Nagasaki Marine Observatory, Japan
Dr. Alexandre Ivanoff	École Supérieure de Physique et de Chimie, Paris, France
Dr. Sheina M. Marshall	The Marine Station, Millport, Scotland
Mr. Jack McLachlan	Oregon State College
Dr. Sigeru Motoda	Hokkaido University, Japan
Mr. Donald G. Murphy	Oregon State College
Dr. Andrew P. Orr	The Marine Station, Millport, Scotland
Dr. Alberto Sáez	National University of Zuila, Venezuela
Dr. Rolf Heinz Siepmann	Kiel, Germany
Mr. Norman Dennis Smith	National Institute of Oceanography, England
Mr. Gordon L. Stamm	Naval Research Laboratory
Dr. Raymond G. Stross	University of Wisconsin
Mr. John H. Steele	The Marine Laboratory, Aberdeen, Scotland
Dr. Roman Vishniac	New York City
Dr. George C. William	Michigan State University
Dr. Jacques S. Zaneveld	Caraibisch Biologisch Institut, Curaçao, Netherlands West Indies

The following personnel, in addition to those otherwise listed, were in the employ of the Institution for the twelve-month period ending December 31, 1958.

Ethel B. Allen
Nellie E. Andersen
Judith A. Ashmore
Nadine N. Athearn
Cyril Backus
Harold Backus
Jeanne M. Backus
Rose L. Barbour
Ann H. Barrett
Joseph R. Barrett, Jr.
Elmer M. Barstow
Martin R. Bartlett
Edward R. Baylor
Henry G. Behrens
James S. Bercaw
Stanley W. Bergstrom
Robert N. Betterley
Forrest W. Blake
Ralph H. Bodman
Georg Boltz
Warren O. Bowman
Mabel D. Bradley
Alvin L. Bradshaw
W. Scott Bray
Joseph C. Brown
Edwin T. Bryant
John Q. Bumer
Charles A. Burnham
John P. Cabral
John V. Cabral

Henry A. Cain
Sybil A. Campbell
Angelo Cangiamilia
Alwyn L. Carter
David F. Casiles
James J. Cavanaugh
Constance W. Chadwick
Margaret A. Chaffee
Agnes C. Chalmers
John A. Christian
Edward H. Chute
William H. Clarkin
Arthur D. Colburn, Jr.
J. William Condon
Hans Cook
Jerome M. Cotter
Brooks W. Coughlin
Marion W. Crocker
Elizabeth S. Curl
Lee C. Davis
C. Godfrey Day
Joseph V. Day
Charles D. Densmore
Richard H. Dimmock
Paul E. Dingwell
William M. Dunkle, Jr.
Stanley N. Eldridge
Davis A. Fahlquist
Louis F. Fernandez
Alice H. Ferris
George A. Ferris
Frederick E. Fielden
Don R. Fink
Stanley O. Fisher
Richard A. Fitzgerald
Donald B. Foster
John G. Fraser
Gloria S. Gallagher
Rosemary Gallagher
William F. Gallagher
Fred Gaskell
James E. Gifford
Barbara L. Gill
Norman Gingrass
Florence E. Glaeser
Carlton W. Grant
James E. Hanks
Kaleroy L. Hatzikon
Carlyle R. Hayes
George L. Hilton
Lloyd D. Hoadley
Harry L. Hodgkins
Sloat F. Hodgson
Paul M. Howe
Myron P. Howland, Jr.
Paul C. Howland
Charles J. Hubbard
Otis E. Hunt
Charles S. Innis, Jr.
Delmar R. Jenkins
Alfred C. John
Barbara Johnson
David C. Johnson
Henry R. Johnson
Yolande A. Kahler
Richard L. Keeler
Willard E. Ketchen
John A. Kostrzewa
Joseph L. Lambert
Delia M. Lavin
Joseph Levine
Thomas Lyon
Colin Dhu Macafee
Duane E. Maddux
George E. Martin
Francis S. Matthews
Clement L. McCann, Jr.
Margaret McCloskey
Eileen M. McCormack
Joseph M. McElliott
David A. McGill
Florence K. Mellor
Francis Minot
Juanita A. Mogardo
Wendell Mordy
Clayton B. Morehouse
Kenneth Morrison
Robert G. Munns
Eugene J. Mysona
James S. Nicolson
Richard V. Olson
Mary Ortolani
Betty P. Ostiguy
Michael Palmieri, Jr.
Gale G. Pasley, Jr.
Helen F. Phillips
Samuel F. Pierce
John M. Pimental
Stanley E. Poole
Mary Dorothy Rogers
Nicholas Rosa
Lawrence Rose
Michael Rosetti
James E. Salthouse
John D. Sandblom
Margaret Scharff
John L. Schilling
Elizabeth H. Schroeder
Harry H. Seibert
William Shields
William S. Shultz
Luther V. Slabaugh
David Snowman
Eloise M. Soderland
Otto Solberg
James H. Souza
Matthew R. Souza
Elizabeth C. Sparks
Charles E. Spooner
Robert J. Stanley
Richard Stansfield
Thomas R. Stetson
Stephen L. Stillman, Jr.
John W. Stimpson
Thomas O. L. Sutcliffe
Herman Tasha
Louis J. Tometich
Wendell K. Tripp
Carl R. von Dannenberg
Jean D. Walker
Robert H. Walker, Jr.
Robert G. Weeks
Phillips B. Wilde
Charles H. Wilkins
George A. Williams
Edward Wilson
Esther N. Wilson
Carleton R. Wing
Warren E. Witzell
Fred C. Woodward, Jr.
Javan D. York
Anita M. Young

V. TREASURER'S REPORT FOR THE YEAR 1958

The accounts for the year 1958 have been audited by Lybrand, Ross Bros. & Montgomery.

The book value of endowment funds at December 31, 1958 was $3,389,617, of which $954,054 represented accumulated net gains from sales of investments. The market value of endowment assets on the same date, including real estate at book amount, was $5,091,900. Endowment fund investments and income received therefrom are summarized in Schedule D.

Income received on endowment assets, including interest charged on the advance to current funds, was $178,607 for the year ended December 31, 1958, compared with $180,593 the previous year. This income represented a return on endowment fund assets of 3.5% at year-end market quotation, 5.3% on the book amount and 7.3% on the contributed amount of the endowment fund.

Endowment income was allocated for 1958 operating expenses at the rate of 5.5% of the book amount of original endowment funds, or $133,129. Of the balance of endowment income, $45,478, there was transferred to the income and salary stabilization reserve $44,810 and to unexpended balance of gifts from Oceanographic Associates as income from investment of life memberships $668. Advances were made from endowment funds to current funds during portions of the year, but all such advances were paid off prior to the end of the year.

Deferred charges amounting to $239,364 (see balance sheet for breakdown) represented expenditures for the benefit of future years. A proportionate part of these charges will be added to current costs, or other appropriate accounts, as the benefits accrue.

The details of unexpended balances of gifts and receipts for research, other than Government, are shown in Schedule C. The income from Woods Hole Oceanographic Associates for the year amounted to $49,606. Expenditures and allocations to specific projects of $15,261, plus $4,042 of life memberships transferred to endowment assets, increased the balance on hand of $59,615 at December 31, 1957 to $89,918 at December 31, 1958.

The Institution's 1958 contribution to the Woods Hole Oceanographic Institution's Employees Retirement Trust amounted to $76,344. The trust is administered by three trustees. The balance of the old Retirement Fund, administered by the Treasurer, amounted to $68,140 as at December 31, 1958. This balance consisted of amounts on deposit in sixteen savings bank accounts held in trust for ten members of the plan. No contributions to the old plan were made in 1958. Interest totalling $2,167 was credited to the savings accounts during the year.

In the financial statements that follow it is interesting to note that for each dollar spent 79.4 cents was spent for direct costs of research activity, 15.8 cents for general and administration expenses and 4.8 cents for plant operation and miscellaneous. Administrative salaries amounted to only 6.4 cents of each dollar of total expense. Included in the 15.8 cents for general and administration expenses was 3.6 cents for staff benefits (group insurance, social security taxes, and contributions to retirement plan).

BALANCE SHEET

As at December 31, 1958

ASSETS

Endowment Fund Assets:		
Investments (Schedule D):		
Bonds (market quotations $1,765,105)		$1,847,508
Stocks (market quotations $3,196,478)		1,411,792
Real estate		128,417
		3,387,717
Cash		1,900
		3,389,617
Plant Fund Assets (note):		
Laboratory plant and equipment		602,429
Vessels and equipment		266,707
Other property		161,541
Total plant		1,030,677
Cash	$185,654	
Receivable from sale of securities	132,685	318,339
		1,349,016
Current Fund Assets:		
Cash		38,735
Accounts receivable:		
U. S. Government	$300,734	
Other	14,719	315,453
Unbilled costs on research contracts:		
U. S. Government	325,628	
Other	42,043	367,671
Supply inventories		28,700
Deferred charges:		
Reconditioning boat Crawford	190,468	
Electronic equipment	24,844	
Other	24,052	239,364
		989,923
		$5,728,556

LIABILITIES

Endowment Funds:		
Unrestricted		$2,016,143
For upkeep of plant		419,420
Accumulated net gain on sale of investments		954,054
		3,389,617
Plant Funds:		
Invested in plant		1,030,677
Fund for purchase and reconditioning of boat Aries		318,339
		1,349,016
Current Liabilities and Funds:		
Accounts payable and accrued expenses		163,336
Contribution payable to employees' retirement plan and trust		76,344
Unexpended balances of gifts and grants for research:		
Government	$174,817	
Other (Schedule C)	98,825	273,642
General fund:		
General plant and equipment reserve	244,084	
Income and salary stabilization reserve	211,399	
Unappropriated	21,118	476,601
		989,923
		$5,728,556

Note — Since 1945 the Institution has provided for depreciation of plant assets other than vessels at annual rates of 2% on buildings and 5% to 33⅓% on equipment, carrying the amounts to general plant and equipment reserve.

STATEMENT OF INCOME, OPERATING EXPENSES AND UNAPPROPRIATED GENERAL FUND

For the Year Ended December 31, 1958

INCOME:		
Receipts for sponsored research:		
For direct costs		$ 2,260,277
For indirect costs		561,294
Fees for use of facilities		102,389
		2,923,960
Endowment income (Schedule D)	$178,607	
Less amounts added to income and salary stabilization reserve ($44,810) and unexpended balance of gifts from Oceanographic Associates as income from investment of life memberships ($668)	45,478	133,129
Miscellaneous		10,129
Total income availed of		3,067,218
OPERATING EXPENSES:		
Direct costs of research activity (Schedule A):		
Salaries and wages		1,043,073
Vessel operations		593,330
Materials and services		637,693
Travel		132,696
		2,406,792
Indirect costs:		
General and administration (Schedule B)	480,467	
Plant operation (Schedule B)	138,207	
Miscellaneous	7,269	625,943
Total operating expenses		3,032,735
EXCESS OF INCOME		34,483
Additions to plant from current funds — books and equipment purchased		25,212
		9,271
UNAPPROPRIATED GENERAL FUND, JANUARY 1, 1958		11,847
UNAPPROPRIATED GENERAL FUND, DECEMBER 31, 1958		$ 21,118

Schedule A

DIRECT COSTS OF RESEARCH ACTIVITY

For the Year Ended December 31, 1958

	Salaries and Wages	Vessel Operations	Materials and Services	Travel	Total
U.S. GOVERNMENT CONTRACTS	$ 923,938	$563,005	$548,482	$121,685	$2,157,110
OTHER SPONSORED RESEARCH	42,861	3,993	49,340	6,973	103,167
Total direct costs of sponsored research.	966,799	566,998	597,822	128,658	2,260,277
INSTITUTION RESEARCH......	76,274	26,332	39,871	4,038	146,515
Total direct costs of research...........	$1,043,073	$593,330	$637,693*	$132,696	$2,406,792

* Includes grants and fellowships:

Other sponsored research...............	$11,750
Institution research....................	20,375
	$32,125

Schedule B

GENERAL AND ADMINISTRATION EXPENSES AND EXPENSES FOR PLANT OPERATION

For the Year Ended December 31, 1958

GENERAL AND ADMINISTRATION

GENERAL EXPENSES:		
Staff benefits:		
Contributions to retirement plan..............................		$76,344
Social security taxes....................................		27,309
Group insurance..		5,133
		108,786
Shop services..		90,202
Housing, net...		3,477
ADMINISTRATION EXPENSES:		
Salaries and wages....................................	$192,587	
Insurance, travel, supplies and other....................	85,415	278,002
		$480,467

PLANT OPERATION

SALARIES AND WAGES..		47,251
PROVISION FOR DEPRECIATION (credited to general plant and equipment reserve)..		31,449
OTHER REPAIR COSTS....................................	17,851	
HEAT, LIGHT AND POWER..................................	22,140	
AMORTIZATION OF COST OF ELECTRONIC EQUIPMENT...........	6,211	
OTHER..	13,305	59,507
		$138,207

Schedule C

SUMMARY OF GIFTS AND RECEIPTS FOR RESEARCH

Year Ended December 31, 1958

	Unexpended Balance January 1, 1958	Received	Expended		Other Charges or (Credits)	Unexpended Balance December 31, 1958
			Direct Costs	Indirect Costs		
American Society of Limnology and Oceanography		$ 605	$ 478	$ 127		
Bermuda Biological Station for Research		3,143	3,025	118		
Commonwealth of Massachusetts — shellfish propagation	$ 1,783	20,144	13,941	7,986		
Esso Research and Engineering Company — foraminifera cataloging		2,892	1,773	1,119		
Manufacture, sale, and calibration of instruments		38,650	44,090	9,496	($8,329) (a) (6,605) (b) (2) (c)	
Lou Marron science fund — pelagic fish studies	254	4,000	3,853	15		$ 386
Massachusetts Institute of Technology — Institute for Atmospheric Research		9,112	6,592	2,520		
Munitalp Foundation — meteorological research	1,700		1,550	150		
National Academy of Sciences:						
Project Nobska		183	183			
Project Piccard		596	596			
National Lead Company		4,755	4,581	174		
David Nutt — Blue Dolphin		75	75			
Oceanographic Associates:						
Deuterium studies	697		466	180		51
Peruvian core analysis	3,106		2,843	263		
Fellowships		11,750	11,750			
Other		2,250	2,250			
Unappropriated	59,615	49,606 (14,000)			4,042 (d) 1,261 (e)	89,918
Research Corporation — instrument fund	2,402				(285) (c)	2,687
Sundry work for others		5,156	4,026	1,130		
Towns of Brookhaven and Islip, New York — Great South Bay Survey		2,000	1,095	122		783
Other gifts		5,000				5,000
	$69,557	$145,917	$103,167	$23,400	($9,918)	$98,825

(a) Charged to income. (b) Charged to other projects. (c) Sales. (d) Life memberships added to endowment. (e) Miscellaneous expenditures.

SCHEDULE D

SUMMARY OF INVESTMENTS

As at December 31, 1958

	Book Amount	% of Total	Market Quotation	% of Total	Income
BONDS:					
U. S. Government	$ 383,796	11.33	$ 375,385	7.37	$ 6,361
Railroad	505,337	14.92	471,581	9.27	20,958
Public utility	395,684	11.68	373,720	7.34	17,571
Industrial	407,654	12.03	385,843	7.58	13,287
Financial and investment	155,037	4.58	158,576	3.12	8,957
Total bonds	1,847,508	54.54	1,765,105	34.68	67,134
STOCKS:					
Preferred	252,508	7.45	239,325	4.70	14,003
Common:					
Public utility	370,056	10.92	772,523	15.18	24,244
Industrial	608,731	17.97	1,819,663	35.75	55,084
Miscellaneous	180,497	5.33	364,967	7.17	13,706
Total common stocks	1,159,284	34.22	2,957,153	58.10	93,034
Total stocks	1,411,792	41.67	3,196,478	62.80	107,037
REAL ESTATE	128,417	3.79	128,417*	2.52	2,845
Total investments	$3,387,717	100.00	$5,090,000	100.00	177,016
INTEREST ON ADVANCE TO CURRENT FUNDS CHARGED TO MISCELLANEOUS OPERATING EXPENSE					1,591
TOTAL ENDOWMENT FUND INCOME					$178,607

*At book amount.

WOODS HOLE OCEANOGRAPHIC INSTITUTION
WOODS HOLE, MASSACHUSETTS

We have examined the balance sheet of Woods Hole Oceanographic Institution as at December 31, 1958 and the related statement of income, operating expenses and unappropriated general fund for the year then ended. Our examination was made in accordance with generally accepted auditing standards, and accordingly included such tests of the accounting records and such other auditing procedures as we considered necessary in the circumstances; however, it was not practicable to confirm receivables from United States Government departments, as to which we have satisfied ourselves by means of other auditing procedures.

In our opinion, the accompanying financial statements present fairly the position of Woods Hole Oceanographic Institution at December 31, 1958 and the results of its operations for the year then ended, on a basis consistent with that of the preceding year.

Boston, Massachusetts
April 28, 1959

LYBRAND, ROSS BROS. & MONTGOMERY

List of Contributions

LIST OF CONTRIBUTIONS

FROM THE WOODS HOLE OCEANOGRAPHIC INSTITUTION

See Author, Subject-Locality, Taxonomic Indexes, published in 1957, for a complete list up to 1956.

No. 701. R. B. Montgomery. Convection of Heat. *Arch. Meteorol., Geoph. u. Bioklim.*, Ser. A, Meteorol. und Geoph., Band 7, pp. 125–132. 1954.

No. 702. Frank J. Mather III. Northerly Occurrences of Warm Water Fishes in the Western Atlantic. *Copeia*, No. 4, pp. 292–293. 1954.

No. 703. C. W. Newton. Analysis and Data Problems in Relation to Numerical Prediction. *Bull. Amer. Meteorol. Soc.*, Vol. 35, No. 7, pp. 287–294. 1954.

No. 704. George L. Clarke. Elements of Ecology. John Wiley & Sons, Inc., New York. 534 pp. 1954. (Not included in *Collected Reprints*).

No. 705. L. van Dam. On the Respiration in Scallops (Lamellibranchiata). *Biol. Bull.*, Vol. 107, No. 2, pp. 192–202. 1954.

No. 706. Joanne Starr Malkus and R. S. Scorer. The Erosion of Cumulus Towers. *Jour. Meteorol.*, Vol. 12, No. 1, pp. 43–57. 1955.

No. 707. Athelstan F. Spilhaus. Sea and Air Resources. *Geogr. Rev.*, Vol. 44, No. 3, pp. 346–351. 1954.

No. 708. Charles J. Fish and Mary Curtis Cobb. Noxious Marine Animals of the Central and Western Pacific Ocean. Fish and Wildlife Service, *Research Report* 36, 45 pp., 1954.

No. 709. P. F. Scholander, Warner E. Love and John W. Kanwisher. The Rise of Sap in Tall Grapevines. *Plant Physiol.*, Vol. 30, No. 2, pp. 93–104. 1955. (Not included in *Collected Reprints*).

No. 710. P. F. Scholander, L. van Dam and Susan I. Scholander. Gas Exchange in the Roots of Mangroves. *Amer. Jour. Bot.*, Vol. 42, No. 1, pp. 92–98. 1955.

No. 711. Duncan C. Blanchard. A Simple Method for the Production of Homogeneous Water Drops down to 1 Micron Radius. *Jour. Colloid Sci.*, Vol. 9, No. 4, pp. 321–328. 1954.

No. 712. John H. Ryther. Ecology of Autotrophic Marine Dinoflagellates with Refence to Red Water Conditions. In: The Luminescence of Biological Systems, F. H. Johnson, Edit., Publ. by Amer. Assoc. Adv. Sci., Washington, pp. 387–414. 1955.

No. 713. Henry Stommel. Serial Observations of Drift Currents in the Central North Atlantic Ocean. *Tellus*, Vol. 6, No. 3, pp. 203–214. 1954.

No. 714. Francis A. Richards. Oxygen in the Ocean. *Geol. Soc. Amer.*, Mem. 67, Vol. 1, Ch. 9, pp. 185–238. 1957.

No. 715. Harry J. Turner, Jr. and J. Arthur Posgay. Sixth Report on Investigations of the Shellfisheries of Massachusetts. *Com. Mass., Dept. Nat. Res., Div. Mar. Fish.*, pp. 1–74. 1953.

No. 716. Joanne Starr Malkus and Claude Ronne. On the Structure of Some Cumulonimbus Clouds which Penetrated the High Tropical Troposphere. *Tellus*, Vol. 6. No. 4, pp. 351–366. 1954.

No. 717. L. V. Worthington. A Preliminary Note on the Time Scale in North Atlantic Circulation. *Deep-Sea Research*. Vol. 1, pp. 244–251. 1954.

No. 718. Arthur R. Miller. Some Suggestions for more prècise Loran Navigation. *Navigation*, Vol. 3, Nos. 1 and 2, pp. 23–29. 1951. (Included in *Collected Reprints* for 1953).

No. 719. Henry B. Bigelow and Isabel Pérez Farfante. Fishes of the Western North Atlantic. Lancelets. *Mem. Sears Found. Mar. Res.*, No. 1, Pt. 1, Ch. 1, pp. 1–28. 1948. (Not included in *Collected Reprints*).

No. 720. Henry B. Bigelow and William C. Schroeder. Fishes of the Western North Atlantic. Cyclostomes. *Mem. Sears Found. Mar. Res.*, No. 1, Pt. 1, Ch. 2, pp. 29–58. 1948. (Not included in *Collected Reprints*).

No. 721. Henry B. Bigelow and William C. Schroeder. Fishes of the Western North Atlantic. Sharks. *Mem. Sears Found. Mar. Res.*, No. 1, Pt. 1, Ch. 3, pp. 59–576. 1948. (Not included in *Collected Reprints*).

No. 722. Arthur H. Clarke, Jr. Some Mollusks from the Continental Slope of Northeastern North America. *Breviora*, No. 40, 11 pp. 1954.

No. 723. C. W. Newton. Frontogenesis and Frontolysis as a Three-Dimensional Process. *Jour. Meteorol.*, Vol. 11, No. 6, pp. 449–461. 1954.

No. 724. Charles B. Officer. Southwest Pacific Crustal Structure. *Trans. Amer. Geophys. Union*, Vol. 36, No. 3, pp. 449–459. 1955.

No. 725. K. G. Wilson and A. B. Arons. Osmotic Pressures of Sea Water Solutions Computed from Experimental Vapor Pressure Lowering. *Sears Found., Jour. Mar. Res.*, Vol.14, No. 2, pp. 195–198. 1955.

No. 726. Joanne Starr Malkus. On the Formation and Structure of Downdrafts in Cumulus Clouds. *Jour. Meteorol.*, Vol. 12, No. 4, pp. 350–354. 1955.

No. 727. Joanne Starr Malkus. The Effects of a Large Island upon the Trade-Wind Air Stream. *Quart. Jour. Roy. Meteor. Soc.*, Vol. 81, No. 350, pp. 538–550. 1955.

No. 728. Paul Ferris Smith. Further Measurements of the Sound Scattering Properties of Several Marine Organisms. *Deep-Sea Research*, Vol. 2, pp. 71–79. 1954.

No. 729. Willard Dow. Underwater Telemetering. *Deep-Sea Research*, Vol. 2, pp. 145–151 (erroneously dated 1954). 1955.

No. 730. John H. Ryther. Inhibitory Effects of Phytoplankton upon the Feeding of *Daphnia magna* with Reference to Growth, Reproduction, and Survival. *Ecology*, Vol. 35, No. 4, pp. 522–533. 1954.

No. 731. Charles B. Officer. A Deep-Sea Seismic Reflection Profile. *Geophysics*, Vol. 20, No. 2, pp. 270–282. 1955.

No. 732. Henry B. Bigelow and William C. Schroeder. Occurrence off the Middle and North Atlantic United States of the Offshore Hake *Merluccius albidus* (Mitchill) 1818, and of the Blue Whiting *Gadus (Micromesistius) poutassou* (Risso) 1826. *Bull. Mus. Comp. Zool.*, Vol. 113, No. 2, pp. 205–226. 1955.

No. 733. John H. Ryther. The Ratio of Photosynthesis to Respiration in Marine Plankton Algae and its Effect upon the Measurement of Productivity. *Deep-Sea Research*, Vol. 2, pp. 134–139 (erroneously dated 1954). 1955.

No. 734. Duncan C. Blanchard. Bursting of Bubbles at an Air-Water Interface. *Nature*, Vol. 173, p. 1048. 1954.

No. 735. Joseph Chase. Winds and Temperatures in Relation to the Brood-Strength of Georges Bank Haddock. *Jour. du Conseil*, Vol 21, No. 1, pp. 17–24. 1955.

No. 736. Grace I. Creitz and Francis A. Richards. The Estimation and Characterization of Plankton Populations by Pigment Analysis. III. A Note on the use of "Millipore" Membrane Filters in the Estimation of Plankton Pigments. *Sears Found., Jour. Mar. Res.*, Vol. 14, No. 3, pp. 211–216. 1955.

No. 737. Charles J. Fish. Preliminary Observations on the Biology of Boreo-Arctic and Subtropical Oceanic Zooplankton Populations. In: Symposium on Marine and Fresh-Water Plankton in the Indo-Pacific, Bangkok, Jan. 25–26, 1954, FAO-UNESCO, Sect. 1, No. 1, pp. 1–7, 1955. (Not included in *Collected Reprints*).

No. 739. William G. Metcalf. On the Formation of Bottom Water in the Norwegian Basin. *Trans. Amer. Geophys. Union*, Vol. 36, No. 4, pp. 596–600. 1955.

No. 740. Andrew F. Bunker. Turbulence and Shearing Stresses Measured over the North Atlantic Ocean by an Airplane-Acceleration Technique. *Jour. Meteorol.*, Vol 12, No. 5, pp. 445–455. 1955.

No. 741. Wilbur Marks and F. Claude Ronne. Aerial Stereo-Photography and Ocean Waves. *Photogr. Engineering*, March 1955, pp. 107–110. 1955.

No. 742. Malcolm S. Gordon. Summer Ecology of Oceanic Birds off Southern New England. *The Auk*, Vol 72, pp. 138–147. 1955.

No. 743. Charles B. Officer. Geologic Interpretation of a Series of Seismic Reflection Profiles from Bermuda to the Continental Margins. *Deep-Sea Research*, Vol. 2, pp. 253–260. 1955.

No. 744. J. W. Kanwisher and Gordon Volkmann. A Scattering Layer Observation. *Science*, Vol. 121, No. 3134, pp. 108–109. 1955.

No. 745. Irving I. Schell. Interrelations of Arctic Ice with the Atmosphere and the Ocean in the North Atlantic — Arctic and Adjacent Areas. *Jour. Meteorol.*, Vol. 13, No. 1, pp. 46–58. 1956.

No. 746. H. G. Farmer, W. Marks, R. G. Walden and G. G. Whitney, Jr. A Technique for Ocean Wave Measurements. In: Proc. First Conf., Ships and Waves, Oct. 1954, Counc. Wave Res. and Soc. Naval Arch. and Mar. Eng., pp. 11–32. 1955.

No. 747. Duncan C. Blanchard. Electrified Droplets from the Bursting of Bubbles at an Air-Sea Water Interface. *Nature*, Vol. 175, No. 4451, pp. 334–336. 1955.

No. 748. E. M. Hulburt. Distribution of Phosphorus in Great Pond, Massachusetts. *Sears Found., Jour. Mar. Res.*, Vol. 15, No. 3, pp. 181–192. 1956.

No. 749. F. C. Fuglister. Alternative Analyses of Current Surveys. *Deep-Sea Research*, Vol. 2, pp. 213–229. 1955.

No. 750. Gilbert L. Voss. The Cephalopoda Obtained by the Harvard-Havana Expedition off the Coast of Cuba in 1938–39. *Bull, Mar. Sci., Gulf and Caribbean*, Vol. 5, No. 2, pp. 81–115. 1955.

No. 751. Frank S. Essapian. Speed-Induced Skin Folds in the Bottle-Nosed Porpoise, *Tursiops truncatus*. *Breviora*, No. 43, 4 pp., 9 Pls. 1955.

No. 752. John P. Barlow. Effect of Wind on Salinity Distribution in an Estuary. *Sears Found., Jour. Mar. Res.*, Vol. 15, No. 3, pp. 193–203. 1956.

No. 753. John P. Barlow. Physical and Biological Processes Determining the Distribution of Zooplankton in a Tidal Estuary *Biol. Bull.*, Vol. 109, No. 2, pp. 211–225. 1955.

No. 754. Alan J. Faller. A Demonstration of Fronts and Frontal Waves in Atmospheric Models. *Jour. Meteorol.*, Vol. 13, No. 1, pp. 1–4. 1956.

No. 755. P. F. Scholander. Evolution of Climatic Adaptation in Homeotherms. *Evolution*, Vol. 9, No. 1, pp. 15–26. 1955.

No. 756. Hilary B. Moore. Variations in Temperature and Light Response within a Plankton Population. *Biol. Bull.*, Vol. 108, No. 2, pp. 175–181. 1955.

No. 757. A. H. Woodcock and W. A. Mordy. Salt Nuclei, Wind and Daily Rainfall in Hawaii. *Tellus*, Vol. 7, No. 3, pp. 291–300. 1955.

No. 758. Floyd M. Soule and J. E. Murray. Physical Oceanography of the Grand Banks Region and the Laborador Sea in 1954. *U. S. Coast Guard Bull.*, No. 40, pp. 79–168. 1955.

No. 759. Bostwick H. Ketchum, Nathaniel Corwin and D. Jean Keen. The Significance of Organic Phosphorus Determinations in Ocean Waters. *Deep-Sea Research*, Vol. 2, pp. 172–181. 1955.

No. 760. Dean F. Bumpus and E. Lowe Pierce. The Hydrography and the Distribution of Chaetognaths over the Continental Shelf off North Carolina. Pap. Mar. Biol. and Oceanogr., *Deep-Sea Research*, Suppl. to Vol. 3, pp. 92–109. 1955. (Included in *Collected Reprints* for 1955, Part II).

No. 761. A. H. Woodcock. Bursting Bubbles and Air Pollution. *Sewage and Industrial Wastes*, Vol. 27, No. 10, pp. 1189–1192. 1955.

No. 762. Gordon A. Riley. Review of the Oceanography of Long Island Sound. Pap. Mar. Biol. and Oceanogr., *Deep-Sea Research*, Suppl. to Vol. 3, pp. 224–238. 1955. (Included in *Collected Reprints* for 1955, Part II).

No. 763. Talbot H. Waterman. Polarization of Scattered Sunlight in Deep Water. Pap. Mar. Biol. and Oceanogr., *Deep-Sea Research*, Suppl. to Vol. 3, pp. 426–434. 1955. (Included in *Collected Reprints* for 1955, Part II).

No. 764. E. M. Hulburt. The Phytoplankton of Great Pond, Massachusetts. *Biol. Bull.*, Vol. 110, No. 2, pp. 157–168. 1956.

No. 765. C. O'D. Iselin. Recent Advances in our Understanding of the Circulation Problem and their Implications. *Sears Found., Jour. Mar. Res.*, Vol. 14, No. 4, pp. 315–322. 1955.

No. 766. John C. Ayers. Population Dynamics of the Marine Clam, *Mya arenaria*. *Limnol. and Oceanogr.*, Vol. 1, No. 1, pp. 26–34. 1956.

No. 767. Edward M. Thorndike. Hydroscopes. *Trans. Amer. Geophys. Union*, Vol. 36, No. 3, pp. 470–472. 1955.

No. 768. A. H. Woodcock and D. C. Blanchard. Tests of the Salt-Nuclei Hypothesis of Rain Formation. *Tellus*, Vol. 7, No. 4, pp. 437–448. 1955.

No. 769. Wilbur Marks and Joseph Chase. Observation of the Growth and Decay of a Wave Spectrum. In: Interaction of Sea and Atmosphere. *Meteorol. Monogr.*, Vol. 2, No. 10, pp. 67–74. 1957.

No. 770. C.-G. Rossby and H. Egnér. On the Chemical Climate and its Variation with Atmospheric Circulation Pattern. *Tellus*, Vol. 7, No. 1, pp. 118–133. 1955.

No. 771. Stefan Machlup and J. B. Hersey. Analysis of Sound-Scattering Observations from Non-Uniform Distributions of Scatterers in the Ocean. *Deep-Sea Research*, Vol. 3, pp. 1–22. 1955.

No. 772. Bostwick H. Ketchum. Distribution of Coliform Bacteria and other Pollutants in Tidal Estuaries. *Sewage and Industrial Wastes*, Vol. 27, No. 11, pp. 1288–1296. 1955.

No. 773. Susan I. Scholander. Land Birds over the Western North Atlantic. *The Auk*, Vol. 72, pp. 225–239. 1955.

No. 774. Harvey R. Bullis, Jr. and F. J. Mather, III. Tunas of the Genus *Thunnus* of the Northern Caribbean. *Novitates*, No. 1765, 12 pp. 1956.

No. 775. Bostwick H. Ketchum and D. Jean Keen. The Accumulation of River Water over the Continental Shelf between Cape Cod and Chesapeake Bay. Pap. Mar. Biol. and Oceanogr., *Deep-Sea Research*, Suppl. to Vol. 3, pp. 346–357. 1955. (Included in *Collected Reprints* for 1955, Part II).

No. 776. Alfred C. Redfield. The Hydrography of the Gulf of Venezuela. Pap. Mar. Biol. and Oceanogr., *Deep-Sea Research*, Suppl. to Vol. 3, pp. 115–133. 1955. (Included in *Collected Reprints* for 1955, Part II).

No. 777. Harry J. Turner, Jr. How Clam Drills Capture Razor Clams. *The Nautilus*, Vol. 69, No. 1, pp. 20–22. 1955.

No. 778. J. W. Kanwisher. Freezing in Intertidal Animals. *Biol. Bull.*, Vol. 109, No. 1, pp. 56–63. 1955.

No. 779. Ruth D. Turner. Scaphopods of the *Atlantis* Dredgings in the Western Atlantic with a Catalogue of the Scaphopod Types in the Museum of Comparative Zoology. Pap. Mar. Biol. and Oceanogr., *Deep-Sea Research*, Suppl. to Vol. 3, pp. 309–320. 1955. (Included in *Collected Reprints* for 1955, Part II).

No. 780. E. Steemann Nielsen. The Production of Antibiotics by Plankton Algae and its Effect upon Bacterial Activities in the Sea. Pap. Mar. Biol. and Oceanogr., *Deep-Sea Research*, Suppl. to Vol. 3, pp. 281–286. 1955. (Included in *Collected Reprints* for 1955, Part II).

No. 781. W. T. Edmondson. Factors Affecting Productivity in Fertilized Water. Pap. Mar. Biol. and Oceanogr., *Deep-Sea Research*, Suppl. to Vol. 3, pp. 451–464. 1955. (Included in *Collected Reprints* for 1955, Part II).

No. 782. Henry C. Stetson. Patterns of Deposition at the Continental Margin. Pap. Mar. Biol. and Oceanogr., *Deep-Sea Research*, Suppl. to Vol. 3, pp. 298–308. 1955. (Included in *Collected Reprints* for 1955, Part II).

No. 783. Harry J. Turner, Jr. and Stanley Scher. Seventh Report on Investigations of the Shellfisheries of Massachusetts. *Com. Mass., Dept. Nat. Res., Div. Mar. Fish.*, 35 pp. 1954.

No. 784. Alfred C. Redfield. Preludes to the entrapment of organic matter in the sediments of Lake Maracaibo. In: Habitat of Oil. Amer. Assoc. Petrol. Geologists, June, 1958.

No. 785. Earl Barrett and Gunnar Brodin. The Acidity of Scandinavian Precipitation. *Tellus*, Vol. 7, No. 2, pp. 251–257. 1955.

No. 786. T. F. Goreau and V. T. Bowen. Calcium Uptake by a Coral. *Science*, Vol. 122, No. 3181, pp. 1188–1189. 1955.

No. 787. Henry B. Bigelow, William C. Schroeder and Stewart Springer. Three New Shark Records from the Gulf of Mexico. *Breviora*, No. 49, 12 pp. 1955.

No. 788. Dean F. Bumpus. The Circulation over the Continental Shelf South of Cape Hatteras. *Trans. Amer. Geophys. Union*, Vol. 36, No. 4, pp. 601–611. 1955.

No. 789. Donald R. Griffin. Hearing and Acoustic Orientation in Marine Animals. Pap. Mar. Biol. and Oceanogr., *Deep-Sea Research*, Suppl. to Vol. 3, pp. 406–417. 1955. (Included in *Collected Reprints* for 1955, Part II).

No. 790. William C. Schroeder. Report on the Results of Exploratory Otter-Trawling along the Continental Shelf and Slope between Nova Scotia and Virginia during the Summers of 1952 and 1953. Pap. Mar. Biol. and Oceanogr., *Deep-Sea Research*, Suppl. to Vol. 3, pp. 358–372. 1955. (Included in *Collected Reprints* for 1955, Part II).

No. 791. L. V. Worthington. A New Theory of Caribbean Bottom-Water Formation. *Deep-Sea Research*, Vol. 3, pp. 82–87. 1955.

No. 792. C. O'D. Iselin. Coastal Currents and the Fisheries. Pap. Mar. Biol. and Oceanogr., *Deep-Sea Research*, Suppl. to Vol. 3, pp. 474–478. 1955. (Included in *Collected Reprints* for 1955, Part II).

No. 793. Barbara Lawrence and William E. Schevill. The Functional Anatomy of the Delphinid Nose. *Bull. Mus. Comp. Zool.*, Vol. 114, No. 4, pp. 103–151. 1956. (Not included in *Collected Reprints*).

No. 794. William S. Von Arx and W. S. Richardson. On the Fine-Structure of the Gulf Stream Front. *Deep-Sea Research*, Vol. 3, pp. 46–65. 1955.

No. 795. P. F. Scholander, L. van Dam, C. Lloyd Claff and J. W. Kanwisher. Micro Gasometric Determination of Dissolved Oxygen and Nitrogen. *Biol. Bull.*, Vol. 109, No. 2, pp. 328–334. 1955.

No. 796. Henry Stommel. Lateral Eddy Viscosity in the Gulf Stream System. *Deep-Sea Research*, Vol. 3, pp. 88–90. 1955.

No. 797. Irving I. Schell. Further Evidence of Dynamic Persistence and of its Application to Foreshadowing. *Jour. Meteorol.*, Vol. 13, No. 5, pp. 471–481. 1956.

No. 798. Nora Gladwin Fairbank. Methods and Preliminary Results in a Study of Minerals from the Eastern Gulf of Mexico. *Jour. Sed. Petrol.*, Vol. 26, No. 3, pp. 268–275. 1956.

No. 799. Henry Stommel, Arnold B. Arons and Duncan Blanchard. An Oceanographical Curiosity: the Perpetual Salt Fountain. *Deep-Sea Research*, Vol. 3, pp. 152–153. 1956.

No. 800. M. S. Gordon and Richard H. Backus. New Records of Labrador Fishes with Special Reference to those of Hebron Fjord. *Copeia*, No. 1, pp. 17–20. 1957.

No. 801. Floyd M. Soule and J. E. Murray. Physical Oceanography of the Grand Banks and the Labrador Sea in 1955. *U. S. Coast Guard Bull.*, No. 41, pp. 59–114. 1956.

No. 802. James M. Moulton and Richard H. Backus. Annotated References Concerning the Effects of Man-Made Sounds on the Movements of Fishes. *Dept. Sea and Shore Fish.*, Augusta, Maine, Fish. Circ. No. 17, 8 pp. 1955.

No. 804. W. V. R. Malkus. Outline of a Theory of Turbulent Shear Flow. *Jour. Fluid Mech.*, Vol. 1, Pt. 5, pp. 521–539. 1956.

No. 805. John Mackiewicz and Richard H. Backus. Oceanic Records of *Lasionycteris noctivagans* and *Lasiurus borealis*. *Jour. Mammalogy*, Vol. 37, No. 3, pp. 442–443. 1956.

No. 806. Allyn C. Vine. Oceanographic Instrumentation. *Science*, Vol. 122, No. 3173, pp. 748–751. 1955.

No. 807. P. F. Scholander and William E. Schevill. Counter-Current Vascular Heat Exchange in the Fins of Whales. *Jour. Appl. Physiol.*, Vol. 8, No. 3, pp. 279–282 1955.

No. 808. E. Steemann Nielsen. The Interaction of Photosynthesis and Respiration and its Importance for the Determination of ^{14}C-Discrimination in Photosynthesis. *Physiologia Plantarum*, Vol. 8, pp. 945–953. 1955.

No. 809. Duncan C. Blanchard. The Supercooling, Freezing and Melting of Giant Waterdrops at Terminal Velocity in Air. Proceedings of the First Conference on the Physics of Cloud Precipitation Particles, Woods Hole, September 7–10, 1955. In: Artificial Stimulation of Rain, pp. 233–249. Pergamon Press, New York, London, Paris. 1957.

No. 810. Karl E. Schleicher and Alvin Bradshaw. A Conductivity Bridge for Measurement of the Salinity of Sea Water. *Jour. du Conseil*, Vol. 22, No. 1, pp. 9–20. 1956.

No. 811. G. W. Morgan. On the Wind-Driven Ocean Circulation. *Tellus*, Vol. 8, No. 3, pp. 301–320. 1956.

No. 812. Duncan C. Blanchard. Discussion of Raindrop Distributions made during Project Shower, Hawaii, 1954. Proceedings of the First Conference on the Physics of Cloud Precipitation Particles, Woods Hole, September 7–10, 1955. In: Artificial Stimulation of Rain, pp. 213–223. Pergamon Press, New York, London, Paris. 1957.

No. 813. R. W. Holmes. The Annual Cycle of Phytoplankton in the Labrador Sea, 1950–51. *Bull. Bingham Oceanogr. Coll.*, Vol. 16, Art. 1, 74 pp. 1956. (Not included in Collected Reprints).

No. 814. Richard H. Backus, Stewart Springer and Edgar L. Arnold, Jr. A Contribution to the Natural History of the White-Tip Shark, *Pterolamiops longimanus* (Poey). *Deep-Sea Research*, Vol. 3, pp. 178–188. 1956.

No. 815. William E. Schevill. *Lagenorhynchus acutus* off Cape Cod. *Jour. Mammalogy*, Vol. 37, No. 1, pp. 128–129. 1956.

No. 816. P. F. Scholander, L. van Dam and Theodore Enns. Nitrogen Secretion in the Swimbladder of Whitefish. *Science*, Vol. 123, No. 3185, pp. 59–60. 1956.

No. 817. Harold E. Edgerton and Lloyd D. Hoadley. Cameras and Lights for Underwater Use. *Jour. Soc. Motion Pict. and Teler. Eng.*, Vol. 64, pp. 345–350. 1955.

No. 818. P. F. Scholander, John W. Kanwisher and D. C. Nutt. Gases in Icebergs. *Science*, Vol. 123, No. 3186, pp. 104–105. 1956.

No. 819. John H. Ryther. Photosynthesis in the Ocean as a Function of Light Intensity. *Limnol. and Oceanogr.*, Vol. 1, No. 1, pp. 61–70. 1956.

No. 820. William S. von Arx. An Experimental Approach to Problems in Physical Oceanography. In: Progress in Physics and Chemistry of the Earth, Vol. 2, pp. 1–29. Pergamon Press, London, New York, Paris. 1957.

No. 821. George L. Clarke and Gunther K. Wertheim. Measurements of Illumination at Great Depths and at Night in the Atlantic Ocean by Means of a New Bathyphotometer. *Deep-Sea Research*, Vol. 3, pp. 189–205. 1956.

No. 822. P. F. Scholander. Hydrostatic Pressure in Coconuts. *Plant Physiol.*, Vol. 30, No. 6, pp. 560–561. 1955.

No. 823. John C. Ayers. A Dynamic Height Method for the Determination of Currents in Deep Lakes. *Limnol. and Oceanogr.*, Vol. 1, No. 3, pp. 150–161. 1956.

No. 824. Parker D. Trask. The *Atlantis* Marine Geological Expedition to Peru and Chile. *Nature*, Vol. 177, pp. 454–455. 1956.

No. 825. John H. Ryther. The Measurement of Primary Production. *Limnol. and Oceanogr.*, Vol. 1, No. 2, pp. 72–84. 1956.

No. 826. Robert L. Miller. Trend Surfaces: Their Application to Analysis and Description of Environments of Sedimentation. 1. The Relation of Sediment-Size Parameters to Current-Wave Systems and Physiography. *Jour. Geology*, Vol. 64, No. 5, pp. 425–446. 1956.

No. 827. Joanne Starr Malkus. On the Maintenance of the Trade Winds. *Tellus*, Vol. 8, No. 3, pp. 335–350. 1956.

No. 828. Alfred C. Redfield and Arthur R. Miller. Water Levels Accompanying Atlantic Coast Hurricanes. In: Interaction of Sea and Atmosphere. *Meteorol. Monogr.*, Vol. 2, No. 10, pp. 1–23. 1957.

No. 829. Arthur R. Miller. The Effect of Steady Winds on Sea Level at Atlantic City. In: Interaction of Sea and Atmosphere. *Meteorol. Monogr.*, Vol. 2, No. 10, pp. 24–31. 1957.

No. 830. Francis A. Richards and Ralph F. Vaccaro. The Cariaco Trench, an Anaerobic Basin in the Caribbean Sea. *Deep-Sea Research*, Vol. 3, pp. 214–228. 1956.

No. 831. David C. Nutt and Lawrence K. Coachman. The Oceanography of Hebron Fjord, Labrador. *Jour. Fish. Res. Bd. Canada*, Vol. 13, No. 5, pp. 709–758. 1956.

No. 832. William E. Schevill and Barbara Lawrence. Food-Finding by a Captive Porpoise (*Tursiops truncatus*). *Breviora*, No. 53, 15 pp. 1956.

No. 833. A. F. Bunker. Turbulence Measurements in a Young Cyclone over the Ocean. *Bull. Amer. Meteorol. Soc.*, Vol. 38, No. 1, pp. 13–16. 1957.

No. 834. Richard H. Backus and J. B. Hersey. Echo-Sounder Observations of Midwater Nets and their Towing Cables. *Deep-Sea Research*, Vol. 3, pp. 237–241. 1956.

No. 835. Joseph Chase. The Bermuda-Azores High Pressure Cell. Its Surface Wind Circulation. *Miscelânea Geofísica*, pp. 29–54. Luanda, Angola. 1956.

No. 837. A. H. Woodcock. Dimorphism in the Portuguese Man-of-War. *Nature*, Vol. 178, No. 4527, pp. 253–255. 1956.

No. 838. E. M. Hulburt. The Taxonomy of Unarmored Dinophyceae of Shallow Embayments on Cape Cod, Massachusetts. *Biol. Bull.*, Vol. 112, No. 2, pp 196–219. 1957.

No. 839. C. B. Officer, J. I. Ewing, R. S. Edwards and H. R. Johnson. Geophysical Investigations in the Eastern Caribbean: Venezuelan Basin, Antilles Island Arc, and Puerto Rico Trench. *Bull. Geol. Soc. Amer.*, Vol. 68, pp. 359–378. 1957.

No. 840. Francis A. Richards. On the State of our Knowledge of Trace Elements in the Ocean. *Geochimica et Cosmochimica Acta*, Vol. 10, No. 4, pp. 241–243. 1956.

No. 841. Henry R. Johnson, Richard H. Backus, J. B. Hersey and D. M. Owen. Suspended Echo-Sounder and Camera Studies of Midwater Sound Scatterers. *Deep-Sea Research*, Vol. 3, pp. 266–272. 1956.

No. 842. John H. Ryther. Interrelation between Photosynthesis and Respiration in the Marine Flagellate, *Dunaliella euchlora*. *Nature*, Vol. 178, pp. 861–862. 1956.

No. 843. Joanne Starr Malkus. Trade Cumulus Cloud Groups: Some Observations Suggesting a Mechanism of Their Origin. *Tellus*, Vol. 9, No. 1, pp. 33–44. 1957.

No. 844. Francis A. Richards. Some Current Aspects of Chemical Oceanography. In: Progress in Physics and Chemistry of the Earth, Vol. 2, pp. 77–128. 1957.

No. 845. Henry Stommel. Florida Straits Transports, 1952–1956. *Bull. Mar. Sci., Gulf and Caribbean*, Vol. 7, No. 3, pp. 252–254. 1957.

No. 846. Henry Stommel. On the Determination of the Depth of No Meridional Motion. *Deep-Sea Research*, Vol. 3, pp. 273–278. 1956.

No. 847. Athelstan Spilhaus. Control of the World Environment. *Geogr. Rev.*, Vol. 46, No. 4, pp. 451–459. 1956.

No. 848. Henry B. Bigelow and William C. Schroeder. A Study of the Sharks of the Suborder Squaloidea. *Bull. Mus. Comp. Zool.*, Vol. 117, No. 1, pp. 1–150. 1957. (Not included in *Collected Reprints*).

No. 849. Duncan C. Blanchard. Electrically Charged Drops from Bubbles in Sea Water and their Meteorological Significance. *Jour. Meteorol.*, Vol. 15, No. 4, pp. 383–396. 1958.

No. 850. von H. Walden and H. G. Farmer. Auswertung von Seegangsregistrierungen des Forschungsschiffes "Atlantis" mit dem "Ship-Borne Wave Recorder" sowie Vergleich mit entsprechenden Seegangsberechnungen aus den Windverhaltnissen (Hindcasting). *Deutsche Hydrogr. Zeitschrift*, Bd. 10, Heft 4, pp. 121–134. 1957.

No. 851. Allyn C. Vine, Some Trends in Oceanographic Instrumentation. *Proc. UNESCO Symp. Phys. Oceanogr.*, Tokyo, 1955: 49–52. 1597. (Not included in *Collected Reprints*).

No. 852. Francis A. Richards and Nathaniel Corwin. Some Oceanographic Applications of Recent Determinations of the Solubility of Oxygen in Sea Water. *Limnol. and Oceanogr.*, Vol. 1, No. 4, pp. 263–267. 1956.

No. 853. Irving I. Schell. On the Nature and Origin of the Southern Oscillation. *Jour. Meteorol.*, Vol. 13, No. 6, pp. 592–598. 1956.

No. 854. Richard H. Backus. Northern Record of the Snake Eel *Ophichthus gomesi* (Castelnau). *Copeia*, No. 1, p. 61. 1957.

No. 855. A. B. Arons and Henry Stommel. A β-Plane Analysis of Free Periods of the Second Class in Meridional and Zonal Oceans. *Deep-Sea Research*, Vol. 4, pp. 23–31. 1956.

No. 856. Gordon Volkmann, John Knauss and Allyn Vine. The Use of Parachute Drogues in the Measurement of Subsurface Ocean Currents. *Trans. Amer. Geophys. Union*, Vol. 37, No. 5, pp. 573–577. 1956.

No. 857. Richard H. Backus. Notes on Western North Atlantic Sharks. *Copeia*, No. 3, pp. 246–248. 1957.

No. 858. George L. Clarke and Richard H. Backus. Measurements of Light Penetration in Relation to Vertical Migration and Records of Luminescence of Deep-Sea Animals. *Deep-Sea Research*, Vol. 4, pp. 1–14. 1956.

No. 859. G. Veronis and Henry Stommel. The Action of Variable Wind Stresses on a Stratified Ocean. *Sears Found., Jour. Mar. Res.*, Vol. 15, No. 1, pp. 43–75. 1956.

No. 860. I. Friedman and A. H. Woodcock. Determination of Deuterium-Hydrogen Ratios in Hawaiian Waters. *Tellus*, Vol. 9, No. 4, pp. 553–556. 1957.

No. 861. J. I. Ewing, C. B. Officer, H. R. Johnson, and R. S. Edwards. Geophysical Investigations in the Eastern Caribbean: Trinidad Shelf, Tobago Trough, Barbados Ridge, Atlantic Ocean. *Bull. Geol. Soc. Amer.*, Vol. 68, pp. 897–912. 1957.

No. 862. James M. Moulton. Influencing the Calling of Sea Robins (*Prionotus* spp.) with Sound. *Biol .Bull.*, Vol. 111, No. 3, pp. 393–398. 1956.

No. 863. S. T. Knott and J. B. Hersey. Interpretation of High-Resolution Echo-Sounding Techniques and their Use in Bathymetry, Marine Geophysics, and Biology. *Deep-Sea Research*, Vol. 4, pp. 36–44. 1956.

No. 864. H. B. Moore and E. G. Corwin. The Effects of Temperature, Illumination, and Pressure on the Vertical Distribution of Zooplankton. *Bull. Mar. Sci., Gulf and Caribbean*, Vol. 6, No. 4, pp. 273–287. 1956.

No. 865. Richard S. Edwards and Francis A. Richards. A Bottom-Water Sampler. *Deep-Sea Research*, Vol. 4, pp. 65–66. 1956.

No. 866. M. S. Rutstein. Flooded Quarries for Experimental Work. *Trans. Amer. Geophys. Union*, Vol. 35, No. 5, pp. 688–690. 1957.

No. 867. Irving Friedman, Daniel R. Norton, Douglas B. Carter and Alfred C. Redfield. The Deuterium Balance of Lake Maracaibo. *Limnol. and Oceanogr.*, Vol. 1, No. 4, pp. 239–246. 1956.

No. 868. M. S. Gordon. Observations on Osmoregulation in the arctic char (*Salvelinus alpinus* L.). *Biol. Bull.*, Vol. 112, No. 1, pp. 28–33. 1957.

No. 869. Helen S. Vishniac. On the Ecology of the Lower Marine Fungi. *Biol. Bull.*, Vol. 111, No. 3, pp. 410–414. 1956.

No. 870. W. S. Wooster and Bostwick H. Ketchum. Transport and Dispersal of Radioactive Elements in the Sea. In: The Effects of Atomic Radiation on Oceanography and Fisheries. Publ. No. 551, Nat. Acad. Sci.-Nat. Res. Council, Chapt. 4, pp. 43–51. 1957.

No. 871. Bostwick H. Ketchum. The Effects of the Ecological System on the Transport of Elements in the Sea. In: The Effects of Atomic Radiation on Oceanography and Fisheries. Publ. No. 551, Nat. Acad. Sci.-Nat. Res. Council, Chapt. 5, pp. 52–59. 1957.

No. 873. Lawrence K. Coachman, E. Hemmingsen and P. F. Scholander. Gas Enclosures in a Temperate Glacier. *Tellus*, Vol. 8, No. 4, pp. 415–423. 1956. (Not included in *Collected Reprints*).

No. 874. J. B. Hersey. Electronics in Oceanography. In: Advances in Electronics and Electron Physics. Vol. 9, pp. 239–295. Academic Press, Inc., New York. 1957. (Not included in *Collected Reprints*.)

No. 875. Duncan C. Blanchard and A. H. Woodcock. Bubble Formation and Modification in the Sea and its Meteorological Significance. *Tellus*, Vol. 9, No. 2, pp. 145–158. 1957.

No. 876. Harry J. Turner, Carl J. George and Joseph H. Connell. Eighth Report on Investigations of the Shellfisheries of Massachusetts. *Com. Mass., Dept. Nat. Res., Div. Mar. Fish.*, 25 pp. 1955.

No. 877. Floyd M. Soule and J. E. Murray. Physical Oceanography of the Grand Banks Region and the Labrador Sea in 1956. *U. S. Coast Guard Bull.*, No. 42, pp. 35–100. 1957.

No. 878. J. W. Kanwisher and H. Leivestad. Thermal Regulation in Whales. *Norwegian Whaling Gazette*, No. 1, pp. 1–5. 1957.

No. 879. P. F. Scholander and L. van Dam. Micro Gasometric Determination of Oxygen in Fish Blood. *Jour. Cell. and Comp. Physiol.*, Vol. 48, No. 3, pp. 529–532. 1956.

No. 880. P. F. Scholander. Observations on the Gas Gland in Living Fish. *Jour. Cell. and Comp. Physiol.*, Vol. 48, No. 3, pp. 523–528. 1956.

No. 881. P. F. Scholander, L. van Dam and Theodore Enns. The Source of Oxygen Secreted into the Swimbladder of Cod. *Jour. Cell. and Comp. Physiol.*, Vol. 48, No. 3, pp. 517–522. 1956.

No. 882. H. L. Sanders. The Cephalocarida and Crustacean Phylogeny. *Syst. Zool.*, Vol. 6, No. 3, pp. 112–129. 1957.

No. 883. John C. Ayers and Roger Bachmann. Simplified Computations for the Dynamic Height Method of Current Determination in Lakes. *Limnol. and Oceanogr.*, Vol. 2, No. 2, pp. 155–157. 1957.

No. 884. John M. Zeigler and F. C. Ronne. Time-Lapse Photography - - an Aid to Studies of the Shoreline. *Research Reviews*, Office of Naval Research, Washington, April, pp. 1–6. 1957.

No. 885. Shannon R. Torphy and John M. Zeigler. Submarine Topography of Eastern Channel, Gulf of Maine. *Jour. Geology*, Vol. 65, No. 4, pp. 433–441. 1957.

No. 886. Harry J. Turner and David L. Belding. The Tidal Migrations of *Donax variabilis* Say. *Limnol. and Oceanogr.*, Vol. 2, No. 2, pp. 120–124. 1957.

No. 887. J. W. Kanwisher. Freezing and Drying in Intertidal Algae. *Biol. Bull.*, Vol. 113, No. 2, pp. 275–285. 1957.

No. 888. J. W. Kanwisher and Alfred Ebeling. Composition of the Swim-Bladder Gas in Bathypelagic Fishes. *Deep-Sea Research*, Vol. 4, pp. 211–217. 1957.

No. 889. A. H. Woodcock and A. T. Spencer. An Airborne Flame Photometer and its Use in the Scanning of Marine Atmospheres for Sea-Salt Particles. *Jour. Meteorol.*, Vol. 14, No. 5, pp. 437–447. 1957.

No. 890. Willem A. van Bergeijk and Emil Witschi. The Basilar Papilla of the Anuran Ear. *Acta Anatomica*, Vol. 30, pp. 81–91. 1957. (Not included in *Collected Reprints*).

No. 891. P. F. Scholander, L. van Dam, J. W. Kanwisher, H. T. Hammel and M. S. Gordon. Supercooling and Osmoregulation in Arctic Fish. *Jour. Cell. and Comp. Physiol.*, Vol. 49, No. 1, pp. 5–24. 1957.

No. 892. P. F. Scholander and L. van Dam. The Concentration of Hemoglobin in Some Cold Water Arctic Fishes. *Jour. Cell. and Comp. Physiol.*, Vol. 49, No. 1, pp. 1–4. 1957.

No. 893. Charles S. Yentsch and John H. Ryther. Short-term Variations in Phytoplankton Chlorophyll and Their Significance. *Limnol. and Oceanogr.*, Vol. 2, No. 2, pp. 140–142. 1957.

No. 894. Richard H. Backus and Harold Barnes. Television-Echo-Sounder Observations by Midwater Sound Scatterers. *Deep-Sea Research*, Vol. 4, pp. 116–119. 1957.

No. 895. Robert G. Walden, David D. Ketchum and David H. Frantz, Jr. Buoy Telemeters Ocean Temperature Data. *Electronics*, Vol. 30, No. 6, pp. 164–167. McGraw Hill Co., New York. 1957.

No. 896. Richard H. Backus. The Fishes of Labrador. *Bull. Amer. Mus. Nat. Hist.*, Vol. 113, Art. 4, pp. 273–337. 1957. (Not included in *Collected Reprints*).

No. 897. Harold Barnes. The Northern Limit of *Balanus balanoides* (L). *Oikos*, Vol. 8, No. 1, pp. 1–15. 1957.

No. 898. Charles S. Yentsch. A Non-Extractive Method for the Quantitative Estimation of Chlorophyll in Algal Cultures. *Nature*, Vol. 179, pp. 1302–1304. 1957.

No. 899. Henry Stommel and George Veronis. Steady Convective Motion in a Horizontal Layer of Fluid Heated Uniformly from Above and Cooled Non-Uniformly from Below. *Tellus*, Vol. 9, No. 3, pp. 401–407. 1957.

No. 900. Arthur R. Miller. The Effects of Winds on Water Levels on the New England Coast. *Limnol. and Oceanogr.*, Vol. 3, No. 1, pp. 1–14. 1958.

No. 901. Frank J. Mather III and Robert H. Gibbs. Distributional Records of Fishes from Waters off New England and the Middle Atlantic States. *Copeia*, No. 3, pp. 242–244. 1957.

No. 902. John H. Ryther and Charles S. Yentsch. The Estimation of Phytoplankton Production in the Ocean from Chlorophyll and Light Data. *Limnol. and Oceanogr.*, Vol. 2, No. 3, pp. 281–286. 1957.

No. 903. W. H. Sutcliffe, Jr. An Improved Method for the Determination of Preserved Plankton Volumes. *Limnol. and Oceanogr.*, Vol. 2, No. 3, pp. 295–296. 1957.

No. 904. Dean F. Bumpus. Surface Water Temperature along Atlantic and Gulf Coasts of the United States. U. S. Fish and Wildlife Service, Spec. Sci. Rept. — Fisheries No. 214, 153 pp. 1957. (Not included in *Collected Reprints*).

No. 905. William D. Athearn. Comparisons of Clay from the Continental Shelf off Long Island with the Gardiners Clay. *Jour. Geology*, Vol. 65, No. 4, pp. 448–449. 1957.

No. 906. John H. Ryther and Charles S. Yentsch. Primary Production of Continental Shelf Waters off New York. *Limnol. and Oceanogr.*, Vol. 3, No. 3, pp. 327–335. 1958.

No. 907. Vaughan T. Bowen and T. T. Sugihara. Strontium 90 in North Atlantic Surface Water. *Proc. Nat. Acad. Sci.*, Vol. 43, No. 7, pp. 576–580. 1957.

No. 908. L. V. Worthington and William E. Schevill. Underwater Sounds Heard from Sperm Whales. *Nature*, Vol. 180, p. 291. 1957.

No. 909. Jan Hahn. Oceanus Goes to the Bottom of the Sea. Reprinted from *Oceanus*, Vol. 5, Nos. 1 and 2, pp. 20–31. 1957.

No. 910. J. C. SWALLOW and L. V. WORTHINGTON. Measurements of Deep Currents in the Western North Atlantic. *Nature*, Vol. 179, pp. 1183–1184. 1957.

No. 911. G. C. MCLEOD. The Effect of Circularly Polarized Light on the Photosynthesis and Chlorophyll *a* Synthesis of Certain Marine Algae. *Limnol. and Oceanogr.*, Vol. 2, No. 4, pp. 360–362. 1957.

No. 912. ROBERT H. GIBBS, JR. A Taxonomic Analysis of *Myctophum affine* and *M. nitidulum*, two Lantern-Fishes Previously Synonymized, in the Western North Atlantic. *Deep-Sea Research*, Vol. 4, pp. 230–237. 1957.

No. 913. E-AN ZEN. Preliminary Report on the Mineralogy and Petrology of Some Marine Bottom Samples off the Coast of Peru and Chile. *Amer. Mineralogist*, Vol. 42, pp. 889–903. 1957.

No. 914. JAMES M. MOULTON. Sound Production in the Spiny Lobster *Panulirus argus* (Latreille). *Biol. Bull.*, Vol. 113, No. 2, pp. 286–295. 1957.

No. 915. JOANNE S. MALKUS. On the Structure and Maintenance of the Mature Hurricane Eye. *Jour. Meteorol.*, Vol. 15, No. 4, pp. 337–349. 1958.

No. 916. G. G. WHITNEY, JR. Factors Affecting the Accuracy of Thermometric Depth Determinations. *Jour. du Conseil*, Vol. 22, No. 2, pp. 167–173. 1957.

No. 917. HENRY STOMMEL. A Survey of Ocean Current Theory. *Deep-Sea Research*, Vol. 4, pp. 149–184. 1957.

No. 918. DEAN F. BUMPUS. Oceanographic Observations 1956, East Coast of the United States. U. S. Fish and Wildlife Service, Spec. Sci. Rept. — Fisheries No. 233, 132 pp. 1957. (Not included in *Collected Reprints*).

No. 919. JOHN M. ZEIGLER, W. D. ATHEARN and H. SMALL. Profiles across the Peru-Chile Trench. *Deep-Sea Research*, Vol. 4, pp. 238–249. 1957.

No. 920. A. H. WOODCOCK. The Release of Latent Heat in Tropical Storms due to the Fall-Out of Sea-Salt Particles. *Tellus*, Vol. 10, No. 3, pp. 355–371. 1958.

No. 921. P. F. SCHOLANDER. Oxygen Dissociation Curves in Fish Blood. *Acta Physiol Scand.*, Vol. 41, No. 4, pp. 340–344. 1957.

No. 922. ROBERT H. GIBBS, JR. Preliminary Analysis of the Distribution of White Marlin, *Makaira albida* (Poey), in the Gulf of Mexico. *Bull. Mar. Sci., Gulf and Caribbean*, Vol. 7, No. 4, pp. 360–369. 1957.

No. 923. ALFRED C. REDFIELD. The Inadequacy of Experiment in Marine Biology. In: Perspectives in Marine Biology. Symposium held at Scripps Inst. of Oceanogr., Univ. Cal., March 24-April 2, 1956. 1958.

No. 924. MARY A. PLUNKETT. The Qualitative Determination of Some Organic Compounds in Marine Sediments. *Deep-Sea Research*, Vol. 4, pp. 259–262. 1957.

No. 926. DEAN F. BUMPUS, JOSEPH CHASE, C. GODFREY DAY, DAVID H. FRANTZ, JR., DAVID D. KETCHUM and ROBERT G. WALDEN. A new Technique for Studying Non-Tidal Drift with Results of Experiments off Gay Head, Mass., and in the Bay of Fundy. *Jour. Fish. Bd. Canada*, Vol. 14, No. 6, pp. 931–944. 1957.

No. 928. H. BARNES and MARGARET BARNES. The Rate of Development of *Balanus balanoides* (L.) Larvae. *Limnol. and Oceanogr.*, Vol. 3, No. 1, pp. 29–32. 1958.

No. 929. Theodore R. Folsom and Allyn C. Vine. On the Tagging of Water Masses for the Study of Physical Processes in the Oceans. In: The Effects of Atomic Radiation on Oceanography and Fisheries. Publ. No. 551. Nat. Acad. Sci.-Nat. Res. Council, Chapt. 12, pp. 121–132. 1957.

No. 930. William S. von Arx. "Dister": A Displacement Sequence Stereoscope. *Jour. Meteorol.*, Vol. 15, No. 2, pp. 230–231. 1958.

No. 931. William S. von Arx. Synoptic Photography. *Weather, Roy. Meteorol. Soc.*, London, pp. 179–197. 1958.

No. 932. Henry B. Bigelow and William C. Schroeder. Four New Rajids from the Gulf of Mexico. *Bull. Mus. Comp. Zool.*, Vol. 119, No. 2, pp. 201–233. 1958.

No. 933. G. Veronis. On the Transient Response of a β-plane Ocean. *Jour. Oceanogr. Soc. Japan*, Vol. 14, No. 1, pp. 1–5. 1958.

No. 934. William S. Richardson and Charles H. Wilkins. An Airborne Radiation Thermometer. *Deep-Sea Research*, Vol. 5, pp. 62–71. 1958.

No. 935. Joyce C. Lewin, R. A. Lewin and D. E. Philpott. Observations on *Phaeodactylum tricornutum. Jour. Gen. Microbiology*. Vol. 18, No. 2, pp. 420–426. 1958.

No. 936. Joyce C. Lewin. The Taxonomic Position of *Phaeodactylum tricornutum. Jour. Gen. Microbiology*. Vol. 18, No. 2, pp. 427–432. 1958.

No. 938. Harry J. Turner. The Effect of Nutrition on the Color of the Callus of *Polinices duplicatus. The Nautilus*, Vol. 72, No. 1, pp. 1–3. 1958.

No. 939. Henry Stommel, A. B. Arons and A. J. Faller. Some Examples of Stationary Planetary Flow Patterns in Bounded Basins. *Tellus*, Vol. 10, No. 2, pp. 179–187. 1958.

No. 940. Howard L. Sanders. Benthic Studies in Buzzards Bay. I. Animal-Sediment Relationships. *Limnol. and Oceanogr.* Vol. 3, No. 3, pp. 245–258. 1958.

No. 941. Dean F. Bumpus and C. Godfrey Day. Drift Bottle Records for the Gulf of Maine and Georges Bank, 1931–56. U.S. Fish and Wildlife Service, Spec. Sci. Rept. — Fisheries No. 242, 61 pp. 1957.

No. 942. Frank J. Mather, III and Robert H. Gibbs, Jr. Distribution of the Atlantic Bigeye Tuna, *Thunnus obesus*, in the western North Atlantic and the Caribbean Sea. *Copeia*, 1958, No. 3, pp. 237–239. 1958.

No. 943. W. V. R. Malkus and G. Veronis. Finite Amplitude Cellular Convection. *Jour. Fluid Mech.*, Vol. 4, Pt. 3, pp. 225–260. 1958.

No. 944. J. B. Hersey and M. S. Rutstein. Reconnaissance Survey of Oriente Deep (Caribbean Sea) with a Precision Echo Sounder. *Bull. Geol. Soc. Amer.*, Vol. 69, pp. 1297–1304. 1958.

No. 945. Alan J. Faller. An Optical Method for the Measurement of Surface Waves in the Laboratory. *Trans. Amer. Geophys. Union*, Vol. 39, No. 4, pp. 716–720. 1958.

No. 946. Bostwick H. Ketchum, John H. Ryther, Charles S. Yentsch and Nathaniel Corwin. Productivity in Relation to Nutrients. *Rapp. et Proc.-Verb., Cons. Internat. Explor. de la Mer*, Vol. 144, pp. 132–140. 1958.

No. 949. H. Barnes and Margaret Barnes. Further Observations on Self-Fertilization in *Chthamalus* sp. *Ecology*, Vol. 39, No. 3, p. 550. 1958.

No. 951. Takashi Ichiye. A Theory of Vertical Structure of Density in the Ocean. *Jour. Oceanogr. Soc. Japan*, Vol. 14, No. 2, pp. 35–40. 1958.

No. 952. Takashi Ichiye. Tsunami Waves—What are known about them—How we have studied them. *The Port Engineer*, Vol. 7, No. 1, pp. 5–19 [1–14]. Calcutta, India. 1958.

No. 953. Henry Stommel. Letter to the Editors: The Abyssal Circulation. *Deep-Sea Research*, Vol. 5, pp. 80–82. 1958.

No. 955. G. C. McLeod. Delayed Light Action Spectra of several Algae in Visible and Ultraviolet Light. *Jour. Gen. Physiol.*, Vol. 42, No. 2, pp. 243–250. 1958.

No. 957. James M. Moulton. The Acoustical Behavior of some Fishes in the Bimini Area. *Biol. Bull.*, Vol. 114, No. 3, pp. 357–374. 1958.

No. 958. Robert L. Miller and John M. Zeigler. A Model Relating Dynamics and Sediment Pattern in Equilibrium in the Region of Shoaling Waves, Breaker Zone, and Foreshore. *Jour. Geology*, Vol. 66, No. 4, pp. 417–441. 1958.

No. 959. Floyd M. Soule and R. M. Morse. Physical Oceanography of the Grand Banks Region and the Labrador Sea in 1957. *U. S. Coast Guard Bull.*, No. 43, pp. 81–131. 1958.

No. 960. James M. Moulton. A Summer Silence of Sea Robins, *Prionotus* spp. *Copeia* 1958, No. 3, pp. 234–235. 1958.

No. 963. Takashi Ichiye. The response of a Stratified Bounded Ocean to Variable Wind Stresses. *Oceanogr. Mag.*, Vol. 10, No. 1, pp. 19–63. Tokyo, Japan. 1958.

No. 965. Theodore J. Smayda. Biogeographical Studies of Marine Phytoplankton. *Oikos*, Vol. 9, No. 2, pp. 158–191. 1958.

No. 968. Bostwick H. Ketchum and Vaughan T. Bowen. Biological factors determining the distribution of radio-isotopes in the sea. Proc. 2nd Internat. Conference on the Peaceful Uses of Atomic Energy, Geneva, Sept. 1–15, 1958. Paper UN402-01C724, 11 pp. 1958.

No. 969. Joanne Starr Malkus. On the Structure of the Trade Wind Moist Layer. *Papers in Physical Oceanography and Meteorology*, Vol. 13, No. 2, pp. 1–47. 1958. (Not included in Collected Reprints.)

No. 970. Vaughan T. Bowen and T. T. Sugihara. Marine Geochemical Studies with Fall-out Radioisotopes. Proc. 2nd Internat. Conference on the Peaceful Uses of Atomic Energy, Geneva, Sept. 1–15, 1958. Paper UN403–01C902, 12 pp. 1958.

No. 972. Charles S. Yentsch and Ralph F. Vaccaro. Phytoplankton Nitrogen in the Oceans. *Limnol. and Oceanogr.*, Vol. 3, No. 4, pp. 443–448. 1958.

No. 976. Alfred C. Redfield. The Biological Control of Chemical Factors in the Environment. *Amer. Scientist*, Vol. 46, No. 3, pp. 205–222. 1958.

No. 977. C. Godfrey Day. Surface Circulation in the Gulf of Maine Deduced from Drift Bottles. U. S. Fish and Wildlife Service, Vol. 58, *Fish. Bull.* 141, pp. 443–472. 1958.

No. 978. John H. Ryther, Charles S. Yentsch and Ralph F. Vaccaro. The Dynamics of a Diatom Bloom. *Biol. Bull.*, Vol. 115, No. 2, pp. 257–268. 1958.

No. 979. A. T. Spencer and D. C. Blanchard. A Portable Raindrop Recorder for Semi-Continuous Determination of Size Distributions. *Trans. Amer. Geophys. Union.* Vol. 39, No. 5, pp. 853–857. 1958.

No. 981. Takashi Ichiye. On Convective Circulation and Density Distribution in a Zonally Uniform Ocean. *Oceanogr. Mag.*, Vol. 10, No. 1, pp. 97–135. Tokyo, Japan, 1958.

No. 983. P. F. Scholander. Counter Current Exchange: A Principle in Biology. *Hvalrådets Skrifter*, No. 44, 24 pp. Oslo. 1958.

No. 994. Gilbert L. Voss. The Cephalopods Collected by the R/V Atlantis during the West Indian Cruise of 1954. *Bull. Mar. Sci., Gulf and Caribbean*, Vol. 8, No. 4, pp. 369–389. 1958.

No. 998. H. Barnes. Regarding the Southern Limits of *Balanus balanoides* (L.) *Oikos*, Vol. 9, No. 2, pp. 139–157. 1958.

No. 1001. L. R. Breslau and H. E. Edgerton. The Luminescence Camera. *Jour. Biol. Photogr. Assoc.*, Vol. 26, No. 2, pp. 49–58, 1958.

No. 981. Takashi Ichiye. On Convective Circulation and Density Distribution in a Zonally Uniform Ocean. *Oceanogr. Mag.*, Vol. 10, No. 1, pp. 97–135. Tokyo, Japan, 1958.

No. 983. P. F. Scholander. Counter Current Exchange: A Principle in Biology. *Hvalrådets Skrifter*, No. 44, 24 pp. Oslo. 1958.

No. 994. Gilbert L. Voss. The Cephalopods Collected by the R/V Atlantis during the West Indian Cruise of 1954. *Bull. Mar. Sci., Gulf and Caribbean*, Vol. 8, No. 4, pp. 369–389. 1958.

No. 998. H. Barnes. Regarding the Southern Limits of *Balanus balanoides* (L.) *Oikos*, Vol. 9, No. 2, pp. 139–157. 1958.

No. 1001. L. R. Breslau and H. E. Edgerton. The Luminescence Camera. *Jour. Biol. Photogr. Assoc.*, Vol. 26, No. 2, pp. 49–58, 1958.